

AD \_\_\_\_\_

Award Number: DAMD17-99-1-9553

TITLE: Mechanisms of Neuronal Apoptosis In Vivo

PRINCIPAL INVESTIGATOR: Lee J. Martin, Ph.D.

CONTRACTING ORGANIZATION: The Johns Hopkins University  
Baltimore, MD 21205

REPORT DATE: February 2004

TYPE OF REPORT: Final

PREPARED FOR: U.S. Army Medical Research and Materiel Command  
Fort Detrick, Maryland 21702-5012

DISTRIBUTION STATEMENT: Approved for Public Release;  
Distribution Unlimited

The views, opinions and/or findings contained in this report are those of the author(s) and should not be construed as an official Department of the Army position, policy or decision unless so designated by other documentation.

20070321262

REPORT DOCUMENTATION PAGE			Form Approved OMB No. 074-0188	
Public reporting burden for this collection of information is estimated to average 1 hour per response, including the time for reviewing instructions, searching existing data sources, gathering and maintaining the data needed, and completing and reviewing this collection of information. Send comments regarding this burden estimate or any other aspect of this collection of information, including suggestions for reducing this burden to Washington Headquarters Services, Directorate for Information Operations and Reports, 1215 Jefferson Davis Highway, Suite 1204, Arlington, VA 22202-4302, and to the Office of Management and Budget, Paperwork Reduction Project (0704-0188), Washington, DC 20503				
1. AGENCY USE ONLY (Leave blank)	2. REPORT DATE February 2004	3. REPORT TYPE AND DATES COVERED Final (1 Jul 1999 - 31 Dec 2003)		
4. TITLE AND SUBTITLE  Mechanisms of Neuronal Apoptosis in Vivo		5. FUNDING NUMBERS  DAMD17-99-1-9553		
6. AUTHOR(S)  Lee J. Martin, Ph.D.				
7. PERFORMING ORGANIZATION NAME(S) AND ADDRESS(ES) The Johns Hopkins University Baltimore, MD 21205  E-Mail: martinl@jhmi.edu		8. PERFORMING ORGANIZATION REPORT NUMBER		
9. SPONSORING / MONITORING AGENCY NAME(S) AND ADDRESS(ES) U.S. Army Medical Research and Materiel Command Fort Detrick, Maryland 21702-5012		10. SPONSORING / MONITORING AGENCY REPORT NUMBER		
11. SUPPLEMENTARY NOTES  Original contains color plates: ALL DTIC reproductions will be in black and white				
12a. DISTRIBUTION / AVAILABILITY STATEMENT Approved for Public Release; Distribution Unlimited			12b. DISTRIBUTION CODE	
13. ABSTRACT (Maximum 200 Words)  Neuronal cell death in the central nervous system (CNS) has broad significance for military personnel in combat and veteran status and civilians. Neuronal cell death in the form of apoptosis or necrosis occurs after exposure to neurotoxins, chemical warfare agents, radiation, viruses, and after seizures, trauma, limb amputation, and hypoxic-ischemia caused by cardiac arrest, stroke, asphyxiation, and increased intracranial pressure. Secondary brain damage can result from hemorrhagic and hypovolemic shock. The goal of this project was to identify mechanisms of neuronal cell death. We discovered that injury-induced neuronal apoptosis in the adult CNS requires the <i>bax</i> gene and involves an upregulation of Bax and its translocation to mitochondria. The Bax upregulation requires a functional <i>p53</i> gene. The early events of target deprivation/axotomy-induced neuronal apoptosis involves oxidative stress, DNA damage, <i>p53</i> phosphorylation, and subcellular redistribution of death proteins. The process of neuronal apoptosis involves a perinuclear accumulation of mitochondria and cytochrome C release from mitochondria and caspase-3 activation. Upstream signals for neuronal apoptosis within the CNS involve the accumulation of specific forms of DNA lesions, including single-strand breaks, that trigger <i>p53</i> activation and downstream cell death. The DNA damage that occurs early during neuronal apoptosis has a reactive oxygen species fingerprint.				
14. SUBJECT TERMS Alzheimer's disease, amyotrophic lateral sclerosis, apoptosis, Bax, brain trauma, cell death, cerebral ischemia, DNA damage, secondary brain damage, mitochondria, oxidative stress, <i>p53</i>			15. NUMBER OF PAGES 463	
			16. PRICE CODE	
17. SECURITY CLASSIFICATION OF REPORT Unclassified	18. SECURITY CLASSIFICATION OF THIS PAGE Unclassified	19. SECURITY CLASSIFICATION OF ABSTRACT Unclassified	20. LIMITATION OF ABSTRACT Unlimited	



## Table of Contents

Cover.....	1
SF 298.....	2
Introduction.....	4
Body.....	5-26
Key Research Accomplishments.....	26-28
Reportable Outcomes.....	28-31
Conclusions.....	31-33
References.....	33-36
Appendices.....	36-461

## INTRODUCTION

The goal of our research supported by the USAMRMC was to further understand the molecular regulation of neuronal death and to identify novel neuroprotection strategies. This objective is fundamental to the Department of Defense and military operations ranging from veteran health care to combat casualty care. This objective is also highly significant for civilian populations as it relates to sporadic and familial neurodegenerative disease and terrorism situations. Neuronal degeneration occurs in many acute and chronic neurological disorders that effect humans and can occur in civilian and military personnel populations. In combat settings, acute neurodegeneration in the brain and spinal cord could occur after exposure to radiation and a variety of neurotoxins, including excitotoxins (e.g., glutamate receptor agonists), mitochondrial poisons (cyanide and 3-nitropropionic acid), and chemical warfare agents such as organophosphate compounds (soman) and mycotoxins (T-2 toxin). Acute neurological injury is also caused by trauma, hypoxia-ischemia (stroke and cardiac arrest), increased intracranial pressure, seizures and status epilepticus, with secondary brain damage resulting from hemorrhagic shock, hypovolemia, hypoxia, hypoglycemia, acidosis, hyperthermia, and asphyxiation. Chronic neurodegeneration occurs in Alzheimer's disease, amyotrophic lateral sclerosis (ALS), Huntington's disease, and Parkinson's disease. Veterans of the Gulf Wars may have an increased incidence of ALS (Charatan, 2002).

The development of effective neuroprotection therapies for these neurodegenerative conditions depends on a better understanding of the principles of selective vulnerability within the central nervous system (CNS) and the mechanisms of neuronal cell death. Our primary goal is to learn about the molecular and biochemical regulation of neuronal cell death using animal and cell culture models of neurodegeneration. Cells can die in different ways. This fundamental idea was proposed first in the early 1970s (Kerr et al., 1972; Schweichel and Merker, 1973). Historically, the death of cells has been classified generally as two distinct types, called apoptosis and necrosis. These two forms of cellular degeneration were originally classified differently because microscopically they differ structurally. The ordered dismantling of selective cells by apoptosis (derived from a Greek word for 'dropping of leaves

from trees') contrasts with the indiscriminant destructiveness of necrosis. Cell death resulting from cytoplasmic swelling and karyolysis has been classified traditionally as necrosis. Currently, the Society of Toxicologic Pathologists recommends the replacement of the term "necrosis" with the term "oncosis", reserving the former to describe dead cells in histological sections regardless of how they died (Levin et al., 1999). Apoptosis was later considered as an example of programmed cell death (PCD) that is a genetically driven form of cell suicide. More recent studies have shown that there are many other routes to cell death, including non-apoptotic PCD and autophagy. The distinctions between different forms of cell death are now becoming blurred with the proposal that cell death could exist as a continuum with apoptosis and necrosis at opposite ends of this continuum (Portera-Cailliau et al., 1997a,b; Martin et al., 1998). Apoptosis and necrosis are two forms of neuronal cell death that are particularly relevant to the pathobiology of neurodegeneration in acute and chronic neurological disorders (Martin, 2002; Appendix) and were the focus of this work.

## **BODY**

### **Hypothesis 1: Neuronal apoptosis in the mammalian CNS has molecular characteristics of programmed cell death (PCD).**

#### **Remote degeneration of neurons after cortical injury has molecular characteristics of PCD**

Neurons in the brain are believed to undergo cytoskeletal changes and retrograde degeneration as a secondary result of target deprivation caused by trauma and stroke and as a primary degenerative process in ALS, Parkinson's disease, and Alzheimer's disease (Martin et al., 1998). To gain insight into the mechanisms of progressive neuronal injury and secondary brain damage, we have studied animal models of axotomy and target deprivation. Ablation of the visual neocortex induces retrograde neuronal degeneration in the dorsal lateral geniculate nucleus (dLGN) of thalamus. The geniculocortical projection neurons die by a morphological process that is unequivocal apoptosis (Al-Abdulla et al., 1998; Al-Abdulla and Martin, 2002). This cell death is preceded by an accumulation of apparently active mitochondria in the perikaryon and might emerge with oxidative damage to genomic DNA of the highly

vulnerable projection neurons (Al-Abdulla and Martin, 1998). Unilateral ablation of the occipital cortex in rat and mouse results in unequivocal end-stage neuronal apoptosis in the dLGN at 6-7 days postlesion (Martin et al., 2001; Appendix). We tested the hypothesis that p53 and Bax regulate this neuronal apoptosis. We found using immunocytochemistry that p53 accumulates in the nucleus of neurons destined to undergo apoptosis. By immunoblotting, p53 levels increase (~150% of control) in the LGN by 5 days after occipital cortex ablation. In nuclear-enriched subcellular fractions, p53 is activated (~3-fold) in the ipsilateral LGN at 5 days postlesion, as shown by DNA binding assay. The levels of procaspase-3 increase at 4 days postlesion, and caspase-3 is activated prominently at 5 days postlesion. To identify if neuronal apoptosis in the adult brain is dependent on p53 and Bax, cortical ablations were done on genetically engineered mice. In *p53<sup>-/-</sup>* mice, the severity of neuronal apoptosis is significantly attenuated (~34%) compared to wildtype mice, and in *bax<sup>-/-</sup>* mice neuronal apoptosis in the dorsal LGN is completely blocked. From these experiments we concluded that: 1) retrograde neuronal death in the adult thalamus after cortical injury is definitely apoptosis and has molecular characteristics of PCD; 2) neuronal apoptosis in the adult CNS requires Bax, and 3) p53 modulates neuronal apoptosis in the adult brain, but apoptosis can also occur independent of p53-mediated mechanisms (Martin et al., 2001; Appendix).

#### **Death proteins in adult dLGN have differential subcellular localizations that change during apoptosis in vivo**

We studied the molecular regulation of target deprivation-induced neuronal apoptosis (Martin et al., 2003, Appendix). Apoptosis is a structurally and biochemically organized form of cell death. The basic machinery of apoptosis is conserved in yeast, hydra, nematode, fruitfly, zebrafish, mouse, and human (Ameisen, 2002). Several families of apoptosis-regulation genes have been identified in mammals. Apoptotic cell death is controlled by the Bcl-2 family (Merry and Korsmeyer, 1997), the caspase family of cysteine-containing, aspartate-specific proteases (Wolf and Green, 1999), the p53 gene family (Levrero et al., 2000), death receptors (Nagata, 1999), and other apoptogenic factors, including cytochrome c. The *bcl-2* protooncogene family is a group of apoptosis regulatory genes encoding for proteins defined by at

least one-conserved Bcl homology domains (BH1-BH4 can be present) that function in the protein-protein interactions (Merry and Korsmeyer, 1997). Of these genes, *bcl-2*, *bcl-x<sub>L</sub>*, and *boo* are antiapoptotic, whereas *bax*, *bcl-x<sub>S</sub>*, *bad*, *bak*, *bid*, *bim*, and *bik* are proapoptotic. The relative levels of cell death proteins were evaluated in different subcellular compartments in adult rat dLGN. Bax immunoreactivity (IR) was much higher in the soluble protein compartment compared to the mitochondria-enriched membrane compartment (Martin et al., 2003, Appendix). In mitochondrial fractions a distinct doublet was observed, corresponding to the detection of  $\alpha$ -Bax and  $\beta$ -Bax at 21 and 24 kDa, respectively. The levels of  $\alpha$ -Bax and  $\beta$ -Bax in the adult dLGN were similar (Martin et al., 2003, Appendix). In contrast to Bax, Bak was much more enriched in the mitochondria-enriched membrane compartment compared to the soluble protein compartment (Martin et al., 2003, Appendix). Bad was enriched in the soluble protein compartment relative to the mitochondrial compartment of the dLGN but was increased in the mitochondria-enriched compartment after injury (Martin et al., 2003, Appendix). The synchronized apoptosis of dLGN projection neurons occurs in association with differential subcellular changes in proapoptotic molecules (Martin et al., 2003, Appendix). Bax increases in mitochondria within 1 day after target deprivation, while Bak increases later after about 4 days. Few studies have demonstrated such a rapid (within 1 day) redistribution of Bax during apoptosis of neurons or of cells in general. Very few studies have addressed the role of Bak in neuronal apoptosis. In CNS neurons, Bax and Bak show an increased level and subcellular redistribution during target deprivation-induced apoptosis, but, interestingly, the timing of the changes is different for these two proapoptotic molecules (Martin et al., 2003). Bax may be a rapid-response protein, whereas Bak may be a delayed-response protein. Bax and Bak may have coordinated hierarchical or independent functions during neuronal apoptosis. Translocated Bax in mitochondria may coalesce with Bak into mitochondria-associated clusters during apoptosis, supporting the idea of a coordinated participation of these two molecules. Bak may therefore be involved in reinforcing the cell death process after Bax engages the process in CNS neurons.

Bad showed an early sustained increased (Martin et al., 2003, Appendix). Neurons are dependent on target or afferent derived neurotrophic factors for survival. Withdrawal of neurotrophins results in neuronal apoptosis. Some neurotrophins possess antiapoptotic activity by interacting with membrane tyrosine kinase receptors linked to phosphoinositide-3 kinase (PI-3 kinase) (Franke et al., 1997). Activation of PI-3 kinase leads to activation of protein kinase B (PKB/Akt) by phosphorylation. Active Akt phosphorylates Bad at serine<sup>136</sup> (del Peso et al., 1997) causing phospho-Bad to disassociate from Bcl-2 or Bcl-X<sub>L</sub> within mitochondrial membranes and to translocate to the cytosol where it is sequestered by protein 14-3-3. This process allows Bcl-2 and Bcl-X<sub>L</sub> to exert their antiapoptotic function(s). Until now we have assumed that occipital cortex ablation induces an in vivo state of target deprivation and neurotrophin withdrawal of dLGN neurons, but, other than the apoptosis of these neurons, evidence to support this assumption has not been forthcoming. The finding that Bad undergoes an early sustained increased in the dLGN, particularly in the mitochondria-enriched fraction, suggests that its phosphorylation and cytosolic sequestration by 14-3-3 are diminished, supporting the proposition that this CNS lesion is an in vivo model of neurotrophin withdrawal-induced neuronal apoptosis.

Cleaved caspase-3 was elevated maximally at 5 and 6 days (Martin et al., 2003, Appendix). Active caspase-3 underwent a subcellular translocation to the nucleus. A dramatic phosphorylation of p53 was detected at 4 days postlesion. Nevertheless we provide some new information on an unsuspected early phase caspase-3 activation and a later phase nuclear translocation of biochemically active caspase-3. Moreover, the presence of cleaved caspase-3 may not be equivalent to the presence of biochemically active caspase-3. It is interesting that the increased activity seen at 1 day postlesion in the soluble fraction did not appear to require additional formation of cleaved subunits. In addition, the massive increase in cleaved caspase-3 in nuclear fractions at 6 days postlesion did not have a corresponding increase in activity. Our previous in vitro data suggests that apoptosis of cortical neurons can involve caspase-3 changes without additional cleavage after an apoptotic stimulus (Lesuisse and Martin, 2002b). It is possible that the early events of apoptosis of mature neurons can be engaged without the formation of additional caspase-3 subunits via proteolysis of proenzyme and that preexisting low levels of cleaved

caspase-3 can play a role, along with other proteins such as Bax, to initiate the death process. Many proteins appear to interact with cleaved caspase-3, as shown by cross-linking experiments, and constitutively cleaved caspase-3 might be regulated by interacting proteins (Lesuisse and Martin, 2002b). In healthy normal cells, cleaved caspase-3 might interact with possible endogenous inhibitor proteins or the subunits may be folded or assembled as inactive enzyme. In this state constitutive cleaved caspase-3 would be inactive and could not execute the apoptotic process. Thus, a rapid increase in caspase-3 activity in mature neurons might occur by mechanisms other proteolytic cleavage of proenzyme, while later events in the apoptotic process, possibly occurring in the nucleus such as activation of DNA fragmentation pathways, appear to require recruitment of additional subunits by proteolysis. However, at near endstage apoptosis cleaved caspase-3 appears to lose its biochemical activity as suggested by our results at 6 days. This result is consistent with the accumulation of cleaved caspase-3 in cellular fragments and apoptotic debris of cortical neurons in vitro (Lesuisse and Martin, 2002b) as well as striatal neurons (Lok and Martin, 2002) and dLGN neurons (Natale et al., 2002) in vivo. The functions of caspase-3 in nervous tissue may be even more complicated than previously realized, as suggested by the transient increase in caspase-3 activity in the nonlesioned dLGN at 5 days postlesion, where no loss of neurons occurs but astroglial activation and induction of p53 in astrocytes has been observed (Martin et al., 2001). By immunoelectron microscopy we have found cleaved caspase-3 at synaptic sites in the adult brain (unpublished observations). In this regard, caspase-3 may function in synaptic plasticity and regeneration rather than cell death.

### **Phosphorylated p53 accumulates in the nucleus during neuronal apoptosis**

Cells that have sustained DNA damage from reactive oxygen species (ROS) and other genotoxic agents undergo apoptosis by engaging molecular cascades involving expression or activation of p53, Bcl-2 family members, and caspases (Polyak et al., 1997). p53 regulates target-deprivation-induced neuronal apoptosis in the dLGN because p53<sup>-/-</sup> mice show less neuronal loss than p53<sup>+/+</sup> mice (Martin et al., 2001). A critical question that remains to be elucidated is how DNA damage is communicated to p53 so that it

becomes activated and functional in neurons. Serine<sup>392</sup>-phosphorylated p53 accumulates in dLGN neurons during their degeneration and this p53 has enhanced DNA binding activity (Martin et al., 2001). We have also found massive accumulation of serine<sup>15</sup>-phosphorylated p53 in the dLGN during apoptosis (Martin et al., 2003). Phospho-p53<sup>Ser15</sup> levels were dramatically elevated in nuclear fractions of the ipsilateral LGN at 4 days postlesion. The increase remained present at 5 days postlesion. At 6 days postlesion ipsilateral levels were not different from contralateral levels. The phosphorylation of p53 at the serine-15 site was specific for the nucleus because phospho-p53<sup>Ser15</sup> was not detected in the soluble fraction. This accumulation was maximal at 4 days after injury, at a time when neurons with accumulated single-stranded DNA (ssDNA) were most numerous (Martin et al., 2003).

#### **The tempo of neuronal apoptosis is accelerated in the immature brain**

The thalamus is a major site of remote neurodegeneration after cortical damage in adult humans and experimental animals. In the adult brain occipital cortex ablation results in degeneration of geniculocortical projection neurons within the dLGN by apoptosis (Al-Abdulla et al., 1998; Martin et al., 2001; Natale et al., 2002), but less is known about thalamic responses to cortical injury in the immature brain. The structural emergence of this apoptosis and its time course are very synchronous, and the process is accelerated in the immature brain. In the adult brain the cell death process is nearly complete by 14 days postlesion, with the bulk of the geniculocortical neuronal apoptosis occurring during the first 7 days postlesion. In the newborn brain the apoptotic process takes 2 days. In newborn mouse Fluorogold-prelabeling showed the apoptosis of thalamocortical projection neurons at 36-48 hours after cortical injury (Natale et al., 2002). The structural progression of apoptosis in the immature dLGN reveals typical chromatolytic morphology by 18-24 hours, followed by cytoplasmic shrinkage and chromatin condensation characteristic of end-stage apoptosis after 36-48 hours. Electron microscopy (EM) confirmed the presence of apoptosis (Natale et al., 2002). This study showed internucleosomal DNA fragmentation and expression of cleaved caspase-3 occurs rapidly, being noted first at 18 hours, well before the peak of apoptotic cell death occurring at 36 hours after cortical damage in the immature brain



(Natale et al., 2002). These data suggest that axotomy/target deprivation-induced cell death in the immature brain differs from that previously reported in adult mice with respect to the time required for progression to cell death.

### **Delayed secondary neuronal apoptosis occurs after hypoxia-ischemia**

Apoptosis of thalamic neurons can occur days after stroke and cardiac arrest. We found that thalamic neuron apoptosis in the rat brain after hypoxia-ischemia (HI) is structurally identical to the apoptosis of thalamic neurons after cortical damage (Northington et al., 2001a; Appendix). We also detected apoptotic cell death in some neuronal groups that are not typically regarded as selectively vulnerable to ischemia (Martin et al., 2000). For example, subsets of granule cells in the dentate gyrus, subsets of granule cells in the cerebellar cortex, and certain neurons in thalamic nuclear groups appear apoptotic. In addition, prominent apoptotic death of white matter oligodendrocytes occurs after HI. The presence of apoptotic death in these groups of cells after global ischemia is possibly related secondarily to target deprivation or to axonal degeneration in response to ischemic degeneration of selectively vulnerable populations of neurons. The apoptosis in thalamic neurons after HI in rat is associated with a rapid increase in the levels of the Fas death receptor and caspase-8 activation (Northington et al., 2001b; Appendix). Concurrently, the levels of Bax in mitochondrial-enriched cell fractions increase. Increased levels of Fas death receptor and Bax and activation of caspase-8 in the thalamus precede the marked activation of caspase-3 and the occurrence of neuronal apoptosis. Thus, as in nonneural tissues, the mechanisms for neuronal apoptosis in different in vivo settings can differ in upstream signals, but they converge on common downstream mechanisms (i.e., the participation of Bax and caspase-3).

### **Rapid subcellular redistribution of Bax precedes caspase-3 and endonuclease activation during excitotoxic neuronal apoptosis**

Excitotoxic activation of glutamate receptors is a common pathophysiological mechanism of neurodegeneration. Neurotoxic activation of glutamate receptors is believed to occur in traumatic brain

injury, cerebral ischemia, epilepsy, ALS, Huntington's disease, and Parkinson's disease (Martin, 2001).

The brain damage induced by excitotoxicity has features of apoptosis and necrosis (Martin, 2002). The precise mechanisms of excitotoxic neuronal apoptosis *in vivo* have not been identified specifically.

Neurons in the immature rodent CNS undergo massive apoptosis in response to glutamate receptor excitotoxicity (Portera-Cailliau et al., 1997a,b). Apoptosis is much more prominent after excitotoxic injury in the immature brain compared to the mature brain (Portera-Cailliau et al., 1997b). Intrastriatal administration of kainic acid (KA) in newborn rodents causes copious apoptosis of striatal neurons (Portera-Cailliau et al., 1997a,b), serving as an unequivocal model of apoptosis in neurons that are selectively vulnerable in Huntington's disease. This apoptosis has been verified structurally with light microscopy and EM and by immunolocalization of cleaved caspase-3 (Lok and Martin, 2002). Ubiquitous apoptosis is observed at 24 hours after the insult. DNA degradation by internucleosomal fragmentation further confirms the presence of apoptosis. Excitotoxic neuronal apoptosis is associated with rapid (within 2 hours after neurotoxin exposure) translocation of Bax and cleaved caspase-3 translocate to mitochondria (Lok and Martin, 2002). We evaluated if caspase-3 is proteolytically cleaved during excitotoxic neuronal apoptosis (Lok and Martin, 2002). The levels of cleaved caspase-3 increase in striatum after KA lesions. Caspase-3 cleavage was detected with two antibodies that bind different epitopes. Formation of cleaved caspase-3 was most prominent between 12 and 24 hours after neurotoxin exposure. Cleaved caspase-3 undergoes an early redistribution into the mitochondrial-enriched fraction by 2 hours postlesion followed by a later increase in the soluble fraction at 12-24 hours. This early translocation of caspase-3 is a very novel finding for neuronal apoptosis. An immunolocalization analysis of cleaved caspase-3 was done during excitotoxic neuronal apoptosis (Lok and Martin, 2002). In the striatum of naïve and PBS-injected P7 pups, only occasional isolated cells showed cleaved caspase-3 IR, consistent with previous observations demonstrating a low level of naturally occurring developmental PCD at this time (Martin, 2001). At 12 hours after intrastriatal injection of KA, a marked increase in cleaved caspase-3 was found throughout the striatum, while much less cleaved caspase-3 was visualized in the non-lesioned striatum. Caspase-3 accumulated in the cytoplasm and nucleus of neurons showing nascent chromatin condensation

at 12 hours. At 24 hours after KA, cleaved caspase-3 was detected in many cells with clearly distinguishable apoptotic nuclei and was also present in cellular debris within the neuropil, while the nonlesioned striatum had rare staining. The prominent formation of cleaved caspase-3 occurred between 6 and 12 hours after the injury, because at 6 hours after the KA lesion the ipsilateral striatum showed only faint staining, and, at 12 hours, the staining for cleaved caspase-3 was intense.

This study (Lok and Martin, 2002) revealed that the ratio of mitochondrial Bax to soluble Bax in normal developing striatum changes prominently with brain maturation. Newborn rat striatum has a much greater proportion of Bax in the mitochondrial fraction with lower levels of soluble Bax. Mature rat striatum has a much larger proportion of Bax in the soluble fraction and low amounts of Bax in the mitochondrial fraction. With brain maturation there is a linear decrease in the ratio of mitochondrial Bax to soluble Bax. This developmental subcellular redistribution of Bax might be related to the observation that immature neurons exhibit a more robust classical apoptosis response compared to adult neurons after brain damage (Martin, 2001).

### **Apoptosis in young and old cortical neurons has different structural, biochemical, and molecular signatures**

Neurons in the cerebral cortex are very sensitive to injury. Neocortical neurons degenerate after hypoxia-ischemia, trauma, neurotoxin exposure, and seizures. We have used animal models of neurodegeneration (e.g., excitotoxins, hypoxia-ischemia) to study cortical neuron pathology, but the mechanisms are difficult to pinpoint in vivo due to the inherent complexity of nervous system tissue. We developed a mouse cortical neuron culture system to study mechanisms of apoptosis in neurons (Lesuisse and Martin, 2002a,b).

Exposure of neurons to the topoisomerase inhibitor camptothecin (CPT) causes apoptosis of neurons (Lesuisse and Martin, 2002a,b Appendix). Apoptosis assays included internucleosomal fragmentation of DNA, morphology, and caspase-3 activation. The timing and magnitude of DNA fragmentation were different in immature (DIV5) and mature (DIV30) neurons. DIV5 neurons showed DNA fragmentation

after 24 hours of CPT. With 24 and 48 hours treatment, long exposures were necessary to visualize a ladder. In contrast, DIV30 neurons, treated with the same concentrations of CPT, showed prominent internucleosomal DNA fragmentation by 8 hours of treatment, peaking at about 24 hours. EM confirmed that mouse cortical cultures treated with CPT at DIV5 and DIV30 were morphologically apoptotic (Lesuisse and Martin, 2002b). The morphology of the chromatin condensation was different at the two ages. The nuclear morphology in the majority of apoptotic DIV5 neurons was similar to classical apoptosis with the formation of uniformly round chromatin masses (Martin et al., 1998; Martin, 2002). Apoptosis in DIV30 neurons was different because large irregularly-shaped chromatin masses were formed.

Mitogen-activated protein kinase (MAPK)/extracellular-regulated protein kinase (Erk) signaling is different in immature and mature cortical neurons during apoptosis (Lesuisse and Martin, 2002b). Erk42/44 phosphorylation occurs in mature neurons during apoptosis but not in immature neurons. Phosphorylated Erk42/44 was not detected in the different subcellular fractions of control DIV5 neurons, and no phosphorylation of Erk42/44 occurred in DIV5 neurons after CPT exposure. In contrast, phosphorylated Erk was detected in control DIV30 neurons and was increased dramatically (over 10-fold for soluble Erk44) after CPT, occurring after 4 h of treatment and remaining at high levels until 8 h and then decreasing. We examined the levels of full-length MEKK1 and putative proapoptotic MEKK1 fragments in nontreated and CPT-treated cortical neuron cultures. Full-length MEKK1 (~160-197 kDa) promotes cell survival, whereas cleaved MEKK1 (~72-95 kDa) promotes apoptosis (Cardone et al., 1997; Widmann et al., 1998). Caspase-3 generates MEKK1 C-terminal fragments that have constitutively active proapoptotic kinase activity (Cardone et al., 1997). CPT-treated DIV5 neurons at 15 and 24 h generated several cleavage products of MEKK1. These cleavage products had sizes (~70-95) that were similar to the reported sizes of the active kinase fragments of MEKK1 that induce apoptosis (Cardone et al., 1997). There was an inverse relationship between the levels of MEKK1 fragments and full-length MEKK1, supporting the conclusion that the immunoreactive proteins at ~70-95 kDa are derived from cleavage of MEKK1 holoenzyme. The formation of MEKK1 C-terminal fragments coincided with the formation of

cleaved caspase-3 in immature neurons. The level of MEKK1 fragments at ~70-95 kDa remained unchanged during apoptosis in mature neurons, while the level of full-length MEKK1 decreased during apoptosis.

Caspase-3 activation is different in immature and mature cortical neurons during apoptosis (Lesuisse and Martin, 2002b). Caspases-3 was evaluated in subcellular fractions of control neurons and CPT treated neurons. Cleaved caspase-3 was evaluated in subcellular fractions of control neurons and CPT treated neurons. In control neurons, cleaved caspase-3 was found primarily in the nuclear fraction with two different antibodies. Control neurons at DIV5 and DIV30 had similar low levels of constitutively cleaved caspase-3 in nuclear fractions. In immature neurons exposed to CPT the levels of cleaved caspase 3 subunits (17-19 kDa) progressively increased in nuclear fractions between 4-24 hours and abruptly increased between 8 and 24 hours in pellet fractions. In contrast, the levels of cleaved caspase-3 did not change in nuclear and pellet fractions of mature neurons after CPT.

**Hypothesis 2: Mitochondria accumulate and release cytochrome c within neurons during apoptosis.**

**Mitochondria accumulate at perinuclear sites in thalamic neurons during apoptosis**

Mitochondria are potent generators of apoptotic stimuli (e.g., ROS) and they serve as reservoirs for apoptotic protease activating factors such as cytochrome c. The mitochondrion integrates death signals mediated by proteins in the Bcl-2 family and releases molecules residing in the mitochondrial intermembrane space, such as cytochrome c, that activate caspase proteases leading to internucleosomal cleavage of DNA. We found that mitochondria accumulate in neurons destined to undergo apoptosis at preapoptotic stages of degeneration. This change may be a general feature of apoptosis in neurons because we have found it in thalamic neurons (Al-Abdulla and Martin, 1998; Northington et al., 2001b,c, Appendix) and motor neurons (Martin and Liu, 2002a, Appendix) during apoptosis in animal models and in human ALS motor neurons (Martin, 2002, Appendix). This perinuclear accumulation of mitochondria has been shown quantitatively by EM and by localization of mitochondrial proteins using

immunocytochemistry and enzyme histochemistry. The mechanisms and consequences of this preapoptotic perinuclear accumulation of mitochondria in neurons need to be studied.

There may be several possible consequences that result from the perinuclear accumulation of mitochondria. Accelerated oxidative damage to genomic DNA may occur (see Hypothesis 3 below), and proapoptotic factors may be released. We found that cytochrome c undergoes an intracellular redistribution in apoptotic neurons (Martin and Liu, 2002a). We directly visualized and quantified cytochrome c in different subcellular compartments specifically in neurons by immuno-EM early in the apoptotic process (Martin and Liu, 2002a). Prior to the structural emergence of apoptosis total cytoplasmic cytochrome c levels increased significantly (147% of contralateral), but the level of mitochondrial-associated cytochrome c immunoreactivity in injured neurons was not different from control. As the apoptotic structure emerged, total cytoplasmic cytochrome c levels were elevated further (170% of control), while mitochondrial-associated cytochrome c was decreased (73% of control) in injured neurons. In neurons with a definite apoptotic structure, mitochondrial cytochrome c levels were only 20% of control, while the level of diffusely distributed cytoplasmic cytochrome c was 281% of control. These experiments showed that mitochondria accumulate and release cytochrome c very early during neuronal apoptosis (days before end-stage apoptosis).

#### **Bax translocates rapidly to mitochondria early during excitotoxic neuronal apoptosis**

The levels of Bax in mitochondrial-enriched and soluble fractions were analyzed during the progression of excitotoxic neuronal apoptosis (Lok and Martin, 2002). Bax levels decreased in the soluble fraction but increased correspondingly in the mitochondrial-enriched fraction early after KA exposure. The increase in Bax within the mitochondrial fraction was maximal within 2 hours after KA. This prominent change at 2 hours after KA was confirmed with two antibodies that detect different epitopes on Bax. Cytochrome c oxidase subunit 1 IR decreased progressively with time after KA. The loss of mitochondrial marker was most marked at 24 hours after KA, consistent with the prominent end-stage apoptosis found at this time point.

**Hypothesis 3: Neuronal apoptosis in vivo evolves in association with oxidative stress.**

Neuronal degeneration can be triggered by oxidative stress, defined as the generation of reactive oxygen species (ROS)/ reactive nitrogen species (RNS) and their attack on cellular molecules. Superoxide and hydroxyl radicals and hydrogen peroxide ( $\text{H}_2\text{O}_2$ ) are common ROS. Nitric oxide (NO) and its derivatives peroxynitrite ( $\text{ONOO}^-$ ) and nitrous anhydride ( $\text{N}_2\text{O}_3$ ) are common RNS. ROS/RNS are constantly formed during normal cellular metabolism. These toxic chemicals can damage protein, lipids, and nucleic acids. Interestingly, some of these radicals have key physiological functions as well. For example, NO functions in neurotransmission, blood flow regulation throughout the body by modulating guanylate cyclase activity and possibly by covalent modification (S-nitrosylation) of proteins, and in immune defense. Cells have evolved a variety of elaborate antioxidant defense enzyme systems to attenuate or neutralize the toxicity of ROS/RNS, including superoxide dismutases, catalase, and glutathione peroxidase. Superoxide dismutases converts superoxide radical to  $\text{H}_2\text{O}_2$  and which is then decomposed by catalase and glutathione peroxidase.

The production of ROS/RNS is increased during apoptosis. NMDA receptors and NO generation might activate two different toxic pathways. One pathway of NO toxicity is based on presynaptic actions. NO, acting as a retrograde messenger, stimulates exocytotic release of neurotransmitter from synaptic vesicles, thereby potentiating glutamate release. A second pathway for NO toxicity is based on the findings that enzymatically produced NO can undergo a variety of nonenzymatic reactions with thiols, metals, and superoxide. NO reacts with superoxide to form  $\text{ONOO}^-$ . The rate constant of the NO-superoxide reaction is  $6.7 \times 10^9 \text{ M}^{-1} \text{ s}^{-1}$ , which is  $\sim 3.5$  times greater than that for the superoxide dismutase-catalyzed decomposition of superoxide.  $\text{ONOO}^-$  can nitrate or hydroxylate protein tyrosine residues, oxidize thiols, or decompose into hydroxyl radical. The possible cytotoxic consequences of  $\text{ONOO}^-$  production include protein damage, DNA damage, poly (ADP-ribose) synthase activation and subsequent depletion of  $\text{NAD}^+$  and ATP, and mitochondrial damage. The targets of  $\text{ONOO}^-$  in neurons remain to be fully identified. We found that the key neuronal enzyme  $\text{Na,K ATPase}$  is a target for  $\text{ONOO}^-$  (Golden et

al., 2003). We also found that  $\text{ONOO}^-$  is a potent DNA damaging agent in neurons by inducing the formation of single-strand breaks, double-strand breaks, and abasic sites (Martin and Liu, 2002b).

DNA damage caused by oxidative stress is a potent signal for cell death (Levine, 1997). Neurons sustain DNA damage (e.g., hydroxyl radical adducts or single-strand breaks) after cerebral ischemia (Martin et al., 2000) and mechanical injury such as axotomy/target deprivation and trauma (Al-Abdulla and Martin, 1998; Martin and Liu, 2002) and in ALS, Alzheimer's disease, and Parkinson's disease. The mechanisms of DNA damage-induced apoptosis in postmitotic cells such as neurons are not understood. The possibility of a pivotal role of oxidative stress-induced DNA damage in human pathobiology underscores the essential need for methods to detect and measure different forms of DNA lesions and their repair in specific populations of cells. Biochemical methods lack cellular resolution. Flow cytometry and terminal deoxynucleotidyl transferase-mediated 3' dUTP nick end labeling are popular methods for determining DNA damage with cellular resolution but they lack the ability to distinguish specific types of DNA lesions.

The comet assay, also known as single cell gel electrophoresis (SCGE), has been used before to identify genomic DNA damage in eukaryotic cells on a single cell basis. The types of DNA lesions detectable by comet assay include SSB, alkali-labile sites (AP sites) and DSB. We used this sensitive and quantitative method for profiling specific DNA lesions induced by neurotoxic agents directly in neurons. The goals of these experiments were to develop a new method to isolate neurons, and, then apply the comet assay to evaluate the vulnerability of the neuronal genome to ROS (Liu and Martin, 2001a,b).

DNA damage was profiled in isolated adult motor neurons (MN) exposed in vitro to  $\text{H}_2\text{O}_2$ , NO donor, and  $\text{ONOO}^-$  using the comet assay (Martin and Liu, 2002b). The formation of different types of genomic DNA lesions induced in neurons by NO donor and  $\text{ONOO}^-$  was profiled by varying pH conditions in the comet assay. The use of different pH conditions during SCGE is a validated approach for discriminating AP sites and strand breaks. A pH of 13, 12, and 7.4 was used to detect alkali-labile AP sites, SSB, and DSB, respectively. MN accumulated DNA-SSB (pH 12) with exposure to the NO donor NONOate. AP sites (pH 13) did not accumulate significantly. The presence of DNA-SSB in MN was dynamic. DNA-



SSB accumulated rapidly in MN, occurring within 30 min exposure and then increased further over the subsequent 30 min, with ~60% of the cells showing DNA damage at 60 min exposure to 100  $\mu$ M NONOate. In contrast, ONOO<sup>-</sup> rapidly induced the formation of alkali-labile sites within 15 min followed by an accumulation of DNA-SSB as alkali-labile sites dissipated. Moreover, ONOO<sup>-</sup> potently induced DNA-DSB (pH 7.4) quickly (within 15 min) in neurons.

### **DNA damage accumulates rapidly in dLGN neurons after target deprivation**

Because p53 was activated in the dLGN at 4 days postlesion, LGN neurons were evaluated for DNA damage at early postlesion time points (Martin et al., 2003, Appendix). DNA damage was assessed with 2 different markers. 8-hydroxydeoxyguanosine (OHdG) IR was seen in the nucleus and cytoplasm of dLGN neurons. It has been shown previously that the intensity of cytoplasmic and nuclear immunolabeling detected with OHdG antibodies can be altered respectively by RNase and DNase pretreatment and by preadsorption of antibody with 8-hydroxyguanosine and 8-hydroxy-2-deoxyguanosine, indicating hydroxyl adduct modified RNA and DNA (Al-Abdulla and Martin, 1998; Martin et al., 1999). Both the overall intensity of staining in labeled neurons and the number immunopositive neurons changed in the dLGN after target deprivation (Martin et al., 2003). The number of neurons with nuclear OHdG IR was increased in the ipsilateral dLGN at 1 through 5 days postlesion. The increase was progressive between 1 and 3 days, peaking at 3 days, and then the number of immunopositive neurons declined. Immunostaining for ssDNA was found primarily in the nucleus, with much fainter cytoplasmic labeling. The number of neurons with ssDNA was also increased in the ipsilateral dLGN. ssDNA-positive neurons were higher than control at 1 through 4 days postlesion. A maximal level was found at 4 days postlesion, corresponding to the spike in p53 phosphorylation (Martin et al., 2003).

### **Motor neuron degeneration in ALS may be oxidative stress-induced, p53-mediated apoptosis**

The degeneration of MN in ALS may be a form of apoptosis (Martin, 1999). This idea is based on morphological and biochemical findings. A staging scheme for the structural progression of MN death

has been devised (Martin, 1999). This staging arrangement reveals that MN degeneration in ALS may be a nonclassical form of apoptosis. After an initial chromatolytic stage, MN progressively undergo attrition of the cell body and dendrites that culminates in a residual MN of only ~20% of normal diameter. During somatodendritic attrition, both the cytoplasm and the nucleus become condensed and dark, consistent with apoptosis. The nuclear condensation in ALS MN differs from classical apoptosis because the chromatin is not discretely organized into uniformly round, dense clumps as in animal models of neuronal apoptosis. The terminal transferase-biotinUTP nick-end labeling (TUNEL) method was used to identify when nuclear DNA fragmentation commences during the staging of MN degeneration in ALS. DNA fragmentation is detected in MN at the somatodendritic attrition and apoptotic stages of neuronal death but not in MN in the chromatolytic stage of degeneration. DNA fragmentation is also found in subsets of pyramidal neurons in ALS motor cortex, but not somatosensory cortex. Immunoblotting experiments of subcellular fractions have shown that Bax and Bak protein levels are increased and Bcl-2 protein level is decreased in selectively vulnerable motor regions, but the levels of Bcl-X<sub>L</sub> are unchanged (Martin, 1999). The biochemical activity of caspase-3 activity is increased selectively in ALS MN regions (Martin, 1999). A DNA fragmentation factor endonuclease is activated, and internucleosomal fragmentation of genomic DNA can be found (Martin, 1999). These findings lead to the hypothesis that an inappropriate re-emergence of a PCD mechanism, involving cytosol-to-membrane and membrane-to-cytosol redistributions of cell death proteins, participates in the pathogenesis of MN degeneration ALS (Martin, 1999). However, precise structure-molecular correlations are needed to validate this MN degeneration staging scheme, and the protein expression data lack resolution for MN-specific abnormalities, despite the use of a micropunch tissue sampling method for anterior horn and motor cortex. There is non-neuronal cell contamination in the samples. The resolution and MN specificity in these experiments need to be enhanced using laser capture microdissection.

Even if MN in ALS die through some form of apoptosis, this outcome might be too late in the degenerative process for antagonism of apoptotic pathways to have any major therapeutic benefit for individuals with ALS. Therefore, it is vital to explore upstream mechanisms for MN degeneration. DNA

damage could be involved in the pathogenesis of ALS (Bradley and Krasin, 1982). A key DNA lesion is OHdG. OHdG is a mutagenic lesion. Most DNA polymerases fail to recognize this mismatch, resulting in base transversions (Norbury and Hickson, 2001). Immunolocalization experiments have shown that OHdG lesions occur directly in ALS MN (Martin, 2001).

The accumulation of DNA damage in MN could be a stimulus for MN degeneration in ALS. This idea is supported by the finding that p53 is activated in MN in human ALS. By immunoblotting, p53 levels increase in vulnerable regions in individuals ALS (Martin, 2000). p53 accumulates specifically in ALS MN. This p53 is functionally active because it is phosphorylated at serine<sup>392</sup> and has increased DNA binding activity (Martin, 2000, 2001).

The accumulation of DNA damage in ALS could also signify perturbations in DNA repair processes. However, the number of studies on DNA repair in ALS is few. We studied the expression and function of the class II apurinic/apyrimidinic endonuclease (APE) in ALS CNS has been studied (Shaikh and Martin, 2002). This protein is interesting to ALS because APE functions as a redox factor (redox factor-1, Ref-1) that facilitates the DNA-binding of transcription factors through redox modulation. APE protein levels and repair activity are increased in ALS MN regions, supporting the possibility that DNA damage is an upstream mechanism for MN degeneration.

#### **RNS attack of the Na,K ATPase $\alpha$ 3 isoform does not occur during striatal neuron necrosis after hypoxia-ischemia (HI)**

Sodium-potassium ATPase (Na, K ATPase) is a ubiquitous cell membrane enzyme vital in the neuron for establishment of cellular volume and the resting membrane potential. In regions of the brain (striatum, thalamus, hippocampus, and somatosensory cortex) selectively vulnerable to HI, high levels of Na/K ATPase activity are present. Furthermore, in our animal model of HI and recovery, we have shown a biphasic pattern of Na, K ATPase inactivation in the striatum (Golden et al., 2001). Enzyme activity acutely decreases at 3 hours post-injury, recovers to near sham control values at 6 h, and then declines to

~55% of control throughout the remainder of recovery. The mechanism by which this inhibition of Na, K ATPase occurs may involve ROS.

ONOO<sup>-</sup> has been described as a potential mediator of cell death in pathological processes. In our piglet model of HI, we demonstrated that neuronal death in the striatum occurs via necrosis, with a burst of oxidative stress and extensive tyrosine nitration of cellular proteins, which serves as a marker of ONOO<sup>-</sup> modification (Martin et al., 2000). We tested the hypothesis that striatal Na, K ATPase is vulnerable to direct, ONOO-mediated attack and that protein nitration in vivo emerges with the known pattern of enzyme inactivation during recovery from HI (Golden et al., 2003). In vitro, reaction of ONOO<sup>-</sup> (100-500  $\mu$ M) with purified Na, K ATPase produced nitration of the  $\alpha$  (catalytic) and  $\beta$  (transport) subunits, as quantified by immunoblots of the reaction products for nitrotyrosine. To evaluate for ONOO<sup>-</sup> damage to Na, K ATPase in vivo, striatal plasma membrane fractions from piglets subjected to asphyxic cardiac arrest and recovery were also studied by immunoprecipitation. During the progression of striatal neurodegeneration and loss of enzyme function 3-24 hours after arrest, nitration of the  $\alpha_3$  (neuronal) isoform of Na, K ATPase was not increased relative to sham control. We conclude that Na, K ATPase is a target of ONOO<sup>-</sup>, but that this mechanism is not responsible for enzyme inactivation after HI.

#### **Hypothesis 4: Antioxidant and caspase inhibitor treatments prevent neuronal apoptosis.**

We believe that DNA damage is an early upstream signal for neuronal apoptosis. This hypothesis is supported by our earlier work and the experiments conducted during the first and second years of this project. For example, thalamic neurons (Al-Abdulla and Martin, 1998) and motor neurons (Martin et al., 1999) sustain hydroxyl radical damage to DNA during apoptosis. Furthermore, using SCGE, we have identified recently that DNA-SSB occur very early in the progression of neuronal apoptosis (Liu and Martin, 2001a,b). This DNA damage found in vivo has the same fingerprint as the DNA damage caused by ROS (Liu and Martin, 2001a,b). We have also found that apoptosis of thalamocortical projection neurons requires the presence of the *Bax* gene and is modified by a functional *p53* gene (Martin et al.,

2001), and that motor neuron death after nerve avulsion is p53- and Bax-dependent apoptosis (Martin and Liu, 2002a). We therefore believe that oxidative damage to DNA is an upstream signal in the mechanisms for neuronal apoptosis.

### **Transgenic antioxidant therapy protects against neuronal apoptosis**

We evaluated if oxidative stress participates in the mechanisms of dLGN neuron apoptosis by determining if antioxidant strategies are neuroprotective in our model. Transgenic and pharmacological antioxidant therapies were used. Transgenic mice overexpressing normal human SOD1 showed a significant attenuation (40%) in the neuronal loss at 7 days postlesion compared to wildtype mice. In contrast, neither trolox nor ascorbate showed any efficacy in preventing neuronal loss in the dLGN after target deprivation. The only known function of SOD1 is catalyzing the dismutation of superoxide anion into  $O_2$  and  $H_2O_2$  (McCord and Fridovich, 1969). Our results directly implicate superoxide, or its derivative  $ONOO^-$ , in the trigger for neuronal apoptosis in vivo. We do not yet know if the protection afforded by enforced SOD1 expression is due to increased SOD1 after target deprivation/axotomy or if the neurons in these animals are intrinsically more resistant to injury due to brain changes that have occurred during their lifetime. We hypothesize that the mechanism of SOD1 neuroprotection in dLGN neurons is through potentiated SOD1 induction early after the injury and attenuation of DNA strand breakage and p53 activation. Previous work on the benefits of antioxidant pharmacotherapy in protecting against target deprivation/axotomy-induced neuronal apoptosis is scant, and existing studies have employed entirely different model systems than that used here.

### **Caspase-3 inhibition blocks neuronal apoptosis induced by DNA damage in immature but not mature neurons**

We evaluated possible neuroprotective effect of caspase-3 inhibition on DNA damage-induced apoptosis of neurons induced by CPT. A cell permeable reversible caspase-3 inhibitor Ac-AAVALLPAVLLALLAPDEV-CHO (Alexis Biochemicals) was tested. Caspase-3 inhibition blocked

CPT-induced apoptosis in immature cortical neurons but not in mature cortical neurons (Lesuisse and Martin, 2002b, Appendix).

### **MEK inhibitors block DNA damage-induced apoptosis in both immature and mature cortical neurons**

We evaluated possible neuroprotective effects of MEK inhibitors on DNA damage-induced apoptosis of neurons induced by CPT. We used inhibitors of MEK1 (PD98059) and MEK1-MEK2 (U0126) (both from Cell Signaling Technology). PD98059 and U0126 were dissolved in 50% ethanol/50% DMSO or 70% methanol/30% DMSO, respectively. Both drugs were used at final concentrations of 100 $\mu$ M, and cells were pretreated for 2 h before exposure to CPT. Both PD98059 and U0126 blocked apoptosis in both DIV5 and DIV25 cortical neurons. The antiapoptotic effects of U0126 were associated with a blockade of alterations in the MAP kinase pathway in CPT treated neurons. U0126 blocked the subcellular translocation of Erk54 from soluble to nuclear compartments and the nuclear accumulation of cleaved caspase-3 in CPT-exposed immature neurons. U0126 blocked the activation of Erk42/44 early in the process of apoptosis in CPT-exposed mature neurons. U0126 also blocked MEKK1 degradation and the formation of the putative proapoptotic MEKK1 fragments and active caspase-3 in immature neurons. Treatment with U0126 further decreased the level of full-length MEKK1 in CPT-exposed mature neurons.

### **Hypothermia attenuates the early NMDA receptor activation, oxidative stress, and neurodegeneration after hypoxia-ischemia (HI)**

The cerebral cortex, hippocampus, basal ganglia, thalamus, and cerebellum are extremely vulnerable to HI. Neuronal necrosis is a major early form of neuropathology occurring after HI, though the mechanisms are defined poorly and strategies for sustained neuroprotection are very limited. We have hypothesized that the mechanisms for the profound degeneration of striatal neurons after HI involve NMDA receptor-mediated excitotoxicity (Martin et al., 2000). Protein phosphorylation is a major

mechanism for regulation of receptor function and plays a role in NMDA receptor modulation and activation. We examined in our piglet model of HI, the protein levels and phosphorylation status of NMDA receptors after HI (Guerguerian et al., 2001). When NMDA receptor subunit-1 (NR1) levels are related to the evolving neuronal cell injury in the putamen, we discovered an interesting association. NR1 levels are lower than baseline when few neurons are damaged, but levels increase as the number of damaged neurons increases. The highest levels of NR1 protein correlate with the highest number of neurons showing injury. Because of this apparent relationship between NR1 levels and accumulating neuronal injury, the levels of a phosphorylated form of NR1 were measured to indirectly analyze NR1 activation after HI. Piglet synaptic membrane fractions of total striatum were probed with antibody recognizing phospho-Ser897 NR1. Incremental increases in the number of injured neurons in the putamen correlate with an increase in phosphoNR1 levels, further suggesting an association between evolving neuronal damage and NR1 activation. The increased phosphoNR1 is not clearly associated with the amount of elapsed time after HI but rather with the specific amount of neuronal damage in the putamen. To identify whether changes in NMDA receptors are subunit specific, selected NR2 subunits were measured. NR2B levels do not change significantly at 3, 6, and 12 hours recovery after HI compared to controls, but, at 24 h after HI, NR2B levels are elevated significantly above control at 24 hours after HI. The levels of NR2B do not relate to the number of damaged putaminal neurons, but the increase is associated with augmented astroglial expression evolving in parallel with the neuronal damage. NR2A levels in striatum of HI piglets are not different from control during the 3-24 h evaluation period. We concluded that NMDA receptor subunits are changed differentially in the striatum after neonatal HI and that abnormal NMDA receptor potentiation through increased NR1 phosphorylation participates in the mechanisms of striatal neuron degeneration after HI.

We found that 24 hours of mild hypothermia (34 °C) with sedation and muscle relaxation after HI profoundly protects against neurodegeneration (Agnew et al., 2003). Moreover, this effect is sustained without deleterious side effects. The neuroprotective effects of hypothermia appear to be mediated by

silencing of NMDA receptor signaling and attenuation of oxidative stress (Agnew et al., 2001). These findings could have pathophysiological and therapeutic relevance for combat casualty care.

#### **KEY RESEARCH ACCOMPLISHMENTS SUPPORTED BY DAMD17-99-1-9553**

- Neuronal apoptosis in the adult brain and spinal cord is controlled by the *bax* gene and is Bax dependent (Martin et al., 2001; Martin and Liu, 2002, Appendix)
- Bax upregulation during neuronal apoptosis requires a functional *p53* gene (Martin et al., 2001; Martin and Liu, 2002, Appendix)
- The neurotoxin kainic acid induces large-scale neuronal apoptosis with structural and molecular characteristics of PCD in developing brain (Lok and Martin, 2002).
- Caspase-3 is activated during trauma- and hypoxia-ischemia-induced neuronal apoptosis in the mature and immature CNS (Martin et al., 2001; Northington et al., 2001b; Martin and Liu, 2002; Natale et al., 2002, Appendix)
- Caspase-3 is activated during excitotoxic neuronal apoptosis (Lok and Martin, 2002).
- Caspase-3 activation coincides with internucleosomal degradation of genomic DNA during neuronal apoptosis (Martin and Liu, 2002a; Lok and Martin, 2002).
- Bax translocates rapidly (within 2 hours) to mitochondria after an excitotoxic stimulus (Lok and Martin, 2002).
- Rapid subcellular redistribution of Bax precedes caspase-3 and endonuclease activation during excitotoxic neuronal apoptosis (Lok and Martin, 2002).
- Mitochondria in the developing brain have more Bax than mitochondria in adult brain (Lok and Martin, 2002).
- A plasma membrane death receptor (Fas) is activated in some forms of CNS neuron apoptosis (Northington et al., 2001, Appendix)



- Mouse cortical neurons can be cultured in a viable state for long-term and can be used to model neuronal development, aging, and death (Lesuisse and Martin, 2002a,b).
- Both immature and mature cortical neurons are capable of activating apoptotic mechanisms induced by DNA damage (Lesuisse and Martin, 2002a).
- Synucleins have differential localizations during cortical neurons development (Lesuisse and Martin, 2002a).
- $\beta$ -synuclein is enriched in dentritic growth cones (Lesuisse and Martin, 2002a).
- Synuclein protein levels do not change at preapoptotic stages of neuronal apoptosis (Lesuisse and Martin, 2002b).
- Immature and mature cortical neurons engage different apoptotic mechanisms involving caspase- and the MAP kinase pathway (Lesuisse and Martin, 2002b).
- Mitochondria are targets of cleaved caspase-3 (Lok and Martin, 2002; Lesuisse and Martin, 2002b).
- Single neurons can be profiled for different DNA lesions (Liu and Martin, 2001a,b).
- AP sites, SSB, and DSB can be profiled in single neurons by the comet assay (Liu and Martin, 2001a,b).
- Different forms of ROS induce different DNA damage signatures in neurons (Liu and Martin, 2001b).
- SOD1 overexpression attenuates neuronal apoptosis in vivo.
- The formation of DNA single-strand breaks is an early upstream signal for Bax- and p53-dependent neuronal apoptosis (Martin and Liu, 2002)
- Inhibition of Na,K ATPase is a pre-necrotic event during acute brain injury (Golden et al., 2001)
- Neuronal Na,K ATPase is a target of ONOO<sup>-</sup> (Golden et al., 2003)
- NMDA receptor activation and oxidative damage are pre-necrotic events during acute brain injury (Guerguerian et al., 2002)
- Caspase-3 and MEK inhibitors block DNA damage-induced neuronal apoptosis (Lesuisse and Martin, 2002b).

- Mild hypothermia with sedation and muscle paralysis cause sustained neuroprotection against acute brain injury without deleterious side effects

## REPORTABLE OUTCOMES

### *Original Full-Length Peer-Reviewed Papers*

- ✓ Martin LJ, Sieber FE and Traystman RJ (2000) Apoptosis and necrosis occur in separate neuronal populations in hippocampus and cerebellum after ischemia and are associated with alterations in metabotropic glutamate receptor signaling pathways. *J Cereb Blood Flow Metab* 20:153-167. **Appendix**
- ✓ Martin LJ, Brambrink AM, Price AC, Kaiser A, Agnew DM, Ichord RN and Traystman RJ (2000) Neuronal death in newborn striatum after hypoxia-ischemia is necrosis and evolves with oxidative stress. *Neurobiol Disease* 7:169-191. **Appendix**
- ✓ Martin LJ, Kaiser A, Yu JW, Natale JE and Al-Abdulla NA (2001) Injury-induced apoptosis of neurons in adult brain is mediated by p53-dependent and p53-independent pathways and requires bax. *J Comp Neurol* 433:299-311. **Appendix**
- ✓ Northington FJ, Ferriero DM, Flock DL and Martin LJ (2001) Delayed neurodegeneration in neonatal rat thalamus after hypoxia-ischemia is apoptosis. *J Neurosci* 21:1931-1938. **Appendix**
- ✓ Liu Z and Martin LJ (2001) Motor neurons rapidly accumulate DNA single-strand breaks after *in vitro* exposure to nitric oxide and peroxynitrite and *in vivo* axotomy. *J Comp Neurol* 432:35-60. **Appendix**
- ✓ Northington FJ, Ferriero DM and Martin LJ (2001) Neurodegeneration in thalamus following neonatal hypoxia-ischemia is programmed cell death. *Dev Neurosci* 23:186-191. **Appendix**
- ✓ Gabrielson KL, Hogue BA, Bohr VA, Cardounel AJ, Nakajima W, Kofler J, Zweier JL, Rodriguez ER, Martin LJ, de Souza-Pinto NC and Bressler J (2001) Mitochondrial neurotoxin 3-nitropropionic acid induces cardiac and neurotoxicity differentially in mice. *Am J Pathol* 159:1507-1520. **Appendix**
- ✓ Northington FJ, Ferriero DM, Graham EM, Traystman RJ and Martin LJ (2001) Early neurodegeneration after hypoxia-ischemia in neonatal rat is necrosis while delayed neuronal death is apoptosis. *Neurobiol Disease* 8:207-219. **Appendix**
- ✓ Golden WC, Brambrink AM, Traystman RJ and Martin LJ (2001) Failure to sustain recovery of Na,K-ATPase function is a possible mechanism for striatal neurodegeneration in hypoxic-ischemic newborn piglets. *Mol Brain Res* 88:94-102. **Appendix**
- ✓ Liu Z and Martin LJ (2001) Isolation of mature spinal motor neurons and single cell analysis using the comet assay of early low-level DNA damage induced *in vitro* and *in vivo*. *J Histochem Cytochem* 49: 957-972. **Appendix**
- ✓ Martin LJ (2001) Neuronal cell death in nervous system development, disease, and injury. *Int J Mol Med* 7:455-478. **Appendix**

✓ ~~Natale~~ JE, Cheng Y and Martin LJ (2002) Thalamic neuron apoptosis emerges rapidly after cortical damage in immature mice. *Neuroscience* 112:665-676. **Appendix**

✓ Martin LJ and Liu Z (2002) Injury-induced spinal motor neuron apoptosis is preceded by DNA single-strand breaks and is p53- and Bax-dependent. *J Neurobiol* 50:181-197. **Appendix**

✓ Ginsberg SD and Martin LJ (2002) Axonal transection in adult rat brain induces transsynaptic apoptosis and persistent atrophy of target neurons. *J Neurotrauma* 19:99-109. **Appendix**

✓ Lesuisse C and Martin LJ (2002) Long term culture of mouse cortical neurons as a model for neuronal development, aging, and death. *J Neurobiol* 51:9-23. **Appendix**

✓ ~~Guerguerian~~ AM, Brambrink AM, Traystman RJ, Haganir RL and Martin LJ (2002) Altered expression and phosphorylation of N-methyl-D-aspartate receptors in piglet striatum after hypoxia-ischemia. *Mol Brain Res* 104:66-80. **Appendix**

✓ Al-Abdulla NA and Martin LJ (2002) Projection neurons and interneurons in the lateral geniculate nucleus undergo distinct forms of degeneration ranging from retrograde and transsynaptic apoptosis to transient atrophy after cortical ablation in rat. *Neuroscience* 115:7-14. **Appendix**

✓ ~~Lok J~~ and Martin LJ (2002) Rapid subcellular redistribution of Bax precedes caspase-3 and endonuclease activation during excitotoxic neuronal apoptosis. *J Neurotrauma* 19:815-828. **Appendix**

✓ ~~Lesuisse~~ C and Martin LJ (2002) Immature and mature cortical neurons engage different apoptotic mechanisms involving caspase-3 and the MAP kinase pathway. *J Cereb Blood Flow Metabol* 22:935-950. **Appendix**

? Shaikh AY and Martin LJ (2002) DNA base-excision repair enzyme apurinic/apyrimidinic endonuclease/redox factor-1 is increased and competent in brain and spinal cord of individuals with amyotrophic lateral sclerosis. *NeuroMolecular Med* 2:47-60. **Appendix**

✓ Martin LJ and Liu Z (2002) DNA damage profiling in motor neurons: a single-cell analysis by comet assay. *Neurochem Res* 27:1093-1104. **Appendix**

Martin LJ, Price AC, McClendon KB, Al-Abdulla NA, Subramaniam JR, Wong PC and Liu Z (2003) Early events of target deprivation/axotomy-induced neuronal apoptosis in vivo: oxidative stress, DNA damage, p53 phosphorylation and subcellular redistribution of death proteins. *J Neurochem* 85:234-247. **Appendix**

Agnew DM, Koehler RC, Guerguerian AM, Shaffner DH, Traystman RJ, Martin LJ and Ichord RN (2003) Hypothermia for 24 hours after asphyxic cardiac arrest in piglets provides striatal neuroprotection that is sustained 10 days after rewarming. *Pediatric Res* 54:1-10.

Liu Z and Martin LJ (2003) The olfactory bulb core is a rich source of neural progenitor and stem cells in adult rodent and human. *J Comp Neurol* 459:368-391.

Golden WC, Brambrink AM, Traystman RJ, Shaffner DH and Martin LJ (2003) Nitration of the Striatal Na, K ATPase  $\alpha 3$  isoform occurs in normal brain development but not during hypoxia-ischemia in newborn piglets. *Neurochem. Res*, in press.

*Reviews and Book Chapters*

Martin LJ, Price AC, Kaiser A, Shaikh AY and Liu Z (2000) Mechanisms for neuronal degeneration in amyotrophic lateral sclerosis and in models of motor neuron death. *Int J Mol Med* 5:3-13. **Appendix**

✓ Martin LJ (2002) Synaptic and neuroglial pathobiology in acute and chronic neurological disorders. In: *Neuroglial in the Aging Brain*. de Vellis J (ed), Humana Press, pp 443-457. **Appendix**

✓ Martin LJ (2002) Apoptosis in CNS development, injury, and disease: contributions and mechanisms. In: *Neuroprotection*. Lo E and Marwah J (eds), Prominent Press, pp 379-412.

✓ Martin LJ (2002) Neurodegenerative disorders of the human brain and spinal cord. In: *Encyclopedia of the Human Brain*. VS Ramachandran (ed), Elsevier Science, Vol 3, pp 441-463. **Appendix**

Martin LJ (2002) Peptides, hormones, and the human brain and spinal cord. In: *Encyclopedia of the Human Brain*. VS Ramachandran (ed), Elsevier Science, Vol 3, pp 797-815, 2002. **Appendix**

Martin LJ (2003) Mechanisms of brain damage in animal models of hypoxia-ischemia in newborns, in *Fetal and Neonatal Brain Injury: Mechanisms, Management, and the Risks of Practice* (Stevenson, D.K. and Sunshine, P. eds.), 2<sup>nd</sup> edition, Oxford University Press, pp 30-57.

#### *Abstracts*

Martin LJ, Kaiser A and Price AC (1999) Oxidative stress and p53 induction may participate in the mechanisms for motor neuron apoptosis in adult spinal cord. *Soc Neurosci Abstr* 25:289.

Northington FJ, Ferriero DM, Traystman RJ and Martin LJ (1999) Early neurodegeneration in forebrain after neonatal hypoxia-ischemia (H/I) is necrosis while delayed neuronal death in thalamus and remote brain regions is apoptosis. *Soc Neurosci Abstr* 25:755.

Martin LJ (2000) Motor neurons have DNA damage and p53 is abnormally elevated and active in the CNS of patients with amyotrophic lateral sclerosis. *Soc Neurosci Abstr* 26:500.

Liu Z and Martin LJ (2000) DNA single-strand breaks occur rapidly in motor neurons in vitro and in vivo after oxidative stress and axotomy. *Soc Neurosci Abstr* 26:331.

Lesuisse C and Martin LJ (2000) Neuronal maturity influences the progression of neuronal apoptosis induced by DNA damage. *Soc Neurosci Abstr* 26:322.

Al-Abdulla NA and Martin LJ (2000) Target-deprived lateral geniculate projection neurons in the adult rat undergo DNA damage and apoptosis while interneurons transiently atrophy. *Soc Neurosci Abstr* 26:331.

Natale JE and Martin LJ (2000) Ablation of occipital cortex in immature mouse brain induces p53 and neuronal apoptosis in the lateral geniculate nucleus. *Soc Neurosci Abstr* 26:1323.

Guerguerian AM, Brambrink A, Martin LA, Traystman RJ and Martin LJ (2000) Expression and phosphorylation of NMDA receptors are altered in striatum early after hypoxia-ischemia in piglets. *Soc Neurosci Abstr* 26:760.

Agnew DM, Koehler RC, Traystman RJ and Martin LJ (2001) Early NMDA receptor activation and oxidative stress coexist and precede striatal neurodegeneration after hypoxic ischemia in piglets and are attenuated with hypothermia. Soc Neurosci Abstr 867.7.

Lok J, Crain BJ and Martin LJ (2001) rapid subcellular redistribution of bax precedes caspase-3 and endonuclease activation during excitotoxic neuronal apoptosis in newborn brain. Soc Neurosci Abstr 20.2.

Northington FJ, Ferriero DM, Hagberg H, Flock DL, Blomgren J and Martin LJ (2001) Neuronal death emerges as a necrosis-apoptosis continuum driven by mitochondria and caspases after neonatal hypoxia-ischemia. Soc Neurosci Abstr 20.6.

Liu Z and Martin LJ (2001) The olfactory bulb is a novel source of neural stem cells in adult CNS: identification, isolation, and culture. Soc Neurosci Abstr 134.7.

Lesuisse CG and Martin LJ (2001) Apoptosis is mediated differentially by MAP kinase and caspase pathways during development of mouse cortical neurons in culture. Soc Neurosci Abstr 655.19.

Martin LJ and Liu Z (2001) Genetic and molecular regulation of motor neuron cell death in spinal cord: apoptosis is p53- and bax-dependent and involves early DNA damage. Soc Neurosci Abstr 767.9.

Liu Z, Xu G, Jankowsky J, Borchelt DR, Price DL and Martin LJ (2002) Neural stem cells in adult olfactory bulb (OB) core can be transplanted and grafted into CNS and are retained in mutant mouse models of amyotrophic lateral sclerosis and Alzheimer's disease. Soc Neurosci Abstr 483.13.

Martin LJ and Liu Z (2002) Neural stem cells from adult rat olfactory bulb core can differentiate into motor neurons. Soc Neurosci Abstr 719.1.

#### **List of Personnel Supported from this Contract**

Lee J. Martin, Ph.D.-PI  
Nael Al-Abdulla, M.D.-Fellow  
Zhiping Liu, M.D., Ph.D.-Postdoctoral Fellow  
Ann Price-Technician

#### **CONCLUSIONS**

The DAMD17-99-1-9553 contract has been highly productive, evolving by incorporating innovative technologies and has always focused on mechanisms of neurodegeneration. Each of the four original hypotheses outlined in our proposal has been addressed and new ground was broken in our study of neuronal apoptosis. DAMD17-99-1-9553 has supported ~24 original peer-reviewed publications and 6 book chapters/reviews on neuronal cell death. This progress has included work on the contribution of apoptosis to retrograde neurodegeneration after target deprivation in adult and newborn brain, the validation of the cortical ablation model as a system to study apoptosis of neurons in a homogeneous

population of cells, the dependence of this apoptosis on Bax and the possible roles of other Bcl-2 family members (eg, Bak and Bad), the regulation of dLGN neuron apoptosis by p53, the identification of ROS/RNS-generated DNA damage as a possible upstream signal for neuron cell death, and the development of a method to profile DNA damage in single neurons using SCGE (comet assay). With the funding provided by the USAMRMC, we have identified molecules that regulate mammalian neuron apoptosis, including p53, Bax, caspases, and protein kinases. We have identified possible upstream mechanisms that trigger neuronal cell death such as DNA damage, MAP kinase signaling, and Na,K ATPase inactivation. These results provide direction and rationale for the future development of anti-apoptosis and anti-necrosis therapies for a variety of neurological disorders.

Under this contract major accomplishments at the technical level have been achieved. We developed neuronal isolation procedures and quantitative and high-resolution assays to study the biochemical and molecular regulation of neuronal cell death (e.g., comet assay, immunogold-EM). The method that we have developed to isolate adult motor neurons can be used in future studies to isolate and profile DNA damage in other populations of cells, such as midbrain dopamine neurons, in other animal models of neurodegeneration. The comet assay can be used to profile DNA damage in single neurons and to screen drugs for neuroprotective actions. Protein translocation and subcellular redistribution can be measured directly in single cells with our immunogold-EM assay. Our long-term cortical neuron culture system can be used to identify the molecular and genetic regulation of DNA damage-induced neuronal apoptosis and to screen antiapoptotic drugs in a relatively homogeneous population of cells. In the future, we plan to use *in vitro* screening of potential antiapoptotic drugs in addition to *in vivo* testing. With our technical approaches we can better identify mechanisms of neurotoxin action as well as reveal the mechanisms of action of neuroprotective drugs.

The work funded through this USAMRMC grant has implications for the understanding and treatment of acute and chronic brain injury as well as secondary neuropathology. Thus, this research has broad significance for military personnel and civilians. The relevance of this work extends to the neurodegeneration after exposure to neurotoxins, including chemical and biological warfare agents, and

radiation. It also embraces the neurodegeneration after head and spinal cord trauma, limb amputation, seizures, and hypoxia-ischemia caused by cardiac arrest, stroke, and increased intracranial pressure. Lastly, this work is also important for the further understanding of the pathogenesis of stroke, Alzheimer's disease, ALS, Huntington's disease, and Parkinson's disease.

## REFERENCES

- Agnew DM, Koehler RC, Traystman RJ and Martin LJ (2001) Early NMDA receptor activation and oxidative stress coexist and precede striatal neurodegeneration after hypoxic ischemia in piglets and are attenuated with hypothermia. Soc Neurosci Abstr 867.7.
- Agnew DM, Koehler RC, Guerguerian AM, Shaffner DH, Traystman RJ, Martin LJ and Ichord RN (2003) Hypothermia for 24 hours after asphyxic cardiac arrest in piglets provides striatal neuroprotection that is sustained 10 days after rewarming. Pediatric Res 54:1-10.
- Al-Abdulla NA and Martin LJ (1998) Apoptosis of retrogradely degenerating neurons occurs in association with the accumulation of perikaryal mitochondria and oxidative damage to the nucleus. Am J Pathol 153: 447-456.
- Al-Abdulla NA and Martin LJ (2002) Projection neurons and interneurons in the lateral geniculate nucleus undergo distinct forms of degeneration ranging from retrograde and transsynaptic apoptosis to transient atrophy after cortical ablation in rat. Neuroscience 115:7-14.
- Al-Abdulla NA, Portera-Cailliau C and Martin LJ (1998) Occipital cortex ablation in adult rat causes retrograde neuronal death in the lateral geniculate nucleus that resembles apoptosis. Neuroscience 86: 191-209.
- Bradley WG and Krasin F (1982) A new hypothesis of the etiology of amyotrophic lateral sclerosis. The DNA hypothesis. Arch Neurol 39:677-680.
- Cardone MH, Salvesen GS, Widmann C, Johnson G, and Frisch SM (1997) The regulation of anoikis: MEKK-1 activation requires cleavage by caspases. Cell 90:315-323.
- Charatan F (2002) US links motor neurone disease with Gulf War service. Brit Med J 324:65.
- del Peso L, González-García M, Page C, Herrera R and Nuñez G. (1997) Interleukin-3-induced phosphorylation of Bad through the protein kinase Akt. Science 278:687-689.
- Franke T.F., Kaplan D.R. and Cantley L.C. (1997) PI3K: downstream AKT ion blocks apoptosis. Cell 88: 435-437.
- Guerguerian AM, Brambrink AM, Traystman RJ, Haganir RL and Martin LJ (2002) Altered expression and phosphorylation of N-methyl-D-aspartate receptors in piglet striatum after hypoxia-ischemia. Mol Brain Res 104:66-80.

Golden WC, Brambrink AM, Traystman RJ and Martin LJ (2001) Failure to sustain recovery of Na,K ATPase function is a possible mechanism for striatal neurodegeneration in hypoxic-ischemic newborn piglets. *Mol Brain Res* 88:94-102.

Golden WC, Brambrink AM, Traystman RJ, Shaffner DH and Martin LJ (2003) Nitration of the Striatal Na, K ATPase  $\alpha 3$  isoform occurs in normal brain development but not during hypoxia-ischemia in newborn piglets. *Neurochem. Res*, in press.

Kerr JFR, Wyllie AH and Currie AR (1972) Apoptosis: a basic biological phenomenon with wide-ranging implications in tissue kinetics. *Br J Cancer* 26:239-257.

Lesuisse C and Martin LJ (2002a) Long term culture of mouse cortical neurons as a model for neuronal development, aging, and death. *J Neurobiol* 51:9-23.

Lesuisse C and Martin LJ (2002b) Immature and mature cortical neurons engage different apoptotic mechanisms involving caspase-3 and the MAP kinase pathway. *J Cereb Blood Flow Metabol* 22:935-950.

Levin S, Bucci TJ, Cohen SM, Fix AS, Hardisty JF, LeGrande EK, Maronpot RR, and Trump BF (1999) The nomenclature of cell death: recommendations of an ad hoc Committee of the Society of Toxicologic Pathologists. *Toxicol Pathol* 27:484-490.

Leverro M, De Laurenzi V, Costanzo A, Sabatini S, Gong J, Wang JYJ and Melino G (2000) The p53/p63/p73 family of transcription factors: overlapping and distinct functions. *J Cell Sci* 113:1661-1670.

Levine AJ (1997) p53, the cellular gatekeeper for growth and division. *Cell* 88:323-331.

Liu Z and Martin LJ (2001a) Motor neurons rapidly accumulate DNA single strand breaks after in vitro exposure to nitric oxide and peroxynitrite and in vivo axotomy. *J Comp Neurol* 432:35-60.

Liu Z and Martin LJ (2001b) Isolation of mature spinal motor neurons and single cell analysis using the comet assay of early low-level DNA damage induced in vitro and in vivo. *J Histochem Cytochem* 49:957-972.

Lok J and Martin LJ (2002) Rapid subcellular redistribution of Bax precedes caspase-3 and endonuclease activation during excitotoxic neuronal apoptosis. *J Neurotrauma* 19:815-828.

Martin LJ (1999) Neuronal death in amyotrophic lateral sclerosis is apoptosis: possible contribution of a programmed cell death mechanism. *J Neuropathol Exp Neurol* 58:459-471.

Martin LJ (2000) p53 is abnormally elevated and active in the CNS of patients with amyotrophic lateral sclerosis. *Neurobiol Disease* 7:613-622.

Martin LJ (2001) Neuronal cell death in nervous system development, disease, and injury. *Int J Mol Med* 7:455-478.

Martin LJ (2002) Apoptosis in CNS development, injury, and disease: contributions and mechanisms. In: *Neuroprotection*. Lo E and Marwah J (eds), Prominent Press, pp 379-412.

Martin LJ, Al-Abdulla NA, Brambrink AM, Kirsch JR, Sieber FE, and Portera-Cailliau C (1998) Neurodegeneration in excitotoxicity, global cerebral ischemia, and target deprivation: a perspective on the contributions of apoptosis and necrosis. *Brain Res Bull* 46:281-309.



- Martin LJ, Sieber FE and Traystman RJ (2000) Apoptosis and necrosis occur in separate neuronal populations in hippocampus and cerebellum after ischemia and are associated with alterations in metabotropic glutamate receptor signaling pathways. *J Cereb Blood Flow Metab* 20: 153-167.
- Martin LJ, Kaiser A, Yu JW, Natale JE and Al-Abdulla NA (2001) Injury-induced apoptosis of neurons in adult brain is mediated by p53-dependent and p53-independent pathways and requires Bax. *J Comp Neurol* 433:299-311.
- Martin LJ and Liu Z (2002a) Injury-induced spinal motor neuron apoptosis is preceded by DNA single-strand breaks and is p53- and Bax-dependent. *J Neurobiol* 50:181-197.
- Martin LJ and Liu Z (2002b) DNA damage profiling in motor neurons: a single-cell analysis by comet assay. *Neurochem Res* 27:1093-1104.
- Martin LJ, Price AC, McClendon KB, Al-Abdulla NA, Subramaniam JR, Wong PC and Liu Z (2003) Early events of target deprivation/axotomy-induced neuronal apoptosis in vivo: oxidative stress, DNA damage, p53 phosphorylation and subcellular redistribution of death proteins. *J Neurochem* 85:234-247.
- McCord JM and Fridovich I (1969) Superoxide dismutase, an enzymic function for erythrocuprein (hemocuprein). *J Biol Chem* 244:6049-6055.
- Merry DE and Korsmeyer SJ (1997) Bcl-2 gene family in the nervous system. *Ann Rev Neurosci* 20:245-267.
- Nagata S (1999) Fas ligand-induced apoptosis. *Annu Rev Genet* 33:29-55.
- Natale JE, Cheng Y and Martin LJ (2002) Thalamic neuron apoptosis emerges rapidly after cortical damage in immature mice. *Neuroscience* 112:665-676.
- Norbury CJ and Hickson ID (2001) Cellular responses to DNA damage. *Annu Rev Pharmacol Toxicol* 41:367-401.
- Northington FJ, Ferriero DM, Graham EM, Traystman RJ and Martin LJ (2001a) Early neurodegeneration after hypoxia-ischemia in neonatal rat is necrosis while delayed neuronal death is apoptosis. *Neurobiol Disease* 8:207-219.
- Northington FJ, Ferriero DM, Flock DL and Martin LJ (2001b) Delayed neurodegeneration in neonatal rat thalamus after hypoxia-ischemia is apoptosis. *J Neurosci* 21:1931-1938.
- Polyak K, Xia Y, Zweier JL, Kinzler KW and Vogelstein B (1997) A model for p53-induced apoptosis. *Nature* 389:300-305.
- Portera-Cailliau C, Price DL and Martin LJ (1997a) Excitotoxic neuronal death in the immature brain is an apoptosis-necrosis morphological continuum. *J Comp Neurol* 378:70-87.
- Portera-Cailliau C, Price DL and Martin LJ (1997b) Non-NMDA and NMDA receptor-mediated excitotoxic neuronal deaths in adult brain are morphologically distinct: further evidence for an apoptosis-necrosis continuum. *J Comp Neurol* 378:88-104.

Schweichel JU and Merker HJ (1973) The morphology of various types of cell death in prenatal tissues. *Teratology* 7:253-266.

Shaikh AY and Martin LJ (2002) DNA base-excision repair enzyme apurinic/apyrimidinic endonuclease/redox factor-1 is increased and competent in brain and spinal cord of individuals with amyotrophic lateral sclerosis. *NeuroMolecular Med* 2:47-60.

Widmann C, Gerwins P, Johnson NL, Jarpe MB and Johnson GL (1998) MEK kinase 1, a substrate for DEVD-directed caspases, is involved in genotoxin-induced apoptosis. *Mol Cell Biol* 18:2416-2429.

Wolf BB and Green DR (1999) Suicidal tendencies: apoptotic cell death by caspase family proteinases. *J Biol Chem* 274:20049-20052.

## **APPENDIX**

### **Reported Outcomes (copies of reprints and preprints)**

24 published full-length papers and 3 book chapters are enclosed in the Appendix.

## Early events of target deprivation/axotomy-induced neuronal apoptosis *in vivo*: oxidative stress, DNA damage, p53 phosphorylation and subcellular redistribution of death proteins

Lee J. Martin,\*† Anne C. Price,\* Karen B. McClendon,\* Nael A. Al-Abdulla,\*†  
Jamuna R. Subramaniam,\* Philip C. Wong\* and Zhiping Liu\*

\*Division of Neuropathology, Department of Pathology and †Department of Neuroscience, Johns Hopkins University School of Medicine, Baltimore, Maryland, USA

†The Wilmer Eye Institute of the Johns Hopkins Hospital, Baltimore, Maryland, USA

### Abstract

The mechanisms of injury- and disease-associated apoptosis of neurons within the CNS are not understood. We used a model of cortical injury in rat and mouse to induce retrograde neuronal apoptosis in thalamus. In this animal model, unilateral ablation of the occipital cortex induces apoptosis of corticopetal projection neurons in the dorsal lateral geniculate nucleus (LGN), by 7 days post-lesion, that is p53 modulated and Bax dependent. We tested the hypothesis that this degenerative process is initiated by oxidative stress and early formation of DNA damage and is accompanied by changes in the levels of pro-apoptotic mediators of cell death. Immunoblotting revealed that the protein profiles of Bax, Bak and Bad were different during the progression of neuronal apoptosis in the LGN. Bax underwent a subcellular redistribution by 1 day post-lesion, while Bak increased later. Bad showed an early sustained increase. Cleaved caspase-3 was elevated maximally at 5 and 6 days. Active caspase-3 underwent a

subcellular translocation to the nucleus. A dramatic phosphorylation of p53 was detected at 4 days post-lesion. DNA damage was assessed immunocytochemically as hydroxyl radical adducts (8-hydroxy-2-deoxyguanosine) and single-stranded DNA. Both forms of DNA damage accumulated early in target-deprived LGN neurons. Transgenic overexpression of superoxide dismutase-1 provided significant protection against the apoptosis but antioxidant pharmacotreatments with trolox and ascorbate were ineffective. We conclude that overlapping and sequential signaling pathways are involved in the apoptosis of adult brain neurons and that DNA damage generated by superoxide derivatives is an upstream mechanism for p53-regulated, Bax-dependent apoptosis of target-deprived neurons.

**Keywords:** Alzheimer's disease, amyotrophic lateral sclerosis, cell death, DNA damage, Parkinson's disease, traumatic brain injury.

*J. Neurochem.* (2003) **85**, 234–247.

Dysregulated apoptosis may contribute to the pathophysiology of CNS damage in acute neuropathological disorders, such as cerebral ischemia (MacManus and Linnik 1997; Martin *et al.* 1998) and CNS trauma (Liu *et al.* 1997; Yakovlev *et al.* 1997; Conti *et al.* 1998), and in chronic neurodegenerative diseases, such as Alzheimer's disease (Anderson *et al.* 1996; Kitamura *et al.* 1999), amyotrophic lateral sclerosis (Martin 1999; Mattson *et al.* 1999) and Parkinson's disease (Burke and Kholodilov 1998). Knowledge of the mechanisms of apoptosis in post-mitotic cells such as neurons is limited compared with non-nervous tissue cells. In cultures of neonatal superior cervical ganglion neurons or cerebellar granular cells (Deckwerth *et al.* 1996; Miller *et al.* 1997; Putcha *et al.* 2001, 2002) and in

developmental models of neuronal death (Deckwerth *et al.* 1996), expression and translocation of the multidomain

Received October 30, 2002; revised manuscript received December 19, 2002; accepted December 20, 2002.

Address correspondence and reprint requests to Dr Lee J. Martin, Johns Hopkins University School of Medicine, Department of Pathology, 558 Ross Building, 720 Rutland Avenue, Baltimore, MD 21205-2196, USA. E-mail: martinl@jhmi.edu

**Abbreviations used:** Cox1, cytochrome *c* oxidase subunit 1; DEVD, Asp-Glu-Val-Asp; dLGN, dorsal lateral geniculate nucleus; DNA-PK, DNA-dependent protein kinase; DSB, double-strand breaks; EM, electron microscopy; IR, immunoreactivity; LGN, lateral geniculate nucleus; OHdG, 8-hydroxy-2-deoxyguanosine; PI-3, phosphoinositide-3 kinase; ROS, reactive oxygen species; SOD1, superoxide dismutase 1; ssDNA, single-stranded DNA; Tg, transgenic.

pro-apoptotic family member Bax are critical for apoptosis of neurons. Bim, a BH3-only protein, also appears to have a pro-apoptotic role in apoptosis of peripheral neurons (Putcha *et al.* 2001). Much less work has been done on the mechanisms of CNS neuron apoptosis *in vivo*. A more complete understanding of the molecular mechanisms that trigger and regulate neuronal apoptosis within the CNS could be therapeutically relevant to acute and chronic neurological disorders.

We used an animal injury model of neurodegeneration to further understand *in vivo* mechanisms of neuronal apoptosis. Ablation of the visual cortex induces retrograde neuronal degeneration in the dorsal lateral geniculate nucleus (dLGN) of thalamus (Lashley 1941; Barron *et al.* 1967; Giolli and Guthrie 1971). The geniculocortical projection neurons die by a morphological process that is unequivocal apoptosis (Al-Abdulla *et al.* 1998; Al-Abdulla and Martin 2002). This cell death is preceded by an accumulation of apparently active mitochondria in the perikaryon and might emerge with oxidative damage to genomic DNA of the highly vulnerable projection neurons (Al-Abdulla and Martin 1998). Apoptosis of geniculocortical projection neurons requires the presence of the *Bax* gene and is modified by a functional *p53* gene, further supporting a role for apoptosis in this neurodegeneration and the possible role of DNA damage as a trigger (Martin *et al.* 2001). Despite this information on the molecular genetics of this neuronal apoptosis, it is still not clear how these neurons die. We tested the hypothesis that neuronal apoptosis in this *in vivo* CNS model is accompanied by changes in the levels of pro-apoptotic mediators of cell death and by the early formation of DNA damage.

## Materials and methods

### Lesion paradigm to study neuronal apoptosis *in vivo*

An occipital cortex aspiration lesion served as the model for producing axotomy and target deprivation of lateral geniculate nucleus (LGN) projection neurons in rat and mouse. The accuracy and reproducibility of this CNS lesion have been described previously (Al-Abdulla *et al.* 1998; Martin *et al.* 2001). Lesions were done on adult (weight ~150–300 g) male Sprague-Dawley rats ( $n = 160$ ), purchased from Charles River Laboratories Inc. (Wilmington, MA, USA) and adult male C57BL/6 mice ( $n = 26$ ). The institutional Animal Care and Use Committee approved the animal protocols. The animals were anesthetized with a mixture of enflurane : oxygen : nitrous oxide (1 : 33 : 66) and placed in a stereotaxic apparatus. The scalp was incised at the midline and a craniotomy was made. The dura was incised with a fresh, sterile 22-gauge needle. The cortex underlying the craniotomy was then aspirated using a blunt-tipped 22-gauge needle connected to a vacuum line, without damaging the surrounding venous sinuses and the underlying hippocampus.

### Immunoblotting for cell death proteins

Bax, Bak, Bad, caspase-3 and phospho-p53 protein levels were measured during the progression of neuronal apoptosis. Samples of

LGN (ipsilateral and contralateral) were collected for immunoblotting at 1, 4, 5 and 6 days after occipital cortex ablation ( $n = 12$ –15 rats/time point). Animals were deeply anesthetized with chloral hydrate, decapitated and the brain was removed quickly and placed on ice. Under a microsurgical stereomicroscope, the cerebral cortex was reflected to visualize the dorsal thalamus. The LGN is readily discernible by surface landmarks. Using iridectomy scissors, the LGN from ipsilateral (target deprived) and contralateral (control) thalamus was microdissected from each rat and frozen quickly in liquid nitrogen. The LGN samples from target-deprived and control sides were pooled from 12–15 rats for each time point. The accuracy of the LGN microdissection was verified by removing LGN samples and then placing the brainstems in 4% paraformaldehyde. Afterwards the brainstems were cryoprotected in phosphate-buffered 20% glycerol, cut and rostral brainstem sections were stained with cresyl violet and viewed microscopically (Fig. 1a).

Microdissected LGN samples were homogenized with a polytron (Brinkmann Instruments, Westbury, NY, USA) in ice-cold 20 mM Tris HCl (pH 7.4) containing 10% (w/v) sucrose, 200 mM mannitol, 20 U/mL aprotinin, 20 µg/mL leupeptin, 20 µg/mL antipain, 20 µg/mL pepstatin A, 20 µg/mL chymostatin, 0.1 mM phenylmethylsulfonyl fluoride, 10 mM benzamidine, 1 mM EDTA and 5 mM EGTA. Crude homogenates were sonicated for 15 s and then centrifuged at 1000  $g_{av}$  for 10 min (4°C), the resulting pellet consisting of the nuclear-enriched fraction was washed (twice) by trituration in homogenization buffer followed by centrifugation and then finally resuspended in homogenization buffer (without sucrose) supplemented with 20% (w/v) glycerol. The supernatant fluid was then centrifuged at 54 000  $g_{av}$  for 20 min (4°C) to yield soluble (S2) and mitochondria-enriched pellet (P2) fractions. The pellet fraction was washed (twice) by trituration in homogenization buffer followed by centrifugation and then finally resuspended in homogenization buffer (without sucrose) supplemented with 20% (w/v) glycerol. Protein concentrations in all fractions were measured by a protein assay (Bio-Rad Laboratories, Hercules, CA, USA) with bovine serum albumin as a standard. This subcellular fractionation protocol has been verified previously in other CNS tissues (Martin 2000) and confirmed in this LGN model (Figs 1b and c; Martin *et al.* 2001) using antibodies to neuronal nuclear protein NeuN (Chemicon, Temecula, CA, USA), lactate dehydrogenase (Rockland Immunochemicals, Gilbertsville, PA, USA) and cytochrome *c* oxidase subunit 1 (Cox1; Molecular Probes, Eugene, OR, USA) to evaluate the purity of nuclear, soluble and mitochondria-enriched protein fractions, respectively.

Proteins from ipsilateral and contralateral LGN samples were subjected to 15% sodium dodecyl sulfate–polyacrylamide gel electrophoresis and transferred to nitrocellulose membrane by electroelution as described by Martin (1999). Several different cell death proteins were evaluated (Table 1). A fusion protein containing amino acids 1–171 of mouse Bax (Santa Cruz Biotechnology, Santa Cruz, CA, USA) served as a positive control for Bax immunoblots. The CNS extracts from Bax<sup>−/−</sup> mice and p53<sup>−/−</sup> mice (Martin *et al.* 2001) as well as peptide competition with an amino terminal peptide of Bax-α (Santa Cruz) were negative controls for Bax blots. A fusion protein containing amino acids 1–211 of human Bak (Santa Cruz) and HeLa and A-431 cell lysates served as positive controls for Bak immunoblots. Peptide competition with an amino terminal peptide of Bak (Santa Cruz) was a negative control for Bak blots. A fusion

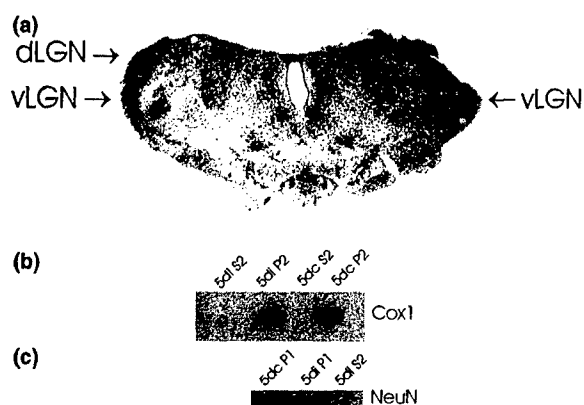


**Fig. 1** Verification of dorsal lateral geniculate nucleus (dLGN) microdissection and tissue subcellular fractionation. (a) Cresyl violet-stained transverse section of a rat thalamus demonstrating the high accuracy of the dLGN microdissection. In this example, the dLGN was removed from only one side of the brain (upper right side) and the ventral LGN (VLGN) is preserved. (b) dLGN ipsilateral (i) and contralateral (c) tissues at 5 days post-lesion (5d) were fractionated into soluble (S2) and pellet (P2) proteins and were subjected to sodium dodecyl sulfate–polyacrylamide gel electrophoresis (SDS–PAGE; each lane contains protein extracts that were pooled from LGN samples from 12 rats), transferred to nitrocellulose membranes and immunoblotted with monoclonal antibody to cytochrome *c* oxidase subunit 1 (Cox1). The high levels of the mitochondrial enzyme Cox1 verified the mitochondria enrichment of the pellet P2 fractions. Cox1 was not detected in the soluble protein (S2) fractions irrespective of whether they were from the target-deprived ipsilateral dLGN or from the control contralateral dLGN. The lesion did not alter the level of Cox1 at 5 days. (c) dLGN contralateral (c) and ipsilateral (i) tissues at 5 days post-lesion (5d) were fractionated into soluble (S2) and nuclear (P1) proteins and were subjected to SDS–PAGE (each lane contains protein extracts that were pooled from LGN samples from 12 rats), transferred to nitrocellulose membranes and immunoblotted with monoclonal antibody to the neuronal nuclear protein NeuN. The high levels of the neuronal nuclear protein verified the nuclear enrichment of the pellet P1 fractions. NeuN was not detected in the soluble protein (S2) fractions irrespective of whether they were from the target-deprived ipsilateral dLGN or from the control contralateral dLGN. The lesion did not alter the level of NeuN for 5 days post-lesion.

**Table 1** Expression profiling of cell death regulators by immunoblotting

Cell death protein	Antibody source	Dilution ( $\mu\text{g/mL}$ )
Bax	Upstate	1
Bax	Santa Cruz	0.4
Bak	Upstate	1
Bad	Transduction Laboratories	0.5
Caspase-3	Santa Cruz	0.4
Cleaved caspase-3	Cell Signaling	1 : 500
Phospho-p53 (Ser15)	Cell Signaling	0.1

protein containing amino acids 1–168 of human Bad (Santa Cruz) served as a positive control for Bad blots. Peptide competition with a carboxy terminal peptide of Bad (Santa Cruz) was a negative control for Bad blots. Caspase-3 was detected with a rabbit polyclonal antibody that binds both the pro-enzyme and the cleaved subunits (Santa Cruz) and a rabbit polyclonal antibody that binds only the cleaved subunits (Cell Signaling Technology, Beverly, MA, USA). The positive control for cleaved caspase was purified active caspase-3 (BioVision Research Products, Palo Alto, CA, USA). The positive control for phospho-p53 was lysates of neurons exposed to the DNA-damaging agent camptothecin (Lesuisse and Martin 2002). The reliability of sample loading and electroblotting in each experiment was evaluated by staining nitrocellulose membranes with Ponceau S before immunoblotting. Blots were blocked with 2.5% non-fat dry milk with 0.1% Tween 20 in 50 mM Tris-buffered saline (pH 7.4) and then incubated overnight at 4°C with antibody. The antibodies were used at concentrations for visualizing immunoreactive proteins within the linear range (Lok and Martin 2002). After the primary antibody incubation, blots were washed and incubated with horseradish peroxidase-conjugated secondary antibody (0.2  $\mu\text{g/mL}$ ), developed with enhanced chemiluminescence (Pierce, Rockford, IL, USA) and exposed to X-ray film. The blots were then reprobed with monoclonal antibodies to synaptophysin (Boehringer Mannheim, Indianapolis, IN, USA) or synapse-associated protein-25 (Sternberger Monoclonals, Lutherville, MD, USA) as controls for protein loading.

To quantify protein immunoreactivity (IR), films were scanned and densitometry was performed as described by Martin (1999). For caspase-3, pro-enzyme and the cleaved subunits were analysed separately. Protein levels were expressed as relative optical density measurements, determined by comparing the density and area (average-integrated optical density) of the immunoreactive bands from ipsilateral LGN samples to corresponding bands in contralateral control lanes in the same blot. Immunodensities for death proteins were normalized to Ponceau S-stained proteins or to synaptic protein IR within the same lanes. Two different normalization procedures were used because different subcellular fractions were analysed. Synaptic proteins were used for the normalization of soluble and pellet fractions, while Ponceau S was used for the normalization of nuclear fractions due to the low level of synaptic proteins in this fraction. The values for each time point were replicated in triplicate or quadruplicate experiments. Comparisons were made between the ipsilateral and contralateral LGN samples at the same post-lesion time point. Statistical analyses of group means and variances were performed using a one-way analysis of variance (ANOVA) followed by a *post-hoc* Newman–Keuls test for individual comparisons.

#### Caspase-3 activity assay

Caspase-3 enzyme activity was measured in LGN samples using a colorimetric assay kit (Chemicon). This assay is based on spectrophotometric detection (405 nm) of the chromophore *p*-nitroaniline after caspase-mediated cleavage from the labeled substrate Asp-Glu-Val-Asp (DEVD)-*p*-nitroaniline. Recombinant human active caspase-3 (Chemicon) was used as a positive control. Caspase-3 inhibitor (Ac-DEVD-CHO) was used as a negative control. Caspase-3 activity was measured in soluble and nuclear fractions of ipsilateral and contralateral LGN samples at 1, 4, 5 and 6 days post-lesion ( $n = 12$  rats/time point). All assays were done in duplicate at two different protein concentrations (50 and 100  $\mu\text{g}$ ). The group means and variances were evaluated by one-way ANOVA and a Newman–Keuls *post-hoc* test.

### Identification of DNA damage

Rats received unilateral occipital cortex ablations and were killed by an overdose of chloral hydrate and perfusion fixation (4% paraformaldehyde) at 1, 2, 3, 4 and 5 days post-lesion ( $n = 4$  rats/time point). The brains were removed from the skull and then cryoprotected in phosphate-buffered 20% glycerol. A peroxidase-antiperoxidase detection method was used for immunocytochemical staining of free-floating brain sections with diaminobenzidine as chromogen. Two different forms of DNA damage were evaluated. Hydroxyl radical damage to DNA was detected with monoclonal antibodies to 8-hydroxy-2-deoxyguanosine (OHdG; QED Bioscience, San Diego, CA, USA, and OXIS International, Portland, OR, USA). These antibodies to OHdG have been evaluated for specificity by multiple approaches (Al-Abdulla and Martin 1998; Martin *et al.* 1999). In competition experiments, sections were reacted with antibody to OHdG that was incubated at 4°C for 24 h with 1000-fold concentrations of OHdG, 8-hydroxyguanosine or guanosine (Martin *et al.* 1999). As additional controls, sections have been digested with DNase (5–10 mg/mL) or RNase (11–50 mg/mL) prior to incubation with OHdG antibody. A monoclonal antibody (Alexis Biochemicals, San Diego, CA, USA) to single-stranded DNA (ssDNA) was also used. The ssDNA immunodetection protocol requires pre-treatment of sections with 0.2 mg/mL saponin and 20 µg/mL proteinase K (20 min at room temperature, 23°C) and then 50% formamide (20 min at 56°C) for DNA denaturation. Staining for ssDNA has been reported to be a specific and sensitive method for the detection of apoptotic cells (Frankfurt *et al.* 1996). Immunolabeled sections were counterstained with cresyl violet. Neurons showing nuclear immunopositivity in the ipsilateral and contralateral dLGN were counted at 1000× magnification in three matched levels from each rat by an observer unaware of experimental history. Careful focusing through the z-axis was used to distinguish nuclear labeling from cytoplasmic labeling. Group means and variances were evaluated statistically by one-way ANOVA and a Newman–Keuls *post-hoc* test.

### Antioxidant gene therapy and pharmacotherapy experiments

We studied whether oxidative stress participates in the mechanisms for retrograde neuronal death in the adult rat brain by determining if antioxidant therapies are neuroprotective by blocking apoptosis. Transgenic (Tg) and pharmacological therapies were used. Unilateral occipital cortex ablations were done on Tg superoxide dismutase-1 (SOD1) mice ( $n = 16$ ) and wild-type non-Tg C57BL/6 mice ( $n = 10$ ). The Tg SOD1 mice carry a 12-kb genomic DNA fragment encoding wild-type human SOD1 (Wong *et al.* 1995). The background strain for these mice is C57BL/6J. Transgenic expression of SOD1 was confirmed by genotyping tail genomic DNA and by immunolocalization of human SOD1 using a human-specific monoclonal antibody to SOD1 (Sigma, St Louis, MO, USA). This transgene product is expressed throughout the CNS of these mice in a pattern that mimics the endogenous protein, but levels of transgene expression and SOD1 activity are seven to 10 times higher than the level of endogenous SOD1 (Wong *et al.* 1995). For pharmacotherapies, we used trolox (6-hydroxy-2,5,7,8-tetramethylchroman-2-carboxylic acid; Calbiochem, San Diego, CA, USA and Aldrich, St Louis, MO, USA) and ascorbic acid (vitamin C) as antioxidants. Trolox, a water- and lipid-soluble vitamin E derivative, is a cell-permeable free radical scavenger that can prevent radiation- and peroxynitrite (ONOO<sup>-</sup>)-induced (Salgo and Pryor 1996) apoptosis

*in vitro* and methylmercury-induced neuronal apoptosis *in vivo* (Usuki *et al.* 2001). Trolox was dissolved in ethanol/saline at a stock concentration of 50 mg/mL. Studies showing the antioxidant actions of ascorbate are numerous (Carr and Frei 1999). Ascorbate was dissolved in saline. Rats ( $n = 40$ ) were treated daily on day 0 (day of lesion) and on post-lesion days 1–5 with trolox (50 mg/kg, i.p.), ascorbic acid (50 mg/kg, i.p.) or the corresponding vehicle. Each treatment group had 10 animals. The Tg and wild-type mice and rats with test therapies were killed by perfusion fixation (4% paraformaldehyde) at 7 days post-lesion. After perfusion-fixation, brains were allowed to remain *in situ* for 1 h before they were removed from the skull. The brains were cryoprotected in 20% glycerol-phosphate-buffered saline, uniformly blocked and frozen under pulverized dry ice. Coronal serial symmetrical sections (40 µm) through the thalamus were cut using a sliding microtome. Serial sections from each mouse and rat brain were mounted on glass slides and stained with cresyl violet for neuronal counting. Neuronal counts in the ipsilateral and contralateral dLGN were determined by an operator unaware of sample experimental history at 1000× magnification using the stereological optical disector method as described (Calhoun *et al.* 1996; Al-Abdulla *et al.* 1998). Neurons without apoptotic structural changes were counted. These criteria included a round, open, pale nucleus (not condensed and stained darkly), granular Nissl staining of the cytoplasm and a major diameter of ~20–25 µm. With these criteria, astrocytes, oligodendrocytes and microglia were excluded from the counts. Neuronal counts were used to determine group means and variances and comparisons among groups were performed using a one-way ANOVA and a *post-hoc* *t*-test.

## Results

### Lateral geniculate nucleus microdissection and subcellular fractionation

The accuracy of the microdissection of the LGN tissue samples for immunoblotting and biochemical assays was confirmed (Fig. 1a). The LGN was isolated from the rat diencephalon with minimal or no contamination of other brain regions. The microdissection was precise for subdivisions within the rat LGN, as demonstrated by the exclusion of the ventral LGN (Fig. 1a).

The subcellular fractions of the dLGN tissue were evaluated for purity after homogenization and centrifugation. High levels of Cox1 IR confirmed the mitochondrial enrichment of the P2 fraction (Fig. 1b). The Cox1 levels were maintained in the mitochondria-enriched fractions of the ipsilateral dLGN for 5 days post-lesion. Soluble protein fractions were enriched in lactate dehydrogenase IR (data not shown) but were devoid of mitochondrial contamination (regardless of injury) based on the absence of Cox1 IR, even after prolonged exposures (Fig. 1b). The nuclear enrichment of the P1 fraction was verified by the high level of the neuron-specific nuclear protein NeuN (Fig. 1c). NeuN levels in the ipsilateral dLGN were maintained for 5 days post-lesion. NeuN was not detected in the S2 or P2 fractions (Fig. 1c).

### Subcellular localization of death proteins in adult dorsal lateral geniculate nucleus

The identification of an immunoreactive band of protein as Bax was demonstrated using mutant mice. This experiment was done because, in our experience, many of the antibodies to Bcl-2 family proteins, particularly those to Bax, are not monospecific. Bax IR was not detected in brain extracts of Bax<sup>-/-</sup> mice ( $n = 2$ ) compared with a strong immunoreactive band at ~20–24 kDa in forebrain extracts of wild-type mice and in rat dLGN (Fig. 2a). As the Bax gene is activated by p53 (Miyashita and Reed 1995), p53<sup>-/-</sup> mice ( $n = 2$ ) were used to show that the levels of this immunoreactive band at ~20–23 kDa were altered by the presence or absence of p53. Forebrain extracts from p53<sup>-/-</sup> mice had diminished levels of Bax compared with wild-type mice. Results with liver extracts were similar (Fig. 2a).

The relative levels of cell death proteins were evaluated in different subcellular compartments in adult rat dLGN. The Bax IR was much higher in the soluble protein compartment compared with the mitochondria-enriched membrane compartment (Fig. 2b). In mitochondrial fractions, a distinct doublet was observed corresponding to the detection of  $\alpha$ -Bax and  $\beta$ -Bax at 21 and 24 kDa, respectively. The levels of  $\alpha$ -Bax and  $\beta$ -Bax in the adult dLGN were similar (Fig. 2b). In contrast to Bax, Bak was much more enriched in the mitochondria-enriched membrane compartment compared with the soluble protein compartment (Fig. 2b). Bad was enriched in the soluble protein compartment relative to the mitochondrial compartment of the dLGN but was increased in the mitochondria-enriched compartment after injury (Fig. 2c).

### The protein expression profiles of Bax, Bak and Bad are different during the progression of neuronal apoptosis in the dorsal lateral geniculate nucleus

Bax levels were changed at early pre-apoptotic stages of neuronal death (Figs 2d and 3a). At 1 day post-lesion, the Bax level was <50% of control in the soluble protein fraction while, in marked contrast, the Bax level was >200% of control in the mitochondria-enriched membrane fraction (Fig. 3a). At 4 and 5 days post-lesion, the Bax levels in the ipsilateral dLGN did not differ significantly from control (Fig. 3a). At 6 days post-lesion, a significant reduction in Bax IR was observed in the soluble protein fraction (Fig. 3a).

Bak levels were altered later in the post-lesion time course. Bak was detected as a prominent band of IR at ~30 kDa. Bak IR in the soluble fraction of the ipsilateral dLGN was not different from control at 1 and 4 days post-lesion but, at 5 and 6 days post-lesion, the Bak level was increased significantly above control level (Fig. 3b). Bak IR in the mitochondria-enriched fraction of the ipsilateral dLGN was significantly increased above contralateral dLGN at 4 and 5 days post-lesion, but returned to control level at 6 days post-lesion (Fig. 3b).

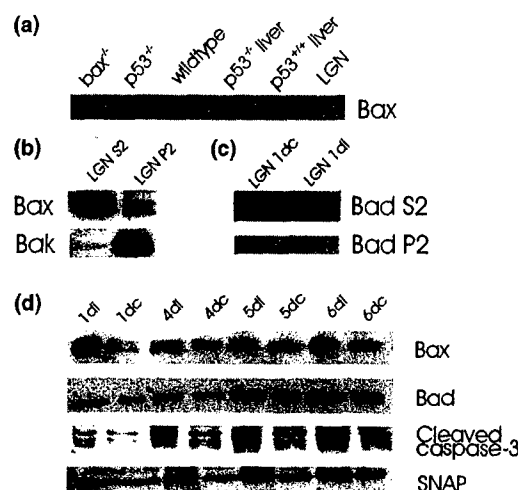


**Fig. 2** Subcellular distributions of cell death proteins. (a) Verification of an immunoreactive protein band as Bax. Soluble protein fractions from Bax-null, p53-null and wild-type mouse forebrains, p53-null and wild-type mouse livers, and rat dorsal lateral geniculate nucleus (dLGN) were subjected to sodium dodecyl sulfate–polyacrylamide gel electrophoresis (SDS-PAGE; 20  $\mu$ g total protein loaded in each lane), transferred to nitrocellulose and probed with polyclonal antibody to Bax (Upstate, Charlottesville, VA, USA). An immunoreactive band was detected at ~20–23 kDa. This band found in rat dLGN was not present in Bax<sup>-/-</sup> mouse brain and was attenuated in p53<sup>-/-</sup> liver. A similar attenuation of Bax protein was found in p53<sup>-/-</sup> liver. (b) dLGN tissues were fractionated into soluble (S2) and mitochondria-enriched pellet (P2) proteins and were subjected to SDS-PAGE (10  $\mu$ g total protein loaded in each lane), transferred to nitrocellulose membranes and immunoblotted with polyclonal antibodies to Bax (Upstate) and Bak (Upstate). Bax was more enriched in the soluble protein compartment compared with the mitochondrial compartment. Bak was more enriched in the mitochondrial compartment compared with the soluble compartment. (c) dLGN tissues were fractionated into soluble (S2) and mitochondria-enriched pellet (P2) proteins and were subjected to SDS-PAGE (10 or 20  $\mu$ g total protein loaded in each lane for S2 and P2, respectively), transferred to nitrocellulose membranes and immunoblotted with polyclonal antibodies to Bad (Transduction Laboratory, San Diego, CA, USA). Bad was more enriched in the soluble protein compartment compared with the mitochondrial compartment. Very low levels of Bad were detected in mitochondrial fractions of normal dLGN (P2, LGN 1dc) only after prolonged exposures. Bad levels were increased in the ipsilateral dLGN soluble compartment as early as 1 day post-lesion (LGN 1di). A corresponding increase in Bad was observed in the ipsilateral dLGN mitochondrial P2 compartment at 1 day post-lesion (LGN 1di). (d) Representative ipsilateral (i) and contralateral (c) dLGN immunoblots for mitochondrial Bax, soluble Bad and nuclear cleaved caspase-3 at 1, 4, 5 and 6 days (d) after occipital cortex ablation. Each lane contains protein extracts from dLGN samples pooled from 12–15 different rats/time point. The synaptic protein synapse-associated protein (SNAP)-25 was used as a normalization control for S2 and P2 blots. See Figs 3 and 4 for densitometric quantification of immunoblots.

Bad levels were changed throughout the entire post-lesion time course (Figs 2d and 3c). Bad was detected as a prominent band of IR at ~23 kDa. Cell lysates from A431

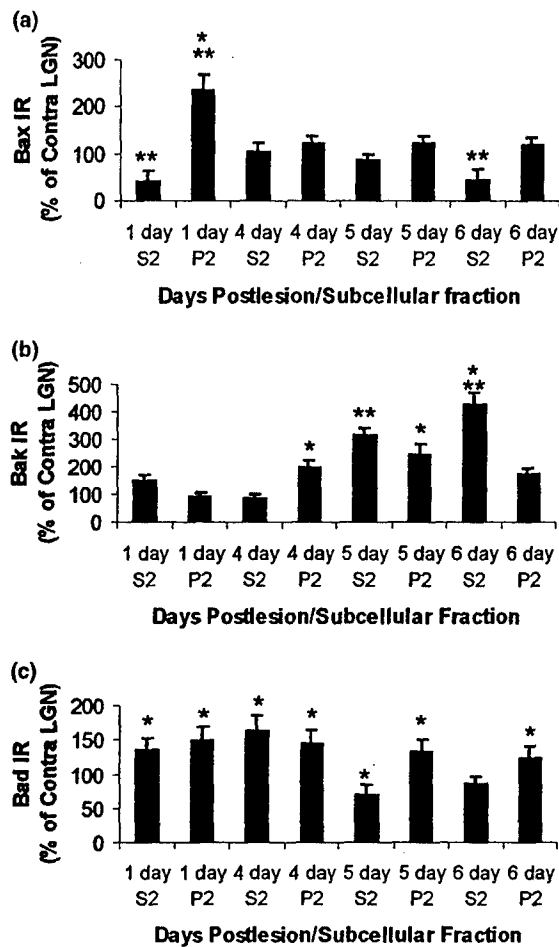


**Fig. 3** Densitometric quantification of protein immunoreactivity (IR) levels for (a) Bax, (b) Bak and (c) Bad in soluble (S2) and mitochondria-enriched (P2) protein fractions as determined by immunoblotting. The values (mean  $\pm$  SD) are represented as percentage of contralateral (contra) non-lesioned dorsal lateral geniculate nucleus (dLGN). Each bar represents data from three different groups of rat dLGN samples (4–6 rats/group) that were microdissected (see Fig. 1a) at each time point after occipital cortex ablation and were pooled for fractionation. The total number of rats represented in each bar is 12–15. The results are derived from three to four different immunoblotting experiments with each of the three different groups of dLGN samples/time point. Significance differences from control dLGN are denoted by \* $p < 0.05$  or \*\* $p < 0.01$ .

cells (human epidermoid carcinoma cell line) were used to detect an immunoreactive band of similar molecular weight (data not shown). Bad IR was increased significantly in both the soluble and membrane fractions of ipsilateral dLGN at 1 and 4 days post-lesion. At 5 day post-lesion, Bad in the soluble compartment was lower than control, while Bad in the mitochondrial compartment was significantly higher than control (Fig. 2c). At 6 days post-lesion, Bad in the mitochondrial compartment remained significantly higher than control, but Bad in the soluble compartment was not different from control (Fig. 2c).

### Caspase-3 is activated in the dorsal lateral geniculate nucleus after occipital cortex ablation

The protein levels of pro-caspase-3 and cleaved caspase-3 subunits were measured in soluble and nuclear fractions of dLGN after target deprivation (Fig. 4). Pro-caspase-3 was detected as a prominent band of IR at  $\sim 32$  kDa. The cleaved subunits were detected at  $\sim 11$  and  $\sim 17$ – $20$  kDa. At 1 day post-lesion, the levels of pro-caspase-3 and cleaved caspase-3 in soluble protein fractions of ipsilateral and contralateral dLGN were similar (Figs 4a and b). At 4 days, the level of pro-caspase-3 in the ipsilateral dLGN was not significantly different from the contralateral dLGN but cleaved caspase-3 was elevated significantly in the ipsilateral dLGN soluble compartment (Figs 4a and b). A further increase in cleaved caspase-3 subunits was observed at 5 days in the soluble compartment, while pro-caspase-3 levels decreased (Figs 4a and b). At 6 days post-lesion, cleaved caspase-3 levels in the ipsilateral dLGN remained higher than in contralateral dLGN, but pro-caspase-3 levels were not significantly different from control (Figs 4a and b). Cleaved caspase-3 was also detected in the dLGN nuclear compartment, consistent with *in vitro* studies of cortical neurons (Lesuisse and Martin 2002). Cleaved caspase-3 levels were elevated significantly in the ipsilateral dLGN nuclear compartment at 4, 5 and 6 days post-lesion, with highest levels at 6 days (Figs 2d and 4c).

The biochemical activity of caspase-3 was measured in soluble and nuclear protein fractions of dLGN after target deprivation (Fig. 5). Caspase-3 enzyme activity was increased significantly in soluble fractions in the ipsilateral dLGN at 1 day (Fig. 5a). Activity was blocked completely in the presence of  $10 \mu\text{M}$  caspase-3 inhibitor Ac-DEVD-CHO (data not shown). Caspase-3 activities in soluble fractions of the ipsilateral and contralateral dLGN were similar at 4 days (Fig. 5a). At 5 days post-lesion, caspase-3 activity was lower in the ipsilateral dLGN compared with the contralateral dLGN which showed significantly higher levels of activity compared with the contralateral dLGN at earlier time points. Caspase-3 activities in the ipsilateral and contralateral dLGN were at baseline levels in the soluble fraction at 6 days (Fig. 5a). Caspase-3 activities in ipsilateral dLGN nuclear fractions at 4 and 5 days post-lesion were increased significantly compared with control but were unchanged at other time points (Fig. 5b).

### Phosphorylated p53 accumulates in the nucleus during dorsal lateral geniculate nucleus neuron apoptosis

Phospho-p53<sup>Ser15</sup> levels were dramatically elevated in nuclear fractions of the ipsilateral LGN at 4 days post-lesion (Fig. 6). The increase remained present at 5 days post-lesion (Fig. 6). At 6 days post-lesion ipsilateral levels were not different from contralateral levels (Fig. 6). The phosphorylation of p53 at the Ser15 site was specific for the nucleus because phospho-p53<sup>Ser15</sup> was not detected in the soluble fraction.



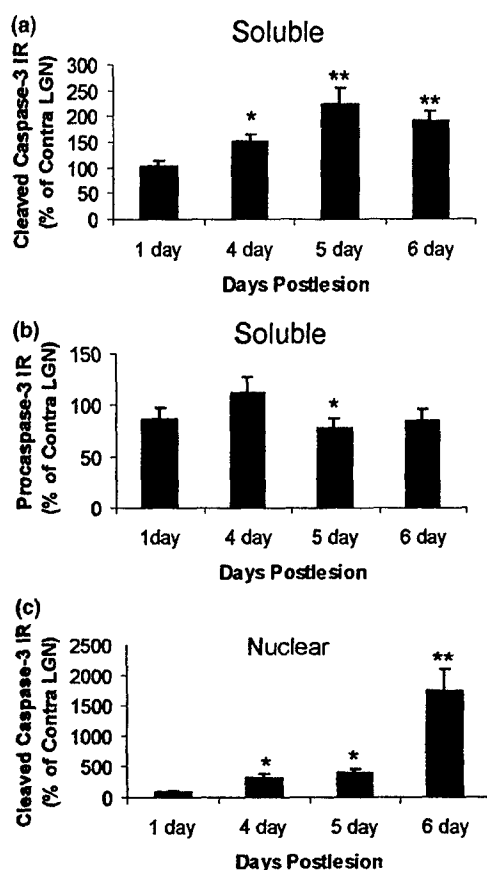


**Fig. 4** Densitometric quantification of protein immunoreactivity (IR) levels for (a) cleaved caspase-3 and (b) pro-caspase-3 in soluble protein fractions and (c) cleaved caspase-3 in nuclear fractions as determined by immunoblotting. The values (mean  $\pm$  SD) are represented as percentage of contralateral (contra) non-lesioned dorsal lateral geniculate nucleus (dLGN). Each bar represents data from three different groups of rat dLGN samples (4–6 rats/group) that were microdissected (see Fig. 1a) at each time point after occipital cortex ablation and were pooled for fractionation. The total number of rats represented in each bar is 12–15. The results are derived from three to four different immunoblotting experiments with each of the three different groups of dLGN samples/time point. Significance differences from control dLGN are denoted by \* $p < 0.05$  or \*\* $p < 0.01$ .

#### DNA damage accumulates rapidly in dorsal lateral geniculate nucleus neurons after target deprivation

As p53 was activated in the dLGN at 4 days post-lesion, LGN neurons were evaluated for DNA damage at early, pre-apoptotic, post-lesion time points (Figs 7 and 8). DNA damage was assessed with two different markers. The OHdG IR was seen in the nucleus and cytoplasm of dLGN neurons (Fig. 7). It has been shown previously that the intensity of cytoplasmic and nuclear immunolabeling detected with OHdG antibodies can be altered, respectively, by RNase and DNase pre-treatment and by pre-adsorption of antibody with 8-hydroxyguanosine and 8-hydroxy-2-deoxyguanosine, indicating hydroxyl adduct modified RNA and DNA

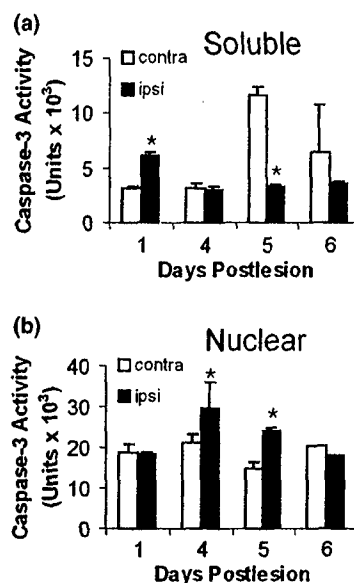


**Fig. 5** Measurement of caspase-3 enzyme activity in (a) soluble and (b) nuclear protein fractions as determined by biochemical spectrophotometric assay. The values (mean  $\pm$  SD) are represented as units of enzyme activity (determined by conversion of absorbency units using a standard curve generated from known caspase-3 units) in contralateral (contra,  $\square$ ) non-lesioned dorsal lateral geniculate nucleus (dLGN) and ipsilateral (ipsi,  $\blacksquare$ ) dLGN at 1, 4, 5 and 6 days after occipital cortex ablation. The total number of rats represented in each bar is 12–15. Significance differences from time-matched control dLGN are denoted by \* $p < 0.05$ .

(Al-Abdulla and Martin 1998; Martin *et al.* 1999). Both the overall intensity of staining in labeled neurons and the number of immunopositive neurons changed in the dLGN after target deprivation. The number of neurons with nuclear OHdG IR was increased in the ipsilateral LGN at 1–5 days post-lesion (Figs 7a and b and 8a). The increase was progressive between 1 and 3 days, peaking at 3 days, and then the number of immunopositive neurons declined. Immunostaining for ssDNA was found primarily in the nucleus, with much fainter cytoplasmic labeling (Figs 7c and d). The number of neurons with ssDNA was also increased in the ipsilateral LGN (Figs 7c and d and 8b). The ssDNA-positive neurons were higher than control at 1–4 days post-lesion. A maximal level was found at 4 days post-lesion (Fig. 8b), corresponding to the spike in p53 phosphorylation (Fig. 6). The accumulation of ssDNA was transient because, at 5 days post-lesion, the number of ssDNA-positive neurons was not different from control (Fig. 8b).

#### Transgenic antioxidant therapy protects dorsal lateral geniculate nucleus neurons after target deprivation

Transgenic and pharmacological antioxidant therapies were used to study whether oxidative stress participates in the mechanisms of LGN neuron apoptosis in the adult brain. Transgenic mice overexpressing normal human SOD1

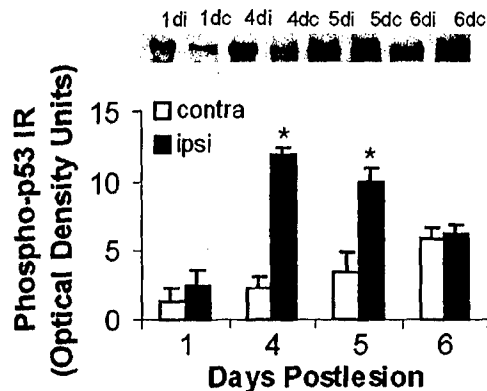


**Fig. 6** Measurement of phosphoSer15-p53 immunoreactivity (IR) in dorsal lateral geniculate nucleus (dLGN) nuclear fractions. The dLGN tissues were fractionated into nuclei-enriched fractions and were subjected to sodium dodecyl sulfate–polyacrylamide gel electrophoresis (20  $\mu$ g total protein loaded in each lane), transferred to nitrocellulose membranes and immunoblotted with antibody to phosphoSer15-p53 (Cell Signaling Technology, Beverly, MA, USA). An immunoblot of ipsilateral (i) and contralateral (c) dLGN nuclear protein at 1, 4, 5 and 6 days post-lesion is shown. The quantitative densitometric measurements of several different blots are shown in the histogram. The values (mean  $\pm$  SD) are represented as average-integrated optical density units in the contralateral (contra,  $\square$ ) non-lesioned dLGN and the ipsilateral (ipsi,  $\blacksquare$ ) target deprived dLGN. Each bar represents data from three different groups of rat dLGN samples (4–6 rats/group) that were microdissected at each time point after occipital cortex ablation and were pooled for fractionation. The total number of rats represented in each bar is 12–15. The results are derived from four different immunoblotting experiments with each of the three different groups of dLGN samples/time point. Significance differences from control dLGN are denoted by \* $p < 0.001$ .

showed a significant attenuation in the neuronal loss at 7 days post-lesion compared with wild-type mice (Fig. 9a). In contrast, neither trolox (Fig. 9b) nor ascorbate (Fig. 9c) showed any efficacy in preventing neuronal loss in the dLGN after target deprivation.

## Discussion

Occipital cortex ablation results in degeneration of geniculocortical projection neurons within the dLGN by apoptosis (Al-Abdulla *et al.* 1998; Martin *et al.* 2001; Natale *et al.* 2002). This system is an excellent model to study induced neuronal apoptosis in the adult and newborn CNS. The structural emergence of this apoptosis and its time course are very synchronous and the process is accelerated in the immature brain. In the adult brain the cell death process is nearly complete by 14 days post-lesion, with the bulk of the geniculocortical neuronal apoptosis occurring during the first 7 days post-lesion. In the newborn brain the apoptotic process takes 2 days. Structurally, this neuronal cell death is characterized by progressive cytoplasmic and nuclear

condensation that is typical of unequivocal apoptosis (Al-Abdulla and Martin 1998; Al-Abdulla *et al.* 1998; Martin *et al.* 1998; Natale *et al.* 2002). The dependence of this cell death on Bax and its regulation by p53 support the conclusion that this geniculocortical projection neuron death is a form of apoptosis (Martin *et al.* 2001). However, the precise mechanisms of this neuron-specific apoptosis need to be further understood.

We first needed to overcome some technical hurdles inherent to *in vivo* models of neurodegeneration that could confound interpretation of the results, namely those related to tissue sampling and processing. The occipital cortex ablation lesion induces apoptosis of neurons within only a relatively small area of brain. Therefore, LGN samples were specifically microdissected to avoid regional contamination. Our precision was better than originally anticipated because the microdissection was selective for subdivisions of the LGN, specifically the dLGN. This anatomical precision is important because the neuronal apoptosis occurs in the dLGN rather than in the ventral LGN that does not have major efferents to cortex (Sefton and Dreher 1985). However, non-neuronal cell contamination is still present in the dLGN samples, but we have not observed apoptosis of glial cells or blood-derived cells in this model in adult animals (Al-Abdulla *et al.* 1998; Martin *et al.* 2001; Al-Abdulla and Martin 2002). We performed a subcellular fractionation analysis because the locations of these cell death proteins contribute to their functional activity. Specific protein markers were used to assess the purity of the fractions. The mitochondrial enrichment of the subcellular fraction was shown by the presence of Cox1. The soluble cytosolic protein compartment was verified by the presence of lactate dehydrogenase. The nuclear enrichment was demonstrated by the presence of NeuN. There was no cross-contamination among these fractions. However, the mitochondria-enriched fraction is likely to contain endoplasmic reticulum and microsome components.

Cells within the dLGN expressed Bax, Bak, Bad and caspase-3 at high levels. These proteins had differential subcellular localizations. Our results on the subcellular distributions of Bax, Bak and Bad in healthy adult rodent CNS tissue are consistent with *in vitro* studies of non-neuronal cells (Wolter *et al.* 1997; Nechushtan *et al.* 2001). Bax and Bad reside primarily in the cytosol, whereas Bak resides primarily in mitochondria. Caspase-3 was found in the soluble protein compartment, as expected, and we showed a novel localization of cleaved caspase-3 with enzymatic activity in the nuclear compartment of nervous tissue.

We further studied the molecular regulation of target deprivation-induced neuronal apoptosis by profiling cell death proteins during the evolution of thalamic neuron apoptosis. Cell death effector proteins are known to undergo changes in their subcellular distributions during apoptosis



**Fig. 7** Identification of DNA damage in dorsal lateral geniculate nucleus (dLGN) neurons after occipital cortex ablation. Brain sections were reacted with monoclonal antibodies to (a and b) 8-hydroxy-2-deoxyguanosine (OHdG) and (c and d) single-stranded DNA (ssDNA) with sites of antibody binding visualized by immunoperoxidase and diaminobenzidine (brown reaction product). Sections exposed to the same antibody were processed using identical conditions and were counterstained with cresyl violet. These examples are from animals at 2 days (OHdG) or 4 days (ssDNA) post-lesion. The OHdG immunoreactivity (IR) in neurons (arrowheads) in the contralateral dLGN (a) was much lower compared with the ipsilateral dLGN (b). Subsets of neurons (see Fig. 8a for quantification) in the ipsilateral dLGN had

intense cytoplasmic and nuclear OHdG IR (b, arrowheads), whereas neurons in the contralateral dLGN had mostly faint cytoplasmic OHdG IR (a, arrowheads). The ssDNA IR in neurons (arrowheads) in the contralateral dLGN (c) was very faint compared with the ipsilateral dLGN (d). In ssDNA preparations, there was some loss of neuropil integrity due to the required DNA denaturation with heat and formaldehyde. Subsets of neurons (see Fig. 8b for quantification) in the ipsilateral dLGN had strong nuclear ssDNA IR (d, arrowheads) whereas neurons in the contralateral dLGN had barely detectable to no staining (c, arrowheads). Scale bar (shown in d) = 25  $\mu$ m (for a and b) and 40  $\mu$ m (for c and d).

leading to multimerization, membrane integration, cytochrome *c* release from mitochondria and caspase activation (Wei *et al.* 2001). We found by immunoblotting that the synchronized apoptosis of dLGN projection neurons occurs in association with differential subcellular changes in pro-apoptotic molecules. Within 1 day of target deprivation, Bax increased in the mitochondria-enriched fraction of dLGN. Bak increased later. Few studies have demonstrated such a rapid (within 1 day) redistribution of Bax during apoptosis of neurons or of cells in general. During excitotoxic neuronal apoptosis, Bax undergoes a subcellular redistribution within 2 h of glutamate receptor activation (Lok and Martin 2002). Very few studies have addressed the role of Bak in neuronal apoptosis. The increased expression of Bak during dLGN neuron apoptosis *in vivo* is a new finding. An *in vitro* study of neonatal peripheral nervous system neurons deprived of nerve growth factor failed to reveal a change in Bak during apoptosis (Putcha *et al.* 2002). However, experiments on non-neuronal cells suggest that Bax and Bak are essentially interchangeable (Wei *et al.* 2001). We found that both Bax and Bak showed an increased expression and subcellular redistribution during target deprivation-induced neuronal

apoptosis within the CNS but, interestingly, the timing of the changes was different for these two pro-apoptotic molecules. Our results on apoptosis of CNS neurons show that Bax is a rapid-response protein whereas Bak is a delayed-response protein. Our results suggest that there may be coordinated hierarchical or independent functions for Bax and Bak during neuronal apoptosis. The idea of a coordinated participation of these two molecules is supported by the finding that Bax translocates to mitochondria and then coalesces with Bak into mitochondria-associated clusters during apoptosis in non-neuronal cells (Nechushtan *et al.* 2001). Bak may, therefore, be involved in reinforcing the cell death process after Bax engages the process in CNS neurons.

Neurons are dependent on target- or afferent-derived neurotrophic factors for survival. Withdrawal of neurotrophins results in neuronal apoptosis. Some neurotrophins possess antiapoptotic activity by interacting with membrane tyrosine kinase receptors linked to phosphoinositide-3 kinase (PI-3 kinase) (Franke *et al.* 1997). Activation of PI-3 kinase leads to activation of protein kinase B (PKB/Akt) by phosphorylation. Active Akt phosphorylates Bad at Ser136 (del Peso *et al.* 1997) causing phospho-Bad to disassociate from Bcl-2

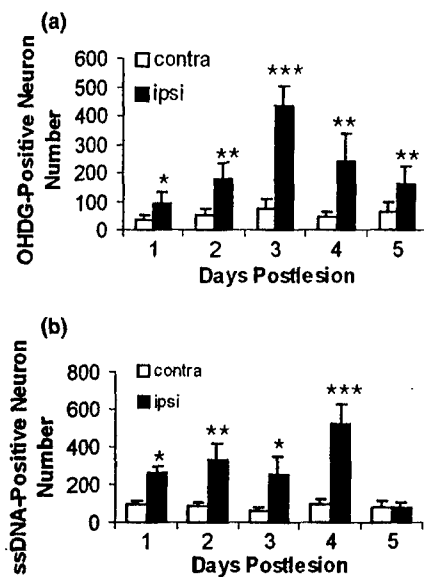


**Fig. 8** Counts of the numbers of neurons with DNA damage in the dorsal lateral geniculate nucleus (dLGN) after occipital cortex ablation. Immunocytochemistry was used to detect (a) 8-hydroxy-2-deoxyguanosine (OHdG) and (b) single-stranded DNA (ssDNA) lesions in neurons in the ipsilateral (ipsi, ■) and contralateral (contra, □) dLGN at 1, 2, 3, 4 and 5 days post-lesion ( $n = 4$  rats/time point). Cells with only nuclear immunoreactivity were counted. The number is immunopositive neurons/mm<sup>2</sup>. The values are mean  $\pm$  SD. Significance differences from control dLGN (contra) are denoted by \* $p < 0.05$ , \*\* $p < 0.01$  or \*\*\* $p < 0.001$ .

or Bcl-X<sub>L</sub> within mitochondrial membranes and to translocate to the cytosol where it is sequestered by protein 14-3-3. This process allows Bcl-2 and Bcl-X<sub>L</sub> to exert their antiapoptotic function(s). Until now we have assumed that occipital cortex ablation induces an *in vivo* state of target deprivation and neurotrophin withdrawal of dLGN neurons but, other than the apoptosis of these neurons, evidence to support this assumption has not been forthcoming. The finding that Bad undergoes an early sustained increase in the dLGN, particularly in the mitochondria-enriched fraction, suggests that its phosphorylation and cytosolic sequestration by 14-3-3 are diminished, supporting the proposition that this CNS lesion is an *in vivo* model of neurotrophin withdrawal-induced neuronal apoptosis.

Because we used a homogenate-based assay of dLGN tissue, we currently assume that the changes in cell death proteins occur in apoptotic corticopetal projection neurons. Neurons are the primary cells that undergo apoptosis in this model as shown directly by electron microscopy (EM) (Al-Abdulla and Martin 1998; Al-Abdulla *et al.* 1998). Although immunoblot analysis of subcellular fractions is commonly used to assay for translocation of proteins, the increase in Bax, Bak and Bad in mitochondria of neurons needs to be shown directly in future studies by quantitative immunogold EM (Martin and Liu 2002a). These

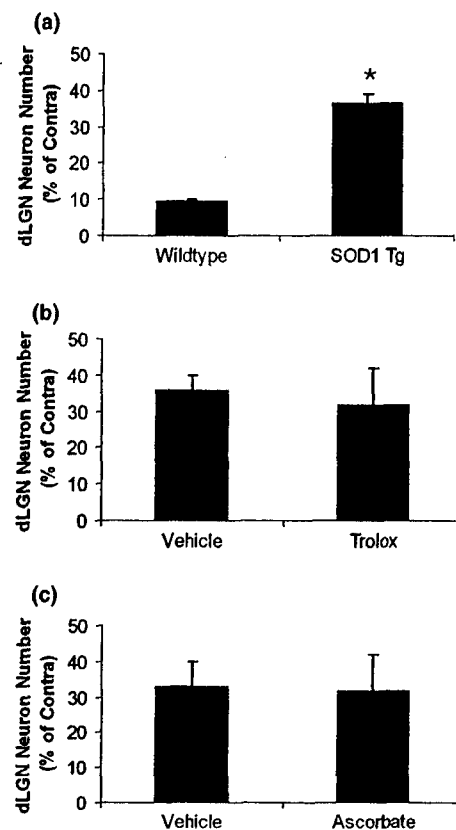


**Fig. 9** Counts of the number of neurons remaining in the dorsal lateral geniculate nucleus (dLGN) at 7 days after occipital cortex ablation in mice with (a) transgenic (Tg) antioxidant enzyme therapy and in rats with pharmacotreatments with (b) trolox or (c) ascorbate. The neuronal number is represented as the mean  $\pm$  SD of the percentage of contralateral (contra) control dLGN neuron number as determined using stereology. Tg mice overexpressing normal human SOD1 were significantly (\* $p < 0.01$ ) protected against the neuronal apoptosis induced by target deprivation compared with wild-type control mice (a). Neither trolox [50 mg/kg, i.p. (b)] nor ascorbate [50 mg/kg, i.p. (c)] for 7 days after the lesion protected against the neuronal apoptosis compared with their respective vehicle controls.

immunolocalization experiments will require the identification of monospecific antibodies that can be used appropriately for immunocytochemistry.

Our results on caspase-3 demonstrate that neuronal apoptosis in this adult *in vivo* CNS model is associated with caspase-3 pro-enzyme cleavage and increased caspase-3 enzyme activity. Cleaved caspase-3 accumulates in different types of neurons destined to undergo apoptosis in several model systems, including dLGN neurons after target deprivation in immature mouse brain (Natale *et al.* 2002), excitotoxically injured striatal neurons in immature rat brain (Lok and Martin 2002) and cortical neurons with DNA damage *in vitro* (Lesuisse and Martin 2002). These results indirectly support the conclusion that dLGN neuron apoptosis induced by target deprivation is caspase dependent.

This interpretation is not novel or surprising when considering that activation of caspase-3 is a major downstream event in several forms of apoptosis (Kuida *et al.* 1996). Work on neuronal apoptosis in another adult *in vivo* CNS model (e.g. retinal ganglion cell axotomy) has revealed caspase dependence by pharmacological inhibition of caspase-3 (Kermer *et al.* 1998). Nevertheless, we provide some new information on an unsuspected early phase caspase-3 activation and a later phase nuclear translocation of biochemically active caspase-3. Moreover, the presence of cleaved caspase-3 may not be equivalent to the presence of biochemically active caspase-3. It is interesting that the increased activity seen at 1 day post-lesion in the soluble fraction did not appear to require additional formation of cleaved subunits. In addition, the massive increase in cleaved caspase-3 in nuclear fractions at 6 days post-lesion did not have a corresponding increase in activity. Our previous *in vitro* data suggest that apoptosis of cortical neurons can involve caspase-3 changes without additional cleavage after an apoptotic stimulus (Lesuisse and Martin 2002). It is possible that the early events of apoptosis of mature neurons can be engaged without the formation of additional caspase-3 subunits via proteolysis of pro-enzyme and that pre-existing low levels of cleaved caspase-3 can play a role, along with other proteins such as Bax, in initiating the death process. Many proteins appear to interact with cleaved caspase-3, as shown by cross-linking experiments, and constitutively cleaved caspase-3 might be regulated by interacting proteins (Lesuisse and Martin 2002). In healthy normal cells, cleaved caspase-3 might interact with possible endogenous inhibitor proteins or the subunits may be folded or assembled as inactive enzyme. In this state, constitutive cleaved caspase-3 would be inactive enzymatically and could not execute the apoptotic process. Thus, a rapid increase in caspase-3 activity in mature neurons might occur by mechanisms other than proteolytic cleavage of pro-enzyme, while later events in the apoptotic process, possibly occurring in the nucleus such as activation of DNA fragmentation pathways, appear to require recruitment of additional subunits by proteolysis. However, at near endstage apoptosis cleaved caspase-3 appears to lose its biochemical activity as suggested by our results at 6 days. This result is consistent with the accumulation of cleaved caspase-3 in cellular fragments and apoptotic debris of cortical neurons *in vitro* (Lesuisse and Martin 2002) as well as striatal neurons (Lok and Martin 2002) and dLGN neurons (Natale *et al.* 2002) *in vivo*. Cleaved caspase-3 has been found in the nucleus of non-neuronal cells (Jurkat cells) undergoing apoptosis (Zhivotovsky *et al.* 1999). The functions of caspase-3 in nervous tissue may be even more complicated than previously realized, as suggested by the transient increase in caspase-3 activity in the non-lesioned dLGN at 5 days post-lesion, where no loss of neurons occurs but astroglial activation and induction of p53 in astrocytes has been observed (Martin *et al.* 2001). By immunoelectron

microscopy we have found cleaved caspase-3 at synaptic sites in the adult brain (unpublished observations). In this regard, caspase-3 may function in synaptic plasticity and regeneration rather than cell death.

DNA damage may be an upstream trigger for dLGN neuron degeneration. We show that dLGN neurons acquire two forms of DNA damage at early pre-apoptotic stages. This genotoxicity was observed as OHdG-DNA lesions and ssDNA lesions. These lesions may be caused by oxidative stress. Several reactive oxygen species (ROS), including  $H_2O_2$ , hydroxyl radical and  $ONOO^-$ , induce DNA damage (Aust and Eveleigh 1999).  $ONOO^-$  is the product of the reaction between nitric oxide and superoxide anion (Beckman 1990) which, by themselves, are not aggressively toxic to DNA. We have found that the neuronal genome is particularly sensitive to  $ONOO^-$ , with this ROS inducing abasic sites, single- and double-strand breaks (Martin and Liu 2002b).  $ONOO^-$  can also cause OHdG lesions through the formation of hydroxyl radical-like intermediates (Coddington *et al.* 1998). It is not yet clear if OHdG-DNA lesions and ssDNA lesions in dLGN neurons are related, because OH-DNA adducts can lead to abasic sites that are converted subsequently to DNA single-strand breaks (Kohn 1991).

We evaluated whether oxidative stress participates in the mechanisms of dLGN neuron apoptosis by determining if antioxidant strategies are neuroprotective in our model. Transgenic overexpression of SOD1 provided significant protection against the apoptosis; however, treatment with trolox and ascorbate were ineffective. The SOD1 overexpression can also block apoptosis of sympathetic ganglion neurons induced by nerve growth factor withdrawal *in vitro* (Greenlund *et al.* 1995). The only known function of SOD1 is catalyzing the dismutation of superoxide anion into  $O_2$  and  $H_2O_2$  (McCord and Fridovich 1969). Our results directly implicate superoxide, or its derivative  $ONOO^-$ , in the trigger for neuronal apoptosis *in vivo*. We do not yet know whether the protection afforded by enforced SOD1 expression is due to increased SOD1 after target deprivation/axotomy or if the neurons in these animals are intrinsically more resistant to injury due to brain changes that have occurred during their lifetime. We hypothesize that the mechanism of SOD1 neuroprotection in dLGN neurons is through potentiated SOD1 induction early after the injury and attenuation of DNA strand breakage and p53 activation. Previous work on the benefits of antioxidant pharmacotherapy in protecting against target deprivation/axotomy-induced neuronal apoptosis is scant and existing studies have employed entirely different model systems from that used here. In an adult rat model of retinal ganglion cell death induced by optic nerve transection, systemic treatment with the unspecific free radical scavenger *N*-tert-butyl-(2-sulphophenyl)-nitron did not protect the neurons (Klöcker *et al.* 1998). However, *N*-tert-butyl-(2-sulphophenyl)-nitron was neuroprotective in an embryonic chick model of retinal ganglion cell axotomy

when the drug was delivered by intraocular injection (Castagné *et al.* 1999). A problem with our study and other studies in rat using systemic treatment is the uncertainty regarding the bioavailability of the antioxidant drug to the damaged neurons. It is possible that the lack of effects with trolox and ascorbate is due to inadequate blood–brain barrier penetration and insufficient brain concentrations, but previous studies using other brain damage models have shown neuroprotective actions at concentrations lower than used here (Usuki *et al.* 2001). As revealed by a study on axotomized ganglion cells in chick embryos (Castagné *et al.* 1999), there may be an optimal dose range for antioxidant neuroprotection in adult rat brain that we missed. Alternatively, unlike enforced expression SOD1, trolox and ascorbate may not have sufficient targeting to specific ROS such as superoxide or ONOO<sup>-</sup>.

Cells that have sustained DNA damage from ROS and other genotoxic agents undergo apoptosis by engaging molecular cascades involving expression or activation of p53, Bcl-2 family members and caspases (Polyak *et al.* 1997). p53 regulates target-deprivation-induced neuronal apoptosis in the dLGN because p53<sup>-/-</sup> mice show less neuronal loss than p53<sup>+/+</sup> mice (Martin *et al.* 2001). A critical question that remains to be elucidated is how DNA damage is communicated to p53 so that it becomes activated and functional in neurons. Ser392-phosphorylated p53 accumulates in dLGN neurons during their degeneration and this p53 has enhanced DNA-binding activity (Martin *et al.* 2001). We now show a massive accumulation of Ser15-phosphorylated p53 in the dLGN during apoptosis. This accumulation was maximal at 4 days after injury, at a time when ssDNA-positive neurons were most numerous; ssDNA is a potent activator of p53 (Jayaraman and Prives 1995). Specific protein kinases transduce the DNA damage signal to p53 by serine phosphorylation. DNA-dependent protein kinase (DNA-PK) and ataxia telangiectasia protein, members of the PI-3 kinase family, phosphorylate p53 at Ser15 and Ser20 (Nakagawa *et al.* 1999; Shangary *et al.* 2000). Casein kinase II phosphorylates p53 at Ser392 (Milne *et al.* 1992). Phosphorylation regulates the interactions of p53 monomers. p53 can form homotetramers and must be in tetrameric form for sequence-specific DNA binding and transcriptional activation (Kohn 1999). Tetramerization is stimulated by phosphorylation of Ser392. This phosphorylation increases 10-fold the association constant for tetramer formation. In non-neuronal cells, DNA-double-strand breaks (DSB) are recognized and bound by the heterodimeric regulatory subunits of DNA-PK (Ku70/80), thereby recruiting the catalytic DNA-PK that phosphorylates p53. In *in vitro* systems, DNA-PK-mediated phosphorylation of p53 at Ser15 alleviates the inhibition by murine double minute-2 and correlates with the stabilization of p53 and its activation as a transcription factor (Shieh *et al.* 1997; Shangary *et al.* 2000). Ataxia telangiectasia protein is required for the phosphory-

lation of p53 at Ser15 and Ser20. *In vitro* studies have shown that DNA-DSB result in Ser15 phosphorylation of p53 and stabilization through a process mediated by ataxia telangiectasia protein (Shangary *et al.* 2000). The transcriptional activity of p53 enhances the expression of Bax and Bak (Pohl *et al.* 1999; Kannan *et al.* 2001). The elevated levels of Bak in the dLGN at 4 days and thereafter could be the result of p53 activation and this mechanism could enforce the apoptotic process initially engaged by a rapid subcellular redistribution of Bax.

This study delineates for the first time the activation of cell death effector mechanisms during target deprivation-induced neuronal death in adult brain that is structurally verified as primarily apoptosis. Pro-apoptotic proteins undergo early and delayed changes in their subcellular distributions during the progression of neuronal apoptosis in adult rat brain. The initiation of this death cascade appears to occur relatively fast, within 1 day of target deprivation. This neuronal apoptosis appears to be mediated by overlapping and sequential signaling pathways with DNA damage generated by superoxide derivatives as an upstream mechanism for p53-regulated, Bax-dependent apoptosis of target-deprived neurons.

### Acknowledgements

This work was supported by grants from the U.S. Public Health Service, National Institutes of Health, National Institute of Neurological Disorders and Stroke (NS34100) and National Institute on Aging (AG16282) and the Department of Defense, U.S. Army Medical Research and Materiel Command (DAMD17-99-1-9553).

### References

- Al-Abdulla N. A. and Martin L. J. (1998) Apoptosis of retrogradely degenerating neurons occurs in association with the accumulation of perikaryal mitochondria and oxidative damage to the nucleus. *Am. J. Pathol.* **153**, 447–456.
- Al-Abdulla N. A. and Martin L. J. (2002) Projection neuron and interneurons in the lateral geniculate nucleus undergo distinct forms of degeneration ranging from retrograde and transynaptic apoptosis to transient atrophy after cortical ablation. *Neuroscience* **115**, 7–14.
- Al-Abdulla N. A., Portera-Cailliau C. and Martin L. J. (1998) Occipital cortex ablation in adult rat causes retrograde neuronal death in the lateral geniculate nucleus that resembles apoptosis. *Neuroscience* **86**, 191–209.
- Anderson A. J., Su J. H. and Cotman C. W. (1996) DNA damage and apoptosis in Alzheimer's disease: Colocalization with c-jun immunoreactivity, relationship to brain area, and effect of postmortem delay. *J. Neurosci.* **16**, 1710–1719.
- Aust A. E. and Eveleigh J. F. (1999) Mechanisms of DNA oxidation. *Proc. Soc. Exp. Biol. Med.* **222**, 246–252.
- Barron K. D., Doolin P. F. and Oldershaw J. B. (1967) Ultrastructural observations on retrograde atrophy of lateral geniculate body. 1. Neuronal alterations. *J. Neuropath. Exp. Neurol.* **26**, 300–326.
- Beckman J. S. (1990) Ischaemic injury mediator. *Nature* **345**, 27–28.
- Burke R. E. and Kholodilov N. G. (1998) Programmed cell death: does it play a role in Parkinson's disease? *Ann. Neurol.* **44**, S1126–S1133.

- Calhoun M. E., Jucker M., Martin L. J., Thinakaran G., Price D. L. and Mouton P. R. (1996) Comparative evaluation of synaptophysin-based methods for quantification of synapses. *J. Neurocytol.* **25**, 821–828.
- Carr A. and Frei B. (1999) Does vitamin C act as a pro-oxidant under physiological conditions? *FASEB J.* **13**, 1007–1024.
- Castagné V., Lefèvre K., Natero R., Becker D. A. and Clarke P. G. H. (1999) An optimal redox status for the survival of axotomized ganglion cells in the developing retina. *Neuroscience* **93**, 313–320.
- Coddington J. W., Hurst J. K. and Lymar S. V. (1998) Hydroxyl radical formation during peroxynitrous acid decomposition. *J. Am. Chem. Soc.* **121**, 2438–2443.
- Conti A. C., Raghupathi R., Trojanowski J. Q. and McIntosh T. K. (1998) Experimental brain injury induces regionally distinct apoptosis during the acute and delayed post-traumatic period. *J. Neurosci.* **18**, 5663–5672.
- Deckwerth T. L., Elliott J. L., Knudson C. M., Johnson E. M. Jr, Snider W. D. and Korsmeyer S. J. (1996) Bax is required for neuronal death after trophic factor deprivation and during development. *Neuron* **17**, 401–411.
- Franke T. F., Kaplan D. R. and Cantley L. C. (1997) PI3K: downstream AKT ion blocks apoptosis. *Cell* **88**, 435–437.
- Frankfurt O. S., Robb J. A., Sugarbaker E. V. and Villa L. (1996) Monoclonal antibody to single-stranded DNA is a specific and sensitive cellular marker for apoptosis. *Exp. Cell Res.* **226**, 387–397.
- Giolli R. A. and Guthrie M. D. (1971) Organization of subcortical projections of visual areas I and II in the rabbit. An experimental degeneration study. *J. Comp. Neurol.* **142**, 351–376.
- Greenlund L. J. S., Deckwerth T. L. and Johnson E. M. Jr (1995) Superoxide dismutase delays neuronal apoptosis: a role for reactive oxygen species in programmed neuronal death. *Neuron* **14**, 303–315.
- Jayaraman L. and Prives C. (1995) Activation of p53 sequence-specific DNA binding by short single strands of DNA requires the p53 C-terminus. *Cell* **81**, 1021–1029.
- Kannan K., Amariglio N., Rechavi G., Jakob-Hirsch J., Kela I., Kaminski N., Getz G., Domany E. and Givol D. (2001) DNA microarrays identification of primary and secondary target genes regulated by p53. *Oncogene* **20**, 2225–2234.
- Kermer P., Klöcker N., Labes M. and Bähr M. (1998) Inhibition of CPP32-like proteases rescues axotomized retinal ganglion cells from secondary cell death in vivo. *J. Neurosci.* **18**, 465–4662.
- Kitamura Y., Taniguchi T. and Shimohama S. (1999) Apoptotic cell death in neurons and glial cells: implications for Alzheimer's disease. *Jpn J. Pharmacol.* **79**, 1–5.
- Klöcker N., Cellerino A. and Bähr M. (1998) Free radical scavenging and inhibition of nitric oxide synthase potentiates the neurotrophic effects of brain-derived neurotrophic factor on axotomized retinal ganglion cells in vivo. *J. Neurosci.* **18**, 1038–1046.
- Kohn K. W. (1991) Principles and practice of DNA filter elution. *Pharmac. Ther.* **49**, 55–77.
- Kohn K. W. (1999) Molecular interaction map of the mammalian cell cycle control and DNA repair systems. *Mol. Biol. Cell* **10**, 2703–2734.
- Kuida K., Zheng T. S., Na S., Kuan C.-Y., Yang D., Karasuyama H., Rakic P. and Flavell R. A. (1996) Decreased apoptosis in the brain and premature lethality in CPP32-deficient mice. *Nature* **384**, 368–372.
- Lashley K. S. (1941) Thalamo-cortical connections of the rats brain. *J. Comp. Neurol.* **75**, 67–121.
- Lesuisse C. and Martin L. J. (2002) Immature and mature cortical neurons engage different apoptotic mechanisms involving caspase-3 and the mitogen-activated protein kinase pathway. *J. Cereb. Blood Flow Metab.* **22**, 935–950.
- Liu X. Z., Xu X. M., Du Hu R. C. *et al.* (1997) Neuronal and glial apoptosis after traumatic spinal cord injury. *J. Neurosci.* **17**, 5395–5406.
- Lok J. and Martin L. J. (2002) Rapid subcellular redistribution of bax precedes caspase-3 and endonuclease activation during excitotoxic neuronal apoptosis. *J. Neurotrauma* **19**, 815–828.
- MacManus J. P. and Linnik M. D. (1997) Gene expression induced by cerebral ischemia: an apoptotic perspective. *J. Cereb. Blood Flow Metab.* **17**, 815–832.
- Martin L. J. (1999) Neuronal death in amyotrophic lateral sclerosis is apoptosis: possible contribution of a programmed cell death mechanism. *J. Neuropathol. Exp. Neurol.* **58**, 459–471.
- Martin L. J. (2000) p53 is abnormally elevated and active in the CNS of patients with amyotrophic lateral sclerosis. *Neurobiol. Dis.* **7**, 613–622.
- Martin L. J. and Liu Z. (2002a) Injury-induced spinal motor neuron apoptosis is preceded by DNA single-strand breaks and is p53- and bax-dependent. *J. Neurobiol.* **5**, 181–197.
- Martin L. J. and Liu Z. (2002b) DNA damage profiling in motor neurons: a single-cell analysis by comet assay. *Neurochem. Res.* **27**, 1089–1100.
- Martin L. J., Al-Abdulla N. A., Brambrink A. M., Kirsch J. R., Sieber F. E. and Portera-Cailliau C. (1998) Neurodegeneration in excitotoxicity, global cerebral ischemia, and target deprivation: a perspective on the contributions of apoptosis and necrosis. *Brain Res. Bull.* **46**, 281–309.
- Martin L. J., Kaiser A. and Price A. C. (1999) Motor neuron degeneration after sciatic nerve avulsion in adult rat evolves with oxidative stress and is apoptosis. *J. Neurobiol.* **40**, 185–201.
- Martin L. J., Kaiser A., Yu J. W., Natale J. E. and Al-Abdulla N. A. (2001) Injury-induced apoptosis of neurons in adult brain is mediated by p53-dependent and p53-independent pathways and requires bax. *J. Comp. Neurol.* **433**, 299–311.
- Mattson M. P., Duan W., Chan S. L. and Camandola S. (1999) Par-4. An emerging pivotal player in neuronal apoptosis and neurodegenerative disorders. *J. Mol. Neurosci.* **13**, 17–30.
- McCord J. M. and Fridovich I. (1969) Superoxide dismutase, an enzymic function for erythrocyte hemocuprein. *J. Biol. Chem.* **244**, 6049–6055.
- Miller T. M., Moulder K. L., Knudson C. M., Creedon D. J., Deshmukh M., Korsmeyer S. J. and Johnson E. M. Jr (1997) Bax deletion further orders the cell death pathway in cerebellar granule cells and suggests a caspase-independent pathway to cell death. *J. Cell Biol.* **139**, 205–217.
- Milne D. M., Palmer R. H. and Meek D. W. (1992) Mutation of the casein kinase II phosphorylation site abolishes the anti-proliferative activity of p53. *Nucl. Acids Res.* **20**, 5565–5570.
- Miyashita T. and Reed J. C. (1995) Tumor suppressor p53 is a direct transcriptional activator of the human bax gene. *Cell* **80**, 293–299.
- Nakagawa K., Taya Y., Tamai K. and Yamaizumi M. (1999) Requirement of ATM in phosphorylation of the human p53 protein at serine 15 following DNA double-strand breaks. *Mol. Cell Biol.* **19**, 2828–2834.
- Natale J. E., Cheng Y. and Martin L. J. (2002) Thalamic neuron apoptosis emerges rapidly after cortical damage in immature mice. *Neuroscience* **112**, 665–676.
- Nechushtan A., Smith C. L., Lamensdorf I., Yoon S.-H. and Youle R. J. (2001) Bax and Bak coalesce into novel mitochondria-associated clusters during apoptosis. *J. Cell Biol.* **153**, 1265–1276.
- del Peso L., González-García M., Page C., Herrera R. and Nufiez G. (1997) Interleukin-3-induced phosphorylation of Bad through the protein kinase Akt. *Science* **278**, 687–689.
- Pohl U., Wagenknecht B., Naumann U. and Weller M. (1999) p53 enhances Bak and CD95 expression in human malignant glioma cells but does not enhance CD95L-induced apoptosis. *Cell Physiol. Biochem.* **9**, 29–37.

- Polyak K., Xia Y., Zweier J. L., Kinzler K. W. and Vogelstein B. (1997) A model for p53-induced apoptosis. *Nature* **389**, 300–305.
- Putcha G. V., Moulder K. L., Golden J. P., Bouillet P., Adams J. A., Strasser A. and Johnson E. M. Jr (2001) Induction of Bim, a proapoptotic BH3-only Bcl-2 family member, is critical for neuronal apoptosis. *Neuron* **29**, 615–628.
- Putcha G. V., Harris C. A., Moulder K. L., Easton R. M., Thompson C. B. and Johnson E. M. Jr (2002) Intrinsic and extrinsic pathway signaling during neuronal apoptosis: lessons from the analysis of mutant mice. *J. Cell Biol.* **157**, 441–453.
- Salgo M. G. and Pryor W. A. (1996) Trolox inhibits peroxynitrite-mediated oxidative stress and apoptosis in rat thymocytes. *Arch. Biochem. Biophys.* **333**, 482–488.
- Sefton A. J. and Dreher B. (1985) *Visual System, in the Rat Nervous System*, Vol. 1: Forebrain and Midbrain (Paxinos G., ed.), pp. 169–221. Academic Press, Orlando.
- Shangary S., Brown K. D., Adamson A. W., Edmonson S., Ng B., Pandita T. K., Yalowich J., Taccioli G. E. and Baskaran R. (2000) Regulation of DNA-dependent protein kinase activity by ionizing radiation-activated Abl kinase is an ATM-dependent process. *J. Biol. Chem.* **275**, 301 613–330 168.
- Shieh S.-Y., Ikeda M., Taya Y. and Prives C. (1997) DNA damage-induced phosphorylation of p53 alleviates inhibition by MDM2. *Cell* **91**, 325–334.
- Usuki F., Yasutake A., Umehara F., Tokunaga H., Matsumoto M., Eto K., Ishiura S. and Higuchi I. (2001) In vivo protection of a water-soluble derivative of vitamin E, Trolox, against methylmercury-intoxication in the rat. *Neurosci. Lett.* **304**, 199–203.
- Wei M. C., Zong W.-X., Cheng E. H.-Y., Lindsten T., Panoutsakopoulou V., Ross A. J., Roth K. A., MacGregor G. R., Thompson C. B. and Korsmeyer S. J. (2001) Proapoptotic Bax and Bak: a requisite gateway to mitochondrial dysfunction and death. *Science* **292**, 727–730.
- Wolter K. G., Hsu Y.-T., Smith C. L., Nechushtan A., Xi X.-G. and Youle R. L. (1997) Movement of Bax from the cytosol to mitochondria during apoptosis. *J. Cell Biol.* **139**, 1281–1292.
- Wong P. C., Pardo C. A., Borchelt D. R., Lee M. K., Copeland N. G., Jenkins N. A., Sisodia S. S., Cleveland D. W. and Price D. L. (1995) An adverse property of a familial ALS-linked SOD1 mutation causes motor neuron disease characterized by vacuolar degeneration of mitochondria. *Neuron* **14**, 1105–1116.
- Yakovlev A. G., Knoblach S. M., Fan L., Fox G. B., Goodnight R. and Faden A. I. (1997) Activation of CPP32-like caspases contributes to neuronal apoptosis and neurological dysfunction after traumatic brain injury. *J. Neurosci.* **17**, 7415–7424.
- Zhivotovsky B., Samali A., Gahm A. and Orrenius S. (1999) Caspases: their intracellular localization and translocation during apoptosis. *Cell Death Diff.* **6**, 644–651.



## FAST TRACK

# Injury-Induced Spinal Motor Neuron Apoptosis Is Preceded by DNA Single-Strand Breaks and Is p53- and Bax-Dependent

Lee J. Martin,<sup>1,2</sup> Zhiping Liu<sup>1</sup>

<sup>1</sup> Department of Pathology, Division of Neuropathology, Johns Hopkins University School of Medicine, Baltimore, Maryland 21205

<sup>2</sup> Department of Neuroscience, Johns Hopkins University School of Medicine, Baltimore, Maryland 21205

Received 12 July 2001; accepted 25 September 2001

**ABSTRACT:** The mechanisms of injury-induced apoptosis of neurons within the spinal cord are not understood. We used a model of peripheral nerve-spinal cord injury in the rat and mouse to induce motor neuron degeneration. In this animal model, unilateral avulsion of the sciatic nerve causes apoptosis of motor neurons. We tested the hypothesis that p53 and Bax regulate this neuronal apoptosis, and that DNA damage is an early upstream signal. Adult mice and rats received unilateral avulsions causing lumbar motor neurons to achieve endstage apoptosis at 7–14 days postlesion. This motor neuron apoptosis is blocked in *bax*<sup>-/-</sup> and *p53*<sup>-/-</sup> mice. Single-cell gel electrophoresis (comet assay), immunocytochemistry, and quantitative immunogold electron microscopy were used to measure molecular changes in motor neurons during the progression of apoptosis. Injured motor neurons accumulate single-strand breaks in DNA by 5 days. p53

accumulates in nuclei of motor neurons destined to undergo apoptosis. p53 is functionally activated by 4–5 days postlesion, as revealed by immunodetection of phosphorylated p53. Preapoptotically, Bax translocates to mitochondria, cytochrome *c* accumulates in the cytoplasm, and caspase-3 is activated. These results demonstrate that motor neuron apoptosis in the adult spinal cord is controlled by upstream mechanisms involving DNA damage and activation of p53 and downstream mechanisms involving upregulated Bax and cytochrome *c* and their translocation, accumulation of mitochondria, and activation of caspase-3. We conclude that adult motor neuron death after nerve avulsion is DNA damage-induced, p53- and Bax-dependent apoptosis. © 2002 John Wiley & Sons, Inc. *J Neurobiol* 50: 181–197, 2002; DOI 10.1002/neu.10026

**Keywords:** amyotrophic lateral sclerosis; *bax*<sup>-/-</sup> mice; DNA damage; *p53*<sup>-/-</sup> mice; spinal cord trauma

## INTRODUCTION

Apoptosis is an organized form of cell death that is mediated by active, intrinsic mechanisms (Yuan and

Yankner, 2000). Apoptosis in the nervous system is important for a variety of reasons. Apoptosis of neurons and non-neuronal cells occurs normally in the developing nervous system (Glücksmann, 1951; Oppenheim, 1991), and defects in apoptosis can cause cerebral malformations during embryogenesis (Kuida et al., 1996; Hakem et al., 1998). Apoptosis might also participate in the pathogenesis of abnormal neuronal death in chronic and acute neuropathological disorders (Martin et al., 1998; Yuan and Yankner, 2000; Martin, 2001). For example, the genes for neuronal apoptosis inhibitory protein and survival motor neuron protein are mutant in some children with pediatric forms of motor neuron disease such as spinal

Correspondence to: L.J. Martin (lmartin@jhmi.edu).

Contract grant sponsors: the U.S. Public Health Service, National Institutes of Health.

Contract grant sponsor: National Institute of Neurological Disorders and Stroke; contract grant number: NS34100.

Contract grant sponsor: National Institute on Aging; contract grant number: AG16282.

Contract grant sponsor: the Department of Defense, U.S. Army Medical Research and Materiel Command; contract grant number: DAMD17-99-1-9553.

© 2002 John Wiley & Sons, Inc.

muscular atrophy (Roy et al., 1995; Lefebvre et al., 1995). The neuronal degeneration in adult types of motor neuron disease such as amyotrophic lateral sclerosis (ALS) is apoptosis (Martin et al., 2000; Martin, 2001). Apoptosis of neurons and nonneuronal cells contributes to the neuropathology in animal models of spinal cord trauma (Liu et al., 1997). Therefore, understanding the molecular regulation of apoptosis is highly relevant to human spinal cord disorders as well as other neurodegenerative disorders of the human central nervous system (CNS).

Motor neurons in individuals with ALS sustain DNA damage (Martin, 2001), and the oncosuppressor protein p53 may participate in the mechanisms of motor neuron apoptosis in ALS (Martin, 2000). This DNA binding protein functions in genome surveillance, DNA repair, and as a transcription factor. p53 commits to death cells that have sustained DNA damage from reactive oxygen species and other genotoxic stresses. The mechanisms by which p53 induces apoptosis are largely unknown. p53 is a direct transcriptional activator of the *bax* gene (Miyashita and Reed, 1995) and a transcriptional repressor of the *bcl-2* gene (Miyashita et al., 1994); thus, apoptosis is thought to be executed by molecular cascades involving expression or activation of p53, Bax, and caspases (Polyak et al., 1997).

The understanding of the mechanisms of apoptosis in nervous system cells is much less advanced compared to cells of non-nervous tissue origin. Studies have shown recently that Bax is critical for apoptosis of neurons in cell culture (Deckwerth et al., 1996; Cregan et al., 1999; Putcha et al., 1999), and is required for neuronal apoptosis during development (Deckwerth et al., 1996). However, the mechanisms of injury-induced neuronal apoptosis within the CNS are much less understood compared to cell culture and developmental paradigms. We used an injury model of neuronal apoptosis within the rodent spinal cord to identify the *in vivo* mechanisms of motor neuron apoptosis. In this model, we have found that sciatic nerve avulsion reliably induces apoptosis of motor neurons (Martin et al., 1999; Liu and Martin, 2001a), although the involvement of apoptosis in the death of adult spinal motor neurons is still controversial (Li et al., 1998; Chan et al., 2001). The evolution of apoptosis in these neurons is associated with oxidative stress and the accumulation of nuclear DNA damage in the form of hydroxyl radical damage (Martin et al., 1999) and single-strand breaks (Liu and Martin, 2001a). We used this model to test the hypothesis that injury-induced apoptosis of motor neurons in the adult spinal cord is controlled by p53, Bax, and caspase-3.

## MATERIALS AND METHODS

### Animals

Adult male rats and gene-deficient and wild-type mice were used for these experiments. Sprague-Dawley rats (Charles River, Wilmington, MA) weighed ~150–200 g. Mice (Jackson Labs) were deficient in the *bax* gene (*bax*<sup>-/-</sup>, *n* = 16) or the *p53* gene (*p53*<sup>-/-</sup>, *n* = 18), and were 6–8 weeks of age when used. Bax-deficient mice were the C57BL/6-Bax<sup>tm1Sjk</sup> congenic strain. p53-deficient mice were the 129/Sv-Trp53<sup>tm1Tyj</sup> strain. C57BL/6 mice (*n* = 20) served as wild-type controls for bax-null mice, and 129/Sv mice (*n* = 18) served as wild-type controls for p53-null mice. The animals were housed in a colony room with a 12 h:12 h light:dark cycle and *ad libitum* access to food and water. The Animal Care and Use Committee of the Johns Hopkins University School of Medicine approved the animal protocol.

### *In Vivo* Model of Motor Neuron Apoptosis

The unilateral sciatic nerve avulsion model was used as an *in vivo* model for apoptosis of spinal motor neurons (Martin et al., 1999; Liu and Martin 2001a). Mice and rats were deeply anesthetized with enflurane/oxygen/nitrous oxide (1:33:66). A midline incision was made in the lateral aspect of the left pelvis and upper hindlimb. The sciatic nerve was located by blunt retraction of the biceps femoris and gluteus muscles, and was tracked proximally to an extravertebral location deep within the pelvis. A steady, moderate traction was applied to the sciatic nerve with forceps until the nerve separated from the spinal cord, resulting in a mixed motor-sensory root avulsion. Muscle retraction was released and the overlying skin was sutured. Postlesion survival times following sciatic nerve avulsion were 1, 2, 3, 4, 5, 7, 9, 10, 12, 14, 21, and 28 days (*n* = 6–8 rats per time point) or 3, 4, 5, 7, 14, 21, and 70 days (*n* = 10–16 mice per time point).

### Quantification of Motor Neurons

Bax-deficient mice and wild-type C57BL/6 mice were sacrificed at 21 days after lesioning, and p53-deficient mice and wild-type 129/Sv mice were sacrificed at 21 and 70 days after lesioning. Animals were anesthetized with an overdose of chloral hydrate and perfused intracardially with ice-cold phosphate buffer-saline (PBS, 100 mM, pH 7.4) followed by ice-cold 4% paraformaldehyde in PBS. After perfusion-fixation, spinal cords were allowed to remain *in situ* for 1 h before they were removed from the vertebral column. After the spinal cords were removed, lumbar enlargements were dissected under a surgical microscope segment by segment and they were cryoprotected in 20% glycerol-PBS, and frozen under pulverized dry ice. Transverse serial symmetrical sections (40  $\mu$ m) through the lumbar cord were cut using a sliding microtome. Serial sections from each mouse

brain were mounted on glass slides and stained with cresyl violet for neuronal counting. Neuronal counts in the ipsilateral and contralateral ventral horns were made at 1000 $\times$  magnification using the stereological optical disector method as described (Calhoun et al., 1996; Al-Abdulla et al., 1998). Motor neurons without apoptotic structural changes (using strict morphological criteria) were counted. These criteria included a round, open, pale nucleus (not condensed and darkly stained), granular Nissl staining of the cytoplasm, and a diameter of  $\sim 30$ – $40\ \mu\text{m}$ . With these criteria, astrocytes, oligodendrocytes, and microglia were excluded from the counts. Neuronal counts were used to determine group means and variances, and comparisons among groups were analyzed using a one-way analysis of variance and a Student's *t* test. The experiments were controlled at two levels. Bax-deficient mice have more neurons than wild-type mice (Deckwerth et al., 1996); therefore, neuronal counts in the contralateral ventral horn always served as controls for the ipsilateral ventral horn in lesioned Bax- and p53-null mice. In addition, neuron counts in wildtype mice served as strain controls.

### Immunolocalization of p53, Bax, Cytochrome *c*, and Active Caspase-3 in Spinal Motor Neurons after Sciatic Nerve Avulsion

The expression and localization patterns of p53, Bax, cytochrome *c*, and caspase-3 were examined in spinal motor neurons during apoptosis at the light microscopic level in rat and mouse. Animals were anesthetized and perfusion-fixed, and the spinal cords were prepared as described above. p53, Bax, and caspase-3 were detected in rat and mouse spinal cord sections using a standard immunoperoxidase method with diaminobenzidine as chromogen. Cytochrome *c* was detected in rat spinal cord sections by immunofluorescence.

The antibodies used for immunocytochemistry have been characterized previously. Three different commercial antibodies to p53 were used. Two of these antibodies recognize p53 regardless of phosphorylation state [BMG-1B1, 1  $\mu\text{g}$  IgG/mL (Roche), and Pab240, 1  $\mu\text{g}$  IgG/mL (Santa Cruz)]. The other p53 antibody that we used detects p53 only when it is phosphorylated at Ser392 (Oncogene), and thus recognizes activated p53 (Levine, 1997). The specificities of these p53 antibodies have been evaluated previously (Martin, 2000; Martin et al., 2001). These antibodies are highly specific for detecting a major protein band at  $\sim 53$  kDa that has the same mobility as recombinant p53. These antibodies supershift p53 in DNA binding experiments (Martin et al., 2001). Immunostaining for Bax was detected with two different antibodies: a rabbit polyclonal antibody that recognizes the N-terminal residues 1–12 of human Bax (Upstate), and a mouse monoclonal antibody to Bax (Pharmingen). Caspase-3 was detected with a rabbit polyclonal antibody that specifically detects the cleaved (active) form of caspase-3; the specificity of this antibody has been confirmed by immunoblotting (Northington et al., 2001). Cytochrome *c* was detected with a rabbit polyclonal anti-

body (Santa Cruz), which has also been characterized by immunoblotting (Martin et al., 2000). Negative control sections were incubated in comparable dilutions of immunoglobulin G or with primary or secondary antibody omitted. For Bax immunostaining, spinal cord sections from *bax*<sup>-/-</sup> mice also served as negative controls.

### Immunogold-EM for Bax and Cytochrome *c* Translocation in Motor Neurons

We directly evaluated whether subcellular translocation of Bax and cytochrome *c* occurs specifically in motor neurons. This analysis has not been done before quantitatively at the cellular level *in situ*, and cannot be done by Western blotting. Rats with sciatic nerve avulsions were perfused with 4% paraformaldehyde/0.5% glutaraldehyde in PBS. Vibratome sections of L5 spinal cord were processed using an immunogold–silver intensification detection system and a flat sample-epon embedding technique to determine the subcellular localization of Bax and cytochrome *c*. Spinal cord sections were preincubated in gelatin–BSA and then incubated (at 4°C) for 3 days with antibody to Bax or cytochrome *c*. After primary antibody incubation, sections were rinsed and incubated (at room temperature) with goat antirabbit IgG conjugated to 1 nm colloidal gold diluted 1:50 for 4 h, followed by silver enhancement solution for 10–20 min (Amersham Life Science, Arlington Heights, IL). L5 ventral horns of immunostained spinal cord sections were microdissected discretely under a microscope. Ipsilateral and contralateral samples were osmicated, dehydrated by graded concentrations of ethanol, and embedded in resin. Plastic blocks containing L5 motor neurons were serially thin sectioned using ultramicrotomes (Sorvall). Ultrathin sections, stained with lead citrate (15 min), were viewed and photographed with a JEOL electron microscope. Electron micrographs of motor neurons were shot by an observer unaware of sample history.

Ipsilateral and contralateral L5 motor neurons from the same sections were compared. Immunogold labeling of mitochondrial and cytosolic compartments was quantified in electron micrographs (shot and enlarged at constant magnification) of contralateral control and ipsilateral lesioned motor neurons at prechromatolytic and chromatolytic stages of apoptosis (Martin et al., 1999) using point-hit counting by an observer unaware of sample history. A plastic, transparent, orthogonal grid (grid point area =  $0.01\ \mu\text{m}^2$ ) was placed on each micrograph, and the number of points that fell on mitochondria were counted along with the number of immunogold particles bound to mitochondria and “free” in the cytosol. The data were analyzed using a one-way analysis of variance and a Student's *t* test.

### Comet Assay

The comet assay is a method for identifying early damage to genomic DNA of eukaryotic cells on a single-cell basis (see Liu and Martin, 2001b, for historical citations). Depending

upon the pH conditions, different types of DNA lesions are detectable in neurons by comet assay, including apurinic/apyrimidinic (AP or alkali-labile sites), single-strand breaks (SSB), and double-strand breaks (Liu and Martin, 2001b). In this study, we were interested in the formation of SSB. These DNA lesions are a loss of a purine or pyrimidine base and the deoxyribose with a cut in the phosphodiester backbone. We tested the hypothesis that DNA-SSB are formed early in the process of motor neuron apoptosis after sciatic nerve avulsion.

Because the comet assay is a single-cell assay, we developed a new method to isolate motor neurons for gel electrophoresis (Liu and Martin, 2001b). This technique can be used to isolate a spinal cord ventral horn cell suspension with a neuronal composition that is ~86% motor neurons (Liu and Martin, 2001a, 2001b). Spinal cords were isolated from adult rats at 5, 7, 10, 14, and 28 days after sciatic nerve avulsions. The animals were anesthetized deeply with a mixture of enflurane/oxygen/nitrous oxide (1:33:66) and then decapitated. The entire lumbar enlargements (divided into ipsilateral and contralateral sides) were used. After removing the pia, lumbar enlargements were dissected segmentally under a surgical microscope, and then the segments were microdissected into gray matter columns of ventral horn without appreciable contamination of dorsal horn and surrounding white matter funiculi. Gray matter tissue columns from ventral horns of lumbar enlargements were collected and rinsed in a cell culture dish on ice containing dissection medium ( $1 \times \text{Ca}^{2+}$  and  $\text{Mg}^{2+}$  free Hanks balanced salt solution, GibcoBRL, Grand Island, NY, supplemented with glucose and sucrose).

To identify DNA damage in motor neurons undergoing apoptosis *in vivo*, the comet assay was used on motor neuron cell suspensions prepared from rats with sciatic nerve avulsions. Motor neurons from ipsilateral or contralateral (control) ventral horns of lumbar enlargements of animals with unilateral sciatic nerve avulsions were subjected directly to comet assay immediately after isolation. All the procedures for comet assay were done under low light to minimize spontaneous DNA damage.

Motor neurons were embedded into agarose gels for electrophoresis. The cell microgels were prepared as layers. The first layer of gel was made by applying 200  $\mu\text{L}$  of regular melting point agarose (0.7%) onto superfrosted glass microscope slides ( $3 \times 1''$ , thickness 1 mm) and a coverslip was laid gently on the agarose. The agarose was allowed to solidify at  $4^\circ\text{C}$ , and the coverslip was removed. Low melting point agarose was prepared in 100 mM PBS and kept at  $37^\circ\text{C}$ . Samples of the motor neuron enriched cell suspension were mixed with the low melting point agarose, and 50  $\mu\text{L}$  of a mixture of cell suspension (containing  $\sim 4.4 \times 10^4$  motor neurons) and low melting point agarose was applied to the first gel layer. The slides were then coverslipped and placed at  $4^\circ\text{C}$  for solidification of the cell suspension-agarose mixture. After the second layer solidified, the coverslips were removed and 100  $\mu\text{L}$  of low melting point agarose was added on top of the cell layer. The gels were

recoverslipped, and the slides were placed on ice for gel solidification.

For the elution of DNA from motor neurons during electrophoresis the cells were lysed and their DNA was denatured. Coverslips were removed from the cell microgels and the slides were covered with 1.5 mL of lysis buffer at pH 10 containing 2.5 M NaCl, 100 mM EDTA, 1% sodium lauryl sarcosine, 10 mM Tris, and Triton X-100 (final concentration 1%, freshly added immediately before use). The cell microgels were lysed for 30 min (at room temperature). After draining, microgels were treated with DNA-unwinding solution (300 mM NaOH, 1 mM EDTA, pH 12) for 30 min (room temperature). A pH 12 is appropriate for SSB detection, because hydrogen bonds destabilize at this pH and double-stranded DNA separates into individual single strands, rendering shorter single-stranded DNA (resulting from SSB) more easily eluted from the nucleus (Liu and Martin, 2001b). The microgels were then placed directly into a horizontal gel electrophoresis chamber filled with DNA-unwinding solution. Gels were run with constant current (300 mA at room temperature) for generally 30 min. After electrophoresis, the microgels were neutralized with 50 mM Tris-HCl (pH 7.5) for 15 min (twice). DNA was visualized with ethidium bromide staining (20  $\mu\text{g}/\text{mL}$ , 20 min at room temperature) after which the microgels were washed and coverslipped. The evaluation and image acquisition were performed using a Zeiss fluorescence microscope as described (Liu and Martin, 2001a, 2001b). Comet measurements were performed as described (Liu and Martin, 2001a, 2001b).

## RESULTS

### Bax Deficiency Prevents Injury-Induced Motor Neuron Apoptosis in Adult Spinal Cord

We used mice with targeted deletions of the *bax* gene (*bax*<sup>-/-</sup>) to test the hypothesis that motor neuron apoptosis in the adult spinal cord is Bax dependent [Fig. 1(A)]. At 21 days after sciatic nerve avulsion, the number of motor neurons in the ipsilateral L5 of wild-type C57BL/6 mice was  $54 \pm 17\%$  (mean  $\pm$  SD) of contralateral L5; in contrast, the number of neurons in the ipsilateral L5 of Bax-deficient mice was  $98.0 \pm 5\%$  (mean  $\pm$  SD) of contralateral L5.

### Loss of p53 Function Protects Adult Motor Neurons from Apoptosis

Mice with targeted inactivation of the *p53* gene (*p53*<sup>-/-</sup>) were used to test the hypothesis that motor neuron apoptosis in adult spinal cord is p53 dependent [Fig. 1(B)]. At 21 days after sciatic nerve avulsion, the number of motor neurons in the ipsilateral L5 of wild-type 129/Sv mice was  $53 \pm 16\%$  (mean  $\pm$  SD)



**Figure 1** Motor neuron apoptosis in adult spinal cord is mediated by Bax and p53. Sciatic nerve avulsions were done on *bax*<sup>+/+</sup> (wild type, *n* = 20) and *bax*<sup>-/-</sup> mice (*n* = 16) or *p53*<sup>+/+</sup> (wild type, *n* = 10) and *p53*<sup>-/-</sup> mice (*n* = 18) that were survived for 21 days. Neurons were counted in the ipsilateral and contralateral (control) L5. Values are mean  $\pm$  standard deviation. *Bax* gene deletion (A) and *p53* gene inactivation (B) completely blocked the injury-induced apoptosis of motor neurons (asterisk, *p* < .05).

of contralateral L5; in contrast, the number of neurons in the ipsilateral L5 of *p53*-deficient mice was  $93 \pm 9.0\%$  (mean  $\pm$  SD) of contralateral L5. Thus, loss of *p53* function protects neurons from apoptosis in the adult brain. To determine whether this effect is sustained, mice were survived for a longer time. At 70 days after sciatic nerve avulsion, the number of neurons in the ipsilateral L5 of wild-type 129/Sv mice was  $50 \pm 15\%$  (mean  $\pm$  SD) of contralateral L5, whereas the number of neurons in the ipsilateral L5 of *p53*-deficient mice was  $90 \pm 10\%$  (mean  $\pm$  SD) of contralateral L5. Thus, deletion of *p53* results in sustained protection against motor neuron apoptosis in spinal cord.

### p53 Accumulation Mediates Motor Neuron Apoptosis after Sciatic Nerve Lesions

In the normal rat and mouse spinal cord the level of immunocytochemically detectable p53 is low. Immunoreactivity is observed mostly in the nuclei of some parenchymal glial cells and ependymal cells lining the central canal. In motor neurons of naive animals, p53 immunoreactivity is observed very rarely. In the non-lesioned (contralateral) side of spinal cord, p53 immunoreactivity is observed in the nucleus of a few

motor neurons in rat [Fig. 2(A) and (C), arrowheads] and mouse [Fig. 3(A) and (C), arrowheads]. In contrast, p53 immunoreactivity accumulates prominently in the nucleus of neurons in the ipsilateral ventral horn of rat [Fig. 2(B) and (D)–(G)] and mouse [Fig. 3(B) and (D)–(G)]. At 1, 2, and 3 days postlesion, the localization of p53 in the ipsilateral ventral horn is not substantially different from the contralateral ventral horn. In ipsilateral motor neurons, p53 immunoreactivity is elevated at 4 days in both rat [Fig. 2(B) and (D)] and mouse [Fig. 3(B) AND (D)] and remains elevated through 7 days postlesion [Figs. 2(F) and 3(D)–(G)]. Lesioned motor neurons in mouse also showed a prominent increase in p53 in the cytoplasm [Fig. 3(D)]. The nuclear sequestration of p53 occurs in motor neurons prior to and during chromatolysis, as shown by cresyl violet counterstaining [Fig. 2(D) and (E), arrowheads]; thus, this is an early event in the staging of motor neuron apoptosis (Martin et al., 1999). p53 immunoreactivity is localized to strands in the nucleus, consistent with a DNA binding protein [Fig. 2(D), double arrows]. There is some induction of p53 in contralateral motor neurons by 7 days, but the difference between ipsilateral and contralateral is dramatic, as demonstrated by counting motor neurons with p53 immunoreactivity. In the rat, at 4 days postlesion the number (% of contralateral) of motor neurons with p53 immunoreactivity was  $162 \pm 4\%$  (mean  $\pm$  SD) and at 7 days postlesion this value increased to  $274 \pm 70\%$ . In motor neurons showing structural characteristics of apoptosis [Figs. 2(F) and 3(G)], and in some preapoptotic chromatolytic motor neurons [Fig. 2(E)] p53 is present in nuclear inclusions. At 7 days postlesion and thereafter, some small nonneuronal cells that are likely to be astroglia show an induction of p53 in ipsilateral ventral horn [Fig. 2(G), dotted arrows].

The functional activation of p53 as a transcription factor in motor neurons was evaluated by immunodetection of phosphorylated p53. The phosphorylation of p53 at Ser392 results in its activation as a DNA binding protein (Levine, 1997). Ser-392-phosphorylated p53 was observed in the cytoplasm and nucleus of ipsilateral motor neurons at 5 days postlesion through 14 days in rat [Fig. 4(A) and (B)] and mouse [Fig. 4(C)] spinal cord.

### Bax Undergoes an Intracellular Redistribution in Motor Neurons during Apoptosis

Bax has a critical role in the apoptotic process in many cells presumably by forming ion-conducting channels in

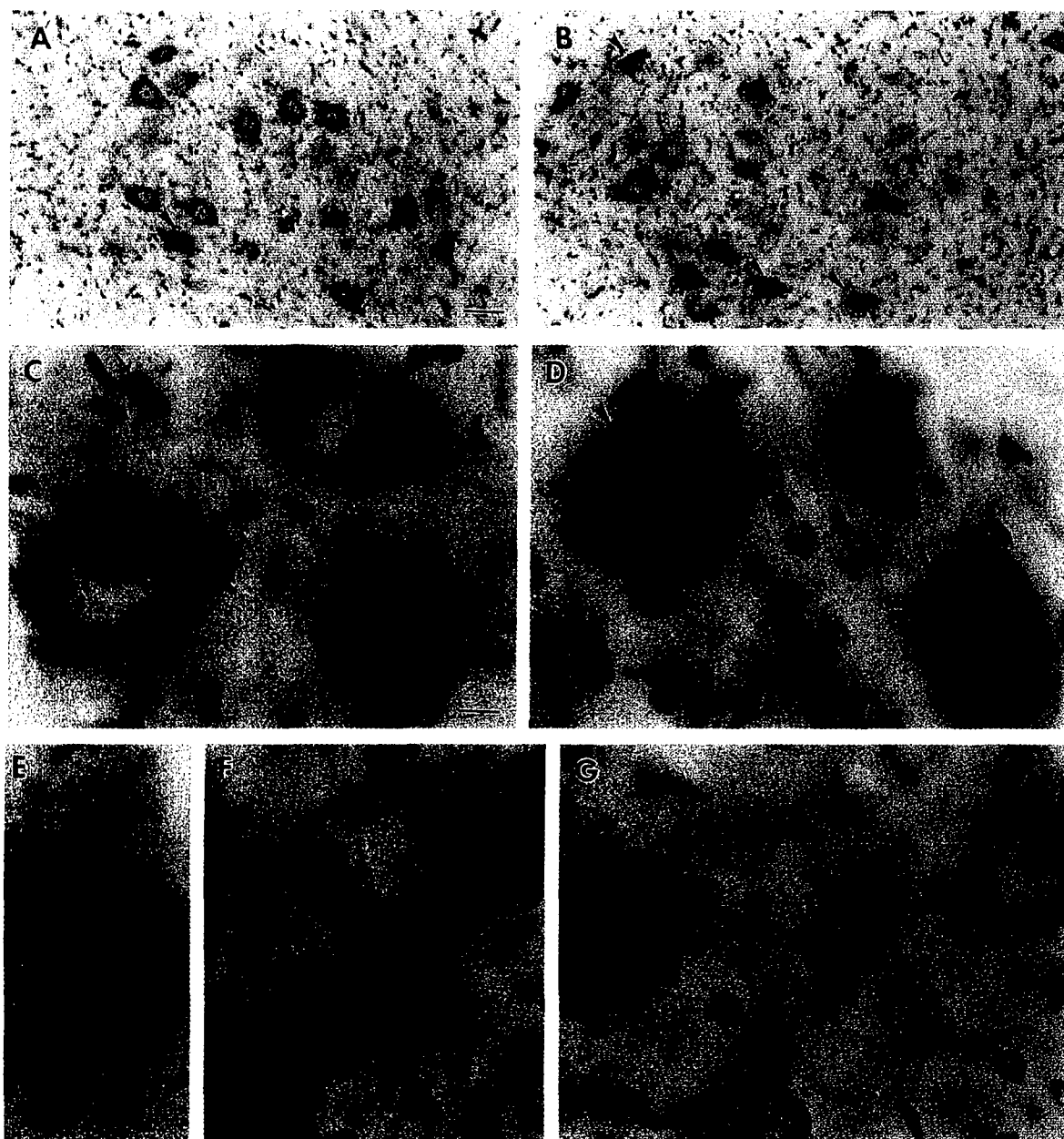


**Figure 2** p53 immunoreactivity accumulates in rat spinal motor neurons after sciatic nerve avulsion. In the nonlesioned side of spinal cord at 4 days, few neurons are immunoreactive for p53 [(A) and (C), arrowheads] and subsets of small glial cells are positive [(C), dotted arrow]. (A) A panoramic view of the contralateral L5 group IX motor neurons at low magnification. (C) A high magnification view of a p53 immunopositive motor neuron (lower right, arrowhead) and a nearby motor neuron with a completely immunonegative nucleus, illustrating the highly selective and rare localization of p53 in individual motor neurons and occasional small nonneuronal cells (top left, dotted arrow) in contralateral side of lumbar spinal cord. In the lesioned side at 4 days, p53 immunoreactivity accumulates in the nucleus of many motor neurons [(B) and (D), arrowheads]. (B) A panoramic view of the ipsilateral L5 group IX motor neurons at low magnification. (D) A high magnification view of p53 immunopositive motor neurons (arrowheads.) In some motor neuron nuclei, p53 immunoreactivity decorates strands in the nucleus [(D), left motor neuron, small double arrows]. In motor neurons in the chromatolytic stage of apoptosis [(E), arrowhead] p53 immunoreactivity aggregates to form novel nuclear inclusions [(E), small double arrows]. As apoptosis progresses to the somatodendritic atrophy stage with nuclear condensation [(F), arrowhead], p53 nuclear inclusions become more prominent as they become dense and dark [(F), top right, small

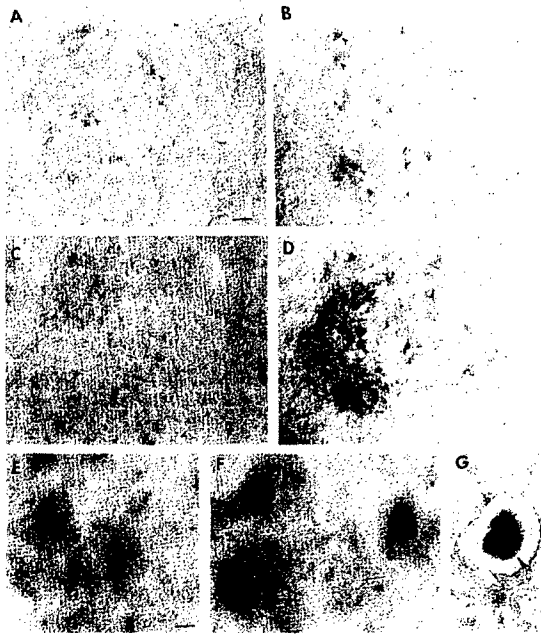


**Figure 3** p53 immunoreactivity accumulates in mouse L5 motor neurons after sciatic nerve avulsion. In the non-lesioned side of spinal cord at 4 days, constitutive levels of p53 are low in motor neurons with only a few neurons showing faint immunoreactivity [(A), arrowheads]. In the lesioned side at 4 days, p53 immunoreactivity is increased in subsets of motor neurons [(B), arrowheads]. In the non-lesioned side of spinal cord at 7 days, very few motor neurons show p53 immunoreactivity, but these immunopositive cells have more intense staining than neurons in the nonlesioned side at 4 days [(C) and (E), arrowheads; compare with (A)]. In contrast in the lesion side, motor neurons show a dramatic upregulation in the levels of p53 [(D) and (F), arrowheads], with immunoreactivity filling the cell. Lesioned motor neurons at 9 days are in the somatodendritic atrophy stage of apoptosis (i.e., they are shrunken and are separated from the surrounding neuropil) and remain p53 positive [(G), arrowhead]. Scale bars: [(A), same for (B)–(D)], 100  $\mu$ m; [(E), same for (F) and (G)], 12  $\mu$ m.

the membrane of mitochondria (Antonsson et al., 1997). Moreover, p53 is a transcriptional activator of the *bax* gene (Miyashita and Reed, 1995), and one pathway through which p53 commits cells to death is Bax up-regulation. We, therefore, evaluated whether Bax immunostaining patterns change in L5 motor neurons after sciatic nerve avulsion rat and mouse (Figs. 5 and 6,

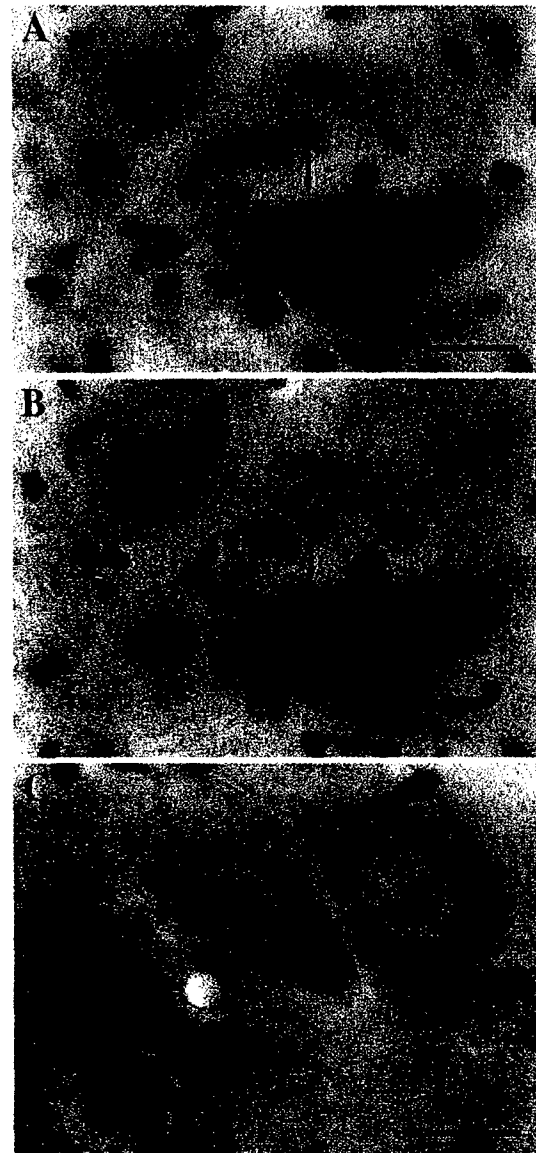


**Figure 4** Immunolocalization of active p53 with antibody to phospho-p53 (ser392) demonstrates nuclear accumulation of active p53 in subsets of ipsilateral L5 motor neurons in rat [(A) and (B), black arrows] and mouse [(C), black arrow] at 5 days postlesion. Photomicrographs in (A) and (B) are of the identical microscopic field but at different z-axis levels showing a nearby unlabeled motor neuron (asterisks). Scale bars: [(A), same for (B)], 22  $\mu$ m; (C), 16  $\mu$ m.

double arrows]. A nearby large nucleus [(F), lower left] contains a p53 nuclear inclusion. Subsets of small nonneuronal cells, most likely astroglia (distinguished by their small size and ellipsoidal pale nucleus), in the ipsilateral L5 express p53 [(G), dotted arrows] in addition to motor neurons (cell at far left center). Scale bars: [(A), same for (B)], 47  $\mu$ m; [(C), same for (D)–(G)], 9  $\mu$ m.

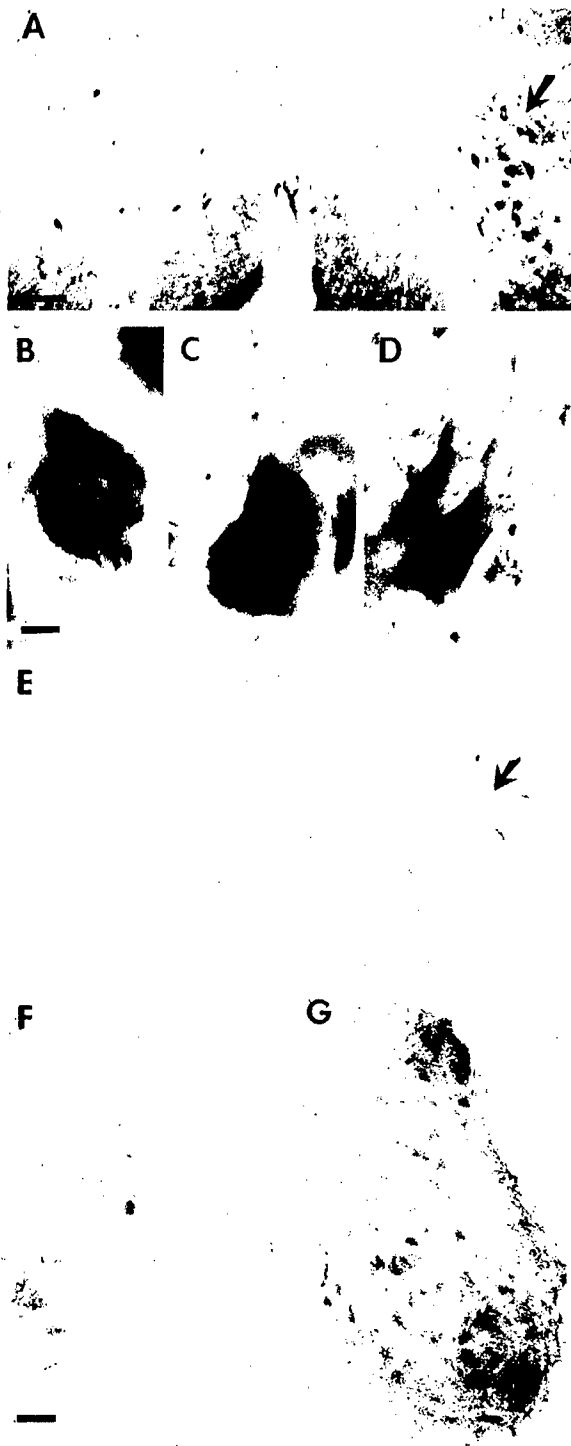


**Figure 5** Immunolocalization of Bax in L5 after sciatic nerve avulsion. (A) In rat L5 at 7 days after lesioning, Bax immunoreactivity is increased dramatically in ipsilateral motor neurons (arrow) compared to the nonlesioned side. Scale bar = 100  $\mu$ m [same for (E)]. (B)–(D) In nonlesioned motor neurons, Bax immunoreactivity is enriched in the cytoplasm and is organized into large Nissl-like aggregates (B). In lesioned motor neurons in the chromatolytic stage of apoptosis at 5–7 days (C) Bax immunostaining is increased, (D) Bax immunoreactivity remains diffusely localized throughout the cell. Scale bar in (B) [same for (C) and (D)] = 4  $\mu$ m. (E) In *bax*<sup>-/-</sup> mice, Bax immunoreactivity is not detectable [using the same antibody as in (A)–(D)] in ipsilateral (arrow) and contralateral sides of L5. Nonspecific staining of microvessels served as a positive control for the immunoperoxidase method. (F) and (G) p53 gene inactivation in mice (F) attenuates the elevation in Bax immunoreactivity seen in wild-type mice (G) after sciatic nerve avulsion. Scale bar (F) = 100  $\mu$ m [same for (G)].

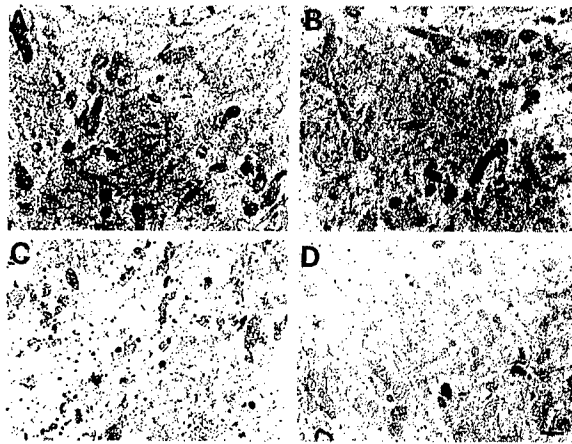


**Figure 6** Immunogold-EM localization of Bax and cytochrome *c* in spinal motor neurons after sciatic nerve avulsion. (A) and (B) Constitutive levels of Bax immunoreactivity (arrowheads) in motor neurons are low in motor neurons in the nonlesioned side of spinal cord (A). Bax is localized to mitochondria (m), endoplasmic reticulum, nuclear envelope, and cytosol [(A), arrowheads]. In lesioned L5 motor neurons at 7 days, Bax immunolabeling of mitochondria and endoplasmic reticulum is increased prominently (B). (C) and (D) In motor neurons in the nonlesioned side of spinal cord, cytochrome *c* immunolabeling is associated primarily with mitochondria (C), often forming clusters of immunoreactivity [see Fig. 7(A)]. In lesioned motor neurons at 7 days postlesion (D), cytochrome *c* is found diffusely in the cytoplasm [see Fig. 7(B)–(D)]. Scale bar in (D), same for (A)–(C)] = 0.1  $\mu$ m.

Table 1). In normal motor neurons of rat and wild-type *bax*<sup>+/+</sup> mice, Bax immunoreactivity is found as large aggregates in the cytoplasm [Fig. 5(B)]. This immunoreactivity has a distribution similar to Nissl substance by light microscopy [Fig. 5(B)]. Immunogold EM confirmed that Bax immunoreactivity is enriched in aggregates of rough endoplasmic reticulum [Fig. 6(A) and (B)]. In lesioned motor neurons undergoing apoptosis,

filling the cytoplasm and the nucleus in a diffuse distribution (see Table 1 for quantification). In lesioned motor neurons in the somatodendritic stage of apoptosis, Bax immunoreactivity remains diffusely localized throughout the cell. Scale bar in (B) [same for (C) and (D)] = 4  $\mu$ m. (E) In *bax*<sup>-/-</sup> mice, Bax immunoreactivity is not detectable [using the same antibody as in (A)–(D)] in ipsilateral (arrow) and contralateral sides of L5. Nonspecific staining of microvessels served as a positive control for the immunoperoxidase method. (F) and (G) p53 gene inactivation in mice (F) attenuates the elevation in Bax immunoreactivity seen in wild-type mice (G) after sciatic nerve avulsion. Scale bar (F) = 100  $\mu$ m [same for (G)].



**Table 1** Quantitative Subcellular Analysis of Bax and Cytochrome *c* in Adult Spinal Motor Neurons Undergoing Injury-Induced Apoptosis

Days After Lesion <sup>a</sup>	Mitochondrial Number <sup>b</sup>		Bax IR <sup>c</sup>		Cytochrome <i>c</i> IR <sup>d</sup>	
	Contra	Ipsi	Total	Mitochondria	Total	Mitochondria
5	0.53 ± 0.18	0.50 ± 0.16	97.5 ± 2.1	91.0 ± 12.7	147 ± 5.1* [ <i>F</i> (1, 5) = 6.93; <i>p</i> = 0.04]	108.6 ± 17.6
7	0.58 ± 0.12	0.85 ± 0.23* [ <i>F</i> (1, 5) = 6.75; <i>p</i> = 0.04]	196.6 ± 4.2* [ <i>F</i> (1, 6) = 6.21; <i>p</i> = 0.03]	400.0 ± 101.0** [ <i>F</i> (1, 6) = 16.12; <i>p</i> = 0.001]	170.8 ± 46.7* [ <i>F</i> (1, 5) = 8.12; <i>p</i> = 0.04]	72.6 ± 10.2** [ <i>F</i> (1, 5) = 17.32; <i>p</i> = 0.005]
9	0.65 ± 0.07	0.76 ± 0.38	92.5 ± 8.4	67.7 ± 9.0** [ <i>F</i> (1, 6) = 14.01; <i>p</i> = 0.005]	281.1 ± 62.3* [ <i>F</i> (1, 5) = 9.01; <i>p</i> = 0.02]	20.4 ± 20.0** [ <i>F</i> (1, 5) = 17.89; <i>p</i> = 0.0001]

<sup>a</sup> The lesion was a unilateral sciatic nerve avulsion in adult (150–200 g) male rat.

<sup>b</sup> Mitochondrial number/μm<sup>2</sup> in ipsilateral (ipsi) and contralateral (contra) L5 motor neurons. Values are mean ± SD based on analysis of serial thin sections of 5–10 group IX motor neurons per side. Single asterisk indicates significantly different (*p* < 0.05) from contralateral side. The calculated *F*-values for the analysis of variance and the post hoc probabilities are indicated for the significant values.

<sup>c</sup> The level of Bax immunoreactivity (IR) in ipsilateral L5 motor neurons is represented as % (mean ± SD) of contralateral L5 motor neurons. Total refers to cytoplasmic Bax immunogold particles (free and organelle-associated) and mitochondrial refers to only mitochondrial-associated Bax immunogold particles. Single asterisk indicates significantly increased (*p* < 0.05) from contralateral side. Double asterisk indicates significantly decreased (*p* < 0.01) from contralateral side. The calculated *F*-values for the analysis of variance and the post hoc probabilities are indicated for the significant values.

<sup>d</sup> The level of cytochrome *c* immunoreactivity (IR) in ipsilateral L5 motor neurons is represented as % (mean ± SD) of contralateral L5 motor neurons. Total refers to cytoplasmic cytochrome *c* immunogold particles (free and organelle-associated) and mitochondrial refers to only mitochondrial-associated cytochrome *c* immunogold particles. Single asterisk indicates significantly increased (*p* < 0.05) from contralateral side. Double asterisk indicates significantly decreased (*p* < 0.01) from contralateral side. The calculated *F*-values for the analysis of variance and the post hoc probabilities are indicated for the significant values.

the pattern of Bax immunostaining changes notably in two ways. In the rat and mouse, Bax immunostaining is enhanced in lesioned motor neurons compared to contralateral motor neurons as revealed by light microscopy [Fig. 5(A)]. Quantitative immunogold EM showed a twofold increase in total Bax immunoreactivity in ipsilateral L5 motor neurons by 7 days [Table 1, Fig. 6(B)]. In addition, Bax immunoreactivity redistributes in lesioned motor neurons. By light microscopy the lesioned L5 motor neurons show a marked increase in Bax levels, and the pattern of Bax immunostaining changes from large aggregates to finer particles within the cytoplasm and nuclear staining [Fig. 5(C) and (D)]. Immunogold EM showed a prominent increase (~400%) in mitochondrial-associated Bax immunoreactivity by 7 days postlesion [Table 1, Fig. 6(B)]. Bax accumulates within mitochondria at perinuclear locations in injured motor neurons [Fig. 6(B)]. This increase in mitochondrial Bax was transient because by 9 days postlesion mitochondrial-associated Bax is significantly lower than contralateral motor neurons and, by light microscopy, there is a corresponding decrease in Bax immunostaining intensity [Fig. 5(D)]. Bax immunostaining was not detectable in nonlesioned and lesioned *bax*<sup>-/-</sup> mice [Fig. 5(E)]. Inactivation of the p53 gene altered the Bax staining patterns. *p53*<sup>-/-</sup> mice had lower constitutive expression of Bax and, after le-

sioning, the enhancement of Bax immunostaining in motor neurons was attenuated [Fig. 5(F) and (G)]. However, *bax* gene deletion did not prevent the induction and activation of p53 in lesioned motor neurons (data not shown).

### Motor Neurons Destined to Undergo Apoptosis Accumulate Mitochondria

We have shown previously that avulsed motor neurons accumulate cytochrome *c* oxidase activity (Martin et al., 1999), but the significance of this finding is not clear. To evaluate possible changes in mitochondrial distribution and number, mitochondria were counted in lesioned and control L5 motor neurons in serial thin sections using EM (Table 1, Fig. 6). At 5 days postlesion, mitochondrial numbers in ipsilateral and contralateral L5 motor neuron perikarya were similar. By 7 days, the number of mitochondria increased significantly (~148% of contralateral) in ipsilateral L5 motor neuron perikarya (Table 1, Fig. 6). At 9 days postlesion the number of intact mitochondria in ipsilateral motor neurons did not differ significantly from contralateral motor neurons (Table 1).

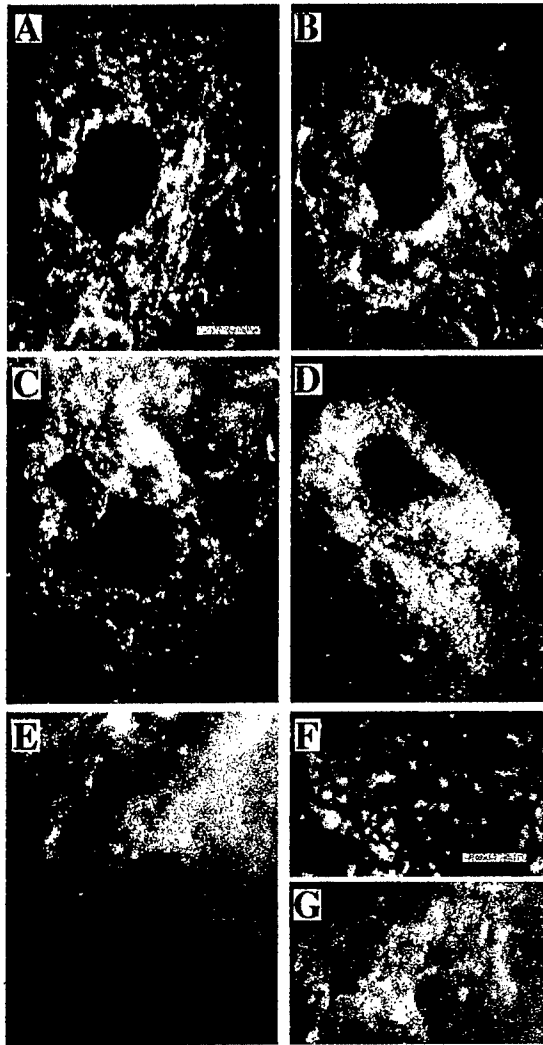


**Figure 7** Immunolocalization of cytochrome *c* in motor neurons after sciatic nerve avulsion in rat. (A) In normal nonlesioned motor neurons (contralateral side at 1 day postlesion), cytochrome *c* is localized to discrete granules distributed throughout the cytoplasm [(F) shows immunoreactivity at greater magnification] in a pattern similar to the distribution of mitochondria. (B) Lesioned motor neurons at 1 day show subtle changes in the distribution of cytochrome *c*. An early sign of injury is accumulation of cytochrome *c* immunoreactivity around the nucleus (in this example the accumulation is most noticeable at the lower right area around the nucleus) and the cytoplasm has less discrete particles compared to contralateral motor neurons [compare with (A)]. (C) Lesioned motor neurons at 2 days begin to show an increase in the staining intensity of cytochrome *c*. (D) At 4 day postlesion motor neurons undergoing apoptosis (note the nuclear shape change) have dramatically elevated cytochrome *c*. (E) At 7 days postlesion, cytochrome *c* appears as fine amorphous, diffusely distributed labeling throughout the cytoplasm in motor neurons [(G) shows immunoreactivity at greater magnification]. Scale bar: [(A), same for (B)–(E)], 14  $\mu$ m; [(F), same for (G)], 7  $\mu$ m.

### Cytochrome *c* Undergoes an Intracellular Redistribution in Apoptotic Motor Neurons

The intracellular localization of cytochrome *c* was evaluated by immunofluorescence in motor neurons during apoptosis (Fig. 7). Cytochrome *c* immunoreactivity in spinal motor neurons appears normally as large granules or vermiform structures scattered throughout the cytoplasm [Fig. 7(A) and (F)]. This pattern of immunolabeling changes quickly in motor neurons after sciatic nerve avulsion. By 1 day postlesion, the cytochrome *c* immunoreactivity redistributes to a perinuclear location in ipsilateral motor neurons [Fig. 7(B)] compared to contralateral motor neurons. At 2 days the level of immunostaining is increased, with large cytoplasmic territories showing intense cytochrome *c* immunoreactivity [Fig. 7(C)]. At 4 days postlesion cytochrome *c* immunoreactivity appears as diffuse fine particles that fill the perikaryal cytoplasm of ipsilateral motor neurons undergoing preapoptotic somatodendritic atrophy [Fig. 7(D)]. At 7 days postlesion two staining patterns emerge in motor neurons ipsilaterally. Some motor neurons in apoptosis are shrunken and round in shape with the cytoplasm filled with finely particulate and diffusely distributed cytochrome *c* immunolabeling [Fig. 7(E) and (G)], while other motor neurons display an inhomogeneous loss of immunostaining. Other motor neurons have labeling similar to the pattern seen at earlier times postlesion. At 14 days postlesion, in addition to the degenerating motor neurons with diffuse cytoplasmic labeling for cytochrome *c*, a few motor neurons in the ipsilateral side of spinal cord display a cytochrome *c* pattern typical of normal neurons and are likely to be recovering from the lesion.

Immunogold EM was used to directly visualize and quantify cytochrome *c* in different subcellular compartments specifically in L5 motor neurons early in the apoptotic process. At 5 days postinjury, total cytoplasmic cytochrome *c* levels were increased significantly (147% of contralateral), but the level of mitochondrial-associated cytochrome *c* immunoreactivity in ipsilateral motor neurons was not different from control (Table 1). At 7 days after avulsion, total cytoplasmic cytochrome *c* levels were elevated further (170% of control), but mitochondrial-associated cytochrome *c* was decreased (73% of control) in lesioned motor neurons [Table 1, Fig. 6(C) and (D)]. By 9 days postlesion, mitochondrial cytochrome *c* levels were only 20% of control, while the level of diffusely distributed cytoplasmic cytochrome *c* was 281% of control (Table 1).

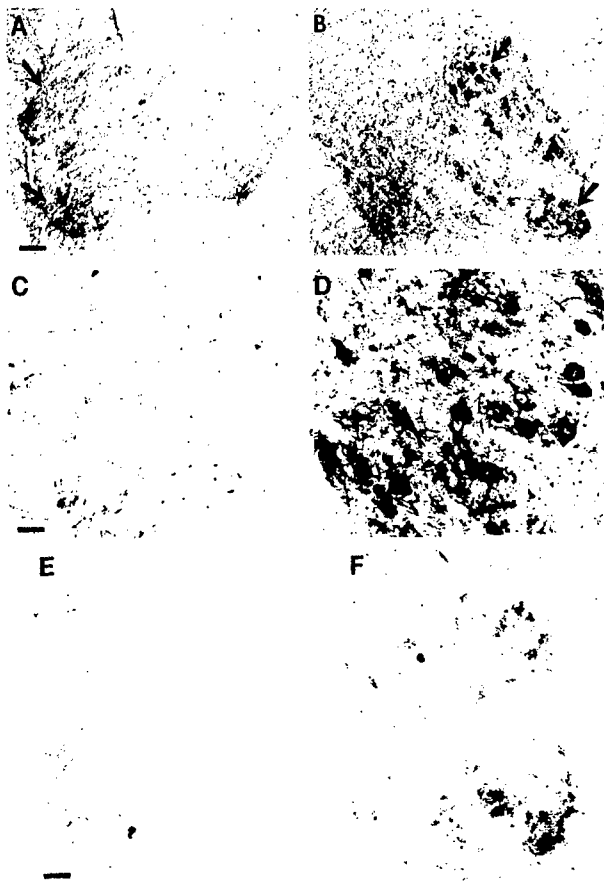


**Figure 8** Caspase-3 is activated in adult motor neurons after injury. (A)–(D) In nonlesioned L5 spinal cord, active caspase-3 is present in the neuropil of the ventral horn [(A), arrows] and in some glial cells (C), but in the lesioned side of L5 [(B), arrows] active caspase-3 is enriched in motor neuron cell bodies and dendrites [(B) and (D)]. Scale bars: [(A), same for (B)], 90  $\mu$ m; [(C), same for (D)], 30  $\mu$ m. (E) and (F) p53 gene inactivation in mice attenuates the caspase-3 activation (E) seen in wild-type mice (F) after sciatic nerve avulsion. Scale bar (E) = 90  $\mu$ m [(same for (F))].

### Caspase-3 Is Activated in Adult Spinal Motor Neurons during Injury-Induced Apoptosis

Activation of caspase-3 is a critical downstream event in many forms of PCD (Kuida et al., 1996). We evaluated if caspase-3 is activated directly in motor neurons during apoptosis using an antibody specific for active caspase-3 (Fig. 8). In normal and lesioned spinal cord, subsets of glial cells showed faint nuclear immunoreactivity for caspase-3. Nuclear labeling for caspase-3 is consistent with subcellular fractionation analyses (Zhivotovsky et al., 1999). Immunoreactivity for cleaved caspase-3 was

also present in the neuropil of normal and lesioned spinal cord. Cleaved caspase-3 was rarely observed in neuronal cell bodies in nonlesioned spinal cords. In rats at 5, 7, 9, and 12 days after sciatic nerve avulsions, a progressive accumulation of active caspase-3 occurred in subsets of ipsilateral motor neurons. Maximal accumulation was observed at 9 and 12 days postlesion [Fig. 8(A)–(D)]. Caspase-3 activation was not observed in lesioned motor neurons in *p53*<sup>−/−</sup> and *bax*<sup>−/−</sup> mice [Fig. 8(E) and (F)], consistent with the lack of injury-induced motor neuron apoptosis in these animals.

### Motor Neurons Accumulate DNA-SSB *In Vivo* Early after Injury

The comet assay was used to evaluate if DNA damage could be an early upstream signal for motor apoptosis, consistent with a p53-mediated mechanism of cell death (Fig. 9, Table 2). At 5 days after unilateral sciatic nerve avulsion, many (26%) lumbar motor neurons from the lesioned side of L5 had comets [Fig. 9(A)], while <2.0% of motor neurons from the nonlesioned side of L5 had comets. The heads of these motor neuron comets were large, round, and bright, and the tails were very short (Table 2), and consisted of scattered large granules close to the head [Fig. 9(A)]. The comet moment, a very sensitive index of early DNA damage (Liu and Martin, 2001b), was low ( $\sim 1.8 \times 10^5$ , Table 2). Motor neurons with comets at 5 days did not have an apoptotic nuclear morphology based on ethidium bromide staining.

The number of motor neurons with DNA damage and the extent of DNA-SSB in motor neurons continued to increase between 5–7 days after sciatic nerve avulsion. At 7 days after sciatic nerve avulsion, the number of motor neuron comets in the lesioned side of spinal cord increased significantly (35%,  $p < .05$ ) compared to 5 days. The comet moment also increased ( $\sim 9.5 \times 10^5$ ) compared to 5 days (Table 2), indicating a progressive formation of DNA-SSB. The DNA content in the heads of these comets was similar to 5 days comets, but the head area was increased (Table 2) indicating looser DNA packaging. These comets had granular tails that were longer than those at 5 days [Fig. 9(B), Table 2]. No motor neuron comets were observed in the nonlesioned side of L5 at 7 days postlesion.

At 10 days after sciatic nerve avulsion subsets of lumbar motor neurons (23%) on the lesioned side were comets. Many of these comets had heads with a coma and a short granular tail [Fig. 9(C)]. Other comets had a small head or no head and a much larger

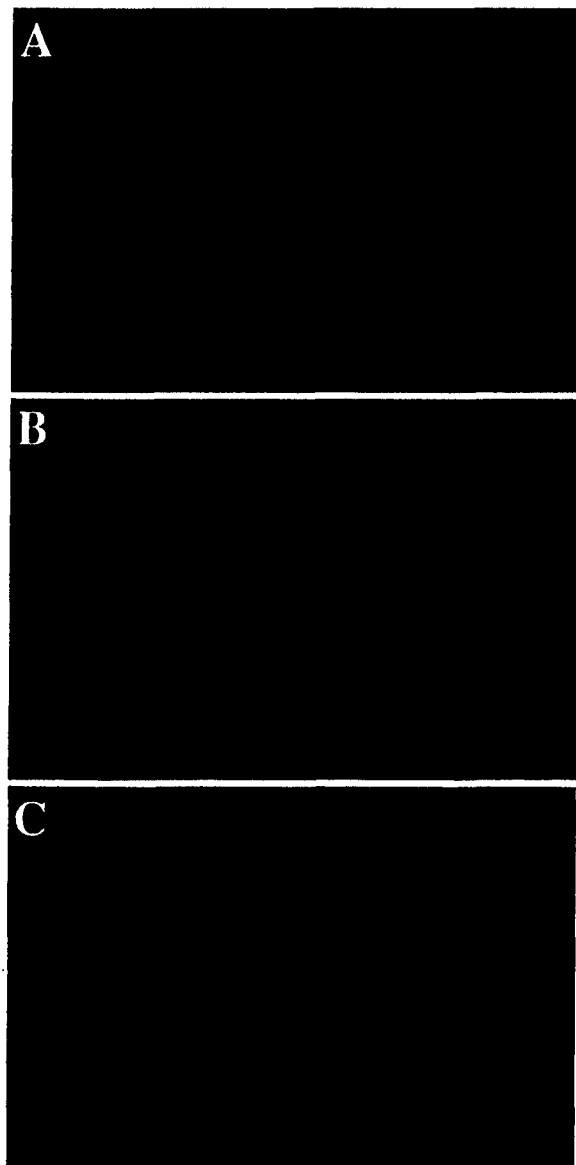


**Figure 9** DNA-SSB occur in motor neurons after unilateral sciatic nerve avulsion as detected with the comet assay. See Table 2 for measurements of DNA damage. (A) At 5 days postlesion, the comet heads are large and round and the tails are very short. (B) At 7 days postlesion, the comet heads are large and the tails are longer than at 5 days, indicating the accumulation of DNA-SSB. (C) At 10 days postlesion, motor neurons comets have an irregular head and a tail formed by scattered large granules, indicating accumulation of many DNA-SSB. Scale bars: [(A), same for (B)], 46  $\mu\text{m}$ ; C, 92  $\mu\text{m}$ .

tail [tail area = 124,199  $\mu\text{m}^2$ , Fig. 9(C), Table 2]. The heads of several comets had a nucleus with round aggregates of chromatin typical of apoptosis [Fig. 9(C)], and the tails were still comprised of large granules, although they were finer than those at 5 and 7 days. These cells had the greatest comet moments

**Table 2** DNA Damage in Motor Neurons after Sciatic Nerve Avulsion as Determined by Comet Assay<sup>a</sup>

Days After Lesion	DNA Intensity		DNA Intensity Ratio: Tail/Head	DNA Area		DNA Area Ratio: Tail/Head	Tail Length	Traditional Comet Moment ( $\times 10^3$ ) <sup>b</sup>	Comet Moment ( $\times 10^3$ ) <sup>c</sup>
	Head	Tail		Head	Tail				
5	201.4 $\pm$ 17.1	71.5 $\pm$ 23.4	0.349 $\pm$ 0.090	965 $\pm$ 139	2482 $\pm$ 1000	2.495 $\pm$ 0.777	65 $\pm$ 19	0.4463 $\pm$ 0.1521	1.8 $\pm$ 0.8
7	217.5 $\pm$ 7.5	95.9 $\pm$ 12.0	0.443 $\pm$ 0.061*	2493 $\pm$ 669*	9776 $\pm$ 1500*	4.083 $\pm$ 0.860*	261 $\pm$ 18*	2.4899 $\pm$ 0.2018*	9.5 $\pm$ 2.5*
			[ <i>F</i> (1, 3) = 10.61; <i>p</i> = 0.04]	[ <i>F</i> (1, 3) = 14.33; <i>p</i> = 0.02]	[ <i>F</i> (1, 3) = 16.72; <i>p</i> = 0.01]	[ <i>F</i> (1, 3) = 11.21; <i>p</i> = 0.03]	[ <i>F</i> (1, 3) = 12.48; <i>p</i> = 0.01]	[ <i>F</i> (1, 3) = 19.27; <i>p</i> = 0.01]	[ <i>F</i> (1, 3) = 21.10; <i>p</i> = 0.01]
10	194.4 $\pm$ 27.3	82.1 $\pm$ 22.8	0.400 $\pm$ 0.100	2517 $\pm$ 1395	24199 $\pm$ 8563*	14.500 $\pm$ 7.500*	315 $\pm$ 9*	2.5762 $\pm$ 0.6694*	19.9 $\pm$ 8.4*
					[ <i>F</i> (1, 2) = 21.23; <i>p</i> = 0.01]	[ <i>F</i> (1, 2) = 22.55; <i>p</i> = 0.01]	[ <i>F</i> (1, 2) = 21.32; <i>p</i> = 0.01]	[ <i>F</i> (1, 2) = 19.02; <i>p</i> = 0.03]	[ <i>F</i> (1, 2) = 21.41; <i>p</i> = 0.01]

<sup>a</sup> See Liu and Martin (2001b) for detailed method for the comet assay. All values are mean  $\pm$  SEM.

\* Significantly different (*p* < 0.05) from earlier time point or from 5 days postlesion. The calculated *F*-values for the analysis of variance and the post hoc probabilities are indicated for the significant values.

<sup>b</sup> Calculated from DNA intensity<sub>tail</sub>  $\times$  tail length (Hellman et al., 1995).

<sup>c</sup> Calculated from DNA intensity<sub>tail</sub>  $\times$  tail area (Liu and Martin, 2001b).

( $\sim 19.9 \times 10^5$ ), indicating accumulated DNA damage in motor neurons at 10 days after sciatic nerve avulsion (Table 2). At 14, 20, and 28 days after sciatic nerve avulsion, no comets were observed in motor neurons from either ipsilateral or contralateral lumbar ventral horns.

## DISCUSSION

Motor neuron apoptosis occurs in humans with ALS and after spinal cord trauma, but the mechanisms are unknown. We used an animal model of motor neuron degeneration to elucidate some of these possible mechanisms (Fig. 10). Avulsion of the sciatic nerve induces motor neuron apoptosis (Martin et al., 1999). Injured motor neurons exhibit metabolic activation and oxidative stress in the form of hydroxyl radical damage to DNA and ONOO<sup>-</sup> damage (Martin et al., 1999). However, another group has reported that adult spinal motor neurons die through nonapoptotic pathways (Li et al., 1998; Chan et al., 2001). This study further supports our earlier conclusion that avulsed adult motor neurons die through apoptotic mechanisms. We now show (Fig. 10) that this process occurs in association with early formation of DNA-SSB, activation and nuclear sequestration of p53, perikaryal and mitochondrial accumulation of Bax, cytochrome *c* redistribution, and activation of caspase-3. Furthermore, we show that apoptosis of motor neurons in adult spinal cord after injury is mediated by Bax and p53.

We found that apoptosis of adult motor neurons requires Bax. Bax gene deletion blocked injury-induced motor neuron apoptosis, Bax accumulation, and caspase-3 activation, but did not prevent activation of p53. Thus, Bax-effector mechanisms for motor neuron apoptosis are downstream from p53. Other experiments have shown that Bax is required for the death of peripheral neurons after neurotrophin withdrawal *in vitro* and neonatal facial motor neurons after axotomy (Deckwerth et al., 1996), as well as thalamic neurons after target deprivation in adult brain (Martin et al., 2001). Bax is important also for developmental programmed cell death of neurons (Deckwerth et al., 1996). Our study demonstrates for the first time that motor neuron apoptosis within the adult spinal cord is Bax dependent, and that the Bax accumulation is dependent on the functional p53 gene.

We have directly shown using immunogold EM that Bax accumulates in mitochondria of injured motor neurons prior to apoptosis. We also demonstrate directly that cytochrome *c* levels increase in the cytoplasm of motor neurons early during apoptosis. Our

study is the first quantitative subcellular localization analysis of Bax and cytochrome *c* in the CNS after injury. Our results are consistent with cell culture experiments showing that redistribution of Bax to mitochondria and release of cytochrome *c* are critical steps in the signaling of apoptosis (Wolter et al., 1997; Putcha et al., 1999). Bax is a member of the *bcl-2* protooncogene family (Merry and Korsmeyer, 1997), and it functions by forming channels in mitochondrial membranes (Antonsson et al., 1997). When active, these channels may allow the release of cytochrome *c* from mitochondria to the cytosol. As revealed here *in vivo*, Bax-dependent, caspase-3 activation is a key determinant in p53-mediated apoptosis of motor neurons. Cell culture models of apoptosis show that activation of caspase-3 occurs when caspase-9 proenzyme is bound by apoptotic protease-activating factor-1 (Apaf-1) in a process initiated by cytochrome *c* and either ATP or dATP (Liu et al., 1996; Li et al., 1997). Apaf-1, a 130 kD protein, serves as a docking protein for procaspase-9 and cytochrome *c* (Li et al., 1997). Apaf-1 becomes activated with the binding and hydrolysis of ATP and the binding of cytochrome *c*, promoting Apaf-1 oligomerization (Zou et al., 1999). This oligomeric complex recruits and activates procaspase-9, and active caspase-9 disassociates from the complex and becomes available to activate caspase-3.

Our *in vivo* study is also novel because we found activation of caspase-3 in adult spinal motor neurons after injury. Prominent activation of caspase-3 occurs between 7 and 9 days postlesion. Activation of caspase-3 in injured motor neurons is a far downstream event. It occurs after the initial formation of DNA-SSB, the activation of p53, and the accumulation and redistribution of Bax and cytochrome *c*. The changes in caspase-3 in apoptotic motor neurons in adult spinal cord are consistent with studies showing that activation of caspase-3 participates in the mechanisms of retinal ganglion neuron death after optic nerve transection (Kermer et al., 1999) and thalamic neuron death after cortical damage (Martin et al., 2001). Active caspase-3 cleaves a protein with DNase activity (DFF-45), and this cleavage activates a pathway leading to the fragmentation of genomic DNA. We have identified previously motor neurons undergoing nuclear DNA fragmentation between 7 and 9 days postlesion (Martin et al., 1999).

We found that p53 regulates motor neuron apoptosis. p53 accumulates in the cytoplasm and is sequestered in the nucleus of motor neurons prior to apoptosis. We also observed for the first time that p53 forms strands and inclusions in the nucleus of motor neurons undergoing apoptosis. This observation was extended by showing that p53 is functionally activated, as in-

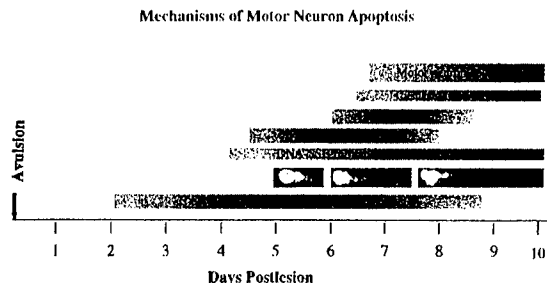


**Figure 10** Diagrammatic representation of the tentative time course of major events associated with apoptosis of motor neurons within the adult spinal cord after injury. Sciatic nerve avulsion (a lesion of motor neurons involving axotomy, target deprivation, and trauma) induces motor neurons to undergo apoptosis by 14 days postlesion (Martin et al., 1999). This apoptosis is mediated by Bax and cytochrome *c* and involves caspase-3 activation as downstream mechanisms. The upstream mechanisms are mediated by p53 in response to DNA SSB. Representative comets found at 5, 7, and 10 days postlesion (from Fig. 9) are superimposed on this time line. The DNA damage progresses as indicated by the progressive elongation of the tail and the DNA clumping in the head. These latter comets (far right profile) correspond to the time of severe DNA fragmentation as detected by *in situ* end-labeling methods (Martin et al., 1999). The initial periods of each step of the cascade may occur sequentially, but after the alteration is engaged there is overlap in the molecular stages of motor neuron apoptosis.

indicated by serine-392 phosphorylation of p53 directly in motor neurons. p53 functions in the elimination and repair of cells that have sustained DNA damage. p53 accumulation in motor neurons most likely signifies DNA damage-induced, p53-mediated apoptosis, because these neurons are terminally differentiated and accumulate DNA-SSB. This conclusion supported by the finding that p53 gene inactivation blocks motor neuron apoptosis.

We have identified previously three structural stages of motor neuron apoptosis *in vivo* (Martin et al., 1999). Neurons pass consecutively through chromatolysis, somatodendritic atrophy, and apoptosis. We have hypothesized that some yet to be identified key events associated with DNA damage occur during chromatolysis that commit neurons to apoptosis (Al-Abdulla et al., 1998; Al-Abdulla and Martin, 1998; Martin et al., 1999). This fate contrasts with other models of axonal injury that induce chromatolysis followed by partial or complete recovery and survival of neurons (Ginsberg and Martin, 1998; Martin et al., 1998). Surprisingly, cytochrome *c* changes occurred very early in the time course of motor neuron apoptosis (Fig. 10). This early accumulation may be due to enhanced synthesis during metabolic activation rather

than mitochondrial release. The nuclear accumulation and activation of p53 occurs during the chromatolytic stage of retrograde neuronal apoptosis at 4 to 5 days postlesion is also a possible key signal for the transition of chromatolytic motor neurons into apoptosis (Fig. 10). p53 activation early in the process of motor neuron apoptosis is consistent with the detection of DNA-SSB in motor neurons by 5 days after injury (Fig. 10). We suspect that the formation of DNA-SSB is an early preapoptotic mechanism of motor neuron death. More work needs to be done to identify the earliest time when DNA-SSB begin to accumulate in injured motor neurons after axonal injury.

Increased levels of p53 result primarily from increased stability of the protein (Levine, 1997). In unstressed cells, the level of p53 protein is low. The half-life of p53 is short (~5–20 min) due to rapid degradation. p53 protein levels can be increased when the half-life of the protein is extended due to diminished degradation. Inhibition of the 26 S proteasome increases p53 levels (Maki et al., 1996). Alternatively, p53 levels can be increased because the rate of initiation of p53 mRNA translation is enhanced (Levine, 1997). p53 exists in a latent, inactive form that requires modification to become active. DNA damage can activate p53 (Levine, 1997). Increases in p53 levels are proportional to the extent of DNA damage, with several different types of DNA lesions being potent signals for p53 activation, including double- and single-strand breaks and adduct formation (Levine, 1997). The induction and activation of p53 in motor neurons undergoing apoptosis is consistent with our comet assay analysis showing early formation of DNA-SSB as an upstream mechanism of neuronal apoptosis.

p53 functions as a DNA transcription factor (Vogelstein and Kinzler, 1992; Miyashita et al., 1994; Miyashita and Reed, 1995; Levine, 1997). The carboxyl terminus of p53 is important for controlling p53–DNA binding functions in response to single strands of DNA (Jayaraman and Prives, 1995). By 5 days after avulsion, nuclear accumulation of phosphorylated p53 is increased markedly in the ipsilateral ventral horn, indicating that the p53 is activated functionally. Promoters that respond to p53 include genes encoding proteins associated with growth control and cell cycle checkpoints and apoptosis. *Bax* (Miyashita and Reed, 1995) and redox-related genes (Polyak et al., 1997) are transcriptional targets of p53. These genes are relevant to motor neuron degeneration because this neuronal death is apoptosis and these neurons sustain damage to DNA (Martin et al., 1999; Liu and Martin, 2001a).

We have identified a direct relationship between

p53 and Bax. In mice with functional p53, Bax immunoreactivity increases in motor neurons undergoing apoptosis, but in  $p53^{-/-}$  mice the Bax accumulation was attenuated and motor neuron loss was blocked. Other *in vivo* studies have shown that loss of p53 function is neuroprotective in paradigms of irradiation (Wood and Youle, 1995), kainate-induced seizures (Morrison et al., 1996), focal ischemia (Crumrine et al., 1994), and target deprivation (Martin et al., 2001). Thus, we document for the first time that p53 mediates injury-induced apoptosis of motor neurons *in vivo*. This modulation of apoptosis may occur through p53 regulation of the Bax gene. The accumulation of Bax protein after the initial activation of p53 is consistent with this interpretation.

In this study, we intentionally used cell-based assays (e.g., immunocytochemistry and single-cell gel electrophoresis) to evaluate changes in p53, Bax, cytochrome c, and caspase-3, and to detect early, low-level DNA damage. We purposefully did not apply tissue homogenate-based assays (e.g., Western and Northern blotting), because motor neurons are relatively few in number compared to the nonmotor neuron cellular compartments in spinal cord. Moreover, we were interested in the cytoplasmic and mitochondrial compartments specifically of motor neurons. Tissue homogenates cannot afford this level of resolution. The small size of rat and mouse ventral horn (compared to human ventral horn) makes micropunching very difficult. Furthermore, changes in p53 and caspase-3 can occur in glial cells, notably astroglia, in response to injury (see Fig. 2; Martin et al., 2001). We also observed that activated caspase-3 accumulates in the neuropil of the lesioned L5, but is not yet clear in which cellular compartment this change occurs. These realities make difficult the appropriate interpretation of homogenate-based assays of tissues with a heterogeneous cellular composition. Therefore, we elected to evaluate motor neurons on a single-cell basis.

The key findings of this study are that apoptosis of motor neurons in the adult spinal cord requires Bax and p53. These findings are consistent with work in other, mostly *in vitro*, models of neuronal death. Despite these similarities, our work is nevertheless novel and important because we used an adult *in vivo* system of motor neuron apoptosis. Furthermore, we have identified a cascade of events leading to motor neuron apoptosis involving DNA-SSB, p53 activation, Bax upregulation and mitochondrial translocation, cytochrome c release, and caspase-3 activation. Considering the vast differences in neuroanatomical and cellular complexity, the identification of several common

neuronal death signaling pathways in *in vitro* and *in vivo* systems is notably exciting.

This proposed mechanism for motor neuron apoptosis in an animal model (Fig. 10) is particularly relevant to the pathogenesis of ALS and to *in vitro* models of motor neuron death. Motor neuron degeneration in ALS may be a form of aberrantly occurring apoptosis (Martin, 1999) that could be mediated by p53 (Martin, 2000) with DNA damage as an upstream pathogenic event (Martin, 2001). Direct evidence for DNA-lesions has been found specifically in upper and lower motor neurons of individuals with ALS (Martin, 2001); however, the possible accumulation of DNA-SSB in ALS motor needs to be evaluated. We have found that reactive oxygen species, including peroxynitrite, are potent inducers of DNA-SSB in motor neurons (Liu and Martin, 2001a, 2001b), and peroxynitrite neurotoxicity has been implicated in ALS. *In vitro* exposure of motor neurons to direct oxidative stress induces accumulation of p53 within the nucleus (Liu and Martin, 2001b) and motor neuron death (Liu and Martin, 2001a). Thus, it appears that the molecular pathogenesis of motor neuron degeneration in our *in vivo* and *in vitro* models of motor neuron disease is similar enough to ALS to warrant further study.

We are grateful for the outstanding technical assistance of Ann Price and Frank Barksdale.

## REFERENCES

- Al-Abdulla NA, Martin LJ. 1998. Apoptosis of retrogradely degenerating neurons occurs in association with the accumulation of perikaryal mitochondria and oxidative damage to the nucleus. *Am J Pathol* 153:447–456.
- Al-Abdulla NA, Portera-Cailliau C, Martin LJ. 1998. Occipital cortex ablation in adult rat causes retrograde neuronal death in the lateral geniculate nucleus that resembles apoptosis. *Neuroscience* 86:191–209.
- Antonsson B, Conti F, Ciavatta A, Montessuit S, Lewis S, Martinou I, Bernasconi L, Bernard A, Mermoud J-J, Mazzei G, Maundrell K, Gambale F, Sadoul R, Martinou J-C. 1997. Inhibition of bax channel-forming activity by bcl-2. *Science* 277:370–372.
- Calhoun ME, Jucker M, Martin LJ, Tinakaran G, Price DL, Mouton PR. 1996. Comparative evaluation of synaptophysin-based methods for quantification of synapses. *J Neurocytol* 25:821–828.
- Chan YM, Wu W, Yip HK, So KF, Oppenheim RW. 2001. Caspase inhibitors promote the survival of avulsed spinal motoneurons in neonatal rats. *NeuroReport* 12:541–545.
- Cregan SP, MacLaurin JG, Craig CG, Robertson GS, Nicholson DW, Park DS, Slack RS. 1999. Bax-dependent

- caspase-3 activation is a key determinant in p53-induced apoptosis in neurons. *J Neurosci* 19:7860–7869.
- Crumrine RC, Thomas AL, Morgan PF. 1994. Attenuation of p53 expression protects against focal ischemic damage in transgenic mice. *J Cereb Blood Flow Metab* 14:887–891.
- Deckwerth TL, Elliott JL, Knudson CM, Johnson EM Jr, Snider WD, Korsmeyer SJ. 1996. Bax is required for neuronal death after trophic factor deprivation and during development. *Neuron* 17:401–411.
- Ginsberg SD, Martin LJ. 1998. Ultrastructural analysis of the progression of neurodegeneration in the septum following fimbria-fornix transection. *Neuroscience* 86:1259–1272.
- Glücksmann A. 1951. Cell deaths in normal vertebrate ontogeny. *Biol Rev* 26:59–86.
- Hakem R, Hakem A, Duncan GS, Henderson JT, Woo M, Soengas MS, Elia A, de la Pompa JL, Kagi D, Khoo W, Potter J, Yoshida R, Kaufman SA, Lowe SW, Penninger JM, Mak TW. 1998. Differential requirement for caspase 9 in apoptotic pathways in vivo. *Cell* 94:339–352.
- Jayaraman L, Prives C. 1995. Activation of p53 sequence-specific DNA binding by short single strands of DNA requires the p53 C-terminus. *Cell* 81:1021–1029.
- Kermer P, Klöcker N, Labes M, Thomsen S, Srinivasan A, Bähr M. 1999. Activation of caspase-3 in axotomized rat ganglion cell in vivo. *FEBS Lett* 453:361–364.
- Kuida K, Zheng TS, Na S, Kuan C-Y, Yang D, Karasuyama H, Rakic P, Flavell RA. 1996. Decreased apoptosis in the brain and premature lethality in CPP32-deficient mice. *Nature* 384:368–372.
- Lefebvre S, Burglen L, Reboullet S, Clermont O, Burlet P, Viollet L, Benichou B, Cruaud C, Millasseau P, Zeviani M, LePaslier D, Frezal J, Cohen D, Weissenbach J, Munnich A, Melki J. 1995. Identification and characterization of a spinal muscular atrophy-determining gene. *Cell* 80:155–165.
- Levine AJ. 1997. p53, the cellular gatekeeper for growth and division. *Cell* 88:323–331.
- Li L, Houenou LJ, Wu W, Lei M, Prevette DM, Oppenheim RW. 1998. Characterization of spinal motoneuron degeneration following different types of peripheral nerve injury in neonatal and adult mice. *J Comp Neurol* 396:158–168.
- Li P, Nijhawan D, Budihardjo I, Srinivasula SM, Ahmad M, Alnemri ES, Wang X. 1997. Cytochrome *c* and dATP-dependent formation of Apaf-1/caspase-9 complex initiates an apoptotic protease cascade. *Cell* 91:479–489.
- Liu X, Kim CN, Yang J, Jemmerson R, Wang X. 1996. Induction of apoptotic program in cell-free extracts: requirement for dATP and cytochrome *c*. *Cell* 86:147–157.
- Liu Z, Martin LJ. 2001a. Motor neurons rapidly accumulate DNA single-strand breaks after *in vitro* exposure to nitric oxide and peroxynitrite and *in vivo* axotomy. *J Comp Neurol* 432:35–60.
- Liu Z, Martin LJ. 2001b. Isolation of mature spinal motor neurons and single cell analysis using the comet assay of early low-level DNA damage induced in vitro and in vivo. *J Histochem Cytochem* 49:957–972.
- Liu XZ, Xu XM, Hu R, Du C, Zhang SX, McDonald JW, Dong HX, Wu YJ, Fan GS, Jacquín MF, Hsu CH, Choi DW. 1997. Neuronal and glial apoptosis after traumatic spinal cord injury. *J Neurosci* 17:5395–5406.
- Maki CG, Huibregtse JM, Howley PM. 1996. *In vivo* ubiquitination and proteasome-mediated degradation of p53. *Cancer Res* 56:2649–2654.
- Martin LJ. 1999. Neuronal death in amyotrophic lateral sclerosis is apoptosis: possible contribution of a programmed cell death mechanism. *J Neuropathol Exp Neurol* 58:459–471.
- Martin LJ. 2000. p53 is abnormally elevated and active in the CNS of patients with amyotrophic lateral sclerosis. *Neurobiol Dis* 7:613–622.
- Martin LJ. 2001. Neuronal cell death in nervous system development, disease, and injury. *Int J Mol Med* 7:455–478.
- Martin LJ, Al-Abdulla NA, Brambrink AM, Kirsch JR, Sieber FE, Portera-Cailliau C. 1998. Neurodegeneration in excitotoxicity, global cerebral ischemia, and target deprivation: a perspective on the contributions of apoptosis and necrosis. *Brain Res Bull* 46:281–309.
- Martin LJ, Kaiser A, Price AC. 1999. Motor neuron degeneration after sciatic nerve avulsion in adult rat evolves with oxidative stress and is apoptosis. *J Neurobiol* 40:185–201.
- Martin LJ, Kaiser A, Yu JW, Natale JE, Al-Abdulla NA. 2001. Injury-induced apoptosis of neurons in adult brain is mediated by p53-dependent and p53-independent pathways and requires Bax. *J Comp Neurol* 433:299–311.
- Martin LJ, Price AC, Kaiser A, Shaikh AY, Liu Z. 2000. Mechanisms for neuronal degeneration in amyotrophic lateral sclerosis and in models of motor neuron death. *Int J Mol Med* 5:3–13.
- Merry DE, Korsmeyer SJ. 1997. Bcl-2 gene family in the nervous system. *Annu Rev Neurosci* 20:245–267.
- Miyashita T, Krajewski S, Krajewska M, Wang HG, Lin HK, Liebermann DA, Hoffman B, Reed JC. 1994. Tumor suppressor p53 is a regulator of *bcl-2* and *bax* gene expression in vitro and in vivo. *Oncogene* 9:1799–1805.
- Miyashita T, Reed JC. 1995. Tumor suppressor p53 is a direct transcriptional activator of the human *bax* gene. *Cell* 80:293–299.
- Morrison RS, Wenzel HJ, Kinoshita Y, Robbins CA, Donehower LA, Schwartzkroin PA. 1996. Loss of the p53 tumor suppressor gene protects neurons from kainate-induced cell death. *J Neurosci* 16:1337–1345.
- Northington FJ, Ferriero DM, Flock DL, Martin LJ. 2001. Delayed neurodegeneration in neonatal rat thalamus after hypoxia-ischemia is apoptosis. *J Neurosci* 21:1931–1938.
- Oppenheim RW. 1991. Cell death during development of the nervous system. *Annu Rev Neurosci* 14:453–501.
- Polyak K, Xia Y, Zweier JL, Kinzler KW, Vogelstein B. 1997. A model for p53-induced apoptosis. *Nature* 389:300–305.
- Putchá GV, Deshmukh M, Johnson EM Jr. 1999. Bax



- translocation is a critical event in neuronal apoptosis: regulation by neuroprotectants, Bcl-2, and caspases. *J Neurosci* 19:7476-7485.
- Roy N, Mahadevan MS, McLean M, Shutler G, Yaraghi Z, Farahani R, Baird S, Besner-Johnston A, Lefebvre C, Kang X, Salih M, Aubry H, Tamai K, Guan X, Ioannou P, Crawford TO, de Jong PJ, Surh L, Ikeda J-E, Korneluk RG, Mackenzie A. 1995. The gene for neuronal apoptosis inhibitory protein is partially deleted in individuals with spinal muscular atrophy. *Cell* 80:167-178.
- Vogelstein B, Kinzler KW. 1992. p53 function and dysfunction. *Cell* 70:523-536.
- Wolter KG, Hsu Y-T, Smith CL, Nechushtan A, Xi X-G, Youle RJ. 1997. Movement of Bax from the cytosol to mitochondria during apoptosis. *J Cell Biol* 139:1281-1292.
- Wood KA, Youle RJ. 1995. The role of free radicals and p53 in neuron apoptosis *in vivo*. *J Neurosci* 15:5851-5857.
- Zou H, Li Y, Liu X, Wang X. 1999. An Apaf-1-cytochrome *c* multimeric complex is a functional apoptosome that activates procaspase-9. *J Biol Chem* 274:11549-11556.
- Yuan J, Yankner BA. 2000. Apoptosis in the nervous system. *Nature* 407:802-809.
- Zhivotovsky B, Samali A, Gahm A, Orrenius S. 1999. Caspases: their intracellular localization and translocation during apoptosis. *Cell Death Diff* 6:644-651.

# Long-Term Culture of Mouse Cortical Neurons as a Model for Neuronal Development, Aging, and Death

Christian Lesuisse,<sup>1</sup> Lee J. Martin<sup>1,2</sup>

<sup>1</sup> Department of Pathology, Division of Neuropathology, Johns Hopkins University School of Medicine, Baltimore, Maryland 21205

<sup>2</sup> Department of Neuroscience, Johns Hopkins University School of Medicine, Baltimore, Maryland 21205

Received 4 May 2001; accepted 9 November 2001

**ABSTRACT:** A long-term cell culture system was used to study maturation, aging, and death of cortical neurons. Mouse cortical neurons were maintained in culture in serum-free medium (Neurobasal supplemented with B27) for 60 days *in vitro* (DIV). The levels of several proteins were evaluated by immunoblotting to demonstrate that these neurons matured by developing dendrites and synapses and remained continuously healthy for 60 DIV. During their maturation, cortical neurons showed increased or stable protein expression of glycolytic enzyme, synaptophysin, synapsin IIa,  $\alpha$  and  $\beta$  synucleins, and glutamate receptors. Synaptogenesis was prominent during the first 15 days and then synaptic markers remained stable through DIV60. Very early during dendritic development at DIV3,  $\beta$ -synuclein (but not  $\alpha$ -synuclein) was localized at the base of dendritic growth cones identified by MAP2 and  $\alpha$ -amino-3-hydroxy-5-methyl-4-isoxazole (AMPA) receptor GluR1. In mature neurons,  $\alpha$  and  $\beta$  synucleins colocalized in pre-synaptic axon terminals. Expression of *N*-methyl-D-aspartate (NMDA) and AMPA receptors preceded the

formation of synapses. Glutamate receptors continued to be expressed strongly through DIV60. Cortical neurons aging *in vitro* displayed a complex profile of protein damage as identified by protein nitration. During cortical neuron aging, some proteins showed increased nitration, while other proteins showed decreased nitration. After exposure to DNA damaging agent, young (DIV5) and old (DIV60) cortical neurons activated apoptosis mechanisms, including caspase-3 cleavage and poly-(ADP)-ribose polymerase inactivation. We show that cultured mouse cortical neurons can be maintained for long term. Cortical neurons display compartmental changes in the localization of synucleins during maturation *in vitro*. These neurons sustain protein nitration during aging and exhibit age-related variations in the biochemistry of neuronal apoptosis. © 2002 Wiley Periodicals, Inc. *J Neurobiol* 51: 9–23, 2002; Published online in Wiley InterScience (www.interscience.wiley.com). DOI 10.1002/neu.10037

**Keywords:** Alzheimer's disease; amyotrophic lateral sclerosis; apoptosis; NMDA receptor; Parkinson's disease; synucleins

## INTRODUCTION

The central nervous system (CNS) is vulnerable to defects, disease, and injury throughout development

and adulthood. Malformations of the CNS during development have major clinical importance (occurring in  $\approx 5$ –10 per 1000 births), causing considerable mortality and morbidity both prenatally and postnatally (Volpe, 1995). Both the immature and the mature CNS are highly vulnerable to toxic and metabolic insults such as oxygen and glucose deprivation occurring during stroke and cardiac arrest. The aging CNS is vulnerable to neurodegenerative diseases such as Alzheimer's disease, amyotrophic lateral sclerosis, Parkinson's disease, and Huntington's disease. In many settings of CNS abnormalities, neurons in the cerebral cortex are very sensitive. In the immature and

Correspondence to: L.J. Martin (lmartin@jhmi.edu).  
Contract grant sponsor: U.S. Public Health Service.  
Contract grant sponsor: National Institutes of Health.  
Contract grant sponsor: National Institute of Neurological Disorders and Stroke; contract grant number: NS34100.  
Contract grant sponsor: National Institute on Aging; contract grant number: AG16282.  
Contract grant sponsor: U.S. Army Medical Research and Materiel Command; contract grant number: DAMD17-99-1-9553.  
© 2002 Wiley Periodicals, Inc.

mature brain, neocortical neurons degenerate after hypoxia-ischemia, trauma, and seizures, and subsets of neocortical neurons degenerate in Alzheimer's disease, amyotrophic lateral sclerosis, Parkinson's disease, and Huntington's disease. Despite many advances in the understanding of mechanisms that cause abnormalities in neuronal development and loss of neuronal viability, effective restorative and therapeutic treatments for most developmental and for all of the neurodegenerative disorders of cortical neurons do not exist.

Animal and cell culture model systems are used to further understand mechanisms of neuronal dysfunction and degeneration. These *in vivo* or *in vitro* systems have particular advantages and limitations. Animal models can be used to reveal many aspects of neuronal development (Martin et al., 1998b; Furuta and Martin, 1999) and neuronal degeneration (Martin et al., 1994, 1998a, 1999, 2001; Portera-Cailliau et al., 1997a, 1997b); however, definitive comprehension of molecular, biochemical, and structural observations is often obscured, due to the inherent complexity of nervous system tissue. The confounders include coincident changes in developing or injured neurons and glial cells, as well as overlapping changes in degenerating neurons and uninjured neurons or injured recovering neurons. Furthermore, cell death in populations of neurons in the CNS is not always uniform. For example, an apoptosis-necrosis cell death continuum has been identified in animal models of excitotoxicity, cerebral ischemia, and axotomy (Martin et al., 1998a). The neuronal death continuum is influenced by the subtype of glutamate receptor that is activated and brain maturity (Martin et al., 1998a; Martin, 2001), but the mechanisms are difficult to pinpoint *in vivo*. With *in vitro* systems, although devoid of an intact tissue environment, homogeneous populations of cells that are undergoing synchronous and uniform changes can be studied, providing the appropriate system is used.

A variety of methods are available for culturing nerve cells. Primary neurons can be cocultured on a feeder layer of glial cells or cultured in media that is serum-supplemented or serum-free (Banker and Goslin, 1991). A glial feeder layer allows neuronal cultures to be studied at relatively low cell densities. Disadvantages of this method are that glial cells proliferate in serum-supplemented media, thus requiring the use of cytotoxic antimetabolic drugs that can damage neurons (Wallace and Johnson, 1989), and, in mixed-cell cultures, neurons are not studied in isolation, thus confounding the identification of neuron-autonomous changes. A major advance in neuronal cell culture occurred with the introduction of serum-

free media (Bottenstein and Sato, 1979). Subsequently, a serum-free medium was introduced that effectively supported primary hippocampal and cortical neurons (Brewer et al., 1993). With primary neuronal culture, the environment can be defined precisely, and neurons can be studied in isolation from other types of cells that can modify neuronal responses directly or indirectly, confounding the interpretation of observations.

Primary neuronal culture is a powerful tool for isolating cellular and molecular mechanisms of neuronal development, aging, and death. However, it has not been a common practice to examine the relationships between neuronal maturity and cell injury at different stages of neuronal development. Few laboratories have reported routine success at culturing primary neurons for up to 4 weeks or longer (Banker and Goslin, 1991; Kuroda et al., 1995; Porter et al., 1997; Brewer, 1997; Aksenova et al., 1999). Moreover, a thorough study that characterizes primary neurons maintained in culture over long term is not available. A goal of this study was to develop and characterize a primary cortical neuron culture system from mouse that remained viable and could be studied over long term. We studied aspects of neuronal maturation, aging, and death. We wanted to demonstrate that these neurons could be maintained viably for up to 60 days in serum-free medium, because relatively few studies exist on neuronal aging *in vitro*. These cultures were characterized extensively with a panel of antibodies to demonstrate their cellular composition, maturation, and viability. The maintained viability of these cultures was further revealed by showing that old cortical neurons, like young neurons, undergo apoptosis in response to DNA damage and can activate similar cell death mechanisms, including caspase-3 activation. We hypothesized that an age-related biochemical phenotype emerges in cultured neurons. We found that protein nitration is an age-related phenotype in neuronal culture. This neuronal culture will be useful for delineating cellular and molecular mechanisms of neuronal development, aging, and death.

## MATERIALS AND METHODS

### Mouse Cortical Neuron Culture

Embryonic day 16 mice were harvested by cesarean section from anesthetized pregnant dams (C57/B6 strain; Charles River). The animal protocol was approved by the Animal Care and Use Committee of the Johns Hopkins University School of Medicine. Cerebral cortices were isolated and

dissociated by 10% (v/v) trypsin (Life Technologies, Bethesda, MD) digestion and trituration with a fire-polished Pasteur pipette. High density cultures ( $10^6$  cells,  $\approx 1000$  cells/mm<sup>2</sup>), plated onto 35 mm tissue culture dishes, were used for Western blot analyses, and lower density cultures ( $2 \times 10^5$  cells,  $\approx 630$  cells/mm<sup>2</sup>), plated onto glass coverslips introduced into 20 mm tissue culture dishes, were used for immunocytochemical studies. Tissue culture dishes were coated with 33  $\mu$ g/mL poly-D-lysine. The cells were plated in Neurobasal medium (Life Technologies) supplemented with B27 (Life Technologies), 300  $\mu$ M glutamine (Life Technologies), 25  $\mu$ M  $\beta$ -mercaptoethanol, and streptomycin/amphotericin B (Life Technologies). Three days after plating, 50% of the medium was changed and subsequently the medium was changed every 6 days. Neuronal cultures were maintained for up to 60 days *in vitro* (DIV60).

## Immunoblotting

Total protein extracts from cortical neuron cultures (three wells for each maturational time point) were lysed in TNE buffer (10 mM Tris-HCL, pH 7.4, 150 mM NaCl, and 5 mM EDTA) containing protease inhibitors (1 mM PMSF, 10  $\mu$ g/mL leupeptin, and 10  $\mu$ g/mL pepstatin A) and detergents (2% SDS, 1% deoxycholate, and 1% NP-40), and sonicated for 15 s. Protein concentrations of each homogenate were determined by protein assay (Pierce, Rockford, IL). Homogenates were diluted further in Laemmli sample buffer.

Protein (20  $\mu$ g) from neuronal cultures were resolved on gradient SDS polyacrylamide gels (4–20%) and transferred to nitrocellulose membranes by electroblotting. Nitrocellulose membranes were preincubated in 5% nonfat dry milk (w/v) in phosphate-buffered saline (PBS). After overnight incubation with the primary antibodies in 5% nonfat dry milk and 0.05% (v/v) Tween-20 prepared in PBS, membranes were rinsed and then incubated with peroxidase-conjugated secondary antibody, and immunoreactive proteins were visualized with enhanced chemiluminescence (Amersham).

A panel of antibodies was used to characterize this neuronal culture system by immunoblotting. The maturation of cortical neuron cultures was evaluated by expression of the glycolytic enzyme glyceraldehyde phosphate dehydrogenase (GAPDH), structural protein  $\beta$ -tubulin, synaptic proteins, and subtypes of glutamate receptors. The neuronal nuclear protein NeuN revealed the relative amount of neurons at different DIVs. The level of NeuN is an accurate estimate of neuronal number in human CNS regions (Martin, 2000, 2001) and in experimental lesions in animals (Martin et al., unpublished observations). The level of glial fibrillary acidic protein (GFAP) was used to evaluate the presence of astrocytes in this cell culture system. Oxidative stress is believed to be a mechanism for cellular aging and disease (Halliwell and Gutteridge, 1986). As a biomarker for cellular aging, we evaluated peroxynitrite (ONOO<sup>-</sup>)-mediated nitration of proteins. Antibodies against GAPDH (Research Diagnostics),  $\beta$ -tubulin (Amersham), NeuN

(Chemicon),  $\alpha$ -synuclein (Transduction Laboratories), NMDAR1 (Pharmingen), synaptophysin SY38 (Boehringer), and synapsin IIa (Transduction Laboratories) were mouse monoclonal. Antibodies against  $\beta$ -synuclein (Oncogene, MA), AMPA receptor GluR2/GluR3 (Martin et al., 1993), nitrotyrosine (Upstate Biotechnology), and GFAP (Dako) were rabbit polyclonal.

## Immunolocalization in Cortical Neuron Cultures

The general method described by Liao and coworkers (1999) was followed. Cells were fixed at DIV3, DIV5, or DIV20 in 4% paraformaldehyde/4% sucrose in PBS (4°C, 20 min) and then with methanol (4°C, 10 min), and then permeabilized in 0.2% Triton X-100 and 10% NGS in PBS (4°C, 10 min), and incubated overnight at 4°C in 10% NGS in PBS with primary antibody (1:1000). The following antibodies were used for immunolocalization: mouse monoclonal antibody against  $\alpha$ -synuclein (Transduction Laboratories, KY) and MAP2 (Boehringer Mannheim Biochemicals), and polyclonal antibody against  $\beta$ -synuclein (Oncogene), synaptophysin (Dako, Denmark), and AMPA receptor GluR1 (Martin et al., 1998b). To identify the compartmental localizations of synucleins, dendritic growth cone markers were MAP2 and GluR1, and a presynaptic marker was synaptophysin. The following secondary antibodies were used: Cy<sup>TM</sup>3-conjugated goat antimouse IgG (Jackson ImmunoResearch Laboratories) and Alexa Fluor<sup>TM</sup>-conjugated goat antirabbit or goat anti-guinea pig (Molecular Probes) diluted at 1:600 in PBS. Digital images were captured with a Zeiss Axiovert/Quantix CCD camera.

## Electron Microscopy (EM) of Cortical Neuron Cultures

Neuronal cultures at DIV5 and DIV25 were evaluated by EM for ultrastructure. Media was removed and the neuronal cultures were washed briefly with PBS and then the cells were fixed with 1% glutaraldehyde in PBS for 1 h. The neuronal cultures were processed for conventional EM directly in culture plates. Plastic embedded neurons were removed from the culture plates as large blocks that were cut into pieces, trimmed, and sectioned for EM.

## DNA Damage-Induced Apoptosis in Cortical Neuron Cultures

Exposure of neurons *in vitro* to camptothecin (CPT), an inhibitor of topoisomerase-I (Hsiang et al., 1985; Bendixen et al., 1990), can induce apoptosis (Morris and Geller, 1996). CPT (Sigma, St. Louis, MO) was dissolved in double-distilled water supplemented with sodium hydroxide and heated at 55°C for 30 min to dissolve the drug completely at a final concentration of 50 mM. CPT was further diluted in Neurobasal medium. At DIV5 and DIV60, mouse cortical neurons were treated for 24 h with 100  $\mu$ M CPT. To

identify apoptosis after exposure to CPT, neurons were harvested for immunoblot analysis of protein extracts using rabbit polyclonal antibodies to cleaved caspase-3 (Cell Signaling) and poly-ADP ribose polymerase (Calbiochem, CA), or neurons were fixed and stained with Hoechst 33258 to assess nuclear morphology.

## RESULTS

### Morphological and Protein Expression Characterization of Mouse Cortical Neuron Cultures

Mouse cortical neurons were cultured over long term. Long-term mouse cortical neuron cultures were only possible when neurons were plated at high density. The cultures were characterized morphologically and biochemically. Under phase contrast microscopy, cortical neurons at DIV5 extended prominent neurites [Fig. 1(A)]. Many of these neurites were dendritic growth cones, identified ultrastructurally by the prominent polyribosomes and the tubulovesicular cisterns [Fig. 1(D,E)]. Few synapses were mature at DIV5, consistent with protein expression data for synaptic markers (Fig. 2), but many nascent synaptic junctions were present [Fig. 1(E)]. At  $\approx$ DIV20–25, cortical neurons [Fig. 1(B)] had large, pyramidal-like cell bodies ( $\approx$ 15–25  $\mu$ m). These neurons were embedded within an elaborate plexus of axons, dendrites, and synapses [Fig. 1(B,E,F)]. Immunoblotting for dendritic and synaptic proteins verified their enrichment (Fig. 2). EM showed that the nuclear morphology of the neurons at DIV5 and DIV20–25 was notably similar, suggesting a uniform population of cells [Fig. 1(D)]. At DIV60, the structural viability of the neurons was still very well maintained as shown by phase contrast microscopy [Fig. 1(C)]. However, it was apparent from phase contrast microscopy that only a subset of the original population of neurons was alive at DIV60 [compare Fig. 1(A) and (C)]. Estimates of cell counts in representative phase contrast photographs revealed that  $\approx$ 40–50% of the original population of cells at DIV5 was surviving at DIV60. These remaining neurons were healthy, as confirmed by protein expression analysis (Fig. 2).

Evaluating the protein expression of the glycolytic enzyme GAPDH, structural and synaptic proteins, and glutamate receptors (Fig. 2) demonstrated the molecular viability of cortical neurons in culture. Extracts of total protein from mouse cortical cultures at DIV5, 10, 15, 20, 25, 30, 40, and 60 were analyzed by immunoblotting. The level of GAPDH, used as a metabolic marker, was maximum (3–4-fold) around DIV25 and remained unchanged through DIV60. The level of the

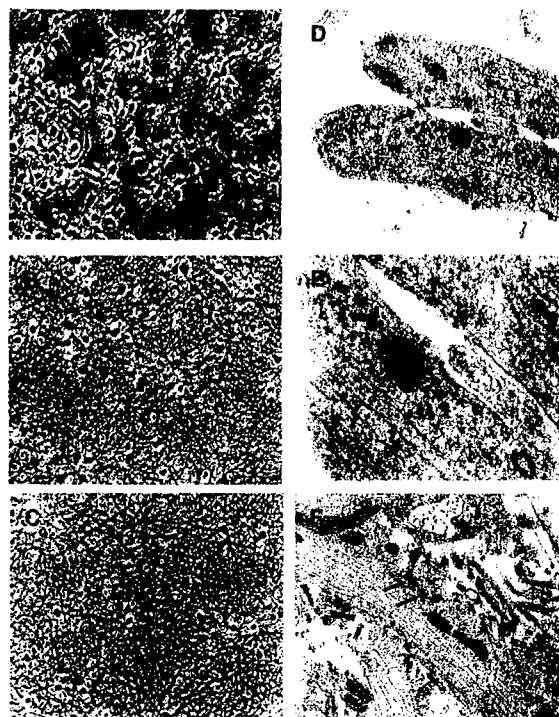


**Figure 1** Mouse cortical neurons mature and remain viable over long term in culture. Light and electron microscopy reveals the dramatic elaboration of the dendritic/axonal plexus of cortical neurons in culture between DIV5 (A, D, E) and DIV25 (B, F), with maintenance of the *in vitro* neuropil compartment through DIV60 (C). At DIV5, many growth cones are present, some of which have nascent synaptic junctions [(D, E), arrows]. By DIV25 the dendrosynaptic architecture is extensively developed [(F), arrows]. Because of the similarities in synaptic marker and cytoskeletal protein expression in cortical neuron cultures from DIV25 through DIV60 (see Figure 2), EM was not done on DIV60 cultures.

structural protein  $\beta$ -tubulin remained constant from DIV5 to DIV60. Interestingly, early in culture (DIV5), the levels of the three neuronal nuclear proteins detected with the NeuN antibody were low (Fig. 2). NeuN levels were greater at DIV10. The levels of NeuN remained relatively stable through DIV40, but by DIV60 NeuN levels declined, consistent with a loss of a subset of neurons.

Expression of synaptic proteins (synaptophysin,  $\alpha$ - and  $\beta$ -synuclein) was very low at DIV5 (i.e., faintly detectable only after prolonged exposure to film; data not shown). This Western blot finding is consistent with the EM analysis showing few synapses [Fig. 1(D,E)]. By DIV10, the expression of these synaptic proteins was increased, detectable with short exposure (Fig. 2). Synaptophysin and  $\alpha$ - and  $\beta$ -synuclein reached highest levels ( $>10$ -fold) at about DIV15–20 and DIV25, respectively. Synapsin IIa protein was

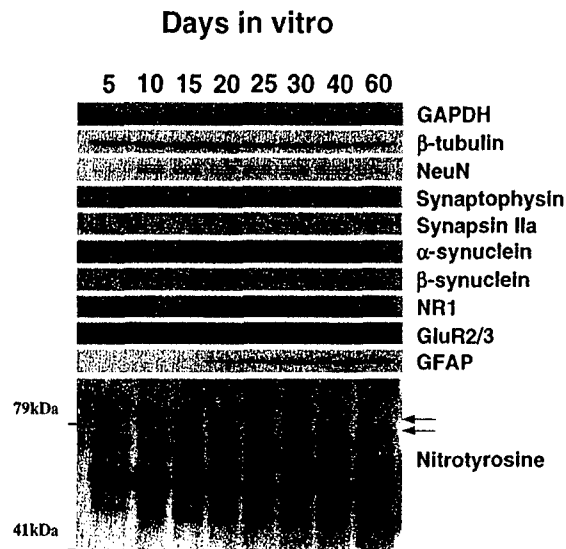


**Figure 2** Molecular maturation and aging of mouse cortical neurons in culture. The maturation and sustained viability of this long-term neuronal culture system were evaluated by the expression of glycolytic protein GAPDH, structural protein  $\beta$ -tubulin, neuronal nucleus protein NeuN, synaptic proteins (synaptophysin, synapsin IIa, and  $\alpha/\beta$ -synucleins), and glutamate receptors (NR1 and GluR2/3). Astroglial contamination was assessed by GFAP levels. To identify an age-related biochemical phenotype, protein nitration was evaluated. For the nitrotyrosine blot, molecular weight standards are shown at left. Selected immunoreactive protein bands are identified (arrows at right). Total proteins were extracted from neuronal cultures at DIV5, 10, 15, 20, 25, 30, 40, and 60. Samples (20  $\mu$ g protein) were fractionated on gradient SDS-PAGE (4–20% gels), transferred to nitrocellulose membranes, and then probed successively or in combination with specific monoclonal or polyclonal antibodies (see Materials and Methods). These results were replicated in three independent experiments.

expressed at appreciable levels only between DIV15–20, reaching highest levels at  $\approx$ DIV30, and then remaining unchanged through DIV60.

The NMDA receptor subunit NR1 and the AMPA receptor subunits GluR2/GluR3 were already expressed by DIV5, thus preceding the synaptic markers (Fig. 2). Glutamate receptor levels increased to a maximum by DIV10–15 ( $>5$ -fold) and then remained unchanged through DIV60. The high level of expression of metabolic enzyme, structural protein, synaptic proteins, and glutamate receptors demonstrates that these mouse cortical neurons remain viable and maintain structural integrity through 60 days in culture. These findings are consistent with the morphological evaluations (Fig. 1). These experiments show that these mouse cortical neurons mature, establish synapses, and remain viable over long term in culture.

Non-neuronal cell contamination of this neuronal culture system was evaluated. Previous studies have reported that astroglia comprise  $<0.5\%$  of the cell population of neurons grown in Neurobasal-B27 (Brewer et al., 1993). Interestingly, by immunoblotting, GFAP was not detected in our mouse cortical neuron cultures until DIV20 (Fig. 2). Levels of GFAP remained relatively constant from DIV20 through DIV60 (Fig. 2).

We tested the hypothesis that an accumulation of protein damage is an age-related phenotype in aging cortical neuron cultures. Protein nitration was evaluated in total protein extracts of neurons from DIV5 to DIV60. A protein band at  $\approx 55$  kD showed particularly prominent nitration in cortical cultures, but the intensity of this band was relatively invariant at different ages (Fig. 2). Other protein bands at about 60–80 kD showed selective increases or decreases in nitration as identified by nitrotyrosine immunoreactivity (Fig. 2, lower panel arrows).

### Immunocytochemical Characterization of Cortical Neuron Cultures

Immunostaining for MAP2 is widely used to identify neurons in culture (Banker and Goslin, 1991). MAP2 immunopositive cells were prevalent in this cortical neuron culture system [Fig. 3(A)], verifying the predominance of neurons in this cell culture. In immature neurons, MAP2 immunoreactivity marked dendritic growth cones of neurons [Fig. 3(A,B,D)], consistent with previous reports (Banker and Goslin, 1991). The GluR1 AMPA receptor also marks dendritic growth cones, as shown in developing rat forebrain by immuno-EM (Martin et al., 1998b). In mouse cortical neuron cultures, GluR1 was also present in dendritic growth cones [Fig. 3(E)].

Little information is available on the developmental expression and localization of synucleins in neurons, despite a possible role for synucleins in the pathogenesis of Parkinson's disease and Alzheimer's disease and in neuronal cell death (Hsu et al., 1998; Ostrerova et al., 1999). Therefore, the immunostaining patterns of synucleins were examined in cortical neuron cultures. In very immature neurons (at DIV3),  $\beta$ -synuclein was localized at dendritic growth cones (Fig. 3). Specifically,  $\beta$ -synuclein was present at the base of dendritic growth cones [Fig. 3(B–E)]. As dendrites grew in length and as presynaptic axon-dendrite interactions were established (between DIV5 and DIV10), growth cones became less prominent, and  $\beta$ -synuclein immunostaining of these structures dissipated [Fig. 4(A,B)].

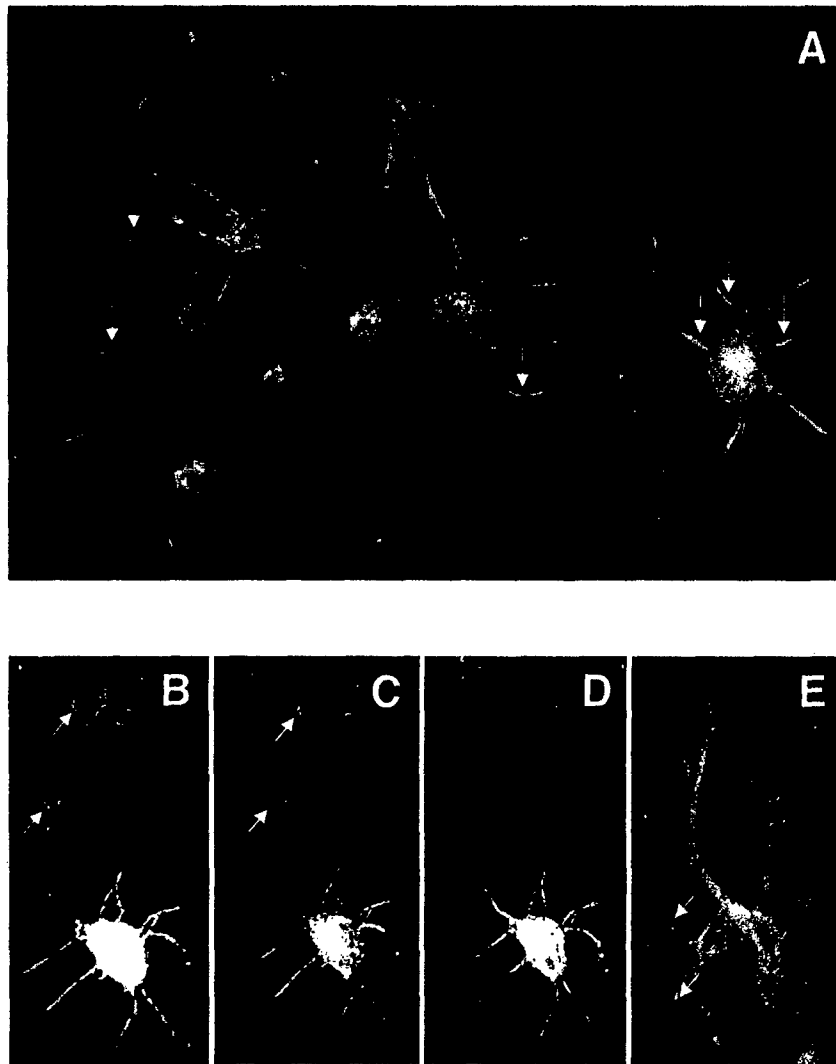


**Figure 3**  $\beta$ -synuclein is present at the base of dendritic growth cones in DIV3 mouse cortical neuron cultures. (A) Double labeling of mouse cortical neurons (at 25X magnification) for MAP2 (red) and  $\beta$ -synuclein (green). Beta-synuclein is targeted to specific dendritic domains (white arrows). Some dendrosomal domains coexpress MAP2 (sites of colocalization of MAP2 and  $\beta$ -synuclein immunoreactivities are yellow), while other dendritic regions have adjacent but non-overlapping sites where MAP2 and  $\beta$ -synuclein are present. (B) A DIV3 cortical neuron [40X magnification, same cell is illustrated in (C) and (D)] showing the localization of MAP2 (red) and  $\beta$ -synuclein (green) and the presence of  $\beta$ -synuclein at the base of dendritic growth cones (arrows). In the cell body and in some dendritic regions MAP2 and  $\beta$ -synuclein colocalize (yellow). (C) Neuron [shown in (B)] observed under the filter for  $\beta$ -synuclein staining only. Beta-synuclein has a prominent somatodendritic localization and is present within dendritic growth cones. (D) Neuron [shown in (B)] observed under the filter for MAP2 staining only. Sites of low MAP2 staining in dendritic growth correspond to locations of intense  $\beta$ -synuclein localization [see (C), arrows]. (E) Localization of AMPA receptor GluR1 (red) and  $\beta$ -synuclein (green) in dendritic growth cones. Beta-synuclein (white arrows pointing to green staining) is at the base of growth cones, whereas GluR1 is localized distally in the growth cone. In the cell body and in some dendritic regions GluR1 and  $\beta$ -synuclein colocalize (yellow).

Beta-synuclein underwent prominent changes in neuronal compartment localization during cortical neuron maturation. The localization of  $\beta$ -synuclein

showed differential dendritic targeting in cortical neurons that was maturation-related. Immunolocalization revealed that  $\beta$ -synuclein is targeted to dendrites of

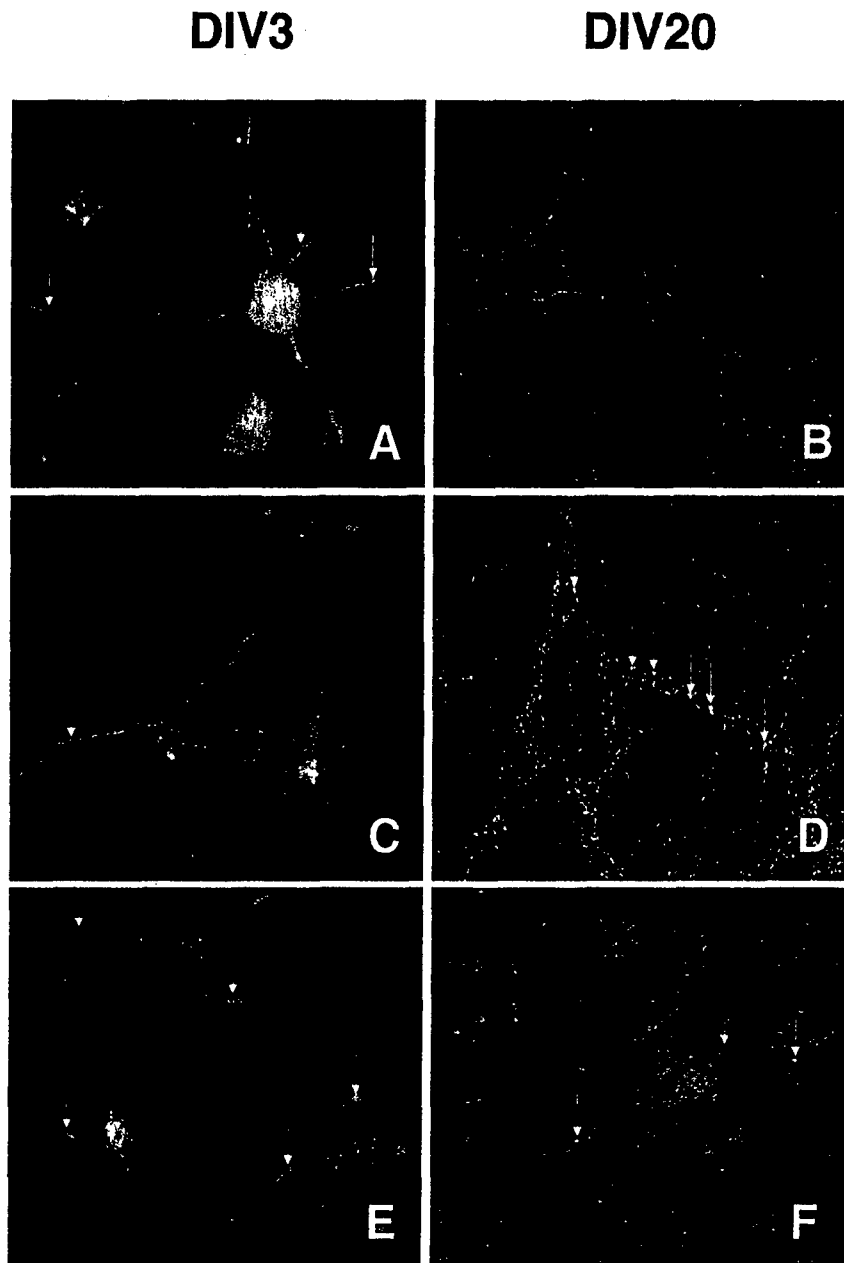


**Figure 4** Maturation-related targeting of synuclein to different neuronal compartments as shown by immunolocalization of  $\alpha/\beta$ -synucleins, MAP2, and synaptophysin in immature (DIV3) and mature (DIV20) cortical neuron cultures. (A, B) In immature neurons (A)  $\beta$ -synuclein (white arrows, green staining) is localized in the cell body and dendrites, identified by MAP2 staining (red). In mature neurons (B), MAP2 is localized throughout the cell body and dendrites (red), while  $\beta$ -synuclein has cell body (green) and presynaptic axon terminal [(B), fine green dots] localizations. (C, D) In immature neurons (C),  $\alpha$ -synuclein is expressed in neuronal cell bodies (red), but not in axons identified by synaptophysin (white arrow, green staining). In mature neurons (D),  $\alpha$ -synuclein (green) has a prominent presence in presynaptic axon terminals (fine green dots) that have a similar appearance and distribution as synaptophysin staining (red). These terminals, many of which show colocalization of  $\alpha$ -synuclein and synaptophysin (white arrows, yellow staining), decorate the surfaces of unstained dendrites and the surface of the cell body (part of this cell is enlarged as Figure 5). (E, F) In immature neurons (E),  $\alpha$ -synuclein is concentrated in neuronal cell bodies (red), and  $\alpha/\beta$ -synucleins colocalize (yellow) in subsets of neuronal cell bodies, but only  $\beta$ -synuclein is found in growing dendrites (white arrows, green staining). In mature neurons (F),  $\alpha/\beta$ -synucleins colocalize (yellow) in subsets of neurons and in numerous presynaptic axon terminals (white arrows, fine yellow dots).



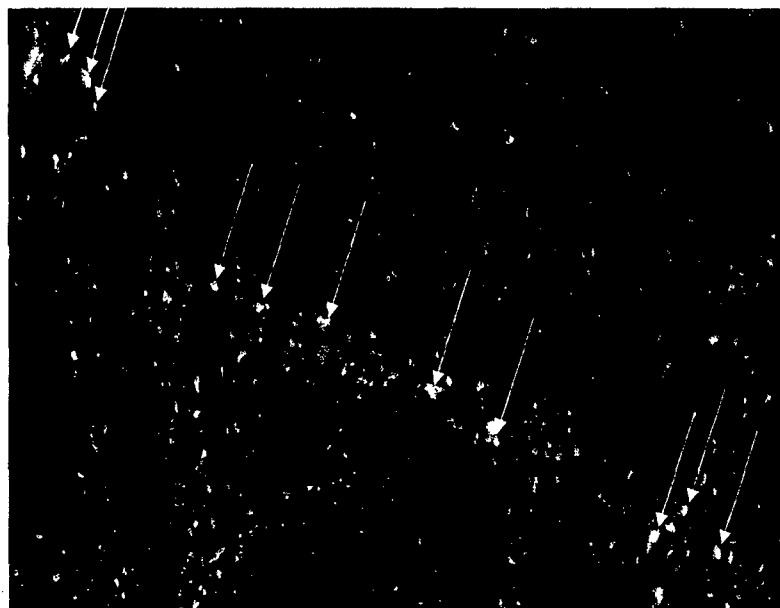


**Figure 5** Presynaptic localization of  $\alpha$ -synuclein in mature cortical neurons. In DIV20 cortical cultures, some large pyramidal neurons expressing synaptophysin (red) are enmeshed in a field of axons and synapses that stain for synaptophysin (red) and  $\alpha$ -synuclein (green). The dendrites of this neuron are not stained for synaptophysin or  $\alpha$ -synuclein but their surfaces are decorated with axodendritic boutons (red, synaptophysin; green,  $\alpha$ -synuclein), with a subset that colocalizes synaptophysin and  $\alpha$ -synuclein (white arrows, yellow staining). Axosomatic boutons *en passage* also colocalize synaptophysin and  $\alpha$ -synuclein (white arrows, yellow staining).

immature neurons but not to dendrites of mature neurons [Fig. 4(A,B)]. Specifically, in DIV3 neurons  $\beta$ -synuclein was often observed in MAP2-positive dendrites, but in DIV20 neurons colocalization of  $\beta$ -synuclein and MAP2 was observed rarely [Fig. 4(A,B)]. Instead, in mature cortical neuron cultures,  $\beta$ -synuclein was found in axon terminals [Fig. 4(B,F)].

In immature cortical neurons,  $\alpha$ -synuclein was not prominently found in dendrites, but was more apparent in neuronal cell bodies [Fig. 4(C)]. As cortical neurons matured and formed synapses,  $\alpha$ -synuclein became localized in presynaptic axon terminals, as evidenced by the colocalization with synaptophysin [Figs. 4(D) and 5]. At DIV20, large synaptophysin-positive, pyramidal cortical neurons were embedded in a network of axons and synapses [Figs. 4(D) and 5]. The surfaces of these pyramidal neurons were decorated with axodendritic and axosomatic synapses (Fig. 5, red synaptophysin, green  $\alpha$ -synuclein), and some of these presynaptic terminals showed colocalization of synaptophysin and  $\alpha$ -synuclein (Fig. 5, yellow identified by white arrows). In mature cortical neurons,  $\alpha$ - and  $\beta$ -synuclein colocalized in axon terminals [Fig. 4(F)] but not in growing dendrites of immature neurons [Fig. 4(E)].

### Old and Young Cortical Neurons Activate Apoptotic Mechanisms in Response to DNA Damage

As an indirect assessment of the viability of remaining cortical neurons, they were exposed to a chemical stressor to induce cell death. We examined whether DIV60 neurons undergo apoptosis or necrosis (or are insensitive to chemical stressor) compared to DIV5 neurons. Hoechst 33258 was used to assess nuclear morphology in control and poisoned cells. The Hoechst 33258 staining pattern in control cells was uniform [Fig. 6(A)], supporting the EM observations that suggested a uniform population of cells. Exposure of neurons to CPT (100  $\mu$ M for 24 h), an inhibitor of topoisomerase-I that causes DNA damage (Hsiang et al., 1985; Bendixen et al., 1990), induced morphologically confirmed apoptosis of cortical neurons [Fig. 6(B)], consistent with the original report (Morris and Geller, 1996). DIV5 and DIV60 mouse cortical neurons were exposed to CPT, and protein extracts were examined for caspase-3 activation and PARP cleavage. PARP cleavage was used as a functional assay for apoptosis in young and old neurons, because PARP cleavage is an indicator of caspase-3 activation (Lazebnik et al., 1994). After insulting the

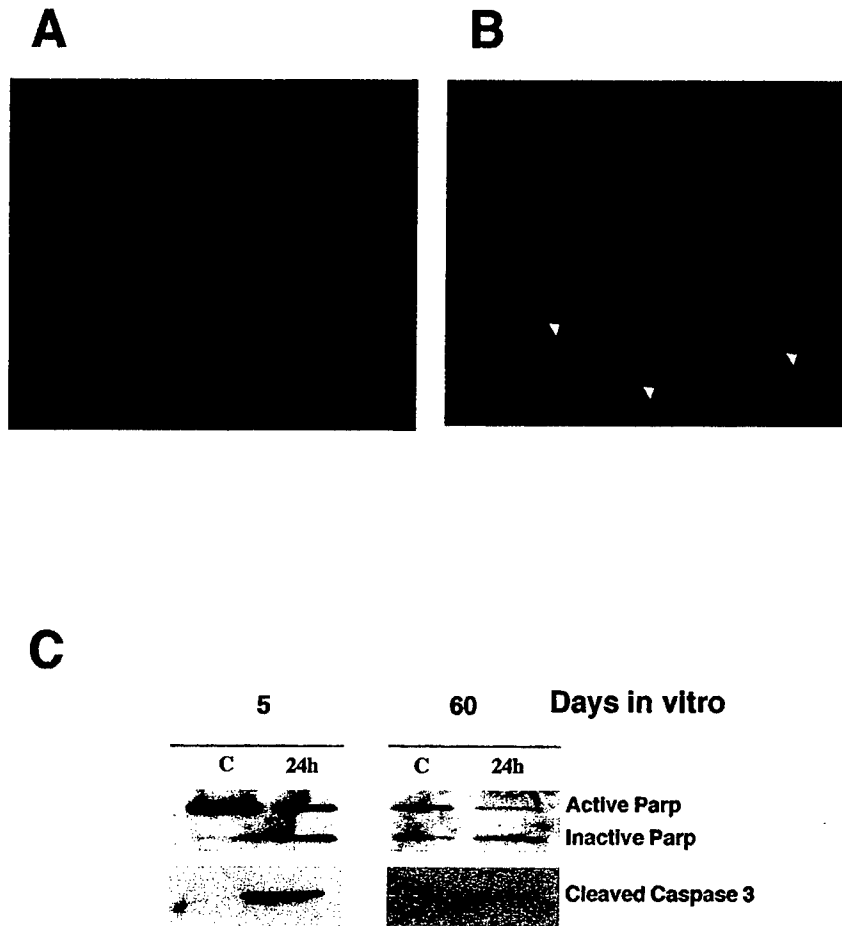


**Figure 6** DNA damage induces apoptosis in young and old cortical neuron cultures. (A) Control cortical neurons at DIV5 stained with Hoechst 33258 showing a uniform normal nuclear morphology. (B) Hoechst 33258 staining of DIV5 neurons undergoing apoptosis (arrowheads) induced by CPT. The nuclear condensation and formation of round blue-staining masses are indicative of apoptosis. The apoptosis was relatively homogeneous and synchronous. (C) Immature (DIV5) and old (DIV60) neurons were exposed to an apoptotic stimulus (DNA damage by CPT), and PARP degradation and caspase-3 cleavage were used to assess activation of apoptosis mechanisms. Total proteins were extracted from DIV5 and DIV60 neuronal cultures that were untreated (control, C) or treated with CPT for 24 h. Samples (20  $\mu$ g protein) were fractionated on gradient SDS-PAGE (4–12% gels), transferred to nitrocellulose membranes, and then probed with antibodies to PARP and cleaved caspase-3. Both DIV5 and DIV60 neurons that were exposed to CPT showed inactivation of PARP and activation of caspase-3. The caspase-3 cleavage was stronger in immature neurons. Exposure of DIV5 blot was shorter than exposure of DIV60 blot.

cells, both DIV5 and DIV60 neurons showed biochemical evidence for apoptosis, as indicated by the increase in cleaved caspase-3 and accumulation of inactivation cleavage products of PARP [Fig. 6(C)].

## DISCUSSION

A goal of this study was to develop and characterize a primary cortical neuron culture system from mouse that remains viable and can be studied over long term.

This work was done because studies of primary neuron cultures at DIV25–30 and beyond are infrequent (Banker and Goslin, 1991; Brewer et al., 1993; Kuroda et al., 1995; Brewer, 1997; Porter et al., 1997; Aksenova et al., 1999). Furthermore, studies demonstrating a thorough characterization of primary neurons maintained in culture over long term are not available. In addition, it is uncommon to examine the effects of cell injury on neurons at different stages of maturity. It is important to study neuronal cultures over long term to provide insight into cell-autono-

mous mechanisms of neuronal aging and death and to identify differential mechanisms regulating neuronal cell death forms that are found in developing and adult CNS (Martin, 2001).

This study documents the feasibility and usefulness of a long-term culture of mouse cortical neurons. This cell system was characterized thoroughly using morphological and immunoblotting methods. The neuronal composition as well as the maturation and viability of these neurons for up to DIV60 were shown by phase contrast microscopy, EM, and immunocytochemistry for MAP2, synaptophysin, and synuclein. These neurons grow very well, as evidenced by the dendritic maturation and synaptogenesis. A comparison of our morphological results with other studies is difficult because most of the published phase contrast images are from hippocampal neuron cultures instead of cortical neuron cultures. Our structural findings were supported by Western blot analyses demonstrating the developmental profiles for synapse markers and glutamate receptors. These markers are often studied in hippocampal neuron culture but not often in cortical neuron culture. The expression of the glycolytic enzyme GAPDH and the structural protein  $\beta$ -tubulin confirmed the sustained viability of these neurons. However, based on phase contrast microscopy and NeuN levels, it seems that only a subset of the original population of neurons survives through DIV60. This is an important distinction between DIV20–25 neurons and DIV60 neurons. Older cultures have fewer neurons than younger mature cultures. Thus, there is spontaneous age-related loss of neurons in this system. The maintained levels of GAPDH and the structural protein  $\beta$ -tubulin reveal that the metabolic and structural integrity of surviving cortical neurons is preserved through DIV60.

The precise extent of cellular homogeneity of this neuronal culture is not yet fully ascertained, but it is predominantly neuronal. There is, however, a low level of astroglial contamination based on GFAP immunoblots. Morphological data derived from phase contrast microscopy, EM, and immunocytochemistry show the predominance of neurons. These neurons can assume pyramidal neuron morphology, but dendritic spines are not prominent as in the *in vivo* state. The nuclear morphology in normal cells stained with Hoechst dye is very similar in the cell population, and, after an apoptotic stimulus, the cells undergo apoptosis synchronously with a similar morphology. Both of these observations indicate a homogeneous population of cells. However, although these cell cultures are mostly neurons, different types of neurons (pyramidal vs. interneurons) could be present, but GABAergic

interneurons comprise <5% of the neurons in rat cortical cultures (De Lima and Voigt, 1997).

## Methodological Considerations

A variety of methods are available for culturing nerve cells. Primary neurons can be cocultured on a glial feeder layer with serum (Banker and Goslin, 1991). Glial cells support neurons in culture (Banker, 1980; Unsicker et al., 1987) through humoral factors released into the culture medium and contact-dependent interactions (Manthorpe et al., 1988). Glial conditioned medium can modify gene expression in rat hippocampal neuron culture, thus glial conditioned medium may also affect neuronal activity (Lesuisse et al., 2000). Astroglia protect neurons in culture from toxicity (Ye and Sontheimer, 1998). Astroglia actively uptake glutamate, which is transformed enzymatically, by glutamine synthetase, to glutamine (Hertz et al., 1983; Schousboe et al., 1977). Glutamine is an important precursor for nucleic acids and proteins and is critical for cellular proliferation.

Primary neurons can be cultured also without a glial feeder layer but in media that is serum-supplemented (Banker and Goslin, 1991). To block potential excitotoxic effects of glutamate in the absence of astroglia and to maintain primary hippocampal neurons for 3–4 weeks, NMDA and AMPA receptors can be blocked by supplementing culture medium with DL-2-amino-5-phosphonovaleric acid and 6-cyano-7-nitroquinoxaline-2,3-dione (Liao et al., 1999). Other investigators use culture medium supplemented with fibroblast growth factor to keep primary neurons alive for over 7 days in culture (Ray et al., 1993). Glial feeder layers, glial conditioned medium, NMDA, and AMPA receptor antagonists, or growth factors are proven devices for maintaining routine long-term primary neuron culture, but they render interpretation of pharmacological and biochemical studies of neurons *in vitro* far more complex.

The application of new serum-free medium supplemented with B27, without added neurotrophic factors or a glial feeder layer, has profoundly improved neuronal survival in culture (Brewer et al., 1993). It was reported originally that in Neurobasal-B27 medium a nearly pure neuronal culture could be maintained for 4 weeks with >90% viability with cells plated at 640/mm<sup>2</sup> and >50% viability of cells plated at 160/mm<sup>2</sup> (Brewer et al., 1993). Assessment of glial contamination was done by immunocytochemical detection of GFAP in DIV4 cultures. Our immunoblotting results for GFAP confirm earlier work (Brewer et al., 1993) and extend the characterization of these cultures by showing the emergence of GFAP at

DIV20. The few astroglia in these cultures may proliferate at DIV15 through DIV25, and then cease to divide after DIV25. However, the low concentrations of amino acids in Neurobasal medium are insufficient for glial proliferation (Brewer et al., 1993). A more likely explanation is that the few astrocytes present early in these cultures upregulate GFAP, but after DIV20 the ratio of glial protein to neuronal protein does not increase.

Despite the introduction of B27-supplemented Neurobasal medium, studies of primary neuron cultures for long term are very rare. Only two other studies have demonstrated the benefit of serum-free B-27 supplemented Neurobasal medium for long-term neuronal culture (Aksenova et al., 1999; Xie et al., 2000). Both of these previous studies used embryonic rat hippocampal neurons instead of embryonic mouse cortical neurons. The molecular viability of the hippocampal neuron cultures was assessed in only one of these studies, using  $\beta$ -actin as a marker, which declined after DIV20 (Aksenova et al., 1999). We evaluated the expression of many proteins in our mouse cortical neuron cultures, including GAPDH,  $\beta$ -tubulin, synaptophysin, synapsin IIa,  $\alpha$ - and  $\beta$ -synucleins, as well as NMDA and AMPA glutamate receptors, and found stable levels up to DIV60.

The paucity of information on long-term neuronal cultures is likely due to the extreme technical difficulty in culturing healthy dissociated primary neurons for durations of 3–4 weeks or longer. Thus, our study helps to fill this gap in the available data on long-term culturing of neurons. Our success in establishing a long-term culture of primary neurons could be attributed to reagents and technique. The use of Neurobasal medium supplemented with B27 is critical. B27 contains several antioxidants (Brewer et al., 1993) with known protective actions on neurons, and we also added  $\beta$ -mercaptoethanol to the medium, which has been found to help sustain viability of mouse cortical neurons in culture (Ishii et al., 1993). Other laboratories usually do not supplement neuronal culture medium with  $\beta$ -mercaptoethanol. The meticulous care in processing cortices from the dissection to dissociation steps may also contribute to the viability (Brewer, 1997). The trypsinization of cortices is an important early step for primary cortical neuron culture. We incubate cortices at 37°C for 20 min in Hanks medium supplemented with 10% (v/v) trypsin solution (Life Technologies; catalogue #15090046). We have observed that the effectiveness of trypsin varies in different batches. Trypsin effectiveness also decreases with storage, possibly due to differences in enzymatic activity; thus, the final concentration of activity used for cortical digestion may vary. We also suspect that

the trituration of cortical digests should not exceed 10–15 times for long-term cultures. Rather than increasing the trituration, it is advisable to routinely chop the tissues into small pieces (as small as possible) and to use more trypsin (up to an additional 20%).

### Protein Nitration Profiling in Aging Mouse Cortical Neuron Cultures

We tested the hypothesis that neurons aging *in vitro* accumulate oxidative damage. Only one other study has reported a progressive increase in oxidative damage in the form of protein carbonyl formation in rat hippocampal neurons aging in culture (Aksenova et al., 1999). The specific type of oxidative damage of interest to us was via ONOO<sup>-</sup> because of its possible role in the pathogenesis of cortical neuron degeneration after cerebral ischemia and in upper motor neurons of individuals with ALS (Beckman et al., 1992; Martin et al., 2000a, 2000b; Martin, 2001). ONOO<sup>-</sup> is a potent and relatively long lived reactive oxygen species, formed by a reaction between superoxide and nitric oxide (NO), which nitrates proteins through the formation of nitrotyrosine (Beckman et al., 1992).

We tested the hypothesis that an accumulation of protein damage is an age-related phenotype in cortical neuron cultures. We used nitrotyrosine formation as a bioassay for age-related oxidative damage to protein in cortical neuron cultures. A band at  $\approx$ 55 kD showed particularly prominent nitration in cortical cultures, but the level of nitration varied little with *in vitro* aging. A similar nitrated protein has been identified *in vivo* in brain that is  $\beta$ -tubulin, and the nitration of  $\beta$ -tubulin increases after cerebral ischemia (Martin et al., 2000a). Other protein bands at about 60–80 kD showed selective increases or decreases in nitration in cortical neuron cultures. The size of these proteins is consistent with the identification of nitrated low molecular weight neurofilament in human CNS (Strong et al., 1998). Our findings are novel because the level of protein nitration changes as cortical neurons age *in vitro*. Interestingly, there appears to be a specific protein nitration profile in aging cortical neurons. Some proteins accumulate nitration, whereas other proteins appear to show reduced nitration. Reduced nitration may be due to decreased nitration of intact protein or to degradation of nitrated protein. To our knowledge, this is a new finding. The source of the NO for the formation of ONOO<sup>-</sup> is presently unknown. Some of these cortical neurons are interneurons (De Lima and Voigt, 1997) and thus may contain NO synthase, thereby providing a source for NO. Maintaining cortical neuron cultures beyond DIV20–25

will allow for further exploration of protein nitration profiling, the proteins that are vulnerable to ONOO<sup>-</sup> attack at different stages of maturation, and the cellular management of nitrated proteins, particularly in older neurons.

### Old Cortical Neurons Can Activate Apoptosis Mechanisms

The structure of neuronal death after brain injury can vary depending on animal age (Martin, 2001). We examined whether older neurons can be stimulated to undergo apoptosis, similar to younger cortical neurons in culture. This experiment was done for two reasons: as an indirect assay of the viability of remaining cortical neurons, and to begin to evaluate if cell death mechanisms in young and old neurons are different or similar. DIV5 and DIV60 neurons were exposed to the DNA damaging agent CPT. Insulted DIV60 neurons, like DIV5 neurons, activated apoptosis mechanisms, such as caspase-3 cleavage and PARP inactivation. However, the magnitude of caspase-3 cleavage in old and young neurons after injury appears to be different. These observations suggest that caspase-3 biochemistry is different in stressed immature and mature neurons, further underscoring the usefulness of the long-term cortical culture. Age-related differences in caspase-3 activation could partly explain observations on age-related differences in neuronal cell death phenotypes that have been identified *in vivo* (Martin, 2001). To better understand the influence of neuronal maturity on neuronal cell death, immature and mature neurons need to be used in *in vitro* models of cell death, once more reinforcing the need for long-term cultures of neurons from the same batches of embryos.

With *in vitro* neuronal death systems the general health of the neurons undergoing the toxicological stress is an important concern. Cell injury paradigms with unhealthy cell systems will not likely yield information that accurately reflects a typical cellular response and will be less relevant to the *in vivo* state. If experiments are done on cells that will die spontaneously near the time at which an insult is delivered, then inappropriate conclusions could be made on the cell death mechanisms. It is important to document the longevity of a neuronal cell culture system. In our study, the cells were maintained until DIV60 and could still activate molecular pathways for apoptosis. Maintaining the cells to DIV60 was arbitrary. The observations on apoptosis attest to the healthy condition of these long-term neuronal cultures and strengthen our confidence that neuronal cell death experiments on fully mature but younger cultures

(e.g., DIV25–30 neurons) will be representative of initially healthy cells that are undergoing a stress or toxin induced death process. This study is the first demonstration of apoptosis in *in vitro* aged neuronal cultures. Old cortical neurons, like young neurons, undergo apoptosis in response to DNA damage and can activate similar cell death mechanisms, including caspase-3 activation.

### Synaptogenesis in Mouse Cortical Neuron Cultures

Mouse cortical neurons in culture can mature into pyramidal-like neurons and develop extensive dendritic and axonal arbors and form numerous synapses. At DIV5, expression of synaptic proteins (synaptophysin,  $\alpha$ - and  $\beta$ -synuclein) was very low. These Western blot observations were confirmed by immunolocalization studies of synaptophysin and by EM. The levels of synaptic proteins were higher at DIV10. Synaptophysin reached highest levels (>10-fold) at  $\approx$ DIV15–20. However, synapsin IIa protein became expressed at appreciable levels only between DIV15–20, reaching highest levels at  $\approx$ DIV30. NMDA receptor subunit NR1 and the AMPA receptor subunits GluR2/GluR3 were expressed by DIV5; thus, glutamate receptor expression precedes the expression of appreciable levels of presynaptic markers. We have made this observation in prior Western blot studies of fetal and postnatal brain development (Martin et al., 1998b; Furuta and Martin, 1999). We also observed with *in vitro* developing cortical neurons that the levels of  $\beta$ -tubulin are surprisingly invariant. In rat brain, the expression of  $\beta$ -tubulin was also found to be unchanged from the embryonic to adult stages (Martin et al., 1998b). It appears that aspects of synaptogenesis in mouse cortical neuron culture are consistent with *in vivo* developmental events related to synapse formation (Knaus et al., 1986; Fletcher et al., 1991; Martin et al., 1998b; Furuta and Martin, 1999).

The functional significance of the observed changes in glutamate receptor expression in developing mouse cortical neurons is not yet clear. Other studies of dissociated cortical neurons cultured from postnatal rat at 1–15 days old have identified normal physiological properties for both NMDA and non-NMDA glutamate receptors (Huettner and Baughman, 1986). In cultures of rat neocortical neurons, the frequency of spontaneous inward events is reported to increase fourfold from DIV6–15 to DIV26–35, suggesting that neurons in culture undergo major functional changes during their maturation (Zona et al., 1994).

## **$\alpha$ and $\beta$ Synucleins Have Distinct Dendritic and Axonal Localizations during Development of Mouse Cortical Neurons in Culture**

In developing mouse cortical neurons we found that  $\alpha$  and  $\beta$  synucleins are localized differentially. Importantly, we observed for the first time that  $\beta$ -synuclein, but not  $\alpha$ -synuclein, is selectively localized within dendritic growth cones. MAP2 and GluR1 were used as known markers for dendrites. Beta-synuclein was present at the base of dendritic growth cones at DIV3, suggesting a function in the formation or guidance of growing dendrites in immature cortical neurons. The visualization of  $\beta$ -synuclein in dendritic growth cones is also another indicator of the integrity of these cultured cortical neurons, because of the relative ease of identifying growth cones in immature cultures using conventional microscopy.

We also found that  $\beta$ -synuclein undergoes prominent changes in neuronal compartment localization during cortical neuron maturation. Although  $\beta$ -synuclein is targeted to dendritic growth cones in immature neurons, in mature neurons  $\beta$ -synuclein is targeted to axon terminals where it colocalizes with  $\alpha$ -synuclein. A synaptic terminal localization for  $\alpha$ - or  $\beta$ -synucleins has been found previously in rat hippocampal neuron cultures at DIV14 (Withers et al., 1997; Murphy et al., 2000) and in adult mouse brain (Hsu et al., 1998). In zebra finch cerebellum, synelfin ( $\alpha$ -synuclein) was found to overlap significantly with a synaptic protein, synaptotagmin, but it remained uncertain whether the localization was at pre- or postsynaptic sites (George et al., 1995). Alpha- and  $\beta$ -synuclein colocalization in synaptic terminals of hippocampal neurons has been shown before (Murphy et al., 2000). We show for the first time a prominent colocalization of  $\alpha$ - and  $\beta$ -synucleins in synaptic terminals of cortical neurons but not in dendrites of DIV20 cortical neurons.

## **CONCLUSION**

The novelty of this study is found in six aspects. First, the feasibility of maintaining a viable long-term primary mouse cortical neuron culture is demonstrated. Second, a thorough characterization of this culture from DIV5 to DIV60 was done using microscopic and immunoblotting methods. Third, old cortical neurons (DIV60), like young neurons, were found to undergo apoptosis in response to DNA damage and can activate similar cell death mechanisms. Fourth, protein nitration is an age-related phenotype in neuronal cul-

ture. Fifth, cortical neurons *in vitro*, like hippocampal neurons, express glutamate receptors prior to the major period of synaptogenesis. Sixth,  $\beta$ -synuclein, but not  $\alpha$ -synuclein, is present in dendritic growth cones in developing neurons, and  $\alpha$ - and  $\beta$ -synucleins are differentially localized in immature neurons but have common presynaptic localizations in mature neurons. This study is the first to evaluate aspects of neuronal development and aging, as well as mechanisms of cell death in immature and mature cortical neurons.

The authors are grateful for the expert technical assistance of Frank Barksdale.

## **REFERENCES**

- Aksenova MV, Aksenov MY, Marksesbery WR, Butterfield DA. 1999. Aging in a dish: age-dependent changes of neuronal survival, protein oxidation, and creatine kinase BB expression in long-term hippocampal cell culture. *J Neurosci Res* 58:308–317.
- Banker G, Goslin K. 1991. Culturing nerve cells. Cambridge, MA: MIT Press. 453 p.
- Banker GA. 1980. Trophic interactions between astroglial cells and hippocampal neurons in culture. *Science* 209: 809–810.
- Beckman JS, Chen J, Ischiropoulos H, Conger KA. 1992. Inhibition of nitric oxide synthesis and cerebral neuroprotection. In: Kriegstein J, Oberpichler-Schwenk H, editors. *Pharmacology of cerebral ischemia*. Stuttgart: Wissenschaftliche Verlagsgesellschaft, p 383–394.
- Bendixen C, Thomsen B, Alsner J, Westergaard O. 1990. Camptothecin-stabilized topoisomerase I-DNA adducts cause premature termination of transcription. *Biochem* 29:5613–5619.
- Bottenstein JE, Sato GH. 1979. Growth of a rat neuroblastoma cell line in serum-free supplemented medium. *Proc Natl Acad Sci USA* 76:514–517.
- Brewer GJ. 1997. Isolation and culture of adult rat hippocampal neurons. *J Neurosci Meth* 71:143–155.
- Brewer GJ, Torricelli JR, Evege EK, Price PJ. 1993. Optimized survival of hippocampal neurons in B27-supplemented Neurobasal, a new serum-free medium combination. *J Neurosci Res* 35:567–576.
- De Lima AD, Voigt T. 1997. Identification of two distinct populations of  $\gamma$ -aminobutyric acideric neurons in cultures of the rat cerebral cortex. *J Comp Neurol* 388:526–540.
- Fletcher TL, Cameron P, De Camilli P, Banker G. 1991. The distribution of synapsin I and synaptophysin in hippocampal neurons developing in culture. *J Neurosci* 11: 1617–1626.
- Furuta A, Martin LJ. 1999. Laminar segregation of the cortical plate during corticogenesis is accompanied by changes in glutamate receptor expression. *J Neurobiol* 39:67–80.

- George JM, Jin H, Woods WS, Clayton DF. 1995. Characterization of a novel protein regulated during the critical period for song learning in the Zebra Finch. *Neuron* 15:361-372.
- Halliwell B, Gutteridge JMC. 1986. Oxygen free radicals and iron in relation to biology and medicine: some problems and concepts. *Arch Biochem Biophys* 246:501-514.
- Hertz L, Yu ACH, Potter RL, Fisher TE, Schousboe A. 1983. Metabolic fluxes from glutamate and towards glutamate in neurons and astrocytes in primary cultures. In: Hertz L, Kvamme E, McGeer EG, Schousboe A, editors. *Glutamine, glutamate and GABA in the central nervous system*. New York: Alan R. Liss, p 327-342.
- Hsiang YH, Hertzberg R, Hecht S, Liu LF. 1985. Camptothecin induced protein-linked DNA breaks via mammalian DNA topoisomerase I. *J Biol Chem* 260:14873-22580.
- Hsu LJ, Mallory M, Xia Y, Veinbergs I, Hashimoto M, Yoshimoto M, Thal LJ, Saitoh T, Masliah E. 1998. Expression pattern of synuclein (Non-A $\beta$  amyloid component of Alzheimer's disease amyloid precursor protein/ $\alpha$ -synuclein) during murine brain development. *J Neurochem* 71:338-344.
- Huettner JE, Baughman RW. 1986. Primary culture of identified neurons from the visual cortex of postnatal rats. *J Neurosci* 6:3044-3060.
- Ishii K, Katayama M, Hori K, Yodoi J, Nakanishi T. 1993. Effects of 2-mercaptoethanol on survival and differentiation of fetal mouse brain neurons cultured in vitro. *Neurosci Lett* 163:159-162.
- Knaus P, Betz H, Rehm H. 1986. Expression of synaptophysin during postnatal development of the mouse brain. *J Neurochem* 47:1302-1304.
- Kuroda Y, Kobayashi K, Ichikawa M, Kawahara M, Muramoto K. 1995. Application of long-term cultured neurons in aging and neurological research: aluminum neurotoxicity, synaptic degeneration and Alzheimer's disease. *Gerontology* 41(suppl 1):2-6.
- Lazebnik YA, Kaufmann SH, Desnoyers S, Poirier GG, Earnshaw WC. 1994. Cleavage of poly(ADP-ribose) polymerase by a proteinase with properties like ICE. *Nature* 317:346-347.
- Lesuisse C, Qiu D, Bose CM, Nakaso K, Rupp F. 2000. Regulation of agrin expression in hippocampal neurons by cell contact and electrical activity. *Brain Res Mol Brain Res* 81:92-100.
- Liao D, Zhang X, O'Brien R, Ehlers MD, Haganir RL. 1999. Regulation of morphological postsynaptic silent synapses in developing hippocampal neurons. *Nature Neurosci* 2:37-43.
- Manthorpe M, Pettman B, Varon S. 1988. Modulation of astroglial cell output of neuronotrophic and neurite promoting factors. In: Norenberg MD, Hertz L, Schousboe A, editors. *The biochemical pathology of astrocytes*. New York: Alan R. Liss, p 41-58.
- Martin LJ. 2000. p53 is abnormally elevated and active in the CNS of patients with amyotrophic lateral sclerosis. *Neurobiol Disease* 7:613-622.
- Martin LJ. 2001. Neuronal cell death in nervous system development, disease, and injury. *Int J Mol Med* 7:455-478.
- Martin LJ, Al-Abdulla NA, Brambrink AM, Kirsch JR, Sieber FE, Portera-Cailliau C. 1998a. Neurodegeneration in excitotoxicity, global cerebral ischemia, and target deprivation: a perspective on the contributions of apoptosis and necrosis. *Brain Res Bull* 46:281-309.
- Martin LJ, Blackstone CD, Levey AI, Haganir RL, Price DL. 1993. AMPA glutamate receptor subunits are differentially distributed in rat brain. *Neuroscience* 53:327-358.
- Martin LJ, Brambrink AM, Price AC, Kaiser A, Agnew DM, Ichord RN, Traystman RJ. 2000a. Neuronal death in newborn striatum after hypoxia-ischemia is necrosis and evolves with oxidative stress. *Neurobiol Disease* 7:169-191.
- Martin LJ, Furuta A, Blackstone CD. 1998b. AMPA receptor protein in developing rat brain: glutamate receptor-1 expression and localization change at regional cellular, and subcellular levels with maturation. *Neuroscience* 83:917-928.
- Martin LJ, Kaiser A, Price AC. 1999. Motor neuron degeneration after sciatic nerve avulsion in adult rat evolves with oxidative stress and is apoptosis. *J Neurobiol* 40:185-201.
- Martin LJ, Kaiser A, Yu JW, Natale JE, Al-Abdulla NA. 2001. Injury-induced apoptosis of neurons in adult brain is mediated by p53-dependent and p53-independent pathways and requires Bax. *J Comp Neurol* 433:299-311.
- Martin LJ, Pardo CA, Cork LC, Price DL. 1994. Synaptic pathology and glial responses to neuronal injury precede the formation of senile plaques and amyloid deposits in the aging cerebral cortex. *Am J Pathol* 145:1358-1381.
- Martin LJ, Price AC, Kaiser A, Shaikh AY, Liu Z. 2000b. Mechanisms for neuronal degeneration in amyotrophic lateral sclerosis and in models of motor neuron death. *Int J Mol Med* 5:3-13.
- Morris EJ, Geller HM. 1996. Induction of neuronal apoptosis by camptothecin, an inhibitor of DNA topoisomerase-I: evidence for cell cycle-independent toxicity. *J Cell Biol* 134:757-770.
- Murphy DD, Rueter SM, Trojanowski JQ, Lee VMY. 2000. Synucleins are developmentally expressed, and  $\alpha$ -synuclein regulates the size of the presynaptic vesicular pool in primary hippocampal neurons. *J Neurosci* 20:3214-3220.
- Osterova N, Petrucelli L, Farrer M, Mehta N, Choi P, Hardy J, Wolozin B. 1999.  $\alpha$ -Synuclein shares physical and functional homology with 14-3-3 proteins. *J Neurosci* 19:5782-5791.
- Porter NM, Thibault O, Thibault V, Chen KC, Landfield PW. 1997. Calcium channel density and hippocampal cell death with age in long-term culture. *J Neurosci* 17:5629-5639.
- Portera-Cailliau C, Price DL, Martin LJ. 1997a. Excitotoxic neuronal death in the immature brain is an apoptosis-necrosis morphological continuum. *J Comp Neurol* 378:70-87.
- Portera-Cailliau C, Price DL, Martin LJ. 1997b. Non-

- NMDA and NMDA receptor-mediated excitotoxic neuronal deaths in adult brain are morphologically distinct: further evidence for an apoptosis-necrosis continuum. *J Comp Neurol* 378:88–104.
- Ray J, Peterson DA, Schinstine M, Gage FF. 1993. Proliferation, differentiation, and long-term culture of primary hippocampal neurons. *Proc Natl Acad Sci USA* 90:3602–3606.
- Schousboe A, Svenneby G, Hertz L. 1977. Uptake and metabolism of glutamate in astrocytes cultured from dissociated mouse brain hemispheres. *J Neurochem* 29:999–1005.
- Simantov R. 1989. Glutamate neurotoxicity in culture depends on the presence of glutamine: Implications for the role of glial cells in normal and pathological brain development. *J Neurochem* 52:1694–1699.
- Strong MJ, Sopper MM, Crow JP, Strong WL, Beckman JS. 1998. Nitration of low molecular weight neurofilament is equivalent in sporadic amyotrophic lateral sclerosis and control cervical spinal cord. *Biochem Biophys Res Comm* 248:157–164.
- Unsicker KH, Richert-Preibsch H, Schmidt R, Pettman B, Labourdette G, Sensenbrenner M. 1987. Astroglial and fibroblast growth factors have neurotrophic functions for cultured peripheral and central nervous systems. *Proc Natl Acad Sci USA* 84:5459–5463.
- Volpe JJ. 1995. *Neurology of the Newborn*. Philadelphia: Saunders. 1450 p.
- Wallace T, Johnson E. 1989. Cytosine arabinoside kills postmitotic neurons: evidence that deoxycytidine may have a role in neuronal survival that is independent of DNA synthesis. *J Neurosci* 9:115–124.
- Withers GS, George JM, Banker GA, Clayton DF. 1997. Delayed localization of synelfin (synuclein, NACP) to presynaptic terminals in cultured rat hippocampal neurons. *Dev Brain Res* 99:87–94.
- Xie C, Marksbery WR, Lovell MA. 2000. Survival of hippocampal and cortical neurons in a mixture of MEM<sup>+</sup> and B27-supplemented neurobasal medium. *Free Rad Biol Med* 28:665–672.
- Ye ZC, Sontheimer H. 1998. Astrocytes protect neurons from neurotoxic injury by serum glutamate. *Glia* 22:237–248.
- Zona C, Palma E, Brancati A, Avoli M. 1994. Age-dependent appearance of synaptic currents in rat neocortical neurons in culture. *Synapse* 18:1–6.



---

ORIGINAL RESEARCH

---

## DNA Base-Excision Repair Enzyme Apurinic/Apyrimidinic Endonuclease/Redox Factor-1 is Increased and Competent in the Brain and Spinal Cord of Individuals with Amyotrophic Lateral Sclerosis

**Arif Y. Shaikh and Lee J. Martin\***

*Departments of Pathology, Division of Neuropathology, and Neuroscience, Johns Hopkins University School of Medicine, 720 Rutland Avenue, 558 Ross Building, Baltimore, MD 21205-2196*

### Abstract

Motor neurons degenerate in amyotrophic lateral sclerosis (ALS). The mechanisms for this neuronal cell death are not known, although apoptosis has been implicated. Oxidative damage to DNA and activation of p53 has been identified directly in motor neurons in cases of ALS. We evaluated whether motor neuron degeneration in ALS is associated with changes in the levels and function of the multifunctional protein apurinic/apyrimidinic endonuclease (APE/Ref-1). APE/Ref-1 functions as an enzyme in the DNA base-excision repair pathway and as a redox-regulation protein for transcription factors. The protein level and localization of APE/Ref-1 are changed in ALS. Immunoblotting showed that APE/Ref-1 protein levels are increased in selectively vulnerable central nervous system (CNS) regions in individuals with ALS compared to age-matched controls. Plasmid DNA repair assay demonstrated that APE from individuals with ALS is competent in repairing apurinic (AP) sites. DNA repair function in nuclear fractions is increased significantly in ALS motor cortex and spinal cord. Immunocytochemistry and single-cell densitometry revealed that APE/Ref-1 is expressed at lower levels in control motor neurons than in ALS motor neurons, which are decreased in number by 42% in motor cortex. APE/Ref-1 is increased in the nucleus of remaining upper motor neurons in ALS, which show a 38% loss of nuclear area. APE-Ref-1 is also upregulated in astrocytes in spinal cord white matter pathways in familial ALS. We conclude that mechanisms for DNA repair are activated in ALS, supporting the possibility that DNA damage is an upstream mechanism for motor neuron degeneration in this disease.

**Index Entries:** Motor neuron; apoptosis; DNA damage; DNA repair; DNA single-strand breaks; programmed cell death; Lou Gehrig's disease.

\*Author to whom all correspondence and reprint requests should be addressed. E-mail: [lmartin@jhmi.edu](mailto:lmartin@jhmi.edu)

## Introduction

Amyotrophic lateral sclerosis (ALS), or motor neurone disease, is still a fatal neurological disease in humans, because it cannot be cured or treated effectively. The disease causes progressive weakness, muscle atrophy, paralysis, and death within 3–5 yr of clinical onset (Kuncl et al., 1992; Rowland and Schneider, 2001). ALS is the third most common neurodegenerative disease with an adult onset (after Alzheimer's disease and Parkinson's disease). The average prevalence of ALS in the 1990s was 5.2 per 100,000 individuals (Worms, 2001). Each year ~5000 Americans are diagnosed with ALS, and, in parts of the United Kingdom, 1 in ~500 deaths is caused by some form of motor neurone disease (Nicholson et al., 2000). The disease attacks motor neurons in the cerebral cortex, brainstem, and spinal cord. The mechanisms for this selective degeneration of motor neurons are not known (Martin et al., 2000; Rowland and Schneider, 2001). The degeneration of upper and lower motor neurons in ALS may be a form of aberrantly occurring apoptosis (Ekegren et al., 1999; Martin, 1999; Mattson et al., 1999; Sathasivam et al., 2001) that could be mediated by p53 (Martin, 2000, 2001), although this idea has been challenged (He and Strong, 2000). The possible involvement of p53 implicates DNA damage as an upstream pathogenic event in motor neuron degeneration in ALS.

It has been proposed previously that DNA damage could be involved in the pathogenesis of ALS (Bradley and Krasin, 1982). This damage is caused possibly by oxidative stress, because 8-hydroxy-2-deoxyguanosine (OHdG) adducts are elevated in individuals with ALS (Fitzmaurice et al., 1996; Ferrante et al. 1997); however, the contributions of motor neurons to the burden of OHdG was uncertain in these studies. Direct evidence for OHdG-DNA lesions specifically in motor neurons of individuals with ALS has been found recently (Martin, 2001). The mechanisms of DNA damage accumulation in neurons are understood poorly. Possible mechanisms for the elevated levels of DNA damage in individuals with ALS include increases in the spontaneous generation of DNA damage by reactive oxygen species (ROS) and defective DNA repair. Nonrepaired or misrepaired DNA causes acquired genetic mutations and genomic instability (Lindahl, 1993) that could contribute to the pathogenesis of motor neuron degeneration in ALS.

Mammalian cells have elaborate DNA repair mechanisms. DNA base-excision repair (BER) is believed to be the major pathway for repairing oxidative damage to DNA (Subba Rao, 1993). BER involves three major classes of DNA repair enzymes: DNA glycosylases, apurinic/apyrimidinic endonucleases (APE), and DNA polymerases. The removal of oxidatively damaged DNA bases by BER involves hydrolysis of the *N*-glycosylase bond between the sugar and the base by a DNA glycosylase. This reaction generates a site that is without a base (i.e., an AP site). A DNA single-strand break (SSB) is induced by hydrolysis of the phosphodiester bond in the DNA backbone by APE, followed by excision of the AP site by exonuclease activity. The gap is filled via nucleotide insertion by DNA polymerase- $\beta$ . Ligation of the 3' and 5' ends by DNA ligase completes the repair process.

There is a paucity of studies on DNA repair in individuals with ALS. The studies available have examined DNA repair in ALS skin fibroblasts (Tandan et al., 1987), lymphocytes (Robison et al., 1993), and postmortem frontal cortex (Kisby et al., 1997). Some of these reports are conflicting. We therefore tested the hypothesis that changes occur in the expression and function of the class II APE in selectively vulnerable regions of central nervous system (CNS) in ALS, specifically in upper cortical and lower spinal motor neurons.

## Methods

### *Human Autopsy Cases and CNS Tissue Sampling*

Patients were diagnosed with ALS by neurological examination using the El Escorial criteria (World Federation of Neurology Research Group on Neuromuscular Diseases, 1994). Postmortem CNS tissues from these individuals were obtained from the Human Brain Resource Center, Division of Neuropathology, Johns Hopkins University School of Medicine. Neuropathological evaluation confirmed the clinical diagnosis of ALS (Martin, 1999). Sporadic ALS comprised the majority (~89%) of the cases studied (Table 1). Postmortem samples of brain and spinal cord from age-matched control individuals without neurological disease ( $n = 6$ ) and patients with ALS ( $n = 16$ ) were selected randomly for analysis of APE/Ref-1 (Table 1). The ages (mean

Table 1  
Human Autopsy Cases From Which CNS Tissues Were Obtained

Group	Case number	Age (years)/sex	Postmortem delay(hours)	Cause of death
Control	487	73/male	22	Pancreatic cancer
	515	62/male	21	Aortic aneurysm
	712	44/female	20	Pneumonia
	719	66/male	10	Myocardial infarction
	961	59/female	6	Myocardial infarction
	993	66/male	12	Prostatic carcinoma
ALS	345	59/female	3	Respiratory arrest
	414	65/male	4	Respiratory arrest
	433	71/male	17	Respiratory arrest
	447	69/female	15	Respiratory arrest
	492	68/female	18	Respiratory arrest
	834	46/male	3	Respiratory arrest
	875	70/female	24	Respiratory arrest
	950	38/male	22	Respiratory arrest
	1014	72/male	5	Respiratory arrest
	1088	66/male	7	Respiratory arrest
	1108	64/female	8	Respiratory arrest
	1151	57/female	14	Respiratory arrest
	1161	47/male	6	Pneumonia
	1169	67/female	15	Respiratory arrest
	1176	27/male	6	Respiratory arrest
	1485	61/female	5	Respiratory arrest

$\pm$  standard deviation) for control and ALS groups were  $62 \pm 10$  yr and  $59 \pm 13$  yr, respectively. The postmortem delays (mean  $\pm$  standard deviation) of the groups were comparable (control,  $15 \pm 7$  h; ALS,  $11 \pm 7$  h).

Very selective and specific CNS tissue samples were used for these experiments. Samples of motor cortex (superior precentral gyrus, leg area), somatosensory cortex, and spinal cord were used for immunoblotting and DNA repair assays. Using a 4- or 2-mm diameter micropunch (Acuderm Inc., Fort Lauderdale, FL), neocortical samples (0.3–0.5 g) and spinal cord samples (0.1–0.3 g) were obtained carefully from fresh-frozen postmortem brain slabs of the right or left hemisphere or from the spinal cord that were stored at  $-70^{\circ}\text{C}$  and warmed to  $-20^{\circ}\text{C}$ . Samples of spinal cord included only the anterior horn gray matter (mostly the group IX column) of cervical or lumbar levels. White matter pathways were avoided. Discretely microdissected punches of the lumbar and cervical spinal cord and the motor and sensory cortical gray matter mantles were used

to make the measurements made here and previously (Martin, 1999, 2000). These samples of motor cortex and spinal cord anterior horn were as selective as could be feasible for motor neuron populations, without using laser capture microscopy.

### Immunoblotting for APE/Ref-1

Subcellular fractions were prepared from human CNS tissues. Nuclear-enriched and soluble protein extracts were prepared by homogenizing tissue samples in cold 20 mM Tris-HCl, pH 7.4, containing 10% (w/v) sucrose, 20 U/mL aprotinin (Trasyol), 20  $\mu\text{g}/\text{mL}$  leupeptin, 20  $\mu\text{g}/\text{mL}$  antipain, 20  $\mu\text{g}/\text{mL}$  pepstatin A, 20  $\mu\text{g}/\text{mL}$  chymostatin, 0.1 mM phenylmethylsulfonyl fluoride (PMSF), 10 mM benzamidine, 1 mM EDTA, and 5 mM EGTA. Homogenates were centrifuged at  $1,000 g_{\text{av}}$  for 10 min ( $4^{\circ}\text{C}$ ), and the resulting pellet (P1 fraction) was resuspended in homogenization buffer (without sucrose) supplemented with 20% (w/v) glycerol. The supernatant was then centrifuged at  $54,000 g_{\text{av}}$  for 20 min ( $4^{\circ}\text{C}$ ) to yield soluble and mem-

brane fractions. Fraction-specific organelle/enzyme markers verified this subcellular fractionation method for human CNS tissues (Martin, 2000). Protein concentrations in different fractions were measured by a Bio-Rad protein assay with bovine serum albumin (BSA) as a standard.

The levels of immunoreactivity for APE/Ref-1 were measured by immunoblotting. Nuclear-enriched and soluble protein extracts (5 and 10  $\mu$ g protein samples) from ALS ( $n = 12$ ) and control ( $n = 6$ ) cases were subjected to 15% sodium dodecyl sulfate polyacrylamide gel electrophoresis (SDS-PAGE) and transferred to nitrocellulose membrane by electroelution as described (Martin, 1999). Sample loading and protein electroblotting was controlled for in each experiment by staining nitrocellulose membranes with Ponceau S before immunoblotting and normalizing subsequent immunoreactivity to Ponceau S-stained protein. Blots were blocked with 2.5% nonfat dry milk with 0.1% Tween 20 in 50 mM Tris-buffered saline (TBS), pH 7.4, then incubated overnight at 4°C with antibody to APE/Ref-1 (Affinity Bioreagents, Golden, CO) used at 200 ng IgG/mL. After the primary antibody incubation, blots were washed and incubated with horseradish peroxidase-conjugated secondary antibody (0.2  $\mu$ g/mL), developed with enhanced chemiluminescence (Pierce), and exposed to X-ray film. Immunoreactive protein was visualized within the linear range.

To quantify APE/Ref-1 immunoreactivity, films were scanned using Adobe Photoshop and an Agfa Arcus Plus scanner (Martin, 1999). Densitometric analysis was performed using signal Analytics IP Lab Gel software. Protein levels were expressed as relative optical density (OD) measurements, determined by comparing the density and area of the immunoreactive bands from ALS cases to corresponding bands in control lanes in the same blot. The measurements for all blots were normalized to total protein loaded as determined by Ponceau S staining. The regional and subcellular values for each ALS and control case (determined from at least three different blots per region and fraction) were used to determine group means and variances.

### **APE Activity Assay**

APE activity in ALS and control CNS samples was measured using a DNA repair assay (Henner et al., 1987). This assay is based on the repair of plas-

mid DNA (pUC18, Amersham) containing AP sites generated *in vitro* by hydrolytic depurination. Plasmid DNA was depurinated by heating (60°C) pUC18 in 3 volumes of 50 mM sodium citrate for 15 min. The assay mixtures contained 100 mM HEPES, pH 8.25, 3 mM MgCl<sub>2</sub>, 500 ng depurinated Form I pUC18 DNA, and nuclear or soluble protein (25 ng-1  $\mu$ g). Assay mixtures (final volume 20  $\mu$ L) were incubated at 37°C for 20 min. The amounts of DNA and protein and the time of reaction were established empirically. Negative controls were denaturation of protein extracts by boiling for 3 min in SDS prior to reacting with plasmid DNA and by reacting damaged DNA without protein extract. Adding DNA-gel loading buffer containing 10% SDS and placing samples on ice terminated the reaction. To resolve repaired and nonrepaired DNA, samples were loaded into agarose gels (0.8%) containing ethidium bromide and were fractionated for 2 h at 60 V. Repaired and nonrepaired DNA bands were visualized with a Stratagene Eagleeye II. Digital images were quantified by densitometry.

### **Immunolocalization of APE/Ref-1**

From ALS ( $n = 16$ ) and control ( $n = 6$ ) cases, paraffin-embedded samples of spinal cord, precentral gyrus (motor cortex), and postcentral gyrus (somatosensory cortex) were sectioned (10  $\mu$ m) and stained with antibody to APE/Ref-1 (10  $\mu$ g IgG/mL) using a standard immunoperoxidase method with diaminobenzidine as chromogen. The high specificity of this antibody is shown by immunoblotting (Fig. 1). Negative control sections, including primary or secondary antibody omission and dilute or denatured primary antibody, did not show immunoreactivity. Some sections were dual-labeled for APE and glial fibrillary acid protein (GFAP) using a sequential antibody detection method (Furuta et al., 1995) with diaminobenzidine and benzidine dihydrochloride as chromogens.

The immunocytochemical preparations were analyzed quantitatively using cell counting and single-cell densitometry. The evaluation focused on motor cortex of control and ALS cases because this is a selectively vulnerable region that generally shows less advanced degeneration than spinal cord anterior horn. Furthermore, the upper motor neurons in ALS are understudied. In carefully matched sections of motor cortex, APE immunoreactivity was measured in individual layer 5 pyramidal neurons.

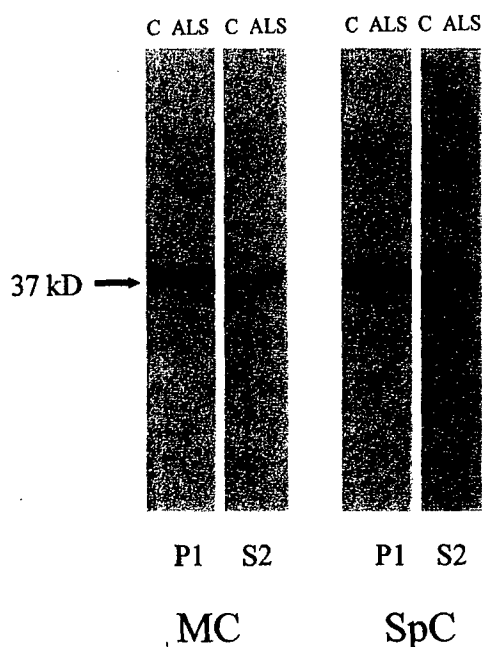


Fig. 1. Antibody to APE/Ref-1 is highly specific in human CNS tissue extracts. Full-length immunoblots of APE/Ref-1 in motor cortex (MC) and spinal cord (SpC) of control (C) and ALS cases. Brain and spinal cord samples were fractionated into nuclear-enriched (P1) and soluble (S2) protein compartments. The APE/Ref-1 antibody detects a single protein band at ~37 kDa.

Images of randomly selected immunoreactive upper motor neurons were captured photographically at 1000× magnification by an observer unaware of case history. For each case, ~30 neurons were acquired. The films of individual motor neurons were scanned and saved as TIFF files. For each neuron, two different measurements were obtained by delineating a region of interest (i.e., nucleus) using densitometry software (Inquiry Software, Loats Associates, Westminster, MD). These measurements were OD and area of the nucleus. Relative APE immunoreactivity was reflected by the average-integrated intensity of emulsion grain density. After the sections were used for single-cell densitometry, they were counterstained with cresyl violet and the number of layer 5 pyramidal neurons was determined by profile counting.

### Data Analysis

The sample populations were selected randomly and were normally distributed (i.e., assumptions for parametric analyses were not violated). The mea-

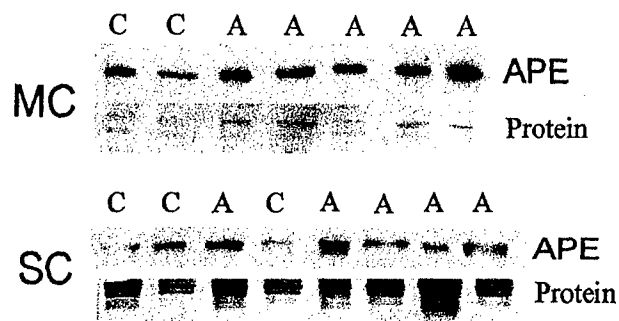


Fig. 2. Representative immunoblots of APE/Ref-1 in soluble (S2) protein fractions of motor cortex (MC, 5 µg of protein loaded) and spinal cord (SC, 10 µg of protein loaded) of control (C) and ALS (A) cases. For each pair, the upper image is an APE/Ref-1 immunoblot and the lower image is a strip showing the Ponceau S staining of the actual nitrocellulose membrane used for the immunoblot. These blots are only two of several blots for each CNS region that were used to generate the quantitative data shown in Fig. 3.

surements that were made were APE/Ref-1 protein levels by immunoblotting and immunocytochemistry, APE enzyme activity, motor neuron number, and nuclear area. The analysis of the measurements was done by comparing age-matched control values to ALS values with one-way analysis of variance. Subsequent statistical evaluation of significance was done using a two sample Student's *t*-test.

## Results

### APE/Ref-1 Protein Levels are Increased in Motor Neuron Regions in ALS

The specificity of the antibody to APE/Ref-1 was evaluated in immunoblots of human CNS tissue extracts (Fig. 1). This antibody is highly specific as shown in full-length blots (Fig. 1). It detects a single band at ~37 kDa. This protein has a size consistent with human APE/Ref-1 (Duguid et al., 1995). The same size of protein is present in nuclear and soluble protein fractions in control and ALS cases (Fig. 1).

The levels of APE/Ref-1 were measured in subcellular protein fractions of CNS tissues from ALS and control cases by immunoblotting (Figs. 2, 3). Soluble protein fractions (S2) of lumbar/cervical spinal cord anterior horn, motor cortex, and somatosensory cortex of ALS and control cases were isolated. The level of APE/Ref-1 was dramatically

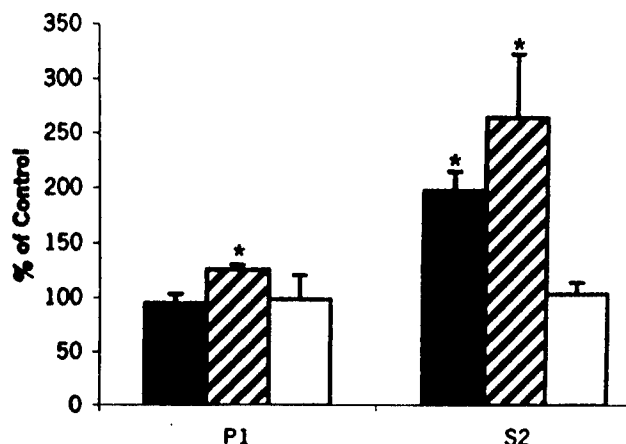


Fig. 3. Measurement of APE/Ref-1 levels in nuclear (P1) and soluble (S2) protein fractions of motor cortex (solid black bars), spinal cord (striped bars), and somatosensory cortex (white bars) of ALS cases. The values (presented as % of control, which is set at 100%) are mean  $\pm$  SD. In ALS motor cortex and spinal cord soluble protein fractions, the levels were increased significantly (asterisk,  $p < 0.01$ ) above control level. In ALS spinal cord nuclear protein fractions (P1), the levels were increased significantly (asterisk,  $p = 0.05$ ) above control level.

increased ( $p < 0.01$ ) in S2 fractions of spinal cord and motor cortex, whereas the level in sensory cortex was not different from age-matched controls (Figs. 2, 3). Nuclear-enriched fractions (P1) of lumbar/cervical spinal cord anterior horn, motor cortex, and somatosensory cortex were isolated from ALS and control cases. The level of APE/Ref-1 was elevated modestly ( $p = 0.05$ ) in P1 fractions of spinal cord, but the levels in motor cortex and sensory cortex were not significantly different from age-matched controls (Fig. 3). These results were replicated in experiments using 5 and 10  $\mu$ g of protein.

### DNA Repair Function of APE is Increased in ALS Motor Neuron Regions

APE functions as a nuclear DNA repair enzyme in the BER pathway (Subba Rao, 1993). We determined the functional capacity of APE in nuclear extracts of human CNS tissue using a DNA repair assay. Agarose gel electrophoresis successfully resolved the damaged and repaired plasmid DNA (Fig. 4). DNA repaired by APE was seen as the upper band (form II). The nonrepaired DNA was seen as the lower band (form I). Denaturation of nuclear protein extracts prior to their use in the assay blocked

DNA repair activity (Fig. 4). DNA repair activity in nuclear fractions of ALS motor cortex and spinal cord appeared elevated compared to control, as suggested by the increased ethidium bromide staining of the upper DNA band, and the corresponding decrease in the intensity of the lower band. Densitometry on the bands revealed an overall significant increase in repaired DNA in the ALS cases compared to controls (Fig. 5).

### APE/Ref-1 Localization is Altered in Motor Neuron Regions in ALS

In the CNS of control humans free of neurological disease (Table 1), immunocytochemically detectable APE/Ref-1 was observed most prominently in glial cell nuclei. These labeled glial cells were found in the parenchyma and white matter (Fig. 6A). APE/Ref-1 immunoreactivity was low in neurons in control CNS, based on one antibody. Only subsets of neurons displayed cytoplasmic and nuclear labeling that was not intense (Fig. 6B). In all cases of ALS, APE/Ref-1 immunoreactivity was detected intensely in the nucleus of subsets of lower spinal motor neurons and upper motor neurons in motor cortex (Fig. 6C, D). Most of these neurons enriched in APE/Ref-1 immunoreactivity were chromatolytic (Fig. 6C) or undergoing somatodendritic attrition (Fig. 6D). In cases of FALS, nonneuronal cells in white matter that appeared to be reactive astrocytes were frequently positive for APE/Ref-1 in spinal cord (most prominently in the corticospinal tracts) and motor cortex (Fig. 6E). Dual labeling of cells for APE and GFAP confirmed that these cells were astroglia (Fig. 6F).

Motor neurons in layer 5 of motor cortex were counted. Sporadic ALS cases had a 42% loss of upper motor neurons compared to age-matched controls (Table 2). Of the remaining upper motor neurons in cases of ALS, ~36% of these cells had a nucleus that was intensely immunoreactive for APE (Table 2), whereas <1% of the motor neurons showed strong APE immunoreactivity in controls (Table 2). The level of APE immunoreactivity in the nucleus of upper motor neurons in ALS cases was ~150% of control (Table 2). There was a 38% loss of nuclear area in these neurons (Table 2).

### Discussion

This study advances the understanding of the pathobiology of ALS by finding an activation of a

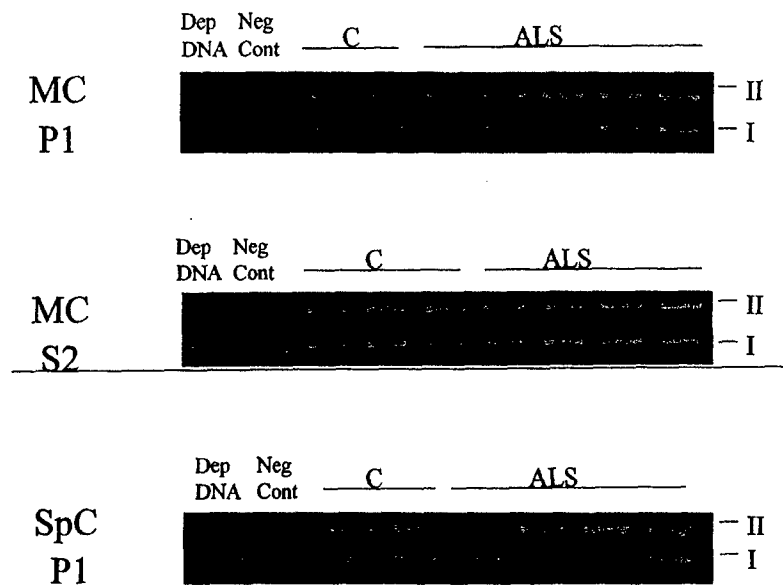


Fig. 4. Repair of AP sites in plasmid DNA by protein extracts of ALS and control (C) CNS tissues. Samples of motor cortex (MC) and spinal cord (SpC) were fractionated into nuclear (P1) and soluble (S2) protein extracts. APE activity was determined by reacting in vitro human protein with depurinated (AP site damaged) pUC18 plasmid DNA (form I) containing ~3-4 AP sites per pUC18 DNA molecule (Henner et al., 1987). The reactions were quenched with SDS. Damaged and repaired plasmid DNA was resolved by electrophoresis in 0.8% agarose and stained with ethidium bromide. Repaired DNA is seen as the upper band (form II), and nonrepaired DNA is seen as the lower band (form I). Reactions with depurinated DNA alone (Dep DNA) and denatured protein extracts (Neg Cont) were negative controls for the assay. The apparent increase in ethidium bromide staining of the upper DNA band and the decrease in the intensity of the lower band indicate that DNA repair activity in nuclear fractions of ALS motor cortex and spinal cord are elevated compared to control. These DNA gels are only three of several gels for each CNS region that were used to generate the quantitative data shown in Fig. 5.

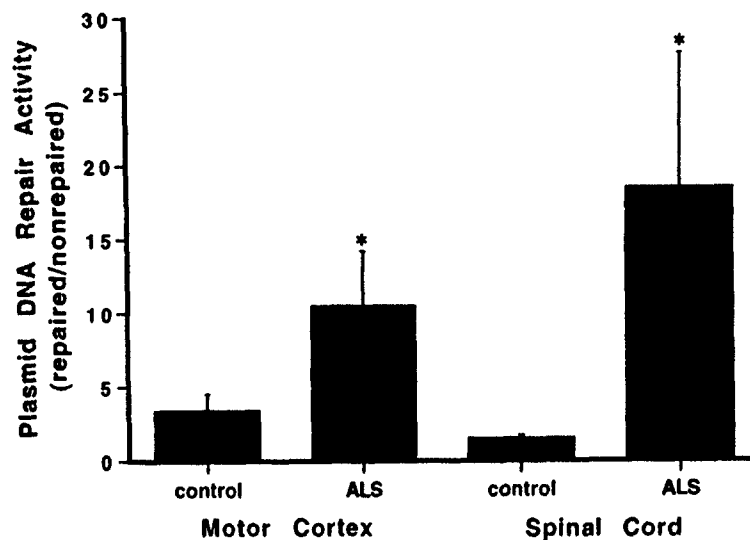
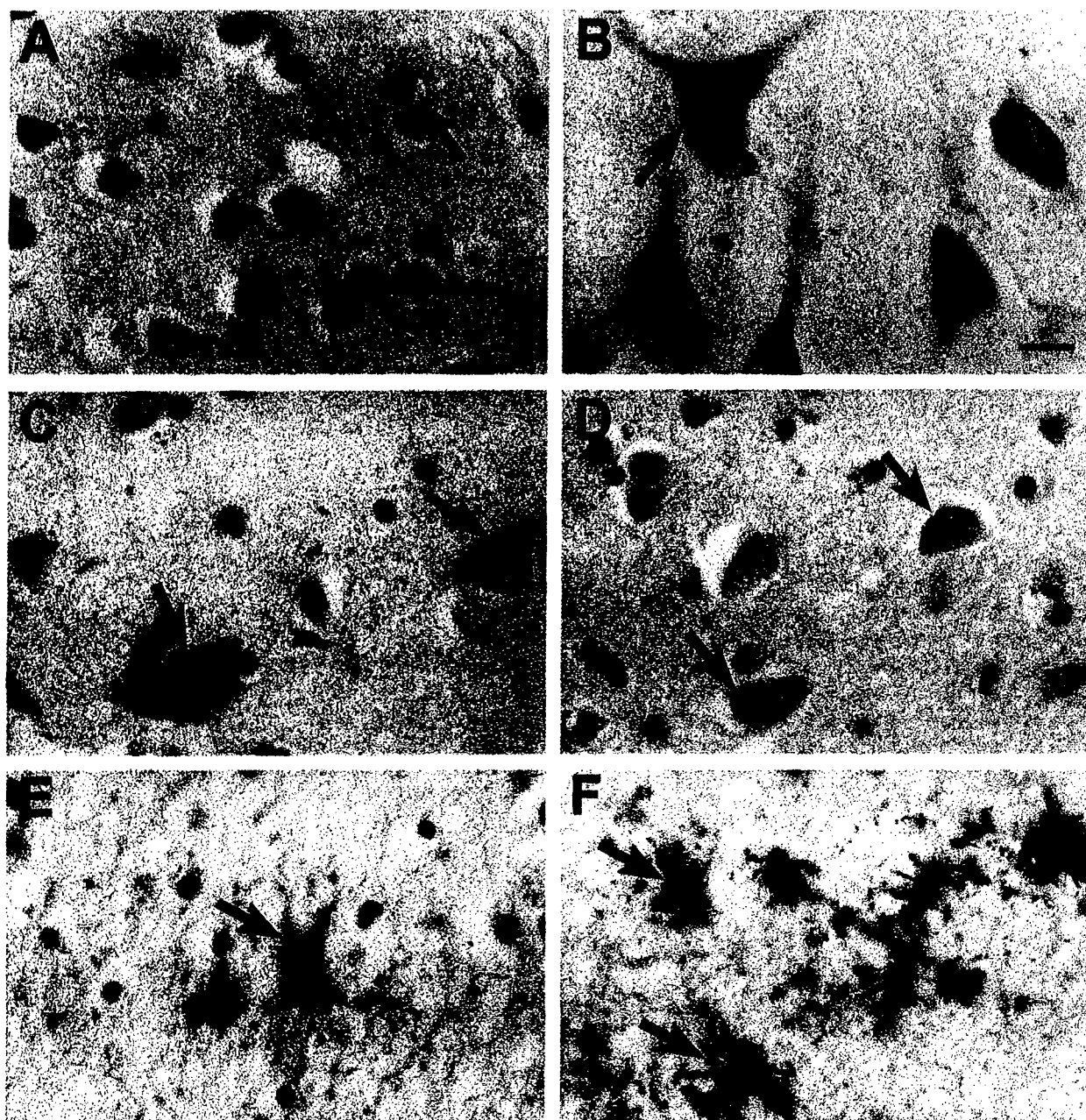


Fig. 5. Quantification of APE activity in nuclear protein fractions of motor cortex and spinal cord of control and ALS cases. The values shown are mean  $\pm$  SEM. Asterisk indicates significant difference ( $p < 0.05$ ) from control.



**Fig. 6.** Localization of APE/Ref-1 in ALS brain and spinal cord. **(A)** and **(B)** In control brain APE is enriched in subsets of glial cell nuclei (**A**, arrows), while upper and lower motor neurons show only faint labeling (**B**, arrow). Scale bar: **(A)** 20  $\mu$ m; **(B)** (same for **C**–**F**), 15  $\mu$ m. **(C)** and **(D)** In ALS, motor neurons in the chromatolytic (**C**, arrows) and somatodendritic atrophy (**D**, arrows) stage of apoptosis (see Martin, 1999 for the staging of motor neuron death in ALS) show strong nuclear labeling for APE/Ref-1. **(E)** and **(F)** In FALS cases, some astroglia-like cells in spinal cord white matter (not included in the micropunched samples used for immunoblots) have strong cytoplasmic immunoreactivity for APE/Ref-1 (**E**, arrow), and subsequent dual labeling for APE/Ref-1 and GFAP (**F**) confirmed that reactive astrocytes are positive for GFAP (**E**, arrows, black labeling) are also APE positive (**E**, arrows, brown labeling).



Table 2  
Upper Motor Neuron Abnormalities in ALS<sup>a</sup>

Group <sup>b</sup>	Neuronal number <sup>c</sup>	APE-positive neurons <sup>d</sup>	Nuclear APE level <sup>e</sup>	Nuclear area
Control	433 ± 62	4 ± 4	133.8 ± 4.9	14897 ± 436
ALS	250 ± 78**	90 ± 46**	198.3 ± 30.0*	9203 ± 2945*

<sup>a</sup>Age-matched neurological disease-free controls ( $n = 6$ ) and sporadic ALS ( $n = 14$ ) cases were used.

<sup>b</sup>All values are mean ± standard deviation. Significant difference from control is indicated by the double asterisk ( $p < 0.01$ ) or single asterisk ( $p < 0.05$ ).

<sup>c</sup>Number of neurons (neurons/mm<sup>2</sup>) in layer 5 of motor cortex.

<sup>d</sup>Number of neurons (neurons/mm<sup>2</sup>) in layer 5 of motor cortex with strong nuclear APE immunopositivity.

<sup>e</sup>Value was determined from the average-integrated optical density of immunoreactivity measured using single-cell densitometry on ~30 layer 5 neurons in each case.

key enzyme that functions in DNA-BER. In mammalian cells, APE corrects AP sites through base incision. Removal of the deoxyribose 5-phosphate and ligation are carried out primarily by DNA polymerase  $\beta$  (pol $\beta$ ), with APE and pol $\beta$  interacting to form a ternary complex comprised of AP-DNA, APE, and pol $\beta$  (Bennet et al., 1997). We found that APE/Ref-1 levels are increased in CNS tissues from patients with ALS. Because BER of DNA is one function of APE/Ref-1, we determined whether there was a corresponding increase in functional activity of APE using an in vitro assay. APE activity is increased in nuclear fractions of motor neurons regions in cases of ALS. Although this finding is consistent with the increased levels of APE/Ref-1 protein, it is important because it demonstrates that the APE is functionally competent.

APE levels and activity are elevated in motor cortex and spinal cord anterior horn, regions that contain motor neurons, but not in nonmotor regions such as the somatosensory cortex, in cases of ALS. APE activity was increased in nuclear fractions of motor cortex without a significant increase in protein; however, we found a loss of neurons in motor cortex, which may deplete nuclear APE. Our tissue homogenate-based assays were not quantitative specifically for motor neurons. Despite using an accurate micropunch technique, nonneuronal cells, motor neurons, and neurons other than motor neurons contribute to the samples. Selective loss of motor neurons could lead to reactive activation of glial cells and a corresponding increase in APE.

Therefore, we used immunocytochemistry to localize APE at the cellular level. Except in some spinal cord white matter pathways in cases of FALS, immunoreactivity for APE was not generally upregulated in astroglia. Immunolocalization experiments showed that APE/Ref-1 is present in motor neurons. We measured APE on a single motor neuron basis using immunocytochemistry and single-cell densitometry. In motor cortex, very few (<1%) upper motor neurons strongly expressed APE in controls; in contrast, APE immunoreactivity was increased dramatically in a significant proportion of remaining motor neurons in ALS. Using single-cell densitometry, APE immunoreactivity was increased in the nucleus of layer 5 motor neurons in individuals with ALS. These motor neurons expressing APE/Ref-1 were injured based on a decrease in nuclear area and other structural features such as chromatolysis and somatodendritic attrition (Martin, 1999). We conclude that DNA repair pathways are activated in vulnerable cells in ALS, supporting the possibility that DNA damage is an upstream mechanism for motor neuron degeneration in this disease.

Our observations on APE/Ref-1 are consistent with current information on the possible mechanisms of motor neuron degeneration in ALS. Motor neurons die selectively in individuals with ALS (Yoshiyama et al., 1994; Ekegren et al., 1999; Martin, 1999). Surprisingly, little attention has been paid to upper motor neurons in ALS with regard to cell loss and molecular mechanisms of degeneration. This

study provides much needed novel data on upper motor neurons in ALS. We found a 42% loss of pyramidal neurons in layer 5 of motor cortex. This result is consistent the loss of the neuronal nuclear protein NeuN found by immunoblotting (Martin, 2001). The death of motor neurons in ALS may be a form of apoptosis based on structural, biochemical, and molecular evidence (Martin, 1999, 2000, 2001), although this interpretation has been contested (He and Strong, 2000). Other groups now believe that apoptosis has a prominent contribution to the pathogenesis of ALS (Mattson et al., 1999; Sathasivam et al., 2001) and in mouse models of FALS (Vukosavic et al., 1999; Gonzalez de Aguilar et al., 2000). However, it is unlikely that apoptosis is the sole defining event in ALS because motor neurons in this disease are believed to be impaired over a long period of time.

It is not yet clear when APE is increased in motor neurons during the disease process of ALS. Motor neurons displaying APE/Ref-1 immunoreactivity in ALS cases are usually in the chromatolytic and somatodendritic atrophy stages of degeneration. It is possible that APE/Ref-1 is induced in response to oxidative stress occurring during the chromatolytic stage of motor neuron degeneration. Recent studies have shown that neurons undergoing apoptosis in animal models pass through three major structural stages of degeneration: chromatolysis, somatodendritic atrophy, and apoptosis (Al-Abdulla and Martin, 1998; Martin et al., 1999; Martin and Liu, 2002). Motor neurons in ALS appear to follow this staging scheme of degeneration (Martin, 1999). Early during chromatolysis in rat motor neurons, mitochondrial metabolic activity is increased and concomitantly OHdG adducts and DNA-SSB are formed in the nucleus (Martin et al., 1999; Martin and Liu, 2002). An increase in APE/Ref-1 in motor neurons in ALS may be indicative of accumulating oxidative damage to DNA during chromatolysis. If DNA damage exceeds repair capacity and if oxidative stress reaches threshold for cell survival, then these events could contribute to the initial molecular signals for the suspected p53-dependent motor neuron apoptosis in this disease (Martin, 2000, 2001).

Elevated APE/Ref-1 in ALS may signify accumulated DNA damage in the form of AP sites in ALS motor neurons. DNA damage is increased in ALS compared to age-matched controls. Elevated levels of oxidatively damaged DNA in the form of DNA adducts (e.g., 8-oxodeoxyguanosine) have

been found in spinal cord tissue of ALS cases (Fitzmaurice et al., 1996). In addition, increased concentrations of hydroxyl radical damaged DNA have been found in the motor cortex of sporadic ALS cases (Ferrante et al., 1997). These studies, however, did not provide evidence for the contribution of motor neurons to the pool of OHdG detected biochemically. We have detected DNA lesions specifically in motor neurons in individuals with ALS (Martin, 2001). Our current data suggest that AP sites also accumulate in ALS motor neurons since APE, which accomplishes the removal of AP sites (Subba Rao, 1993), is increased. DNA damage in ALS may accumulate because of increased generation of spontaneous DNA lesions caused by free radicals or through defective DNA repair mechanisms (Tandan et al., 1987; Kisby et al., 1997). Defective repair of DNA in ALS could be the result of loss-of-function mutations in APE/Ref-1. Missense mutations in APE were found in 8 of 11 ALS cases (Olkowski, 1998). However, other studies have found that APE mutations do not occur in a large number of ALS cases (Hayward et al., 1999; Tomkins et al., 2000).

It is not yet clear whether the increased activity of APE in ALS motor neurons is compensatory and beneficial or is deleterious. A gain of function in APE could result from increased oxidative stress and DNA damage. A gain of function as a consequence of dysregulated DNA repair enzyme activity could cause nuclease attacks on undamaged DNA, resulting in subsequent accumulation of DNA damage and spontaneous acquired mutations (Branum et al., 2001). To remove AP sites APE cleaves DNA adjacent to the AP site and creates DNA-SSB (Subba Rao, 1993). DNA-SSB can activate p53-dependent apoptosis (Jayaraman and Prives, 1995). In animal models of motor neuron degeneration, DNA-SSB have been detected in motor neurons early in the process of p53-dependent apoptosis (Martin and Liu, 2002). The possibility that DNA-SSB participate in the pathogenesis of ALS is consistent with our previous studies of p53 activation in ALS motor neurons (Martin, 2000, 2001). It will now be necessary to investigate other enzymes in the BER pathway to determine if they are functioning appropriately in ALS. For example, APE could be functioning normally or is augmented in the presence of dysfunctional downstream DNA polymerase- $\beta$ , or APE could be responding to hyperactive upstream DNA glycosylases, thereby contributing to the accumulation of DNA-SSB. Thus,

increased activity of APE and possibly other DNA repair enzymes specifically in motor neurons with superimposed stressors could contribute to the mechanisms of DNA damage in ALS. DNA repair defects may not emerge in invulnerable cells because they are divorced from other injurious stresses or risk factors. An acquired DNA repair abnormality may be one of many cell stresses for motor neurons that define their selective vulnerability in ALS.

DNA damage is an upstream signal that activates PCD mechanisms (Levine, 1997). Several different types of DNA lesions are potent signals for p53 activation, including double-strand breaks (DSB), SSB, adduct formation, as well as insertion/deletion mismatches (Jayaraman and Prives, 1995; Levine, 1997). The most frequent DNA damage is the formation of AP sites, and AP sites are converted to SSB in motor neurons (Liu and Martin, 2001b), possibly through the activity of APE (Subba Rao, 1993). AP lesions occur spontaneously and are induced by ionizing radiation, UV irradiation, chemically initiated hydrolysis, oxidizing agents, as well as by removal of modified bases by DNA glycosylases that function in BER. Estimates indicate that a human cell sustains ~10,000 DNA lesions per day due to metabolism-generated free radicals (Subba Rao, 1993) and 2,000–10,000 DNA purine bases turnover daily because of hydrolytic depurination and subsequent repair (Lindahl, 1993). AP sites are mutagenic. The transduction mechanisms by which DNA damage is converted to proapoptosis signals are poorly delineated in neurons. However, a variety of molecules, mostly protein kinases (e.g., DNA-protein kinase, ATM, MEKK-1, and c-Abl) have been identified that contribute to early apoptotic signaling and may link DNA damage to p53 activation by phosphorylation in non-neuronal cells (Kohn, 1999). p53 activation has been found in ALS motor neurons (Martin, 2001) and in animal models of motor neuron apoptosis (Liu and Martin, 2001b; Martin and Liu, 2002).

Our findings dispute the only other study of APE levels and activity in ALS that reported a loss of protein and enzyme function (Kisby et al., 1997). An unspecified region of frontal cortical tissue was evaluated in the earlier study (Kisby et al., 1997). We specifically evaluated selectively vulnerable and nonvulnerable regions of neocortex. We analyzed APE/Ref-1 in confirmed nuclear-enriched and soluble fractions, and the measurements were normalized for total protein. In these and other aspects,

the experimental designs of the two studies are very different.

APE/Ref-1 is of particular interest to ALS because human APE is also a multifunctional protein that functions as a redox factor (redox factor-1, Ref-1). This protein regulates intracellular redox state. It reduces cysteine residues in several DNA binding proteins (Xanthoudakis and Curran, 1992). APE/Ref-1 facilitates the DNA-binding of numerous transcription factors through redox modulation (Xanthoudakis and Curran, 1992). Thus, an increase in APE/Ref-1 is consistent with the role of oxidative stress in the pathogenesis of ALS. Mutations have been identified in the gene for superoxide dismutase-1 (SOD1) in a small subset of individuals with FALS (Rosen et al., 1993; Deng et al., 1993). Mutant SOD1 may acquire a neurotoxic gain in function, converting this enzyme from a protein with antioxidant-antiapoptotic functions to a protein with oxidative stress- and apoptosis-promoting effects (Rabizadeh et al., 1995). Peroxidase activity of mutant SOD1 is increased compared to wild-type SOD1 (Wiedau-Pazos et al., 1996). This gain-of-function enhances the production of hydroxyl and superoxide radicals, and possibly the formation of peroxynitrite by the combination of superoxide and nitric oxide (Beckman et al., 1993; Wiedau-Pazos et al., 1996). These altered properties of mutant SOD1 have not yet been causally linked specifically to motor neuron damage in ALS. However, DNA damage from hydroxyl radicals has been found in cases of ALS (Ferrante et al., 1997; Martin, 2001) and in mutant SOD1 mice (Warita et al., 2001). Recent *in vitro* experiments show that exposure of motor neurons to nitric oxide (NO) donors,  $H_2O_2$ , or NO donor plus  $H_2O_2$  induces rapidly AP sites and SSB in DNA and causes motor neuron degeneration structurally similar to that found in ALS (Liu and Martin, 2001a,b). Peroxynitrite induces AP sites, SSB and DSB in motor neuron DNA (Liu and Martin, 2001b). In an *in vivo* model of motor neuron apoptosis, AP sites and SSB accumulate slowly in injured motor neurons before apoptotic nuclear features emerge, and the DNA damage fingerprint is similar to NO toxicity (Liu and Martin, 2001a). Therefore, different experimental systems with motor neurons show that when these cells are challenged by oxidative stress and axotomy, they accumulate DNA damage early in their degeneration and that the formation of peroxynitrite is involved in the neurotoxic mechanisms. In support of our observations, it has been shown that NO

inactivates DNA repair enzymes and leads to DNA damage (Jaiswal et al., 2000).

We have proposed that oxidative stress-induced DNA damage is an upstream signal for motor neuron degeneration in ALS (Martin, 2001). It was proposed nearly 20 years ago that DNA damage has a role in the pathogenesis of ALS (Bradley and Krasin, 1982). It has been discovered only recently that these patients accumulate DNA lesions specifically in motor neurons (Martin, 2001) and that p53 may be involved in the mechanisms of motor neuron degeneration in ALS through apoptosis (Martin, 1999; Martin 2000). The finding that APE/Ref-1 is elevated in ALS further supports the possibility that oxidative stress-induced or hyperactive APE-induced DNA damage contributes to the pathogenesis of ALS.

## Acknowledgments

We thank Ann Price and Frank Barksdale for their outstanding technical assistance. This research was supported by the U.S. Public Health Service, National Institute of Neurological Disorders and Stroke (NS34100) and National Institute on Aging (AG16282), and the Department of Defense, U.S. Army Medical Research and Materiel Command (DAMD17-99-1-9553).

## References

- Al-Abdulla, N. A. and Martin, L. J. (1998) Apoptosis of retrogradely degenerating neurons occurs in association with the accumulation of perikaryal mitochondria and oxidative damage to the nucleus. *Am. J. Pathol.* **153**, 447–456.
- Beckman, J. S., Carson, M., Smith, C. D., and Koppenol, W. H. (1993) ALS, SOD and peroxynitrite. *Nature* **364**, 584.
- Bradley, W. G. and Krasin, F. (1982) A new hypothesis of the etiology of amyotrophic lateral sclerosis. The DNA hypothesis. *Arch. Neurol.* **39**, 677–680.
- Bennett, R. A., Wilson, D. M., Wong, D., and Demple, B. (1997) Interaction of human apurinic endonuclease and DNA polymerase  $\beta$  in the base excision repair pathway. *Proc. Natl. Acad. Sci. USA* **94**, 7166–7169.
- Branum, M. E., Reardon, J. T., and Sancar, A. (2001) DNA repair excision nuclease attacks undamaged DNA. A potential source of spontaneous mutations. *J. Biol. Chem.* **276**, 25,421–25,426.
- Deng, H.-X., Hentati, A., Tainer, J. A., Iqbal, Z., Cayabyab, A., Hung, W.-Y., et al. (1993) Amyotrophic lateral sclerosis and structural defects in Cu,Zn superoxide dismutase. *Science* **261**, 1047–1051.
- Duguid, J. R., Eble, J. N., Wilson, T. M., and Kelley, M. R. (1995) Differential cellular and subcellular expression of the human multifunctional apurinic/apyrimidinic endonuclease (APE/ref-1) DNA repair enzyme. *Cancer Res.* **55**, 6097–6102.
- Ekegren, T., Grundström, E., Lindholm, D., and Aquilino, S.-M. (1999) Upregulation of Bax protein and increased DNA degradation in ALS spinal cord motor neurons. *Acta Neurol. Scand.* **100**, 317–321.
- Ferrante, R. J., Browne, S. E., Shinobu, L. A., Bowling, A. C., Baik, M. J., MacGarvey, U., et al. (1997) Evidence of increased oxidative damage in both sporadic and familial amyotrophic lateral sclerosis. *J. Neurochem.* **69**, 2064–2074.
- Fitzmaurice, P. S., Shaw, I. C., Kleiner, H. E., Miller, R. T., Monks, T. J., Lau, S. S., et al. (1996) Evidence for DNA damage in amyotrophic lateral sclerosis. *Muscle Nerve* **19**, 797–798.
- Furuta, A., Price, D. L., Pardo, C. A., Troncoso, J. C., Xu, Z., Taniguchi, N., and Martin, L. J. (1995) Localization of superoxide dismutases in Alzheimer's disease and Down's syndrome neocortex and hippocampus. *Am. J. Pathol.* **146**, 357–367.
- Gonzalez de Aguilar, J. L., Gordon, J. W., Rene, F., de Tapia, M., Lutz-Bucher, B., Gaiddon, C., and Loeffler, J. P. (2000) Alteration of the Bcl-x/Bax ratio in a transgenic mouse model of amyotrophic lateral sclerosis: evidence for the implication of the p53 signaling pathway. *Neurobiol. Dis.* **7**, 406–415.
- Hayward, C., Colville, S., Swingle, R. J., and Brock, D. J. H. (1999) Molecular genetic analysis of the APEX nuclease gene in amyotrophic lateral sclerosis. *Neurology* **52**, 1899–1901.
- He, B. P. and Strong, M. J. (2000) Motor neuronal death in sporadic amyotrophic lateral sclerosis (ALS) is not apoptotic: a comparative study of ALS and chronic aluminium chloride neurotoxicity in New Zealand white rabbits. *Neuropathol. Appl. Neurobiol.* **26**, 150–160.
- Henner, W. D., Kiker, N. P., Jorgensen, T. J., and Muck, J.-N. (1987) Purification and amino-terminal amino acid sequence of an apurinic/apyrimidinic endonuclease from calf thymus. *Nucleic Acids Res.* **15**, 5529–5544.
- Jaiswal, M., LaRusso, N. F., Burgart, L. J., and Gores, G. J. (2000) Inflammatory cytokines induce DNA damage and inhibit DNA repair in cholangiocarci-

- noma cells by a nitric oxide-dependent mechanism. *Cancer Res.* 60, 184–190.
- Jayaraman, L. and Prives, C. (1995) Activation of p53 sequence-specific DNA binding by short single strands of DNA requires the p53 C-terminus. *Cell* 81, 1021–1029.
- Kisby, G. E., Milne, J., and Sweatt, C. (1997) Evidence of reduced DNA repair in amyotrophic lateral sclerosis brain tissue. *NeuroReport* 8, 1337–1340.
- Kohn, K. W. (1999) Molecular interaction map of the mammalian cell cycle control and DNA repair systems. *Mol. Biol. Cell* 10, 2703–2734.
- Kuncl, R. W., Crawford, T. O., Rothstein, J. D., and Drachman, D. B. (1992) Motor neuron diseases, in *Diseases of the Nervous System. Clinical Neurobiology* (Asbury, A. K., McKhann, G. M., and McDonald, W. I., eds.), WB Saunders, Philadelphia, PA, pp. 1179–1208.
- Levine, A. J. (1997) p53, the cellular gatekeeper for growth and division. *Cell* 88, 323–331.
- Lindahl, T. (1993) Instability and decay of the primary structure of DNA. *Nature* 362, 709–715.
- Liu, Z. and Martin, L. J. (2001a) Motor neurons rapidly accumulate DNA single-strand breaks after in vitro exposure to nitric oxide and peroxynitrite and in vivo axotomy. *J. Comp. Neurol.* 432, 35–60.
- Liu, Z. and Martin, L. J. (2001b) Isolation of mature spinal motor neurons and single cell analysis using the comet assay of early low-level DNA damage induced in vitro and in vivo. *J. Histochem. Cytochem.* 49, 957–972.
- Martin, L. J. (1999) Neuronal death in amyotrophic lateral sclerosis is apoptosis: possible contribution of a programmed cell death mechanism. *J. Neuropathol. Exp. Neurol.* 58, 459–471.
- Martin, L. J., Kaiser, A., and Price, A. C. (1999) Motor neuron degeneration after sciatic nerve avulsion in adult rat evolves with oxidative stress and is apoptosis. *J. Neurobiol.* 40, 185–201.
- Martin, L. J., Price, A. C., Kaiser, A., Shaikh, A. Y., and Liu, Z. (2000) Mechanisms for neuronal degeneration in amyotrophic lateral sclerosis and in models of motor neuron death. *Int. J. Mol. Med.* 5, 3–13.
- Martin, L. J. (2000) p53 is abnormally elevated and active in the CNS of patients with amyotrophic lateral sclerosis. *Neurobiol. Dis.* 7, 613–622.
- Martin, L. J. (2001) Neuronal cell death in nervous system development, disease, and injury. *Int. J. Mol. Med.* 7, 455–478.
- Martin, L. J. and Liu, Z. (2002) Injury-induced spinal motor neuron apoptosis is preceded by DNA single-strand breaks and is p53- and Bax-dependent. *J. Neurobiol.* 50, 181–197.
- Mattson, M. P., Duan, W., Chan, S. L., and Camandola, S. (1999) Par-4. An emerging pivotal player in neuronal apoptosis and neurodegenerative disorders. *J. Mol. Neurosci.* 13, 17–30.
- Nicholson, S. J., Witherden, A. S., Hafezparast, M., Martin, J. E., and Fisher, E. M. C. (2000) Mice, the motor system, and human motor neuron pathology. *Mammalian Genome* 11, 1041–1052.
- Olkowski, Z. L. (1998) Mutant AP endonuclease in patients with amyotrophic lateral sclerosis. *NeuroReport* 9, 239–242.
- Rabizadeh, S., Butler Gralla, E., Borchelt, D. R., Gwinn, R., Valentine, J. S., Sisodia, S., et al. (1995) Mutations associated with amyotrophic lateral sclerosis convert superoxide dismutase from an antiapoptotic gene to a proapoptotic gene: studies in yeast and neural cells. *Proc. Natl. Acad. Sci. USA* 92, 3024–3028.
- Robison, S. H., Tandan, R., and Bradley, W. G. (1993) Repair of N-methylpurines in DNA from lymphocytes of patients with amyotrophic lateral sclerosis. *J. Neurol. Sci.* 115, 201–207.
- Rosen, D. R., Siddique, T., Patterson, D., Figlewicz, D. A., Sapp, P., Hentati, A., et al. (1993) Mutations in Cu/Zn superoxide dismutase gene are associated with familial amyotrophic lateral sclerosis. *Nature* 362, 59–62.
- Rowland, L. P. and Shneider, N. A. (2001) Amyotrophic lateral sclerosis. *N. Engl. J. Med.* 344, 1688–1700.
- Sathasivam, S., Ince, P. G., and Shaw, P. J. (2001) Apoptosis in amyotrophic lateral sclerosis: a review of the evidence. *Neuropathol. Appl. Neurobiol.* 27, 257–274.
- Subba Rao, K. (1993) Genomic damage and its repair in young and aging brain. *Mol. Neurobiol.* 7, 23–48.
- Tandan, R., Robison, S. H., Munzer, J. S., and Bradley, W. G. (1987) Deficient DNA repair in amyotrophic lateral sclerosis cells. *J. Neurol. Sci.* 79, 189–203.
- Tomkins, J., Dempster, S., Banner, S. J., Cookson, M. R., and Shaw, P. J. (2000) Screening of AP endonuclease as a candidate gene for amyotrophic lateral sclerosis. *NeuroReport* 11, 1695–1697.
- Vukosavic, S., Dubois-Dauphin, M., Romero, N., and Przedborski, S. (1999) Bax and Bcl-2 interaction in a transgenic mouse model of familial amyotrophic lateral sclerosis. *J. Neurochem.* 73, 2460–2468.
- Warita, H., Hayashi, T., Murkami, T., Manabe, Y., and Abe, K. (2001) Oxidative damage to mitochondrial DNA in spinal motoneurons of transgenic ALS mice. *Brain Res. Mol. Brain Res.* 89, 147–152.
- Wiedau-Pazos, M., Goto, J. J., Rabizadeh, S., Gralla, E. B., Roe, J. A., Lee, M. K., et al. (1996) Altered reactivity of superoxide dismutase in familial amyotrophic lateral sclerosis. *Science* 271, 515–518.

- World Federation of Neurology Research Group on Neuromuscular Diseases (1994) El Escorial world federation of neurology criteria for the diagnosis of amyotrophic lateral sclerosis. *J. Neurol. Sci.* **124**(Suppl), 96–107.
- Worms, P. M. (2001) The epidemiology of motor neuron diseases: a review of recent studies. *J. Neurol. Sci.* **191**, 3–9.
- Yoshiyama, Y., Yamada, T., Asanuma, K., and Asahi, T. (1994) Apoptosis related antigen, Le<sup>y</sup> and nick-end labeling are positive in spinal motor neurons in amyotrophic lateral sclerosis. *Acta Neuropathol.* **88**, 207–211.
- Xanthoudakis, S. and Curran, T. (1992) Identification and characterization of Ref-1, a nuclear protein that facilitates AP-1 DNA-binding activity. *EMBO J.* **11**, 653–665.

## Rapid Subcellular Redistribution of Bax Precedes Caspase-3 and Endonuclease Activation during Excitotoxic Neuronal Apoptosis in Rat Brain

JOSEPHINE LOK<sup>1</sup> and LEE J. MARTIN<sup>2,3</sup>

### ABSTRACT

Neuronal apoptosis is induced prominently in the newborn rodent brain by glutamate receptor excitotoxicity and related insults, including trauma and hypoxia-ischemia. However, the molecular mechanisms of this neurodegeneration are unclear. We tested the hypothesis that changes in the subcellular distribution of the proapoptotic protein Bax precede the activation of downstream apoptosis-effector mechanisms such as caspase-3 cleavage and endonuclease activation during the progression of excitotoxic neuronal apoptosis in the striatum of newborn rat. Kainic acid (4 nmol) was injected into striatum of anesthetized 7-day-old rats, and the animals were killed at 2, 6, 12, and 24 h postinsult. Controls were age-matched, vehicle-injected, or naive rats. Counts of ultrastructurally confirmed striatal neuron apoptosis in brain sections were highest at 24 h. Striatal tissue was microdissected and fractionated into cytosolic, mitochondrial-, and nuclear-enriched compartments. Immunoblots showed that Bax translocates from the cytosol fraction to the mitochondrial fraction, with maximal translocation by 2 h in the absence of changes in mitochondrial accumulation. Cleaved caspase-3 levels increase progressively in both cytosolic and mitochondrial fractions between 6 and 24 h. Cleaved caspase-3 accumulates in apoptotic striatal neurons as shown by immunolocalization. Internucleosomal fragmentation of DNA coincides with caspase-3 cleavage. We conclude that rapid translocation of Bax to mitochondria precedes caspase-3 and endonuclease activation during excitotoxic neuronal apoptosis in newborn rat brain and that initiation of this death cascade occurs within 2 h after glutamate receptor activation.

**Key words:** brain trauma; glutamate receptor; mitochondria; neonatal brain injury; neuronal cell death

### INTRODUCTION

**A**POPTOSIS IS A FORM OF CELL DEATH that is organized and mediated by active, intrinsic mechanisms (Kerr and Harmon, 1991). In the nervous system, apoptosis is important for several reasons. Neurons and nonneuronal

cells in the developing nervous system normally undergo apoptosis through programmed cell death (Glücksmann, 1951; Oppenheim, 1991; Martin, 2001), and defective apoptosis during CNS development can cause profound cerebral malformations (Kuida et al., 1996; Hakem et al., 1998; Yoshida et al., 1998). Neurons in the immature ro-

Departments of <sup>1</sup>Anesthesiology & Critical Care Medicine, <sup>2</sup>Neuroscience, and <sup>3</sup>Pathology, Division of Neuropathology, Johns Hopkins University School of Medicine, Baltimore, Maryland.

dent CNS undergo vigorous, structurally confirmed apoptosis in response to a variety of injuries. These injurious stimuli include hypoxia-ischemia (Northington et al., 2001a,b), trauma (Bittigau et al., 1999), axotomy and target deprivation (LaVelle and LaVelle, 1958; Torvik, 1976; Martin, 2001), and glutamate receptor excitotoxicity (Portera-Cailliau et al., 1997a,b). In some forms of brain injury, the type of neuronal death (i.e., necrosis versus apoptosis) is influenced by CNS maturity. Apoptosis is much more prominent after injury in the immature brain compared to the mature brain (Portera-Cailliau et al., 1997b), but unequivocal neuronal apoptosis is also found in the adult CNS after injury (Martin, 2001). Therefore, understanding the molecular regulation of apoptosis is relevant to not only nervous system development but also neurodegeneration in pathological conditions affecting the CNS of fetuses, newborns, and adults.

The understanding of the mechanisms of apoptosis in postmitotic cells such as neurons is less advanced compared to nonneural cells. Nevertheless, seminal work has been done on the mechanisms of apoptosis in cultured neurons deprived of neurotrophin (Deckwerth et al., 1996; Easton et al., 1997; Putcha et al., 1999). These studies have established that neuronal apoptosis induced *in vitro* by trophic factor deprivation depends on Bax and its mitochondrial translocation. Some of the critical molecules that control injury-induced neuronal apoptosis in the developing (Martinou et al., 1994; Farlie et al., 1995; Deckwerth et al., 1996) and adult (Martin et al., 2001; Martin and Liu, 2002) CNS have been identified. However, these previous studies have used models of axotomy and target deprivation. The mechanisms of neuronal apoptosis in excitotoxicity-related insults in the developing brain are largely unknown. We tested the hypothesis that a change in the subcellular distribution of the proapoptotic protein Bax is an early event during the progression of excitotoxic neuronal apoptosis in newborn rat brain.

## MATERIALS AND METHODS

### Animals

Animal care was provided in accordance with the National Institutes of Health Guide for the Care and Use of Laboratory Animals. The Animal Care and Use Committee of the Johns Hopkins University School of Medicine approved the animal protocol. All efforts were made to minimize both the suffering and the number of animals used. Timed-pregnant Sprague-Dawley rats were purchased from Charles River Laboratory (Wilmington, MA). The day of delivery was designated as P0. Pups were housed with a nursing mother in the laboratory an-

imal suite with an ambient temperature of 23°C, 12-h light/dark cycle, and *ad libitum* access to food and water.

At 7 days of age, kainic acid (KA) was injected into the striatum of rat pups. Postnatal day 7 (P7) was chosen because naturally occurring programmed cell death in striatum is near completion at this time (Martin, 2001) and because P7 rats are used commonly in a model neonatal hypoxia-ischemia, which induces striatal neuron apoptosis (Nakajima et al., 2000; Northington et al., 2001b). KA (Sigma, St. Louis, MO) was dissolved in 100 mM phosphate-buffered saline (PBS, pH 7.4) and was stored in the dark at -20°C until used. Pups were deeply anesthetized (enflurane/nitrous oxide/oxygen) and were placed in a neonatal rat stereotaxic apparatus (Stoelting, Wood Dale, IL). Surgical anesthesia was maintained with enflurane and nitrous oxide. Body temperature was maintained with external warming. The scalp was cleaned with betadine and 70% isopropyl alcohol prior to making a midsagittal incision. A burr hole in the skull over the right hemisphere was made with a dental drill. KA (4 nmol, 300 nL total volume) or an equal volume of PBS was injected stereotaxically with a Hamilton syringe into the striatum (0.5 mm anterior and 1.5 mm lateral to Bregma; 2.5 mm ventral to the dura). The neurotoxin and buffer were injected over 1 min, and the needle was left in place for 5 min before it was withdrawn slowly.

After the intracerebral injections, the animals were sacrificed at 2, 6, 12, and 24 h. Pups were triaged into two groups for different types of experiments. Some animals were perfusion fixed for neuropathological analysis of the brain by light and electron microscopy (EM). Other animals were quickly decapitated and their brains were rapidly removed for biochemical experiments. For homogenate-based assays, the ipsilateral and contralateral striata from at least four to six animals were pooled for each time point. Controls animals were rats that were injected with PBS and rats that were naive and received no injections.

### Structural Analysis of Neuronal Apoptosis

For histological studies, pups were anesthetized with 8% chloral hydrate (6 mg/g body weight, ip). The pups were perfusion-fixed through the left ventricle with 20 mL of PBS (100 mM, pH 7.4) followed by 4% paraformaldehyde in PBS (120 mL). Brains were allowed to fix *in situ* for 2 h and then were removed from the skull, cryoprotected in 20% glycerol, and frozen, and then serial coronal sections (40  $\mu$ m in thickness) were cut through the entire striatum using a sliding microtome. Every fifth section was mounted on gelatin-coated microscope slides, dried, dehydrated with alcohols, defatted with xylene, and stained with cresyl violet.



At 24 h postlesion, KA- and PBS-injected rat pups ( $n = 2$  per time-point) were injected with an overdose of chloral hydrate and were perfused for EM with 1% paraformaldehyde/0.1% glutaraldehyde in 100 mM phosphate buffer followed by 2% paraformaldehyde/2% glutaraldehyde in phosphate buffer. Brains were postfixed *in situ* with the same fixative. The striatal samples were microdissected from each brain, rinsed in 100 mM phosphate buffer, placed in 2% osmium tetroxide for 2 h, dehydrated and embedded in plastic. Semithin sections (1  $\mu\text{m}$ ) stained with 1% toluidine blue were screened for areas of interest, and then thin sections were cut on an ultramicrotome (Sorvall, Norwalk, CT), contrasted with uranyl acetate and lead citrate, and viewed with a Jeol 100S electron microscope.

#### *Quantification of Apoptotic Cells in the Striatum*

Cresyl violet-stained sections were used to count end-stage apoptotic cells in the striatum of pups at 2, 6, 12, and 24 h after the excitotoxic lesion. Apoptotic cells were shrunken and round with a translucent rim of cytoplasm, detached from surrounding neuropil, and with two or more sharply delineated, uniformly dense, smooth, round, regularly shaped discrete masses of dark purple chromatin. Counts of end-stage apoptotic cells were made in six, nonoverlapping high-power fields ( $1,000\times$ ) in the middle of each striatum in the rostrocaudal axis. Each field was counted twice with the mean number of apoptotic cells reported.

#### *DNA Fragmentation Analysis*

To identify the pattern of DNA fragmentation after excitotoxic lesions, DNA was extracted from nuclear-enriched fraction isolated from microdissected ipsilateral or contralateral striatum from PBS-injected and KA-injected pups that survived for 2, 6, 12, and 24 h. Striatal samples were treated with proteinase K overnight, genomic DNA was extracted with phenol/chloroform/isoamyl alcohol. DNA concentration was determined spectrophotometrically. After digesting RNA with DNase-free RNase followed by repurification, DNA ( $\sim 2 \mu\text{g}$ ) was end-labeled with digoxigenin-11-dd-UTP using terminal deoxynucleotidyl transferase. DNA was fractionated in a 1.5% agarose gel, transferred to a nylon membrane, and crosslinked with ultraviolet light. Membranes were incubated in 2% nucleic acid blocking reagent containing antidigoxigenin Fab fragments (Boehringer Mannheim) conjugated to alkaline phosphatase (7.5 Units), and detected with disodium 3-(4-methoxyspiro[1,2-dioxetane-3,2'-(5''-chloro)tricyclo[3.3.1]decan-4-yl) phenyl phosphate (CSPD, Boehringer Mannheim) followed by exposure to Kodak X-Omat AR film.

#### *Measurement of Cell Death Proteins by Immunoblotting*

Striatal tissue was homogenized and separated into subcellular fractions enriched in soluble proteins (S2), mitochondrial membranes (P2), and nuclei (P1). The nuclear fractions were used for genomic DNA extractions. The level of Bax and caspase-3 immunoreactivity in P2 and S2 fractions at each time point was measured by immunoblotting. Subcellular fractions were prepared by homogenizing striatal samples in cold 20 mM Tris HCl (pH 7.4) containing 10% (wt/vol) sucrose, 20 U/mL aprotinin (Trasylol), 20  $\mu\text{g}/\text{mL}$  leupeptin, 20  $\mu\text{g}/\text{mL}$  antipain, 20  $\mu\text{g}/\text{mL}$  pepstatin A, 20  $\mu\text{g}/\text{mL}$  chymostatin, 0.1 mM phenylmethylsulfonyl fluoride, 10 mM benzamidine, 1 mM EDTA, and 5 mM EGTA. Homogenates were centrifuged at  $1,000g_{\text{av}}$  for 10 min ( $4^\circ\text{C}$ ), and the resulting pellet (P1 fraction) was resuspended in homogenization buffer (without sucrose) supplemented with 20% (wt/vol) glycerol. The supernatant was then centrifuged at  $54,000g_{\text{av}}$  for 20 min ( $4^\circ\text{C}$ ) to yield soluble (S2) and membrane (P2) fractions. This subcellular fractionation method has been verified by organelle/enzyme markers (Martin, 2000). Protein concentrations in different fractions were measured by a Bio-Rad protein assay with bovine serum albumin as a standard.

Protein (20  $\mu\text{g}$  for Bax; 25–40  $\mu\text{g}$  for caspase-3 blots) from P2 and S2 fractions were resolved by SDS-PAGE and transferred to nitrocellulose filters by electroblotting. The reliability of sample loading and electroblotting in each experiment was evaluated by staining nitrocellulose membranes with Ponceau S before immunoblotting. Nitrocellulose membranes were blocked in 2.5% or 5% (w/v) nonfat dry milk in Tris-buffered saline (TBS). The following antibodies were used: rabbit polyclonal antibodies against Bax N-terminus (Upstate, antibody 06-499), Bax N-terminus (Santa Cruz, antibody N-20), caspase-3 (Santa Cruz, antibody H-277), cleaved caspase-3 (Cell Signaling Technology, antibody D175), and monoclonal antibody to cytochrome c oxidase subunit 1 (Molecular Probes). After overnight incubation with the primary antibodies in TBS supplemented with nonfat dry milk and 0.05% or 0.1% (v/v) Tween-20, membranes were rinsed and then incubated with peroxidase-conjugated secondary antibody, and immunoreactive proteins were visualized with enhanced chemiluminescence (Amersham or Pierce) and exposure to radiographic film.

To quantify Bax, caspase-3, and cytochrome c oxidase subunit 1 (Cox1) immunoreactivity, films were scanned and analyzed by densitometry. Protein levels were expressed as relative optical density measurements. The measurements were normalized to protein loaded in each lane as determined by total protein staining of gels. Im-

munoblotting results were replicated in two to four different experiments.

### *Immunolocalization of Cleaved Caspase-3 in Neonatal Striatum after KA Lesions*

The localization of cleaved caspase-3, presumably representing active caspase-3, was examined in striatum during apoptosis at the light microscopic level in rat pups. Caspase-3 was detected using a standard immunoperoxidase method with diaminobenzidine as chromogen. Brain sections that were near adjacent to those used for cresyl violet staining and cell counting were used. Caspase-3 was detected with a rabbit polyclonal antibody (Cell Signaling Technology, D175) that specifically detects a cleaved (active) form of caspase-3; the specificity of this antibody was confirmed by immunoblotting. Immunocytochemical sections were viewed without counterstaining and then with cresyl violet counterstaining to visualize apoptotic cells.

## RESULTS

### *KA Lesions Induce Large-Scale Neuronal Apoptosis in Neonatal Rat Brain*

The striatum is composed of a population of neurons that is relatively homogeneous morphologically as seen by cresyl violet staining (Fig. 1A). KA induces prominent apoptosis of these neurons in newborn rat striatum (Fig. 1). The apoptosis was identified by light microscopy (Fig. 1B,C), EM (Fig. 1D), and internucleosomal fragmentation of DNA (Fig. 1G). The morphology of this degeneration is very indicative of apoptosis. In cresyl violet-stained sections, neuronal cell bodies are shrunken and chromatin is aggregated into multiple small, round masses or into few, larger, dense chromatin masses (Fig. 1B,C). Most of the end-stage apoptosis emerges between 12 and 24 h after the insult (Fig. 1F). At 24 h after excitotoxic exposure, neuronal apoptosis is widespread with thousands of striatal cells at or near end-stage apoptosis (Fig. 1C,F). EM was used to confirm the apoptosis. By 24 h postlesion, the ultrastructure of degenerating neurons is characterized by prominent cytoplasmic and nuclear condensation with chromatin compaction into uniformly large round clumps within the nucleus (Fig. 1D). Based on cell size, nuclear morphology and number present, these apoptotic profiles appear to be neurons at low magnification. This interpretation was confirmed by EM evidence at high magnification revealing that these cells are contacted by residual axosomatic synapses (Fig. 1E).

The pattern of genomic DNA fragmentation in the

striatum was used as a marker for cell death. An internucleosomal ("ladder") pattern of DNA fragmentation is prominent in the ipsilateral striatum at 12 and 24 h after unilateral intrastratial injection of KA (Fig. 1G). A faint ladder is present at 6 h (Fig. 1G). Between 12 and 24 h, the DNA fragmentation progresses from higher molecular weight forms to lower molecular weight DNA fragments (Fig. 1G). Genomic DNA extracted from the contralateral striatum from the same KA-injected pups and from PBS controls had no detectable DNA fragmentation at the same recovery times (Fig. 1G).

### *Validation of Immunoblot Assay System*

Demonstrating that proteins were measured within the linear range of detection validated the immunoblot assay (Fig. 2). Gels were loaded with increasing amounts of total protein and probed with antibodies to Bax (Fig. 2, left panel) or Cox1 (Fig. 2, right panel). The detection of Bax in the soluble fraction was linear between 1 and 30  $\mu$ g of total protein (Fig. 2, left panel). The detection of Cox1 in mitochondrial fractions was linear between 5 and 30  $\mu$ g of total protein (Fig. 2, right panel).

### *Bax Levels in Striatal Mitochondrial Fractions Change with Maturation*

Animal age influences the induction of neuronal apoptosis (Martin et al., 1998). After KA lesions, newborn rat pups exhibit a more robust classical apoptosis response compared to adult rats (Portera-Cailliau et al., 1997a,b). Similarly, after brain trauma and cerebral hypoxia-ischemia (Northington et al., 2001b; Martin, 2001), the classical apoptosis component of the neurodegeneration is more prominent in newborn rodents compared to adults. To begin to understand this age-related cell death response *in vivo*, the subcellular distribution of Bax was examined in the developing rat striatum.

From naive rats, striatal samples were microdissected and fractionated by differential centrifugation into mitochondrial-enriched (P2) and soluble (S2) compartments (Fig. 3A). The mitochondrial fraction is enriched in the mitochondrial membrane protein Cox1 (Fig. 2, right panel, and Fig. 3B). Soluble fractions did not contain Cox1 (data not shown). The ratio of mitochondrial Bax to soluble Bax is higher in the immature striatum compared to the mature striatum (Fig. 3A,C). In the immature striatum, more Bax is present in the mitochondrial compartment compared to the soluble compartment; in contrast, in the adult striatum, more Bax is present in the soluble fraction compared to the mitochondrial compartment. This change occurs gradually with maturation, during which time mitochondrial protein increases (Fig. 3B,D).

# MECHANISMS OF EXCITOTOXIC NEURONAL DEATH

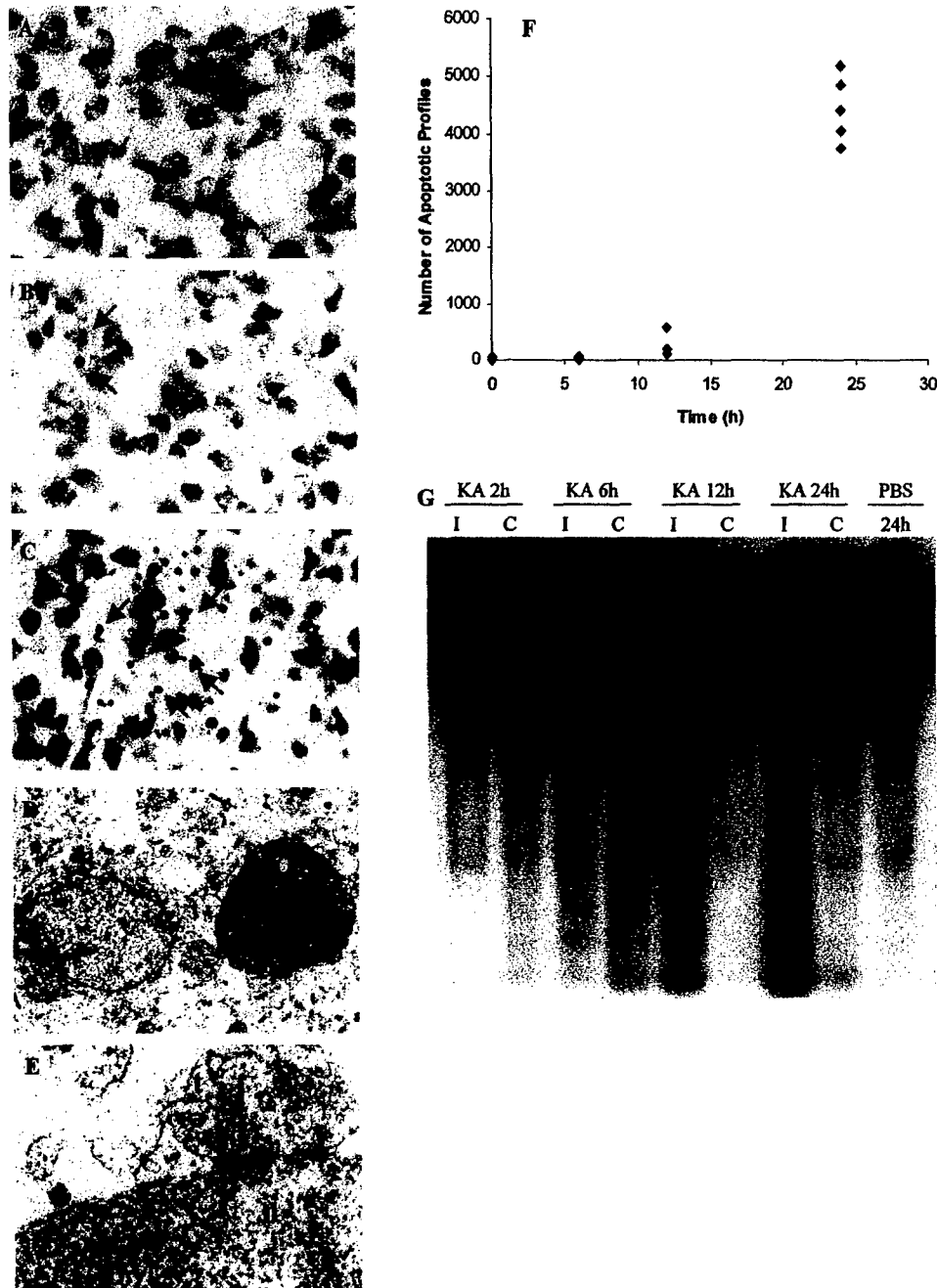


**FIG. 1.** Intrastratial excitotoxic lesions in newborn rat induce copious apoptosis. (A–C) Cresyl violet-stained sections of P7 rat pup brain showing the normal immature striatum with a uniform population of neurons (A) and the KA-lesioned striatum with neuronal apoptosis at 12 h (B, arrows) and 24 h (C, arrows). (D) EM confirms the apoptosis of striatal neurons (cell at right) after excitotoxic injury with KA. A normal cell is shown (at left) for comparison. The apoptotic neuron (n) has a dark cytoplasm and the chromatin is packaged into uniformly dark, round masses. (E) EM reveals that apoptotic cells are unequivocally neurons (n) because they are contacted by presynaptic terminals (t) that form axosomatic synapses (arrow). (F) Counts of apoptotic cells/mm<sup>2</sup> after intrastratial injection of KA. Each data point is one P7 rat. (G) Biochemical verification of striatal cell apoptosis after KA lesions. DNA fragmentation analysis of nuclear fraction-extracted genomic DNA of lesioned (ipsilateral, I) and non-lesioned (contralateral, C) P7 rat striatum at 2, 6, 12, and 24 h postinjection. At 6 h, DNA fragmentation is faint. At 12 h, an internucleosomal ladder is observed, with a larger proportion of high molecular weight fragments. At 24 h, there is prominent DNA fragmentation, with a larger proportion of low molecular weight fragments, consistent with increasing endonuclease activity. Internucleosomal DNA fragmentation was not observed in the striatum of PBS-injected pups.

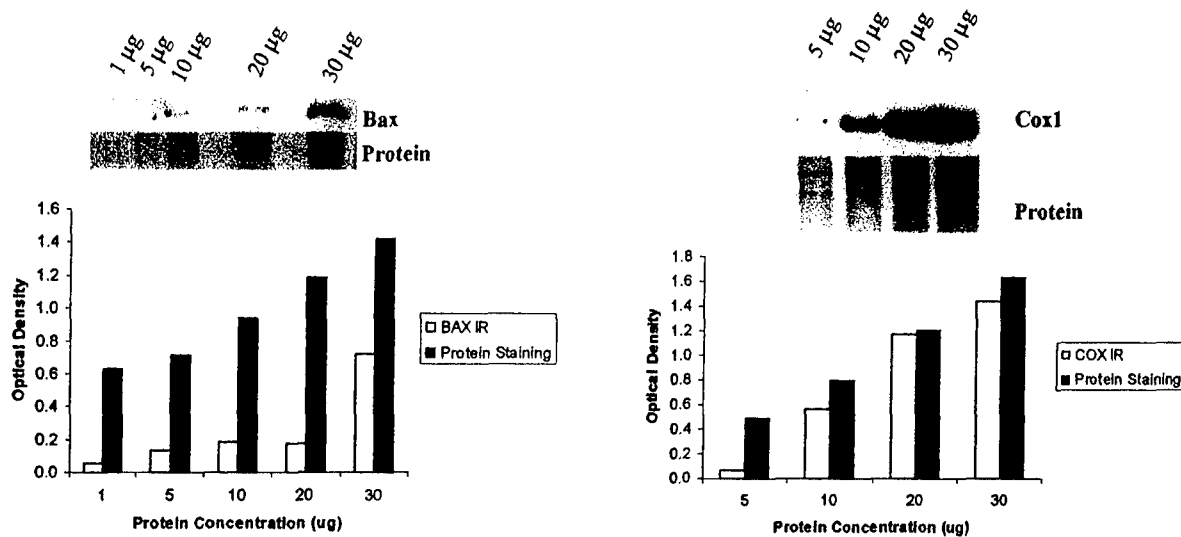


**FIG. 2.** Immunoblot detection of proteins within the linear range. Immunoblot of Bax in soluble fractions of developing rat striatum (left panel). The corresponding protein stain of the gel is shown. The graph shows the optical density of Bax immunoreactivity (IR) at different concentrations of total protein subjected to SDS-PAGE. Immunoblot of Cox1 in mitochondrial fractions of developing rat striatum (right panel). The corresponding protein stain of the gel is shown. The graph shows the optical density of Cox immunoreactivity (IR) at different concentrations of total protein subjected to SDS-PAGE.

#### *Bax Translocates Rapidly into the Mitochondrial Fraction Early During Excitotoxic Neuronal Apoptosis in Newborn Rat Striatum*

The levels of Bax in mitochondrial-enriched and soluble fractions were analyzed during the progression of excitotoxic neuronal apoptosis (Fig. 4). Bax levels decrease in the soluble fraction but increase correspondingly in the mitochondrial-enriched fraction early after KA exposure (Fig. 4A–C). The increase in Bax within the mitochondrial fraction is maximal within 2 h after KA (Fig. 4B,C). This prominent change at 2 h after KA was confirmed with two antibodies that detect different epitopes of the protein (Fig. 4B,C). Cox1 immunoreactivity decreases progressively with time after KA. The loss of mitochondrial marker is most marked at 24 h after KA (Fig. 4D), consistent with the prominent end-stage apoptosis found at this time point (Fig. 1C,E,G).

#### *Caspase-3 is Cleaved During Excitotoxic Neuronal Apoptosis in the Newborn Rat Striatum*

Activation of caspase-3 is a critical downstream event in many forms of PCD (Kuida et al., 1996). We evaluated if caspase-3 is proteolytically cleaved during excitotoxic neuronal apoptosis. The levels of cleaved caspase-3 increase in striatum after KA lesions (Fig. 5). Formation of cleaved caspase-3 is most prominent between 12 and 24 h after lesioning (Fig. 5B,C). The caspase-3 cleavage was detected with two antibodies that bind different epitopes. One antibody (Santa Cruz) revealed that cleaved

caspase-3 undergoes an early redistribution into the mitochondrial-enriched fraction by 2 h postlesion followed by a later increase in the soluble fraction at 12–24 h (Fig. 5C). An early translocation of caspase-3 is consistent with subcellular fractionation analyses of induced apoptosis in HeLa cells (Zhivotovsky et al., 1999).

An immunocytochemical localization analysis was done using the antibody that recognizes only cleaved caspase-3 (Fig. 6). In the striatum of naive and PBS-injected P7 pups, only occasional isolated cells show cleaved caspase-3 immunoreactivity (not shown), consistent with previous observations demonstrating a low level of naturally occurring developmental programmed cell death at this time (Martin, 2001). At 12 h after intrastriatal injection of KA, a marked increase in cleaved caspase-3 is found throughout the striatum (Fig. 6A,C,D), while much less cleaved caspase-3 is visualized in the contralateral striatum (Fig. 6B). After KA lesions, cleaved caspase-3 is detected primarily in neurons based on size, morphology, and distribution (Fig. 6C). Caspase-3 accumulates in the cytoplasm and nucleus of neurons showing nascent chromatin condensation at 12 h (Fig. 6D). At 24 h after KA, cleaved caspase-3 is detected in many cells with clearly distinguishable apoptotic nuclei and is also present in cellular debris within the neuropil (Fig. 6E,F), while the contralateral striatum has rare staining (Fig. 6G). The prominent formation of cleaved caspase-3 occurs between 6 and 12 h after the injury, because at 6 h after the KA lesion the ipsilateral striatum shows only faint staining (Fig. 6H), but at 12 h the staining for cleaved caspase-3 is intense (Fig. 6A).

## MECHANISMS OF EXCITOTOXIC NEURONAL DEATH

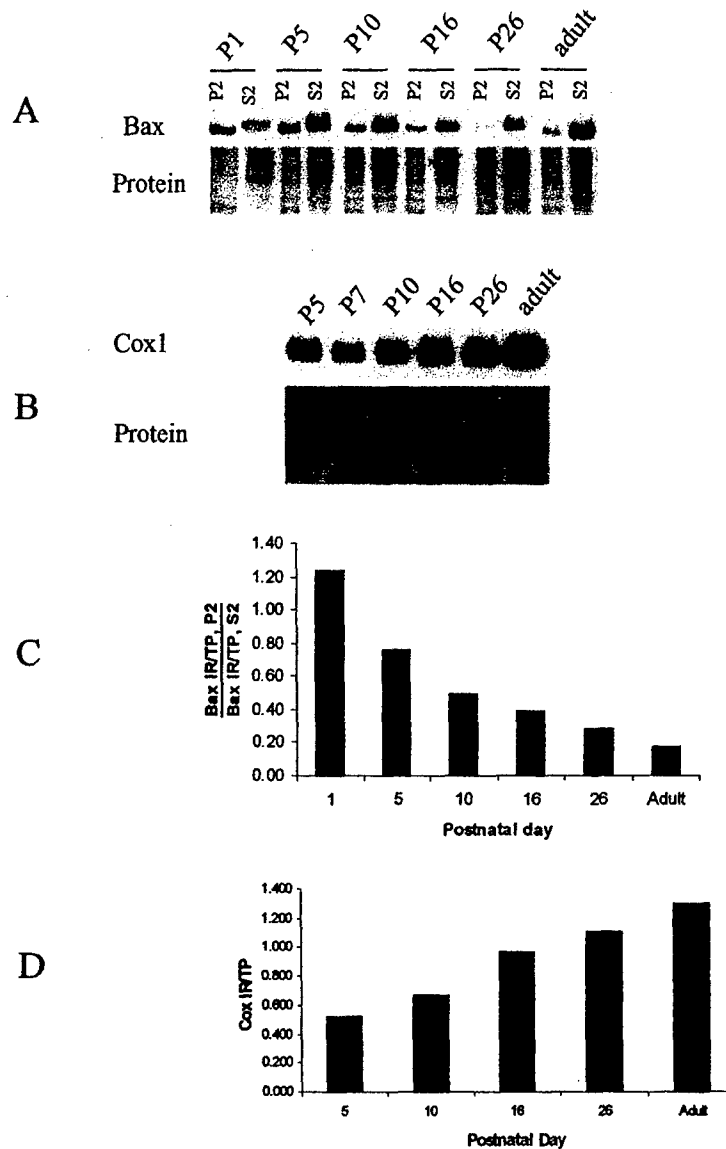


**FIG. 3.** The subcellular distribution of Bax changes during brain maturation. (A) Immunoblots of Bax in mitochondrial-enriched (P2) and soluble (S2) fractions of developing rat striatum at postnatal (P) days 1, 5, 10, 16, and 26, and in adult rat. The corresponding protein stain of the gel is shown for normalization to total protein. (B) Immunoblot of Cox1 levels in mitochondrial (P2) fractions in striatum of developing rats from postnatal day 1 (P1) to adult. Cox1 was not detected in the S2 fraction (not shown). The corresponding protein stain of the gel is shown for normalization to total protein. (C) Ratio of mitochondrial (P2) Bax to soluble (S2) Bax in striatum from normal rats at postnatal days 1, 5, 7, 10, 16, and 26 and in adult rat. Striatal samples were fractionated into mitochondrial-enriched and soluble fractions. Amount of Bax is indicated by the ratio of Bax immunoreactivity (IR) in immunoblots over total protein (TP). (D) Cox1 levels (used as an indirect marker for mitochondrial abundance) increase during postnatal maturation of the striatum. P2 fractions were probed for Cox1 by immunoblotting and presented as the ratio of Cox1 immunoreactivity (IR) over total protein (TP).

## DISCUSSION

Brain damage is a leading cause of pediatric morbidity and mortality. A large proportion of pediatric brain injuries results from two primary insults, mainly hypoxia-ischemia and trauma (Kochanek et al., 2000). Although

the initial pathophysiology of these two processes is quite distinct from each other, current data suggest that they have common molecular pathways that lead to neuronal death. Excitotoxic activation of glutamate receptors seems to be shared by both cerebral ischemia and trauma (MacManus and Buchan, 2000; Martin, 2001). Neuronal

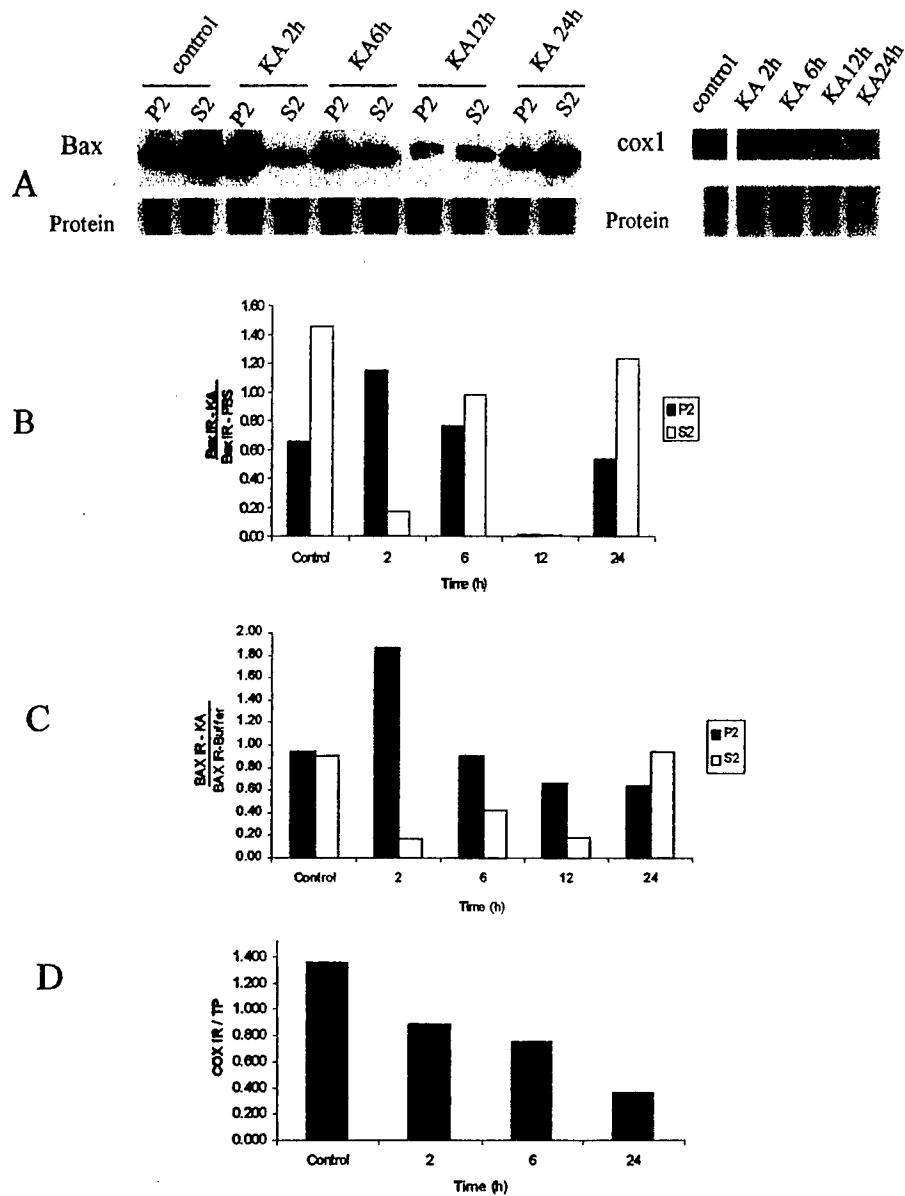


**FIG. 4.** Bax rapidly redistributes to the mitochondrial compartment early during excitotoxic neuronal apoptosis. (A) Immunoblots of Bax in mitochondrial (P2) and soluble (S2) fractions of striatum isolated from P7 rat at 2, 6, 12, and 24 h after KA (top left). Cox-1 levels in mitochondrial (P2) fractions during excitotoxic neuronal apoptosis (top right). The corresponding total protein staining of the gel is shown for normalization to protein loading. (B) Quantification of Bax immunoreactivity (IR) in mitochondrial (P2) and soluble (S2) fractions of P7 rat striatum at 2, 6, 12, and 24 h after KA. Bax was detected using a rabbit polyclonal IgG antibody (Upstate 06-499) that recognizes residues 1-21 of human Bax. Each bar represents the ratio of Bax IR (normalized to protein loading) in KA-injected animals over Bax immunoreactivity (normalized to protein loading) in PBS-injected animals. Control animals did not receive either injection. (C) Quantification of Bax immunoreactivity (IR) in mitochondrial (P2) and soluble (S2) fractions of P7 rat striatum at 2, 6, 12, and 24 h after KA. Bax IR was detected with polyclonal IgG antibody whose epitope maps at the amino terminus of human Bax (Santa Cruz, N-20). Each bar represents the ratio of Bax IR (normalized to protein loading) in KA-injected animals over Bax immunoreactivity (normalized to protein loading) in PBS-injected animals. Control animals did not receive either injection. (D) Mitochondrial quantity in striatal tissue (P2 fractions) after KA injection. P2 fractions were probed with antibody to Cox1, and mitochondrial protein content is indicated by the ratio of Cox1 immunoreactivity over total protein.

# MECHANISMS OF EXCITOTOXIC NEURONAL DEATH

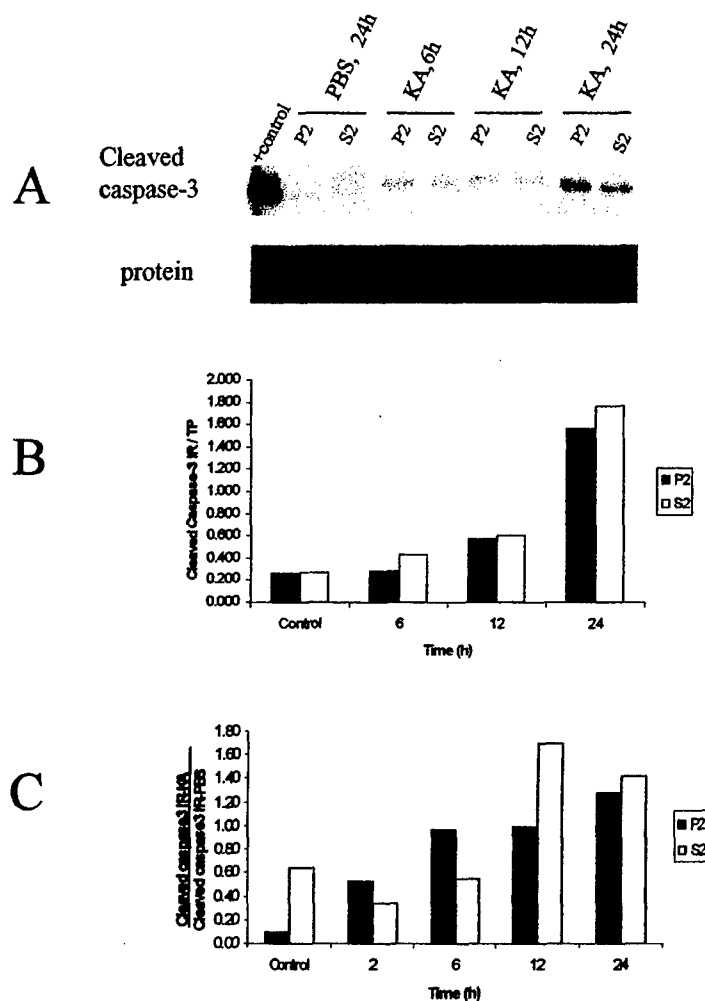


**FIG. 5.** Cleavage of caspase-3 during excitotoxic neuronal apoptosis. (A) Immunoblot for cleaved caspase-3 in mitochondrial-enriched (P2) and soluble (S2) fractions of striatum isolated from P7 rat at 6, 12, and 24 h after KA. The corresponding protein stain of the gel is shown for normalization to total protein. Caspase-3 is activated during excitotoxic neuronal apoptosis. The positive control for cleaved caspase-3 (far left lane) is cell lysates of C6 cells treated with 250  $\mu$ g/mL cytochrome C. (B,C) Quantification of caspase-3 activation during excitotoxic neuronal apoptosis. Bars in each histogram represents the amount of cleaved caspase-3 immunoreactivity as detected with antibody that specifically detects cleaved subunits (B, D175) and antibody that detects proenzyme and cleaved caspase-3 (C, H-277). Amount of cleaved caspase-3 is expressed as cleaved caspase-3 immunoreactivity (IR) over total protein.

apoptosis is a prominent feature of the brain damage induced in the newborn rodent brain by glutamate receptor excitotoxicity (Portera-Cailliau et al., 1997a,b) and related insults, including hypoxia-ischemia (Northington et al., 2001a,b) and trauma (Bittigau et al., 1999). Despite the prominent contribution of apoptotic neurodegeneration to the evolution of neonatal brain injury in rodents, the mechanisms of excitotoxic neuronal apoptosis are still not understood. A better understanding of this process in a newborn rodent model of brain injury may provide useful therapeutic directions for brain injury in human newborns.

We used an animal model of neurodegeneration induced by KA to identify biochemical correlates of excitotoxic neuronal apoptosis in the neonatal rat striatum. This brain region in newborns is highly vulnerable to excitotoxicity (Portera-Cailliau et al., 1997a) and hypoxia-ischemia (Northington et al., 2001b). We have shown elsewhere (Portera-Cailliau et al., 1997a,b) and here that intracerebral administration of this neurotoxin causes copious neuronal apoptosis in the striatum. The apoptosis was verified structurally with light microscopy and EM, and by immunolocalization of cleaved caspase-3. Ubiquitous apoptosis was observed at 24 h after the insult.

DNA degradation by internucleosomal fragmentation further confirmed the presence of apoptosis.

Excitotoxic neuronal apoptosis was associated with rapid changes in cell death proteins. Within 2 h after neurotoxin exposure, Bax increased in the mitochondria-enriched fraction of striatum, as shown by immunoblotting. The mitochondrial enrichment of the subcellular fraction was verified by the presence of Cox1. This is the first demonstration of such a rapid redistribution of Bax during apoptosis of neurons and cells in general. We used a homogenate-based assay of striatal tissue, so we currently assume that the increase occurs in striatal neurons. Neurons are the primary cells that undergo apoptosis in this model as shown directly by EM and by the immunolocalization of cleaved caspase-3. Although immunoblot analysis of subcellular fractions is commonly used to assay for translocation of proteins, the increase in Bax in mitochondria of neurons needs to be shown directly in future studies by quantitative immunogold EM (Martin and Liu, 2002). We also found, surprisingly, with one of two antibodies that detect cleaved fragments of caspase-3, a rapid increase in cleaved caspase-3 in mitochondria. These antibodies recognize different epitopes on the caspase-3 molecule. The extensive proteolytic processing of this protein could generate cleavage products of different sizes that are differentially detected with these antibodies, revealing a complex targeting of this protein. We are not certain but this difference with the two caspase-3 antibodies may provide insight into the processing and subcellular targeting of caspase-3 fragments in apoptotic neurons. Translocation of active caspase-3 to mitochondria has been found previously in Jurkat cells undergoing apoptosis (Zhivotovsky et al., 1999). We confirmed by immunocytochemistry that cleaved caspase-3 accumulates in the cytoplasm of neurons. This study demonstrates for the first time the activation of cell death effector mechanisms during excitotoxic neuronal death in newborn rat brain that was structurally verified as primarily apoptosis. The initiation of this death cascade and the possible commitment to apoptosis occur relatively fast, within 2 h after glutamate receptor activation, and involves a subcellular redistribution of cell death proteins and caspase-3 activation. These findings are particularly relevant to newborn brain damage after hypoxia-ischemia (Northington et al., 2001a,b) and trauma, and to some age-related neurodegenerative diseases, such as amyotrophic lateral sclerosis, in which neuronal apoptosis and a redistribution of cell death proteins including Bax, have been discovered (Martin, 1999, 2001).

The findings reported in this study provide novel information on the progression of neuronal apoptosis specifically in the immature brain after injury. Copious

end-stage apoptosis is present in the striatum, as observed in Nissl, EM, and immunocytochemical preparations at 24 h after an excitotoxic lesion. Structural evidence for apoptosis (i.e., chromatin condensation) begins to emerge between 6 and 12 h postlesion by light microscopy. Thus, the emergence and completion of the structural process of neuronal apoptosis is relatively rapid (~12 h) in neonatal rat striatal neurons. At 6 h postlesion, faint internucleosomal fragmentation of DNA was detected, and at 12 and 24 h the ladder pattern was pronounced with progressive formation of lower molecular weight fragments of DNA. Apparently in immature striatal neurons, large-scale genomic DNA fragmentation coincides with the formation of large, round nuclear masses characteristic of apoptosis. Similarly, the cleavage of caspase-3, a protease whose activation can lead directly to an apoptotic phenotype, was first prominent in the ipsilateral striatum at 12 h postlesion. The increase in cleaved caspase-3 was greatest at 24 h postlesion. Cleaved caspase-3 was present in cells with an end-stage apoptotic morphology and in cellular debris. Taken together, these results suggest that neurons in the striatum after an excitotoxic insult are committed to apoptosis between 6 and 12 h after the lesion, and this process advances quickly to end-stage death by 24 h.

The contribution of apoptotic mechanisms to excitotoxic death of neurons has been examined in neuronal culture. However, these studies have provided conflicting results. In primary culture of mouse cortical cells, KA exposure induced an increase in Bax protein, and *bax* gene deficiency significantly protected cells against KA receptor toxicity (Xiang et al., 1998). However, NMDA receptor toxicity in mouse cerebellar granule neurons (Miller et al., 1997) and mouse cortical cells (Dargusch et al., 2001) was not Bax related. *In vitro* studies of caspase activation in excitotoxic cell death are also conflicting. Glutamate (100  $\mu$ M) stimulation of mouse cortical cells did not cause an increase in caspase activity (Johnson et al., 1999), but NMDA-treated rat cortical cells showed increased caspase activity (Tenneti and Lipton, 2000). These conflicting results may be due to the finding that activation of different subtypes of glutamate receptors appears to activate different cell death pathways (Portera-Cailliau et al., 1997b). The *in vitro* data that are most relevant to and consistent with our *in vivo* study support a role for Bax in KA-induced neuronal apoptosis (Xiang et al., 1998). Future studies need to examine the effects of *bax* gene deficiency on KA-induced neuronal apoptosis in the neonatal mouse brain.

Our results on glutamate receptor-mediated excitotoxic neuronal apoptosis in neonatal rat are consistent with previous results from our laboratory using a neonatal rat



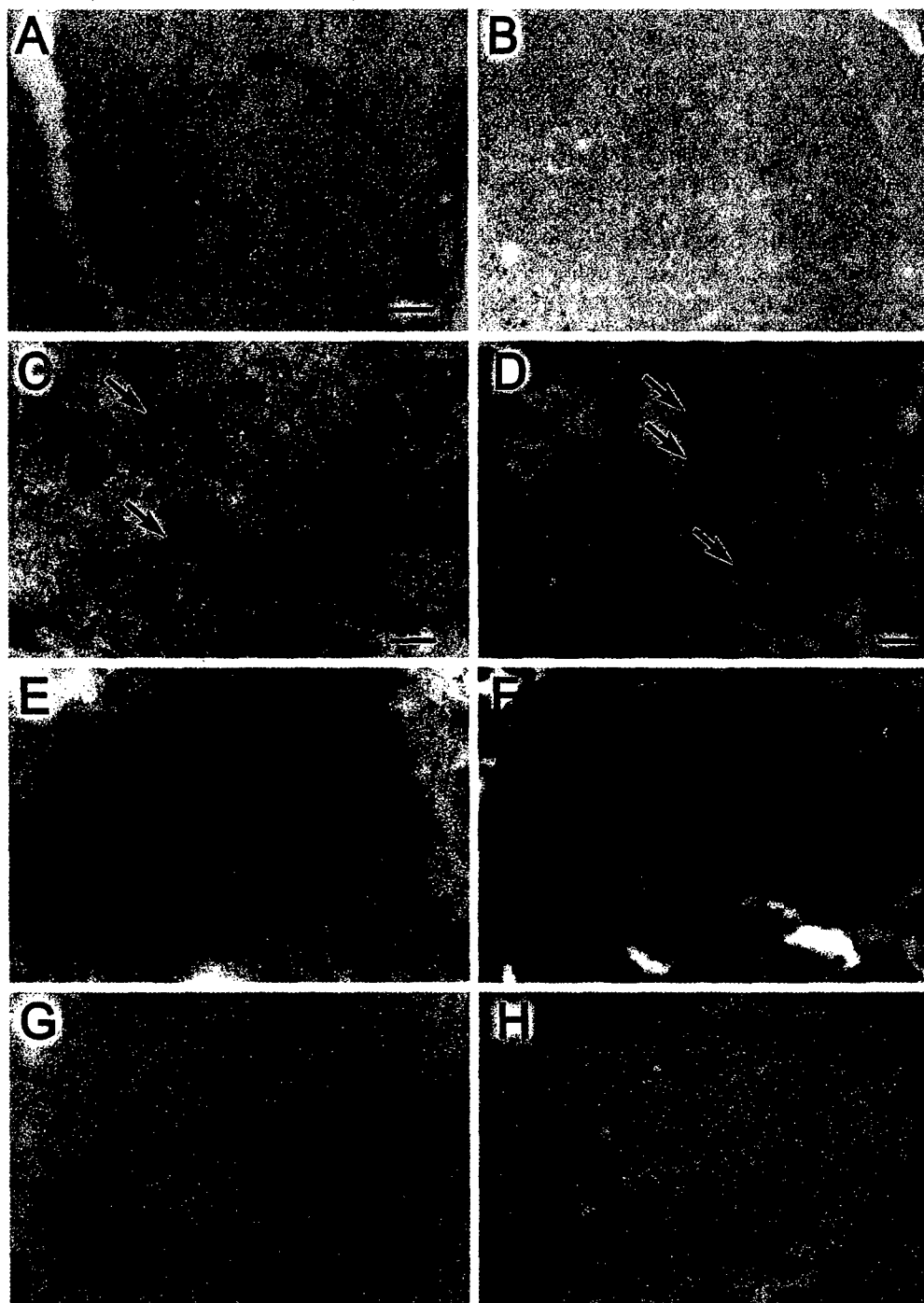


**FIG. 6.** Immunolocalization of cleaved caspase-3 in neonatal rat striatum after excitotoxic lesions. (A) At 12 h after KA, cleaved caspase-3 (brown staining) is prominent in the ipsilateral striatum. The artifact is the needle track. Bar = 200  $\mu$ m (same for B and H). (B) Immunoreactivity for cleaved caspase-3 in the contralateral striatum (opposite side to that shown in A) at 12 h after KA is very low and is restricted to isolated cells at periventricular locations (upper right corner). (C) Many neurons in the ipsilateral striatum at 12 h after KA have cleaved caspase-3 (arrows). Bar = 25  $\mu$ m (same for E and G). (D) Immunoperoxidase sections counterstained with cresyl violet (purple staining) revealed that many striatal cells with cleaved caspase-3 at 12 h after KA are neurons with nascent chromatin condensation (arrows). (E) At 24 h after KA, cleaved caspase-3 immunoreactivity (brown staining) is mostly dispersed throughout the neuropil of the ipsilateral striatum. (F) Immunoperoxidase sections counterstained with cresyl violet (purple staining) revealed that cleaved caspase-3 immunoreactivity at 24 h after KA localized to cellular debris and end-stage apoptotic cells. (G) Immunoreactivity for cleaved caspase-3 in the contralateral striatum (opposite side to that shown in E) at 24 h after KA is very low and is restricted to occasional isolated cells. (H) Immunoreactivity for cleaved caspase-3 in the ipsilateral striatum at 6 h after KA is barely detectable.

model of hypoxia-ischemia. During apoptosis of neurons after hypoxia-ischemia, the levels of Bax in the mitochondria-enriched cell fraction increased, and cytochrome c accumulated in the soluble protein compartment (Northington et al., 2001a). This apoptosis was associated with a rapid increase in the levels of the Fas death receptor in cell membranes and caspase-8 cleavage (Northington et al., 2001a). Increased levels of Fas death receptor and Bax, cytochrome c accumulation, and caspase-8 cleavage were upstream to marked cleavage of caspase-3.

Excitotoxic and ischemic neurodegeneration in the immature brain is phenotypically heterogeneous and regionally specific. Neurodegeneration in specific regions is model- or species-related. In neonatal rat exposed to excitotoxins (Portera-Cailliau et al., 1997a,b) and ischemia (Northington et al., 2001a,b), structural and biochemical studies show that neuronal necrosis is prominent in cerebral cortex, whereas apoptosis is prominent in striatum, hippocampus, thalamus, and brainstem. Furthermore, a hybrid form of cell death with characteristics of both necrosis and apoptosis appears widely in hippocampus and striatum. In contrast, in 7-day-old piglet the primary neurodegeneration after hypoxia-ischemia is categorically necrosis (Martin et al., 2000). The mechanisms that account for the differences in animals are unclear, as are the mechanisms that channel neurons into necrotic, apoptotic, and hybrid cell death. Some studies have shown that the level of intracellular ATP can direct cell death down different pathways (Leist et al., 1997). The maturity of the brain and the subtype of glutamate receptor that is activated influence cell death along a so-called apoptosis-necrosis cell death continuum (Portera-Cailliau et al., 1997a,b; Martin et al., 1998; Martin, 2001). Hence, neuronal death induced by excitotoxicity, hypoxia-ischemia, and trauma might not be the same in mature and immature brain and may vary in different populations of neurons.

Neurons in newborn rodents exhibit a more robust classical apoptosis response compared to the adults after brain damage (Martin, 2001). Our study identifies a possible explanation for this phenomenon. We found developmental changes in the subcellular distribution of Bax. The ratio of mitochondrial Bax to soluble Bax in normal developing striatum changes prominently with brain maturation. Newborn rat striatum has a much greater proportion of Bax in the mitochondrial fraction with lower levels of soluble Bax. Mature rat striatum has a much larger proportion of Bax in the soluble fraction and low amounts of Bax in the mitochondrial fraction. With brain maturation there is a linear decrease in the ratio of mitochondrial Bax to soluble Bax. Age-related differences in mitochondrial quantity do not ap-

pear to account for the changes in the subcellular distribution of Bax. In fact, the amount of mitochondrial protein increases with maturation as determined by the levels of Cox1. The greater proportion of Bax in the mitochondrial compartment of newborn brain may prime neurons for apoptosis after injury, allowing immature neurons to engage classical apoptosis pathways more readily than mature neurons. However, the presence of Bax in mitochondria per se is insufficient to induce apoptosis because mitochondrial Bax is found in the normal developing striatum at times with infrequent apoptosis; therefore, other molecules have a role in the regulation of injury-induced neuronal apoptosis.

## ACKNOWLEDGMENTS

We are grateful for the outstanding technical assistance of Ann Price and Frank Barksdale. This work was supported by grants from the U.S. Public Health Service, National Institutes of Health, National Institute of Neurological Disorders and Stroke (NS34100) and National Institute on Aging (AG16282) and the Department of Defense, U.S. Army Medical Research and Materiel Command (DAMD17-99-1-9553).

## REFERENCES

- BITTIGAU, P., SIFRINGER, M., POHL, D., et al. (1999). Apoptotic neurodegeneration following trauma is markedly enhanced in the immature brain. *Ann. Neurol.* **45**, 724-735.
- DARGUSCH, R., PIASECKI, D., TAN, S., et al. (2001). The role of Bax in glutamate-induced nerve cell death. *J. Neurochem.* **76**, 295-301.
- DECKWERTH, T.L., ELLIOTT, J.L., KNUDSON, C.M., et al. (1996). Bax is required for neuronal death after trophic factor deprivation and during development. *Neuron* **17**, 401-411.
- EASTON, R.M., DECKWERTH, T.L., PARSADANIAN, A.S.H., et al. (1997). Analysis of the mechanisms of loss of trophic factor dependence associated with neuronal maturation: a phenotype indistinguishable from Bax deletion. *J. Neurosci.* **17**, 9656-9666.
- FARLIE, P.G., DRINGEN, R., REES, S.M., et al. (1995). Bcl-2 transgene expression can protect neurons against developmental and induced cell death. *Proc. Natl. Acad. Sci. USA* **92**, 4397-4401.
- GLÜCKSMANN, A. (1951). Cell deaths in normal vertebrate ontogeny. *Biol. Rev.* **26**, 59-86.
- HAKEM, R., HAKEM, A., DUNCAN, G.S., et al. (1998). Dif-

# MECHANISMS OF EXCITOTOXIC NEURONAL DEATH

- ferential requirement for caspase 9 in apoptotic pathways *in vivo*. *Cell* **94**, 339–352.
- JOHNSON, M.D., KINOSHITA, Y., XIANG, H., et al. (1999). Contribution of p53-dependent caspase activation to neuronal cell death declines with neuronal maturation. *J. Neurosci.* **19**, 2996–3006.
- KERR, J.F.R., and HARMON, B.V. (1991). Definition and incidence of apoptosis: an historical perspective, in: *Apoptosis: The Molecular Basis of Cell Death*. L.D. Tomei, and F.O. Cope (eds), Cold Spring Harbor Laboratory Press: Cold Spring Harbor, New York, pps. 5–29.
- KOCHANNEK, P.M., CLARK, R.S., RUPPEL, R.A., et al. (2000). Biochemical, cellular, and molecular mechanisms in the evolution of secondary damage after severe traumatic brain injury in infants and children: lessons learned from the bedside. *Pediatr. Crit. Care Med.* **1**, 4–19.
- KUIDA, K., ZHENG, T.S., NA, S., et al. (1996). Decreased apoptosis in the brain and premature lethality in CPP32-deficient mice. *Nature* **384**, 368–372.
- LAVELLE, A., and LAVELLE, F.W. (1958). The nucleolar apparatus and neuronal reactivity in injury during development. *J. Exp. Zool.* **137**, 285–315.
- LEIST, M., SINGLE, B., CASTOLDI, A.F., et al. (1997). Intracellular adenosine triphosphate (ATP) concentration: a switch in the decision between apoptosis and necrosis. *J. Exp. Med.* **185**, 1481–1486.
- LIU, X., ZOU, H., SLAUGHTER, C., et al. (1997). DFF, a heterodimeric protein that functions downstream of caspase-3 to trigger DNA fragmentation during apoptosis. *Cell* **89**, 175–184.
- MACMANUS, J.P., and BUCHAN, A.M. (2000). Apoptosis after experimental stroke: fact or fashion? *J. Neurotrauma* **17**, 899–914.
- MARTIN, L.J. (1999). Neuronal death in amyotrophic lateral sclerosis is apoptosis: possible contribution of a programmed cell death mechanism. *J. Neuropathol. Exp. Neurol.* **58**, 459–471.
- MARTIN, L.J. (2000). p53 is abnormally elevated and active in the CNS of patients with amyotrophic lateral sclerosis. *Neurobiol. Dis.* **7**, 613–622.
- MARTIN, L.J. (2001). Neuronal cell death in nervous system development, disease, and injury. *Int. J. Mol. Med.* **7**, 455–478.
- MARTIN, L.J., and LIU, Z. (2002). Injury-induced spinal motor neuron apoptosis is preceded by DNA single-strand breaks and is p53- and bax-dependent. *J. Neurobiol.* **50**, 181–197.
- MARTIN, L.J., AL-ABDULLA, N.A., BRAMBRINK, A.M., et al. (1998). Neurodegeneration in excitotoxicity, global cerebral ischemia, and target deprivation: a perspective on the contributions of apoptosis and necrosis. *Brain Res. Bull.* **46**, 281–309.
- MARTIN, L.J., BRAMBRINK, A.M., PRICE, A.C., et al. (2000). Neuronal death in newborn striatum after hypoxia-ischemia is necrosis and evolves with oxidative stress. *Neurobiol. Dis.* **7**, 169–191.
- MARTIN, L.J., KAISER, A., YU, J.W., et al. (2001). Injury-induced apoptosis of neurons in adult brain is mediated by p53-dependent and p53-independent pathways and requires Bax. *J. Comp. Neurol.* **433**, 299–311.
- MARTINO, J.-C., DUBOIS-DAUPHIN, M., STAPLE, J.K., et al. (1994). Overexpression of bcl-2 in transgenic mice protects neurons from naturally occurring cell death and experimental ischemia. *Neuron* **13**, 1017–1030.
- MILLER, T.M., MOULDER, K.L., KNUDSON, C.M., et al. (1997). Bax deletion further orders the cell death pathway in cerebellar granule cells and suggests a caspase-independent pathway to cell death. *J. Cell Biol.* **139**, 205–217.
- NAKAJIMA, W., ISHIDA, A., LANGE, M.S., et al. (2000). Apoptosis has a prolonged role in the neurodegeneration after hypoxic ischemia in the newborn rat. *J. Neurosci.* **20**, 7994–8004.
- NORTHINGTON, F.J., FERRIERO, D.M., FLOCK, D.L., et al. (2001a). Delayed neurodegeneration in neonatal rat thalamus after hypoxia-ischemia is apoptosis. *J. Neurosci.* **21**, 1931–1938.
- NORTHINGTON, F.J., FERRIERO, D.M., GRAHAM, E.M., et al. (2001b). Early neurodegeneration after hypoxia-ischemia in neonatal rat is necrosis while delayed neuronal death is apoptosis. *Neurobiol. Dis.* **8**, 207–219.
- OPPENHEIM, R.W. (1991). Cell death during development of the nervous system. *Annu. Rev. Neurosci.* **14**, 453–501.
- PORTERA-CAILLIAU, C., PRICE, D.L., and MARTIN, L.J. (1997a). Excitotoxic neuronal death in the immature brain is an apoptosis-necrosis morphological continuum. *J. Comp. Neurol.* **378**, 70–87.
- PORTERA-CAILLIAU, C., PRICE, D.L., and MARTIN, L.J. (1997b). Non-NMDA and NMDA receptor-mediated excitotoxic neuronal deaths in adult brain are morphologically distinct: further evidence for an apoptosis-necrosis continuum. *J. Comp. Neurol.* **378**, 88–104.
- PUTCHA, G.V., DESHMUKH, M., and JOHNSON, E.M., JR. (1999). Bax translocation is a critical event in neuronal apoptosis: regulation by neuroprotectants, Bcl-2, and caspases. *J. Neurosci.* **19**, 7476–7485.
- TENNETI, L., and LIPTON, S.A. (2001). Involvement of activated caspase-3-like proteases in *N*-methyl-D-aspartate-induced apoptosis in cerebrocortical neurons. *J. Neurochem.* **74**, 134–142.
- TORVIK, A. (1976). Central chromatolysis and the axon reaction. A reappraisal. *Neuropathol. Appl. Neurobiol.* **2**, 423–432.

LOK AND MARTIN

XIANG, H., KINOSHITA, Y., KNUDSON, C.M., et al. (1998).  
Bax involvement in p53-mediated neuronal cell death. *J. Neurosci.* **18**, 1363-1373.

YOSHIO, H., KONG, Y.-Y., YOSHIDA, R., et al. (1998).  
Apaf1 is required for mitochondrial pathways of apoptosis  
and brain development. *Cell* **94**, 739-750.

ZHIVOTOVSKY, B., SAMALI, A., GAHM, A., et al. (1999).  
Caspases: their intracellular localization and translocation  
during apoptosis. *Cell Death Diff.* **6**, 644-651.

Address reprint requests to:

*Lee J. Martin, Ph.D.*

*Department of Pathology*

*Johns Hopkins University School of Medicine*

*720 Rutland Ave., 558 Ross Bldg.*

*Baltimore, MD 21205-2196*

*E-mail: lmartin@jhmi.edu*

ARTICLE

## Isolation of Mature Spinal Motor Neurons and Single-cell Analysis Using the Comet Assay of Early Low-level DNA Damage Induced In Vitro and In Vivo

Zhiping Liu and Lee J. Martin

Departments of Pathology (ZL,LJM), Division of Neuropathology, and Neuroscience (LJM), Johns Hopkins University School of Medicine, Baltimore, Maryland

**SUMMARY** We developed an isolation technique for motor neurons from adult rat spinal cord. Spinal cord enlargements were discretely microdissected into ventral horn tissue columns that were trypsin-digested and subjected to differential low-speed centrifugation to fractionate ventral horn cell types. A fraction enriched in  $\alpha$ -motor neurons was isolated. Motor neuron enrichment was verified by immunofluorescence for choline acetyltransferase and prelabeling axon projections to skeletal muscle. Adult motor neurons were isolated from naïve rats and were exposed to oxidative agents or were isolated from rats with sciatic nerve lesions (avulsions). We tested the hypothesis, using single-cell gel electrophoresis (comet assay), that hydrogen peroxide, nitric oxide, and peroxynitrite exposure in vitro and axotomy in vivo induce DNA damage in adult motor neurons early during their degeneration. This study contributes three important developments in the study of motor neurons. It demonstrates that mature spinal motor neurons can be isolated and used for in vitro models of motor neuron degeneration. It shows that adult motor neurons can be isolated from in vivo models of motor neuron degeneration and evaluated on a single-cell basis. This study also demonstrates that the comet assay is a feasible method for measuring DNA damage in individual motor neurons. Using these methods, we conclude that motor neurons undergoing oxidative stress from reactive oxygen species and axotomy accumulate DNA damage early in their degeneration. (*J Histochem Cytochem* 49:957-972, 2001)

**KEY WORDS**

amyotrophic lateral sclerosis  
apoptosis  
axotomy  
DNA single-strand breaks  
single-cell gel electrophoresis

GENOTOXICITY, caused by DNA damage, is believed to contribute to the mechanisms of human aging and disease (Lindahl 1993; Subba Rao 1993). Its importance ranges broadly from cancer to neurological disorders. DNA damage can be mutagenic, contributing to tumor formation in breast, colorectal, and lung cancers. DNA damage can also induce apoptosis, possibly contributing to the abnormal neuronal degeneration in amyotrophic lateral sclerosis (ALS), Alzheimer's disease, and Parkinson's disease (Kisby et al. 1999; Martin 1999; Martin et al. 2000).

A variety of endogenous or intrinsic and exogenous or environmental factors can cause DNA damage (Lindahl 1993; Subba Rao 1993). Endogenous sources include reactive oxygen species (ROS) and oxidative stress generated by cellular metabolism, temperature, errors in DNA replication and repair, high levels of glucose and other reducing sugars, and methylation. Intrinsically generated DNA damage occurs as mismatched base pairs, base structure alterations such as tautomeric shifts and deamination, base adducts (e.g., hydroxylation), and base deletions causing apurinic/apyrimidinic (AP) sites (alkali-labile sites), single-strand breaks (SSBs), and double-strand breaks (DSBs). Estimates indicate that a human cell sustains ~10,000 lesions per day due to metabolism-generated free radicals (Subba Rao 1993) and 2000-10,000 DNA purine bases turn over daily because of hydrolytic depurination and subsequent repair (Lindahl 1993).

Correspondence to: Lee J. Martin, PhD, Johns Hopkins Univ. School of Medicine, Dept. of Pathology, 558 Ross Building, 720 Rutland Ave., Baltimore, MD 21205-2196. E-mail: [lmartin@jhmi.edu](mailto:lmartin@jhmi.edu)

Received for publication March 12, 2001; accepted March 14, 2001 (1A5500).

Environmental sources of DNA damage include dietary mutagenic chemicals, ultraviolet and ionizing radiation such as X-rays and  $\gamma$ -rays, free radicals, and heavy metals. These exogenous agents can cause crosslinks, adducts, and oxidative cleavage. Many of these types of DNA damage can be converted from one form to another form. For example, the interaction of DNA with hydroxyl radicals yields a variety of lesions, including base adducts, strand breaks, and sugar modifications; in addition, AP sites are converted into SSBs if not repaired.

DNA lesions can be evaluated by a variety of methods. Some methods are quantitative and other methods are qualitative. The methods for DNA damage detection can be broadly classified as biochemical and in situ detection methods. DNA filter elution assay is a powerful biochemical method for the determination of DNA strand breaks, apurinic/aprimidinic (alkali-labile) sites, and crosslinks (Kohn 1991). Another method is the detection of nucleoside adducts in digests of DNA extracts with high-performance liquid chromatography (Ames 1989). Gel electrophoresis is another reliable and major means for detecting genomic DNA damage (i.e., DNA fragmentation) in tissue/cell extracts. Flow cytometry for sorting cells on the basis of DNA quantity, indicating DNA damage, is also a good method for quantification of numbers of cells with DNA damage and severity of DNA damage. The most popular in situ method for DNA damage is the terminal deoxynucleotidyl transferase-mediated 3' dUTP nick end-labeling (TUNEL) technique (Gavrieli et al. 1992). Neuroscientists often use this method to observe cell death in nervous system disease and injury.

We are interested in developing sensitive and quantitative assays for detecting genotoxicity directly in motor neurons because of its relevance to ALS (Martin 2000; Martin et al. 2000). Single-cell gel electrophoresis, also called the "comet" assay, is a method for identifying early damage to genomic DNA of eukaryotic cells on a single-cell basis (Östling and Johanson 1984; Singh et al. 1988; Kindzelskii and Petty 1999; Morris et al. 1999; Tice et al. 2000). The types of DNA lesions detectable by comet assay include SSBs, alkali-labile sites (AP sites), and DSBs. Based on the principles of alkaline elution, the comet assay detects early DNA damage, which is of particular importance in investigating the mechanisms of cell death, particularly apoptosis. SSBs and DSBs are strong signals for activation of p53-mediated cell death (Jayaraman and Prives 1995). p53 is activated or induced in cells undergoing DNA damage-induced apoptosis. This pathway may participate in the mechanisms of motor neuron degeneration in ALS (Martin 2000). The goals of these experiments were first, to develop a new method to isolate and study adult motor neurons

and, second, to apply the comet assay to study of DNA damage in motor neurons.

## Materials and Methods

### Animals and Tissues

Adult male Sprague-Dawley rats (Charles River; Wilmington, MA) weighing ~150–200 g were used for these experiments. Naïve rats without experimental manipulations and rats with experimental manipulations were used in these experiments. The manipulations performed were retrograde tracing of motor neurons and avulsion of the sciatic nerve. The institutional Animal Care and Use Committee approved the animal protocols. The animals were housed in a colony room with a 12 hr:12 hr light:dark cycle and ad libitum access to food and water.

### Retrograde Tracing of Spinal Motor Neurons

Rats ( $n=2$ ) were anesthetized deeply with enflurane:oxygen:nitrous oxide (1:33:66) and, using sterile surgery, the sciatic nerve was exposed within the middle of the upper hindlimb. The nerve was transected by cutting and 50  $\mu$ l of 2.5% DAPI was applied to the proximal nerve stump for 1 hr using tracer-saturated Gelfoam placed in a sterile Eppendorf tube. The incision was closed with the bottom of the Eppendorf tube containing DAPI remaining applied to the proximal stump of the sciatic nerve. The animals were allowed to survive for 48 hr before they were sacrificed.

### Sciatic Nerve Avulsion Model of Motor Neuron Apoptosis

The unilateral sciatic nerve avulsion model was used as an in vivo model of spinal motor neuron apoptosis (Martin et al. 1999; Liu and Martin 2001). Rats were anesthetized deeply with enflurane:oxygen:nitrous oxide (1:33:66). With sterile surgery, a midline incision was made in the lateral aspect of the left pelvis and upper hindlimb. The sciatic nerve was located by blunt retraction of the biceps femoris and gluteus muscles and was tracked proximally to an extravertebral location deep within the pelvis. A steady, moderate traction was applied to the sciatic nerve with forceps until the nerve separated from the spinal cord, resulting in a mixed motor-sensory root avulsion. Muscle retraction was released and the overlying skin was sutured. The animals ( $n=2-4$  rats per time point) were allowed to live for 5, 7, 10, 14, or 28 days after sciatic nerve avulsion.

### Preparation of Spinal Cord Tissue for Isolation of Mature Motor Neurons

Spinal cords were isolated from adult rats that were anesthetized deeply with a mixture of enflurane:oxygen:nitrous oxide (1:33:66) and then decapitated. From rats without experimental lesions, cervical and lumbar enlargements were used. The two enlargements of the spinal cord contain the majority of the spinal motor neurons. From rats exposed to tracers and from rats with sciatic nerve avulsions, only the entire lumbar enlargements (divided into ipsilateral and contralateral sides) were used. After removal of the pia, lumbar/cervical enlargements were dissected segmentally under a

surgical microscope and then the segments were microdissected into gray matter columns of ventral horn without appreciable contamination of dorsal horn and surrounding white matter funiculi. Spinal motor neurons are large neurons locating in Lamina IX of spinal cord. Gray matter tissue columns from spinal cord ventral horns of lumbar/cervical enlargements were collected and rinsed in a cell culture dish on ice containing dissection medium [ $1 \times \text{Ca}^{2+}$  and  $\text{Mg}^{2+}$ -free Hanks balanced salt solution (Gibco BRL; Grand Island, NY) supplemented with glucose and sucrose]. These tissues were used to prepare motor neuron cell suspensions.

### Preparation of Adult Spinal Motor Neuron-enriched Cell Suspensions

**Digestion of Spinal Cord Ventral Horns.** Ventral horn samples were digested (20 min) with 0.25% trypsin-EDTA (Gibco) in a tissue culture incubator (5%  $\text{CO}_2$  and 95% air at 37°C). This mixture was titrated gently with a transfer pipette. The tissue digested was transferred to a 5-ml centrifugation tube on ice, and the remaining small pieces of ventral horn gray matter were further digested in trypsin-EDTA (16 min). The total cell suspension was then centrifuged at different speeds for cell sorting.

### Sorting of Cell Suspensions

To isolate a spinal motor neuron-enriched fraction, tissue digests were centrifuged (Beckman GPR model centrifuge) at 200 rpm (20  $g_{av}$ ) for 5 min (4°C). The supernatant was collected and then centrifuged at 400 rpm (50  $g_{av}$ ), 800 rpm (160  $g_{av}$ ), and then 2500 rpm (1400  $g_{av}$ ). After each spin (for 5 min), the pellet was resuspended in 100  $\mu\text{l}$  PBS, pH 7.4, fixed with 1 ml of 4% paraformaldehyde (4°C for 1 hr) for cell characterization using immunocytochemistry, TUNEL, or cresyl violet staining.

### Characterization of Sorted Cell Suspensions

The cells were repelleted after fixation and each pellet was resuspended with 250  $\mu\text{l}$  PBS. An aliquot of cell suspension (50  $\mu\text{l}$ ) was applied to a gelatin-coated slide and a coverslip (24 mm  $\times$  30 mm) was gently overlaid to form a monolayer of cells. The slides were then air-dried. Air-dried slides were rinsed (1 hr) in PBS to separate the slides from the coverslips. The cells did not attach to the coverslips because they were not coated with adhesive; instead, the cells were attached to the gelatin-coated slides. The cells were permeabilized (30 min) in 1% Triton X-100 and then treated (30 min) with 1% bovine serum albumin (BSA). The cells were probed with antibodies to neuronal nucleus protein (NeuN, diluted 1:20), a neuron-specific marker (Chemicon International; Temecula, CA), choline acetyltransferase (ChAT, diluted 1:5), a marker for motor neurons in rat spinal cord enlargements (Roche Molecular Biochemicals; Indianapolis, IN), glial fibrillary acidic protein (GFAP, diluted 1:20), an astroglial marker (DAKO; Glostrup, Denmark), CD11b/c IgG<sub>2a</sub> (OX-42, diluted 1:20), a microglial/macrophage marker (Harlan Sera-Lab; Sussex, UK). Diluted primary antibodies were applied to the slides and the slides were incubated (24 hr at room temperature) in a humidified box. After primary antibody incubation, the slides were rinsed in PBS. Alexa-

conjugated anti-mouse IgG (diluted 1:100; Molecular Probes, Eugene, OR) was used to visualize NeuN, ChAT, and OX-42, and Cascade blue-conjugated anti-rabbit IgG (diluted 1:100; Molecular Probes) was used to visualize GFAP. The slides were incubated (4 hr at RT) in a humidified dark box. The slides were washed and coverslipped with propidium iodide/antifade (Ventana; Tucson, Arizona). The slides were observed and photographed under a Zeiss fluorescence microscope. The preparation of cell suspensions from rats used for retrograde tracing of motor neurons was identical to that described above. The slides were coverslipped with or without propidium iodide/antifade and were observed under the same fluorescence microscope but with UV emission.

### Counting of Different Cell Types in Cell Suspensions

To identify the cell fraction that was enriched in motor neurons, neurons marked with cell-specific antibodies were counted. The total number of neurons was estimated by comparing the number of NeuN-positive cells to the total number of cells identified by propidium iodide staining plus NeuN staining. To determine the proportion of spinal motor neurons in the cell suspensions, the percentage of ChAT-positive cells relative to NeuN-positive cells was calculated. To determine the proportion of spinal motor neurons issuing sciatic nerve axons, the fraction of DAPI-positive cells relative to the total number of NeuN-positive cells was also calculated. The numbers of labeled cells from six different microscopic fields ( $\times 400$ ) were averaged from each case and then a total mean was derived from the preparations from three different cases.

### Immunoblotting

Immunoblotting was used to identify ChAT immunoreactivity in lysates of motor neuron cell suspensions to additionally verify the presence of a motor neuron phenotype in this fraction. The cells were pelleted, washed, and lysed in buffer. Samples (20  $\mu\text{g}$  of total protein) were fractionated by SDS-PAGE. Proteins were electroeluted onto nitrocellulose sheets. Blots were washed with 50 mM Tris-buffered saline (TBS) and blocked in 2.5% nonfat milk in 50 mM TBS/0.1% Tween-20. ChAT immunoreactivity was detected with a monoclonal antibody (Incstar, Stillwell, MN) used at a concentration of 1  $\mu\text{g}$  IgG/ml. Immunoreactivity was visualized with enhanced chemiluminescence.

### In Vitro Exposure of Motor Neurons to ROS

We tested the hypothesis that adult motor neurons rapidly accumulate genomic DNA lesions in response to oxidative stress. Motor neuron-enriched cell suspensions were exposed to  $\text{H}_2\text{O}_2$ , NO donors,  $\text{H}_2\text{O}_2$  + NO donor, and  $\text{ONOO}^-$ . Two different NO donors were used: sodium nitroprusside (SNP; Sigma, St Louis, MO) and *N*-(2-aminoethyl)-*N*-(2-hydroxyl-nitrosohydrazino)-1,2-ethylenediamine (spermine-NONOate; OXIS International, Portland, OR). Spermine-NONOate was used because this agent can maintain long exposure to steady-state generation of NO (Hrabie et al. 1993). Motor neurons were also exposed directly to  $\text{ONOO}^-$  (Alexis; San Diego, CA).  $\text{ONOO}^-$  is a potent and relatively long-lived ROS formed by a reaction between  $\text{O}_2^-$  and NO (Beckman et al. 1993).

Motor neuron cell suspensions (the 400 rpm preparation) were prepared from naïve rats. Motor neurons were exposed to SNP at concentrations of 10, 100, and 300  $\mu$ M for different durations ranging from 15 min to 4 hr. Identical cell suspensions were exposed to spermine-NONOate at concentrations of 10 and 100  $\mu$ M for 30 min, 1 hr, and 2 hr. Alternatively, motor neurons were treated with ONOO<sup>-</sup> at concentrations of 10 and 100  $\mu$ M for 15 min, 30 min, and 1 hr. These exposures were done in medium containing 90% Neurobasal-A (Gibco), 5% horse serum, 5% fetal bovine serum (both sera were heat-inactivated) and  $1 \times$  glutamine (Gibco) in a tissue culture incubator (containing 5% CO<sub>2</sub> and 95% air, 37°C) for the different times. For controls, samples of the same cell suspensions were incubated in medium for the same time in the absence of SNP, with spermine tetrahydrochloride/sodium nitrite (NO<sub>2</sub><sup>-</sup>) or with decomposed ONOO<sup>-</sup> in alkaline solution. After exposure, the treatment groups were collected in 5-ml centrifuge tubes and repelleted at 4°C for 5 min. Each pellet was resuspended and subjected to the comet assay.

### Comet Assay

**Preparation of Cell Microgels on Slides.** To detect DNA damage in individual cells, motor neuron cell suspensions that were exposed to H<sub>2</sub>O<sub>2</sub>, NO donor, H<sub>2</sub>O<sub>2</sub>/SNP, and ONOO<sup>-</sup> were analyzed by the comet assay. In addition, to identify DNA damage in motor neurons undergoing apoptosis *in vivo*, the comet assay was used on motor neuron cell suspensions prepared from rats with sciatic nerve avulsions. The 400 rpm cell preparations from ipsilateral or contralateral sides of ventral horns of lumbar enlargements of animals with unilateral sciatic nerve avulsions were subjected directly to comet assay immediately after they were sorted and repelleted. All the procedures for comet assay were done under low light to minimize spontaneous DNA damage.

Our method for the comet assay on motor neurons is based mainly on the original protocol for lymphocytes (Singh et al. 1988). Many details were modified in the procedure for our application. The cell microgels were prepared as layers. The first layer of gel was made by applying 200  $\mu$ l of regular melting point agarose (0.7%) onto superfrosted glass microscope slides (3"  $\times$  1", thickness 1 mm) and a coverslip was laid gently on the agarose. The agarose was allowed to solidify at 4°C and the coverslip was removed. Low melting-point agarose was prepared in 100 mM PBS and kept at 37°C. Samples of the motor neuron-enriched cell suspension were mixed with the low melting-point agarose and 50  $\mu$ l of a mixture of cell suspension (containing  $\sim 4.4 \times 10^4$  motor neurons) and low melting-point agarose was applied to the first gel layer. The slides were then coverslipped and placed at 4°C for solidification of the cell suspension-agarose mixture. After the second layer solidified, the coverslips were removed and 100  $\mu$ l of low melting-point agarose was added on top of the cell layer. The gels were re-coverslipped and the slides were placed on ice for gel solidification.

For preparing microgels, we compared two brands of low melting-point agarose (at the same concentrations) from different companies: Gibco BRL LMP agarose (cat. no. 15517-022) and FMC BioProducts SeaPlaque GTG agarose (cat.

no. 50110). We found that the FMC agarose was the best for our purpose.

**Lysis of Cells, DNA Unwinding, Gel Electrophoresis, and DNA Staining.** Coverslips were removed from the cell microgels and the slides were covered with 1.5 ml of lysis buffer at pH 10 (for alkaline conditions) or pH 8.6 (for neutralized conditions) containing 2.5 M NaCl, 100 mM EDTA, 1% sodium lauryl sarcosine, 10 mM Tris, and Triton X-100 (final concentration 1%, freshly added immediately before use). The cell microgels were lysed for 30 min (at RT). After draining, microgels were treated with DNA-unwinding solution (300 mM NaOH, 1 mM EDTA, generally at pH 12 unless otherwise stated) for 30 min at RT. In some experiments, the effects of DNA unwinding solution/electrophoresis buffer pH on comet patterns were studied. Three different pH conditions were used: pH  $\geq 13$ , pH 12, and pH 7.4. Loss of a purine or pyrimidine base from the DNA sugar-phosphate backbone facilitates an alkali-catalyzed  $\beta$ -elimination of the 3'-phosphate (Kohn 1991). At pH  $\geq 13$ , alkali-labile sites are converted to SSB (Kohn 1991). A pH of 12 is reported to be appropriate for SSB detection because hydrogen bonds destabilize at this pH and double-stranded DNA separates into individual single strands, rendering shorter single-stranded DNA (resulting from SSBs) more easily eluted from the nucleus (Tice et al. 2000). Neutral conditions are used to detect double-strand breaks because under neutral pH conditions DNA remains double-stranded and regions containing DSBs will allow the DNA to migrate more readily in an electrophoretic field (Singh et al. 1988; Kohn 1991). The microgels were then placed directly into a horizontal gel electrophoresis chamber filled with DNA-unwinding solution. Gels were run with constant current (300 mA at RT) for usually 20 min. After electrophoresis, the microgels were neutralized with 50 mM Tris-HCl (pH 7.5) for 15 min (twice). DNA was visualized with ethidium bromide staining (20  $\mu$ g/ml, 20 min at RT), after which the microgels were washed and coverslipped. The evaluation and image acquisition were performed using a Zeiss fluorescence microscope.

### Counting Comets in Microgels

The number of cells with comets were counted in microgels prepared from motor neurons exposed to ROS *in vitro* and from motor neurons isolated from *in vivo* axotomy experiments. For cell preparations exposed to H<sub>2</sub>O<sub>2</sub>, NO donor, H<sub>2</sub>O<sub>2</sub>/SNP or ONOO<sup>-</sup>, cells incubated for the same time in medium without oxidant were used as controls. Three to five separate experiments from different animals were done for each type of *in vitro* oxidant exposure experiment. For the unilateral sciatic nerve avulsion experiments, comet assays were performed on two to four rats for each recovery time (5, 7, 10, 14, or 28 days). The contralateral (unlesioned) side of the spinal cord from rats with sciatic nerve avulsions was used as the control for each time point. The number of comets and large intact cell nuclei regarded as motor neurons stained by ethidium bromide were counted in six microscopic views at  $\times 200$  from microgels of treated cells and from sciatic nerve avulsion animals. The percentages of comets relative to the total number of cells (total number of comets and total number of intact cell nuclei)



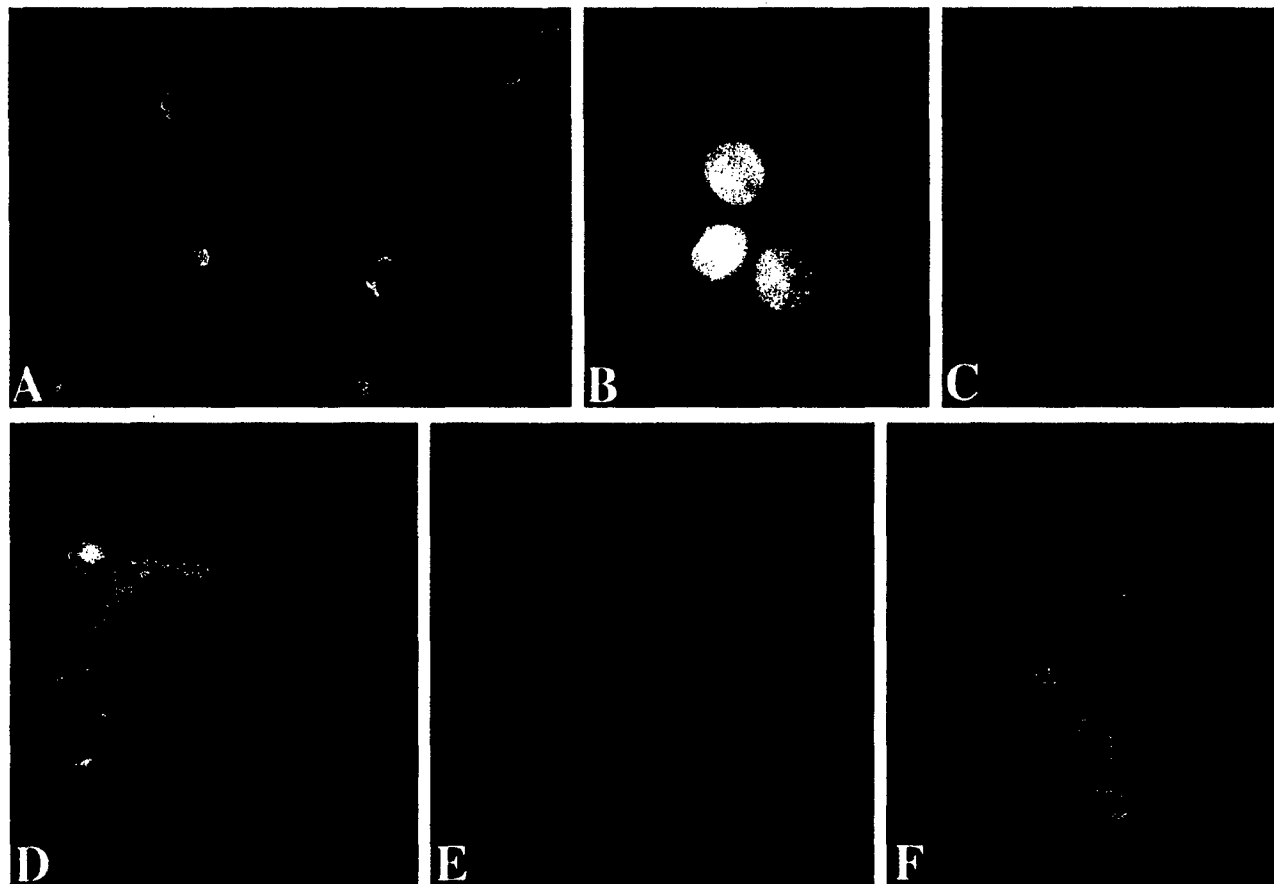


**Figure 1** Characterization of the motor neuron-enriched cell suspension isolated from adult rat spinal cord ventral horn. (A) Immunocytochemical labeling for NeuN (green) shows that most (~84%) of the cells in the 400 rpm preparation are neurons. The green fluorescence is localized in nuclei of neurons. Bar = 22  $\mu$ m (same for F). (B) In the 400 rpm cell suspension, most of the cells are ChAT-positive (green cytoplasmic labeling). Bar = 10  $\mu$ m (same for C). (C) Propidium iodide nuclear staining (red) of cells shown in B. (D,E) GFAP-positive astroglial processes (blue staining) are observed in the 400 rpm cell suspension. Some astroglial processes are attached to large neurons (red in E). Bar in D = 18  $\mu$ m (same for E). (F) Prelabeling lumbar motor neurons with retrograde tracer DAPI (blue) shows that most of the  $\alpha$ -motor neurons with sciatic nerve axons sort into the 400 rpm cell suspension.

were determined and group means were calculated. The data were analyzed using a Student's *t*-test.

#### TUNEL

Motor neuron cell suspensions exposed to NONOate (10  $\mu$ M or 100  $\mu$ M) or corresponding vehicle (10  $\mu$ M or 100  $\mu$ M spermine/ $\text{NO}_2^-$ ) were analyzed with TUNEL. Cells were fixed in 4% paraformaldehyde overnight. They were pelleted and washed with PBS (pH 7.4), and then mounted on gelatin-coated slides by coverslipping to form a cell monolayer and allowed to air-dry. The slides were rinsed in PBS for 1 hr to separate the coverslip from the slides. A modified enhanced TUNEL procedure was used. The cells were rinsed in 1% Triton X-100 for 1 hr and washed with PBS before they were rinsed with terminal deoxynucleotidyl transferase (TdT) buffer (containing 30 mM Tris, pH 7.2, 140 mM sodium cacodylate, 3 mM cobalt chloride) for 20 min. The TdT buffer was changed to fresh TdT buffer (0.5 ml/slide) containing TdT (0.02U/ $\mu$ l) and biotin-16-dUTP (50  $\mu$ M) (both reagents were from Roche Molecular Biochemistry) and the slides were incubated at 37°C for 2 hr.

The reaction was terminated by incubating the slides in SSC (300 mM sodium chloride, 30 mM sodium citrate) for 15 min. The slides were then incubated in avidin-biotin-peroxidase complex for 2 hr at RT. After washing with PBS, the slides were stained with DAB/ $\text{H}_2\text{O}_2$  for 20 min. Some of the slides were counterstained with cresyl violet and were observed and photographed.



**Figure 2** Immunoblot for ChAT in motor neuron cell suspensions. ChAT (detected as a major band at ~67 kD) is enriched in lysates of cell suspensions, confirming the presence of a motor neuron phenotype. Molecular mass markers (in kD) are indicated at right. The levels of immunoreactivity are similar in motor neurons incubated for 30 min with 100  $\mu$ M  $\text{ONOO}^-$  (Lane 1) or vehicle (Lane 2), indicating no generalized degradation of cells.

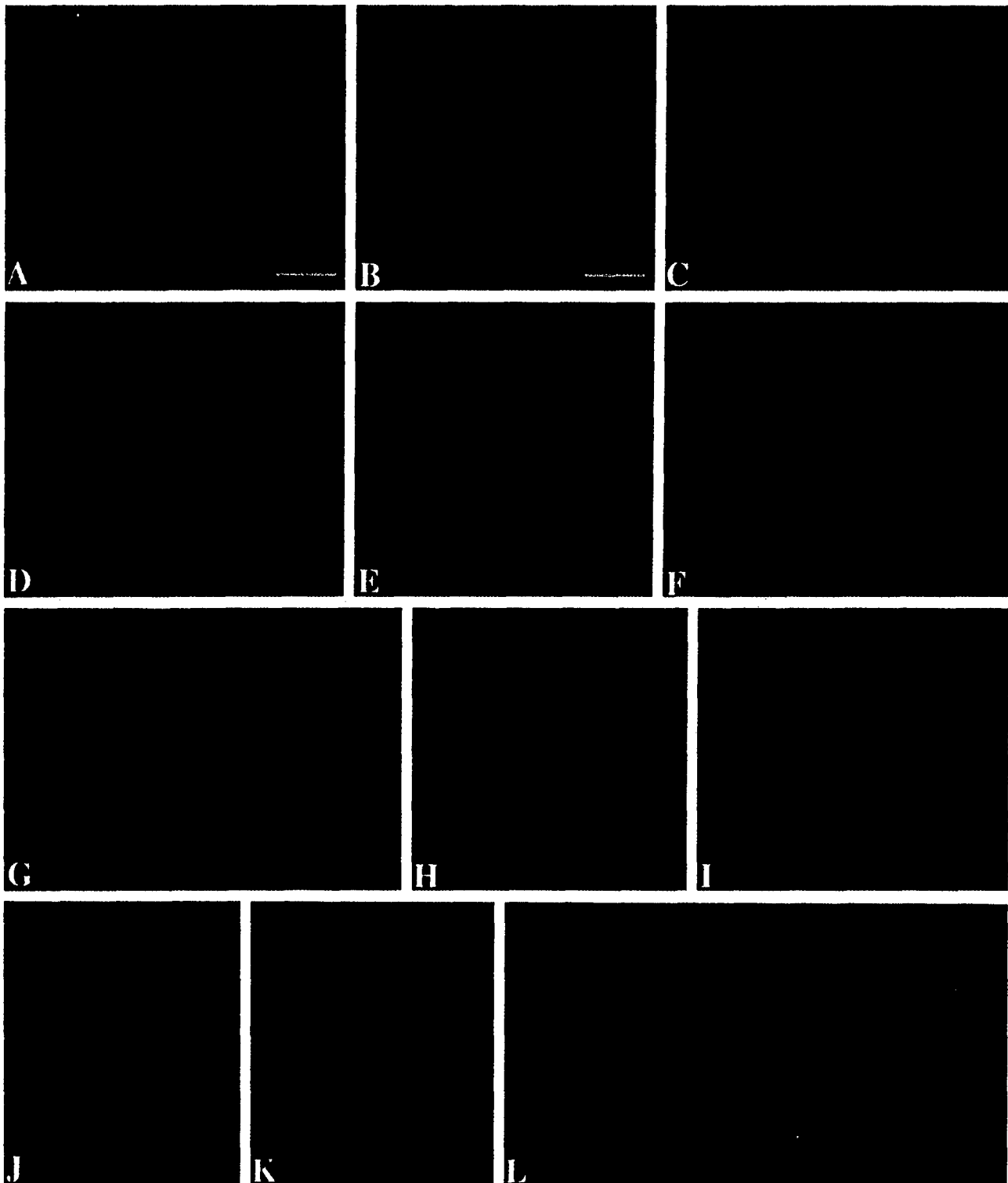


**Figure 3** Alkaline (pH 12) comet assay on isolated motor neurons after exposure to ROS or axotomy. (A) Appearance of normal cells and comet in the microgels from control sample. The 400 rpm cell preparation was incubated for 15 min in neurobasal-A medium. A single background comet is observed. The comet head is large and round but not homogeneously labeled with ethidium bromide. The comet tail is short and granular. The majority of cells have normal nuclei without tails, revealing no detectable DNA damage. Bar = 112  $\mu$ m. (B) Comet in cells exposed to 1 mM  $H_2O_2$  in neurobasal-A medium for 15 min. The comet has a round head and a short neck between head and tail. Bar = 56  $\mu$ m (same for C-L). (C) Comet in cells exposed to 1 mM  $H_2O_2$  in MEM for 30 min. The comet head is small and the tail is broad and spindle shaped. This pattern of comet indicates that the DNA damage is more severe than other patterns. (D,E). Comets in motor neurons exposed to 10  $\mu$ M SNP for 30 min. The comets are numerous and have a head with a halo and a short granular tail (detailed morphol-

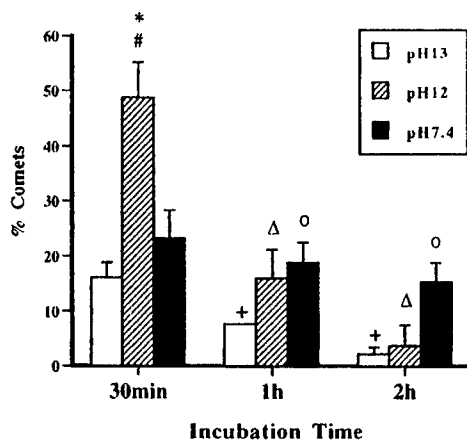


**Figure 4** Histogram of percentage of comets detected using different pH conditions for the comet assay. Motor neurons were incubated in MEM alone for 30 min, 1 hr, or 2 hr. Alkali-labile sites/SSBs (at pH 13), SSBs (at pH 12), and DSBs (at pH 7.4) all exist in spontaneously degenerating motor neurons. Motor neurons with SSBs are significantly more numerous at 30 min compared to comet numbers at pH 13 (\*,  $p < 0.05$ ) and pH 7.4 (\*,  $p < 0.05$ ). With increased incubation time, the number of comets visualized at pH 13 and pH 12 decreases, indicating a decrease in the formation of AP sites (+,  $p < 0.05$  for pH 13 compared to earlier pH 13 time point) and SSBs ( $\Delta$ ,  $p < 0.05$ , pH 12 compared to 30-min pH 12 time point). In contrast, the number of comets detected at pH 7.4 remains comparatively stable, indicating that the level of DNA DSBs is relatively invariant. Therefore, the detection of AP sites and SSB is transient.  $^o$ ,  $p < 0.05$ , pH 13, compared to time matched pH 7.4 samples.

#### Double Labeling of Comet Assay Microgels with Immunocytochemistry

We evaluated the feasibility of characterizing motor neuron comets by immunocytochemistry. Motor neurons were examined for expression of survival motor neuron (SMN) protein and p53 in microgels after comet assay. Coverslips from microgels of motor neurons exposed to either  $H_2O_2$  (for SMN) or NONOate (for p53) were removed after they were stained with ethidium bromide and observed for comets. Mouse monoclonal antibodies were used to localize SMN (Transduction Laboratories; Lexington, KY) and p53 (Santa Cruz; Santa Cruz, CA). Microgels were incubated with primary antibody dilutions (1:250 for SMN and 1:50 for p53) for 24 hr at RT. The slides were washed with PBS, then incubated (1:50–1:100 dilution) with Alexa-conjugated anti-

mouse IgG for 2 hr at RT. Afterwards, the slides were washed and re-coverslipped for observation and photography.

#### Results

New approaches need to be developed to study mechanisms of degeneration of adult motor neurons. Specifically, sensitive quantitative assays for specific types of DNA lesions need to be identified to study the possible role of DNA damage in the upstream mechanisms of motor neuron apoptosis. We developed and characterized a novel short-term, motor neuron-enriched cell suspension system to evaluate the formation of DNA damage directly in individual adult spinal motor neurons.

#### Purification of a Motor Neuron-enriched Cell Suspension

Ventral horns of cervical/lumbar enlargements of adult rat spinal cord were microdissected and subjected to mild dissociation with trypsin-EDTA. The total cell suspension was fractionated by low-speed centrifugation. The different cellular fractions were examined for NeuN, ChAT, GFAP, and OX-42 immunofluorescence, and for DAPI fluorescence to identify  $\alpha$ -motor neurons giving rise to sciatic nerve axons. One fraction was identified that is enriched in motor neurons. In the 400 rpm fraction of digests of ventral horn enlargements, neurons comprise ~84% of the total cell number (NeuN-positive cells/total cells, i.e., NeuN-positive cells and cells stained with propidium iodide; Figure 1A). Of these neurons, ~86% are motor neurons (ChAT-positive cells/NeuN-labeled cells; Figures 1B and 1C). Of these motor neurons, ~72% are  $\alpha$ -motor neurons giving rise to sciatic nerve axons (by DAPI sciatic nerve tracing; Figure 1F). Some motor neurons are entirely or partially surrounded by fragments of astroglial processes (Figures 1D and 1C), but GFAP-positive cells are rarely present in this fraction. OX-42-positive microglial cells are present only occasionally (not shown). Immunoblotting evaluation of

ogy of two comets is shown in E). Exposure to 10  $\mu M$  NONOate shows a similar comet morphology. (F) Motor neuron comet induced by 100  $\mu M$  SNP for 1 hr. This type of comet is a typical pattern for exposure to NO donors. The comet head is irregularly shaped, with clumped and granular DNA. The tail is very long and granular. This comet morphology is characteristic of apoptotic motor neurons. Exposure of isolated motor neurons to 100  $\mu M$  NONOate for 1 hr or longer induces similar patterns. (G) Motor neuron comet induced by SNP + 1 mM  $H_2O_2$ , showing severe DNA damage, as demonstrated by the long broad tail and small head (much of the genomic DNA has been eluted from the cell). (H) Prolonged exposure of motor neurons to SNP + 1 mM  $H_2O_2$  (for 4 hr) induces comets with shorter tails and irregular heads, with many small irregular DNA clumps in the nucleus. (I) Motor neurons exposed briefly (15–30 min) to ONOO<sup>-</sup> display comets with ambiguous granular heads and long granular tails similar to the pattern after exposure to NO donor at higher doses or longer times. (J) At 5 days after sciatic nerve avulsion, the comet assay identified motor neurons at very early stages of DNA damage. These comets had very short granular tails composed of large granules close to the head, indicating a few genomic DNA SSBs. (K) At 7 days after the lesion, motor neuron comets have a longer tails compared to 5-day comets, demonstrating that DNA damage progresses. (L) At 10 days after sciatic nerve avulsion, the comets have very long tails with large scattered granules, further indicating a slowly evolving but accumulating level of DNA damage in motor neurons.

**Table 1** Quantification of DNA damage in motor neuron comets induced by different ROS in vitro<sup>a</sup>

Treatment	Comet pattern <sup>b</sup>	DNA Intensity <sup>c</sup>		DNA intensity ratio (tail:head)	DNA Area		DNA area ratio (tail:head)	Tail length	Traditional comet moment ( $\times 10^4$ ) <sup>d</sup>	Comet moment ( $\times 10^5$ ) <sup>e</sup>
		Head	Tail		Head	Tail				
Control	3A	196.8 $\pm$ 13.4	52.5 $\pm$ 9.9	0.27 $\pm$ 0.05	2113 $\pm$ 751	3368 $\pm$ 1335	1.7 $\pm$ 0.3	88 $\pm$ 10	0.46 $\pm$ 0.10	1.7 $\pm$ 0.6
SNP (10 $\mu$ M)	3E	225.9 $\pm$ 3.8	100.2 $\pm$ 14.2	0.44 $\pm$ 0.06	2523 $\pm$ 596	12,868 $\pm$ 1808	5.4 $\pm$ 0.8	234 $\pm$ 24*	2.32 $\pm$ 0.24*	12.6 $\pm$ 0.97*
SNP (100 $\mu$ M)	3F	156.7 $\pm$ 17.9	58.4 $\pm$ 12.4	0.37 $\pm$ 0.06	1859 $\pm$ 480	26,477 $\pm$ 4810	16.8 $\pm$ 7.1	337 $\pm$ 19**	1.95 $\pm$ 0.34*	15.3 $\pm$ 3.6**
NONOate	7A	205.3 $\pm$ 12.1	68.3 $\pm$ 8.9	0.33 $\pm$ 0.03	3450 $\pm$ 1048	14,495 $\pm$ 5664	4.2 $\pm$ 1.0	242 $\pm$ 26*	1.67 $\pm$ 0.36*	8.2 $\pm$ 2.4*
SNP + H <sub>2</sub> O <sub>2</sub>	3G	124.2 $\pm$ 27.4	40.7 $\pm$ 11.6	0.35 $\pm$ 0.14	670 $\pm$ 389	29,327 $\pm$ 4573	74.9 $\pm$ 50.0	377 $\pm$ 21*	1.56 $\pm$ 0.48*	12.3 $\pm$ 5.1*
ONOO <sup>-</sup>	3I	172.3 $\pm$ 16.4	61.2 $\pm$ 10.5	0.36 $\pm$ 0.06	1442 $\pm$ 655	28,032 $\pm$ 2872	25.4 $\pm$ 11.7	366.2 $\pm$ 15.2*	2.24 $\pm$ 0.44*	17.3 $\pm$ 4.1*

<sup>a</sup>All values are mean  $\pm$  SEM; \*, significantly different ( $p < 0.05$ ) from control; \*\*, significantly different ( $p < 0.05$ ) from lower concentration.

<sup>b</sup>Representative comet patterns are shown in Figure 3 (for control, SNP, SNP + H<sub>2</sub>O<sub>2</sub>, and ONOO<sup>-</sup>) or Figure 7 (for NONOate) and are identified by the corresponding panel letter.

<sup>c</sup>See Figure 5 for delineation of comet head and tail.

<sup>d</sup>Calculated from DNA intensity<sub>tail</sub>  $\times$  tail length (Hellman et al. 1995).

<sup>e</sup>Calculated from DNA intensity<sub>tail</sub>  $\times$  tail area.

fraction for ChAT confirmed the presence of motor neurons in this fraction (Figure 2).

#### DNA Damage Is Rapidly Induced and Accumulates in Motor Neurons Undergoing Oxidative Stress

Motor neuron cell suspensions were exposed to H<sub>2</sub>O<sub>2</sub>, NO donor, H<sub>2</sub>O<sub>2</sub>/SNP, or ONOO<sup>-</sup>. Control cells were exposed to vehicle and incubated in medium for the same time. Comet assays were done at pH 12 (at this pH hydrogen bonds in DNA destabilize, causing strand separation). Comets were observed with each

treatment (Figure 3). Each treatment gave consistent results, with the major comet pattern generated from each exposure being highly reproducible (Figure 3). Figure 3 shows the most common patterns of comets after different treatments.

In microgels of control samples, the nuclei of many intact cells stained with ethidium bromide. Motor neurons with intact genomic DNA in gels stained with ethidium bromide have an evenly stained, smooth round nucleus without a tail (Figure 3A), indicating no DNA damage. In control motor neuron suspensions incubated in Neurobasal-A medium, the percentage of comets is  $\sim 10\%$  or less. Control comets have a large round head, densely labeled with ethidium bromide, and a short granular tail, composed of large scattered granules (Figure 3A). We have reported previously (Liu and Martin 2001) that viability of adult motor neurons in suspension is influenced by culture medium. Neurobasal medium is much better than MEM for maintaining adult motor neurons in vitro. Isolated mature motor neurons produce high levels of O<sub>2</sub><sup>-</sup> and spontaneously degenerate in MEM (Liu and Martin 2001). We used this system to evaluate the effects of DNA-unwinding solution pH on comet detection. At 30 min of incubation, many more motor neuron comets are observed at pH 12 compared to the number at pH 13 and 7.4 (Figure 4). In addition, the number of comets decreases over time (Figure 4). These results indicate that DNA SSBs are formed rapidly and accumulate transiently in dying motor neurons.

A comparison of control comets (Figure 3A) with comets induced by H<sub>2</sub>O<sub>2</sub> (Figure 3B) and NO donors (Figures 3D–3H) shows the striking difference in the comet profiles and amount (Table 1) of DNA damage. With 1 mM H<sub>2</sub>O<sub>2</sub> exposure in neurobasal-A medium, the comets have a round head, a tail with fine gran-

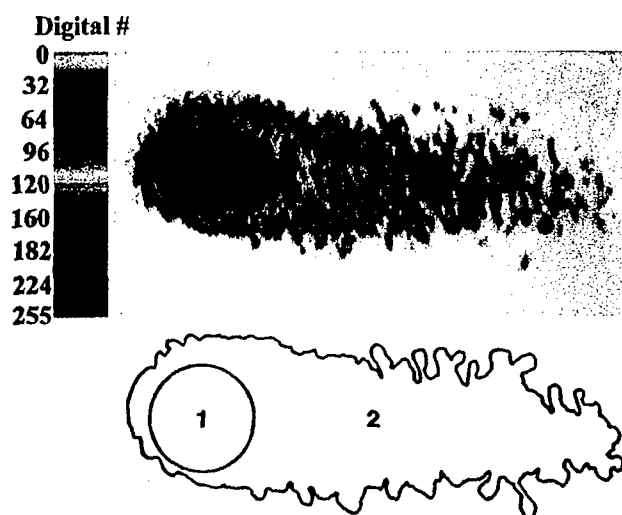


**Figure 5** Measurement of DNA damage in motor neurons with the comet assay. Digital image (upper image) of a motor neuron comet (the tail and the head comprise the comet) found in microgels after single-cell gel electrophoresis. Ethidium bromide staining of DNA is in pseudocolor. Each color indicates a different DNA content, with black indicating highest DNA intensity (background color has the intensity of 0). Comet contour (lower image) delineating comet head (1) and tail (2).

ules, and a short neck between head and tail (Figure 3B). With 1 mM  $H_2O_2$  exposure in MEM, the comets have huge spindle-shaped tails with a small round head (Figure 3C), indicating severe DNA damage and elution from the cell. Exposure to NO donors generates consistent comet profiles depending on exposure concentration and duration. In general, with exposure to 10  $\mu$ M SNP or NONOate for 15 min, 30 min, or even 1 hr, the comet head has a halo composed of large granules, with a short granular tail (Figures 3D and 3E). With 100  $\mu$ M or higher doses, or with 10  $\mu$ M for more than 1 hr of exposure, the head halo is less prominent but the tail length increases (Table 1), and it is still composed of scattered large granules (Figure 3F). Another comet pattern that shows severe DNA damage is found after motor neurons are exposed to 100  $\mu$ M SNP with 1 mM  $H_2O_2$  (Figure 3G). With these comets the head is small and the tail is long and wide; the degree of DNA damage is severe (Table 1). With increased exposure to 100  $\mu$ M SNP with 1 mM  $H_2O_2$ , the comet head contains some clumped DNA, as shown by ethidium bromide staining (Figure 3H). We have found previously that the combination of SNP with 1 mM  $H_2O_2$  induces severe protein nitration in motor neuron suspensions (Liu and Martin 2001), indicating the formation of  $ONOO^-$  by the reaction of NO with  $O_2^-$ . We therefore exposed motor neurons to  $ONOO^-$  directly, and the majority of comets have granular heads and long granular tails (Figure 3I; Table 1). The DNA damage profiles of NO donors, NO donor plus  $H_2O_2$ , and  $ONOO^-$  are similar.

#### Measurement of DNA Damage

The comet moment is regarded as one of the best indices of induced DNA damage in cells (Singh et al. 1988; Hellman et al. 1995). The extent of DNA damage was determined by measuring the displacement of DNA between the cell nucleus (i.e., the comet head) and the tail (Table 1). Cells with more DNA damage show an increased migration of DNA in the direction of electrophoresis (Östling and Johanson 1984; Singh et al. 1988). DNA migration length is believed to be directly related to fragment size, and it is believed migration is proportional to the level of SSBs and alkali-labile sites (Tice et al. 2000). DNA density and comet moments for individual motor neurons were measured using the fluorescence intensity of ethidium bromide-stained DNA (Figure 5). Randomly selected comets (~10–30 comets in each treatment group) were captured as digital images using Inquiry software (Loats Associates; Westminster, MD). Comets were saved in TIFF format. Each comet was used to obtain several measurements by delineating the region of interest (Figure 5). DNA intensity<sub>head</sub>, DNA intensity<sub>tail</sub>, area<sub>head</sub>, and area<sub>tail</sub> were measured. Tail length was measured

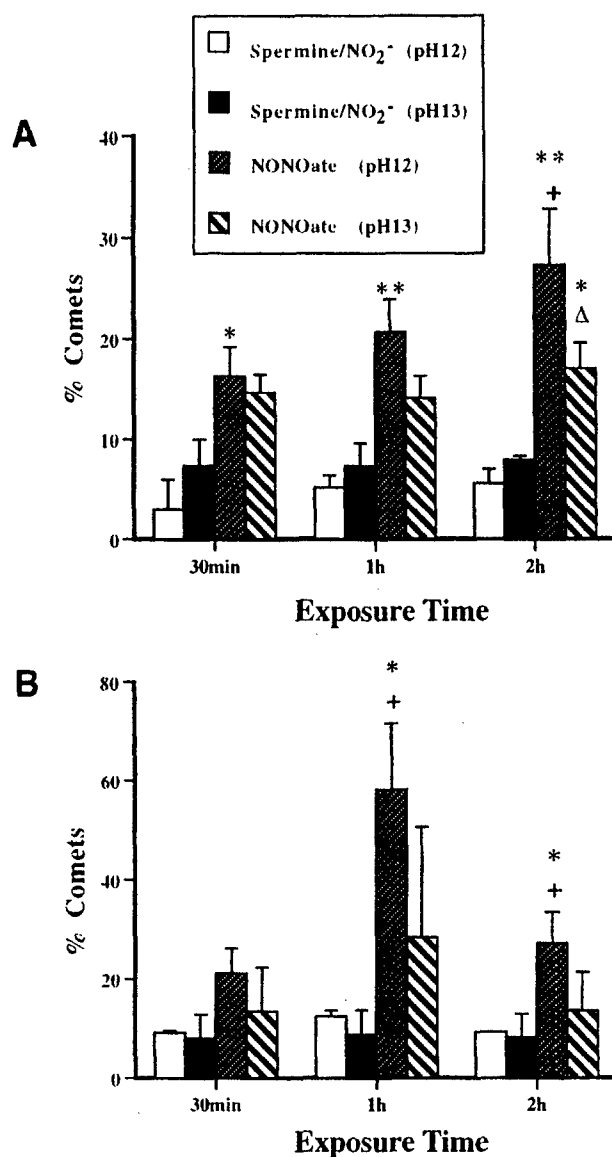


**Figure 6** Comet assay analysis of different forms of DNA damage induced in motor neurons exposed to NO donor. (A) Histogram of percentage of comets induced by 10  $\mu$ M NONOate. No significant increases in % comets are observed in control groups with increased incubation time at both pH 12 and pH 13. The number of motor neurons with SSBs after NONOate exposure is significantly higher than the comet number in time-matched control motor neurons at each time examined (\* $p < 0.05$  and \*\* $p < 0.01$ ). In addition, the number of cells with SSBs increases with increased exposure time (\*,  $p < 0.05$  2-hr exposed cells compared to 30-min exposed cells). In contrast, the number of comets at pH 13 (alkali-labile sites/SSBs) is not different from time-matched controls, except for 2 hr exposure (\*,  $p < 0.05$ ), and the number does not change with increased exposure time. The number of cells with SSBs (pH 12) is significantly higher ( $\Delta$ ,  $p < 0.05$ ) at 2 hr than the number of cells with alkali-labile sites/SSBs (pH 13). (B) Histogram of comet percentage after exposure of motor neurons to 100  $\mu$ M NONOate. The number of comets with SSB is significantly higher at 1 hr and 2 hr compared to time-matched controls (\*,  $p < 0.05$ ) and significantly higher at 1 hr compared to 30-min exposed cells, but significantly lower at 2 hr compared to 1 hr (\*,  $p < 0.05$ ). The number of comets detected at pH 13 did not differ significantly from time-matched controls.

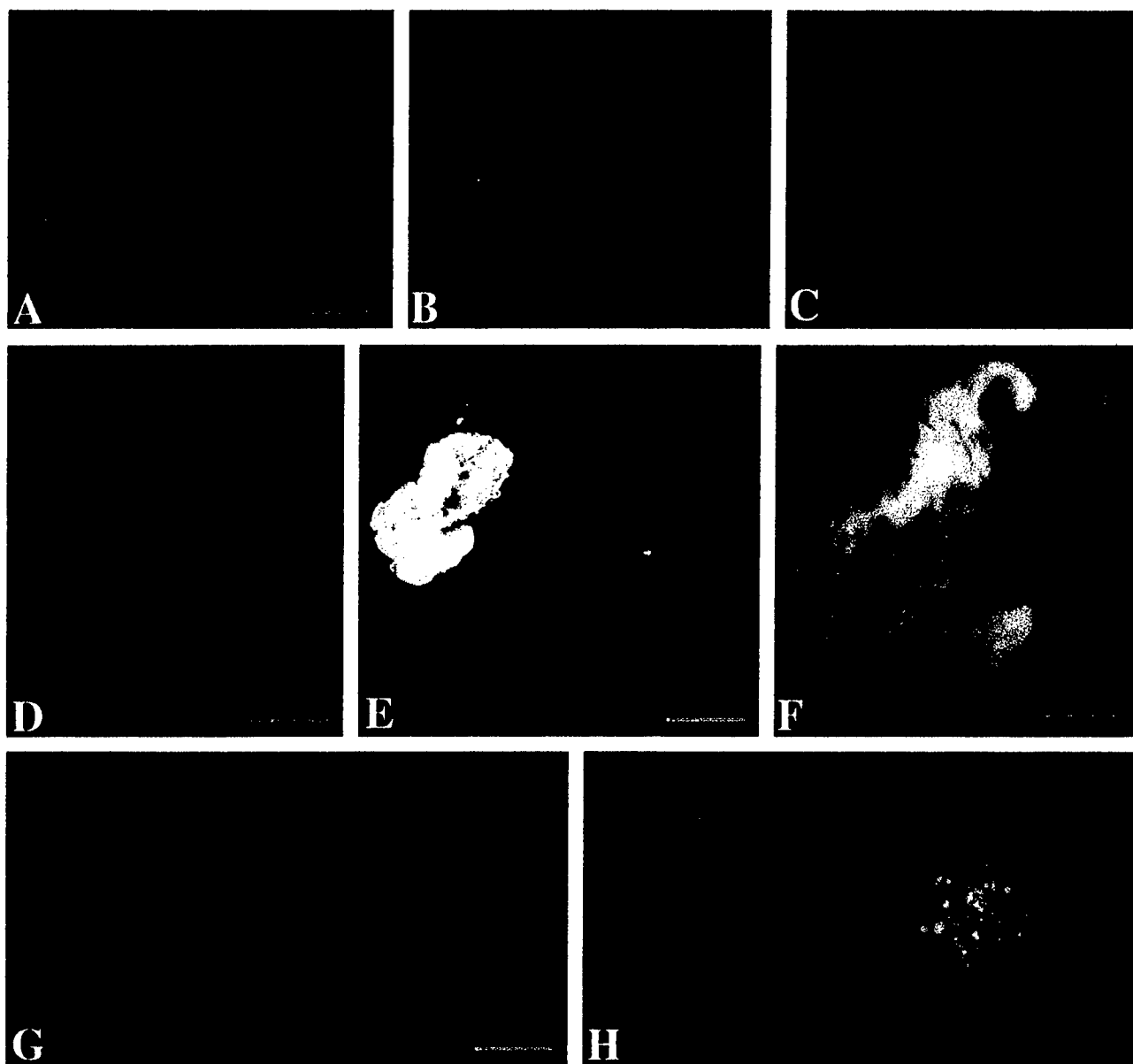


**Figure 7** Comet morphology at different pH conditions and comet assay combined with immunocytochemistry in microgels. (A) At pH 12, motor neurons exposed to NONOate (10  $\mu$ M, 30 min) have comets with prominent halos and short granular tails (under exposure to show the head core clearly). Bar = 56  $\mu$ m (same for B and C). (B) At pH 13, motor neuron comets (in cells with the identical experimental treatment as in A) have no halos and display longer highly granular tails. The comet morphologies at pH 13 compared to pH 12 reveal that the head halo observed at pH 12 contains AP sites that are converted into SSBs that appear as DNA granules that are eluted out of head. (C) ONOO<sup>-</sup> (100  $\mu$ M, 30 min) induces DSBs in motor neurons as indicated by comets with short tails and irregular heads detected at pH 7.4. (D–F) Immunophenotyping of comets. Motor neuron comet (D) induced by exposure to 10 mM H<sub>2</sub>O<sub>2</sub> and visualized with ethidium bromide. Bar = 75  $\mu$ m. The comet head is positive for SMN (green in E), confirming that the cell is a motor neuron. Bar = 94  $\mu$ m. SMN immunoreactivity in the nucleus has a fibrillar structure (green in F) that surrounds the DNA core (red ethidium bromide staining in F). Bar = 19  $\mu$ m. (G,H) p53 is expressed in motor neurons exposed to NONOate. Although these cells are not showing comets (G) the DNA staining (red in G) is suggestive of apoptosis, particularly in the cell on the left the DNA is condensed as a single large mass and the cell on the right has several mini-masses. Bar = 33  $\mu$ m (same for H). These cells are immunoreactive for p53 (green in H). In the cell at advanced apoptosis, the p53 staining is faint (cell at left), whereas in cell in the active stage of DNA condensation (cell at right), p53 immunoreactivity is prominent and appears bound to DNA granules.

from the center of the head to the end of the tail. Relative DNA content is reflected by the average integrated intensity of fluorescence. The amount of DNA damage for each cell is derived from the calculation of

the comet moment (Hellman et al. 1995; Petersen et al. 2000). We calculated the comet moment by two different methods. The traditional calculation is DNA intensity<sub>tail</sub>  $\times$  tail length (Hellman et al. 1995). Be-

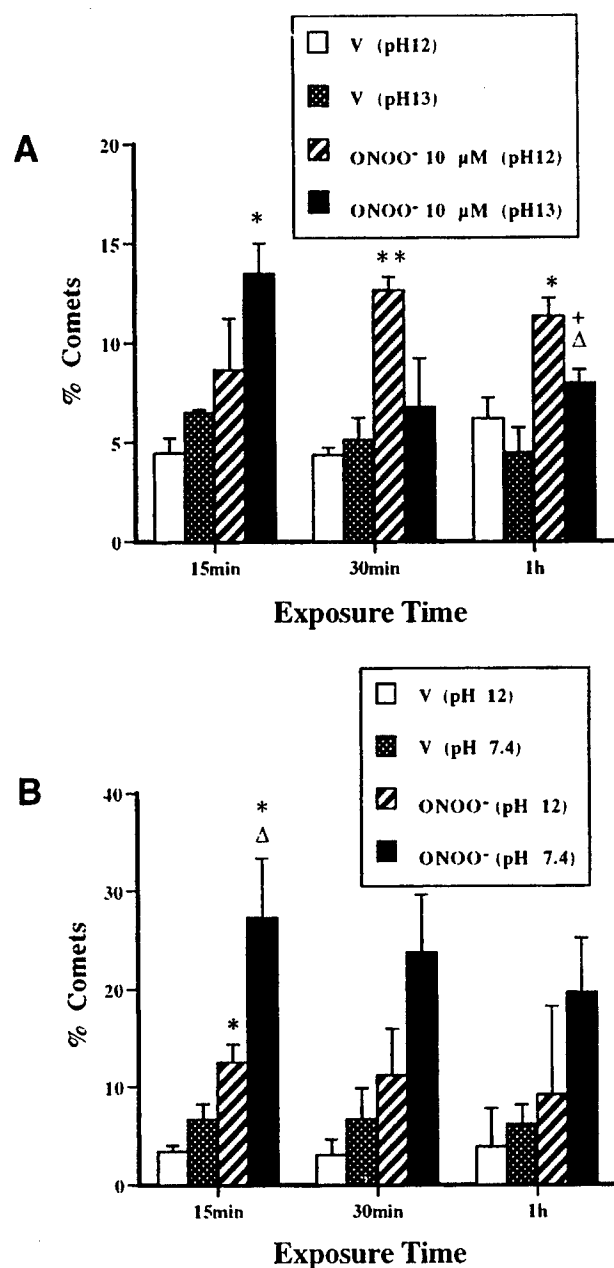


**Figure 8** Comet assay analysis of different forms of DNA damage induced in motor neurons exposed to ONOO<sup>-</sup>. (A) Histogram of percentage of comets induced by exposure to 10 μM ONOO<sup>-</sup> or vehicle (V) in neurobasal-A. Comet assays were done at pH 12 and 13. The comet number in motor neurons exposed to ONOO<sup>-</sup> for 15 min is prominent at pH 13 (\*,  $p < 0.05$  compared to the time- and pH-matched control cells), but comet number decreased with increased exposure time (\*,  $p < 0.05$  for 1-hr exposed cells compared to 15-min exposed, pH-matched cells). The number of comets in identical samples at pH 12 increases significantly as exposure time increases (\*,  $p < 0.05$ ; \*\*,  $p < 0.01$  compared to time-matched control cells at pH 12). At 1-hr exposure to ONOO<sup>-</sup>, number of comets detected at pH 12 (cells with SSBs) is significantly greater (<sup>Δ</sup>,  $p < 0.05$ ) than the number of comets detected at pH 13 (cells with AP sites/SSBs). (B) Histogram of % comets induced by exposure to 100 μM ONOO<sup>-</sup> or vehicle (V) in neurobasal-A. Comet assays were done at pH 12 and 7.4. DNA damage as DSBs (as revealed with comet assay under neutralized conditions) is very prominent

cause this equation does not take into consideration the broadness of the tail, we also calculated the comet moment from DNA intensity<sub>tail</sub> × area<sub>tail</sub>.

The comets in control motor neurons have low moments ( $\sim 1.7 \times 10^5$ ; Table 1). The comet moments in motor neurons exposed to ROS are significantly higher than those of controls (Table 1). These measurements show that NO, NO plus H<sub>2</sub>O<sub>2</sub>, and ONOO<sup>-</sup> induce DNA damage directly in motor neurons. In addition, the results show that the comet moment is a sensitive measure of DNA damage in motor neurons.

#### DNA Damage Occurs Early in Motor Neurons Undergoing Apoptosis In Vivo

We applied the comet assay to an in vivo model of motor neuron apoptosis in adult spinal cord. Sciatic nerve avulsion in adult rat causes apoptosis of lumbar motor neurons over 7–14 days (Martin et al. 1999). To identify whether DNA lesions occur in motor neurons early during the progression of apoptosis in vivo, the comet assay was used on motor neurons isolated from rats with sciatic nerve avulsions. With the same dissection and dissociation as mentioned above, the ipsilateral and contralateral motor neuron columns in the lumbar enlargement from sciatic nerve-avulsed animals were separately isolated and directly analyzed with the comet assay after cell sorting. We detected DNA damage in lumbar motor neurons injured by sciatic nerve avulsion. Motor neurons from the contralateral side did not show comets at any time. In contrast, as early as 5 days after sciatic nerve avulsion, the comet assay shows DNA damage, with comet profiles having a large head and a very short tail (Figure 3J). At 7 days after sciatic nerve avulsion, the comet head is looser and tail is longer (Figure 3K) than at 5 days. At 10 days after sciatic nerve avulsion, some of the comets have small heads and very long granular tails (Figure 3L), whereas others have a head with a big halo and a short granular tail (Liu and Martin 2001). Both are similar to the comet patterns observed after motor neurons are exposed to NO donors (Figures 3D–3F). At 14 and 28 days after sciatic nerve avulsion, no comets are observed in motor neurons from either ipsilateral or contralateral lumbar ventral horns.

(\*,  $p < 0.05$  compared to time- and pH-matched control cells and <sup>Δ</sup>,  $p < 0.05$  compared to pH 12 cells). In contrast, motor neurons with SSBs as revealed with comet assay under alkaline conditions (pH 12) are not as numerous as motor neurons with DSBs, although the number of cells with SSBs is still significantly higher than time-matched control cells at 15 min (\*,  $p < 0.05$ ). The results indicate that ONOO<sup>-</sup> rapidly and strongly induces severe DNA damage in motor neurons.

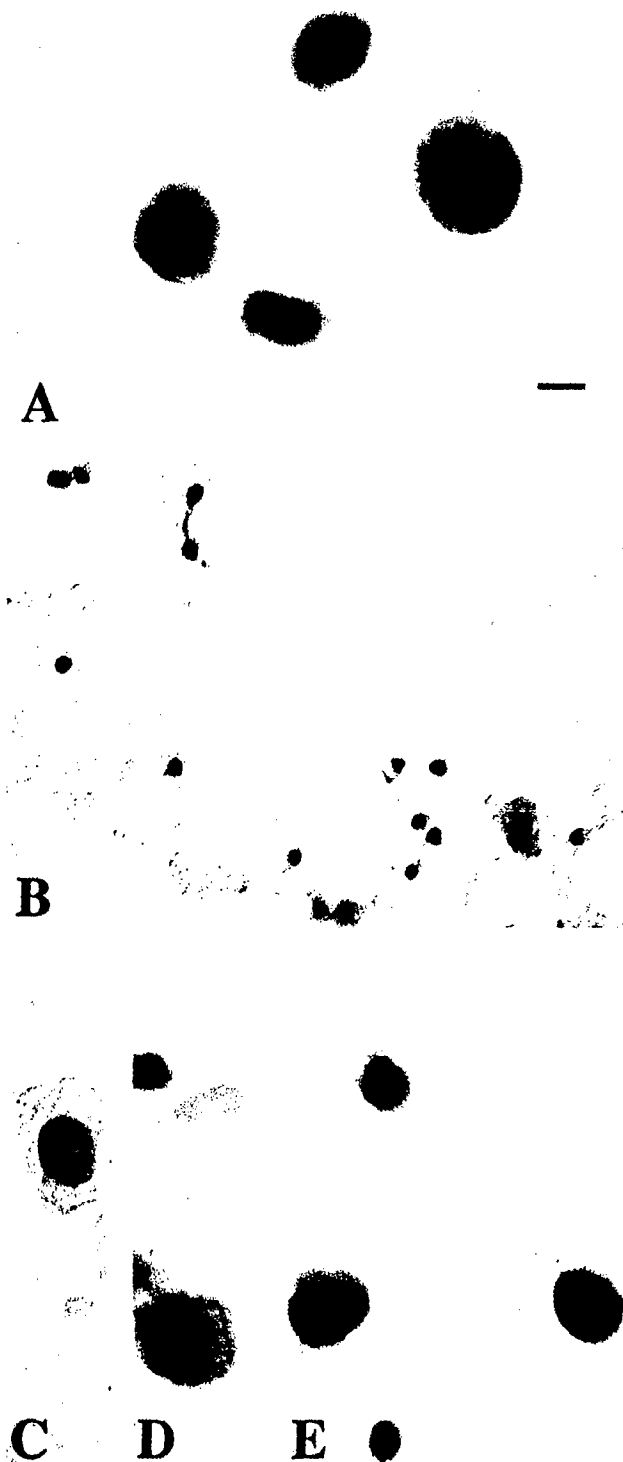


**Figure 9** DNA fragmentation in motor neurons exposed to NO donor as analyzed by TUNEL. Adult motor neurons were isolated, exposed *in vitro* to 10  $\mu$ M NONOate or vehicle for 30 min, washed, and mounted on slides. (A) Time-matched, vehicle-treated control motor neurons are not TUNEL positive (no brown staining is observed). These cells were counterstained with cresyl violet to visualize the large round motor neurons isolated by our technique. (B)

#### Identification of Different Types of DNA Damage in Motor Neurons by Varying pH Conditions

The use of different pH conditions during electrophoresis is an approach to discriminate between DNA strand breaks and alkali-labile sites (Tice et al. 2000). This approach has been validated (Tice et al. 2000) but it has not been applied to neurons. At pH  $\geq 13$ , alkali-labile sites are thought to be converted into SSBs, and DNA crosslinking diminishes migration of DNA strand breaks. At pH 13, we did not observe comets in motor neurons exposed to 10 mM  $H_2O_2$  in neurobasal-A for several durations (30, 45, 60, and 90 min). At pH 12, many comets are observed after exposure of motor neurons to 10 mM  $H_2O_2$  (Liu and Martin 2001). These results with neurons are consistent with results from non-neuronal cells showing that  $H_2O_2$  mainly induces SSBs (SSBs:DSBs  $\sim 1:2000$ ) instead of DSB or alkali-labile sites (Singh et al. 1988; Horváthová et al. 1999). We conclude that comet assay conditions using pH 12 electrophoresis buffer are appropriate for detecting primarily DNA SSBs in motor neurons induced by  $H_2O_2$ .

We evaluated the types of DNA damage (SSBs or alkali-labile sites) induced in motor neurons exposed to NO (Figure 6). At two different concentrations of NONOate (10 and 100  $\mu$ M, exposure for 1 or 2 hr), the number of comets detected at pH 12 was generally greater than the number observed at pH 13. The comet morphology was different at pH 12 and, compared to pH 13 (Figures 7A and 7B). At pH 12, comets had prominent halos and short tails (Figure 7A), and comets at pH 13 had no halos and long granular tails (Figure 7B). At pH conditions of 12.6 or higher, alkali-labile sites are converted to SSBs and, therefore a pH  $\geq 13$  maximizes the detection of alkali-labile sites as SSBs (Kohn 1991). The presence of increased DNA migration from motor neurons at pH 13 indicates specifically the induction of alkali-labile sites, as well as SSBs, by NO donor. The formation of DNA SSBs is very dynamic. Exposure of motor neurons to 10  $\mu$ M causes a progressive accumulation of DNA SSBs over a 2-hr period, while the level of alkali-labile

Panoramic view showing many TUNEL-positive motor neurons (brown cells) after exposure to NONOate. (C–E) Morphological progression of NO-induced apoptosis of adult spinal motor neurons *in vitro* as detected with TUNEL. At early stages of apoptosis, DNA fragmentation is diffuse throughout the nucleus, but the nuclear membrane is intact with no leakage of DNA fragments into the cytoplasm (C). Cells progress to show faint cytoplasmic labeling (lower cell in D). Not all motor neurons show DNA fragmentation after exposure to NO donor (unlabeled upper cell in D). End-stage apoptotic motor neurons (E) show TUNEL staining of DNA that is organized into dense round masses surrounded by a lighter-staining cytoplasm, typical of apoptosis. Bars: A = 7  $\mu$ m (same for C–E); B (same bar as in A) = 40  $\mu$ m.



sites is relatively invariant (Figure 6A). With exposure of motor neurons to 100  $\mu\text{M}$  NONOate, a prominent peak in the number of comets detected at pH 12 is observed at 1 hr (Figure 6B). The DNA SSBs are formed within a 30-min time window. Therefore, motor neurons exposed to NO rapidly form DNA SSBs and alkali-labile sites.

The types of DNA damage were analyzed in motor neurons exposed to ONOO<sup>-</sup> (Figure 8). ONOO<sup>-</sup> induces rapid formation of alkali-labile sites, followed by an accumulation of SSBs while alkali-labile sites decline (Figure 8A). In addition, ONOO<sup>-</sup> induces DSBs (pH 7.4) very quickly in motor neurons (Figures 7C and 8B). These changes in motor neuron DNA were not the result of generalized cellular degradation because ChAT levels remained stable (Figure 2). Therefore, ONOO<sup>-</sup> is a potent DNA-damaging agent that concurrently induces alkali-labile sites, SSBs, and DSBs in motor neurons.

#### TUNEL Analysis of Isolated Adult Motor Neurons Exposed to NO Donor

TUNEL is a commonly used method for detecting DNA damage in cells. For comparison with the comet assay, we used the TUNEL method on motor neurons exposed to NO donor. Motor neuron cell suspensions were exposed to NONOate (10  $\mu\text{M}$  or 100  $\mu\text{M}$ ) or corresponding vehicle (10  $\mu\text{M}$  or 100  $\mu\text{M}$  spermine/NO<sub>2</sub><sup>-</sup>). TUNEL confirmed that NO is toxic to motor neurons because many motor neurons were TUNEL-positive after exposure to NONOate (Figures 9B–9E) but not after exposure to spermine/NO<sub>2</sub><sup>-</sup> (Figure 9A). TUNEL staining ranged from light (Figures 9C and 9D) to very dark and aggregated (Figure 9E). However, the types of DNA damage could not be ascertained with the TUNEL method; yet, a major advantage of the TUNEL method over the comet assay is that the morphological progression of motor neuron apoptosis is better appreciated with the TUNEL method (Figure 9E).

#### Combination of Comet Assay with Immunocytochemistry

We evaluated whether comet assay and immunocytochemical techniques could be combined. This combination is desirable because information on the expression of specific proteins is helpful for understanding the mechanisms of DNA damage-induced motor neuron apoptosis (Martin et al. 2000). Survival motor neuron (SMN) protein, a motor neuron protein that functions in cell survival (Liu and Dreyfuss 1996), is detectable in microgels after the comet assay in the 400 rpm cell preparation (Figures 7D–7F), further confirming that these cells are motor neurons. Although cytoplasmic proteins are degraded by the lysis

procedure, SMN has a nuclear localization and appears fibrous under alkaline conditions (Figure 7F). p53 immunoreactivity is also detected in the cells after comet procedures. p53 is a known DNA-binding protein. Cells without tails showed p53 immunoreactivity. Some positive cells had faint labeling, with a nucleus that was small and shrunken with DNA condensed after the SSB stage (Figure 7G). Other cells had nuclei with p53 granules, some of which co-localized with DNA granules (Figure 7G and 7H). This pattern was observed frequently in motor neurons exposed to NO donor.

#### Discussion

This work advances the study of motor neurons in three ways. It shows that mature spinal motor neurons can be isolated and used for in vitro models of neurotoxicity. This demonstration was extended by showing that adult motor neurons can also be isolated from in vivo models of motor neuron degeneration and evaluated for DNA damage using single-cell analysis. This study also shows for the first time that the comet assay is a useful method for measuring distinct DNA lesions in individual motor neurons. Using the comet assay with different pH conditions, we identified the coexistence of different types of early DNA damage in motor neurons. This approach may enable the study of motor neuron disease to move in new directions, particularly with regard to understanding mechanisms of DNA damage-induced apoptosis of motor neurons, which is relevant to ALS (Martin 2000).

#### Mature Motor Neurons Can Be Studied In Vitro

We developed a new approach to study mature motor neurons by creating a short-term, motor neuron-enriched cell suspension isolated from spinal cord ventral horn enlargements of adult rat. The motor neuron enrichment of this cell system was confirmed by immunophenotyping (e.g., ChAT, NeuN, and SMN), retrograde tracing, and immunoblotting. Electron microscopy has also been used to confirm the presence of motor neurons in this preparation (Liu and Martin 2001). This isolation technique for adult motor neurons can be applied successfully to paradigms of in vivo motor neuron injury (e.g., axotomy) to understand mechanisms of motor neuron degeneration using in vitro assays.

We took advantage of the structural features (i.e., their large size) of adult motor neurons and the large difference in size between spinal motor neurons and surrounding cells in the ventral horn to assist in their isolation by centrifugation. With strict microdissection and appropriate dissociation, our cell-sorting method may also be useful for isolating other populations of selectively vulnerable neurons, including cere-

bellar Purkinje cells, CA1 pyramidal neurons, and nigral dopaminergic neurons. This procedure could be highly applicable for Purkinje cells because these neurons are much larger than any adjacent cells, although the appropriate centrifugation speeds and times need to be identified for neuronal types other than spinal motor neurons.

This method is an important technical advancement in the field of motor neuron degeneration because very few methods are available to study motor neurons *in vitro*. Embryonic motor neuron cultures are a widely used *in vitro* system (Henderson et al. 1995), but these are immature neurons in a low-density culture. A recognized limitation of our model is the relatively short viability of adult motor neurons in suspension (~40% survival at 24 hr after isolation; Liu and Martin 2001), but long-term viability is also a problem with embryonic motor neurons, such that these cells are usually studied for only 24–48 hr after plating. There are several advantages of our mature motor neuron system. First, the cells are adult neurons and, because neuronal maturity appears to influence cell death mechanisms (Portera-Cailliau et al. 1997), this system may be more relevant than embryonic cell models for understanding motor neuron degeneration in ALS. Second, injured motor neurons can be isolated from adult animals after *in vivo* spinal cord or peripheral nerve manipulations. Similar experimental manipulations cannot be done with embryonic systems. Third, our isolation technique yields a high density of motor neurons (i.e., large number of cells) that can be used not only for comet assay and immunocytochemical methods but also for biochemical assays (e.g., immunoblotting and Southern blotting). Fourth, this isolation approach can be extended to adult transgenic mouse models of motor neuron degeneration. Fifth, our *in vitro* cell system can be used as a high-throughput screening system for environmental, synthetic, or biological compounds for neurotoxic (genotoxic), neuroprotective, or survival activities on adult motor neurons.

#### Early DNA Damage in Motor Neurons Can Be Measured with the Comet Assay

Since Kohn discovered that single-strand DNA is eluted rapidly under the alkaline condition from cells onto filters, the alkaline elution method has been used to detect and measure low-level DNA damage in eukaryotic cells (Kohn et al. 1976). This principle guided the development of a new method for analyzing DNA damage at the level of individual cells using single-cell gel electrophoresis (Östling and Johanson 1984; Singh et al. 1988). The comet assay detects DNA SSBs at pH ~12, DNA DSBs at neutralized conditions, DNA–DNA or DNA–protein crosslinking, alkali-labile sites

that cause SSBs under alkali conditions (pH >12.6), and damage to purine and pyrimidine bases (AP sites). The comet assay is sensitive enough for detecting one break per  $2 \times 10^{10}$  Daltons of DNA in lymphocytes (Singh et al. 1988). However, very few studies have applied the comet assay to neurons (Lai and Singh 1995; Morris et al. 1999; Liu and Martin 2001). In our description here, we used two different models of motor neuron degeneration to evaluate the feasibility of the comet assay for detecting early low-level DNA damage.

For one approach, we isolated motor neurons using our new method and exposed these cells *in vitro* to different ROS, followed by analysis by the comet assay. Motor neuron-enriched cell suspensions were exposed to  $H_2O_2$ , NO donors,  $H_2O_2$  + NO donor, and  $ONOO^-$ . We tested the hypothesis that oxidative stress causes adult motor neurons to accumulate DNA damage. We used different pH conditions during electrophoresis to discriminate between DNA strand breaks and alkali-labile sites in motor neurons. Interestingly, we found that different ROS induce different DNA damage signatures in neurons, which has not been shown before.  $H_2O_2$  induces primarily SSBs in motor neurons, consistent with previous reports using non-neuronal cells (Horváthová et al. 1999). NO donors induce alkali-labile (AP) sites and also SSBs, whereas  $ONOO^-$  induces a combination of SSBs, DSBs, and AP sites.

In the other model we used an *in vivo* lesion that induces motor neuron apoptosis (Martin et al. 1999). After this lesion, motor neurons were isolated during the early progression of degeneration and analyzed by the comet assay. Motor neurons in the unlesioned side of spinal cord did not show comets at any time (Liu and Martin 2001). In the lesioned side, motor neurons at 5 days after sciatic nerve avulsion had DNA damage, as detected with the comet assay. At this time, TUNEL labeling is negative in motor neurons (Martin et al. 1999). The motor neuron comets have a large head and a very short tail at 5 days post lesion. DNA damage in motor neurons was also detected at 7 days after sciatic nerve avulsion. The comet heads are looser and tails are longer than at 5 days. At 7 days post lesion, the TUNEL method slightly detects DNA damage in the ipsilateral side of lumbar spinal cord after sciatic nerve avulsion (Martin et al. 1999). At 10 days post lesion, the comet assay reveals motor neurons with more advanced comets than at earlier time points, indicating accumulating DNA damage. Beyond 10 days, motor neuron comets were not detected in the 400 rpm fraction but were detected in higher-speed centrifugation fractions (Liu and Martin 2001), indicating that the cells are now lighter, and possibly hypoploid, due to the apoptotic process (Martin et al. 1999). An increase in DNA SSBs could be caused by

an increased rate of DNA lesion formation or a reduction in DNA repair mechanisms (Lai and Singh 1995). The comets of motor neurons after avulsion and the comets of motor neurons exposed to NO donor *in vitro* are similar on the basis of comet morphology. Because avulsion-induced motor neuron death is apoptosis (Martin et al. 1999), comet patterns consisting of prominent DNA granules within the heads and tails are therefore signatures of apoptosis in neurons.

The comet assay has advantages over other more frequently used methods for detecting DNA damage (e.g., nick end-labeling methods such as TUNEL). It appears that assays for single-stranded DNA are more sensitive and specific than TUNEL for apoptosis. We have confirmed indirectly the sensitivity of comet assay detection of DNA SSBs as an early and sensitive marker for apoptosis. We found that DNA SSBs are visualized prominently in avulsed motor neurons at least 2 days before the detection of DNA fragmentation by TUNEL (Martin et al. 1999) and 5 days before round DNA-containing aggregates are detected in the nucleus (Liu and Martin 2001). The results indicate that the comet assay is more sensitive than the TUNEL method for showing DNA damage. Moreover, in motor neurons exposed to oxidative stress, DNA SSBs are detected prominently before morphological evidence for chromatin condensation and electrophoretic detection of internucleosomal DNA fragmentation (Liu and Martin 2001). In addition, the comet assay reveals the type of DNA damage (e.g., SSBs, DSBs, and AP sites), depending on the conditions. Another benefit of the comet assay is that comets can be classified into categories or stages of DNA damage, by morphology, by measuring tail length, and by digital image analysis of comets for DNA intensity and comet moment.

Previous studies using the comet assay have not combined this method with immunophenotyping of neuronal populations with DNA damage. We anticipated that some nuclear proteins would retain antigenicity in comet assay microgels. This suspicion was confirmed. Motor neurons contained SMN within the nucleus. In cell cultures (Liu and Dreyfuss 1996) and in rat spinal cord (Pagliardini et al. 2000), SMN has been localized in nuclear structures called gems that are associated with coiled bodies. SMN functions in the processing of pre-mRNA (Liu and Dreyfuss 1996). We found a nuclear localization in rat motor neurons as well and also report the novel observation that, after alkaline denaturation, SMN possesses an interesting fibrous structure. We also found that p53 is induced in motor neurons exposed to NO donor (Figure 7G) and that some of these cells are apoptotic based on morphology (Figure 7H) and TUNEL (Figure 9E). We also found that NO donors induce DNA SSBs and AP sites in motor neurons (Figure 6). Because DNA

SSBs are potent activators of p53 (Jayaraman and Prives 1995; Levine 1997), early formation and accumulation of oxidative stress-induced DNA-SSB in adult motor neurons could be a primary signal for motor neuron apoptosis. However, cells expressing p53 generally did not display comets at pH 12 (as did cells expressing SMN), although nuclear morphology indicated apoptosis in many cells. It is possible that the DNA damage in these motor neurons advanced beyond SSBs, suggesting that p53 activation occurs later than SSBs, and therefore SSB could be an upstream signaling mechanism for motor neuron cell death as in non-neuronal cells.

### Acknowledgments

Supported by grants from the US Public Health Service, the National Institutes of Health, National Institute of Neurological Disorders and Stroke (NS34100), and National Institute on Aging (AG16282), and the Department of Defense, US Army Medical Research and Materiel Command (DAMD17-99-1-9553).

### Literature Cited

- Ames BN (1989) Endogenous DNA damage as related to cancer and aging. *Mutat Res* 214:41–46
- Beckman JS, Carson M, Smith CD, Koppenol WH (1993) ALS, SOD and peroxynitrite. *Nature* 364:548
- Gavrieli Y, Sherman Y, Ben-Sasson SA (1992) Identification of programmed cell death *in situ* via specific labeling of nuclear DNA fragmentation. *J Cell Biol* 119:493–501
- Hellman B, Vaghef H, Boström B (1995) The concept of tail moment and tail inertia in the single cell gel electrophoresis assay. *Mutat Res* 336:123–131
- Henderson CE, Bloch-Gallego E, Camu W (1995) Purified embryonic motoneurons. In Cohen J, Wilkin G, eds. *Nerve Cell Culture: a Practical Approach*. London, Oxford University Press, 69–81
- Horváthová E, Slameňová D, Gábelová A (1999) Use of single cell gel electrophoresis (comet assay) modifications for analysis of DNA damage. *Gen Physiol Biophys* 18:70–74
- Hrabie JA, Klose JR, Wink DA, Keefer LK (1993) New nitric oxide-releasing zwitterions derived from polyamines. *J Org Chem* 58:1472–1476
- Jayaraman L, Prives C (1995) Activation of p53 sequence-specific DNA binding by short single strands of DNA requires the p53 C-terminus. *Cell* 81:1021–1029
- Kindzelskii AL, Petty HR (1999) Ultrasensitive detection of hydrogen peroxide-mediated DNA damage after alkaline single cell gel electrophoresis using occultation microscopy and TUNEL labeling. *Mutat Res* 426:11–22
- Kisby GE, Kabel H, Hugon J, Spencer P (1999) Damage and repair of nerve cell DNA in toxic stress. *Drug Metab Rev* 31:589–618
- Kohn KW (1991) Principles and practice of DNA filter elution. *Pharmacol Ther* 49:55–77
- Kohn KW, Erickson LC, Ewig RAG, Friedman CA (1976) Fractionation of DNA from mammalian cells by alkaline elution. *Biochemistry* 15:4629–4637
- Lai H, Singh NP (1995) Acute low-intensity microwave exposure increases DNA single-strand breaks in rat brain cells. *Bioelectromagnetics* 16:207–210
- Levine AJ (1997) p53, the cellular gatekeeper for growth and division. *Cell* 88:323–331
- Lindahl T (1993) Instability and decay of the primary structure of DNA. *Nature* 362:709–715

- Liu Q, Dreyfuss G (1996) A novel nuclear structure containing the survival of motor neurons protein. *EMBO J* 15:3555-3565
- Liu Z, Martin LJ (2001) Motor neurons rapidly accumulate DNA single strand breaks after in vitro exposure to nitric oxide and peroxynitrite and in vivo axotomy. *J Comp Neurol* 432:35-60
- Martin LJ (1999) Neuronal death in amyotrophic lateral sclerosis is apoptosis: possible contribution of a programmed cell death mechanism. *J Neuropathol Exp Neurol* 58:459-471
- Martin LJ (2000) p53 is abnormally elevated and active in the CNS of patients with amyotrophic lateral sclerosis. *Neurobiol Dis* 7:613-622
- Martin LJ, Kaiser A, Price AC (1999) Motor neuron degeneration after sciatic nerve avulsion in adult rat evolves with oxidative stress and is apoptosis. *J Neurobiol* 40:185-201
- Martin LJ, Price AC, Kaiser A, Shaikh AY, Liu Z (2000) Mechanisms for neuronal degeneration in amyotrophic lateral sclerosis and in models of motor neuron death. *Int J Mol Med* 5:3-13
- Morris EJ, Drexler JC, Cheng K-Y, Wilson PM, Gin RM, Geller HM (1999) Optimization of single-cell gel electrophoresis (SCGE) for quantitative analysis of neuronal DNA damage. *Bio-Techniques* 26:282-289
- Östling O, Johanson KJ (1984) Microelectrophoretic study of radiation-induced DNA damage in individual mammalian cells. *Biochem Biophys Res Commun* 123:291-298
- Pagliardini S, Giavazzi A, Setola V, Lizier C, DiLuca M, DeBiasi S, Battaglia G (2000) Subcellular localization and axonal transport of the survival motor neuron (SMN) protein in the developing rat spinal cord. *Hum Mol Genet* 9:47-56
- Petersen AB, Gniadecki R, Wulf HC (2000) Laser scanning cytometry for comet assay analysis. *Cytometry* 39:10-15
- Portera-Cailliau C, Price DL, Martin LJ (1997) Non-NMDA and NMDA receptor-mediated excitotoxic neuronal deaths in adult brain are morphologically distinct: further evidence for an apoptosis-necrosis continuum. *J Comp Neurol* 378:87-104
- Singh NP, McCoy MT, Tice RR, Schneider EL (1988) A simple technique for quantitation of low levels of DNA damage in individual cells. *Exp Cell Res* 175:184-191
- Subba Rao K (1993) Genomic damage and its repair in young and aging brain. *Mol Neurobiol* 7:23-48
- Tice RR, Agurell E, Anderson D, Burlison B, Hartmann A, Kobayashi H, Miyamae Y, Rojas E, Ryu J-C, Sasaki YF (2000) Single cell gel/comet assay: guidelines for in vitro and an in vivo genetic toxicological testing. *Environ Mol Mutagen* 35:206-221

## Neuronal Death in Newborn Striatum after Hypoxia-Ischemia Is Necrosis and Evolves with Oxidative Stress

Lee J. Martin,<sup>\*,†,1</sup> Ansgar M. Brambrink,<sup>‡,2</sup> Ann C. Price,<sup>\*</sup>  
Adeel Kaiser,<sup>\*</sup> Dawn M. Agnew,<sup>§</sup> Rebecca N. Ichord,<sup>†</sup>  
and Richard J. Traystman<sup>†</sup>

<sup>\*</sup>Department of Pathology, Division of Neuropathology, <sup>†</sup>Department of Neuroscience,  
<sup>‡</sup>Department of Anesthesiology and Critical Care Medicine, and <sup>§</sup>Department of Neurology,  
Johns Hopkins University School of Medicine; and <sup>1</sup>School of Nursing,  
University of Maryland, Baltimore, Maryland

Received September 21, 1999; revised December 16, 1999; accepted January 31, 2000

The mechanisms for neurodegeneration after hypoxia-ischemia (HI) in newborns are not understood. We tested the hypothesis that striatal neuron death is necrosis and evolves with oxidative stress and selective organelle damage. Piglets (~1 week old) were used in a model of hypoxia-asphyxia and survived for 3, 6, 12, or 24 h. Neuronal death was progressive over 3–24 h recovery, with ~80% of putaminal neurons dead at 24 h. Striatal DNA was digested randomly at 6–12 h. Ultrastructurally, dying neurons were necrotic. Damage to the Golgi apparatus and rough endoplasmic reticulum occurred at 3–12 h, while most mitochondria appeared intact until 12 h. Mitochondria showed early suppression of activity, then a transient burst of activity at 6 h, followed by mitochondrial failure (determined by cytochrome c oxidase assay). Cytochrome c was depleted at 6 h after HI and thereafter. Damage to lysosomes occurred within 3–6 h. By 3 h recovery, glutathione levels were reduced, and peroxynitrite-mediated oxidative damage to membrane proteins, determined by immunoblots for nitrotyrosine, occurred at 3–12 h. The Golgi apparatus and cytoskeleton were early targets for extensive tyrosine nitration. Striatal neurons also sustained hydroxyl radical damage to DNA and RNA within 6 h after HI. We conclude that early glutathione depletion and oxidative stress between 3 and 6 h reperfusion promote damage to membrane and cytoskeletal proteins, DNA and RNA, as well as damage to most organelles, thereby causing neuronal necrosis in the striatum of newborns after HI. © 2000 Academic Press

**Key Words:** apoptosis; cerebral palsy; cytochrome c; DNA damage; mitochondria; RNA oxidation

### INTRODUCTION

Hypoxia-ischemia (HI) in newborns is a major cause of pediatric mortality and morbidity and causes brain damage resulting in life-long neurobehavioral handicaps. In human newborns (Volpe, 1995; Roland *et al.*, 1998; Maller *et al.*, 1998) and in some pediatric animal models (Martin *et al.*, 1997a,b), HI causes a character-

istic encephalopathy, with basal ganglia and somatosensory systems showing selective vulnerability. However, the mechanisms that cause this brain damage in HI neonates remain unclear. Glutamate receptor-mediated excitotoxic cell injury is a possible mechanism for this neuronal degeneration following HI in newborns (Olney, 1994; Martin *et al.*, 1998a). Using a newborn piglet model of cardiac arrest that causes reproducible damage to the basal ganglia (Martin *et al.*, 1997b,c), we found that the protein levels of specific subtypes of glutamate transporters (e.g., GLT1 and EAAC1) are reduced in striatum at 24 h recovery and thereafter (Martin *et al.*, 1997c) and that functional

<sup>1</sup> To whom correspondence and reprint requests should be addressed at Ross Bldg., Rm 558, 720 Rutland Ave, Baltimore, MD 21205. Fax: (410) 955-9777. E-mail: [lmartin@welchlink.welch.jhu.edu](mailto:lmartin@welchlink.welch.jhu.edu).

<sup>2</sup> Present address: Department of Anesthesiology, Johannes Gutenberg-University, Mainz, Germany.

transport of glutamate is impaired in striatal synaptosomes by 6–12 h after HI (Natale *et al.*, 1999). The concept that excitotoxicity participates in the mechanisms for neuronal degeneration resulting from perinatal HI is supported by studies showing that the NMDA receptor antagonist MK-801 ameliorates brain damage in HI neonatal rats (McDonald *et al.*, 1987; Ford *et al.*, 1989). However, neither MK-801 (LeBlanc *et al.*, 1991) nor AMPA receptor antagonists (LeBlanc *et al.*, 1995; Martin *et al.*, 1997a; Brambrink *et al.*, 1999) afford neuroprotection in clinically relevant models of newborn HI. Although glutamate receptor excitotoxicity continues to be a potential mechanism for neurodegeneration in the perinatal period, the precise cellular and molecular pathways for neuronal death *in vivo* remain poorly understood.

Depending on the type of cell and on the stimulus, cells typically die in either of two ways generally described as apoptosis or necrosis (Kerr *et al.*, 1972; Martin *et al.*, 1998a). These two forms of cell death are thought to differ fundamentally at structural and mechanistic levels. Apoptosis is a structurally organized, programmed cell death that is mediated by active, intrinsic mechanisms. In contrast, cellular necrosis is thought to be structurally a more rapid and random degeneration resulting from extrinsic insults to the cells, such as abrupt environmental perturbations (e.g., osmotic, thermal, toxic, or traumatic) and departures from physiological conditions, involving disruption of plasma membrane structural and functional integrity, rapid influx of  $\text{Na}^+$ ,  $\text{Ca}^{2+}$ , and water, cell swelling, and subsequent dissolution of the cell (Choi, 1992). More recent experiments have revealed that the death of neurons can also be a hybrid of apoptosis and necrosis with overlapping characteristics (Portera-Cailliau *et al.*, 1997a,b). Some studies have suggested that neuronal death after HI in newborns is apoptosis (Beilharz *et al.*, 1995; Hill *et al.*, 1995; Cheng *et al.*, 1998). However, this conclusion is controversial (Martin *et al.*, 1998a). Neurodegeneration in the newborn striatum is advanced at 24 h after HI (Martin *et al.*, 1997c). Therefore, we tested the hypothesis that the progression of striatal neuron death after HI is rapid and necrotic structurally, but evolves orderly with successive subcellular abnormalities in different organelles, similar to excitotoxic neuronal necrosis (Portera-Cailliau *et al.*, 1997a,b). Because reactive oxygen species (ROS) are potent mediators of cell necrosis (McCord, 1985; Halliwell and Gutteridge, 1986), we also determined if striatal neuron death after HI emerges in association with acute oxidative stress and

ROS-mediated damage to membrane proteins and nucleic acids.

## MATERIALS AND METHODS

### Piglet Model of HI

The animal protocol was approved by the Animal Care and Use Committee of the Johns Hopkins Medical Institutions and was described previously (Martin *et al.*, 1997a,b,c; Brambrink *et al.*, 1999). This piglet model was adopted because of its relevance to HI encephalopathy in human newborns and children (Johnston, 1998). One-week-old male or female piglets (~3 kg) were anesthetized with intraperitoneal (ip) sodium pentobarbital (65 mg/kg), intubated, and ventilated mechanically. Using sterile surgery, femoral arterial and venous catheters were placed into the thoracic aorta and inferior vena cava, respectively, and were tunneled subcutaneously exiting the skin for long-term access. Cephalothin (50 mg/kg) prophylaxis was administered intravenously. Oxygenation, ventilation, and acid-balance were all maintained at normal values. Rectal temperature was maintained at 38.5–39.5°C. Piglets received a maintenance infusion of intravenous lactated Ringer's solution (10 mg/kg/h), with additional analgesia and neuromuscular blockade provided by bolus intravenous fentanyl (10 µg/kg) and pancuronium (0.3 mg/kg), respectively. Baseline arterial blood gases, pH, hemoglobin, glucose, lactate, pulse rate, and blood pressure were measured (Brambrink *et al.*, 1999).

Piglets were then exposed to 30 min of hypoxia ( $\text{SaO}_2$  30%), followed by 5 min of ventilation with room air ( $\text{SaO}_2$  65%), and then 7 min of airway occlusion ( $\text{SaO}_2$  5%), resulting in asphyxic cardiac arrest (Brambrink *et al.*, 1999). Piglets were resuscitated by ventilation with 100%  $\text{O}_2$ , manual chest compressions, intravenous epinephrine (0.1 mg/kg), and intravenous sodium bicarbonate (1 mEq/kg) until return of spontaneous circulation, usually within 2–3 min. Defibrillation (2 joules/kg) was performed for ventricular fibrillation, with intravenous lidocaine (1 mg/kg) if multiple defibrillations were required. Approximately 90% of piglets were successfully resuscitated. Piglets were allowed to awaken and were extubated when able to maintain spontaneous oxygenation and ventilation, usually within 8 h. Piglets drank formula milk, usually by 24 h recovery, or were tube fed if necessary. Animals ( $n = 23$ ) were recovered for 3, 6, 12, or 24 h after the return of spontaneous circulation. Sham con-

trol animals ( $n = 8$ ) were anesthetized and subjected to the surgical preparation but not the HI.

### Preparation of Brain Samples

Piglet brains were harvested freshly for protein and DNA gel analyses and for biochemical assays, or were perfusion-fixed for *in situ* DNA fragmentation analysis, immunocytochemistry, enzyme histochemistry, and electron microscopy. Animals for fresh brain tissue ( $n = 3$  or 4 per recovery time) were anesthetized deeply with sodium pentobarbital (65 mg/kg, ip) and exsanguinated with ice-cold phosphate-buffered saline (PBS). Brains were removed rapidly and placed on wet ice. The cerebrum was transected midsagittally, and the hemispheres were subdivided to obtain samples from the striatum (including putamen, caudate, internal capsule, nucleus accumbens). These samples were flash-frozen in cold isopentane and stored at  $-70^{\circ}\text{C}$  until used for extractions. From the left hemisphere of each of these animals, a thin brain slab containing the striatum was immersion fixed in 5% acrolein and processed for paraffin histology for quantification of neuronal damage in hematoxylin & eosin (H&E) stained sections.

Piglets for fixed brain tissue ( $n = 2$  or 3 per recovery time) were anesthetized deeply with sodium pentobarbital (65 mg/kg, ip) and exsanguinated with ice-cold PBS, then perfused intraaortically for 20 min with ice-cold 4% paraformaldehyde plus 1% glutaraldehyde. Brains were removed and bisected midsagittally, and each hemisphere cut into 1-cm slabs. The left forebrain was used for paraffin histology and electron microscopy (EM). The right forebrain was cryoprotected in 20% glycerol-PBS for 24 h, frozen, and serial 40- $\mu\text{m}$  sections through striatum were cut on a sliding microtome. Sections were stored in antifreeze buffer at  $-20^{\circ}\text{C}$  until they were used for DNA end-labeling, immunocytochemistry, and enzyme histochemistry.

### Neuropathology, TUNEL, and Electron Microscopy

For quantification of neuronal degeneration after HI in all piglets ( $n = 31$ ), coronal samples of striatum from the left hemisphere were paraffin-processed, and sections (10- $\mu\text{m}$ -thick) were stained with H&E and the terminal transferase-mediated biotin-dUTP nick-end labeling (TUNEL) method for *in situ* detection of nuclear DNA fragmentation as described (Portera-Cailliau *et al.*, 1997a,b; Martin *et al.*, 1997c; Al-Abdulla *et al.*, 1998). The TUNEL method was used to identify

dying cells after HI, although this technique is not specific for apoptosis (Grasl-Kraupp *et al.*, 1995; Martin *et al.*, 1998a, 2000). Comparable levels of the striatum from sham and HI piglets were used to determine the severity of striatal injury at 3, 6, 12, and 24 h recovery. In H&E sections, the density of principal striatal neurons and the percentage of remaining neurons with ischemic cytopathology were determined from six nonoverlapping, random 1000x microscopic fields in the putamen. The criteria for neuronal injury were cytoplasmic eosinophilia and vacuolation, perikaryal shrinkage, and nuclear pyknosis. H&E sections were also used for measurements of principal striatal neuron cell body volume and nuclear volume using ocular filar micrometry at 1000x. Neuronal cell body and nuclear volumes were calculated from  $V = \pi/6(ab^2)$ , where  $a$  = diameter of the major axis and  $b$  = the diameter of the minor axis (Martin *et al.*, 1986). In TUNEL preparations, the density of dying cells was determined by parcellating the putamen into six divisions and counting the number of TUNEL-positive nuclei in six microscopic fields at 1000x.

To determine whether the neuronal degeneration after HI has the structure of apoptosis, necrosis, or a hybrid form of death (Portera-Cailliau *et al.*, 1997a,b), samples (3 mm<sup>3</sup>) of putamen from control and HI piglets (3, 6, 12, and 24 h) were osmicated, embedded in plastic, and evaluated by EM. Ischemic neurodegeneration was evaluated using ultrastructural criteria for cellular necrosis and apoptosis that we have described previously using *in vivo* models of neuronal degeneration (Portera-Cailliau *et al.*, 1997a,b; Al-Abdulla *et al.*, 1998; Martin *et al.*, 1998a, 1999, 2000).

### DNA Isolation and Agarose Gel Electrophoresis

Because the TUNEL method identifies DNA fragmentation independent of mechanisms (Grasl-Kraupp *et al.*, 1995; Portera-Cailliau *et al.*, 1997a; Martin *et al.*, 1998a), we evaluated striatal neuropathology based on DNA fragmentation patterns in agarose gels. Genomic DNA was isolated from samples of sham control piglets ( $n = 2$ ) and HI piglets at 3, 6, 12, and 24 h recovery (two animals/time). Striatal samples were homogenized in DNA extraction buffer containing 10 mM Tris (pH 7.4), 10 mM NaCl, 25 mM EDTA, 1% SDS, 1 mg/ml proteinase K, and incubated in the same buffer overnight at  $37^{\circ}\text{C}$ . DNA was extracted with an equal volume of salt saturated-phenol:chloroform:isoamyl alcohol (10:10:1) and the recovered aqueous phase was extracted with diethyl ether. DNA was precipitated with ethanol (2.5 vol). The DNA pellet was dissolved

in  $0.1\times$  SSC and incubated ( $37^{\circ}\text{C}$ ) with DNase-free RNase A (0.1 mg/ml) for 1 h and then overnight ( $37^{\circ}\text{C}$ ) with 0.1 mg/ml proteinase K. DNA was reextracted, precipitated, and dissolved in TE buffer. DNA samples were fractionated by agarose gel (1.2%) electrophoresis and were evaluated by ethidium bromide staining and by end labeling. For end labeling, DNA samples ( $\sim 1.0\text{ }\mu\text{g}$ ) were 3'-end labeled with digoxigenin-11-ddUTP using terminal transferase (Boehringer-Mannheim), precipitated, resuspended in TE buffer, fractionated, and transferred to nylon membrane followed by UV-crosslinking. Membranes were incubated in 2% nucleic acid blocking reagent (Boehringer-Mannheim) and then in blocking reagent containing 75 mU/ml antidigoxigenin Fab fragments conjugated to alkaline phosphatase (Boehringer-Mannheim). After washing, membranes were reacted with CSPD detection reagent (Boehringer-Mannheim) and exposed to Kodak X-OMAT film to visualize DNA.

### Immunoblot Analyses

Striatal samples (0.4–0.6 g from each piglet) for immunoblot analysis were homogenized with a Brinkman Polytron in ice-cold homogenization buffer (20 mM Tris-HCl, pH 7.4, with 10% sucrose, 1 mM EDTA, 5 mM EGTA, 20 U/ml Traysol, 20  $\mu\text{g}/\text{ml}$  leupeptin, 20  $\mu\text{g}/\text{ml}$  antipain, 20  $\mu\text{g}/\text{ml}$  pepstatin, 20  $\mu\text{g}/\text{ml}$  chymostatin, 0.1 mM phenylmethylsulfonyl fluoride, and 10 mM benzamidin). Crude homogenates were centrifuged at  $1,000g_{av}$  for 10 min at  $4^{\circ}\text{C}$ . The supernatant (S1 fraction) was then centrifuged at  $114,000g_{av}$  for 20 min. The resulting supernatant (S2 soluble fraction) was collected, and the pellet (P2 mitochondrial-enriched, membrane fraction) was washed in homogenization buffer (without sucrose) three times by resuspension, each followed by centrifugation at  $114,000g_{av}$  for 20 min. The washed membrane fraction was resuspended fully in this buffer supplemented with 20% (wt/vol) glycerol. Protein concentrations in soluble and membrane fractions were measured by a Bio-Rad protein assay with bovine serum albumin as a standard. Samples were stored at  $-70^{\circ}\text{C}$ .

Frozen striatal membrane and soluble fractions were thawed to  $4^{\circ}\text{C}$ , and samples (10  $\mu\text{g}$  of total protein) were fractionated by sodium dodecyl sulfate-polyacrylamide gel electrophoresis (SDS-PAGE). Proteins were transferred electrophoretically to nitrocellulose filters. Gels were stained with Coomassie blue, and nitrocellulose membranes were briefly stained with Ponceau S to verify uniform protein transfer. Blots were washed with 50 mM Tris-buffered saline

(TBS) and subsequently blocked in 2.5% nonfat milk in 50 mM TBS/0.1% Tween 20. As a marker for peroxynitrite-mediated damage to protein tyrosines in membrane fractions, nitrotyrosine modification of proteins was detected with monoclonal and polyclonal antibodies (Upstate Biotechnology, Lake Placid, NY) used at a concentration of 1  $\mu\text{g}$  IgG/ml. Peroxynitrite is a potent and relatively long lived ROS formed by a reaction between superoxide and nitric oxide (Beckman *et al.*, 1992). Subcellular fractions were also evaluated with organelle-specific antibodies to identify damage to these intracellular compartments over 24 h recovery. Blots of membrane proteins were probed with a monoclonal antibody (0.5  $\mu\text{g}$  IgG/ml) to human cytochrome c oxidase subunit I (Molecular Probes, Eugene, OR) or a monoclonal antibody (3.4  $\mu\text{g}$  IgG/ml) to rat Golgi 58K protein (Sigma, St. Louis, MO) as markers for mitochondria and the Golgi apparatus, respectively. Golgi 58K protein is a peripheral Golgi membrane protein that functions in microtubule binding (Bloom and Brashear, 1989). Blots of cytosolic proteins were probed with monoclonal antibody (100 ng IgG/ml) to pigeon cytochrome c (PharMingen, San Diego, CA) or with polyclonal antibodies (1  $\mu\text{g}$  IgG/ml) to KDEL proteins (Affinity BioReagents, Golden, CO), as markers for mitochondrial membrane damage and degradation of cytochrome c and for endoplasmic reticulum (ER) membrane damage and release of ER lumenal proteins, respectively. The KDEL sequence at protein C-termini is an ER retention signal (Munro and Pelham, 1987). Primary antibodies to these proteins in soluble fractions were diluted in 2.5% nonfat milk or normal goat serum (NGS) prepared with 50 mM TBS/0.1% Tween 20. Blots were incubated with antibody overnight at  $4^{\circ}\text{C}$ . After the primary antibody incubation, the blots were washed and incubated (0.2  $\mu\text{g}/\text{ml}$ ) with goat anti-rabbit or goat anti-mouse IgG conjugated to horseradish peroxidase (Bio-Rad). Blots were again washed, and immunoreactive proteins were visualized within the linear range with an enhance chemiluminescence detection system (Amersham or Pierce) and exposed to radiographic film.

To identify proteins that are possible targets of nitrotyrosine modification, we used immunoprecipitation. Subcellular fractions (50  $\mu\text{g}$  protein) were reacted overnight with monoclonal antibody to tubulin (Amersham). Immunocomplexes were captured with protein A-agarose bead slurry, washed, and subjected to SDS-PAGE for subsequent analysis by western blotting with polyclonal antibodies to nitrotyrosine. For negative control experiments, nitrotyrosine antibodies



were neutralized with nitrotyrosine-molecular weight standards (Upstate).

Protein levels were quantified densitometrically using a Macintosh Adobe Photoshop program, and analyzed using Signal Analytics IP Lab Gel software. Protein levels were expressed as percentage of control by comparing density of the protein band scanned to density of the same band in the control lane of the same blot. For a quantitative control for equal protein loading in each lane, blots of membrane proteins were reprobed (0.06  $\mu\text{g}/\text{ml}$ ) with a mouse monoclonal antibody to synaptophysin (Boehringer Mannheim), a membrane protein involved in synaptic vesicle fusion. The levels of synaptophysin (p38) in HI piglet striatum are not changed before 24 h recovery (Martin *et al.*, 1997b). The levels of nitrotyrosine-modified proteins, cytochrome c oxidase subunit I, and Golgi 58K protein were corrected for relative synaptophysin immunodensity. For a quantitative control for equal protein loading in each lane in blots of striatal soluble proteins, blots were reprobed (40–80 ng IgG/ml) with a mouse monoclonal antibody to tyrosine hydroxylase (Boehringer-Mannheim), the enzyme involved in dopamine synthesis in nigrostriatal terminals, or a mouse monoclonal antibody (1:2000) to synapse-associated protein-25 (SNAP-25, Sternberger Monoclonals). Nerve terminal degeneration in HI piglet striatum does not occur until after 24 h recovery (Martin *et al.*, 1997b,c). Thus, cytochrome c and KDEL protein levels in the cytosolic compartment were corrected for relative tyrosine hydroxylase or SNAP-25 immunodensity.

#### Cytochrome c Oxidase Assay

A colorimetric assay (Wharton and Tzagoloff, 1967) was used for biochemical measurements of cytochrome c oxidase (COX) activity in homogenates of control striatum ( $n = 3$ ) and HI piglet ( $n = 2$  or 3/time point) striatum at 3, 6, 12, and 24 h after reperfusion. Reduced cytochrome c (ferrocytochrome c) was prepared freshly for each experiment by mixing 1% cytochrome c (Sigma) with sodium hydrosulfite in potassium phosphate buffer. Samples (20  $\mu\text{g}$  protein) of mitochondrial-enriched membrane fractions were reacted with ferrocytochrome c in potassium phosphate buffer (10 mM, pH 7.0) at room temperature. The decrease in absorbance was measured spectrophotometrically at 550 nm every 15 s. The activity of COX was defined in terms of the first-order velocity constant.

#### Acid Phosphatase Assay

HI and reperfusion are known to effect the stability and permeability of lysosomes (Frederiks and Marx, 1989). As an index of lysosomal membrane damage and destabilization of lysosomes (Frederiks and Marx, 1989; van Noorden, 1991), acid phosphatase activity was measured in cytosolic protein fractions of control striatum ( $n = 3$ ) and HI piglet ( $n = 2$  or 3/time point) striatum at 3, 6, 12, and 24 h recovery. In 2.5-ml plastic cuvettes, samples of soluble protein fractions (500 or 1000  $\mu\text{g}$  total protein) were mixed at room temperature with 15 mM *o*-carboxyphenyl-phosphate in 150 mM sodium acetate buffer (pH 5.0) in a final reaction volume of 1.5 or 2.0 ml. The  $\Delta_{\text{Abs}}$  was measured with a spectrophotometer (Pharmacia) over 2 min at 300 nm. Purified potato acid phosphatase (Boehringer-Mannheim) was used as a positive control (0.6–6 U/ml). Reactions were run in the absence or presence of the acid phosphate inhibitor sodium fluoride (Sigma). Acid phosphatase activity, based on results of triplicate experiments, was expressed as percentage of control.

#### Glutathione Assay

The levels of glutathione (GSH and GSSG) in soluble protein fractions of control piglet striatum ( $n = 3$ ) and HI piglet striatum at 3, 6, 12, and 24 h reperfusion ( $n = 2$  or 3/time point) were measured using a modification of the method of Tietze (Tietze, 1969). Disposable cuvettes were loaded with 650  $\mu\text{l}$  of 100 mM potassium phosphate buffer (pH 7.5) containing 5 mM EGTA, 100  $\mu\text{g}/\text{ml}$  5,5'-dithiobis(2-nitrobenzoic acid), and 320  $\mu\text{g}/\text{ml}$  NADPH. To this reaction mixture, 2 U/ml of GSH reductase and striatal soluble protein (500  $\mu\text{g}$ ) were added (with a final reaction volume of 1 ml), and the  $\Delta_{\text{Abs}}$  was measured immediately with a spectrophotometer (Pharmacia) over 4 min at 412 nm. GSH levels, based on results of duplicate experiments, were expressed as percentage of control.

#### Immunocytochemical Analyses of Organelles and Oxidative Damage

Brain sections from perfusion-fixed control piglets ( $n = 3$ ) and HI piglets at 3, 6, 12, and 24 h reperfusion ( $n = 2$  or 3/time point) were removed from antifreeze buffer and washed in TBS. Free-floating sections were pretreated with  $\text{H}_2\text{O}_2$ /methanol (to eliminate endogenous peroxidase activity), rinsed, and then with sodium borohydride (for antigen retrieval), and blocked

in NGS. Sections were incubated for 48 h at 4°C with primary antibodies (see below). After primary antibody incubation, sections were incubated sequentially with affinity-purified F(ab)<sub>2</sub> fragments of goat anti-rabbit or anti-mouse IgG (Cappel) and then affinity-purified monoclonal goat anti-rabbit or goat anti-mouse antibody conjugated to horseradish peroxidase (Sternberger Monoclonals). Sites of antibody binding were visualized with H<sub>2</sub>O<sub>2</sub> and diaminobenzidine as a chromogen.

Several different antibodies were used as immunocytochemical probes to identify the progression of subcellular abnormalities in striatal neurons after HI. As organelle probes, we used monoclonal antibody to Golgi 58K protein (15 µg IgG/ml) for the Golgi apparatus, monoclonal antibody (1 µg IgG/ml) to COX subunit I for mitochondria, polyclonal rabbit antibody (200 ng IgG/ml, Santa Cruz) to Rab5A for early endosomes (Simons and Zerial, 1993), and polyclonal rabbit antibody (10 µg IgG/ml, Affinity BioReagents) to KDEL sequence-containing proteins for the ER. To determine if striatal neurons undergo oxidative stress, peroxynitrite-mediated damage to proteins was identified using antibodies to nitrotyrosine (3 µg IgG/ml), and hydroxyl radical damage to DNA and RNA was detected with monoclonal antibody (30 µg IgG/ml) to 8-hydroxy-2'-deoxyguanosine (QED Bioscience, Inc and PharMingen, San Diego, CA). These antibodies react with hydroxyl radical modified DNA and RNA (Al-Abdulla and Martin, 1998; Martin et al., 1999). For competition controls, sections were reacted with antibody to 8-hydroxy-2'-deoxyguanosine (OHdG) that was incubated at 4°C for 24 h with 1000-fold concentrations of OHdG, 8-hydroxyguanosine (OHG) or guanosine (Cayman Chemical, Ann Arbor, MI). As additional controls, sections were digested with DNase (5–10 mg/ml) or RNase (11–50 mg/ml) prior to incubation with OHdG antibody.

### Cytochrome c Oxidase Enzyme Histochemistry

To assay for mitochondrial function with spatial resolution, the COX histochemical method of Wong-Riley (1979) was used as described previously (Martin et al., 1997a,b). Forebrain sections from control piglets ( $n = 3$ ) and HI piglets ( $n = 2$  or 3/time point) were incubated concomitantly with freshly prepared enzymatic reaction medium consisting of 100 mM phosphate buffer (pH 7.4), 0.1% horse heart cytochrome c, 117 mM sucrose, and 1.4 mM diaminobenzidine tetrahydrochloride (Wong-Riley, 1979). The enzymatic specificity of this reaction in piglet brain has been

TABLE 1

Progression of Neuronal Degeneration in the Striatum after HI<sup>a</sup>

Group	Percentage neuronal damage	Neuronal density (cells/mm <sup>2</sup> )
Control	0.4 ± 0.4	572.9 ± 22.3
3-h	15.7 ± 3.3 <sup>b,c</sup>	515.5 ± 14.0
6-h	30.9 ± 4.7 <sup>b,c</sup>	550.0 ± 14.1
12-h	47.2 ± 7.6 <sup>b,c</sup>	535.0 ± 23.4
24-h	78.8 ± 3.9 <sup>b,c</sup>	395.2 ± 19.8 <sup>b</sup>

<sup>a</sup> Percentage of principal neurons with damage and neuronal density in the putamen of control and ischemic piglets at 3, 6, 12, and 24 h after HI. Measurements were made in H&E-stained sections. Percentage neuronal damage was estimated by identifying the fraction of neurons with ischemic cytopathology relative to the total number of neurons in microscopic fields of the striatum. All values are mean ± SEM.

<sup>b</sup> Significantly different ( $P < 0.05$ ) from control.

<sup>c</sup> Significantly different ( $P < 0.05$ ) from preceding recovery time.

shown (Martin et al., 1997b). After the reaction, sections were rinsed in phosphate buffer, mounted on glass slides, and coverslipped. Histochemical COX enzyme activity was quantified densitometrically using an image-processing system as described (Martin et al., 1997a,b).

### Statistical Analysis of Data

All histological and biochemical measurements were made in duplicate or triplicate. Statistical analysis of measurements for percentage neuronal damage and neuronal and TUNEL-positive cell densities were performed using one-way analysis of variance. If there were significant differences among the group means as indicated by the  $F$  test, group means were further analyzed using Newman-Keuls test. Protein levels determined by immunoblotting were expressed as percentage of sham-control piglets. Mean percentages were compared among 3, 6, 12, and 24 h recovery groups by a Wilcoxon signed rank test. The level of significance was  $P < 0.05$  in all tests.

## RESULTS

### Striatal Neuron Death after HI in Newborns Is Rapid and Progressive over 24 h

Prominent neuronal degeneration in the striatum of HI piglets occurred during 3 to 24 h recovery (Table 1; Fig. 1). Neurons were distinguished from glial and inflammatory cells by strict perikaryal and nuclear

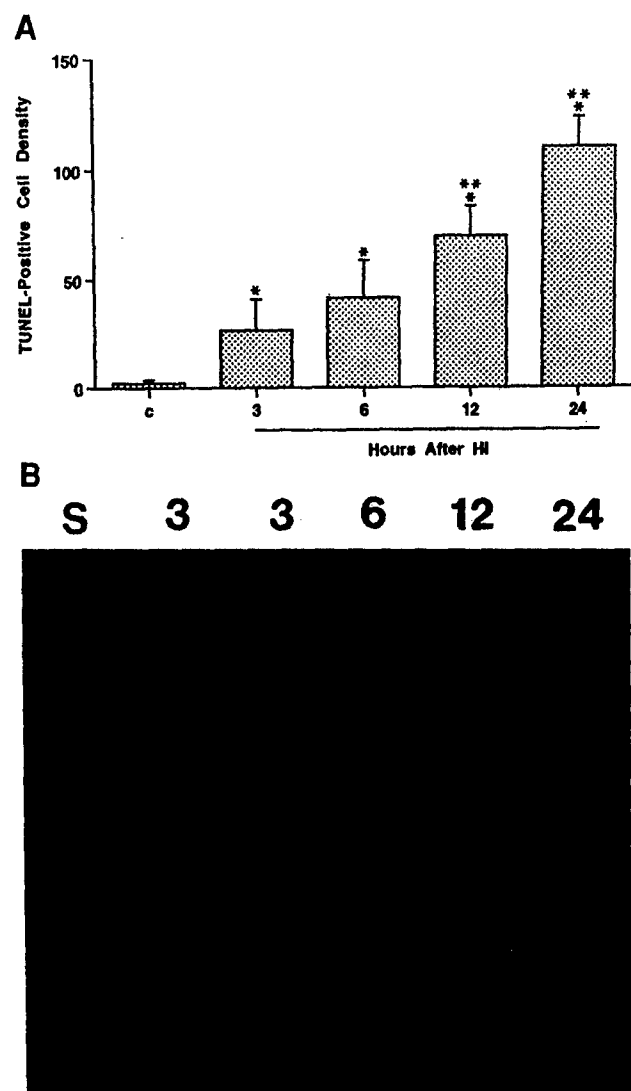


**FIG. 1.** DNA fragmentation begins by 3 h after HI and is progressive and consistent with cellular necrosis. (A) Striatal neuron death (in putamen) in control piglets (C) and piglets at 3, 6, 12, and 24 h after HI. TUNEL-positive cell densities (cells/mm<sup>2</sup>) are mean  $\pm$  SEM. Asterisk indicates significant difference ( $P < 0.05$ ) from control. Double asterisk indicates significant difference ( $P < 0.05$ ) from control, 3 h and 6 h after HI. (B) Agarose gel fractionation of DNA isolated from the striatum of sham control piglets (S) and piglets at 3, 6, 12, and 24 h after HI. Maximal, random digestion of DNA occurs between 3 and 12 h recovery. At 24 h, most of the DNA digestion has advanced to small fragments that are not retained in agarose gels, but these DNA fragments are detectable by TUNEL in individual cells in striatal sections.

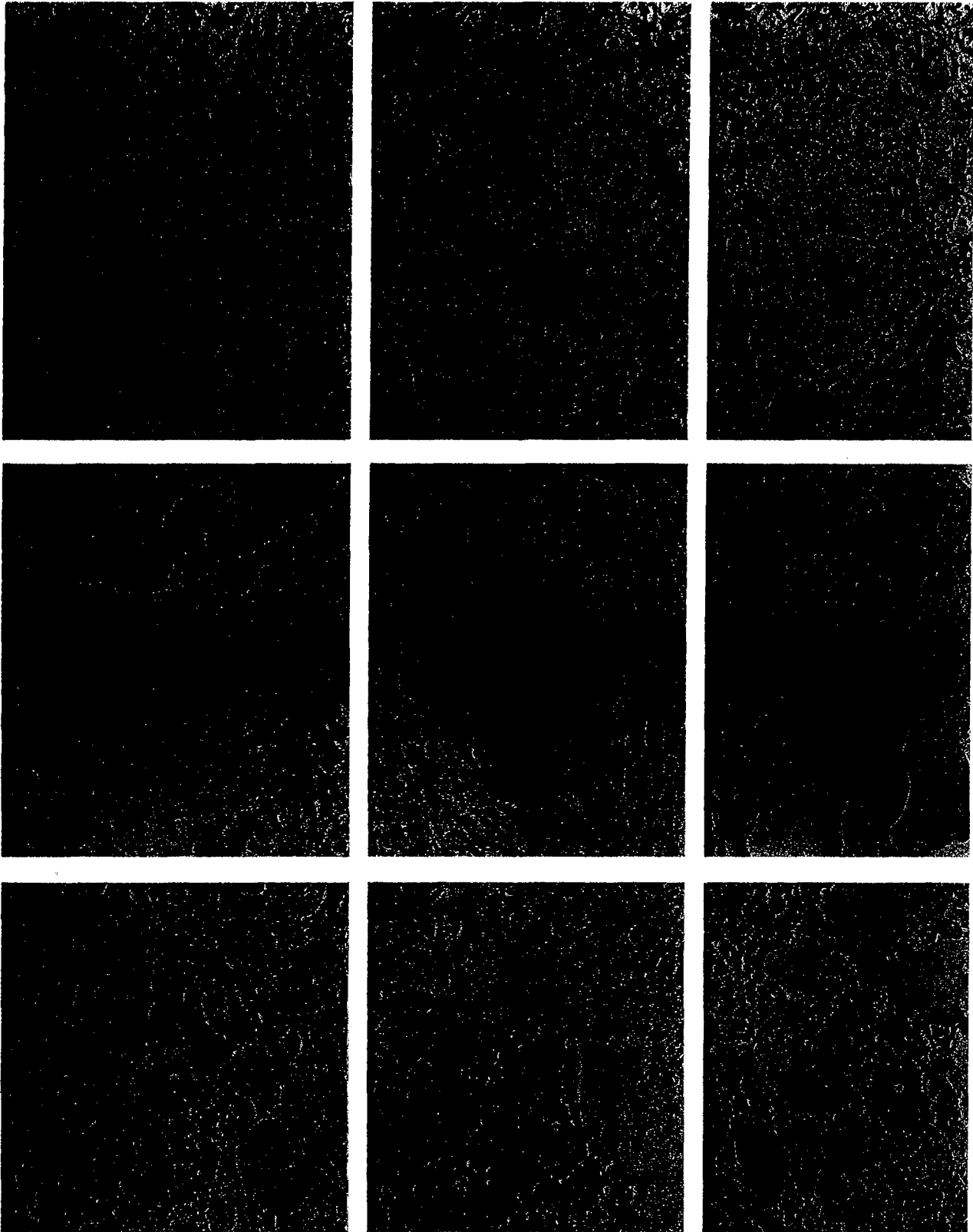
morphological criteria in H&E-stained sections (Martin *et al.*, 1997b,c). Neuronal injury was progressive, with percentage neuronal damage correlating significantly with time after HI (Table 1). In contrast, during early recovery, astroglia may be uninjured (Martin *et*

*al.*, 1997c; Natale *et al.*, 1999). At 24 h after HI, neuronal density was reduced significantly, and ~79% of remaining principal neurons within the putamen were degenerating (Table 1), consistent with our previous findings at 24 h after HI (Martin *et al.*, 1997c).

The progression of striatal neuron injury revealed by H&E staining was paralleled by the occurrence of DNA fragmentation (Fig. 1). In TUNEL preparations counterstained with cresyl violet, nuclear DNA fragmentation in striatal neurons was progressive over 3–24 h after HI (Fig. 1A). During this time course, the majority of TUNEL-positivity was associated with neurons, because most glial cell death in striatum occurs after 24 h in this model, and the DNA condensation patterns in neurons and glia are distinct morphologically (Martin *et al.*, 1997c). By gel electrophoresis, the pattern of fragmentation in genomic DNA extracts of the striatum of HI piglets was consistent with cellular necrosis, with prominent random digestion of DNA occurring at 6 and 12 h after HI (Fig. 1B).

#### **The Ultrastructure of Striatal Neuron Death after HI Is Necrosis**

The structural progression of principal striatal neuron death in 1-week-old HI piglets was determined by EM (Figs. 2 and 3). The degeneration of these neurons was not apoptosis or a hybrid form of apoptosis and necrosis, based on previously established criteria for neuronal death (Portera-Cailliau *et al.*, 1997a,b; Al-Abdulla *et al.*, 1998; Al-Abdulla and Martin, 1998; Martin *et al.*, 1998a, 1999, 2000). Striatal neuron degeneration in newborn piglet brain during the first 24 h after HI is necrosis (Figs. 2 and 3). Both the cytoplasm and the nucleus undergo ultrastructural changes typical of cellular necrosis, with the main features being swelling of the cell body, swelling and degeneration of organelles, extensive cytoplasmic vacuolation, irregular clumping of chromatin and nuclear membrane disintegration, destruction of plasma membrane integrity, and eventual dissolution of the cell (Fig. 2). By 3 h reperfusion, the cell body of striatal neurons swells and many vacuoles are formed in the cytoplasm (Fig. 2B). Morphometric analysis showed that the volume of striatal neuron cell bodies (cytoplasm and nucleus) was  $1265.7 \pm 98.9 \mu\text{m}^3$  (mean  $\pm$  SEM) in control piglets, while, at 3 h after HI, striatal neuron cell body volume was  $1716.4 \pm 129.9 \mu\text{m}^3$  (corresponding to a significant 36% increase in cell body volume). In contrast, the volume of striatal neuron nuclei was  $527.6 \pm 37.6 \mu\text{m}^3$  (mean  $\pm$  SEM) in control piglets, and, at 3 h after HI, striatal neuron nuclear volume was  $388.2 \pm$



52.8  $\mu\text{m}^3$  (corresponding to a significant 26% decrease in nuclear volume). These measurements demonstrate that the cell body swelling is due the cytoplasmic swelling. Shrinkage of the nucleus coincides with incipient condensation of the nuclear matrix at 3 h after HI (Fig. 2B). The condensation of the nuclear matrix progresses during 6–12 h (Fig. 2), consistent with the progression and pattern of DNA fragmentation (Fig. 1). By 6 h, the rough ER dilates severely (Fig. 2C). Progressive cellular condensation commences by 12 h (Figs. 2D–2F). Between 6 and 12 h, the neurons become dark (osmophilic) and assume an angular shape, and the nucleus becomes pyknotic and forms irregularly shaped clumps of chromatin that are distributed throughout the nucleus with a darkened matrix. While nuclear pyknosis and chromatin condensation into irregular clumps is observed in these dying neurons, this pattern was very dissimilar to that found in neuronal apoptosis (Portera-Cailliau *et al.*, 1997a,b; Al-Abdulla *et al.*, 1998; Martin *et al.*, 1998a, 1999, 2000). During this process, the nucleolus remains obvious (Fig. 2, asterisks), this feature is distinct from the early disassembly of the nucleolus in apoptosis (Martin *et al.*, 1998a). Subsequently, the condensed cell body and nucleus disintegrate between 12 and 24 h, as cellular debris is dispersed into the extracellular compartment (Figs. 2F and 2G), consistent with the loss of neuronal density observed at 24 h (Table 1) and severe tissue inflammation thereafter (Martin *et al.*, 1997c).

Striatal neuron necrosis after HI evolves as a sequence of organelle abnormalities (Fig. 3), similar to the sequence found with NMDA receptor-mediated excitotoxic neuronal necrosis (Portera-Cailliau *et al.*, 1997a). By 3 h and progressing through 12 h after HI, neurons accumulate many, clear, round, membrane-bound vacuoles (Figs. 3B–3E) that may be derived

from vesiculation of the Golgi apparatus (Donaldson *et al.*, 1990; Pavelka and Ellinger, 1993) or from increased formation of plasma membrane-derived endosomes (Simons and Zerial, 1993). By 6 h, the ER dilates severely, resulting in the formation of large cisterns, and the potential space between the apposing membranes of the nuclear envelope also dilates due to its continuity with the ER (Fig. 3C). ER swelling is associated with release of ER-bound ribosomes, and disaggregation of cytoplasmic polyribosomes to form monosomes. Between 6 and 12 h after HI, the ER collapses and becomes fragmented, and the nuclear membrane becomes discontinuous (Figs. 3C and 3D). ER collapse and fragmentation, ribosome release, and polysomal disaggregation coincide with the homogenization and darkening of the cytoplasmic matrix. During the first 12 h after HI, mitochondria appear to accumulate within the cell bodies of striatal neurons, and most mitochondria remain intact until about 6–12 h (Figs. 3B–3D), and then they swell and vacuolate and undergo cristaeolysis. At the time when most mitochondria show ultrastructural damage (i.e., at 12–24 h after HI), the plasma membrane ruptures and the condensed cytoplasm and fragmented nucleus are dispersed into the neuropil (Figs. 3F–3I).

#### Damage to the Golgi Apparatus and ER Occur Early after HI

We performed immunoblot and immunocytochemical experiments with specific organelle protein antibodies to identify the subcellular origin of the numerous vacuoles that accumulate in striatal neurons after HI and to identify possible molecular correlates of the structural abnormalities in organelles found by EM. To determine whether the Golgi apparatus or plasma

**FIG. 2.** EM analysis of striatal neuron degeneration in HI piglets. A normal principal striatal neuron from control piglet (A) is shown for comparison with neurons from piglets at 3, 6, 12, and 24 h after HI (B–I) arranged in a temporal sequence to show the predominant ultrastructural evolution of ischemic neuron necrosis. This neuronal death is not completely synchronized, because dying neurons can be found at different stages of degeneration at most times after HI; however, the neuronal profiles shown for each time represent the predominant stage of degeneration. Asterisks identify the nucleolus (when present in the plane of section). By 3 h after HI (B), the neuronal cell body swells (see text for measurements) and numerous, clear vacuoles are formed within the cytoplasm, increasing progressively over 9–12 h (C–E). At 6 h after HI (C), the arrays of rough ER are severely dilated (D, E) and then become fragmented, and the mitochondria become dark and condensed, as the cytoplasmic matrix becomes progressively dark and homogeneously granular. The overall contour of the cell changes from a round shape (A–C) to a fusiform or angular shape (D, E), as the neurons become shrunken 6–12 h after HI (F). Concurrently, during the first 12 h after HI, the nucleus shrinks (see text for measurements at 3 h) and the nuclear matrix progressively becomes uniformly dark (C–E) as numerous small, irregular clumps of chromatin are formed throughout the condensing nucleus (F). The nucleolus (asterisks) still remains prominent throughout this process (B–D), even until ultimate neuronal disintegration (G–I). Between 12 and 24 h, injured cells disintegrate as the dark, severely vacuolated cytoplasm, containing few discernible but very swollen mitochondria, undergoes dissolution, while the nucleus progressively forms more chromatin clumps and undergoes karyolysis (G–I). The cytoplasmic and nuclear debris is liberated into the surrounding neuropil (I). This neurodegeneration is structurally necrotic. Scale bar (A), 1.3  $\mu\text{m}$  (same for B–I).

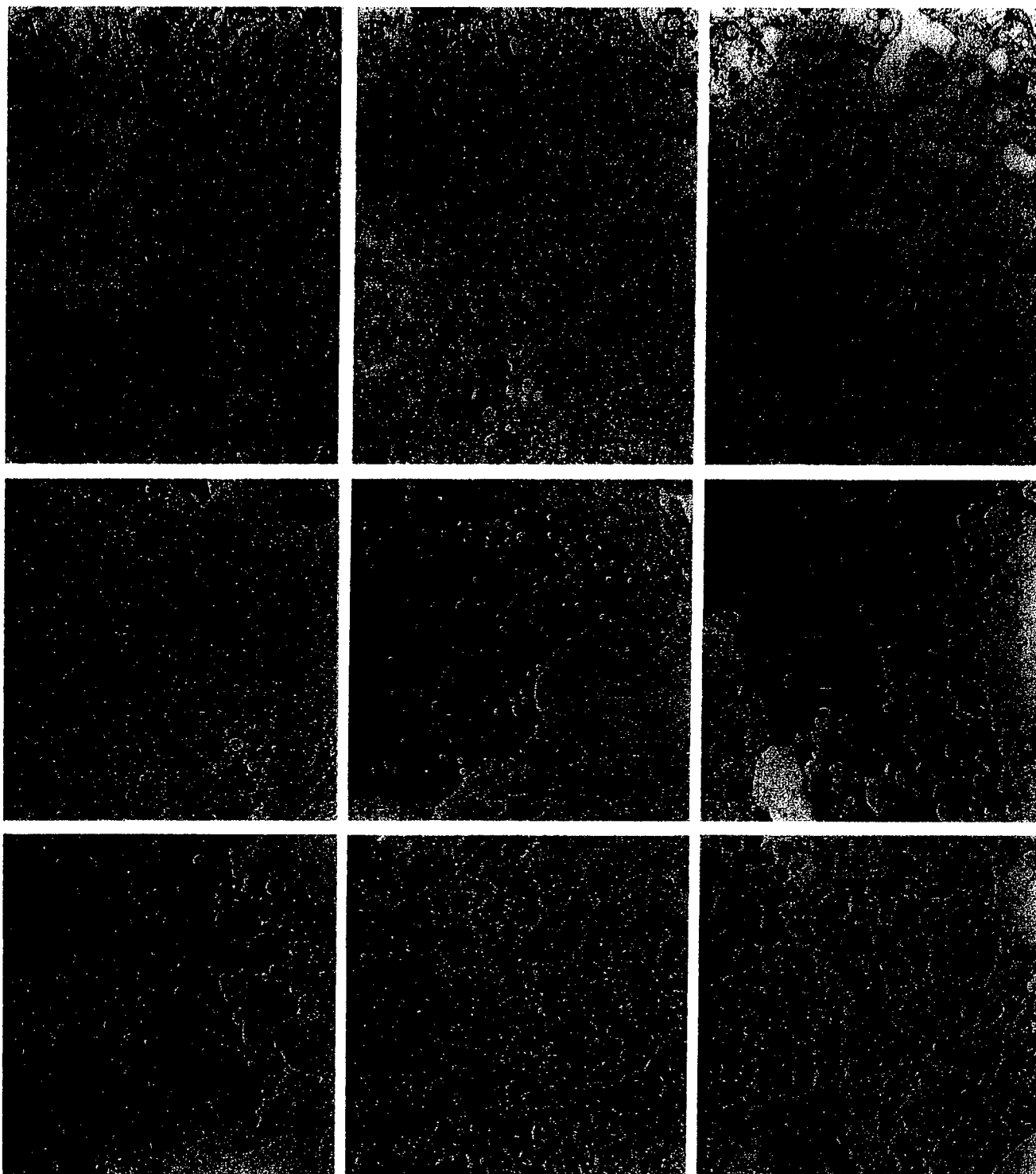


**FIG. 3.** Death of striatal neurons after HI progresses as a sequence of organelle abnormalities. (A) In control piglet, normal, principal, striatal neurons have abundant polyribosomes distributed throughout the cytoplasmic matrix, intact arrays of rough ER (rer) and Golgi stacks (g) and uniformly shaped mitochondria (m) with intact cristae. The nucleus (Nu) has a predominantly pale matrix and is surrounded by a continuous, bilaminar nuclear membrane (arrow). (B) By 3 h after HI, many clear vacuoles (asterisks) appear to be derived from swelling and vesiculation of the Golgi apparatus. The rough ER appears relatively normal, and the mitochondria are intact structurally but appear condensed. (C–E) By 6 h after HI, numerous vacuoles accumulate (asterisks) as the surrounding cytoplasmic matrix becomes progressively granular and dark. The rough ER becomes severely dilated, and ribosomes become unbound from the rough ER membrane. Polyribosomes disaggregate into

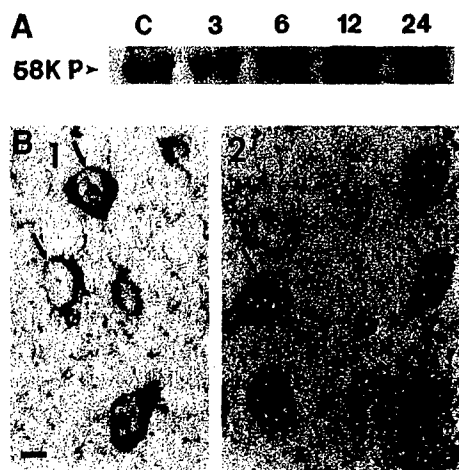


FIG. 4. The Golgi apparatus fragments early after HI. (A) Immunoblot analysis of the Golgi membrane protein (58K P) in subcellular membrane fractions of striatum from control (c) and HI piglets at 3, 6, 12, and 24 h postinsult. The levels of 58K protein are maintained until 24 h after HI. (B) Immunolocalization of Golgi 58K protein (black immunoperoxidase staining) shows the normal perinuclear location of the Golgi apparatus in control striatal neurons (1, arrows) and the prominent fragmentation of the Golgi apparatus and formation of vesicles in striatal neurons by 6 h after HI (2, arrows). Scale bar (B1, same for 2), 10  $\mu$ m.

membrane endosomes are sources of the cytoplasmic vacuoles, antibodies to Golgi 58K protein and Rab5A were used. Golgi 58K protein levels in striatum remained unchanged ( $P < 0.05$ ) until 24 h after HI (Fig. 4A), at which time levels were reduced significantly ( $P < 0.05$ ) to ~50% of control, consistent with loss of striatal neurons (Table 1). However, despite maintained levels of protein at 3–12 h after HI, immunolocalization of Golgi 58K protein revealed that the Golgi apparatus in striatal neurons is dispersed and fragmented early after HI (Fig. 4B). In contrast, intracellular Rab5A immunoreactivity was lost in striatal neurons early after HI, while Rab5A immunoreactivity increased markedly in nonneuronal cells that ap-

peared to be microglia (Fig. 5). Therefore, the numerous vacuoles that accumulate within striatal neurons early after HI are likely to be derived from the Golgi apparatus rather than from the plasma membrane.

EM revealed that the ER undergoes massive swelling prior to its fragmentation (Figs. 2 and 3). We used antibodies to ER resident, KDEL sequence-containing proteins to track the progression of damage to the ER. In soluble protein fractions of control piglet striatum, protein disulfide isomerase (PDI), a luminal ER-resident ~57 kDa protein (Munro and Pelham, 1987; Jiang *et al.*, 1999), is undetectable or at very low levels (Fig. 6A). In contrast, as early as 3 h after HI, PDI levels in soluble protein fractions are detected at high levels compared to control piglet striatum (Fig. 6A). PDI levels remain high through 12 h after HI and then levels begin to dissipate by 24 h, consistent with the conclusion that active neuronal necrosis has tapered-off by 24 h. Immunolocalization of KDEL-proteins showed faint cytoplasmic labeling of striatal neurons in controls (Fig. 6B, 1); in contrast, the cytoplasm of striatal neurons was intensely immunoreactive at 6 and 12 h after HI (Fig. 6B, 2, 3). These results are consistent with the EM observations of ER dilatation and fragmentation at 6–12 h after HI, and they suggest that these structural changes are associated with ER membrane damage and release of ER resident proteins into the cytosol or increased accessibility of antibodies to KDEL proteins within ER fragments.

#### **Striatal Mitochondria after HI Show Early Functional Suppression Followed by Transient Activation and Then Failure**

EM showed that at 3 h after HI most mitochondria appear structurally intact, but at 6 h a subset of mitochondria swells and lyses while others appear to remain intact, and at 12 h most mitochondria are swollen and lytic (Figs. 2 and 3). Biochemical assay of COX in mitochondrial-enriched organelle fractions of piglet

monosomes, and these free ribosomes are dispersed in the cytoplasm causing the matrix to become granular. Most mitochondria appear condensed but a subset is very swollen and exhibits cristaeolysis. The nucleoplasmic matrix progressively becomes darker and the chromatin undergoes condensation into small clumps of various sizes (asterisks, D, E), while the nuclear membrane (solid black arrow) becomes less discernible and is breached in some locations (C and D, open arrows). (F) At 12 h after HI, the cytoplasmic matrix is homogeneously dark and most organelles are no longer discernible, except for swollen and degenerating mitochondria. Numerous vacuoles containing membranous debris are formed in the cytoplasm as more mitochondria degenerate and undergo cristaeolysis. The nuclear chromatin becomes prominently aggregated into clumps of various shapes and sizes, as the surrounding nucleoplasmic matrix becomes uniformly dark and the nuclear envelope loses integrity. (G, H) At 12–24 h after HI, the dark and condensed cytoplasm, containing degenerated mitochondria, undergoes fragmentation as the plasma membrane ruptures. The nucleus, containing chromatin clumps (asterisk), is no longer surrounded by an intact nuclear membrane and undergoes karyolysis. (I) At end-stage degeneration, cytoplasmic debris and nuclear debris with chromatin clumps (asterisk) are dispersed into the surrounding neuropil. Scale bar (A), 0.5  $\mu$ m (same for B–I).

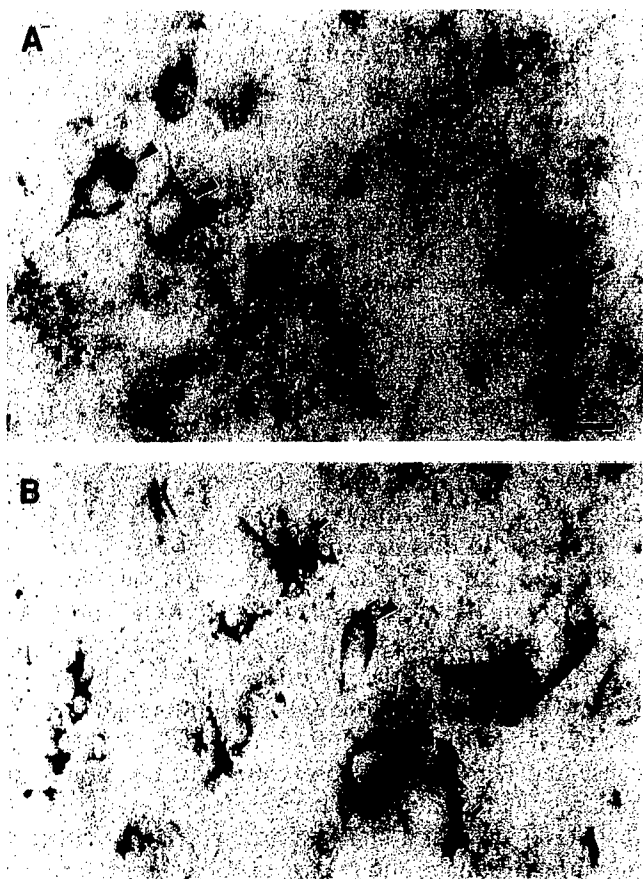


**FIG. 5.** Cell type-dependent changes in the endosomal compartment occur after HI as demonstrated by the immunolocalization of the plasma membrane early-endosome protein Rab5A. (A) In control striatal neurons (arrowheads), Rab5A-labeled endosomes fill the cytoplasm, and in some neurons (upper left arrowhead) Rab5A immunoreactivity is present as discrete particles on or near the cell surface. Nonneuronal cells and their processes in control striatum are only faintly immunoreactive for Rab5A. Scale bar, 8  $\mu$ m (same for B). (B) At 6 h after HI, endosomal labeling of striatal neurons is markedly deficient (arrowhead), and cells that appear to be microglia are intensely immunoreactive for Rab5A (open arrows).

striatum revealed time-dependent functional changes. Activity was 37, 163, 72, and 81% of control at 3, 6, 12, and 24 h, respectively (Fig. 7A). COX subunit I levels were measured by immunoblotting in these same subcellular fractions. Piglet COX subunit I was detected as two major bands, corresponding to an ~40 kDa monomer and a multimeric high molecular mass aggregate, consistent with the migration pattern of purified bovine COX (Fig. 7B). These forms of COX change differentially after HI. At 3 h, COX subunit I immunoreactivity (both monomeric and aggregated forms) was reduced markedly (Fig. 7B). The levels of the COX subunit I monomer returned to control

amounts at 6 h and then were decreased at 12 and 24 h (Fig. 7B). In contrast, levels of the aggregated form of COX subunit I were increased at 6–24 h after HI compared to control (Fig. 7B). To visualize mitochondria in piglet brain sections, COX subunit I antibodies were used for immunocytochemistry. Immunolocalization of COX subunit I in control striatum showed a finely particulate distribution within the neuropil (Fig. 7C, 1), consistent with a mitochondrial localization in cellular processes. After HI, the finely particulate COX subunit I immunoreactivity dissipated in the neuropil and many larger, swollen particles were formed (Fig. 7C, 2, 3). In addition, COX subunit I immunoreactivity

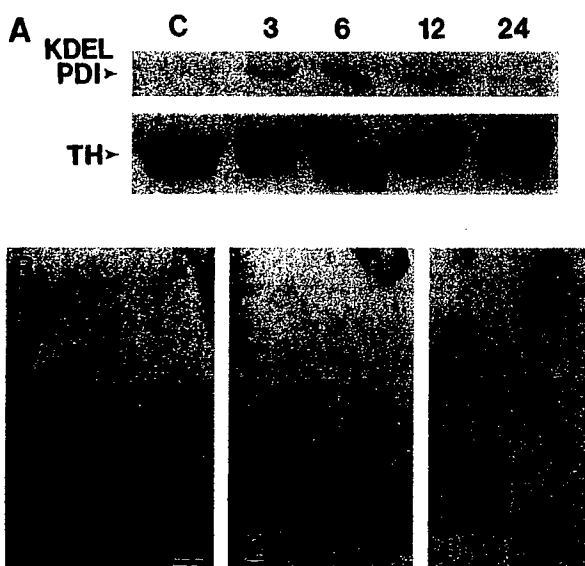


**FIG. 6.** The ER is damaged early after HI. (A) Immunoblot analysis of the KDEL sequence-containing ER luminal protein, protein disulfide isomerase (PDI), in nondetergent solubilized cytosolic fractions of striatum from control (c) and HI piglets at 3, 6, 12, and 24 h postinsult. In control striatum, PDI levels are undetectable because it is retained with the luminal compartment of the ER. At 3, 6, and 12 h after HI, PDI levels are markedly elevated in the soluble compartment compared to control, but by 24 h PDI levels are dissipating. Blots were reprobated with antibody to tyrosine hydroxylase (TH) as a protein loading control. (B) In control striatal neurons, immunolocalization of KDEL proteins (gray immunoperoxidase staining) shows diffuse cytoplasmic labeling consistent with specific ER localization (1, arrows). Scale bar (B1, same for 2 and 3), 10  $\mu$ m. At 3 h after HI, the cytoplasmic immunoreactivity (black immunoperoxidase labeling) for KDEL proteins is increased in striatal neurons (2, arrows) with the most intense staining occurring peripherally in the cell body, consistent with the ER redistribution seen by EM (compare with Fig. 2B). At 12 h after HI, immunoreactivity for KDEL proteins is enriched highly in striatal neurons with shrunken and angular morphologies (arrows) at a time when the ER undergoes fragmentation as shown by EM (compare with Figs. 2 and 3).



accumulated transiently (notably at 6 h) in neuronal cell bodies, with some of this immunoreactivity appearing to delineate swollen mitochondria (Fig. 7C, 2, 3), consistent with the EM findings (compare Figs. 3D and 3E with Fig. 7C, 2, 3). To examine COX activity with greater spatial resolution in piglet brain sections, COX activity was assayed with a histochemical method, and reaction product was quantified by densitometry. These results generally paralleled the data obtained by biochemical assay and were most notable because histochemical activity for COX in putamen was increased at 6 h (Fig. 7D), consistent with the biochemical assay for COX (Fig. 7A).

### **Cytochrome c Is Depleted in Striatum after HI**

The EM showed progressive structural damage to mitochondria, and the COX assays showed a temporal profile of mitochondrial suppression (at 3 h), activation (at 6 h), and then suppression (after 6 h) during striatal neuron necrosis. Therefore, we measured cytochrome c levels in piglet striatum as another marker for mitochondrial damage and metabolic impairment. Scant information is known about cytochrome c in pig brain. Under our assay conditions, we could detect amounts of cytochrome c as low as 500 pg (Fig. 8A). Procine brain cytochrome c migrated as a monomer of ~12 kDa and as dimers and multimers, similar to purified horse heart cytochrome c (Fig. 8A). Piglet brain cytochrome c was measured in the range of 5 ng, corresponding to ~0.05% of total soluble protein (Fig. 8A). Cytochrome c levels were normal at 3 h after HI, but by 6 h after HI and thereafter, cytochrome c was reduced to ~55% of control (Fig. 8B).

### **Lysosomal Membrane Integrity in Striatum Is Compromised by 6 h after HI**

To understand some of the possible mechanisms for striatal neuron necrosis after HI, acid phosphatase activity was measured in soluble protein fractions (unexposed to detergent solubilization) of control and HI piglets (Table 2). This biochemical assay serves as an index of lysosomal membrane damage and destabilization and release of hydrolytic enzymes into the cytosol (Frederiks and Marx, 1989; van Noorden, 1991). In the presence of sodium fluoride (10 mM), acid phosphatase activity was inhibited ~95% (data not shown). Acid phosphatase activity was increased significantly above control levels at 6, 12, and 24 h after

HI (Table 2), demonstrating that damage to lysosomal membranes in striatum occurs between 3 and 6 h after HI.

### **Glutathione Levels in Striatum Are Depleted by 3 h after HI**

A potent stimulus for cellular necrosis is oxidative stress (McCord, 1985). GSH functions in antioxidant mechanisms as a free radical scavenger, and the levels of GSH are often used as an index of oxygen radical production (Mizui *et al.*, 1992). Therefore, we measured GSH levels in piglet striatum after HI (Table 3). GSH in soluble protein fractions was significantly reduced to ~80% of control at 3 and 6 h after HI but returned to control levels by 12 h after HI (Table 3), demonstrating that oxidative stress occurs early (by 3 h) after HI newborn in piglets, but that this stress in the form of glutathione depletion is transient.

### **Peroxynitrite Damage to Striatal Membrane Proteins Occurs after HI**

To determine if HI produces oxidative damage, striatal membrane fractions were immunoblotted for nitrotyrosine-modified proteins as a marker for peroxynitrite-mediated oxidative damage (Fig. 9A). An intensely reacting band of proteins at ~50 kDa showed nitration in control striatum. The nitrotyrosine-modification of this ~50-kDa protein was increased at 6 h after HI. Immunoprecipitation experiments demonstrated that this nitrotyrosine-modified, ~50-kDa protein is tubulin and that tubulin nitration is markedly increased by 6 h after HI (Fig. 9B). Another prominent band of nitrotyrosine immunoreactivity was detected at ~68–70 kDa (Fig. 9A), probably corresponding to nitration of the low molecular weight neurofilament (Strong *et al.*, 1998). This ~68- to 70-kDa protein band showed nitrotyrosine modification above control at 3, 6, 12, and 24 after HI, with maximal nitration occurring at 6 h (Fig. 9A). To identify directly that neurons in the striatum sustain peroxynitrite-mediated oxidative damage after HI, brain sections from perfusion-fixed piglets were reacted with nitrotyrosine antibodies. In control piglet striatum, nitrotyrosine immunoreactivity was not detectable by immunocytochemistry (Fig. 9C, 1). Early after HI, striatal neurons showed intense nitrotyrosine immunoreactivity (Fig. 9C, 2, 3). In many putaminal neurons at 3 and 6 h after HI, nitrotyrosine immunoreactivity was lo-

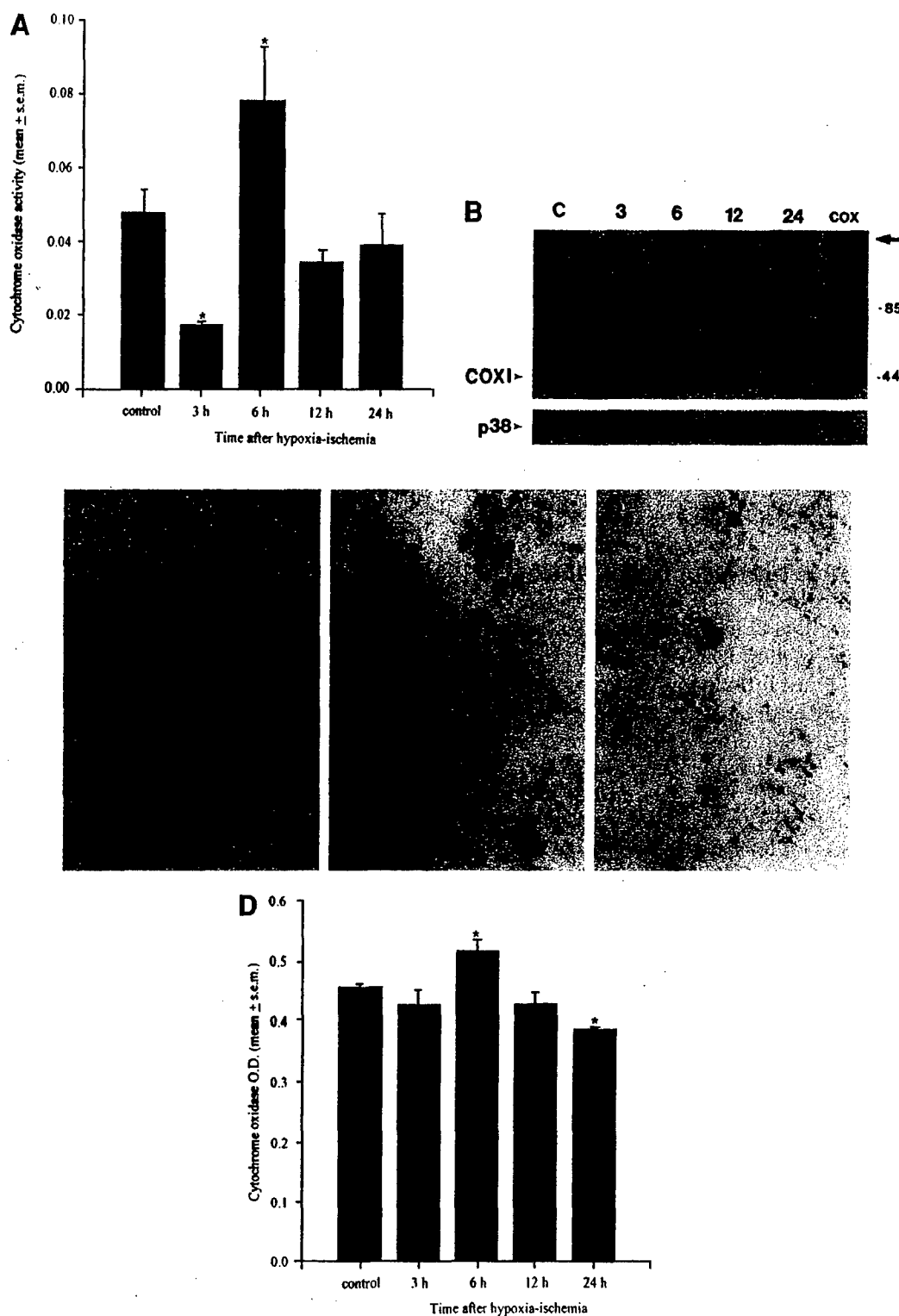


**FIG. 7.** Mitochondria undergo functional, molecular, and structural abnormalities in HI piglet striatum. (A) In mitochondrial-enriched subcellular fractions of control and HI piglet striatum ( $n = 2-3$  per group), biochemical assay for COX activity shows a transient suppression of mitochondrial function at 3 h after HI, followed by a large burst of activity at 6 h recovery, and then reduced mitochondrial function thereafter. Asterisk indicates significant difference ( $P < 0.05$ ) from control. (B) Immunoblot analysis of COX subunit I in mitochondrial-enriched fractions of striatum from control (c) and HI piglets at 3, 6, 12, and 24 h postinsult ( $n = 2-3$  per group). Purified bovine COX (right

calized at a perinuclear location (Fig. 9C, 2), and at 12 h after HI this immunoreactivity was dispersed throughout the cytoplasm as small packets in subsets of neurons (Fig. 9C, 3). This localization of nitrotyrosine immunoreactivity was very reminiscent of the vesiculation and fragmentation of the Golgi apparatus observed by EM (Figs. 2 and 3) and light microscopy (Fig. 4B). To identify if Golgi apparatus-associated proteins are damaged by peroxynitrite radicals, we examined the possible colocalization of Golgi 58K protein and nitrotyrosine immunoreactivities by immunofluorescence. Striatal neurons in HI piglets showed precise colocalization of nitrotyrosine and Golgi 58K protein immunoreactivities (Fig. 10). These results demonstrate that peroxynitrite-mediated oxidative damage to membrane proteins occurs in the piglet striatum early after HI and that proteins associated with the Golgi apparatus are targets of peroxynitrite radicals.

#### **Hydroxyl Radical Damage to DNA and RNA Occurs in Striatal Neurons after HI**

To identify other possible forms of oxidative stress and other macromolecular targets of oxidative stress during the progression of neuronal necrosis after HI, we determined if nucleic acids are damaged by hydroxyl radicals using monoclonal antibodies that react with hydroxydeoxyguanosine (OHdG) and hydroxyguanosine (OHG) (Fig. 11). The characterization of these antibodies has been shown previously (Al-Abdulla and Martin, 1998; Martin *et al.*, 1999). These antibodies also weakly react with normal guanosine (Martin *et al.*, 1999), consistent with the faint cytoplasmic labeling suggestive of an RNA pattern in striatal neurons of control piglets (Fig. 11A). However, the pattern and intensity of immunoreactivity for OHG and OHdG was very different in piglet striatum after HI (Figs. 11B–11E). The intensity of immunoreactivity

in the cytoplasm of neurons and in the neuropil was much greater in striatum at 3 and 6 h after HI compared to controls. In addition, intense nuclear labeling occurred only in striatal neurons in HI piglets (Figs. 11C and 11D). Nonneuronal cells such as vascular endothelial cells also exhibited oxidative damage to DNA after HI (Fig. 11D). Digestion of RNA in brain sections with DNase-free RNase eliminated the cytoplasmic labeling of neurons and the neuropil labeling in HI piglet striatum, revealing the prominent nuclear immunoreactivity (Fig. 11D). Digestion of DNA with DNase diminished the nuclear labeling of striatal neurons in HI piglets (Fig. 11E). PreadSORption of OHdG antibodies with OHdG or OHG prior to the immunocytochemistry selectively competed the labeling in the different cellular compartments (data not shown), similar to experiments shown previously (Al-Abdulla and Martin, 1998; Martin *et al.*, 1999). These results demonstrate that both RNA and DNA undergo prominent hydroxyl radical damage early after HI.

#### **DISCUSSION**

We studied striatal neurodegeneration in a newborn animal model of HI that causes brain damage very similar to the pattern of injury found in human newborns that have experienced HI (Martin *et al.*, 1997a,b,c; Johnston, 1998). The clinical and neuropathological features of our piglet model are very different from those of the more commonly used newborn rat models (Martin *et al.*, 1997a; Brambrink *et al.*, 1999). Using this model, we tested the hypothesis that striatal neuron death is necrosis and evolves with oxidative stress and selective damage to organelles. The early neurodegeneration in newborn piglet striatum after HI is cellular necrosis and evolves rapidly through mechanisms associated with oxidative stress. A major strength of this study is that it consolidates in

lane) was used as a positive control. Molecular mass standards (in kDa) are indicated at right. Arrow identifies high molecular mass (> 200 kDa) multimeric complexes containing COX subunit I. Blots were reprobbed with antibody to synaptophysin (p38) as a protein loading control. (C) Immunolocalization of mitochondria using antibody to COX subunit I. In control putamen (C1), mitochondria (grey immunoperoxidase staining) are localized as fine particles distributed diffusely throughout the neuropil without intense cytoplasmic labeling of striatal neuron cell bodies. Scale bar (C1, same for 2 and 3), 8  $\mu$ m. At 6 h after HI, mitochondria accumulate within the cell bodies of striatal neurons (2, broad black arrowheads), as demonstrated by the cytoplasmic immunoreactivity (black immunoperoxidase labeling) for COX subunit I, while the neuropil immunoreactivity dissipates. Subsets of mitochondria within cellular processes in the neuropil (2, open arrows) and in neuronal cell bodies (2, broad black arrowheads) are dilated, consistent with the mitochondrial swelling seen by EM (compare with Fig. 3). At 12 h after HI, immunoreactivity for COX subunit I is reduced throughout the neuropil of putamen and many of the remaining mitochondria are swollen (3, open arrows), consistent with the disintegration of mitochondria found by EM. (D) Densitometric histochemical assay for COX enzyme activity in control and HI piglet putamen also revealed a transient elevation in mitochondrial function at 6 h recovery. Asterisks indicate significant difference ( $P < 0.05$ ) from control followed by a loss of function at 24 h.

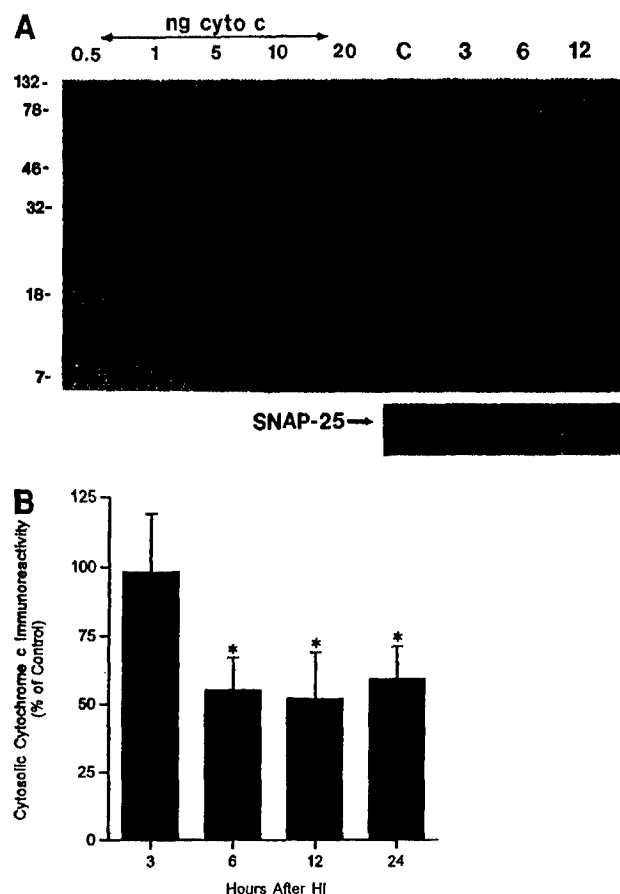


**FIG. 8.** Characterization of cytochrome c in pig brain and changes after HI: cytochrome c is depleted during striatal neuron necrosis. (A) Cytochrome c in piglet brain extracts was evaluated by immunoblotting and was compared to purified horse heart cytochrome c as a standard. Lanes were loaded with varying amounts of purified cytochrome c (0.5, 1, 5, 10, or 20 ng) or with 10 µg total soluble protein from striatal extracts of control (C) and HI (3, 6, or 12 h recovery) piglets. Molecular weight standards (in kDa) are shown at left. Purified cytochrome c monomer is detected at a molecular mass of ~12 kDa. The upper bands in the cytochrome c lanes are due to dimers or multimers of cytochrome c. Immunoreactive bands with similar mobilities are detected in piglet brain extracts. Blots were reprobed with synapse-associated protein-25 (SNAP-25) as a loading control for piglet extracts. (B) Densitometric analysis of cytochrome c protein levels in soluble fractions of striatum from piglets recovered for 3, 6, 12, or 24 h after HI. Cytochrome c immunodensity (2–3 piglets per group) was corrected for nerve terminal marker immunodensity in the same sample, then expressed as percentage control. Values are mean  $\pm$  SEM. Asterisk indicates significant difference ( $P < 0.05$ ) from control and 3 h after HI.

one set of experiments several observations previously reported as isolated fragments in less comprehensive papers. Furthermore, this study clarifies the controversial contributions of neuronal necrosis versus apoptosis to striatal degeneration after HI in newborns,

**TABLE 2**

Lysosomal Destabilization in Striatum after HI

Time after HI	Acid phosphatase activity (Percentage of control) <sup>a</sup>
3 h	119.7 $\pm$ 20.5
6 h	143.7 $\pm$ 16.1 <sup>b</sup>
12 h	149.7 $\pm$ 15.9 <sup>b</sup>
24 h	181.0 $\pm$ 5.2 <sup>b</sup>

<sup>a</sup> See methods for assay. All values are mean  $\pm$  SEM.

<sup>b</sup> Significantly different ( $P < 0.05$ ) from control.

notably by demonstrating in piglets that neuronal apoptosis does not have a major contribution to this degeneration during the first 24 h after the hypoxic-asphyxic cardiac arrest. Apoptosis of neurons and neuroglia may, however, have a more prominent contribution to the neuropathology after HI in newborns as a form of delayed or secondary cell death that is related to target deprivation of interconnected brain regions (Martin et al., 1997b, 1998a).

### Neuronal Death in Striatum Begins Rapidly after HI and Is Necrosis

Striatal neuron degeneration begins before 3 h after HI and is progressive during the first 24 h after the insult. This degeneration is necrosis. Specific organelles are not targeted selectively. The nucleus, Golgi apparatus, ER, lysosomes, mitochondria, and cytoskeleton are all damaged. Proteins and nucleic acids (both RNA and DNA) are damaged by ROS. Protein constituents of the Golgi apparatus and/or Golgi complex-associated proteins (e.g., cytoskeletal proteins) are direct targets of peroxynitrite radicals. Thus, the damage is indiscriminate at the subcellular level and is consistent with acute oxidative stress. This

**TABLE 3**

Glutathione Levels in Striatum after HI

Time after HI	Glutathione level (percentage of control) <sup>a</sup>
3 h	81.3 $\pm$ 1.7 <sup>b</sup>
6 h	80.7 $\pm$ 0.6 <sup>b</sup>
12 h	91.0 $\pm$ 3.7
24 h	95.0 $\pm$ 2.5

<sup>a</sup> See methods for assay. All values are mean  $\pm$  SEM.

<sup>b</sup> Significantly different ( $P < 0.05$ ) from control.

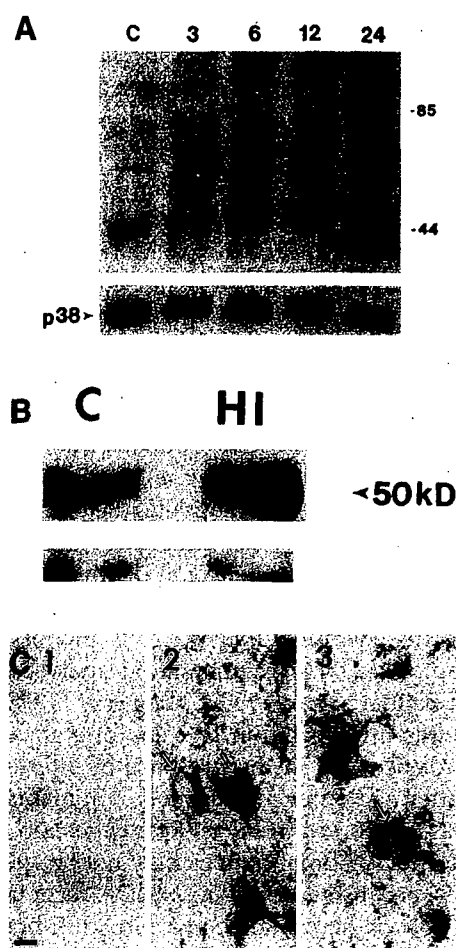


**FIG. 9.** Peroxynitrite-mediated oxidative damage to proteins occurs early after HI. (A) Immunoblot of nitrotyrosine-modified membrane proteins in striatum from control (c) and ischemic piglets at 3, 6, 12, and 24 h after HI. Molecular mass markers (in kDa) are indicated at right. Prominent increases in nitration after HI occur in proteins at ~50 and ~68 kDa. Blots were reprobed with antibody to synaptophysin (p38) as a protein loading control. (B) Immunoprecipitation demonstrated that tubulin (with a molecular mass of ~50 kDa) is a nitrated protein in control striatum (c). After HI, nitrotyrosine modification of tubulin is increased in striatum at 6 h (HI). Nitrotyrosine modification of a low molecular mass fragment of tubulin or a protein that interacts with tubulin (lower panels) is unchanged after HI. (C) Immunolocalization of nitrated proteins in striatal neurons after HI. In control striatum (C1), nitrotyrosine immunoreactivity is not detectable, but, at 6 (2) and 12 h (3) after HI, striatal neurons (open arrows) are intensely immunoreactive for nitrotyrosine. At 6 h after HI many neurons have a perinuclear localization of nitrotyrosine immunoreactivity, while at 12 h after HI, nitrotyrosine immunoreactivity is dispersed throughout the cytoplasm of striatal neurons. This pattern is reminiscent of the structural changes in the Golgi apparatus (see Figs. 2-4). Scale bar (C1, same for 2 and 3), 8  $\mu$ m.

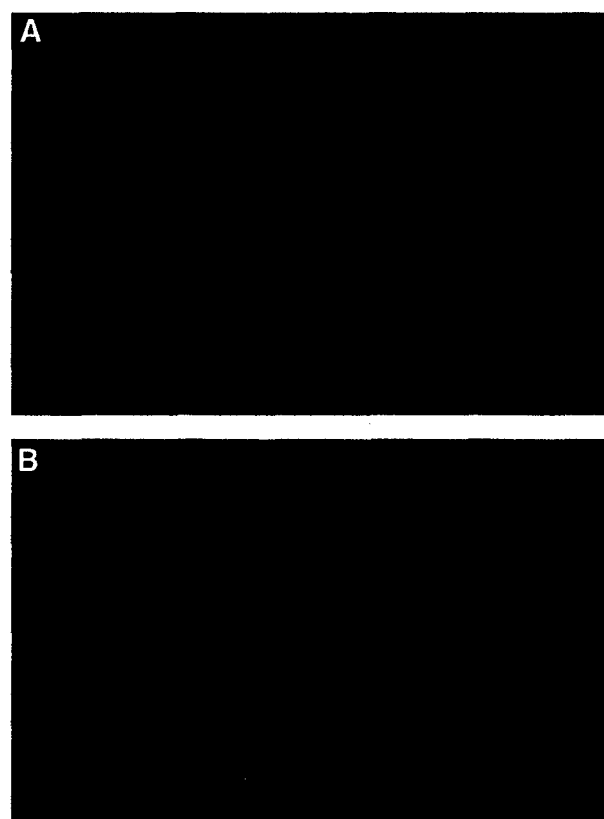
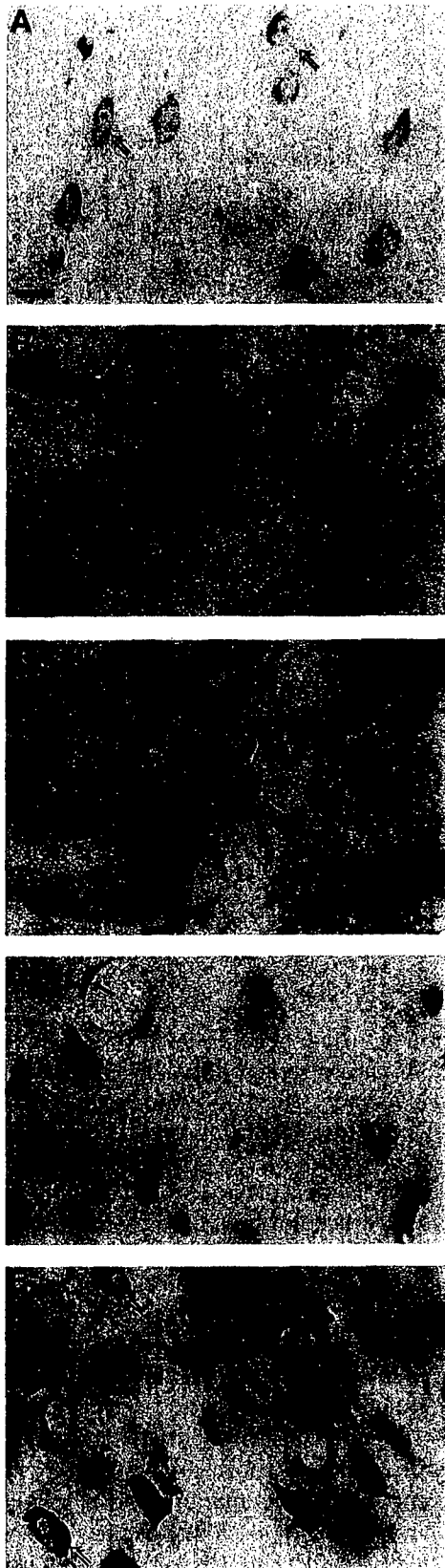


**FIG. 10.** Double-label immunofluorescence for nitrotyrosine (A, green FITC labeling) and Golgi 58K protein (B, red Texas red labeling) demonstrates that nitrotyrosine immunoreactivity (A, arrowhead) occurs at fragments of the Golgi apparatus (B, arrowhead) in striatal neurons at 6 h after HI. Scale bar in A, 4  $\mu$ m.

conclusion is further substantiated by the depletion of GSH by 3 h. This degeneration of striatal neurons after HI is very distinct structurally and biochemically from neuronal apoptosis (Martin *et al.*, 1998a). It is also distinct from non-NMDA glutamate receptor-mediated excitotoxic neuronal apoptosis, but it is very similar to NMDA receptor-mediated excitotoxic neuronal necrosis (Portera-Cailliau *et al.*, 1997a). Based on the onset of neuronal damage, the rate of progression of neuronal death, and on the widespread subcellular damage, we conclude that early neurodegeneration in striatum after HI in newborns is oxidative stress-induced cellular necrosis.

Our results demonstrating that neuronal death in the striatum of HI newborn piglets is necrosis differs from recent conclusions made by other groups using neonatal rats (Hill *et al.*, 1995; Beilharz *et al.*, 1995; Cheng *et al.*, 1998). This discrepancy regarding the occurrence of neuronal apoptosis after HI is partly due



to differences in the criteria for apoptosis, differences in the comprehensiveness of the EM analysis, and to differences in the animal species used for the experimental injury. It was reported that the ultrastructure of neuronal degeneration was apoptosis after HI in 1-week-old rat (Cheng *et al.*, 1998). However, this ultrastructure would be interpreted as necrosis by us and others (present study and Martin *et al.*, 1998a, 2000; Ishimaru *et al.*, 1999). The nuclear pyknosis with condensation of chromatin into many small, irregularly shaped clumps in ischemic neurons contrasts with the formation of few, uniformly dense and regularly shaped chromatin aggregates which occurs in neuronal apoptosis (Portera-Cailliau *et al.*, 1997a; Al-Abdulla *et al.*, 1998; Martin *et al.*, 1998a, 1999, 2000; Ishimaru *et al.*, 1999). Alternatively, the data from neonatal rats may support our concept of the apoptosis-necrosis continuum for neuronal death (Portera-Cailliau *et al.*, 1997a,b; Martin *et al.*, 1998a) in that this neuronal degeneration may be a hybrid of necrosis and apoptosis. DNA fragmentation analyses (Hill *et al.*, 1995; Beilharz *et al.*, 1995; Cheng *et al.*, 1998) would support this interpretation, in view of a structure indicative of necrosis in the presence of internucleosomal laddering. Internucleosomal fragmentation of DNA was not found in HI piglets. Digestion of DNA in an internucleosomal pattern may not be specific for apoptosis, because it occurs in NMDA receptor-mediated excitotoxic neuronal necrosis in adult brain (Portera-Cailliau *et al.*, 1997a) and in neuronal culture (Gwag *et al.*, 1997), and in cells undergoing necrosis induced by calcium ionophores and heat shock (Collins *et al.*, 1992). Moreover, *in situ* end-labeling methods for DNA fail to discriminate among apoptotic and

**FIG. 11.** Prominent hydroxyl radical damage to RNA and DNA occurs in striatal neurons after HI. (A) In control striatal neurons (open arrows) faint labeling of the cytoplasm is detected with OHdG/OHG antibodies, corresponding to RNA labeling, while the nucleus (asterisks) and the neuropil is free of immunoreactivity. Scale bar, 25  $\mu$ m (same for B-E). (B) By 6 h after HI, the cell bodies and processes of striatal neurons (open arrows) have intense cytoplasmic OHdG/OHG immunoreactivity. (C) By 12 h after HI, striatal neurons (open arrows) display intense OHdG/OHG immunoreactivity within the cytoplasm and the nucleus. (D) RNase digestion abolished the prominent cytoplasmic and neuropil labeling for OHG in striatal neurons after HI, revealing the intense nuclear labeling for OHdG (open arrows). Hydroxyl radical damage to DNA also occurs in vascular endothelial cells at 6 h after HI (solid black arrow). (E) In striatal neurons (open arrows) at 12 h after HI, DNase treatment diminished the labeling for OHdG within the nucleus (asterisk).

necrotic cell deaths (Grasl-Kraupp *et al.*, 1995; Portera-Cailliau *et al.*, 1997a; Martin *et al.*, 1998a) and can also detect DNA fragments during DNA synthesis (Lockshin and Zakeri, 1994). Additional observations demonstrating that a pan-caspase inhibitor is neuroprotective in neonatal rats after HI suggests a possible contribution of neuronal apoptosis (Cheng *et al.*, 1998) to this neuropathology; however, many caspase family members function in the proteolytic processing of proinflammatory cytokines, thus neuroprotective effects of pharmacological inhibition of all caspases may be mediated by mechanisms other than blocking apoptosis (e.g., anti-inflammation).

Furthermore, the rat pup model of neonatal HI and our newborn piglet model of HI are different from physiological, clinical, and neuropathological standpoints and are likely to exhibit different responses to injury. Rat pups and piglets (and other artiodactylous ungulates) near the day of birth are at very different stages of maturation with respect to glutamate receptors and glutamate transporters (Martin *et al.*, 1997c; Furuta *et al.*, 1997; Martin *et al.*, 1998b; Furuta and Martin, 1999; Northington *et al.*, 1998). In both pig and human, the peak of the brain growth spurt occurs near term, whereas that of rat occurs at about 7 days postnatally (Dobbing and Sands, 1979). Moreover, in pig, the percentage of adult brain weight at birth is much closer to human compared to that of rat (Dobbing and Sands, 1979). These fundamental neurobiological issues are very important when considering the relevance of experimental animals as models for brain injury in human newborns.

### **Striatal Neurons Undergo Widespread Organelle Damage after HI**

Most organelles in vulnerable neurons are damaged after ischemia. Organelles that function in protein synthesis and posttranslational modification (i.e., the ER, polysomes, and Golgi apparatus) become structurally abnormal early after ischemia and are persistently abnormal during the process of neurodegeneration (Kirino *et al.*, 1984; Petito and Pulsinelli, 1984; Rafols *et al.*, 1995). Perturbations in the ER, ribosomes, and Golgi apparatus are consistent with the finding that total protein synthesis is severely reduced by 6 h after transient global forebrain ischemia and is reduced persistently in selectively vulnerable neurons (Thilmann *et al.*, 1986; Araki *et al.*, 1990). The ER damage and release of luminal chaperone proteins found in HI piglets suggests that appropriate protein folding is also likely to be compromised. Our findings that the Golgi apparatus is structurally abnor-

mal and its protein constituents are possible targets of peroxynitrite radicals are consistent with other observations. Golgi membranes in neurons undergo lipid peroxidation after global ischemia (Rafols *et al.*, 1995). Furthermore, the finding that lysosomal membranes become destabilized in striatum after HI is consistent with results showing that lysosomal membrane stability is disrupted in liver after ischemia-reperfusion (Frederiks and Marx, 1989). Lysosomal instability and release of hydrolytic enzymes into the cytosol may propagate cellular necrosis by further damaging membranous organelles (Farber *et al.*, 1981).

Abnormalities in mitochondrial structure occur during cellular necrosis and can be produced when mitochondrial ATP synthesis fails and plasma membrane function is impaired (Laiho *et al.*, 1975). We found that mitochondrial function is suppressed at 3 h after HI, is sharply increased by 6 h reperfusion, and then mitochondrial enzymatic activity is lost. COX subunit I protein levels drop abruptly by 3 h after HI, followed by a return to baseline, and then a loss of protein is sustained. The loss of enzyme function and immunological delectability of protein at 3 h may reflect acute inactivation and epitope modification or proteolysis of mitochondrial proteins, possibly resulting from changes in intracellular pH and ionic strength, thermodynamic stability, or changes in the interactions of COX with endogenous modifiers such as ROS or other proteins (Bolli *et al.*, 1985; Wolff and Dean, 1986; Davies, 1987; Capaldi *et al.*, 1990). Mitochondrial proteins undergo oxidative inactivation by peroxynitrite. COX is a target of peroxynitrite-mediated inactivation (Bolaños *et al.*, 1995). In addition,  $H_2O_2$  production can lead to formation of hydroxyl radicals and then lipid hydroperoxides that can damage mitochondrial membranes and inhibit mitochondrial functions (Ravindranath and Reed, 1990). The transient elevation of COX activity and reappearance of protein levels at 6 h suggests that the changes found at 3 h may be reversible. The enzyme complex may renature or undergo reversed modification or reversible inhibition, or rapid synthesis (COX subunit I is made intramitochondrially) (Capaldi, 1990; Bolli *et al.*, 1995). Moreover, we found that COX subunit I protein aggregates, forming large multimeric complexes after HI. This change in COX may signify increased covalent protein-protein interactions due to sulfhydryl oxidation and perturbations in redox state and is possibly related to the depletion of GSH levels early after HI. Loss of protein thiols by oxidation can lead to abnormalities in mitochondrial protein function and mitochondrial membrane permeability (Ravindranath and Reed, 1990).

Mitochondrial failure after HI is also suspected because cytochrome c is depleted. Cytochrome c has been identified as an apoptotic protease activating factor. Its regulated release from mitochondria and interactions with other proteins participate in the mechanisms for programmed cell death (Li *et al.*, 1997). However, cytochrome c translocation and cytoplasmic accumulation alone are insufficient for neuronal apoptosis (Deshmukh and Johnson, 1998). Cytochrome c accumulation in CNS tissue soluble fractions is presumed to be a marker for neuronal apoptosis after ischemia (Fujimura *et al.*, 1998). However, in the presence of widespread structural and biochemical abnormalities in striatum after HI, release of cytochrome c from mitochondria after ischemia is unlikely to be a physiologically regulated event, nor is it likely that downstream effector mechanisms for apoptosis are operative in striatal neurons after ischemia. Indeed, we found that cytochrome c is depleted in striatal cytosolic extracts after HI. This abnormality is consistent with mitochondrial failure, impaired oxidative phosphorylation, and neuronal necrosis. Importantly, the loss of cytochrome c may contribute to the oxidative stress by mobilizing iron from heme groups during its proteolysis. Overall, these changes point toward acute mitochondrial dysfunction contributing to the pathobiology of neuronal necrosis in the newborn striatum after HI.

#### **Tubulin Is a Target of Oxidative Stress after HI in Newborn Brain**

We found that tubulin is a target of extensive tyrosine nitration after HI. Tubulin is the major cytoskeletal protein in neurons that forms the microtubule network (Brady, 1991). Microtubules serve as tracks for the movement of mitochondria and lysosomes, and they are important in establishing and maintaining the shape, structural integrity, locations, and functions of the Golgi apparatus, ER, and mitochondria (Brady, 1991). Amino acid modification of tubulin by posttranslational nitrotyrosination causes microtubule dysfunction by a nitric oxide-dependent mechanism (Eiserich *et al.*, 1999), consistent with our finding that tubulin is a target of peroxynitrite. It is possible that nitrotyrosination of tubulin and microtubule dysfunction participate in the mechanisms for the organelle abnormalities that occur in striatal neurons after HI, including dispersion of the Golgi apparatus, dilation of the ER, accumulation and swelling of mitochondria, and destabilization of lysosomes. When cells are exposed to agents that perturb microtubule assembly,

the ER network redistributes, contracts, and then collapses towards the nucleus (Lee and Chen, 1988), and the Golgi apparatus fragments into small vesicles that are dispersed throughout the cytoplasm (Donaldson *et al.*, 1990; Pavelka and Ellinger, 1993). These changes are similar to those that we have found in striatal neurons after HI. Thus, oxidative damage to tubulin and microtubule dysfunction may provide a molecular mechanism for some of the subcellular abnormalities occurring in striatal neurons after HI.

#### **Oxidative Stress Is a Mechanism for Striatal Neuron Necrosis in Newborns after HI**

We found evidence for an early loss of antioxidant capacity and oxidative damage to proteins and nucleic acids. By 3 to 6 h after HI, GSH was depleted, peroxynitrite damaged membrane proteins (specifically Golgi-associated proteins), and nitration of tubulin increased. In addition, nucleic acids were damaged by hydroxyl radicals. Peroxynitrite oxidation of nucleosides may not be a major pathway (Uppu *et al.*, 1996). A more likely pathway for nucleoside oxidation by hydroxyl radical is from the transitional metal (iron)-catalyzed, Haber-Weiss- and Fenton-type reactions that use superoxide and  $H_2O_2$  as substrates, respectively, thereby producing hydroxyl radicals (Boveris and Cadenas, 1997). Interestingly, redox-active heme and nonheme iron from cytochrome c breakdown may support hydroxyl radical formation in the cytosol and RNA oxidation.

The mitochondrial alterations that occur in dying striatal neurons after HI support our conclusion that oxidative stress participates in the mechanisms of neuronal necrosis. Mitochondria accumulated in the cell bodies of neurons by 6 h of reperfusion, and mitochondrial function was increased transiently at 6 h after reperfusion. Mitochondrial accumulation could be due to interruption of mitochondrial trafficking because of tubulin/microtubule perturbations or to dendritic attrition because dendrites are damaged early after ischemia (Kitagawa *et al.*, 1989; Yamamoto *et al.*, 1990). Alternatively, mitochondrial accumulation may be due to cell body shrinkage after the initial swelling stage during 3 h recovery. A possible consequence of this accumulation is that mitochondria are in closer proximity to each other and to the nucleus and other organelles within the perikaryon. The mitochondrial electron-transfer chain is a primary generator of superoxide and peroxide, and damaged mitochondria are believed to produce even more superoxide ion (Boveris and Cadenas, 1997). Excessive



generation of superoxide occurs in piglet brain during asphyxia-reventilation (Pourcyrus *et al.*, 1993). In addition, depletion of GSH has been shown to lead to mitochondrial swelling and lysis and then cellular necrosis (Meister, 1995), consistent with the abnormalities we observed by EM. We also found that depletion of GSH precedes mitochondrial swelling and lysis and loss of cytochrome c. Thus, mitochondrial accumulation and activation may be important mechanistically because peroxynitrite and hydroxyl radicals are highly reactive and short-lived (Boveris and Cadenas, 1997) and, therefore, need to be generated at sites near target organelles and macromolecules.

### Conclusion

In a piglet model of HI brain damage in newborns, striatal neuron necrosis evolves rapidly. It is likely that widespread oxidative damage to organelles and macromolecules is a primary mechanism for striatal neurodegeneration. Based on the observations made here with this piglet model, neuroprotection strategies for the amelioration or prevention of the acute striatal damage in HI newborns should be implemented immediately after HI, before depletion of glutathione, oxidative stress, and subcellular injury. This information is important for the management of basal ganglia damage and neurological abnormalities in HI human newborns.

### ACKNOWLEDGMENTS

This study was funded by grants from the NIH-NINDS (NS34100 and NS20020) NIH-NIA (AG16282) and the U.S. Army Medical Research and Materiel Command (DAMD17-99-1-9553).

### REFERENCES

- Al-Abdulla, N. A., Portera-Cailliau, C., & Martin, L. J. (1998) Occipital cortex ablation in adult rat causes retrograde neuronal death in the lateral geniculate nucleus that resembles apoptosis. *Neuroscience* 86, 191-209.
- Al-Abdulla, N. A., & Martin, L. J. (1998) Apoptosis of retrogradely degenerating neurons occurs in association with the accumulation of perikaryal mitochondria and oxidative damage to the nucleus. *Am. J. Pathol.* 153, 447-456.
- Araki, T., Kato, H., Inoue, T., & Kogure, K. (1990) Regional impairment of protein synthesis following brief cerebral ischemia in the gerbil. *Acta Neuropathol.* 79, 501-505.
- Beckman, J. S., Chen, J., Ischiropoulos, H., & Conger, K. A. (1992) Inhibition of nitric oxide synthesis and cerebral neuroprotection. In: *Pharmacology of Cerebral Ischemia* (J. Kriegstein and H. Oberpichler-Schwenk, Eds.), pp. 383-394. Wissenschaftliche Verlagsgesellschaft, Stuttgart.
- Beilharz, E. J., Williams, C. E., Dragunow, M., Sirimanne, E. S., & Gluckman, P. D. (1995) Mechanisms of delayed cell death following hypoxic-ischemic injury in the immature rat: Evidence for apoptosis during selective neuronal loss. *Mol. Brain Res.* 29, 1-14.
- Bloom, G. S., & Brashear, T. A. (1989) A novel 58-kDa protein associates with the Golgi apparatus and microtubules. *J. Biol. Chem.* 264, 16083-16092.
- Bolaños, J. P., Heales, S. J. R., Land, J. M., & Clark, J. B. (1995) Effect of peroxynitrite on the mitochondrial respiratory chain: Differential susceptibility of neurones and astrocytes in primary culture. *J. Neurochem.* 64, 1965-1972.
- Bolli, R., Nalecz, K. A., & Azzi, A. (1985) The interconversion between monomeric and dimeric bovine heart cytochrome c oxidase. *Biochimie* 67, 119-128.
- Boveris, A., & Cadenas, E. (1997) Cellular sources and steady-state levels of reactive oxygen species. In: *Oxygen, Gene Expression, and Cellular Function* (L. Biadasz Clerch & D. J. Massaro, Eds.), pp. 1-25. Marcel Dekker, New York.
- Brady, S. T. (1991) Molecular motors in the nervous system. *Neuron* 7, 521-533.
- Brambrink, A. M., Martin, L. J., Hanley, D. F., Becker, K. Y., Koehler, R. C., & Traystman, R. J. (1999) Effects of the AMPA receptor antagonist NBQX on the outcome of newborn pigs after asphyxial cardiac arrest. *J. Cereb. Blood Flow Metab.* 19, 927-938.
- Capaldi, R. A. (1990) Structure and function of cytochrome c oxidase. *Annu. Rev. Biochem.* 59, 569-596.
- Cheng, Y., Deshmukh, M., D-Costa, A., Demare, J. A., Gidday, J. M., Shah, A., Sun, Y., Jacquin, M. F., Johnson, Jr., E. M., & Holtzman, D. M. (1998) Caspase inhibitor affords neuroprotection with delayed administration in a rat model of neonatal hypoxic-ischemic brain injury. *J. Clin. Invest.* 101, 1992-1999.
- Choi, D. W. (1992) Excitotoxic cell death. *J. Neurobiol.* 23, 1261-1276.
- Collins, R. J., Harmon, B. V., Gobé, V. C., & Kerr, J. F. R. (1992) Internucleosomal DNA cleavage should not be the sole criterion for identifying apoptosis. *Int. J. Radiat. Biol.* 61, 451-453.
- Corbett, E. F., Oikawa, K., Francois, P., Tessier, D. C., Kay, C., Bergeron, J. J. M., Thomas, D. Y., Krause, K.-H., & Michalak, M. (1999) Ca<sup>2+</sup> regulation of interactions between endoplasmic reticulum chaperones. *J. Biol. Chem.* 274, 6203-6211.
- Davies, K. J. (1987) Protein damage and degradation by oxygen radicals. I. General aspects. *J. Biol. Chem.* 262, 9895-9901.
- Deshmukh, M., & Johnson, Jr., E. M. (1998) Evidence of a novel event during neuronal death: Development of competence-to-die in response to cytoplasmic cytochrome c. *Neuron* 21, 695-705.
- Dobbing, J., & Sands, J. (1979) Comparative aspects of the brain growth spurt. *Early Hum. Dev.* 3, 79-83.
- Donaldson, J. G., Lippincott-Schwartz, J., Bloom, G. S., Kreis, T. E., & Klausner, R. D. (1990) Dissociation of a 110-kD peripheral membrane protein from the Golgi apparatus is an early event in brefeldin A action. *J. Cell Biol.* 111, 2295-2306.
- Eiserich, J. P., Estévez, A. G., Bamberg, T. V., Ye, Y. Z., Chumley, P. H., Beckman, J. S., & Freeman, B. A. (1999) Microtubule dysfunction by posttranslational nitrotyrosination of  $\alpha$ -tubulin: A nitric oxide-dependent mechanism of cellular injury. *Proc. Natl. Acad. Sci. USA* 96, 635-6370.
- Farber, J. L., Chien, K. R., & Mittnacht, Jr., S. (1981) The pathogenesis of irreversible cell injury in ischemia. *Am. J. Pathol.* 102, 271-281.
- Ford, L. M., Sanberg, P. R., Norman, A. B., & Fogelson, M. H. (1989) MK-801 prevents hippocampal neurodegeneration in neonatal hypoxic-ischemic rats. *Arch. Neurol.* 46, 1090-1096.

- Frederiks, W. M., & Marx, F. (1989). Changes in acid phosphatase activity in rat liver after ischemia. *Histochemistry* 93, 161-166.
- Fujimura, M., Morita-Fujimura, Y., Murkami, K., Kawase, M., & Chan, P. K. (1998) Cytosolic redistribution of cytochrome c after transient focal cerebral ischemia in rats. *J. Cereb. Blood Flow Metab.* 18, 1239-1247.
- Furuta, A., Rothstein, J. D., & Martin, L. J. (1997) Glutamate transporter protein subtypes are expressed differentially during rat CNS development. *J. Neurosci.* 17, 8363-8375.
- Furuta, A., & Martin, L. J. (1999) Laminar segregation of the cortical plate during corticogenesis is accompanied by changes in glutamate receptor expression. *J. Neurobiol.* 39, 67-80.
- Grasl-Kraupp, B., Ruttkay-Nedecky, B., Koudelka, H., Bukowska, K., Bursch, W., & Schulte-Hermann, R. (1995) In situ detection of fragmented DNA (TUNEL assay) fails to discriminate among apoptosis, necrosis, and autolytic cell death: A cautionary note. *FASEB J.* 21, 1465-1468.
- Gwag, B. J., Koh, J. Y., DeMaro, J. A., Ying, H. S., Jacquin, M., & Choi, D. W. (1997) Slowly triggered excitotoxicity occurs by necrosis in cortical cultures. *Neuroscience* 77, 393-401.
- Halliwell, B., & Gutteridge, J. M. C. (1986) Oxygen free radicals and iron in relation to biology and medicine: some problems and concepts. *Arch. Biochem. Biophys.* 246, 501-514.
- Hill, I. E., MacManus, J. P., Rasquinha, I., & Tuor, U. I. (1995) DNA fragmentation indicative of apoptosis following unilateral cerebral hypoxia-ischemia in the neonatal rat. *Brain Res.* 676, 398-403.
- Ishimaru, M. J., Ikonomidou, C., Tenkova, T. L., Der, T. C., Dikranian, K., Sesma, M. A., & Olney, J. W. (1990) Distinguishing excitotoxic from apoptotic neurodegeneration in the developing rat brain. *J. Comp. Neurol.* 408, 461-476.
- Jiang, X.-M., Fitzgerald, M., Grant, C. M., & Hogg, P. J. (1999) Redox control of exofacial protein thiols/disulfides by protein disulfide isomerase. *J. Biol. Chem.* 274, 2416-2423.
- Johnston, M. V. (1998) Selective vulnerability in the neonatal brain. *Ann. Neurol.* 44, 155-156.
- Kerr, J. F. R., Wyllie, A. H., & Currie, A. R. (1972) Apoptosis: A basic biological phenomenon with wide-ranging implications in tissue kinetics. *Br. J. Cancer* 26, 239-257.
- Kirino, T., Tamura, A., & Sano, K. (1984) Delayed neuronal death in rat hippocampus following transient forebrain ischemia. *Acta Neuropathol.* 64, 139-147.
- Kitagawa, K., Matsumoto, M., Niinobe, M., Mikoshiba, K., Hata, R., Ueda, H., Handa, N., Fukunaga, R., Isaka, Y., Kimura, K., & Kamada, T. (1989) Microtubule-associated protein 2 as a sensitive marker for cerebral ischemic damage. Immunohistochemical investigation of dendritic damage. *Neuroscience* 31, 401-411.
- Laiho, K. U., & Trump, B. J. (1975) Studies on the pathogenesis of cell injury. Effects of inhibitors of metabolism and membrane function on the mitochondria of Ehrlich ascites tumor cells. *Lab. Invest.* 32, 163-182.
- LeBlanc, M. H., Vig, V., Smith, B., Parker, C. C., Evans, O. B., & Smith, E. E. (1991) MK-801 does not protect against hypoxic-ischemic brain injury in piglets. *Stroke* 22, 1270-1275.
- LeBlanc, M. H., Li, X. Q., Huang, M., Patel, D. M., & Smith, E. E. (1995) AMPA antagonist LY293558 does not affect the severity of hypoxic-ischemic injury in newborn pigs. *Stroke* 26, 1908-1915.
- Lee, C., & Chen, L. B. (1988) Dynamic behavior of endoplasmic reticulum in living cells. *Cell* 54, 37-46.
- Li, P., Nijhawan, D., Budihardjo, I., Srinivasula, S. M., Ahmad, M., Alnemri, E. S., & Wang, X. (1997) Cytochrome c and dATP-dependent formation of Apaf-1/caspase-9 complex initiates an apoptotic protease cascade. *Cell* 91, 479-489.
- Lockshin, R. A., & Zakeri, A. (1994) Programmed cell death: Early changes in metamorphosing cells. *Biochem. Cell Biol.* 72, 589-596.
- Maller, A. I., Hankins, L. L., Yeakley, J. W., & Butler, I. J. (1998) Rolandic type cerebral palsy in children as a pattern of hypoxic-ischemic injury in the full-term neonate. *J. Child Neurol.* 13, 313-321.
- Martin, L. J., Doeblner, J. A., & Anthony, A. (1986) Cytophotometric analysis of neuronal chromatin and RNA changes in oxotremorine-treated rats. *Proc. Soc. Exp. Biol. Med.* 181, 41-48.
- Martin, L. J., Brambrink, A., Koehler, R. C., & Traystman, R. J. (1997a) Neonatal asphyxial brain injury is neural system preferential and targets sensory-motor networks. In: *Fetal and Neonatal Brain Injury: Mechanisms, Management, and the Risks of Practice* (D. K. Stevenson and P. Sunshine, Eds.), pp. 374-399. Oxford Univ. Press, New York.
- Martin, L. J., Brambrink, A., Koehler, R. C., & Traystman, R. J. (1997b) Primary sensory and forebrain motor systems in the newborn brain are preferentially damaged by hypoxia-ischemia. *J. Comp. Neurol.* 377, 262-285.
- Martin, L. J., Brambrink, A. M., Lehmann, C., Portera-Cailliau, C., Koehler, R., Rothstein, J., & Traystman, R. J. (1997c) Hypoxia-ischemia causes abnormalities in glutamate transporters and death of astroglia and neurons in newborn striatum. *Ann. Neurol.* 42, 335-348.
- Martin, L. J., Al-Abdulla, N. A., Brambrink, A. M., Kirsch, J. R., Sieber, F. E., & Portera-Cailliau, C. (1998a) Neurodegeneration in excitotoxicity, global cerebral ischemia, and target deprivation: A perspective on the contributions of apoptosis and necrosis. *Brain Res. Bull.* 46, 281-309.
- Martin, L. J., Furuta, A., & Blackstone, C. D. (1998b) AMPA receptor protein in developing rat brain: Glutamate receptor-1 expression and localization change at regional, cellular, and subcellular levels with maturation. *Neuroscience* 83, 917-928.
- Martin, L. J., Kaiser, A., & Price, A. C. (1999) Motor neuron degeneration after sciatic nerve avulsion in adult rat evolves with oxidative stress and is apoptosis. *J. Neurobiol.* 40, 185-201.
- Martin, L. J., Sieber, F. E., & Traystman, R. J. (2000) Apoptosis and necrosis occur in separate neuronal populations in hippocampus and cerebellum after ischemia and are associated with differential alterations in metabotropic glutamate receptor signaling pathways. *J. Cereb. Blood Flow Metab.* 20, 153-167.
- McCord, J. M. (1985) Oxygen-derived free radicals in postischemic tissue injury. *N. Engl. J. Med.* 312, 159-163.
- Meister, A. (1995) Mitochondrial changes associated with glutathione deficiency. *Biochimica et Biophysica Acta* 1271, 35-42.
- McDonald, J. W., Silverstein, F. S., & Johnston, M. V. (1987) MK-801 protects the neonatal brain from hypoxic-ischemic damage. *Eur. J. Pharmacol.* 140, 359-361.
- Mizui, T., Kinouchi, H., & Chan, P. H. (1992) Depletion of brain glutathione by buthionine sulfoximine enhances cerebral ischemic injury in rats. *Am. J. Physiol.* 262, H313-H317.
- Munro, S., & Pelham, H. R. (1987) A C-terminal signal prevents secretion of luminal ER proteins. *Cell* 48, 899-907.
- Natale, J. E., Brambrink, A. M., Traystman, R. J., & Martin, L. J. (1999) Hypoxia-ischemia in newborn piglets produces early defects in striatal high-affinity glutamate uptake. *Pediatric Res.* 45, 345A.
- Northington, F. J., Traystman, R. J., Koehler, R. C., Rothstein, J. R., & Martin, L. J. (1998) Regional and cellular expression of glial (GLT1) and neuronal EAAC1 glutamate transporter proteins in ovine fetal brain. *Neuroscience* 85, 1183-1194.

- Olney, J. W. (1994) Excitatory transmitter neurotoxicity. *Neurobiol. Aging* 15, 259-260.
- Pavelka, M., & Ellinger, A. (1993) Early and late transformations occurring at organelles of the Golgi area under the influence of brefeldin A: An ultrastructural and lectin cytochemical study. *J. Histochem. Cytochem.* 41, 1031-1042.
- Petito, C. K., & Pulsinelli, W. A. (1984) Sequential development of reversible and irreversible neuronal damage following cerebral ischemia. *J. Neuropathol. Exp. Neurol.* 43, 141-153.
- Portera-Cailliau, C., Price, D. L., & Martin, L. J. (1997a) Non-NMDA and NMDA receptor-mediated excitotoxic neuronal deaths in adult brain are morphologically distinct: Further evidence for an apoptosis-necrosis continuum. *J. Comp. Neurol.* 378, 88-104.
- Portera-Cailliau, C., Price, D. L., & Martin, L. J. (1997b) Excitotoxic neuronal death in the immature brain is an apoptosis-necrosis morphological continuum. *J. Comp. Neurol.* 378, 70-87.
- Pourcyrous, M., Leffler, C. W., Bada, H. S., Korones, S. B., & Busija, D. W. (1993) Brain superoxide anion generation in asphyxiated piglets and the effect of indomethacin at therapeutic dose. *Pediatric Res.* 34, 366-36.
- Rafols, J. A., Daya, A. M., O'Neil, B. J., Krause, G. S., Neumar, R. W., & White, B. C. (1995) Global brain ischemia and reperfusion: Golgi apparatus ultrastructure in neurons selectively vulnerable to death. *Acta Neuropathol.* 90, 17-30.
- Ravindranath, V., & Reed, D. J. (1990) Glutathione depletion and formation of glutathione-protein mixed disulfide following exposure of brain mitochondria to oxidative stress. *Biochem. Biophys. Res. Comm.* 169, 1-75-1079.
- Roland, E. H., Poskitt, K., Rodriguez, E., Lupton, B. A., & Hill, A. (1998) Perinatal hypoxic-ischemic thalamic injury: Clinical features and neuroimaging. *Ann. Neurol.* 44, 161-166.
- Simons, K., & Zerial, M. (1993) Rab proteins and road maps for intracellular transport. *Neuron* 11, 789-799.
- Strong, M. J., Sopper, M. M., Crow, J. P., Strong, W. L., & Beckman, J. S. (1998) Nitration of the low molecular weight neurofilament is equivalent in sporadic amyotrophic lateral sclerosis and control cervical spinal cord. *Biochem. Biophys. Res. Commun.* 248, 157-164.
- Thilmann, R., Xie, Y., Kleihues, P., & Kiessling, M. (1986) Persistent inhibition of protein synthesis precedes delayed neuronal death in postischemic gerbil hippocampus. *Acta Neuropathol.* 71, 88-93.
- Tietze, F. (1969) Enzymic method for quantitative determination of nanogram amounts of total and oxidized glutathione: Applications to mammalian blood and other tissues. *Anal. Biochem.* 27, 502-522.
- Uppu, R. M., Cueto, R., Squadrito, G. L., Salgo, M. G., & Pryor, W. A. (1996) Competitive reactions of peroxynitrite with 2'-deoxyguanosine and 7,8-dihydro-8-oxo-2'-deoxyguanosine (8-oxodG): Relevance to the formation of 8-oxodG in DNA exposed to peroxynitrite. *Free Rad. Biol. Med.* 21, 407-411.
- Van Noorden, C. J. F. (1991) Assessment of lysosomal function by quantitative histochemical and cytochemical methods. *Histochem. J.* 23, 429-435.
- Volpe, J. J. (1995) *Neurology of the Newborn*. Saunders, Philadelphia.
- Wang, C. C. (1998) Protein disulfide isomerase assists protein folding as both an isomerase and a chaperone. *Ann. N.Y. Acad. Sci.* 864, 9-13.
- Wharton, D. C., & Tzagoloff, A. (1967) Cytochrome oxidase from beef heart mitochondria. *Methods Enzymol.* 10, 245-250.
- Wolff, S. P., & Dean, R. T. (1986) Fragmentation of proteins by free radicals and its effect on their susceptibility to enzymic hydrolysis. *Biochem. J.* 234, 399-403.
- Wong-Riley, M. T. T. (1979) Changes in the visual system of monocularly sutured or enucleated cats demonstrable with cytochrome oxidase histochemistry. *Brain Res.* 171, 11-28.
- Yamamoto, K., Hayakawa, T., Mogami, H., Akai, F., & Yanagihara, T. (1990) Ultrastructural investigation of the CA1 region of the hippocampus after transient cerebral ischemia in gerbils. *Acta Neuropathol.* 80, 487-492.

---

## Rapid Publication

---

# Injury-Induced Apoptosis of Neurons in Adult Brain Is Mediated by p53-Dependent and p53-Independent Pathways and Requires Bax

LEE J. MARTIN,<sup>1,2\*</sup> ADEEL KAISER,<sup>1</sup> JONATHAN W. YU,<sup>1</sup> JOANNE E. NATALE,<sup>3</sup>  
AND NAEL A. AL-ABDULLA<sup>1,4</sup>

<sup>1</sup>Department of Pathology, Division of Neuropathology, Johns Hopkins University School of Medicine, Baltimore, Maryland 21205

<sup>2</sup>Department of Neuroscience, Johns Hopkins University School of Medicine, Baltimore, Maryland 21205

<sup>3</sup>Department of Anesthesiology/Critical Care Medicine, Johns Hopkins University School of Medicine, Baltimore, Maryland 21287

<sup>4</sup>Wilmer Eye Institute, Johns Hopkins University School of Medicine, Baltimore, Maryland 21287

---

### ABSTRACT

The mechanisms of injury-induced apoptosis of neurons within the CNS are not understood. We used a model of cortical injury in rat and mouse to induce retrograde neuronal apoptosis in thalamus. In this animal model, unilateral ablation of the occipital cortex causes unequivocal apoptosis of corticopetal projection neurons in the dorsal lateral geniculate nucleus (LGN) by 7 days postlesion. We tested the hypothesis that p53 and Bax regulate this retrograde neuronal apoptosis. We found, by using immunocytochemistry, that p53 accumulates in nuclei of neurons destined to undergo apoptosis. By immunoblotting, p53 levels increase (~150% of control) in nuclear-enriched fractions of the ipsilateral LGN by 5 days after occipital cortex ablation. p53 is functionally activated in nuclear fractions of the ipsilateral LGN at 5 days postlesion, as shown by DNA binding assay (~fourfold increase) and by immunodetection of phosphorylated p53. The levels of procaspase-3 increase at 4 days postlesion, and caspase-3 is activated prominently at 5 days postlesion. To identify whether neuronal apoptosis in the adult brain is dependent on p53 and Bax, cortical ablations were done on *p53* and *bax* null mice. Neuronal apoptosis in the dorsal LGN is significantly attenuated (~34%) in *p53*<sup>-/-</sup> mice. In lesioned *p53*<sup>+/-</sup> mice, Bax immunostaining is enhanced in the ipsilateral dorsal LGN and Bax immunoreactivity accumulates at perinuclear locations in dorsal LGN neurons. The enhancement and redistribution of Bax immunostaining is attenuated in lesioned *p53*<sup>-/-</sup> mice. Neuronal apoptosis in the dorsal LGN is blocked completely in *bax*<sup>-/-</sup> mice. We conclude that neuronal apoptosis in the adult thalamus after cortical injury requires Bax and is modulated by p53. *J. Comp. Neurol.* 433: 299–311, 2001. © 2001 Wiley-Liss, Inc.

**Indexing terms:** Alzheimer's disease; amyotrophic lateral sclerosis; DNA damage; programmed cell death; head trauma; tumor suppressor protein

---

Grant sponsor: U.S. Public Health Service, National Institutes of Health, National Institute of Neurological Disorders and Stroke, and National Institute on Aging; Grant numbers: NS34100, AG16282; Grant sponsor: Department of Defense, U.S. Army Medical Research and Materiel Command; Grant number: DAMD17-99-1-9553.

\*Correspondence to: Lee J. Martin, Ph.D., Johns Hopkins University School of Medicine, Department of Pathology, 558 Ross Building, 720 Rutland Avenue, Baltimore, MD 21205-2196. E-mail: lmartin@jhmi.edu

Received 15 September 2000; Revised 1 February 2001; Accepted 19 February 2001

Apoptosis is an organized form of cell death that is mediated by active, intrinsic mechanisms (Arends et al., 1990; Kerr and Harmon, 1991). Apoptosis in the nervous system is important for a variety of reasons. Apoptosis of neurons and nonneuronal cells occurs normally in the developing nervous system (Glücksmann, 1951; Oppenheim, 1991), and defects in apoptosis can cause cerebral malformations during central nervous system (CNS) development (Kuida et al., 1996; Hakem et al., 1998). Apoptosis might also participate in the pathogenesis of abnormal neuronal death in chronic and acute neuropathologic disorders. For example, the genes for neuronal apoptosis inhibitory protein and survival motor neuron protein are either deleted partially or are mutant in some children with pediatric forms of motor neuron disease such as spinal muscular atrophy (Roy et al., 1995; Lefebvre et al., 1995). The neuronal and glial degeneration in age-related neurodegenerative disorders such as Alzheimer's disease and amyotrophic lateral sclerosis also may be forms of apoptosis (Anderson et al., 1996; Kitamura et al., 1999; Martin et al., 2000a). In acute neurologic disorders, apoptosis of neurons and nonneuronal cells may contribute to the neuropathology in animal models of cerebral ischemia (MacManus et al., 1997; Martin et al., 1998, 2000b) and spinal cord trauma (Liu et al., 1997). Therefore, understanding the molecular regulation of apoptosis is relevant to not only nervous system development but also neurodegeneration in pathologic conditions.

Apoptosis can be induced by the oncosuppressor protein p53 (Vogelstein and Kinzler, 1992; Levine, 1997). This DNA binding protein functions in genome surveillance, DNA repair, and as a transcription factor. p53 commits to death cells that have sustained DNA damage from reactive oxygen species and other genotoxic agents. The mechanisms by which p53 induces apoptosis are largely unknown. p53 is a direct transcriptional activator of the *Bax* gene (Miyashita and Reed, 1995) and a transcriptional repressor of the *Bcl-2* gene (Miyashita et al., 1994); thus, apoptosis is thought to be executed by molecular cascades involving expression or activation of p53, Bax, and caspases (Polyak et al., 1997).

The understanding of the mechanisms of apoptosis in nervous system cells is less advanced compared with cells of nonnervous tissue origin. Seminal studies have shown recently that Bax is critical for apoptosis of neurons in cell culture (Deckwerth et al., 1996; Miller et al., 1997; Putcha et al., 1999) and is required for neuronal apoptosis during development (Deckwerth et al., 1996). However, the mechanisms of injury-induced neuronal apoptosis within the CNS are much less understood as compared with cell culture and developmental paradigms. We used an injury model of unequivocal neuronal apoptosis within the rodent brain to identify the *in vivo* mechanisms of neuronal apoptosis. In this model, occipital cortex ablation reliably induces neuronal apoptosis in the dorsal lateral geniculate nucleus (dLGN) of thalamus (Agarwala and Kalil, 1998; Al-Abdulla and Martin, 1998; Al-Abdulla et al., 1998). The evolution of apoptosis in these neurons is associated with oxidative stress and the accumulation of nuclear DNA damage (Al-Abdulla and Martin, 1998). We used this model to test the hypothesis that injury-induced apoptosis of neurons in the adult brain is controlled by p53, Bax, and caspase-3.

## MATERIALS AND METHODS

### Animals

Adult male rats and mice were used for these experiments. Sprague-Dawley rats (Charles River, Wilmington, MA) weighed ~150–200 g. Mice (Jackson Labs) were deficient in the *bax* gene (*bax*<sup>-/-</sup>, *n* = 16) or the *p53* gene (*p53*<sup>-/-</sup>, *n* = 10) and were 6–8 weeks of age when used. Bax-deficient mice were the C57BL/6-Bax<sup>tm1Sjk</sup> congenic strain. p53-deficient mice were the 129/Sv-Trp53<sup>tm1Tyi</sup> strain. C57/B6 mice (*n* = 20) served as wild-type controls for *bax*-null mice, and 129/SV mice (*n* = 10) served as wild-type controls for p53-null mice. The animals were housed in a colony room with a 12 hour:12 hour-light/dark cycle and ad libitum access to food and water. The Animal Care and Use Committee of the Johns Hopkins University School of Medicine approved the animal protocol.

### In vivo model of neuronal apoptosis

A unilateral occipital cortex ablation served as the model for producing axotomy and target deprivation of neurons and subsequent apoptosis selectively in the dLGN (Al-Abdulla et al., 1998; Al-Abdulla and Martin, 1998). Rats and mice were anesthetized with a mixture of enflurane:oxygen:nitrous oxide (1:33:66) and placed in a stereotaxic apparatus. After a midline scalp incision, a craniotomy was made and the dura was incised by using a sharp 22-gauge needle. The cortex underlying the craniotomy was then aspirated by using a blunt-tipped 22-gauge needle connected to a vacuum line, without damaging the surrounding venous sinuses and the underlying hippocampus (Fig. 1A). Postlesion survival times after occipital cortex ablation were 1, 2, 3, 4, 5, 6, 7, and 14 days.

### Retrograde labeling of corticopetal projection neurons in mouse dLGN

The retrograde tracer Fluoro-Gold (FG, Fluorochrome, Inc., Englewood, CO) was injected into mouse visual cortex to identify corticopetal projection neurons in the dLGN. An occipital craniotomy was performed, and 100 nl of 5% FG in deionized-distilled H<sub>2</sub>O was injected into the cortex as described (Al-Abdulla and Martin, 1998). Three days later, the mice (*n* = 5) were lesioned with an occipital cortex ablation as described above. FG-injected mice with occipital cortex ablations survived for 4 days. Corticopetal projection neurons were identified by direct fluorescence as described (Al-Abdulla et al., 1998; Martin et al., 1999).

### Quantification of neurons

At 7 and 14 days after occipital cortex ablation, Bax-deficient mice, p53-deficient mice, and wild-type mice were anesthetized with an overdose of chloral hydrate and perfused intracardially with ice-cold phosphate buffer-saline (PBS, 100 mM, pH 7.4), delivered by a perfusion pump, followed by 4% paraformaldehyde in ice-cold PBS. After perfusion-fixation, brains were allowed to remain *in situ* for 1 hour before they were removed from the skull. After the brains were removed, they were cryoprotected in 20% glycerol-PBS, uniformly blocked, and frozen under pulverized dry ice. Coronal serial symmetrical sections (40  $\mu$ m) through the thalamus were cut by using a sliding microtome. Serial sections from each mouse brain were mounted on glass slides and stained with cresyl violet for neuronal counting. Neuronal counts in the ipsilateral and contralateral dLGN were made at 1,000 $\times$  magnification.

by using the stereologic optical dissector method as described (Calhoun et al., 1996; Al-Abdulla et al., 1998). Neurons without apoptotic structural changes (by using strict morphologic criteria, see Fig. 1Aa) were counted. These criteria included a round, open, pale nucleus (not condensed and darkly stained), granular Nissl staining of the cytoplasm, and a diameter of ~20–25  $\mu$ m. With these criteria, astrocytes, oligodendrocytes, and microglia were excluded from the counts. Neuronal counts were used to determine group means and variances and comparisons among groups were performed by using a one-way analysis of variance and a Student's *t*-test. The experiments were controlled for at two levels. Bax-deficient have more neurons than wild-type mice (Deckwerth et al., 1996), therefore, neuronal counts in the contralateral dLGN always served as controls for the ipsilateral dLGN in lesioned Bax- and p53-null mice. In addition, neuron counts in wild-type mice served as strain controls.

### Localization of p53 and Bax in dLGN after occipital cortex ablation

We evaluated whether the localizations of p53 and Bax are changed in dLGN neurons after cortical damage. Rats at 1, 3, 4, 5, 6, and 7 days postlesion (*n* = 4 to 6 per time point) and mice at 5, 6, and 7 days postlesion (*n* = 4–10 per time point) were used for the immunocytochemical detection of p53. p53<sup>-/-</sup> and wild-type mice at 5 and 7 days postlesion (*n* = 5 per time point) were used for the immunocytochemical detection of Bax. These animals were anesthetized and perfusion-fixed, and the brains were prepared as described above. p53 and Bax were detected in rat or mouse brain sections by using a standard immunoperoxidase method with diaminobenzidine as chromogen and cresyl violet counterstaining. Three different commercial antibodies to p53 were used. Two of these antibodies recognize p53 regardless of phosphorylation state (BMG-1B1, 1  $\mu$ g IgG/ml [Boehringer-Mannheim] and Pab240, 1  $\mu$ g IgG/ml [Santa Cruz]). The other p53 antibody used detects p53 only when it is phosphorylated at Ser392 (Oncogene) and, thus, recognizes activated p53 (Levine, 1997). The specificities of these p53 antibodies were demonstrated by immunoblotting (see below and data not shown). These antibodies are highly specific for detecting a major protein band at ~53 kDa that has the same mobility as recombinant p53. Furthermore, p53 immunoreactivity detected with these antibodies is exclusively nuclear and is found only in subsets of cells. Immunostaining for Bax was detected with a rabbit polyclonal antibody that recognizes the *N*-terminus (Upstate). Negative control sections were incubated in comparable dilutions of immunoglobulin G or with primary or secondary antibody omitted.

### Immunoblotting for p53 and caspase-3

Rats were used to measure p53 and caspase-3 protein levels during the progression of neuronal apoptosis. Samples of LGN (ipsilateral and contralateral) were collected for immunoblotting at 1, 4, 5, and 6 days after occipital cortex ablation (*n* = 10–17 rats per time point). Animals were deeply anesthetized with chloral hydrate, decapitated, and the brain was removed quickly and placed on ice. Under a microsurgical stereomicroscope, the cerebral cortex was reflected to visualize the dorsal thalamus. The LGN is readily discernible by surface landmarks. By using iridectomy scissors, the LGN from ipsilateral (target de-

prived) and contralateral (control) thalamus was microdissected from each rat and frozen quickly on dry ice. LGN samples from target-deprived and control sides were pooled for each time point. The accuracy of the LGN microdissection was verified. LGN samples were removed, and then brainstems were immersion-fixed in 4% paraformaldehyde. Afterward, the brainstems were cryoprotected, cut, and rostral brainstem sections were stained with cresyl violet and viewed microscopically (data not shown).

LGN samples were homogenized in cold 20 mM Tris HCl (pH 7.4) containing 10% (wt/vol) sucrose, 20 U/ml aprotinin (Trasylol), 20  $\mu$ g/ml leupeptin, 20  $\mu$ g/ml antipain, 20  $\mu$ g/ml pepstatin A, 20  $\mu$ g/ml chymostatin, 0.1 mM phenylmethylsulfonyl fluoride, 10 mM benzamidine, 1 mM EDTA, and 5 mM EGTA. Crude homogenates were centrifuged at 1,000 *g*<sub>av</sub> for 10 minutes (4°C), and the resulting pellet consisting of the nuclear-enriched fraction was resuspended in homogenization buffer (without sucrose) supplemented with 20% (wt/vol) glycerol. The supernatant was then centrifuged at 54,000 *g*<sub>av</sub> for 20 minutes (4°C) to yield soluble and membrane fractions. This subcellular fractionation protocol has been verified (Martin, 2000). Protein concentrations in nuclear and soluble fractions were measured by a Bio-Rad protein assay with bovine serum albumin as a standard.

Immunoreactivities for p53 and caspase-3 were measured in the LGN after occipital cortex ablation. Nuclear-enriched and soluble cell fractions from ipsilateral and contralateral LGN samples were subjected to 15% sodium dodecyl sulfate polyacrylamide gel electrophoresis (SDS-PAGE) and transferred to nitrocellulose membrane by electroelution as described (Martin, 1999). The positive control for p53 was purified human recombinant p53 (Oncogene Research Products). The positive control for active caspase was purified active caspase-3 (BioVision Research Products). The reliability of sample loading and electroblotting in each experiment was evaluated by staining nitrocellulose membranes with Ponceau S before immunoblotting. Blots were blocked with 2.5% nonfat dry milk with 0.1% Tween 20 in 50 mM Tris-buffered saline (pH 7.4), then incubated overnight at 4°C with antibody. Two different p53 antibodies were purchased commercially and were a sheep anti-human recombinant p53 (BMG-1B1, Boehringer Mannheim) and a mouse monoclonal antibody to p53- $\beta$ -galactosidase fusion protein containing the p53 domain corresponding to amino acids 156–214 (Pab240, Santa Cruz). The neuronal nuclear-enrichment of the LGN subcellular fractions was verified by the presence of the neuronal nuclear protein NeuN (Martin, 2000; data not shown), as detected with a mouse monoclonal antibody (Chemicon). Caspase-3 was detected with a rabbit polyclonal antibody that binds both the proenzyme and the active subunits (Santa Cruz). The antibodies were used at the following concentrations to visualize immunoreactive proteins within the linear range: 2–3  $\mu$ g IgG/ml (BMG-1B1), 1–2  $\mu$ g IgG/ml (Pab240), 0.2–0.4  $\mu$ g IgG/ml (NeuN), and 0.4  $\mu$ g IgG/ml (caspase-3). After the primary antibody incubation, blots were washed and incubated with horseradish peroxidase-conjugated secondary antibody (0.2  $\mu$ g/ml), developed with enhanced chemiluminescence (Pierce), and exposed to x-ray film. The blots were then reprobed with a monoclonal antibody to synaptophysin (Boehringer Mannheim) or synapse-associated protein-25 (SNAP-25) as controls for protein loading.

To quantify p53, caspase-3, and synaptic protein immunoreactivities, films were scanned and densitometry was performed as described (Martin, 1999). Because the antibody to caspase-3 detects both the proenzyme and the active subunit, these proteins were analyzed separately. Protein levels were expressed as relative optical density measurements, determined by comparing the density and area of the immunoreactive bands from ipsilateral LGN samples to corresponding bands in contralateral control lanes in the same blot. The immunodensities for p53 and caspase-3 were normalized to synaptic proteins. The values for each time point were replicated in triplicate or quadruplicate experiments. Comparisons were made between the ipsilateral and contralateral LGN samples at the same postlesion time point. The group means and variances were evaluated by one-way analysis of variance, and subsequent statistical evaluations for significance were made by using a two-sample Student's *t*-test.

### p53-DNA binding assay

We evaluated whether p53 in LGN samples had competent DNA binding activity. A p53-consensus, double stranded oligonucleotide (Santa Cruz, sc2579) was 3'-end labeled with digoxigenin-11-ddUTP by using terminal transferase (Boehringer Mannheim), precipitated, and resuspended in TE buffer. DNA-p53 binding reactions were carried out at room temperature for 40 minutes with 1 ng DNA probe and 20  $\mu$ g nuclear extract protein (from ipsilateral and contralateral LGN samples) in 10 mM Tris buffer (pH 7.5), 50 mM NaCl, 5 mM MgCl<sub>2</sub>, 1 mM dithiothreitol, 1 mM EDTA, 5% glycerol, and 2  $\mu$ g herring sperm DNA. For supershift assays, nuclear fractions were incubated (1 hour at room temperature) with p53 antibody (10  $\mu$ g/ml) before the reaction with oligonucleotide. Negative controls for the p53-DNA binding assay were nuclear fractions from brain and liver of *p53*<sup>-/-</sup> mice. The samples were resolved by electrophoresis through a nondenaturing 4% polyacrylamide gel (pre-run for 30 minutes at 33 V) and transferred overnight to nylon membrane followed by ultraviolet cross-linking. Membranes were incubated in 2% nucleic acid blocking reagent (Boehringer Mannheim) and then in blocking reagent containing 75 mU/ml anti-digoxigenin Fab fragments conjugated to alkaline phosphatase (Boehringer Mannheim). After washing, membranes were reacted with CSPD detection reagent (Boehringer Mannheim) and exposed to Kodak X-OMAT film to visualize DNA. Films were scanned and DNA binding was measured by densitometry.

## RESULTS

### Occipital cortex ablation in adult mouse causes neuronal apoptosis in the dLGN

This model of neuronal apoptosis in rat has been characterized previously (Al-Abdulla et al., 1998; Al-Abdulla and Martin, 1998; Martin et al., 1998). We have adapted this model of occipital cortex ablation to the mouse brain (Fig. 1A). The results in wild-type C57/B6 and 129/SV mice are similar to the data obtained in rat; therefore, they are described only briefly. The visual cortex was ablated in mouse, as verified by injecting occipital neocortex with FG and retrogradely labeling the projection neurons in the dLGN (Fig. 1A). The lesion in mouse brain is consistent. The interanimal variability is minimal in the

extent of the cortical aspiration in the anterior-posterior and medial-lateral axes and in the depth of the lesion. It extends throughout the entire thickness of the cortex at the lesion site, but the underlying hippocampus is spared (Fig. 1A). This cortical lesion in adult wild-type C57/B6 and 129/SV mice causes significant apoptosis of dLGN neurons (~90% loss of neurons, see below) over a period of 7 days (Fig. 1Aa-d). During this period the majority of dLGN neurons pass consecutively through chromatolysis (Fig. 1Ab), condensation of chromatin into several round mini-masses (Fig. 1Ac), and then apoptosis (Fig. 1Ad). This progression of neuronal apoptosis *in vivo* has been described before (Al-Abdulla et al., 1998; Martin, 1999; Martin et al., 1999). Tract-tracing with FG shows that these apoptotic neurons are geniculocortical projection neurons (Fig. 1B, inset).

### p53 accumulates in dLGN neurons after occipital cortex lesions

In normal rat and mouse brain, the level of immunocytochemically detectable p53 is low. Immunoreactivity is observed mostly in the nuclei of some parenchymal glial cells and ependymal cells lining the ventricular system. p53 immunoreactivity is rarely observed in the nucleus of neurons in control brain (Fig. 2A,E). After occipital cortex ablation, p53 immunoreactivity accumulates in the nucleus of neurons in the ipsilateral dLGN of rat (Fig. 2B) and mouse (Fig. 2F). At 1 day and 2 days postlesion, the localization of p53 in the ipsilateral dLGN does not differ from the contralateral dLGN. In ipsilateral dLGN neurons, p53 immunoreactivity is elevated at 4 days through 6 days postlesion and is most prominent at 5 days. This accumulation of p53 in neurons is much more conspicuous in the mouse brain compared with the rat brain (Fig. 2B,F). At 6 days postlesion, some astroglia show an induction of p53 in both ipsilateral and contralateral dLGN (Fig. 2C,D).

### p53 levels increase in nuclear fractions of the LGN after occipital cortex ablation

To confirm the immunocytochemical findings, p53 levels in rat LGN after occipital cortex ablation were measured by immunoblotting. p53 in rat brain tissue is resolved at ~53 kDa as two closely migrating immunoreactive bands (Fig. 3) by SDS-PAGE (15% gels), consistent with phosphorylated and dephosphorylated forms of p53 (Levine, 1997). These immunoreactive bands migrate as a major single band in 10% gels (data not shown). The migration of these immunoreactive proteins from rat LGN coincides with the migration and detection of purified human-p53 by SDS-PAGE (Fig. 3). At 5 days postlesion, p53 levels are increased significantly ( $P < 0.05$ ) in the ipsilateral LGN ( $150\% \pm 13\%$  of control, mean  $\pm$  SEM). At 6 days postlesion, p53 levels are not different ( $92\% \pm 3\%$  of control, mean  $\pm$  sem) from the contralateral LGN. Experiments with the two different antibodies to p53 showed similar results.

### p53-DNA binding is elevated transiently in the LGN after occipital cortex ablation

The functional activation of p53 as a transcription factor in nuclear extracts of target-deprived and control LGN samples was evaluated by gel shift assay (Fig. 4). The specificity of p53-DNA binding was demonstrated by the



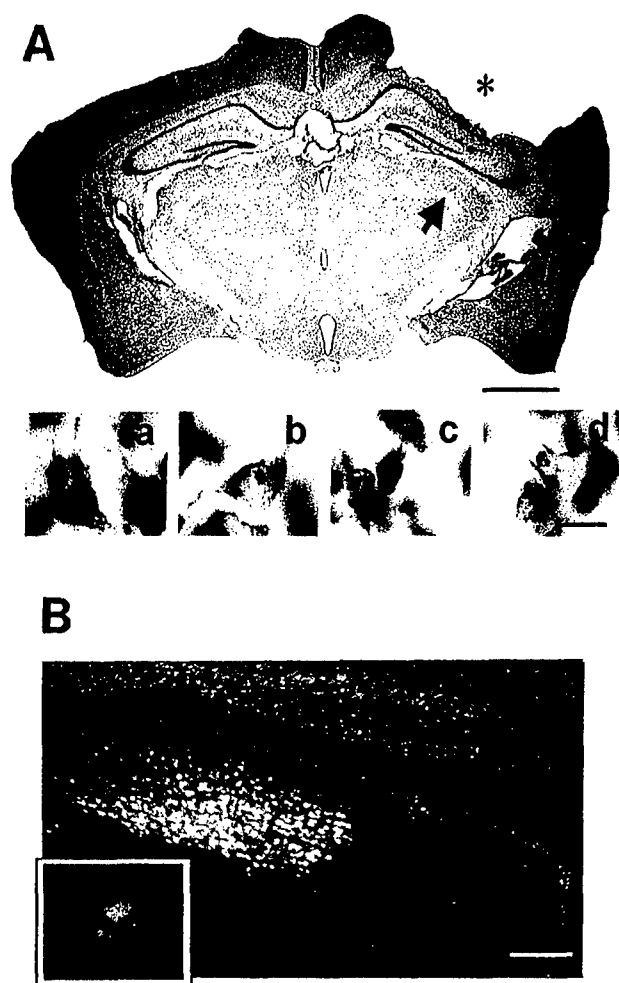


**Fig. 1.** Occipital cortex ablation causes apoptosis of geniculocortical projection neurons in mouse brain. **A:** Nissl-stained section demonstrating the cortical aspiration lesion (asterisk) in mouse brain. The medial-lateral extent of the cortical lesion involves occipital cortex subdivisions Oc1, Oc2M, and Oc2L. The depth of the lesion consistently reaches the corpus callosum, but the underlying hippocampus remains intact. The lateral geniculate nucleus (LGN) ipsilateral to the lesion is identified (arrow). Neurons are shown at the different stages during the progression of neuronal apoptosis in the ipsilateral dLGN. These stages have been described (Al-Abdulla et al., 1998; Martin et al., 1999). **a:** A normal dLGN neuron; **b:** a neuron in the chromatolytic stage; **c:** a neuron in early apoptosis showing nascent chromatin condensation into mini-masses; **d:** a neuron at endstage apoptosis with at least two, discrete, large round nuclear masses. **B:** Corticopetal projection neurons undergo apoptosis in the dLGN after cortical ablation in mouse. After Fluoro-Gold (FG) injection into the mouse occipital cortex, the dLGN is strongly labeled (yellow cells), showing that these cells are geniculocortical projection neurons. Pre-labeling of neurons with FG before ablation identifies these apoptotic neurons as geniculocortical projection neurons (inset). By fluorescence microscopy, cytoplasmic FG labeling (yellow granules) is detected within a neuron in apoptosis, as revealed by Hoechst 33258 staining in the nucleus showing (light blue) the condensed chromatin. Scale bar = 1.5 mm in A; 50  $\mu$ m in d (applies to a–d); 200  $\mu$ m in B.

absence of signal when nuclear extracts of brain and liver from  $p53^{-/-}$  mice were used in the binding reactions. A prominent p53-DNA complex was found in liver nuclear extracts of wild-type mice (Fig. 4, bracket in lane L<sup>+/+</sup>). A

less prominent p53-DNA complex was found in total brain nuclear extracts of wild-type mice (Fig. 4, lane B<sup>+/+</sup>). A p53-DNA complex was not found in liver and brain of  $p53^{-/-}$  mice (Fig. 4, lanes L<sup>-/-</sup> and B<sup>-/-</sup>). DNA binding also disappeared when labeled probe was omitted, when an excess of unlabeled oligonucleotide was included, when nuclear protein fractions were omitted (not shown). In nuclear fractions of LGN at 5 day postlesion, two p53-DNA complexes were observed (Fig. 4, brackets in lane 5di). The presence of p53-DNA binding complexes with different mobilities in gel shift assay is consistent with the finding that oligomers of p53 bind DNA (Levine, 1997). p53-DNA binding was increased markedly ( $385.0\% \pm 17.6\%$  of control, mean  $\pm$  SD) at 5 days in ipsilateral LGN compared with contralateral LGN, corresponding to an ~fourfold increase in DNA binding of p53 (Fig. 4, brackets in lane 5di). Supershift analysis with 5 days ipsilateral LGN samples revealed an additional band that was shifted to higher molecular masses by p53 antibody (Fig. 4, lane 5di + p53 Ab). In contrast, at 6 days when neuronal apoptosis is advanced structurally, the binding activity of p53 in ipsilateral LGN was similar to the contralateral LGN (Fig. 4, lanes 6dc and 6di). The functional activation of p53 at 5 days postlesion was confirmed by the immunocytochemical localization of phosphorylated p53 (Fig. 5). Serine-392-phosphorylated p53 was observed in the nucleus of neurons in the ipsilateral dorsal LGN (Fig. 5A) but not in contralateral LGN neurons (Fig. 5B).

### Caspase-3 is activated in the LGN after occipital cortex ablation

Activation of caspase-3 is a major downstream event in most forms of PCD (Kuida et al., 1996). The levels of procaspase-3 and active caspase-3 subunits were measured by immunoblotting soluble protein fractions of discrete LGN microdissections from rats at 1, 4, 5, and 6 days after the cortical lesion (Fig. 6). Procaspase-3 was detected as a prominent band of immunoreactivity at ~32 kDa, and the active subunits were detected at ~17–20 kDa (Fig. 6A). At 1 day postlesion, the levels of procaspase-3 and active caspase-3 are unchanged (being similar to naïve animals); however, at 4 days, the levels of procaspase-3 and activated caspase are both significantly elevated (Fig. 6B). A prominent peak in caspase-3 activation occurs at 5 days as procaspase-3 levels return to control levels. At 6 days postlesion, caspase-3 activation is attenuated significantly compared with 5 days, although levels of active caspase-3 remain higher than in the control LGN (Fig. 6B).

### Loss of the p53 tumor suppressor function protects neurons from apoptosis

Mice with targeted deletions of the p53 gene ( $p53^{-/-}$ ) were used to test the hypothesis that neuronal apoptosis in adult brain is p53-dependent (Fig. 7). At 7 days after occipital cortex ablation, the number of neurons in the ipsilateral dLGN of wild-type 129/SV mice was  $13.4\% \pm 2.9\%$  (mean  $\pm$  SEM) of contralateral dLGN; in contrast, the number of neurons in the ipsilateral dLGN of  $p53^{-/-}$  mice was  $47.0\% \pm 11.0\%$  (mean  $\pm$  SEM) of contralateral dLGN. Thus, loss of p53 function protects neurons from apoptosis in the adult brain.

p53 functions as a transcription factor (Levine, 1997). We found that p53-DNA binding is markedly elevated in



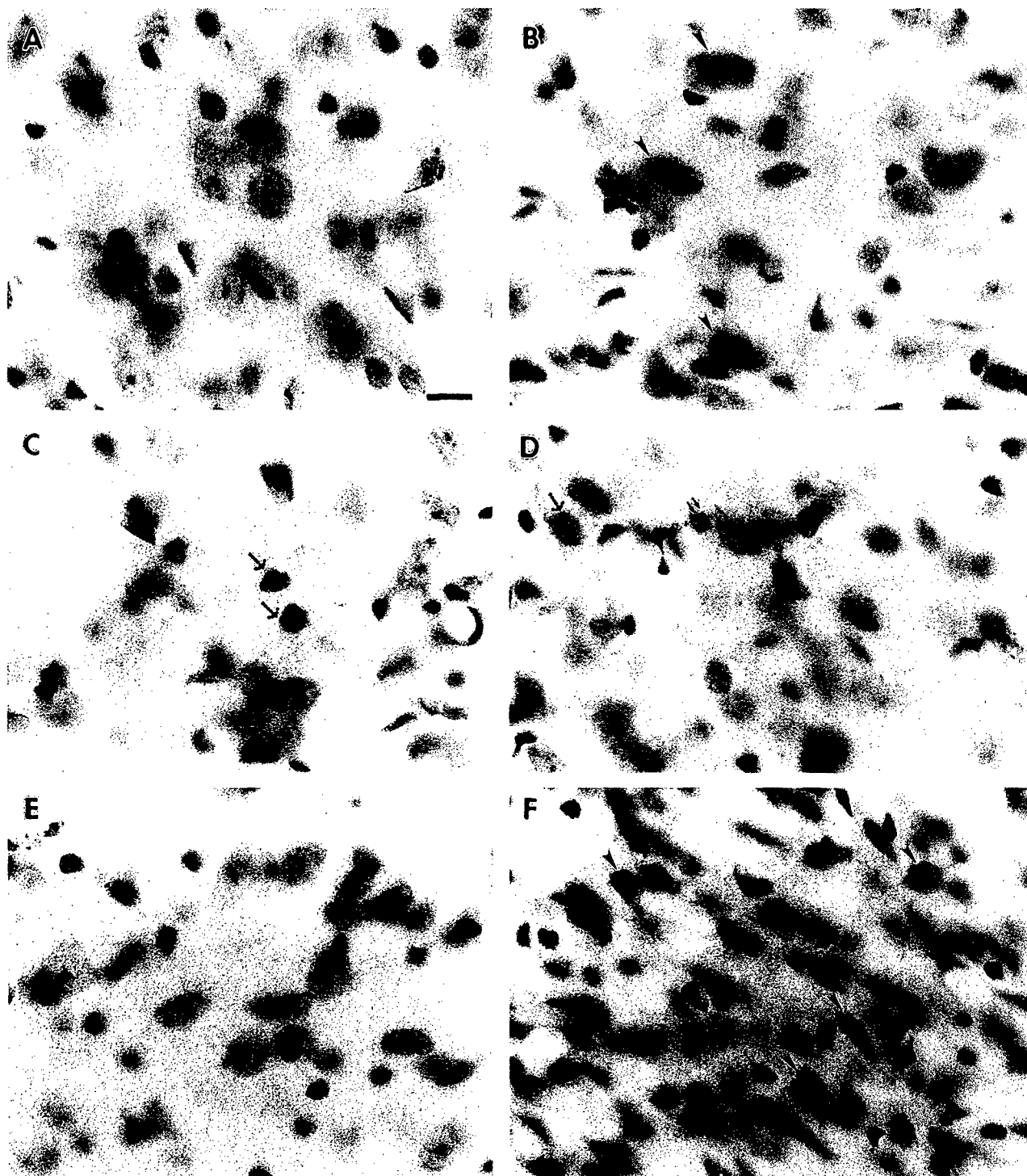


Fig. 2. p53 immunoreactivity accumulates in neuronal nuclei in the dorsal lateral geniculate nucleus (dLGN) after occipital cortex lesions. In rat brain at 5 days postlesion, neurons in the contralateral dLGN are not immunoreactive for p53 (A), but in the ipsilateral dLGN, p53 immunoreactivity has accumulated in the nucleus of neurons (B, arrowheads). C: In rat brain at 6 days postlesion, subsets of small cells with an astroglial morphology (including an ellipsoidal pale nucleus and radiating processes) in the contralateral dLGN now

have nuclear p53 immunoreactivity (dotted arrows). D: Reactive astroglia (dotted arrow) in the ipsilateral dLGN express p53, but end-stage apoptotic neurons (small, double arrows) are not immunoreactive. In mouse brain at 5 days postlesion, neurons in the contralateral dLGN are not immunoreactive for p53 (E), but in the ipsilateral dLGN, p53 immunoreactivity has accumulated in the nucleus of many neurons (F, arrowheads). Scale bar = 10  $\mu$ m in A (applies to A-F).

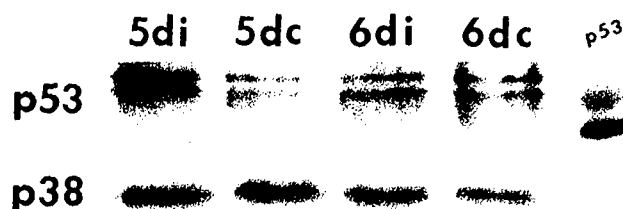


Fig. 3. p53 increases transiently in rat lateral geniculate nucleus (LGN) after occipital cortex ablation. Immunoblot analysis of p53 levels in the nuclear fractions of microdissected ipsilateral and contralateral LGN samples at 5 and 6 days postlesion. Purified, recombinant p53 was used as a positive control (far right lane). p53 is increased in the ipsilateral LGN at 5 days (5di) compared with the contralateral LGN (5dc). At 6 days postlesion, the ipsilateral LGN (6di) is not significantly different from control (6dc). In the contralateral LGN at 6 days (6dc), the levels of p53 are significantly greater than in the contralateral LGN at 5 days (5dc). Each lane represents extracts from pooled LGN samples from 10–17 rats. See text for quantitative measurements using densitometry. Synaptophysin (p38) was used as a loading control.



Fig. 4. p53 is activated transiently in rat lateral geniculate nucleus (LGN) after occipital cortex ablation. Electrophoretic mobility shift assay for p53-DNA binding function in nuclear fractions of microdissected ipsilateral and contralateral LGN samples at 5 and 6 days postlesion. Nuclear extracts were incubated with digoxigenin-labeled p53 consensus oligonucleotide and p53-DNA binding was detected with antibodies to digoxigenin. Negative controls were nuclear fractions from brain (B<sup>-/-</sup>) and liver (L<sup>-/-</sup>) of p53<sup>-/-</sup> mice, demonstrating the specificity of this assay. Brackets identify p53-DNA complexes (in lanes L<sup>+/+</sup>, 5di, and 5di + p53Ab). Supershift analysis (lane 5di + p53Ab) revealed an additional band (uppermost band) shifted to a higher molecular mass. p53-DNA binding activity is greatly increased (fourfold) in the ipsilateral LGN at 5 days postlesion. The discrete, nonspecific DNA-protein complex (just above the free probe) is relatively equal across all lanes, indicating similar protein loading. Each lane represents extracts from pooled LGN samples from 10–17 rats. fp, free probe. See Results section for measurements.

nuclear extracts of the LGN at 5 days postlesion (Fig. 4), consistent with p53 activation through phosphorylation (Fig. 5A). p53 is a transcriptional activator of the *bax* gene (Miyashita and Reed, 1995), and one pathway through which p53 commits cells to death is Bax up-regulation. We therefore evaluated whether Bax immunostaining patterns change in the LGN after occipital cortex lesions in mice (Fig. 8). In wild-type p53<sup>+/+</sup> mice at 5 days after

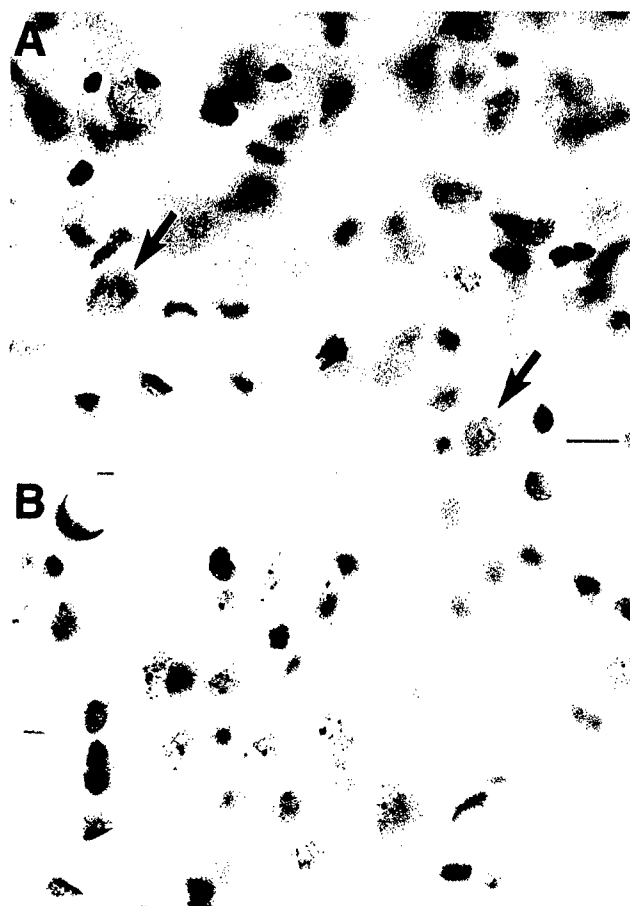


Fig. 5. Immunolocalization of active p53 with antibody to phospho-p53 (ser392) demonstrates nuclear accumulation of active p53 in subsets of ipsilateral dorsal lateral geniculate nucleus (dLGN) neurons (arrows, A) at 5 days postlesion, whereas contralateral dLGN neurons (B) have no immunoreactivity. Scale bar = 20 μm in A (applies to A,B).

lesioning, Bax immunostaining is more prominent in the ipsilateral LGN compared with the contralateral LGN, but the staining in the ventral LGN was similar (Fig. 8A,B). Neurons in the dorsal LGN of p53<sup>+/+</sup> mice show marked accumulation or redistribution of Bax immunoreactivity within the perikaryon (Fig. 8C,D). Specifically, Bax accumulates at perinuclear locations in injured dorsal LGN neurons (Fig. 8D, arrowheads). In contrast, in p53<sup>-/-</sup> mice at 5 days after lesioning, the enhancement of Bax immunostaining in the dorsal LGN is attenuated (Fig. 8E,F).

### Bax is required for retrograde neuronal apoptosis in thalamus after cortical injury

We used mice with targeted deletions of the *bax* gene (bax<sup>-/-</sup>) to test the hypothesis that neuronal apoptosis in the adult brain is Bax-dependent (Fig. 9). At 7 days after occipital cortex ablation, the number of neurons in the ipsilateral dLGN of wild-type C57/B6 mice was 9.0% ± 1.0% (mean ± SEM) of contralateral dLGN; in contrast, the number of neurons in the ipsilateral dLGN of Bax-deficient mice was 88.0% ± 10.0% (mean ± SEM) of con-

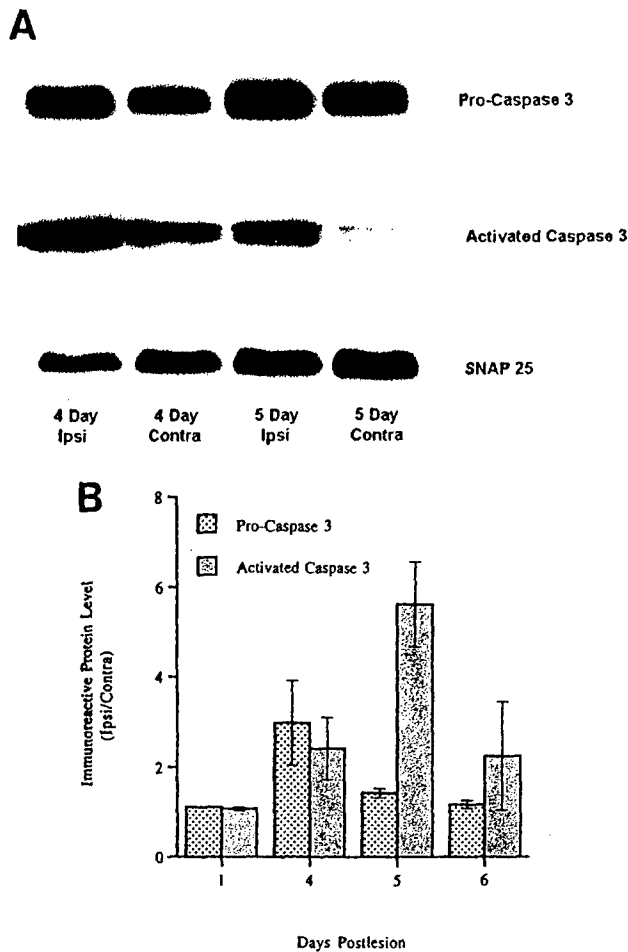


Fig. 6. Caspase-3 is increased and activated transiently in rat lateral geniculate nucleus (LGN) after occipital cortex ablation. **A:** Immunoblot analysis of procaspase-3 and activated caspase-3 in the soluble fractions of microdissected ipsilateral (Ipsi) and contralateral (Contra) LGN samples at 1, 4, 5, and 6 days postlesion. Synaptophysin (p38) was used as a loading control. **B:** Densitometric quantification of procaspase 3 and activated caspase-3 levels. Values are mean  $\pm$  standard deviation. The level of procaspase is increased significantly ( $P < 0.05$ ) at 4 days postlesion. The levels of activated caspase-3 are increased significantly ( $p < 0.05$ ) at 4, 5, and 6 days postlesion, with peak activation occurring at 5 days postlesion. Each lane represents extracts from pooled LGN samples from 10–17 rats.

tralateral dLGN. To determine whether this effect is sustained, mice were survived for twice as many days. At 14 days after occipital cortex ablation, the number of neurons in the ipsilateral dLGN of wild-type C57/B6 mice was  $9.3\% \pm 2.0\%$  (mean  $\pm$  SEM) of contralateral dLGN, whereas the number of neurons in the ipsilateral dLGN of Bax-deficient mice was  $95.0\% \pm 9.0\%$  (mean  $\pm$  SEM) of contralateral dLGN. Thus, deletion of Bax results in sustained protection against neuronal apoptosis in brain.

## DISCUSSION

Ablation of the occipital cortex causes neurodegeneration in the dLGN (Fig. 10). This retrograde neuronal degeneration is apoptosis in rat (Agarwala and Kalil, 1998; Al-Abdulla et al., 1998; Al-Abdulla and Martin, 1998). In

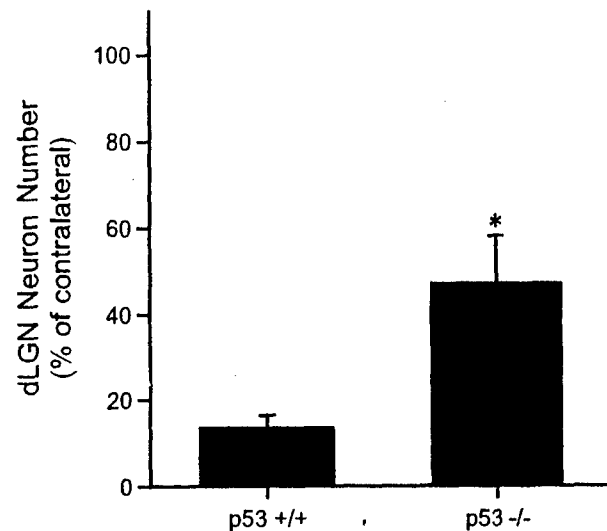


Fig. 7. Loss of functional p53 protects neurons from apoptosis after cortical damage. Occipital cortex lesions were done on  $p53^{+/+}$  (wild-type,  $n = 10$ ) and  $p53^{-/-}$  mice ( $n = 10$ ) that were survived for 7 days. Neurons were counted in the ipsilateral and contralateral (control) dorsal lateral geniculate nucleus (dLGN). Values are mean  $\pm$  SEM. p53 deficiency caused significant ( $*P < 0.05$ ) protection against apoptosis of LGN neurons.

mouse, the neurodegeneration in the LGN after occipital cortex ablation is also apoptosis, as shown here. This study was undertaken to begin to identify the genetic and molecular regulation of neuronal apoptosis in vivo induced by axonal injury and target deprivation. Retrograde degeneration of neurons may occur in human adult-onset neurodegenerative disease, including Alzheimer's disease and motor neuron disease (Saper et al., 1985; German et al., 1987; Pearson and Powell, 1989; Martin et al., 1998), and also in human brain trauma, notably in thalamus (Adams et al., 2000). Our results extend our understanding of the in vivo mechanisms neuronal apoptosis in the adult brain by demonstrating that it requires Bax and is modulated by p53. Cortical damage-induced, retrograde neuronal apoptosis in thalamus occurs in association with nuclear sequestration and activation of p53, perikaryal accumulation of Bax, as well as induction and activation of caspase-3 (Fig. 10). Interestingly, however, this neuronal apoptosis may occur by both p53-dependent and p53-independent mechanisms, but Bax is required for injury-induced apoptosis of neurons in adult thalamus.

p53 is altered during the progression of neuronal apoptosis in the LGN, leading to the suspicion that p53 participates in mechanisms of this neuronal death. We found that p53 accumulates in neuronal nuclei before apoptosis, and p53 protein levels increase transiently in nuclear extracts of LGN. This observation was extended by showing that p53 is functionally activated, as indicated by DNA-binding activity and p53 phosphorylation. However, the results gleaned by immunoblotting and DNA binding assay must be interpreted with some caution, because these observations are based on brain fractions of mixed neuron and glial cell populations. The more easily interpretable changes occur at 5 days postlesion. At 5 days, DNA binding activity is increased in the ipsilateral LGN and immunolocalization shows nuclear accumulation of

p53 in neurons. This p53 is activated because it is phosphorylated, as also shown by direct immunolocalization in neurons. At 6 day postlesion, the interpretation is more nebulous than at 5 days, because subsets of astroglial cells are immunopositive in ipsilateral and contralateral LGN at 6 days. This change most likely signifies astroglial

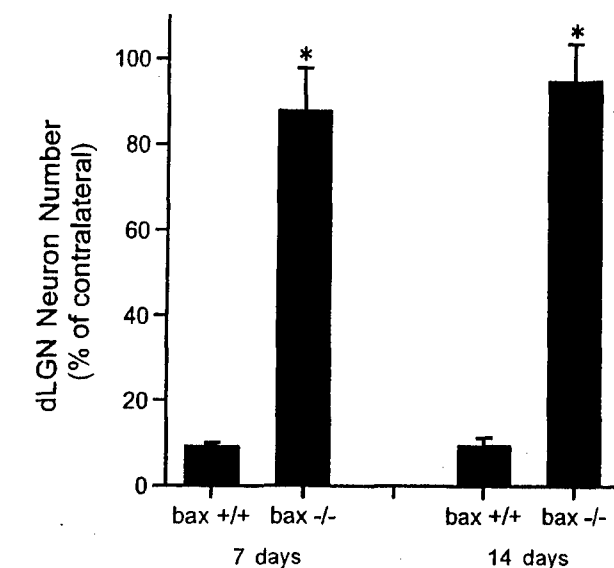
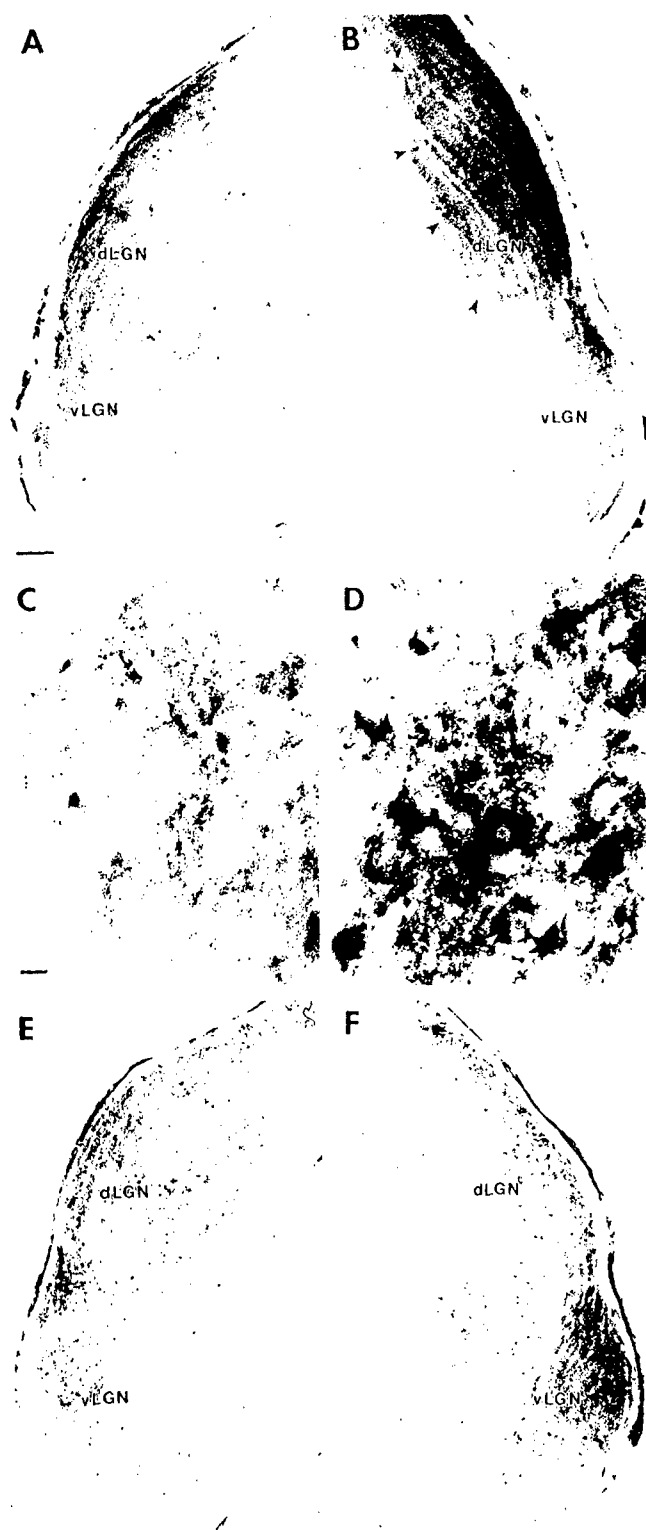


Fig. 9. Neuronal apoptosis in thalamus after cortical damage requires Bax. Occipital cortex lesions were done on *bax*<sup>+/+</sup> (wild type, *n* = 20) and *bax*<sup>-/-</sup> mice (*n* = 16) that were survived for 7 and 14 days. Neurons were counted in the ipsilateral and contralateral (control) dorsal lateral geniculate nucleus (dLGN). Values are mean  $\pm$  SEM. Bax deficiency completely blocked the apoptosis of dLGN neurons, and this effect was sustained (\**P* < 0.05).

activation, even in the unlesioned LGN. p53 functions in the elimination and repair of cells that have sustained DNA damage. The accumulation of p53 in different types of cells (neurons versus glia) within the LGN may reflect similar or different cellular events. p53 accumulation in LGN neurons most likely signifies DNA damage-induced apoptosis, because these neurons are terminally differentiated. In contrast, p53 induction in astroglia may signify metabolic activation and DNA damage-induced cell cycle/growth arrest, possibly to allow for repair of damaged DNA, or it may signify apoptosis of subsets of astroglial cells.

We have identified previously three structural stages of neuronal apoptosis *in vivo* (Al-Abdulla et al., 1998; Al-Abdulla and Martin, 1998; Martin et al., 1999). After axotomy and target deprivation, neurons pass consecutively through chromatolysis, somatodendritic shrinkage, and apoptosis. We have hypothesized that some yet to be identified key events associated with DNA damage occur during chromatolysis that commit neurons to apoptosis (Al-Abdulla et al., 1998; Al-Abdulla and Martin, 1998;

Fig. 8. p53 deficiency attenuates changes in Bax localization in the lateral geniculate nucleus (LGN) after cortical lesions. In *p53*<sup>+/+</sup> mice at 5 days postlesion (A–D), Bax immunoreactivity is elevated in the ipsilateral dorsal LGN (B, dLGN) compared with the contralateral dLGN (A), but staining is unaltered in the ventral LGN (vLGN). Bax immunoreactivity markedly accumulates in neurons (D, asterisks) at perinuclear locations (D, white arrowheads) in the ipsilateral dLGN, while much fainter Bax immunoreactivity is observed in the contralateral dLGN (C). E, F: In *p53*<sup>-/-</sup> mice, Bax immunostaining is similar in the ipsilateral (F) and contralateral (E) dLGN at 5 days postlesion. Scale bars = 120  $\mu$ m in A (applies to A, B, E, F); 10  $\mu$ m in C (applies to C, D).

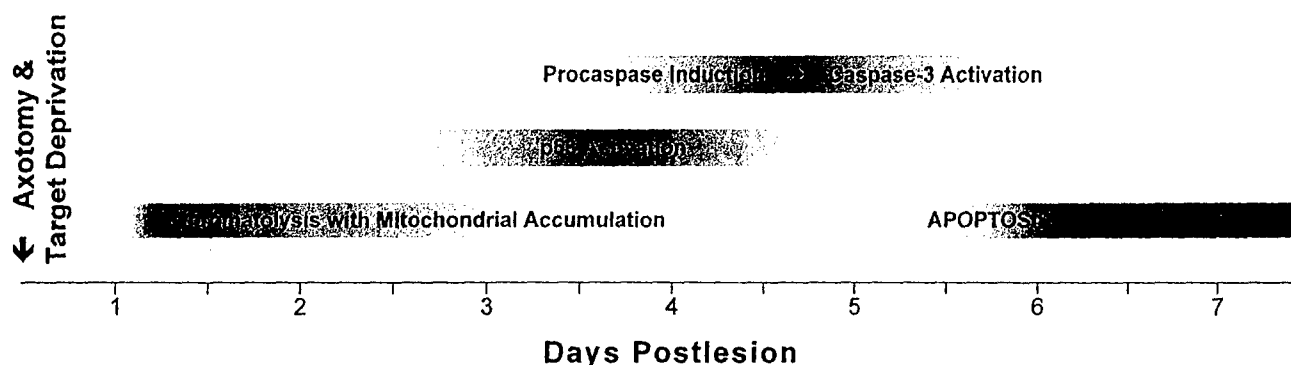


Fig. 10. Diagrammatic representation of the tentative time course of major events associated with injury-induced apoptosis of neurons within the adult brain after cortical injury. Ablation of the occipital cortex (a form of axotomy and target deprivation) induces thalamic neurons in the dorsal lateral geniculate nucleus (dLGN) to undergo apoptosis at 6–7 days postlesion (Al-Abdulla et al., 1998; Al-Abdulla

and Martin, 1998). This apoptosis is Bax-dependent and involves caspase-3 activation as downstream mechanisms. The upstream mechanisms seem to be p53-dependent and p53-independent and may involve activation of nuclear DNA-damage signaling pathways (Al-Abdulla and Martin, 1998) in response to oxidative stress during chromatolysis.

Martin et al., 1999). This fate contrasts with other models of axonal injury that induce chromatolysis followed by recovery, rescue, and regeneration of neurons (Martin et al., 1998). In our cortical ablation model, the nuclear accumulation and activation of p53 occurs during the chromatolytic stage of retrograde neuronal apoptosis at 3 to 5 days postlesion and, thus, is possibly a key signal for the transition of chromatolytic dLGN neurons into apoptosis (Fig. 10).

Increased levels of p53 result primarily from increased stability of the protein (Levine, 1997). In unstressed cells, the level of p53 protein is low. The half-life of p53 is short (~5–20 minutes) due to rapid degradation. p53 protein levels can be increased when the half-life of the protein is extended due to diminished degradation. Inhibition of the 26S proteasome increases p53 levels (Maki et al., 1996). Alternatively, p53 levels can be increased because the rate of initiation of p53 mRNA translation is enhanced (Levine, 1997). p53 exists in a latent, inactive form that requires modification to become active. DNA damage can activate p53 (Levine, 1997). Increases in p53 levels are proportional to the extent of DNA damage, with several different types of DNA lesions being potent signals for p53 activation, including double- and single-strand breaks and adduct formation (Levine, 1997). In a different model of axonal injury-induced neuronal apoptosis, we have found that DNA single-strand breaks are formed at preapoptotic stages of degeneration (Liu and Martin, 2001). The induction and activation of p53 in LGN neurons undergoing apoptosis is consistent with early DNA damage as an upstream mechanism of neuronal apoptosis (Al-Abdulla and Martin, 1998).

p53 functions as a DNA transcription factor (Vogelstein and Kinzler, 1992; Miyashita et al., 1994; Miyashita and Reed, 1995; Levine, 1997). The carboxyl terminus of p53 is important for controlling p53-DNA binding functions in response to single strands of DNA (Jayaraman and Prives, 1995). Therefore, to determine whether there is a corresponding increase in transcription factor activity of p53, two experiments were performed. At 5 days after cortical damage, p53-DNA binding activity and nuclear accumulation of phosphorylated p53 are increased markedly in the ipsilateral LGN, indicating that the p53 is activated

functionally. By binding to promoters, p53 activates the transcription of many genes. Promoters that respond to p53 include genes encoding proteins associated with growth control and cell cycle checkpoints (e.g., p21<sup>Waf1/Cip1</sup>, Gadd45, Mdm2, PCNA, cyclin D1, and cyclin G) and apoptosis (e.g., Bax, Bcl-2, Bcl-x<sub>L</sub>, and Fas). *Bax* (Miyashita and Reed, 1995) and redox-related genes (Polyak et al., 1997) are key transcriptional targets of p53 with regard to neuronal apoptosis. These genes are relevant to LGN neuron degeneration because this neuronal death is apoptosis and these neurons sustain oxidative damage to DNA (Al-Abdulla and Martin, 1998). In this study, we identified a direct relationship between p53 and Bax. In mice with functional p53, Bax immunoreactivity accumulates in neurons undergoing apoptosis in the LGN, but in mice deficient in p53, the Bax accumulation is attenuated.

We found that loss of p53 function by targeted mutation of the p53 gene attenuated significantly the magnitude of neuronal death. Other *in vivo* studies have shown that loss of p53 function is neuroprotective in paradigms of irradiation (Wood and Youle, 1995), kainate-induced seizures (Morrison et al., 1996), and focal ischemia (Crumrine et al., 1994). Thus, we document for the first time that p53 modulates axotomy/target deprivation-induced apoptosis of neurons *in vivo*. This modulation of apoptosis may occur in part through regulation of Bax levels. However, p53 deficiency does not completely rescue LGN neurons from apoptosis, as does Bax deficiency. Thus, p53 modulates neuronal death, and Bax functions downstream of p53 in this model of neuronal apoptosis *in vivo*. This modulation of apoptosis may stem from p53 having DNA repair functions as well as proapoptotic functions. Therefore, it is evident from the partial rescue that this form of neuronal apoptosis can also occur independent of p53 as well. A similar attenuation of neuronal apoptosis occurs in p53-deficient mice after adrenalectomy (Sakhi et al., 1996). Because apoptosis of LGN neurons can occur in the absence of functional p53, changes in p53 during the chromatolytic stage of retrograde neuronal apoptosis cannot be solely the key signal for commitment of chromatolytic LGN neurons to apoptosis (Fig. 10). Granule cells in cerebellum can undergo apoptosis that is p53-dependent

and p53-independent, depending on the initiating stimulus that triggers DNA damage (Wood and Youle, 1995). Based on our observations, it is likely that both p53-dependent and p53-independent pathways for apoptosis are operative in the death mechanisms of LGN neurons. Therefore, further studies must be conducted to identify the signals upstream from Bax that modify the commitment of neurons to apoptosis in thalamus after cortical injury.

Because deletion of the p53 gene protects only partially against neuronal apoptosis within the brain, the nuclear sequestration and activation of p53 are not absolute requirements for the progression of apoptosis in all dLGN neurons. However, it is noteworthy that two genes (p73 and p63) have been identified that have significant sequence homology to p53 (Mills et al., 1999). These p53 homologues may participate in the mechanisms of neuronal apoptosis in the absence of p53. p73 can activate p53-responsive promoters and can induce apoptosis when overexpressed in p53-deficient tumor cells (Fang et al., 1999). p63 isoforms contain transactivation domains that can transactivate p53 reporter genes and induce apoptosis (White and Prives, 1999). Deletion of p73 seems to have greater effects in the nervous system compared with p53 (Yang et al., 2000). Therefore, in the absence of p53, the possible contributions of p73 and p63 in neuronal apoptosis need to be explored.

We found that apoptosis of LGN neurons requires Bax. This conclusion is based on the finding the LGN neurons in Bax-deficient mice do not undergo apoptosis after occipital cortex ablation. By extending the postlesion survival time, we found that the rescue of neurons is sustained. Other experiments have shown that Bax is required for peripheral neuron death after neurotrophin withdrawal in vitro and neonatal facial motor neurons after axotomy (Deckwerth et al., 1996). Bax deficiency blocks apoptosis of cerebellar cultured granule neurons induced by low potassium (Miller et al., 1997). Bax is important also for developmental PCD of neurons (Deckwerth et al., 1996). However, our study demonstrates, for the first time, that axotomy/target deprivation-induced retrograde neuronal death within the adult CNS is Bax-dependent apoptosis and that the Bax accumulation is dependent on the presence of the functional p53 gene. The Bax accumulation coincides with our previous demonstration that mitochondria accumulate in a perinuclear location at 3 to 5 days postlesion (Fig. 10; Al-Abdulla and Martin, 1998). The perikaryal accumulation of both Bax and mitochondria in neurons undergoing apoptosis in vivo is consistent with cell culture experiments showing that redistribution of Bax to mitochondria is a critical early step in the promotion of apoptosis by Bax (Wolter et al., 1997; Putcha et al., 1999).

Bax is a member of the *Bcl-2* protooncogene family (Merry and Korsmeyer, 1997). Bax is thought to function by forming channels in mitochondrial membranes (Antonsson et al., 1997). When active, these channels may allow the release of cytochrome c from mitochondria to the cytosol. In neuronal cell culture, Bax-dependent, caspase-3 activation is a key determinant in p53-induced apoptosis (Cregan et al., 1999). Other cell culture models of apoptosis show that activation of caspase-3 occurs when caspase-9 proenzyme is bound by apoptotic protease-activating factor-1 (Apaf-1) in a process initiated by cytochrome c and either ATP or dATP (Liu et al., 1996; Li et

al., 1997). Apaf-1, a 130-kD protein, serves as a docking protein for procaspase-9 and cytochrome c (Li et al., 1997). Apaf-1 becomes activated with the binding and hydrolysis of ATP and the binding of cytochrome c, promoting Apaf-1 oligomerization (Zou et al., 1999). This oligomeric complex recruits and activates procaspase-9, and active caspase-9 disassociates from the complex and becomes available to activate caspase-3.

Our in vivo study of LGN neuron apoptosis is also important because we found changes in caspase-3. A large increase in procaspase-3 levels occurs at 4 days postlesion, suggesting a transcriptional/translational event, and then a prominent activation of caspase-3 occurs at 5 days postlesion, indicating a posttranslational proteolytic event. Caspase-3 is activated constitutively in the LGN, consistent with other studies in brain (Mooney and Miller, 2000). Constitutive levels of active caspase-3 in CNS extracts may reflect glial cell turnover. Interestingly, the level of activated caspase-3 decreased in the contralateral LGN at 5 days postlesion. This change seems to coincide with p53 accumulation in subsets of astroglia and their morphologic activation, thus, decreased levels of active caspase-3 mirror astrogliosis. In contrast, the enhanced activation of caspase-3 or maintenance of constitutive levels of active caspase-3 in the ipsilateral LGN coincides with the neuronal accumulation of p53 and Bax proteins and neuronal apoptosis. In the ipsilateral LGN, it is possible that active caspase-3 decreases in the glial cell compartment undergoing reactive changes and increases in the neuronal compartment undergoing apoptosis. Unfortunately, we did not do immunolocalization experiments with the caspase-3 antibody used here, because the results would not be clearly interpretable because this antibody, like most caspase-3 antibodies available, detects both the proenzyme and the active subunit. The changes in caspase-3 that we found by immunoblotting in our model of neuronal apoptosis with the adult brain are consistent with studies showing that activation of caspase-3 participates in the mechanisms of retinal ganglion neuron death after optic nerve transection (Kermer et al., 1998, 1999). Once activated, caspase-3 cleaves a protein with DNase activity (DFF-45), and this cleavage activates a pathway leading to the fragmentation of genomic DNA. We have identified dLGN neurons undergoing nuclear DNA fragmentation at 6 and 7 days postlesion (Al-Abdulla et al., 1998; Al-Abdulla and Martin, 1998).

The key findings of this study are that neuronal apoptosis in the adult CNS is modulated by p53 and requires Bax. These findings are consistent with work in other, mostly in vitro, models of neuronal death. Our work is nevertheless novel and important because we used an adult in vivo CNS model system of neuronal apoptosis. We found many consistencies with in vitro paradigms. Considering the vast differences in neuroanatomic and cellular complexity, the identification of several common neuronal death signaling pathways in in vitro and in vivo systems is unusual and exciting, because this is not always the case. For example, different results have been observed among in vivo and in vitro neuronal excitotoxicity models (Portera-Cailliau et al., 1997). Our model of cortical damage-induced retrograde neuronal apoptosis is relevant to acute neurologic disorders in human, such as traumatic and ischemic brain damage (Adams et al., 2000), and adult-onset neurodegenerative diseases in human (Martin et al., 2000a). The identification of the ge-

netic and molecular basis of neuronal death in vivo is essential, because ultimately, it is much more appropriate to test new therapies for neuroprotection in relevant in vivo systems compared with in vitro systems.

## ACKNOWLEDGMENTS

We thank Ms. Ann Price and Mr. Frank Barksdale for their expert technical assistance.

## LITERATURE CITED

- Adams JH, Graham DI, Jennett B. 2000. The neuropathology of the vegetative state after an acute brain insult. *Brain* 123:1327-1338.
- Agarwala S, Kalil RE. 1998. Axotomy-induced neuronal death and reactive astrogliosis in the lateral geniculate nucleus following a lesion of the visual cortex in the rat. *J Comp Neurol* 392:252-263.
- Al-Abdulla NA, Martin LJ. 1998. Apoptosis of retrogradely degenerating neurons occurs in association with the accumulation of perikaryal mitochondria and oxidative damage to the nucleus. *Am J Pathol* 153:447-456.
- Al-Abdulla NA, Portera-Cailliau C, Martin LJ. 1998. Occipital cortex ablation in adult rat causes retrograde neuronal death in the lateral geniculate nucleus that resembles apoptosis. *Neuroscience* 86:191-209.
- Anderson AJ, Su JH, Cotman CW. 1996. DNA damage and apoptosis in Alzheimer's disease: colocalization with c-jun immunoreactivity, relationship to brain area, and effect of postmortem delay. *J Neurosci* 16:1710-1719.
- Antonsson B, Conti F, Ciavatta A, Montessuit S, Lewis S, Martinou I, Bernasconi L, Bernard A, Mermoud J-J, Mazzei G, Maundrell K, Gambale F, Sadoul R, Martinou J-C. 1997. Inhibition of bax channel-forming activity by bcl-2. *Science* 277:370-372.
- Arends MJ, Morris RG, Wyllie AH. 1990. Apoptosis: the role of endonuclease. *Am J Pathol* 136:593-608.
- Calhoun ME, Jucker M, Martin LJ, Thinakaran G, Price DL, Mouton PR. 1996. Comparative evaluation of synaptophysin-based methods for quantification of synapses. *J Neurocytol* 25:821-828.
- Cregan SP, MacLaurin JG, Craig CG, Robertson GS, Nicholson DW, Park DS, Slack RS. 1999. Bax-dependent caspase-3 activation is a key determinant in p53-induced apoptosis in neurons. *J Neurosci* 19:7860-7869.
- Crumrine RC, Thomas AL, Morgan PF. 1994. Attenuation of p53 expression protects against focal ischemic damage in transgenic mice. *J Cereb Blood Flow Metab* 14:887-891.
- Deckwerth TL, Elliott JL, Knudson CM, Johnson EM Jr, Snider WD, Korsmeyer SJ. 1996. Bax is required for neuronal death after trophic factor deprivation and during development. *Neuron* 17:401-411.
- Fang L, Lee SW, Aaronson SA. 1999. Comparative analysis of p73 and p53 regulation and effector functions. *J Cell Biol* 147:823-830.
- Glücksmann A. 1951. Cell deaths in normal vertebrate ontogeny. *Biol Rev* 26:59-86.
- German DC, White CL, Sparkman DR. 1987. Alzheimer's disease: neurofibrillary tangles in nuclei that project to the cerebral cortex. *Neuroscience* 21:305-312.
- Hakem R, Hakem A, Duncan GS, Henderson JT, Woo M, Soengas MS, Elia A, de la Pompa JL, Kagi D, Khoo W, Potter J, Yoshida R, Kaufman SA, Lowe SW, Penninger JM, Mak TW. 1998. Differential requirement for caspase 9 in apoptotic pathways in vivo. *Cell* 94:339-352.
- Jayaraman L, Prives C. 1995. Activation of p53 sequence-specific DNA binding by short single strands of DNA requires the p53 C-terminus. *Cell* 81:1021-1029.
- Kermer P, Klöcker N, Labes M, Bähr M. 1998. Inhibition of CPP-32-like proteases rescues axotomized retinal ganglion cells from secondary cell death in vivo. *J Neurosci* 18:4656-4662.
- Kermer P, Klöcker N, Labes M, Thomsen S, Srinivasan A, Bähr M. 1999. Activation of caspase-3 in axotomized rat ganglion cell in vivo. *FEBS Lett* 453:361-364.
- Kerr JFR, Harmon BV. 1991. Definition and incidence of apoptosis: an historical perspective. In: Tomei LD, Cope FO, editors. *Apoptosis: the molecular basis of cell death*. Cold Spring Harbor, NY: Cold Spring Harbor Laboratory Press. p 5-29.
- Kitamura Y, Taniguchi T, Shimohama S. 1999. Apoptotic cell death in neurons and glial cells: implications for Alzheimer's disease. *Jpn J Pharmacol* 79:1-5.
- Kuida K, Zheng TS, Na S, Kuan C-Y, Yang D, Karasuyama H, Rakic P, Flavell RA. 1996. Decreased apoptosis in the brain and premature lethality in CPP32-deficient mice. *Nature* 384:368-372.
- Lefebvre S, Burglen L, Reboullet S, Clermont O, Burlet P, Viollet L, Benichou B, Cruaud C, Millasseau P, Zeviani M, LePaslier D, Frezal J, Cohen D, Weissenbach J, Munnich A, Melki J. 1995. Identification and characterization of a spinal muscular atrophy-determining gene. *Cell* 80:155-165.
- Levine AJ. 1997. p53, the cellular gatekeeper for growth and division. *Cell* 88:323-331.
- Li P, Nijhawan D, Budihardjo I, Srinivasula SM, Ahmad M, Alnemri ES, Wang X. 1997. Cytochrome c and dATP-dependent formation of Apaf-1/caspase-9 complex initiates an apoptotic protease cascade. *Cell* 91:479-489.
- Liu X, Kim CN, Yang J, Jemmerson R, Wang X. 1996. Induction of apoptotic program in cell-free extracts: requirement for dATP and cytochrome c. *Cell* 86:147-157.
- Liu XZ, Xu XM, Hu R, Du C, Zhang SX, McDonald JW, Dong HX, Wu YJ, Fan GS, Jacquin MF, Hsu CH, Choi DW. 1997. Neuronal and glial apoptosis after traumatic spinal cord injury. *J Neurosci* 17:5395-5406.
- Liu Z, Martin LJ. 2001. Motor neurons rapidly accumulate DNA single-strand breaks after in vitro exposure to nitric oxide and peroxynitrite and in vivo axotomy. *J Comp Neurol* 432:35-60.
- MacManus JP, Rasquinha I, Tuor U, Preston E. 1997. Detection of higher-order 50- and 10-kbp DNA fragments before apoptotic internucleosomal cleavage after transient cerebral ischemia. *J Cereb Blood Flow Metab* 17:376-387.
- Maki CG, Huibregtse JM, Howley PM. 1996. In vivo ubiquitination and proteasome-mediated degradation of p53. *Cancer Res* 56:2649-2654.
- Martin LJ. 1999. Neuronal death in amyotrophic lateral sclerosis is apoptosis: possible contribution of a programmed cell death mechanism. *J Neuropathol Exp Neurol* 58:459-471.
- Martin LJ. 2000. p53 is abnormally elevated and active in the CNS of patients with amyotrophic lateral sclerosis. *Neurobiol Dis* 7:613-622.
- Martin LJ, Al-Abdulla NA, Brambrink AM, Kirsch JR, Sieber FE, Portera-Cailliau C. 1998. Neurodegeneration in excitotoxicity, global cerebral ischemia, and target deprivation: a perspective on the contributions of apoptosis and necrosis. *Brain Res Bull* 46:281-309.
- Martin LJ, Kaiser A, Price AC. 1999. Motor neuron degeneration after sciatic nerve avulsion in adult rat evolves with oxidative stress and is apoptosis. *J Neurobiol* 40:185-201.
- Martin LJ, Price AC, Kaiser A, Shaikh AY, Liu Z. 2000a. Mechanisms for neuronal degeneration in amyotrophic lateral sclerosis and in models of motor neuron death. *Int J Mol Med* 5:3-13.
- Martin LJ, Sieber FE, Traystman RJ. 2000b. Apoptosis and necrosis occur in separate neuronal populations in hippocampus and cerebellum after ischemia and are associated with differential alterations in metabotropic glutamate signaling pathways. *J Cereb Blood Flow Metab* 20:153-167.
- Merry DE, Korsmeyer SJ. 1997. Bcl-2 gene family in the nervous system. *Annu Rev Neurosci* 20:245-267.
- Mills AA, Zheng B, Wang XJ, Vogel H, Roop DR, Bradley A. 1999. p63 is a p53 homologue required for limb and epidermal morphogenesis. *Nature* 398:708-713.
- Miller TM, Moulder KL, Knudson CM, Creedon DJ, Deshmukh M, Korsmeyer SJ, Johnson EM Jr. 1997. Bax deletion further orders the cell death pathway in cerebellar granule cells and suggests a caspase-independent pathway to cell death. *J Cell Biol* 139:205-217.
- Miyashita T, Reed JC. 1995. Tumor suppressor p53 is a direct transcriptional activator of the human bax gene. *Cell* 80:293-299.
- Miyashita T, Krajewski S, Krajewska M, Wang HG, Lin HK, Liebermann DA, Hoffman B, Reed JC. 1994. Tumor suppressor p53 is a regulator of Bcl-2 and bax gene expression in vitro and in vivo. *Oncogene* 9:1799-1805.
- Mooney SM, Miller MW. 2000. Expression of Bcl-2, Bax, and caspase-3 in the brain of the developing rat. *Brain Res Dev Brain Res* 123:103-117.
- Morrison RS, Wenzel HJ, Kinoshita Y, Robbins CA, Donehower LA, Schwartzkroin PA. 1996. Loss of the p53 tumor suppressor gene protects neurons from kainate-induced cell death. *J Neurosci* 16:1337-1345.

- Oppenheim RW. 1991. Cell death during development of the nervous system. *Annu Rev Neurosci* 14:453-501.
- Pearson RCA, Powell TPS. 1989. The neuroanatomy of Alzheimer's disease. *Rev Neurosci* 2:101-120.
- Polyak K, Xia Y, Zweier JL, Kinzler KW, Vogelstein B. 1997. A model for p53-induced apoptosis. *Nature* 389:300-305.
- Portera-Cailliau C, Price DL, Martin LJ. 1997. Non-NMDA and NMDA receptor-mediated excitotoxic neuronal deaths in adult brain are morphologically distinct: further evidence for an apoptosis-necrosis continuum. *J Comp Neurol* 378:88-104.
- Putcha GV, Deshmukh M, Johnson EM Jr. 1999. Bax translocation is a critical event in neuronal apoptosis: regulation by neuroprotectants, Bcl-2, and caspases. *J Neurosci* 19:7476-7485.
- Roy N, Mahadevan MS, McLean M, Shutler G, Yaraghi Z, Farahani R, Baird S, Besner-Johnston A, Lefebvre C, Kang X, Salih M, Aubry H, Tamai K, Guan X, Ioannou P, Crawford TO, de Jong PJ, Surh L, Ikeda J-E, Korneluk RG, Mackenzie A. 1995. The gene for neuronal apoptosis inhibitory protein is partially deleted in individuals with spinal muscular atrophy. *Cell* 80:167-178.
- Sakhi S, Gilmore W, Tran ND, Schreiber SS. 1996. p53-deficient mice are protected against adrenalectomy-induced apoptosis. *Neuroreport* 8:233-235.
- Saper CB, German DC, White CL. 1985. Neuronal pathology in the nucleus basalis and associated cell groups in senile dementia of the Alzheimer's type: possible role in cell loss. *Neurology* 35:1089-1095.
- Vogelstein B, Kinzler KW. 1992. p53 function and dysfunction. *Cell* 70:523-536.
- White E, Prives C. 1999. DNA damage enables p73. *Nature* 399:734-737.
- Wolter KG, Hsu Y-T, Smith CL, Nechushtan A, Xi X-G, Youle RJ. 1997. Movement of Bax from the cytosol to mitochondria during apoptosis. *J Cell Biol* 139:1281-1292.
- Wood KA, Youle RJ. 1995. The role of free radicals and p53 in neuron apoptosis in vivo. *J Neurosci* 15:5851-5857.
- Yang A, Walker N, Bronson R, Kaghad M, Oosterwegel M, Bonnin J, Vagner C, Bonnet H, Dikkes P, Sharpe A, McKeon F, Caput D. 2000. p73-deficient mice have neurological, pheromonal and inflammatory defects but lack spontaneous tumors. *Nature* 404:99-103.
- Zou H, Li Y, Liu X, Wang X. 1999. An Apaf-1-cytochrome *c* multimeric complex is a functional apoptosome that activates procaspase-9. *J Biol Chem* 274:11549-11556.



## Axonal Transection in Adult Rat Brain Induces Transsynaptic Apoptosis and Persistent Atrophy of Target Neurons

STEPHEN D. GINSBERG<sup>1,\*</sup> and LEE J. MARTIN<sup>1,2</sup>

### ABSTRACT

We used the fimbria-fornix (FF) transection model of axonal injury to test the hypothesis that transneuronal degeneration occurs in the adult central nervous system in response to deafferentation. The medial mammillary nucleus, pars medialis (MMNm) was analyzed by light and electron microscopy at 3, 7, 14, and 30 days, and 6 months after unilateral FF transection in adult rat to identify the time course of neuronal responses in a remote target. Presynaptic terminals and neuronal cell bodies degenerated in the MMNm ipsilateral to FF transection. Terminal degeneration occurred predominantly at 3 and 7 days postlesion. Between 14 and 30 days postlesion, neuronal number in the MMNm decreased (~20%). Two forms of neuronal degeneration were found in the MMNm after deafferentation. Some neurons died apoptotically. Other neurons underwent vacuolar degeneration. In these latter neurons, somatodendritic pathology occurred at 14 and 30 days and 6 months postlesion. The ultrastructure of this vacuolar degeneration was characterized by disorganization of the cytoplasm, formation of membrane-bound vacuolar cisternae and membranous inclusions, loss of organelles, cytoplasmic pallor, and chromatin alterations. This study shows that both anterograde axonal degeneration and transneuronal degeneration occur in a fornical target after FF axon transection. This transneuronal degeneration can be classified as sustained neuronal atrophy or transsynaptic apoptosis.

**Key words:** afferent-derived trophic support; apoptosis; axotomy; deafferentation; mammillary nucleus; transneuronal injury; traumatic brain injury; fimbria-fornix

### INTRODUCTION

**H**EAD TRAUMA is a leading cause of neurologic disability in children and adults (Adams et al., 1982). White matter damage is a frequent consequence of head trauma in humans (Adams et al., 1982) and experimental animals (Erb and Povlishock, 1988; Maxwell et al., 1997; Povlishock and Jenkins, 1995). Axons are very sensitive to trauma. Axons are transected acutely after severe injury, and they also undergo nondisruptive injury

that culminates in delayed secondary axotomy (Maxwell et al., 1997). In human traumatic brain injury, this secondary axotomy is believed to be more prominent than direct axonal transection (Maxwell et al., 1997). Damage to white matter bundles can cause neurodegeneration in remote locations and functional deficits. Axonal afferent-target disconnection can develop within hours after the trauma (Povlishock and Jenkins, 1995). However, the structure of remote degeneration of target regions after axonal injury is incompletely characterized and the mech-

The <sup>1</sup>Department of Pathology, Division of Neuropathology, and the <sup>2</sup>Department of Neuroscience, Johns Hopkins University School of Medicine, Baltimore, Maryland.

\*Current address: Nathan Kline Institute, Department of Psychiatry, New York University School of Medicine.

anisms of target degeneration after afferent axotomy are not understood. Traumatic injury to axons can activate molecular mechanisms associated with necrosis and apoptosis (Graham et al., 2000). Apoptotic mechanisms are activated directly in axons (Büki et al., 2000), but the responses of neurons in target regions of damaged axons have not been evaluated.

Appropriate model systems need to be developed to understand the relationships between neurodegeneration in targets and injury to afferent axons. The mammillary body is a diencephalic component of the limbic system Papez circuit (Papez, 1937), which is believed to be critical for learning, memory, and emotive responses (Amaral, 1987; MacLean, 1952). This nucleus receives synaptic afferents from the hippocampal formation and tegmental brainstem nuclei, and in turn, relays signals to the anterior thalamic nuclei and cingulate cortex. The mammillary body is a group of nuclei divisible into medial and lateral subdivisions based upon cytoarchitecture and innervation from the postcommissural fornix (Allen and Hopkins, 1988; Krieg, 1932; Nauta and Haymaker, 1969; Rose, 1939). The mammillary body receives its major forebrain afferents from subicular neurons via the fimbria-fornix (FF) system (Allen and Hopkins, 1989; Canteras et al., 1992; Namura et al., 1994; Swanson and Cowan, 1975), with the subiculomammillary projection coursing topographically through the postcommissural fornix and terminating predominantly in the medial mammillary nucleus (MMN). Fornical lesions can cause memory impairments in human, monkey, and rat (Gaffan and Gaffan, 1991; Mahut, 1972; Moudgil et al., 2000; Saunders and Weiskrantz, 1989; Tonkiss and Rawlins, 1992). Mammillary body degeneration occurs in individuals with Korsakoff's syndrome, with this neuropathology differing from that seen in temporal lobe amnesias (Mair et al., 1979; Squire et al., 1990); furthermore, magnetic resonance imaging has identified a reduction in mammillary body size during aging (Raz et al., 1992).

After FF transection, anterograde degeneration of axotomized subicular terminals occurs within the mammillary body, notably the MMN, as demonstrated by light microscopy (Guillery, 1956; Nauta, 1956). Furthermore, transneuronal degeneration of MMN neurons after cortical ablation (including damage to the hippocampus and limbic cortex) and FF transection was described originally by Gudden (1880) and was found by light microscopy in several species, especially when lesions are made in the immature brain (Allen, 1944; Bleier, 1969). This neuropathology may be a form of deafferentation-induced neuronal degeneration. However, the effects of FF transection on the survival and structure of mammillary neurons of adult rat brain have not been evaluated. The present study was undertaken to characterize early

and delayed cellular and subcellular pathology within the MMN after transection of the FF in adult rat. The MMNm was evaluated for anterograde degeneration, and potential transneuronal degeneration.

## MATERIALS AND METHODS

### *Axonal pathway lesion model*

Adult (150–200 g) male Sprague-Dawley rats (Charles River, Wilmington, MA;  $n = 64$ ) were used. The Animal Care and Use Committee of the Johns Hopkins University School of Medicine approved the animal protocol. Rats were anesthetized with a mixture of enflurane/oxygen/nitrous oxide (1:33:66) and placed in a stereotaxic apparatus. After a midline scalp incision, a 1.5-mm-wide craniotomy centered ~1.0 mm caudal to bregma and 1.0 mm lateral to the midline was performed. After the overlying motor-sensory cortex and white matter were removed by aspiration, the FF was transected, avoiding damage to the anterior thalamic nuclei, septal nuclei, and rostral pole of the hippocampus (Ginsberg and Martin, 1998; Ginsberg et al., 1996, 1999). To control for effects of the surgical manipulation not related to the FF transection, a control cerebral cortex/corpus callosum aspiration (CC) lesion was performed at the same rostrocaudal level as the FF transection. Rats that did not undergo surgery served as normal controls.

### *Brain preparation for light microscopy*

Four short-term time points (3, 7, 14, and 30 days postlesion) and one longer term time point (6 months postlesion) were chosen for light and electron microscopic analyses. After the appropriate postlesion interval ( $n = 6$ –7 per time point for FF transection;  $n = 2$  per time point for CC lesions;  $n = 2$  untreated controls), rats were anesthetized with sodium pentobarbital (70 mg/kg, i.p.) and sacrificed by intraaortic perfusion with 1% paraformaldehyde in ice-cold phosphate buffer (0.12 M, pH 7.4) delivered by a perfusion pump (36 mL/min) for 1 min followed by 4% paraformaldehyde in ice-cold phosphate buffer for 20 min delivered at the same flow rate. Brains were removed from the skull, blocked in the coronal plane and postfixed in 4% paraformaldehyde for 2 h at 4°C. Tissue blocks were cryoprotected in 30% sucrose in phosphate buffer prior to being frozen in isopentane chilled by dry ice. A one in 12 series of 40- $\mu$ m-thick tissue sections throughout the forebrain, ranging from ~2.7 mm rostral to bregma to ~8.3 mm caudal to bregma (Paxinos and Watson, 1986), was stained with cresyl violet to evaluate the efficacy of the lesions and to delineate nuclear boundaries within the mammillary body

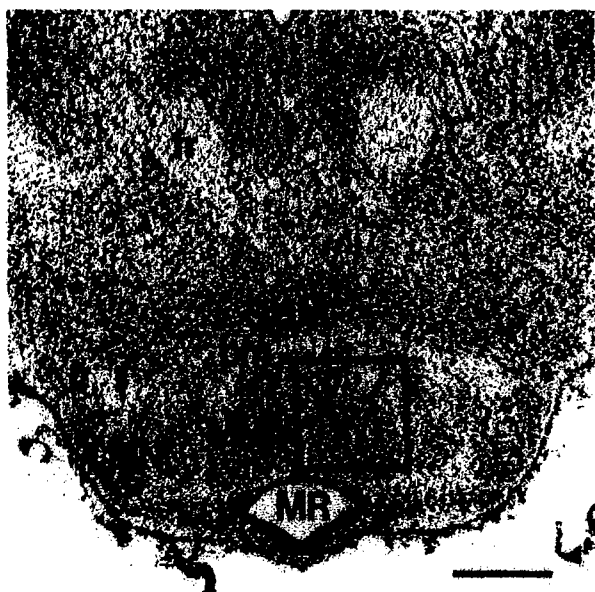


**FIG. 1.** Low-power photomicrograph of a Nissl-stained section through the mammillary complex of a control rat. The box delineates the region of the MMNm subdissected for electron microscopic evaluation. Bar = 500  $\mu$ m. f, postcommissural fornix; fr, fasciculus retroflexus; LMN, lateral mammillary nucleus; MMN, medial mammillary nucleus; MR, mammillary recess of the third ventricle; pm, principal mammillary tract; SUM, supramammillary nucleus.

(Fig. 1). Representative maps of Nissl-stained sections throughout the mammillary complex were created using a video-based imaging system (Ginsberg et al., 1995; Martin et al., 1993).

#### Cell counting

Coronal serial symmetrical sections (40  $\mu$ m) through the hypothalamus were cut using a sliding microtome. Serial sections from each rat brain were mounted on glass slides and stained with cresyl violet for neuronal counting. Neuronal counts in the ipsilateral and contralateral MMNm were made at  $\times 1,000$  magnification using the stereological optical fractionator method as described (Al-Abdulla et al., 1998; Calhoun et al., 1996). Neurons without apoptotic structural changes were counted using strict morphological criteria. These criteria included a round, open, pale nucleus (not condensed and darkly stained), granular Nissl staining of the cytoplasm, and a diameter of  $\sim 10$ – $20$   $\mu$ m. With these criteria, astrocytes, oligodendrocytes, and microglia were excluded from the counts. Neuronal counts were used to determine group means and variances and comparisons among groups were performed using a one-way analysis of variance and a Student's *t* test.

#### Brain preparation for electron microscopy

After the appropriate postlesion interval ( $n = 3$ – $4$  per time point for FF transection;  $n = 2$ – $3$  per time point for CC lesions;  $n = 2$  untreated controls), rats were anesthetized with sodium pentobarbital and vasodilated with 0.1% sodium nitrite in phosphate-buffered saline and anticoagulated with 0.1% heparin sodium in phosphate-buffered saline injected into the spleen. Rats were exsanguinated with 1% paraformaldehyde/0.1% glutaraldehyde in ice-cold phosphate buffer delivered intraaortically by a perfusion pump (36 mL/min) for 1 min followed by 2% paraformaldehyde/2% glutaraldehyde in ice-cold phosphate buffer delivered at the same flow rate for 25 min. Brains were left in the skull overnight in 1% paraformaldehyde/0.1% glutaraldehyde in phosphate buffer at 4°C.

The size and location of the FF transection or the CC lesion were evaluated grossly in coronal slabs and microscopically in Nissl-stained preparations of frozen sections processed throughout the lesion site. Microdissected samples from the MMNm (Fig. 1) for each postlesion time point were trimmed to  $\sim 4 \times 2 \times 2$  mm (length/width/depth), rinsed in phosphate buffer, placed in 2% osmium tetroxide for 2 h, dehydrated, and embedded in plastic. Mid-rostrocaudal mammillary samples were taken at the midline dorsal to the mammillary recess of the third ventricle, effectively excluding the lateral mammillary, tuberomammillary, and arcuate nuclei. Microdissected MMNm samples were processed at the same time for each postlesion time point to control for potential changes in osmophilia. The rostral face of each sample was notched prior to osmication, to ensure proper orientation for embedding. Semithin sections (1  $\mu$ m) and thin sections (gold interference color) were cut on an ultramicrotome (Sorvall, Norwalk, CT). A rostrocaudal survey was prepared by processing semithin and thin sections from multiple blocks at the five postlesion time points. Selected semithin sections were stained with 1% toluidine blue and selected thin sections were contrasted with uranyl acetate and lead citrate. Thin sections were viewed with a Phillips CM12 or a Jeol 100S electron microscope. The investigators were blind to the treatment conditions of the thin sections. Peters et al. (1991) was consulted for general CNS ultrastructure. In addition, the work of Allen and Hopkins (1988, 1989) was used specifically as references for MMNm ultrastructure.

## RESULTS

Transection of the FF interrupted fibers of the dorsal fornix and fimbria with no involvement of the anterior thalamic nuclei or the cingulate cortex, and relatively lit-

tle damage to the hippocampal formation, consistent with previous studies (Ginsberg and Martin, 1998; Ginsberg et al., 1996, 1999). The CC lesions damaged the motor-sensory cortex and corpus callosum, similar to the FF transection, but the FF was undamaged. These lesions did not directly damage the mammillary body, and there was no evidence for intracranial swelling and compression of the ventral surface of the brain.

The MMN is a distinct part of the mammillary complex (Guillery, 1956; Krieg, 1932; Nauta, 1956). The dorsal border is the principal mammillary tract and the supra-mammillary nucleus, the lateral border is the lateral mammillary nucleus and the postcommissural fornix, and the ventral border is the mammillary recess of the third ventricle (Fig. 1). The MMN is subdivided into the MMNm, MMN pars lateralis, and the MMN pars basalis based upon cell packing density (Allen and Hopkins, 1988; Krieg 1932). The MMNm has a relatively homogeneous population of densely packed, darkly stained neurons evenly distributed within both hemispheres. By light microscopy, no qualitative differences were discernable in the number of neurons in Nissl-stained sections and in 1  $\mu$ m-thick plastic sections of the ipsilateral and contralateral sides of the MMNm in rats with FF tran-

sections at 3, 7, 14, and 30 days and 6 months postlesion (Fig. 2A–D). However, detailed stereologic cell counting revealed a 20% loss of neurons in the ipsilateral MMNm at 30 days postlesion (Fig. 3A). At this time point, the contralateral MMNm contained  $51,900 \pm 10,500$  (mean  $\pm$  SD), while the ipsilateral MMNm contained  $41,520 \pm 13,575$ . This loss of neurons may be attributed to transsynaptic apoptosis in the MMNm because apoptotic profiles were identified in the ipsilateral MMNm (Figs. 3B and 4C).

Early axonal and/or terminal degeneration and progressive somatodendritic abnormalities after the lesion were identified in toluidine blue-stained semithin sections of the MMNm ipsilateral to the FF transection. Specifically, dark puncta were observed within the neuropil at 3 and 7 days postlesion, suggesting terminal degeneration, although little somatodendritic changes occurred at these early time points after the lesion (Fig. 2E). By 14 and 30 days postlesion, apparent terminal degeneration was less evident in the neuropil (Fig. 2F). Neuronal degeneration, however, was more apparent, as vacuoles were observed within the cell bodies and proximal dendrites (Fig. 2F). A few dark puncta were visible occasionally within the MMNm neuropil contralateral to the

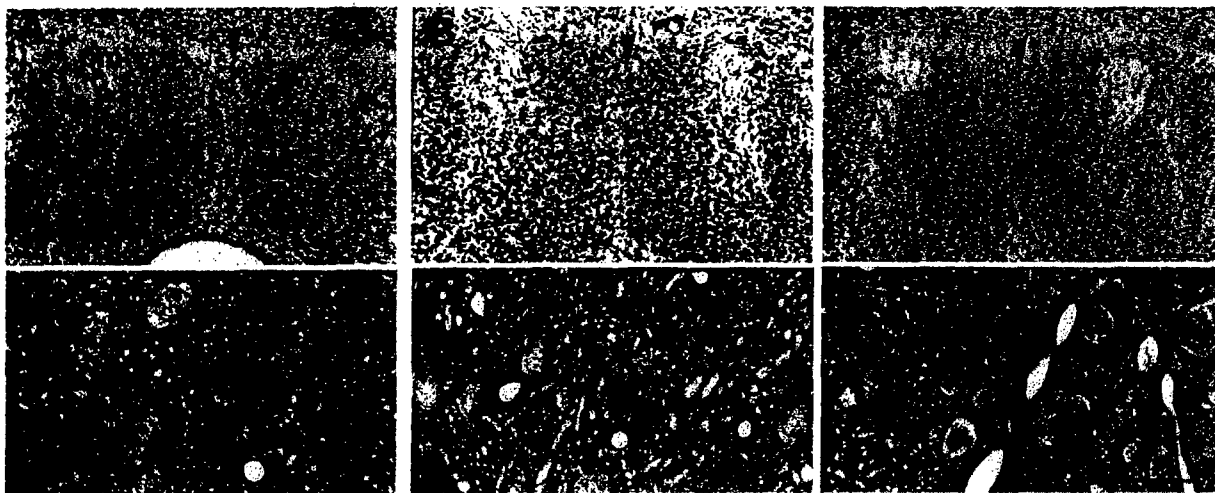


**FIG. 2.** Terminal degeneration and cellular alterations after unilateral FF transections and control CC lesions in Nissl-stained sections (A–C) and toluidine blue-stained 1- $\mu$ m-thick plastic sections (D–F) of the MMNm. The side ipsilateral to the FF and CC lesions is to the right for A–C. The arrowhead indicates the midline for A–C. MMN, medial mammillary nucleus; pm, principal mammillary tract. Bar 100  $\mu$ m (A–C); 25  $\mu$ m (D–H). (A) 14 days post-CC lesion. No qualitative differences are observed between the ipsilateral and contralateral sides. (B) 3 days post-FF transection. Little qualitative differences in cell number, size, or staining intensity are observed at this early postlesion time point. (C) 14 days post-FF transection. Similar to B, qualitative differences between the ipsilateral and contralateral sides are difficult to detect by light microscopy. (D) 14 days post-CC lesion. The morphology of these neurons is characteristic of normal MMNm perikarya. The cell bodies are enriched in Nissl substance and do not contain dilated cisternae. Dark puncta within the neuropil are not detected. (E) 3 days post-FF transection. Dark puncta (arrowheads) are observed throughout the neuropil, indicating anterograde degeneration of terminals within the MMNm after unilateral FF transection. (F) 30 days post-FF transection. Astrocytes and microglial cells (arrowheads) appose MMNm neuronal perikarya. Vacuolated neurons are also observed consistently within the MMNm.

# TARGET DEGENERATION AFTER DEAFFERENTATION

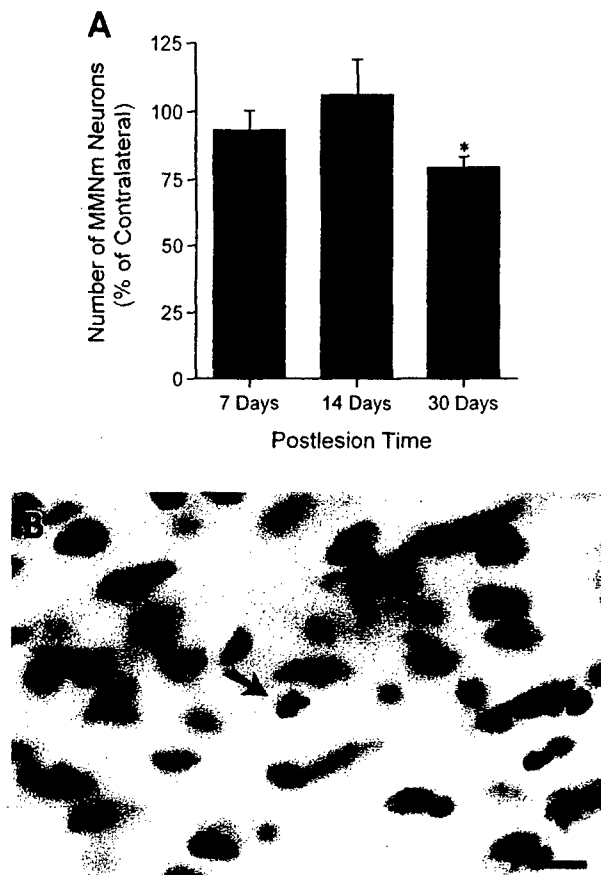


**FIG. 3.** Neuronal loss occurs in the mammillary body after transection of the fornix. **(A)** Neuronal counts in the MMNm after fornical deafferentation. Values are mean  $\pm$  standard deviation. A significant (asterisk,  $p < 0.05$ ) reduction in total neuron number is observed at 30 days postlesion, but not at 7 and 14 days after the lesion. **(B)** Apoptotic cells are encountered occasionally in the ipsilateral MMNm at 30 day postlesion. The cells (arrow) are close to endstage apoptosis according to the staging scheme previously described for neuronal apoptosis *in vivo* (Martin et al., 1998, 1999; Martin, 2001). These cells are classified as apoptotic based on the cellular shrinkage and chromatin condensation into several round masses. EM verified that this degeneration was apoptosis (see Fig. 4C). Bar = 20  $\mu$ m.

FF transection at 3 and 7 days postlesion, suggesting minor degeneration of terminals from the crossed subiculum-mammillary projection (Allen and Hopkins, 1989; Swanson and Cowan, 1975, 1977).

EM was used to characterize this cytopathology at the subcellular level. Normal MMNm neurons appeared as small, ovoid perikarya with eccentric, infolded nuclei and prominent nucleoli (Fig. 4A). The cytoplasm of cell body and proximal dendritic compartments is organized with endoplasmic reticulum, polyribosomes, Golgi apparatus, and mitochondria. No somatodendritic pathology was de-

tected within the MMNm in unoperated controls, after CC lesions, or contralateral to the FF transection at any of the five postlesion time points.

After unilateral FF transection, axonal abnormalities were seen by EM in the MMNm (Figs. 4 and 5). Presynaptic terminal degeneration was identified at 3 and 7 days postlesion ipsilateral to the FF transection (Fig. 5A). Degenerating terminals formed asymmetrical (Gray Type I) axodendritic, and less frequently, axosomatic synaptic contacts within the ipsilateral MMNm (Fig. 5A). Degenerating terminals were observed infrequently contralateral to the FF transection at 3 and 7 days postlesion, consistent with the evaluations of toluidine blue-stained semithin sections (Fig. 2F). Qualitatively, at 14 and 30 days postlesion, terminal degeneration within the MMNm was less prominent than at 3 and 7 days postlesion. However, preterminal neurites with aggregates of mitochondria were observed consistently throughout the neuropil at 6 months postlesion within the MMNm that were not observed at the four earlier postlesion time points (Fig. 5C,D), indicative of long-term changes.

After unilateral FF transection at 14–30 days postlesion, the ultrastructural pathology (Figs. 4 and 5) found within the cell bodies and dendrites was characterized primarily by organelle poverty and the formation of membrane-bound vacuolar cisternae and inclusions. At 14 days, neurons with a very rarefied cytoplasm were observed (Fig. 4B). This cytoplasmic pallor appeared to be due to loss or redistribution of organelles. In these neurons there was a paucity of endoplasmic reticulum, Golgi apparatus, polyribosomes, and mitochondria, but the nucleus appeared mostly normal with prominent nucleoli (Fig. 4B). At 30 days, these atrophic neurons persisted. Dendritic shafts within the MMNm at 30 days postlesion contained prominent membranous inclusions (Fig. 5B). In addition, at 30 days, a few apoptotic neurons were encountered (Fig. 4C). These neurons were identified as apoptotic because they possessed both nuclear and cytoplasmic changes consistent with apoptosis (Martin et al., 1998). The nucleus contained condensed chromatin appearing as caps or crescents abutting the nuclear envelope (Fig. 4C, white arrows). Furthermore, the cytoplasm was dark and condensed and contained intact mitochondria. These cells were identified as neurons because they possessed remnants of synaptic junctions on the cell membrane.

At 6 months, apoptotic neurons were not encountered, but some atrophic neurons still persisted in the MMNm. These MMNm neurons displayed cytoplasmic disorganization, large somatic membrane-bound vacuolar cisternae, and dispersion of chromatin throughout the nucleoplasmic matrix ipsilateral to the FF transection, similar to observations at 30 days postlesion. The nuclear

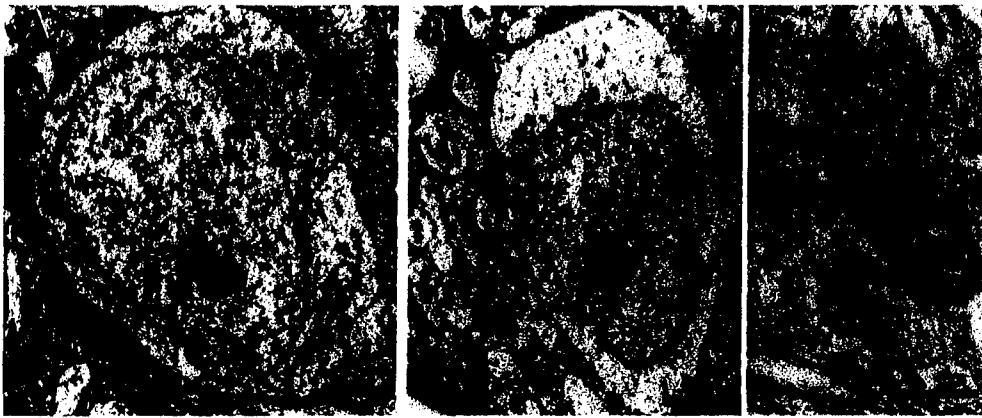


**FIG. 4.** Electron micrographs of MMNm neuronal cell bodies ipsilateral to CC lesions and FF transections. (A) 14 days post-CC lesion. MMNm neurons have a normal structure, including an ovoid cell body with an infolded nucleus and well-organized, granular cytoplasm with rough endoplasmic reticulum, polyribosomes, mitochondria, lysosomes, and Golgi apparatus. Phagocytic cells are not numerous in the neuropil. (B) 14 days post-FF transection. MMNm neurons are damaged. The cell bodies appear pale and reduced in size. Most neurons are organelle-poor and contain disorganized cytoplasm. Compared to normal (A), the nucleus appears smaller and the chromatin is finely dispersed throughout the nucleoplasmic matrix. (C) 30 days post-FF transection. Apoptotic neurons are found. These dying neurons are shrunken and are characterized by chromatin condensation as caps and crescents along the nuclear envelope (white arrows) and cytoplasmic condensation with intact mitochondria. Bars = 1  $\mu$ m (A, B); 0.5  $\mu$ m (C).

changes within these vacuolated neurons (Fig. 5C) were not typical of either neuronal necrosis or apoptosis (Martin et al., 1998). Many of these neuronal cell bodies were surrounded by glial cells, typically oligodendrocytes or microglia (Fig. 5C). At later postlesion time points, aberrant preterminal neurites that contained aggregates of pleomorphic mitochondria were found in the neuropil (Fig. 5C,D). Because no physiological or anatomical evidence exists for a reciprocal projection from the MMNm to the hippocampus or subiculum (Namura et al., 1994; Swanson and Cowan 1975, 1977), it is likely that these somatodendritic alterations are a form of transneuronal degeneration.

## DISCUSSION

We found that axonal bundle transection in the adult CNS induces two forms of remote degeneration in the deafferented target region. One type of neurodegeneration is transsynaptic neuronal atrophy that is characterized morphologically by intracellular vacuolar pathology. This neuronal damage is persistent, as evidenced by the time course evaluation. The other form of neurodegeneration is transsynaptic apoptosis. These observations are important for the further elucidation of mechanisms of remote neurodegeneration and delayed neurologic deficit after traumatic damage to white matter tracts.

### *Experimental lesion design*

We hypothesized that FF transection would cause neuronal damage in the mammillary body consistent with transneuronal degeneration. We selected this system because the MMNm does not project directly to the hippocampus or subiculum (Namura et al., 1994; Swanson and Cowan 1975, 1977). Therefore, changes in MMNm neurons are due to deafferentation rather than retrograde responses. We assessed by light microscopy, stereological counting, and EM the MMNm after FF transection in adult rat. This was done to characterize cellular and subcellular degeneration after lesioning the major forebrain source of afferents to this nucleus. Care was taken to avoid damaging the anterior thalamic nuclei or cingulate cortex in order to avoid potential retrograde degeneration of MMNm neurons that innervate these regions. Unilateral lesions allowed comparison of the involved ipsilateral side to the side contralateral to the lesion in each animal. However, some subiculomammillary fibers are crossed fornical projections (Allen and Hopkins, 1989; Swanson and Cowan, 1975, 1977) and may undergo structural alterations after unilateral FF transection. Therefore, surgical and unoperated controls were also evaluated in this study. Following unilateral FF transection, no somatodendritic changes were observed (although slight, but consistent, terminal degeneration was found) within the contralateral MMNm; moreover, no changes were observed within the ipsilateral and con-

# TARGET DEGENERATION AFTER DEAFFERENTATION

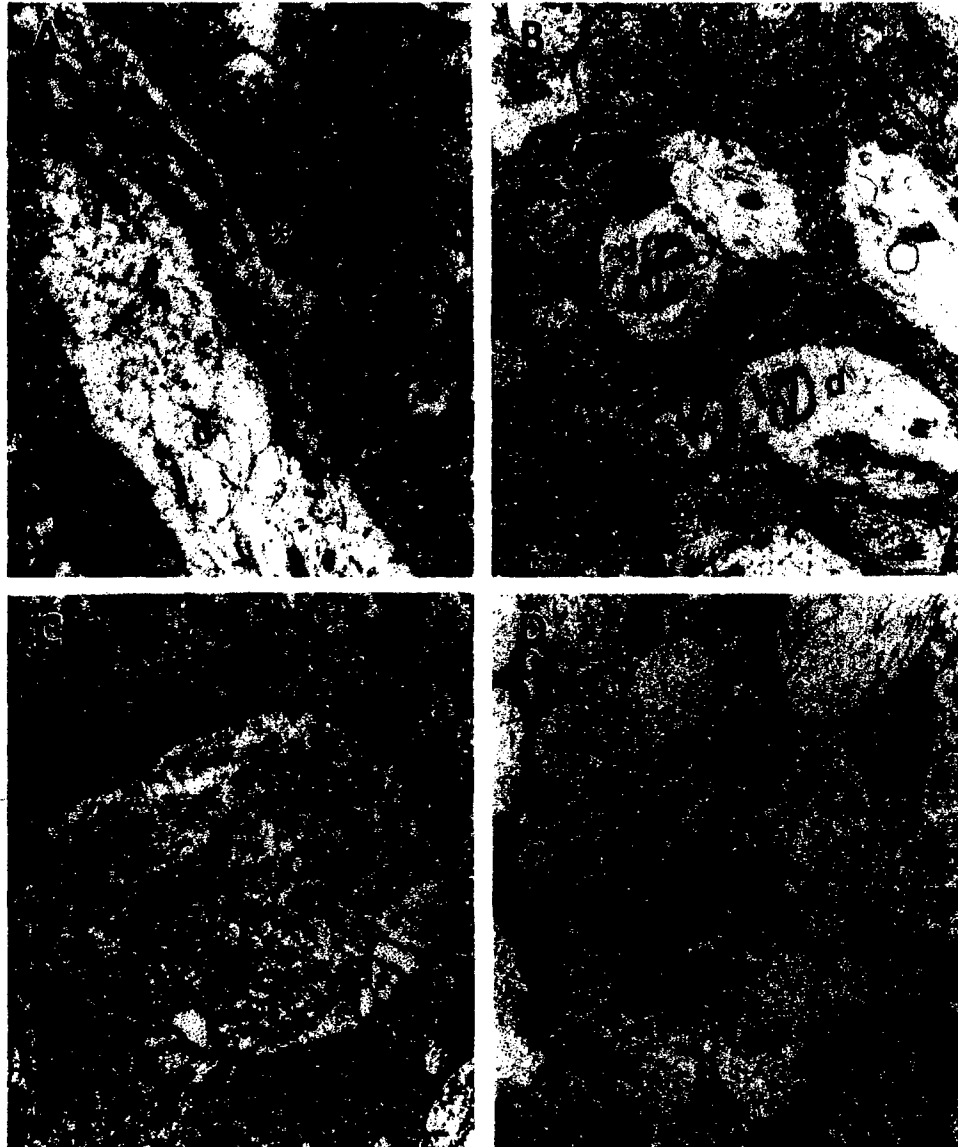


**FIG. 5.** Progression of neurodegeneration by EM within the ipsilateral MMNm following unilateral FF transection. (A) 7 days postlesion. A dark degenerating terminal (asterisk) forms an asymmetrical, axodendritic synapse with a dendrite (d) cut in longitudinal profile. Several nondegenerating terminals (t) also form asymmetrical synapses with the same dendrite. Bar = 0.5  $\mu$ m. (B) 30 days postlesion. Some dendrites (d) contain membranous inclusions. Two nondegenerating terminals (t) form synapses with the dendritic profiles. Bar = 0.5  $\mu$ m. (C) 6 months postlesion. Neuronal cell bodies continue to display evidence for injury, including cytoplasmic vacuolar cisternae (asterisks). Note the organelles within the remaining cytoplasmic matrix are unevenly distributed. Additionally, aggregates of pleomorphic mitochondria are observed within preterminal neurites (arrows) in the surrounding neuropil. Bar = 1  $\mu$ m. (D) 6 months postlesion. Similar to C, axonal neurites filled with mitochondria occur in the neuropil. Bar = 0.5  $\mu$ m.

tralateral MMNm following the CC lesions or in unoperated controls.

This experimental brain injury model is a direct axonal transection lesion. In human head trauma, the majority of white matter damage is believed to be nondisruptive

(Maxwell et al., 1997). A nondisruptive white matter lesion differs from acute axonal transection in that the axotomy is delayed. Nevertheless, both forms of axonal injury can cause afferent deprivation of target neurons, although the timing would differ.

*The MMNm is partially deafferented after FF transection*

Anterograde degeneration occurs within the mammillary complex after FF transection. This observation has been demonstrated previously by light microscopy using silver degeneration methods and by the loss of synaptosomal glutamate uptake (Guillery, 1956; Nauta, 1956; Storm-Mathisen and Opsahl, 1978; Walaas and Fonnum, 1980). Surprisingly, this change has not been verified ultrastructurally. Our EM results demonstrate the axonal and terminal pathology within the MMNm after unilateral FF transection. Degenerating terminals form Gray Type I asymmetric contacts with postsynaptic targets, suggesting that these terminals are glutamatergic. The morphology of these degenerating subicular terminals is consistent with combined EM-tract tracing experiments that demonstrate subicular afferents form asymmetrical, putative excitatory, synaptic contacts within the mammillary body, whereas tegmental afferents form symmetrical, putative inhibitory, synaptic contacts within this nucleus (Allen and Hopkins, 1989).

After FF transection, the majority of terminal degeneration in the MMNm occurs at 3 and 7 days postlesion; axonal pathology is found at 14 and 30 days postlesion. However, swollen axonal neurites are found regularly within the MMNm at 6 months postlesion, revealing long-term structural changes. Swollen axonal neurites were not found within the MMNm at any of the four earlier postlesion time points or within the septal nuclei at 6 months after FF transection (Ginsberg and Martin, 1998). Taken together, these structural changes demonstrate that the MMNm is partially deafferented after FF transection. This injury is characterized by a rapid terminal degeneration (initial onset at 3–7 days postlesion), followed by a delayed, long-term neuritic response of axons. The latter alteration may reflect a sprouting/reinnervation response. For example, sprouting of fornical fibers following transection of the postcommissural fornix has been identified within the posterior hypothalamus in adult rat (Stichel et al., 1995).

*Transsynaptic degeneration of MMNm neurons occurs after FF transection*

Neuronal cell bodies within the MMNm are lost after FF transection as determined using strict stereological methods. We found a 20% reduction in the number of neurons in the MMNm at 30 days postlesion. Two major forms of neurodegeneration were identified in the MMNm. One form was vacuolar pathology and another form was apoptosis. Neither forms of neurodegeneration occurred in controls (i.e., after CC lesions or in the contralateral MMNm). The majority of neurons underwent

progressive somatodendritic shrinkage, disorganization of the cytoplasm, formation of membrane-bound vacuolar cisternae and membranous inclusions, loss of organelles, and dispersion of chromatin throughout the nucleoplasmic matrix. These changes were found at 14–30 days and 6 months postlesion; thus, it occurred after the major wave of terminal degeneration.

Neuronal apoptosis was observed by light microscopy and EM. The structure resembled classic apoptosis that is programmed cell death (Martin, 2001; Martin et al., 1998, 1999). The apoptosis was less prominent than the vacuolar and pale neuron degeneration. This apoptosis may be independent of the vacuolar pathology. If these forms of degeneration are part of the same process, then it remains uncertain at which point the MMNm neurons enter the process of apoptosis. These neurons may enter the apoptotic process directly from a severely atrophic or a non-atrophic intermediate. However, we have not observed such intermediates occurring at time points directly prior to MMNm neuron apoptosis.

These neuronal changes do not represent a retrograde chromatolytic response due to damage of MMNm targets (e.g., anterior thalamic nuclei), and MMNm neurons are not axotomized or deprived of their targets, because no physiological nor anatomical evidence exists for efferent projections from the MMNm coursing within the FF (Allen and Hopkins, 1989; Namura et al., 1994; Swanson and Cowan, 1975, 1977). Therefore, this neuronal pathology within the MMNm after unilateral FF transection is transneuronal degeneration. Our work directly confirms earlier interpretations that transneuronal injury occurs within the mammillary body after limbic decortication or FF transection (Allen, 1944; Bleier, 1969; Gudden, 1880). Furthermore, this study expands these previous observations by revealing two forms of neurodegeneration and by providing ultrastructural evidence of long-term neuronal atrophy in the form of cell body and dendritic pathology.

The vacuolar degeneration in neurons within the MMNm following unilateral FF transection has some ultrastructural similarities to excitotoxic damage caused by excessive activation of glutamate receptors in hypothalamus and septum (Ginsberg et al., 1999; Olney, 1969; Olney et al., 1971). An explanation for this observation is that fornical efferents from the hippocampal formation to the hypothalamus are glutamatergic (Storm-Mathisen and Opsahl, 1978; Walaas and Fonnum, 1980) and that severing FF axons may cause traumatic depolarization and release of presynaptic glutamate (Ramnath and Strange, 1992; Schramm et al., 1990; Takahashi et al., 1995) into extracellular interstitium of the MMNm. This acute event may promote sublethal injury, rather than lethal neurotoxicity, within postsynaptic, somatodendritic targets. This interpretation would be consistent with the



## TARGET DEGENERATION AFTER DEAFFERENTATION

absence of cell loss before 30 days postlesion. In addition, hypothalamic neurons, particularly MMN neurons, express a variety of *N*-methyl-D-aspartate (NMDA) and non-NMDA receptors (Ginsberg et al., 1995; Martin et al., 1993). We have found that NMDA receptor antagonists (Ginsberg et al., 1999) can attenuate transneuronal degeneration in other brain regions. This sustained somatodendritic pathology within the MMNm following FF transection also resembles subcellular pathology within the midline thalamic nuclei and mammillary body following thiamine deficiency, a paradigm used as an animal model of Korsakoff's syndrome (Zhang et al., 1995). Interestingly, somatodendritic alterations caused by thiamine deficiency are ameliorated by the administration of NMDA receptor antagonists (Langlais and Mair, 1990). Thus glutamate receptor excitotoxicity may contribute to the mechanisms for transneuronal degeneration within the MMNm after FF transection.

Another interpretation of the findings is that the transneuronal apoptosis and the apparent neuronal atrophy are due to chronic insufficiencies in neurotrophic support derived from the hippocampus. As in immature neurons (Mount et al., 1993), insufficient activation of glutamate receptors may be a mechanism for neuronal atrophy, possibly due to chronic glutamatergic deafferentation. In addition, neurotrophin signaling may be inadequate for maintaining healthy neurons in the MMN after FF transection. Several neurotrophins are expressed highly in hippocampus (Golden et al., 1998; Langlais and Mair, 1990) and are transported anterogradely to target regions and released presynaptically (Altar et al., 1997; Heymach and Barres, 1997). In any event, it appears that these MMNm neurons survive after FF transection, rather than die, and they exist in an atrophic state, possibly because of an inadequate supply of trophic factors. The identification of the neurotrophic factors for MMN neurons may be important for understanding the mechanisms for transsynaptic apoptosis and chronic neuronal atrophy in the adult brain and long term deficits in memory. Therapeutic interventions such as neurotrophin delivery or enhanced neurotrophin synthesis are particularly pertinent to related traumatic brain injury paradigms of neuronal degeneration where neuronal repair is a desired outcome.

## CONCLUSION

Unilateral FF transection causes rapid terminal degeneration (at 3–7 days) as well as delayed and long-term somatodendritic pathology (at 14–30 days and 6 months) within the mammillary body. Therefore, the MMNm appears to be vulnerable to deprivation of its principal glutamatergic, forebrain afferent source. This neuronal de-

generation occurs as two forms; transsynaptic apoptosis and transneuronal atrophy. This lesion is a useful model system for the identification of the mechanisms of transneuronal degeneration possibly caused by excitotoxicity or loss of afferent-derived trophic support.

## ACKNOWLEDGMENTS

We thank Ann Price and Frank Barksdale for their expert technical assistance. This study was funded by grants from the U.S. Public Health Service, National Institutes of Health, National Institute of Neurological Disorders and Stroke (NS34100) and National Institute on Aging (AG16282) and the U.S. Army Medical Research and Materiel Command (DAMD17-99-1-9553) to L.J.M. and a grant from the Alzheimer's Disease Association (NIRG-00-2250) to S.D.G.

## REFERENCES

- ADAMS, J.H., GRAHAM, D.I., MURRAY, L.S., et al. (1982). Diffuse axonal injury due to nonmissile head injury in humans: an analysis of 45 cases. *Ann. Neurol.* **12**, 557–563.
- AL-ABDULLA, N.A., PORTERA-CAILLIAU, C., and MARTIN, L.J. (1998). Occipital cortex ablation in adult rat causes retrograde neuronal death in the lateral geniculate nucleus that resembles apoptosis. *Neuroscience* **86**, 191–209.
- ALLEN, G.V., and HOPKINS, D.A. (1988). Mammillary body in the rat: a cytoarchitectonic, Golgi, and ultrastructural study. *J. Comp. Neurol.* **275**, 39–64.
- ALLEN, G.V., and HOPKINS, D.A. (1989). Mammillary body in the rat: topography and synaptology of projections from the subicular complex, prefrontal cortex, and midbrain tegmentum. *J. Comp. Neurol.* **286**, 311–336.
- ALLEN, W.F. (1944). Degeneration in the dog's mammillary body and Ammon's horn following transection of the fornix. *J. Comp. Neurol.* **80**, 283–291.
- ALTAR, C.A., CAI, N., BLIVEN, T., et al. (1997). Anterograde transport of brain-derived neurotrophic factor and its role in the brain. *Nature* **389**, 856–860.
- AMARAL, D.G. (1987) Memory: anatomical organization of candidate brain regions, in: *Handbook of Physiology, Section 1: The Nervous System, Vol. V, Higher Functions of the Brain, Part 1*. V.B. Mountcastle (eds.), American Physiological Society: Bethesda, MD, pp. 211–294.
- BLEIER, R. (1969). Retrograde transsynaptic cellular degeneration in mammillary and ventral tegmental nuclei following limbic decortication in rabbits of various ages. *Brain Res.* **15**, 365–393.
- BÜKI, A., OKONKWO, Q.O., WANG, K.W.W., et al. (2000).

- Cytochrome c release and caspase activation in traumatic axonal injury. *J. Neurosci.* **20**, 2825–2834.
- CALHOUN, M.E., JUCKER, M., MARTIN, L.J., et al. (1996). Comparative evaluation of synaptophysin-based methods for quantification of synapses. *J. Neurocytol.* **25**, 821–828.
- CANTERAS, N.S., SIMERLY, R.B., and SWANSON, L.W. (1992). Projections of the ventral premammillary nucleus. *J. Comp. Neurol.* **324**, 195–212.
- ERB, D.E., and POVLISHOCK, J.T. (1988). Axonal damage in severe traumatic brain injury: an experimental study in cat. *Acta Neuropathol.* **76**, 347–358.
- GAFFAN, D., and GAFFAN, E.A. (1991). Amnesia in man following transection of the fornix. A review. *Brain* **114**, 2611–2618.
- GINSBERG, S.D., PRICE, D.L., BLACKSTONE, C.D., et al. (1995). Non-NMDA glutamate receptors are present throughout the primate hypothalamus. *J. Comp. Neurol.* **353**, 539–552.
- GINSBERG, S.D., ROTHSTEIN, J.D., PRICE, D.L., et al. (1996). Fimbria-fornix transections selectively down-regulate subtypes of glutamate transporter and glutamate receptor proteins in septum and hippocampus. *J. Neurochem.* **67**, 1208–1216.
- GINSBERG, S.D., and MARTIN, L.J. (1998). Ultrastructural analysis of the progression of neurodegeneration in the septum following fimbria-fornix transection. *Neuroscience* **86**, 1259–1272.
- GINSBERG, S.D., PORTERA-CAILLIAU, C., and MARTIN, L.J. (1999). Fimbria-fornix transection and excitotoxicity produce similar neurodegeneration in the septum. *Neuroscience* **88**, 1059–1071.
- GOLDEN, J.P., BALOH, R.H., KOTZBAUER, P.T., et al. (1998). Expression of neurturin, GDNF, and their receptors in the adult mouse CNS. *J. Comp. Neurol.* **398**, 139–150.
- GRAHAM, D.I., McINTOSH, T.K., MAXWELL, W.L., et al. (2000). Recent advances in neurotrauma. *J. Neuropathol. Exp. Neurol.* **59**, 641–651.
- GUDDEN, B. (1880). Beitrag zur kenntniss des corpus mammillare und der sogenannten schenkel fornix. *Arch Psychiatr. Nervenkr.* **11**, 428–452.
- GUILLERY, R.W. (1956). Degeneration in the postcommisural fornix and the mammillary peduncle of the rat. *J. Anat.* **90**, 350–371.
- HEYMACH, J.V., and BARRES, B.A. (1997). Neurotrophins moving forward. *Nature* **389**, 789–791.
- KRIEG, W.J.S. (1932). The hypothalamus of the albino rat. *J. Comp. Neurol.* **55**, 19–89.
- LANGLAIS, P.J., and MAIR, R.G. (1990). Protective effects of the glutamate antagonist MK-801 on pyrimethamine-induced lesions and amino acid changes in rat brain. *J. Neurosci.* **10**, 1664–1674.
- MACLEAN, P.D. (1952). Some psychiatric implications of physiological studies on frontotemporal portion of limbic system (visceral brain). *Electroencephalogr. Clin. Neurophysiol.* **4**, 407–418.
- MAHUT, H. (1972). A selective spatial deficit in monkeys after transection of the fornix. *Neuropsychologia* **10**, 65–74.
- MAIR, W.G.P., WARRINGTON, E.K., and WEISKRANTZ, L. (1979). Memory disorder in Korsakoff's psychosis: a neuropathological and neuropsychological investigation of two cases. *Brain* **102**, 749–783.
- MARTIN, L.J., BLACKSTONE, C.D., LEVEY, A.I., et al. (1993). Cellular localizations of AMPA glutamate receptors within the basal forebrain magnocellular complex of rat and monkey. *J. Neurosci.* **13**, 2249–2263.
- MARTIN, L.J., AL-ABDULLA, N.A., BRAMBRINK, A.M., et al. (1998). Neurodegeneration in excitotoxicity, global cerebral ischemia, and target deprivation: a perspective on the contributions of apoptosis and necrosis. *Brain Res. Bull.* **46**, 281–309.
- MARTIN, L.J., KAISER, A., and PRICE, A.C. (1999). Motor neuron degeneration after sciatic nerve avulsion in adult rat evolves with oxidative stress and is apoptosis. *J. Neurobiol.* **40**, 185–201.
- MARTIN, L.J. (2001). Neuronal cell death in nervous system development, disease, and injury. *Int. J. Mol. Med.* **7**, 455–478.
- MAXWELL, W.L., POVLISHOCK, J.T., and GRAHAM, D.I. (1997). A mechanistic analysis of nondisruptive axonal injury. *J. Neurotrauma* **14**, 419–440.
- MOUDGIL, S.S., AZZOUZ, M., AL-AZZAZ, A., et al. (2000). Amnesia due to fornix infarction. *Stroke* **31**, 1418–1419.
- MOUNT, H., DREYFUS, C.F., and BLACK, I.B. (1993). Purkinje cell survival is differentially regulated by metabotropic and ionotropic excitatory amino acid receptors. *J. Neurosci.* **13**, 3173–3179.
- NAMURA, S., TAKADA, M., KIKUCHI, H., et al. (1994). Topographical organization of subicular neurons projecting to subcortical regions. *Brain Res. Bull.* **35**, 221–231.
- NAUTA, W.J.H. (1956). An experimental study of the fornix system in the rat. *J. Comp. Neurol.* **104**, 247–272.
- NAUTA, W.J.H., and HAYMAKER, W. (1969). Hypothalamic nuclei and fiber connections, in: *The Hypothalamus*. W. Haymaker, E. Anderson, and W.J.H. Nauta (eds.), C.C. Thomas: Springfield, pp. 136–209.
- OLNEY, J.W. (1969). Brain lesions, obesity, and other disturbances in mice treated with monosodium glutamate. *Science* **164**, 719–721.
- OLNEY, J.W., HO, O.L., and RHEE, V. (1971). Cytotoxic effects of acidic and sulphur-containing amino acids on the infant mouse central nervous system. *Exp. Brain Res.* **14**, 61–76.

# TARGET DEGENERATION AFTER DEAFFERENTATION

- PAPEZ, J.W. (1937). A proposed mechanism of emotion. *Arch. Neurol. Psychiatry* **38**, 725-743.
- PAXINOS, G., and WATSON, C. (1986). *The Rat Brain in Stereotaxic Coordinates*. Academic Press: Sydney.
- PETERS, A., PALAY, S.L., and WEBSTER, H.F. (1991). *The Fine Structure of the Nervous System*. Oxford University Press: New York.
- POVLISHOCK, J.T., and JENKINS, L.W. (1995). Are the pathological changes evoked by traumatic brain injury immediate and irreversible? *Brain Pathol.* **5**, 415-426.
- RAMNATH, R.R., STRANGE, K.R., and ROSENBERG, P.A. (1992). Neuronal injury evoked by depolarizing agents in rat cortical cultures. *Neuroscience* **51**, 931-939.
- RAZ, N., TORRES, I.J., and ACKER, J.D. (1992). Age-related shrinkage of the mammillary bodies: *in vivo* MRI evidence. *Neuroreport* **3**, 713-716.
- ROSE, J. (1939). The cell structure of the mammillary body in the mammals and in man. *J. Anat.* **74**, 91-115.
- SAUNDERS, R.C., and WEISKRANTZ, L. (1989). The effects of fornix transection and combined fornix transection, mammillary body lesions and hippocampal ablations on object-pair association memory in the rhesus monkey. *Behav. Brain Res.* **35**, 85-94.
- SCHRAMM, M., EIMERL, S., and COSTA, E. (1990). Serum and depolarizing agents cause acute neurotoxicity in cultured cerebellar granule cells: role of the glutamate receptor responsive to *N*-methyl-D-aspartate. *Proc. Natl. Acad. Sci. U.S.A.* **87**, 1193-1197.
- SQUIRE, L.R., AMARAL, D.G., and PRESS, G.A. (1990). Magnetic resonance imaging of the hippocampal formation and mammillary nuclei distinguish medial temporal lobe and diencephalic amnesia. *J. Neurosci.* **10**, 3106-3117.
- STICHEL, C.C., WUNDERLICJ, M.E., SCHWAB, M.E., et al. (1995). Clearance of myelin constituents an axonal sprouting in the transected postcommissural fornix of the adult rat. *Eur. J. Neurosci.* **7**, 401-411.
- STORM-MATHISEN, J., and OPSAHL, M.E. (1978). Aspartate and/or glutamate may be transmitters in hippocampal efferents to septum and hypothalamus. *Neuroscience* **9**, 65-70.
- SWANSON, L.W., and COWAN, W.M. (1975). Hippocampo-hypothalamic connections: origin in subicular cortex, not amon's horn. *Science* **189**, 303-304.
- SWANSON, L.W., and COWAN, W.M. (1977). An autoradiographic study of the organization of the efferent connections of the hippocampal formation in the rat. *J. Comp. Neurol.* **172**, 49-84.
- TAKAHASHI, M., LIOU, S.-Y., and KUNIHARA, M. (1995).  $Ca^{2+}$ - and  $Cl^{-}$ -dependent, NMDA receptor-mediated neuronal death induced by depolarization in rat hippocampal organotypic cultures. *Brain Res.* **675**, 249-256.
- TONKISS, J., and RAWLINS, J.N.P. (1992). Mammillary body lesions and restricted subicular output lesions produce long-lasting DRL performance impairments in rats. *Exp. Brain Res.* **90**, 572-582.
- WALAAS, I., and FONNUM, F. (1980). Biochemical evidence for glutamate as a transmitter in hippocampal efferents to the basal forebrain and hypothalamus in the rat brain. *Neuroscience* **5**, 1691-1698.
- ZHANG, S.X., WEILERSBACHER, G.S., HENDERSON, S.W., et al. (1995). Excitotoxic cytopathology, progression, and reversibility of thiamine deficiency-induced diencephalic lesions. *J. Neuropathol. Exp. Neurol.* **54**, 255-267.

Address reprint requests to:

Lee J. Martin, Ph.D.

Johns Hopkins University School of Medicine

Department of Pathology

558 Ross Building

720 Rutland Avenue

Baltimore, MD 21205-2196

E-mail: lmartin@jhmi.edu

## Immature and Mature Cortical Neurons Engage Different Apoptotic Mechanisms Involving Caspase-3 and the Mitogen-Activated Protein Kinase Pathway

\*Christian Lesuisse and \*†Lee J. Martin

Departments of \*Pathology, Division of Neuropathology, and †Neuroscience, Johns Hopkins University School of Medicine, Baltimore, Maryland, U.S.A.

**Summary:** The authors used cultured mouse cortical neurons to study mechanisms of DNA damage-induced apoptosis in immature and mature neurons. Neurons were maintained viably for 60 days *in vitro* (DIV60). The increased levels of glutamate receptors, synaptic proteins, and glycolytic enzyme were used to track maturation. Exposure of neurons to the DNA-damaging agent camptothecin induced apoptosis in immature (DIV5) and mature (DIV25–30) neurons. Internucleosomal fragmentation of DNA emerged more rapidly in mature neurons than in immature neurons. Immunoblotting revealed that cleaved caspase-3 increased in apoptotic DIV5 neurons but not in DIV30 neurons, but immunolocalization showed accumulation of cleaved caspase-3 in DIV5 and DIV30 neurons. A reversible caspase-3 inhibitor blocked apoptosis in DIV5 neurons but not

in DIV30 neurons. Phosphorylation of extracellular signal-regulated kinase/mitogen-activated protein kinase (Erk/MAP kinase)-42/44 occurred preapoptotically in mature but not immature neurons, while Erk54 nuclear translocation and MAP kinase kinase kinase-1 cleavage into putative caspase-3-generated proapoptotic fragments occurred in DIV5 but not DIV30 neurons. Inhibition of Erk activation with MAP kinase kinase inhibitor blocked apoptosis at both ages. The results show that immature and mature cortical neurons engage different signaling mechanisms in MAP kinase and caspase pathways during apoptosis; thus, neuron age influences the mechanisms and progression of apoptosis. **Key Words:** Alzheimer's disease—Amyotrophic lateral sclerosis—Cortical neuron culture—DNA damage—Ischemic neuronal death—MEKK1.

Understanding the molecular regulation of apoptosis is relevant to neuronal death in nervous system development and to neurodegeneration in pathological conditions affecting the CNS of individuals throughout fetal, newborn, childhood, and adult life. Defective apoptosis can cause cerebral malformations during CNS development (Hakem et al., 1998; Kuida et al., 1996). Dysregulated apoptosis contributes to the pathogenesis of CNS damage in acute neuropathological disorders, such as cerebral ischemia (MacManus et al., 1997; Martin et al., 1998; Martin et al., 2000) and spinal cord trauma (Liu et al., 1997), and in chronic neurodegenerative diseases,

such as Alzheimer disease (Anderson et al., 1996; Kitamura et al., 1999) and amyotrophic lateral sclerosis (Martin, 1999, 2001). The state of CNS maturity at the time of injury appears to influence the emergence of different types of cell death and the rate of cell death (Martin et al., 1998; Martin, 2001; Martin et al., 2001; Natale et al., 2002; Portera-Cailliau et al., 1997).

DNA damage is a potent signal for apoptosis (Levine, 1997). Neurons sustain DNA damage (e.g., hydroxyl radical adducts or single-strand breaks) after cerebral ischemia (Martin et al., 2000) and axotomy/target deprivation (Al-Abdulla and Martin, 1998; Martin and Liu, 2002). Cells that have sustained DNA lesions can undergo apoptosis by engaging molecular cascades involving expression, activation by phosphorylation or proteolysis, or translocation of p53, Bax, and caspases (Polyak et al., 1997). Recently, the extracellular signal-regulated protein kinase/mitogen-activated protein kinase (Erk/MAP kinase) pathway, including the upstream MAP kinase kinase kinase-1 (MEKK1) and MAP kinase kinase (MEK), have been implicated in the signaling of apoptosis in response to DNA damage in nonneuronal

Received February 6, 2002; final version received April 12, 2002; accepted April 12, 2002.

This work was supported by grants from the U.S. Public Health Service, National Institutes of Health, National Institute of Neurological Disorders and Stroke (NS34100) and National Institute on Aging (AG16282), and the U.S. Army Medical Research and Materiel Command (DAMD17-99-1-9553).

Address correspondence and reprint requests to Dr. Lee J. Martin, Johns Hopkins University School of Medicine, Department of Pathology, 558 Ross Building, 720 Rutland Avenue, Baltimore, MD 21205-2196, U.S.A.; e-mail: lmartin@jhmi.edu

cells (Widmann et al., 1998). Erk activation may also have a role in excitotoxic (Jiang et al., 2000) and ischemic (Alessandrini et al., 1999) neuronal death, but the link to DNA damage in neurons is unknown.

The mechanisms of DNA damage-induced apoptosis in postmitotic cells such as neurons are much less understood compared with cells of nonnervous tissue origin. Relatively few *in vitro* model systems have been developed to evaluate mechanisms of DNA damage-induced neuronal apoptosis. Generally, these models are exposure to  $\gamma$ -irradiation, ultraviolet light, cytosine arabinoside, or topoisomerase inhibitors such as etoposide or camptothecin (CPT) (Morris and Gellar, 1996; Park et al., 1997; Park et al., 1998). This study focused on CPT-induced neuronal apoptosis. The few available studies on CPT-induced apoptosis of cortical neurons or sympathetic neurons have suggested that the death process requires p53 (Johnson et al., 1999; Xiang et al., 1998), supporting the idea that CPT neurotoxicity involves DNA damage. However, the roles of caspases in CPT-induced neuronal apoptosis are unclear because some studies have shown that caspase inhibitors block (Johnson et al., 1999; Stefanis et al., 1999) or fail to block (Park et al., 1997) apoptosis, and caspase-3 deletion may only delay neuronal death (Keramaris et al., 2000). The role of the MAP kinase pathway in DNA damage-induced apoptosis of neurons is virtually unexplored. In this study, we used a mouse cortical neuron culture model to further delineate the molecular mechanisms of DNA damage-induced neuronal apoptosis. We tested the hypothesis that apoptosis mechanisms are different in neurons at different maturational ages. Specifically, we examined whether MAP kinase signaling participates in the mechanisms of DNA damage-induced neuronal apoptosis *in vitro*, and whether MAP kinase and caspase pathways and Bcl-2 family members are activated or modulated similarly or differently in immature and mature neurons. We found prominent molecular and biochemical differences during the progression of apoptosis in immature neurons compared with mature neurons. These differences were reflected in the time course or magnitude of internucleosomal DNA fragmentation, caspase-3 and MEKK1 cleavage, and Erk activation.

## MATERIALS AND METHODS

### Murine cortical neuron culture

Mouse cortical neuron cultures were prepared as described previously (Lesuisse and Martin, 2002). The Animal Care and Use Committee of the Johns Hopkins University School of Medicine approved the animal protocol. Cerebral cortices were dissected from embryonic day 16 mice (C57 strain, Charles River) and dissociated by treatment with 0.25% trypsin (Life Technologies, Rockville, MD, U.S.A.) followed by trituration with a fire-polished Pasteur pipette. Cells ( $10^6$ ) were plated onto 35-mm tissue culture dishes coated with 33  $\mu$ g/mL

poly-D-Lysine. The cells were plated in Neurobasal medium (Life Technologies) supplemented with B27 (Life Technologies), and 25  $\mu$ mol/L  $\beta$ -mercaptoethanol and streptomycin/amphotericin B (Life Technologies). Fifty percent of the medium was changed 3 days after plating and subsequently every 6 days. Neuronal cultures were maintained for up to 60 days *in vitro* (DIV60). The astroglial contamination of the cell culture was low. We have shown by immunoblotting that glial fibrillary acidic protein is undetectable at DIV5 and low at DIV25 (Lesuisse and Martin, 2002). By immunoblotting, the detection of markers for microglia and oligodendroglia is similarly low (Martin and Lesuisse, unpublished data, 2002). Another group has reported a nearly pure neuronal culture using similar conditions with B27 supplementation and low glutamine concentration to limit growth of glia (Brewer et al., 1993). For every experiment that was performed on cortical neurons at different *in vitro* ages, the cells in the different age groups were prepared from the same original dissociated cells, so that appropriate comparisons could be made (Lesuisse and Martin, 2002).

### Camptothecin-induced apoptosis

Neurons were stimulated to undergo apoptosis *in vitro* by treatment with CPT, an inhibitor of topoisomerase-I (Bendixen et al., 1990; Hsiang et al., 1985). Camptothecin (Sigma, St. Louis, MO, U.S.A.) was dissolved in double-distilled water supplemented with sodium hydroxide and heated at 55°C for 30 minutes to solubilize completely the drug at a final concentration of 50 mmol/L, and was further diluted in Neurobasal medium. At DIV5 or DIV25–30, mouse cortical neurons were treated with 1, 10, or 100  $\mu$ mol/L CPT for 4, 8, 24, 48, or 72 hours. A cell-permeable reversible caspase-3 inhibitor Ac-AAVALLPAVLLALLAPDEV-CHO (Alexis Biochemicals, San Diego, CA, U.S.A.) and an inhibitor of MEK1/2 (U0126) (Cell Signaling Technology) were evaluated for effects on blocking neuronal apoptosis. Caspase-3 inhibitor was dissolved in DMSO (20-mmol/L stock). U0126 was dissolved in 50% ethanol/50% DMSO or 70% methanol/30% DMSO (50-mmol/L stock). The drugs were used at final concentrations of 10 and 100  $\mu$ mol/L in cultures. Caspase-3 inhibitors are often used at this concentration range (Park et al., 1997; Stefanis et al., 1999). Cells were pretreated for 2 hours before exposure to CPT. Neuronal cultures were used for quantification of apoptosis, protein/DNA extractions, or electron microscopy (EM). For quantification of neuronal apoptosis, cultures were stained with a nuclear dye (Hoechst 33258), digital images were captured from six nonoverlapping microscopic fields (20 $\times$  objective), and apoptotic nuclei were counted. The analysis of the cell counts was performed using ANOVA, and subsequent statistical post hoc evaluation of significance was performed using the Student's *t*-test.

### Genomic DNA fragmentation analysis

Cortical neurons (from three different platings) cultured in 35-mm plates were washed twice in ice-cold phosphate-buffered saline (PBS), resuspended in 300  $\mu$ L DNA extraction buffer (10 mmol/L Tris, pH 7.4; 10 mmol/L NaCl; 25 mmol/L EDTA) containing 100  $\mu$ g proteinase K (Boehringer, Mannheim, Germany) and incubated at 37°C overnight. DNA was purified by phenol/chloroform extraction and resuspended in 200  $\mu$ L TE. Approximately 20 microliters of each sample was fractionated in 1.5% TBE agarose gels containing ethidium bromide. DNA was visualized with a Fluor-S Multimager (Bio-Rad, Hercules, CA).

### Cellular and subcellular fractionation and immunoblotting

Total cell extracts were used to characterize normal developing cultures at DIV5 to DIV60. For total protein extracts, cortical neuron cultures (three wells for each maturational time point, two different platings) were lysed in TNE buffer (10 mmol/L Tris-HCL, pH 7.4; 150 mmol/L NaCl; 5 mmol/L EDTA) containing protease inhibitors (1 mmol/L PMSF, 10  $\mu$ g/mL leupeptin, 10  $\mu$ g/mL pepstatin A) and detergents (2% SDS, 1% deoxycholate, 1% NP-40), and sonicated for 15 seconds.

Subcellular fractionations were performed on CPT-treated neurons. DIV5 and DIV25–30 cortical neuron cultures (three different platings) were treated with 100  $\mu$ mol/L CPT, and cells were harvested 4, 8, and 24 hours later. Soluble, insoluble, and nuclear proteins were analyzed by Western blot analysis to identify changes in the levels or activation of death and survival proteins and changes in organelle and synapse markers during the progression of neuronal apoptosis. For subcellular fractionations, cortical neurons (18 wells for each treatment) were resuspended in 200 mmol/L mannitol, 70 mmol/L sucrose, 1 mmol/L EGTA, and 10 mmol/L HEPES (pH 7.5) containing protease inhibitors (1 mmol/L PMSF, 10  $\mu$ g/mL leupeptin, 10  $\mu$ g/mL pepstatin A), homogenized in a glass-Teflon grinder with 10 up-and-down strokes, and centrifuged at 1,000 *g* to collect the nuclear fraction. The nuclear fraction was resuspended in the same extraction buffer and homogenized for the second time in a glass-Teflon grinder. The soluble and insoluble (pellet) fractions were isolated by centrifugation of the supernatant at 100,000 *g*. Protein concentrations of each homogenate were determined by protein assay (Pierce, Rockford, IL, U.S.A.). Homogenates were diluted further in Laemmli sample buffer.

Protein (20  $\mu$ g) from neuronal cultures was resolved on gradient SDS polyacrylamide gels (4–20%) and transferred to nitrocellulose filter membranes by electroblotting. Nitrocellulose membranes were blocked in 5% (w/v) nonfat dry milk in PBS. After overnight incubation with the primary antibodies in PBS supplemented with 5% nonfat dry milk and 0.05% (v/v) Tween-20, membranes were rinsed and then incubated with peroxidase-conjugated secondary antibody. Immunoreactive proteins were visualized with enhanced chemiluminescence (Amersham).

The developmental maturation of cortical neuron cultures was evaluated by expression of subtypes of glutamate receptors, synaptic proteins, a glycolytic enzyme, and death/survival proteins. Protein expression profiles were also evaluated during the progression of neuronal apoptosis after exposure to CPT. The following antibodies were used for immunoblotting: monoclonal antibodies against  $\alpha$ -synuclein (Transduction Laboratories, Lexington, KY, U.S.A.), cytochrome *c* oxidase subunit I (Molecular Probes, Eugene, OR, U.S.A.), glyceraldehyde phosphate dehydrogenase (Research Diagnostics, Flanders, NJ, U.S.A.), p53 (Pharmingen, San Diego, CA, U.S.A.), NMDA receptor R1 subunit (Pharmingen), synaptophysin (Boehringer), pan-Erk (Transduction Laboratories), active Erk42–44 (Promega), and poly-ADP ribose polymerase (PARP; Calbiochem, San Diego, CA, U.S.A.); and rabbit polyclonal antibodies against  $\beta$ -synuclein (Oncogene Science, Cambridge, MA, U.S.A.), AMPA receptor subunits GluR2/3 (Martin et al., 1993), Bcl-2 (N-19; Santa Cruz Biochemicals, Santa Cruz, CA, U.S.A.), caspase-3 (H-277; Santa Cruz), cleaved caspase-3 (D175; Cell Signaling Technology), Bcl-x<sub>L</sub> (Ab-3; Calbiochem), Bak (N-terminal; Upstate Biotechnology, Lake Placid, NY, U.S.A.), Bax (N-terminal, Santa Cruz), and

MEKK1 (Santa Cruz). A synthetic peptide (Santa Cruz) was used to perform peptide competition experiments for MEKK1.

### Protein crosslinking and immunoprecipitation

Interactions between cleaved caspase-3 and other proteins were studied. Cortical neurons were treated for 24 hours with CPT and then incubated for 20 minutes with 1 mmol/L dithio-bis-succinimidyl-propionate (DSP; Pierce). The cells were rinsed, lysed, and proteins were extracted as described previously. Proteins (200  $\mu$ g) were immunoprecipitated with antibody to cleaved caspase-3 (D175; Cell Signaling Technology) and resolved on gradient SDS polyacrylamide gels with or without  $\beta$ -mercaptoethanol in the loading buffer (DSP-crosslinked proteins are thiol cleavable). Proteins were transferred to nitrocellulose and blots were probed with antibody to cleaved caspase-3 (D175).

### Immunocytochemistry

Immunofluorescence was used to visualize cleaved caspase-3 in nontreated and CPT-treated cortical neurons. Cells were fixed in 4% paraformaldehyde/4% sucrose in PBS (4°C, 20 minutes) and then with methanol (4°C, 10 minutes), and then permeabilized in 0.2% Triton X-100, 10% NGS in PBS (4°C, 10 minutes), and incubated overnight at 4°C in 10% NGS in PBS with primary antibody to cleaved caspase-3 (D175, 1:1000). Antibody binding was visualized with Alexa Fluor-conjugated goat antirabbit (Molecular Probes) that was diluted at 1:600 in PBS. Digital images were captured with a Zeiss Axiovert/Quantix CCD camera.

### Electron microscopy

Neuronal cultures treated with CPT at DIV5 and DIV25 were used for EM. Media were removed and the neuronal cultures were washed briefly with PBS, and the cells were fixed with 1% glutaraldehyde in PBS for 1 hour. Cells were processed for conventional EM directly in culture plates. Plastic-embedded neurons were removed from the culture plates as large blocks that were cut into pieces. Plastic blocks containing neurons were trimmed and sectioned for EM.

## RESULTS

### Mouse cortical neuron cultures mature and remain viable for the long-term

To study the effects of DNA damage on neurons at different stages of maturity, we used a long-term culture system of mouse cortical neurons that were maintained in an extremely viable state (Fig. 1). At DIV5 cortical neurons are bipolar with prominent neurites (Figs. 1A and 1D). At DIV25, cortical neurons are large and are embedded within a dense plexus of axons and dendrites that form numerous synaptic junctions (Figs. 1B, 1E, and 1F). The neurons have abundant polyribosomes distributed throughout the cytoplasmic matrix, intact arrays of rough endoplasmic reticulum and Golgi stacks, and uniformly shaped mitochondria with intact cristae. The nucleus has a predominantly pale matrix and is surrounded by a continuous, bilaminar nuclear membrane. The structural viability was well preserved in old DIV60 neurons (Fig. 1C).

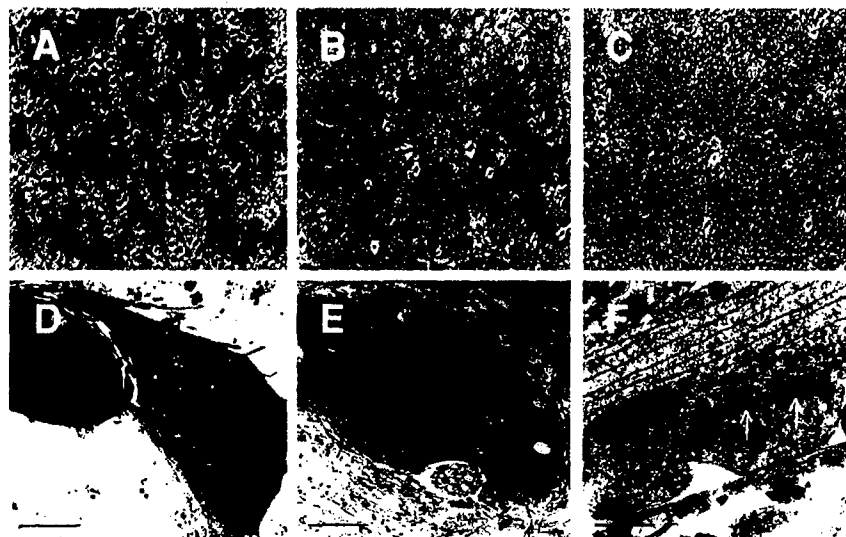


**FIG. 1.** Mouse cortical neurons mature and can remain viable over the long term in culture. (A–C) Light microscopy shows the progressive elaboration of the dendritic/axonal plexus of cortical neurons in culture from DIV5 (days *in vitro*: 5) (A) to DIV25 (B), and then DIV60 (C). (D–F) Electron microscopy shows the change in neurons from a bipolar morphology at DIV5 (D) to pyramidal cell-like cortical neuron morphology at DIV25 (E). The synaptodendritic compartment undergoes considerable maturation between DIV5 and DIV25 (see Fig. 2 for levels of glutamate receptors and synaptic proteins). At DIV25, the synaptodendritic structure is well developed (F), as evidenced by numerous axodendritic synaptic junctions (arrows).

To characterize the molecular viability of this long-term neuronal culture system, we evaluated the expression of glutamate receptors, synaptic proteins, and apoptosis-regulating proteins (Fig. 2). Total protein extracts from mouse cortical cultures at DIV5, 10, 15, 20, 25, 30, 40, and 60 were analyzed by immunoblotting. Expression of the NMDA receptor subunit NR1 and the AMPA receptor subunits GluR2/GluR3 was already detectable by DIV5 (Fig. 2A). Glutamate receptor levels increased to a maximum by DIV10–15 and then remained unchanged through DIV60. The levels of synaptic proteins (synaptophysin,  $\alpha$ -synuclein, and  $\beta$ -synuclein) were very low at DIV5 (detectable only after prolonged exposure to film, data not shown). By DIV10, the expression of these synaptic proteins was detectable with short exposure (Fig. 2A). Synaptophysin,  $\alpha$ -synuclein, and  $\beta$ -synuclein reached highest levels at about DIV15–20 and DIV25, respectively. As a metabolic marker, GAPDH (a glycolytic protein) was analyzed. The level of GAPDH peaked at approximately DIV25 and remained unchanged until after DIV40, and by DIV60 had decreased less than 30% (Fig. 2A). The high level of expression of NMDA and non-NMDA glutamate receptors, synaptic proteins, and metabolic enzyme suggests that our mouse cortical neuron culture remains viable over the long-term (60 days in culture).

Several proteins that function in cell death or survival were evaluated during the maturation of cortical neuron cultures from DIV5 to DIV60. These experiments provided important normative data because these proteins were also evaluated during CPT-induced apoptosis. The p53 in mouse cortical cultures was resolved as multiple immunoreactive bands at approximately 53 kD (Fig. 2B), consistent with phosphorylated and dephosphorylated forms of p53 (Levine, 1997). These immunoreactive proteins had mobilities similar to purified recombinant p53 (data not shown). The levels of apparent phosphorylated

and dephosphorylated forms of p53 reached a maximum in expression at approximately DIV10–15, after which cortical neurons downregulated p53. Procaspase-3 was highly expressed by DIV5–10, decreased by more than 50% by DIV15, and was expressed at low levels after DIV20. PARP levels peaked at DIV5, and by DIV10 had declined by more than 90%. Inactivation cleavage products of PARP (85 kD) were low under normal culture conditions. Bak expression increased threefold to fourfold between DIV5 and DIV15, and after DIV30 Bak decreased slightly (less than 50%). In contrast, the level of expression of its homologue protein, Bax, was very high at DIV5 and DIV10 and then decreased progressively to low levels at DIV60. The level of expression of the antiapoptotic protein Bcl-x<sub>L</sub> did not change significantly during the 60 days in culture, while Bcl-2 expression increased fivefold to 10-fold between DIV5 and DIV25 and remained high through DIV60.

Erk42 levels increased threefold to fivefold from DIV5 to DIV10 and remained unchanged through DIV60 (Fig. 2C). Erk44 was only weakly detectable from DIV5 to DIV60. Erk54 protein expression was high at DIV5, and levels decreased slightly over the 60 days in culture.

#### The progression of apoptosis is different in immature and mature cortical neurons

Internucleosomal fragmentation of DNA was used as an assay for apoptosis in cortical neuron cultures treated with 1, 10, or 100  $\mu$ M CPT for 4, 8, 24, 48, or 72 hours. Camptothecin induced internucleosomal DNA fragmentation in neuronal cultures treated at DIV5 and DIV30. The timing and magnitude of DNA fragmentation were different in immature and mature neurons (Fig. 3A). The DIV5 neurons showed DNA fragmentation after 24 hours of CPT treatment. With 24 and 48 hours of treatment, long exposures were necessary to visualize a ladder (compare the DNA markers in both gels in Fig.

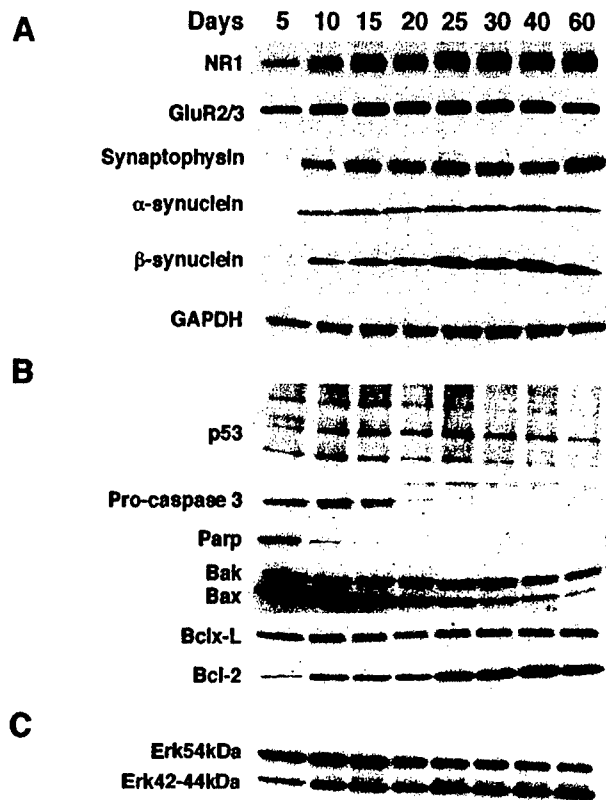


**FIG. 2.** Molecular maturation of mouse cortical neurons in culture. The maturation and sustained viability of this long-term neuronal culture system were evaluated by the expression of glutamate receptors, synaptic proteins, and apoptosis-regulating proteins. For dendritic, synaptic, and metabolic maturation, NR1, GluR2/GluR3, synaptophysin,  $\alpha$ / $\beta$ -synucleins, and GAPDH (a glycolytic protein) were evaluated (**A**). Several cell death/survival proteins were evaluated (**B**), including p53, procaspase 3, poly-ADP ribose polymerase (PARP), Bak, Bax, Bcl-x<sub>L</sub>, Bcl-2, and extracellular signal-regulated kinase (Erk)-54 and Erk44/42 (**C**). Total proteins were extracted from neuronal cultures at DIV5 (days *in vitro*: 5), 10, 15, 20, 25, 30, 40 and 60. Samples (20  $\mu$ g protein) were fractionated on gradient SDS-PAGE (4–20% gels), transferred to nitrocellulose membranes, and then probed successively or in combination with specific monoclonal or polyclonal antibodies (see Materials and Methods). These results were reproduced in two different platings and at least three different immunoblots per antibody.

3A). In contrast, DIV30 neurons treated with the same concentrations of CPT showed prominent internucleosomal DNA fragmentation at 8 hours of treatment, with a peak at approximately 24 hours of treatment (Fig. 3A). Results of gel electrophoresis suggested that concentrations of CPT ranging from 1 to 100  $\mu$ mol/L did not seem to influence significantly the magnitude of internucleosomal fragmentation of DNA degradation in cultures of different ages. However, light microscopy revealed that 100  $\mu$ mol/L CPT appeared to induce a more robust and reliable apoptotic response than the lower CPT concentrations in neurons of different ages (data not shown). Therefore, subsequent toxicologic experiments were done using 100  $\mu$ mol/L CPT.

Electron microscopy confirmed that mouse cortical cultures treated with CPT at DIV5 and DIV30 were morphologically apoptotic (Figs. 3B and 3C). The morphology of the chromatin condensation was different at the two ages. The nuclear morphology in the majority of apoptotic DIV5 neurons was similar to classical apoptosis with the formation of uniformly round chromatin masses (Martin et al., 1998). Apoptosis in DIV30 neurons was different because large, irregularly shaped chromatin masses were formed.

#### Caspase-3 cleavage is different in immature and mature neurons undergoing camptothecin-induced apoptosis

Caspase-3 was evaluated in subcellular fractions of control neurons and CPT-treated neurons (Fig. 4). The purity of the fractions generated by the subcellular fractionation method has been confirmed (Martin, 1999, 2001; Fig. 8). Caspase-3 proenzyme levels were very

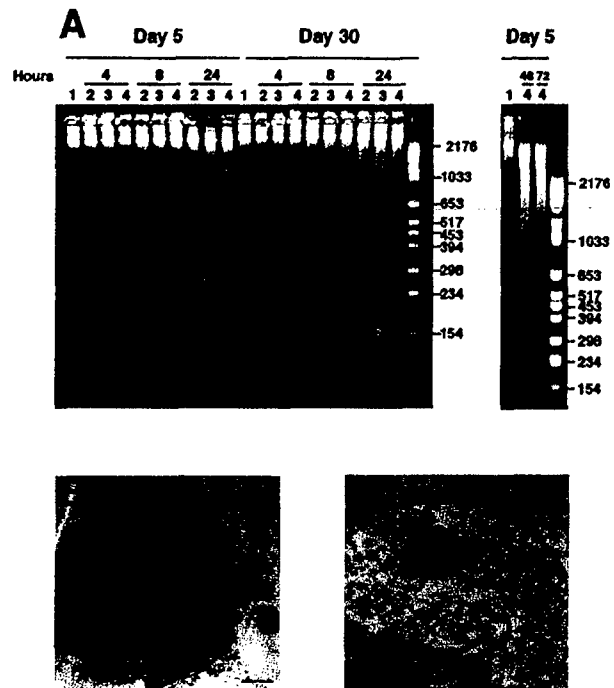


**FIG. 3.** The emergence of DNA fragmentation and chromatin condensation is different in immature and mature cortical neurons treated with camptothecin (CPT). (**A**) Internucleosomal fragmentation of DNA occurs earlier and more strongly in cortical neurons at DIV30 (days *in vitro*: 30) exposed to CPT compared with DIV5 neurons treated similarly. Neurons were exposed to vehicle (1) or to 1  $\mu$ mol/L (2), 10  $\mu$ mol/L (3), or 100  $\mu$ mol/L (4) CPT for 4, 8, 24, 48, or 72 hours. DNA was extracted from neuronal cultures and separated on conventional agarose gels (1.5% w/v). DNA molecular weight markers are shown in the far right lane of each gel. Note that gels with DNA extracts of cultures treated with CPT for 48 and 72 hours required long exposures (see overexposed DNA standards) to visualize the ladder. These results were reproduced in three different platings and at least three different gels. (**B** and **C**) Electron microscopic confirmation of the apoptosis induced by CPT in DIV5 neurons (**B**) and DIV30 neurons (**C**). The chromatin is condensed into large round masses (**B**) or large irregular masses (**C**).



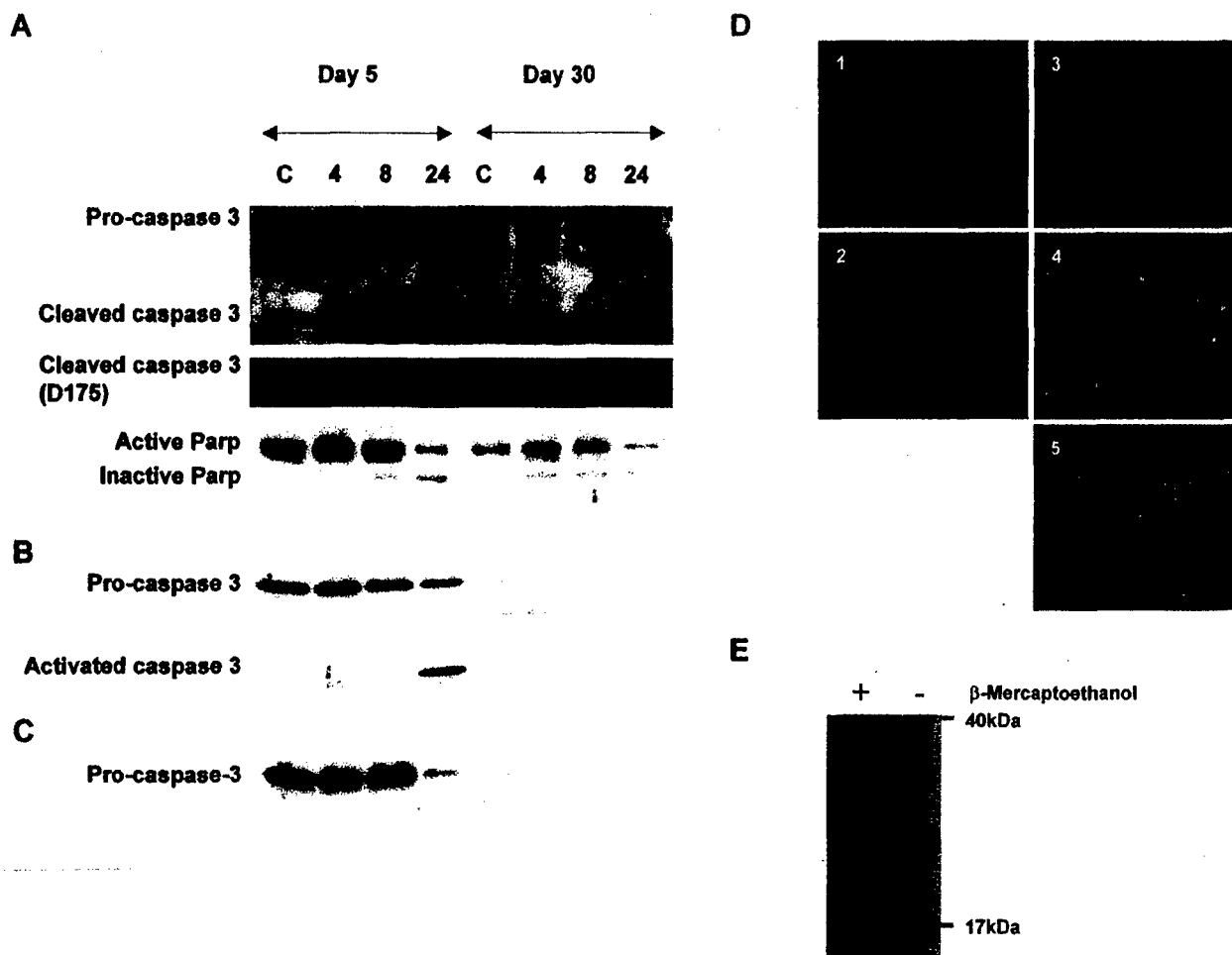


**FIG. 4.** Caspase-3 cleavage is different in immature and mature cortical neurons undergoing camptothecin (CPT)-induced apoptosis. (**A–C**) DIV5 (days *in vitro*: 5) and DIV30 mouse cortical neurons were treated with vehicle (control, C) or with 100  $\mu\text{mol/L}$  CPT for 4, 8, or 24 hours (18 wells per treatment) and collected for subcellular fractionation into nuclear (**A**), pellet (**B**), and soluble (**C**) fractions. In DIV5 neurons, but not in DIV30 neurons, cleaved caspase-3 accumulated progressively in nuclear fractions as revealed by the formation of a 17-kd cleavage product (**A**). Although a low constitutive level of cleaved caspase-3 was detected in DIV30 neurons, this level did not change during apoptosis (**A**). There was a coinciding degradation of poly-ADP ribose polymerase (PARP) with the formation of an 85-kd fragment in both DIV5 neurons (short exposure of blot) and DIV30 neurons (long exposure of blot), indicating activation of caspase (**A**). In pellet fractions of DIV5 neurons exposed to CPT (**B**) cleaved caspase-3 accumulated as proenzyme levels decreased. Major changes in proenzyme and cleaved caspase-3 were not detected in pellet fractions of DIV30 neurons. In soluble fractions of DIV5 neurons, caspase-3 proenzyme level decreased but cleaved caspase-3 was undetectable; in contrast, low constitutive levels of proenzyme were found in DIV30 neurons and no changes were observed. These results were reproduced in three different platings and at least three different immunoblots per antibody. (**D**) Immunolocalization of cleaved caspase-3 in immature and mature cortical neurons undergoing apoptosis. Mouse cortical neurons were cultured on glass slides. At DIV5 (1 and 3) or DIV30 (2, 4, and 5) cells were exposed to vehicle (1 and 2) or CPT for 24 hours (3 and 5) or 8 hours (4). Cleaved caspase-3 was localized (green staining) with a specific antibody (D175) selective for a cleaved product of approximately 17 to 20 kd. Cells were counterstained with a blue nuclear dye (Hoechst 33258) to show normal and apoptotic nuclei. In control neurons, cleaved caspase-3 immunoreactivity was detected in few cells at DIV5 (1) and DIV30 (2). In contrast, strong staining for cleaved caspase-3 (green labeling) was detected in both DIV5 and DIV30 neurons treated with CPT. Apoptosis is evident by the nuclear condensation. In CPT-treated DIV5 neurons at 24 hours, cleaved caspase-3 accumulated in the perikaryal cytoplasm and in processes (3). The CPT-treated DIV30 neurons showed prominent accumulation of cleaved caspase-3 in apoptotic nuclei and nuclear debris at 24 hours (5). At earlier time points (8 hours), the CPT-treated DIV30 neurons showed striking accumulation of cleaved caspase-3 in the cell body and nucleus of apoptotic neurons (4). (**E**) Cleaved caspase-3 in neurons interacts with many proteins. Cortical neurons (DIV5) were stimulated to undergo apoptosis, proteins were crosslinked, cells were lysed, and cleaved caspase-3 was immunoprecipitated. Immunoprecipitates were fractionated by SDS-PAGE with (+) or without (–)  $\beta$ -mercaptoethanol to cleave thiol-crosslinked proteins, transferred to nitrocellulose, and blotted for cleaved caspase-3. Many proteins between 17 and 40 kd bind to cleaved caspase-3.

different in total extracts of developing and mature neuronal cultures (Fig. 2B). Caspase-3 proenzyme was found in nuclear, pellet, and soluble protein fractions (Figs. 4A to 4C). The DIV5 cortical neurons had higher

levels of proenzyme in nuclear (Fig. 4A), pellet (Fig. 4B), and soluble (Fig. 4C) fractions than DIV30 neurons. In control DIV30 neurons, full-length caspase-3 was highest in the nuclear fraction (Fig. 4A). After exposure

to CPT, proenzyme levels were decreased at 24 hours in DIV5 neuron-soluble (Fig. 4C) and pellet (Fig. 4B) fractions, but were unchanged in nuclear (Fig. 4A) fractions. In CPT-treated DIV30 neurons, caspase-3 proenzyme levels were increased modestly in nuclear fractions (Fig. 4A) but were unchanged in pellet and soluble fractions (Figs. 4A and 4B).

Cleaved caspase-3 was evaluated in subcellular fractions of control neurons and CPT-treated neurons (Fig. 4). In control neurons, cleaved caspase-3 was found primarily in the nuclear fraction with two different antibodies (Figs. 4A and 4B). Control neurons at DIV5 and DIV30 had similar low levels of constitutively cleaved caspase-3 in nuclear fractions. In DIV5 neurons exposed to CPT, the levels of cleaved caspase-3 subunits (17–19 kD) progressively increased in nuclear fractions between 4 and 24 hours (Fig. 4A), and abruptly increased between 8 and 24 hours in pellet fractions (Fig. 4B). In contrast, the levels of cleaved caspase-3 did not change in nuclear and pellet fractions of DIV30 neurons after CPT treatment.

Cortical neurons were examined for cleaved caspase-3 using immunocytochemistry. Cleaved caspase-3 immunoreactivity (detected with D175 antibody) was rarely observed in control cells, but was seen infrequently in isolated apoptotic cells in control cultures at DIV5 and DIV30 (Figs. 4D1, 2). After CPT exposure, DIV5 and DIV30 neurons showed different immunolocalization patterns for cleaved caspase-3. In DIV5 neurons with 24-hour CPT exposure, cleaved caspase-3 was observed in the perikaryal cytoplasm and nucleus and in neuronal processes in the surrounding matrix (Fig. 4D3). In DIV30 neurons with 8-hour CPT exposure, cleaved caspase-3 immunoreactivity was prominent in the perikaryal cytoplasm and nucleus (Fig. 4D4), and with 24-hour CPT exposure cleaved caspase-3 was localized to cellular debris of apoptotic neurons (Fig. 4D5). Apoptotic cells incubated with secondary antibody without prior treatment with cleaved caspase-3 antibody did not show labeling (data not shown).

Immunofluorescence due to nonspecific secondary antibody binding to degenerating neurons *in vitro* has not been observed with the concentration used in the present study (Lesuisse and Martin, 2002). Similar patterns of specific labeling for cleaved caspase-3 have been seen in apoptotic striatal neurons *in vivo* (Lok and Martin, 2002) and apoptotic thalamic neurons *in vivo* (Natale et al., 2002).

The levels of PARP were examined by immunoblotting because this DNA repair enzyme is cleaved and inactivated by active caspase-3 (Lazebnik et al., 1994). The levels of intact PARP are much higher in DIV5 neurons compared with DIV30 neurons. PARP was inactivated in CPT-treated DIV5 and DIV30 neurons, as seen by the formation of an 85-kD cleavage product (Fig.

4A), indicating the activation of caspase-3. The cleavage of PARP occurred earlier in DIV30 neurons compared with DIV5 neurons.

#### **Cleaved caspase-3 interacts with many proteins**

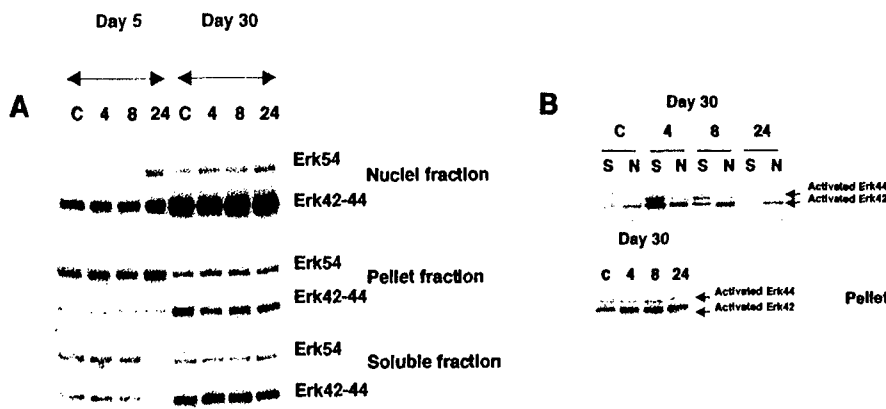
To understand the seemingly discrepant immunoblotting and immunolocalization results on cleaved caspase-3 during CPT-induced apoptosis, we hypothesized that cleaved caspase-3 forms complexes with other proteins that could serve as a pool of constitutively cleaved, inactive caspase-3. The DSP crosslinking and immunoprecipitation showed that cleaved caspase-3 in cortical neurons binds many proteins of different sizes (Fig. 4E, right lane). As a negative control, protein interactions involving cleaved caspase-3 were reversed by  $\beta$ -mercaptoethanol, resulting in a single major 17-kD band of cleaved caspase-3 (Fig. 4E, left lane).

#### **Mitogen-activated protein kinase signaling is different in immature and mature cortical neurons during camptothecin-induced apoptosis**

Components of the MAP kinase pathway were evaluated in subcellular fractions of control and CPT-treated DIV5 and DIV30 neurons. In control neurons, Erk54 was higher in nuclear fractions of mature neurons, but Erk54 was higher in the pellet and soluble fractions of immature neurons (Fig. 5A). Changes in Erk after CPT treatment were different in neuronal cultures at different ages. In DIV5 neuron nuclei, Erk54 levels were increased approximately fivefold after 24 hours of CPT exposure, whereas in DIV30 neuron nuclei only a 1.5-fold increase in Erk54 occurred after 24-hour CPT exposure (Fig. 5A). Erk54 levels in the pellet fraction increased slightly (< 50%) in DIV5 neurons after 24-hour exposure to CPT, but no change occurred in DIV30 neurons (Fig. 5A). Erk54 levels in the soluble compartment decreased by more than 50% in DIV5 neurons between 8 and 24 hours of CPT treatment, but Erk54 levels did not change in soluble fractions of DIV30 neurons (Fig. 5A).

Erk42/44 levels in nuclear, pellet, and soluble fractions were lower in DIV5 neurons compared with DIV30 neurons (Fig. 5A). Total Erk42/44 levels in DIV5 and DIV30 neurons during CPT-induced apoptosis did not change in the different subcellular fractions, except for a loss in the soluble fraction of DIV5 neurons at 24 hours (Fig. 5A).

Active Erk levels were different in immature and mature control neurons and in neurons responding to DNA damage. Phosphorylated Erk42/44 was not detected in the different subcellular fractions of control DIV5 neurons, and no phosphorylation of Erk42/44 occurred in DIV5 neurons after CPT exposure (data not shown). In contrast, phospho-Erk was detected in control DIV30 neurons (Fig. 5B). Activated Erk42 levels were generally higher than activated Erk44 levels in nuclear, soluble, and pellet fractions. The pellet fraction had the highest



constitutive control levels in DIV30 neurons. Changes in Erk42/44 levels were not observed during apoptosis. In contrast, prominent phosphorylation of Erk42/44 occurred in DIV30 neurons exposed to CPT (B). Activation of Erk (detected with phospho-Erk antibody) occurred in soluble (S), nuclear (N), and insoluble (pellet) fractions. These results were reproduced in three different platings and at least four different immunoblots per antibody.

level of activated Erk42 (Fig. 5B). Phospho-Erk42/44 levels in nuclear and soluble fractions increased dramatically ( $> 10$ -fold for soluble Erk44) after CPT after 4 hours of treatment (Fig. 5B) and remained high until 8 hours of treatment, after which levels decreased. Activated Erk42/44 levels in the pellet fraction were approximately double control levels at 4 and 8 hours (Fig. 5B).

#### A reversible caspase-3 inhibitor blocks apoptosis in immature neurons and MEK inhibition blocks apoptosis in immature and mature neurons

Caspase-3 is activated in cortical neurons undergoing CPT-induced apoptosis, based on immunoblotting or immunolocalization for cleaved caspase-3 and on PARP cleavage. Furthermore, Erk42/44 is activated prominently in DIV30 neurons, but not in DIV5 neurons. To determine whether these pathways are participating in the mechanisms of apoptosis in cortical neurons induced by CPT, cells were treated either with inhibitors of

caspase-3 or with MEK. Caspase-3 inhibition blocked CPT-induced apoptosis in DIV5 but not DIV25 cortical neurons (Fig. 6). The MEK1/2 inhibitor U0126 blocked apoptosis in both DIV5 and DIV25 cortical neurons (Fig. 6). The neuroprotection was more dramatic in DIV5 neurons. In control cells not exposed to CPT, U0126 induced apoptosis in DIV25 neurons but not in DIV5 neurons (Fig. 6).

We evaluated if the antiapoptotic effects of U0126 were associated with a blockade of alterations in the MAP kinase pathway in CPT-treated neurons (Fig. 7). In CPT-treated DIV5 neurons, U0126 blocked the subcellular translocation of Erk54 from soluble to nuclear compartments and the nuclear accumulation of cleaved caspase-3 (Fig. 7A). Evidence for Erk42/44 activation and translocation in DIV5 neurons during apoptosis was not observed (Fig. 5A); thus, these events were not studied in cells treated with CPT and U0126. In CPT-treated DIV25 neurons, U0126 blocked the activation of

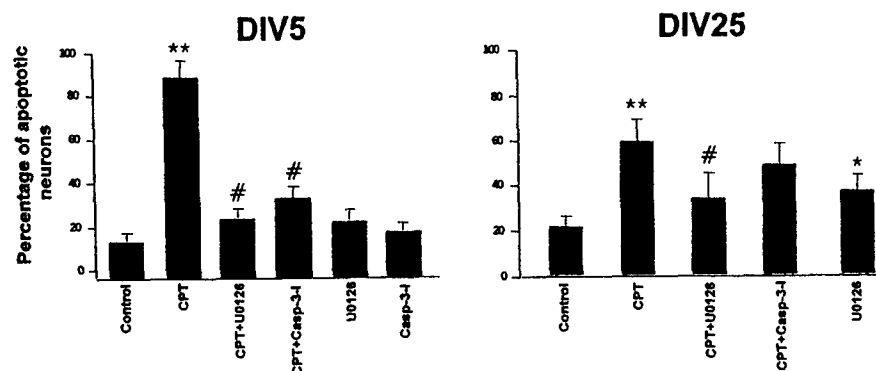


**FIG. 6.** The effects of drugs on camptothecin (CPT)-induced apoptosis in immature and mature cortical neurons are different. Immature cortical neuron cultures at DIV5 (days *in vitro*: 5; left) and mature cortical neuron cultures at DIV25 (right) were treated as controls or were exposed to 100  $\mu$ M CPT for 24 hours alone or with prior exposure (2-hour pretreatment) to cell-permeable reversible caspase-3 inhibitor (Casp-3-I) or the MEK1/2 inhibitor U0126, or were treated with only U0126 or caspase-3 inhibitor. Hoechst 33258 staining was used to determine the percentages of apoptotic neurons.

toxic neurons. The values are mean  $\pm$  SD. Results shown are from experiments using inhibitors at 100- $\mu$ M/L concentrations. Similar results were obtained using inhibitors at 10- $\mu$ M/L concentrations. These results were reproduced in three different platings. In DIV5 neurons, CPT induced significant ( $**P < 0.001$ ) apoptosis compared with the control. The U0126 and caspase-3 inhibitor significantly ( $#P < 0.001$ ) attenuated the CPT-induced apoptosis in DIV5 neurons. In DIV25 neurons, CPT induced significant ( $**P < 0.01$ ) apoptosis compared with the control. U0126 significantly ( $#P < 0.05$ ) attenuated the CPT-induced apoptosis in DIV25 neurons. In DIV25 neurons not exposed to CPT, U0126 caused a significant ( $*P < 0.05$ ) induction of apoptosis compared with the control. MEK, MAP kinase kinase.

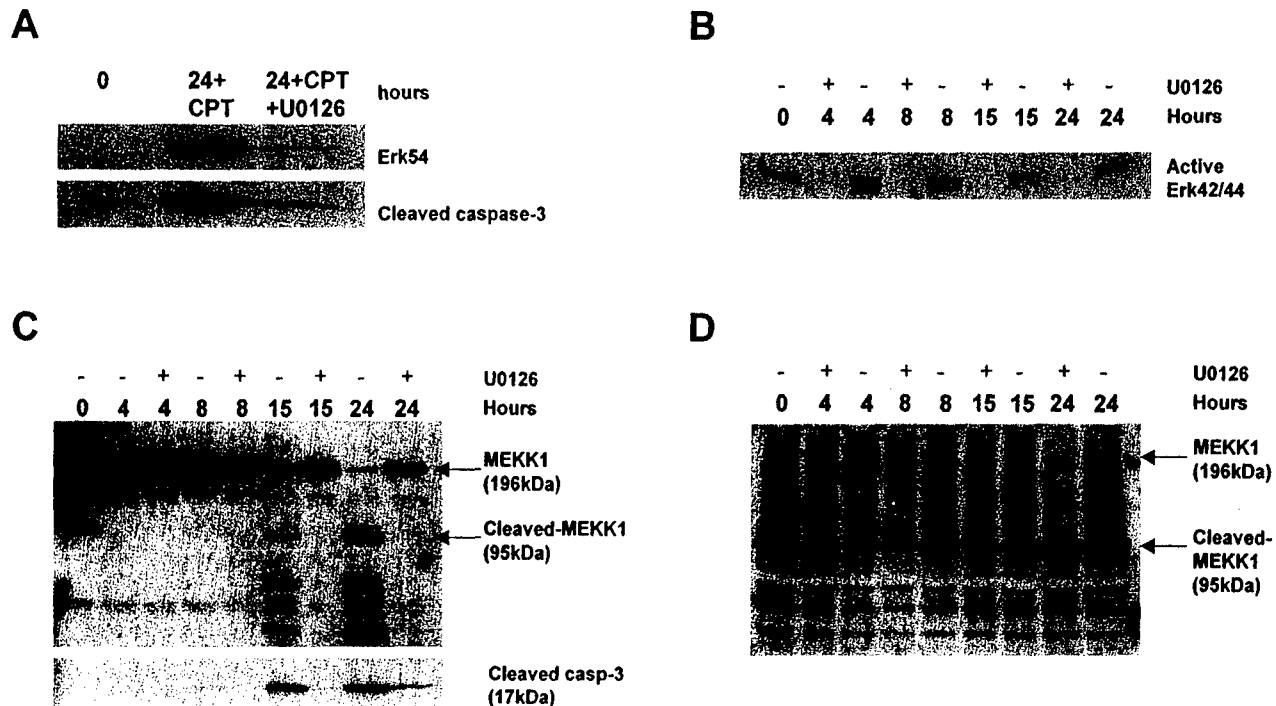


**FIG. 7.** Different components of the MAP kinase pathway are activated in immature and mature cortical neurons undergoing apoptosis and are blocked by an inhibitor of MEK (U0126). **(A)** DIV5 (days *in vitro*: 5) cortical neurons were treated with vehicle (0) or camptothecin (CPT) for 24 hours with or without pretreatment with U0126. Erk54 translocation to the nucleus and caspase-3 cleavage during CPT-induced apoptosis are blocked by U0126. **(B)** DIV25 cortical neurons were treated with vehicle (0) or CPT for 4, 8, 15, and 24 hours with (+) or without (-) pretreatment with U0126. The activation of Erk42/44 during CPT-induced apoptosis is blocked by U0126. **(C)** DIV5 cortical neurons were treated with vehicle (0) or CPT for 4, 8, 15, and 24 hours with (+) or without (-) pretreatment with U0126. MEKK1 is cleaved into putative apoptotic fragments (95 kd) during CPT-induced apoptosis. There is a corresponding loss of full-length (prosurvival) MEKK1 (196 kd). Cleaved MEKK1 is present at 15 hours with further accumulation at 24 hours. Significant accumulation of cleaved caspase-3 (lower blot) coincided with MEKK1 cleavage, consistent with a positive-feedback loop (Cardone et al., 1997). U0126 blocks the cleavage of MEKK1 and caspase-3. **(D)** DIV25 (days *in vitro*: 25) cortical neurons were treated with vehicle (0) or CPT for 4, 8, 15, and 24 hours with (+) or without (-) pretreatment with U0126. Cleaved MEKK1 is constitutively present in mature neurons, and levels do not change during apoptosis. In neurons treated with CPT alone, there is a loss of full-length MEKK1 (196 kd), and U0126 in combination with CPT further promotes the loss of full-length MEKK1. These results were reproduced in three different platings. Erk, extracellular signal-regulated kinase; MAP, mitogen-activated protein; MEK, MAP kinase kinase; MEKK1, MAP kinase kinase kinase-1.

Erk42/44 early in the process of apoptosis, and this block in Erk42/44 activation was sustained (Fig. 7B).

The MAP kinase pathway can function in DNA damage-induced apoptosis through MEKK1 in nonneuronal cells. Full-length MEKK1 (~160 to 197 kd) promotes cell survival, whereas cleaved MEKK1 (~72 to 95 kd) promotes apoptosis (Cardone et al., 1997; Widmann et al., 1998). Caspase-3 generates MEKK1 C-terminal fragments that have constitutively active proapoptotic kinase activity (Cardone et al., 1997). We examined the levels of full-length MEKK1 and putative proapoptotic MEKK1 fragments in nontreated and CPT-treated cortical neuron cultures. In control DIV5 neurons, a single major immunoreactive band of approximately 196 kd was detected (Fig. 7C), corresponding to full-length MEKK1. In CPT-treated neurons at 4 and 8 hours, only one major band of approximately 196 kd was still detected, and the levels were similar to control (Fig. 7C). In contrast, in CPT-treated neurons at 15 and 24 hours, several cleavage products of MEKK1 were observed. MEKK1 cleavage was greater at 24 hours compared with

15 hours (Fig. 7C). These cleavage products had sizes (~70 to 95) that were similar to the reported sizes of the active kinase fragments of MEKK1 that induce apoptosis (Cardone et al., 1997). The detection of these immunoreactive bands with the MEKK1 antibody was blocked by competition with a synthetic peptide corresponding to the C-terminal domain of MEKK1 (data not shown). There was an inverse relationship between the levels of MEKK1 fragments and full-length MEKK1, supporting the conclusion that the immunoreactive proteins at approximately 70 to 95 kd are derived from cleavage of MEKK1 holoenzyme. The levels of full-length MEKK1 decreased correspondingly at 15 hours, and were very low at 24 hours, at a time when the level of immunoreactive MEKK1 fragments was greatest (Fig. 7C). The formation of MEKK1 C-terminal fragments coincided with the formation of cleaved caspase-3 in DIV5 neurons (Fig. 7C, lower blot). U0126 blocked MEKK1 degradation and the formation of the putative proapoptotic MEKK1 fragments and active caspase-3 in immature neurons (Fig. 7C). Mature neurons had lower

levels of full-length MEKK1 and greater amounts of constitutively cleaved MEKK1 C-terminal fragments compared with immature neurons. The level of MEKK1 fragments at approximately 70 to 95 kd remained unchanged during apoptosis (Fig. 7D). However, the level of full-length MEKK1 decreased during apoptosis (Fig. 7D). Treatment with U0126 further decreased the level of full-length MEKK1 in CPT-exposed mature neurons (Fig. 7D).

#### Subcellular levels of p53, Bcl-2 family members, and synuclein proteins in cortical neurons and changes during camptothecin-induced apoptosis

We evaluated p53 in three subcellular fractions of cortical neurons. p53 was detected in nuclear and pellet fractions of DIV5 and DIV30 neurons, but was not present in soluble fractions of DIV5 neurons (Fig. 8). Overall no major changes in the levels occurred early during apoptosis.

The levels of three Bcl-2 family members were evaluated in nuclear fractions of cortical neurons (Fig. 8, nuclear). Bak and Bcl-2, but not Bax, were detected in nuclear fractions of mouse cortical neurons. The presence of Bcl-2 in the nucleus is consistent with its localization to the nuclear envelope (Lithgow et al., 1994), but the presence of Bak in the nuclear fraction is a novel finding. Both Bak and Bcl-2 levels were higher in mature neurons compared with immature neurons. The level of Bcl-2 in DIV5 neurons decreased markedly with CPT for 24 hours, but Bcl-2 levels did not change in CPT-treated DIV30 neurons (Fig. 8, nuclei). Bak levels were unchanged in apoptotic DIV5 and DIV30 neurons (Fig. 8, nuclei).

The insoluble pellet fraction of mouse cortical neurons was identified as the mitochondrial-enriched fraction based on the high level of Cox1 (Fig. 8, pellet). The mitochondrial fraction contained Bax, Bak, Bcl-x<sub>L</sub>, and Bcl-2, consistent with the localization of some of these proteins in mitochondrial membranes in nonneuronal cells (Lithgow et al., 1994) and neurons (Martin and Liu, 2002). Bak and Bcl-2 were higher in mitochondrial fractions of mature neurons, but Bax and Bcl-x<sub>L</sub> were higher in mitochondrial fractions of immature neurons. A dramatic loss of Cox1 in DIV5 and DIV30 neurons with 24-hour exposure to CPT showed that mitochondrial integrity was compromised between 8 and 24 hours during apoptosis (Fig. 8, pellet). Electron microscopy confirmed the degeneration of mitochondria by 24 hours of treatment (Figs. 3B and 3C). Late changes occurred in the levels of Bcl-2 family members in the mitochondrial-enriched membrane fraction during cortical neuron apoptosis (Fig. 8, pellet). In DIV5 neurons exposed to CPT, the levels of Bax and Bak decreased dramatically (> 50%). In contrast, in DIV30 neurons, Bax and Bak levels did not change conspicuously during apoptosis (Fig. 8,

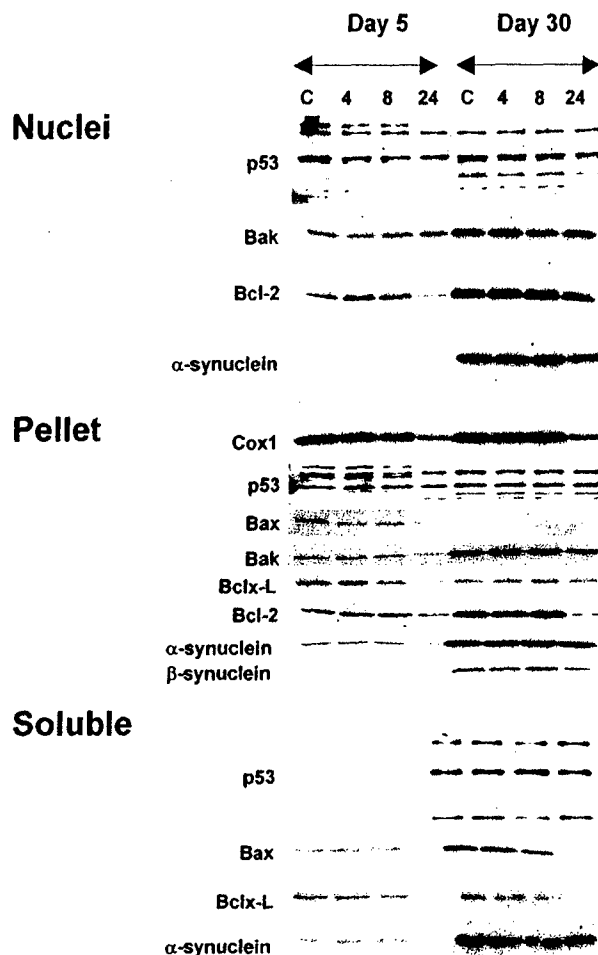


**FIG. 8.** Subcellular levels of p53, Bcl-2 family members, and synuclein proteins during camptothecin (CPT)-induced neuronal apoptosis. DIV5 (days *in vitro*: 5) and DIV30 mouse cortical neurons were treated with vehicle (control, C) or with 100  $\mu$ M/L CPT for 4, 8, or 24 hours (18 wells per treatment) and collected for subcellular fractionation into nuclear, pellet, and soluble fractions and subsequent analysis by immunoblotting. Nuclear fractions were evaluated for p53, Bak, Bcl-2, and  $\alpha$ -synuclein. Mitochondrial-enriched pellet fractions were analyzed for Cox1, p53, Bax, Bak, Bcl-x<sub>L</sub>, Bcl-2, and  $\alpha/\beta$ -synucleins. The mitochondrial enrichment of this fraction was confirmed by the high levels of Cox1. Bax, Bak, Bcl-x<sub>L</sub>, and Bcl-2 were reduced at 24 hours in DIV5 neurons. Bcl-2 was lost in DIV30 neurons. Soluble fractions were evaluated for p53, Bax, Bcl-x<sub>L</sub>, and  $\alpha$ -synuclein. p53 was not detected in soluble fractions. DIV5 neurons showed loss of Bax, Bcl-x<sub>L</sub> and  $\alpha$ -synuclein at 24 hours. DIV30 neurons showed a loss of Bax and Bcl-x<sub>L</sub> at 24 hours. These results were reproduced in three different platings and at least three different immunoblots per antibody.

pellet). The level of Bcl-x<sub>L</sub> decreased by more than 50% in DIV5 neurons after 24 hours of treatment with CPT, but remained unchanged in DIV30 neurons treated similarly. Bcl-2 levels decreased in neurons at both ages between 8 and 24 hours of treatment.

In the soluble fraction of control cortical neurons, Bax and Bcl-x<sub>L</sub> were detected, but Bak and Bcl-2 were not detected (Fig. 8, soluble). Bax was more enriched in soluble fractions of neurons at DIV30 compared with

DIV5 neurons. Bax levels decreased by more than 90% by 24 hours of CPT treatment at both ages. The level of Bcl-x<sub>L</sub> was similar in control cortical neurons at DIV5 and DIV30, and decreased by more than 50% between 8 and 24 hour of treatment with CPT.

Synuclein proteins function in apoptosis (Ostrerova et al., 1999). Major changes in their levels were not detected early during apoptosis of mouse cortical neurons (Fig. 8; nuclei, pellet, and soluble fractions). More interesting was the finding of differential localization in subcellular fractions.  $\beta$ -synuclein was not present in nuclear or soluble fractions of neurons at DIV5 and DIV30 or in the pellet fraction of DIV5 neurons; however,  $\beta$ -synuclein was present selectively in the pellet fraction of mature neurons.

## DISCUSSION

The degeneration of neurons *in vivo* induced by excitotoxicity and axotomy-target deprivation appears to be influenced by CNS maturity (Martin, 2001; Martin et al., 2001; Natale et al., 2002; Portera-Cailliau et al., 1997). Thus, neuronal death might be different in immature and mature neurons. Here, we tested the hypothesis that signaling mechanisms for DNA damaged-induced apoptosis in immature and mature neurons are different. We found that immature and mature neurons engage different apoptotic mechanisms during apoptosis *in vitro*. To classify the cell death in our study as apoptosis, we used DNA fragmentation patterns, morphology, caspase-3 and MEKK1 cleavage, and sensitivity to caspase inhibition. Caspase and MAP kinase pathways have different contributions to CPT-induced apoptosis in immature and mature cortical neurons *in vitro*. Apoptotic immature and mature neurons were different in terms of structure and fragmentation of DNA, cleavage of caspase-3 and MEKK1, nuclear translocation of Erk54, and phosphorylation of Erk42/44 (Fig. 9). A caspase-3 inhibitor blocked apoptosis in immature neurons but not in mature neurons, while a MEK inhibitor blocked apoptosis in neurons at both ages. These results show for the first time that young and older cortical neurons use different molecular mechanisms for apoptosis.

### Development of a new long-term cell culture model to study apoptosis in neurons at different ages

To evaluate the molecular mechanisms of apoptosis in neurons at different ages, a healthy long-term neuronal culture system was required. We established a long-term primary neuronal culture system using mouse cortical neurons and conducted a thorough morphologic and biochemical characterization to demonstrate the legitimacy of this neuronal system. Dendritic, synaptic, and metabolic markers revealed the relative immaturity or maturity of these neurons. These cortical neuron cultures undergo robust dendritic maturation as shown by the

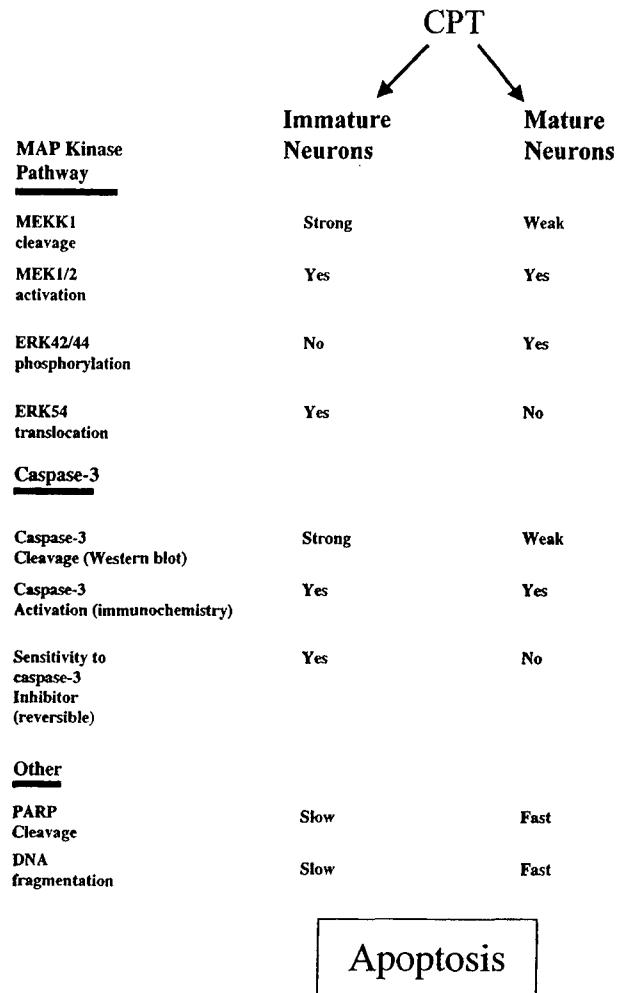


**FIG. 9.** Diagram contrasting some of the different and similar molecular mechanisms that are engaged during camptothecin (CPT)-induced apoptosis of immature and mature mouse cortical neurons. Erk, extracellular signal-regulated kinase; MAP, mitogen-activated protein; MEK, MAP kinase kinase; MEKK1, MAP kinase kinase kinase-1; PARP, poly-ADP ribose polymerase.

expression of NMDA and AMPA receptors, prominent synapse formation as revealed by the expression of synaptophysin and synucleins, and metabolic maturation as shown by the expression of the glycolytic enzyme GAPDH. These cells remain healthy for at least 60 days, as evidenced by a sustained expression of glutamate receptors, synaptic proteins, Erk, and GAPDH. Morphologic assessments by light microscopy and EM confirmed the maturation and sustained viability of these neurons. The ability to maintain these cells to DIV60 attests to the healthy condition of these long-term neuronal cultures and strengthens our confidence that neuronal cell death experiments of fully mature but younger cultures (e.g., DIV30 neurons) will be representative of initially healthy cells that are undergoing a stress-induced or toxin-induced death process.

We used CPT to induce apoptosis in cortical neurons at different stages of maturation. A DNA-damaging

agent was used as an apoptotic stimulus because DNA lesions contribute to the pathogenesis of CNS injury in children and adults (Kohji et al., 1998; Martin, 2001). Furthermore, upper cortical motor neuron degeneration in amyotrophic lateral sclerosis is a form of apoptosis that may be mediated by p53 mechanisms triggered by DNA damage (Martin, 2001). The induction of neuronal apoptosis after exposure to CPT has been shown previously (Morris and Geller, 1996; Park et al., 1997; Stefanis et al., 1999; Xiang et al., 1998). In nonneuronal cells, this poisoning may involve the stabilization of topoisomerase-DNA complexes and premature termination of transcription (Bendixen et al., 1990; Hsiang et al., 1985) as well as the formation of DNA single-strand breaks (Nieves-Neira and Pommier, 1999).

#### **The progression of DNA fragmentation is different in immature and mature neurons undergoing apoptosis**

DNA fragmentation was different in immature and mature cortical neurons undergoing apoptosis. Internucleosomal fragmentation of DNA occurred earlier and more prominently in DIV30 neurons than in DIV5 neurons (Fig. 9). The differences in DNA degradation patterns may reflect the participation of different endonucleases in the death of immature and mature neurons or different types of chromatin degradation early during apoptosis. Immature neurons may generate larger fragments (> 50 kb) early during apoptosis that are undetectable by conventional agarose gel electrophoresis (MacManus et al., 1997). Other studies have shown that apoptosis can occur in some cells without internucleosomal fragmentation of DNA (Tomei et al., 1993). The finding of a study of muscle cells that internucleosomal cleavage of DNA during apoptosis varies depending on the degree of differentiation (Fimia et al., 1996) is consistent with our results. Inactivation of the DNA repair enzyme PARP also occurred more rapidly in older neurons compared with young neurons. It is interesting that both DNA fragmentation and PARP cleavage were observed earlier in older neurons, despite more apoptosis in CTP-treated young neurons. The explanation for this observation is uncertain because of insufficient information on quantitative relationships between the fragmentation of DNA and death of single cells. In CTP-treated neurons, EM revealed that the morphology of the chromatin condensation into discrete aggregates were different in immature and mature neurons, with the immature neuron morphology being identical to that found in classical apoptosis (Martin et al., 1998). These results support the conclusion that mechanisms of DNA degradation and condensation are different in young and mature neurons. These data extend earlier structural studies suggesting that the apoptotic process is different in immature and

mature neurons (Martin et al., 1998; Portera-Cailliau et al., 1997).

#### **Caspase-3 cleavage is more prominent in immature neurons than in mature neurons during apoptosis**

The processing of caspase-3 during apoptosis of cortical neurons is maturation dependent. Low constitutive levels of cleaved caspase-3 were detected by immunoblotting in control and CPT-treated immature and mature neurons. Caspase-3 cleavage products increased dramatically in immature neurons but not in mature neurons undergoing apoptosis. Cleaved caspase-3 accumulated in nuclear and mitochondrial-enriched fractions. A nuclear and mitochondrial translocation of cleaved caspase-3 in apoptotic immature cortical neurons is supported by findings in apoptotic nonneuronal cells *in vitro* (Zhivotovsky et al., 1999) and in striatal neurons undergoing excitotoxic death in newborn brain (Lok and Martin, 2002). In apoptotic mature cortical neurons, we did not find increased caspase-3 cleavage products in immunoblots of different subcellular fractions. However, immunolocalization showed a prominent presence of cleaved caspase-3 in apoptotic mature neurons that was not seen in control neurons. In both CPT-treated immature and mature neurons, PARP was inactivated, indicating activation of caspases (Lazebnik et al., 1994). It is therefore possible that apoptosis of mature neurons does not require formation of additional caspase-3 subunits via proteolysis of proenzyme, and that preexisting low levels of cleaved caspase-3 are sufficient to execute the death process. The rapid and robust internucleosomal fragmentation of DNA and the early PARP inactivation in apoptotic mature neurons (Fig. 9) are consistent with this possibility. Constitutively cleaved caspase-3 may be regulated by other proteins that function as endogenous inhibitors of cleaved caspase-3. This idea is in part supported by our crosslinking results. Some of these proteins that bind cleaved caspase-3 are likely to be substrates, but some could be negative regulators. In unstressed normal cells, cleaved caspase-3 might interact with possible inhibitor proteins or the subunits may be folded or assembled as inactive enzyme. This could explain the lack of immunoreactivity in control cells because the epitope that is recognized by the cleaved caspase-3 antibody is masked. In this state, constitutive cleaved caspase-3 would be inactive and could not execute the apoptotic process. Thus, activation of caspase-3 in mature neurons may occur by mechanisms other than proteolytic cleavage of proenzyme. It is also possible that apoptosis in young and older neurons has varying contributions of caspase-3-independent mechanisms.

Immature and mature neurons were different in their sensitivity to caspase-3 inhibitor. A reversible caspase-3 inhibitor had significant antiapoptotic actions in DIV5 neurons but not in DIV30 neurons. To our knowledge,

this is the first demonstration of antiapoptotic actions of a reversible caspase-3 inhibitor in neurons (other studies have used irreversible inhibitors). This finding suggests that apoptosis in immature neurons may be caspase-3-dependent, whereas apoptosis of mature neurons is caspase-3-independent. However, the robust presence of cleaved caspase-3 observed directly in apoptotic mature neurons and the PARP cleavage would argue against this conclusion or in favor of the involvement of other caspases. It is not yet evident where caspase inhibitors act in intact cells to inhibit caspase activity. Inhibition of caspase-3 may occur in the cytoplasm, but the main action of active caspase-3 may be in the nucleus in mature neurons. This peptide inhibitor might not "see" existing cleaved caspase-3 in the nucleus. Furthermore, a peptide that is a reversible caspase-3 inhibitor would have to compete with endogenous protein inhibitors. Alternatively, caspases other than caspase-3 may be activated in apoptotic cortical neurons. Different types of caspase inhibitors need to be used to further evaluate the role of caspase-3 and other caspases in apoptosis of mature cortical neurons.

Previous studies have not clearly identified the role of caspases in CPT-induced apoptosis of immature neurons. Others have reported protection against CPT-induced apoptosis with 100  $\mu\text{mol/L}$  caspase-3 inhibitor in rat embryonic cortical neurons at DIV1 (Stefanis et al., 1999) and mouse telencephalic neuron cultures at DIV4 (Johnson et al., 1999). Caspase inhibition partially protected against and delayed CPT-induced apoptosis in mouse embryonic cortical neurons at DIV2 (Keramaris et al., 2000). However, other experiments have failed to block CPT-induced neuronal apoptosis with caspase inhibitor (Park et al., 1997). Moreover, caspase-3 deletion in caspase-3<sup>-/-</sup> mice appears to only delay the neuronal death by 24 hours (Keramaris et al., 2000). We found with a caspase-3 inhibitor a near complete block of CPT-induced apoptosis of immature cortical neurons at 24 hours.

#### **Mitogen-activated protein kinase pathway participates in the mechanisms of neuronal apoptosis**

The MAP kinase pathway functions in the regulation of cellular proliferation, differentiation, survival, and death (Cardone et al., 1997; English et al., 1999), although in postmitotic cells (such as neurons) the functions of this pathway are much less understood. Our study shows that different downstream (Erk42/44 and Erk54) and upstream (MEKK1) components of the MAP kinase pathway are enlisted during CPT-induced apoptosis in mature and immature neurons.

In CPT-treated mature neurons, phosphorylated Erk42/44 was sequestered in the nucleus early (4 hours) after exposure. A parallel decrease in the level of phos-

phorylated Erk42/44 in the soluble fraction suggests translocation from the cytoplasm to the nucleus. The phosphorylation and nuclear accumulation of Erk42/44 preceded the internucleosomal fragmentation of DNA (detected robustly at 8 hours). When activated, Erk42/44 translocates to the nucleus to phosphorylate target proteins, including transcription factors (Elk, Sap, and Sp1) and histone proteins (English et al., 1999), many of which are involved in apoptosis. This nuclear translocation of active Erk42/44 may function as a preapoptotic signal or a transient, compensatory survival signal in mature neurons. There is precedence for Erk activation functioning proapoptotically in mesangial cells (Ishikawa and Kitamura, 1999) and neuronal cells (Sato et al., 2000; Stanciu and DeFrance, 2002; Stanciu et al., 2000) after oxidative stress. We observed that blocking Erk activation by MEK inhibition protects cortical neurons against apoptosis, supporting a proapoptotic role for Erk activation in mature neurons.

Phosphorylation of Erk42/44 was not observed during the progression of apoptosis in immature neurons at DIV5. However, U0126 also blocked apoptosis in CPT-treated DIV5 neurons. The increased level of Erk54 could explain the apoptotic activity of the MAP kinase pathway in DIV5 neurons after exposure to CPT. This 54-kd protein detected with a pan-Erk antibody may be related to the Erk family (Keel et al., 1995). Erk54 has kinase activity and may be an isoform of Erk44 (Keel et al., 1995); however, Erk54 is distinct from Erk42/44 based on size, chromatographic properties, and substrate specificity (Kyriaks and Auruch, 1990). Because the level of Erk54 decreased dramatically (> 80%) in the soluble fraction, Erk54 (rather than Erk42/44) appears to be translocated to the nucleus in immature neurons but not mature neurons. This translocation of Erk54 coincided with the prominent nuclear accumulation of cleaved caspase-3. Both of these molecular events were blocked by MEK inhibition, which strongly protected DIV5 neurons against apoptosis.

MEKK1 could also account for the proapoptotic activity of the MAP kinase pathway in cortical neurons. This upstream kinase in the MAP kinase cascade also has dual functions. Full-length MEKK1 promotes cell survival, whereas MEKK1 C-terminal fragments promote apoptosis (Cardone et al., 1997; Widmann et al., 1998). Caspases act as switches to convert MEKK1 from a survival signal to a proapoptotic effector. MEKK1 fragments have constitutive kinase activity that can activate caspases, comprising a positive-feedback loop for driving apoptosis (Cardone et al., 1997). MEKK1 activity is required for apoptosis in nonneuronal cells after DNA damage (Widmann et al., 1998). We show for the first time that MEKK1 appears to have a role in neuronal apoptosis induced by DNA damage. This role might be



different in immature and mature neurons stimulated to undergo apoptosis as well as in unstressed normal neurons. For instance, cleaved MEKK1 levels were constitutively higher in mature neurons than in immature neurons, suggesting that C-terminal fragments of MEKK1 are inactive as proapoptotic kinases in mature neurons. Major C-terminal fragments of MEKK1 were not present constitutively in immature neurons. However, during CPT-induced apoptosis of immature cortical neurons, the formation of C-terminal fragments of MEKK1 coincided with caspase-3 cleavage and decreased full-length MEKK1. In contrast, during CPT-induced apoptosis of mature cortical neurons, levels of major C-terminal fragments of MEKK1 did not appear to change, but levels of full-length (survival) MEKK1 declined, suggesting different mechanisms for MEKK1 processing and stabilization in mature and immature neurons. The loss of full-length MEKK1 may be sufficient to engage apoptosis in mature neurons. The antiapoptotic actions of U0126 could be mediated by the prevention of MEKK1 cleavage in immature neurons, but this is unlikely the case in mature neurons because MEK inhibition enhanced the loss of full-length MEKK1 during apoptosis. Thus, the primary antiapoptotic action of U0126 in mature neurons may be through blockade of Erk42/44 activation with a feedback modulation of MEKK1.

The duality of the MAP kinase pathway in regulating cell death or survival has been realized previously. In nonneuronal cells, basal constitutive activity of Erk functions in cell survival, whereas a transient upregulation of Erk induces apoptosis (Ishikawa and Kitamura, 1999). Depending on the cell type and context, Erk signaling can participate in neuronal survival (Hetman et al., 1999) or neuronal death (Sato et al., 2000; Stanciu et al., 2000). A neuronal study revealed that Erk activation by neurotrophin is important for survival of rat cortical neurons *in vitro* (Hetman et al., 1999). However, activation of Erk42/44 might contribute to neuronal apoptosis in some *in vitro* models of neurotoxicity (Jiang et al., 2000; Stanciu et al., 2000), although the mechanisms are not known. We found that the MAP kinase pathway has a survival function in unstressed mature DIV30 neurons but not in unstressed immature DIV5 neurons. Specifically, MEK inhibition induced apoptosis in healthy, unstressed mature neurons but not in immature neurons (Fig. 6). This finding is consistent with the observation that DIV5 neurons do not require constitutive phosphorylation of Erk42/44. Therefore, Erk42/44 phosphorylation is less important as a survival signal in unstressed immature neurons compared with mature neurons. However, in mature and immature neurons undergoing genotoxic stress, the MAP kinase pathway assumes a proapoptotic function (Figs. 6 and 9). The proapoptotic activity of Erk in immature neurons with DNA damage did not appear to require phosphorylation of Erk42/44.

Our study is the first to reveal a proapoptotic function of Erk during DNA damage-induced neuronal apoptosis that may be unrelated to Erk42/44 phosphorylation.

#### **Roles of p53 and Bax during camptothecin-induced cortical neuronal apoptosis require further examination**

Camptothecin neurotoxicity may involve p53 and Bax. Neuronal death induced by CPT in granule neurons is blocked in cells deficient in p53 and Bax (Xiang et al., 1998). We did not, however, observe increased p53 and Bax protein levels in different subcellular fractions (nuclear, insoluble/pellet, and soluble) of DIV5 and DIV30 cortical neurons exposed to CPT. An early change in the intracellular localization of Bax has been found in apoptotic nonneuronal cells, with a redistribution of soluble Bax to mitochondria promoting cell death (Wolter et al., 1997). In human colon adenocarcinoma cells treated with CPT, Bax redistributes from the cytosol to organelle membranes within 1 or 2 hours after drug exposure (Gajkowska et al., 2001). During striatal neuron apoptosis in newborn rat brain, Bax translocates to mitochondrial membranes within 2 hours after the stimulus (Lok and Martin, 2002). In cultured cortical neurons, the levels of Bax in the mitochondrial-enriched cell fraction and soluble fraction decreased dramatically between 8 and 24 hours after exposure to CPT. However, an early subcellular translocation of Bax could have been missed because our earliest time point was 4 hours after CPT; moreover, p53 activation (phosphorylation) needs to be evaluated in our system. Additional experiments are necessary to define the role of Bax and p53 in CPT-induced cortical neuron apoptosis.

#### **CONCLUSIONS**

Apoptotic cell death mechanisms in immature and mature cortical neurons are different (Fig. 9). Young and old neurons may use different caspase-3 activation mechanisms and enlist different components of the MAP kinase pathway during apoptosis. Caspase-3 activation by proenzyme cleavage occurs more strongly in apoptotic immature neurons compared with older neurons. The cleavage of full-length MEKK1 into putative proapoptotic fragments also occurs more prominently in immature neurons versus mature neurons. In contrast, Erk42/44 is strongly activated in mature neurons undergoing apoptosis but not in immature neurons, while Erk54 increases in immature but not mature neurons. Our experiments show for the first time that the developmental maturity or age of neurons influences the mechanisms of apoptosis induced by DNA damage and that pharmacologic therapies for the protection of young and older neurons might be different.

**Acknowledgments:** The authors are grateful for the expert technical assistance of Frank Barksdale and Ann Price.

## REFERENCES

- Al-Abdulla NA, Martin LJ (1998) Apoptosis of retrogradely degenerating neurons occurs in association with the accumulation of perikaryal mitochondria and oxidative damage to the nucleus. *Am J Pathol* 153:447-456
- Alessandrini A, Namura S, Moskowitz MA, Bonventre JV (1999) MEK1 protein kinase inhibition protects against damage resulting from focal cerebral ischemia. *Proc Natl Acad Sci U S A* 96:12866-12869
- Anderson AJ, Su JH, Cotman CW (1996) DNA damage and apoptosis in Alzheimer's disease: Colocalization with c-jun immunoreactivity, relationship to brain area, and effect of postmortem delay. *J Neurosci* 16:1710-1719
- Bendixen C, Thomsen B, Alsner J, Westergaard O (1990) Camptothecin-stabilized topoisomerase I-DNA adducts cause premature termination of transcription. *Biochemistry* 29:5613-5619
- Brewer GJ, Torricelli JR, Evege EK, Price PJ (1993) Optimized survival of hippocampal neurons in B27-supplemented Neurobasal, a new serum-free medium combination. *J Neurosci Res* 35:567-576
- Cardone MH, Salvesen GS, Widmann C, Johnson G, Frisch SM (1997) The regulation of anoikis: MEKK-1 activation requires cleavage by caspases. *Cell* 90:315-323
- English J, Pearson G, Wilsbacher J, Swantek J, Karandikar M, Xu S, Cobb MH (1999) New insights into the control of MAP kinase pathways. *Exp Cell Res* 253:255-270
- Fimia GM, Gottifred V, Passananti C, Malone R (1996) Double-stranded internucleosomal cleavage of apoptotic DNA is dependent on the degree of differentiation in muscle cells. *J Biol Chem* 271:15575-15579
- Gajkowska B, Motyl T, Olszewska-Badarczuk, Godlewski MM (2001) Expression of Bax in cell nucleus after experimentally induced apoptosis revealed by immunogold and embedment-free electron microscopy. *Cell Biol Int* 25:725-733
- Hakem R, Hakem A, Duncan GS, Henderson JT, Woo M, Soengas MS, Elia A, de la Pompa JL, Kagi D, Khoo W, Potter J, Yoshida R, Kaufman SA, Lowe SW, Penninger JM, Mak TW (1998) Differential requirement for caspase 9 in apoptotic pathways *in vivo*. *Cell* 94:339-352
- Hetman M, Kanning K, Cavanaugh JE, Xia Z (1999) Neuroprotection by brain-derived neurotrophic factor is mediated by extracellular signal-regulated kinase and phosphatidylinositol 3-kinase. *J Biol Chem* 274:22569-22580
- Hsiang YH, Hertzberg R, Hecht S, Liu LF (1985) Camptothecin induced protein-linked DNA breaks via mammalian DNA topoisomerase I. *J Biol Chem* 260:14873-14878
- Ishikawa Y, Kitamura M (1999) Dual potential of extracellular signal-regulated kinase for the control of cell survival. *Biochem Biophys Res Comm* 264:696-701
- Jiang Q, Gu Z, Zhang G, Jing G (2000) Diphosphorylation and involvement of extracellular signal-regulated kinases (ERK1/2) in glutamate-induced apoptotic-like death in cultured rat cortical neurons. *Brain Res* 857:71-77
- Johnson MD, Kinoshita Y, Xiang H, Ghatan S, Morrison RS (1999) Contribution of p53-dependent caspase activation to neuronal cell death declines with neuronal maturation. *J Neurosci* 19:2996-3006
- Keel BA, Hildebrandt JM, May JV, Davis JS (1995) Effects of epidermal growth factor on the tyrosine phosphorylation of mitogen-activated protein kinases in monolayer cultures of porcine granulosa cells. *Endocrinology* 136:1197-1204
- Keramaris E, Stefanis L, MacLaurin J, Harada N, Takaku K, Ishikawa T-O, Taketa MM, Robertson GS, Nicholson DW, Slack RS, Park DS (2000) Involvement of caspase 3 in apoptotic death of cortical neurons evoked by DNA damage. *Mol Cell Neurosci* 15:368-379
- Kitamura Y, Taniguchi T, Shimohama S (1999) Apoptotic cell death in neurons and glial cells: implications for Alzheimer's disease. *Jpn J Pharmacol* 79:1-5
- Kohji T, Hayashi M, Shioda K, Minagawa M, Morimatsu Y, Tamagawa K, Oda M (1998) Cerebellar neurodegeneration in human hereditary DNA repair disorders. *Neurosci Lett* 243:133-136
- Kuida K, Zheng TS, Na S, Kuan C-Y, Yang D, Karasuyama H, Rakic P, Flavell RA (1996) Decreased apoptosis in the brain and premature lethality in CPP32-deficient mice. *Nature* 384:368-372
- Kyriakis JM, Avruch J (1990) pp54 Microtubule-associated protein-2 kinase: a novel serine/threonine protein kinase regulated by phosphorylation and stimulated by poly-L-lysine. *J Biol Chem* 265:17355-17363
- Lazebnik YA, Kaufmann SH, Desnoyers S, Poirier GG, Earnshaw WC (1994) Cleavage of poly(ADP-ribose) polymerase by a proteinase with properties like ICE. *Nature* 371:346-347
- Lesuisse C, Martin LJ (2002) Long-term culture of mouse cortical neurons as a model for neuronal development, aging, and death. *J Neurobiol* 51:9-23
- Levine AJ (1997) p53, the cellular gatekeeper for growth and division. *Cell* 88:323-331
- Lithgow T, van Driel R, Bertram JF, Strasser A (1994) The protein product of the oncogene *bcl-2* is a component of the nuclear envelope, the endoplasmic reticulum, and the outer mitochondrial membrane. *Cell Growth Differ* 5:411-417
- Liu XZ, Xu XM, Hu R, Du C, Zhang SX, McDonald JW, Dong HX, Wu YJ, Fan GS, Jacquin MF, Hsu CH, Choi DW (1997) Neuronal and glial apoptosis after traumatic spinal cord injury. *J Neurosci* 17:5395-5406
- Lok J, Martin LJ (2002) Rapid subcellular distribution of bax precedes caspase-3 and endonuclease activation during excitotoxic neuronal apoptosis in rat brain. *J Neurotrauma*, in press
- MacManus JP, Rasquinha I, Tuor U, Preston E (1997) Detection of higher-order 50- and 10-kbp DNA fragments before apoptotic internucleosomal cleavage after transient cerebral ischemia. *J Cereb Blood Flow Metab* 17:376-387
- Martin LJ (1999) Neuronal death in amyotrophic lateral sclerosis is apoptosis: possible contribution of a programmed cell death mechanism. *J Neuropathol Exp Neurol* 58:459-471
- Martin LJ (2001) Neuronal cell death in nervous system development, disease, and injury. *Int J Mol Med* 7:455-478
- Martin LJ, Blackstone CD, Levey AI, Hagan RL, Price DL (1993) AMPA glutamate receptor subunits are differentially distributed in rat brain. *Neuroscience* 53:327-358
- Martin LJ, Al-Abdulla NA, Brambrink AM, Kirsch JR, Sieber FE, Portera-Cailliau C (1998) Neurodegeneration in excitotoxicity, global cerebral ischemia, and target deprivation: a perspective on the contributions of apoptosis and necrosis. *Brain Res Bull* 46:281-309
- Martin LJ, Sieber FE, Traystman RJ (2000) Apoptosis and necrosis occur in separate neuronal populations in hippocampus and cerebellum after ischemia and are associated with alterations in metabotropic glutamate receptor signaling pathways. *J Cereb Blood Flow Metab* 20:153-167
- Martin LJ, Kaiser A, Yu JW, Natale JE, Al-Abdulla NA (2001) Injury-induced apoptosis of neurons in adult brain is mediated by p53-dependent and p53-independent pathways and requires bax. *J Comp Neurol* 433:299-311
- Martin LJ, Liu Z (2002) Injury-induced spinal motor neuron apoptosis is preceded by DNA single-strand breaks and is p53- and bax-dependent. *J Neurobiol* 5:181-197
- Morris EJ, Geller HM (1996) Induction of neuronal apoptosis by camptothecin, an inhibitor of DNA topoisomerase-I: evidence for cell cycle-independent toxicity. *J Cell Biol* 134:757-770
- Natale JE, Cheng Y, Martin LJ (2002) Thalamic neuron apoptosis emerges rapidly after cortical damage in immature mice. *Neuroscience*, in press
- Nieves-Neira W, Pommier Y (1999) Apoptotic response to camptothecin and 7-hydroxystaurosporine (UCN-01) in the 8 human breast cancer cell lines of the NCI anticancer drug screen: multifactorial relationships with topoisomerase I, protein kinase C, Bcl-2, p53, MDM-2 and caspase pathways. *Int J Cancer* 82:396-404
- Ostrerova N, Petrucelli L, Farrer M, Mehta N, Choi P, Hardy J, Wolozin B (1999)  $\alpha$ -Synuclein shares physical and functional homology with 14-3-3 proteins. *J Neurosci* 19:5782-5791
- Park DS, Morris EJ, Greene LA, Geller HM (1997) C1/S cell cycle blockers and inhibitors of cyclin-dependent kinases suppress camptothecin-induced neuronal apoptosis. *J Neurosci* 17:1256-1270
- Park DS, Morris EJ, Stefanis L, Troy CM, Shelanski ML, Geller HM, Greene LA (1998) Multiple pathways of neuronal death induced by

- DNA-damaging agents, NGF deprivation, and oxidative stress. *J Neurosci* 18:830-840
- Polyak K, Xia Y, Zweier JL, Kinzler KW, Vogelstein B (1997) A model for p53-induced apoptosis. *Nature* 389:300-305.
- Portera-Cailliau C, Price DL, Martin LJ (1997) Non-NMDA and NMDA receptor-mediated excitotoxic neuronal deaths in adult brain are morphologically distinct: further evidence for an apoptosis-necrosis continuum. *J Comp Neurol* 378:88-104
- Satoh T, Nakatsuka D, Watanabe Y, Nagata I, Kikuchi H, Namura S (2000) Neuroprotection by MAPK/ERK kinase inhibition with U0126 against oxidative stress in a mouse neuronal cell line and rat primary cultured cortical neurons. *Neurosci Lett* 288:163-166
- Stanciu M, Wang Y, Kentor R, Burke N, Watkins S, Kress G, Reynolds I, Klann E, Angiolieri MR, Johnson JW, DeFranco DB (2000) Persistent activation of ERK contributes to glutamate-induced oxidative toxicity in a neuronal cell line and primary cortical neuron cultures. *J Biol Chem* 275:12200-12206
- Stanciu M and DeFranco DB (2002) Prolonged nuclear retention of activated extracellular signal-regulated protein kinase promotes cell death generated by oxidative toxicity or proteasome inhibition in a neuronal cell line. *J Biol Chem* 277:4010-1017
- Stefanis L, Park DS, Friedman WJ, Greene LA (1999) Caspase-dependent and -independent death of camptothecin-treated embryonic cortical neurons. *J Neurosci* 19:6235-6247
- Tomei LD, Shapiro JP, Cope FO (1993) Apoptosis in C3H/10T<sup>1/2</sup> mouse embryonic cells: evidence for internucleosomal DNA modification in the absence of double-strand cleavage. *Proc Natl Acad Sci U S A* 90:853-857
- Widmann C, Gerwins P, Johnson NL, Jarpe MB, Johnson GL (1998) MEK kinase 1, a substrate for DEVD-directed caspases, is involved in genotoxin-induced apoptosis. *Mol Cell Biol* 18:2416-2429
- Wolter KG, Hsu YT, Smith CL, Nechushtan A, Xi XG, Youle RJ (1997) Movement of Bax from the cytosol to mitochondria during apoptosis. *J Cell Biol* 139:1281-1292
- Xiang H, Kinoshita Y, Knudson CM, Korsmeyer SJ, Schwartzkroin PA, Morrison RS (1998) Bax involvement in p53-mediated neuronal cell death. *J Neurosci* 18:1363-1373
- Zhivotovsky B, Samali A, Gahm A, Orrenius S (1999) Caspases: their intracellular localization and translocation during apoptosis. *Cell Death Differ* 6:44-651

# Motor Neurons Rapidly Accumulate DNA Single-Strand Breaks After In Vitro Exposure to Nitric Oxide and Peroxynitrite and In Vivo Axotomy

ZHIPING LIU<sup>1</sup> AND LEE J. MARTIN<sup>1,2\*</sup>

<sup>1</sup>Department of Pathology, Johns Hopkins University School of Medicine, Baltimore, Maryland 21205-2196

<sup>2</sup>Department of Neuroscience, Johns Hopkins University School of Medicine, Baltimore, Maryland 21205-2196

## ABSTRACT

The mechanisms of neuronal degeneration in motor neuron disease are not fully understood. We tested the hypothesis that oxidative stress in vitro and axotomy in vivo induce single-strand breaks (SSB) in DNA, a form of early DNA damage, in adult motor neurons early during their degeneration. We developed and characterized a novel cell suspension system enriched in motor neurons from adult rat spinal cord ventral horn. This cell system is ~84% neurons, with ~86% of these neurons being motor neurons; ~72% of these motor neurons are  $\alpha$ -motor neurons. Motor neuron viability in suspension is ~100% immediately after isolation and ~61% after 12 hours of incubation. During incubation, isolated motor neurons generate high levels of superoxide. We used single-cell gel electrophoresis (comet assay) to detect DNA-SSB in motor neurons. Exposure of motor neurons to nitric oxide (NO) donors (sodium nitroprusside or NONOate),  $H_2O_2$ , or NO donor plus  $H_2O_2$  rapidly induces DNA-SSB and causes motor neuron degeneration, the occurrence of which is dose and time related, as represented by comet formation and cell loss. Motor neuron toxicity is potentiated by cotreatment with NO donor and  $H_2O_2$  (at nontoxic concentrations alone). Peroxynitrite causes DNA-SSB in motor neurons. The DNA damage profiles (shown by the comet morphology and moment) of NO donors, NO donor plus  $H_2O_2$ , and peroxynitrite are similar. In an in vivo model of motor neuron apoptosis, DNA-SSB accumulate slowly in avulsed motor neurons before apoptotic nuclear features emerge, and the comet fingerprint is similar to NO toxicity. We conclude that motor neurons challenged by oxidative stress and axotomy accumulate DNA-SSB early in their degeneration and that the formation of peroxynitrite is involved in the mechanisms. *J. Comp. Neurol.* 432:35–60, 2001. © 2001 Wiley-Liss, Inc.

**Indexing terms:** amyotrophic lateral sclerosis; apoptosis; DNA damage; single-cell gel electrophoresis; spinal cord injury; superoxide

The degeneration of motor neurons in spinal cord, brainstem, and cerebral cortex is the cause of amyotrophic lateral sclerosis (ALS; for review, see Martin et al., 2000). This degeneration may be a form of aberrantly occurring apoptosis (Martin, 1999) that is mediated by p53 (Martin, 2000a), implicating DNA damage as an upstream pathogenic event. Injury to peripheral nerves in experimental animal models also causes apoptosis of spinal motor neurons that is associated with DNA damage (Martin et al., 1999a) and p53 induction (Martin et al., 1999b). Oxidative stress has been implicated in the pathogenesis of both ALS (Fitzmaurice et al., 1996; Ferrante et al. 1997) and motor neuron apoptosis after experimental lesion-

ing (Martin et al., 1999a). A few studies have found oxidative damage to DNA (in the form of 8-hydroxy-2-

Grant sponsor: U.S. Public Health Service, National Institutes of Health, the National Institute of Neurological Disorders and Stroke and the National Institute on Aging; Grant numbers: NS34100, AG16282; Grant sponsor: Department of Defense, U.S. Army Medical Research and Materiel Command; Grant number: DAMD17-99-1-9553.

\*Correspondence to: Lee J. Martin, Ph.D., Johns Hopkins University School of Medicine, Department of Pathology, 558 Ross Building, 720 Rutland Avenue, Baltimore, MD 21205-2196. E-mail: lmartin@jhmi.edu

Received 18 October 2000; Revised 8 December 2000; Accepted 8 December 2000.

deoxyguanosine adducts) in individuals with ALS (Fitzmaurice et al., 1996; Ferrante et al., 1997), and this type of DNA damage occurs specifically within motor neurons in these patients (Martin, 2000b). Similar oxidative damage to DNA is found directly in motor neurons after axotomy (Martin et al., 1999a), but it is not yet known with certainty whether DNA damage is an early upstream signal for motor neuron death or whether this damage is a consequence of degeneration.

DNA damage is a highly diverse and complicated process. DNA damage occurs in many different forms, including apurinic/apyrimidinic sites, double- and single-strand breaks, adduct formation, thymidine dimers, crosslinks, and insertion/deletion mismatches (Subba Rao, 1993). Single-strand breaks (SSB) in DNA are the earliest and major type of DNA damage among the several forms and are potent signals for apoptosis (Levine, 1997). Cells that have sustained DNA damage from reactive oxygen species (ROS) and other genotoxic agents undergo apoptosis by engaging molecular cascades involving expression or activation of p53, Bax, and caspases (Polyak et al., 1997). It is possible that motor neurons in the adult brain and spinal cord are particularly sensitive to oxidative stress by forming DNA-SSB, thereby providing a signal for motor neurons to undergo apoptosis. We therefore evaluated whether oxidative stress induces DNA-SSB in adult motor neurons *in vitro* and whether DNA-SSB occur in adult motor neurons early in the progression of apoptosis *in vivo*.

New approaches need to be developed to study the degeneration of adult motor neurons, and sensitive assays for specific types of DNA lesions need to be identified to study the possible role of DNA damage in the mechanisms for motor neuron apoptosis. We used two different model systems of motor neuron degeneration. We developed and characterized a novel short-term, motor neuron-enriched cell suspension system to evaluate the formation of DNA-SSB directly in adult spinal motor neurons exposed *in vitro* to hydrogen peroxide ( $H_2O_2$ ), nitric oxide (NO) donors, and peroxynitrite ( $ONOO^-$ ). DNA-SSB in single motor neurons were detected by using the single-cell gel electrophoresis method, also known as the *comet assay*. The comet assay is an established method for identifying strand breaks in DNA in single cells (Singh et al., 1988; Kindzelskii and Petty, 1999; Morris et al., 1999; Tice et al., 2000). We also applied this assay to an *in vivo* system of motor neuron degeneration, the sciatic nerve avulsion model in adult rat (Martin et al., 1999a), to determine the kinetics of DNA-SSB in spinal motor neurons during apoptosis.

## MATERIALS AND METHODS

### Animals and tissues

Male Sprague-Dawley rats (Charles River, Wilmington, MA), weighing ~150–200 g, were used for these experiments. The animals were housed in a colony room with a 12-hour/12-hour light/dark cycle and *ad libitum* access to food and water. The Animal Care and Use Committee of the Johns Hopkins University School of Medicine approved the animal protocol. Naive rats without experimental manipulations and rats with experimental manipulations were used in these experiments. The manipulations used were retrograde tracing of motor neurons and sciatic nerve avulsions.

Spinal cord tissues for motor neuron cell suspension preparations were harvested from animals that were anesthetized deeply with a mixture of enflurane/oxygen/nitrous oxide (1:33:66) and then decapitated. The cervical and lumbar enlargements from rats without experimental lesions were removed. The entire lumbar enlargements (divided into ipsilateral and contralateral sides) were used from rats exposed to tracers and from rats with sciatic nerve avulsions. After removing the pia, lumbar/cervical enlargements were dissected under a surgical microscope segment by segment, and then the segments were microdissected into gray matter columns of ventral horn without appreciable contamination of dorsal horn and surrounding white matter funiculi.

For retrograde labeling of motor neurons, rats were anesthetized deeply with enflurane/oxygen/nitrous oxide (1:33:66), and, under sterile conditions, the sciatic nerve was exposed within the middle of the upper hindlimb. The nerve was transected by cutting, and either 50  $\mu$ l of 2% nuclear yellow (NY) or 2.5% 4,6-diamidino-2-phenylindole (DAPI) was applied to the proximal nerve stump for 1 hour by using tracer-saturated Gelfoam placed in a sterile Eppendorf tube. The animal incision was closed with the bottom of Eppendorf tube containing NY or DAPI remaining applied to the proximal stump of the sciatic nerve. Two animals were used for each tracer. The animals were allowed to survive for 48 hours before they were killed.

The unilateral sciatic nerve avulsion model was used as an *in vivo* model for apoptosis of spinal motor neurons (Martin et al., 1999a). Rats were anesthetized deeply with enflurane/oxygen/nitrous oxide (1:33:66). A midline incision was made in the lateral aspect of the left pelvis and upper hindlimb. The sciatic nerve was located by blunt retraction of the biceps femoris and gluteus muscles and was tracked proximally to an extravertebral location deep within the pelvis. A steady, moderate traction was applied to the sciatic nerve with forceps until the nerve separated from the spinal cord, resulting in a mixed motor-sensory root avulsion. Muscle retraction was released, and the overlying skin was sutured. Postlesion survival times following sciatic nerve avulsion were 5, 7, 10, 14, and 28 days ( $n = 2-4$  rats per time point).

### Preparation, sorting, characterization, and counting of cell suspensions enriched in motor neurons

**Preparation of cell suspensions from spinal cord ventral horns.** After quick isolation, gray matter tissue columns from spinal cord ventral horns of lumbar/cervical enlargements were collected and rinsed in a cell culture dish on ice containing dissection medium ( $1 \times Ca^{2+}/Mg^{2+}$ -free Hanks' balanced salt solution; GibcoBRL, Grand Island, NY, supplemented with glucose and sucrose). After they had been cut into smaller pieces, ventral horn samples were digested (20 minutes) with 0.25% trypsin-EDTA (Gibco) in a tissue culture incubator (5%  $CO_2$  and 95% air, at 37°C). This mixture was titrated gently with a transfer pipette. The cell suspension was transferred to a 5-ml centrifugation tube on ice, and the remaining small pieces of ventral horn gray matter were further digested in trypsin-EDTA (16 minutes). The total cell suspension was then centrifuged at different speeds for cell sorting.

**Sorting of cell suspensions.** To isolate a spinal motor neuron-enriched fraction, cell suspensions were centri-

fuged (Beckman GPR model centrifuge) at 200 rpm (20  $g_{av}$ ) for 5 minutes (4°C). The supernatant was collected and then centrifuged at 400 rpm (50  $g_{av}$ ), 800 rpm (160  $g_{av}$ ), and then 2,500 rpm (1,400  $g_{av}$ ). After each spin (for 5 minutes), the pellet was resuspended in 100  $\mu$ l phosphate-buffered saline (PBS, pH 7.4), fixed with 1 ml of 4% paraformaldehyde (4°C for 1 hour), and then characterized by using immunocytochemistry or cresyl violet staining.

**Characterization of sorted cell suspensions.** Cell suspensions from the ventral horns of cervical and lumbar enlargements after sorting by differential centrifugation were characterized by immunofluorescence. After fixation, the cells were repelleted, and each pellet was resuspended with 250  $\mu$ l PBS. An aliquot of cell suspension (50  $\mu$ l) was applied to a gelatin-coated slide, and a coverslip (24  $\times$  30 mm) was overlaid gently to form a monolayer of cells. The slides were then air-dried. The following antibodies were used: a mouse monoclonal anti-neuronal nucleus (NeuN, diluted 1:20), a neuron-specific marker (Chemicon, Temecula, CA); a mouse monoclonal anti-choline acetyltransferase (CAT, diluted 1:5), a marker for motor neurons in rat spinal cord enlargements (Roche Molecular Biochemicals, Indianapolis, IN); a rabbit polyclonal anti-gial fibrillary acidic protein (GFAP; diluted 1:20), an astroglial marker (DAKO, Glostrup, Denmark); and a monoclonal mouse anti-CD11b/c IgG2a (OX-42, diluted 1:20), a microglial/macrophage marker (Harlan Sera-Lab, Crawley Down, England).

Air-dried slides were rinsed (1 hour) in PBS to separate the slides from the coverslips. The cells did not attach to the coverslips because they were not coated with adhesive; instead, the cells were attached to the gelatin-coated slides. The cells were permeabilized (30 minutes) in 1% Triton X-100 and then treated (30 minutes) with 1% bovine serum albumin (BSA). Diluted primary antibodies were applied to the slides, and the slides were incubated (24 hours at room temperature) in a humidified box. After primary antibody incubation, the slides were rinsed in PBS. Alexa-conjugated anti-mouse IgG (diluted 1:100, Molecular Probes, Eugene, OR) was used to visualize NeuN, CAT, and OX-42, and Cascade blue-conjugated anti-rabbit IgG (diluted 1:100; Molecular Probes) was used to visualize GFAP. The slides were incubated (4 hours at room temperature) in a humidified, dark box. The slides were washed and coverslipped with propidium iodide/antifade (Ventana, Tucson, AZ). The slides were observed and photographed under a Zeiss fluorescence microscope. The preparation of cell suspensions from rats used for retrograde tracing of motor neurons was identical to that described above. The slides were coverslipped with or without propidium iodide/antifade and were observed under the same fluorescence microscope but with UV emission.

**Counting of different cell types in cell suspensions.** To identify the cell fraction that was enriched in motor neurons, the specific types of cells were identified by cell-specific markers and were counted. To estimate the total number of neurons, the number of NeuN positive-cells was compared with the total number of cells identified by propidium iodide staining plus NeuN staining. The percentage of CAT-positive cells relative to NeuN-positive cells was calculated to determine the proportion of spinal motor neurons in the cell suspensions. The fraction of DAPI- or NY-positive cells relative to the total number of NeuN-positive cells was also calculated to determine the proportion of spinal motor neurons issuing sciatic nerve

axons. The numbers of labeled cells from six different microscopic fields (400 $\times$ ) were averaged from each case, and then a total mean was derived from the preparations from three different cases. The viability of the cell suspensions was measured by the trypan blue assays and counting cells in a hemocytometer with phase contrast microscopy. Viability, as determined by exclusion of trypan blue, was evaluated immediately after the cells were isolated and after incubation for 6, 12, and 24 hours.

### Detection of superoxide ( $\text{O}_2^-$ ) in motor neurons

The dye hydroethidium (HE) detects  $\text{O}_2^-$  in living cells through its oxidative conversion to ethidium bromide by  $\text{O}_2^-$  radical (Rothe and Valet, 1990). We used HE to measure  $\text{O}_2^-$  production in motor neuron cell suspensions. After cell sorting, the 400 rpm cell isolates from ventral horns of cervical and lumbar enlargements were resuspended in either minimum essential medium (MEM) or Neurobasal-A supplemented with 5% horse serum, 5% fetal bovine serum (both sera were heat inactivated), and 1 $\times$  glutamine (Gibco). Aliquots (2 ml) of resuspended cells were incubated (5%  $\text{CO}_2$  and 95% air, 37°C) for 0, 30, or 60 minutes, after which 10  $\mu$ l of 63.5 mM HE (Molecular Probes) in dimethylformamide was added to each sample. Cells were incubated for an additional 15 minutes. Cell suspensions were collected and repelleted, and the cell pellet was washed with PBS and then fixed in 4% paraformaldehyde overnight. After fixation the cells were repelleted and mounted on coated slides. The cells were quickly viewed by fluorescence microscopy under both 421- and 593-nm emission filters, and images were captured on color slide film and digitized. Image analysis was used to measure  $\text{O}_2^-$  production by the conversion of blue to red color in isolated cells.

### Exposure of motor neuron-enriched cell suspensions to $\text{H}_2\text{O}_2$ , NO donors, and ONOO $^-$

We determined whether adult motor neurons that are challenged with oxidative stress accumulate SSB in DNA. Motor neuron-enriched cell suspensions were exposed to  $\text{H}_2\text{O}_2$  and NO donors. Two different NO donors were used: sodium nitroprusside (SNP; Sigma, St. Louis, MO) and N-(2-aminoethyl)-N-(2-hydroxyl-nitrosohydrazino)-1,2-ethylenediamine (spermine-ONOOate; OXIS, Portland, OR). Spermine-ONOOate was used because this agent can maintain long exposure to steady-state generation of NO (Hrabie et al., 1993). A combination of  $\text{H}_2\text{O}_2$  and SNP was also used. Motor neurons were also exposed directly to ONOO $^-$  (Alexis, San Diego, CA). ONOO $^-$  is a potent and relatively long-lived ROS formed by a reaction between  $\text{O}_2^-$  and NO (Beckman et al., 1993).

Motor neuron cell suspensions (the 400-rpm preparation) were prepared from naive rats. To identify the optimal cell culture medium for these experiments, cell suspensions of adult motor neurons were incubated in either MEM or Neurobasal-A (without B27) and were evaluated for DNA damage. Baseline DNA damage in controls was significantly less in motor neurons incubated in Neurobasal-A (see Results). We concluded that Neurobasal-A is better than MEM for survival of adult motor neurons. Motor neuron cell suspensions were exposed to different doses of  $\text{H}_2\text{O}_2$  in a medium containing 90% Neurobasal-A (Gibco),

5% horse serum, 5% fetal bovine serum (both sera were heat inactivated), and 1× glutamine (Gibco). The cells were exposed to  $H_2O_2$  in a tissue culture incubator (containing 5%  $CO_2$  and 95% air, 37°C) for the different times. For controls, cells were not exposed to  $H_2O_2$  but were incubated for the same times in medium. After exposure, the treatment groups were collected into 5-ml centrifuge tubes and repelleted at 4°C for 5 minutes. Each pellet was resuspended and subjected to the comet assay.

Motor neuron cell suspensions (400 rpm preparation) were prepared from naive rats. Motor neurons were exposed to SNP at concentrations of 10, 100, 300, and 800  $\mu M$  for different durations ranging from 15 minutes to 4 hours. Identical cell suspensions were exposed to spermine-NONOate at concentrations of 10 and 100  $\mu M$  for 30 minutes, 1 hour, and 2 hours. Motor neurons were also exposed to  $H_2O_2$ /SNP simultaneously for the same durations as exposure to SNP alone. In addition, motor neurons were treated with  $ONOO^-$  at concentrations of 10 and 100  $\mu M$  for 15 minutes, 30 minutes, and 1 hour. These exposures were done in medium containing 90% Neurobasal-A (Gibco), 5% horse serum, 5% fetal bovine serum (both sera were heat inactivated), and 1× glutamine (Gibco) in a tissue culture incubator (containing 5%  $CO_2$  and 95% air, 37°C) for the different times. For controls, samples of the same cell suspensions were incubated in medium for the same time in the absence of SNP, with spermine tetrahydrochloride/sodium nitrite ( $NO_2^-$ ), or with decomposed  $ONOO^-$  in alkaline solution.

### Comet assay

To detect DNA-SSB on an individual cell basis, motor neuron cell suspensions that were exposed to  $H_2O_2$ , NO donor,  $H_2O_2$ /SNP, and  $ONOO^-$  were analyzed by the comet assay. In addition, to identify DNA-SSB in motor neurons undergoing apoptosis *in vivo*, the comet assay was used on motor neuron cell suspensions prepared from rats with sciatic nerve avulsions. The 400-rpm cell preparations from ipsilateral or contralateral sides of ventral horns of lumbar enlargements of animals with unilateral sciatic nerve avulsions were subjected directly to comet assay immediately after they were sorted and repelleted. All the procedures for the comet assay were done under low light to minimize spontaneous DNA damage.

**Preparation of cell microgels on slides.** The cell microgels were prepared as layers. The first layer of gel was made by applying 200  $\mu l$  of regular melting point agarose (0.7%) on individual superfrosted glass microscope slides (3 × 1 inches, thickness 1 mm), and a coverslip was laid gently on the agarose. After gel solidification at 4°C, the coverslip was removed, and 50  $\mu l$  of a mixture of cell suspension (containing  $\sim 4.4 \times 10^4$  motor neurons) and low-melting-point agarose was applied to the first gel layer. The low-melting-point agarose was prepared in 0.1 M PBS and kept at 37°C, and the cell suspension-agarose mixture was maintained at 37°C. The slides were then coverslipped and placed at 4°C for solidification of the cell suspension-agarose mixture. After the second layer solidified, the coverslips were removed, and 100  $\mu l$  of low-melting-point agarose was added on top of the cell layer. The gels were recoverslipped, and the slides were placed on ice for gel solidification.

**Lysis of cells, DNA unwinding, gel electrophoresis, and DNA staining.** Coverslips were removed from the cell microgels, and the slides were covered with 1.5 ml of

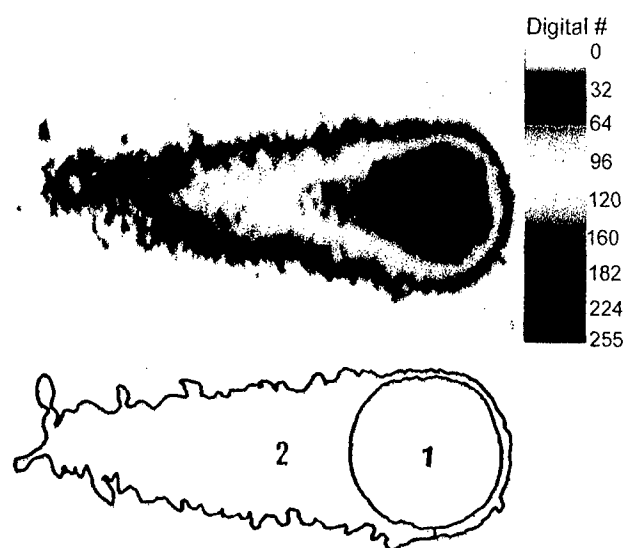


Fig. 1. DNA damage in motor neurons as visualized with the comet assay. Digital image (upper image) of a motor neuron comet (the tail and the head comprise the comet) found in microgels after single-cell gel electrophoresis. Ethidium bromide staining of DNA is in pseudocolor. Each color indicates a different DNA content, with black indicating the highest DNA intensity. (Background color has the intensity of 0.) Comet contour (lower image) delineating comet head (1) and tail (2).

lysis buffer (pH 10) containing 2.5 M NaCl, 100 mM EDTA, 1% sodium lauryl sarcosine, 10 mM Tris, and Triton X-100 (final concentration 1%, freshly added immediately before use). Microgels of oxidant- and vehicle-treated cells were lysed for 30 minutes at room temperature. Microgels of cells prepared from avulsion rats were lysed for 1 hour at room temperature. After draining, microgels were treated with DNA-unwinding solution (300 mM NaOH, 1 mM EDTA, pH 12) for 30 minutes. After DNA unwinding, the microgels were placed in a horizontal gel electrophoresis chamber filled with DNA-unwinding solution and subjected to electrophoresis (300 mA) for 20 minutes (oxidant/control treated cell preparations) or 30 minutes (lesioned/unlesioned sciatic nerve avulsion samples). After neutralizing microgels with 0.4 M Tris-HCl (pH 7.5) for 20 minutes, they were stained (30 minutes) with 20  $\mu g/ml$  ethidium bromide. Subsequently, the gels were washed and coverslipped. The evaluation and image acquisition were performed by using a Zeiss fluorescence microscope.

**Counting comets and intact cells in cell microgels.** The numbers of cells with comets (Fig. 1) were counted in microgels prepared from motor neurons exposed to oxidants *in vitro* and from motor neurons isolated from *in vivo* avulsion experiments. For cell preparations exposed to  $H_2O_2$ , NO donor,  $H_2O_2$ /SNP, or  $ONOO^-$ , cells incubated for the same time in medium with vehicle, without oxidant, were used as controls. Three to five separate experiments from different animals were done for each type of *in vitro* oxidant exposure experiment. For the unilateral sciatic nerve avulsion experiments, comet assays were performed on two to four rats for each recovery time (5, 7, 10, 14, and 28 days). The contralateral (unlesioned) side of



the spinal cord from rats with sciatic nerve avulsions was used as the control for each time point. The numbers of comets and large intact cell nuclei regarded as motor neurons stained by ethidium bromide were counted in six microscopic views at 200 $\times$  from microgels of treated cells and from sciatic nerve avulsion animals. The percentage of comets relative to the total number of cells (total number of comets and total number of intact cell nuclei) was determined, and group means were calculated. The data were analyzed by using a Student's *t*-test.

### Quantification of DNA damage

Individual comets were captured as digital images for quantification of DNA density and comet moments as measured by the fluorescence intensity of ethidium bromide-stained DNA (Fig. 1). Cells with more DNA damage show an increased migration of DNA in the direction of electrophoresis (Ostling and Johanson, 1984; Singh et al., 1988). Randomly selected comet images were acquired by using Inquiry software (Loats Associates, Westminster, MD). In each treatment group, ~10–30 comets were acquired. Comets were saved in TIFF format. From each comet, several measurements were made by delineating the region of interest (Fig. 1). These measurements were DNA intensity<sub>head</sub>, DNA intensity<sub>tail</sub>, area<sub>head</sub>, and area<sub>tail</sub>. Tail length was measured from the center of the head to the end of the tail. The extent of DNA damage was quantified by measuring the displacement of DNA between the cell nucleus (i.e., the comet head) and the tail. Relative DNA content was reflected by the average-integrated intensity of fluorescence. The amount of DNA damage for each cell was derived from the calculation of the comet moment (Hellman et al., 1995; Peterson et al., 2000). We calculated the comet moment by two different methods. The traditional calculation is DNA intensity<sub>tail</sub>  $\times$  tail length (Hellman et al., 1995). However, this equation does not take into consideration the broadness of the tail; therefore, we also calculated the comet moment from DNA intensity<sub>tail</sub>  $\times$  area<sub>tail</sub>. The comet moment is regarded as one of the best indices of induced DNA damage in cells (Singh et al., 1988; Hellman et al., 1995).

### DNA fragmentation analysis of motor neuron-enriched cell suspensions exposed to oxidative stress

We used standard DNA gel electrophoresis to detect DNA damage for a comparison with the comet assay. Immediately after sorting the ventral horn cell preparations, the 400-rpm cell suspensions from both cervical and lumbar enlargements (*n* = 13 rats) were divided into wells. These motor neuron-enriched cell suspensions were treated with either 10 mM H<sub>2</sub>O<sub>2</sub>, 10  $\mu$ M SNP, or vehicle in medium for 60 and 90 minutes. The cells were then collected and repelleted. Samples with the same treatments were pooled, and genomic DNA was extracted. Three separate experiments were performed.

**Agarose gel electrophoresis for DNA fragmentation.** To identify the pattern of DNA fragmentation after oxidative stress, DNA was extracted from motor neuron-enriched cell suspensions exposed to H<sub>2</sub>O<sub>2</sub> or NO donor and their vehicle/time controls. Immediately after the exposure, the cells were pelleted, washed in PBS, repelleted, and then lysed with 1% sodium dodecyl sulfate (SDS) in lysis buffer. The samples were treated with Proteinase K overnight, and then genomic DNA was ex-

tracted with phenol/chloroform/isoamyl alcohol. After digestion of RNA with DNase-free RNase followed by repurification, DNA (10  $\mu$ g) from each sample was end-labeled with digoxigenin as described (Portera-Cailliau et al., 1997; Martin, 1999). DNA was fractionated in a 1.5% agarose gel, transferred to nylon membrane, UV-crosslinked, incubated with a digoxigenin antibody conjugated to alkaline phosphatase, and detected with Lumi Phos 530 (Boehringer Mannheim, Indianapolis, IN) followed by exposure to Kodak X-Omat AR film (Eastman Kodak, Rochester, NY).

### Structural analysis of motor neuron-enriched cell suspensions

We evaluated the structure of adult motor neuron cell suspensions and the structural changes in these cells exposed to H<sub>2</sub>O<sub>2</sub> and NO donor. After sorting, control and treated motor neurons (prepared from three rats for each condition) were fixed with 1% glutaraldehyde and 2% paraformaldehyde and processed for plastic embedding as described (Martin et al., 1999a). Motor neuron cell pellets were cut at 1  $\mu$ m and stained with toluidine blue for high-resolution light microscopy and were also thin-sectioned for electron microscopy.

### Immunoblot analysis of protein nitration

We used protein nitration to track the presence of ONOO<sup>-</sup> (Beckman et al., 1993). Motor neuron cell suspensions were exposed to H<sub>2</sub>O<sub>2</sub>, SNP, NONOate, SNP + H<sub>2</sub>O<sub>2</sub>, ONOO<sup>-</sup>, and respective control applications. The cells were pelleted, washed, and lysed in buffer. Samples (20  $\mu$ g of total protein) were fractionated by SDS-polyacrylamide gel electrophoresis. Proteins were electroeluted onto nitrocellulose sheets. Gels were stained with Coomassie blue, and nitrocellulose membranes were briefly stained with Ponceau S to verify uniform protein transfer. Blots were washed with 50 mM Tris-buffered saline (TBS; pH 7.4), and subsequently blocked in 2.5% nonfat milk in 50 mM TBS/0.1% Tween-20. Nitrotyrosine modification of proteins was detected with polyclonal antibodies (Upstate Biotechnology, Lake Placid, New York) used at a concentration of 1  $\mu$ g IgG/ml. Nitrated proteins were visualized with enhanced chemiluminescence.

## RESULTS

### Motor neurons can be isolated from adult spinal cord and studied in cell suspension

To study the mechanisms of specific types of DNA damage induced in adult spinal motor neurons by oxidative stress *in vitro* and axotomy *in vivo*, model systems for isolating adult motor neurons and for detecting early DNA damage in individual motor neurons needed to be developed. When microdissected samples of spinal ventral horn are exposed to mild digestion and then fractionated by differential low-speed centrifugation, a cell suspension comprised mostly of motor neurons was isolated. Most of the large neurons are found in the 400-rpm pellet, with most of the cells in this fraction being motor neurons (Figs. 2, 4Aa,b,k).

After resuspending the 400-rpm pellet, the cell suspension was even, without visible tissue pieces. Microscopically, most cells are uniformly round, large spheres (volumes of ~98–653  $\mu$ m<sup>3</sup>) or mid-sized (volumes of ~32–63



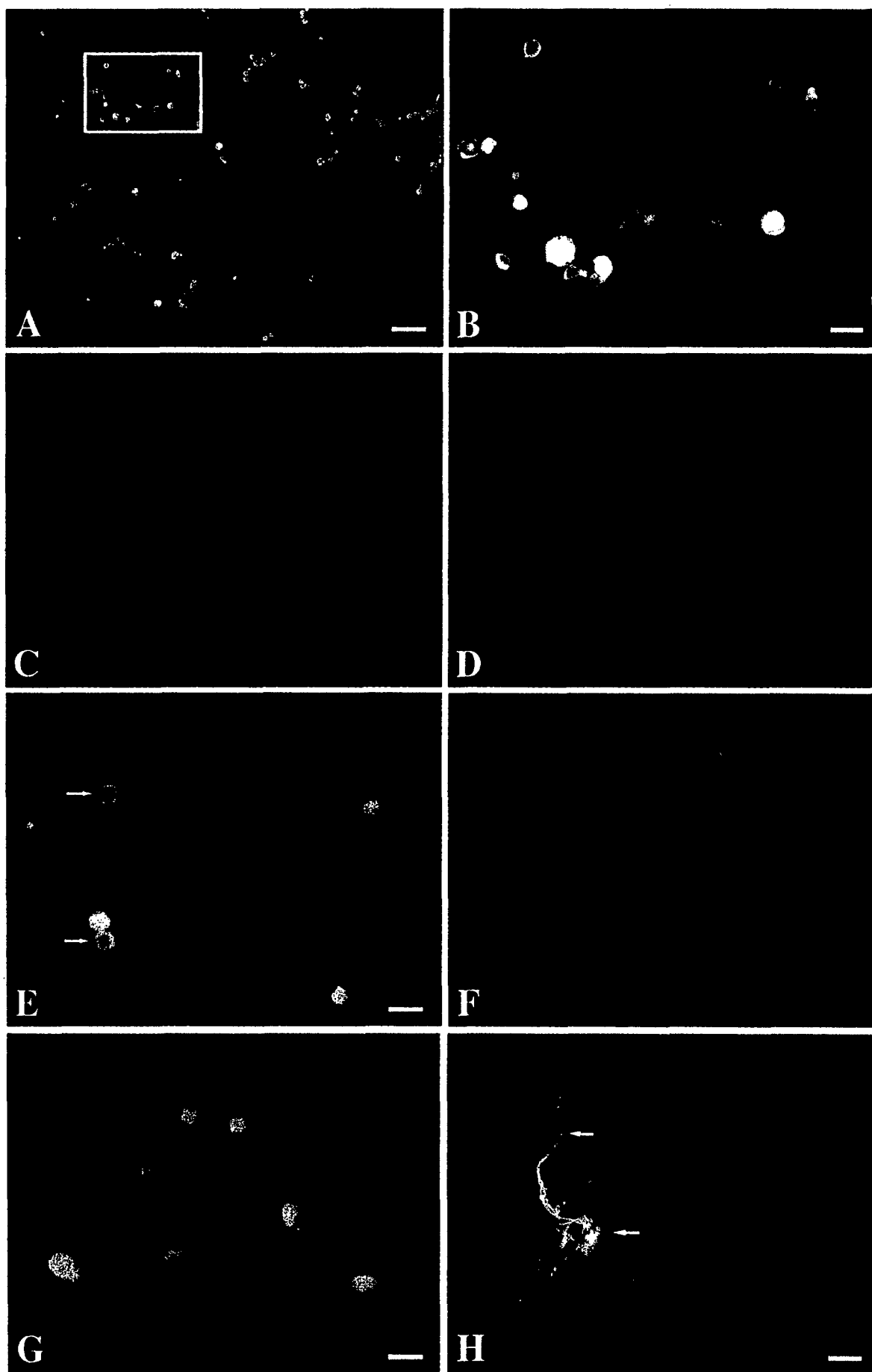


Figure 2

$\mu\text{m}^3$ ) (Figs. 2, 4Aa,b,k). These cells are neurons, as identified by nuclear staining for NeuN (Fig. 2A,B) and are motor neurons as determined by cytoplasmic CAT immunofluorescence (Fig. 2E,F) and retrograde labeling with NY and DAPI (Fig. 2G). Motor neuron nuclei show strong labeling for NeuN that blocked staining with propidium iodide. Only very small cells without NeuN reactivity (glial cells) could be counterstained with propidium iodide (Fig. 2C,D). CAT staining was localized in cell perikarya, and thus the nuclei were counterstained with propidium iodide (Fig. 2E,F). A few large cells were entirely or partially surrounded by astroglial processes, as revealed by GFAP staining (Fig. 2H). GFAP-positive cells are rarely present, but GFAP-positive fragments of astroglial processes are scattered throughout the motor neuron-enriched cell suspension, with only occasional OX-42-positive microglial cells being identified. The large nuclei of motor neurons are easily distinguished from the very small nuclei of glial and endothelial cells.

Cell counting confirmed that ~84% of the cells are neurons in this suspension of the 400-rpm pellet from cervical and lumbar ventral horns (Fig. 2A). Of these neurons, ~86% are spinal motor neurons by cytoplasmic CAT positivity (Fig. 2E). Retrograde tracing revealed that ~72% of cells in the 400-rpm cell suspensions from lumbar enlargements were DAPI labeled (Fig. 2G); thus these cells are  $\alpha$ -motor neurons with axons in the sciatic nerve. The total number of motor neurons in the 400-rpm cell suspension (from spinal cord enlargements) was estimated at  $4.0 \times 10^6 \pm 0.22 \times 10^6$  (mean  $\pm$  SEM).

The cellular compositions of the fractions yielded by the other centrifugation speeds are distinctly different from that found at 400 rpm. Mostly small-sized cells and fewer mid-sized cells are found in the cell suspensions made from the 800-rpm pellet. Individual glial cells and small cell clusters formed by three to five glial cells are found. Cell sizes range from 10 to  $51 \mu\text{m}^3$ . The smaller cells are mostly glia. The larger cells in the 800-rpm fractions are similar in size to the smaller cells in the 400-rpm fraction. These cells of  $\sim 50 \mu\text{m}^3$  are mostly smaller neurons. Only

Fig. 2. Isolation of adult spinal motor neurons. A: The majority of cells (~84% of the total number of cells) in the 400-rpm preparation are NeuN positive (green), demonstrating that these cells are neurons. (Box delineates area shown in B). B: NeuN immunofluorescence (green) is intense in the nuclei of these neurons, whereas the cytoplasm is labeled weakly or not labeled. C: Propidium iodide (PI, red) counterstaining of cell suspensions immunolabeled for NeuN (identical field as shown in A) reveals that NeuN-positive cells exclude PI. Very small nonneuronal glial cells are labeled with PI but not for NeuN. D: PI staining identifies the glial cell nuclei in samples stained for NeuN (same field as shown in B). E,F: In the 400-rpm cell suspension, most of the neurons (~86% of total NeuN-positive cells) and 72% of the total cells are choline acetyltransferase (CAT) positive (E). CAT immunoreactivity is localized in the perikarya of motor neurons with PI nuclear staining (E, arrows, and F, red). G: Prelabeling lumbar motor neurons with the retrograde tracer DAPI (blue) shows that most of the  $\alpha$ -motor neurons with sciatic nerve axons sort into the 400-rpm cell suspension, and they comprise ~62% of the total cells. H: Very few GFAP-positive astroglial cells are present, but scattered GFAP processes (blue staining, arrows) are observed in the 400-rpm cell suspension. Some astroglial processes are attached to large neurons (red). Cell percentages are derived from at least three separate experiments. Scale bars =  $112 \mu\text{m}$  in A (also applies to C);  $28 \mu\text{m}$  in B (also applies to D);  $18 \mu\text{m}$  in E (also applies to F);  $10 \mu\text{m}$  in G;  $12 \mu\text{m}$  in H.

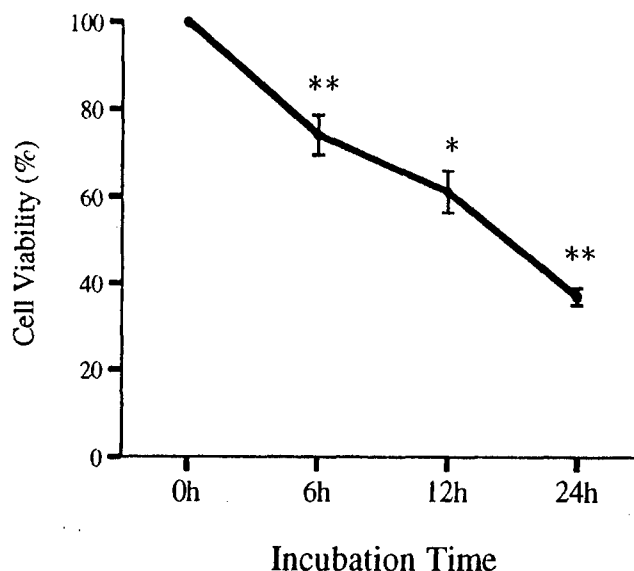


Fig. 3. Viability of adult motor neurons in cell suspension over 24 hours of incubation in supplemented Neurobasal-A, as evaluated by trypan blue staining. The number of viable cells and the total number of cells (viable cells plus trypan blue-stained cells) were counted in a hemocytometer under phase contrast microscopy. \*\*, Significant difference ( $P < 0.01$ ); \*, significant difference ( $P < 0.05$ ), both compared with the earlier time point.

rarely are large, CAT-positive or DAPI-labeled cells observed in the cell suspensions from the 800-rpm fraction. In the cell suspensions from the 2500-rpm pellets, the largest cell bodies are  $\sim 11 \mu\text{m}^3$  (which is similar in size to the smallest cells in the 800-rpm fraction). Tiny cell bodies and cellular processes are observed within the 2500-rpm cell suspensions. The composition of the 200-rpm fraction (it was too loose to be a pellet) is heterogeneous and contains partially digested white matter with aggregates of glial cells. This fraction contains many microvessel fragments composed of endothelial cells (cell body diameters  $\sim 2.5 \times 15 \mu\text{m}$ ) and attached perivascular cells. Most of these cells have small cell bodies (volumes  $\sim 36.8$ – $50.1 \mu\text{m}^3$ ) and appear to be astroglia as revealed by cresyl violet and propidium iodide staining. Isolated cells that appear to be neurons are rarely found in the 200-rpm fraction, indicating that the mild tissue digestion was effective and that neurons are liberated from the tissue but did not pellet after very low-speed centrifugation.

To evaluate the viability of the motor neuron cell suspensions, we used the trypan blue assay (Fig. 3). Immediately after the preparation of the cell suspension, isolated motor neurons excluded trypan blue. At 6 and 12 hours of incubation, 74% and 61% of motor neurons are viable, respectively. At 24 hours of incubation, 37% of the motor neurons still remain viable.

### Oxidative stress accelerates the degeneration of adult motor neurons in vitro

We evaluated by light and electron microscopy the structure of adult motor neurons in cell suspension (Fig. 4A). Isolated motor neurons are adendritic and axonless. The cell body of control motor neurons is preserved after

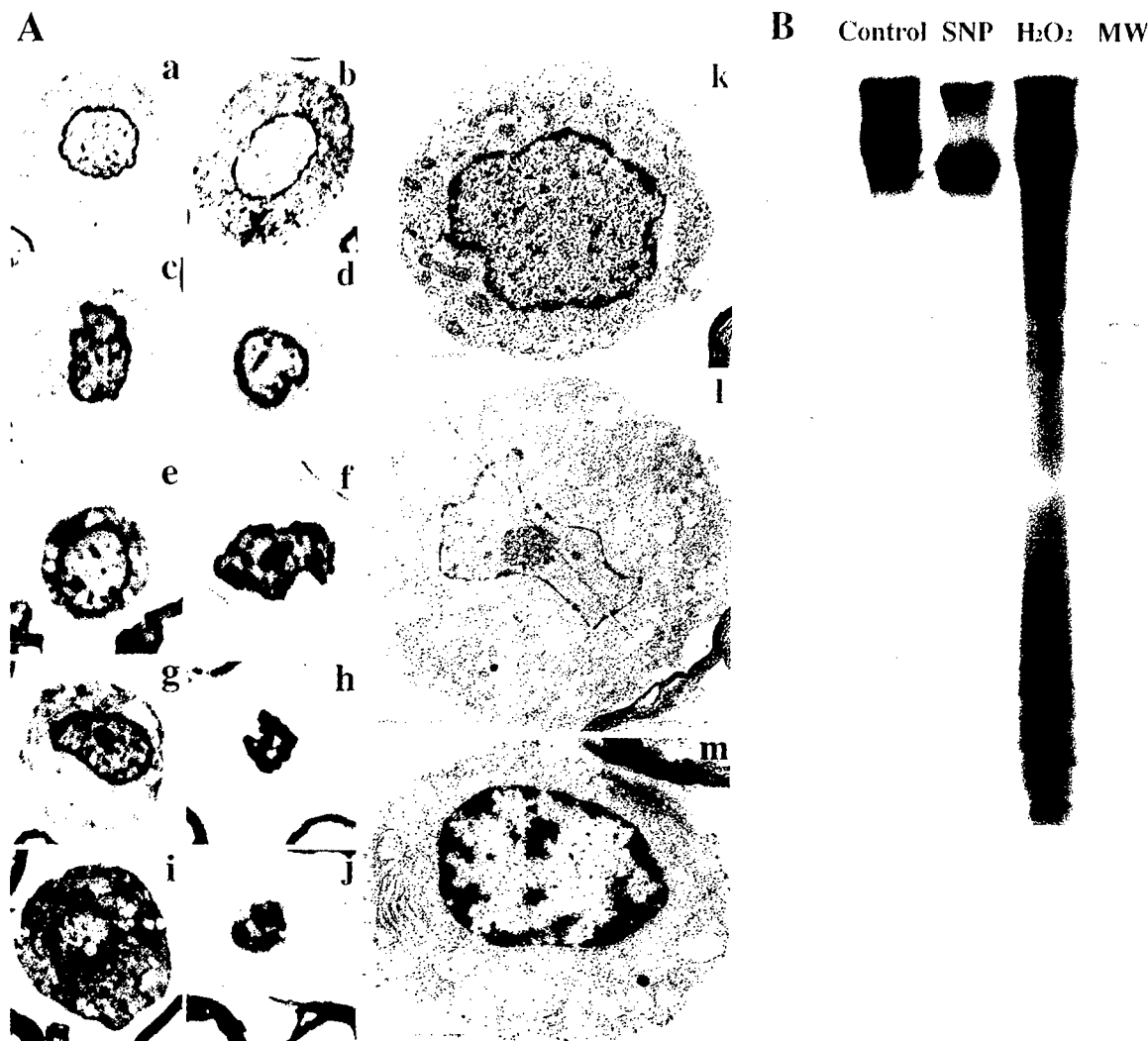


**Fig. 4.** Adult motor neurons in suspension degenerate after exposure to oxidative agents. **A:** Structural analysis of motor neuron degeneration. **a-j:** 1- $\mu$ m-thin plastic sections. **a,b:** Motor neurons incubated for 15 minutes (**a**) and 90 minutes (**b**) in supplemented Neurobasal medium under control conditions. The cells are round, with a nucleus containing dispersed chromatin surrounded by mostly intact cytoplasm, although some vacuoles are present. **c,d:** Motor neurons incubated for 15 minutes (**c**) and 60 minutes (**d**) in 10  $\mu$ M SNP. At 15 minutes, the nucleus appears relatively normal; however, at 1 hour, the nucleus shows clumping of chromatin. Many more mitochondria are swollen compared with control (see **l**). **e,f:** Motor neurons incubated for 15 minutes (**e**) and 60 minutes (**f**) in 100  $\mu$ M SNP. At 15 minutes, the motor neurons are similar to those seen at 1 hour with exposure to 10  $\mu$ M SNP, and at 1 hour the nucleus shows prominent chromatin clumping. **g,h:** Motor neurons incubated for 15 minutes (**g**) and 60 minutes (**h**) in 10  $\mu$ M SNP plus 1 mM  $H_2O_2$ . Motor neurons undergo both cytoplasmic and nuclear condensation at 15 minutes; at 1 hour, the nucleus is condensed and the cytoplasm then becomes paler. **i,j:** Motor neurons incubated for 15 minutes (**i**) and 60 minutes (**j**) in 100  $\mu$ M SNP plus 1 mM  $H_2O_2$ . The cytoplasmic damage is more severe compared with 10  $\mu$ M SNP plus 1 mM  $H_2O_2$ ; particularly at 1 hour it is fragmented. **k:** The ultrastructure of time-control (90 minutes) motor neurons is normal. Most of the mitochondria are

intact and not swollen, and the cytoplasmic matrix is enriched in ribosomes and rough endoplasmic reticulum. The nucleus has dispersed chromatin. **l:** After exposure to 10  $\mu$ M SNP for 1 hour, the cytoplasm is dark and severely vacuolated (corresponding to massively swollen mitochondria), and the nucleus is condensing. **m:** After exposure to 10  $\mu$ M SNP plus 1 mM  $H_2O_2$  for 15 minutes, mitochondria are swollen, and the chromatin is condensing at the periphery of the nucleus. **B:** Gel electrophoresis analysis of DNA damage in motor neuron cell suspensions. Motor neuron cell suspensions were time-controls or were exposed to 10  $\mu$ M SNP or 10 mM  $H_2O_2$  for 60 minutes. Genomic DNA was extracted, end-labeled with digoxigenin, fractionated (1.5% gel), and transferred to a nylon membrane, after which DNA was visualized with antibodies to digoxigenin. Genomic DNA was intact in control motor neurons. In motor neurons treated with NO donor, the genomic DNA band was slightly lower in size compared with control. In motor neurons exposed to  $H_2O_2$ , genomic DNA was fragmented as a coexisting smear-ladder pattern. Molecular weight (MW) standards (in base pairs) are: from top to bottom- 2176, 1766, 1230, 1033, 653, 517, 453, 394, 298, 234, and 220. Data were replicated in three experiments. Scale bar (shown in **a**) = 4.61  $\mu$ m in **a**; 4.94  $\mu$ m in **b**; 3.8  $\mu$ m in **c-e**; 3.17  $\mu$ m in **f**; 4.16  $\mu$ m in **g**; 3.28  $\mu$ m in **h**; 4.75  $\mu$ m in **i**; 2.74  $\mu$ m in **j**. Scale bars = 2.52  $\mu$ m in **k**; 3.27  $\mu$ m in **l**; 4.68  $\mu$ m in **m**.

15 and 90 minutes of incubation in Neurobasal-A medium (Fig. 4Aa,b,k). These cells are large and round with a large nucleus containing dispersed chromatin throughout nu-

cleoplasmic matrix. The cell membrane and the nuclear membrane are intact. Most mitochondria are intact. A few large vacuoles are present in the cytoplasm in some motor

neurons (Fig. 4Ab). These vacuoles appear to be derived from distended cisterns of the Golgi apparatus or from swollen mitochondria. These data show that motor neuron cell bodies appear healthy after isolation and brief incubation in culture.

Isolated motor neurons degenerate after exposure to NO donor and NO donor +  $H_2O_2$ . After a 15-minute exposure to 10  $\mu M$  SNP, motor neurons exhibit nascent chromatin condensation that is more prominent at 1 hour of exposure (Fig. 4Ac,d,l). This early chromatin condensation along the nuclear envelope is found at early stages of apoptosis (Portera-Cailliau et al., 1997a). SNP also induces massive swelling and degeneration of motor neuron mitochondria (Fig. 4Al). The nuclear condensation and chromatin clumping is much more prominent after exposure to 100  $\mu M$  SNP (Fig. 4Ae,f). After exposure to the combination of SNP +  $H_2O_2$ , both cytoplasmic and nuclear condensation is obvious at 15 minutes, and, by 1 hour, the nuclear condensation is very pronounced (Fig. 4Ag-j,m).

### DNA damage in motor neurons caused by $H_2O_2$ and NO donors is different

For a quick assessment of DNA damage in motor neuron cell suspensions, we used gel electrophoresis (Fig. 4B). A hybrid of internucleosomal fragmentation and random fragmentation of DNA is observed in motor neurons exposed to  $H_2O_2$  for 60 (Fig. 4B) and 90 minutes. In contrast, with 10  $\mu M$  SNP, the genomic DNA retains a high molecular weight, although this high molecular weight DNA is slightly lower than control (Fig. 4B). No obvious fragmentation is found in control samples incubated for the same time (Fig. 4B).

### DNA-SSB are rapidly induced and accumulate in motor neurons undergoing oxidative stress

To identify and measure DNA-SSB in motor neurons, the comet assay was used (Figs. 1, 5A). A typical comet viewed microscopically consists of a bright nucleus and a hazy, luminous coma, that together form the head of the comet. The tail can vary in shape and length, ranging from 1 to >1000  $\mu m$ . The specificity of this assay for DNA-SSB is determined by the alkaline conditions for cell lysis, DNA unwinding, and gel electrophoresis (Singh et al., 1988; Kohn, 1991; Tice et al., 2000). Performing the assay under neutral conditions generates a distinct pattern (Tice et al., 2000; Liu and Martin, unpublished observations). The amount (content) of migrating, damaged DNA is related both to the number of DNA-SSB and the size of the strands.

Motor neurons with intact genomic DNA in gels stained with ethidium bromide have an evenly stained, smooth round nucleus without a tail (Fig. 5Aa), indicating no DNA-SSB. In contrast, cells with DNA-SSB have a tail and a stained nucleus (Fig. 5Aa-e). Comets were classified as new comets or mature comets. New comets have a very large, round, and brightly stained head and a very short tail formed by DNA granules very close to the head (Fig. 13b). Motor neurons with new comets have nascent, very early DNA damage, presumably consisting of very large DNA fragments indicating few DNA-SSB (low DNA damage) as quantified by the low comet moments (Table 1). Mature comets have longer tails and smaller heads (Fig. 5Ba-e) and higher comet moments (Table 1). Motor

neurons with mature comets have progressive DNA damage, although the DNA damage in these cells is still at an early stage, because the alkaline condition is favorable for the unwinding and electrophoresis of only DNA-SSB. Generally, the sizes of new comet heads are larger than intact cell nuclei, indicating that the packaging of genomic DNA is loose because of DNA-SSB and consequent DNA unwinding.

We first identified an optimal medium for adult motor neurons by comparing DNA damage in cells incubated in MEM or Neurobasal-A (Fig. 5C). In control motor neurons incubated in MEM, ~50% of these cells have DNA damage by 30 minutes after isolation (Fig. 5C); therefore, MEM does not sustain the viability of isolated adult motor neurons. In contrast, in control motor neuron-enriched cell suspensions incubated in Neurobasal-A medium, the majority of motor neurons have intact DNA, although a background number of comets is observed (Fig. 5A,C,D). The number of background comets is higher ( $P < 0.05$ ) at 30, 60, and 90 minutes compared with 15 minutes (Fig. 5C,D), although from 15 to 90 minutes in Neurobasal-A medium, this value remains at ~10% or lower. Control samples were also evaluated at 4, 6, 8, and 12 hours of incubation. Even at 12 hours in Neurobasal-A medium, most of the cells embedded in the microgels are intact. The overall cell number in microgels of untreated motor neurons does not change appreciably over 12 hours of incubation (Figs. 6C, 7C). Meanwhile, the comet patterns change slowly with increased time in medium, indicating that DNA damage is progressing very slowly (Fig. 5A). In controls at 15 minutes, with the background percent of comets ~4.4% (Fig. 5Aa,b,D), most of the comets are new comets with low comet moments ( $\sim 1.4 \times 10^5$ ; Table 1). At 0.5, 1, 1.5, and 2 hours and even longer incubation times (4, 6, 8, and 12 hours), the comets remain few in number (Fig. 5D). The comet heads are still large and brightly stained, and the tails, although longer than at 15 minutes, consist of scattered, granular DNA fragments (Fig. 5Ac-e). The comet moment of these rare cells is greater than at 15 minutes ( $\sim 9.6 \times 10^5$ ; Table 1).

With a 15-minute exposure to 10 mM  $H_2O_2$ , the number of comets in motor neuron cell suspensions increases significantly ( $P < 0.05$ ) to 19%, compared with control (Fig. 5Ba,D). These comets have a large, round and densely stained head with a tail length <310  $\mu m$  (but much longer than the tail of comets in the 15-minute controls; Fig. 5Ab). The tails are formed of fine DNA granules and are distinctly different from the control comet tails formed by large DNA granules (compare comets in Fig. 5Ac and Ba). This pattern (Fig. 5Ba) reveals that by 15 minutes of exposure to  $H_2O_2$ , the extent of DNA damage in motor neurons is already greater than control comets.

With 30 minutes of exposure to 10 mM  $H_2O_2$ , the number of comets increases compared with control and 15 minutes of  $H_2O_2$  exposure (Fig. 5Bb,c,D). About 26% of the motor neurons have DNA damage. Two comet patterns predominate. Some comets have a small head and a long (~620  $\mu m$ ), thin tail (Fig. 5Bb, Table 1) with significantly greater comet moments ( $\sim 20.1 \times 10^5$ ; Table 1), representing smaller DNA fragments. Other comets have a head with an intensely stained core and a halo as well as a tail longer than 310  $\mu m$  (Fig. 5Bc). The tails are still visibly granular with finer granules than those motor neurons treated for 15 minutes with  $H_2O_2$ .

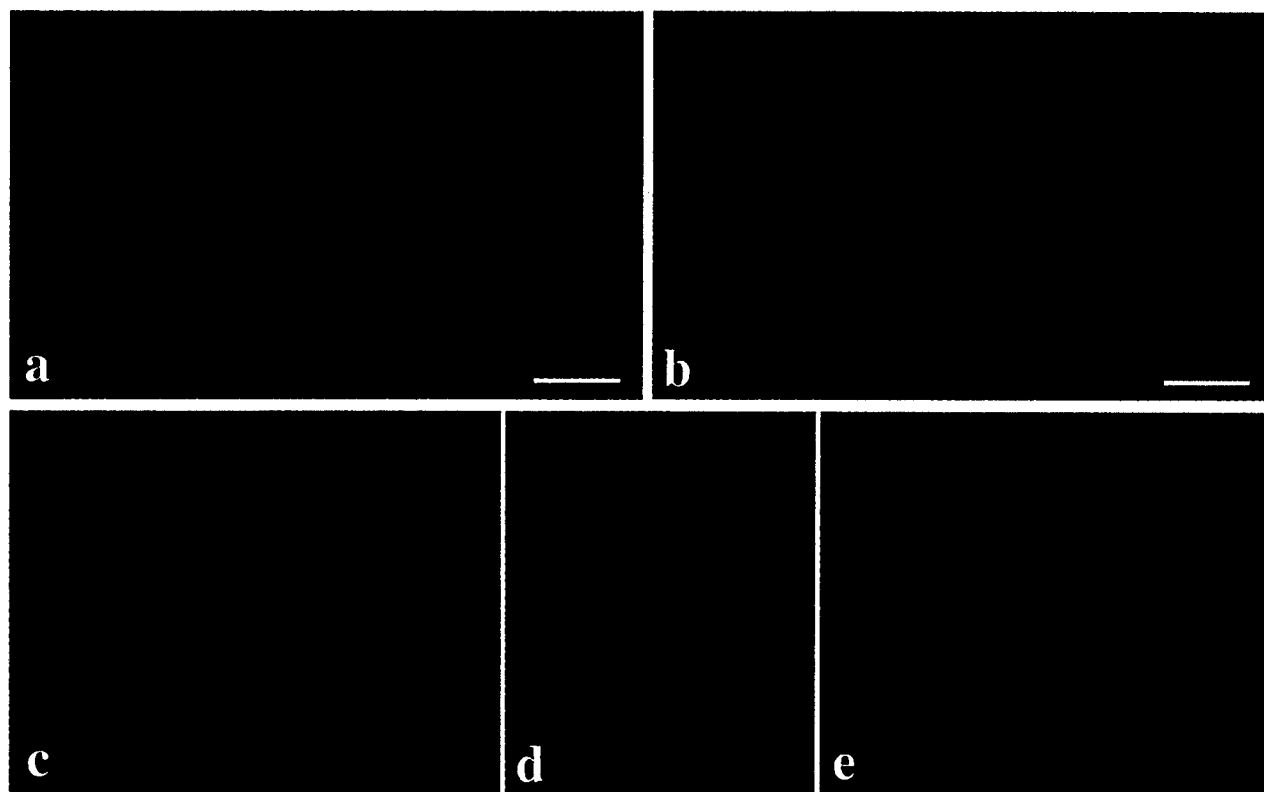
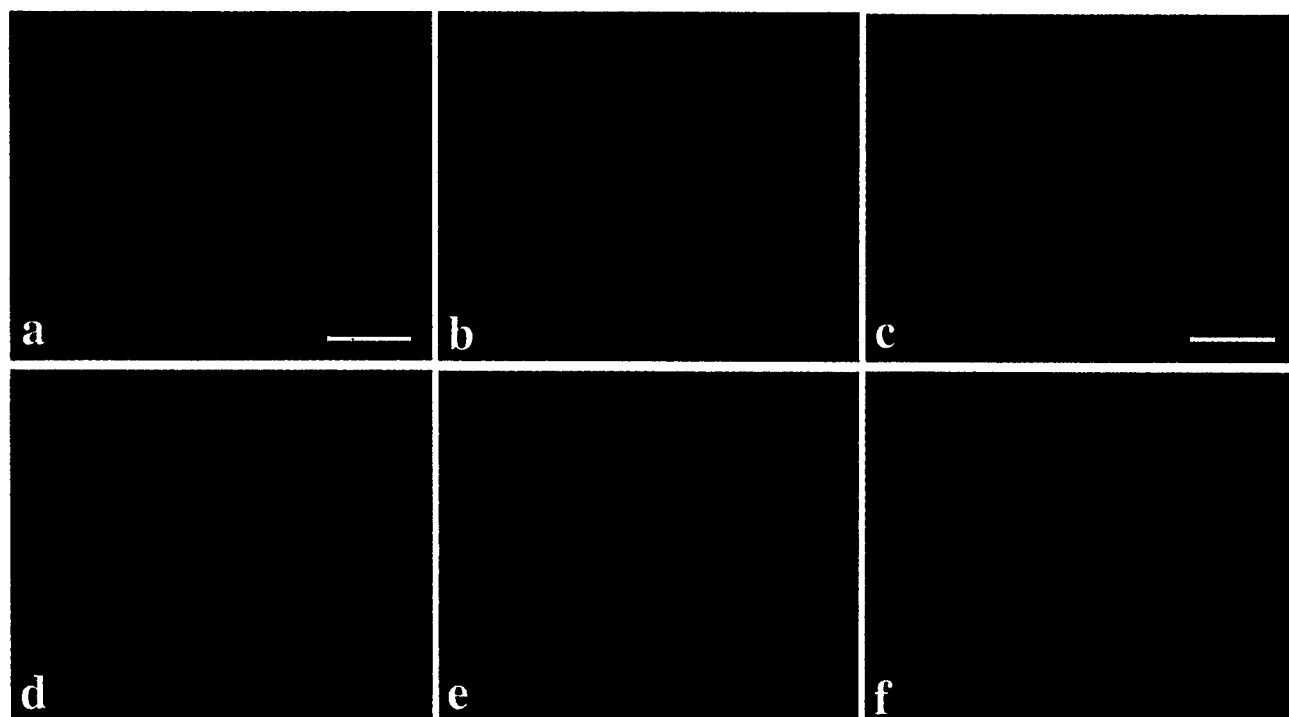
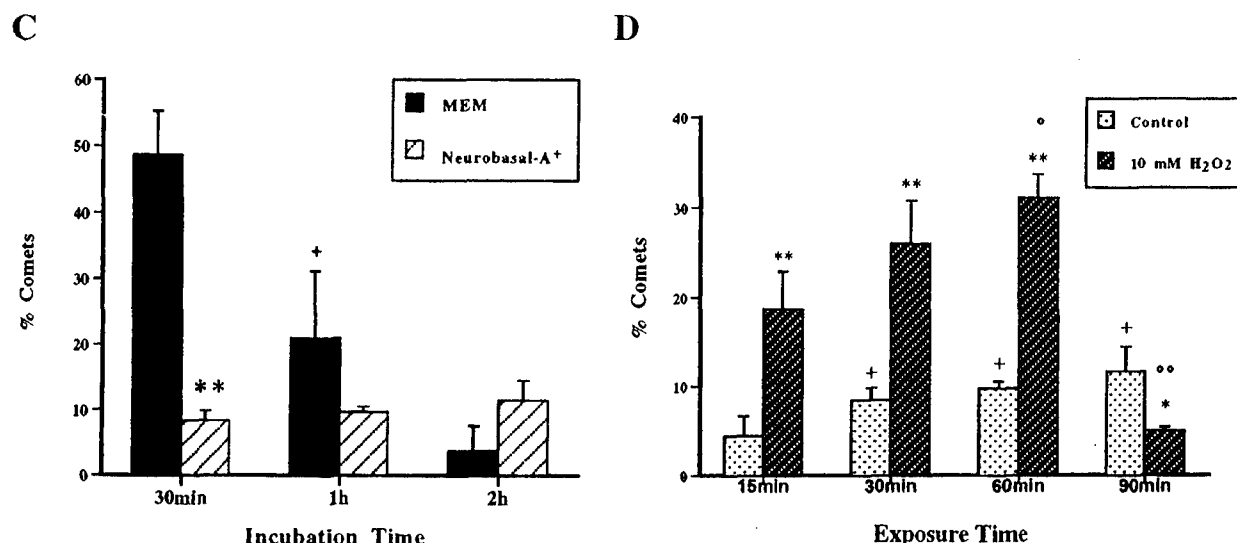
**A****B**

Figure 5



**Fig. 5.** DNA-SSB in motor neurons as revealed by the comet assay. **A:** A few motor neuron comets are occasionally observed in control groups. **a:** Panoramic view of the cell distribution and a single comet in a microgel from a 400-rpm cell suspension incubated for 15 minutes under control conditions. The cell nuclei and the comet are stained with ethidium bromide (red). Many large intact nuclei without comets are seen. **b:** Single motor neuron comet at higher magnification. The comet consists of a head and a short tail. **c:** A motor neuron comet in a 1-hour control group with scattered large granules of DNA fragments in the comet tail. **d:** At 2 hours in the control groups, the comet head is still large and the tail is still short and is comprised of fine DNA granules. **e:** An intact nucleus and a comet from a control group at 4 hours. The comet head is still large and the tail is still short and granular. **B:** Motor neuron comets observed frequently after exposure to 10 mM H<sub>2</sub>O<sub>2</sub>. **a:** After 15 minutes of exposure to H<sub>2</sub>O<sub>2</sub>, the comet heads are smaller and the tails longer than control comets, but the heads are more regular and the tails shorter than those comets seen after 1 hour of exposure (compare with **Bd** and **Be**). A large intact nucleus is shown for comparison with the comets. **b,c:** Comets observed after 30 minutes of exposure to H<sub>2</sub>O<sub>2</sub>. A dense DNA core is surrounded by a less dense and reticular halo or coma of DNA. **d,e:** After 60 minutes of exposure to H<sub>2</sub>O<sub>2</sub>, the comet heads are more irregular and the tails are very long (>620  $\mu$ m or even longer than 1 mm) and discontinuous. **f:** After 90 minutes of exposure to 10 mM H<sub>2</sub>O<sub>2</sub>, DNA damage is very severe and nuclei have large, irregular

fibrous heads, indicating the unwinding and uncoiling of genomic DNA. The tail of this comet is short and stained faintly, indicating few DNA-SSB remaining. **C:** Evaluation of medium effects on spontaneous DNA damage in motor neurons. Adult motor neurons were isolated and resuspended in minimum essential medium (MEM) or supplemented Neurobasal-A (Neurobasal-A<sup>+</sup>) and incubated for 30, 60, or 120 minutes. DNA damage (as reflected by comet number) is significantly lower in Neurobasal-A (\*\*,  $P < 0.005$  compared with MEM at 30 minutes). +, Significantly different ( $P < 0.05$ ) compared with 30 minutes of MEM. These observations were replicated in three different experiments. **D:** Histogram of the percentage of comets in both control and 10 mM H<sub>2</sub>O<sub>2</sub>-treated motor neurons. Values are mean  $\pm$  SEM. In controls, the background number of comets is significantly greater (+,  $P < 0.05$ ) at 30, 60, and 90 minutes compared with 15 minutes. Exposure to 10 mM H<sub>2</sub>O<sub>2</sub> increases significantly (\*\*,  $P < 0.01$ ) the percentage of comets in motor neurons at 15, 30, and 60 minutes compared with the respective time-controls. With 60 minutes of exposure to 10 mM H<sub>2</sub>O<sub>2</sub>, the number of comets is significantly increased (o,  $P < 0.05$ ) compared with 15 minutes of exposure. With 90 minutes of exposure, the number of comets decreases significantly compared with 90 minutes control (\*,  $P < 0.05$ ) and compared with 60 minutes of H<sub>2</sub>O<sub>2</sub> (oo,  $P < 0.01$ ). These observations were replicated in three different experiments. Scale bars in **A** = 192  $\mu$ m in **a**; 48  $\mu$ m in **b** (also applies to **c-e**). Scale bars in **B** = 192  $\mu$ m in **a** (also applies to **c-e** and **f**); 48  $\mu$ m in **c** (also applies to **e** and **f**).

The DNA damage in motor neurons treated with H<sub>2</sub>O<sub>2</sub> progressed with longer exposure. With 60 minutes of exposure to 10 mM H<sub>2</sub>O<sub>2</sub>, 31% of motor neurons have comets (Fig. 5D). The comet heads are small and irregular or are loosely stained "ghost" heads, and the tails are generally very long (>620  $\mu$ m) compared with 30 minutes of exposure (Fig. 5Bd,e). These tails have a finely particulate DNA staining. Motor neuron comets with discontinuous tails comprised of two separate parts (with a total length longer than 1 mm) are seen frequently (Fig. 5Bd), although both parts still have very fine DNA granules. With 90 minutes of exposure to 10 mM H<sub>2</sub>O<sub>2</sub>, the percentage of comets decreases significantly compared with control and 60 minutes of H<sub>2</sub>O<sub>2</sub> exposure (Fig. 5D), although the number of comets in the control group at 90 minutes of incubation is similar to controls at 30 minutes (Fig. 5D). Comets observed with 90 minutes of exposure to 10 mM H<sub>2</sub>O<sub>2</sub> have heads with loosely packed and fibrous DNA and tails that are faint and short (Fig. 5Bf). This comet pattern is typical of DNA damage that has advanced beyond DNA-

SSB to double-strand breaks (Liu and Martin, unpublished observations).

Exposure of motor neuron cell suspensions to 1 mM H<sub>2</sub>O<sub>2</sub> gave surprising results (Fig. 6B). The percentage of comets decreased significantly to a very low level at 15 minutes, 30 minutes, and 1, 2, 4, 6, and 8 hours (data are not shown for 4, 6, and 8 hours) compared with control (Fig. 6B). The few comets detected had a specific pattern. These comets have a large, round head and a wide tail with a neck (Fig. 9a,b). The tail is composed of very fine granules, and the comet moment is significantly greater than the typical control comet moment (Table 1).

### NO-induced DNA damage in motor neurons is dose and time related

NO has been implicated in the degeneration of motor neurons in individuals with ALS (Beckman et al., 1993) and in animal models (Wu and Li, 1993; Martin et al., 1999a). By using our cell suspension preparation and the

TABLE 1. DNA Damage in Motor Neurons Exposed to Oxidative Stress In Vitro as Determined by Comet Assay<sup>1</sup>

Treatment	Comet pattern <sup>2</sup>	DNA intensity <sup>3</sup>		DNA intensity ratio (tail/head)	DNA area		DNA area ratio (tail/head)	Tail length	Traditional comet moment ( $\times 10^4$ ) <sup>4</sup>	Comet moment ( $\times 10^5$ ) <sup>5</sup>
		Head	Tail		Head	Tail				
Control	b <sup>6</sup>	189.5 $\pm$ 12.2	54.4 $\pm$ 9.7	0.29 $\pm$ 0.04	1550 $\pm$ 296	2794 $\pm$ 854	1.8 $\pm$ 0.4	81 $\pm$ 4	0.44 $\pm$ 0.07	1.4 $\pm$ 0.4
Control	d <sup>7</sup>	202.6 $\pm$ 15.6	72.7 $\pm$ 6.3	0.36 $\pm$ 0.03	1949 $\pm$ 555	13264 $\pm$ 2119	7.3 $\pm$ 1.4	195 $\pm$ 24	1.41 $\pm$ 0.15	9.6 $\pm$ 1.9
H <sub>2</sub> O <sub>2</sub>										
1 mM	m	177.3 $\pm$ 15.0	74.0 $\pm$ 2.6	0.4 $\pm$ 0.02	2290 $\pm$ 229	16967 $\pm$ 2202	7.6 $\pm$ 1.7	203 $\pm$ 3*	1.49 $\pm$ 0.04*	12.6 $\pm$ 2.1*
10 mM	j	196.7 $\pm$ 4.2	64.1 $\pm$ 3.7	0.33 $\pm$ 0.03	2621 $\pm$ 438	31078 $\pm$ 3882	12.2 $\pm$ 2.5	401 $\pm$ 7*+	2.57 $\pm$ 0.13*+	20.1 $\pm$ 3.5*+
SNP										
10 $\mu$ M	e	217.5 $\pm$ 6.5	80.4 $\pm$ 11.3	0.37 $\pm$ 0.05	3516 $\pm$ 466	4878 $\pm$ 660	1.4 $\pm$ 0.2	107 $\pm$ 5*	0.86 $\pm$ 0.08*	3.9 $\pm$ 0.7*
10 $\mu$ M	g	228.2 $\pm$ 0.8	98.5 $\pm$ 11.5	0.43 $\pm$ 0.05	2396 $\pm$ 259	12531 $\pm$ 1666	5.3 $\pm$ 0.6	252 $\pm$ 22*	2.45 $\pm$ 0.18*	12.1 $\pm$ 1.0*
300 $\mu$ M	h	160.0 $\pm$ 18.1	60.9 $\pm$ 12.0	0.38 $\pm$ 0.06	2032 $\pm$ 314	25442 $\pm$ 4577	13.0 $\pm$ 2.6	333 $\pm$ 18*+	2.00 $\pm$ 0.34*	15.5 $\pm$ 4.0*+
NONOate	o	198.7 $\pm$ 9.8	62.3 $\pm$ 2.3	0.32 $\pm$ 0.02	2762 $\pm$ 515	10783 $\pm$ 3018	4.1 $\pm$ 1.2	230 $\pm$ 20*	1.43 $\pm$ 0.11*	6.7 $\pm$ 1.9*
SNP + H <sub>2</sub> O <sub>2</sub>	l	115.4 $\pm$ 15.7	49.5 $\pm$ 9.1	0.45 $\pm$ 0.10	530 $\pm$ 372	30028 $\pm$ 6481	101.2 $\pm$ 64.6	393 $\pm$ 18*	1.94 $\pm$ 0.16*	15.3 $\pm$ 5.9*
ONOO	p	169.8 $\pm$ 17.8	56.6 $\pm$ 8.7	0.34 $\pm$ 0.05	1280 $\pm$ 455	27602 $\pm$ 3430	25.5 $\pm$ 9.8	368 $\pm$ 20*	2.08 $\pm$ 0.35*	15.7 $\pm$ 3.3*

<sup>1</sup>All values are mean  $\pm$  SEM. \*, significantly different ( $P < 0.05$ ) from control (b pattern). +, significantly different ( $P < 0.05$ ) from lower concentration.

<sup>2</sup>Representative comet patterns are shown in Figure 13 and are identified by the corresponding panel letter.

<sup>3</sup>See Figure 1 for delineation of comet head and tail.

<sup>4</sup>Calculated from DNA intensity<sub>tail</sub>  $\times$  tail length (Hellman et al., 1995).

<sup>5</sup>Calculated from DNA intensity<sub>tail</sub>  $\times$  tail area.

<sup>6</sup>Most frequent control comet.

<sup>7</sup>Infrequent control comet, most likely reflecting rapidly dying motor neuron due directly to the isolation procedure.

comet assay, we tested the hypothesis that NO causes DNA damage in motor neurons. Two different NO donors were used for comparison (SNP and NONOate). Both NO donors induce dose- and time-related DNA damage in motor neurons.

Exposure to different concentrations of SNP for different durations induces DNA-SSB. Exposure to 10  $\mu$ M SNP causes a time-dependent increase in the percent comets from 15 to 60 minutes (Fig. 6A,B). Some of the early appearing comets most likely disappeared between two successive times according to the comet pattern analysis (Fig. 6A). At 15 minutes, most of the comets have large heads, being either packed densely or displaying a very bright granular coma around the head (Fig. 6Aa,b). The tails, when present, blend with the coma and are granular, short, and broad. The comet moment is low ( $\sim 3.9 \times 10^5$ ; Table 1). At 30 minutes, the cores of most of the comet heads are smaller and the tails are longer than those at 15

minutes (Fig. 6Ac,d). The number of comets in the 30-minute SNP-exposed cells is significantly greater than that at 15 minutes; thus new comets are formed. After 1 hour of exposure, the number of comets further increases (Fig. 6B), and their tails are long (Fig. 6Ae,f). These comets have higher moments ( $\sim 12.1 \times 10^5$ , Table 1). At 2 hours after exposure, the percentage of comets decreases compared with 1 hour but is still greater than control (Fig. 6B). Interestingly, most of these comets have a dense core head with a coma, and a broad, short, granular tail, indicating they are new comets, instead of matured comets from 60 minutes (Fig. 6Ag,h). The absence of significant change in motor neuron number from 15 minutes to 2 hours of exposure to 10  $\mu$ M (Fig. 6C) indicates that many of these motor neurons remain in the cell suspension after they transiently display their comet.

Motor neurons exposed to 100  $\mu$ M SNP show an abrupt increase in the percentage of comets at 15 minutes, but

Fig. 6. Comet assay on motor neuron cell suspensions exposed to 10  $\mu$ M SNP, 1 mM H<sub>2</sub>O<sub>2</sub> or 10  $\mu$ M SNP plus 1 mM H<sub>2</sub>O<sub>2</sub>. **A:** Comet profiles after exposure to 10  $\mu$ M SNP. **a:** Comets in cells exposed to 10  $\mu$ M SNP for 15 minutes have bright, large heads and very short, broad tails formed by large granules of DNA. **b:** A typical comet (from Aa) observed with 10  $\mu$ M SNP for 15 minutes. A nucleus with intact DNA is nearby. **c:** The comets in the motor neurons exposed to 10  $\mu$ M SNP for 30 minutes are more numerous than at 15 minutes, and their tails are longer. **d:** Typical comets (from Ac) observed with 10  $\mu$ M SNP for 30 minutes. **e:** After 1 hour of exposure to 10  $\mu$ M SNP, the tails of comets are longer than the earlier time points. **f:** The tail of a comet (from Ae) is much longer, but still granular. **g:** The comets of cells exposed to 10  $\mu$ M SNP for 2 hours have a similar pattern as some of the comets in samples exposed to 10  $\mu$ M SNP for 1 hour, but the nuclei appear swollen in many cells compared with the 1-hour exposed samples. **h:** Comet (from g) after exposure to 10  $\mu$ M SNP for 2 hours showing a short tail that merges with the comet of the head. **B:** Histogram of comets. Values are mean  $\pm$  SEM. Compared with the untreated control cells, the percentage of comets decreases significantly (\*\*,  $P < 0.01$ ) after exposure to 1 mM H<sub>2</sub>O<sub>2</sub> for 30, 60, and 90 minutes. In contrast, 10  $\mu$ M SNP induces a marked increase (\*\*,  $P < 0.01$ ) in the number of comets at 15, 30, and 60 minutes of exposure compared with control cells. This increase in comets is significantly (+,  $P < 0.01$ ) time related (e.g., 15 minutes vs 30 minutes, 30 minutes vs 1 hour, and 15 minutes vs 1 or 2 hours). At 2 hours, the percent comets in 10  $\mu$ M SNP-exposed motor neurons decreases sig-

nificantly ( $P < 0.01$ ) compared with 1 hour. After exposure of motor neurons to 10  $\mu$ M SNP plus 1 mM H<sub>2</sub>O<sub>2</sub>, the percent comets is decreased significantly (\*,  $P < 0.05$  or \*\*,  $P < 0.01$ ) at 30 minutes, 1 hour, and 2 hours compared with the corresponding control cells. Among the 10  $\mu$ M SNP plus 1 mM H<sub>2</sub>O<sub>2</sub> exposure times, the percent comets increases significantly (+,  $P < 0.05$ ) between 1 and 2 hours. The percent comets in the motor neurons exposed to 10  $\mu$ M SNP is significantly higher (oo,  $P < 0.01$ ) than the percent comets found with 1 mM H<sub>2</sub>O<sub>2</sub>, or 10  $\mu$ M SNP plus 1 mM H<sub>2</sub>O<sub>2</sub> at 30 minutes, 1 hour, and 2 hours. There is no significant difference among corresponding cells exposed to 1 mM H<sub>2</sub>O<sub>2</sub> or 10  $\mu$ M SNP plus 1 mM H<sub>2</sub>O<sub>2</sub>. These observations were replicated in three different experiments. **C:** Histogram of the number of cells in the comet assay microgels. Value are mean  $\pm$  SEM. Cell number is not significantly different among the untreated control groups over 2 hours. Decreases in cell number are found at 1 hour (\* $P < 0.05$ ) and 2 hours (\*\* $P < 0.01$ ) after 1 mM H<sub>2</sub>O<sub>2</sub> compared with 15 minutes after H<sub>2</sub>O<sub>2</sub> and at 1 and 2 hours after 10  $\mu$ M SNP compared with 15 minutes after SNP; however, no decreases are found relative to time-matched controls. The most prominent decrease in cell number is observed in motor neurons exposed to 10  $\mu$ M SNP plus 1 mM H<sub>2</sub>O<sub>2</sub> compared with the corresponding control groups and to treatments with either 1 mM H<sub>2</sub>O<sub>2</sub> or 10  $\mu$ M SNP alone. These observations were replicated in three different experiments. Scale bars = 280  $\mu$ m in a (also applies to c,e,g); 70  $\mu$ m in h (also applies to b,d,f).

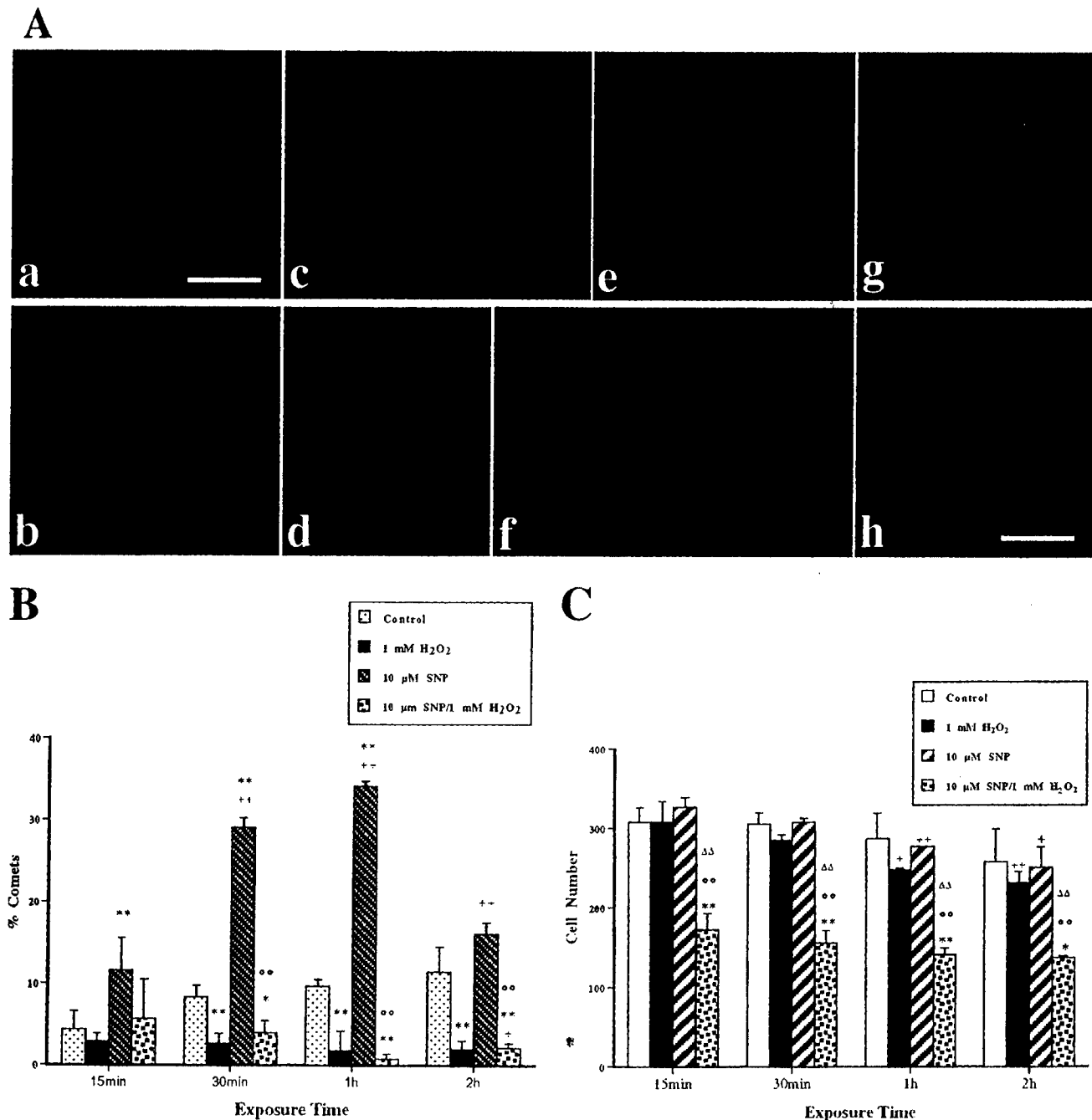


Figure 6

the number of comets does not change over 2 hours (Fig. 7B). The comet patterns are similar to those observed with 10  $\mu$ M of SNP exposure (Fig. 7A). With brief exposure (15 minutes), many of the comets are new comets (Fig. 7Aa,b). With longer exposure times, mature comets predominate with corresponding greater comet moments (Fig. 7Ac,d). The heads of these long-tailed comets have a very specific profile (Fig. 7Ad); notably they possess DNA-poor foci in the core. No significant change occurs in motor neuron number between 15 minutes to 2 hours of exposure compared with time-matched controls (Fig. 7C), further indi-

cating that the formation of comets comprised of DNA-SSB is transient and reflects early DNA damage. With 2 hours of exposure to 100  $\mu$ M SNP, some nuclei of motor neurons are large, swollen, and vacuolated (Fig. 7Ae), although some new comets are present. These two profiles reflect different stages of DNA damage during motor neuron degeneration.

After exposure to 300 or 800  $\mu$ M SNP, the number of comets decreases compared with lower concentrations of SNP, and the decrease in cell density with longer incubation is more obvious than with lower dose exposures (data



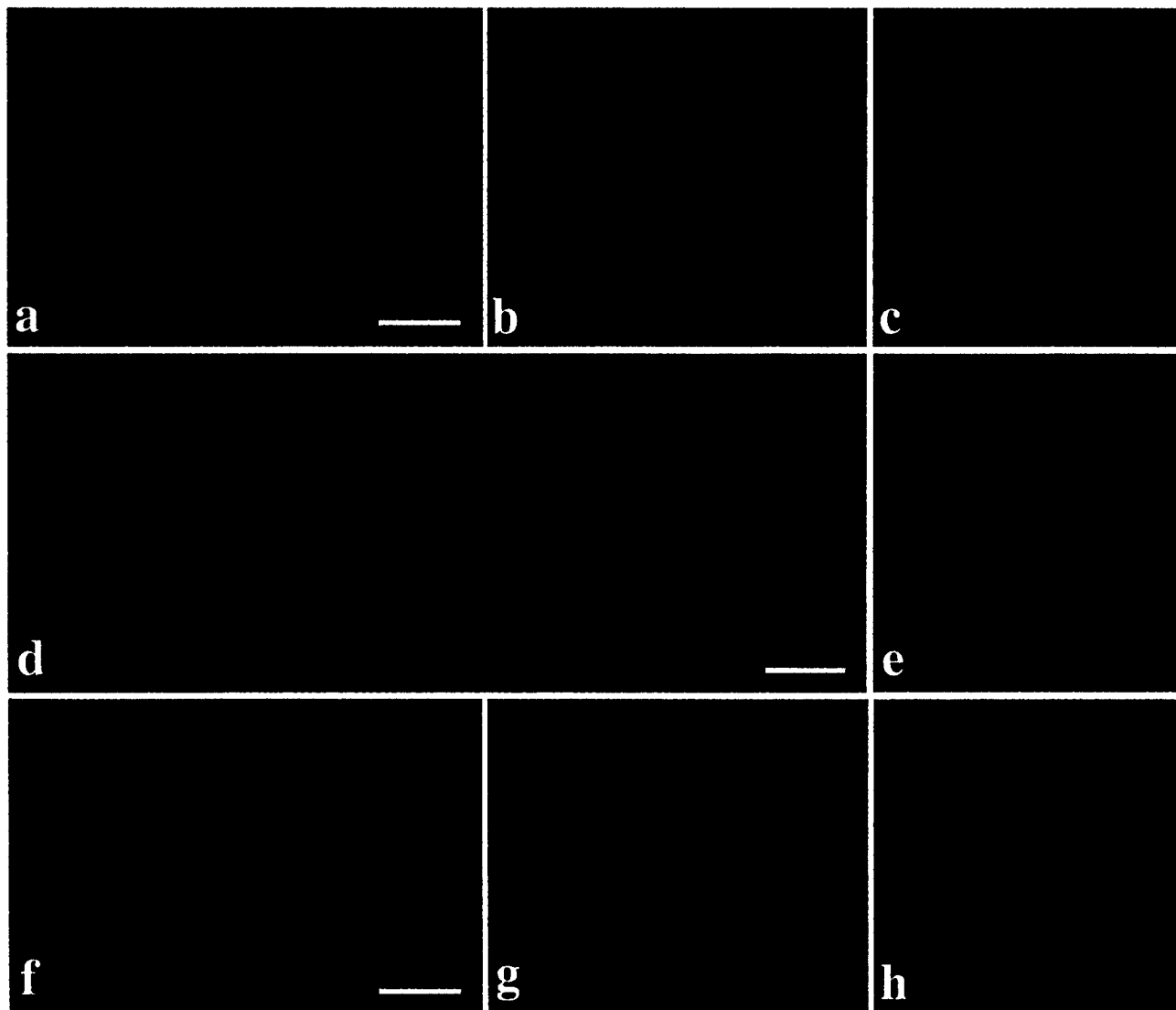
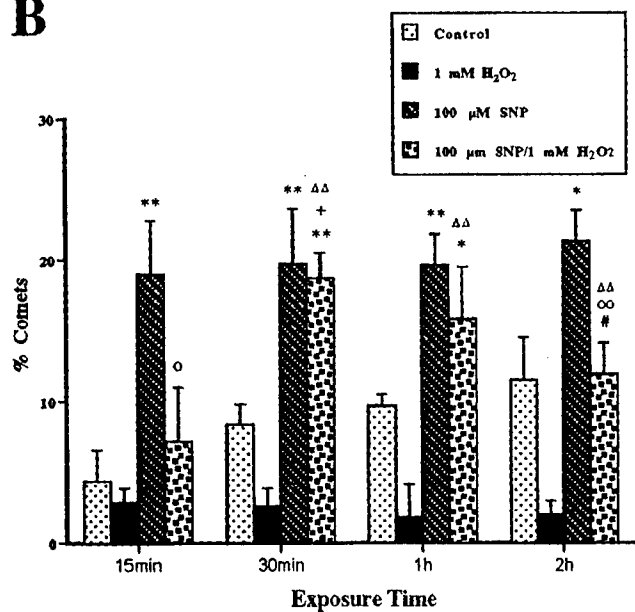
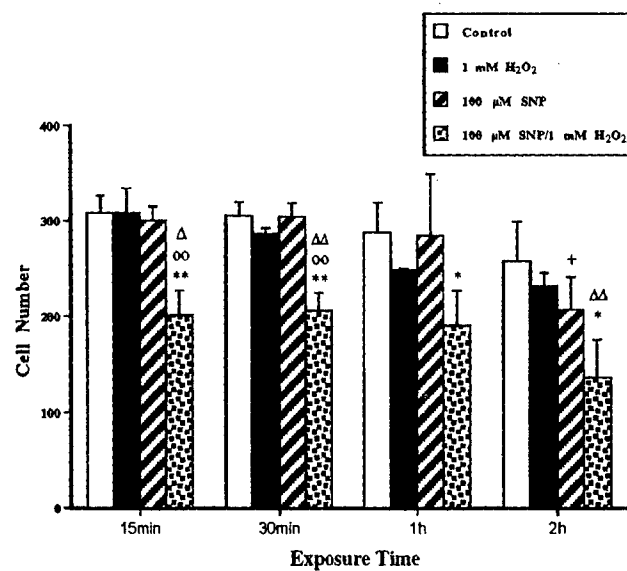
**A****B****C**

Figure 7

not shown). With these higher SNP concentrations, a different type of comet profile emerges. The DNA staining of the heads is faint and loosely granulated or clumped, and the heads exhibit a range of sizes from either large to very small (Fig. 7Af–h). The tails are usually broad and very granular, particularly for the comets with the smaller heads (Fig. 7Af–h). The moments ( $\sim 15.5 \times 10^5$ ; Table 1) are significantly greater than the moments for control and 10  $\mu\text{M}$  SNP.

Findings made with SNP, which is a commonly used NO donor, were compared with those caused by continuous generation of NO from spermine-NONOate, which has a half-life of NO release of  $\sim 4$  hours (Hrabie et al., 1993). NONOate induces a concentration-dependent formation of DNA-SSB (Fig. 8A,B). At 10  $\mu\text{M}$  (Fig. 8B), the number of comets is significantly higher than control, but this level is relatively invariant over 2 hours of exposure ( $\sim 16$ – $27\%$  comets). NONOate at 100  $\mu\text{M}$  (Fig. 8B) causes a greater increase in comet number that is time dependent, with maximum formation of comets ( $\sim 58\%$ ) at 1 hour. Essentially all of these comets are new comets with moments greater than the predominant control comet (Fig. 8A; Table 1), consistent with the formation of early DNA-SSB in the absence of cell loss (Fig. 8C).

### NO synergies with $\text{H}_2\text{O}_2$ in killing motor neurons

Combined exposure to SNP and  $\text{H}_2\text{O}_2$  is potentially toxic to motor neurons. Because  $\text{H}_2\text{O}_2$  at a concentration of 10 mM causes prominent DNA damage (Fig. 5B,D; Table 1), whereas, in contrast, 1 mM  $\text{H}_2\text{O}_2$  decreases comet number in motor neurons (Figs. 6B, 7B), we evaluated whether 1 mM  $\text{H}_2\text{O}_2$  protected against SNP-mediated damage. Co-exposure to 10  $\mu\text{M}$  SNP and 1 mM  $\text{H}_2\text{O}_2$  induces prominent cell loss by 15 minutes (Fig. 6C). This loss of motor neurons is found consistently through 2 hours. Many nu-

clear fragments of motor neurons are found throughout the microgels (Fig. 9c–f), and, therefore, the magnitude of cell loss may be underestimated. Some motor neurons have new comets, whereas the DNA in other nuclei is condensed and margined at the periphery with the center of the nucleus low in DNA (Fig. 9d), indicating severe DNA damage. The heads of other comets are very small with tightly packed DNA, whereas their tails are comparatively large and smear-like with a spindle shape and a narrow neck between the head and the tail (Fig. 9e,g,h). Based on the comet moment, the DNA damage is augmented (Table 1) compared with 10  $\mu\text{M}$  SNP comets. When motor neurons are exposed to 100  $\mu\text{M}$  SNP and 1 mM  $\text{H}_2\text{O}_2$ , cell loss is rapid (Fig. 7C), and cellular fragmentation is more obvious (Fig. 9f). Furthermore, the number of comets is greater than the number in each corresponding time in the 10  $\mu\text{M}$  SNP plus 1 mM  $\text{H}_2\text{O}_2$  groups (Figs. 6B, 7B).

### ONOO<sup>-</sup> induces DNA-SSB in motor neurons

Motor neuron cell suspensions were exposed to ONOO<sup>-</sup>. ONOO<sup>-</sup> at concentrations of 10 and 100  $\mu\text{M}$  induced DNA-SSB, as demonstrated by the significant increase in the percent comets compared with control (Fig. 10B). The formation of DNA-SSB occurred rapidly with both concentrations causing similar DNA damage (Fig. 10A,B) and cell loss (Fig. 10C). The typical comets at 15–30 minutes of exposure have long granular tails (Fig. 10Aa,b) and high comet moments (Table 1). Motor neurons exposed to 10  $\mu\text{M}$  ONOO<sup>-</sup> for longer times (1 hour) or 100  $\mu\text{M}$  ONOO<sup>-</sup> for shorter times (30 minutes) induced comets with patterns similar to the comets induced by SNP +  $\text{H}_2\text{O}_2$  (Fig. 10Ac,d), suggesting that ONOO<sup>-</sup> is involved in the synergistic toxicity of NO donor and  $\text{H}_2\text{O}_2$ .

We used protein nitration to track the presence of ONOO<sup>-</sup> in motor neurons (Fig. 11). High levels of nitrated

Fig. 7. Comet assay on motor neurons exposed to 100  $\mu\text{M}$  SNP, 1 mM  $\text{H}_2\text{O}_2$ , and 100  $\mu\text{M}$  SNP plus 1 mM  $\text{H}_2\text{O}_2$ . **A:** Comet profiles in cells treated with 100 and 300  $\mu\text{M}$  SNP. **a:** Panoramic view of cells and comets after 30 minutes of exposure to 100  $\mu\text{M}$  SNP. **b:** Two comets (from a) with large heads, conspicuous comas, and short granular tails. **c:** A comet after exposure to 100  $\mu\text{M}$  SNP for 1 hour displays a smaller head and longer granular tail than those shown for 30 minutes of exposure. An intact nucleus is seen at the left of the comet. **d:** Mature comet from cells exposed to 100  $\mu\text{M}$  SNP for 1 hour with a head containing a DNA-poor core and a very long tail. **e:** With 2 hours of exposure to 100  $\mu\text{M}$  SNP, comets can be found with large heads and diffuse comas and short granular tails, indicating DNA damage is at an earlier stage. However, some nuclear profiles are large, swollen, and vacuolated. These two patterns may reflect different stages of DNA damage. **f–h:** With 4 hours of exposure to 300  $\mu\text{M}$  SNP, comet patterns are very distinct. The heads of the comets are different in their DNA quantities (Table 1). The comet in f has a granular head, and the comet in g has a smaller head than that in f; the comet in h has almost no head. The tails of these comets are composed of large granules typical of the SNP pattern. **B:** Histogram of the number of comets in microgels. Values are mean  $\pm$  SEM. The percentages of comets in all the groups exposed to 100  $\mu\text{M}$  SNP are significantly higher than in the corresponding control groups, demonstrating that SNP at this dose induces DNA damage in many cells. The level of significance is greater in the 15-minute, 30-minute, and 1-hour groups (\*,  $P < 0.01$ ) compared with the 2-hour group (\*,  $P < 0.05$ ). Exposure time-effects are not apparent with 100  $\mu\text{M}$  SNP, reflecting that the formation of DNA-SSB is transient rather than sustained; thus comets appear and disappear. Comet percentages in cells exposed to 100  $\mu\text{M}$  SNP plus 1 mM  $\text{H}_2\text{O}_2$  are increased signifi-

cantly at 30 minutes ( $P < 0.01$ ) and 1 hour ( $P < 0.05$ ), compared with untreated controls, with comet numbers peaking at 30 minutes. With 100  $\mu\text{M}$  SNP plus 1 mM  $\text{H}_2\text{O}_2$ , the percentages of comets at most times (30 minutes, 1 hour, and 2 hours) were significantly higher ( $\Delta\Delta$ ,  $P < 0.01$ ) compared with the number of comets in cells exposed to 1 mM  $\text{H}_2\text{O}_2$ , but cells exposed to 100  $\mu\text{M}$  SNP plus 1 mM  $\text{H}_2\text{O}_2$  for 15 minutes ( $\circ$ ,  $P < 0.05$ ) and 2 hours ( $\circ\circ$ ,  $P < 0.01$ ) have significantly lower percentages of comets compared with the 100  $\mu\text{M}$  SNP groups. At 2 hours of exposure to 100  $\mu\text{M}$  SNP plus 1 mM  $\text{H}_2\text{O}_2$ , the percentage of comets is significantly ( $\#$ ,  $P < 0.05$ ) lower compared with 1 hour of exposure to the same treatment. With 30 minutes of exposure to 100  $\mu\text{M}$  SNP plus 1 mM  $\text{H}_2\text{O}_2$ , the comet number was significantly higher ( $+$ ,  $P < 0.05$ ) than at 15 minutes. These observations were replicated in three different experiments. **C:** Histogram of cell number in the comet assay microgels. Values are mean  $\pm$  SEM. With 1 hour of exposure to 100  $\mu\text{M}$  SNP alone, cell number is lower relative to 15 minutes; however, compared with time-matched control cells, cell number is unchanged after exposure to 100  $\mu\text{M}$  SNP alone. Control and 1 mM  $\text{H}_2\text{O}_2$  exposure groups are the same as those shown in Figure 6C. A prominent loss of cells occurs at all times after exposure to 100  $\mu\text{M}$  SNP plus 1 mM  $\text{H}_2\text{O}_2$  (\*,  $P < 0.01$ , for 15 and 30 minutes; \*,  $P < 0.05$  for 1 and 2 hours) compared with their control groups. Comparison among groups exposed to 100  $\mu\text{M}$  SNP plus 1 mM  $\text{H}_2\text{O}_2$  and groups exposed to 100  $\mu\text{M}$  SNP shows that cell number is significantly ( $\circ\circ$ ,  $P < 0.01$ ) lower in the former groups at 15 and 30 minutes. Comparison between groups exposed to 100  $\mu\text{M}$  SNP plus 1 mM  $\text{H}_2\text{O}_2$  and groups exposed to 1 mM  $\text{H}_2\text{O}_2$  showed that cell number is significantly lower ( $\Delta$ ,  $P < 0.05$ ;  $\Delta\Delta$ ,  $P < 0.01$ ) in former groups at 15 minutes, 30 minutes, and 2 hours. Scale bars = 220  $\mu\text{M}$  in a; 55  $\mu\text{M}$  in d (also applies to b,c,e); 52  $\mu\text{M}$  in f (also applies to g,h).

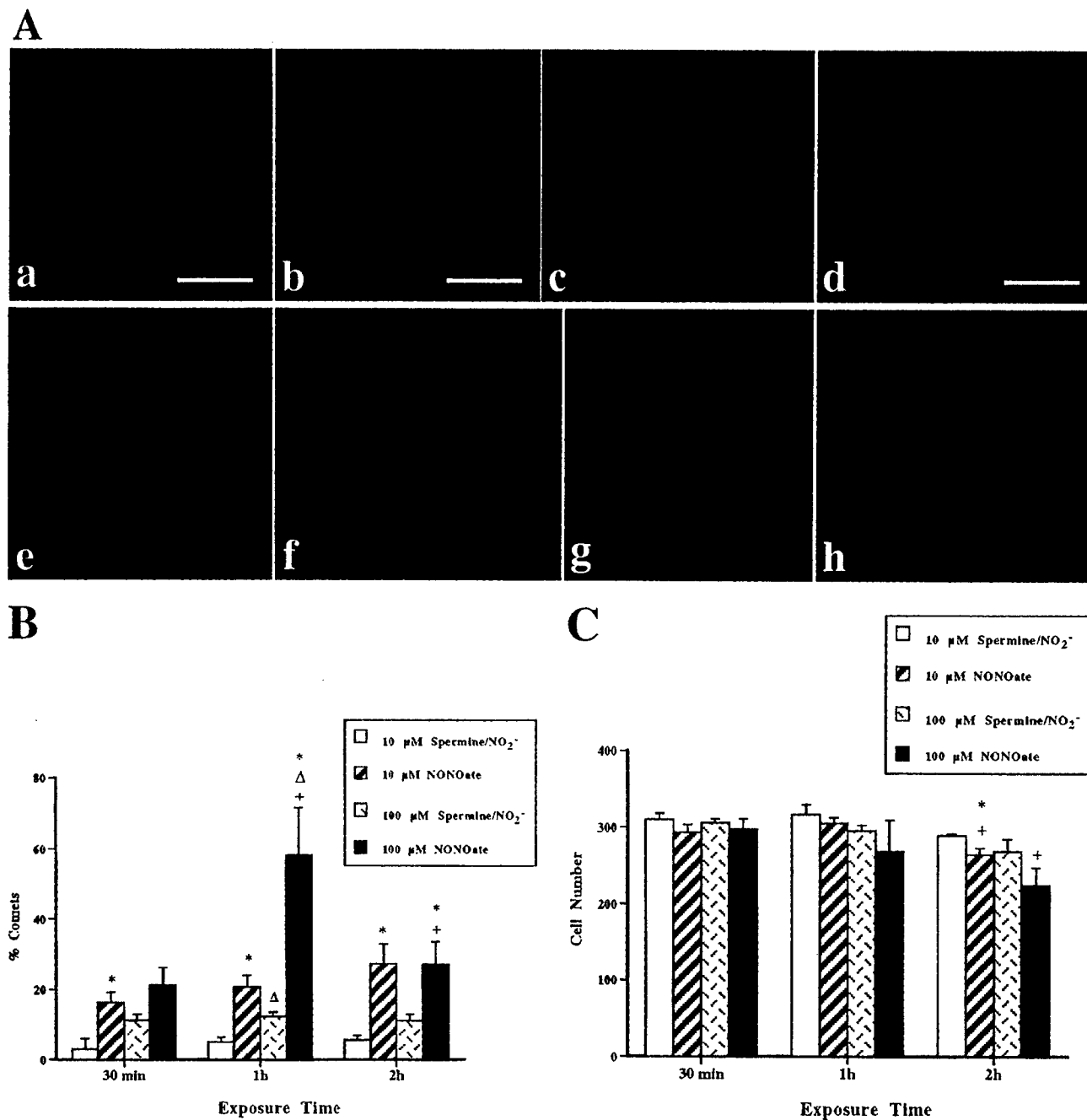


Fig. 8. Comet assay on motor neurons exposed to NONOate. **A:** Comet profiles in cells treated with 10 or 100  $\mu\text{M}$  NONOate. **a:** Control cells treated with 10  $\mu\text{M}$  spermine/ $\text{NO}_2^-$  for 2 hours show few comets. **b,c:** NO generation induces a continuous accumulation of DNA-SSB in motor neuron comets after exposure to 10  $\mu\text{M}$  NONOate for 1 hour (b) or 2 hours (c). **d:** The typical comets induced by 10  $\mu\text{M}$  NONOate have bright, large heads and short tails formed by large granules of DNA. **e,f:** Motor neuron comets after exposure to 100  $\mu\text{M}$  NONOate for 30 minutes (e) or 1 hour (f). **g:** The typical comets induced by 100  $\mu\text{M}$  NONOate have bright, large heads with a prominent coma and very short, broad tails. **h:** Motor neurons exposed to 100  $\mu\text{M}$  NONOate for 2 hours display comets with very granular,

reticulated heads and short, faint tails, indicating severe DNA damage. **B:** Histogram of the number of comets in microgels of motor neurons exposed to NONOate. Values are mean  $\pm$  SEM. \*, Significantly different ( $P < 0.05$ ) from time-matched control;  $\Delta$ , significantly different ( $P < 0.05$ ) from the 10  $\mu\text{M}$  dose at the same exposure time; +, significantly different ( $P < 0.05$ ) from earlier time points. **C:** Histogram of cell number in the comet assay microgels. Values are mean  $\pm$  SEM. \*, Significantly different ( $P < 0.05$ ) from time-matched control; +, significantly different ( $P < 0.05$ ) from corresponding 30-minute value. Scale bars = 140  $\mu\text{m}$  in a; 280  $\mu\text{m}$  in b (also applies to c,e,f); 70  $\mu\text{m}$  in d (also applies to g,h).

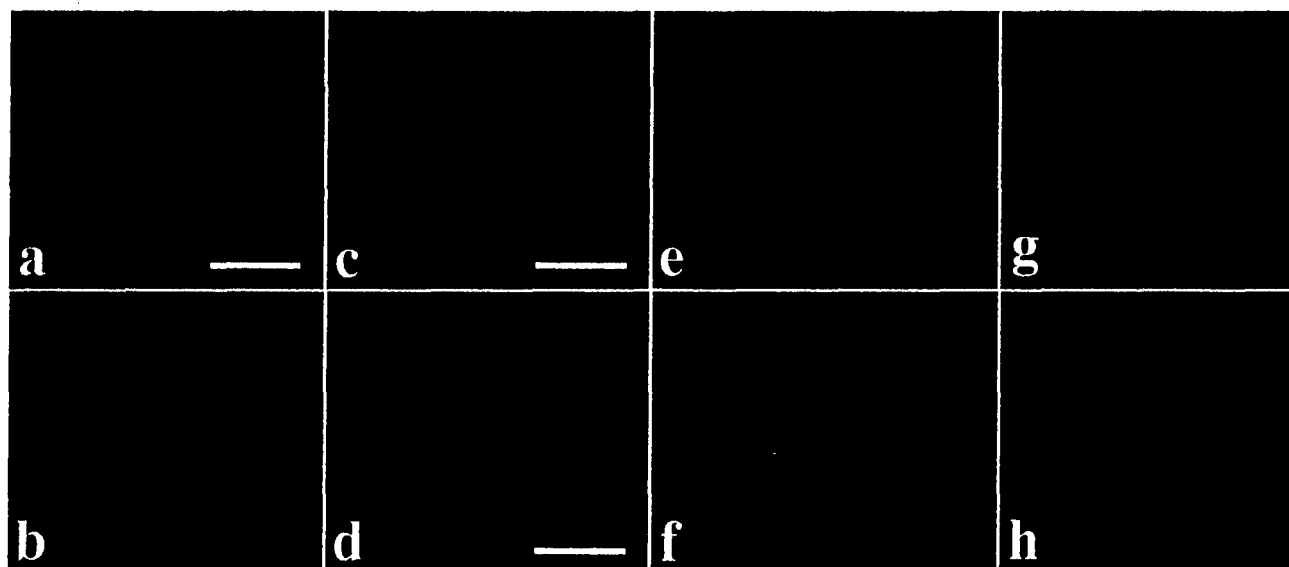


Fig. 9. Comets in motor neurons exposed to 1 mM  $\text{H}_2\text{O}_2$  alone or 1 mM  $\text{H}_2\text{O}_2$  plus different doses of SNP (10, 100, or 300  $\mu\text{M}$ ). **a:** Most nuclei in the cells exposed to 1 mM  $\text{H}_2\text{O}_2$  for 15 minutes are large and intact without DNA damage. The comets typically found after exposure to 1 mM  $\text{H}_2\text{O}_2$  have a large head and short tail with a narrow neck. **b:** After exposure to 1 mM  $\text{H}_2\text{O}_2$  for 6 hours, the comet patterns are similar to the pattern found at 15 minutes. **c:** After exposure of cells to 100  $\mu\text{M}$  SNP and 1 mM  $\text{H}_2\text{O}_2$  for 15 minutes, cell density is low (see Fig. 6C). Large cells (i.e., motor neurons) are particularly sensitive to oxidants. Some large neuronal comets have irregular heads. **d:** Two neuronal comets (shown at higher magnification from c) with one comet having a large round head with a prominent coma and a short, faint tail, and the other comet having an irregular head. **e:** Ex-

posure of cells to 100  $\mu\text{M}$  SNP and 1 mM  $\text{H}_2\text{O}_2$  for 15 minutes also produced another comet pattern. The heads of these comets are very small and the tails are very long with a narrow neck, indicate severe DNA damage. **f:** After cells were exposed to 100  $\mu\text{M}$  SNP and 1 mM  $\text{H}_2\text{O}_2$  for 15 minutes, normal cell nuclei are observed rarely, but swollen nuclei and nuclear fragments containing DNA are observed frequently. **g:** Comets found after exposure to 10  $\mu\text{M}$  SNP plus 1 mM  $\text{H}_2\text{O}_2$  for 30 minutes have pale DNA staining in the tail. **h:** A comet (after exposure to 300  $\mu\text{M}$  SNP plus 1 mM  $\text{H}_2\text{O}_2$  for 4 hours) with a head that is fragmenting, indicating a late stage of nuclear damage and severe DNA damage. Scale bars = 140  $\mu\text{m}$  in a (also applies to e,g,h); 280  $\mu\text{m}$  in c (also applies to b); 70  $\mu\text{m}$  in d (also applies to f).

proteins are found in motor neuron lysates after exposure to  $\text{ONOO}^-$ . Protein nitration is also found at high levels in motor neurons after exposure to SNP +  $\text{H}_2\text{O}_2$ , demonstrating indirectly the formation of  $\text{ONOO}^-$ . Interestingly, high levels of nitrated proteins are also detected in motor neurons treated with NO donor alone (Fig. 11).  $\text{ONOO}^-$  produces the most severe protein nitration, and SNP +  $\text{H}_2\text{O}_2$  induces a similar pattern, revealing the presence of  $\text{ONOO}^-$ .

$\text{ONOO}^-$  is formed from the combination of NO and  $^-\text{O}_2$  (Beckman et al., 1993); therefore, we suspected that isolated motor neurons produce high levels of endogenous  $^-\text{O}_2$ . Motor neurons were stained with HE to detect  $^-\text{O}_2$  (Fig. 12). This experiment confirmed that isolated motor neurons produce  $^-\text{O}_2$  and that a higher level of  $^-\text{O}_2$  production (or increased half-life of  $^-\text{O}_2$ ) is associated with enhanced DNA damage in motor neurons (Figs. 5C, 12E).

#### Comet patterns in motor neurons reveal the severity and progressiveness of DNA damage and suggest common mechanisms of neurotoxicity

Motor neurons display a variety of comet patterns (Fig. 13). The nuclei of healthy motor neurons are similar in size and DNA staining regardless of lysis, unwinding, and electrophoresis of DNA. These nuclei are round and are stained very brightly (Fig. 13a). This type of nucleus is found in control groups at every time point and in groups treated with 1 mM  $\text{H}_2\text{O}_2$  (early times, such as 15 minutes,

30 minutes, 1 hour, and 2 hours), 10 mM  $\text{H}_2\text{O}_2$  and NO donor (15 and 30 minutes), and in motor neurons at 5 days after avulsion (see below for details).

The most frequent new comet pattern is one with a large, round, densely staining head and a short, granular tail (Table 1) consisting of large granules close to the head (Fig. 13b). The moment of this comet pattern was low (Table 1). The majority of background comets detected in control motor neurons have this profile (even at 12 hours). This comet type occurs more frequently in motor neurons treated for short durations (15 minutes) with 10 mM  $\text{H}_2\text{O}_2$  or 10, 100, 300, or 800  $\mu\text{M}$  SNP. Other new comets consist of a head with a densely staining round core surrounded by a dense DNA halo (Fig. 13c) occasionally found in control groups, or large granules (Fig. 13e) found in NO donor-treated motor neurons. The comet moment analysis (Table 1) suggests that these comets represent nascent DNA damage at few sites with the formation of large DNA single strands.

Mature comets have longer tails compared with new comets (Table 1). Newly matured comets have a large, densely stained head and a tail shorter than 620  $\mu\text{m}$  formed by scattered large granules (Fig. 13d). This type of comet occurs occasionally in some untreated motor neurons incubated from 1 to 12 hours and probably represents background dying cells after dissection from spinal cord and trypsin digestion. NO donor-treated motor neurons have a characteristic type of mature comet, appearing with a large head and very bright halo, and a longer tail

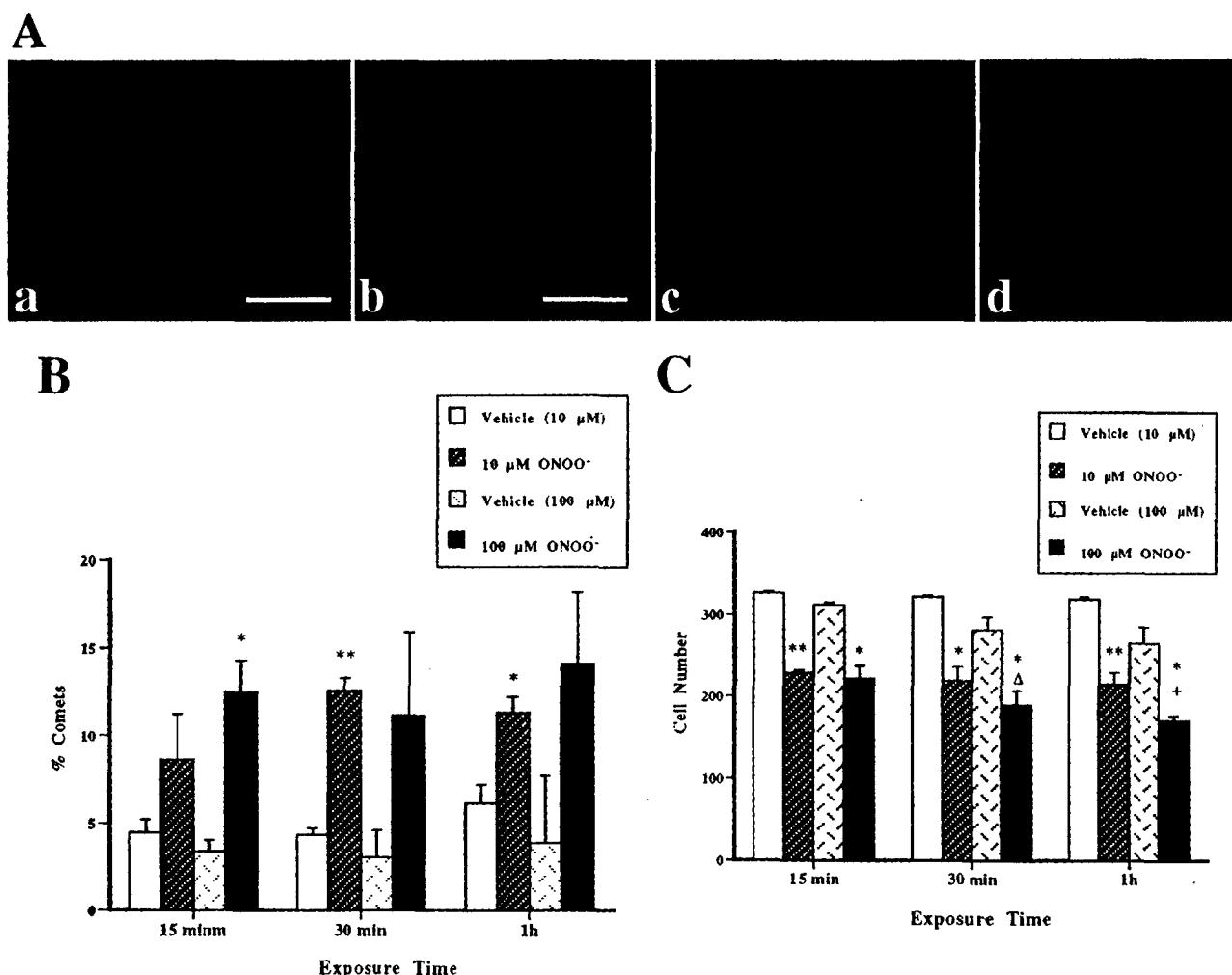


Fig. 10. Comet assay on motor neurons exposed to ONOO<sup>-</sup>. A: Motor neuron comets after exposure to 10  $\mu\text{M}$  ONOO<sup>-</sup> for 15 minutes (a), 30 minutes (b), or 1 hour (c) or to 100  $\mu\text{M}$  ONOO<sup>-</sup> for 30 minutes (d). Note that 10  $\mu\text{M}$  ONOO<sup>-</sup> exposure for 1 hour induces motor neuron comets similar to 10  $\mu\text{M}$  SNP + 1 mM H<sub>2</sub>O<sub>2</sub>, whereas 100  $\mu\text{M}$  ONOO<sup>-</sup> exposure for 30 minutes induces motor neuron comets similar to 100  $\mu\text{M}$  SNP + 1 mM H<sub>2</sub>O<sub>2</sub>. B: Histogram of the number of comets in microgels of motor neurons exposed to ONOO<sup>-</sup>. Vehicles are alkaline-decomposed ONOO<sup>-</sup> at the corresponding doses. Values are mean  $\pm$  SEM. \*, Significantly different ( $P < 0.05$ ) from time-matched control; \*\*, significantly different ( $P < 0.01$ ) from time-matched control. These

observations were replicated in three different experiments. C: Histogram of motor neuron number in the comet assay microgels. Vehicles are alkaline-decomposed ONOO<sup>-</sup> at the corresponding doses. Values are mean  $\pm$  SEM. \*, Significantly different ( $P < 0.05$ ) from time-matched control; \*\*, significantly different ( $P < 0.01$ ) from time-matched control;  $\Delta$ , significantly different ( $P < 0.05$ ) from 10- $\mu\text{M}$  dose at the same exposure time; +, significantly different ( $P < 0.05$ ) from the 30-minute group. These observations were replicated in three different experiments. Scale bars = 140  $\mu\text{m}$  in a; 70  $\mu\text{m}$  in b (also applies to c,d).

(~310  $\mu\text{m}$ ) consisting of very scattered large granules (Fig. 13f,o). This comet morphology is found most frequently with 10  $\mu\text{M}$  SNP and NONOate at 30 minutes or 1 hour. This pattern indicates that DNA damage progressed from the new comets, as indicated by the greater comet moment (Table 1).

The mature comet morphology is more variable than with the new comets. Mature comets can display medium-sized heads and densely staining, intermediate tail lengths (>310  $\mu\text{m}$ ). Some motor neuron comets have a head with a bright granular halo and a wide granular tail as broad as the head coma (Fig. 13g). This type of mature comet is also typical for NO donor exposure, but the DNA damage is more extensive compared with the new comets observed with NO donors.

The DNA-SSB are much more prevalent in these motor neurons compared with motor neurons with new comets, because the tail was very broad and there are many granules. Another type of comet typical of NO donor exposure (with higher dose and/or longer exposure time) is a very progressed form (Fig. 13h). The head consists of only scattered large granules, and the tail is also composed of large granules and is long (~620  $\mu\text{m}$  or longer). This comet morphology is very similar to the comets found in motor neurons exposed to ONOO<sup>-</sup> (Fig. 13p). Some of these comets had irregular heads with a blebbing nucleus containing round, DNA masses similar to apoptosis (Fig. 13k).

In motor neurons treated with 10 mM H<sub>2</sub>O<sub>2</sub>, characteristic comet patterns emerge. At 30 minutes, motor neuron

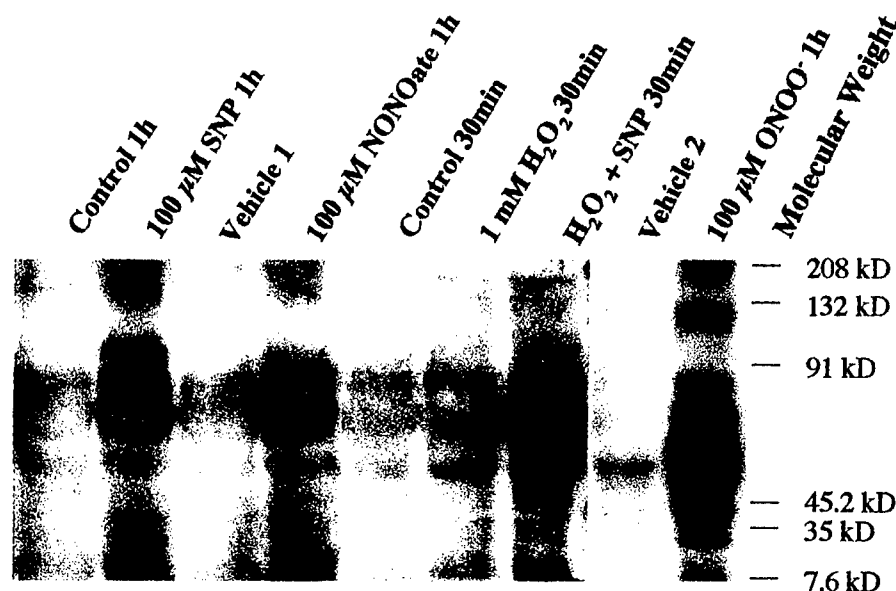


Fig. 11. Immunoblots of nitrotyrosine-modified proteins in motor neuron cell lysates after exposure to NO donors,  $H_2O_2$ , and  $ONOO^-$ . Molecular mass markers (in kD) are indicated at right. Prominent increases in protein nitration occur after exposure of motor neurons to

SNP, SNP +  $H_2O_2$ , NONOate, and  $ONOO^-$ . Vehicle 1 (100  $\mu M$  spermine/ $NO^-$ ) is control for 100  $\mu M$  NONOate. Vehicle 2 (alkaline-decomposed  $ONOO^-$ ) is control for 100  $\mu M$   $ONOO^-$ .

comets have a densely staining core in the head and a circular profile of DNA around the core (Fig. 13i). These heads are much smaller than the new comet heads with this halo pattern (Fig. 13c). The tails consisted of fine granules, indicating that the DNA-SSB are numerous and the lengths of the DNA single strands in the tail are shorter than those in the comets typically found with SNP. In motor neurons treated with 10 mM  $H_2O_2$  for longer times (30 minutes or 1 hour), comets have a small densely stained head and thin, long tails (620  $\mu m$  or longer) consisting of fine granules (Fig. 13j). Apparently, the DNA damage progressed further, and the single strands of DNA fragments are more numerous and shorter (Table 1).

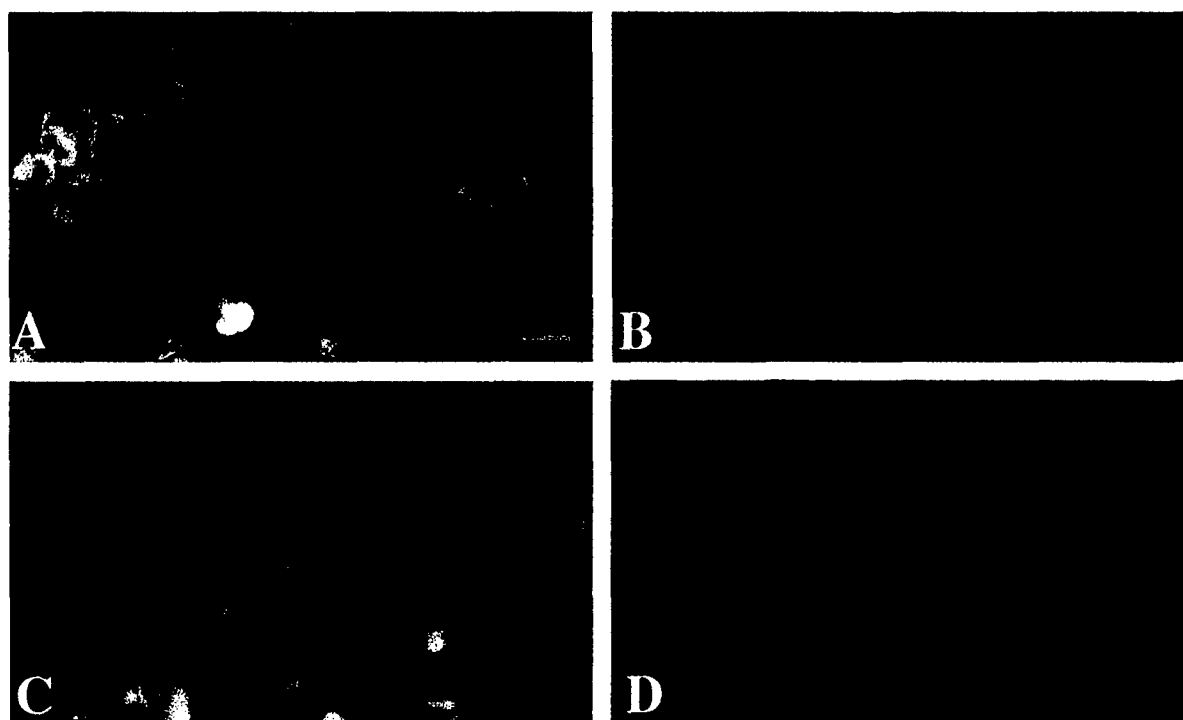
In motor neurons exposed to 1 mM  $H_2O_2$ , there is a specific neuronal comet pattern, in the presence of decreased comet numbers. The head is large and round, typical of neuronal comets. The tail of these comets has a narrow neck, and the broad part of the tail is short and consists of very fine granules (Fig. 13m). The large part of the tail may consist of short DNA single strands because they appear as fine particles rather than large granules. The DNA damage may accumulate very rapidly and then cease, consistent with the shape of the broad tail with a narrow neck.

Two typical types of comets are observed in motor neurons exposed to SNP and  $H_2O_2$ , with severe nuclear DNA damage. One comet profile has an irregular head, displaying either nuclear blebbing with round, apoptotic-like chromatin masses (Fig. 13k) or fragmentation (data not shown). Another comet pattern has very small heads, and the tails are very long with a neck (Fig. 13l). Most of the comets associated with cells exposed to SNP plus  $H_2O_2$  are stained incompletely and faintly with ethidium bromide. This comet pattern is similar to a pattern found under neutralized elution conditions (data not shown) and thus may reflect some double-stranded DNA breaks.

### Motor neurons accumulate DNA-SSB in vivo early after injury and the comet pattern is similar to DNA damage induced by NO donor exposure in vitro

The comet assay was applied to an in vivo model of motor neuron degeneration (Fig. 14; Table 2). At 5 days after unilateral sciatic nerve avulsion, many (26%) lumbar motor neurons from the lesioned side have comets (Fig. 14B), but very few motor neurons (1.8%) from the unlesioned side have comets. The heads of these motor neuron comets are large, round and bright, and the tails are very short (Table 2) and consist of scattered large granules close to the heads (Fig. 14Aa,b). The comet moment is low ( $\sim 1.6 \times 10^5$ ; Table 2). Motor neurons at 5 days did not have an apoptotic nuclear morphology based on ethidium bromide staining and previous observations (Martin et al., 1999a).

At 7 days after sciatic nerve avulsion, the number of motor neuron comets in the lesioned side of spinal cord increases significantly (35%,  $P < 0.05$ ) compared with 5 days (Fig. 14B). The comet moment also increases compared with 5 days (Table 2), indicating a progressive formation of DNA-SSB. These comets have large heads and short granular tails that are longer than those at 5 days (Fig. 14Ac,d; Table 2). These comets appear as intermediates between control comets (Fig. 13b or d) and comets from motor neurons exposed to NO donors (Fig. 13e or f), but they are most similar to NO donor-induced new comets (Fig. 13e). Thus, both the number of motor neurons with DNA damage and the extent of DNA-SSB in these motor neurons increase between 5 and 7 days after sciatic nerve avulsion. Motor neurons at 7 days did not exhibit apoptotic nuclear features (e.g., chromatin condensation into round clumps) based on ethidium bromide staining and previous evaluations (Martin et al., 1999a). No comets



E

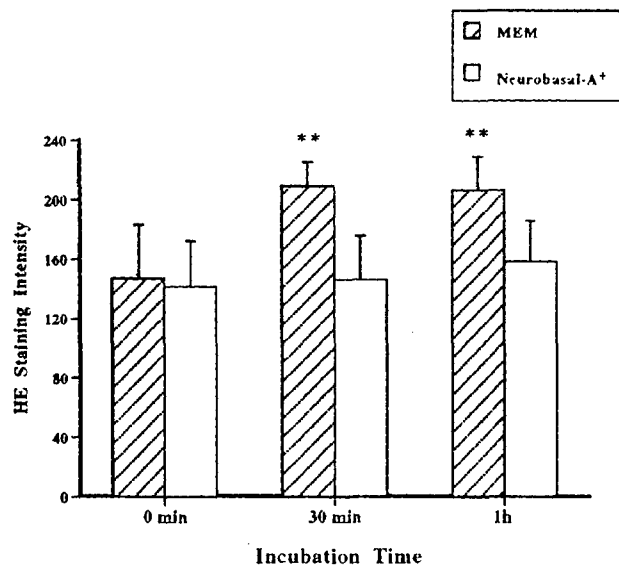


Fig. 12. Detection of endogenous  $\text{O}_2^-$  in living motor neurons. A-D: HE staining of motor neurons incubated in minimum essential medium (MEM) (A, B) or supplemented Neurobasal-A (C, D) for 30 minutes prior to the detection of  $\text{O}_2^-$ . Panel pairs (A, B and C, D) are the same cells viewed under different emission filters. Blue (A, C) indicates unconverted HE and red (B, D) reveals  $\text{O}_2^-$  converted dye.  $\text{O}_2^-$  production is greater in the MEM-incubated motor neurons.

E: Histogram of the comparison of  $\text{O}_2^-$  production in isolated motor neurons incubated in MEM or Neurobasal-A (with supplements) for 0 minutes (immediately after isolation), 30 minutes, or 1 hour.  $\text{O}_2^-$  production is significantly greater (\*\*,  $P < 0.001$ ) in MEM-incubated motor neurons at 30 minutes and 1 hour. Scale bar = 50  $\mu\text{m}$  in a (also applies to b-d).

are found with motor neurons from the unlesioned side at 7 days post lesion.

Subsets of lumbar motor neurons (23%) on the lesioned side have comets at 10 days after sciatic nerve avulsion (Fig. 14). Many of these comets have heads with a coma

and a short granular tail (Fig. 14Ae). Other comets have a small head or no head and a much longer tail (as long as 1240  $\mu\text{m}$ ; Fig. 14Ag,f; Table 2). These comet patterns (Fig. 14Ae,g) are similar to comets in motor neurons induced by SNP (Fig. 13f, h). The heads of many of these comets have

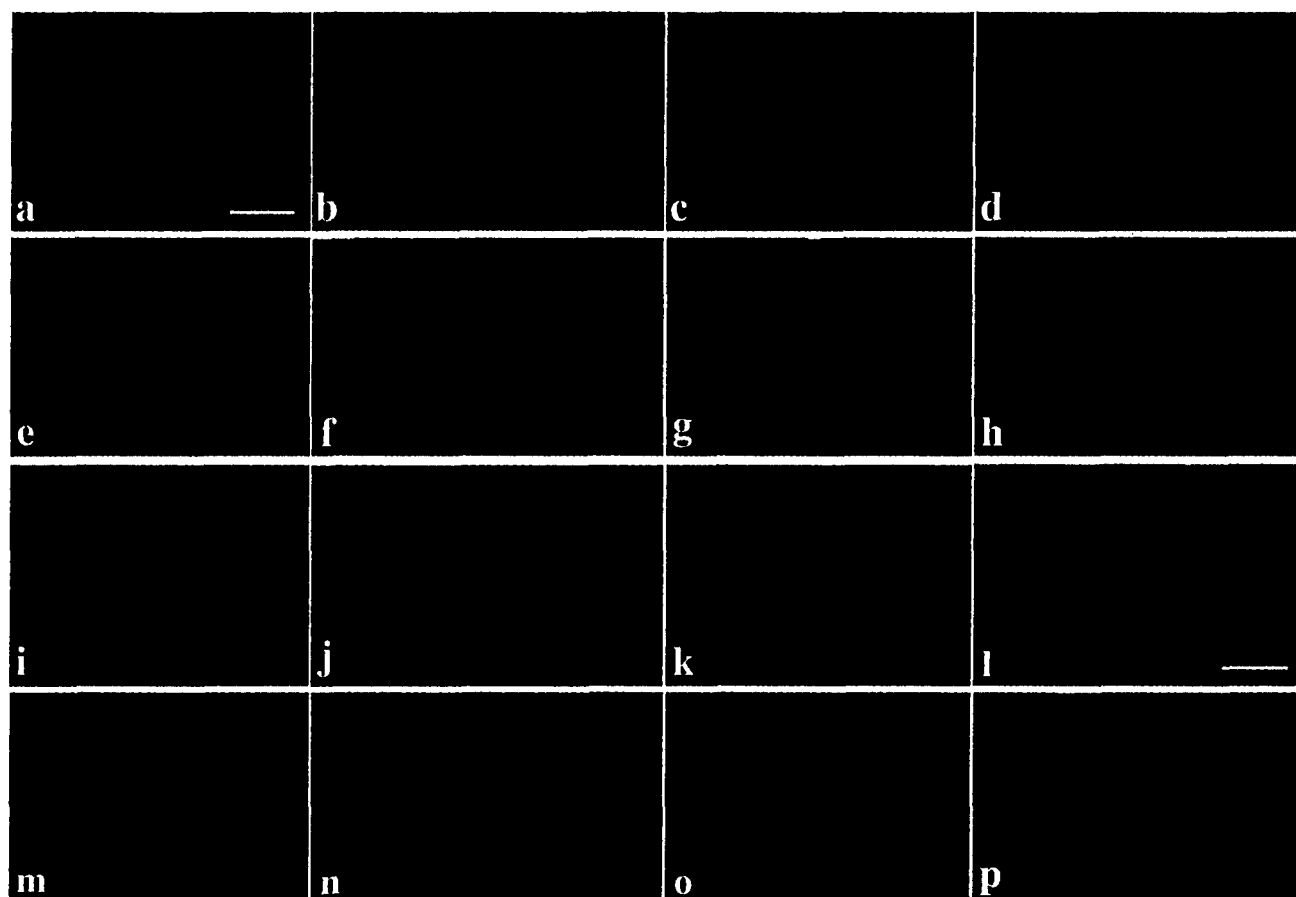


Fig. 13. Gallery of neuronal comet patterns observed by single-cell gel electrophoresis and ethidium bromide staining. **a**: A large intact motor neuron nucleus. The DNA is stained brightly, but no comet is present. **b**: A typical new comet with a large head and a very short tail, consisting of a few large granules. This type of comet appears infrequently as background comets in control cells and much more frequently in cells exposed to 10  $\mu$ M SNP for a short time (15 minutes), and in lumbar motor neurons at 5 days after sciatic nerve avulsion. **c**: A comet with a head surrounded by a halo and a very short tail. **d**: A comet with a longer tail consisting of scattered large granules. This comet type is observed occasionally in control samples incubated for >2 hours, indicating slowly accumulated DNA damage. **e**: Comets with a large intensely staining head surrounded by a very bright coma. These comets are often observed in neurons exposed to 10  $\mu$ M SNP and NONOate and in lumbar motor neurons at 10 days after sciatic nerve avulsion. **f**: Comets (more mature than those shown in **e**) with a bright head and coma and a longer tail formed by very scattered large granules. This is the typical pattern of comets in motor neurons exposed to NO. **g**: Comets with a dissipating head and broad tail composed of more densely distributed granules. This is a mature comet pattern (from the comets shown in **e** or **f**) observed in cells exposed to lower concentrations of NO donor (10  $\mu$ M SNP and NONOate). **h**: Typical comet pattern with cells exposed to higher doses of

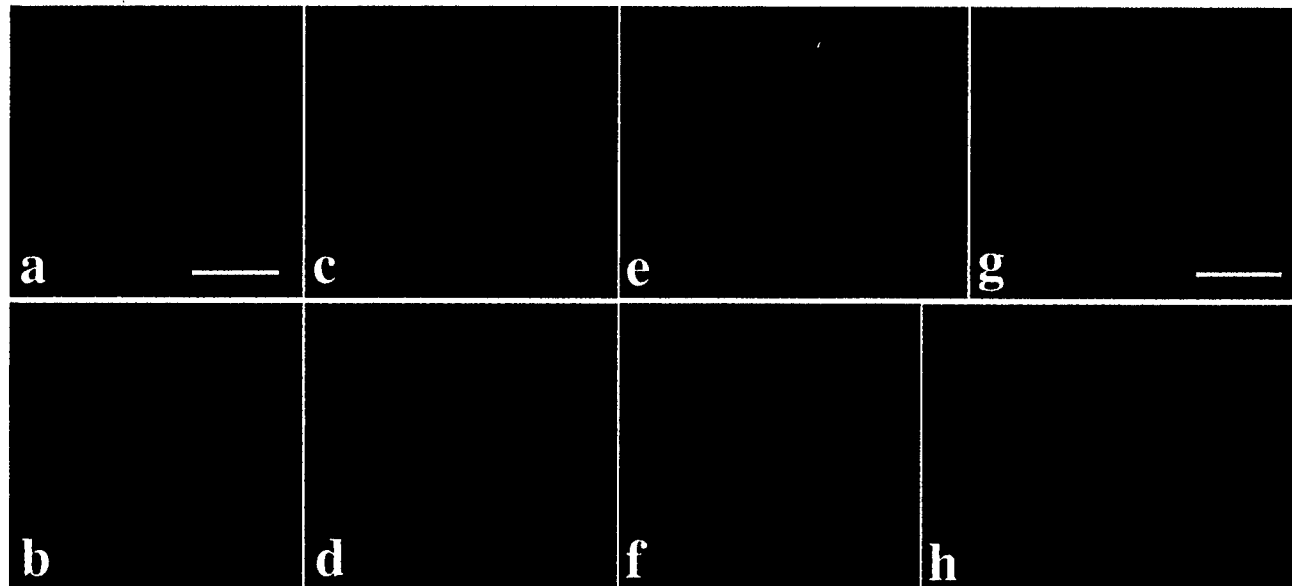
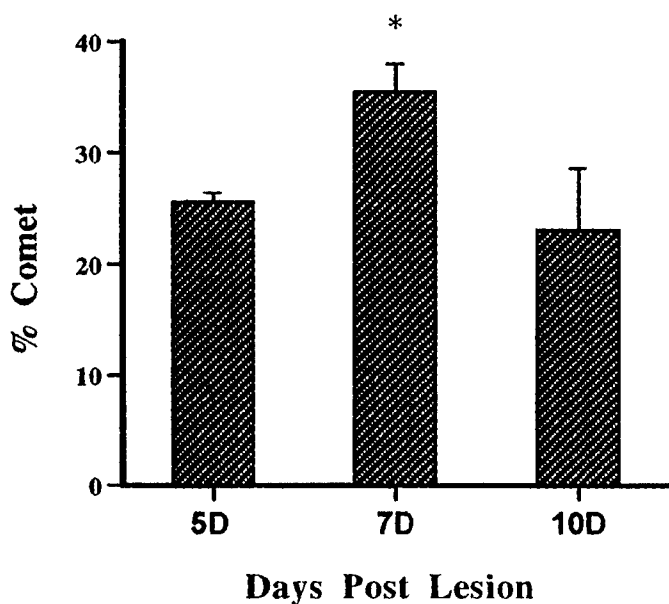
SNP (300 or 800  $\mu$ M) or to 100  $\mu$ M SNP and NONOate for a longer time (2–4 hours). The heads are small and granular and the tails consist of very large granules. **i**: A comet with a distinct head consisting of a halo surrounding a core (from cells exposed to 10 mM  $H_2O_2$  for 30 minutes). **j**: A comet with a small head and very long thin tail found in cells exposed to 10 mM  $H_2O_2$  for 30 or 60 minutes. **k**: Comets with irregular heads and faintly staining tails are observed in motor neurons exposed to 100  $\mu$ M (or 10  $\mu$ M) SNP plus 1 mM  $H_2O_2$  for 15 minutes, 30 minutes, or 1 hour. **l**: A comet from SNP +  $H_2O_2$  (1 mM) exposed (1 hour) motor neurons with a head that is very small and a tail that is very long with a narrow faintly stained neck. This comet is in a field of swollen nuclei or nuclear fragments. **m**: Comets from cells exposed to 1 mM  $H_2O_2$  for 15 minutes show a typical pattern. This pattern is a large head and a short broad tail with a short neck. **n**: Comet from cells exposed to 1 mM  $H_2O_2$  in MEM. **o**: Most common comet morphology found with motor neurons after exposure to NONOate (10  $\mu$ M). Note the similarity to SNP-exposed motor neurons (see **f** and **g**). **p**: Most common comet morphology in motor neurons exposed to ONOO $^-$  (10  $\mu$ M) for 15–30 minutes. This comet pattern is similar to the pattern found with higher dose SNP or longer time exposure to lower doses. Scale bars = 49  $\mu$ m in **a** (also applies to **b**–**i**, **k**, **m**–**p**); 98  $\mu$ m in **l** (also applies to **j**).

a nucleus round aggregates of chromatin typical of apoptosis (Fig. 14Af), and the tails are still comprised of large granules, though they are finer than those at 5 and 7 days. These cells have the greatest comet moments (Table 2), indicating accumulated DNA damage in apoptotic motor neurons at 10 days after sciatic nerve avulsion.

The 800-rpm cell suspension was also evaluated to identify motor neurons with comets, because these cells may be lighter after advanced DNA damage and are not pre-

cipitated at 400 rpm. Comets are found in the 800-rpm cell suspensions, particularly at 10 days after avulsion (Fig. 14Ah). No comets are observed in the 400- and 800-rpm cell suspensions from ventral horns of the unlesioned spinal cord at 10 days post lesion. At 14, 20, and 28 days after sciatic nerve avulsion, no comets are observed in motor neurons from either ipsilateral or contralateral lumbar ventral horns, despite the presence of apoptotic profiles ipsilaterally at these times.



**A****B**

**Fig. 14.** DNA-SSB occur in motor neurons after unilateral sciatic nerve avulsion. **A:** Motor neuron comets after unilateral sciatic nerve avulsion. **a:** At 5 days post lesion, the comet heads are large and round, and the tails are very short. **b:** A typical 5-day comet (from a) with a short tail. **c:** At 7 days post lesion, the comet heads are large and the tails are longer than at 5 days, indicating the accumulation of DNA-SSB. **d:** A typical 7-day comet (from c) with a tail that is formed by scattered, large DNA granules. These comets are very similar to those produced by SNP but not  $H_2O_2$ . **e-g:** At 10 days the similarities between the comets produced by axotomy and those produced by SNP become much more prominent. The comets shown in e have heads with a granular coma and granular tails similar to the comets found in cells exposed to 10 or 100  $\mu M$  SNP. Some comets have an irregular

head and a granular tail (shown in f). Other comets (shown in g) have longer tails formed by scattered large granules. **h:** At 10 days after the lesion, motor neurons comets can be found in the 800-rpm cell suspensions. These comets have long tails, indicating accumulation of many DNA-SSB. **B:** Percent comets in lumbar motor neuron cell suspensions (400-rpm preparations) from the lesioned side of the spinal cord. The percentage of comets (compared with the total number of large cells embedded) increased significantly (\*,  $P < 0.05$ ) between 5 days (5D) and 7 days (7D) post lesion (with significantly more comets at 7 days compared with 5 days) and then decreased at 10 days (10D) post lesion. Scale bars = 140  $\mu m$  in a (also applies to c,h); 70  $\mu m$  in g (also applies to b,d-f).

TABLE 2. DNA Damage in Motor Neurons After Sciatic Nerve Avulsion as Determined by Comet Assay<sup>1</sup>

Survival time (days)	Comet pattern <sup>2</sup>	DNA intensity <sup>3</sup>		DNA intensity ratio (tail/head)	DNA area		DNA area ratio (tail/head)	Tail length	Traditional comet moment ( $\times 10^4$ ) <sup>4</sup>	Comet moment ( $\times 10^5$ ) <sup>5</sup>
		Head	Tail		Head	Tail				
5	b	201.4 $\pm$ 17.4	70.4 $\pm$ 21.9	0.344 $\pm$ 0.086	988 $\pm$ 143	2338 $\pm$ 985	2.33 $\pm$ 0.79	64 $\pm$ 17	0.43 $\pm$ 0.15	1.6 $\pm$ 0.8
7	d	219.5 $\pm$ 7.1	92.1 $\pm$ 9.3	0.420 $\pm$ 0.042	2138 $\pm$ 303	9136 $\pm$ 1554	4.32 $\pm$ 0.84	265 $\pm$ 20*	2.42 $\pm$ 0.19*	8.5 $\pm$ 1.6*
10	f	168.7 $\pm$ 16.2	70.6 $\pm$ 11.2	0.421 $\pm$ 0.061	2882 $\pm$ 1607	25377 $\pm$ 7860	11.44 $\pm$ 4.55	322 $\pm$ 10*	2.26 $\pm$ 0.33	18.9 $\pm$ 8.5*

<sup>1</sup>All values are mean  $\pm$  SEM. \*, significantly different ( $P < 0.05$ ) from earlier time point.

<sup>2</sup>Representative comet patterns are shown in Figure 14A and are identified by the corresponding panel letter.

<sup>3</sup>See Figure 1 for delineation of comet head and tail.

<sup>4</sup>Calculated from DNA intensity<sub>tail</sub>  $\times$  tail length (Hellman et al., 1995).

<sup>5</sup>Calculated from DNA intensity<sub>tail</sub>  $\times$  tail area.

## DISCUSSION

This study evaluates mechanisms of motor neuron degeneration. We studied the formation of DNA damage in motor neurons because of the selective vulnerability of these cells in ALS. This study is novel for several reasons. First, we developed a new approach to study adult motor neurons. Second, we characterized a new assay to study DNA damage in motor neurons. Third, we found that degenerating adult motor neurons in vitro rapidly accumulate SSB in DNA after exposure to oxidative stress. Specifically, we found that  $H_2O_2$ , NO, and ONOO<sup>-</sup> are potent inducers of DNA-SSB in motor neurons and that ONOO<sup>-</sup> formation is a major final common mediator. Fourth, by extending the analysis to motor neuron degeneration in an animal model, we found that DNA-SSB accumulate early during the progression of motor neuron apoptosis in vivo. Fifth, the early DNA damage fingerprint in motor neurons destined to undergo apoptosis in vivo (Martin et al., 1999a) has a pattern similar to NO and ONOO<sup>-</sup> toxicity in vitro.

### Adult motor neurons can be studied in vitro

We developed a new model system to study motor neuron degeneration. Motor neurons from adult spinal cord cannot be cultured; therefore, we created a short-term, motor neuron-enriched cell suspension isolated from spinal cord ventral horn enlargements of adult rat. This method is an important technical advancement in the study of motor neurons. After digestion of ventral horn tissue columns in trypsin, adult motor neurons are isolated by centrifugation, yielding a motor neuron-enriched cell suspension. The motor neuron enrichment of this cell system was confirmed by immunophenotyping (e.g., CAT and NeuN), retrograde tracing, and electron microscopy. These motor neurons become spherical and are viable after dissociation and isolation. The majority of these motor neurons remain viable over short-term incubation (up to 12 hours after isolation), and ~40% of these cells are still viable at 24 hours of incubation in supplemented Neurobasal medium.

An important aspect of this cell system is that the motor neurons are initially viable after their isolation, and then viability is lost progressively. This loss of viability is associated with the formation of vacuoles within the cytoplasm. Our electron microscopic data reveal that these vacuoles are likely to be derived from degenerating mitochondria. Early after isolation when these cell suspensions are exposed to  $H_2O_2$ , NO, and ONOO<sup>-</sup>, the motor neurons rapidly degenerate. Thus, this in vitro system can

be used to study accelerated motor neuron degeneration in suspensions exposed to toxins and slower motor neuron degeneration in untreated cell suspensions. This isolation technique for adult motor neurons can be applied successfully to paradigms of in vivo motor neuron injury (e.g. axotomy) to understand mechanisms of motor neuron degeneration. However, the relatively short viability of adult motor neurons in suspension is a distinct limitation of the model, and attempts to extend their viability are under way.

This acute model of adult rat spinal motor neuron degeneration is relevant to ALS. Despite the acute paradigm, the system can be used to identify disease mechanisms that may be operational in ALS. For instance, motor neuron degeneration in ALS has been identified to be a form of apoptosis (Martin, 1999) that may be induced by the accumulation of DNA damage and mediated by p53 (Martin, 2000a,b). The degeneration of adult motor neurons in our model has some structural features in common with the degeneration of motor neurons in ALS (Martin, 1999), and this degeneration may be a form of apoptosis. Morphological (nuclear condensation) and biochemical (internucleosomal fragmentation of DNA) indices of apoptosis were detected in motor neurons exposed acutely to NO donors or  $H_2O_2$ . The accelerated neurodegeneration is strikingly similar to the motor neuron degeneration found in transgenic mice with forced expression of SOD1 mutations (Dal Canto and Gurney, 1994) identified in individuals with familial ALS (Deng et al., 1993; Rosen et al., 1993). Interestingly, motor neuron degeneration in patients with familial ALS is accelerated compared with individuals with sporadic ALS. As in our acute model of motor neuron degeneration, the degeneration of motor neurons in familial ALS may be mediated by the formation of ONOO<sup>-</sup> (Beckman et al., 1993). Our in vitro motor neuron system is very different from cultured embryonic motor neurons (Henderson et al., 1995). However, our interest is in evaluating mechanisms of degeneration of adult motor neurons and effects of ROS on DNA stability in motor neurons because of the relevance to ALS, which is an adult-onset disease. Furthermore, neurodegeneration can vary depending on neuronal maturity (Portera-Cailliau et al., 1997), and DNA repair capacity displays age-related differences in the CNS (Subba Rao, 1993). We were interested specifically in determining whether  $H_2O_2$ , NO, and ONOO<sup>-</sup> cause DNA-SSB in mature motor neurons and whether DNA-SSB occur early during the in vivo progression of motor neuron apoptosis in the adult spinal cord.

### Comet assay is a feasible method for measuring DNA damage in neurons

We demonstrate for the first time the usefulness of the single-cell gel electrophoresis method (comet assay) for identifying and measuring the occurrence and progression of early DNA damage in individual motor neurons that are injured by ROS *in vitro* and axotomy *in vivo*. Damage to DNA occurs in many forms. At least six general types of DNA are known, such as apurinic/apyrimidinic sites, altered bases, thymidine dimers, crosslinks, double-strand breaks, and SSB (Subba Rao, 1993). The comet assay is an established method for identifying strand breaks in DNA (Singh et al., 1988; Kindzelskii and Petty, 1999; Morris et al., 1999), and its validation has been described (Tice et al., 2000). Based on the principles of alkaline elution (Kohn, 1991), the comet assay is the most sensitive method available for detecting DNA-SSB in individual cells (Ostling and Johanson, 1984; Singh et al., 1988; Hellman et al., 1995; Kindzelskii and Petty, 1999; Morris et al., 1999). The comet assay is sensitive enough for detecting one break per  $2 \times 10^{10}$  daltons of DNA (Singh et al., 1988). The exquisite sensitivity of this assay is revealed further by the detection of subtle DNA-SSB in a small percentage of untreated control motor neurons. A low level of spontaneous comets is found, but this DNA damage is not resolved in standard DNA gels, thus confirming that the comet assay is a sensitive method for detecting early DNA damage in individual cells. Comet formation in this small subset of control cells is related possibly to damage during isolation and to excessive generation of  $\cdot\text{O}_2$ . In fact, we found that these isolated motor neurons generate  $\cdot\text{O}_2$ .

The comet assay has advantages over other more frequently used methods for detecting DNA damage (e.g., nick-end labeling methods such as TUNEL) because it reveals the type of DNA damage (e.g., SSB, double-strand breaks, and alkali labile sites) depending on conditions. Furthermore, assays for single-stranded DNA are more sensitive and specific than TUNEL for apoptosis (Frankfurt et al., 1996). Moreover, the types of DNA damage detected by the comet assay and TUNEL are distinct, with TUNEL detecting late-stage DNA fragmentation (Frankfurt et al., 1996). We have confirmed indirectly the sensitivity of comet assay detection of DNA-SSB as an early and sensitive marker for apoptosis. We observed that DNA-SSB are visualized prominently in avulsed motor neurons at least 2 days before the detection of DNA fragmentation by TUNEL (Martin et al., 1999a) and 5 days before round DNA-containing aggregates are detected in the nucleus (Fig. 14f). Moreover, in motor neurons exposed to oxidative stress, DNA-SSB are detected prominently prior to morphological evidence for chromatin condensation and electrophoretic detection of internucleosomal DNA fragmentation (Fig. 4). Another benefit of the comet assay is that comets can be analyzed by visually dividing them into categories or stages of DNA damage, by measuring tail length, and by digital image analysis of comets for DNA intensity and comet moment. We conclude that the comet assay is a feasible approach to quantify specific types of DNA damage in single neurons induced by neurotoxic agents and traumatic injury *in vitro* and *in vivo*.

### $\text{H}_2\text{O}_2$ has dose-related effects on the formation of DNA-SSB in adult motor neurons

We show that motor neurons are highly vulnerable to oxidative stress by rapidly accumulating DNA damage. Motor neurons are sensitive to  $\text{H}_2\text{O}_2$ . DNA-SSB are induced prominently by  $\text{H}_2\text{O}_2$ , as evidenced by the increase in comet percentage and comet moment as well as the comet patterns. The concentration of  $\text{H}_2\text{O}_2$  that induced DNA-SSB is relatively high (10 mM), possibly because we used Neurobasal-A medium that is free of potentially toxic ferrous ions (Brewer et al., 1993). Lower concentrations of  $\text{H}_2\text{O}_2$  (1 mM) did not generate much DNA damage in this medium. Previous studies have shown that  $\text{H}_2\text{O}_2$  induces DNA damage in leukocytes (Singh et al., 1988; Kindzelskii and Petty, 1999), HeLa cells (Szmigiero and Studzian, 1988), and fibroblasts (Horváthová et al., 1999). SSB are the predominant form of DNA damage produced by  $\text{H}_2\text{O}_2$ , with the ratio of double-strand to single-strand DNA breaks estimated to be 1 to 2000. This is the first demonstration of the formation of DNA-SSB in motor neurons after exposure to  $\text{H}_2\text{O}_2$ . Based on the comet analysis obtained at 15, 30, and 60 minutes of exposure to 10 mM  $\text{H}_2\text{O}_2$ , a progressive accumulation of DNA-SSB occurs in motor neurons. Our quantitative analysis shows that the DNA content in the heads becomes lesser (the heads become smaller) and the DNA content in the tails becomes greater (the tails become longer); thus, there is a shift to the mature comet pattern as the comet moment increases. At 90 minutes of exposure, motor neurons have passed the comet moment for DNA-SSB; thus DNA-SSB are less frequently detected, because damage has advanced mostly to double-strand breaks. Alternatively, motor neurons with DNA damage may disappear from the preparation because they are smaller and lighter or broken and thus are not captured by repelleting. These explanations may account for the decreased comet number and cell density after 90 minutes of exposure.

In the presence of 1 mM  $\text{H}_2\text{O}_2$ , motor neuron comet number is decreased compared with controls. The explanation for this finding is uncertain. Mechanisms for DNA repair may be stimulated in motor neurons exposed to low concentrations of  $\text{H}_2\text{O}_2$ , so that fewer DNA-SSB are detected. The kinetics of DNA repair are very rapid, with significant repair of DNA-SSB in leukocytes occurring within 2 minutes after irradiation (Mendiola-Cruz and Morales-Ramírez, 1999). DNA-SSB are repaired by DNA repair enzymes, some of which are enriched in motor neurons (Duguid et al., 1995). Thus, DNA-SSB occurring spontaneously may be repaired. Motor neurons might display comets perhaps only when levels of nonrepaired or misrepaired DNA damage are above a threshold level. Alternatively, lower concentrations of  $\text{H}_2\text{O}_2$  may be insufficient for inducing DNA damage in healthy motor neurons in suspension for a short time (possibly related to the low level of iron in the Neurobasal medium), but it may enhance DNA damage in already dying/injured motor neurons (background comets) that then disappear from the 400-rpm preparation when repelleting after exposure. However, 1 mM  $\text{H}_2\text{O}_2$  exposure for up to 2 hours was not sufficient to cause a loss of cells compared with time-matched controls. Therefore, sublethal oxidant activation of DNA repair pathways in motor neurons is a possibility.

### NO toxicity to motor neuron DNA is mediated by ONOO<sup>-</sup>

NO toxicity is believed to participate in the pathogenesis of motor neuron degeneration in ALS (Beckman et al., 1993) and in experimental models (Wu and Li, 1993; Martin et al., 1999a). We tested the hypothesis that motor neurons exposed to NO accumulate DNA damage. We found that DNA-SSB are formed in motor neurons exposed to two different NO donors. However, because NO per se does not cause breakage to plasmid DNA (Salgo et al., 1995; Inoue and Kawanishi, 1995), DNA-SSB in motor neurons might not be caused directly by NO. We also found that direct exposure of motor neurons to ONOO<sup>-</sup> induces DNA-SSB in motor neurons. We verified the presence of ONOO<sup>-</sup> in NO donor- and ONOO<sup>-</sup>-treated motor neuron cell suspensions by detecting nitrotyrosine formation in immunoblots. Experiments with plasmid DNA have shown that NO and <sup>-</sup>O<sub>2</sub> in combination or ONOO<sup>-</sup> alone induce DNA damage (Salgo et al., 1995; Inoue and Kawanishi, 1995). ONOO<sup>-</sup> at concentrations as low as 1 μM causes prominent DNA-SSB, with much higher concentrations (>1 mM) needed for double-strand DNA breaks (Szabó and Ohshima, 1997). ONOO<sup>-</sup> is formed very rapidly by NO competing with superoxide dismutase for <sup>-</sup>O<sub>2</sub> (Beckman et al., 1993). We found in our motor neuron cell suspension that endogenous production of <sup>-</sup>O<sub>2</sub> is augmented in motor neurons, most likely because of injury related to dissection and digestion. This finding is consistent with previous studies showing that motor neurons become metabolically activated after axonal injury (Martin et al., 1999a). We conclude that NO toxicity in adult motor neurons directly involves the formation of DNA-SSB through ONOO<sup>-</sup>. A similar mechanism may be operational in the evolution of motor neuron pathology in ALS.

When motor neurons are exposed to NO donor in the presence of H<sub>2</sub>O<sub>2</sub> (at a concentration that is apparently subthreshold for DNA damage, or possibly even protective in Neurobasal-A medium), the combination is potentially neurotoxic. For example, exposure of motor neurons to both SNP (10 or 100 μM) and 1 mM H<sub>2</sub>O<sub>2</sub> induces DNA damage and motor neuron loss that are much more severe than that caused by either SNP (10, 100, 300, or 800 μM) or 1 mM H<sub>2</sub>O<sub>2</sub> alone. It is possible that SNP-donated NO and H<sub>2</sub>O<sub>2</sub> (or secondary products of H<sub>2</sub>O<sub>2</sub>) and endogenously generated <sup>-</sup>O<sub>2</sub> are interacting to enhance toxicity. This enhanced toxicity may be related to the formation of ONOO<sup>-</sup>, as verified by the formation of ONOO<sup>-</sup> with the detection of protein nitration in SNP + H<sub>2</sub>O<sub>2</sub>-treated motor neurons. H<sub>2</sub>O<sub>2</sub> can interact with iron and copper through the Fenton reaction to produce highly reactive hydroxyl radicals that attack DNA and induce strand breaks and base modifications (Halliwell and Gutteridge, 1986). The NO donor SNP contains iron. Thus, another possibility includes SNP-derived, iron-catalyzed oxidation reactions with H<sub>2</sub>O<sub>2</sub> and the formation of DNA-SSB from hydroxyl radicals.

Motor neurons exposed to NO donors and ONOO<sup>-</sup> accumulate DNA damage that is different from damage caused by H<sub>2</sub>O<sub>2</sub>. These differences are found in the varying comet shapes and DNA staining patterns of the comets and the comet moments. Thus, it is reasonable to believe that the resulting DNA damage is different after exposure to different oxidants. With NO donors and ONOO<sup>-</sup>, DNA granules are prominent within the heads and tails of new comets and early mature comets and are very scattered in

the heads of advanced comets. These ethidium bromide-positive large granules are likely to be very large single-strand fragments of DNA. NO donors generated comet patterns similar to ONOO<sup>-</sup>. In contrast, with H<sub>2</sub>O<sub>2</sub>, DNA damage occurs first at peripheral chromatin domains and then the inner nuclear core chromatin, as reflected by comets with discrete halos and comets with very small heads and tails comprised of fine granules. The lengths of DNA fragments caused by H<sub>2</sub>O<sub>2</sub> exposure are probably very different from the DNA damage caused by NO. This conclusion is supported by DNA fragmentation analysis.

To identify relationships between DNA damage detected by the comet assay and DNA gel electrophoresis, motor neuron cell suspensions were exposed to H<sub>2</sub>O<sub>2</sub> or NO donor, and genomic DNA was extracted for gel electrophoresis. The DNA fragmentation coincides with the comet assay for the cells exposed to H<sub>2</sub>O<sub>2</sub> for 60 minutes, which detected ~31% comets and most of the comet tails are discontinuous. H<sub>2</sub>O<sub>2</sub> induced a prominent smear-ladder hybrid of DNA fragments in motor neurons. This pattern is consistent with the comet assay finding showing tails consisting of very fine DNA granules. These tails are apparently internucleosomal and random fragments of DNA. Thus, H<sub>2</sub>O<sub>2</sub> causes many smaller DNA fragments because of numerous SSB. In contrast, motor neurons exposed (for 60 minutes) to SNP contain high molecular weight genomic DNA. Therefore, the large DNA granules typical of the NO donor comet patterns are likely to be high molecular fragments of DNA caused by relatively fewer SSB. Thus, different oxidants cause distinct DNA damage fingerprints, and different chromatin domains (Ferreira et al., 1997) in motor neurons may have differential vulnerabilities to ROS.

### DNA-SSB accumulate progressively in motor neurons after axotomy with a comet profile similar to NO toxicity

We applied the comet assay to an in vivo model of motor neuron apoptosis in adult spinal cord. Sciatic nerve avulsion in adult rat causes apoptosis of lumbar motor neurons over 7–14 days (Martin et al., 1999a). These motor neurons exhibit oxidative stress in the form of hydroxyl radical damage to DNA and ONOO<sup>-</sup> damage. We have observed previously that, at 7 days after the lesion, subsets of motor neurons are undergoing DNA fragmentation as detected weakly by TUNEL assay. Here, we found early DNA damage in motor neurons at 5 days after the lesion. Furthermore, the current study corroborates previous observations (Martin et al., 1999a) by showing that isolated motor neurons after avulsion show morphological evidence of apoptotic chromatin condensation at 10 days after injury. The comet assay revealed a progressive accumulation of DNA-SSB in motor neurons during 5–10 days post lesion. The comet moments increase progressively (Table 2). This observation is also consistent with our preliminary observations showing p53 accumulation in the nucleus of avulsed motor neurons 7–10 days post lesion (Martin et al., 1999b). The comets of motor neurons after avulsion and the comets of motor neurons exposed to NO in vitro are similar. Because avulsion-induced motor neuron death is apoptosis (Martin et al., 1999a), comet patterns consisting of prominent DNA granules within the heads and tails are therefore signatures of apoptosis in neurons.

These findings support and extend the conclusion that NO toxicity is a mechanism for motor neuron apoptosis in the adult spinal cord (Martin et al., 1999a), through the formation of DNA-SSB by ONOO<sup>-</sup>. Because DNA-SSB are potent activators of p53 (Jayaraman and Prives, 1995), early formation and accumulation of DNA-SSB in adult motor neurons could be a primary signal for motor neuron apoptosis, possibly through p53-mediated pathways (Martin et al., 1999b). This proposed mechanism for motor neuron apoptosis in an animal model is particularly relevant to the pathogenesis of ALS (Beckman et al., 1993; Martin, 2000a).

## ACKNOWLEDGMENTS

We are grateful for the technical assistance of Frank Barksdale.

## LITERATURE CITED

- Beckman JS, Carson M, Smith CD, Koppenol WH. 1993. ALS, SOD and peroxynitrite. *Nature* 364:548.
- Brewer GJ, Torricelli JR, Evege EK, Price PJ. 1993. Optimized survival of hippocampal neurons in B27-supplemented Neurobasal™, a new serum-free medium combination. *J Neurosci Res* 35:567-576.
- Del Canto MC, Gurney ME. 1994. Development of central nervous system pathology in a murine transgenic model of human amyotrophic lateral sclerosis. *Am J Pathol* 145:1271-1280.
- Duguid JR, Eble JN, Wilson TM, Kelly MR. 1995. Differential and subcellular expression of the human multifunctional apurinic/apyrimidinic endonuclease (APE/ref-1) DNA repair enzyme. *Cancer Res* 55:6097-6102.
- Deng H-X, Hentati A, Tainer JA, Iqbal Z, Cayabyab A, Hung W-Y, Getzoff ED, Hu P, Herzfeldt B, Roos RP, Warner C, Deng G, Soriano E, Smyth C, Parge HE, Ahmed A, Roses AD, Hallett RA, Pericak-Vance MA, Siddique T. 1993. Amyotrophic lateral sclerosis and structural defects in Cu,Zn superoxide dismutase. *Science* 261:1047-1051.
- Ferrante RJ, Browne SE, Shinobu LA, Bowling AC, Baik MJ, MacGarvey U, Kowall NW, Brown RH JR, Beal MF. 1997. Evidence of increased oxidative damage in both sporadic and familial amyotrophic lateral sclerosis. *J Neurochem* 69:2064-2074.
- Ferreira J, Paoletti G, Ramos C, Lamond AI. 1997. Spatial organization of large-scale chromatin domains in the nucleus: a magnified view of single chromosome territories. *J Cell Biol* 139:197-1610.
- Fitzmaurice PS, Shaw IC, Kleiner HE, Miller RT, Monks TJ, Lau SS, Mitchell JD, Lynch PG. 1996. Evidence for DNA damage in amyotrophic lateral sclerosis. *Muscle Nerve* 19:797-798.
- Frankfurt OS, Robb JA, Sugarbaker EV, Villa L. 1996. Monoclonal antibody to single-stranded DNA is a specific and sensitive cellular marker of apoptosis. *Exp Cell Res* 226:387-397.
- Halliwell B, Gutteridge JMC. 1986. Oxygen free radicals and iron in relation to biology and medicine: some problems and concepts. *Arch Biochem Biophys* 246:501-514.
- Hellman B, Vaghef H, Boström B. 1995. The concept of tail moment and tail inertia in the single cell gel electrophoresis assay. *Mutat Res* 336:123-131.
- Henderson CE, Bloch-Gallego E, Camu W. 1995. Purification and culture of embryonic motor neurons. In: Cohen J, Wilkin G, editors: *Neuronal cell culture: a practical approach*. Oxford: IRL Press. p 69-81.
- Horváthová E, Slameňová, Gábelová A. 1999. Use of single cell gel electrophoresis (comet assay) modifications for analysis of DNA damage. *Gen Physiol Biophys* 18:70-74.
- Hrabie JA, Klose JR, Wink DA, Keefer LK. 1993. New nitric oxide-releasing zwitterions derived from polyamines. *J Org Chem* 58:1472-1476.
- Inoue S, Kawanishi S. 1995. Oxidative DNA damage induced by simultaneous generation of nitric oxide and superoxide. *FEBS Lett* 371:86-88.
- Jayaraman L, Prives C. 1995. Activation of p53 sequence-specific DNA binding by short single strands of DNA requires the p53 C-terminus. *Cell* 81:1021-1029.
- Kindzelskii AL, Petty HR. 1999. Ultrasensitive detection of hydrogen peroxide-mediated DNA damage after alkaline single cell gel electrophoresis using occultation microscopy and TUNEL labeling. *Mutat Res* 426:11-22.
- Kohn KW. 1991. Principles and practice of DNA filter elution. *Pharmacol Ther* 49:55-77.
- Levine AJ. 1997. p53, the cellular gatekeeper for growth and division. *Cell* 88:323-331.
- Martin LJ. 1999. Neuronal death in amyotrophic lateral sclerosis is apoptosis: possible contribution of a programmed cell death mechanism. *J Neuropathol Exp Neurol* 58:459-471.
- Martin LJ. 2000a. p53 is abnormally elevated and active in the CNS of patients with amyotrophic lateral sclerosis. *Neurobiol Dis* 7:613-622.
- Martin LJ. 2000b. Motor neurons have DNA damage and p53 is abnormally elevated and active in patients with amyotrophic lateral sclerosis. *Neurosci Abstr* 26:500.
- Martin LJ, Kaiser A, Price AC. 1999a. Motor neuron degeneration after sciatic nerve avulsion in adult rat evolves with oxidative stress and is apoptosis. *J Neurobiol* 40:185-201.
- Martin LJ, Kaiser A, Price AC. 1999b. Oxidative stress and p53 induction may participate in the mechanisms for motor neuron apoptosis in adult spinal cord. *Soc Neurosci Abstr* 25:289.
- Martin LM, Price AC, Kaiser A, Shaikh AY, Liu Z. 2000. Mechanisms for neuronal degeneration in amyotrophic lateral sclerosis and in models of motor neuron death. *Int J Mol Med* 5:3-13.
- Mendiola-Cruz MT, Morales-Ramírez P. 1999. Repair kinetics of gamma-ray induced DNA damage determined by single cell gel electrophoresis assay in murine leukocytes in vivo. *Mutat Res* 433:45-52.
- Morris EJ, Drexler JC, Cheng K-Y, Wilson PM, Gin RM, Geller HM. 1999. Optimization of single-cell gel electrophoresis (SCGE) for quantitative analysis of neuronal DNA damage. *Biotechniques* 26:282-289.
- Ostling O, Johanson KJ. 1984. Microelectrophoretic study of radiation-induced DNA damage in individual mammalian cells. *Biochem Biophys Res Commun* 123:291-298.
- Peterson AB, Gniadecki R, Wulf HC. 2000. Laser scanning cytometry for comet assay analysis. *Cytometry* 39:10-15.
- Polyak K, Xia Y, Zweier JL, Kinzler KW, Vogelstein B. 1997. A model for p53-induced apoptosis. *Nature* 389:300-305.
- Portera-Cailliau C, Price DL, Martin LJ. 1997. Non-NMDA and NMDA receptor-mediated excitotoxic neuronal deaths in adult brain are morphologically distinct: further evidence for an apoptosis-necrosis continuum. *J Comp Neurol* 378:87-104.
- Rosen DR, Siddique T, Patterson D, Figiwick DA, Sapp P, Hentati A, Donaldson D, Goto J, O'Regan JP, Deng H-X, Rahmani Z, Krizus A, McKenna-Yasek D, Cayabyad A, Gaston AM, Berger R, Tanzi RE, Halperin JJ, Harzfeldt B, Van den Bergen R, Hung W-Y, Bird T, Deng G, Mulder DW, Smyth C, Laing NG, Soriano E, Pericak-Vance MA, Haines J, Rouleau GA, Gusella JS, Horvitz HR, Brown RH. 1993. Mutations in Cu/Zn superoxide dismutase gene are associated with familial amyotrophic lateral sclerosis. *Nature* 362:59-62.
- Rothe G, Valet G. 1990. Flow cytometric analysis of respiratory burst activity in phagocytes with hydroethidine and 2',7'-dichlorofluorescein. *J Leuk Biol* 47:440-448.
- Salgo MG, Stone K, Squadrito GL, Battista JR, Pryor WA. 1995. Peroxynitrite causes DNA nicks in plasmid pBR322. *Biochem Biophys Res Commun* 210:1025-1030.
- Singh NP, McCoy MT, Tice RR, Schneider EL. 1988. A simple technique for quantitation of low levels of DNA damage in individual cells. *Exp Cell Res* 175:184-191.
- Subba Rao K. 1993. Genomic damage and its repair in young and aging brain. *Mol Neurobiol* 7:23-48.
- Szabó C, Ohshima H. 1997. DNA damage induced by peroxynitrite: subsequent biological effects. *Nitric Oxide Biol Chem* 1:373-385.
- Szmigiero L, Studzani K. 1988. H<sub>2</sub>O<sub>2</sub> as a DNA fragmenting agent in the alkaline elution interstrand crosslinking and DNA-protein crosslinking assays. *Anal Biochem* 168:88-93.
- Tice RR, Agurel E, Anderson D, Burlison B, Hartmann A, Kobayashi H, Miyamae Y, Rojas E, Ruy J-C, Sasaki YF. 2000. Single cell gel/comet assay: guidelines for in vitro and in vivo genetic toxicological testing. *Environ Mol Mutagen* 35:206-221.
- Wu W, Li L. 1993. Inhibition of nitric oxide synthase reduces motoneuron death due to spinal root avulsion. *Neurosci Lett* 153:121-124.

# Olfactory Bulb Core is a Rich Source of Neural Progenitor and Stem Cells in Adult Rodent and Human

ZHIPING LIU<sup>1</sup> AND LEE J. MARTIN<sup>1,2\*</sup>

<sup>1</sup>Department of Pathology, Division of Neuropathology, Johns Hopkins University School of Medicine, Baltimore, Maryland 21205

<sup>2</sup>Department of Neuroscience, Johns Hopkins University School of Medicine, Baltimore, Maryland 21205

## ABSTRACT

The olfactory bulb (OB) core is an extension of the rostral migratory stream and thus is a potential source of neural progenitor and neural stem cells. We characterized *in vivo* and *in vitro* neuronal progenitor and neural stem cells in the adult OB core. In mouse and rat, bromodeoxyuridine (BrdU) labeling showed that the OB core accumulates newly replicated cells. Nestin, a neuroepithelial stem cell marker, was enriched in the OB core. BrdU-positive cells were immunolabeled for nestin and TUC4, a marker for early postmitotic neurons. The distributions of cells labeled for BrdU, TUC4, and nestin were similarly concentrated in the OB core. Nestin- and TUC4-positive cells were also found in the OB of young and aged humans. Isolated and cultured OB core cells from adult rat and mouse had the capacity to generate numerous neurospheres. Adult OB core neurospheres were cryopreserved and subsequently cultured. Single cell clonal analysis of neurospheres revealed the capacity for self-renewal and multipotency. Cultured adult OB core cells differentiated into neurons, astrocytes, and oligodendrocytes. Some neurons expressed choline acetyltransferase, substance P, and glutamic acid decarboxylase. Basic fibroblast growth factor potentiated the self-renewal of cells and  $\beta$ -nerve growth factor stimulated differentiation. OB-derived neural stem cells in coculture with skeletal muscle cells were induced to become neurons expressing choline acetyltransferase and substance P and formed neuromuscular synaptic junctions on myocytes displaying acetylcholinesterase-positive motor end plates. Cocultured OB-derived neural stem cells with myoblast cells also generated nonneural cell progeny. We conclude that the adult mammalian OB core is a reservoir of neural progenitor cells and pluripotent neural stem cells. *J. Comp. Neurol.* 459:368–391, 2003. © 2003 Wiley-Liss, Inc.

**Indexing terms:** amyotrophic lateral sclerosis; motor neuron; neural transplantation; neuronal replacement; pluripotent stem cell; subventricular zone

Neuronal loss is a feature of chronic and acute neurological disorders. Selective degeneration of populations of neurons occurs in adult- and pediatric-onset neurodegenerative disorders such as Alzheimer's disease, amyotrophic lateral sclerosis, Huntington's disease, Parkinson's disease, and spinal muscular atrophy. Less selective neuronal degeneration occurs after acute neurological insults such as cerebral ischemia and trauma. No proven cures or effective therapies are available that can either prevent nerve cell loss or replenish neurons in the human brain and spinal cord to restore neurological function. The replacement of lost or damaged neurons by neural progenitor cells or neural stem cells (NSC) is a distant hope for the treatment of many neurological disorders. Stem cells are undifferentiated cells that have the ability to undergo numerous divisions and self-renewal in culture and to

Grant sponsor: U.S. Public Health Service, National Institutes of Health, the National Institute of Neurological Disorders and Stroke and the National Institute on Aging; Grant numbers: NS34100, AG16282; Grant sponsor: Department of Defense, U.S. Army Medical Research and Materiel Command; Grant number: DAMD17-99-1-9553; Grant sponsor: The ALS Association.

\*Correspondence to: Lee J. Martin, Johns Hopkins University School of Medicine, Department of Pathology, 558 Ross Building, 720 Rutland Avenue, Baltimore, MD 21205-2196.

Received 19 July 2002; Revised 15 January 2003; Accepted 17 January 2003

DOI 10.1002/cnc.10664

Published online the week of March 24, 2003 in Wiley InterScience (www.interscience.wiley.com).

TABLE 1. Summary of experiments on the in vivo and in vitro characterization of adult rodent OB core cells

Experiment	Markers	Animals/Number	Quantitative analysis
In vivo	BrdU, TUC4, Nestin, TuJ1, BrdU/TUC4, BrdU/Nestin	Rats/n = 13 (3–5 rats/time point) Mice/n = 13 (3–5 mice/time point)	BrdU single labeling, TUC4/BrdU and Nestin/BrdU double labeling
In vitro	Single culture	Rats/n = 12 Mice/n = 10 (data not shown) GFP mice/n = 5 <sup>1</sup>	MAP5, TuJ1, TUC4, GFAP, MBP, Nestin, BrdU (after growth factor stimulation), ChAT, SP, GAD
	Coculture	Rats/n = 12 Mice/n = 11 GFP mice/n = 5	ChAT, SP, ChAT/GAD double labeling

<sup>1</sup>The same GFP mice were used for single and coculture experiments.

differentiate into multilineage, functionally specialized cells (Potten, 1997; Rao, 1999; Gökhan and Mehler, 2001). Much more information is needed on the sources of NSC, their biology, and application to animal models of disease to appropriately ascertain the value of cell-based therapy for brain and spinal cord degeneration.

Multipotent NSC can be found in the embryonic, neonatal, and adult mammalian CNS (Reynolds and Weiss, 1992; Morshead et al., 1994; Gritti et al., 1996; Kuhn et al., 1997; Luskin et al., 1997; Palmer et al., 1997; Chiasson et al., 1999). The forebrain subventricular zone (SVZ) and dentate gyrus are considered to be the major sources of self-renewing, multipotent NSC (Reynolds and Weiss, 1992; Reynolds and Weiss, 1996; Palmer et al., 1997). NSC in the adult SVZ form a cellular continuum with the core of the olfactory bulb (OB) through an extension called the rostral migratory stream (RMS). Cells that originate from the anterior SVZ (SVZa) migrate within the RMS to reside within the OB. Thus, the OB core is considered to be the anterior-most part of the SVZ (Smart, 1961; Altman, 1969; Luskin, 1993; Lois and Alvarez-Buylla, 1994). The SVZ contains at least four different cell types divisible by morphology and molecular markers (Jankovski and Sotelo, 1996; Alvarez-Buylla and García-Verdugo, 2002). Type A cells are young migrating neurons (neuroblasts) that form chains of cells that are ensheathed by astrocytes (type B cells). Highly proliferative neural precursor cells (type C cells) form clusters next to the chains of migrating neurons. A layer of ependymal cells (type E cells) separates the SVZ from the ventricular cavity. The primary precursors of new neurons in the SVZ now appear to be the astrocytes (Alvarez-Buylla and García-Verdugo, 2002).

Most of the previous work on NSC in the SVZ-RMS-OB system has been done in the neonatal and adult SVZ and RMS, with less attention being paid to the OB core of the adult brain. The adult OB has a prominent ependymal/subependymal core (Paxinos and Watson, 1986; Franklin and Paxinos, 1997), and, historically, it is one of the few regions of the mammalian central nervous system (CNS) that displays prominent postnatal neurogenesis (Hinds, 1968; Altman, 1969; Bayer 1983; Luskin, 1993; Kaplan and Hinds, 1997). Compared to the dentate gyrus, the OB is believed to have more extensive neurogenesis in the adult brain, although this belief may need to be re-examined (Cameron and McKay, 2001). However, NSC intrinsic to the adult RMS and OB have been found only recently (Liu and Martin, 2001; Gritti et al., 2002), despite the earlier work on postnatal neurogenesis in the OB. The NSC in the adult mouse OB core were found to exhibit self-renewal and multipotency by in vitro clonal analysis (Gritti et al., 2002). It is not known if NSC in the adult OB

are common among species, if they have the potential to become specific types of neurotransmitter-specific neurons, and if they have pluripotent capacity.

In search of sources of NSC in the adult mammalian CNS with more convenient accessibility and usefulness for potential cell therapy, we studied the core in the adult OB for neural progenitor and NSC. We show that the adult mouse, rat, and human OB core is a rich source of neural progenitor and multipotent NSC. By coculturing these NSC with skeletal muscle cells, these cells can be induced to differentiate into neurotransmitter-specific neurons and can generate nonneural cell progeny; thus, adult OB core NSC also have pluripotent potential.

## MATERIALS AND METHODS

### Animals

For in vivo and in vitro studies of OB core cells, adult male Sprague-Dawley rats (weighing 200–250 g, Charles River, Wilmington, MA) and adult male C57BL/6J mice (weighing 23–25 g, Jackson Lab) were used. The Animal Care and Use Committee of the Johns Hopkins Medical Institutions approved animal protocols. The experiments are summarized in Table 1.

### In vivo cell proliferation assay using BrdU

Cell proliferation in adult mouse and rat OB was identified using the thymidine analog bromodeoxyuridine (BrdU) to track DNA synthesis (del Rio and Soriano, 1989). Animals were treated with BrdU (Roche Molecular Biochemicals, Indianapolis, IN) twice daily (at 8 a.m. and 8 p.m., 25 mg/kg in normal saline, i.p.) for 2 days or 6 days. The short and longer time points were used to determine if the OB accrues newly replicated cells, although this design cannot determine the site of most of the cell replication. In neonatal rat (postnatal day 2), Luskin and co-workers have reported (Smith and Luskin, 1998) that the cell cycle length is longer in RMS cells (17.3 h) compared to SVZa cells (14 h). The use of adult animals and the more anterior location of the OB core might extend the cycle length, so longer exposures to BrdU were used. At 12 hours after the final BrdU injection, the animals were euthanized. For a short exposure time point, mice were injected with a single dose of BrdU (50 mg/kg) and euthanized 12 hours later. All animals were perfused transcardially with normal saline for exsanguination, followed by 4% paraformaldehyde in 100 mM phosphate buffer (PB, pH 7.4). The brains were removed and postfixed in the same fixative for 2 hours and then placed in 20% glycerol-PB (pH 7.4) overnight at 4°C. The OB were cut



into serial coronal, sagittal, or horizontal sections with a freezing microtome ( $n = 3-5$  animals per condition). The average total numbers of sections generated from a mouse OB cut coronally (35  $\mu\text{m}$ ), sagittally (40  $\mu\text{m}$ ), or horizontally (40  $\mu\text{m}$ ) were 64, 40, and 57, respectively. The average total number of sections generated from a rat OB cut coronally (35  $\mu\text{m}$ ) was 125. The sections were collected in phosphate-buffered saline (PBS, pH 7.4) for immediate use or were stored in antifreeze buffer at  $-20^{\circ}\text{C}$ . From the complete set of serial sections from each OB, a one in ten (rats,  $\sim 13$  sections) or a one in five (mice, 8–13 sections) subset of sections was used for either cresyl violet staining, BrdU detection, or immunophenotyping of OB cells with antibodies to nestin, TUC4, and class III  $\beta$ -tubulin. Nestin, an intermediate filament protein, is considered currently to be the best marker for NSC and neuroepithelial cells (Lendahl et al., 1990; Chiasson et al., 1999; Rao, 1999). TUC4 (Turned On After Division [TOAD]/Unc-33-like phosphoprotein-1 [Ulip-1]/Collapsin Response-Mediated Protein-4 [CRMP-4] family) functions in axonal growth and was used to mark newborn neurons prior to overt differentiation (Quinn et al., 1999). The specificity of TUC4 as a neuronal marker in the CNS has been demonstrated by double-labeling and immunoelectron microscopy (Fernández et al., 2002; Bédard et al., 2002). Class III  $\beta$ -tubulin, identified with TuJ1 antibody, was used as a neuron-specific marker (Lee et al., 1990).

### BrdU immunocytochemistry

OB sections were rinsed with PBS, and then DNA was denatured by incubating sections in 50% formamide/2 $\times$  standard saline citrate (SSC) for 2 hours at  $65^{\circ}\text{C}$  and then in 2N HCl (37 $^{\circ}\text{C}$  for 30 minutes). The sections were rinsed in 100 mM boric acid for 10 minutes and then in PBS followed by PBS containing 1% bovine serum albumin (BSA) and 0.4% Triton X-100 for 30 minutes at room temperature. The sections were incubated in mouse monoclonal anti-BrdU antibody (Roche Molecular Biochemicals, Indianapolis, IN) at a concentration of 250 ng/ml for 12 hours at  $4^{\circ}\text{C}$ . After primary antibody incubation the sections were rinsed in PBS and incubated in biotinylated anti-mouse IgG (Vector Laboratories, Burlingame, CA) for 4 hours at room temperature. Sections were rinsed in PBS and treated with 0.6%  $\text{H}_2\text{O}_2$  in PBS for 30 minutes to inactivate endogenous peroxidase, followed by additional rinses, and then incubation in ABC for 2 hours at room temperature. Antibody binding was visualized with 0.025% DAB and 0.003%  $\text{H}_2\text{O}_2$  in Tris-HCl (pH 7.4) for 10 minutes. Reacted OB sections were rinsed in PBS, mounted on glass slides, air-dried, and coverslipped with or without counterstaining. Sections were observed and analyzed using a Zeiss Axiophot microscope. BrdU-positive cells in the OB core of mouse and rat sections were counted (at 1000 $\times$ ) in matched levels for each of the conditions. The analysis of the cell counts was done by ANOVA. Subsequent statistical post-hoc evaluation of significance was done using a Student's *t*-test.

### In vivo identification of NSC and newborn neurons in adult OB core

OB sections from rat and mouse (from the same animals used for BrdU incorporation) were used for nestin, TUC4, and class III  $\beta$ -tubulin localization. OB sections were rinsed thoroughly in PBS after peroxidase inactivation, incubated in PBS containing 1% BSA and 0.4% Triton

X-100 for 30 minutes, and then reacted (24 hours at room temperature) with monoclonal anti-nestin IgG (Chemicon International, Temecula, CA) at 1:500, polyclonal rabbit anti-TUC4 (Chemicon) at 1:1000, or polyclonal rabbit TuJ1 (Covance, Berkeley, CA) at 1:10,000. Sites of antibody binding were detected with biotinylated secondary antibody (1:100, 4 hours at room temperature), ABC (according to manufacturer's instructions, 2 hours at room temperature), and then 0.025% DAB and 0.003%  $\text{H}_2\text{O}_2$  in Tris-HCl (pH 7.4) for 10 minutes. Reacted sections were mounted on glass slides and coverslipped.

OB sections from rat and mouse (the same source and same selecting frequency as the BrdU sections) were used for BrdU/TUC4 and BrdU/nestin double immunolabeling. TUC4 or nestin were visualized with the ABC method as detailed above, and then the sections were incubated sequentially in avidin and then biotin (both for 30 minutes) to block biotin and avidin binding sites. The sections were then processed to visualize BrdU incorporation, as mentioned above (for BrdU/nestin dual labeling a rat antibody to BrdU [Harlan] was used at 1:200), but antibody sites were visualized with 0.025% DAB, 0.003%  $\text{H}_2\text{O}_2$  with 0.05%  $\text{CoCl}_2$  in Tris-HCl (pH 7.4) to generate a black-blue reaction product. Cells double labeled for BrdU/TUC4 and BrdU/nestin in the OB core of mouse were counted (at 1000 $\times$ ) in serial sections spanning the mid to posterior levels of the OB. The analysis of the cell counts was done by ANOVA. Subsequent statistical post-hoc evaluation of significance was done using a Student's *t*-test.

### Human OB immunophenotyping

OB were removed from formaldehyde fixed autopsy brains from elderly individuals ( $n = 8$ )  $82 \pm 8$  (mean  $\pm$  standard deviation (SD)) years of age and from younger individuals (27 and 40 years of age). The postmortem delays were 4–8 hours. The OB were washed with 100 mM PB and were rinsed in 20% glycerol in PB overnight before they were cut into 40  $\mu\text{m}$  sagittal or coronal sections with a freezing microtome. The average total number of sections generated from a human OB cut sagittally (40  $\mu\text{m}$ ) was 42. Sections from each human OB (1 in 5 subsampling frequency,  $\sim 7$  sections/marker) were used to localize TUC4, TuJ1, nestin, and vimentin with a method similar to that used on rat and mouse OB sections. TUC4 and TuJ1 antibodies were the same as those used for rat and mouse. Nestin was detected with a human-specific antibody (Chemicon, 1:500). Vimentin was used as a glial cell progenitor marker and was detected with a mouse monoclonal antibody (Sigma, Louis, MO) at 1:400. Double-label immunocytochemistry was used for colocalization of TUC4 and a neuron-specific nuclear protein (NeuN) as well as TUC4 and the astroglia-specific marker glial fibrillary acidic protein (GFAP) to corroborate the localization of TUC4 in neurons (and its absence in astrocytes) in the adult human OB. For TUC4/NeuN labeling, sections were reacted with TUC4 antibodies and developed with DAB and then, after re-blocking and peroxidase inactivation, were reacted with monoclonal antibody to NeuN (Chemicon, 1:100) and developed with cobalt-DAB. For TUC4/GFAP labeling, sections were reacted with monoclonal antibody to GFAP (Roche, 1:50) and developed with DAB and then, after re-blocking and peroxidase inactivation, were reacted with TUC4 antibody and developed with cobalt-DAB. Quantification was not done on human OB sections due to the few number of cases with precisely



matched ages and because of the more complex architecture of the human OB compared to the rodent OB.

### Isolation and culture of NSC from adult rat and mouse OB core

The OB core (ependymal/subependymal layer) was isolated from rat and mouse for *in vitro* studies (Table 1). Rats and mice were anesthetized deeply with oxygen: nitrous oxide:enflurane (33:66:1) and decapitated. The entire brain was removed and rinsed briefly in dissection medium. Both OB were separated from the brain (only the anterior "free" bulbs without the portion underneath the frontal lobe), transferred to another dish containing dissection medium, and a dorsal midsagittal cut was made to expose the OB core. Under a surgical microscope, the ependymal/subependymal zone (identified by its location and glistening appearance) was carefully microdissected (see white rectangles in Figs. 1A and 2A for the region that was microdissected). On either side of the OB midline, ~0.5 mm samples in rat and ~0.25 mm samples in mouse were discretely excised. The samples were collected in a dish containing ice-cold dissecting medium (Hank's salt balanced solution,  $\text{Ca}^{++}$  and  $\text{Mg}^{++}$  free, Gibco). After cutting samples into smaller pieces, they were incubated ( $37^{\circ}\text{C}$ , 5%  $\text{CO}_2$ , and 95% air) in 0.25% trypsin-EDTA for 20 minutes and were triturated gently to dissociate cells. Aliquots of OB core dissociated cell suspensions were seeded on poly-D-lysine coated 35-mm diameter wells (Costar) at cell densities of  $\sim 6 \times 10^5/\text{ml}$  (one rat OB was used to seed four 35-mm wells; one mouse OB was used to seed one 35-mm well). Dulbecco's modified Eagle's medium (DMEM) (Gibco/Life Technologies, Rockville, MD, Cat. # 11965-092) containing L-glutamine, high glucose, and supplemented with 10% fetal bovine serum (FBS), 10% heat inactivated horse serum, B27 (Gibco), DNase I, and antibiotics (100 U/ml penicillin and 100  $\mu\text{g}/\text{ml}$  streptomycin) was used for cell seeding.

OB core cells were studied using population and clonal analyses. Twenty-four hours after seeding, the medium in wells containing attached cells, attached spheres, and floating spheres was removed to another well (floating spheres were removed and transferred to new wells), and fresh medium was added to the seeded well with attached cells/spheres for population analysis. The medium for attached cells/spheres was DMEM supplemented with L-glutamine, 5% horse serum, and antibiotics. Thereafter, the medium was changed once in 3 days. Floating cells/

spheres were passaged by periodically transferring floating spheres to new wells. The medium for growing neurospheres was DMEM supplemented with L-glutamine, 5% FBS, and 5% horse serum, high glucose, and antibiotics (growth medium). Some neurospheres were cryopreserved for further analysis to assess multipotency. For clonal analysis to assess self-renewal and multipotency, fresh spheres (after at least 9 passages) or cryopreserved and thawed spheres were mechanically dissociated to single cell suspensions, and individual cells were transferred to single chambers in 96 well plates with growth medium. After 3–5 days, the single cells formed clones, and clones formed floating spheres that were transferred to coated 35-mm wells for further replication and then differentiation for 2–3 weeks.

### In vitro exposure of adult OB core NSC to growth factors

Attached primary OB core cells and their spheres were isolated and cultured as above from adult rats ( $n = 8$ ). At day 3 *in vitro* (DIV3), the medium was changed to serum-free, B27-supplemented DMEM containing 10 ng/ml or 100 ng/ml  $\beta\text{NGF}$  (R&D Systems) or 10 ng/ml or 100 ng/ml bFGF (R&D Systems). Control wells were treated with vehicle (1% BSA in PBS). On the following day the cells were exposed to the same quantities of growth factors or vehicle with or without 5  $\mu\text{M}$  BrdU. More floating spheres were formed. The attached cells/spheres were incubated for another 24 hours, fixed with 2% paraformaldehyde for 2 hours, and used for immunolocalization of BrdU and class III  $\beta$  tubulin (TuJ1 antibody). BrdU and class III  $\beta$  tubulin were also evaluated for colocalization using the ABC method for BrdU and immunofluorescence for class III  $\beta$  tubulin. We used bFGF (FGF-2) based on the work of others. bFGF has been used as a mitogen to expand NSC from adult mouse striatum (Gritti et al., 1996) and adult rat SVZ (Kuhn et al., 1997). bFGF is a potent stimulus for clonal colonies of undifferentiated embryonic stem cell lines to generate neurospheres *in vitro* (Troppe et al., 2001).  $\beta$ -NGF was used as a neurotrophin. It has been shown that the high affinity NGF receptor *trkA* is present in the adult rodent OB (Horikawa et al., 1999).

To quantify the effects of  $\beta$ -NGF or bFGF, cells stained for BrdU or TuJ1 were either counterstained faintly with hematoxylin (for counting of total cell number) or were not counterstained (for confirmation of total cell number counts under phase contrast). Cells were counted with a

**Fig. 1 (Overleaf.)** Adult mouse OB core is a reservoir of newly generated cells and contains numerous newborn neurons and NSC. **A:** Low magnification view of a cresyl violet stained coronal section (35  $\mu\text{m}$ ) showing the location and size of the ependymal/subependymal layer (white box) in the posterior OB. The ependymal/subependymal layer is referred to here as OB core. **B:** Higher magnification of boxed area delineated in A. The cell density in the core appears high. **C:** The cells are small and packed tightly. Many cells (from a sagittal section) are elongated and narrow (arrowheads). Cells are present undergoing mitosis (arrows). The upper mitotic cell is enlarged in the insert. **D:** At 12 hours after a single BrdU pulse, BrdU-positive cells are found in the OB core. These replicating cells typically appear as daughter pairs (inset). **E:** BrdU labeling of the OB core in a mouse injected 2 days with BrdU (50 mg/kg/day) and then sacrificed. BrdU-positive cells are concentrated in the core that is surrounded by the granule cell layer (gcl). The density of BrdU labeled cells is higher than with a single pulse and 12-hour survival. **F:** Higher magnification of boxed area in

E showing the nuclear morphology and relative density of these newly replicated cells. **G:** BrdU labeling in the OB in a mouse injected 6 days with BrdU (same dose per day as mentioned in E and then sacrificed) showing prominent labeling of the core (the density is higher than with 2 days injection) that extends around the ventral surface of the accessory olfactory bulb but not major labeling of the gcl. **H:** Higher magnification of boxed area in G showing the high density of labeled cells. **I:** The distribution of nestin immunoreactive cells is similar to the distribution of BrdU labeled cells. **J:** The distribution of TUC4 immunoreactive cells is similar to the distribution of BrdU labeled cells. **K:** Class III  $\beta$ -tubulin is enriched in the OB core. The pattern overlaps with that seen with nestin and TUC4. **L:** High magnification of nestin staining in the OB core showing labeling of small cell and processes. **M:** High magnification of TuJ1 staining in the OB core showing labeling of small cell and processes. Scale bars = 200  $\mu\text{m}$  in A; 25  $\mu\text{m}$  in B (applies to F,H–K); 10  $\mu\text{m}$  in C (applies to L and M, for insert of C, bar is 4.3  $\mu\text{m}$ ); 33  $\mu\text{m}$  in D; 100  $\mu\text{m}$  in E (applies to G).

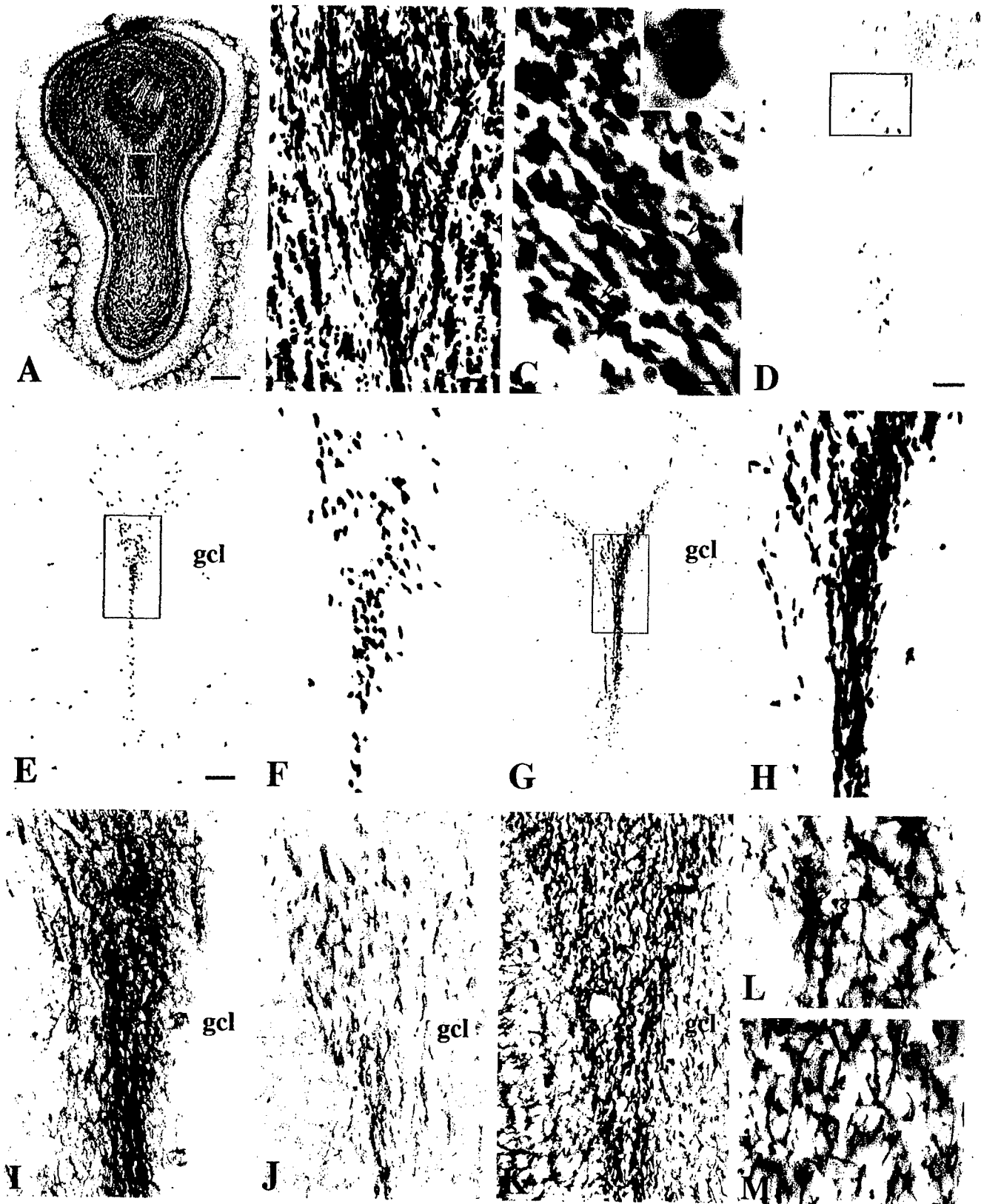


Figure 1

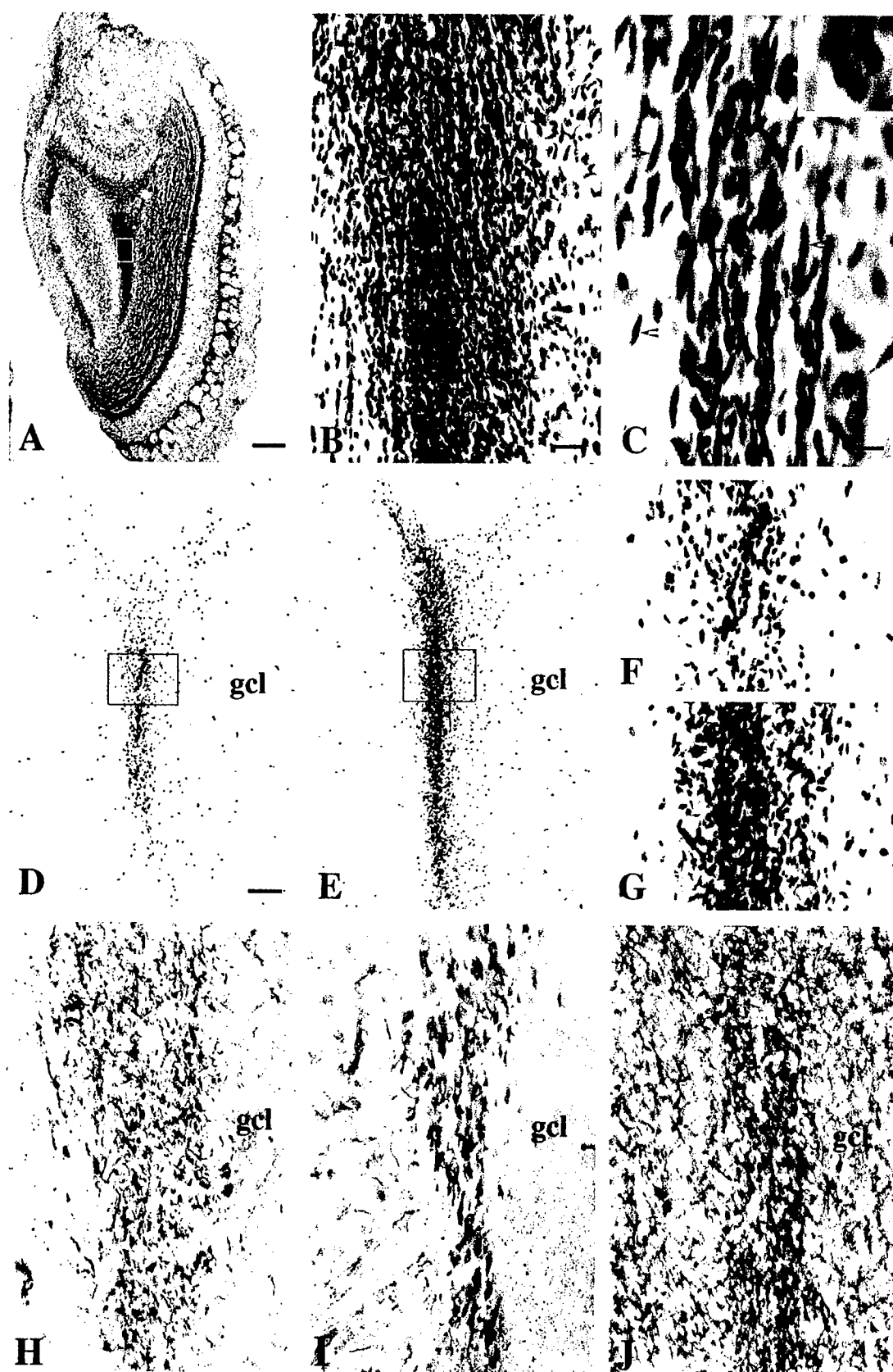


Figure 2

10× objective (six different microscopic fields, area = 2.4 mm<sup>2</sup>). Colonies of cells and attached, dispersed neurospheres were counted with a 4× objective (10 different microscopic fields, area = 6 mm<sup>2</sup>) using an Olympus inverted microscope. For each condition, at least three experiments with different batches of cultures were repeated and cells were counted. The average total number of cells, number of BrdU labeled cells for each condition, the average percentage of BrdU labeled cells to total number of cells, and the percentage of TuJ1 labeled cells to the total number of cells were calculated and analyzed. The numbers of colonies and colony sizes were also counted and the averages were calculated. The criteria for a colony included a minimum of six cells in a cluster or close population with these cells having a similar morphology (cell body shape and size, and the cell process number, length, and pattern). The cell process pattern was defined by whether the processes were straight, curved, or bifurcating.

### Coculture of NSC from adult OB core with muscle cells

NSC from the ependymal/subependymal layer of adult rat ( $n = 8$ ) and mouse ( $n = 6$ ) OB were cocultured with muscle cells to evaluate the capacity of adult NSC to develop into a specific type of neuron (i.e., motor neuron). OB core NSC were also cocultured with muscle cells to evaluate their potential to generate nonneural progeny (i.e., muscle cells). Transgenic adult male mice ( $n = 3$ , 6–8 weeks old, line C57BL/6-TgN[ACTbEGFP]10sb, Jackson Laboratory) expressing green fluorescent protein (GFP) were used as a source of OB core cells for coculture experiments to assess pluripotency. A mouse myoblast cell line (G8, skeletal) and a rat myoblast cell line (L6, skeletal) (both from ATCC) were used. The cells were cultured, subcultured, and stored according to the user's manual instructions. Briefly, the cells were thawed in the vial within 2 minutes in a 37°C water bath and were poured

into complete culture medium. After spinning the cells briefly, they were resuspended and seeded in complete medium. For mouse myoblast cells, the culture medium contained 10% FBS, 10% horse serum (heat inactivated) in DMEM with penicillin (100 U/ml) and streptomycin (100 µg/ml). For rat myoblasts, complete culture medium was 10% FBS in DMEM with penicillin (100 U/ml) and streptomycin (100 µg/ml). After the cells were subcultured twice, they were seeded at a density of  $\sim 3 \times 10^5$  and cultured with 5% FBS (for rat myoblast cells) or 5% FBS and 5% horse serum (for mouse myoblast cells). The cells proliferated very rapidly, and fused and differentiated into multinucleated striated myotubes by DIV6.

For coculture of OB core cells with muscle cells, two different approaches were used. NSC from rat or mouse OB were cocultured with the corresponding muscle cell line. Myoblasts were added to cultured OB-NSC at DIV2, or newly isolated OB-NSC were seeded on cultured myoblasts. Either way, the seeding cell density was  $\sim 6 \times 10^5$  for NSC and  $\sim 3 \times 10^5$  for myoblast cells. Controls were time-matched single cultures of OB-NSC from the same OB core cell preparations as those used for coculture (i.e., cells were not mixed and cultured with muscle cells) as well as single cultures of muscle cells. The culture medium for the first seeding or second seeding was the complete culture medium for myoblast cells (mentioned above) supplemented with B27 (Gibco). The medium was changed 24 hours later with the percentage of sera reduced to 5% each. The cells were cocultured for 4–8 additional days and the medium was changed every 3 days and every day after 5 days. The cells were washed with PBS (pH 7.4) and fixed with 2% paraformaldehyde for 2 hours at 4°C.

### Immunophenotyping cultured and cocultured adult OB core neural progenitor cells and NSC

A panel of markers was used to characterize cultured and cocultured OB cells. Nestin was used to detect neuroepithelial and NSC. TUC4, TuJ1, MAP5, MAP2, synaptophysin, choline acetyltransferase (ChAT), glutamic acid decarboxylase (GAD), and substance P (SP) were used as neuron markers or specific neuron type markers. GFAP was used as an astrocyte marker. Myelin basic protein and O4 were used as oligodendrocyte markers. Myosin was used as a muscle cell marker. BrdU incorporation was used as a marker for OB cell proliferation *in vitro*. The procedures for immunocytochemistry were similar to the protocol used on OB tissue sections (except for BrdU detection the cells were not exposed to formamide/2× SSC for 2 hours at 65°C, but were directly treated with 2N HCl). Specifically, cells were treated with blocking/permeabilization solution (1% BSA and 0.4% Triton-x in PBS) for 30 minutes and then primary antibody for 24–36 hours. Primary antibodies to nestin, MAP5 (Sigma, St. Louis, MO), MAP2 (Sigma), synaptophysin (Roche Molecular Biochemicals), myelin basic protein (SMI-99, Sternberger Monoclonals Inc.) and O4 (Chemicon, Temecula, CA) are mouse monoclonal antibodies. Antibodies to GFAP (DAKO), TUC4, TuJ1, and GAD (Sigma) are rabbit polyclonal antibodies. In cocultures, ChAT was detected with a goat polyclonal antibody (Chemicon), SP was detected with a rabbit polyclonal antibody (Instar), and skeletal muscle cells were detected with an antibody to myosin heavy chain (Zymed, San Francisco, CA). The antibodies

**Fig. 2 (Overleaf.)** The adult rat OB core accumulates newly replicated cells and contains numerous newborn neurons and NSC. **A:** Cresyl violet stained coronal section (35 µm) from posterior OB of adult rat showing the location of NSC (white box). The dark black center area is the OB core. This area was microdissected and dissociated for cell culture (see Fig. 5). **B:** Higher magnification of the boxed area in A showing the extremely high density of cells in the OB core. **C:** High magnification of core area in a cresyl violet stained horizontal section (40 µm) of OB. The cells that comprise this region are small and have an elongated shape (arrowheads) typical of migrating cells. These cells can proliferate (arrow). The inset shows a cell in anaphase. **D:** BrdU incorporation into rat OB core cells (2 days BrdU injection) showing the distribution and density of newborn cells. BrdU-positive cells are concentrated in the core. Fewer labeled cells are seen in the granule cell layer (gcl). **E:** BrdU incorporation into OB core cells (6 days BrdU injection) showing the distribution and density of newborn cells. The labeling is greater compared to 2 day BrdU treatment. **F:** Higher magnification of boxed area in D showing BrdU labeling of cell nuclei and their density. **G:** Higher magnification of boxed area in E showing that many more labeled cells are present compared to F. **H:** The distribution of the NSC/neuroepithelial cell marker nestin overlaps with the core area delineated by cresyl violet staining and BrdU labeling. The labeled cells localize in the midline of the OB. **I:** The distribution of TUC4 coincides with the core area delineated by BrdU and nestin labeling. **J:** The enrichment of class III  $\beta$ -tubulin in the OB core has a distribution that overlaps with nestin and TUC4. Abbreviation: gcl, granule cell layer. Scale bars = 320 µm in A, 25 µm in B (applies to F–J), 10 µm in C, 100 µm in D (applies to E).

were used at the following dilutions: nestin (1:500), MAP2 (1:400), MAP5 (1:125), synaptophysin (1:50), SMI 99 (1:5000), O4 (1:100), TUC4 (1:1000), TuJ1 (1:10000), GFAP (1:100), ChAT (1:10), GAD (1:500), SP (1:200), and myosin (1:50). For immunoperoxidase detection, the secondary antibody was a biotinylated IgG (Vector) used at 1:100. After incubation in ABC for 2 hours (according to insert instructions), immunoreactivity was visualized with 0.025% DAB/0.003% H<sub>2</sub>O<sub>2</sub>. Cell cultures were evaluated with an Olympus inverted microscope. For immunofluorescent detection, the secondary antibodies were cascade blue-conjugated goat anti-rabbit IgG, Alexa-conjugated goat anti-mouse IgG, and biotinylated goat anti-mouse IgM (1:100)/streptavidin-Texas red (all fluorescent conjugates were used at 1:300). Immunofluorescence was examined with a Zeiss Axiphot microscope. OB core cell single cultures and cocultures that were stained for cell type and neuron-specific markers were studied quantitatively. The numbers of immunoreactive cells in single 35-mm wells (2–3 wells) were determined from six microscopic fields using a 20× objective. Cultures stained with TuJ1 antibody were used to compare the morphology of differentiating cells in 12 microscopic fields using a 10× objective.

Cocultures were also characterized using acetylcholinesterase (AChE) enzyme histochemistry (Tago et al., 1986) to identify neurons and neuromuscular junctions. Sites of enzyme activity were visualized directly in the culture plates by a chromogenic reaction with nickel-DAB. AChE is concentrated at motor end-plates in the synaptic cleft where it is mainly associated with the outer surface of the sarcolemma (Lentz, 1969).

Cocultures at DIV8 were examined by electron microscopy (EM) for the formation of synaptic contacts. Media was removed and the cultures were washed briefly with PBS and then the cells were fixed with 0.5% glutaraldehyde in 2% paraformaldehyde/PB for 1 hour. Some cultures were used to localize synaptophysin with a mouse monoclonal antibody to synaptophysin and an immunoperoxidase method with DAB as chromogen. The cultures were processed for conventional EM directly in culture plates as described (Lesuisse and Martin, 2002). Briefly, plastic embedded cultures were removed from the culture plates as plastic disks that were cut into pieces. Plastic blocks were inspected for immunolabeled neurons and axons under a microscope, and blocks containing immunolabeled profiles were trimmed and sectioned for EM. Thin sections were viewed and photographed with a JEOL electron microscope.

The original images used for figure construction were generated either on black-and-white or color photographic film that was scanned using an Agfa Vision 35 scanner and Adobe Photoshop 4.0 software or as JPEG image files captured using a SPOT digital camera and SPOT Advanced software (Diagnostic Instruments). JPEG files were converted to Photoshop files and the figures were composed using Adobe Photoshop 4.0 software.

## RESULTS

### OB core of adult mouse and rat is a reservoir of NSC and neuronal progenitor cells

The OB of adult mouse (Fig. 1A,B) and rat (Fig. 2A,B) has a conspicuous core of numerous, densely packed cells,

TABLE 2. Counts of BrdU labeled adult OB core cells in vivo

Animal	BrdU treatment/ Survival	BrdU-positive cell density (cells/mm <sup>2</sup> ) <sup>1</sup>
Mouse	1 injection/12 hours	1278 ± 95
	2 injections per day/2 days	3911 ± 318*
	2 injections per day/6 days	11500 ± 833**
Rat	2 injections per day/2 days	9900 ± 133*
	2 injections per day/6 days	nd <sup>2</sup>

<sup>1</sup>Cells were counted in the OB core at levels that were matched in the anterior-posterior axis. Values are mean ± standard deviation (n = 3 animals per condition). Single asterisk (\*) denotes significant difference ( $P < 0.001$ ) compared to 12 hours. Double asterisk (\*\*) denotes significant difference ( $P < 0.001$ ) compared to 2 days. Plus (+) denotes significant difference ( $P < 0.001$ ) compared to 2-day mouse.

<sup>2</sup>Not determined. The BrdU labeled cells were too numerous (appearing as aggregates of indistinguishable cells) to count reliably in 35 µm thick sections.

as seen in cresyl violet stained coronal sections. This region is usually identified as the ependymal/subependymal layer of the OB in brain atlases (Paxinos and Watson, 1986; Franklin and Paxinos, 1997). The olfactory ventricle is obliterated and cannot be seen. The typical cuboidal ependymal cells are not observed; instead, these cells have a long slender shape in mouse (Fig. 1C) and rat (Fig. 2C), typical of migrating cells (Rakic, 1972). The cells in the OB core are small (short axis ~2–4 µm) and packed tightly (Figs. 1B,C; 2B,C). The cell number appears considerable. This is implied from the boxed area (shown in the photomicrographs) representing an area of OB core in a 35 µm section from a fixed mouse OB ~2.2 mm in length (anterior tip to frontal lobe) or from a fixed rat OB ~4.3 mm in length (anterior tip to frontal lobe). These cells are arranged around the ventral portion of accessory olfactory bulb. In both mouse and rat OB core, cells can be observed at different stages of mitosis, such as prophase (Fig. 1C and insert), metaphase, anaphase (Fig. 2C and insert), and telophase.

The OB core accumulates replicating cells. Incorporation of BrdU was evaluated at 12 hours after a single injection and at 2 and 6 days after consecutive injections. The BrdU positive cells in mouse (Fig. 1D–H) and rat (Fig. 2D–G) have distributions matching the cell dense core zone seen by cresyl violet staining. The number of positive cells in the mouse OB core at 12 hours after a BrdU injection was significantly lower than the number of labeled cells after 2 and 6 days treatment (compare Figs. 1D,E,G; see counts in Table 2). With a single BrdU injection, the cells labeled lightly and usually appeared as pairs, suggesting daughter cells (Fig. 1D inset). In addition, with a single BrdU pulse, many of the positive cells had BrdU immunoreactivity aggregated at the margin of the nucleus, indicative of a cell in late prophase (as shown in Fig. 1C). The BrdU labeling of OB core cells in mouse was significantly greater after 6 days injection compared to the labeling seen after 2 days injection (Table 2). The granule cell layer had fewer BrdU-positive cells than the core (Figs. 1D,E,G; 2D,E).

Staining for nestin showed that NSC are concentrated in the adult OB core. Nestin-positive cells and processes were present in the OB core in a distribution mirroring the locations of BrdU-positive cells in mouse (Fig. 1I,L) and rat (Fig. 2H). Nestin-immunoreactive cells were elongated and slender with long, thin processes. In mice injected with BrdU for 2 days, 33% ± 4% (mean ± SD) of BrdU-positive cells was nestin-positive. Nestin immunoreactivity in the granule cell layer was localized mostly to blood vessels (Fig. 2H).

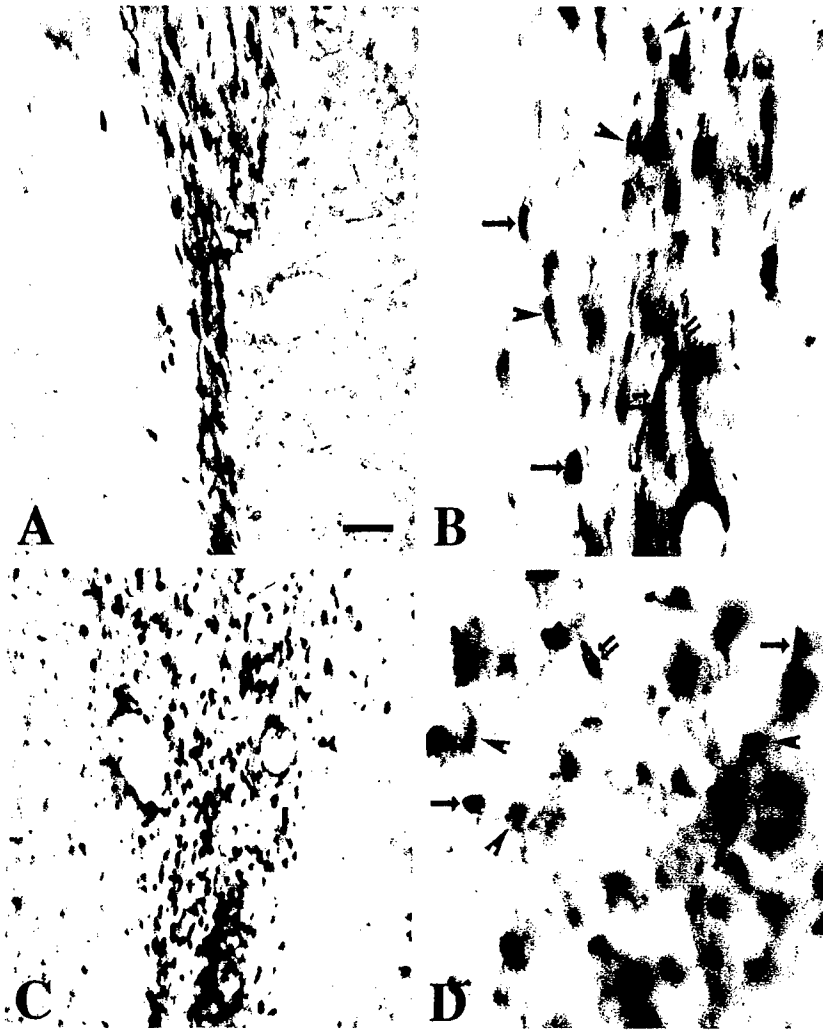


Fig. 3. Newly born cells in the adult OB core express a newborn neuron marker. **A:** Colocalization of BrdU and TUC4 in newborn neurons in the OB core of mouse. The brown- and yellow-colored cells are TUC4 positive newborn neurons, while the dark blue or black identifies BrdU labeled nuclei. Their distributions overlap. **B:** Subsets of cells in the mouse OB core are single-labeled for TUC4 in the cytoplasm (arrowheads, brown/yellow color) or BrdU in the nucleus (black or blue, single arrows). Other cells are double labeled with

brown in the cytoplasm and dark blue or black in the nucleus (double arrows) **C:** Colocalization of TUC4 and BrdU in rat OB core confirms the overlapping distributions. **D:** Some cells are double labeled for TUC4 and BrdU (double arrows, brown is TUC4 immunoreactivity and black/blue is BrdU immunoreactivity) or single-labeled for either TUC4 or BrdU (single arrows identify BrdU labeled cells and single arrowheads identify TUC4 labeled cells). Scale bar (shown in A) = 25  $\mu$ m in A, 7.5  $\mu$ m in B, 150  $\mu$ m in C, 10  $\mu$ m in D.

The adult OB core contains numerous newborn neurons as shown by staining for the growth cone protein TUC4. Many TUC4-positive cells were observed in the OB core of adult mouse (Fig. 1J) and rat (Fig. 2I). The distributions of TUC4-expressing newborn neurons mirrored the BrdU-positive cells (Fig. 1J) and overlapped with the region of the OB core that was the most highly enriched in class III  $\beta$ -tubulin (Fig. 1K,M). The morphology of the TUC4-positive cells matched the pattern seen by Nissl staining (Fig. 1J). They generally had a primitive morphology (i.e., elongated and slender with few neurites). Occasional TUC4-positive cells were seen in the granule cell layer (data not shown). BrdU and TUC4 were colocalized in OB core cells in mouse (Fig. 3A,B) and rat (Fig. 3C,D), defining the presence of neuronal progenitor cells in the OB core. In mice injected with BrdU for 2 days,  $31\% \pm$

$11\%$  (mean  $\pm$  SD) of BrdU-positive cells was TUC4-positive.

#### Adult human OB is a rich source of newborn neurons and NSC

The adult human OB was evaluated for neuronal progenitor cells and NSC. Cresyl violet staining of sagittal sections showed that the human OB is densely populated with small cells (Fig. 4A). The human OB contains a population of numerous cells with a morphology that was similar to OB core cells in rat and mouse, but the cell packing density appeared lower in the OB of aged human (Fig. 4B). Immunophenotyping of OB sections from young and aged individuals revealed the presence of many TUC4 expressing newborn neurons (Fig. 4A,C,D) and neurons expressing class III  $\beta$  tubulin (Fig. 4K). Cells immunop-

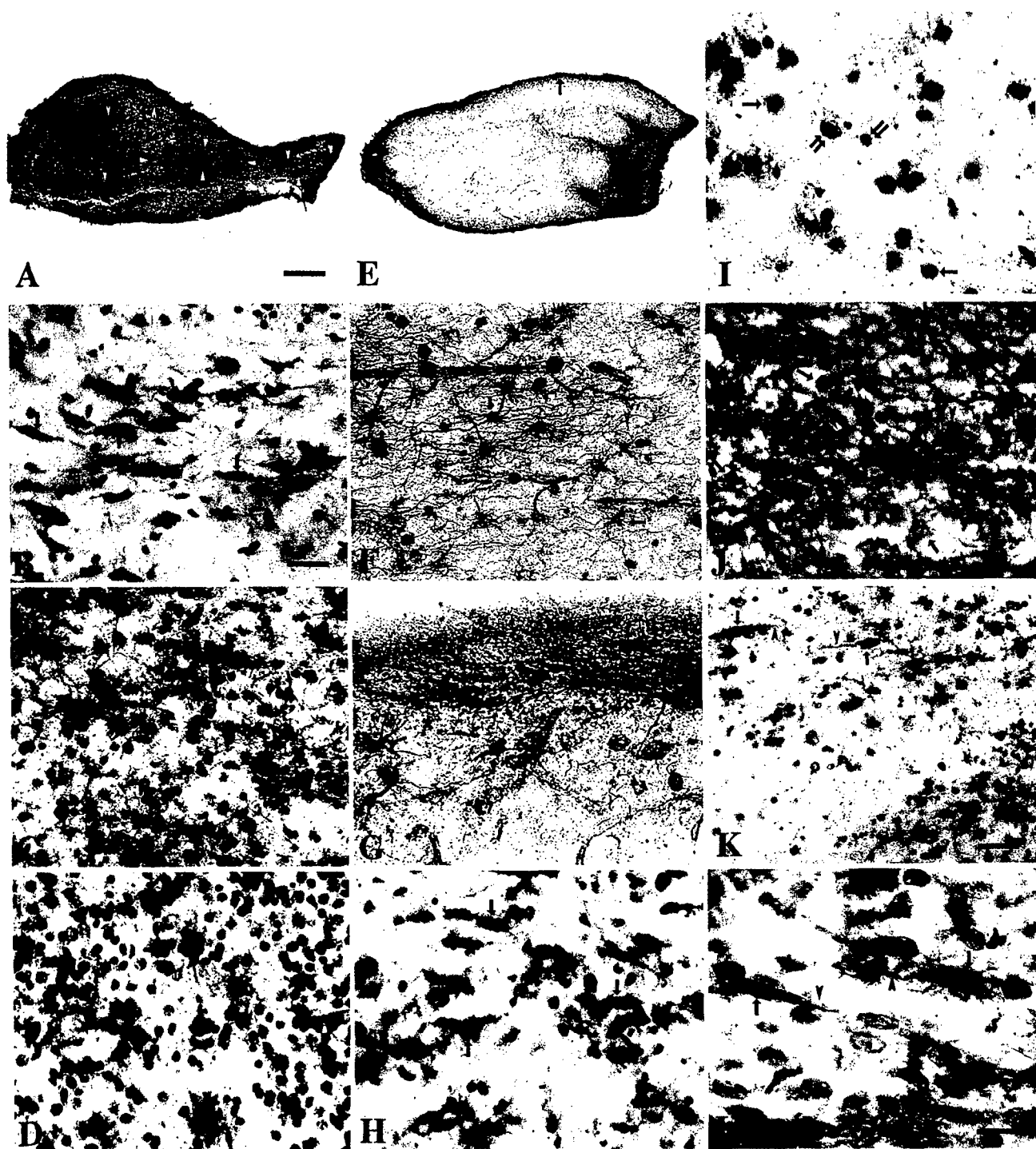


Figure 4

sitive for TUC4 or class III  $\beta$  tubulin did not have an astroglial or oligodendroglial morphology. Double labeling showed that many TUC4-positive cells were also positive for NeuN (Fig. 4I) but not for GFAP (Fig. 4J), confirming their neuronal identity. The OB of young and aged humans also contained numerous cells expressing the NSC/neuroprogenitor cell marker nestin (Fig. 4E-H). These

cells were concentrated at the posterior end of the human OB near the olfactory tract and around the accessory olfactory nucleus (Fig. 4E). Nestin-positive cells are also concentrated within the superficial, olfactory nerve layer of the OB (Fig. 4E,G). Cells positive for the neuroepithelial/glia cell progenitor marker vimentin were also enriched in these areas of the OB in young and aged humans (Fig. 4L).



### Cells from adult OB core form clonally-derived neurospheres in vitro and are multipotent NSC

Adult rat and mouse OB core cells were isolated by microdissection and trypsinization and studied in vitro. Adult OB core cells from both species can generate numerous neurospheres (Fig. 5). Population analysis of rat OB core sphere growth revealed sphere densities (spheres/mm<sup>2</sup>, mean  $\pm$  SD) of  $206 \pm 13$  and  $707 \pm 53$  at 4 and 7 days of culturing, respectively. OB core neurospheres had the ability to undergo serial passaging and cryopreservation. Single cell clonal analysis on OB core neurospheres from adult rat and mouse was performed to provide conclusive evidence for clonal origin of the neurospheres and their self-renewal and sustained multipotency (Fig. 5). OB core-generated primary neurospheres and cryopreserved-thawed neurospheres were dissociated into single cells and cultured individually (Fig. 5A). Individual OB core cells generated secondary neurospheres (Fig. 5B) and continued to generate higher-passaged spheres with longer time in culture (Fig. 5C). Floating spheres became attached neurospheres (Fig. 5D). Many attached spheres were positive for neuron-specific tubulin (Fig. 5E), indicating clonally derived neural progenitors. OB core derived clonal neurospheres were multipotent as shown by the expression of class III  $\beta$  tubulin, GFAP, and O4 in attached nondispersed spheres (Fig. 5F,G,a,b,c) and in attached dispersed cells from clonal spheres (Fig. 5H).

Primary cultures of cells (as a population of mixed dissociated cells and attached spheres, as opposed to clonally generated cells) derived from adult rat and mouse OB core were made successfully for evaluating population multipotency (Fig. 6). Phase contrast microscopy revealed the viability and growth of OB core cells at DIV3 (Fig. 6A) and DIV8 (Fig. 6B). These cells retained the ability to replicate as shown by BrdU labeling (Fig. 6C) and to form colonies (Fig. 6C–K). Immunostaining for nestin showed that subsets of cells derived from OB core and subsequently formed spheres are NSC (Fig. 6D, Table 3). At DIV8, about 44% of the total cells in culture were nestin positive. The morphology of nestin-positive cells was very distinctive.

Some nestin cells had an undifferentiated morphology and were globular, whereas other nestin-positive cells were angular with rapier-like processes (Fig. 6D).

Primary cultures generated from OB core primary cells and their spheres were characterized quantitatively (Table 3) to evaluate multipotency. We used antibodies that mark immature neurons (MAP5, TuJ1, and TUC4), astrocytes (GFAP), and oligodendrocytes (myelin basic protein, MBP). Subsets of cells from the OB core cells and their spheres became definite neurons (Fig. 6E–I; Table 3). Counts of DIV8 cells that were strongly labeled for a neuronal marker and had a definite neuronal morphology were ~5%–7% for TuJ1, TUC4, and MAP5 (Table 3). Staining patterns for MAP5 nicely revealed the apparent viability and maturation of these neurons in vitro. At DIV4 the developing neurons had bipolar cell bodies and thick growing dendrites with conspicuous growth cones (Fig. 6E). At DIV8, neurons had multipolar shapes with slender, branching dendrites (Fig. 6F). Some MAP5 faintly labeled cells were globular and did not have the typical morphology of immature or mature neurons. These cells were present throughout the entire culture period (Fig. 6E,F, arrows) for up to DIV45. These cells were similar in morphology to the globular nestin-positive cells (Fig. 6D) and could be NSC committed recently to become young neurons, or they may be neuronal progenitor cells with the capacity for self-renewal and the product of asymmetrical mitosis (one daughter cell becomes neuronal progenitor and the other progeny remains an NSC). Small subsets of similar cells were strongly labeled with antibodies to neuron-specific tubulin (Fig. 6G, arrows) and TUC4 (Fig. 6H,I). Glial cell markers were detected in cells that were morphologically distinct from neurons (Fig. 6J–L). GFAP was expressed in ~31% of the total cells at DIV8 (Table 3). These GFAP-positive cells were identifiable as protoplasmic astrocytes (Fig. 6J) or fibrous astrocytes (Fig. 6K). Protoplasmic astrocytes have irregular cell bodies with broad processes (Fig. 6J), while fibrous astrocytes have round cell bodies with many thin processes (Fig. 6K). In contrast, a much smaller percentage (2%) of these cultured cells at DIV8 expressed an oligodendrocyte marker

**Fig. 4 (Overleaf.)** The OB in elderly and young adult humans has copious newborn neurons and NSC. **A:** Sagittal section of an aged human OB immunolabeled for TUC4 (brown-black color) and counterstained with cresyl violet. The human OB is densely populated with small cells as shown by cresyl violet staining. A high concentration of TUC4 staining is present in the OB core (delineated by small white arrowheads) and within the olfactory nerve layer (OB surface). **B:** Cresyl violet staining shows that cells (arrows) in the OB core of aged individuals have a morphology that is similar to the cells in the OB core of rodents (mouse and rat). **C:** Many newborn neurons are present in the OB of elderly humans as identified by the expression of TUC4 (brown labeling). Cresyl violet counterstaining reveals the cells not immunolabeled. **D:** The OB core of young adult humans also contains subsets of cells that are TUC4-positive (brown labeling), while other cells (cresyl violet counterstaining) are not immunopositive. **E:** Sagittal section of aged human OB immunolabeled for nestin. High levels of nestin immunoreactivity (brown color) are present in the posterior OB core (arrowhead) and the shell (arrow, olfactory nerve layer). **F:** Nestin-positive cell bodies and processes (arrows, brown labeling) in elderly human OB core. **G:** Nestin-positive cell bodies and processes (arrows, brown labeling) in the olfactory nerve and glomerular layers of the elderly human OB. **H:** The OB core of young adult humans contains many cells that are nestin-positive

(arrows, brown labeling, cells are seen in their long axis), while other cells (cresyl violet counterstaining) are not immunopositive. **I:** TUC4 and NeuN colocalize in human OB core cells. TUC4 was visualized with DAB (brown color) and NeuN was detected with cobalt-DAB (blue staining). Single-labeled TUC4 cells (single arrow) are present, but many TUC4-positive cells coexpress NeuN (double arrows). Most of the double-stained cells are incompletely labeled and both brown and dark blue/black can be seen. **J:** TUC4 and GFAP do not colocalize in human OB cells. TUC4 was visualized with cobalt-DAB (blue color) and GFAP was detected with DAB (brown staining). TUC4-positive cells (single arrows) and GFAP-positive cells (arrowheads) are different populations of cells. Although these cells intermingle and overlap, careful focusing through the z-axis verified the absence of colocalization of TUC4 and GFAP. **K:** The human OB is enriched in TuJ1. The neurons (arrows) show strong somatodendritic labeling (brown color) with one or two processes (arrowheads) similar to the neuronal labeling in rodents (mouse and rat). The uneven cell density may be attributable to fiber bundles. **L:** The neuroepithelial/glial progenitor cell marker vimentin is expressed in human OB cells (arrows, brown labeling). The cells extend neurites (arrowheads) typical of migrating cells. Cresyl violet counterstaining reveals the cells not immunolabeled. Scale bars = 1236  $\mu$ m in A (applies to E), 32  $\mu$ m in B (applies to C,D,F–J), 46  $\mu$ m in K, 12  $\mu$ m in L.



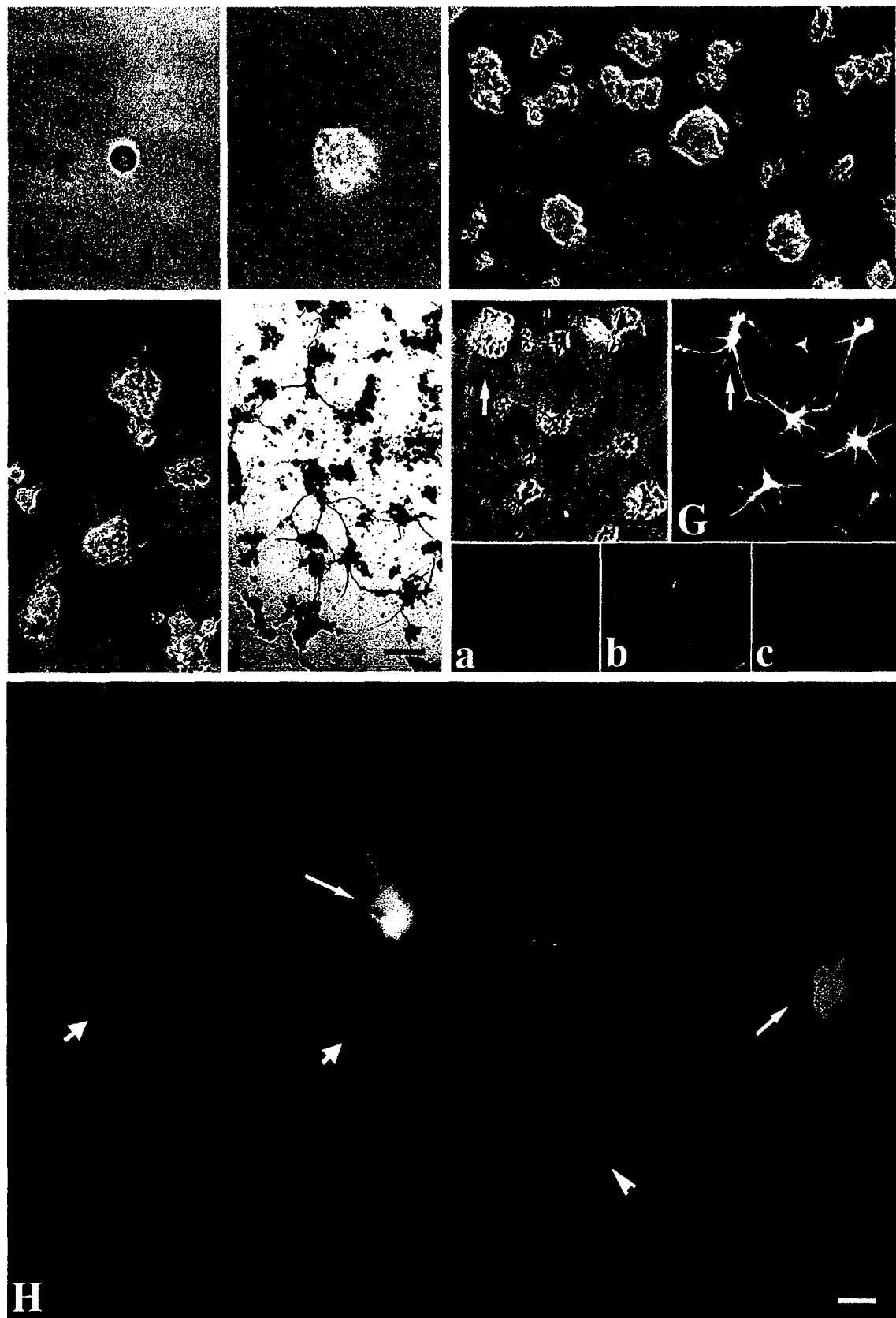


Figure 5

(Fig. 6L; Table 3). These results demonstrate the multipotency of adult OB core cells by both clonal and population analyses.

### In vitro expansion and differentiation of adult OB core NSC stimulated with growth factors

We evaluated the responsiveness of cells derived from adult OB core and their primary spheres to growth factors in vitro. Primary cultures were stimulated with 10 or 100 ng/ml bFGF or  $\beta$ -NGF, and proliferation and differentiation potential were evaluated. Attached colonies with BrdU incorporation were used as a measure of cell proliferation, and TuJ1 labeling of cells was used as a marker for neuronal differentiation.

Isolated BrdU-positive cells in control cultures (i.e., cells treated with 1% BSA in PBS as vehicle) were scattered throughout the cultures at DIV4. Baseline proliferation capacity of isolated OB core-NSC was high, as ~45% of the total cells were BrdU labeled (Figs. 7A,B, 8A). However, the number of colonies (attached, dispersing neurospheres) was low and colony size was small in control cells (Table 4). NSC proliferation was stimulated by bFGF (Figs. 7C,D; 8A,B). The number of BrdU-positive cells after bFGF exposure (100 ng/ml) was significantly higher than control cells and NGF (100 ng/ml) stimulated cells (Figs. 7C–F; 8A,B). BrdU-positive cells often appeared as clusters. Total cell number was also significantly higher in bFGF stimulated (100 ng/ml) cultures compared to control and NGF treated cultures (Fig. 8B). The percentage and total number of BrdU-positive cells in NGF treated cultures was not significantly different from control (Figs. 7E–H; 8A,B); however, the total number of cells after NGF stimulation was higher than control (Fig. 8B). Colony number and size were higher in bFGF (100 ng/ml) treated cultures compared to control and 100 ng/ml  $\beta$ -NGF treated cultures (Table 4). A lower concentration of bFGF (10 ng/ml) also stimulated proliferation of neural progenitor cells, but the proliferation response was less obvious than that achieved with 100 ng/ml. The percentage of TuJ1-positive cells in bFGF treated cultures was similar to control, while NGF stimulation increased in the percentage of TuJ1-positive cells (Fig. 8C). NGF at 10 ng/ml induced a classic NGF response ("halo effect") in cultured OB core NSC (Fig. 7G,H). Colocalization of BrdU and TuJ1 re-

vealed that a large proportion (>50%) of the replicated cells became neurons (Fig. 7I,J).

### NSC from the adult OB core can differentiate into specific types of neurons and distribute terminals on muscle cells

We examined the potential of NSC from the adult OB to differentiate into specific types of neurons by their coculture with skeletal muscle cells. The myoblasts proliferated very rapidly and fused into myotubes after confluence (Fig. 9A, rat myoblasts cultured for 6 days). With two different coculture approaches at different durations of coculture, the NSC distributed throughout the culture well among the muscle cells and were easily distinguishable from the muscle cells using neuron specific markers (Fig. 9). Both coculture approaches were successful (Fig. 9B–K) and yielded similar results for the same coculture times. Many TuJ1-positive neurons were present in 4-day (Fig. 9B,C) and 8-day cocultures (Fig. 9F). At coculture day 4, 56% and 44% of the class III  $\beta$ -tubulin-positive neurons were bipolar or multipolar, respectively. At coculture day 8, 36% and 64% of the class III  $\beta$ -tubulin-positive neurons were bipolar or multipolar, respectively. MAP2 immunostaining was fainter on coculture day 4 (Fig. 8D) compared to the intense labeling on coculture day 8 (Fig. 9E). MAP2 positive neurons were morphologically immature at coculture day 4 (Fig. 9D) compared to labeled cells at coculture day 8 (Fig. 9E). Day 4 cells had shorter processes and smaller cell bodies than day 8 neurons. The synaptic protein synaptophysin was also strongly expressed in many adult OB core-derived neurons cocultured with muscle cells (Fig. 9G–K). These neurons displayed prominent varicosities along their arborized axons that resembled *boutons en passage* on muscle cells (Fig. 9I). These processes were distributed throughout the culture on muscle cells, suggesting innervation of muscle cells. These neurons also showed the potential to form synapses either recurrently or with other neurons, as shown by the formation of perisomatic (Fig. 9J) and peridendritic (Fig. 9K) boutons that were positive for synaptophysin.

OB derived NSC were induced to differentiate structurally and neurochemically into different types of neurotransmitter-specific neurons. Single and cocultures were evaluated for cholinergic (ChAT and AChE), peptidergic (SP), and GABAergic (GAD) neurons. Neurons im-

Fig. 5 (Overleaf.) Single cell clonal analysis of adult OB core neurosphere cells demonstrating self-renewal and multipotency. **A:** Floating spheres derived from OB core cells can be cryopreserved and then subsequently thawed and passaged. Phase contrast microscopy showing a single cell from a dissociated cryopreserved primary neurosphere derived from the adult rat OB core. Single cells were transferred to different wells (1 cell/well) for clonal analysis. **B:** Secondary floating neurosphere (at DIV3) derived from a single cell (phase contrast microscopy). **C:** Numerous floating neurospheres are derived from a single cell after several passages for 2–3 weeks (phase contrast microscopy). **D:** Higher-passaged attached neurospheres are found during the entire culture period (phase contrast microscopy). Attached neurospheres remain viable (bright halos) and extend neurites. **E:** Many attached spheres flattened and are positive for class III  $\beta$  tubulin. **F:** Phase contrast image of higher-passaged spheres that were allowed to attach for characterization of multipotency (shown in G). The white arrow identifies the same neurospheres that are shown

in G (see white arrow) and in a, b, and c at higher magnification. **G:** Triple immunofluorescence staining (triple exposure) for class III  $\beta$  tubulin (blue), GFAP (green), and O4 (red) showing the multipotency of higher-passaged OB spheres. Pink represents the overlap of red (O4) and blue (class III  $\beta$  tubulin) fluorescence. All of the cells/spheres shown are also seen under phase contrast (see F). A sphere (white arrow) is shown to be multipotent under different filters at higher magnification in lower panels to show staining for class III  $\beta$  tubulin (a, blue), GFAP (b, green), and O4 (c, red). **H:** Cells derived from attached dispersed adult OB core spheres (7 days after conditioned medium) were multipotent as demonstrated by triple immunofluorescence staining for class III  $\beta$  tubulin (blue, short broad arrows), GFAP (green, thin arrows), and O4 (red, arrowhead). Some cells in a primitive stage of differentiation expressed more than one cell type marker, notably neuronal and oligodendrocyte markers. Scale bars = 20  $\mu$ m in A (applies to B–D), 40  $\mu$ m in E, 32  $\mu$ m in F (applies to G), 12  $\mu$ m in H.

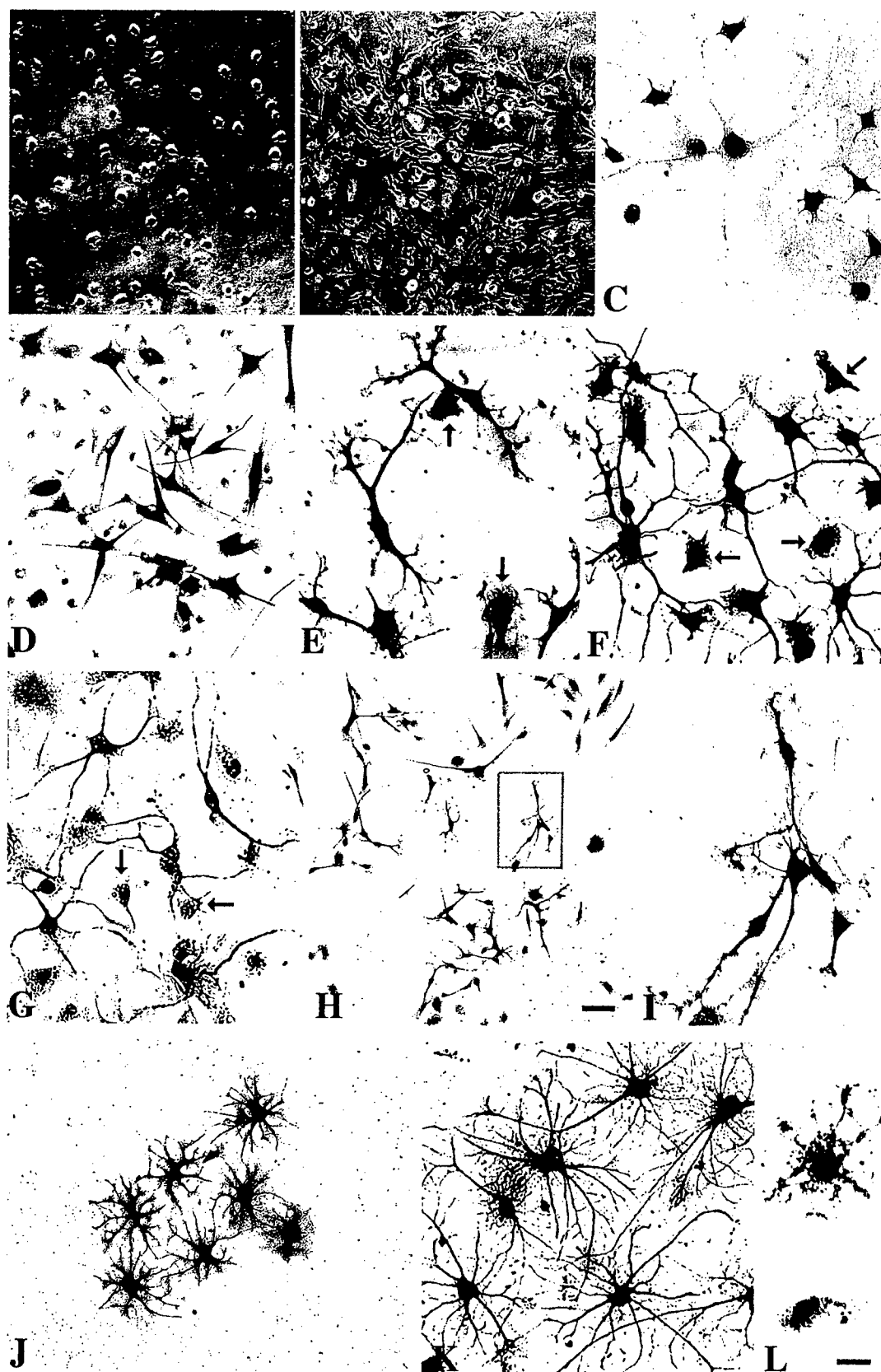


Figure 6

TABLE 3. Immunophenotypic identification of adult rat OB core primary cells in vitro

Cell type marker	Percentage of cells <sup>1</sup>
Nestin	43.6 ± 1.9 <sup>2</sup>
TUC4	5 ± 1.4
TuJ1	5 ± 1.8
MAP5	7 ± 2.5
GFAP	30.9 ± 8.5
MBP	2.4 ± 1.0

<sup>1</sup>Percentage of the total cells in single 35-mm wells (including NSC and definite neurons and glial cells) at DIV8. Only intense, completely labeled cells were counted. Faintly labeled presumptive progenitor cells were not included in the counts. Values are mean ± standard deviation.

<sup>2</sup>In DIV45 cultures the percentage of nestin-positive cells was 12.6 ± 4.8%.

munoreactive for ChAT, SP, and GAD were found in single cultures (Table 5). At coculture day 4, subsets of neurons were strongly immunoreactive for ChAT (Fig. 10A; Table 5). More ChAT-positive cells were found in cocultures compared to single cultures of OB core cells (Table 5). Some of these ChAT-positive neurons were large multipolar neurons (Fig. 10B), which were rarely seen in single cultures. The number of ChAT-positive cells increased significantly with time in coculture (Table 5). Large multipolar neurons were also AChE-positive (Fig. 10C). Evidence for the formation of neuromuscular junctions was obtained using AChE histochemistry to identify motor end plates on muscle cells. AChE-positive motor end plates were distributed throughout the cocultures along myocytes (Fig. 10D). Immuno-EM was used to definitively show the formation of synapses in NSC-muscle cell cocultures. Synaptophysin-positive axon terminals formed neuromuscular junctions with the presence of a synaptic cleft (Fig. 10E,F). SP-positive neurons bearing a unipolar/bipolar morphology were present in the cocultures (Fig. 9G). The number of SP-positive neurons was significantly higher in cocultures compared to single cultures of OB core cells (Table 5). GAD-positive neurons were also present in single and cocultures. Their numbers decreased significantly with time in coculture, compared to the single cultures (Table 5). The GAD-positive cells were mostly small and bipolar, regardless of culture condition. GAD immunoreactivity did not colocalize with ChAT in large multipolar neurons in cocultures.

## Adult mouse OB core NSC are pluripotent

OB core cells were evaluated for pluripotency. OB core cells were isolated from transgenic GFP mice. These cells could be cultured with maintained high levels of GFP without silenced expression (Fig. 11A). Several different events appeared to occur simultaneously when GFP mouse OB core cells and spheres were cocultured with mouse myoblasts. At coculture day 5, ~7–9% of OB core cells expressing GFP had adopted the morphology of multipolar neurons (Fig. 11B). Other GFP cells remained round without neurites or had 1–2 short neurites or became spindle-like (Fig. 11C) or remained as neurospheres (Fig. 11F). Many other GFP cells (~30–50%) at coculture day 5 showed a myocyte morphology (Fig. 11D,E). All of these myocyte-like cells had at least one prominent broad elongated process. Some of these cells were multinucleated (Fig. 11E) with GFP revealing the nuclei. On the 5th day of coculture about 30% of the GFP cells had the morphology of young myotubes and expressed myosin heavy chain (Fig. 11F–J).

## DISCUSSION

We conducted an *in vivo* and *in vitro* analysis of OB core cells to extend the understanding of the location, properties, and potential of NSC in the adult mammalian brain. Our interest in the OB was sparked because this region in the adult brain could be a potential accessible source of NSC for cell therapy in neurological disorders (Liu and Martin, 2001; Gritti et al., 2002). The OB core of adult mouse and rat contains numerous newly replicated cells. Many of these cells expressed newborn neuron or NSC markers. The *in vitro* characterization of adult rat and mouse OB core cells showed that these cells have self-renewal capacity and can generate clonal neurospheres that can be serially passaged and cryopreserved with maintained multipotentiality for generating neurons, astrocytes, and oligodendrocytes. Their number can be expanded using growth factors. When these cells are cocultured with skeletal muscle cells, they can be induced to become neurons that have a specific morphology and express specific neurotransmitter markers. Adult OB core cells also can become muscle cells. Thus adult OB core cells fulfill the criteria for pluripotent NSC (Potten, 1997; Rao, 1999; Gökhan and Mehler, 2001).

Fig. 6 (Overleaf.) Primary cultured cells derived from adult rat OB core cells and their neurospheres display NSC characteristics, including nestin expression, strong replication capacity, and multipotency. A,B: Phase contrast images of OB core cell cultures at 3 days (A) and 8 days (B) after seeding and sphere attachment. Cells at DIV3 are round and extend neurites. In DIV8 cultures, a subset of cells remains round while other cells are fusiform and extend processes. Note the high viability (bright halos), the good morphology, and the increased cell density (at DIV8 compared to DIV3). C: BrdU incorporation of OB core cells at DIV4. Numerous cells are BrdU positive. D: These cell cultures can be maintained for up to DIV45, and subsets of cells continue to express nestin. E: Cells at DIV4 express MAP5 (a marker for immature neurons). The cell body and the processes are strongly labeled. Growth cones are also seen. The expression of MAP5 drops when the neurons mature (data not shown). Some cells remain undifferentiated in morphology but also express MAP5 (arrows) and are found within clusters of neurons, possibly representing neuronal progenitors resulting from asymmetrical mitosis. F: MAP5 labeling of

cells from adult OB at DIV8. Compared to the neurons at DIV4, neurons at DIV8 have multipolar cell bodies and long slender processes. Many fewer growth cones are present. Subsets of MAP5-positive cells without a definite neuronal morphology are also present (arrows). G: TuJ1 labeled neurons in the culture from adult OB at day DIV8. TuJ1 antibody specifically identifies neuron-specific class III  $\beta$ -tubulin. Morphologically undifferentiated TuJ1-positive cells are present (arrows) among the clusters of neurons. H: TUC4 labeling of OB cells at DIV4 (the boxed area is shown in panel I). I: Higher magnification of boxed area in panel H showing TUC4 labeling of neurons and their processes and growth cones. J: A dispersing clonal aggregate of GFAP-positive protoplasmic astrocytes at DIV4. K: Cluster of GFAP-positive fibrous astrocytes. These cells are distinct morphologically from protoplasmic astrocytes (shown in panel J). L: Some cells in adult OB core cultures differentiate into oligodendrocytes expressing myelin basic protein. Scale bar = 92  $\mu$ m in H (applies to B), 48  $\mu$ m in A, 23  $\mu$ m in L (applies to C–G, I–K).

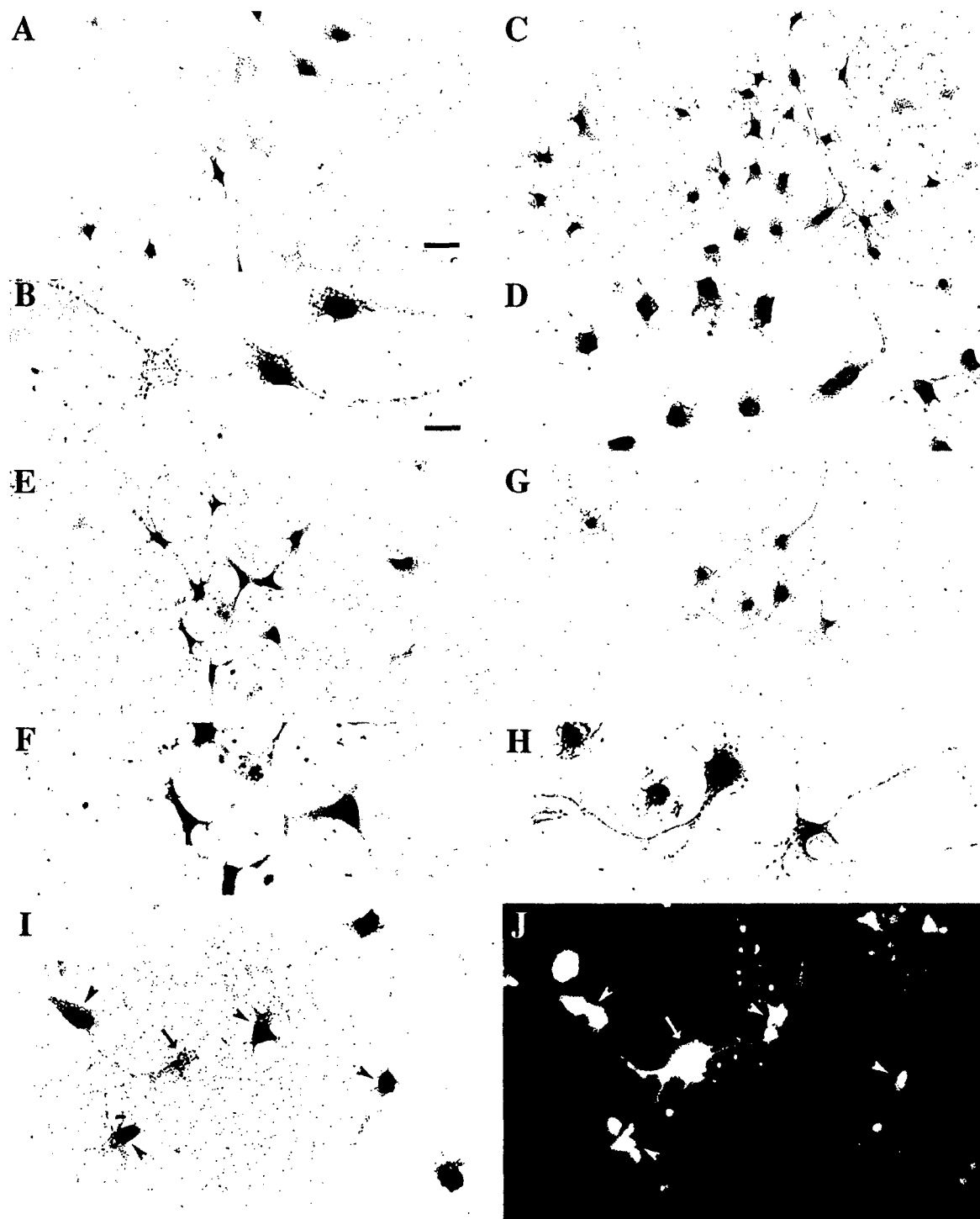


**Fig. 7.** Adult OB core NSC respond to growth factors in vitro. Adult OB cell cultures were exposed to bFGF and  $\beta$ -NGF at DIV3 in DMEM without serum. Cell proliferation was assayed by BrdU incorporation. The responses in the different treatment groups are illustrated as image pairs (A,B; C,D; E,F; G,H) of low and higher magnification views showing the generality of the response (low magnification) and the morphology of the cells (high magnification). BrdU-positive cells have black nuclei. **A,B:** Cells from a vehicle treated culture. Untreated cells have a strong potential for proliferation. In nonreplicating cells, BrdU is assimilated but is not incorporated into the nucleus (see cell in B at left). **C,D:** Cells in a culture treated with bFGF (100 ng/ml). Cell proliferation was promoted strongly by 100 ng/ml bFGF (see Fig. 8A,B and Table 4 for quantification). Many of the BrdU-positive cells have immature morphologies with numerous short neurites. **E,F:** A cell colony from a culture treated with  $\beta$ -NGF (100 ng/ml). The cells appear larger with more

dendritic development than the bFGF-treated cells. **G,H:** Cells treated with  $\beta$ -NGF (10 ng/ml). Some cells show a classic NGF response with numerous radiating neurites (cells at left have "halo effect"), although other cells show more advanced dendritic differentiation (cell at right). **I,J:** Colocalization of BrdU (I) and TuJ1 (J). BrdU was detected with the ABC method using DAB, and TuJ1 staining was detected with immunofluorescence (seen as white because of black-and-white photography). These same cells are shown in both panels. Most of the replicating cells become neurons (arrowheads) as shown by the colocalization of nuclear BrdU labeling (I, black DAB) and the cytoplasmic labeling for neuron-specific tubulin (I, white labeling). The cell without BrdU labeling (I, arrow) is well-differentiated neuron because of tubulin expression (J, arrow). Scale bars = 50  $\mu$ m in A (applies to C,E,G), 25  $\mu$ m in B (applies to D,F,H,I,J).

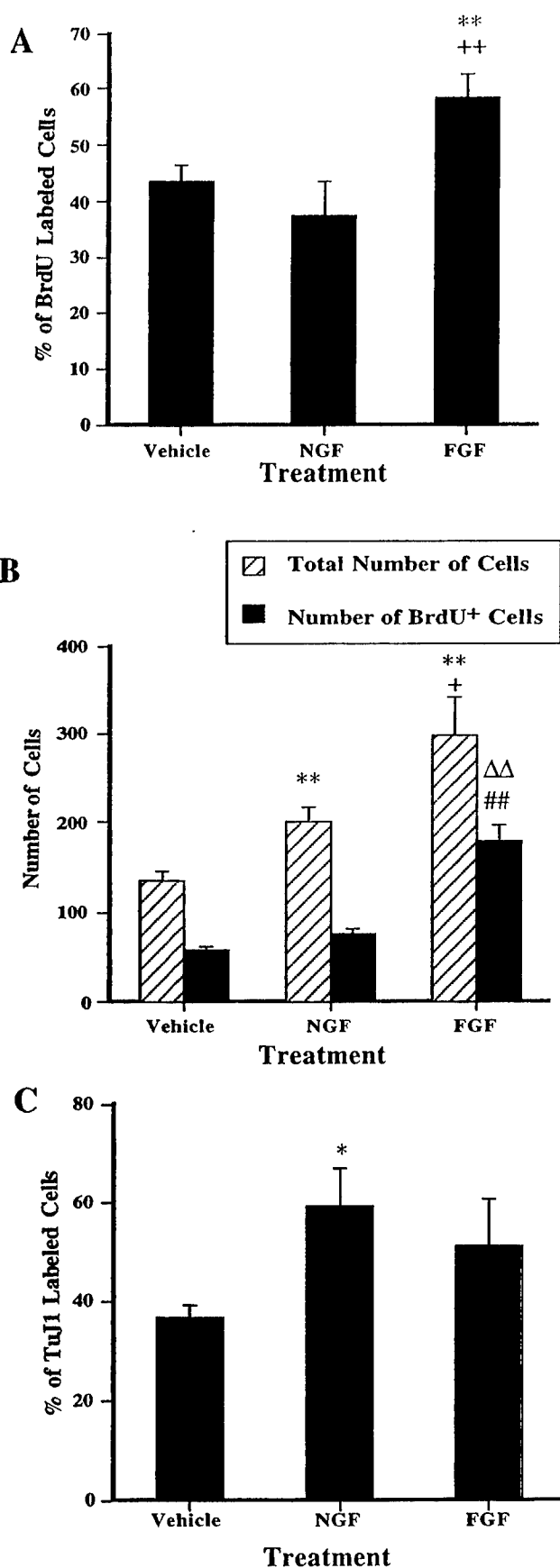


TABLE 4. NSC from adult rat OB core respond to growth factors in vitro

Treatment <sup>1</sup>	Number of colonies <sup>2</sup>	Range in cell number/colony (average colony size)	Number of colonies counted for size determination
Vehicle	1.2	6-13 (7.6)	18
βNGF	1.9	6-23 (10.4)	20
bFGF	5.5	6-36 (15.0)	50

<sup>1</sup>Values are derived from 3-5 35-mm wells for each condition.

<sup>2</sup>The value represents the average number of colonies (attached, dispersed neurospheres) per field based on 30 microscopic fields (at 40×) for each treatment.

### Adult brain OB core is a reservoir of newly generated neuronal progenitor cells and NSC

We found that the OB core of adult mouse and rat contains copious newly born cells in vivo. This finding is important because, although persistent cell division in the adult mouse and rat OB has been documented (Hinds, 1968; Altman, 1969; Kaplan and Hinds, 1977; Bayer, 1983), definitive evidence for the birth of neurons specifically within the adult OB core is uncommon. Most studies have focused on the granule cell layer and have resorted to tentative cell type identification, rather than specific cell immunophenotyping. Only one prior study (Zigova et al., 1998) has found newly generated neurons specifically in the adult rat OB core (subependymal zone). The presence of large numbers of newly generated cells in the adult OB core is likely to be due to both high birth rate and accumulation of migrating newborn cells. The cell proliferation was a mixture of neurogenesis and NSC expansion because BrdU colocalized with a specific newborn neuron marker (TUC4) and an NSC marker (nestin), respectively. The overall distribution of TUC4 expressing cells in the OB core was almost identical to that of BrdU labeling, and was also similar to nestin and class III β-tubulin localizations. This information is new, in that nestin and TUC4 positive cells have not been shown before in the adult OB core of mouse, rat, or human. The classification of these cells according to the scheme developed for the SVZ (Alvarez-Buylla and García-Verdugo, 2002) is tentative. The TUC4-positive cells are likely to be similar to the type

Fig. 8. Quantification of adult OB core NSC responses to growth factors in vitro. **A:** Percentage of BrdU labeled cells relative to the total number of cells in cultures exposed to β-NGF, bFGF, or vehicle (1% BSA in PBS). The number of BrdU labeled cells in bFGF treated culture is significantly higher than that in NGF-treated (\*\*,  $P < 0.01$ ) and vehicle-treated (++,  $P < 0.01$ ) cultures, indicating bFGF promotes expansion of NSC from adult OB core. The percentages of both NGF and vehicle treated cultures were similar. **B:** Total number of cells and total number of BrdU labeled cells in cultures treated with β-NGF, bFGF, and vehicle. Both the total number of cells (\*\*,  $P < 0.01$ ) and the total number of BrdU labeled cells (ΔΔ,  $P < 0.01$ ) in bFGF treated cultures are significantly higher than vehicle-treated cells. The total number of cells in NGF treated cultures is significantly higher than vehicle-treated cells (\*\*,  $p < 0.01$ ). The total number of cells (+,  $p < 0.05$ ) and total number of BrdU labeled cells (##,  $P < 0.01$ ) are significantly higher in bFGF-treated cultures compared to NGF-treated cultures. **C:** Percentage of TuJ1 labeled cells in cultures treated with β-NGF, bFGF, and vehicle. The number of TuJ1-labeled neurons is significantly higher in β-NGF treated cultures compared to vehicle-treated cells (\*,  $P < 0.01$ ). bFGF treatment had no significant effect on TuJ1 labeling.

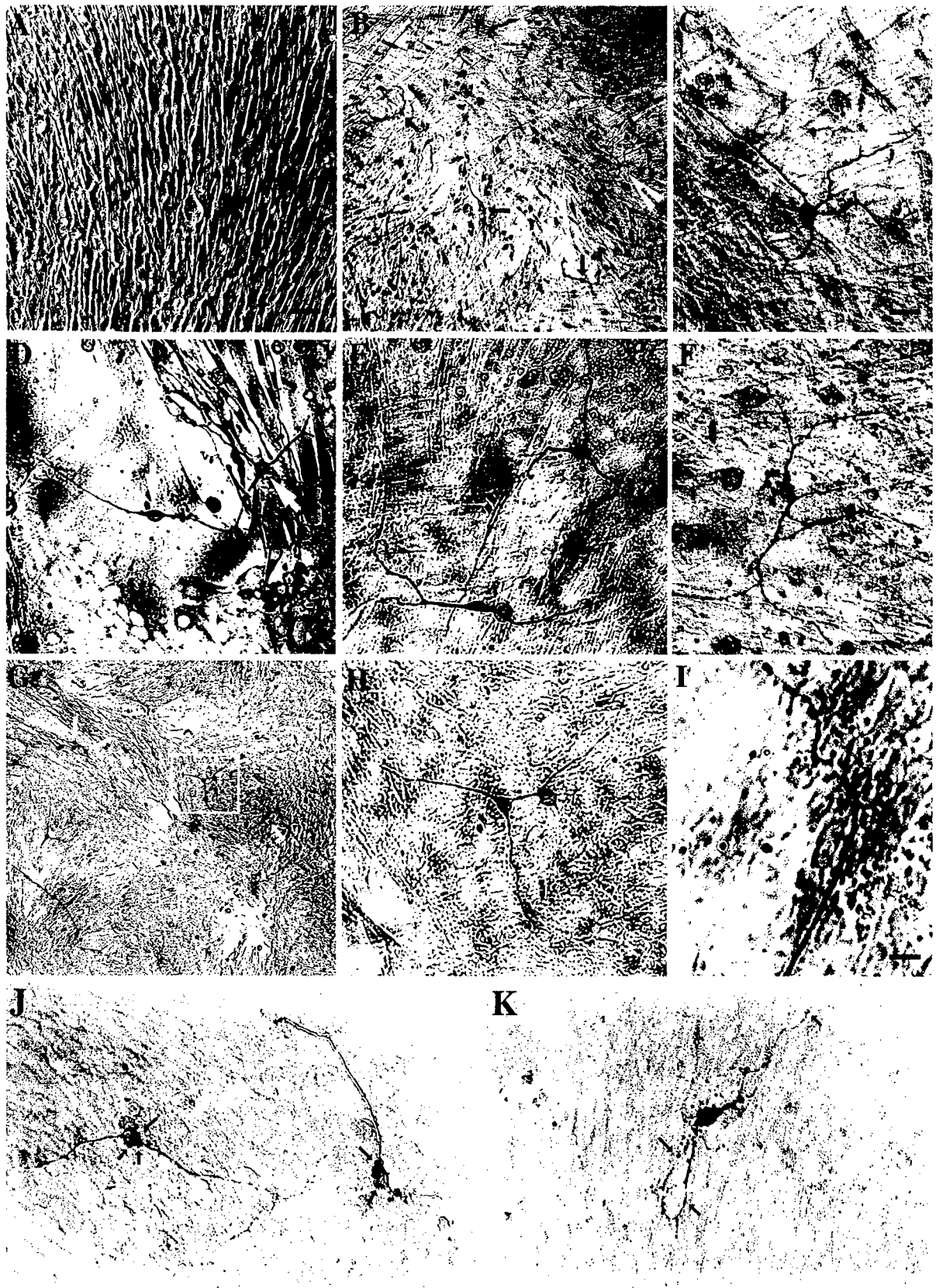


Figure 9

TABLE 5. Adult rat OB core NSC cocultured with muscle cells show induction of neurotransmitters

Neurotransmitter marker	Number of immunopositive cells <sup>1</sup>		
	Single culture <sup>2</sup>	Coculture (4 days) <sup>3</sup>	Coculture (8 days) <sup>4</sup>
ChAT	22 ± 5	61 ± 8*	146 ± 26**
Substance P	10.5 ± 0.5	nd	29.5 ± 1.5*
GAD	21 ± 1.3	15.7 ± 1.1*	12.5 ± 1.5*

<sup>1</sup>Number of immunoreactive cells in single 35-mm wells (2–3 wells) determined from 6 microscopic fields at 20×. Values are mean ± standard deviation. nd, not determined. Single asterisk (\*) denotes significant difference ( $P < .001$ ) compared to single culture. Double asterisk (\*\*) denotes significant difference ( $P < .001$ ) compared to 4 day coculture.

<sup>2</sup>Single cultures were used at DIV10.

<sup>3</sup>Cocultures at 4 days were at a total of 6 days in vitro (2 days of single culture + 4 days of coculture with muscle cells).

<sup>4</sup>Cocultures at 8 days were at a total of 10 days in vitro (2 days of single culture + 8 days of coculture with muscle cells).

A cells within the SVZ (Alvarez-Buylla and García-Verdugo, 2002), and thus are young migrating neurons or neuronal progenitor cells. BrdU and TUC4 colocalized in ~31% of OB core cells (with 2 days BrdU incorporation). Thus, a significant proportion of newly replicated cells found in the adult OB core have become newborn neurons soon after they are born, or cells in the adult OB core newly committed to be neurons retain the capacity to replicate as neuronal progenitors. This latter possibility has been suggested to occur in the neonatal RMS (Menezes et al., 1995). Other BrdU-positive cells were nestin-positive NSC (33% with 2 days BrdU incorporation), indicating *in vivo* expansion of the NSC population within the RMS or OB. The identity of the cells positive for nestin is more complicated because neuroepithelial stem cells, neuron-restricted precursor cells, glial-restricted precursor cells, oligodendrocyte/astrocyte precursor cells, and some differentiated astrocytes can express nestin (Rao, 1999). The nestin-positive cells in the OB core may be similar to the type B and C cells. Type B cells are astrocytes (Alvarez-Buylla and García-Verdugo, 2002). Type C cells are thought to be the highly proliferative neural precursor cells within the SVZ and are usually labeled by <sup>3</sup>H-thymidine (Alvarez-Buylla and García-Verdugo, 2002). However, type A and type B cells can replicate as well. An important distinction is that type A cells isolated from the SVZ do not appear to self-renew *in vitro*, whereas type B and type C cells appear to generate large colonies of type A young neurons (Lim and Alvarez-Buylla, 1999). We found that isolated OB core cells self-renewed *in vitro* and

generated neurons, further narrowing the possibility that these cells could be similar to the type C cells of the SVZ or they may be the same population of cells. The OB core is considered the anterior-most part of the RMS and thus is an extension of the SVZa (Smart, 1961; Altman, 1969; Luskin, 1993; Lois and Alvarez-Buylla, 1994). Cell proliferation has been found along the RMS from the SVZa to the OB core in adult mouse (Smart, 1961) and neonatal rat (Luskin, 1993; Smith and Luskin, 1998; Coskun and Luskin, 2001). Cells with neuronal and astrocytic identities comprise this system in adult mouse (Jankovski and Sotelo, 1996). The new *in vivo* information we provide here is that the adult mouse and rat OB core is a major repository of newborn neurons, neuronal progenitor cells, and NSC, but the specific origins of these cells requires further study. The OB core appears to be much more than the mere destination of RMS cells derived from the SVZa. The OB core in the adult may be a major source of NSC by virtue of a very active RMS that supplies it (Zigova et al., 1998), and itself being a generator of NSC and neuronal progenitor cells. The anatomical location of the OB makes this structure accessible for harvesting large numbers of NSC and neuronal progenitor cells from the adult CNS.

A determination of the precise fraction of cells that are born specifically within the OB core is difficult, because this region is supplied continuously with cells from the RMS, where proliferation is more active (Coskun and Luskin, 2001), and because cells appear to migrate out of the core (see Figure 2D–G). A portion of this cell replication seems to occur directly within the OB core. Evidence for mitosis in the adult OB core was shown (see Figures 1C and 2C). The BrdU data suggest replication of cells directly in the OB core. With a single BrdU pulse and 12-hour survival, the BrdU labeled cells in the OB core appeared as daughter pairs in close proximity (see Figure 1D), and most positive cells had incompletely labeled nuclei with BrdU immunoreactivity that was aggregated at the margin of the nucleus, appearing as condensed chromosomes as in cells at late prophase. The amount of cell replication that occurs in the OB core appears to be more robust than recognized previously. A recent study of the adult dentate gyrus has revealed a magnitude of cell proliferation much greater than previously realized (Cameron and McKay, 2001). More experiments need to be done to determine the amount of cell replication that is intrinsic to the adult OB core.

**Fig. 9 (Overleaf.)** Adult OB core-derived NSC generate neuronal progeny when cocultured with myoblast cells. **A:** Cultured rat skeletal myoblast cells at DIV6 form fused confluent sheets. **B:** Coculture of OB core NSC with rat myoblasts. DIV2 OB core NSC were mixed with myoblasts and cultured for an additional 4 days. TuJ1 localization reveals that neurons structurally differentiate as bipolar (black arrows) and multipolar cells (white arrowhead). **C:** Higher magnification of the neuron (white arrowhead in B) with a multipolar structural phenotype. **D:** MAP2 localization in DIV3 OB core NSC that were mixed with rat myoblasts and cultured for an additional 4 days. Faintly labeled bipolar neurons (white arrow) appear less mature than neurons cocultured for longer times (see E). **E:** Cocultures at DIV7 (coDIV7) have neurons that show advanced structural differentiation and dark staining for MAP2. The processes are longer and the staining is stronger than coDIV4 neurons (D). **F:** CoDIV7 neurons also

show strong staining for TuJ1. The neuronal processes are long and ramified with numerous varicosities distributed on muscle cells. Compare the neurons to TuJ1 labeling of coDIV4 neurons (Fig. 9) and OB core neurons cultured alone (Fig. 6G). **G:** DIV3 OB core cells cocultured with myoblast cells for 5 more days express the presynaptic vesicle protein synaptophysin (white arrows). **H:** Higher magnification of neurons (boxed area in panel G) strongly immunopositive for synaptophysin. **I:** Arborized synaptophysin-positive preterminal axon distributes terminals (arrows) on muscle cells. Numerous isolated synaptophysin-positive terminal boutons are present on the muscle cells. **J:** Neurons at coDIV8 have perisomatic terminals (arrows) labeled for synaptophysin. **K:** Neurons at coDIV8 have peridendritic terminals (arrows) labeled for synaptophysin. Scale bars = 92 µm in A (applies to B,G), 23 µm in C (applies to D–F,H,J,K), 10 µm in I.



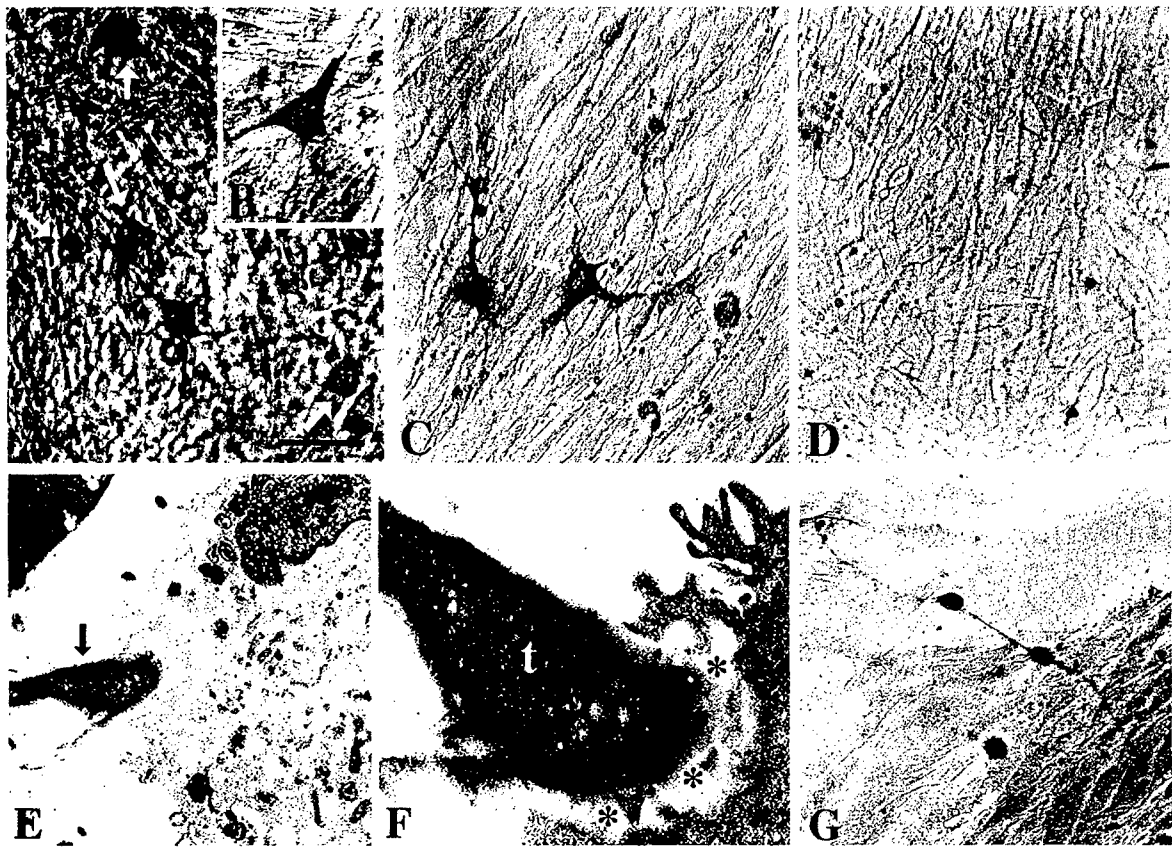


Fig. 10. Adult OB core cells can differentiate into neurons with different phenotypes and can distribute boutons on muscle cells. **A:** ChAT protein expression is strongly induced in OB core-derived neurons (white arrows) when cocultured with muscle cells (see Table 5 for quantification). Many of these ChAT expressing cells can become large multipolar neurons (see cell in **B**). **B:** ChAT-positive multipolar neuron generated from OB core NSC in coculture with muscle cells. **C:** Subsets of OB derived cells can become large multipolar AChE-positive neurons (arrows) when cocultured with muscle cells. **D:** AChE histochemistry reveals the formation of boutons and motor end plates (arrows) on skeletal muscle cells. **E:** Immuno-EM demon-

strates that OB derived neurons can form neuromuscular junctions when cocultured with muscle cells. An axon terminal immunolabeled for synaptophysin (arrow) is establishing a nascent synaptic junction (shown, rotated  $\sim 45^\circ$ , at higher magnification in **F**) with a muscle cell (at right). **F:** At the site of membrane contact between the axon terminal (t) and the muscle cell, a synaptic cleft is forming (asterisks) and the muscle cell sarcolemma is folded extensively. **G:** Subsets of OB derived cells cocultured with muscle cells are induced to express SP (white arrows, see Table 5 for quantification) and have a bipolar or unipolar morphology. Scale bar (shown in **A**) = 49  $\mu\text{m}$  in **A**, 45  $\mu\text{m}$  (applies to **B-D, G**), 0.5  $\mu\text{m}$  in **E**, 0.2  $\mu\text{m}$  in **F**.

### Adult OB core contains pluripotent NSC

We isolated and cultured adult OB core cells to study their NSC characteristics. This detailed *in vitro* characterization of OB core NSC is a very important contribution of this study. Only one other group has isolated and studied *in vitro* NSC from the adult rodent OB core (Gritti et al., 2002). They showed evidence for multipotent NSC in the adult mouse OB core (Gritti et al., 2002). Our work confirms and extends this recent study. We showed that adult rat OB core cells have the cardinal features of NSC by population and formal clonal analyses. Adult OB core cells display long-term self-renewal capacity and the ability to generate clones, express nestin, and differentiate *in vitro* into neurons, astrocytes, and oligodendrocytes. Their ability to proliferate *in vitro* is consistent with our *in vivo* BrdU results. Isolated OB core cells replicated vigorously to generate primary neurospheres that were capable of generating secondary- and higher-passaged spheres. These neurospheres could be cryopreserved and subsequently passaged. OB core-derived cells were responsive

to both bFGF and  $\beta$ -NGF, but the responses were different. bFGF further promoted the proliferation of these cells. bFGF increased the number of colonies and colony cell number. In contrast,  $\beta$ -NGF increased the number of neurons (identified by TuJ1 positivity), possibly through effects on differentiation or survival. The only similar study done on adult mouse OB (Gritti et al., 2002) did not evaluate differential responses of OB core cells to growth factors. Other studies have successfully propagated *in vitro* neural progenitor cells isolated from adult mouse and rat SVZ and hippocampus (Kuhn et al., 1997; Chiasson et al., 1999). Our study is the first to demonstrate the isolation, propagation, and differentiation of large numbers of multipotent NSC from the adult rat OB, specifically the OB core. The ability of these cells to respond to growth factors attests to their general viability *in vitro*. Our clonal analysis showed unequivocal evidence for the multipotency of adult OB core cells. This multipotency was demonstrated at the level of individual spheres, clonal cells, and OB core-derived primary cell cultures.

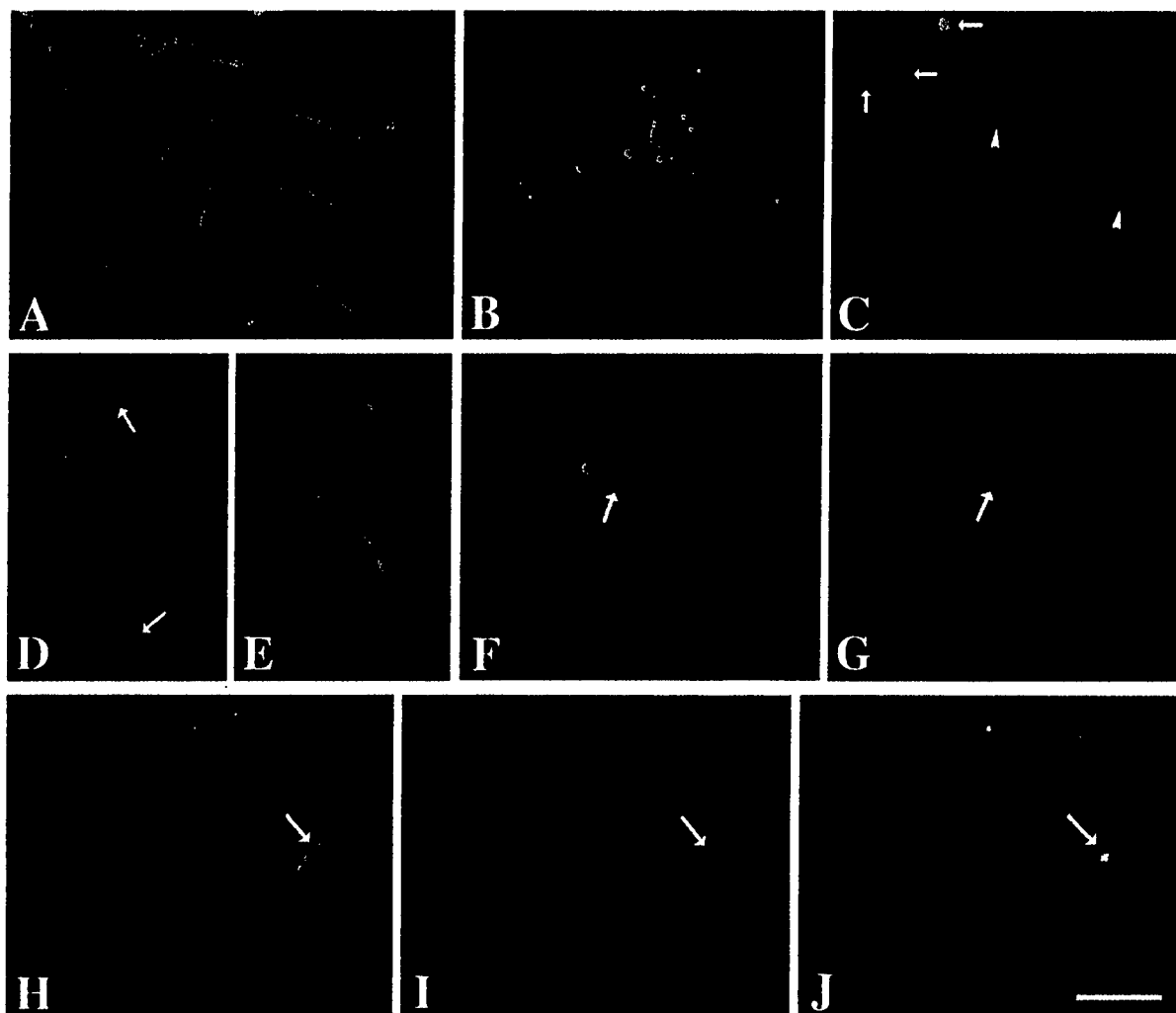


**Fig. 11.** Adult OB core NSC are pluripotent. Primary culture (A) of cells derived from OB core neurospheres of transgenic GFP mice and neurospheres cocultured with mouse skeletal muscle cells for 5 days (B–J). **A:** GFP is localized throughout the cytoplasm and in the nucleus (see cells in lower left corner for clear nuclear localization) of OB core cells. **B:** Some OB core derived GFP cells differentiate into multipolar neurons. **C:** Some OB core cells remain round without neurites or have 1–2 short neurites (arrows) or become spindle-like (arrow-heads). **D:** Many other cocultured GFP cells showed a myocyte morphology. All of these cells had at least one prominent broad elongated

process and a GFP-positive nucleus (arrows). **E:** Some of these GFP cells that appear to be differentiating into myocytes were multinucleated. **F–I:** Subsets of young myotubes are GFP-positive (F and H, arrows). GFP-OB cell neurospheres are still present (F, lower right). GFP cell-derived myotubes express myosin heavy chain (G and I, arrows). Note that the GFP labeling is homogeneous throughout the cytoplasm (rather than particulate). **J:** Overlay of images shown in panels H and I demonstrating the colocalization of green and red (seen as yellow) in a myotube expressing GFP and myosin (arrow). Scale bar (shown in J) = 115  $\mu\text{m}$  (applies to A–J).

Our results are different from the results of an *in vitro* study of SVZa cells from newborn (P0) rat brain showing that most (~90%) of the cells at DIV3 are TuJ1-positive, although the number of GFAP positive cells increased with longer durations in culture (Luskin et al., 1997). Independent groups now confirm the *in vitro* multipotency of adult mammalian OB core-derived NSC.

We suspected the possibility of OB core cell transdifferentiation into nonneural cells *in vitro* and evaluated their potential pluripotency using GFP transgenic mice. This suspicion was based on the observation that the total number of neural cells in mouse OB core cell-muscle cell cocultures appeared to be decreased after 8 days, without obvious signs of increased death. Pluripotency was not evaluated in the only other study of NSC in the adult OB

(Gritti et al., 2002). We found that freshly isolated OB core cells and cell spheres became skeletal muscle cells when cocultured with myoblasts. We interpret this phenomenon as transdifferentiation, rather than cell fusion (Ying et al., 2002), because OB core-GFP cells appeared to pass through recordable morphological stages of differentiation. We did not find evidence for myocytes originating directly from large multipolar neurons. Described simplistically, this process begins with round cells that extend neurites to become bipolar cells that progressively elongate and broaden their processes. Multinucleation appears to occur and then expression of muscle cell specific protein. High levels of GFP were localized in the nucleus of OB core cells, and most of the differentiating myocytes, some of which were multinucleated, had strong nuclear

GFP. OB core cell-derived myocytes at different stages of morphological differentiation had homogeneous GFP signal throughout the cytoplasm. It is unlikely that this observation is the result of myocytes engulfing debris of GFP cells, because the labeling was not particulate within the cytoplasm, indicative of lysosomes. The pluripotency of NSC from the adult mammalian CNS has been identified only recently (Bjornson et al., 1999; Galli et al., 2000; Clarke et al., 2000; Rietze et al., 2001). Other groups have demonstrated that NSC isolated from adult mouse periventricular region can generate skeletal muscle cells (Galli et al., 2000; Clarke et al., 2000; Rietze et al., 2001).

### **NSC from adult OB core have the capacity to differentiate into morphologically and neurochemically distinct types of neurons**

Cells derived from the neonatal rat SVZ are capable of expressing GABA (Luskin, 1993), and neuronal progeny from the adult mouse RMS can express ChAT, GABA, and glutamate (Gritti et al., 2002). We examined NSC from adult OB in single and cocultures for their capacity to differentiate into specific types of neurons. The successful maturation and vitality of these neurons *in vitro* was evident by comparing the morphology of Tuj1-stained cells at different times in culture. Generally, there was a shift in shape from bipolar to multipolar with longer time in culture. Some cells that were multipolar, expressed ChAT and synaptophysin, and formed terminal boutons on myocytes. Based on the quantification of ChAT-positive cells in single cultures and cocultures, the presence of muscle cells induces the ChAT phenotype. The myocytes possessed AChE-positive motor end plates, consistent with a cholinergic innervation. Thus, OB core NSC may have the capacity to differentiate into motor neurons. OB-derived cells also differentiated into neurons with a bipolar morphology and expressed SP or GAD. The expression of SP also appeared to be induced by the presence of muscle cells. In coculture, the number of GAD-positive cells decreased as the number of ChAT-positive cells increased with longer time in coculture. The magnitude of change in the ChAT induction was dramatic (200–500% increases) compared to the loss of GAD cells (25–40% decreases). It is not clear whether the GAD-positive cells are losing their phenotype, selectively dying, or becoming the cholinergic cells. It may not be the latter because of the lack of reciprocity. The cholinergic cells must be derived from other major sources of cells. Our results further demonstrate the versatility of NSC derived from the adult OB core by the epigenetic induction of neurotransmitter marker expression by another type of cell.

### **Adult human OB contains NSC and newborn neurons**

This study shows for the first time the location of NSC and neuronal progenitor cells in the adult human OB. With regard to the presence of these cell populations in the OB, the work on the human brain is more difficult to interpret with certainty, as compared to the work on the rat and mouse brain, because the BrdU experiments in the animals helped to support the contention that NSC are present and that neurogenesis is ongoing. Therefore, with the human OB, we had to rely on immunocytochemical data. There were at least two related concerns to overcome

with this experimental design. One concern is the antibody markers used to identify NSC and newborn neurons and whether the labeled cells can be called justifiably NSC or newborn neurons. The second concern is deciphering whether the labeling, notably in the older cases studied, is confounded by an age-related process. These concerns were neutralized by using highly specific antibodies that have been characterized by other groups and by studying the OB from aged humans as well as young adult humans as controls. Numerous cells in the OB of young and aged humans are positive for nestin, vimentin, and TUC4. The nestin and vimentin staining in the OB of aged humans could be a reflection of gliosis due secondarily to the aging process. However, staining for nestin was also strong in the OB of young adult individuals; thus, it is likely that a true population of NSC is being identified and it is not likely to be due solely to an age-related gliotic process and the detection of glia or glial progenitors. Our observations have additional significance because we identified newborn neurons in the OB of young adult and aged individuals. TUC4 and NeuN (but not TUC4 and GFAP) colocalized in these cells supporting the contention that neurogenesis in the human OB is a continuing process. This colocalization fulfills a standard for identifying a cell as a newborn neuron in the absence of BrdU data (Rakic, 2002). Our study supports a recent *in vitro* study showing that NSC can be isolated from the human OB and cultured (Pagano et al., 2000). Another recent study has identified NSC in the adult human nasal neuroepithelium (Roisen et al., 2001). Our observations in the human brain are consistent with studies on the nonhuman primate brain revealing the presence of proliferating neurons in the RMS (Pencea et al., 2001; Kornack and Rakic, 2001). It is nevertheless essential to show the existence and location of NSC directly in the human CNS, because human and nonhuman primates differ in many aspects of forebrain organization (Martin et al., 1991). A previous study has reported that cell proliferation in the OB is diminished in senescent mice (Tropepe et al., 1997). Much more work is needed on these cells in the human OB at different ages to appreciate fully their abundance, characteristics, and versatility as NSC, as well as their potential applications to human disease.

### **Significance of NSC in the adult OB**

This work is new because the OB is not usually considered as a major source of NSC and neural progenitor cells and because this reservoir of pluripotent NSC is found in the adult brain. The OB core cells are particularly interesting because within this population some cells are differentiating while other cells are migrating. Other novel aspects of this study include the demonstration that these cells can be driven to become neurons that express specific neurotransmitters and to become muscle cells. This major population of cells can be found in the OB of adult mouse, rat, and human. Thus, we have identified a major alternative source of NSC other than NSC derived from fetal/embryonic tissues and from cell lines. The potential of adult OB cells to become specific types of neurotransmitter-expressing neurons, glial cells, and muscle cells warrants animal studies evaluating the effectiveness of these NSC in replacing or rescuing neurons, glia, and muscle cells in animal models of disease or trauma.

## ACKNOWLEDGEMENTS

We are grateful for the outstanding technical assistance of Frank Barksdale, and we thank the staff of the Human Brain Resource Center at Johns Hopkins Medical Institutions.

## LITERATURE CITED

- Altman J. 1969. Autoradiographic and histological studies of postnatal neurogenesis. I.V. Cell proliferation and migration in the anterior forebrain, with special reference to persisting neurogenesis in the olfactory bulb. *J Comp Neurol* 137:433–458.
- Alvarez-Buylla A, García-Verdugo JM. 2002. Neurogenesis in adult subventricular zone. *J Neurosci* 22:629–634.
- Bayer SA. 1983. <sup>3</sup>H-Thymidine-radiographic studies of neurogenesis in the rat olfactory bulb. *Exp Brain Res* 50:329–340.
- Bédard A, Lévesque M, Bernier PJ, Parent A. 2002. The rostral migratory stream in adult squirrel monkeys: contribution of new neurons to the olfactory tubercle and involvement of the antiapoptotic protein Bcl-2. *Eur J Neurosci* 16:1917–1924.
- Bjornson CRR, Rietze RL, Reynolds BA, Magli MC, Vescovi AL. 1999. Turning brain into blood: a hematopoietic fate adopted by adult neural stem cell in vivo. *Science* 283:534–537.
- Cameron HA, McKay RDG. 2001. Adult neurogenesis produces a large pool of new granule cells in the dentate gyrus. *J Comp Neurol* 435:406–417.
- Chiasson BJ, Tropepe V, Morshead CM, van der Kooy D. 1999. Adult mammalian forebrain ependymal and subependymal cells demonstrate proliferative potential, but only subependymal cells have neural stem cell characteristics. *J Neurosci* 19:4462–4471.
- Clarke DL, Johansson CB, Wilbertz J, Veress B, Nilsson E, Karlström, Lendahl U, Frisén. 2000. Generalized potential of adult neural stem cells. *Science* 288:1660–1663.
- Coskun V, Luskin MB. 2001. The expression pattern of the cell cycle inhibitor p19<sup>INK4d</sup> by progenitor cells of the rat embryonic telencephalon and neonatal anterior subventricular zone. *J Neurosci* 21:3092–3103.
- del Río JA, Soriano E. 1989. Immunocytochemical detection of 5'-bromodeoxyuridine incorporation in the central nervous system of the mouse. *Devel Brain Res* 49:311–317.
- Fernández A, Radmilovich M, Trujillo-Cenóz O. 2002. Neurogenesis and gliogenesis in the spinal cord of turtles. *J Comp Neurol* 453:131–144.
- Fiocco R, Cossu G, Vescovi AL. 2000. Skeletal myogenic potential of human and mouse neural stem cells. *Nat Neurosci* 3:986–991.
- Franklin KBJ, Paxinos G. 1997. The mouse brain in stereotaxic coordinates. San Diego: Academic Press.
- Galli R, Borello U, Gritti A, Minasi MG, Bjornson C, Coletta M, Mora M, De Angelis MGC, Gökhan S, Mehler MF. 2001. Basic and clinical neuroscience applications of embryonic stem cells. *Anat Rec* 265:142–156.
- Gritti A, Parati EA, Cova L, Frolichsthal P, Galli R, Wanke E, Faravelli L, Morassutti DJ, Roisen F, Nickel DD, Vescovi AL. 1996. Multipotential stem cells from the adult mouse brain proliferate and self-renew in response to basic fibroblast growth factor. *J Neurosci* 16:1091–1100.
- Gritti A, Bonfanti L, Doetsch F, Caille I, Alvarez-Buylla A, Lim DA, Galli R, García-Verdugo JM, Herrera DG, Vescovi AL. 2002. Multipotent neural stem cells reside into the rostral extension and olfactory bulb of adult rodents. *J Neurosci* 22:437–445.
- Hinds JW. 1968. Autoradiographic study of histogenesis in the mouse olfactory bulb. I. Time of origin of neurons and neuroglia. *J Comp Neurol* 134:287–304.
- Horiikawa I, Miwa T, Ishimaru T, Furukawa M, Kata T, Moriizumi T. 1999. TrkA expression in olfactory epithelium and bulb during development. *NeuroReport* 10:2205–2208.
- Jankovski A, Sotelo C. 1996. Subventricular zone-olfactory bulb migratory pathway in the adult mouse: cellular composition and specificity as determined by heterochronic and heterotopic transplantation. *J Comp Neurol* 371:376–396.
- Kaplan MS, Hinds JW. 1997. Neurogenesis in the adult rat: electron microscopic analysis of light radioautographs. *Science* 197:1092–1094.
- Kornack DR, Rakic P. 2001. The generation, migration, and differentiation of olfactory neurons in the adult primate brain. *Proc Natl Acad Sci USA* 98:4752–4757.
- Kuhn HG, Winkler J, Kempermann G, Thal LJ, Gage FH. 1997. Epidermal growth factor and fibroblast growth factor-2 have different effects on neural progenitors in the adult rat brain. *J Neurosci* 17:5820–5829.
- Lee MK, Tuttle JB, Rebhun LI, Cleveland DW, Frankfurter A. 1990. The expression and posttranslational modification of a neuron-specific  $\beta$ -tubulin isotype during chick embryogenesis. *Cell Motil Cytoskeleton* 17:118–132.
- Lendahl U, Zimmerman LB, McKay RDG. 1990. CNS stem cells express a new class of intermediate filament protein. *Cell* 60:585–595.
- Lentz TL. 1969. Development of the neuromuscular junction. 1. Cytological and cytochemical studies on the neuromuscular junction of differentiating muscle in the regenerating limb of the newt *Triturus*. *J Cell Biol* 42:431–443.
- Lesuisse C, Martin LJ. 2002. Long-term culture of mouse cortical neurons as a model for neuronal development, aging, and death. *J Neurobiol* 51:9–23.
- Lim DA, Alvarez-Buylla A. 1999. Interaction between astrocytes and adult subventricular zone precursors stimulates neurogenesis. *Proc Natl Acad Sci USA* 96:7526–7531.
- Liu Z, Martin LJ. 2001. The olfactory bulb is a novel source of neural stem cells in adult CNS: identification, isolation, and culture. *Soc Neurosci Abstr* 27:134.7.
- Lois C, Alvarez-Buylla A. 1994. Long-distance neuronal migration in the adult mammalian brain. *Science* 264:1145–1148.
- Luskin MB. 1993. Restricted proliferation and migration of postnatally generated neurons derived from the forebrain subventricular zone. *Neuron* 11:173–189.
- Luskin MB, Zigova T, Soteres BJ, Stewart RR. 1997. Neuronal progenitor cells derived from the anterior subventricular zone of the neonatal rat forebrain continue to proliferate in vitro and express a neuronal phenotype. *Mol Cell Neurosci* 8:351–366.
- Martin LJ, Powers RE, Dellovade TL, Price DL. 1991. The bed nucleus-amygdala continuum in human and monkey. *J Comp Neurol* 309:445–485.
- Menezes JRL, Smith CM, Nelson KC, Luskin MB. 1995. The division of neuronal progenitor cells during migration in the neonatal mammalian forebrain. *Mol Cell Neurosci* 6:496–508.
- Morshead CM, Reynolds BA, Craig CG, McBurney MW, Staines WA, Morassutti D, Weiss S, van der Kooy D. 1994. Neural stem cells in the adult mammalian forebrain: a relatively quiescent subpopulation of subependymal cells. *Neuron* 13:1071–1082.
- Pagano SF, Impagnatiello F, Girelli M, Cova L, Grioni E, Onofri M, Cavallaro M, Etteri S, Vitello F, Giombini S, Solero CL, Parati EA. 2000. Isolation and characterization of neural stem cells from the adult human olfactory bulb. *Stem Cells* 18:295–300.
- Palmer TD, Takahashi J, Gage FH. 1997. The adult rat hippocampus contains primordial neural stem cells. *Mol Cell Neurosci* 8:389–404.
- Paxinos G, Watson C. 1986. The rat brain in stereotaxic coordinates. San Diego: Academic Press.
- Pencea V, Bingaman KD, Freedman LJ, Luskin MB. 2001. Neurogenesis in the subventricular zone and rostral migratory stream of the neonatal and adult primate forebrain. *Exp Neurol* 172:1–6.
- Potten CS. 1997. *Stem Cells*. San Diego: Academic Press. 474 p.
- Quinn CC, Gray GE, Hockfield S. 1999. A family of proteins implicated in axon guidance and outgrowth. *J Neurobiol* 41:158–164.
- Rakic P. 1972. Mode of cell migration to the superficial layers of fetal monkey neocortex. *J Comp Neurol* 145:61–84.
- Rakic P. 2002. Adult neurogenesis in mammals: an identity crisis. *J Neurosci* 22:614–618.
- Rao MS. 1999. Multipotent and restricted precursors in the central nervous system. *Anat Rec* 257:137–148.
- Reynolds BA, Weiss S. 1992. Generation of neurons and astrocytes from isolated cells of the adult mammalian central nervous system. *Science* 255:1707–1710.
- Reynolds BA, Weiss S. 1996. Clonal and population analyses demonstrate that an EGF-responsive mammalian embryonic CNS precursor is a stem cell. *Dev Biol* 175:1–13.
- Rietze RL, Valcanis H, Brooker GF, Thomas T, Voss AK, Bartlett PF. 2001. Purification of a pluripotent neural stem cell from the adult mouse brain. *Nature* 412:736–739.
- Roisen FJ, Klueber KM, Lu CL, Hatcher LM, Dozier A, Shields CB, Maguire S. 2001. Adult human olfactory stem cells. *Brain Res* 890:11–22.

- Smart I. 1961. The subependymal layer of the mouse brain and its cell production as shown by radioautography after thymidine- $H^3$  injection. *J Comp Neurol* 116:325-347.
- Smith CM, Luskin MB. 1998. Cell cycle length of olfactory bulb neuronal progenitors in the rostral migratory stream. *Devel Dyn* 213:220-227.
- Tago H, Kimura H, Maeda T. 1986. Visualization of detailed acetylcholinesterase fiber and neuron staining in rat brain by a sensitive histochemical procedure. *J Histochem Cytochem* 34:1431-1438.
- Tropepe V, Craig CG, Morshead CM, van der Kooy D. 1997. Transforming growth factor- $\alpha$  null and senescent mice show decreased neural progenitor cell proliferation in the forebrain subependyma. *J Neurosci* 17:7850-7859.
- Tropepe V, Hitoshi S, Sirard C, Mak TW, Rossant J, van der Kooy D. 2001. Direct neural fate specification from embryonic stem cells: a primitive mammalian neural stem cell stage acquired by a default mechanism. *Neuron* 30:65-78.
- Ying Q-L, Nichols J, Evans EP, Smith AG. 2002. Changing potency by spontaneous fusion. *Nature* 416:545-548.
- Zigova T, Pencea V, Wiegand SJ, Luskin MB. 1998. Intraventricular administration of BDNF increases the number of newly generated neurons in the adult olfactory bulb. *Mol Cell Neurosci* 11:234-245.

# Neuronal cell death in nervous system development, disease, and injury (Review)

LEE J. MARTIN

Departments of Pathology, Division of Neuropathology, and Neuroscience,  
Johns Hopkins University School of Medicine, Baltimore, MD, USA

Received February 22, 2001; Accepted March 5, 2001

**Abstract.** Neuronal death is normal during nervous system development but is abnormal in brain and spinal cord disease and injury. Apoptosis and necrosis are types of cell death. They are generally considered to be distinct forms of cell death. The re-emergence of apoptosis may contribute to the neuronal degeneration in chronic neurodegenerative disease, such as amyotrophic lateral sclerosis and Alzheimer's disease, and in neurological injury such as cerebral ischemia and trauma. There is also mounting evidence supporting an apoptosis-necrosis cell death continuum. In this continuum, neuronal death can result from varying contributions of coexisting apoptotic and necrotic mechanisms; thus, some of the distinctions between apoptosis and necrosis are becoming blurred. Cell culture and animal model systems are revealing the mechanisms of cell death. Necrosis can result from acute oxidative stress. Apoptosis can be induced by cell surface receptor engagement, growth factor withdrawal, and DNA damage. Several families of proteins and specific biochemical signal-transduction pathways regulate cell death. Cell death signaling can involve plasma membrane death receptors, mitochondrial death proteins, proteases, kinases, and transcription factors. Players in the cell death and cell survival orchestra include Fas receptor, Bcl-2 and Bax (and their homologues), cytochrome c, caspases, p53, and extracellular signal-regulated protein kinases. Some forms of cell death require gene activation, RNA synthesis, and protein synthesis, whereas others forms are transcriptionally-translationally-independent and are driven by posttranslational mechanisms such as protein phosphorylation and protein translocation. A better understanding of the molecular mechanisms of neuronal cell death in nervous system development, injury and disease can lead to new therapeutic approaches for the prevention of neurodegeneration and neurological disabilities and will expand the field of cell death biology.

## Contents

1. Cell death classification
2. The cell death continuum
3. Molecular control of apoptosis
4. Apoptosis is regulated cell death
5. Death proteins can be regulated by phosphorylation
6. Death receptors can mediate apoptosis
7. Tumor suppressor proteins mediate apoptosis
8. Naturally-occurring PCD occurs in the developing nervous system
9. Signaling pathways modulate neuronal survival
10. Neuronal cell death in disorders of the human CNS
11. Neuronal degeneration after cerebral ischemia
12. Possible mechanisms driving the apoptosis-necrosis cell death continuum
13. Neuronal death in models of axotomy and target deprivation
14. Perspective on neurodegeneration in animal models of human neurological disorders

## 1. Cell death classification

Cell death is a concept. Pathologists conceived cell death as a mechanism of disease (1). The death of cells (or the absence of appropriate cell death) is now recognized to have pathological and normal physiological importance. It is important for normal histogenesis (2-4) and cellular kinetics of healthy and malignant tissue (5). Cell death occurs through many pathways and has been classified generally as two distinct types, called apoptosis and necrosis, because they differ structurally and biochemically. These distinctions are now becoming blurred. Recently it has been realized that cell death exists as a continuum with apoptosis and necrosis at opposite ends of this continuum (6-9).

**Classical apoptosis.** Apoptosis is normal in most tissues. It is critical for the normal growth and differentiation of organ systems in vertebrates and invertebrates (3,4,10,11). For example, the cells comprising the interdigital webs undergo massive apoptosis (necrosis contributes as well) to establish the pattern of the fingers and toes. Apoptosis is normal in the developing nervous system of invertebrates and vertebrates

---

**Correspondence to:** Dr Lee J. Martin, Johns Hopkins University School of Medicine, Department of Pathology, 558 Ross Building, 720 Rutland Avenue, Baltimore, MD 21205-2196, USA  
E-mail: lmartin@jhmi.edu

**Key words:** Alzheimer's disease, amyotrophic lateral sclerosis, cell death, cerebral ischemia, motor neuron degeneration, stroke, traumatic brain injury, apoptosis-necrosis continuum

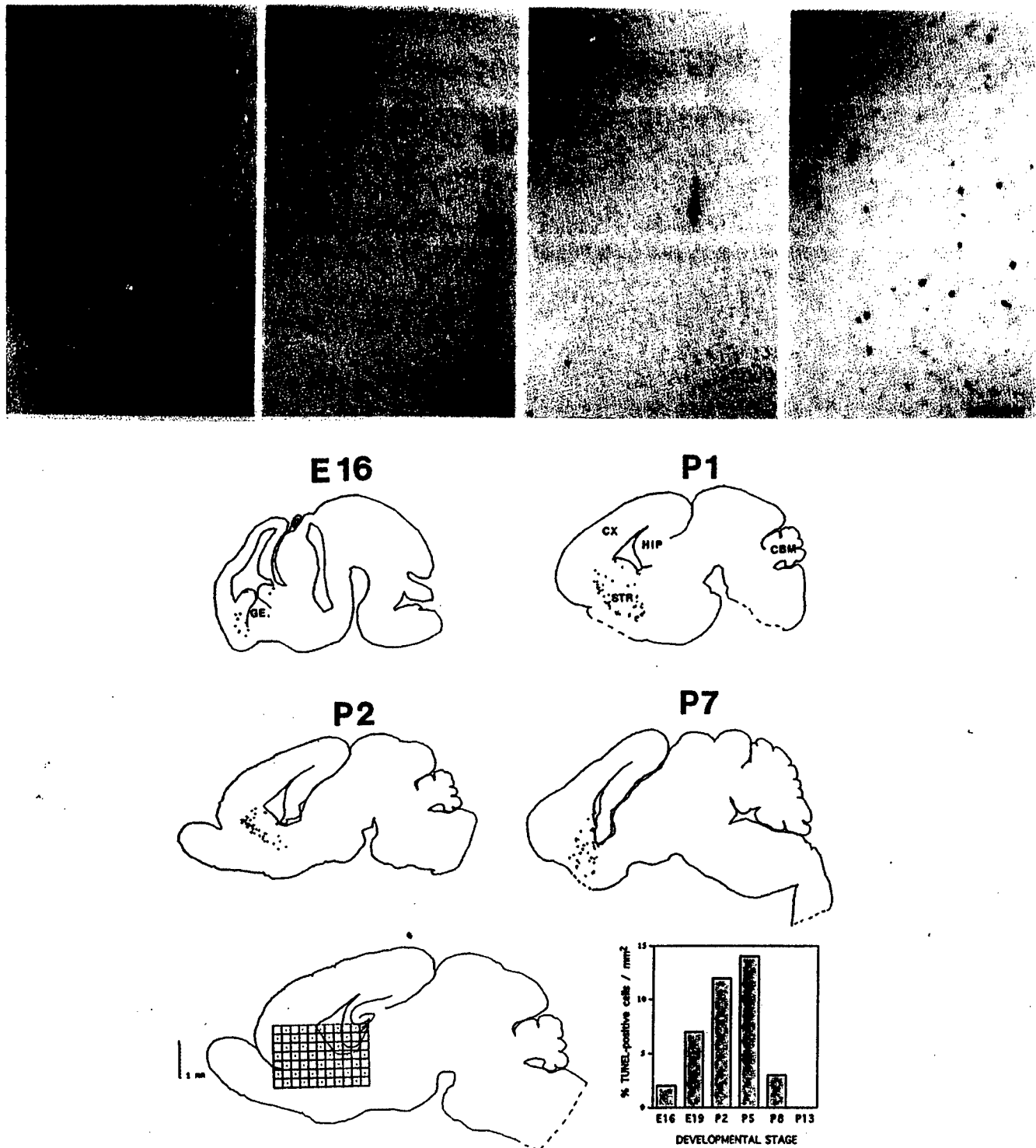


Figure 1. Naturally occurring cell death in the developing brain. Dying cells were identified by deoxy-UTP-biotin nick-end labeling (TUNEL) as a marker for DNA fragmentation. In postnatal day 1 rat brain (top panel), apoptosis (black arrows) is found in cerebral cortex (A), hippocampus (B; so, stratum oriens; sp, stratum pyramidale; sr, stratum radiatum; sl, stratum lacunosum-moleculare), striatum (C), and inferior colliculus (D). Scale bar, 125  $\mu$ m. Distribution and quantification of TUNEL-positive cells in the striatum of developing rat (bottom panel) at embryonic day 16 (E16) and postnatal days (P1, P2, and P7). The images are contours of midsagittal sections of brain. Each dot is a TUNEL-positive cell. TUNEL-positive cells were counted using a grid overlay on similar midsagittal sections (lower left). Dotted boxes indicate the areas where neurons were counted under high magnification. The values (mean cells/mm<sup>2</sup>) are represented graphically (lower right). CBM, cerebellum; CX, cerebral cortex; GE, ganglionic eminence; HIP, hippocampus; STR, striatum.

(Fig. 1). In the developing chick nervous system, large numbers (~50%) of sensory and spinal motor neurons undergo apoptosis (2,12). In the rodent nervous system, apoptosis occurs as well (Figs. 1 and 2). Studies on developmental cell death need to

be done in primates. Apoptosis occurs continuously in cell populations that undergo slow proliferation (e.g., liver and adrenal gland) or rapid proliferation (e.g., epithelium of intestinal crypts) (13,14), and it occurs as a normal event in

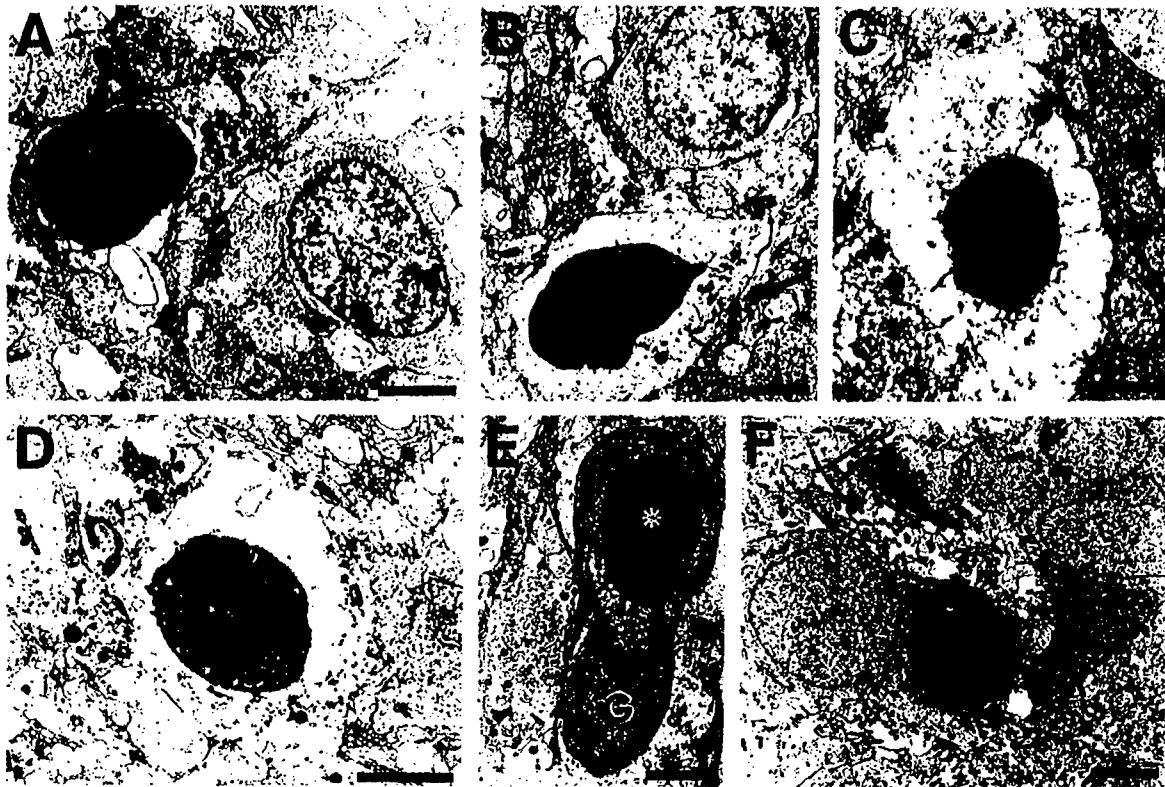


Figure 2. Structural analysis of naturally-occurring apoptosis in newborn rat brain with electron microscopy. A, In cells undergoing PCD (dark cell at left), both the nucleus and cytoplasm condense, and uniformly round, chromatin masses are formed in the nucleus. B-D, The condensation advances and the cell detaches from the surrounding neuropil, as the condensed cytoplasm is enveloped by glial processes (black arrow in B). E and F, The nuclear debris (asterisk in panel E) is phagocytosed by glial cells (G in panel E). Scale bars, 3 µm.

Table I. Molecular regulation of apoptosis.

Bcl-2 family		Caspase family	IAP family	Tumor suppressor family
Antiapoptotic proteins	Proapoptotic proteins			
Bcl-2 <sup>a</sup>	Bax <sup>a</sup>	Apoptosis 'initiators': caspase-2, -8, -9, -10	NAIP SMN	p53 <sup>a</sup> p63 p73
Bcl-x <sub>L</sub>	Bak <sup>a</sup>	Apoptosis 'executioners': caspase-3 <sup>a</sup> , -6, -7	IAP1	
Bcl-2	Bcl-x <sub>S</sub> Bad Bid Bik	Cytokine processors: caspase-1, -4, -5, -11, 12, -14	IAP2 XIAP	

<sup>a</sup>Identifies proteins that have significantly altered levels in individuals with ALS.

the deletion of lymphocyte clones after an immune response (15). Apoptosis is also a feature of the atrophy and involution of hormone-sensitive tissues, occurring in some cell types after hormone withdrawal in the prostate (16), adrenal cortex (14), and endometrium (5). Thus, apoptosis serves as an antagonist to mitosis for the controlled elimination of cells that are excessive and unnecessary. Apoptosis is also used to eliminate

preneoplastic and malignant cells as a mechanism to prevent carcinogenesis. Apoptosis is physiological programmed cell death (PCD) because it is mediated by active, intrinsic mechanisms requiring specific molecules (Table I). However, not all forms of PCD occur by apoptosis (17,18).

Classical apoptosis has a distinctive structure (Fig. 2). It has a type I morphology as defined by Clarke (19). The cell



shrinks and is dismantled into packages in a regulated manner. Nuclear breakdown is orderly. The chromatin condenses into sharply delineated, uniformly dense masses that appear as crescents abutting the nuclear envelope or as smooth, round masses within the nucleus (Fig. 2). Cytoplasmic breakdown is also orderly. The cytoplasm condenses (as reflected by a darkening of the cell in electron micrographs, see Fig. 2), and subsequently the cell shrinks in size, while the plasma membrane remains intact. Condensation of the cytoplasm can be associated with the formation of translucent cytoplasmic vacuoles derived from the endoplasmic reticulum or the Golgi apparatus. It is thought that the mitochondria are normal and are required for apoptosis. Subsequently, the nuclear and plasma membranes become convoluted, and, then the cell undergoes a process called budding. In this process, the nucleus, containing smooth, uniform masses of condensed chromatin (Fig. 2), undergoes fragmentation in association with the condensed cytoplasm, forming cellular debris (called apoptotic bodies) composed of pieces of nucleus surrounded by cytoplasm with closely packed and apparently intact organelles. A double membrane surrounds some nuclear fragments, but others are not membrane bound. Apoptotic cells express markers (e.g., phosphatidylserine or sugars) on their surface for recognition by phagocytes. The final phase of apoptosis *in vivo* is phagocytosis of cellular debris (Fig. 2). Naturally-occurring PCD (Fig. 2) is the 'gold standard' for apoptosis to which other forms of cell death should be compared for classification (8,9).

**Non-apoptotic PCD.** Apoptosis and PCD are not interchangeable terms (17). Cells can die by non-apoptotic forms of PCD, employing PCD mechanisms distinct from apoptosis (17,18). The structure of non-apoptotic PCD can be similar to the type II (autophagic) form of cell death (19). Cells undergoing autophagic death show extensive degradation of cytoplasmic organelles prior to nuclear destruction. There is no internucleosomal fragmentation of DNA during non-apoptotic PCD (17,18).

Variants of classical apoptosis or non-classical apoptosis can occur during nervous system development (19,20) and also in nervous system pathophysiology (6-9). Non-classical forms of apoptosis occur in the nervous system after exposure to neurotoxins (6,7), hypoxia-ischemia (21,22), and in human neurodegenerative disease (23-25).

**Cell necrosis.** Necrosis is cell death (Fig. 3c, d and f) initiated by rapid and severe failure to sustain homeostasis. The process of cellular necrosis involves damage to the structural and functional integrity of the cell plasma membrane and associated enzymes (e.g., Na,K ATPase), rapid metabolic failure, and abrupt influx of ions and H<sub>2</sub>O. It is believed that cellular necrosis is the passive result of departures from physiological conditions rather than from a specific molecular program within dying cells (Fig. 4). However, specific signaling pathways may still cause cellular necrosis.

The morphology of classic necrosis is very distinct from classic apoptosis (Figs. 2 and 3). The shape of the moribund cell is maintained until it disintegrates *in vivo*. It is generally thought that a necrotic cell is not dismantled orderly. The salient features are clumping of chromatin, swelling and

degeneration of organelles, destruction of membrane integrity, and dissolution of the cell. The nuclear pyknosis occurs as condensation of chromatin into many irregularly shaped, small clumps, sharply contrasting with the formation of few, uniformly dense and regularly shaped chromatin aggregates that occurs in apoptosis (compare Figs. 2 and 3). The nuclei of necrotic cells do not bud to form discrete, membrane-bound fragments, as in apoptosis. These differences in the condensation of nuclear chromatin in pure apoptosis and necrosis are very diagnostic. However, between these two extremes, the morphological variants of chromatin condensation are numerous (Fig. 4).

Although it is generally believed that cellular necrosis is a random destructive process, we have found that during cellular necrosis, organelles undergo distinctive structural changes that appear to be sequentially ordered rather than random (7,26). Ribosomes disassociate from the rough endoplasmic reticulum and polyribosomes disaggregate, resulting in many monomeric ribosomes that are found 'free' in the cytoplasm, causing the cytoplasmic matrix to appear dense and granular. The cisterns of the endoplasmic reticulum and Golgi apparatus dilate, fragment, and vesiculate, and the plasma membrane undergoes a process called blebbing. The mitochondria undergo sequential changes that include contraction or condensation of the inner membrane and dissipation of matrical granules (C phase), inner membrane swelling and cristaeolysis (S phase), formation of flocculent aggregates, and then disintegration (27). The molecular mechanisms for the changes in organelle structure that occur during necrotic cell death still have not been identified. Some of these organelle abnormalities are reversible, if homeostasis is restored early enough (28).

## 2. The cell death continuum

Wyllie proposed that apoptosis could be induced by injurious stimuli of lesser amplitude than insults causing necrosis (29). Cell culture toxicological studies have verified that stimulus intensity influences the mode of cell death (30,31), although the modes of cell death are still viewed as mechanistically distinct.

We have proposed that cell death occurs as an apoptosis-necrosis continuum. In this continuum, cell death occurs as hybrids ranging from apoptosis to necrosis (Figs. 4 and 5). We found that the death of neurons is not always strictly apoptosis or necrosis, according to a traditional binary classification of cell death. Neuronal death also occurs as intermediate or hybrid forms of cell death with coexisting characteristics (Fig. 5) that lie along a structural continuum with apoptosis and necrosis at the extremes (6,7).

It appears that the maturity of the brain and the subtype of glutamate receptor (GluR) that is activated influence cell death along this continuum (6,7). Hence, neuronal death induced by excitotoxicity is not the same in mature and immature brain and may not be identical in every neuron. Different survival and death signaling mechanisms (Fig. 6) may modulate neuronal death pathways depending on neuronal maturity (32). In addition, variations in neuronal death may arise from the high diversity in the expression, localization, and function of GluR subtypes and second messenger systems in the developing and mature CNS (33-38).

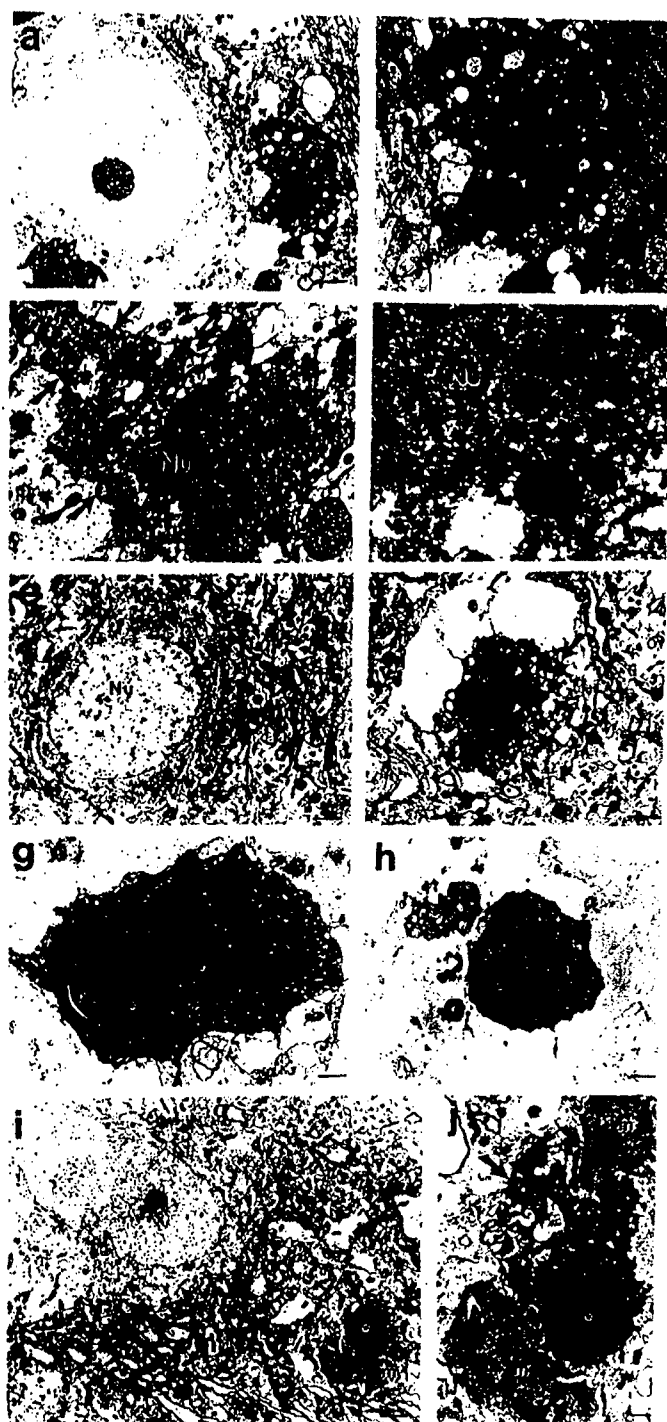


Figure 3. Neuronal death after cerebral ischemia ranges from apoptosis to necrosis. a and b, Striatal neuron death (black arrow in a; shown a higher magnification in b) after global ischemia in adult cat can occur as hybrids of apoptosis and necrosis (see Figs. 4 and 5 for hybrid forms of neuronal cell death). The chromatin condenses as large irregular clumps (white arrowheads) abutting the nuclear envelope. The cytoplasm is vacuolated and contains large swollen mitochondria and degenerating mitochondria. Scale bars, 3.5 (a) and 2 (b)  $\mu\text{m}$ . c and d, CA1 pyramidal neuronal death (black arrows in c; part of this neuron is shown at higher magnification in d) after global ischemia in adult cat is mostly necrosis (similar to NMDA receptor excitotoxicity). The typical ischemic CA1 pyramidal neuron has a nucleus (Nu) that undergoes chromatin condensation as many small, irregular clumps (asterisks) that are dispersed throughout the nucleus. The cytoplasm is severely vacuolated and fragmented. Scale bars, 0.5 (c) and 0.2 (d)  $\mu\text{m}$ . e, Normal striatal neuron (black arrows) in a 10-day-old piglet. The nucleus (Nu) is large and contains dispersed chromatin. Scale bar, 2  $\mu\text{m}$ . f, At 24 h after recovery from hypoxic-asphyxial cardiac arrest, the majority of neurons (black arrows) in putamen have undergone necrosis characteristic of NMDA receptor mediated excitotoxicity. Many small, irregular clumps of chromatin (small white arrowheads) are dispersed throughout the nucleus (Nu). The cytoplasm is severely vacuolated and fragmented. Scale bar, 6.25 (f)  $\mu\text{m}$ . g and h, Delayed degeneration of thalamic neurons after HI in newborn rat (7-day-old) is classical apoptosis. At 24-48 h after HI, neurons in the ventrobasal nuclear complex show nuclear (Nu) condensation, with the formation of uniformly, dense round chromatin aggregates (asterisks), and cytoplasmic condensation with the accumulation of numerous mitochondria. Later in the process of thalamic neuron apoptosis after ischemia, glial processes engulf nuclear fragments with round chromatin masses (asterisk, h) and cytoplasmic fragments. Scale bars, 3  $\mu\text{m}$ . i and j, Apoptosis occurs in thalamic neurons (black arrows) after ablation of the occipital cortex in adult rat. This neurodegeneration in the LGN occurs over 5-7 days and has the features of classical apoptosis, including nuclear packaging into uniformly dense, round chromatin masses (asterisks), cytoplasmic condensation and perforation by glia, and phagocytosis by microglia (m). Scale bars, 7  $\mu\text{m}$ .

The structure of the typical apoptosis-necrosis hybrid form of cell death has been revealed in different models of neurodegeneration. Excitotoxic brain injury is one model that reveals the death hybrid (Fig. 7). They are best seen with non-NMDA GluR receptor excitotoxicity (Fig. 7) in immature and mature rat brain (6-9) and with hypoxia-ischemia in neonatal rat (21,22). These hybrids can also be found in human neurodegenerative disease, notably amyotrophic lateral sclerosis (ALS). Apoptosis-necrosis hybrids also occur in mouse cortical neurons exposed to DNA-damaging agents *in vitro* (32). Hybrid cells undergo progressive compaction of chromatin into few, discrete, large, irregularly shaped clumps (Figs. 3a, b,

4 and 5). This morphology contrasts with the formation of few, uniformly shaped, dense, round masses in classic apoptosis and the formation of numerous, smaller, irregularly shaped chromatin clumps in classic necrosis. The cytoplasmic changes in hybrid cells generally appear more similar to necrosis than apoptosis, but differ in severity.

This new concept of an apoptosis-necrosis cell death continuum could be important for understanding neuronal degeneration in human neurological disorders and cell death in general, and thus may be important for the prevention of neuronal loss in human neurological disorders and the induction of desirable cell death in cancer. Much more work needs to be done. We need to identify the relationships between mechanisms of neuronal death and the structure of dying neurons in human neurodegenerative diseases as well as in animal and cell culture models of neurotoxicity, aging and disease. This is important particularly for addressing hypotheses as to whether PCD and apoptosis are equivalent and whether apoptosis and necrosis are mutually exclusive forms of cell death. Furthermore, if brain maturity dictates how neurons die, then, in humans, neuronal degeneration in adults may be

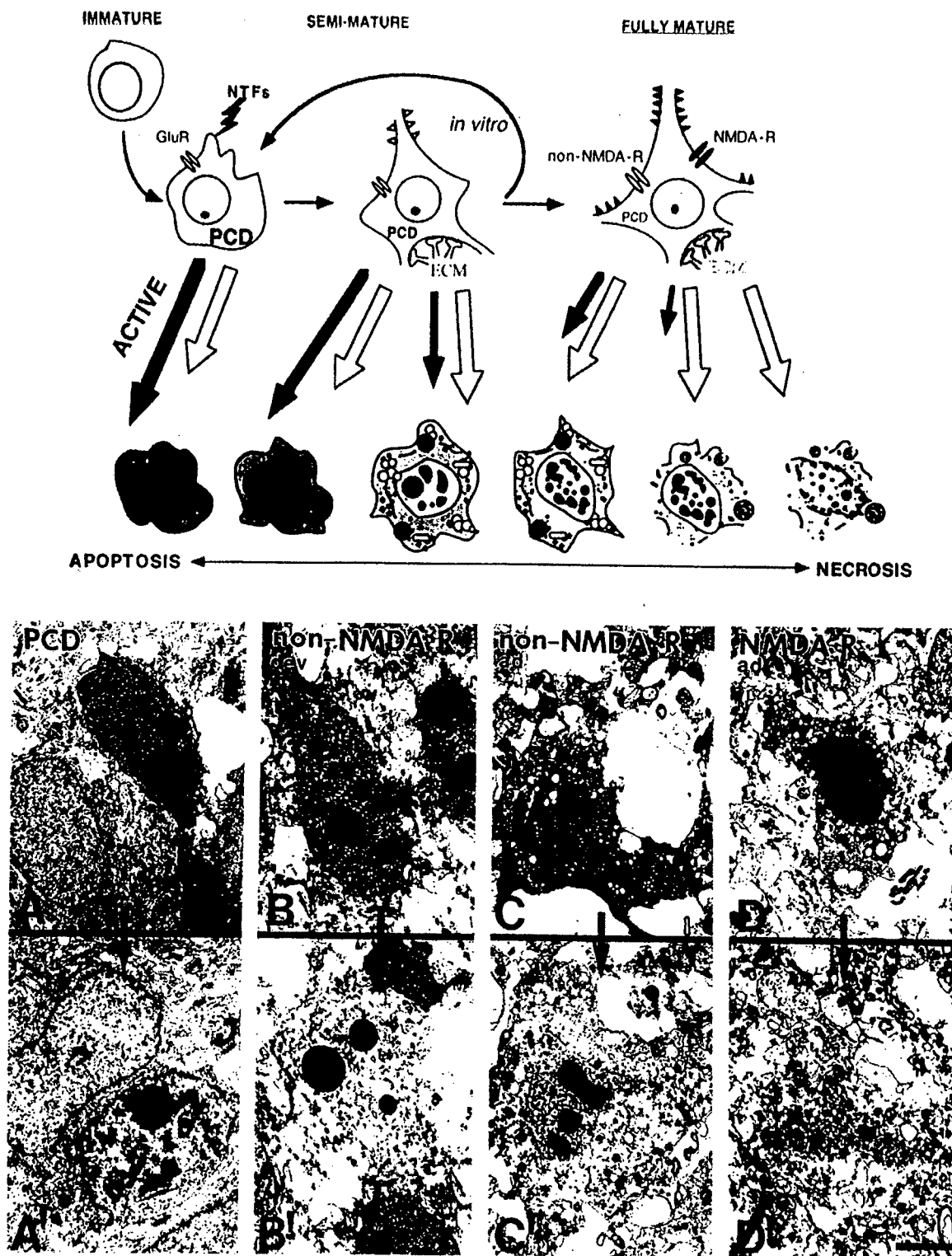


Figure 4. Neuronal cell death occurs as an apoptosis-necrosis continuum. Cartoon (upper panel) showing the potential relationships among naturally occurring programmed cell death (PCD) and induced neuronal cell death, as mediated by differential contributions of active mechanisms (black arrows) and passive mechanisms (open arrows) along the apoptosis-necrosis continuum. This cell death continuum for neuronal degeneration is influenced by the degree of neuronal maturity and the subtype of GluR that is activated, as well as possibly other factors, including cell type and the composition of the cytoskeleton and extracellular matrix (ECM). The sizes of the arrows vary according to the relative contributions of the different mechanisms. Neurons in the developing CNS at immature and semi-mature states undergo PCD in response to neurotrophin (NTF) deprivation, and GluR activation. Semi-mature neurons that are removed from the developing brain are prone to undergo apoptosis when used for *in vitro* manipulations. Excitotoxic neuronal death induced by NMDA receptor (NMDA-R) and non-NMDA GluR (non-NMDA-R) in the developing brain can resemble classic apoptosis, classic necrosis, and hybrid forms of cell death. However, in the fully mature adult CNS, excitotoxic cell death can resemble classic necrosis (NMDA receptor toxicity) or a hybrid of apoptosis-necrosis (non-NMDA receptor toxicity), with primarily passive mechanisms operating in the former and a combination of passive and active mechanisms operating in the latter. Depending on the neuronal groups, axotomy and target deprivation in the adult CNS can cause neuronal injury (atrophy but not death) with necrotic-like features or neuronal death that resembles apoptosis. Lower panel, electron micrographs of striatal neurons at relatively 'early' (A, B, C, D) and 'late' (A', B', C', D') stages of degeneration. Developmental PCD of neurons in postnatal day 8 striatum is a 'gold standard' for neuronal apoptosis (A, A'). Non-NMDA GluR excitotoxicity induces apoptosis in developing (dev) rat striatum (B, B'). Non-NMDA GluR excitotoxicity induces apoptosis-necrosis hybrids in adult (ad) rat striatum (C, C'). NMDA receptor excitotoxicity induces necrosis in adult (ad) rat striatum (D, D'). A continuous spectrum of cell death morphologies can be identified ranging from classical apoptosis (A) to classical necrosis (D). Scale bars = 10  $\mu$ m.

## DEVELOPMENT

## APOPTOSIS

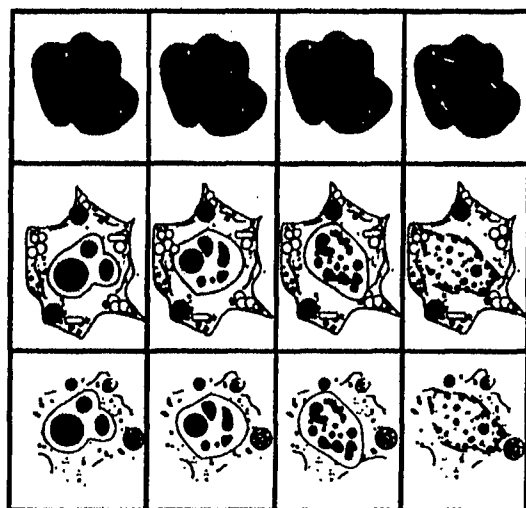
NECROSIS  
ADULT

Figure 5. Diagram summarizing the concept of the apoptosis-necrosis continuum of neuronal cell death. This concept may also be relevant to cell death in general. This matrix shows the numerous possible morphologies of neurons during cell death near or at the terminal stages of degeneration. Combining different nuclear morphologies and cytoplasmic morphologies depicts a two-dimensional, non-linear spectrum or gradient of possible degenerative morphologies. The influences of neuronal maturity and glutamate receptor subtype correspond to the diagonal axis of the apoptosis-necrosis continuum. In the extreme upper left cell, nuclear and cytoplasmic morphologies combine to form a classical apoptotic neuron that is typical of naturally occurring PCD during nervous system development. In contrast, in the extreme lower right cell, the merging of necrotic nuclear and necrotic cytoplasmic morphologies forms a typical necrotic neuron resulting from NMDA receptor excitotoxicity and cerebral ischemia. Between these two extremes hybrids of cell death can be produced with varying contributions of apoptosis and necrosis. We have never found neurons degenerating with a necrotic nucleus surrounded by an apoptotic cytoplasm (upper right cell). The typical apoptosis-necrosis hybrid morphology is best exemplified by neurons in the adult CNS dying from non-NMDA GluR-mediated excitotoxicity. Other apoptosis-necrosis hybrid forms of neuronal cell death occur after cerebral ischemia and in chronic neurodegenerative disease such as ALS.

fundamentally different from neuronal degeneration in infants and children. This suspicion is supported by experiments showing that apoptosis mechanisms are different in immature neurons compared to mature neurons (32).

### 3. Molecular control of apoptosis

Apoptosis is cell death that is organized. An orderly dismantling of a cell requires active, intrinsic mechanisms. Horvitz and colleagues using the nematode *Caenorhabditis elegans* have pioneered the understanding of the genetic control of developmental cell death, with this death being regulated predominantly by three genes (*ced-3*, *ced-4*, and *ced-9*) which have mammalian homologues. Several families of genes that regulate apoptosis have been identified in mammals (Table I): the Bcl-2 family (39); the caspase family of cysteine-containing, aspartate-specific proteases (40); the inhibitor of

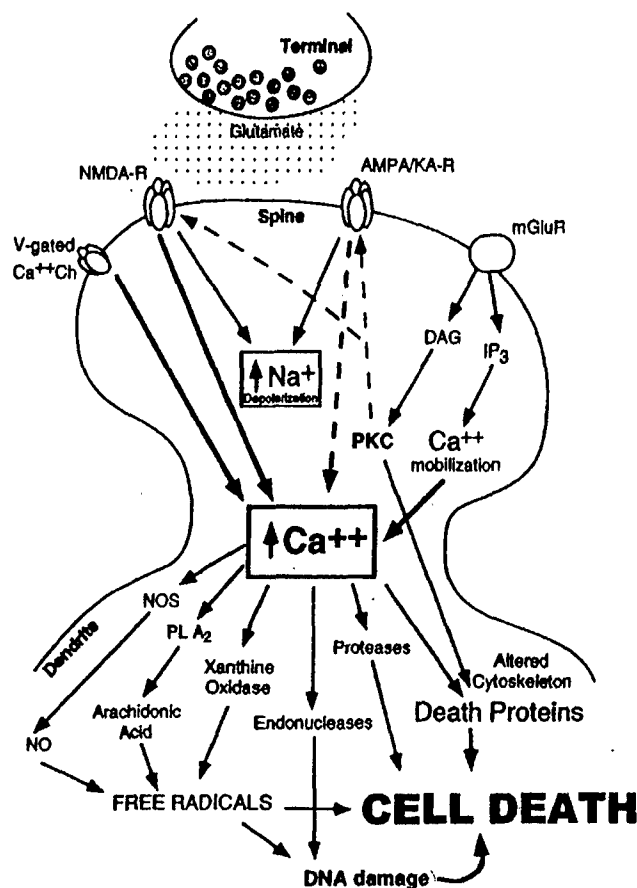


Figure 6. Summary diagram of signal transduction mechanisms related to excitotoxic neuronal death. The diagram summarizes the prominent post-synaptic intracellular pathways that lead to neuronal injury and death resulting from excitotoxic activation of GluR. AMPA/KA-R,  $\alpha$ -amino-3-hydroxy-5-methyl-4-isoxazole propionate and kainate receptors; DAG, diacylglycerol; IP<sub>3</sub>, inositol trisphosphate; mGluR, metabotropic glutamate receptor; NMDA-R, *N*-methyl-*D*-aspartate receptor; NO, nitric oxide; NOS, NO synthase; PKC, protein kinase C; PLA<sub>2</sub>, phospholipase A<sub>2</sub>; V-gated Ca<sup>2+</sup> Ch, voltage-gated Ca<sup>2+</sup> channel.

apoptosis protein (IAP) family (41); and the p53 gene family (42,43).

**Bcl-2 family of proapoptotic and antiapoptotic proteins.** The *bcl-2* proto-oncogene family is a group of apoptosis regulatory genes encoding for proteins defined by homology domains (BH1-BH4) that function in the protein-protein interaction (39). Steady-state protein-protein interactions among members of the Bcl-2 family influence cellular survival and death. Bcl-2, Bcl-x<sub>L</sub>, and Boo are antiapoptotic; while Bax, Bcl-x<sub>s</sub>, Bad, Bak, Bid, Bik, Bim, and Mtd (called matador) are proapoptotic (Table I). Bcl-2 is localized in the outer mitochondrial membrane, the endoplasmic reticulum, and the nuclear membrane (44). Bcl-2 family members may function by conformation-induced insertion into the outer mitochondrial membrane to form channels or pores, because Bcl-x<sub>L</sub> possesses structural similarities to the pore-forming subunit of diphtheria toxin (45). Bcl-2 family members can form homodimers with themselves or heterodimers and higher order multimers with other family members. For example, Bax forms homodimers or heterodimers with either Bcl-2 or Bcl-x<sub>L</sub>. When Bax and

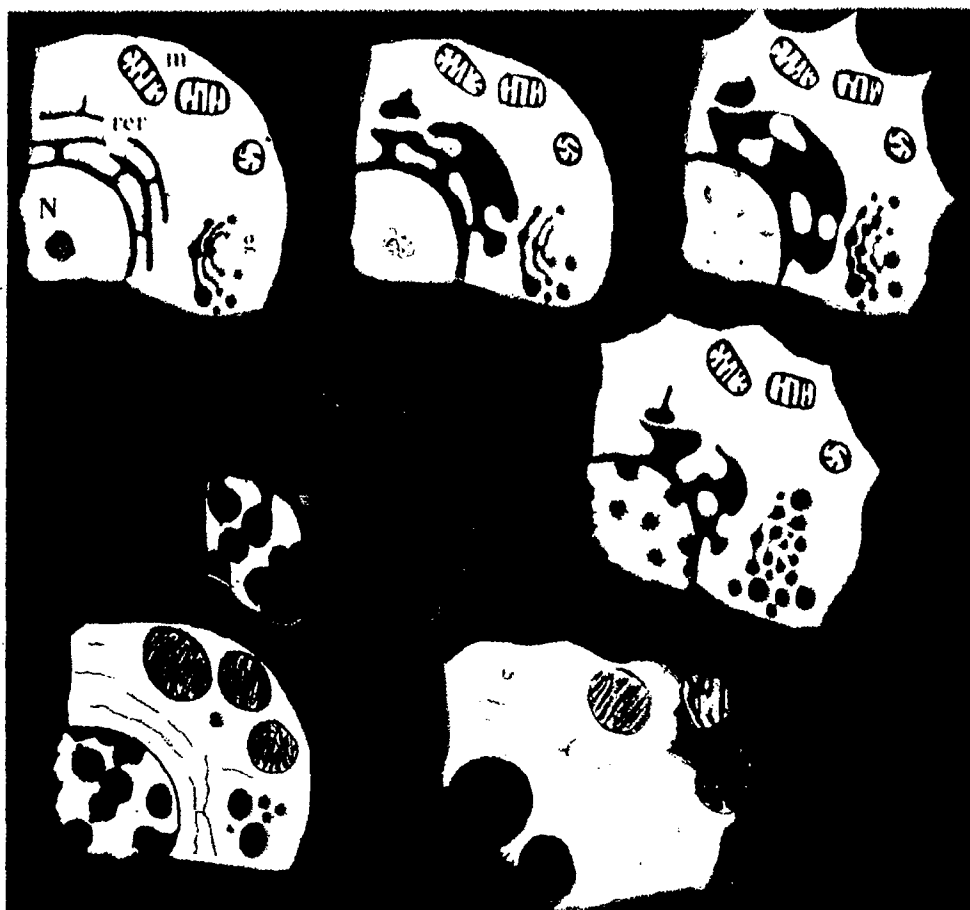


Figure 7. Diagram of organelle changes that occur during neuronal apoptosis induced by GluR excitotoxicity. The proposed succession of subcellular alterations is illustrated in a single representative neuron starting in a normal state (upper left image) and terminating in apoptosis (lower right image). A highly ordered progression of organelle damage occurs during excitotoxic neuronal apoptosis *in vivo* that sequentially involves the rough endoplasmic reticulum (ret), the Golgi apparatus (Golgi), and mitochondria (m) and nucleus (N). Excitotoxic neuronal apoptosis evolves as four sequential stages: endoplasmic reticulum stress (phase 1), Golgi apparatus stress (phase 2), mitochondrial stress and nuclear condensation (phase 3), and plasma membrane breach and phagocytosis stage (phase 4). During phase 1, the endoplasmic reticulum dilates and collapses (small double arrows) and ribosomes dissociate. During phase 2, the Golgi apparatus fragments, liberating numerous vacuoles (v). During phase 3, mitochondria swell and chromatin condensation mechanisms are activated.

Bak are present in excess, the antiapoptotic activity of Bcl-2 is antagonized. The formation of Bax homodimers promotes apoptosis, whereas Bax heterodimerization with either Bcl-2 or Bcl-x<sub>L</sub> prevents apoptosis. Some Bcl-2 members interact with other types of proteins that are non-Bcl-2 members (e.g., Raf-1). Some proapoptotic proteins such as Mtd function independently of heterodimerization with survival promoting Bcl-2 and Bcl-x<sub>L</sub> (46).

**Caspase family of cell death enzymes.** Caspases (cysteiny aspartate-specific proteinases) are cysteine proteases that have a near absolute requirement for aspartic acid in the P<sub>1</sub> position. Fourteen members have been identified so far (40). Caspases exist as constitutively expressed proenzymes (30–50 kDa) in healthy cells. The protein contains three domains, an amino-terminal prodomain, a large subunit (~20 kDa), and a small subunit (~10 kDa). Caspases are activated by regulated proteolysis of proenzyme, although some caspase proenzymes (e.g., caspase-9) have low activity without processing (47). ‘Initiator’ caspases activate ‘executioner’ caspases (Table I). Other caspase family members function in inflammation by processing pro-inflammatory cytokines

(Table I). Activation of caspases involves proteolytic processing between domains, and then association of large and small subunits to form a heterodimer, with two heterodimers associating to form a tetramer that has two independently functioning catalytic sites. Active caspases have numerous target proteins (48). Caspases cleave nuclear proteins [e.g., polyADP-ribose polymerase (PARP), DNA-dependent protein kinase, heteronuclear ribonucleoproteins, transcription factors or lamins], cytoskeletal proteins (e.g., actin and fodrin), and cytosolic proteins (e.g., other caspases, protein kinases, Bid, and DNases).

Different caspase cascades, not necessarily exclusive, mediate apoptosis. One pathway involves cytochrome c release from mitochondria, promoting the activation of caspase-9 through Apaf-1 and then caspase-3 activation (49). Another pathway involves the activation of cell-surface death receptors, including Fas and tumor necrosis factor receptor, leading to caspase-8 activation that in turn cleaves and activates downstream caspases such as caspase-3, -6, and -7 (50,51).

**Inhibitor of apoptosis protein (IAP) family.** To prevent unwanted apoptosis in normal cells, the activity of proapoptotic

proteins must be neutralized. In addition to using Bcl-2, Bcl-x<sub>L</sub> and Boo, cells actively antagonize death with the IAP family (41,52). This family includes X chromosome-linked IAP, IAP1, IAP2, and NAIP (neuronal apoptosis inhibitory protein). Survival motor neuron, a protein that is mutant in infants with spinal muscular atrophy, is another apoptosis inhibitory protein. An identified function of IAPs is suppression of proteolytic processing of caspases (53). Procaspase-9 is a major target of IAPs. However, IAPs do not prevent caspase-8-induced proteolytic processing of procaspase-3. IAPs also block apoptosis by reciprocal interactions with the transcription factor NF $\kappa$ B (52). Proteins exist that inhibit mammalian IAPs. A mitochondrial protein called Smac (for second mitochondria-derived activator of caspases) or DIABLO (for direct IAP-binding protein with low pI) inactivate the anti-apoptotic actions of IAPs (54,55).

#### 4. Apoptosis is regulated cell death

Caspase-3 activation is believed to be a major commitment step for apoptosis. In cell culture models of apoptosis, caspase-3 activation occurs when caspase-9 proenzyme (Apaf-3) is bound by Apaf-1 in a process initiated by cytochrome c (also known as Apaf-2) and either ATP or dATP (49,56). Cytosolic ATP or dATP are required cofactors for cytochrome c-induced caspase activation. Apaf-1, a protein homologous to ced-4, is a docking protein for procaspase-9 (Apaf-3) and cytochrome c (49). Apaf-1 is activated by ATP binding and hydrolysis. ATP hydrolysis and cytochrome c binding promote Apaf-1 oligomerization (57). The oligomeric complex recruits and activates procaspase-9. Caspase-9 then disassociates from the complex and activates caspase-3. IAPs act to block apoptosis at this caspase-9 initiation event (53). Activated caspase-3 then negatively or positively modifies several proteins by cleavage. Caspase-3 inactivates the DNA repair enzyme PARP (58), and it activates a DNA fragmentation factor (DFF) with DNase activity that mediates regulated fragmentation of genomic DNA and chromatin condensation (59,60). DFF is a heterodimeric protein composed of 45 kDa (DFF45) and 40 kDa (DFF40) subunits. DFF45 is a chaperone protein that inhibits the nuclease activity of DFF40. Cleavage of DFF45 by caspase-3 inactivates the inhibitory action on DFF40, allowing DFF40 to oligomerize and cleave DNA by introducing double-strand breaks (61).

The regulated release of initiation factors from mitochondrion is a key event in apoptosis. It is believed that early during apoptosis, cytochrome c is liberated into the cytosol from mitochondria (62,63). A flavoprotein that shares homology with bacterial oxidoreductases, called apoptosis-inducing factor (AIF), is also released from the mitochondrial intermembrane space and is translocated to the nucleus (64). Release of apoptogenic proteins may occur through mechanisms that involve the formation of membrane channels comprised of Bax (65), Bax and the adenine nucleotide translocator (66), and the voltage dependent anion channel (67). The voltage dependent anion channel protein is a subunit of the mitochondrial permeability transition pore. This pore is a large channel that, when open, causes rapid loss of mitochondrial membrane potential and mitochondrial swelling. Bcl-2 and Bcl-x<sub>L</sub> block the release of cytochrome c and AIF

(62-64) from mitochondria and thus the activation of caspase-3 (49,56). The blockade of cytochrome c release from mitochondria by Bcl-2 and Bcl-x<sub>L</sub> (56,68) is caused by inhibition of Bax channel-forming activity in the outer mitochondrial membrane (65) or by modulation mitochondrial membrane potential and volume homeostasis (68). Bcl-x<sub>L</sub> also has anti-apoptotic activity by interacting with Apaf-1 and caspase-9 and inhibiting the Apaf-1-mediated maturation of caspase-9 (69). Boo can inhibit Bak- and Bik-induced apoptosis (but not Bax-induced cell death) possibly through heterodimerization and by interactions with Apaf-1 and caspase-9 (70).

#### 5. Death proteins can be regulated by phosphorylation

Apoptosis-regulatory proteins undergo posttranslational modification that modulates their function. Bcl-2 family members and caspase-9 are regulated by protein phosphorylation. Serine phosphorylation of Bcl-2 inactivates its anti-apoptotic activity (71). In addition to interacting with homologous proteins, Bcl-2 can associate with non-homologous proteins, including the protein kinase Raf-1 (72). Bcl-2 targets Raf-1 to mitochondrial membranes, allowing this kinase to phosphorylate Bad at serine residues. The phosphatidylinositol 3-kinase (PI3-K) -Akt pathway also regulates the function of Bad (73,74) and caspase-9 (75) through phosphorylation. In the presence of trophic factors, Bad is phosphorylated. Phosphorylated Bad translocates to the cytosol and interacts with soluble protein 14-3-3 and, when bound to protein 14-3-3, Bad is unable to interact with Bcl-2 and Bcl-x<sub>L</sub>, thereby promoting survival (76). Conversely, when Bad is dephosphorylated by calcineurin, it dissociates from protein 14-3-3 in the cytosol and translocates to the mitochondria, thereby engaging proapoptotic activity. Non-phosphorylated Bad heterodimerizes with membrane-associated Bcl-2 and Bcl-x<sub>L</sub>, thereby displacing Bax from Bax-Bcl-2 and Bax-Bcl-x<sub>L</sub> dimers and promoting cell death (77).

#### 6. Death receptors can mediate apoptosis

Cell death by apoptosis can also be initiated at the cell membrane by surface receptors that function as death receptors (15,50). The tumor necrosis factor (TNF) receptor family functions as death receptors. Fas (CD95/Apo-1) and p75 (low-affinity NGF receptor) are family members. Fas-mediated apoptosis is independent of new RNA or protein synthesis. Apoptosis is initiated at the cell surface by aggregation (trimerization) of Fas. The activation of Fas is induced by the binding of the multivalent Fas ligand (FasL), a member of the TNF-cytokine family. FasL is expressed on activated T cells and natural killer cells. Clustering of Fas by FasL recruits Fas-associated death domain (FADD), a cytoplasmic adapter molecule that functions in the activation of the caspase 8-Bid pathway, thus forming the 'death-induced signaling complex' (DISC) (51). In this pathway, Bid (a proapoptotic family member that is a substrate for caspase-8) is cleaved in the cytosol, and then truncated Bid translocates to mitochondria, thereby functioning as a transducer of Fas apoptotic signals at the cell plasma membrane to mitochondria (51). Bid translocation from the cytosol to mitochondrial membranes is

associated with a conformational change in Bax (that is prevented by Bcl-2 and Bcl-x<sub>L</sub>) and is accompanied by release of cytochrome c from mitochondria (78).

## 7. Tumor suppressor proteins mediate apoptosis

The oncosuppressor protein p53 induces apoptosis (42,43,79). The p53 gene mutated in about half of all human cancers. Loss of p53 function results in neoplasm because normal apoptosis fails. The identification of two homologues, p63 and p73, places p53 in family of related DNA binding proteins (43). These proteins function in genome surveillance, DNA repair, and as transcription factors. p53 functions in growth arrest and/or apoptosis. p53 commits to death cells that have sustained DNA damage from free radicals, irradiation, and other genotoxic agents. p53 rapidly accumulates in response to DNA damage. This rapid regulation is mediated by post-translational modification such as phosphorylation and acetylation.

The mechanisms by which p53 induces apoptosis are not fully understood. Promoters that respond to p53 include genes encoding proteins associated with growth control and cell cycle checkpoints (e.g., p21<sup>Waf1/Cip1</sup>, Gadd45, Mdm2, PCNA, cyclin D1, and cyclin G) and apoptosis (e.g., Bax, Bcl-2, Bcl-x<sub>L</sub>, and Fas). p53 is a direct transcriptional activator of the human *bax* gene (80) and a transcriptional repressor of the *bcl-2* gene (81). p53 also activates the transcription of redox-related genes (42). Bcl-2 can function as an antiapoptotic protein by inhibiting nuclear import of p53 after DNA damage (82). The carboxyl terminus of p53 is important for controlling p53-DNA-binding functions in response to single strands of DNA (83).

## 8. Naturally-occurring PCD occurs in the developing nervous system

The concept of neurodegeneration occurring normally as PCD in the developing nervous system (Figs. 1 and 2) was a novel idea (2,12). PCD is important for the matching of neuronal population size to target size, and it is thought to be controlled largely by a limiting supply of target-derived trophic factors (84) and by afferent synaptic activity (85,86).

As anticipated from the work of Horvitz and others in nematodes, cell death proteins control developmental PCD in the mammalian nervous system. The numbers of neurons may be increased (presumably resulting from deficient apoptosis) in some CNS regions in transgenic mice that overexpress the *bcl-2* gene (87-89), mice with *bax* gene-inactivation (90), and mice with gene deletions in caspase-3 (91), caspase-9 (92,93), and Apaf-1 (94). Homozygous deficiency in caspase-3, caspase-9, and Apaf-1 are embryonic lethal and cause cerebral malformations. Bax, Bcl-2, and p53 homozygous deficient mice all survive to adulthood, but Bcl-2-deficient mice show progressive degeneration of motor neurons after the PCD period during early postnatal development (95).

## 9. Signaling pathways modulate neuronal survival

Cell survival signaling is the counterpart to cell death signaling. Neurotrophins act as target- or afferent-derived growth

factors for specific populations of neurons and exert survival-promoting effects on immature and adult neurons. In the traditional neurotrophin concept, neurotrophins function by binding to specific high-affinity tyrosine kinase receptors on the presynaptic terminal, followed by internalization, and then retrograde transport of the neurotrophin-receptor complex to the neuronal cell body where it regulates neuronal differentiation and survival.

Links between cell survival signaling through neurotrophins and cell death signaling are beginning to be found. For example, survival effects of nerve growth factor on sympathetic neurons are mediated by Ras (96). Ras proteins are GDP/GTP-regulated switches that interact with exchange proteins that facilitate cycling between an active GTP-bound state and an inactive GDP-bound state. Extracellular signal regulated kinases (ERK1 and ERK2) regulate the exchange factors. In neurons, Ras suppresses the levels or activities of c-jun, p53 and Bax through PI3-K and ERK (96). Insulin-like growth factor-I acts through similar kinases that inactivate caspase-9 and Bad by phosphorylation (97).

## 10. Neuronal cell death in disorders of the human CNS

Neuronal degeneration causes many neurological disorders that effect humans. Chronic neurodegeneration occurs in Alzheimer's disease (AD), ALS, Parkinson's disease, and Huntington's disease. Acute neurodegeneration results from trauma, hypoxia-ischemia (stroke and cardiac arrest), neurotoxins, radiation, and seizures. It has been theorized only recently that an abnormal activation of apoptosis in neurons may play a role in the disease process in humans with neurological injury. For postmitotic cells, apoptosis has irreplaceable consequences. However, much more work is necessary to accurately assess the contribution of apoptosis to the neurodegeneration in chronic and acute neuropathological disorders. Deciphering the contributions of the different types of cell death in neurological diseases of the human CNS will advance the understanding of disease mechanisms.

*Motor neuron degeneration in ALS may occur by DNA damage-induced, p53-mediated apoptosis.* ALS is characterized clinically by progressive weakness, muscle atrophy, and eventual paralysis and death within 3 to 5 years of clinical onset. It is one of the most common neurodegenerative diseases with an adult onset. The incidence of ALS is 1-2 per 100,000 individuals. ALS is neuropathologically characterized by progressive degeneration of upper and lower motor neurons in the brain and spinal cord. The loss of motor neurons in spinal cord, brainstem, and motor cortex is the cause of ALS (Figs. 8 and 9).

Aberrantly occurring apoptosis may be the cause of motor neuron loss in ALS (23,98). Motor neurons undergo DNA fragmentation and are eliminated with minimal inflammatory changes (Figs. 8 and 9). In postmortem samples of ALS motor cortex and spinal cord, Bax and Bak protein levels are increased and Bcl-2 protein levels are decreased in mitochondrial enriched fractions. Coimmunoprecipitation experiments demonstrate that Bax-Bax interactions are greater in the mitochondrial-enriched membrane compartment of ALS motor cortex compared to controls, whereas Bax-Bcl-2 interactions



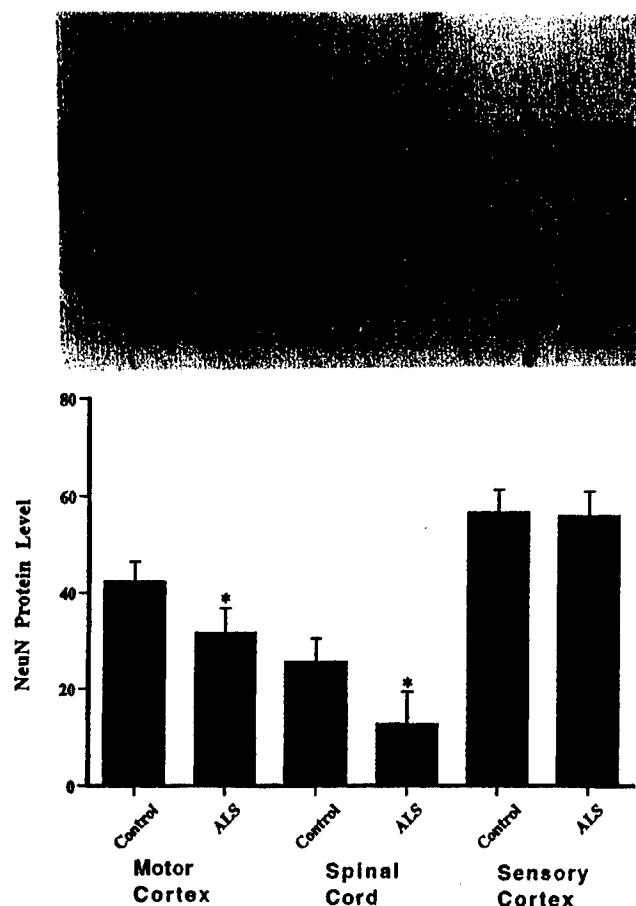


Figure 8. Motor neurons are lost in patients with ALS. In normal control individuals (upper panel, left), the anterior horns of the spinal cord are populated with many large, multipolar motor neurons (arrows). In ALS spinal cord (upper panel, right), the anterior horns are depleted of large multipolar motor neurons, and remaining motor neurons are condensed and shrunken (arrows). Scale bar, 200  $\mu$ m. Measurements of the levels of a neuron specific marker NeuN (a mammalian neuron nuclear protein) by immunoblotting show that NeuN is significantly reduced (asterisk  $p < 0.05$ ) in ALS motor cortex and spinal cord anterior horn but not in sensory cortex.

are decreased in the membrane compartment of ALS motor cortex compared to controls. Bax translocation to mitochondria (99) and Bax-dependent caspase-3 activation (100) are critical events for neuronal PCD apoptosis in *in vitro* systems. In ALS, we have found that caspase-3 activity is elevated, DFF45 is activated, and internucleosomal fragmentation of DNA occurs. Therefore, an inappropriate re-emergence of a PCD mechanism, involving cytosol-to-membrane and membrane-to-cytosol redistributions of cell death proteins, participates in the pathogenesis of motor neuron degeneration ALS (23,98).

p53 may participate in the mechanisms of motor neuron apoptosis in ALS (Figs. 10 and 11). Motor neurons in individuals with ALS sustain DNA damage (Fig. 10B, C and E). Other groups have found DNA damage in individuals with ALS (101). This damage may be caused by free radical attack (102,103) and defective DNA repair (104,105). We have found direct evidence (Fig. 10B, C and E) for DNA lesions specifically in motor neurons of individuals with ALS (24). This finding is important because DNA damage is a potent signal for apoptosis. The accumulation of DNA damage in motor neurons could be a possible cause of motor neuron apoptosis in ALS. p53 levels increase in vulnerable regions in individuals ALS (Fig. 11) (24,25). p53 accumulates in motor neurons in patients with ALS (Fig. 10A and C-E). This p53 is functionally active because it is phosphorylated (Fig. 10F). Neurons that accumulate DNA damage show activated p53 (Fig. 10E). The accumulation of DNA damage in motor neurons is thus a possible upstream pathogenic mechanism in ALS.

It is important to understand mechanisms of DNA damage in motor neurons. Mutations have been identified in the gene

for superoxide dismutase-1 (SOD1) in a small subset of individuals with familial ALS (106,107). Thus, inherited mechanisms for DNA damage may involve mutant SOD1 and nitric oxide (NO)-mediated toxicity via peroxynitrite (108). Mutant SOD1 may acquire a neurotoxic gain in function, converting this enzyme from a protein with antioxidant-antiapoptotic functions to a protein with apoptosis-promoting effects (109). SOD1 also has peroxidase activity, and this peroxidase activity is enhanced in mutant SOD1 compared to normal SOD1 (110). This gain-of-function augments the production of hydroxyl and superoxide radicals, and possibly the formation of peroxynitrite by the combination of superoxide and NO (108,110). These altered properties of mutant SOD1 have not yet been causally linked specifically to motor neuron damage in ALS. However, DNA damage from hydroxyl radicals (24,103) and protein damage from peroxynitrite (111,112) have been found in cases of ALS. Direct oxidation of nucleosides by peroxynitrite may not be a major pathway (113). A more likely pathway for the oxidation of nucleosides is through hydroxyl radicals formed by the transitional metal (iron)-catalyzed, Haber-Weiss and Fenton-type reactions (114). This DNA damage may be related to abnormal accumulation of mitochondria in motor neurons, possibly resulting from impaired axonal transport (115) and target deprivation (116). These possible mechanisms become more plausible in light of recent findings in our laboratory with animal models.

Induced apoptosis of motor neurons is associated with accumulation of mitochondria, peroxynitrite formation and hydroxyl radical damage to DNA (116) and p53 accumulation (117). We have used single-cell gel electrophoresis (comet



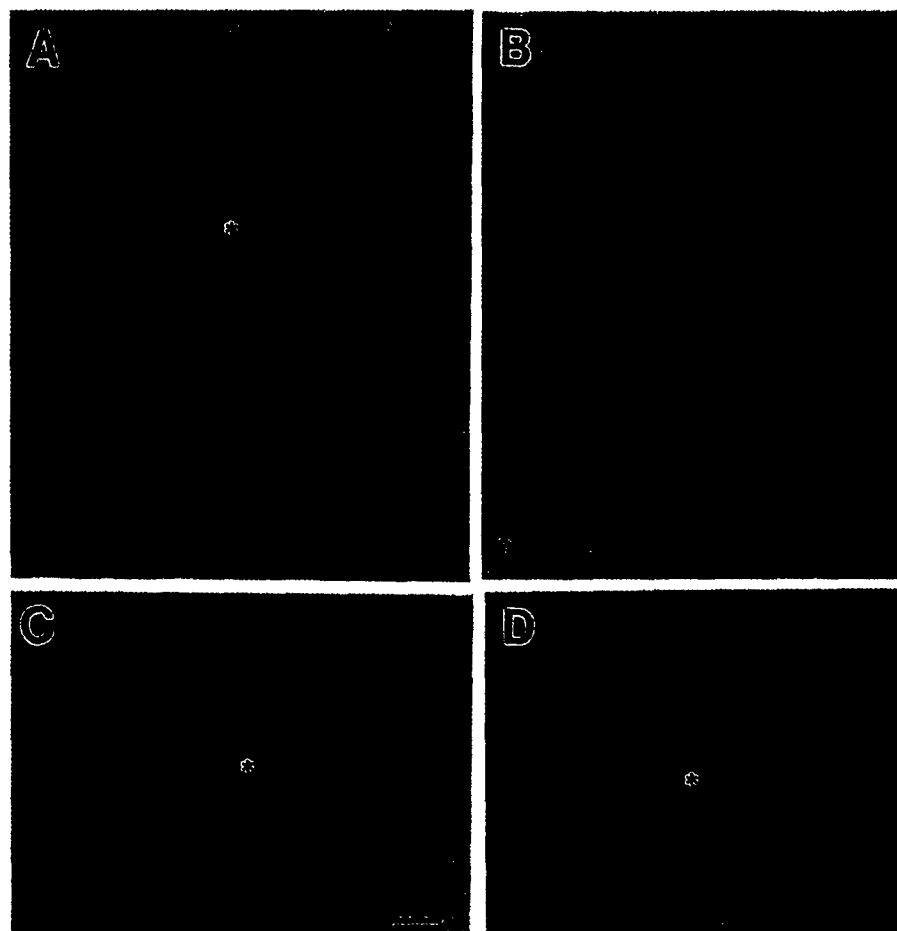


Figure 9. Motor neuron degeneration in ALS is a form of apoptosis. A, Normal appearing spinal motor neuron with a large, multipolar cell body and a large nucleus (asterisk) containing reticular network of chromatin and a large nucleolus. Scale bar, 7  $\mu$ m (same for B). B, Near endstage apoptotic motor neuron in ALS (arrow). The cell has shrunk to about 10% of normal size and has become highly condensed. C and D, Nuclear DNA fragmentation (asterisk, brown labeling) occurs in motor neurons in patients with ALS as the nucleus condenses (asterisks) and the cell shrinks. Scale bar (C), 7  $\mu$ m (same for D).

assay) to detect DNA-SSB in motor neurons (118). Exposure of motor neurons to NO donors,  $H_2O_2$ , and NO donor plus  $H_2O_2$  induces rapidly DNA-SSB and causes motor neuron degeneration. Peroxynitrite causes DNA-SSB in motor neurons. DNA-SSB accumulate slowly in injured motor neurons prior to apoptosis and the comet fingerprint is similar to NO toxicity. Thus, motor neurons challenged by oxidative stress and axotomy accumulate DNA-SSB early in their degeneration. The formation of peroxynitrite appears to be involved in the mechanisms of DNA damage upstream to p53 mediated apoptosis of motor neurons.

*The contribution of apoptosis to Alzheimer's disease is unresolved.* AD causes profound degeneration cerebral cortex and loss of neurons in neocortex and hippocampus (119-121). AD is the most common type of dementia occurring in middle and late life, affecting 7-10% of individuals >65 years of age and possibly 40% of people >80 years of age (122). The prevalence of AD is increasing proportionally to increased life expectancy (estimates predict that ~25% of the population will be >65 years of age in the year 2050). In the United States, AD now affects >4 million people (123).

AD occurs in different forms. Most cases of AD have unknown etiologies and are called sporadic. A small percentage

of AD cases, particularly those with early onset, are familial and are inherited. The disease is autosomal dominant linked to mutations in the genes encoding amyloid precursor protein (APP) (124-126) or presenilin proteins (127,128). For late onset sporadic cases, a variety of risk factors have been identified in addition to old age. The apolipoprotein E (apoE) allele is a susceptibility locus with the apoE4 type showing dose-dependent contributions (129). Cardiovascular disease and head trauma are additional risk factors for AD (122). The formulation of effective therapeutic strategies for the treatment of AD rests on the clarification of the mechanisms of neuronal death in this disease.

The mechanisms that cause the profound degeneration of cortical neurons in AD are not known. Arguments have been presented suggesting that AD-related neurodegeneration is apoptosis (130) and is not apoptosis (131,132). Among many others, the possible mechanisms for neuronal death in AD may involve presynaptic afferent defects (133,134), postsynaptic NMDA receptor abnormalities (135), and altered processing of APP and presenilin proteins. APP is the source of amyloid- $\beta$  protein (A $\beta$ ). The amyloid hypothesis of AD is based on the premise that generation of A $\beta$  by cleavage of APP is a critical pathogenic mechanism. Overexpression and intracellular accumulation of APP activates caspase-3 (136). APP is a

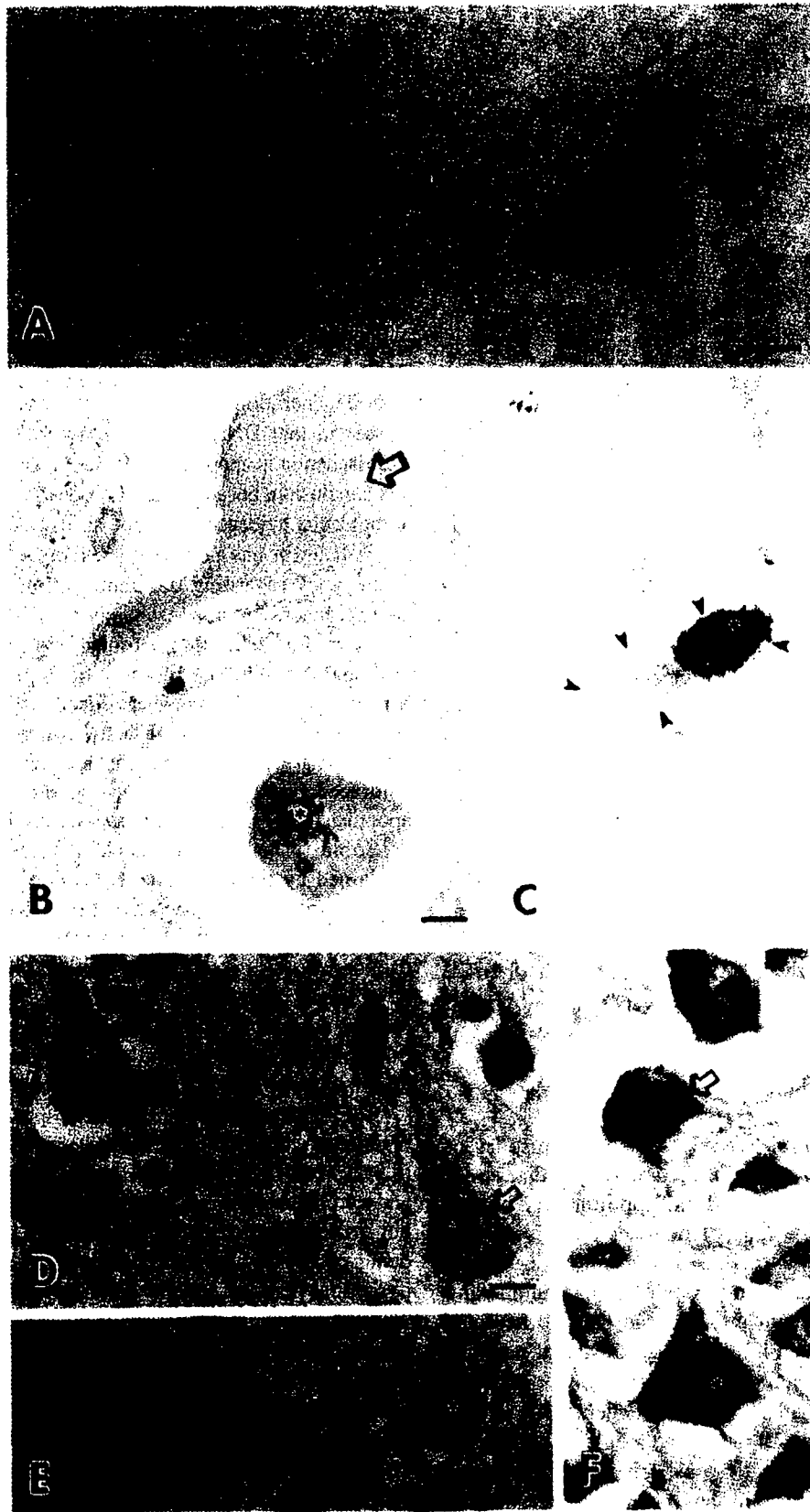


**Figure 10.** Motor neuron apoptosis in ALS may occur by a DNA damage-induced, p53-mediated mechanism. **A,** In individuals with ALS, p53 accumulates in the nucleus (asterisk, brown labeling) of spinal motor neurons. Nearby neuron (open arrow) has an unlabeled nucleus for comparison. Scale bar, 10  $\mu$ m. **B,** Nuclear DNA damage (asterisk, green crystalline labeling) accumulates in motor neurons in ALS spinal cord. DNA damage was detected with antibodies to 8-hydroxy-2-deoxyguanosine. Nearby motor neuron (open arrow) is unlabeled. Scale bar, 10  $\mu$ m (same for C). **C,** Motor neurons in ALS spinal cord with genomic DNA damage accumulate nuclear p53 (asterisk). A motor neuron is delineated with small black arrowheads. The green crystalline labeling against brown p53 immunoreactivity reveals DNA damage in the nucleus. **D,** p53 also accumulates in the nucleus (asterisk, brown labeling) of pyramidal neurons in ALS motor cortex. Nearby pyramidal cortical neuron (open arrow) has an unlabeled nucleus for comparison. Scale bar, 10  $\mu$ m. **E,** Motor neurons in ALS motor cortex with genomic DNA damage accumulate nuclear p53 (asterisk). The green crystalline labeling against brown p53 immunoreactivity shows DNA damage in the nucleus. Nearby pyramidal neuron (open arrow) exhibits DNA damage (green crystalline labeling) but no p53 immunoreactivity. **F,** Active (phosphorylated) p53 accumulates in the nucleus of ALS motor neurons (asterisk, brown labeling) as detected with phospho-p53 antibodies. Nearby pyramidal neuron (open arrow) is not labeled.

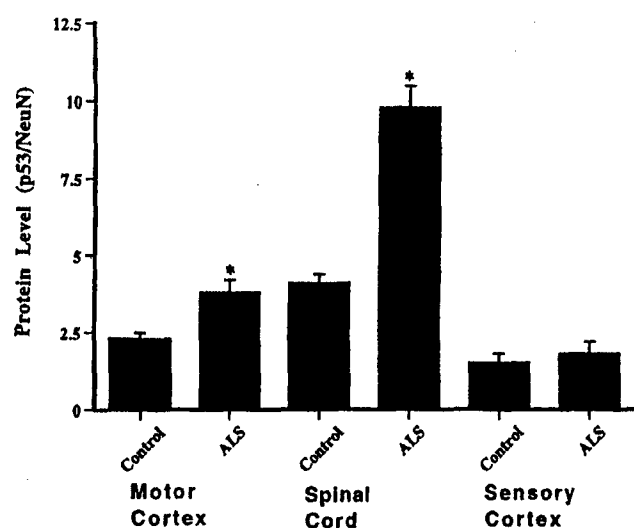


Figure 11. The levels of p53 are elevated in spinal cord and motor cortex in patients with ALS. p53 was measured by immunoblot analysis (asterisk, significantly different,  $p < 0.05$ , from control).

target of caspase-3 (137), and APP cleavage by caspase-3 or caspase-6 may promote A $\beta$  formation (138,139). Thus, increased production of A $\beta$  may be a consequence of neuronal apoptosis. A $\beta$  can induce apoptosis (140) and necrosis (141) in neuronal cell culture. Caspase-12 has been implicated in cortical neuron apoptosis *in vitro* induced by A $\beta$  (142). Presenilin proteins are also substrates for caspase-3 (143). Presenilin proteins have a widespread distribution throughout the CNS (144) and can influence mitochondrial regulation of apoptosis, such as Bax activation and cytochrome c release, through interactions with Bcl-X<sub>L</sub> (145). However, the real contribution of apoptosis to the neurodegeneration in AD still remains to be definitively ascertained.

### 11. Neuronal degeneration after cerebral ischemia

Neurons die after cerebral hypoxia-ischemia. Episodes of cerebral hypoxia-ischemia (HI) can occur during cardiac arrest, stroke, asphyxia, drowning, and cardiopulmonary bypass surgery. Specific populations of neurons show selective vulnerability or sensitivity to HI. Striatal neurons degenerate earlier than CA1 pyramidal neurons of hippocampus and Purkinje cells of cerebellum that undergo delayed neuronal death (DND) (8,9,26,146-148). The mechanisms of neuronal death after cerebral ischemia are not completely understood. Structurally and mechanistically, cellular degeneration in non-nervous tissues caused by HI has been thought to be necrosis (14,27,150). However, recently, postischemic degeneration of neurons in rats and gerbils has been considered to be apoptosis mediated by PCD mechanisms (151-155). The notion that selectively vulnerable neurons undergo apoptosis after ischemia is very controversial (8,9,26,149,156,157) and should be examined more critically. Ischemic DND might be better classified according to the concept of the apoptosis-necrosis continuum (Figs. 3-5) (6-9). The accurate identification of the contributions of apoptosis and necrosis to neuronal death after ischemia has critical therapeutic relevance and needs to be clarified soon in animals models, because antiapoptotic

therapies have been suggested, possibly prematurely, for human clinical trials for the treatment of brain ischemia (158).

*Neurodegeneration after cerebral ischemia can be explained by the apoptosis-necrosis cell death continuum.* Previous studies have suggested that DND in hippocampus is apoptosis. This idea was based originally on the finding that systemic treatment with protein synthesis inhibitors protected against CA1 neuron loss after global ischemia (148,159), although protein synthesis inhibitors cause hypothermia, which is neuroprotective. However, other studies did not confirm that protein and RNA synthesis inhibitors ameliorate postischemic DND in CA1 and structural analysis argued against this neurodegeneration as PCD (156). More recent studies have reasserted that DND of CA1 pyramidal neurons in rodents after ischemia is apoptosis (153-155,160). Other studies reject this conclusion, because unambiguous structural, biochemical, or molecular evidence for apoptosis of CA1 pyramidal neurons in adult brain has not been presented (8,9,149,157). This discrepancy regarding the contribution of apoptosis to the neurodegeneration after ischemia may be due to differences in criteria for identifying neuronal apoptosis at the structural level and to limitations of tissue homogenate-based analysis. It is also possible that neuronal death after ischemia requires descriptions based on cell death concepts that are broader than a binary classification scheme for cell death. We have embraced fuzzy logic (161) to develop the concept of the apoptosis-necrosis cell death continuum (6-9).

Some forms of neuronal death after ischemia can be explained by the apoptosis-necrosis cell death continuum. This neurodegeneration may fall along a structural and mechanistic continuum. As with non-NMDA GluR-mediated excitotoxicity (Figs. 4 and 7), ischemic neuronal death could be a hybrid of apoptosis and necrosis (Figs. 3-5), with this degeneration not strictly apoptosis or necrosis, according to the traditional binary classification of cell death, but occurring as intermediate or hybrid forms with coexisting characteristics.

The degeneration of neurons in the adult and immature brain after global ischemia vindicates the cell death continuum (8,9,21,22,26,149,162,163). DND of CA1 pyramidal neurons and cerebellar Purkinje neurons in mature brain is similar, but striatal neuron death can be different structurally from the death of CA1 neurons (Fig. 3) (8,149). The DND of CA1 pyramidal neurons and Purkinje cells after ischemia in the adult brain falls much closer to the cellular necrosis end of the continuum rather than the classical apoptosis end, whereas striatal neuron death is a very clear hybrid form. In the adult brain, degeneration of CA1 pyramidal neurons and Purkinje cells after ischemia is very distinct from typical neuronal apoptosis, but some neurons have features similar to non-NMDA GluR-mediated excitotoxic neuronal apoptosis, while most degenerating neurons are very similar to NMDA receptor-mediated excitotoxic neuronal necrosis (Figs. 3 and 4). Our interpretations of observations made in cat and dog hippocampus are similar to those made in non-human primate and human (164). In adult striatum after ischemia, neuronal death is also quite different from classical apoptosis, with most neurons having features similar to non-NMDA GluR-mediated excitotoxic neuronal apoptosis or NMDA receptor-mediated excitotoxic neuronal necrosis (Figs. 3 and 4). Ischemic

neurodegeneration is characterized by irregular clumping of chromatin (into many small or few large aggregates), swelling and degeneration of mitochondria, extensive cytoplasmic vacuolation, destruction of plasma membrane integrity, and eventual dissolution of the cell. The nuclear pyknosis with condensation of chromatin into many small, irregularly shaped clumps in ischemic neurons is a contrasting pattern to the formation of few, uniformly dense and regularly shaped chromatin aggregates that typify neuronal apoptosis. However, the organization of the chromatin into few large, chromatin aggregates is a feature typical of the apoptosis-necrosis hybrid cell (Fig. 3-5).

Misunderstanding about the contribution of apoptosis to the neurodegeneration after cerebral ischemia is realized further from studies using DNA fragmentation as the primary criterion for apoptosis. Many studies, using *in situ* DNA end labeling methods, have shown that vulnerable populations of neurons undergo nuclear DNA fragmentation following global cerebral ischemia in the adult brain (149,151-153). However, these methods, based on terminal deoxynucleotidyl transferase and DNA polymerase, are not discriminating among apoptotic and necrotic cell deaths (7,8,165). DNA end-labeling can also detect DNA fragments during DNA synthesis (166). Therefore, DNA end-labeling data cannot be interpreted as solely apoptosis without correlated structural data (167).

DNA fragmentation after global ischemia in adult brain has also been studied by gel electrophoresis. In DNA extracts of adult rat or gerbil brain after transient global forebrain ischemia, internucleosomal fragmentation has been detected and has been interpreted as apoptosis occurring by PCD mechanisms (151-153,168,169). Exceptions to the specificity of internucleosomal DNA fragmentation for apoptosis have been found. It occurs in ischemic liver necrosis (170), in NMDA receptor-mediated excitotoxic neuronal necrosis in adult brain (7) and neuronal culture (171,172), and in cells undergoing necrosis induced by  $\text{Ca}^{2+}$  ionophores and heat shock (167). The DNA fragmentation detected after cerebral ischemia differs from DNA fragmentation occurring in archetypal apoptosis because the fragments have staggered ends with a 3' recess of ~8-10 nucleotides (173). Thus, based on DNA fragmentation patterns, death of neurons after ischemia is neither classical apoptosis nor classical necrosis (173). The apoptosis-necrosis cell death continuum (6,7) can be used to classify both the structure and biochemistry of ischemic neuronal death.

The analysis of DNA fragmentation patterns (and protein levels) in brain extracts is confounded by homogenization of tissues comprised of heterogeneous cell types (nervous tissue is not a homogeneous cell population). Thus the evaluation of information on a cell by cell basis is not possible. Non-neuronal cells (e.g., astrocytes, oligodendrocytes, inflammatory cells, and vascular cells) also die following ischemia-reperfusion, and some of these non-neuronal cells die apoptotically (8,162). As concluded in previous accounts (7,8,150,167,174), cell structure is still the best indicator for classifying cell death *in vivo*. We have found that random and internucleosomal DNA fragmentation can coexist (149). This result could be interpreted as hybrid forms of cell death or as necrosis and apoptosis occurring in different cells that coexist spatially and regionally.

The contribution of apoptosis to the neuronal death after cerebral ischemia has also been evaluated by measuring gene expression and protein levels of cell death proteins in tissue homogenates or tissue sections. Bax mRNA increases in both vulnerable and less vulnerable regions postischemia (160). Changes in mRNA levels after cerebral ischemia are difficult to interpret in the presence of sustained damage to organelles that function in protein synthesis and posttranslational processing (8). These organelle perturbations may render the translation and formation of mature products inefficient. By immunoblotting, Bax protein in hippocampus is increased transiently at 6 h postischemia but then returns to control levels (154). We have not found changes in Bax protein levels in hippocampus at 1 and 7 days after ischemia, but we have observed an increase in Bax in cerebellum at 7 days after ischemia (149). It is possible that this change in Bax reflects apoptosis of granule neurons (rather than Purkinje neurons) in cerebellum (149). However, a sustained postischemic increase in Bax protein levels has been shown in hippocampus but not cerebellum (160), although the contributions of different cells to this observation have not been identified. Many existing immunocytochemical analyses of cell death proteins after ischemia are difficult to interpret because highly specific antibodies need to be used (many of the currently available antibodies to death proteins of the Bcl-2 family should not be used due to the lack of monospecificity). Furthermore, the function of cell death proteins of the Bcl-2 family relies on subcellular translocation, phosphorylation, and protein-protein interactions. More useful information could be obtained on the role cell death proteins after ischemia by analyses focusing on subcellular fractions, subcellular localization, phosphorylation status, and protein interactions.

Recent studies have maintained that cytochrome c release from mitochondria into the cytosol is involved in the death of CA1 neurons after global ischemia (155). However, such results are not clearly interpretable. The change might not reflect events occurring in neurons specifically, because brain tissue was used to prepare soluble extracts. The change could reflect release or abnormal import of cytochrome c into mitochondria due to subcellular damage, and, if it is release, it could be non-physiological and spontaneous due to mitochondrial disruption rather than physiologically regulated release.

Experiments with transgenic mice and gene manipulations are used to decipher a possible role for neuronal apoptosis after cerebral ischemia. Bcl-2 overexpression in transgenic mice reduces hippocampal pyramidal neuron degeneration after global ischemia (175). However, the effect of Bcl-2 transgene expression cannot yet be ascribed specifically to antiapoptotic activity, because this protein has additional functions in injured neurons, including axonal regeneration (176) and blocking the release of calcium from the ER (177). Drug-induced and virally mediated overexpression of NAIP also protects CA1 neuron degeneration after global ischemia (178), but it is still not certain whether this protection results directly from blocking apoptotic mechanisms in CA1 pyramidal neurons. These manipulations could protect or alter the functioning of neurons (e.g., interneurons or upstream presynaptically-coupled neurons) other than CA1 pyramidal neurons that then protect against GluR-mediated excitotoxic neuronal death of CA1 neurons.

Caspases have been studied after cerebral ischemia. The mRNA and protein levels for caspase-1 increase in hippocampus following global ischemia in gerbils, but this change is associated with inflammatory cells rather than selectively vulnerable CA1 pyramidal neurons (169). After global ischemia in rat, caspase-3 mRNA levels progressively increase in CA1 at 24-72 h, although most neurons are already lost by 72 h, while caspase-3 mRNA is transiently elevated in dentate gyrus granule cells at 8 h postischemia (179). This latter pattern would be consistent with a role for caspase-3 in dentate gyrus granule neuron apoptosis that has been identified (149). Existing immunocytochemical analyses of caspases after ischemia are difficult to interpret because of proenzyme detection. Many of the currently available antibodies to caspase-3 are not monospecific for the active forms.

*Classical apoptosis of granule neurons occurs after ischemia.* The degeneration of granule neurons in dentate gyrus and cerebellum after global ischemia sharply contrasts with the degeneration of CA1 neurons and Purkinje cells (149). Granule neuron death after ischemia closely resembles apoptosis. Thus, granule neurons provide an internal standard of classical apoptosis to which CA1 pyramidal neuron and cerebellar Purkinje cell degeneration after ischemia can be compared to demonstrate that the death of these latter neurons clearly differs from classical apoptosis. The death of granule neurons is characterized by condensation of chromatin into few, large round clumps or crescentic caps, aggregation and lamination of the cytoskeleton, and cellular shrinkage. Membranous organelles, including mitochondria, remained intact until the late stages of apoptosis. Apoptosis of granule neurons is similar to the apoptosis in non-neuronal tissues (150,174), in developing brain during naturally occurring PCD of neurons (Fig. 2) (6), and in some neuronal groups after axotomy/target deprivation (Fig. 3) (116,180).

The death of granule neurons after ischemia may have more than one trigger. Granule neuron apoptosis may be a direct consequence of the HI. Alternatively, it may be secondary to degeneration of hippocampal pyramidal neurons and cerebellar Purkinje cells and is a form of target deprivation-induced apoptosis, similar to thalamic neuron death after cortical lesions (8,180,181) and motor neuron degeneration after axotomy (116,118). We know that the distribution of brain damage after HI follows a connectivity-related distribution (182). The apoptosis of granule neurons is consistent with this idea and may possibly explain the contradictory evidence for apoptosis in hippocampal pyramidal neurons found in homogenate-based biochemical experiments.

It is still uncertain however whether the absence of a classic apoptotic structure in selectively vulnerable neurons after ischemia is sufficient evidence to exclude the possibility that PCD mechanisms are operative. We conclude that neuronal death in the mature (adult) CNS after global ischemia exists as more than one temporally overlapping forms in hippocampus and cerebellum: necrosis or necrosis-apoptosis hybrids of selectively vulnerable neurons and classical apoptosis of granule neurons (149).

*Neurodegeneration after cerebral ischemia in immature brain.* Neurodegeneration in the immature brain is phenotypically

heterogeneous and regionally specific. We have also found that the neurodegeneration in specific regions is model- or species-related. For example, neuronal apoptosis is much more prominent in newborn rat models of HI (21,22,163) compared to newborn piglet models of HI (26,162,183).

The cell death continuum is revealed fully in a neonatal rat (7-day-old) model of HI. In this model, neuronal cell death occurs as several forms, including necrosis, apoptosis, and hybrids of necrosis and apoptosis (21,22,163). From structural and biochemical evaluations of the injured cerebral hemisphere, neuronal necrosis predominates in cerebral cortex, necrosis-apoptosis hybrids occur in hippocampus and striatum, and classical apoptosis is prominent in thalamus and brainstem. The thalamic neuron apoptosis in the neonatal rat brain after HI is structurally identical to the apoptosis of thalamic neurons after cortical injury (Fig. 3) (22,163). HI in the neonatal rat causes severe infarction of cerebral cortex (22), and we speculate that this thalamic neuron apoptosis is caused by neurotrophin withdrawal resulting from target deprivation, as in an occipital cortex ablation model (180,181). The apoptosis in thalamic neurons after HI in neonatal rat is associated with a rapid increase in the levels of the Fas death receptor and caspase-8 activation (163). Concurrently, the levels of Bax in mitochondrial-enriched cell fractions increase and cytochrome c accumulates in the soluble protein compartment. Increased levels of Fas death receptor and Bax, cytochrome c accumulation, and activation of caspase-8 in the thalamus precede the marked activation of caspase-3 and the occurrence of neuronal apoptosis.

Contrasting with findings in neonatal rat striatum after HI, the death of striatal neurons after HI in piglets (10-day-old) is categorically necrosis (26). This neuronal death evolves over 24 h with a specific temporal pattern of subcellular organelle damage and biochemical defects (26,183). Damage to the Golgi apparatus and rough endoplasmic reticulum occurs at 3-12 h, while most mitochondria appear intact until 12 h. Mitochondria undergo an early suppression of activity, then a transient burst of activity at 6 h after the insult, followed by mitochondrial failure. Cytochrome c is depleted at 6 h after HI and thereafter. Damage to lysosomes occurs within 3-6 h. By 3 h recovery, glutathione levels are reduced, and peroxynitrite-mediated oxidative damage to membrane proteins occurs at 3-12 h. The Golgi apparatus and cytoskeleton are early targets for extensive tyrosine nitration. Striatal neurons also sustained hydroxyl radical damage to DNA and RNA within 6 h after HI. This work demonstrates that neuronal necrosis in the striatum evolves rapidly and is possibly driven by early glutathione depletion and oxidative stress by 3-6 h recovery from HI.

The rat pup and piglet models of newborn HI are different physiologically and neuropathologically. Rat pups and piglets near the day of birth are at very different stages of maturation with respect to glutamate receptors and glutamate transporters (35,37,162,184). The peak of the brain growth spurt occurs near term in pig and human, whereas this peak occurs at about 7 days postnatally in rat (185). Moreover, the percentage of adult brain weight at birth in pig is much closer to human compared to that of rat (185). These fundamental neurobiological differences are very important when considering the relevance of experimental animals as models for brain injury in human newborns.

## 12. Possible mechanisms driving the apoptosis-necrosis cell death continuum

The intensity of the insult and the rate of injury are important regulators of the commitment process for cell death (29). In neurons, the rate at which oxidative stress evolves may dictate the type of neuronal cell death (8). A variety of subcellular and molecular alterations may drive the cell death continuum.

Intracellular ion concentrations and ion flux may determine where neurons fall along the cell death continuum (Fig. 6). Severe  $\text{Ca}^{2+}$  overload causes acute swelling and necrosis (186). However, elevated intracellular  $\text{Ca}^{2+}$  in moderation is a survival signal and is antiapoptotic by stimulating  $\text{Ca}^{2+}$ /calmodulin-dependent protein kinase kinase which activates Akt that then phosphorylates Bad, thereby permitting its interaction with protein 14-3-3 and thus its inactivation (187). Both apoptosis and necrosis are induced in embryonic striatal neurons by  $\text{Ca}^{2+}$  ionophore (188). It is possible to envision that flux of intracellular  $\text{Ca}^{2+}$  and monovalent cations ranging from subtle to severe could modulate neuronal survival and death along an apoptosis-necrosis continuum.

The status of mitochondria may modulate the cell death continuum. Mitochondria release proapoptotic factors by mechanisms that are still not clear (49,56,62-64). Mitochondria swelling and breaches in the outer mitochondrial membrane can trigger release of proapoptotic factors (68) and can cause ATP depletion and  $\text{Ca}^{2+}$  efflux (186). The severity and rate of mitochondrial changes may be key regulators of cell death, with rapid, high amplitude perturbations causing necrosis (27,28), slow low amplitude regulated changes inducing apoptosis, and intermediate perturbations causing hybrids of necrosis and apoptosis. Interestingly, in dying neurons, mitochondria do not behave uniformly even within individual cells (6). During neuronal cell death, some mitochondria swell and the inner membranes undergo cristaeolysis, but other mitochondria do not appear to become structurally defective. Abnormalities in mitochondrial membranes can occur during cellular necrosis (27) and apoptosis (68). Moreover, both apoptotic and necrotic cell deaths can be preceded by release of cytochrome c (189). Therefore, it is important to delineate whether release of cytochrome c is physiologically regulated and whether downstream players in the apoptosis cascade are in place and intact. The severity of these perturbations may not only influence the mode of cell death as either apoptosis or necrosis, but may also regulate the overlapping contributions of apoptosis and necrosis in hybrid neurons.

Organelles that function in protein synthesis and post-translational modification could also modulate the balance of apoptosis and necrosis in the death continuum. Stimuli that cause stress to the endoplasmic reticulum (ER) and Golgi apparatus can induce apoptosis (142,190). The mechanisms for ER control of cell death may be related to  $\text{Ca}^{2+}$  release, Bcl-2 function, caspase activation (142) and changes in protein synthesis and folding. An increase in cytosolic free  $\text{Ca}^{2+}$  is a well-known stimulus for apoptosis; however,  $\text{Ca}^{2+}$  promotes cellular survival as well.  $\text{Ca}^{2+}$  release from the ER can stimulate apoptosis independent of mitochondria (191). Bcl-2 can repress apoptosis by inhibiting ER-associated  $\text{Ca}^{2+}$  efflux (177). Caspase-12 mediates ER stress-related apoptosis in cortical neuron cultures (142). Structural and biochemical alterations

occur in the ER and Golgi apparatus in neurons early after excitotoxicity and ischemia (6,7). The ER damage is persistent during the process of excitotoxic and ischemic neurodegeneration (6-8,26,147). Structural perturbations in CA1 pyramidal neurons coincide with severe and sustained reductions in total protein synthesis by 6 h following transient global forebrain ischemia (192-194). In sympathetic ganglion neuron cultures, inhibition of protein synthesis induces apoptosis (195). Early abnormalities also occur in the Golgi apparatus (26,196). In cell culture models, agents that disrupt the Golgi apparatus and cause Golgi fragmentation induce apoptosis in neurons (190), but the mechanisms are unclear. The Golgi apparatus may transduce proapoptotic signals through caspase-2 (197). It is possible to envision that gradations in damage to the ER and Golgi apparatus (Fig. 7) may cause a wide range of disturbances in ER-Golgi function and cause hybrids of cell death with features of apoptosis and necrosis.

Perturbations in cytoskeletal dynamics can sway the cell death process. The cytoskeleton is a major target for chemotherapeutic agents that induce apoptosis by depolymerization or stabilization of the cytoskeletal network. Chemical-induced perturbations in actin and microtubules induce apoptosis. Cytoskeletal disintegration occurs early after ischemia, particularly in dendrites, before the degeneration of neuronal cell bodies (198,199). Within minutes after transient forebrain ischemia, spectrin is proteolysed in CA1 prior to neuronal death (200,201). This cytoskeletal disruption is NMDA receptor mediated (200,201) through calpain activation (201). Thus, it is possible that graded alterations in GluR<sup>+</sup> activity and disturbances in cytoskeletal dynamics play a role in the apoptosis-necrosis death continuum after cerebral ischemia.

## 13. Neuronal death in models of axotomy and target deprivation

Animal models of axotomy (axon cutting or transection) and target deprivation (target removal or ablation) can be used to identify mechanisms of progressive and delayed neuronal degeneration. These models are relevant to chronic degenerative diseases and acute disorders, including ischemia and trauma that affect the human brain or spinal cord. Models of axotomy/target deprivation-induced neuronal death provide a structural, biochemical, and molecular 'gold standard' for induced neuronal apoptosis *in vivo* that may occur by PCD mechanisms.

*Cortical and spinal cord injury models of neuronal apoptosis.* The progression of neuronal degeneration and the likelihood of subsequent neuronal death or recovery and survival in axotomy/target deprivation models are modifiable. These events are influenced by the residence of cell body of an axotomized neuron within the peripheral nervous system or CNS, location of axonal trauma in relation to the cell body, and maturity of the nervous system at the time of injury. Peripheral neurons regenerate their axons more readily than central neurons after axotomy, and the more proximal the injury is to the cell body, the greater the likelihood of neuronal death. Furthermore, in the immature brain and spinal cord, axotomized neurons often die much more rapidly than adult

neurons (202-204). The mechanisms for this neuronal age- or maturity-related effect on the rate of neuronal degeneration are not understood, but the signal transduction mechanisms of neuronal apoptosis are different in immature and mature neurons (32).

Several lines of evidence support the conclusion that neuronal death induced by axotomy and trophic factor withdrawal can be apoptosis. In transgenic newborn mice, Bcl-2 overexpression ameliorates motor neuron death induced by facial nerve transection (205), sciatic nerve transection (88), or optic nerve transection (89). Inhibition of caspase-1 and caspase-2 blocks apoptosis of dorsal root and sympathetic ganglion neurons after nerve growth factor withdrawal (206,207), and inhibition of caspase activity protects axotomized retinal ganglion cells from death after optic nerve transection in adult rat (208). Inhibition of caspase-1 also arrests apoptosis of motor neurons *in vitro* induced by neurotrophin withdrawal and PCD of motor neurons *in vivo* during the period of naturally occurring cell death (209).

We have developed and characterized brain and spinal cord injury models of neuronal apoptosis. In one model, ablation of the occipital cortex induces neuronal apoptosis in the dorsal lateral geniculate nucleus (LGN) of thalamus (180,181,204, 210). In another model, avulsion of the sciatic nerve induces apoptosis of motor neurons in lumbar spinal cord (116,118).

Unilateral ablation of the occipital cortex in adult rat and mouse causes unequivocal neuronal apoptosis in the dorsal LGN at 6-7 days postlesion (Fig. 3) (180,181,210). Thus, retrograde neuronal death in the adult brain is apoptosis. This neuronal apoptosis in the adult CNS requires Bax and is modulated by p53, but it can also occur independent of p53 (181).

Neuronal death mechanisms in the mature and immature CNS are dissimilar in the timing of the death process. The process of neuronal apoptosis is accelerated in immature CNS compared to adult CNS. Thalamic neurons in adult and immature brain die similarly after cortical injury, but neuronal apoptosis occurs much faster in the immature brain (204). In newborn mice (10-day-old), nuclear p53 accumulation and internucleosomal fragmentation of DNA coincide at 24 h postlesion, and maximal neuronal apoptosis occurs at 36 h postlesion. This time course contrasts sharply with the time course of neuronal apoptosis in the adult brain. Thus, neuronal apoptosis occurs more rapidly in the immature brain compared to adult brain (which occurs over 6-7 days), although p53-modulated mechanisms may participate in both the adult and newborn brain.

Apoptosis of thalamic neurons occurs in different CNS injury paradigms, such as cortical ablation and HI. We wanted to determine whether the mechanisms of neuronal apoptosis are similar in different types of CNS insults. Interestingly, the mechanisms of thalamic neuron death in our different models have some similar and different components, although both are apoptosis. Thus, mechanisms for neuronal apoptosis in different *in vivo* settings can differ in upstream signals, but they converge on common downstream mechanisms (i.e., the participation of Bax and caspase-3).

Mitochondria accumulate at perinuclear locations early during the progression of neuronal apoptosis *in vivo* (116, 163,210). The mechanisms for this mitochondrial redistribution

in neurons early during apoptosis are not known. In non-neuronal cell systems *in vitro* this redistribution may be an active part of cell signaling mechanisms for apoptosis (51). Although similar events occur in neurons *in vivo* (116,163,210), it is not yet clear whether this redistribution is an active part of the death signaling mechanisms or a consequence of early events during neuronal apoptosis. A sustained accumulation of active mitochondria in the vicinity of the nucleus may provide a source of reactive oxygen species or apoptotic protease activating factors.

Oxidative damage to nucleic acids and proteins occurs during neuronal apoptosis in the adult CNS (116,210). Hydroxyl radical-modification of DNA and RNA and peroxynitrite-modification of proteins occur during the progression of neuronal apoptosis in *in vivo* settings. Oxidative damage to DNA is a possible upstream signal for neuronal apoptosis *in vivo*. This hypothesis is supported by experiments demonstrating thalamic neurons (210) and motor neurons (116) sustain hydroxyl radical damage to DNA during apoptosis. Furthermore, by single-cell gel electrophoresis (comet assay), DNA single-strand breaks occur very early in the progression of motor neuron apoptosis (118). This DNA damage found *in vivo* has the same fingerprint as the DNA damage caused by peroxynitrite (118). DNA damage occurs in many different forms, including apurinic/apyrimidinic sites, double- and single-strand breaks, adduct formation, thymidine dimers, crosslinks, and insertion/deletion mismatches (211). Single strand breaks in DNA are the earliest and major type of DNA damage among the several forms and are potent signals for apoptosis (79,83). We believe that oxidative damage to DNA in the form of single strand breaks is an upstream signal in the mechanisms of p53-modulated, Bax-dependent neuronal apoptosis *in vivo* (181).

#### 14. Perspective on neurodegeneration in animal models of human neurological disorders

Neuronal cell death in the CNS following injury can coexist as apoptosis, necrosis, and hybrid forms along an apoptosis-necrosis continuum. These different forms of cell death have varying contributions to the neuropathology resulting from excitotoxicity, cerebral ischemia, and target deprivation/axotomy. Degeneration of different populations of cells (neurons and non-neuronal cells) may be mediated by distinct or common causal mechanisms that can temporally overlap and perhaps differ mechanistically in the rate of progression of cell death. The range in neuronal death phenotypes is likely to be influenced by many factors. Maturity of the CNS at the time of injury and the subtypes of GluRs that are activated influence neuronal death. The mechanistic rate of evolving injury can also influence the cell death process. For example, oxidative stress evolves slowly in target deprivation/axotomy, and the neurodegeneration is apoptosis. In contrast, oxidative stress evolves acutely with HI injury, and the majority of early occurring neurodegeneration in selectively vulnerable regions is necrosis. DND after cerebral ischemia can be necrosis, necrosis-apoptosis hybrids, and apoptosis.

Neuronal death may be mediated by common upstream mechanisms that differ mechanistically in the rate (days versus hours) and severity of cellular stress. Cellular stress



can destroy neurons through pathways causing apoptosis and necrosis. It will be important to evaluate the specific mechanisms of neuronal necrosis *in vivo* to compare with the mechanisms of neuronal apoptosis *in vivo*. These comparisons will provide valuable information on the signaling pathways that dictate neuronal cell death. We believe that such comparisons will also aid in validating and understanding the concept of the cell death continuum. Understanding the cellular and molecular mechanisms of neuronal cell death can lead to new therapeutic approaches critical for the future prevention of neurodegeneration in chronic and acute neurological disorders and can expand the field of cell death biology.

### Acknowledgments

I am thankful for the birth of my beautiful twin daughters, Isabella and Gabrielle (born July 24, 2000); they have enriched my life forever. Dr L.J. Martin is supported by grants from the U.S. Public Health Service, National Institutes of Health, National Institute of Neurological Disorders and Stroke (NS 34100) and National Institute on Aging (AG16282) and the U.S. Army Medical Research and Materiel Command (DAMD17-99-1-9553). The author is grateful for the outstanding technical assistance of Ann Price and Frank Barksdale. Thanks are extended to Carlos Portera-Cailliau, Nael Al-Abdulla, Chun-I Sze, Akiko Furuta, Adeel Kaiser, Jeffrey Kirsch, Frederick Sieber, Zhiping Liu, Christian Lesuisse, Ansgar Brambrink, Frances Northington, JoAnne Natale, Chris Golden, and Dawn Agnew for their contributions in his laboratory.

### References

1. Virchow R: In: Cellular Pathology as Based Upon Physiological and Pathological Histology. Churchill, London, 1985.
2. Hamburger V and Levi-Montalcini R: Proliferation, differentiation and degeneration in the spinal ganglia of the chick embryo under normal and experimental conditions. *J Exp Zool* 111: 457-501, 1949.
3. Glücksmann A: Cell deaths in normal vertebrate ontogeny. *Biol Rev* 26: 59-86, 1951.
4. Saunders JW: Death in embryonic systems. *Science* 154: 604-612, 1966.
5. Kerr JFR, Wyllie AH and Currie AR: Apoptosis: a basic biological phenomenon with wide-ranging implications in tissue kinetics. *Br J Cancer* 26: 239-257, 1972.
6. Portera-Cailliau C, Price DL and Martin LJ: Excitotoxic neuronal death in the immature brain is an apoptosis-necrosis morphological continuum. *J Comp Neurol* 378: 70-87, 1997.
7. Portera-Cailliau C, Price DL and Martin LJ: Non-NMDA and NMDA receptor-mediated excitotoxic neuronal deaths in adult brain are morphologically distinct: further evidence for an apoptosis-necrosis continuum. *J Comp Neurol* 378: 88-104, 1997.
8. Martin LJ, Al-Abdulla NA, Brambrink AM, Kirsch JR, Sieber FE and Portera-Cailliau C: Neurodegeneration in excitotoxicity, global cerebral ischemia, and target deprivation: a perspective on the contributions of apoptosis and necrosis. *Brain Res Bull* 46: 281-309, 1998.
9. Martin LJ, Portera-Cailliau C, Ginsberg SD and Al-Abdulla NA: Animal models and degenerative disorders of the human brain. *Lab Anim* 27: 18-25, 1998.
10. Lockshin RA and Williams CM: Programmed cell death: II. Endocrine potentiation of the breakdown of the intersegmental muscles of silkworms. *J Insect Physiol* 10: 643-649, 1964.
11. Tata JR: Requirement for RNA and protein synthesis for induced regression of tadpole tail in organ culture. *Dev Biol* 13: 77-94, 1966.
12. Hamburger V: Cell death in the development of the lateral motor column of the chick embryo. *J Comp Neurol* 160: 535-546, 1975.
13. Bursch W, Paffe S, Putz B, Barthel G and Schulte-Hermann R: Determination of the length of the histological stages of apoptosis in normal liver and in altered hepatic foci of rats. *Carcinogenesis* 11: 847-853, 1990.
14. Wyllie AH, Kerr JFR and Currie AR: Cell death: the significance of apoptosis. *Int Rev Cytol* 68: 251-306, 1980.
15. Nagata S: Fas ligand-induced apoptosis. *Annu Rev Genet* 33: 29-55, 1999.
16. Kerr JFR and Searle J: Deletion of cells by apoptosis during castration-induced involution of the rat prostate. *Virchows Arch (B)* 13: 87-102, 1973.
17. Schwartz LM, Smith SW, Jones MEE and Osborne BA: Do all programmed cell deaths occur via apoptosis? *Proc Natl Acad Sci USA* 90: 980-984, 1993.
18. Amin F, Bowen ID, Szegei Z, Mihalik R and Szende B: Apoptotic and non-apoptotic modes of programmed cell death in MCF-7 human breast carcinoma cells. *Cell Biol Int* 24: 253-260, 2000.
19. Clarke PGH: Developmental cell death: morphological diversity and multiple mechanisms. *Anat Embryol* 181: 195-213, 1990.
20. Pilar G and Landmesser L: Ultrastructural differences during embryonic cell death in normal and peripherally deprived ciliary ganglia. *J Cell Biol* 68: 339-356, 1976.
21. Nakajima W, Ishida A, Lange MS, Gabrielson KL, Wilson MA, Martin LJ, Blue ME and Johnston MV: Apoptosis has a prolonged role in the neurodegeneration after hypoxic ischemia in the newborn rat. *J Neurosci* 20: 7994-8004, 2000.
22. Northington FJ, Ferriero DM, Graham EM, Traystman RJ and Martin LJ: Early neurodegeneration after hypoxia-ischemia in neonatal rat is necrosis while delayed neuronal death is apoptosis. *Neurobiol Disease* (In press).
23. Martin LJ: Neuronal death in amyotrophic lateral sclerosis is apoptosis: possible contribution of a programmed cell death mechanism. *J Neuropathol Exp Neurol* 58: 459-471, 1999.
24. Martin LJ: Motor neurons have DNA damage and p53 is abnormally elevated and active in the CNS of patients with amyotrophic lateral sclerosis. *Soc Neurosci Abstr* 26: 500, 2000.
25. Martin LJ: p53 is abnormally elevated and active in the CNS of patients with amyotrophic lateral sclerosis. *Neurobiol Disease* 7: 613-622, 2000.
26. Martin LJ, Brambrink AM, Price AC, Kaiser A, Agnew DM, Ichord RN and Traystman RJ: Neuronal death in newborn striatum after hypoxia-ischemia is necrosis and evolves with oxidative stress. *Neurobiol Disease* 7: 169-191, 2000.
27. Trump BJ, Goldblatt PJ and Stowell RE: Studies on necrosis of mouse liver *in vitro*. Ultrastructural alterations in the mitochondria of hepatic parenchymal cells. *Lab Invest* 14: 343-371, 1964.
28. Allen TD: Ultrastructural aspects of cell death. In: *Perspectives on Mammalian Cell Death*. Potten CS (ed). Oxford University Press, New York, pp39-65, 1987.
29. Wyllie AH: Apoptosis: cell death under homeostatic control. *Arch Toxicol Suppl* 11: 3-10, 1987.
30. Lennon SV, Martin SJ and Cotter TG: Dose-dependent induction of apoptosis in human tumour cell lines by widely diverging stimuli. *Cell Prolif* 24: 203-214, 1991.
31. Fernandes RS and Cotter TG: Apoptosis or necrosis: intracellular levels of glutathione influence mode of cell death. *Biochem Pharmacol* 48: 675-681, 1994.
32. Lesuisse C and Martin LJ: Neuronal maturity influences the progression of neuronal apoptosis induced by DNA damage. *Soc Neurosci Abstr* 26: 322, 2000.
33. Nakanishi S: Molecular diversity of glutamate receptors and implications for brain function. *Science* 258: 597-603, 1992.
34. Martin LJ, Blackstone CD, Levey AI, Huganir RL and Price DL: AMPA glutamate receptor subunits are differentially distributed in rat brain. *Neuroscience* 53: 327-358, 1993.
35. Martin LJ, Furuta A and Blackstone CD: AMPA receptor protein in developing rat brain: GluR1 expression and localization change at regional, cellular, and subcellular levels with maturation. *Neuroscience* 83: 917-928, 1998.
36. Brennan EM, Martin LJ, Johnston MV and Blue ME: The ontogeny of non-NMDA glutamate receptors in rat barrel field cortex. II.  $\alpha$ -AMPA and kainate receptors. *J Comp Neurol* 386: 29-45, 1997.
37. Furuta A and Martin LJ: Laminar segregation of the cortical plate during corticogenesis is accompanied by changes in glutamate receptor expression. *J Neurobiol* 39: 67-80, 1999.



38. Portera-Cailliau C, Price DL and Martin LJ: *N*-methyl-*D*-aspartate receptor proteins NR2A and NR2B are differentially distributed in the developing rat central nervous system as revealed by subunit-specific antibodies. *J Neurochem* 66: 692-700, 1996.
39. Merry DE and Korsmeyer SJ: Bcl-2 gene family in the nervous system. *Annu Rev Neurosci* 20: 245-267, 1997.
40. Wolf BB and Green DR: Suicidal tendencies: apoptotic cell death by caspase family proteinases. *J Biol Chem* 274: 20049-20052, 1999.
41. Liston P, Roy N, Tamai K, Lefebvre C, Baird S, Cherton-Horvat G, Farahani R, McLean M, Ikeda J-E, MacKenzie A and Korneluk RG: Suppression of apoptosis in mammalian cells by NAIP and a related family of IAP genes. *Nature* 379: 349-353, 1996.
42. Polyak K, Xia Y, Zweier JL, Kinzler KW and Vogelstein B: A model for p53-induced apoptosis. *Nature* 389: 300-305, 1997.
43. Leverro M, De Laurenzi V, Costanzo A, Sabatini S, Gong J, Wang JYJ and Melino G: The p53/p63/p73 family of transcription factors: overlapping and distinct functions. *J Cell Sci* 113: 1661-1670, 2000.
44. Lithgow T, van Driel R, Bertram JF and Strasser A: The protein product of the oncogene *bcl-2* is a component of the nuclear envelope, the endoplasmic reticulum, and the outer mitochondrial membrane. *Cell Growth Differ* 5: 411-417, 1994.
45. Muchmore SW, Sattler M, Liang H, Meadows RP, Harlan JE, Yoon HS, Nettekheim D, Chang BS, Thompson CB, Wong SL and Fesik SW: X-ray and NMR structure of human Bcl-x<sub>L</sub>, an inhibitor of programmed cell death. *Nature* 381: 335-341, 1999.
46. Inohara N, Ekhterae D, Garcia I, Carria R, Merino J, Merry A, Chen S and Núñez G: Mtd, a novel Bcl-2 family member activates apoptosis in the absence of heterodimerization with Bcl-2 and Bcl-x<sub>L</sub>. *J Biol Chem* 273: 8705-8710, 1998.
47. Stennicke HR, Deveraux QL, Humke EW, Reed JC, Dixit VM and Salvesen GS: Caspase-9 can be activated without proteolytic processing. *J Biol Chem* 274: 8359-8362, 1999.
48. Schwartz LM and Milligan CE: Cold thoughts of death: the role of ICE proteases in neuronal cell death. *Trends Neurosci* 19: 555-562, 1996.
49. Li P, Nijhawan D, Budihardjo I, Srinivasula SM, Ahmad M, Alnemri ES and Wang X: Cytochrome c and dATP-dependent formation of Apaf-1/caspase-9 complex initiates an apoptotic protease cascade. *Cell* 91: 479-489, 1997.
50. Cleveland JL and Ihle JN: Contenders in FasL/TNF death signaling. *Cell* 81: 479-482, 1995.
51. Li H, Zhu H, Xu C-J and Yuan J: Cleavage of Bid by caspase 8 mediates the mitochondrial damage in the Fas pathway of apoptosis. *Cell* 94: 491-501, 1998.
52. LaCasse EC, Baird S, Korneluk RG and MacKenzie AE: The inhibitors of apoptosis (IAPs) and their emerging role in cancer. *Oncogene* 17: 3247-3259, 1998.
53. Deveraux QL, Roy N, Stennicke HR, Van Arsdalet T, Zhou Q, Srinivasula SM, Alnemri ES, Salvesen GS and Reed JC: IAPs block apoptotic events induced by caspase-8 and cytochrome c by direct inhibition of distinct caspases. *EMBO J* 17: 2215-2223, 1998.
54. Du C, Fang M, Li Y, Li L and Wang X: Smac, a mitochondrial protein that promotes cytochrome c-dependent caspase activation by eliminating IAP inhibition. *Cell* 102: 33-42, 2000.
55. Verhagen AM, Ekert PG, Pakusch M, Silke J, Connolly LM, Reid GE, Moritz RL, Simpson RJ and Vaux DL: Identification of DIABLO, a mammalian protein that promotes apoptosis by binding to and antagonizing IAP proteins. *Cell* 102: 43-53, 2000.
56. Liu X, Kim CN, Yang J, Jemmerson R and Wang X: Induction of apoptotic program in cell-free extracts: requirement for dATP and cytochrome c. *Cell* 86: 147-157, 1996.
57. Zou H, Li Y, Liu X and Wang X: An Apaf-1-cytochrome c multimeric complex is functional apoptosome that activates procaspase-9. *J Biol Chem* 274: 11549-11556, 1999.
58. Lazebnik YA, Kaufmann SH, Desnoyers S, Poirier GG and Earnshaw WC: Cleavage of poly(ADP-ribose) polymerase by a proteinase with properties like ICE. *Nature* 371: 346-347, 1994.
59. Liu X, Zou H, Slaughter C and Wang X: DFF, a heterodimeric protein that functions downstream of caspase-3 to trigger DNA fragmentation during apoptosis. *Cell* 89: 175-184, 1997.
60. Liu X, Li P, Widlak P, Zou H, Luo X, Garrard WT and Wang X: The 40-kDa subunit of DNA fragmentation factor induces DNA fragmentation and chromatin condensation during apoptosis. *Proc Natl Acad Sci USA* 95: 8461-8466, 1998.
61. Liu X, Zou H, Widlak P, Garrard W and Wang X: Activation of the apoptotic endonuclease DFF40 (caspase-activated DNase or nuclease). *J Biol Chem* 274: 13836-13840, 1999.
62. Kluck RM, Bossy-Wetzel E, Green DR and Newmeyer DD: The release of cytochrome c from mitochondria: a primary site for bcl-2 regulation of apoptosis. *Science* 275: 1132-1136, 1997.
63. Yang J, Liu X, Bhalla K, Kim CN, Ibrado AM, Cai J, Peng TI, Jones DP and Wang X: Prevention of apoptosis by bcl2: release of cytochrome c from mitochondria blocked. *Science* 275: 1129-1132, 1997.
64. Susin SA, Lorenzo HK, Zamzami N, Marzo I, Snow BE, Brothers GM, Mangion J, Jacotot E, Constantini P, Loeffler M, Larochette N, Goodlett DR, Aebersold R, Siderovski DP, Penninger JM and Kroemer G: Molecular characterization of mitochondrial apoptosis-inducing factor. *Nature* 397: 441-446, 1999.
65. Antonsson B, Conti F, Ciavatta A, Montessuit S, Lewis S, Martinou I, Bernasconi L, Bernard A, Mermod J-J, Mazzei G, Maundrell K, Gambale F, Sadoul R and Martinou J-C: Inhibition of bax channel-forming activity by bcl-2. *Science* 277: 370-372, 1997.
66. Marzo I, Brenner C, Zamzami N, Jürgensmeier JM, Susin SS, Vieira HLA, Prévost M-C, Xie Z, Matsuyama S, Reed JC and Kroemer G: Bax and adenine nucleotide translocator cooperate in the mitochondrial control of apoptosis. *Science* 281: 2027-2031, 1998.
67. Shimizu S, Ide T, Yanagida T and Tsujimoto Y: Electrophysiological study of a novel large pore formed by Bax and the voltage-dependent anion channel that is permeable to cytochrome c. *J Biol Chem* 275: 12321-12325, 2000.
68. Vander Heiden MG, Chandel NS, Williamson EK, Schumacker PT and Thompson CB: Bcl-x<sub>L</sub> regulates the membrane potential and volume homeostasis of mitochondria. *Cell* 91: 627-637, 1997.
69. Hu Y, Benedict MA, Wu D, Inohara N and Núñez G: Bcl-x<sub>L</sub> interacts with Apaf-1 and inhibits Apaf-1-dependent caspase-9 activation. *Proc Natl Acad Sci USA* 95: 4386-4391, 1998.
70. Song Q, Kuang Y, Dixit VM and Vincenz C: Boo, a negative regulator of cell death, interacts with Apaf-1. *EMBO J* 18: 167-178, 1999.
71. Halder S, Jena N and Croce CM: Inactivation of Bcl-2 by phosphorylation. *Proc Natl Acad Sci USA* 92: 4507-4511, 1995.
72. Wang H-G, Rapp UR and Reed JC: Bcl-2 targets the protein kinase raf-1 to mitochondria. *Cell* 87: 629-638, 1996.
73. Datta SR, Dudek H, Tao X, Masters S, Fu H, Gotoh Y and Greenberg ME: Akt phosphorylation of Bad couples survival signals to the cell-intrinsic death machinery. *Cell* 91: 231-241, 1997.
74. Del Peso L, González-García M, Page C, Herrera R and Núñez G: Interleukin-3-induced phosphorylation of bad through the protein kinase Akt. *Science* 278: 687-689, 1997.
75. Cardone MH, Roy N, Stennicke HR, Salvensen GS, Franke TF, Stanbridge E, Frisch S and Reed JC: Regulation of cell death protease caspase-9 by phosphorylation. *Science* 282: 1318-1321, 1998.
76. Zha J, Harada H, Yang E, Jockel J and Korsmeyer SJ: Serine phosphorylation of death agonist Bad in response to survival factor results in binding to 14-3-3 not Bcl-x<sub>L</sub>. *Cell* 87: 619-628, 1996.
77. Yang E, Zha J, Jockel J, Boise LH, Thompson CB and Korsmeyer SJ: Bad, a heterodimeric partner for Bcl-x<sub>L</sub> and Bcl-2, displaces Bax and promotes cell death. *Cell* 80: 285-291, 1995.
78. Desagher S, Osen-Sand A, Nichols A, Eskes R, Montessuit S, Lauper S, Maundrell K, Antonsson B and Martinou J-C: Bid-induced conformational change of bax is responsible for mitochondrial cytochrome c release during apoptosis. *J Cell Biol* 144: 891-901, 1999.
79. Levine AJ: p53, the cellular gatekeeper for growth and division. *Cell* 88: 323-331, 1997.
80. Miyashita T and Reed JC: Tumor suppressor p53 is a direct transcriptional activator of the human *bax* gene. *Cell* 80: 293-299, 1995.
81. Miyashita T, Krajewski S, Krajewska M, Wang HG, Lin HK, Liebermann DA, Hoffman B and Reed JC: Tumor suppressor p53 is a regulator of *bcl-2* and *bax* gene expression *in vitro* and *in vivo*. *Oncogene* 9: 1799-1805, 1994.
82. Beham A, Marin MC, Fernandez A, Herrmann J, Brisbay S, Tari AM, Lopez-Berestein G, Lozano G, Sarkiss M and McDonnell TJ: Bcl-2 inhibits p53 nuclear import following DNA damage. *Oncogene* 15: 2767-2772, 1997.

83. Jayaraman L and Prives C: Activation of p53 sequence-specific DNA binding by short single strands of DNA requires the p53 C-terminus. *Cell* 81: 1021-1029, 1995.
84. Oppenheim RW: Cell death during development of the nervous system. *Annu Rev Neurosci* 14: 453-501, 1991.
85. Linden R: The survival of developing neurons: a review of afferent control. *Neuroscience* 58: 671-682, 1994.
86. Clarke PGH and Egloff M: Combined effects of deafferentation and de-efferentation on isthmo-optic neurons during the period of their naturally occurring cell death. *Anat Embryol* 179: 103-108, 1988.
87. Martinou JC, Dubois-Dauphin M, Staple JK, Rodriguez I, Frankowski H, Missotten M, Albertini P, Talabot D, Catsicas S, Pietra C and Huarte J: Overexpression of bcl-2 in transgenic mice protects neurons from naturally occurring cell death and experimental ischemia. *Neuron* 13: 1017-1030, 1994.
88. Farlie PG, Dringen R, Rees SM, Kannourakis G and Bernard O: Bcl-2 transgene expression can protect neurons against developmental and induced cell death. *Proc Natl Acad Sci USA* 92: 4397-4401, 1995.
89. Bonfanti L, Strettoi E, Chierzi S, Cenni MC, Liu X-H, Martinou J-C, Maffei L and Rabacchi SA: Protection of retinal ganglion cells from natural and axotomy-induced cell death in neonatal transgenic mice overexpressing bcl-2. *J Neurosci* 16: 4186-4194, 1996.
90. Deckwerth TL, Elliott JL, Knudson CM, Johnson EM, Snider WD and Korsmeyer SJ: Bax is required for neuronal death after trophic factor deprivation and during development. *Neuron* 17: 401-411, 1996.
91. Kuida K, Zheng TS, Na S, Kuan C-Y, Yang D, Karasuyama H, Rakic P and Flavell RA: Decreased apoptosis in the brain and premature lethality in CPP32-deficient mice. *Nature* 384: 368-372, 1996.
92. Kuida K, Haydar TF, Kuan C-Y, Gu Y, Taya C, Karasuyama H, Su MS-S, Rakic P and Flavell RA: Reduced apoptosis and cytochrome c-mediated caspase activation in mice lacking caspase-9. *Cell* 94: 325-337, 1998.
93. Hakem R, Hakem A, Duncan GS, Henderson JT, Woo M, Soengas MS, Elia A, de la Pompa JL, Kagi D, Khoo W, Potter J, Yoshida R, Kaufman SA, Lowe SW, Penninger JM and Mak TW: Differential requirement for caspase 9 in apoptotic pathways *in vivo*. *Cell* 94: 339-352, 1998.
94. Yoshio H, Kong Y-Y, Yoshida R, Elia AJ, Hakem A, Hakem R, Penninger JM and Mak TW: Apaf1 is required for mitochondrial pathways of apoptosis and brain development. *Cell* 94: 739-750, 1998.
95. Michaelidis TM, Sendtner M, Cooper JD, Airaksinen MS, Holtmann B, Meyer M and Thoenen H: Inactivation of bcl-2 results in progressive degeneration of motoneurons, sympathetic and sensory neurons during early postnatal development. *Neuron* 17: 75-89, 1996.
96. Mazzoni IE, Said FA, Aloyz R, Miller FD and Kaplan D: Ras regulates sympathetic neuron survival by suppressing the p53-mediated cell death pathway. *J Neurosci* 19: 9716-9721, 1999.
97. Kermer P, Klöcker N, Labes M and Bähr M: Insulin-like growth factor-I protects axotomized rat retinal ganglion cells from secondary death via PI3-K-dependent Akt phosphorylation and inhibition of caspase-3 *in vivo*. *J Neurosci* 20: 722-728, 2000.
98. Martin LJ, Price AC, Kaiser A, Shaikh AY and Liu Z: Mechanisms for neuronal degeneration in amyotrophic lateral sclerosis and in models of motor neuron death. *Int J Mol Med* 5: 3-13, 2000.
99. Putcha GV, Deshmukh M and Johnson EM Jr: Bax translocation is a critical event in neuronal apoptosis: regulation by neuro-protectants, Bcl-2, and caspases. *J Neurosci* 19: 7476-7485, 1999.
100. Cregan SP, MacLaurin JG, Craig CG, Robertson GS, Nicholson DW, Park DS and Slack RS: Bax-dependent caspase-3 activation is a key determinant in p53-induced apoptosis in neurons. *J Neurosci* 19: 7860-7869, 1999.
101. Bradley WG and Krasin F: A new hypothesis of the etiology of amyotrophic lateral sclerosis. The DNA hypothesis. *Arch Neurol* 39: 677-680, 1982.
102. Fitzmaurice PS, Shaw IC, Kleiner HE, Miller RT, Monks TJ, Lau SS, Mitchell JD and Lynch PG: Evidence for DNA damage in amyotrophic lateral sclerosis. *Muscle Nerve* 19: 797-798, 1996.
103. Ferrante RJ, Browne SE, Shinobu LA, Bowling AC, Baik MJ, MacGarvey U, Kowall NW, Brown RH Jr and Beal MF: Evidence of increased oxidative damage in both sporadic and familial amyotrophic lateral sclerosis. *J Neurochem* 69: 2064-2074, 1997.
104. Tandan R, Robison SH, Munzer JS and Bradley WG: Deficient DNA repair in amyotrophic lateral sclerosis cells. *J Neurol Sci* 79: 189-203, 1987.
105. Kisby GE, Milne J and Sweatt C: Evidence of reduced DNA repair in amyotrophic lateral sclerosis brain tissue. *Neuroreport* 8: 1337-1340, 1997.
106. Rosen DR, Siddique T, Patterson D, Figlewicz DA, Sapp P, Hentati A, Donaldson D, Goto J, O'Regan JP, Deng H-X, Rahmani Z, Krizus A, McKenna-Yasek D, Cayabyab A, Gaston AM, Berger R, Tanzi RE, Halperin JJ, Harzfeldt B, Van den Bergh R, Hung W-Y, Bird T, Deng G, Mulder DW, Smyth CA, Laing NG, Soriano E, Pericak-Vance MA, Haines J, Rouleau GA, Gusella JS, Horvitz HR and Brown RH: Mutations in Cu/Zn superoxide dismutase gene are associated with familial amyotrophic lateral sclerosis. *Nature* 362: 59-62, 1993.
107. Deng H-X, Hentati A, Tainer JA, Iqbal Z, Cayabyab A, Hung W-Y, Getzoff ED, Hu P, Herzfeldt B, Roos RP, Warner C, Deng G, Soriano E, Smyth C, Parge HB, Ahmed A, Roses AD, Hallewell RA, Pericak-Vance MA and Siddique T: Amyotrophic lateral sclerosis and structural defects in Cu, Zn superoxide dismutase. *Science* 261: 1047-1051, 1993.
108. Beckman JS, Carson M, Smith CD and Koppenol WH: ALS, SOD and peroxynitrite. *Nature* 364: 584, 1993.
109. Rabizadeh S, Butler Gralla E, Borchelt DR, Gwinn R, Valentine JS, Sisodia S, Wong P, Lee M, Hahn H and Bredesen DE: Mutations associated with amyotrophic lateral sclerosis convert superoxide dismutase from an antiapoptotic gene to a proapoptotic gene: studies in yeast and neural cells. *Proc Natl Acad Sci USA* 92: 3024-3028, 1995.
110. Wiedau-Pazos M, Goto JJ, Rabizadeh S, Gralla EB, Roe JA, Lee MK, Valentine JS and Bredesen DE: Altered reactivity of superoxide dismutase in familial amyotrophic lateral sclerosis. *Science* 271: 515-518, 1996.
111. Abe K, Pan L-H, Watanabe M, Kato T and Itoyama Y: Induction of nitrotyrosine-like immunoreactivity in the lower motor neuron of amyotrophic lateral sclerosis. *Neurosci Lett* 199: 152-154, 1995.
112. Beal MF, Ferrante RJ, Browne SE, Matthews RT, Kowall NW and Brown RH: Increased 3-nitrotyrosine in both sporadic and familial amyotrophic lateral sclerosis. *Ann Neurol* 42: 646-654, 1997.
113. Uppu RM, Cueto R, Squadrito GL, Salgo MG and Pryor WA: Competitive reactions of peroxynitrite with 2'-deoxyguanosine and 7,8-dihydro-8-oxo-2'-deoxyguanosine (8-oxodG): relevance to the formation of 8-oxodG in DNA exposed to peroxynitrite. *Free Radic Biol Med* 21: 407-411, 1996.
114. Boveris A and Cadenas E: Cellular sources and steady-state levels of reactive oxygen species. In: *Oxygen, Gene Expression, and Cellular Function*. Biadasz Clerch L and Massaro DJ (eds). Marcel Dekker, New York, pp1-25, 1997.
115. Sasaki S and Iwata M: Impairment of fast axonal transport in the proximal axons of anterior horn neurons in amyotrophic lateral sclerosis. *Neurology* 47: 535-540, 1996.
116. Martin LJ, Kaiser A and Price AC: Motor neuron degeneration after sciatic nerve avulsion in adult rat evolves with oxidative stress and is apoptosis. *J Neurobiol* 40: 185-201, 1999.
117. Martin LJ, Kaiser A and Price AC: Oxidative stress and p53 induction may participate in the mechanisms for motor neuron apoptosis in adult spinal cord. *Soc Neurosci Abstr* 25: 289, 1999.
118. Liu Z and Martin LJ: Motor neurons rapidly accumulate DNA single-strand breaks after *in vitro* exposure to nitric oxide and peroxynitrite and *in vivo* axotomy. *J Comp Neurol* 432: 35-60, 2001.
119. Troncoso JC, Martin LJ, Dal Forno G and Kawas CH: Neuropathology in controls and demented subjects from the Baltimore Longitudinal Study of Aging. *Neurobiol Aging* 17: 365-371, 1996.
120. Mouton PR, Martin LJ, Calhoun ME, Dal Forno G and Price DL: Cognitive decline strongly correlates with cortical atrophy in Alzheimer's disease. *Neurobiol Aging* 19: 371-377, 1998.
121. West MJ, Kawas CH, Martin LJ and Troncoso JC: The CA1 region of the human hippocampus is a hot spot in Alzheimer's disease. *Ann N Y Acad Sci* 908: 255-259, 2000.
122. Katzman R: Education and the prevalence of dementia and Alzheimer's disease. *Neurology* 43: 13-20, 1993.
123. Olshansky SJ, Carnes BA and Cassel CK: The aging of the human species. *Sci Am* 268: 46-52, 1993.
124. Chartier-Harlin M-C, Crawford F, Houlden H, Warren A, Hughes D, Fidani L, Goate A, Rossor M, Roques P, Hardy J and Mullan M: Early-onset Alzheimer's disease caused by mutations at codon 717 of the  $\beta$ -amyloid precursor protein gene. *Nature* 353: 844-846, 1991.

125. Goate A, Chartier-Harlin M-C, Mullan M, Brown J, Crawford F, Fidani L, Giuffra L, Haynes A, Irving N, James L, Mant R, Newton P, Rooke K, Roques P, Talbot C, Pericak-Vance M, Roses A, Williamson R, Rossor M, Owen M and Hardy J: Segregation of a missense mutation in the amyloid precursor protein gene with familial Alzheimer's disease. *Nature* 349: 704-706, 1991.
126. Naruse S, Igarashi S, Kobayashi H, Aoki K, Inuzuka T, Kaneko K, Shimizu T, Iihara K, Kojima T, Miyatake T and Tsuji S: Mis-sense mutation Val->Ile in exon 17 of amyloid precursor protein gene in Japanese familial Alzheimer's disease. *Lancet* 337: 978-979, 1991.
127. Campion D, Flaman JM, Brice A, Hannequin D, Dubois B, Martin C, Moreau V, Charbonnier F, Didierjean O, Tardieu S, Penet C, Puel M, Pasquier F, Ledoze F, Bellis G, Calenda A, Heilig R, Martinez M, Mallet J, Bellis M, Clergetdarpoux F, Agid Y and Frebourg T: Mutations of the presenilin 1 gene in families with early-onset Alzheimer's disease. *Hum Mol Genet* 4: 2373-2377, 1995.
128. Sherrington R, Rogaev EI, Liang Y, Rogaeva EA, Levesque G, Ikeda M, Chi H, Lin C, Li G, Holman K, Tsuda T, Mar L, Foncin JF, Bruni AC, Montesi MP, Sorbi S, Rainero I, Pinessi L, Nee L, Chumakov I, Pollen D, Brookes A, Sanseau P, Polinsky RJ, Wasco W, Da Silva HAR, Haines JL, Pericak-Vance MA, Tanzi RE, Roses AD, Fraser PE, Rommens JM and St George-Hyslop PH: Cloning of a gene bearing missense mutations in early-onset familial Alzheimer's disease. *Nature* 375: 754-760, 1995.
129. Roses AD: Apolipoprotein E alleles as risk factors in Alzheimer's disease. *Annu Rev Med* 47: 387-400, 1996.
130. Anderson AJ, Su JH and Cotman CW: DNA damage and apoptosis in Alzheimer's disease: colocalization with c-jun immunoreactivity, relationship to brain area, and effect of postmortem delay. *J Neurosci* 16: 1710-1719, 1996.
131. Lucassen PJ, Chung WCJ, Kamphorst W and Swaab DF: DNA damage distribution in the human brain as shown by *in situ* end labeling; area-specific differences in aging and Alzheimer's disease in the absence of apoptotic morphology. *J Neuropathol Exp Neurol* 56: 887-900, 1997.
132. Stadelmann C, Brück W, Bancher C, Jellinger K and Lassmann H: Alzheimer's disease: DNA fragmentation indicates increased neuronal vulnerability, but not apoptosis. *J Neuropathol Exp Neurol* 57: 456-464, 1998.
133. Sze C-I, Troncoso JC, Kawas C, Mouton P, Price DL and Martin LJ: Loss of the presynaptic vesicle protein synaptophysin in hippocampus correlates with cognitive decline in Alzheimer's disease. *J Neuropathol Exp Neurol* 56: 933-994, 1997.
134. Sze C-I, Bi H, Kleinschmidt-DeMasters BK, Filley CM and Martin LJ: Selective regional loss of exocytotic presynaptic vesicle proteins in Alzheimer's disease. *J Neurol Sci* 175: 81-90, 2000.
135. Sze C-I, Bi H, Kleinschmidt-DeMasters BK, Filley CM and Martin LJ: N-Methyl-D-aspartate receptor subunit proteins and their phosphorylation status are altered selectively in Alzheimer's disease. *J Neurol Sci* 182: 151-159, 2001.
136. Uetsuki T, Takemoto K, Nishimura I, Okamoto M, Niinobe M, Momoi T, Miura M and Yoshikawa K: Activation of neuronal caspase-3 by intracellular accumulation of wild-type Alzheimer amyloid precursor protein. *J Neurosci* 19: 6955-6964, 1999.
137. Weidemann A, Paliga K, Dürrwang U, Reinhard FBM, Schuckert O, Evin G and Masters CL: Proteolytic processing of the Alzheimer's disease amyloid precursor protein within its cytoplasmic domain by caspase-like proteases. *J Biol Chem* 274: 5823-5829, 1999.
138. Gervais FG, Xu D, Robertson GS, Vaillancourt JP, Zhu Y, Huang J, LeBlanc A, Smith D, Rigby M, Shearman MS, Clarke EE, Zheng H, van der Ploeg LH, Ruffolo SC, Thornberry NA, Xanthoudakis S, Zamboni RJ, Roy S and Nicholson DW: Involvement of caspases in proteolytic cleavage of Alzheimer's amyloid- $\beta$  precursor protein and amyloidogenic A $\beta$  peptide formation. *Cell* 97: 395-406, 1999.
139. LeBlanc A, Liu H, Goodyer C, Bergeron C and Hammond J: Caspase-6 role in apoptosis of human neurons, amyloidogenesis, and Alzheimer's disease. *J Biol Chem* 274: 23426-23436, 1999.
140. Loo DT, Copani A, Pike CJ, Whittemore ER, Walencewicz AJ and Cotman CW: Apoptosis is induced by  $\beta$ -amyloid in cultured central nervous system neurons. *Proc Natl Acad Sci USA* 90: 7951-7955, 1993.
141. Behl C, Davis JB, Klier FG and Schubert D: Amyloid  $\beta$  peptide induces necrosis rather than apoptosis. *Brain Res* 645: 253-264, 1994.
142. Nakagawa T, Zhu H, Morishima N, Li E, Xu J, Yankner BA and Yuan J: Caspase-12 mediates endoplasmic reticulum-specific apoptosis and cytotoxicity by amyloid- $\beta$ . *Nature* 403: 98-103, 2000.
143. Kim T-W, Pettingell WH, Jung Y-K, Kovacs DM and Tanzi RE: Alternative cleavage of Alzheimer-associated presenilins during apoptosis by a caspase-3 family protein. *Science* 277: 373-376, 1997.
144. Lee MK, Slunt HH, Martin LJ, Thinakaran G, Kim G, Gandy SE, Seeger M, Koo E, Price DL and Sisodia SS: Expression of presenilin 1 and 2 (PS1 and PS2) in human and murine tissues. *J Neurosci* 16: 7513-7525, 1996.
145. Passer BJ, Pellegrini L, Vito P, Ganjei K and D'Adamio L: Interaction of Alzheimer's presenilin-1 and presenilin-2 with Bcl-X<sub>L</sub>. *J Biol Chem* 274: 24007-24013, 1999.
146. Ito U, Spatz M, Walker JT and Klatzo I: Experimental cerebral ischemia in mongolian gerbils. I. Light microscopic observations. *Acta Neuropathol* 32: 209-223, 1975.
147. Kirino T: Delayed neuronal death in the gerbil hippocampus following ischemia. *Brain Res* 239: 57-69, 1982.
148. Goto K, Ishige A, Sekiguchi K, Iizuka S, Sugimoto A, Yuzurihara M, Aburada M, Hosoya E and Kogure K: Effects of cycloheximide on delayed neuronal death in rat hippocampus. *Brain Res* 534: 299-302, 1990.
149. Martin LJ, Sieber FE and Traystman RJ: Apoptosis and necrosis occur in separate neuronal populations in hippocampus and cerebellum after ischemia and are associated with alterations in metabotropic glutamate receptor signaling pathways. *J Cereb Blood Flow Metab* 20: 153-167, 2000.
150. Kerr JFR and Harmon BV: Definition and incidence of apoptosis: an historical perspective. In: *Apoptosis: The Molecular Basis of Cell Death*. Tomei LD and Cope FO (eds). Cold Spring Harbor Laboratory Press, Cold Spring Harbor, New York, pp5-29, 1991.
151. Héron A, Pollard H, Dessi F, Moreau J, Lasbennes F, Ben-Ari Y and Charriaud-Marlangue C: Regional variability in DNA fragmentation after global ischemia evidenced by combined histological and gel electrophoresis observations in the rat brain. *J Neurochem* 61: 1973-1976, 1993.
152. MacManus JP, Hill IE, Preston E, Rasquinha I, Walker T and Buchan AM: Differences in DNA fragmentation following transient cerebral ischemia or decapitation ischemia in rats. *J Cereb Blood Flow Metab* 15: 728-737, 1995.
153. Nitatori T, Sato N, Waguri S, Karasawa Y, Araki H, Shibana K, Kominami E and Uchiyama Y: Delayed neuronal death in the CA1 pyramidal cell layer of the gerbil hippocampus following transient ischemia is apoptosis. *J Neurosci* 15: 1001-1011, 1995.
154. Krajewski S, Mai JK, Krajewska M, Sikorska M, Mossakowski MJ and Reed JC: Upregulation of bax protein levels in neurons following cerebral ischemia. *J Neurosci* 15: 6364-6376, 1995.
155. Sugawara T, Fujimura M, Morita-Fujimura Y, Kawase M and Chan PH: Mitochondrial release of cytochrome c corresponds to the selective vulnerability of hippocampal CA1 neurons in rats after transient global cerebral ischemia. *J Neurosci* 19: RC39, 1-6, 1999.
156. Deshpande J, Bergstedt K, Linden T, Kalimo H and Wieloch T: Ultrastructural changes in the hippocampal CA1 region following transient cerebral ischemia: evidence against programmed cell death. *Exp Brain Res* 88: 91-105, 1992.
157. Colbourne F, Sutherland GR and Auer RN: Electron microscopic evidence against apoptosis as the mechanism of neuronal death in global ischemia. *J Neurosci* 19: 4200-4210, 1999.
158. Schulz JB, Weller M and Moskowitz MA: Caspases as treatment targets in stroke and neurodegenerative diseases. *Ann Neurol* 45: 421-429, 1999.
159. Shigeno T, Yamasaki Y, Kato G, Kusaka K, Mima T, Takakura K, Graham DI and Furukawa S: Reduction of delayed neuronal death by inhibition of protein synthesis. *Neurosci Lett* 120: 117-119, 1990.
160. Chen J, Zhu RL, Nakayama M, Kawaguchi K, Jin K, Stetler RA, Simon RP and Graham SH: Expression of the apoptosis-effector gene, *bax*, is upregulated in vulnerable hippocampal CA1 neurons following global ischemia. *J Neurochem* 67: 64-71, 1996.
161. Kosko B: *Fuzzy Thinking*. Harper-Collins, London, p318, 1994.

162. Martin LJ, Brambrink AM, Lehmann C, Portera-Cailliau C, Koehler R, Rothstein J and Traystman RJ: Hypoxia-ischemia causes abnormalities in glutamate transporters and death of astroglia and neurons in newborn striatum. *Ann Neurol* 42: 335-348, 1997.
163. Northington FJ, Ferriero DM, Flock DL and Martin LJ: Delayed neurodegeneration in neonatal rat thalamus after hypoxia-ischemia is apoptosis. *J Neurosci* (In press).
164. Yamashima T: Implications of cysteine proteases calpain, cathepsin and caspase in ischemia neuronal death of primates. *Prog Neurobiol* 62: 273-295, 2000.
165. Grasl-Kraupp B, Ruttkay-Nedecky B, Koudelka H, Bukowska K, Bursch W and Schulte-Hermann R: *In situ* detection of fragmented DNA (TUNEL assay) fails to discriminate among apoptosis, necrosis, and autolytic cell death: a cautionary note. *FASEB J* 21: 1465-1468, 1995.
166. Lockshin RA and Zakeri A: Programmed cell death: early changes in metamorphosing cells. *Biochem Cell Biol* 72: 589-596, 1994.
167. Collins RJ, Harmon BV, Gobé VC and Kerr JFR: Internucleosomal DNA cleavage should not be the sole criterion for identifying apoptosis. *Int J Radiat Biol* 61: 451-453, 1992.
168. Okamoto M, Matsumoto M, Ohtsuki T, Taguchi A, Mikoshiba K, Yanagihara T and Kamada T: Internucleosomal DNA cleavage involved in ischemia-induced neuronal death. *Biochem Biophys Res Commun* 196: 1356-1362, 1993.
169. Bhat RV, DiRocco R, Marcy VR, Flood DG, Zhu Y, Dobrzanski P, Siman R, Scott R, Contreras PC and Miller M: Increased expression of IL1 $\beta$  converting enzyme in hippocampus after ischemia: selective localization in microglia. *J Neurosci* 16: 4146-4154, 1996.
170. Fukuda K, Kojiro M and Chiu JF: Demonstration of extensive chromatin cleavage in transplanted Morris hepatoma 7777 tissue: apoptosis or necrosis? *Am J Pathol* 142: 935-946, 1993.
171. Gwag BJ, Koh JY, DeMaro JA, Ying HS, Jacquin M and Choi DW: Slowly triggered excitotoxicity occurs by necrosis in cortical cultures. *Neuroscience* 77: 393-401, 1997.
172. Sohn S, Kim EY and Gwag BJ: Glutamate neurotoxicity in mouse cortical neurons: atypical necrosis with DNA ladders and chromatin condensation. *Neurosci Lett* 240: 147-150, 1997.
173. MacManus JP, Fliss H, Preston E, Rasquinha I and Tuor U: Cerebral ischemia produces ladder DNA fragments distinct from cardiac ischemia and archetypal apoptosis. *J Cereb Blood Flow Metabol* 19: 502-510, 1999.
174. Kerr JFR, Gobé GC, Winterford CM and Harmon BV: Anatomical methods in cell death. In: *Cell Death*. Schwartz LM and Osborne BA (eds). Academic Press, New York, pp1-27, 1995.
175. Kitagawa K, Matsumoto M, Tsujimoto Y, Ohtsuki T, Kuwabara K, Matsushita K, Yang G, Tanabe H, Martinou J-C, Hori M and Yanagihara T: Amelioration of hippocampal neuronal damage after global ischemia by neuronal overexpression of Bcl-2 in transgenic mice. *Stroke* 29: 2616-2621, 1998.
176. Chen DF, Schneider GE, Martinou J-C and Toneyawa S: Bcl-2 promotes regeneration of severed axons in mammalian CNS. *Nature* 385: 434-439, 1997.
177. Lam M, Dubyak G, Chen G, Nufiez G, Miesfeld RL and Distelhorst CW: Evidence that BCL-2 represses apoptosis by regulating endoplasmic reticulum-associated Ca<sup>2+</sup> fluxes. *Proc Natl Acad Sci USA* 91: 6569-6573, 1994.
178. Xu DG, Crocker SJ, Doucet J-P, St-Jean M, Tamai K, Hakim AM, Ikeda J-E, Liston P, Thompson CS, Korneluk RG, MacKenzie A and Robertson GS: Elevation of neuronal expression of NAIP reduces ischemic damage in the rat hippocampus. *Nat Med* 3: 997-1004, 1997.
179. Chen J, Nakayama T, Jin K, Stetler RA, Zhu RL, Graham SH and Simon RP: Induction of caspase-3-like protease may mediate delayed neuronal death in the hippocampus after transient cerebral ischemia. *J Neurosci* 18: 4914-4928, 1998.
180. Al-Abdulla NA, Portera-Cailliau C and Martin LJ: Occipital cortex ablation in adult rat causes retrograde neuronal death in the lateral geniculate nucleus that resembles apoptosis. *Neuroscience* 86: 191-209, 1998.
181. Martin LJ, Kaiser A, Yu JW, Natale JE and Al-Abdulla NA: Injury-induced apoptosis of neurons in adult brain is mediated by p53-dependent and p53-independent pathways and requires bax. *J Comp Neurol* (In press).
182. Martin LJ, Brambrink A, Koehler RC and Traystman RJ: Primary sensory and forebrain motor systems in the newborn brain are preferentially damaged by hypoxia-ischemia. *J Comp Neurol* 377: 262-285, 1997.
183. Golden WC, Brambrink AM, Traystman RJ and Martin LJ: Failure to sustain recovery of Na,K ATPase function is a possible mechanism for striatal neurodegeneration in hypoxic-ischemic newborn piglets. *Mol Brain Res* (In press).
184. Furuta A, Rothstein JD and Martin LJ: Glutamate transporter protein subtypes are expressed differentially during rat CNS development. *J Neurosci* 17: 8363-8375, 1997.
185. Dobbing J and Sands J: Comparative aspects of the brain growth spurt. *Early Hum Dev* 3: 79-83, 1979.
186. Choi DW: Excitotoxic cell death. *J Neurobiol* 23: 1261-1276, 1992.
187. Yano S, Tokumitsu H and Soderling TR: Calcium promotes cell survival through CaM-K kinase activation of the protein-kinase-B pathway. *Nature* 396: 584-587, 1998.
188. Petersén Á, Castilho RF, Hansson O, Wieloch T and Brundin P: Oxidative stress, mitochondrial permeability transition and activation of caspases in calcium ionophore A23187-induced death of cultured striatal neurons. *Brain Res* 857: 20-29, 2000.
189. Li Y-Z, Li CJ, Ventura Pinto A and Pardee AB: Release of mitochondrial cytochrome C in both apoptosis and necrosis induced by  $\beta$ -lapachone in human carcinoma cells. *Mol Med* 5: 232-239, 1999.
190. Yardin C, Terro F, Esclaire F, Rigaud M and Hugon J: Brefeldin A-induced apoptosis is expressed in rat neurons with dephosphorylated tau protein. *Neurosci Lett* 250: 1-4, 1998.
191. Jiang S, Chow SC, Nicotera P and Orrenius S: Intracellular Ca<sup>2+</sup> signals activate apoptosis in thymocytes: studies using the Ca<sup>2+</sup>-ATPase inhibitor thapsigargin. *Exp Cell Res* 212: 84-92, 1994.
192. Thilmann R, Xie Y, Kleihues P and Kiessling M: Persistent inhibition of protein synthesis precedes delayed neuronal death in postischemic gerbil hippocampus. *Acta Neuropathol* 71: 88-93, 1986.
193. Araki T, Kato H, Inoue T and Kogure K: Regional impairment of protein synthesis following brief cerebral ischemia in the gerbil. *Acta Neuropathol* 79: 501-505, 1990.
194. Furuta S, Ohta S, Hatakeyama T, Nakamura K and Sakaki S: Recovery of protein synthesis in tolerance-induced hippocampal CA1 neurons after transient forebrain ischemia. *Acta Neuropathol* 86: 329-336, 1993.
195. Sugita M, Morita T and Yonesaki T: Puromycin induces apoptosis of developing chick sympathetic neurons in a similar manner to NGF-deprivation. *Zool Sci* 12: 419-425, 1995.
196. Petito CK and Pulsinelli WA: Sequential development or reversible and irreversible neuronal damage following cerebral ischemia. *J Neuropathol Exp Neurol* 43: 141-153, 1984.
197. Mancini M, Machamer CE, Roy S, Nicholson DW, Thornberry NA, Casciola-Rosen LA and Rosen A: Caspase-2 is localized at the Golgi complex and cleaves golgin-160 during apoptosis. *J Cell Biol* 149: 603-612, 2000.
198. Kitagawa K, Matsumoto M, Niinobe M, Mikoshiba K, Hata R, Ueda H, Handa N, Fukunaga R, Isaka Y, Kimura K and Kamada T: Microtubule-associated protein 2 as a sensitive marker for cerebral ischemic damage. Immunohistochemical investigation of dendritic damage. *Neuroscience* 31: 401-411, 1989.
199. Yamamoto K, Hayakawa T, Mogami H, Akai F and Yanagihara T: Ultrastructural investigation of the CA1 region of the hippocampus after transient cerebral ischemia in gerbils. *Acta Neuropathol* 80: 487-492, 1990.
200. Seubert P, Lee K and Lynch G: Ischemia triggers NMDA receptor-linked cytoskeletal proteolysis in hippocampus. *Brain Res* 492: 366-370, 1989.
201. Roberts-Lewis JM, Savage MJ, Marcy VR, Pinsker LR and Siman R: Immunolocalization of calpain I-mediated spectrin degradation to vulnerable neurons in the ischemic gerbil brain. *J Neurosci* 14: 3934-3944, 1994.
202. LaVelle A and LaVelle FW: The nucleolar apparatus and neuronal reactivity in injury during development. *J Exp Zool* 137: 285-315, 1958.
203. Torvik A: Central chromatolysis and the axon reaction. A reappraisal. *Neuropathol Appl Neurobiol* 2: 423-432, 1976.
204. Natale JE and Martin LJ: Ablation of occipital cortex in immature mouse brain induces p53 and neuronal apoptosis in the lateral geniculate nucleus. *Soc Neurosci Abstr* 26: 1323, 2000.
205. Dubois-Dauphin M, Frankowski H, Tsujimoto Y, Huarte J and Martinou JC: Neonatal motoneurons overexpressing the bcl-2 protooncogene in transgenic mice are protected from axotomy-induced cell death. *Proc Natl Acad Sci USA* 91: 3309-3313, 1994.

206. Gagliardini V, Fernandez P, Lee RKK, Drexler HCA, Rotello RJ, Fishman MC and Yuan J: Prevention of vertebrate neuronal death by *crmA* gene. *Science* 263: 826-828, 1994.
207. Deshmukh M, Vasilakos J, Deckwerth TL, Lampe PA, Shivers BD and Johnson EM: Genetic and metabolic status of NGF-deprived sympathetic neurons saved by an inhibitor of ICE family proteases. *J Cell Biol* 135: 1341-1354, 1996.
208. Kermer P, Klöcker N, Labes M and Bähr M: Inhibition of CPP-32-like proteases rescues axotomized retinal ganglion cells from secondary cell death *in vivo*. *J Neurosci* 18: 4656-4662, 1998.
209. Milligan CE, Prevett D, Yaginuma H, Homma S, Cardwell C, Fritz LC, Tomaselli KJ, Oppenheim RW and Schwartz LM: Peptide inhibitors of the ICE protease family arrest programmed cell death of motoneurons *in vivo* and *in vitro*. *Neuron* 15: 385-393, 1995.
210. Al-Abdulla NA and Martin LJ: Apoptosis of retrogradely degenerating neurons occurs in association with the accumulation of perikaryal mitochondria and oxidative damage to the nucleus. *Am J Pathol* 153: 447-456, 1998.
211. Subba Rao K: Genomic damage and its repair in young and aging brain. *Mol Neurobiol* 7: 23-48, 1993.



## THALAMIC NEURON APOPTOSIS EMERGES RAPIDLY AFTER CORTICAL DAMAGE IN IMMATURE MICE

J. E. NATALE,<sup>a,b,\*</sup> Y. CHENG<sup>a</sup> and L. J. MARTIN<sup>c,d</sup>

<sup>a</sup>Research Center for Genetic Medicine, Children's National Medical Center, 111 Michigan Avenue, NW, Washington, DC 20010-2970, USA

<sup>b</sup>Neuroscience Research Center, Children's Research Institute, George Washington University School of Medicine, Washington, DC, USA

<sup>c</sup>Department of Pathology, Division of Neuropathology, Johns Hopkins University School of Medicine, Baltimore, MD, USA

<sup>d</sup>Department of Neuroscience, Johns Hopkins University School of Medicine, Baltimore, MD, USA

**Abstract**—In adults and children, head trauma can have long-term neuropathological and functional consequences. The thalamus is a major site of remote neurodegeneration after cortical damage in adult humans and experimental animals, but less is known about thalamic responses to cortical injury in the immature brain. This study introduces an *in vivo* model of axotomy/target deprivation-induced neuronal apoptosis in the dorsal lateral geniculate nucleus of the thalamus produced by unilateral ablation of the occipital cortex in the immature mouse. We specifically examined whether occipital cortex ablation in the immature brain causes apoptotic death of projection neurons in the dorsal lateral geniculate nucleus. After unilateral occipital cortex aspiration, 10-day-old C57BL/6 mice were recovered for up to 28 days. Fluorogold-prelabeled thalamocortical projection neurons were apoptotic at 36–48 h after ablation. The structural progression of apoptosis in the immature lateral geniculate nucleus reveals typical chromatolytic morphology by 18–24 h, followed by cytoplasmic shrinkage and chromatin condensation characteristic of end-stage apoptosis after 36–48 h. Electron microscopy confirmed the presence of apoptosis. This study shows internucleosomal DNA fragmentation and expression of cleaved caspase-3 occurs rapidly, being noted first at 18 h, well before the peak of apoptotic cell death occurring at 36 h after cortical damage in the immature brain.

From these data we suggest that axotomy/target deprivation-induced cell death in the immature brain may: (1) differ from that previously reported in adult mice with respect to the time required for progression to cell death; (2) be mediated by caspase-3 activation. © 2002 IBRO. Published by Elsevier Science Ltd. All rights reserved.

**Key words:** axotomy, brain injury, caspase-3, DNA damage, neuronal cell death, retrograde neurodegeneration.

Axotomy, target deprivation, and neurotrophin withdrawal may participate in the evolution of the neuropathology of a wide range of pediatric and adult neurological diseases, including hypoxia-ischemia, traumatic brain injury (TBI), stroke, spinal muscular atrophy, amyotrophic lateral sclerosis, and Alzheimer's disease. Development of effective therapies for these neurodegenerative disorders depends on understanding the principles of selective vulnerability and the mechanisms of cell death. There is a growing appreciation that the response to injury by the immature brain differs from the adult brain. In this regard, it is known that the extent of functional recovery after damage to the CNS is influ-

enced by many factors, including the maturity of the CNS at the time of the lesion. Furthermore, neuroprotective strategies are likely to be different in the immature and adult CNS. For example, after TBI in adult rats, *N*-methyl-D-aspartate (NMDA) receptor activation has been linked to cell death because NMDA receptor antagonism ameliorates cell loss (Faden et al., 1989). However, in rat pups pharmacological antagonism of NMDA receptors after TBI exacerbates neuronal death, implicating relationships between cell death signaling and neuronal maturity (Pohl et al., 1999). Therefore, a critical examination of cell death in the CNS with regard to brain maturity is essential to the development of approaches to limit cell death in neurodegenerative disease.

After cortical injury produced by stroke, TBI, or hypoxia-ischemia, neurological outcome is determined not only by the cell death produced by the cortical injury itself, but also by retrograde degeneration of thalamocortical fibers (Iizaka et al., 1990; Rink et al., 1995; Conti et al., 1998; Pohl et al., 1999; Nakajima et al., 2000; Northington et al., 2001). In a cortical impact model of TBI in immature animals, a biphasic pattern of neurodegeneration is observed (Rink et al., 1995;

\*Corresponding author. Tel.: +1-202-884-4710; fax: +1-202-884-6014.

E-mail address: jnatale@cnmc.org (J. E. Natale).

**Abbreviations:** EDTA, ethylenediaminetetraacetic acid; EGTA, ethyleneglycol-bis(β-aminoethyl)-*N,N,N',N'*-tetraacetic acid; EM, electron microscopy; FG, fluorogold; LGN, lateral geniculate nucleus; NMDA, *N*-methyl-D-aspartate; PBS, phosphate-buffered saline; TBI, traumatic brain injury; TUNEL, terminal deoxynucleotidyl transferase (TdT)-mediated deoxyuridine triphosphate (dUTP)-biotin nick end labeling; UV, ultraviolet.

Conti et al., 1998; Pohl et al., 1999). Initially, cell death is limited to the area of parietal cortex directly underlying the impact (Pohl et al., 1999). By 24 h after impact, cortical projection neurons in the dorsolateral thalamus die by apoptosis. A similar pattern of delayed cell death was observed in the thalamus 14 days after impact injury to the ipsilateral cortex in adult rats (Conti et al., 1998). Thus secondary apoptosis mediates the delayed pathogenic processes that extend the extent of brain injury. This observation has lead us to adapt a model of target deprivation-induced neurodegeneration to compare the process of secondary neurodegeneration in the developing and mature brain.

Animal models of axotomy and target deprivation in the CNS provide a relatively simple and reliable paradigm for the study of neuronal injury progression and degeneration (Ross and Ebner, 1990; Agarwala and Kalil, 1998; Al-Abdulla and Martin, 1998; Al-Abdulla et al., 1998). One model, unilateral ablation of the occipital cortex in the adult mammalian brain, reproducibly produces retrograde degeneration and elimination of subsets of neurons in the ipsilateral dorsal lateral geniculate nucleus (LGN) through bona fide apoptosis (Al-Abdulla and Martin, 1998; Al-Abdulla et al., 1998). Because geniculocortical projection neurons target highly focal regions of visual cortex with minimal collateralization, target deprivation in this system causes a rapid, synchronized death of neurons in the dorsal LGN of adult rodents (Barron et al., 1973; Agarwala and Kalil, 1998; Al-Abdulla and Martin, 1998; Al-Abdulla et al., 1998; Martin et al., 2001). In this model of unilateral occipital cortex ablation in the adult CNS, neurodegeneration of the LGN neurons evolves morphologically over 7 days through classical chromatolysis to apoptosis (Al-Abdulla et al., 1998).

The objective of this study was to develop and characterize an *in vivo* model of delayed neurodegeneration in the immature mouse brain. We specifically examined whether occipital cortex ablation in the immature CNS would cause death of projection neurons in the dorsal LGN. Furthermore, we describe the temporal progression of this neurodegeneration with neuropathological and ultrastructural morphology, cleaved caspase-3 expression, and DNA fragmentation patterns.

#### EXPERIMENTAL PROCEDURES

Animal care was provided in accordance with the National Institutes of Health Guide for the Care and Use of Laboratory Animals. The Animal Care and Use Committee of the Johns Hopkins University School of Medicine approved the animal protocol. All efforts were made to minimize both the suffering and the number of animals used.

##### *Lesion paradigm to study retrograde degeneration of LGN neurons*

Eight-day-old C57BL/6 mouse pups and nursing mothers were purchased from Charles River Laboratory (Wilmington, MA, USA). Pups were housed with a nursing mother in the laboratory animal suite with an ambient temperature of 20°C, a 12-h light/dark cycle, and *ad libitum* access to food and water.

At 10 days of age, body weight and gender were determined prior to induction of anesthesia with enflurane and nitrous oxide in oxygen. Pups were placed in a mouse stereotaxic apparatus (Stoelting, Wood Dale, IL, USA) while surgical anesthesia was maintained with enflurane and nitrous oxide. Ambient temperature was 25°C and body temperature was maintained with external warming. The scalp was cleaned with betadine and 70% isopropyl alcohol prior to making a midsagittal incision, exposing the sagittal suture from the bregma to the lamdoidal suture. A 3×3-mm cranial flap was made by lifting and folding a rectangular bone flap along the medial aspect; the medial side was located 1 mm lateral to the midline and the caudal side was 1 mm rostral to the lambda. The right occipital cortex was aspirated using a blunt-tipped 20-gauge needle connected to low-grade suction, without damaging surrounding venous sinuses or underlying hippocampus (Fig. 2A). The bone flap was then replaced, and the scalp closed with 5-0 nylon suture. When pups were able to ambulate, they were returned to the cage with the nursing mother. Postlesion survival times after occipital cortex ablation were 6, 12, 18, 24, 30, 36, 48, 72 h, 7 and 28 days (*N*=four males and four females for each time point). Pups in the sham groups underwent the same operative procedure, craniotomy without lifting the bone flap, then scalp closure and recovery (*N*=4 at each time point). Pup brains were either perfusion fixed for histological analysis or retrieved fresh for biochemical analyses.

##### *Retrograde labeling of corticopetal projection neurons in the dorsal LGN*

In another series of experiments, unilateral injections of the retrograde tracer fluorogold (FG; Fluorochrome, Inc, Englewood, CA, USA) were made into the visual cortex of 9-day-old mouse pups (*N*=8). The right skull was exposed in anesthetized pups as described above. Through a burr hole located 1 mm lateral to the midline and 1 mm rostral to the lambda (Rosen et al., 2000), 0.5 µl of 5% FG in deionized, distilled water was injected over 10 min using a 25-gauge, 1-µl blunt-tip syringe. One day later, six pups underwent occipital cortex ablation as described above, and recovered for 24, 36, or 48 h. Three days after FG injection, the remaining two pups were anesthetized, perfused, and the brains cut into coronal sections as described above for light microscopy. Sections were mounted on glass slides, dried, counterstained with Hoechst 33258 (5 µg/µl, Molecular Probes, Eugene, OR, USA), and viewed by fluorescence microscopy.

##### *Light microscopic evaluation of neurodegeneration in the dorsal LGN*

At the 10 postlesion times described above, body weight was measured and pups were anesthetized with intraperitoneal administration of 6 mg/g body weight chloral hydrate (8%). The pups were perfused through the left ventricle with 20 ml phosphate-buffered saline (PBS, 100 mM, pH 7.4), then perfusion fixed with 4% paraformaldehyde in PBS (120 ml). Brains were removed from the skull, cryoprotected in 20% glycerol, frozen, and then serial 40-µm coronal sections were cut from the frontal pole through the brain stem using a sliding microtome. Every fifth section was mounted on gelatin-coated microscope slides, dried, dehydrated with alcohols, and stained with Cresyl Violet for 90 s. Slides were rinsed with distilled water to remove excess stain, then immersed in 70% and 95% ethanol to destain the tissue until the white matter tracts were milky white. Selected sections containing LGN (sections from two pups per time point) were mounted on subbed slides, dried, and stained with Hoechst 33258 (5 µg/µl) to label nucleic acid with blue fluorescence.

##### *TUNEL labeling to identify dying cells in the LGN after occipital cortex ablation*

At 12, 24, 36, and 48 h after occipital ablation, terminal



deoxynucleotidyl transferase (TdT)-mediated deoxyuridine triphosphate (dUTP)-biotin nick end labeling (TUNEL) was performed as previously described (Portera-Cailliau et al., 1997). Mounted coronal sections were incubated with 20 µg/ml proteinase K (Boehringer Mannheim, Basel, Switzerland) for 15 min in phosphate buffer. Endogenous peroxidases were inactivated with 2.5% hydrogen peroxide. Sections were incubated in TdT buffer and biotinylated dUTP for 60 min. Two sections, serving as negative controls, were processed in parallel without TdT buffer and biotinylated dUTP. After stopping the reaction, sections were blocked with 2.5% non-fat milk, and then incubated in avidin peroxidase. Sections were finally processed with a standard diaminobenzidine chromogenic reaction.

#### *Cleaved caspase-3 immunofluorescence in the immature dorsal LGN*

Paraformaldehyde-fixed coronal brain sections from mouse pups 12, 18, 24, 36 and 72 h postlesion were washed with PBS, then blocked with 10% normal goat serum in 0.3% Triton X-100 for 30 min at room temperature. Sections were then incubated overnight at 4°C in a rabbit polyclonal antibody that detects cleaved caspase-3 (1:100, Cell Signaling Technology, Beverly, MA, USA) in 0.2% Triton X-100. On immunoblots, this antibody detected a single band at 20 kDa (Fig. 6G). After washing with PBS, half of the sections were processed for fluorescent immunolabel, while the others were processed for chromogenic immunodetection. For fluorescent labeling, the sections were placed in secondary antibody solution containing 2% normal goat serum, 0.2% Triton X-100, and affinity-purified donkey anti-rabbit IgG conjugated to Cy3 (1:100, Jackson ImmunoResearch Laboratories, Inc., West Grove, PA, USA) for 1 h while protected from light. These sections were washed in PBS, mounted on gelatin-coated slides, coverslipped with Gel/Mount (Biomedex, Foster City, CA, USA), and viewed under a fluorescent microscope (Nikon Microphot FXA). For chromogenic immunodetection, the sections were placed in secondary antibody solution containing 2% normal goat serum, 0.1% Triton X-100, and affinity-purified goat anti-rabbit IgG (1:100, Cappel, ICN Pharmaceuticals, Aurora, OH, USA) for 1 h. After rinsing, the sections were incubated in rabbit peroxidase anti-peroxidase in 2% normal goat serum for 1 h. Sections were processed with a standard peroxide-diaminobenzidine chromogenic reaction. After immunostaining, the sections were washed in PBS, mounted on gelatin-coated slides, air dried, dehydrated, and counterstained with Cresyl Violet as described above. Two additional sections were incubated without the addition of cleaved caspase-3 antibody and processed along with the sections described above.

#### *Quantification of apoptotic cells in the immature dorsal LGN*

Cresyl Violet-stained sections were used to count end-stage apoptotic cells in the dorsal and ventral LGN of mouse pups at the 10 postlesion times described above after unilateral occipital cortex ablation. Brain sectioning, section mounting, and staining are described above. The serially mounted, stained coronal brain sections were reviewed under low magnification (12.5×) to identify the five (11–17-day-old pups) or seven (38-day-old pups) consecutive sections that included the ipsilateral or contralateral LGN. The third or fourth of these five or seven sections represents the mid-level through each LGN in the rostrocaudal axis. Counts of end-stage apoptotic cells were made in two, non-overlapping high power fields (1000×) at this level. Each field was counted in triplicate with the mean number of apoptotic cells reported. Apoptotic cells were identified by a rounded, condensed, translucent rim of cytoplasm, detached from surrounding neuropil, with two or more sharply delineated, uniformly dense, smooth, round, regularly shaped discrete masses of dark purple chromatin (Fig. 4E and F).

#### *Ultrastructural analysis of neuronal death in the dorsal LGN after occipital cortex ablation*

After 18, 24, and 36 h postlesion, mouse pups ( $N=2$  per time point) were anesthetized with chloral hydrate as described above, an incision was made to expose the abdominal contents, and 0.1 ml sodium nitrate and 20 units of heparin (Sigma, St. Louis, MO, USA) were injected into the spleen. A thoracotomy exposed the heart for insertion of a 23-gauge needle into the left ventricle to deliver 20 ml 1% paraformaldehyde/0.1% glutaraldehyde in 0.1 M phosphate buffer followed by 120 ml 2% paraformaldehyde/2% glutaraldehyde in phosphate buffer. Brains were postfixed *in situ* with the same fixative. The LGNs ipsilateral and contralateral to the cortical lesion were microdissected from each brain, rinsed in 0.1 M phosphate buffer, placed in 2% osmium tetroxide for 2 h, dehydrated and embedded in plastic. Semithin sections (1 µm) stained with 1% Toluidine Blue were screened for area of interest, then thin sections were cut on an ultramicrotome (Sorvall, Norwalk, CT, USA), contrasted with uranyl acetate and lead citrate, and viewed with a Jeol 100S electron microscope.

#### *Agarose gel electrophoresis for DNA fragmentation*

For regional biochemical analyses, the brain was removed from anesthetized mice surviving 18 and 24 h after occipital cortex ablation or sham lesioned ( $N=20$  in each group). The brain was placed on a plate of ice under a stereomicroscope and the cortex reflected to expose the dorsal thalamus. Surface landmarks delineated the LGN. From each animal, the ipsilateral (target-deprived) and contralateral (control) LGN were microdissected and immediately frozen in chilled isopentane (−40°C). For each time point, either ipsilateral or contralateral LGN tissue from 20 brains were pooled. We verified the accuracy of the LGN microdissection by removing LGN samples, immersion fixing the hindbrain in 4% paraformaldehyde, then cryoprotected in 20% glycerol. The rostral hindbrain was cut into 40-µm sections on a sliding microtome, then stained with Cresyl Violet and viewed microscopically (data not shown).

LGN samples were homogenized with a polytron in cold homogenization buffer with protease inhibitors (20 mM Tris-HCl, pH 7.4, with 10% sucrose, 1 mM EDTA, 5 mM EGTA, 20 U/ml Traysol, 20 µg/ml leupeptin, 20 µg/ml antipain, 20 µg/ml pepstatin, 20 µg/ml chymostatin, 0.1 mM phenylmethylsulfonyl fluoride, 10 mM benzamide; Sigma, St. Louis, MO, USA), then centrifuged at 1000×g for 10 min at 4°C. To identify the pattern of DNA fragmentation in the LGN after occipital ablation, DNA was extracted from this nuclear-enriched pellet obtained from microdissected ipsilateral or contralateral LGN from sham-lesioned and recovered pups 18 and 24 h after occipital ablation. LGN samples were treated with proteinase K overnight, and genomic DNA was extracted with phenol:chloroform:isoamyl alcohol. DNA concentration was determined spectrophotometrically. After digesting RNA with DNase-free RNase followed by repurification, DNA (2 µg) was end-labeled with digoxigenin. DNA was fractionated in a 1.5% agarose gel, transferred to a nylon membrane and crosslinked with ultraviolet (UV) light. Membranes were incubated in 2% nucleic acid blocking reagent containing anti-digoxigenin Fab fragments (Boehringer Mannheim) conjugated to alkaline phosphatase (7.5 units), and detected with disodium 3-(4-methoxyphosphoryl)-2-dioxetane-3,2'-(5'-chloro)tricyclo[3.3.1]decane-4-yl phenyl phosphate (CSPD, Boehringer Mannheim) followed by exposure to Kodak X-Omat AR film.

#### *Statistical analyses*

GraphPad Prism, v. 3.02 (San Diego, CA, USA) was used for statistical analysis. Weight gain was compared between groups using the one-way analysis of variance (ANOVA) with post hoc Newman-Keuls multiple comparisons test. Apoptotic cell counts in the ipsilateral dorsal LGN were compared to the con-



tralateral dorsal LGN or ipsilateral ventral LGN by the paired Wilcoxon-matched pairs test. These comparisons were undertaken separately in sham and injured animals at each time period. For each recovery time period, apoptotic cell counts in ipsilateral dorsal LGN, ipsilateral ventral LGN, contralateral dorsal LGN, and contralateral ventral LGN were compared to the corresponding region in sham-ablated animals using the Mann-Whitney *U*-test. For all tests, criterion alpha was set at  $<0.05$ . Data are reported as means  $\pm$  S.E.M. for each group.

## RESULTS

### *Unilateral occipital cortex ablation is a reproducible brain lesion in the 10-day-old mouse pup*

Aspiration of the right occipital cortex is well tolerated by 10-day-old C57BL/6 mouse pups. Three percent of pups died during anesthetic induction. Postoperative mortality was  $<2\%$ , and was accounted for by maternal cannibalism. By 10 min after the procedure, pups were walking and feeding. Some small differences were found in weight gain early after the lesion (Fig. 1). However, by

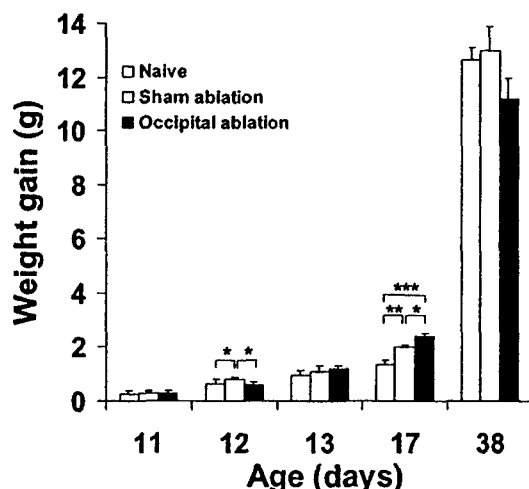


Fig. 1. Growth after unilateral occipital lobe ablation in 10-day-old mouse pups. Eight naive pups were weighed at 11, 12, 13, 17 and 38 days of age. Open bars ( $\pm$  S.E.M.) show the mean weight gain in g from baseline weight at 10 days of age. Average body weight of 10-day-old pups was  $4.2 \pm 0.1$  g. In a second group of 10-day-old pups, anesthesia with unilateral craniotomy was performed without disruption of the dura or cortical ablation. Pups were recovered for 1, 2, 3, 7, or 28 days ( $N=4$  at each time point). Shaded bars ( $\pm$  S.E.M.) show the mean weight gain at each time. Sham cortical ablation did not alter weight gain in mouse pups. In a third group of 10-day-old pups, anesthesia, unilateral craniotomy, and occipital cortex ablation was performed. As above, pups were recovered for 1, 2, 3, 7, or 28 days ( $N=8$  at each time point). Black bars ( $\pm$  S.E.M.) show mean weight gain at each time point. One and 3 days after unilateral occipital ablation, pups continue to feed and grow at the same rate as age-matched naive pups or sham-ablated pups. However, at 2 days after ablation, sham-ablated pups gained more weight than either age-matched naive pups, or occipital-ablated pups ( $P<0.05$ ). By 7 days after surgery, both sham and occipital cortex-ablated groups gained more weight than age-matched naive pups ( $P<0.01$  and  $P<0.001$  respectively), while occipital cortex-ablated pups gained more weight than sham-ablated pups ( $P<0.05$ ).

28 days after surgery, there was no difference in weight gain between groups.

The extent of the occipital cortex lesion is shown in Fig. 2A. Unilateral occipital cortex ablation produced a consistent lesion  $5.4 \pm 0.5$  mm<sup>3</sup> in volume and extending through the entire thickness of the cortex. The underlying hippocampus and surrounding dural sinuses were spared (Fig. 2A). Neither clinical seizure activity nor overt motor dysfunction were observed during the recovery period. In sham-lesioned animals, removal of the bone flap alone, without aspiration of cortex, produced visible but less extensive occipital cortex damage (Fig. 2C).

### *The dorsal LGN has established projections to the occipital cortex in 10-day-old mouse pups*

The area of cortex that was ablated in the 10-day-old mouse pup is the termination zone of corticopetal projection neurons in the dorsal LGN as identified by FG tracing (Fig. 2A, box, area of enlargement in Fig. 2B). FG is present in thalamocortical neurons as cytoplasmic, somatodendritic, and axonal aggregates (Fig. 2B, inset). These small granules within the perikaryal cytoplasm are consistent with the accumulation of this retrograde tracer within vesicles. This is the typical pattern of FG distribution (Schmued and Fallon, 1986). Few FG-positive neurons were detected in the ipsilateral ventral LGN nuclei, but no cells in the contralateral ventral LGN showed FG uptake.

### *Cells in the dorsal LGN degenerate with a pattern consistent with apoptosis following occipital cortex ablation*

TUNEL-positive cells were detected in the ipsilateral dorsal LGN 12, 24, 36, and 48 h postlesion, peaking at 36 h (Fig. 3A). However, no TUNEL staining was present in the contralateral dorsal LGN at any time point after unilateral occipital ablation. TUNEL-positive cells were identified as neurons based on previously described characteristics, notably cell size and the pattern of nuclear condensation (Al-Abdulla and Martin, 1998). In dying neurons, chromatin clumps had dense TUNEL reactivity (Fig. 3B), consistent with nuclear chromatin pattern identified by Cresyl Violet (Fig. 4) or Hoescht stain (Fig. 3D, F) of apoptotic neurons. This nuclear morphology is characteristic of apoptosis in neurons (Martin et al., 1998). In some TUNEL-positive neurons, there was lighter staining of the nuclear core (Fig. 3C). No staining was observed when TdT buffer and biotinylated dUTP were omitted (results not shown).

To determine whether these dying cells are thalamocortical neurons, FG was injected into the right occipital cortex prior to ablation. In a FG-injected, non-ablated mouse brain, FG is present in the cytoplasm and somatodendritic process of a thalamocortical neuron in the ipsilateral dorsal LGN (Fig. 2B, inset, Fig. 3E). Figure 3F illustrates the distinctive apoptotic phenotype in a thalamocortical neuron after occipital ablation, identified by coalescence of FG vesicles occurring in the condens-

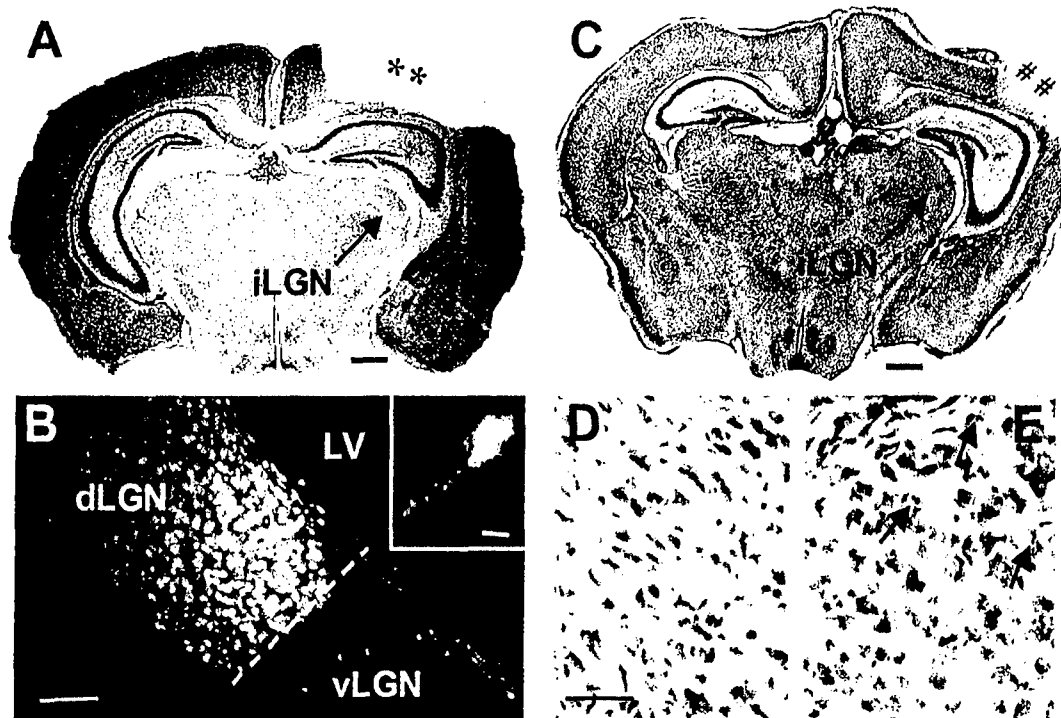


Fig. 2. Dorsal LGN projections to the occipital cortex in 10-day-old mouse pups. (A) Low-magnification view of a 40- $\mu$ m-thick Cresyl Violet-stained coronal section at level of the LGN. Lesion, indicated by \*\*, extends through all layers of the occipital cortex, sparing the hippocampus and corpus collosum inferiorly, and the cingulate gyrus medially. Box outlines the ipsilateral LGN region from a non-injured brain that is enlarged in (B). Scale bar = 600  $\mu$ m. (B) Thalamocortical connectivity in a naive 10-day-old mouse pup. Under UV light, cortical projection neurons in the dorsal LGN are labeled with bright yellow FG after injection of this retrograde tracer into the occipital cortex. By contrast, thalamic neurons in the ventral LGN (vLGN) show scant FG tracer. Digital image brightness adjusted to reduce background signal in the lateral ventricle. LV, lateral ventricle. Thalamocortical projection neurons contain FG aggregated in a somatodendritic distribution (B, inset). (C) Low-magnification view of a 40- $\mu$ m-thick Cresyl Violet-stained coronal section of a representative brain 36 h after sham occipital cortex lesion. Removal of the cranial bone flap caused minimal occipital cortex damage (\*\*). (D) Cellular morphology in the contralateral dorsal LGN (dLGN) 36 h after sham lesion. No apoptotic cells are identified. Scale bar = 40  $\mu$ m. (E) In a comparative view of the ipsilateral dorsal LGN in the same section 36 h after sham lesion, three apoptotic cells are identified (black arrows). Scale bars = 600  $\mu$ m (A, C); 80  $\mu$ m (B); 40  $\mu$ m (D, E); 5  $\mu$ m (B, inset).

ing cytoplasm, while the nucleus has condensed into several small, round aggregates characteristic of apoptosis.

The temporal and structural progression of axotomy-induced thalamocortical neuronal degeneration was examined in Cresyl Violet-stained coronal sections from mouse pups after occipital cortex ablation. Apoptotic cells in the ipsilateral and contralateral thalamic dorsal and ventral LGN, characterized by the morphology seen in Fig. 4E and F, were counted at 10 time points after unilateral occipital ablation (Table 1). The low number of apoptotic cells in the ipsilateral ventral LGN, and contralateral nuclei are consistent with the level of programmed cell death in the immature brain (Parnavelas et al., 1977). At 36 and 48 h after ablation, apoptotic cell counts in the ipsilateral dorsal LGN were higher than in the ipsilateral ventral LGN or the contralateral dorsal LGN. Sham-ablated groups showed no significant difference in apoptotic cell counts in any of the four thalamic nuclei. However, there were more apoptotic cells in the ipsilateral dorsal LGN from ablated mice compared to time-matched sham-ablated groups at 36 and 48 h after ablation. Figure 2E shows the extent of apoptosis in the

dorsal LGN 36 h after occipital ablation (arrows), compared to the contralateral dorsal LGN (Fig. 2D). Gender did not significantly influence apoptotic cell counts (data not shown).

Neurons in the dorsal LGN passed through the chromatolytic stage 18–24 h after occipital ablation, then underwent apoptosis that was completed by 48–72 h postlesion (Fig. 4). In chromatolytic neurons, the nucleus became eccentric and the neuron appears to swell. Subsequently, after the chromatolytic stage, there was shrinkage of the cell body and dendrites, and the Nissl substance dispersed creating a less dense cytoplasm (Fig. 4B, C). Clumping of chromatin into multiple small masses ('minimass stage') further lightened the cytoplasm and distinguished entry into the apoptotic stage (Fig. 4D). Further coalescence of minimasses into larger, dense chromatin masses characterized entry into end-stage apoptosis (Fig. 4E, F). At this point, the cellular debris has fully condensed chromatin surrounded by translucent cytoplasm. This progression of neuronal death replicated the morphology of apoptosis found in *in vivo* paradigms of neuronal apoptosis in mature neurons.

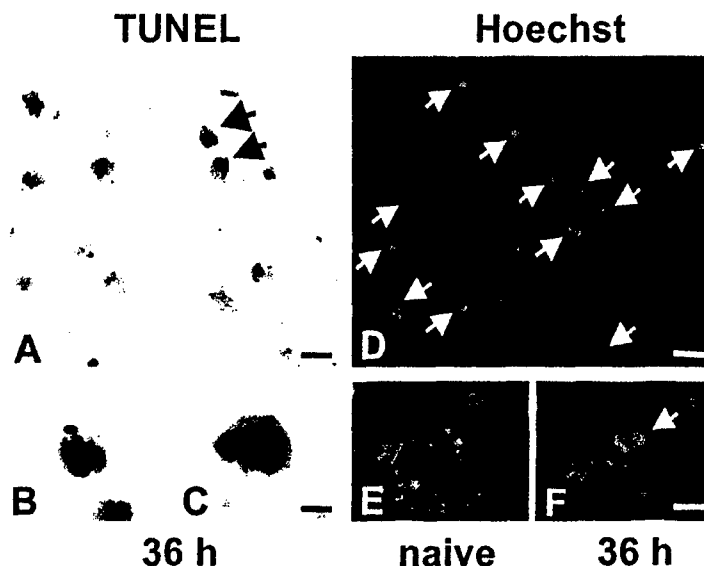


Fig. 3. Apoptotic neurodegeneration of the ipsilateral dorsal LGN following occipital cortex ablation. (A) High-magnification image from the ipsilateral dorsal LGN 36 h after occipital ablation stained with TUNEL method. Black arrows indicate neurons with dense TUNEL nuclear reactivity. (B) Degenerating neuron with nuclear TUNEL reactivity characteristic of apoptosis. (C) Other degenerating neurons have lighter staining of the nuclear core surrounded by dense TUNEL-positive nuclear matrix. (D) High magnification of near adjacent section through the ipsilateral dorsal LGN 36 h after occipital ablation stained with Hoechst 33258 shows widespread apoptotic cells with bright blue-stained, round, chromatin clumps (white arrows). (E) LGN neurons project to the ipsilateral occipital cortex in immature mouse pups. One day after FG injection into the occipital cortex, FG aggregates (colored arrow) are present in the cytoplasm and somatodendritic processes of a thalamocortical projection neuron in the ipsilateral LGN. (F) Thalamocortical projection neurons show apoptotic morphology after occipital ablation. A FG-labeled thalamocortical projection neuron (colored arrow) in the ipsilateral LGN has chromatin clumps (white arrow) 36 h after occipital ablation. Scale bars = 8  $\mu$ m (A); 5  $\mu$ m (B, C); 10  $\mu$ m (D); 4  $\mu$ m (E, F).

#### *Electron microscopy (EM) identifies prominent apoptosis in the dorsal LGN after cortical ablation in immature brain*

With EM, many apoptotic cells were found throughout the dorsal LGN (Fig. 5). At 18 h after cortical ablation, some neurons in the LGN showed early structural features of apoptosis, notably darkening of the cytoplasm and nascent chromatin condensation in the nucleus (Fig. 5A). By 24 h postlesion, the ultrastructure of degenerating LGN cells was characterized by progressive cytoplasmic and nuclear condensation with chromatin compaction into uniformly large round clumps within the nucleus (Fig. 5B). Based on cell size and number present, these apoptosis profiles were considered to be neurons. At 36 h postlesion, macrophages/microglia were observed engulfing apoptotic debris (Fig. 5C).

#### *Expression of cleaved caspase-3 in the dorsal LGN precedes apoptosis identified structurally*

Expression of cleaved caspase-3 serves as a biochemical marker of cells undergoing apoptosis. The cleaved caspase-3 antibody detected a single cleaved form at 20 kDa (Fig. 6P) in human T lymphocyte leukemia whole cell lysates (HuT). Using this antibody, cleaved caspase-3 immunostaining localized to both the cytoplasm and nucleus in neurons (Fig. 6I, inset, K, and L). No cleaved caspase-3 immunostaining was detected 12 h after occi-

pital ablation. However, cleaved caspase-3 expression was detected in neurons at 18 h postlesion (Fig. 6G, K, and L). By 24 h, there was robust cleaved caspase-3 immunofluorescence (Fig. 6H) that remained through 36 h (Fig. 6I). Furthermore, at 36 h postlesion, cleaved caspase-3 immunoreactivity localized to the cytoplasm of

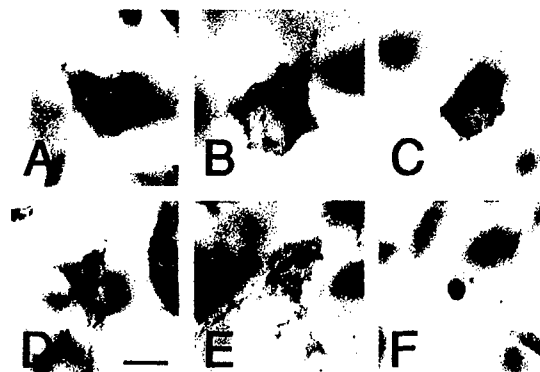


Fig. 4. Structural progression of axotomy-induced apoptosis in LGN neurons in 10-day-old mice. (A) Normal neuronal morphology is found in a naive 10-day-old pup. (B, C) Representative neurons show chromatolytic phenotype with eccentric placement of the nucleus and cellular condensation 18–24 h postlesion. (D, E) Representative neurons show further cell shrinkage with condensation of chromatin into dense, round aggregates 36–48 h postlesion. (F) End-stage neurons are characterized by pale cytoplasm, loss of nuclear membrane, dense, round chromatin, and small size. Scale bar = 5  $\mu$ m.

Table 1. Apoptotic cell counts in the LGN after unilateral occipital ablation

	Apoptotic cells/mm <sup>2</sup>			
	Dorsal LGN		Ventral LGN	
	Ipsilateral	Contralateral	Ipsilateral	Contralateral
6 h	0.00 ± 0.00	0.00 ± 0.00	0.00 ± 0.00	0.00 ± 0.00
6 h sham	0.00 ± 0.00	0.00 ± 0.00	0.00 ± 0.00	0.00 ± 0.00
12 h	2.93 ± 1.69	2.83 ± 1.63	2.13 ± 0.92	1.09 ± 0.75
12 h sham	0.03 ± 0.03	0.03 ± 0.03	0.10 ± 0.10	0.03 ± 0.03
18 h	2.40 ± 1.57	0.01 ± 0.01	2.80 ± 1.27	0.40 ± 0.40
18 h sham	1.07 ± 1.07	0.03 ± 0.03	3.20 ± 1.85	1.07 ± 1.07
24 h	8.77 ± 5.70	0.01 ± 0.01	2.80 ± 1.27	0.01 ± 0.01
24 h sham	0.52 ± 0.35	0.02 ± 0.02	0.05 ± 0.05	0.02 ± 0.02
30 h	170 ± 12.2 <sup>§§</sup>	0.02 ± 0.03 <sup>***</sup>	1.56 ± 1.11 <sup>##</sup>	0.80 ± 0.52
30 h sham	30.4 ± 15.8	0.02 ± 0.03	0.02 ± 0.02	0.02 ± 0.02
36 h	217 ± 8.98 <sup>§</sup>	0.40 ± 0.40 <sup>***</sup>	0.01 ± 0.01 <sup>##</sup>	0.80 ± 0.52
36 h sham	48.8 ± 18.8	0.03 ± 0.03	0.03 ± 0.03	1.07 ± 1.07
48 h	131 ± 10.0 <sup>§§</sup>	0.01 ± 0.01 <sup>**</sup>	0.01 ± 0.01 <sup>##</sup>	0.01 ± 0.01
48 h sham	34.4 ± 18.1	0.02 ± 0.02	0.02 ± 0.02	0.02 ± 0.02
72 h	10.4 ± 3.80	0.01 ± 0.01 <sup>*</sup>	1.60 ± 0.60	0.40 ± 0.40
72 h sham	8.50 ± 3.81	0.03 ± 0.03	0.03 ± 0.03	0.03 ± 0.03
7 days	2.32 ± 2.02	0.01 ± 0.01	0.91 ± 0.92	0.00 ± 0.00
7 days sham	4.80 ± 1.33	0.01 ± 0.01	0.01 ± 0.01	0.00 ± 0.00
28 days	0.00 ± 0.00	0.00 ± 0.00	0.00 ± 0.00	0.00 ± 0.00
28 days sham	0.00 ± 0.00	0.00 ± 0.00	0.00 ± 0.00	0.00 ± 0.00

N=8 for occipital ablation groups, N=4 for sham groups. Values are mean ± S.E.M. Ipsilateral vs. contralateral, \**P* < 0.05, \*\**P* < 0.01, \*\*\**P* < 0.001, Wilcoxon signed rank test; ipsilateral dorsal vs. ipsilateral ventral, ##*P* < 0.01, Wilcoxon signed rank test; ipsilateral dorsal vs. ipsilateral dorsal sham, §*P* < 0.05, §§*P* < 0.01, Mann-Whitney *U*-test.

LGN cells with end-stage apoptotic phenotype (Fig. 6M and N). Sparse cleaved caspase-3-positive cells remain at 72 h postlesion (Fig. 6J). The contralateral dorsal LGN in the same coronal sections for each time point showed rare cleaved caspase-3-expressing cells (Fig. 6A–E). When the primary antibody was omitted, background staining was observed due to non-specific binding of the secondary fluorescent antibody with an appearance similar to immunostaining in the contralateral dorsal LGN (data not shown).

#### *Internucleosomal fragmentation of DNA precedes apoptosis end-stage in the LGN*

The pattern of genomic DNA fragmentation in the LGN was used as a marker for early cell death. An internucleosomal ('ladder') pattern of DNA fragmentation was present in the ipsilateral LGN at 18 and 24 h after unilateral occipital cortex ablation (Fig. 7). This pattern is characteristic of many forms of apoptosis (Compton, 1992). Genomic DNA extracted from the contralateral LGN in the same mice showed no DNA fragmentation at the same recovery times.

#### DISCUSSION

This study provides novel information on the temporal progression of subcortical delayed neuronal apoptosis in the immature brain after cortical injury. Specifically, we show the upstream biochemical/molecular mechanisms of neuronal apoptosis in the thalamus after cortical damage, including DNA fragmentation and cleavage of cas-

pase-3, are engaged within the first 18–24 h and precede structural cell death. This time course is consistent with a mechanism initiated by neurotrophin withdrawal as evaluated *in vitro* with PC12 cells (Pittman et al., 1993). We anticipate that the implementation of postulated neuroprotective interventions after this time, perhaps targeted at limiting caspase-3 activation, would be ineffective in this model of remote degeneration.

#### *Expression of cleaved caspase-3 precedes apoptosis identified structurally*

Structural evidence for apoptosis began to emerge approximately 24 h postlesion by light microscopy and approximately 18 h postlesion by EM. By 36 h postlesion massive end-stage apoptosis was present in the dorsal LGN observed in Nissl, TUNEL, and EM preparations. Therefore, the structural process of neuronal apoptosis occurs over 6–18 h in immature thalamic neurons after axotomy. Although evaluation of Cresyl Violet-stained sections showed no evidence for necrotic cell death in the LGN, we recognize that TUNEL-positive cells may represent necrotic or apoptotic cell death. Therefore it would be premature to conclude that in this model of subcortical delayed cell death, apoptotic phenotype occurs to the exclusion of necrotic cell death. We also demonstrate that biochemical events associated with apoptosis precede the development of the apoptotic phenotype. At both 18 and 24 h postlesion, internucleosomal fragmentation of DNA was detected (Fig. 7). Thus in immature thalamic neurons, genomic DNA fragmentation preceded the major structural events in the nucleus. Similarly, cleaved caspase-3, a protease whose activation



can lead directly to an apoptotic phenotype, was first detected in neurons in the ipsilateral dorsal LGN 18 h postlesion (Fig. 6). By 24 and 36 h postlesion, caspase-3 cleavage was widespread in the dorsal LGN. Specifically, cleaved caspase-3 expression co-localized to cells with end-state apoptotic morphology, suggesting a role for caspase-3 activation in this model of apoptosis. The mediating effect of caspase-3 is further substantiated by low apoptotic cell counts at 24 h postlesion (Table 1) when cleaved caspase-3 expression is high (Fig. 6H), suggesting that cleaved caspase-3 expression *precedes* apoptotic cell death.

Cleaved caspase-3 expression is present in the ipsilateral ventral LGN (Fig. 6), raising the possibility that caspase-3 activation may be an epiphenomenon of cortical ablation. However, cleaved caspase-3 expression in the ventral LGN was not unexpected. Geniculate neurons projecting to the occipital cortex in the 10-day-old pup are not exclusively localized to the dorsal LGN as shown in Fig. 2B. Here, FG injected into the occipital cortex is retrogradely transported to thalamic cell bodies primarily in the dorsal LGN, but labeled neurons are present in the ventral LGN. These ventral LGN neurons would be at risk for target deprivation-induced apoptosis in this model system. In fact, a low number of apoptotic cells are present in the ipsilateral ventral LGN (Table 1), but this experiment was not powered to detect a difference in apoptotic cell counts between the ipsilateral and contralateral ventral LGN. Since *both* apoptotic cell death and cleaved caspase-3 were observed in the ventral LGN, caspase-3 activation is not an epiphenomenon of cortical ablation.

*Thalamocortical projection neurons in the ipsilateral dorsal LGN undergo apoptosis after unilateral occipital cortex ablation*

Previous studies in rat and mouse have shown that unilateral ablation of the occipital cortex produces retrograde degeneration of LGN neurons, resulting in cell loss and subsequent atrophy of the LGN (Barron et al., 1973; Ross and Ebner, 1990; Al-Abdulla et al., 1998; Agarwala and Kalil, 1998). We have demonstrated that this degeneration is apoptosis in the 10-day-old mouse pup. The presence of TUNEL-positive cells only in the ipsilateral LGN after right occipital ablation indicates that retrograde neuronal degeneration occurs in a localized region. Furthermore, to determine if the focal location of neuronal death is related to geniculocortical connectivity in 10-day-old mouse pup, the retrograde

Fig. 5. EM demonstrating prominent apoptosis in the LGN after cortical ablation in 10-day-old mouse. (A) At 18 h postlesion, many cells in the LGN show early structural features of apoptosis, notably darkening of the cytoplasm and nascent chromatin condensation in the nucleus (Nu). (B) At 24 h postlesion, LGN neurons show unequivocal ultrastructural features of apoptosis, including the dark condensed cytoplasm and the large round masses of chromatin within the nucleus. (C) At 36 h postlesion, debris from apoptotic cells (asterisk) is engulfed by macrophages/microglia (m). Scale bars = 0.5  $\mu$ m (C); 1  $\mu$ m (A, B).

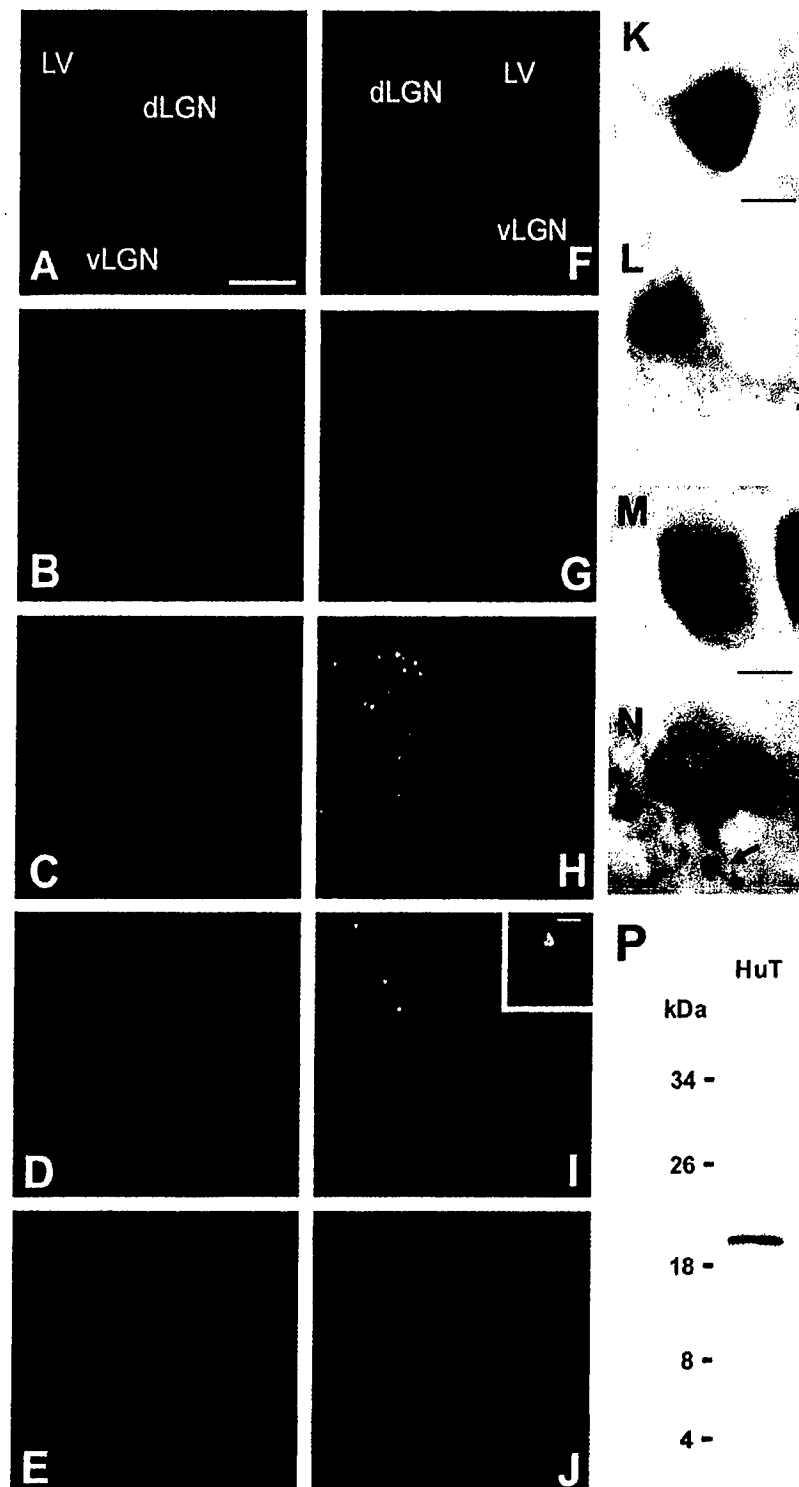


Fig. 6 (Caption overleaf).

tracer FG was applied to the occipital cortex. The distribution of thalamocortical projection neurons identified by the retrograde tracer FG was localized to the ipsilateral dorsal LGN, consistent with the localization in adult mice (Martin et al., 2001). Similarly, other investigators

have demonstrated that injection of brain-derived neurotrophic factor into the occipital cortex of adult rats results in neuronal labeling of the dorsal LGN (Sobrevela et al., 1996; Mufson et al., 1999). Retrograde transport of neurotrophic factors along thalamocortical



Fig. 7. Internucleosomal pattern of genomic DNA fragmentation patterns in the LGN as a marker of early cell death. Agarose gel electrophoresis of genomic DNA from LGN obtained at 0, 18, and 24 h after unilateral occipital ablation. Internucleosomal pattern of DNA fragmentation (arrows) is present in the lesioned (Ipsi) LGN but not in the non-lesioned (Contra) LGN of 10-day-old mice.

axons may provide the trophic support required to sustain viability degeneration of thalamic neurons. In our injury paradigm, it has been suggested that occipital ablation reduces trophic support to the dorsal LGN, resulting in neurodegeneration. The anatomic distribution of FG-positive neurons in the dorsal LGN is consistent with this suggestion.

#### Brain maturity alters the rate of apoptosis

Our group has previously characterized the morphology of LGN neuronal degeneration and its time course in the adult mouse (Martin et al., 2001). In adult C57BL/6 mice, neuronal apoptosis after occipital cortex ablation resulted in maximal neuronal loss 7 days after occipital cortex ablation. Although more rapid, the progression of the morphological phenotype of axotomy-induced apoptosis in the 10-day-old mouse brain (Fig. 4) was similar to the pattern described in the mature rodent brain. Morphologically, our results in this murine model confirm that immature neurons die following injury with apoptotic morphology. LaVelle described a similar age-

dependent rate of neurodegeneration after facial nerve axotomy in hamsters (LaVelle and LaVelle, 1958), but this degeneration was not identified as apoptotic. Several explanations for this age-dependent rate of axotomy-induced neurodegeneration can be considered. First, the age-related rate of progression in apoptosis may be determined by the time required for survival of signal loss in thalamic neurons. In the immature brain, the shorter distances and briefer time to loss of signal would lead to earlier cell death. Second, immature neurons have less fully developed arborization of the somatodendritic architecture (Parnavelas et al., 1977), leading to diminished afferent-derived support. Third, axonal collateralization is less extensive in the immature brain (Fricke and Cowan, 1977), leaving an immature neuron with fewer sources of retrograde-derived neurotrophic support than a mature neuron. Fourth, immature neurons may express different complements of cell adhesion molecules than mature neurons, and thus increasing the likelihood of apoptosis (Meridith et al., 1993; Frisch and Francis, 1994; Ruoslahti and Reed, 1994).

Young neurons are highly dependent on neurotrophin support. For example, as neurons mature *in vitro* they become much less acutely dependent on nerve growth factor (Easton et al., 1997). In this regard, it may also be useful to recognize the neurodevelopmental context within which injury and subsequent apoptosis occurs (Portera-Cailliau et al., 1997; Pohl et al., 1999). Programmed cell death is a cell autonomous elimination strategy of normal nervous system development and extends into the postnatal period (Oppenheim, 1991). Thus, there may be fewer intrinsic 'survival' mechanisms or less evolved compensatory responses to injury in the immature brain where many neurons are redundant and must die.

#### Retrograde degeneration contributes to neuronal death after TBI

Outcome from TBI or cortical infarction is determined by the cell death produced by the cortical injury itself, and by loss of neuronal and non-neuronal cells in regions remote to the areas receiving the direct impact (Iizaka et al., 1990). In experimental TBI, controlled cortical contusion and fluid percussion injury produce both necrotic and apoptotic cell death at the site of impact (Rink et al., 1995; Yakovlev et al., 1997; Conti et al., 1998;

Fig. 6. Cleaved caspase-3 expression in the LGN after occipital cortex ablation. (A-E) Cleaved caspase-3 is present in only a few scattered cells in the left (contralateral) dorsal LGN (dLGN) and ventral LGN (vLGN) at 12, 18, 24, 36 and 72 h after occipital cortex ablation in 10-day-old mouse pups. LV, lateral ventricle. (F) Similarly, no cells expressing cleaved caspase-3 are identified in the ipsilateral LGN at 12 h postlesion. (G) However, cleaved caspase-3 is present in cells in the ipsilateral (right) dorsal LGN at 18 h postlesion. (H, I) By 24 h, there was robust cleaved caspase-3 immunofluorescence in the dorsal LGN that remained through 36 h. (J) Cleaved caspase-3 expression was undetectable in the ipsilateral LGN by 72 h after occipital cortex ablation. (I, inset) Cleaved caspase-3 immunostaining localized to both the cytoplasm and nucleus in LGN neurons. (K, L) Cleaved caspase-3 immunoreactivity (brown reaction product) localizes to the cytoplasm and nucleus of ipsilateral LGN neurons 18 h after occipital cortex ablation. (M, N) Cleaved caspase-3 immunoreactivity (brown reaction product) localizes to the cytoplasm and cytoplasmic fragments (arrow) of LGN cells with end-stage apoptotic phenotype (Cresyl Violet staining) at 36 h after occipital cortex ablation. Contrast adjusted to sharpen digital images (K-N). (P) Immunoblot showing detection of cleaved caspase-3 as a single band at 20 kDa in human T lymphocyte leukemia whole cell lysates (HuT). Scale bars = 150  $\mu$ m (A-J); 15  $\mu$ m (I, inset); 5  $\mu$ m (K, L); 2  $\mu$ m (M, N).

Newcomb et al., 1999). In these models, neurodegeneration after TBI is not limited to the impact site, but extends to subcortical regions (Conti et al., 1998; Newcomb et al., 1999; Bittigau et al., 1999; Pohl et al., 1999; Clark et al., 2000). We present an *in vivo* model of cortical damage with remote thalamic neuronal death that is likely to be very similar to the delayed apoptosis resulting from cortical trauma. Our study indicates that this remote delayed apoptosis is related to target deprivation.

#### Methodological considerations

Our model has several important advantages for studying the mechanisms of neuronal apoptosis. First, it is an *in vivo* model that produces *bona fide* neuronal death with a structure of apoptosis that evolves reproducibly over a highly synchronous time course of 7 days in adult mice (Martin et al., 2001) and 1–2 days in 10-day-old mice. Second, this lesion produces remote neurodegeneration, without accompanying secondary brain responses. These responses, including seizures, hyperthermia, alterations in cerebral blood flow, or ischemia, and systemic perturbations, such as hypoxia or hypotension are common in hypoxic-ischemic or brain impact paradigms of neurodegeneration. Third, based on thalamo-cortical projections, a predictable and localized area of at-risk neurons can be identified and sampled for biochemical and molecular analyses. As a consequence, the 'dilutional effect' of non-affected neurons is decreased and the high density of affected neurons increases the probability of identifying pathobiological patterns specific to the axotomized, 'at-risk' neurons. Thus, the identification of a relatively narrow window for cell death makes this lesion a very efficient assay system for the study of neuronal apoptosis *in vivo*. Finally, this study introduces and characterizes a new *in vivo* model of delayed neurodegeneration in mouse pups that permits

long-term recovery without significant morbidity. We make this statement based on weight gain as a meaningful surrogate for such adverse sequelae. As shown in Fig. 1, there were significant but trivial differences in weight gain observed in two of the five ages when comparing naive, sham, and injured animals. In fact, naive mouse pups showed significantly less weight gain than age-matched brain injured pups at one time point, although there was no consistent pattern favoring one group over the other. Taken together, these results provide evidence that there was not significant operative morbidity in recovered animals.

Acute neurological injury caused by stroke, birth asphyxia, or head trauma often results in lifelong impairment of physical, cognitive, and psychosocial functioning in both adults and children (NIH Consensus Statement, 1998). Despite its public health importance, pediatric brain injury remains incompletely understood, in part because relevant clinical and animal studies lag behind those for adults. Since the limited availability of human tissue precludes comprehensive mechanistic analyses, animal models of injury and the sequelae of this brain damage are essential tools. We describe here the development and characterization of a reliable *in vivo* model of cortical injury-induced thalamic neuron apoptosis in the developing brain.

**Acknowledgements**—The authors are grateful for the expert technical assistance of Ann Price, Frank Barksdale, and Lauren White. Ms. White was supported by the Smith College Summer Preceptorship Program. This study was supported by grants from the U.S. Public Health Service, National Institutes of Health, National Institute of Aging AG16282 (L.J.M.) and the Department of Defense, U.S. Army Medical Research and Material Command DAMD17-99-1-9553 (L.J.M.), and the U.S. Public Health Service, National Institutes of Health, National Institute of Child Health and Development, Child Health Research Center at Children's National Medical Center, Child Health Research Career Development Award (J.E.N.).

#### REFERENCES

- Agarwala, S., Kalil, R.E., 1998. Axotomy-induced neuronal death and reactive astrogliosis in the lateral geniculate nucleus following lesion of the visual cortex in the rat. *J. Comp. Neurol.* 392, 252–263.
- Al-Abdulla, N.A., Martin, L.J., 1998. Apoptosis of retrogradely degenerating neurons occurs in association with the accumulation of perikaryal mitochondria and oxidative damage to the nucleus. *Am. J. Pathol.* 153, 447–456.
- Al-Abdulla, N.A., Portera-Cailliau, C., Martin, L.J., 1998. Occipital cortex ablation in adult rat causes retrograde neuronal death in the lateral geniculate nucleus that resembles apoptosis. *Neuroscience* 86, 191–209.
- Barron, K.D., Means, E.D., Larsen, E., 1973. Ultrastructure of retrograde degeneration in thalamus of rat. *J. Neuropathol. Exp. Neurol.* 32, 218–244.
- Bittigau, P., Siffringer, M., Pohl, D., Stadthaus, D., Ishimaru, M., Shimizu, H., Ikeda, M., Lang, D., Speer, A., Olney, J.W., Ikonomidou, C., 1999. Apoptotic neurodegeneration following trauma is markedly enhanced in the immature brain. *Ann. Neurol.* 45, 724–735.
- Clark, R.S., Kochanek, P.M., Watkins, S.C., Chen, M., Dixon, C.E., Seidberg, N.A., Melick, J., Loeffert, J.E., Nathaniel, P.D., Jin, K.L., Graham, S.H., 2000. Caspase-3 mediated neuronal death after traumatic brain injury in rats. *J. Neurochem.* 74, 740–753.
- Compton, M.M., 1992. A biochemical hallmark of apoptosis: Internucleosomal degradation of the genome. *Cancer Metastasis Rev.* 11, 105–119.
- Conti, A.C., Raghupathi, R., Trojanowski, J.Q., McIntosh, T.K., 1998. Experimental brain injury induces regionally distinct apoptosis during the acute and delayed post-traumatic period. *J. Neurosci.* 18, 5663–5672.
- Easton, R.M., Deckwerth, T.L., Parsadanian, A.S., Johnson, E.M., 1997. Analysis of the mechanisms of loss of trophic factor dependence associated with neuronal maturation: A phenotype indistinguishable from bax deletion. *J. Neurosci.* 17, 9656–9666.
- Faden, A.I., Demediuk, P., Panter, S.S., Vink, R., 1989. The role of excitatory amino acids and NMDA receptors in traumatic brain injury. *Science* 244, 798–800.
- Fricke, R., Cowan, W.M., 1977. An autoradiographic study of the development of the entorhinal and commissural afferents to the dentate gyrus of the rat. *J. Comp. Neurol.* 173, 231–250.
- Frisch, S.M., Francis, H., 1994. Disruption of epithelial cell-matrix interactions induces apoptosis. *J. Cell Biol.* 124, 619–626.
- Iizaka, H., Sakatani, K., Young, W., 1990. Neuronal damage in the rat thalamus after cortical infarcts. *Stroke* 21, 790–794.



- LaValle, A., LaVelle, F.W., 1958. The nucleolar apparatus and neuronal reactivity to injury during development. *J. Exp. Zool.* 137, 285–315.
- Martin, L.J., Al-Abdulla, N.A., Brambrink, A.M., Kirsch, J.R., Sieber, F.E., Portera-Cailliau, C., 1998. Neurodegeneration in excitotoxicity, global cerebral ischemia, and target deprivation: A perspective on the contributions of apoptosis and necrosis. *Brain Res. Bull.* 46, 281–309.
- Martin, L.J., Kaiser, A., Yu, J.W., Natale, J.E., Al-Abdulla, N.A., 2001. Injury-induced apoptosis of neurons in adult brain is mediated by p53-dependent and p53-independent pathways and requires bax. *J. Comp. Neurol.* 433, 299–311.
- Meredith, J.E., Fazeli, B., Schwartz, M.A., 1993. The extracellular matrix as a survival factor. *Mol. Biol. Cell* 4, 953–961.
- Mufson, E.J., Kronin, J.S., Sendera, T.J., Sobrievila, T., 1999. Distribution and retrograde transport of trophic factors in the central nervous system: Functional implications for the treatment of neurodegenerative diseases. *Prog. Neurobiol.* 57, 451–484.
- Nakajima, W., Ishida, A., Lang, M.S., Gabrielson, K.L., Wilson, M.A., Martin, L.J., Blue, M.E., Johnston, M.V., 2000. Apoptosis has a prolonged role in the neurodegeneration after hypoxia ischemia in the newborn rat. *J. Neurosci.* 20, 7994–8004.
- Newcomb, J.K., Zhao, X., Pike, B.R., Hayes, R.L., 1999. Temporal profile of apoptotic-like changes in neurons and astrocytes following controlled cortical impact injury in the rat. *Exp. Neurol.* 158, 76–88.
- Northington, F.J., Ferriero, D.M., Flock, D.L., Martin, L.J., 2001. Delayed neurodegeneration in the neonatal rat thalamus after hypoxia-ischemia is apoptosis. *J. Neurosci.* 21, 1931–1938.
- Oppenheim, R.W., 1991. Cell death during development of the nervous system. *Annu. Rev. Neurosci.* 14, 453–501.
- Parnavelas, J.G., Mounty, E.J., Bradford, R., Lieberman, A.R., 1977. The postnatal development of neurons in the dorsal lateral geniculate nucleus of the rat: A Golgi study. *J. Comp. Neurol.* 171, 481–500.
- Pittman, R.N., Wang, S., DiBenedetto, A.J., Mills, J.C., 1993. A system for characterizing cellular and molecular events in programmed neuronal cell death. *J. Neurosci.* 13, 3669–3680.
- Pohl, D., Bittigau, P., Ishimaru, M., Stadthaus, D., Hübner, C., Olney, J.W., Turkski, L., Ikonomidou, C., 1999. N-methyl-D-aspartate antagonists and apoptotic cell death triggered by head injury in developing rat brain. *Proc. Natl. Acad. Sci. USA* 96, 2508–2513.
- Portera-Cailliau, C., Price, D.L., Martin, L.J., 1997. Excitotoxic neuronal death in the immature brain is an apoptosis-necrosis morphological continuum. *J. Comp. Neurol.* 378, 70–87.
- NIH Consensus Statement, 1998. Rehabilitation of Persons with Traumatic Brain Injury. NIH Consensus Statement 16, pp. 1–41.
- Rink, A., Fung, K., Trojanowski, J., Lee, V.M., Neugebauer, E., McIntosh, T., 1995. Evidence of apoptotic cell death after experimental traumatic brain injury in the rat. *Am. J. Pathol.* 147, 1575–1583.
- Rosen, G.D., Williams, A.G., Capra, J.A., Connolly, M.T., Cruz, B., Lu, L., Airey, D.C., Kulkarni, K., Williams, R.W., 2000. The Mouse Brain Library@www.mbl.org. *Int. Mouse Genome Conference* vol. 14, p. 166.
- Ross, D.T., Ebner, F.F., 1990. Thalamic retrograde degeneration following cortical injury: an excitatory process? *Neuroscience* 35, 525–550.
- Ruosiahti, E., Reed, J.C., 1994. Anchorage dependence, integrins, and apoptosis. *Cell* 77, 477–478.
- Schmued, L.C., Fallon, J.H., 1986. Fluoro-gold: a new fluorescent retrograde axonal tracer with numerous unique properties. *Brain Res.* 377, 147–154.
- Sobrievila, T., Pagcatipunan, M., Kroin, J.S., Mufson, E.J., 1996. Retrograde transport of brain-derived neurotrophic factor (BDNF) following infusion in neo- and limbic cortex in the rat: relationship to BDNF mRNA expressing neurons. *J. Comp. Neurol.* 375, 417–444.
- Yakovlev, A.G., Knoblach, S.M., Fan, L., Fox, G.B., Goodnight, R., Faden, A.I., 1997. Activation of CPP32-like caspases contributes to neuronal apoptosis and neurological dysfunction after traumatic brain injury. *J. Neurosci.* 17, 7415–7424.

(Accepted 20 February 2002)

## DNA Damage Profiling in Motor Neurons: A Single-Cell Analysis by Comet Assay

Lee J. Martin<sup>1,2,3</sup> and Zhiping Liu<sup>1</sup>

(Accepted July 22, 2002)

We developed a method to measure DNA damage in single motor neurons (MN). A cell fraction enriched in viable  $\alpha$ -motor neurons was isolated from adult rat spinal cord. This cell preparation was used to measure the vulnerability of the MN genome to different reactive oxygen species (ROS). MN were exposed in vitro to hydrogen peroxide, nitric oxide and peroxynitrite. Specific types of DNA lesions (e.g., abasic sites, single-strand breaks, and double-strand breaks) were measured using single-cell gel electrophoresis (comet assay). The MN genome was very susceptible to attack by ROS. Different ROS induced different DNA damage profiles in MN. MN were also isolated from adult rats with sciatic nerve avulsions to show that DNA damage emerges early during their degeneration in vivo. This study demonstrates that the comet assay is a feasible method for profiling DNA lesions in the genome of single MN. Viable mature MN can be isolated and used for in vitro models of MN genotoxicity and can be isolated from in vivo models of MN degeneration for profiling DNA damage on a single-cell basis.

**KEY WORDS:** Amyotrophic lateral sclerosis; apoptosis; axotomy; DNA single-strand breaks; single-cell gel electrophoresis.

### INTRODUCTION

DNA damage has been implicated in the mechanisms of aging (1,2) and in the pathogenesis of many human diseases, including cancer and neurological disorders ranging from stroke to amyotrophic lateral sclerosis (ALS), Alzheimer's disease, and Parkinson's disease (3–6). Endogenous and environmental agents can cause DNA damage in cells (1,2). Endogenous factors are reactive oxygen species (ROS) generated

by cellular metabolism, temperature, errors in DNA replication and repair, high level of glucose and other reducing sugars, and methylation. Intrinsically generated DNA lesions occur as mismatched base pairs, base structure alterations such as tautomeric shifts and deamination, base adducts (e.g., hydroxylation), and base deletions causing apurinic/apyrimidinic (AP) sites (alkali-labile sites), single-strand breaks (SSB), and double strand-breaks (DSB). Metabolism-generated ROS can cause ~10,000 lesions/day in the genome of a human cell (2), and purine base turnover in DNA, resulting from hydrolytic depurination and subsequent repair, is ~2000–10,000 bases/day (1). The different forms of DNA damage can be converted from one form to another type. Hydroxyl radical attack on DNA induces base adducts and then strand breaks, because AP sites are converted into SSB if not repaired (2). In addition to the intrinsically-generated lesions to DNA, dietary mutagenic chemicals, ultraviolet and ionizing

<sup>1</sup> Department of Pathology, Division of Neuropathology, Johns Hopkins University School of Medicine, Baltimore, MD 21205.

<sup>2</sup> Department of Neuroscience, Johns Hopkins University School of Medicine, Baltimore, MD 21205.

<sup>3</sup> Address reprint request to: Lee J. Martin, Ph.D., Johns Hopkins University School of Medicine, Department of Pathology, 558 Ross Building, 720 Rutland Avenue, Baltimore, MD 21205-2196. Tel: (410) 502-5170; Fax: (410) 955-9777; E-mail: martinl@jhmi.edu

radiation such as X-rays and  $\gamma$ -rays, and heavy metals are environmental agents that damage the genome, causing DNA crosslinks, adducts, and oxidative cleavage (2).

The pivotal role of DNA damage in human pathobiology underscores the essential need for methods to detect and measure DNA lesions and their repair in specific populations of cells. The DNA filter elution assay is a powerful biochemical method for the determination of DNA strand breaks, AP sites, and crosslinks (7). Nucleoside adducts can be measured in digests of DNA extracts with high performance liquid chromatography. However, these methods lack cellular resolution. Popular methods for determining DNA damage with cellular resolution (e.g., flow cytometry and terminal deoxynucleotidyl transferase-mediated 3' dUTP nick end labeling), however, lack the ability to distinguish specific types of DNA lesions. We were interested in developing and implementing sensitive and quantitative assays for profiling specific DNA lesions directly in neurons, specifically motor neurons (MN), because of the possible role of DNA damage in the pathogenesis of ALS (4,5,8) and other neurological disorders. The comet assay, also known as single cell gel electrophoresis (SCGE), has been used to identify genomic DNA damage in eukaryotic cells on a single cell basis (9–13). The types of DNA lesions detectable by comet assay include SSB, alkali-labile sites (AP sites) and DSB. We envisioned that the comet assay could be used to profile DNA damage directly in MN. The goals of these experiments were to develop a new method to isolate adult MN, and, then apply the comet assay to evaluate the vulnerability of the MN genome to ROS and axonal injury.

## EXPERIMENTAL PROCEDURE

**Animals and Preparation of Spinal Cord Tissue for Isolation of Mature MN.** The institutional Animal Care and Use Committee approved the animal protocols. Adult (2–3 months old, ~150–200 g) male Sprague-Dawley rats (Charles River, Wilmington, MA) were used for these experiments. To prelabel  $\alpha$ -MN, rats ( $n = 4$ ) were anesthetized deeply with enflurane/oxygen/nitrous oxide (1:33:66), and the sciatic nerve was exposed unilaterally and transected distally. Gelfoam that was saturated with 2.5% 4-6-diamidino-2-phenylindol (DAPI) was applied to the proximal nerve stump for 1 h. The animals were allowed to survive for 48 h before they were killed. For a MN degeneration paradigm a unilateral sciatic nerve avulsion was used to induce apoptosis as described (14,15). Lesioned rats ( $n = 2$ –4 per time point) were allowed to live for 5, 7, 10, 14, and 28 days after the injury.

Spinal cords were isolated from rats after deep anesthetization and then decapitation. Cervical and lumbar enlargements were used from naive rats without experimental manipulations. Only the lum-

bar enlargement (divided into ipsilateral and contralateral sides) was used from rats exposed to DAPI and from rats with sciatic nerve avulsions. After removing the pia, spinal cord enlargements were dissected segment-by-segment under a surgical microscope, and then the segments were microdissected into columns of ventral horn gray matter (Fig. 1) without appreciable contamination from the dorsal horn and the surrounding white matter funiculi. Tissue samples were collected and rinsed in a cell culture dish on ice containing dissection medium (1x  $\text{Ca}^{2+}$  and  $\text{Mg}^{2+}$  free Hanks balanced salt solution, GibcoBRL, Grand Island, NY, supplemented with glucose and sucrose). These tissues were used to isolate MN.

**Preparation of MN Enriched Cell Suspensions.** Ventral horn samples were digested (20 min) with 0.25% trypsin-EDTA (Gibco) in a tissue culture incubator (5%  $\text{CO}_2$  and 95% air, at 37°C) and then triturated gently with a transfer pipette (Fig. 1). The tissue digests were transferred to a 5 ml-centrifugation tube on ice, and the remaining small pieces of gray matter were further digested in trypsin-EDTA (~15 min). The total cell suspension was then subjected to differential low speed centrifugation for cell sorting (Fig. 1) to isolate a spinal MN-enriched fraction. Tissue digests were centrifuged (Beckman GPR model centrifuge) at 200 rpm (20  $g_{av}$ ) for 5 min (4°C)

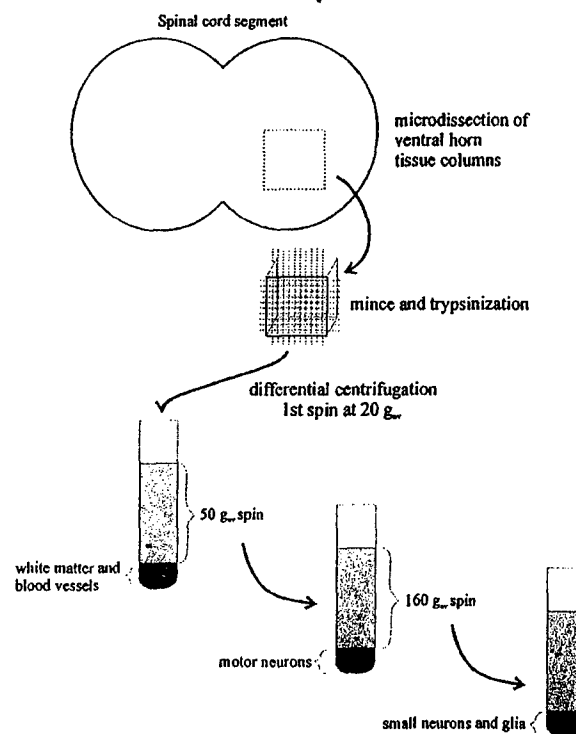


**Fig. 1.** Diagram of the isolation method for MN from adult rat spinal cord. Under a surgical microscope ventral horn gray matter tissue columns are microdissected from isolated cervical/lumbar spinal cord segments and then minced and trypsinized. Tissue digests are subjected to low speed differential centrifugation to fractionate the different cell types. Ventral horn gray matter was fractionated into different pellets (black components at tube bottoms) by sequential centrifugation of supernatant fractions (gray component in tubes). The different pellet fractions were analyzed microscopically and were found to contain white matter and blood vessels (P1), MN (P2), and small neurons and glia (P3).

to remove white matter and blood vessels (P1 fraction) and then the supernatant (S1 fraction) was collected and centrifuged at 400 rpm (50  $g_{av}$ ) to yield S2 and P2 fractions. The supernatant (S2) was again collected and centrifuged at 800 rpm (160  $g_{av}$ ) to yield S3 and P3 fractions. After each spin (for 5 min), the pellet (Fig. 1) was resuspended in 100  $\mu$ l phosphate-buffered saline (PBS, pH 7.4) and fixed with 4% paraformaldehyde (4°C for 1 h) for immunophenotypic characterization of cell types.

**Immunophenotyping Sorted Cell Suspensions.** The cells were gently repelleted after fixation, and each pellet was resuspended with 250  $\mu$ l PBS. Aliquots of cell suspension (50  $\mu$ l) were applied to gelatin-coated slides as a cell monolayer and air-dried. The cells were permeabilized (30 min) in 1% Triton X-100 and then treated (30 min) with 1% bovine serum albumin. The cells were probed (24 h at room temperature) with antibodies to neuronal nucleus protein (NeuN, diluted 1:20, Chemicon International Inc., Temecula, CA), a neuron-specific marker, choline acetyltransferase (ChAT, diluted 1:5, Roche Molecular Biochemicals, Indianapolis, IN), a marker for MN in spinal cord enlargements, glial fibrillary acidic protein (GFAP, diluted 1:20, DAKO, Denmark), an astroglial marker, and CD11b/c IgG2a (OX-42, diluted 1:20, Harlan Sera-Lab, England), a microglial/macrophage marker. Alexa conjugated anti-mouse IgG (diluted 1:100, Molecular Probes, Eugene, OR) was used to visualize NeuN, ChAT and OX-42, and Cascade blue conjugated anti-rabbit IgG (diluted 1:100, Molecular Probes) was used to visualize GFAP. Preparation of cell suspensions from rats used for retrograde tracing of MN was identical to that described above.

Neurons that were marked with cell type-specific antibodies were counted to identify the cell fraction that was enriched in MN. The total number of neurons was determined by counting the number of NeuN positive cells and the total number of cells identified by propidium iodide staining (a general nuclear dye) plus NeuN staining. The percentage of ChAT positive cells relative to NeuN positive cells was used to determine the proportion of MN in the cell suspensions. The fraction of DAPI positive cells (that issued sciatic nerve axons) relative to the total number of NeuN positive cells was used to determine the proportion of  $\alpha$ -MN. The numbers of labeled cells from 6 different microscopic fields (at 400 $\times$ ) were averaged from each case and then a total mean was derived from the preparations from different rats ( $n = 6$ ).

**In Vitro Exposure of Spinal MN to ROS.** MN were isolated from naive rat spinal cord and were exposed to different ROS. Treatments were done in medium containing 90% Neurobasal-A (Gibco), 5% horse serum, 5% fetal bovine serum (both sera were heat inactivated) and 1 $\times$  glutamine (Gibco) in a tissue culture incubator (containing 5% CO<sub>2</sub> and 95% air, 37°C). Hydrogen peroxide (H<sub>2</sub>O<sub>2</sub>) was used at a concentration of 1 mM. Two different nitric oxide (NO) donors were used: sodium nitroprusside (SNP, Sigma, St. Louis, MO) and N-(2-aminoethyl)-N-(2-hydroxyl-nitrosohydrazino)-1,2-ethylenediamine (spermine-NONOate, OXIS, International, Portland, OR). Spermine-NONOate was used because the in vitro generation of NO is slower than SNP and is steady state (16). Cells were exposed to SNP (10 and 100  $\mu$ M) or spermine-NONOate 10 and 100  $\mu$ M for 15, 30, 60, and 120 min. MN were also exposed directly to peroxy-nitrite (ONOO<sup>-</sup>, Alexis, San Diego, CA) at concentrations of 10 and 100  $\mu$ M for 15, 30, and 60 min. ONOO<sup>-</sup> is a potent and relatively long-lived ROS formed by a reaction between superoxide and NO (17). For controls, samples of the same isolated MN were incubated in medium for the same time in the absence of H<sub>2</sub>O<sub>2</sub> or SNP, with spermine tetrahydrochloride/sodium nitrite (NO<sub>2</sub><sup>-</sup>) as a control for NONOate, or with decomposed ONOO<sup>-</sup> in alkaline solution. After exposure, the cells in the different treatment groups were collected

into 5 ml centrifuge tubes and gently repelleted at 4°C for 5 min. Each cell pellet was resuspended and analyzed with the comet assay.

**Comet Assay.** The comet assay was used to profile DNA damage in MN exposed to ROS in vitro and in MN from ipsilateral (lesioned) or contralateral (nonlesioned) lumbar spinal cord of rats with unilateral sciatic nerve avulsions. Cell microgels were prepared on slides (Fig. 2). The method for the comet assay on MN was based mainly on the original protocol for experiments on lymphocytes (10). Many details were modified in the procedure for our application. The procedures for comet assay were done under low light to minimize environmentally induced DNA damage. The cell microgels were prepared as layers. The first layer of gel was made by applying 200  $\mu$ l of regular melting point agarose (0.7%) onto superfrosted glass microscope slides (3"  $\times$  1", thickness 1mm) and then laying a coverslip gently on the agarose. The agarose was allowed to solidify at 4°C, and the coverslip was removed. Low-melting point agarose was prepared in 100 mM PBS and kept at 37°C. MN were mixed

## DNA Damage Profiling in Motor Neurons by Single Cell Gel Electrophoresis (Comet Assay)

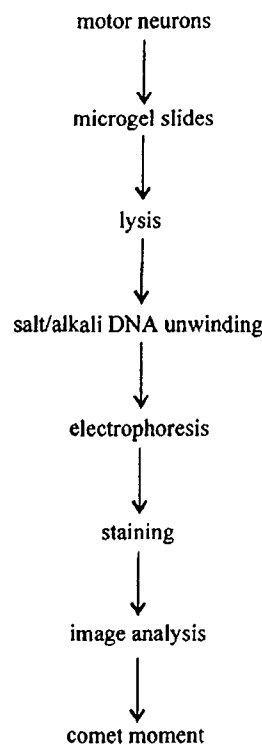


**Fig. 2.** Flow diagram of the method to profile DNA damage in MN at the single-cell level using the comet assay. Isolated cells are cast into microgels by mixing cells in low melting-point agarose and casting the gel on a glass microscope slide. The cells are lysed and the slides are inserted into an electrophoresis unit in buffer at a specified pH for DNA unwinding. Electrophoresis of DNA is then initiated and the DNA is allowed to migrate from the nucleus. The microgels are stained with ethidium bromide for DNA detection and comet moment analysis.

with the low melting point agarose, and 50  $\mu$ l of a mixture of cell suspension (containing  $\sim 4.4 \times 10^4$  MN) in low-melting point agarose was applied to the first gel layer. The slides were then coverslipped and placed at 4°C for solidification of the cell suspension-agarose mixture. After the second layer solidified, the coverslips were removed and 100  $\mu$ l of low-melting point agarose was added on top of the cell layer. The gels were recoverslipped, and the slides were placed on ice for gel solidification.

Coverslips were removed from the slides and the cell microgels were covered with lysis buffer (pH 10) containing 2.5 M NaCl, 100 mM EDTA, 1% sodium lauryl sarcosine, 10 mM Tris, and 1% Triton X-100. The cell microgels were lysed for 30 min (at room temperature). After draining, microgels were treated with DNA-unwinding solution (300 mM NaOH, 1 mM EDTA, at pH 12 unless indicated otherwise) for 30 min (room temperature). The effects of DNA unwinding solution/electrophoresis buffer pH on comet profiles were also evaluated at pH 13 and pH 7.4. Loss of a purine or pyrimidine base from the DNA sugar-phosphate backbone facilitates an alkali-catalyzed  $\beta$ -elimination of the 3'-phosphate (7). At pH  $\geq$  13, these alkali-labile sites are converted to SSB (7). DNA-SSB are detected at pH 12, while DNA-DSB are detected at more neutral conditions (7). The microgels were then placed directly into a horizontal gel electrophoresis chamber filled with DNA-unwinding solution. Gels were run with constant current (300 mA at room temperature) for generally 20 min. After electrophoresis, the microgels were neutralized with 50 mM Tris-HCl (pH 7.5) for 15 min (twice). DNA was visualized with ethidium bromide staining (20  $\mu$ g/ml, 20 min at room temperature) after which the microgels were washed and coverslipped. Comet evaluation and image acquisition were performed using a Zeiss Axiophot microscope.

**Comet Counting and Measurement of DNA Damage.** The comet profiles (Fig. 3) were analyzed by counting the number of MN with comets and by directly measuring the DNA damage in these comets. The number of cells with comets was counted in microgels prepared from MN exposed to ROS *in vitro* and from MN isolated from *in vivo* axotomy experiments. The number of comets and large intact cell nuclei regarded as MN stained by ethidium bromide were counted in 6 microscopic views at 200 $\times$  from microgels of ROS treated cells and from sciatic nerve avulsion animals. The percentages of comets relative to the total number of cells (total number of comets and total number of intact cell nuclei) were determined and group means were calculated. The data were analyzed using a Student's *t* test.

The extent of DNA damage was determined by measuring the displacement of DNA between the cell nucleus (i.e., the comet head) and the tail (Fig. 3). This measurement is designated as the comet moment. The comet moment is believed to be the best index of DNA damage in cells (10,18). Cells with more DNA damage (Fig. 3, compare 3A to 3B) show an increased migration of DNA in the direction of electrophoresis (9,10). DNA density and comet moments for individual MN were measured using the fluorescence intensity of ethidium bromide-stained DNA (Fig. 3). Randomly selected comets ( $\sim 10$ –30 comets in each treatment group) were captured as digital images using Inquiry software (Loats Associates, Westminster, MD). Comets were saved in TIFF format. Each comet was used to obtain several measurements by delineating the head and tail. DNA intensity<sub>head</sub>, DNA intensity<sub>tail</sub>, area<sub>head</sub>, and area<sub>tail</sub> were measured. Tail length was measured from the center of the head to the end of the tail. Relative DNA content is reflected by the average-integrated intensity of fluorescence. The amount of DNA damage for each cell was derived from the calculation of the comet moment using the equation  $\text{DNA intensity}_{\text{tail}} \times \text{area}_{\text{tail}}$  (19,20). The data were analyzed using a Student's *t* test.

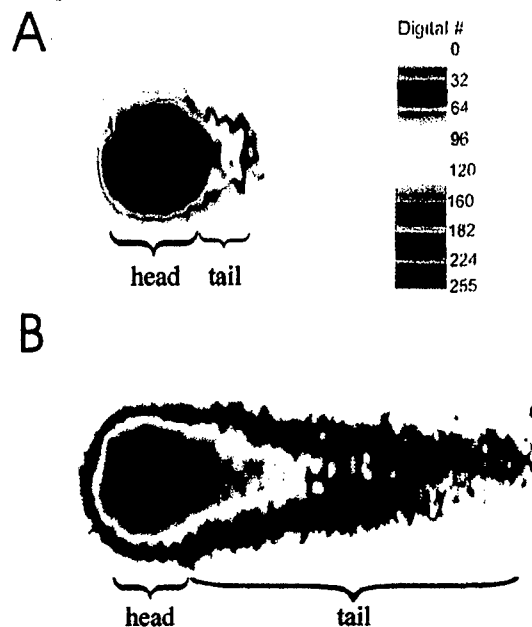


**Fig. 3** Detection of DNA damage in MN with the comet assay. Digital images of MN comets (the tail and the head comprise the comet) in microgels after SCGE. Ethidium bromide staining of DNA is in pseudocolor (color scale is shown at upper right). Each color indicates a different DNA level, with black indicating highest DNA intensity (background color has the intensity of 0). Cells with DNA damage present as comets with tails formed by migrating DNA from the head (nucleus). The images have very distinct head and tail profiles. The upper comet profile (A) has a large head and a very short tail, while the lower comet profile (B) has a smaller head and a long tail.

## RESULTS

**Isolation of MN from Adult Spinal Cord.** MN were isolated by discrete microdissection of ventral horn gray matter columns followed by trypsin digestion and differential low-speed centrifugation to fractionate ventral horn cell types (Fig. 1). Nissl staining (Fig. 4A) and NeuN immunofluorescence (Fig. 4B, C) revealed that the 400 rpm fraction (P2 fraction) was enriched in large neurons. MN enrichment was verified by immunofluorescence for ChAT (Fig. 4D–F) and prelabeling axonal projections in the sciatic nerve (Fig. 4G). Neurons comprised  $\sim 84\%$  of the total cell number (NeuN-positive cells/total cells stained with propidium iodide) in the 400 rpm fraction of digests of ventral horn enlargements. Of these neurons,  $\sim 86\%$  were MN (ChAT-positive cells/NeuN-labeled cells), and of these MN,  $\sim 72\%$  were  $\alpha$ -MN giving rise to sciatic nerve axons. The total number of MN that were isolated from combined cervical and lumbar enlargements was calculated to be  $4.0 \times 10^6 \pm 0.22 \times 10^6$ .

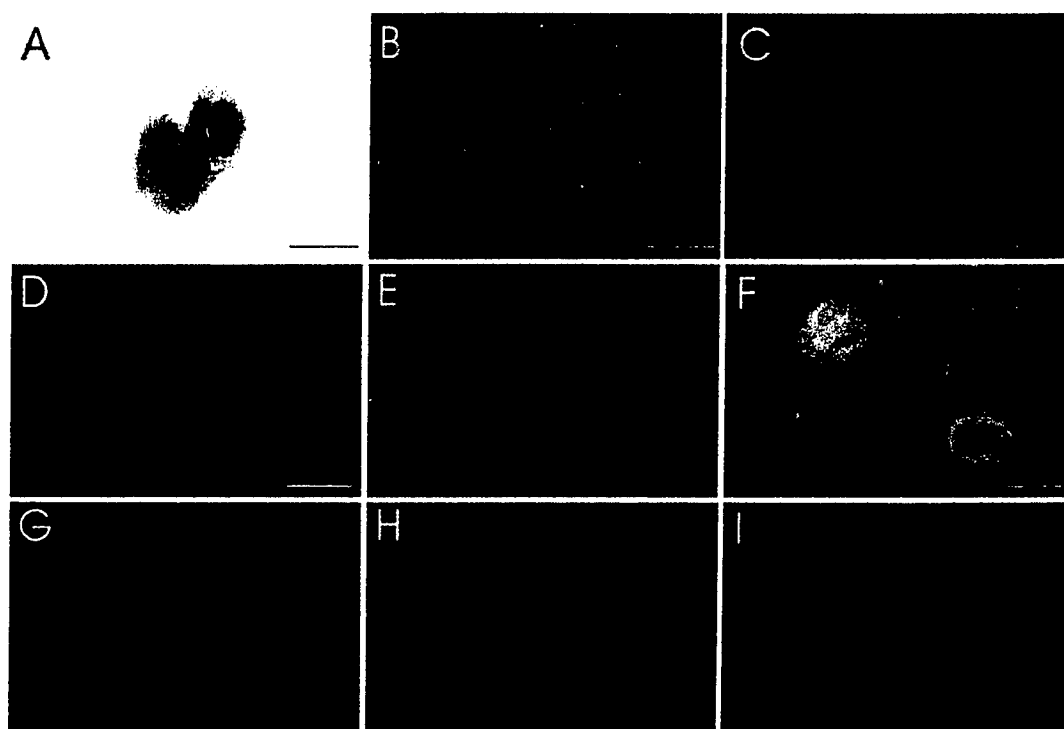


**Fig. 4.** Characterization of the MN enriched cell suspension isolated from adult rat spinal cord ventral horn. **A.** Cresyl violet staining of MN isolates in P2 fraction. The cells lose their multipolar morphology and appear as large round or ovoid nucleated cells. **B and C.** Immunocytochemical labeling for NeuN (green) shows that most of the cells in the 400 rpm preparation (P2 fraction) are neurons. The green immunofluorescence is localized in neuronal nuclei (**C**). **D.** Popidium iodide nuclear staining (red) of cells shows the cell density in the 400 rpm cell suspension (P2 fraction). **E.** Same microscopic field as that shown in **D** but viewing ChAT immunofluorescence. Most of the cells are ChAT-positive (green labeling). **F.** High magnification double exposure of popidium iodide and ChAT staining to show the perikaryal labeling for ChAT (green). **G.** Prelabeling lumbar MN with retrograde tracer DAPI (blue) shows that  $\alpha$ -MN with sciatic nerve axons sort into the 400 rpm cell suspension (P2 fraction). **H and I.** Popidium iodide nuclear staining (**H**, red) of cells showing the cell density in the microscopic field compared to the same microscopic field viewing GFAP immunofluorescence (**I**, blue). GFAP-positive astroglial processes (blue staining) are observed in the 400 rpm cell suspension. Some astroglial processes are attached to large neurons (red in **E**). Scale bars: **A**, 50  $\mu$ m; **B**, 480  $\mu$ m; **C**, 100  $\mu$ m; **D** (same for **E**, **G**, **H**, **I**), 192  $\mu$ m; **F**, 40  $\mu$ m.

GFAP-positive cell bodies were present occasionally in this fraction, although many fragments of astroglial processes were observed, some of which enveloped large cells (Fig. 4H, I). Microglial cells were rarely present in this fraction (not shown).

The viability of isolated MN was determined by trypan blue assay (Fig. 5). Freshly isolated MN completely excluded trypan blue. In Neurobasal-A medium, 74% and 61% of MN were viable at 6 and 12 hours in vitro (HIV), respectively. At HIV24, 37% of the MN were still viable.

#### DNA Damage Profiling in MN Exposed to ROS

DNA damage was profiled in individual MN exposed in vitro to  $H_2O_2$ , NO donor, and  $ONOO^-$  using the comet assay. Control cells were exposed to vehicle and

were incubated in medium for the same time in vitro. Comets were observed with each treatment. Figure 6 shows the common patterns of comets after different treatments. These assays were done at pH 12 (hydrogen bonds in DNA destabilize causing strand separation at this pH). Each treatment gave consistent results, with the major comet pattern generated from each exposure being highly reproducible (Fig. 6).

The background DNA damage was very low in control cell preparations. The vast majority of cells in microgels of control cells (time-matched for cells exposed to ROS) had intact genomic DNA (Fig. 6A–C). MN with intact DNA had a nucleus that was stained evenly with ethidium bromide and was smooth and round without a tail (Fig. 6A–C), demonstrating no elution of genomic DNA and indicating no DNA damage. Relatively few of the control cells displayed comets at 15 min (Fig. 6A), 30 min (Fig. 6B), 60 min, 120 min

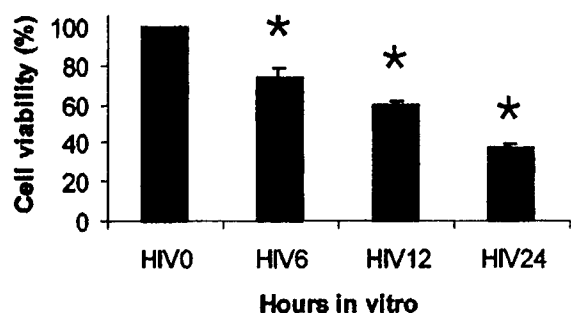


Fig. 5. Viability of adult MN after isolation and incubation for up to 24 hours in vitro (HIV). The number of viable cells and the total number of cells (viable cells plus trypan blue-stained cells) were counted in a hemocytometer under phase contrast microscopy. Asterisk denotes significant difference ( $p < 0.05$ ) compared to the earlier time point.

(Fig. 6C), and up to 240 min of incubation. Quantitative analysis of control MN suspensions incubated in Neurobasal-A medium with or without vehicle showed that the % comets was ~10% or lower (Figs. 6A–C, 7A, 8A, 9A) during an incubation period of 120 min. At 15 min, ~4% of total number of control cells had comets (Fig. 6A, 7A). This background level increased to ~10% between 15 min to 30 min in vitro and then remained stable through 120 min (Figs. 7A). The mean comet moment in control cells was  $1.4 \times 10^5$  (Fig. 8B). To determine the reproducibility of MN cell capture after in vitro incubation and microgel preparation, cells were counted in microgels. Microgel cell number remained constant (Fig. 7B).

ROS caused DNA damage in MN. NO donors and ONOO<sup>-</sup> increased significantly the comet number compared to time-matched controls (Figs. 6D–H, 8A, 9). More DNA-SSB comets were observed with SNP compared to NONOate and ONOO<sup>-</sup> (Fig. 8A). Surprisingly, cells treated with 1 mM H<sub>2</sub>O<sub>2</sub> had fewer comets compared to control (Fig. 8A, H<sub>2</sub>O<sub>2</sub> vs control-1). The moments of MN comet profiles induced by SNP, NONOate, ONOO<sup>-</sup>, and H<sub>2</sub>O<sub>2</sub> were dramatically higher than control comet moments (Fig. 8B). This difference in the formation of DNA-SSB was also reflected by differences in comet tail length (Fig. 8C) and the elution of DNA from the head to the tail (Fig. 8D). Comet tail length was generally highest with ONOO<sup>-</sup> exposure. Microgel cell number in ROS treated MN was similar to time-matched vehicle controls (not shown).

The comet morphologies in control and ROS treated MN were different (Fig. 6). Exposure to NO donors and ONOO<sup>-</sup> generated consistent comet profiles depending on exposure concentration and duration. Generally, with exposure to 10  $\mu$ M SNP or

NONOate for 15 min, 30 min and 60 min, the comet head had a bright coma composed of large granules, with a short granular tail (Fig. 6D, F). With 100  $\mu$ M or higher doses, or with 10  $\mu$ M for more than 1h exposure, the coma of the head became less prominent and the tail length was increased (Fig. 6E, G). ONOO<sup>-</sup> produced a distinct comet profile in MN. ONOO<sup>-</sup> induced comets had long tails with a paddle-like shape and a head that was small and ambiguous or undetectable (Fig. 6H).

The formation of different types of genomic DNA lesions induced in MN by NO donor and ONOO<sup>-</sup> was profiled by varying pH conditions in the comet assay (Fig. 9). The use of different pH conditions during SCGE is a validated approach for discriminating AP sites and strand breaks (13). A pH of 13, 12, and 7.4 was used to detect alkali-labile AP sites, SSB, and DSB, respectively. MN accumulated DNA-SSB (pH 12) with exposure to the NO donor NONOate (Fig. 9A). AP sites (pH 13) did not accumulate significantly (Fig. 9A). The presence of DNA-SSB in MN was dynamic. DNA-SSB accumulated rapidly in MN, occurring within 30 min exposure and then increased further over the subsequent 30 min, with ~60% of the cells revealing the presence of DNA damage at 60 min exposure to 100  $\mu$ M NONOate (Fig. 9A). In contrast, ONOO<sup>-</sup> rapidly induced the formation of alkali-labile sites within 15 min followed by an accumulation of DNA-SSB as alkali-labile sites dissipated (Fig. 9B). Moreover, ONOO<sup>-</sup> potentially induced DNA-DSB (pH 7.4) quickly (within 15 min) in MN (Fig. 9C).

#### DNA Damage Profiling in MN Injured *in Vivo*

To track DNA damage in cells degenerating in vivo, the comet assay was used on lumbar MN isolated from rats with unilateral sciatic nerve avulsions. This lesion induces MN apoptosis over a period of 10 days (14,15). Nonlesioned control MN from the contralateral side of lumbar spinal cord rarely displayed comets throughout the entire time course (Figs. 6I, 10A). The infrequent comets that were observed in MN from the nonlesioned side of lumbar spinal cord had very low comet moments (Fig. 10B). In contrast, at 5 days after sciatic nerve avulsion, the comet assay revealed DNA-SSB in ~26% of ipsilateral MN (Fig. 10A), with comet profiles having a relatively normal sized head and a very short tail (Fig. 6J). At 5 days, the comet moments were low in lesioned MN but were nevertheless significantly greater than comet moments in contralateral MN (Fig. 10B). At 7 days after sciatic nerve avulsion,

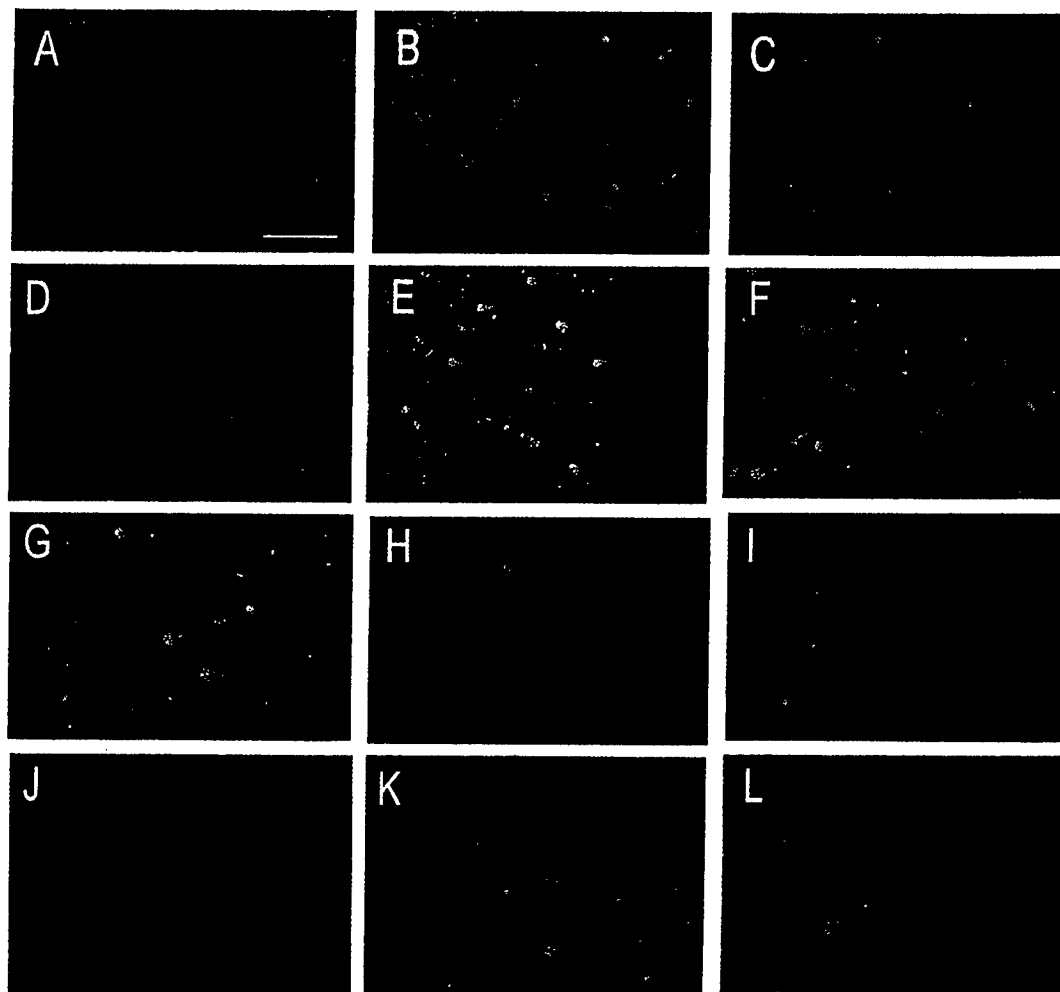


**Fig. 6.** Alkaline (pH 12) comet assay on isolated MN after exposure to ROS in vitro or axotomy in vivo. **A.** Appearance of normal cells and comets in the microgels from control sample. The 400 rpm (P2 fraction) cell preparation was incubated for 15 min in Neurobasal A medium. Microgels were stained with ethidium bromide (red). The majority of nuclei are normal without tails, revealing very little detectable DNA damage in the form of SSB. Only three background comets are seen in this image. **B.** Control MN incubated with spermine tetrahydrochloride/sodium nitrite (control for NONOate) for 60 min displayed very few comets (only one comet is seen in this image). The cells shown in panel B are at a higher magnification than the cells shown in panel A. **C.** Control MN incubated in vehicle for 120 min also displayed very few comets (only two comets are seen in this image). **D.** Comets in MN exposed to 10  $\mu$ M SNP for 15 min. The comet number is increased compared to control. The comets have a head with a prominent coma and a broad short tail. **E.** Comets in MN exposed to 10  $\mu$ M NONOate for 60 min. The comets have prominent tails. **F.** High magnification of MN comets induced by 10  $\mu$ M SNP for 30 min. These comets have distinct signatures consisting of a prominent coma and a broad tail. The comet profiles are very uniform. **G.** High magnification of MN comets induced by 10  $\mu$ M NONOate for 30 min. The tails are not as broad as those seen with 10  $\mu$ M SNP for 30 min. **H.** MN exposed to ONOO<sup>-</sup> for 30 min display a distinct signature. Some comets have ambiguous granular heads and long granular paddle-shaped tails. **I.** MN isolated from the lumbar spinal cord contralateral to the side of the sciatic nerve avulsion usually had very little detectable DNA damage. In this image of contralateral MN at 7 days postlesion, no comets are seen. **J.** At 5 days after sciatic nerve avulsion, MN have early DNA damage in the form of SSB. These comets had very short tails, indicating a few genomic DNA-SSB. **K.** At 7 days after the lesion, MN comets have prominent comas (halos) and longer tails compared to 5-day comets, demonstrating that DNA-SSB accumulate progressively. **L.** At 10 days after sciatic nerve avulsion, the comets are conspicuous and have extremely long tails with large scattered granules, further indicating a slowly evolving and accumulating level of DNA-SSB in MN. Scale bar (shown in A): 500  $\mu$ m for A, D, E; 200  $\mu$ m for B, C, F, G, H; 400  $\mu$ m for I; 160  $\mu$ m for J, K, L.

the number of MN comets was increased significantly (Fig. 10A). The comet head was expanded with a brilliant coma and a tail that was longer (Fig. 6K) compared to comets seen in lesioned MN at 5 days. The

moment of 7-day comets was significantly greater than contralateral MN comets and was increased significantly compared to lesioned MN at 5 days (Fig. 10B). At 10 days after sciatic nerve avulsion, the comet



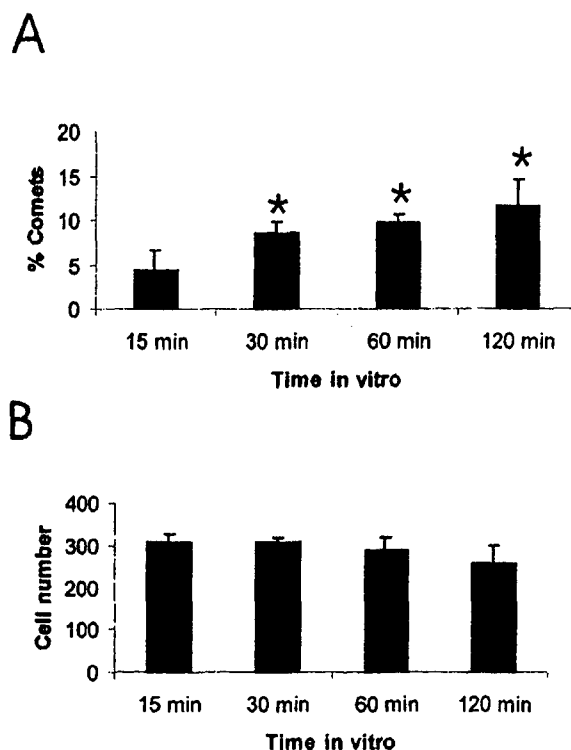


Fig. 7. Time course analysis of % comets and cell number in nontreated control MN. A. Comet number in cells incubated in Neurobasal-A for 15, 30, 60, and 120 min to determine the level of background comets (at pH 12). Values are mean  $\pm$  standard deviation. The % background comets became stable between 15–30 min (\* indicates significant difference from 15 min,  $p < 0.05$ ). B. MN number in microgels of cells incubated in Neurobasal-A for 15, 30, 60, and 120 min. The number of ethidium bromide-stained, large intact cell nuclei regarded as MN were counted in 6 microscopic views of the microgels at 200 $\times$ . Cell number did not change.

B. Comet moment (means  $\pm$  standard deviation) after 30 min exposure to 1 mM  $H_2O_2$ , 10  $\mu$ M SNP, 10  $\mu$ M NONOate, or 10  $\mu$ M ONOO $^-$ . Comet moments in control groups were not significantly different; therefore, an average control value is presented. Single asterisk denotes significant difference ( $p < 0.05$ ) from control. Double asterisk denotes significant difference ( $p < 0.05$ ) from control and other treatment groups. C. Comet tail length (mean  $\pm$  standard deviation) after 30 min exposure to 1 mM  $H_2O_2$ , 10  $\mu$ M SNP, 10  $\mu$ M NONOate, or 10  $\mu$ M ONOO $^-$ . Comet tail lengths in control groups were not significantly different; therefore, an average control value is presented. Single asterisk denotes significant difference ( $p < 0.05$ ) from control. Double asterisk denotes significant difference ( $p < 0.01$ ) from control and other treatment groups. D. Ratio of DNA area in comet tail and head (mean  $\pm$  standard deviation) after 30 min exposure to 1 mM  $H_2O_2$ , 10  $\mu$ M SNP, 10  $\mu$ M NONOate, or 10  $\mu$ M ONOO $^-$ . Single asterisk denotes significant difference ( $p < 0.05$ ) from control. Double asterisk denotes significant difference ( $p < 0.01$ ) from control and other treatment groups.

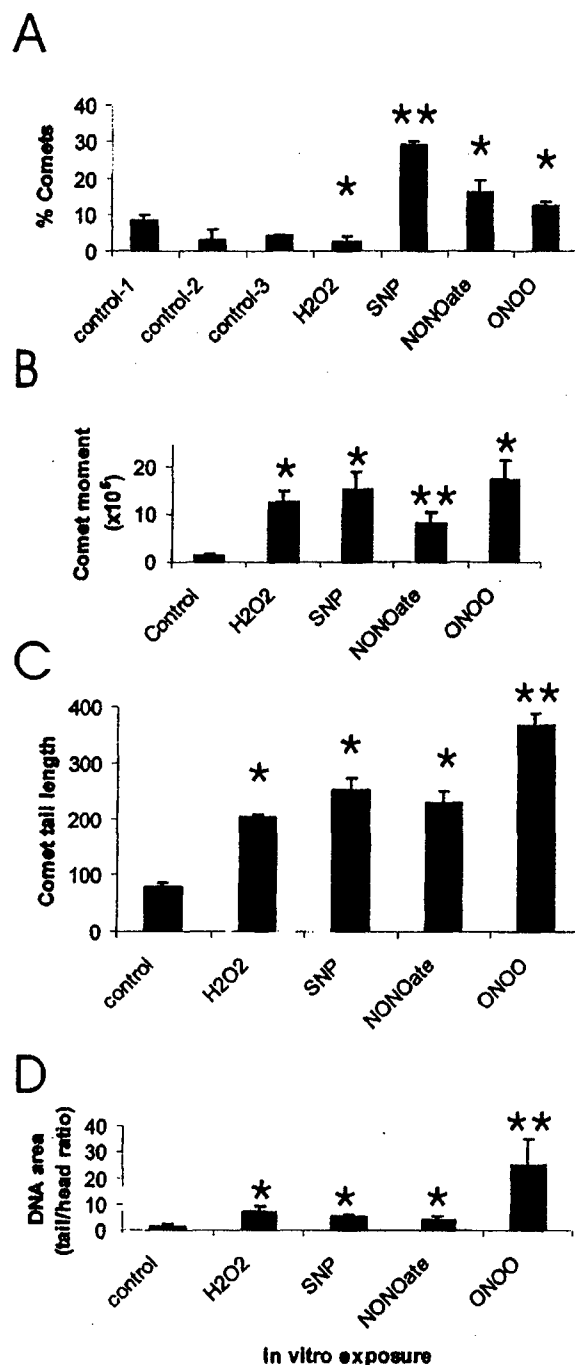
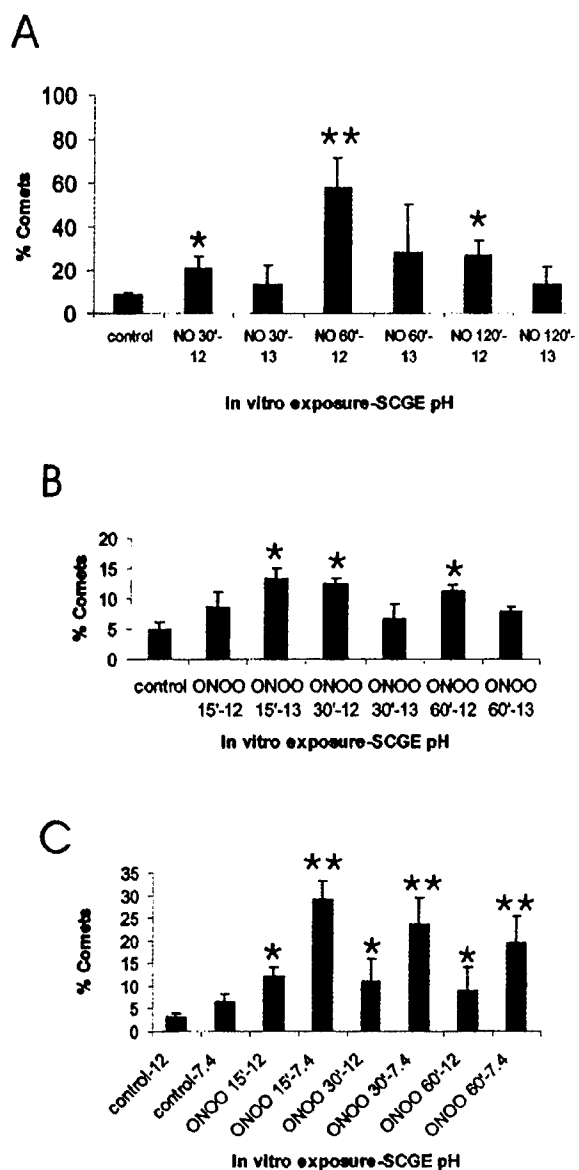


Fig. 8. DNA damage profiling in MN exposed to ROS in vitro. A. Comet number after 30 min exposure to 1 mM  $H_2O_2$ , 10  $\mu$ M SNP, 10  $\mu$ M NONOate, or 10  $\mu$ M ONOO $^-$ . Control groups are cells in medium alone (control-1 for  $H_2O_2$  and SNP), spermine/ $NO_2$  (control-2 for NONOate), and decomposed alkaline ONOO $^-$  (control-3). Values are mean  $\pm$  standard deviation. Single asterisk denotes significant difference ( $p < 0.05$ ) from corresponding control. Double asterisk denotes significant difference from corresponding control and  $H_2O_2$  ( $p < 0.01$ ) and from NONOate and ONOO $^-$  ( $p < 0.05$ ).



**Fig. 9.** DNA lesion-specific profiling in MN exposed to ROS in vitro by SCGE. Different pH conditions for the comet assay were used to distinguish alkali-labile sites/SSB (at pH 13), SSB (at pH 12), and DSB (at pH 7.4). **A.** Comet number after exposure to 10  $\mu$ M NONOate (NO) for 30, 60, and 120 min. SCGE was done at pH 12 or 13. Values are mean  $\pm$  standard deviation. Single asterisk denotes significant difference ( $p < 0.05$ ) from control. Double asterisk denotes significant difference from control ( $p < 0.01$ ) and other treatment groups ( $p < 0.05$ ). No significant increases in % comets were observed in control groups with increased incubation time at both pH 12 and pH 13. The number of MN with SSB after NONOate exposure was significantly higher than the comet number in time matched control MN at each time examined. At 60 and 120 min, the number of MN with SSB (pH 12) was significantly higher ( $p < 0.05$ ) than the number of MN with alkali-labile sites/SSB (pH 13). The number of comets at pH 13 (alkali-labile sites/SSB) was not different from controls and the number did not change with increased exposure time. **B.** Histogram of % comets induced by exposure to 10  $\mu$ M

number was lower compared to 7 days (23% vs 36; pc). However, the existing 10-day comets had spectacular heads with large loose comas and very long granular tails (Fig. 6L) with very high comet moments (Fig. 10B). Comets were observed rarely in MN from ipsilateral lumbar ventral horns at 14 and 28 days after sciatic nerve avulsion.

## DISCUSSION

DNA damage has been implicated in the mechanisms of cellular aging and disease. A major neurological disease that appears to involve DNA damage in its pathogenesis is ALS (4,5,8). 8-hydroxy-2-deoxyguanosine (OHdG) adducts are elevated in postmortem CNS tissue extracts from individuals with ALS (21,22). Direct evidence for OHdG-DNA lesions specifically in MN of individuals with ALS has been found recently (5). Indirect evidence for DNA damage in ALS is also available. The protein levels and enzyme activity of apurinic/apyrimidinic endonuclease, an enzyme that functions in the DNA base-excision repair pathway, are elevated selectively in MN regions in ALS (6). Furthermore, p53 is activated in MN regions in individuals with ALS (4). The involvement of DNA damage as an upstream stimulus for MN degeneration has been shown in animal and cell culture models. OHdG lesions and DNA-SSB accumulate in MN during p53-dependent apoptosis in rat and mouse (14,15). In mouse cortical neuron cultures the DNA topoisomerase inhibitor camptothecin is a potent inducer of apoptosis (23,24), presumably by inducing the formation of DNA-SSB (25). DNA damage may therefore be pivotal in the pathogenesis of lower and upper MN degeneration in ALS.

ONOO<sup>-</sup> or vehicle (control). SCGE was done at pH 12 and 13. The comet number in MN exposed to ONOO<sup>-</sup> for 15 min was prominent at pH 13 (\*,  $p < 0.05$  compared to the time and pH matched control cells), but comet number decreased relative to 15 min exposure with increased exposure time. The number of comets in identical samples at pH 12 increased significantly as exposure time increased (\*,  $p < 0.05$  compared to control cells at pH 12). At 60 min exposure to ONOO<sup>-</sup> number of comets detected at pH 12 (cells with SSB) was significantly more ( $p < 0.05$ ) than the number of comets detected at pH 13 (cells with alkali-labile sites/SSB). **C.** Histogram of % comets induced by exposure to 100  $\mu$ M ONOO<sup>-</sup> or vehicle (control). SCGE was done at pH 12 and 7.4. ONOO<sup>-</sup> induced prominent DNA-DSB (pH 7.4) with 15 min exposure and longer time (\*\*,  $p < 0.01$  as compared to time and pH matched control cells and  $p < 0.05$  compared to pH 12 cells). In contrast, MN with DNA-SSB (pH 12) were not as numerous as MN with DSB, although the number of cells with SSB was still significantly higher than time matched control cells (\*,  $p < 0.05$ ).

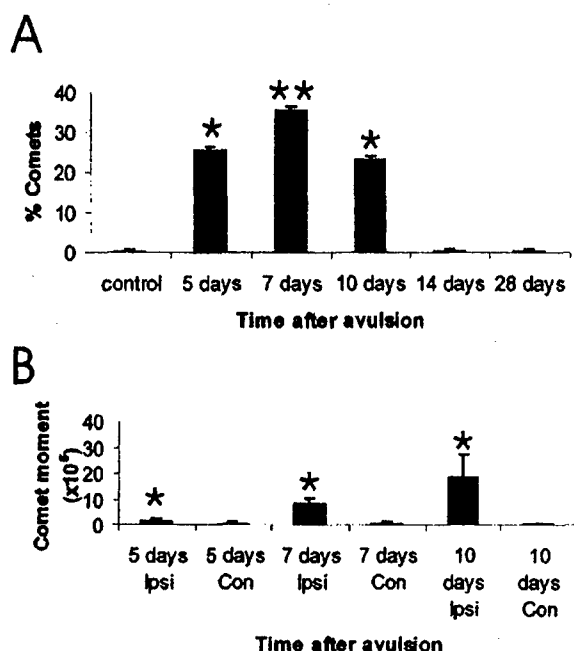


**Fig. 10.** DNA damage profiling (pH 12 for SSB) in MN injured in vivo by sciatic nerve avulsion. **A.** Percent comets in lumbar MN from the lesioned side of spinal cord. Values are mean  $\pm$  standard deviation. The percentage of comets (relative to total number of large cells in the microgels) was significantly higher at 5 days (\*,  $p < 0.05$ ), 7 days (\*\*,  $p < 0.01$ ), and 10 days (\*,  $p < 0.05$ ) postlesion compared to control contralateral side (comets were rarely detected). Comet number was significantly higher ( $p < 0.05$ ) at 7 days compared to 5 and 10 days. Comets were rarely seen in the 400 rpm fraction (P2 fraction) at 14 and 28 days. **B.** Injured MN showed a progressive increase in comet moment, indicating a progressive accumulation of DNA-SSB. Values are mean  $\pm$  standard deviation. In the rare comets found in nonlesioned contralateral (Con) MN at 5, 7, and 10 days postlesion, the comet moments were low. Comet moments in ipsilateral (Ipsi) lesioned MN at 5, 7, and 10 days postlesion were significantly greater than their corresponding contralateral controls (asterisks,  $p < 0.05$  for 5 days,  $p < 0.01$  for 7 days,  $p < 0.001$  for 10 days). Comet moments increased significantly in injured MN with time postlesion ( $p < 0.05$ , 7 days vs 5 days, 10 days vs 7 days) and were greatest at 10 days. Examples of corresponding comets are shown in Figure 6J–L.

Quantitative assays need to be developed for profiling specific types of DNA lesions in mature MN at the single-cell level. The fulfillment of this need is a two-stage process. The first stage requires the development of an approach to isolate mature MN, and then the second stage is the employment of a reliable and sensitive method to detect DNA lesions in single cells. In this study, we show that viable MN can be isolated from the adult spinal cord and that these MN can be used to profile the emergence of DNA lesions at the single-cell level.

We found that MN for the adult spinal cord can be isolated and postlesioned (Fig. 10). It is likely that the large

size adult MN contributes to the ability to isolate these neurons by differential centrifugation. The MN enrichment of this cell system was documented by immunophenotyping for ChAT and axonal tract tracing. This work confirms our previous results using this MN isolation method (19,20). We anticipate that other large neurons (e.g., dopaminergic nigral neurons and cerebellar Purkinje cells) could be isolated using this method and profiled for DNA damage. The current inability to culture isolated adult MN, and the resulting short-term viability of adult MN in suspension, is a disadvantage of our system, but an  $\sim 37\%$  survival at HIV24 is a reasonable starting point for future studies on extending the viability of these MN with different media and growth factor supplements.

This method is an important technical advancement in the field of MN biology because only one other method is available to study MN in vitro. Embryonic rat spinal cord MN can be isolated and cultured (26); however, these cells are immature MN cultured at low density. Long-term viability is also a difficulty with embryonic rat MN, because these cells are usually studied at 24–48 hours after plating. Compared to the embryonic MN culture model, our in vitro system using mature MN has several notable advantages. The cells are adult neurons. This is important because neuronal maturity appears to influence cell death mechanisms in vivo and in vitro (5,24,27) as well as DNA repair mechanisms (2); thus, our system may be more relevant than embryonic cell models for understanding MN biology and for modeling degeneration of MN in ALS. In addition, injured MN can be isolated from adult animals after in vivo spinal cord or peripheral nerve manipulations. Similar experimental manipulations have not been done with embryonic mammalian systems. Our isolation technique yields a high number of spinal  $\alpha$ -MN ( $\sim 4 \times 10^6$ /rat) that can be studied in vitro at high density. The cells can be used for comet assay and immunocytochemical methods and for biochemical and molecular assays. This in vitro MN system can be used as a high throughput screening system for testing the neurotoxic (genotoxic) or neuroprotective activities of environmental, synthetic, or biological compounds on adult MN.

We used the comet assay to profile the emergence of genomic DNA damage in neurons after in vitro exposure to ROS and after in vivo axotomy. The majority of past and current publications on the comet assay have studied nonneuronal cells. Others (12,28) and we (19,20) have recently demonstrated the feasibility and innovative utility of the comet assay in neuronal systems. This assay is the only known method to track

specific DNA lesions and DNA repair at the single-cell level. This assay is based on the fundamental principle that single strand DNA elutes rapidly under alkaline conditions from cells onto filters (29). This principle was then extended to the analysis of DNA damage in individual cells using SCGE (9,10). The comet assay detects DNA-SSB at pH ~12, DNA-DSB at neutralized conditions, DNA-DNA or DNA-protein crosslinking, alkali-labile sites that cause SSB under alkali conditions (pH > 12.6) and damage to purine and pyrimidine bases (AP sites). At pH conditions of 12.6 or higher, alkali-labile sites are converted SSB, and, thus, a pH  $\geq$  13 maximizes the detection of alkali-labile sites as SSB (7). The sensitivity of the comet assay is reported to be exquisite, detecting one break per  $2 \times 10^{10}$  Daltons of DNA in lymphocytes (10).

We tested the hypothesis that ROS cause adult MN to accumulate DNA damage. MN were exposed *in vitro* to  $H_2O_2$ , NO donors, and  $ONOO^-$ . Different pH conditions were used during electrophoresis to discriminate between DNA strand breaks and alkali-labile sites in MN. We found that different ROS induce different DNA damage profiles in MN.  $H_2O_2$  and NO induce primarily SSB in MN, whereas  $ONOO^-$  induces a combination of SSB, DSB, and alkali-labile sites (AP sites). The genotoxic actions of  $ONOO^-$  in MN were dramatic. The formation of DNA-SSB in MN is very dynamic. Exposure of MN to the NO donor  $NONOate$  caused a progressive accumulation of DNA-SSB over a 1 h period, while the level of alkali-labile sites was relatively invariant. DNA-SSB are formed in MN within a 30 min window of time. Thus, MN exposed to NO rapidly form DNA-SSB.

MN comet number decreased compared to control in the presence of 1 mM  $H_2O_2$ . The explanation for this finding is uncertain. It is possible that this concentration of  $H_2O_2$  may be insufficient for inducing DNA damage in healthy MN in suspension for a short time (possibly related to antioxidant enzymes in the Neurobasal medium), but it may enhance DNA damage in already dying/injured MN (background comets) that then disappear from the 400 rpm preparation with repelleting after exposure. However, 1 mM  $H_2O_2$  exposure for up to 2 h did not cause a loss of cells compared to time-matched controls (data not shown). Alternatively, DNA-SSB occurring spontaneously in isolated MN could be repaired. DNA repair mechanisms may be stimulated in MN exposed to low concentrations of  $H_2O_2$ , so that fewer DNA-SSB are detected. The kinetics of DNA repair is very rapid. In leukocytes DNA-SSB can be repaired within 2 minutes after irradiation (30).

We also tested the hypothesis that MN accumulate DNA damage after axonal injury *in vivo* using a sciatic nerve avulsion model. MN had accumulated DNA-SSB by 5 days after injury. The accumulation of DNA-SSB after injury was progressive over 5–10 days postlesion as revealed by the comet moments. This finding supports and extends the conclusion that DNA damage is a stimulus for MN apoptosis in the adult spinal cord (14). The accumulation of DNA-SSB could be a primary upstream signal for MN apoptosis by engaging p53-mediated pathways (15).

## ACKNOWLEDGMENTS

This work was supported by grants from the U.S. Public Health Service, National Institutes of Health, National Institute of Neurological Disorders and Stroke (NS34100) and National Institute on Aging (AG16282) and the Department of Defense, U.S. Army Medical Research and Materiel Command (DAMD17-99-1-9553).

## REFERENCES

1. Lindahl, T. 1993. Instability and decay of the primary structure of DNA. *Nature* 362:709–715.
2. Subba Rao, K. 1993. Genomic damage and its repair in young and aging brain. *Mol. Neurobiol.* 7:23–48.
3. Kisby, G. E., Kabel, H., Hugon, J., and Spencer, P. 1999. Damage and repair of nerve cell DNA in toxic stress. *Drug Metabol. Rev.* 31:589–618.
4. Martin, L. J. 2000. p53 is abnormally elevated and active in the CNS of patients with amyotrophic lateral sclerosis. *Neurobiol. Dis.* 7:613–622.
5. Martin, L. J. 2001. Neuronal cell death in nervous system development, disease, and injury. *Int. J. Mol. Med.* 7:455–478.
6. Shaikh, A. Y. and Martin, L. J. 2002. DNA base-excision repair enzyme apurinic/aprimidinic endonuclease/redox factor-1 is increased and competent in the brain and spinal cord of individuals with amyotrophic lateral sclerosis. *Neuromol. Med.* 2:47–60.
7. Kohn, K. W. 1991. Principles and practice of DNA filter elution. *Pharmac. Ther.* 49:55–77.
8. Bradley, W. G. and Krasin, F. 1982. A new hypothesis of the etiology of amyotrophic lateral sclerosis. The DNA hypothesis. *Arch. Neurol.* 39:677–680.
9. Östling, O. and Johansson, K. J. 1984. Microelectrophoretic study of radiation-induced DNA damage in individual mammalian cells. *Biochem. Biophys. Res. Commun.* 123:291–298.
10. Singh, N. P., McCoy, M. T., Tice, R. R., and Schneider, E. L. 1988. A simple technique for quantitation of low levels of DNA damage in individual cells. *Exp. Cell Res.* 175:184–191.
11. Kindzelskii, A. L. and Petty, H. R. 1999. Ultrasensitive detection of hydrogen peroxide-mediated DNA damage after alkaline single cell gel electrophoresis using occultation microscopy and TUNEL labeling. *Mutat. Res.* 426:11–22.
12. Morris, E. J., Drexler, J. C., Cheng, K.-Y., Wilson, P. M., Gin, R. M., and Geller, H. M. 1999. Optimization of single-cell gel electrophoresis (SCGE) for quantitative analysis of neuronal DNA damage. *BioTechniques* 26:282–289.
13. Tice, R. R., Agurell, E., Anderson, D., Burlison, B., Hartmann, A., Kobayashi, H., Miyamae, Y., Rojas, E., Ryu, J.-C., and Sasaki, Y. F. 2000. Single cell gel/comet assay: guidelines for

- in vitro and an in vivo genetic toxicological testing. *Environ. Mol. Mutag.* 35:206–221.
14. Martin, L. J., Kaiser, A., and Price, A. C. 1999. Motor neuron degeneration after sciatic nerve avulsion in adult rat evolves with oxidative stress and is apoptosis. *J. Neurobiol.* 40:185–201.
  15. Martin, L. J. and Liu, Z. 2002. Injury-induced spinal motor neuron apoptosis is preceded by DNA single-strand breaks and is p53- and bax-dependent. *J. Neurobiol.* 5:181–197.
  16. Hrabie, J. A., Klose, J. R., Wink, D. A., and Keer, L. K. 1993. New nitric oxide-releasing zwitterions derived from polyamines. *J. Org. Chem.* 58:1472–1476.
  17. Beckman, J. S., Carson, M., Smith, C. D., and Koppenol, W. H. 1993. ALS, SOD and peroxynitrite. *Nature* 364:548.
  18. Hellman, B., Vaghef, H., and Boström, B. 1995. The concept of tail moment and tail inertia in the single cell gel electrophoresis assay. *Mutat. Res.* 336:123–131.
  19. Liu, Z. and Martin, L. J. 2001. Motor neurons rapidly accumulate DNA single strand breaks after in vitro exposure to nitric oxide and peroxynitrite and in vivo axotomy. *J. Comp. Neurol.* 432:35–60.
  20. Liu, Z. and Martin, L. J. 2001. Isolation of mature spinal motor neurons and single cell analysis using the comet assay of early low-level DNA damage induced in vitro and in vivo. *J. Histochem. Cytochem.* 49:957–972.
  21. Fitzmaurice, P. S., Shaw, I. C., Kleiner, H. E., Miller, R. T., Monks, T. J., Lau, S. S., Mitchell, J. D., and Lynch, P. G. 1996. Evidence for DNA damage in amyotrophic lateral sclerosis. *Muscle Nerve* 19:797–798.
  22. Ferrante, R. J., Browne, S. E., Shinobu, L. A., Bowling, A. C., Baik, M. J., MacGarvey, U., Kowall, N. W., Brown, R. H., Jr., and Beal, M. F. 1997. Evidence of increased oxidative damage in both sporadic and familial amyotrophic lateral sclerosis. *J. Neurochem.* 69:2064–2074.
  23. Lesuisse, C. and Martin, L. J. 2002. Long-term culture of mouse cortical neurons as a model for neuronal development, aging, and death. *J. Neurobiol.* 51:9–23.
  24. Lesuisse, C. and Martin, L. J. 2002. Immature and mature cortical neurons engage different apoptotic mechanisms involving caspase-3 and the MAP kinase pathway. *J. Cereb. Blood Flow Metab.* 22:935–950.
  25. Nieves-Neira, W. and Pommier, Y. 1999. Apoptotic response to camptothecin and 7-hydroxystaurosporine (UCN-01) in the 8 human breast cancer cell lines of the NCI anticancer drug screen: multifactorial relationships with topoisomerase I, protein kinase C, Bcl-2, p53, MDM-2 and caspase pathways. *Int. J. Cancer* 82:396–404.
  26. Henderson, C. E., Bloch-Gallego, E., and Camu, W. 1995. Purified embryonic motoneurons. Pages 69–81, in Cohen, J. and Wilkin, G. (eds.), *Nerve Cell Culture: A Practical Approach*. Oxford University Press, London.
  27. Portera-Cailliau, C., Price, D. L., and Martin, L. J. 1997. Non-NMDA and NMDA receptor-mediated excitotoxic neuronal deaths in adult brain are morphologically distinct: further evidence for an apoptosis-necrosis continuum. *J. Comp. Neurol.* 378:87–104.
  28. Lai, H. and Singh, N. P. 1995. Acute low-intensity microwave exposure increases DNA single-strand breaks in rat brain cells. *Bioelectromagnetics* 16:207–210.
  29. Kohn, K. W., Erickson, L. C., Ewig, R. A. G., and Friedman, C. A. 1976. Fractionation of DNA from mammalian cells by alkaline elution. *Biochemistry* 15:4629–4637.
  30. Mendiola-Cruz, M. T. and Morales-Ramirez, P. 1999. Repair kinetics of gamma-ray induced DNA damage determined by single cell gel electrophoresis assay in murine leukocytes in vivo. *Mutat. Res.* 433:45–52.

# Mitochondrial Toxin 3-Nitropropionic Acid Induces Cardiac and Neurotoxicity Differentially in Mice

Kathleen L. Gabrielson,\* Barbara A. Hogue,<sup>†</sup>  
Vilhelm A. Bohr,<sup>†</sup> A. J. Cardounel,<sup>‡</sup>  
Waco Nakajima,\*\* Julia Kofler,<sup>§</sup> Jay L. Zweier,<sup>‡</sup>  
E. Rene Rodriguez,<sup>¶</sup> Lee J. Martin,<sup>¶</sup>  
Nadja C. de Souza-Pinto,<sup>†</sup> and Joseph Bressler<sup>||</sup>

*From the Division of Comparative Medicine and the Departments of Medicine (Cardiology Division),<sup>†</sup> Anesthesiology,<sup>‡</sup> and Pathology,<sup>§</sup> School of Medicine; and the Department of Environmental Health Sciences,<sup>||</sup> Division of Toxicological Sciences, and Kennedy Krieger Institute, School of Public Health, The Johns Hopkins University, Baltimore, Maryland; the Laboratory of Molecular Genetics,<sup>¶</sup> National Institutes of Health, National Institute of Aging, Gerontology Research Center, Baltimore, Maryland; and the Department of Pediatrics,\* School of Medicine, Akita University, Hondo, Akita, Japan*

We investigated the effects of 3-nitropropionic acid (3NPA), a previously characterized neurotoxin, in four strains of mice to better understand the molecular basis of variable host responses to this agent. Unexpectedly, we found significant cardiac toxicity that always accompanied the neurotoxicity in all strains of mice in acute and subacute/chronic toxicity testing. Caudate putamen infarction never occurred without cardiac toxicity. All mouse strains tested are sensitive to 3NPA although the C57BL/6 and BALB/c mice require more exposure than 129SVEMS and FVB/n mice. Cardiac toxicity alone was found in 50% of symptomatic mice tested and morphologically, the cardiac toxicity is characterized by diffuse swelling of cardiomyocytes and multifocal coagulative contraction band necrosis. In subacute to chronic exposure, atrial thrombosis, cardiac mineralization, cell loss, and fibrosis are combined with cardiomyocyte swelling and necrosis. Ultrastructurally, mitochondrial swelling occurs initially, followed by disruption of myofilaments. Biochemically, isolated heart mitochondria from the highly sensitive 129SVEMS mice have a significant reduction of succinate dehydrogenase activity, succinate oxygen consumption rates, and heart adenosine triphosphate after 3NPA treatment. The severity of morphological changes parallels the biochemical alterations caused by 3NPA, consistent with cardiac toxicity being a consequence of the effects of 3NPA on succinate dehydrogenase. These experiments show, for the first time, that 3NPA has important cardiotoxic effects as well as neurotoxic effects, and that cardiac toxicity possibly result-

**ing from inhibition of the succinate dehydrogenase in heart mitochondria, contributes to the cause of death in 3NPA poisoning in acute and subacute/chronic studies in mice. (*Am J Pathol* 2001, 159:1507-1520)**

3-Nitropropionic acid (3NPA) is a natural environmental toxin made by various plants and fungi. Human 3NPA intoxication has occurred in China via ingestion of fungal contaminated sugarcane,<sup>1,2</sup> yet 3NPA contamination of various foodstuffs (corn, peanuts, sugarcane) is not monitored by regulatory agencies. 3NPA induces neurodegeneration in the caudate putamen in humans and experimental animals, resembling Huntington's disease.<sup>3-8</sup> Consequently, 3NPA poisoning is used primarily as an animal model of selective neurodegeneration. The mechanism of toxicity is thought to be because of the irreversible, covalent binding of 3NPA with subsequent inhibition of succinate dehydrogenase (SDH), an enzyme of the citric acid cycle that transfers electrons to the electron transport chain via its complex II function.<sup>9,10</sup> Thus, a major factor in 3NPA toxicity is because of cellular and mitochondrial stress seen with metabolic impairment.

Differential neurotoxic effects of 3NPA have been identified between rats and mice,<sup>11</sup> as mice seem resistant and require more 3NPA exposure, and between the mice carrying the Huntington's disease mutation and their wild-type littermates.<sup>12,13</sup> Additionally, various strains of rats exhibit differential sensitivity to 3NPA,<sup>14</sup> however previous investigations of 3NPA toxicity have not considered strain differences in mouse models. Significant variation has been found between mouse strains in response to neurological injury resulting from other neurotoxins such as kainic acid and 1-methyl-4-phenyl-1,2,3,6-tetrahydropyridine,<sup>15,16</sup> as well as hypoxia and ischemia reperfusion mouse models.<sup>17,18</sup> We investigated the effects of 3NPA on the same strains of inbred mice, C57BL/6, BALB/c, FVB/n, and 129SVEMS strains, which showed differential sensitivity to the neurotoxin kainic acid. We were interested if certain strains of mice were less sen-

Supported by T32 ES07141 (to K. L. G.), the National Institute of Environmental Health Sciences (grant ES03819, NIEHS), the National Institutes of Health (grant NIA AG16282 to L. J. M.), the Department of Defense, United States Army Medical Research and Materiel Command (DAMD 17-99-1-9553 to L. J. M.), and RO1 ES08785 NIEHS (to J. B.).

Accepted for publication July 17, 2001.

Address reprint requests to Kathleen L. Gabrielson, D.V.M., Ph.D., 720 Rutland Ave., Ross 459, Comparative Medicine, School of Medicine, Baltimore, Maryland 21205. E-mail: kgabrieli@jhmi.edu.

sitive to neurological injury. The significance of this would be of great importance in strain background selection in genetic engineering of mice and the interpretation of these studies.

Furthermore, because the heart, similar to the brain, has a tremendous dependence on mitochondrial function and oxidative metabolism for the production of ATP, we investigated the effects of 3NPA on the heart in this experimental protocol. Our finding of 3NPA-induced cardiac pathology, which varied between mouse strains, was then followed up by investigation of biochemical mechanisms of cardiac toxicity in the most sensitive and least sensitive mouse strains.

## Materials and Methods

### Animals and Materials

BALB/c and C57BL/6 mice (8- to 10-week-old males) were purchased from Hilltop Labs (Philadelphia, PA). FVB/n and 129SVEMS mice (8- to 10-week-old males) were purchased from the Jackson Laboratory (Bar Harbor, ME). All of the mice were housed in groups of five on a 12-hour light/dark schedule. Mice were allowed free access to mouse lab chow and water. All experiments were performed in accordance to the Guidelines for the Use and Care of Laboratory Animal (NIH Publication 85-23).

### Drug Administration and Experimental Groups

3NPA (Aldrich Chemical Co., Milwaukee, WI) was made fresh daily and dissolved in isotonic saline (20 mg/ml) without neutralization, passed through a 0.2- $\mu$ m filter to remove any bacterial contamination, and administered by intraperitoneal injection. Mice were numbered, weighed, and injected daily between 11:00 a.m. and 1:00 p.m. Two dosing protocols were used.

#### Protocol 1 Acute Toxicity

This 3NPA-dosing protocol was adapted from the original mouse protocol for Webster Swiss mice used by Gould and Gustine.<sup>7</sup> Saline or 3NPA was administered to 4 to 6 mice per strain/treatment (C57BL/6, BALB/c, 129SVEMS, and FVB/n) for two injections, 100 mg/kg 3NPA, 24 hours apart, and survival was assessed at 48 hours after the first injection. In this survival study, mice were monitored every 15 minutes throughout a 12-hour period and were euthanized using criteria described below based on clinical signs. In another series of structural and biochemical studies, this same protocol was used, except mice were euthanized at 24 hours after the first dose or 1 hour after the second dose to harvest tissues for electron microscopy ( $n = 10$ /strain/treatment), ATP analysis ( $n = 3$  to 6/strain/treatment), or isolate heart mitochondria for metabolic studies ( $n = 3$  to 4/strain/treatment).

#### Protocol 2 Subacute/Chronic Toxicity

3NPA (75 mg/kg/day) was given to the above strains of mice to model a subacute/chronic exposure. Mice were monitored every 15 minutes throughout a 12-hour period and euthanized based on clinical signs as described below.

### 3NPA-Induced Clinical Signs in Mice

With protocol 2, exposing mice to a more chronic, lower dose exposure of 3NPA, more consistent neurological signs were observed, accompanied by neuropathology. The majority of mice dosed with 3NPA developed a characteristic, progressive neurological disorder, clinically recognized in three stages referred to as stage I, II, and III, similar to the disorder seen in the 3NPA-treated rats.<sup>8</sup>

In stage I, symptomatic mice were hypoactive but retained a normal posture and gait. These mice had minimal grooming activity and interaction with other mice. In stage II, there was an increase in spontaneous motor activity, which was characterized by a wobbly gait (ataxia), tremors, and a frequency to fall to one side with short episodes of paddling.

Finally, stage III was characterized by a reduction in motor hyperactivity with ventral or lateral recumbency (moribund state) and frequently bilateral hindlimb extension (more pronounced in protocol 2). Occasionally mice would have a seizure ( $<10\%$  of FVB/n mice) when aroused.

Other clinical signs included weight loss (20%) that usually began 2 to 3 days before stage III signs were observed. Stage III mice routinely were hypothermic, with body temperatures as low as 29°C compared to 38°C in control mice. Body temperatures were monitored using a Mallinckrodt Mon-a-therm model 6510 system (Mallinckrodt Medical Inc., St Louis, MO) with rectal probe attachment. Additionally, hypothermic moribund mice, which never progressed through neurological stages, seemed to be in cardiopulmonary failure, characterized by respiratory signs (labored breathing) and possibly impaired perfusion (bluish distal extremities).

Criteria for euthanasia and evaluation: the moribund mice described above were immediately euthanized and histologically examined. Additionally, all mice with stage III neurological signs were euthanized and histologically examined. Mice that died acutely without significant clinical signs during the day of observation (15%) were also examined and each of the above groups were included in Figure 1, Table 1, or Table 2.

### Light Microscopy

For necropsy, mice exhibiting the above clinical signs were anesthetized with metaphane, perfused via left ventricle with 10% buffered formalin or tissues were fixed in formalin by immersion-fixation. Tissues were processed for standard hematoxylin and eosin staining (H&E). Because of the acute deaths in mice using protocol 1, with inconsistent neurological signs, multiple organs were ex-

**Table 1.** Survival Rate (in %) of Four Mouse Strains after 3NPA Treatment (Protocol 1)

Strain	Number of mice	Survival rate (48 hours), %
C57BL/6	5	100
BALB/c	6	84
FVB/n	4	25
129SVEMS	5	20

Eight-week-old male mice (C57BL/6, BALB/c, FVB/n, and 129SVEMS strains) were intraperitoneally treated with 2 doses, 100 mg/kg 3NPA at 0 and 24 hours and survival rate was assessed at 48 hours after the first injection. This treatment protocol was based on the original mouse protocol developed by Gould and Gustine.<sup>7</sup> Mice included in this study were observed every 15 minutes over a 12-hour period for 48 hours after the first 3NPA dose and were euthanized using criteria described in the Materials and Methods section based on clinical signs. Chi-square Fisher's exact analysis on these mice showed a significant difference in survival between C57BL/6 mice compared to FVB/n ( $P = 0.048$ ) and C57BL/6 compared to 129SVEMS mice ( $P = 0.048$ ). Comparison of Balb/c mice with other strains did not reach the 0.05 level of significance. Significant cardiac injury was found in all mice that were euthanized or died after exposure to 3NPA in this study.

amined in protocols 1 and 2 (heart, lungs, liver, kidneys, pancreas, and intestines) to identify other organ pathological injury and the likely cause of sudden death. After it was determined that only the heart and brain (specifically caudate putamen) were affected and no other organs showed significant pathology, only the brain and heart were examined in subsequent studies.

### Characterization and Grading of 3NPA-Induced Cardiac Toxicity

C57BL/6 mice ( $n = 7$ ) were compared to 129SVEMS mice ( $n = 7$ ) treated with two doses of 3NPA (100 mg/kg; 0 and 24 hours) and perfused with a 1% paraformaldehyde and 1.25% glutaraldehyde solution 1 hour after the

**Table 2.** Incidence of Lesions and Tissues Injured (Caudate Putamen, Heart, or Both) in Mice Treated with 75 mg/kg/day of 3NPA (Protocol 2)

Mouse strain	Number of mice	Type of lesion		
		Heart only	Brain only	Heart and brain
C57BL/6	17	10	0	7
BALB/c	16	3	0	13
FVB/n	8	6	0	2
129SVEMS	8	4	0	4

Mice included in this study were observed every 15 minutes over a 12-hour period for consecutive days of 3NPA dosing as described in the Materials and Methods section. Mice included in this table were euthanized due to stage III neurological signs (mice with heart and brain lesions above) or if clinically moribund (mice with only heart lesions above) as described in the Materials and Methods section and in Figure 1.

second injection. Saline-treated controls ( $n = 6$  per strain) were compared to the 3NPA treatment groups. This time point was used because 129SVEMS mice would commence to die shortly (1 to 2 hours) after the second injection. The degree of cardiac cellular swelling, necrosis, mineralization, and hemorrhage were assessed on toluidine blue-stained histological sections. Twenty representative heart sections per mouse were graded semiquantitatively on a scale of 0 to 4 (0, absent; 1, minimal; 2, mild; 3, moderate; 4, severe) and averaged according to previously published criteria.<sup>19</sup> For cellular swelling the following scores were used: 1, microscopic foci of cellular swelling that involve a few cardiomyocytes in one location in the atria, ventricles, and septum; 2, cellular swelling foci consisting of a few cardiomyocytes involving more than one of the above locations; 3, small localized, multiple foci of cellular swelling involving more than one area; and 4, large diffuse cellular swelling involving the ventricular walls and septum. Necrosis was scored as follows: 1, microscopic foci of necrosis that involve a few cardiomyocytes in one location in the atria, ventricles, and septum; 2, necrotic foci consisting of a few cardiomyocytes involving more than one of the above locations; 3, small localized, multiple foci of necrosis involving more than one area; and 4, large diffuse necrotic foci involving the ventricular walls and septum. Mineralization was scored as follows: 1, microscopic foci of mineralization that involve a few cardiomyocytes in one location in the atria, ventricles, and septum; 2, mineralization foci consisting of a few cardiomyocytes involving more than one of the above locations; 3, small localized, multiple foci of mineralization involving more than one area; and 4, large diffuse mineralization foci involving the ventricular walls and septum. Hemorrhage was scored as follows: 1, occasional erythrocytes in the interstitium; 2, small groups of erythrocytes in the interstitium; 3, large groups of erythrocytes in the interstitium; and 4, diffuse large accumulation of erythrocytes in the interstitium.

### Electron Microscopy

129SVEMS and C57BL/6 mice were compared by ultrastructural analysis of caudate putamen and heart at the

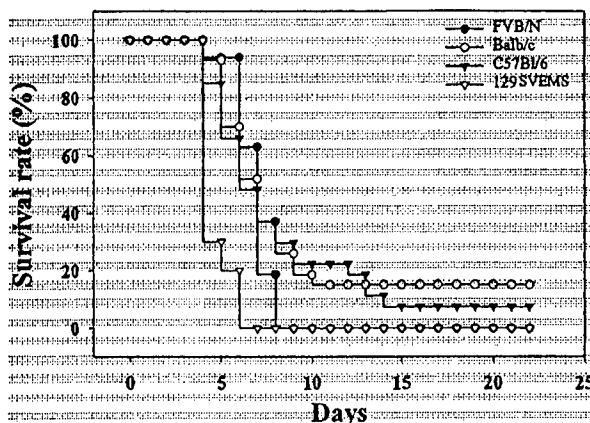


**Figure 1.** 129SVEMS and FVB/n mice show increased sensitivity to 3NPA compared to C57BL/6 and BALB/c mice in protocol 2 (75 mg/kg/day 3NPA). Modified Kaplan-Meier survival curve. Mice included in this study were observed every 15 minutes throughout a 12-hour period for consecutive days of 3NPA dosing as described in Materials and Methods. These mice were euthanized because of stage III neurological signs (mice with heart and brain lesions from Table 2) or if clinically moribund (mice with only heart lesions from Table 2) as described in Materials and Methods. Strain differences in lesions are presented in Table 2. Fifteen percent of BALB/c mice and 7.4% of C57BL/6 mice did not present clinical signs throughout the 22-day experiment demonstrating an intrastrain and interstrain variability in resistance to 3NPA.



time point that was used for mitochondrial biochemical analysis and whole heart adenosine triphosphate (ATP) evaluation. Ten mice per group were treated intraperitoneally with saline or 100 mg/kg of 3NPA given at 0 and 24 hours and sacrificed at 1 hour after the second injection. Mice were anesthetized with metaphane and perfused by intracardiac perfusion via the left ventricle. One percent paraformaldehyde in phosphate buffer was used to clear the blood from vessels followed by a 1% paraformaldehyde and 1.25% glutaraldehyde in phosphate buffer using a 20 ml/minute flow rate. The brain and hearts were removed and placed in the glutaraldehyde fixative overnight. Tissues were trimmed to a 1 to 2 mm<sup>3</sup>, postfixed in osmium, processed, and embedded in epoxy resin. Blocks were cut in 1- $\mu$ m sections, stained with toluidine blue, and screened by light microscopy. Thin sections were cut, stained with lead acetate and uranyl acetate, and representative samples were viewed with a Jeol electron microscope.

#### *Heart Mitochondrial Isolation*

Various biochemical parameters were compared in isolated mitochondria from saline- or 3NPA-treated (protocol 1) 129SVEMS and C57BL/6 mice. Mitochondria were isolated from mice (single hearts) using Nargarse digestion as described by Hansford and colleagues.<sup>20</sup> Mice were euthanized by cervical dislocation and decapitation. Hearts were quickly removed and washed free of blood in 0.25 mol/L sucrose, 10 mmol/L hepes and 1 mmol/L EGTA isolation buffer. Hearts were then cut into 1-mm<sup>3</sup> pieces and homogenized for 8 minutes (3 strokes/minute) in a glass-Teflon homogenizer with 10 ml of sucrose buffer and 0.7 mg Nargarse enzyme per heart. The homogenate was spun at 8500  $\times$  g for 8 minutes, the pellet was resuspended in 5 ml of isolation buffer, and rehomogenized (10 strokes total). The homogenate was spun at 500  $\times$  g for 12 minutes. The supernatant containing mitochondria was centrifuged at 9500  $\times$  g for 9 minutes to pellet mitochondria. The pellet was gently resuspended and spun at 8500  $\times$  g to pellet only unbroken mitochondria. The last pellet was resuspended in the above described sucrose/hepes buffer without the addition of EGTA. Mitochondrial proteins were measured using the method of Lowery and colleagues.<sup>21</sup>

#### *SDH Activity in Heart Mitochondria*

SDH activity was measured in isolated heart mitochondria from three to four mice per strain in the saline controls and the 3NPA-treated mice (protocol 1). Heart mitochondrial protein (100  $\mu$ g) was solubilized in a 0.01% Triton X solution in an incubation buffer of 0.05 mol/L potassium phosphate, 0.02 mol/L succinate, 50  $\mu$ mol/L 2,6-dichlorophenolindophenol, 2  $\mu$ g/ml antimycin A, rotenone 2  $\mu$ g/ml, 2 mmol/L KCN, and 50  $\mu$ mol/L decylubiquinone.<sup>22</sup> Briefly, SDH activity was measured by the rate of reduction of decylubiquinone using the substrate succinate by following the secondary reduction of the dye 2,6-dichlorophenolindophenol. The reaction was fol-

lowed spectrophotometrically by a decrease in absorbance at 600 nm for 3 minutes at 30°C.

#### *Oxygen Consumption*

Oxygen consumption rates in heart mitochondria (protocol 1) were measured at 28°C with a Clark-type O<sub>2</sub> electrode. Mitochondria (0.25 mg) were added to a 1-ml aliquot of respiration buffer containing 0.12 mol/L KCl, 20 mmol/L K Hepes, pH 7.4, 5 mmol/L K phosphate, 5 mmol/L succinate, and 1  $\mu$ mol/L rotenone. Respiration was measured without ADP (state IV) and after the addition of 0.5 mmol/L ADP (state III).<sup>22</sup>

#### *Cardiac ATP Analysis*

Using protocol 1, C57BL/6 and 129SVEMS mice, 3NPA ( $n = 6$  per strain) or saline ( $n = 3$ ) was administered at 0 and 24 hours. One hour after the second injection, mice were anesthetized with 0.5 mg/g of chloral hydrate and endotracheally intubated with a 22-gauge catheter (2N1116; Baxter, Deerfield, IL). Mice were ventilated using a Harvard apparatus rodent ventilator (no. 680) on room air with a respiratory rate 150/minute and tidal volume set at 0.125 ml.<sup>23</sup> The tidal volume was adjusted to ensure an arterial carbon dioxide tension within the physiological range. The thorax was opened and while the lungs were being ventilated, the hearts were freeze-clamped by a pre-cooled metal clamp that was immediately immersed into liquid nitrogen. The heart samples were ground to fine powder under liquid nitrogen and extracted and homogenized in ice cold 0.4 mol/L perchloric acid. The denatured protein was pelleted and reserved for protein analysis.<sup>21</sup> The acid extract was neutralized with equal volumes of 0.4 mol/L KHCO<sub>3</sub>. Each extract was subjected to nucleotide analysis using gradient ion-pair reversed-phase liquid chromatography.<sup>24</sup> HPLC separation was performed using an ESA (Chelmsford, MA) solvent delivery system with a 3- $\mu$ m symmetry C18 column (3.9  $\times$  150 mm inner diameter) from Waters Corporation (Milford, MA). Separation was performed by reverse-phase chromatography using an isocratic mobile phase consisting of buffer A (35 mmol/L KH<sub>2</sub>PO<sub>4</sub>, 6 mmol/L tetrabutylammonium hydrogensulfate, pH 6.0, 125 mmol/L ethylenediaminetetraacetic acid) and buffer B (a mixture of buffer A and HPLC-grade acetonitrile in a ratio of 1:1, v/v), filtered through a 0.2- $\mu$ m membrane filter and helium degassed. The flow rate was set at 1.0 ml/minute and detection was performed at 260 nm using an ESA variable wavelength UV/V is absorbance detector.

#### *Statistical Analysis*

Survival data from protocol 1 was compared by chi-square Fisher's exact analysis. SDH activity and ATP analysis were analyzed by analysis of variance followed by Bonferroni's post hoc test. Heart lesion severity scores (cellular swelling, necrosis, hemorrhage, and mineralization) were analyzed by the Kruskal-Wallis rank test. A  $P$  value  $<0.05$  was considered statistically significant. All data are presented as mean  $\pm$  SEM.

## Results

### *3NPA-Induced Mortality Is Mouse Strain- and Dose-Dependent*

In 3NPA protocol 1 (100 mg/kg, two doses at 0 and 24 hours) C57BL/6 mice and BALB/c mice had significantly better survival at 48 hours compared to the FVB/n mice and 129SVEMS mice (Table 1). Frequent monitoring of mice was performed (every 15 minutes) throughout a 12-hour period. Mice were euthanized when first observed in the recumbent hypothermic condition (more prevalent in FVB/n and 129SVEMS mice) because it was found that disease progression occurs rapidly in these strains and mice in this state die suddenly.

When comparing mouse strains to each other, neurological signs were inconsistently seen between strains in mice treated with this 3NPA treatment paradigm adapted from the original 3NPA mouse study.<sup>7</sup> In the original pilot study ( $n = 4$  to 6 mice) presented in Table 1, none of the mice presented neurological signs up to 48 hours after the initial injection. The majority of FVB/n and 129SVEMS mice became acutely moribund after the second injection. These mice either died during the observation period or were euthanized based on clinical signs. In later studies using the protocol 1 dosing paradigm, 40% of the C57BL/6 mice progressed to stage II (ataxia and tremors) 1 hour after the second injection, while 129SVEMS mice would infrequently show neurological signs because of a moribund condition (recumbency, nonambulatory state).

Because our initial goal was to study 3NPA-induced neurodegeneration between strains of mice, we reasoned that the cause of death, which prevented the development of overt neurotoxicity, may be avoided if we lowered the 3NPA dose. In a second study (protocol 2), a lower daily dose of 3NPA was used (75 mg/kg) for consecutive days until specific neurological signs (ataxia and tremors initially with progression to hindlimb extension) were observed. More reproducible neurological signs were observed with this protocol and neurodegeneration was found to accompany and precede mortality in all mouse strains tested. When comparing the four strains of mice, signs of toxicity were evident in mice as early as day 5 to day 14 with daily exposure to 75 mg/kg. In contrast, in the 100 mg/kg (2 doses, 24 hours apart) study, signs of toxicity occur 1 hour after the second dose especially in the 129SVEMS and FVB/n mice.

Survival curves for protocol 2 (Figure 1) illustrate the time course variability between the mouse strains in survival after 3NPA treatment. By day 9, 100% of the 129SVEMS and FVB/n mice had died or were euthanized. In contrast, 30% of the C57BL/6 mice and 26% of the BALB/c mice remained without exhibiting any clinical signs in the 3NPA treatment group. Between days 15 to 22, no additional mice in the remaining strains (C57BL/6 and BALB/c) showed clinical signs. On day 22 of dosing, the saline-treated and 3NPA-treated mice that had not presented clinical signs were euthanized and histologically analyzed. Fifteen percent of BALB/c mice and 7.4% of C57BL/6 mice (presented in Figure 1) did not present

clinical signs throughout the 22-day experiment demonstrating an intrastrain and interstrain variability in resistance to 3NPA. In contrast, all of the 129SVEMS and FVB/n mice treated in this protocol with 3NPA either showed clinical signs and were euthanized or died suddenly by day 9 of 3NPA treatment, demonstrating a lack of resistance in these strains to 3NPA.

### *3NPA Causes Strain- and Dose-Dependent Caudate Putamen and Cardiac Toxicity*

A histological survey from protocol 1 revealed toxicity in the heart, a finding that had not been previously reported in any species. One hundred percent of the mice that died or were euthanized within the first 48 hours of the first dose (Table 1) had only acute cardiac injury (see Figure 3B). There was no evidence of histological injury in saline-treated controls.

In attempts to avoid the acute mortality and predominant cardiac toxicity seen in protocol 1, the 3NPA daily dose was decreased to 75 mg/kg for another series of studies (protocol 2). A histological survey of multiple organs was performed to correlate with clinical signs and the cause of death in 3NPA-treated mice. With this protocol, a much higher incidence in caudate putamen infarction was observed, although cardiac injury was still a confounding problem and was present in 100% of the mice tested. 3NPA treatment either induced heart lesions alone (myocardial cellular swelling and necrosis with frequent atrial thrombosis) (Figure 2) (23 of 49 mice) or in combination with caudate putamen infarction (26 of 49 mice). There were no examples of mice with only caudate putamen infarction. Table 2 summarizes the incidence and tissues injured in mice treated with 3NPA from the four mouse strains tested in the protocol 2.

### *3NPA-Induced Caudate Putamen Pathology*

One hundred percent of the mice exhibiting hindlimb extension (euthanized in stage III) had severe damage in the caudate putamen including widespread cellular swelling, necrosis, edema, and mild to moderate hemorrhage (infarction) (Figure 2F). Occasional small vessel microthrombi were found in the caudate putamen in areas adjacent to infarcts. Saline-treated mice showed no morphological injury in the caudate putamen (Figure 2E). Infarcts were bilateral in the majority of mice. The infarcts were centered on the dorsal-lateral caudate putamen. In some mice, that showed transient inconsistent neurological signs, removed from the study and examined 7 days later, the caudate putamen also showed evidence of chronic injury with white matter bundles positioned in close proximity to each other because of substantial neuronal loss (Figure 2G). Ten percent of the treated mice (FVB/n and 129SVEMS) were observed to have seizures that were associated with unilateral infarcts that extended into the globus pallidus, thalamus, hippocampus, cingulate and motor cortex, as well as caudate putamen.

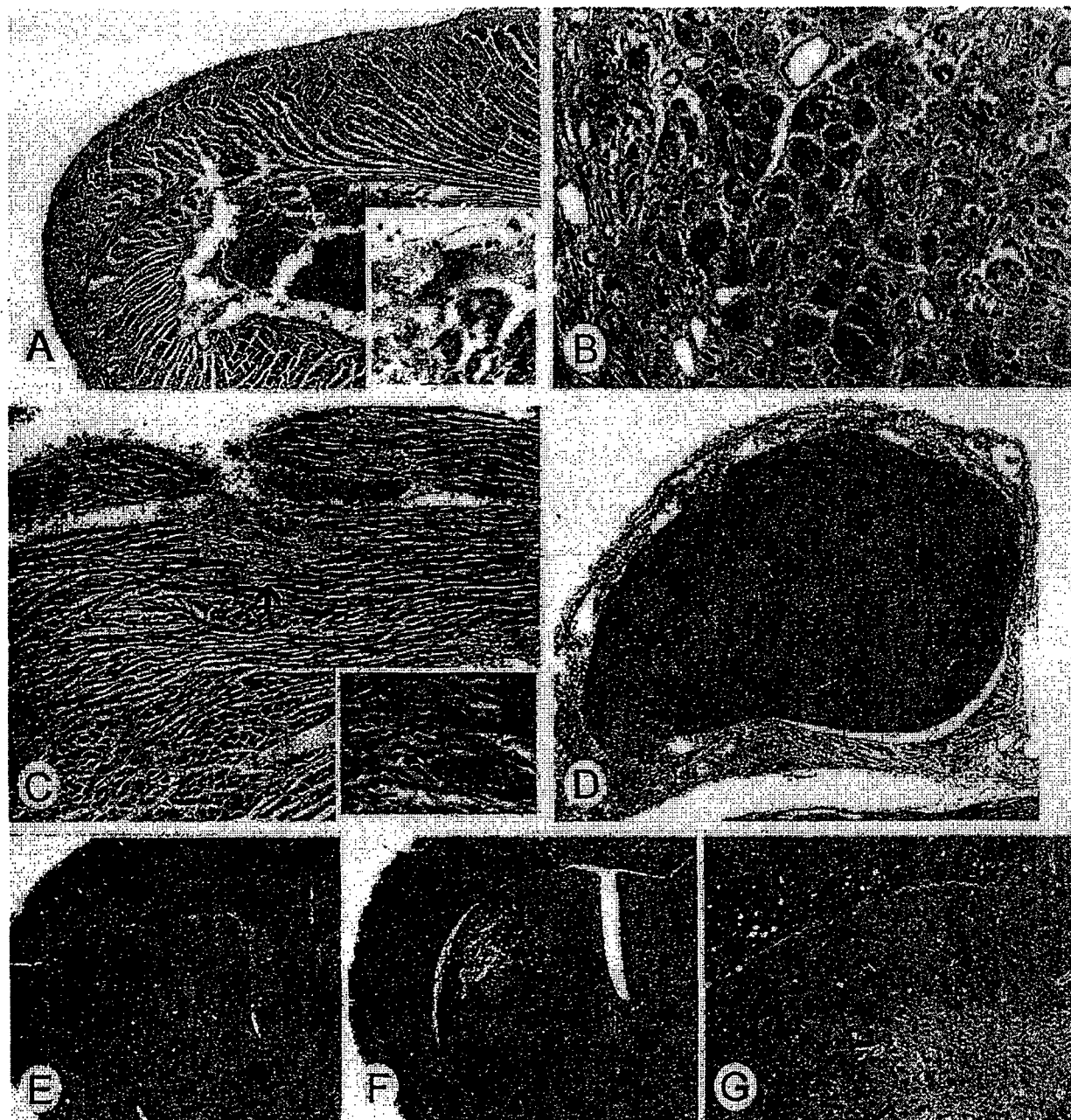


**Figure 2.** 3NPA treatment induces cardiac and caudate putamen injury in mice. **A** to **D** are representative light micrographs of 3NPA-induced lesions in the heart (H&E stain). **A:** Left ventricle showing a band of marked epicardial pallor (original magnification,  $\times 24$ ). The *inset* represents an area of transition between the epicardial swollen (pale) myocytes and the deeper (darker) myocytes (original magnification,  $\times 100$ ). **B:** An area of cardiac myocyte loss, interstitial fibrosis, and mineralization present in a subacute-treated mouse is shown (original magnification,  $\times 100$ ). **C:** Several foci of inflammatory mononuclear cell infiltrates (*arrow*) are noted (original magnification,  $\times 30$ ). Myocyte necrosis and cellular infiltrate are shown (*inset*; original magnification,  $\times 80$ ). **D:** Organizing thrombus filling the atrial cavity (original magnification,  $\times 24$ ). **E** to **G** are representative light micrographs of the caudate putamen (H&E stain). **E:** Normal caudate putamen from saline-treated mouse (original magnification,  $\times 10$ ). **F:** Caudate putamen from 3NPA-treated mouse with infarct (note area of pallor) in the dorsal lateral aspect (original magnification,  $\times 10$ ). **G:** Caudate putamen from 3NPA-treated mouse with cellular loss, glial proliferation, and hemosiderin-laden mononuclear cells. Note the white matter tracts are positioned closer together (resolving infarct) (original magnification,  $\times 60$ ).

### 3NPA Acute Toxicity Induces Cardiomyocyte Cellular Swelling and Necrosis

In protocol 1, two morphological patterns were observed in cardiomyocytes, frequently seen in adjacent cells (cellular swelling and necrosis). Cardiomyocytes exhibited multifocal to diffuse cellular swelling, characterized by increased pallor (Figure 2A and Figure 3D) and promi-

nent eosinophilic granulation (swollen mitochondria) and occasional microvacuolation. Swollen mitochondria are easily seen on the toluidine blue sections (Figure 3B). Multifocal coagulative necrosis of cardiomyocytes was characterized by cardiomyocytes with homogeneous intensively eosinophilic cytoplasm (hematoxylin and eosin), loss of striations, and irregular contraction bands (Figure 3C, toluidine blue).

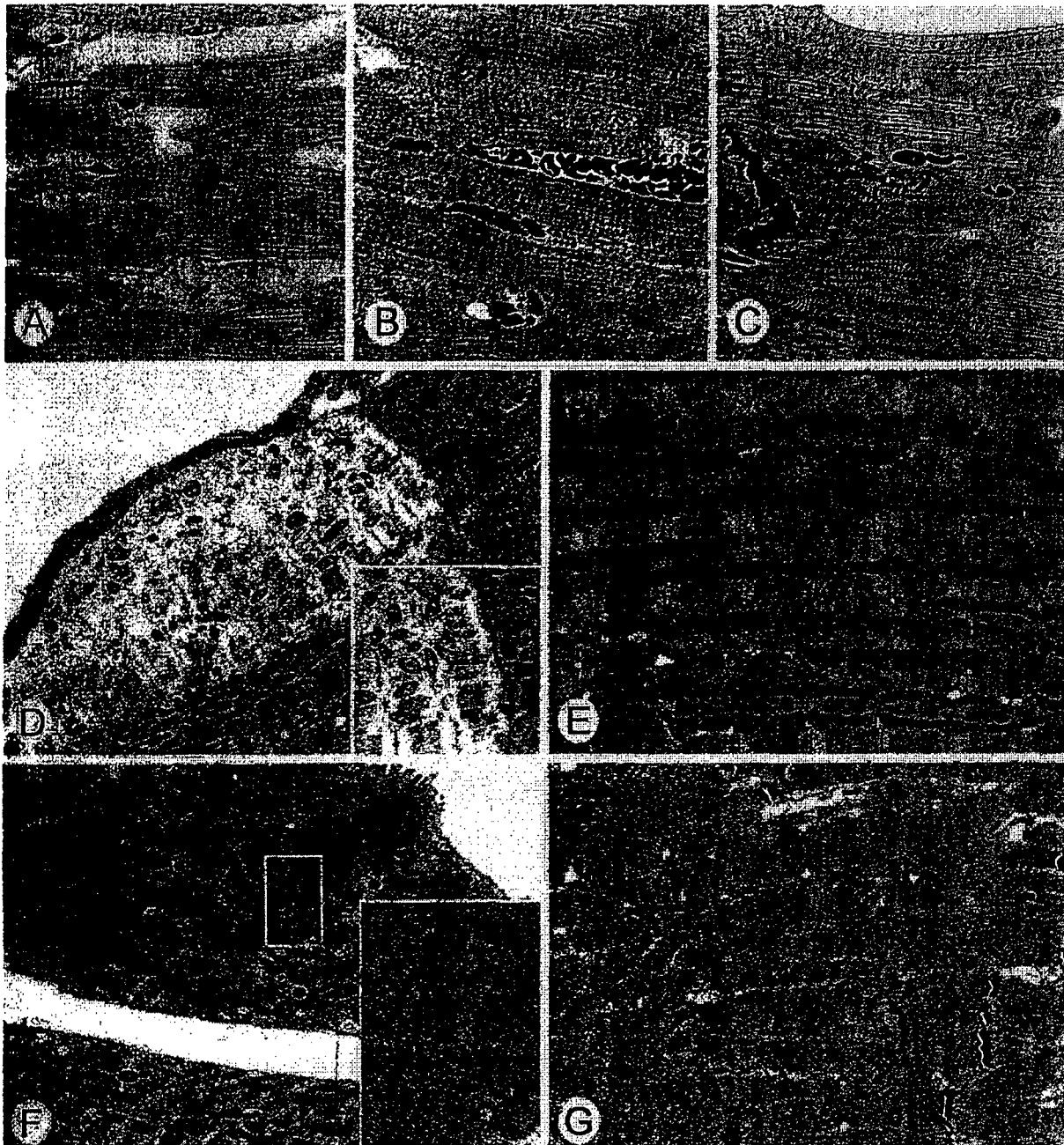


**Figure 3.** 3NPA treatment induces cardiac injury in mice. **A to C** are representative light micrographs of toluidine blue-stained 1- $\mu$ m-thick plastic-embedded sections of mouse hearts (original magnification,  $\times 600$ ). **A:** Normal heart saline-treated mouse. **B:** Myocardial cellular swelling, mitochondrial enlargement, and focal hemorrhage. **C:** Myocardial contraction band necrosis. **D to G** are representative examples of electron micrographs from mouse hearts. **D:** Epicardial myocyte showing myofilament disruption and swollen mitochondria adjacent to less affected cell (original magnification,  $\times 3000$ ). The **inset** shows a comparison of the pale myocyte to an adjacent myocyte separated by an intercalated disk (original magnification,  $\times 5000$ ). Note the dark electron-dense mitochondria with abnormal morphology within the affected myocyte. **E:** Normal control myocyte (original magnification,  $\times 6000$ ). **F:** Myocyte showing contraction band necrosis and swollen mitochondria (original magnification,  $\times 4000$ ). The **inset** shows the aggregated disrupted myofilament (original magnification,  $\times 12,000$ ). **G:** Swollen mitochondria are present in this cardiac myocyte. These mitochondria are larger than control, but they do not show the abnormal morphology and electron density noted in the myocytes with myofilament disruption shown in **D**. Note the good preservation of the sarcomeres.

In the protocol 2, in addition to cellular swelling and necrosis, bilateral atrial thrombosis (Figure 2D), cardiomyocyte mineralization, cellular loss, and fibrosis (Figure 2B) were present. Neutrophils were associated with the superficial atrial endocardium and endothelium attached to atrial thrombi. With the exception of thrombi, inflamma-

tory cells were rarely seen in acute toxicity associated with cellular swelling and myocardial necrosis.

In the several mice that showed transient inconsistent neurological signs and were removed from the study, and examined 7 days after the last 3NPA injection, cardiac macrophage and fibroblastic remodeling after necrosis

**Table 3.** Incidence and Severity of Cardiac Myocyte Cellular Swelling and Necrosis in the Most Sensitive (129SVEMS) and Least Sensitive (C57BL/6) Strain

Strain/treatment group	Number of mice	Cellular swelling scores					Necrosis scores				
		0	1	2	3	4	0	1	2	3	4
129 mice/3NPA	7	0	0	0	0	7*	0	0	0	1	6*
129 mice/saline	6	6	0	0	0	0	6	0	0	0	0
C57 mice/3NPA	7	0	3	2	2	0	2	2	2	1	0
C57 mice/saline	6	6	0	0	0	0	6	0	0	0	0

129SVEMS and C57BL/6 mice were treated with 3NPA (100 mg/kg, 2 doses 0 and 24 hours), sacrificed 1 hour after the 2nd dose, and lesions were scored and analyzed.

\*Lesion scores significantly more severe than controls ( $P < 0.05$  by Kruskal-Wallis rank test).

was evident (Figure 2C). In two C57BL/6 mice that survived to day 22 in protocol 2, without neurological signs, mild to moderate multifocal cardiomyocyte cellular loss and fibrosis was observed but no caudate putamen pathology was found in these mice.

#### *129SVEMS Mice Are More Vulnerable to 3NPA Cardiac Toxicity Compared to C57BL/6 Mice*

Because C57BL/6 and 129SVEMS mice show the extremes of interstrain variability to 3NPA-induced mortality in various dosing protocols, we hypothesized that 129SVEMS mice would have more significant cardiac injury compared to the more resistant C57BL/6 mice when compared at the same time point using protocol 1. Four morphological components were recognized and separately scored (Tables 3 and 4) by a semiquantitative method described in Materials and Methods. The incidence and severity of lesions was greater in the 129SVEMS mice compared to the C57BL/6 mice. Only 3NPA-treated 129SVEMS mice lesions scores were significantly ( $P < 0.001$ ) more severe than those of control mice compared to C57BL/6 mice.

#### *Electron Microscopy Shows that Mitochondria in Brain and Heart Are Major Targets for 3NPA Toxicity*

Ultrastructural evaluation of the heart revealed 129SVEMS mice had more severe damage compared to the C57BL/6 mice. 129SVEMS mice showed extensive diffuse myocardial cellular swelling compared to mild, multifocal areas myocardial swelling in the hearts of C57BL/6 mice. Acute ultrastructural changes included cellular swelling, disrupted myofilaments and markedly swollen mitochondria.

Mitochondrial swelling may have occurred early in the progression of pathology, as it was found alone in many cardiomyocytes without cardiomyocyte myofilament disruption (Figure 3, B and G). Mitochondrial swelling always accompanied cellular swelling and disruption of myofilaments (Figure 3F).

Ultrastructural assessment of heart and brain revealed a temporal relationship between the injury in the two organs. Heart ultrastructural lesions appeared before caudate putamen infarction. Some mice had severe heart damage and no or mild caudate putamen injury. In the 129SVEMS mice, in cases in which the heart damage was extensive, caudate putamen neurons were affected as described below (Figure 4, A and B).

Caudate putamen from 3NPA-treated mice had a distinctive ultrastructural pathology at a timepoint that preceded infarction. Damage was more prominent in 129SVEMS mice compared to C57BL/6 mice. The major ultrastructural abnormalities occurred in neurons and could be classified as cell body or axonal degeneration. The pathology in neuronal cell bodies predominated in the dorsolateral caudate putamen. The neurons were angular rather than round, suggesting shrinkage (Figure 4, A and B). These degenerating neurons had a very dark and granular cytoplasmic matrix because of fine particles, possibly free ribosomes, within the cytoplasm. Cytoplasmic vacuoles were present. Most of the vacuoles were derived from swollen mitochondria, because remnants of cristae were present within the vacuole. Other mitochondria in surrounding neuropil structures appeared normal. The Golgi apparatus was also swollen in these neurons. These abnormal neuronal cell bodies typically had a nucleus with a dark nucleoplasmic matrix with nascent chromatin condensation along the nuclear envelope. Many dark neurons were surrounded partially by swollen astroglial processes characterized by a pale

**Table 4.** Incidence and Severity of Myocardial Hemorrhage and Mineralization in the Most Sensitive (129SVEMS) and Least Sensitive (C57BL/6) Strain

Strain/treatment group	Number of mice	Hemorrhage scores					Mineralization scores				
		0	1	2	3	4	0	1	2	3	4
129 mice/3NPA	7	3	1	2	1	0	5	2	0	0	0
129 mice/saline	6	6	0	0	0	0	6	0	0	0	0
C57 mice/3NPA	7	6	0	1	0	0	7	0	0	0	0
C57 mice/saline	6	6	0	0	0	0	6	0	0	0	0

129SVEMS and C57BL/6 mice were treated with 3NPA (100 mg/kg, 2 doses 0 and 24 hours), sacrificed 1 hour after the 2nd dose, and lesions were scored and analyzed.



**Figure 4.** 3NPA treatment induces neuronal degeneration in 129SVEMS mice. **A** and **B** are electron micrographs from the caudate putamen of a 129SVEMS mouse with severe myocardial injury. **A:** A dark shrunken degenerating caudate putamen neuron (small arrowhead) adjacent to a normal neuron (large arrowhead). Adjacent normal myelinated axons are at the bottom right of the micrograph (original magnification,  $\times 4000$ ). **B:** Dark shrunken neuron (original magnification,  $\times 10,000$ ) with swollen mitochondria (small box) (original magnification,  $\times 11,000$ ) and adjacent to a swollen astroglial process (large box) (original magnification,  $\times 17,000$ ). This cell can be identified as a neuron because of the axosomatic synaptic junction (inset, top left, arrowhead).

cytoplasmic matrix, few organelles, and membranous cisterns. In the caudate putamen of C57BL/6 mice, axonal pathology was found in white matter bundles. Individual myelinated axons, found among normal axons, were prominently dark. These abnormal axons had a normal caliber and normal myelin sheath and were not dystrophic but contained neurofilament accumulations.

### *3NPA Induces a Reduction in Heart Mitochondrial SDH Activity and Oxygen Consumption Rates*

Because extensive ultrastructural mitochondrial swelling was observed in the heart, a variety of mitochondrial metabolic endpoints were examined at the time point used in the ultrastructural studies to verify the metabolic significance of the mitochondrial swelling. SDH activity was measured in isolated heart mitochondria from saline- and 3NPA-treated 129SVEMS and C57BL/6 mice in protocol 1. Compared to the controls, 3NPA-treated 129SVEMS mice had a significant decrease in SDH ac-

tivity compared to the 3NPA-treated C57BL/6 mice (Figure 5A). Control 129SVEMS mice SDH activity was significantly higher compared to the control C57BL/6 mice. Oxygen consumption rates using succinate as a substrate (SDH substrate) were also higher in the 129SVEMS mouse controls compared to the C57BL/6 mice (Figure 5B). This is consistent with the finding that the control 129SVEMS mice have a higher SDH activity. SDH enzyme activity and oxygen consumption rates were significantly reduced in both C57BL/6 and 129SVEMS mice after two doses of 100 mg/kg 3NPA compared to the controls. Oxygen consumption rates were significantly lower in the 129SVEMS mice compared to the C57BL/6 mice after only one dose of 3NPA suggesting an increased metabolic vulnerability in the 129SVEMS strain at this earlier time point.

### *3NPA Induces a Significant Reduction of Cardiac ATP in 129SVEMS Mice*

Other metabolic indices were analyzed to better understand mechanisms underlying interstrain mortality and morphological differences. We hypothesized that heart ATP values could predict the more susceptible strain. Because there was no current example in the literature for freeze-clamping the mouse heart from an *in vivo* preparation to analyze ATP, we used a method developed for rats. Intubated and room air-ventilated rats have been used to assess whole heart ATP levels.<sup>25</sup> We used this method, because mice that were not intubated in our pilot studies had low ATP values in all treatment groups. Figure 5C summarizes the mean ATP values from 3NPA-treated mice in protocol 1. Compared to 129SVEMS controls, only 3NPA-treated 129SVEMS mice had significantly lower ATP values. 3NPA-treated C57BL/6 mice did show the trend for ATP reduction, although it did not reach a 0.05 level of significance.

### *Discussion*

Genetic differences between mouse strains can modulate responses to various perfusion insults or toxins.<sup>15,26–29</sup> We have determined that mouse strain differences can also modulate the response to 3NPA toxicity based on mortality, pathology, and biochemical analysis. 129SVEMS and FVB/n mice are more susceptible to 3NPA compared to the C57BL/6 and BALB/c mice in acute and subacute/chronic exposures. This pattern of vulnerability among strains is the same pattern found in kainic acid toxicity.<sup>15</sup> However, unlike the kainic acid study, the finding of cardiac toxicity with 3NPA most likely influences the pattern of mortality seen between strains.

We used a mouse 3NPA-dosing protocol adapted from that of Gould and Gustine<sup>7</sup> from the original 3NPA Swiss Webster mouse study. We modified their protocol by lowering the 3NPA dose from 120 mg/kg to 100 mg/kg and used only two doses given 24 hours apart. For our protocol, as in the Gould and Gustine protocol, we also did not neutralize 3NPA solutions before injection. The



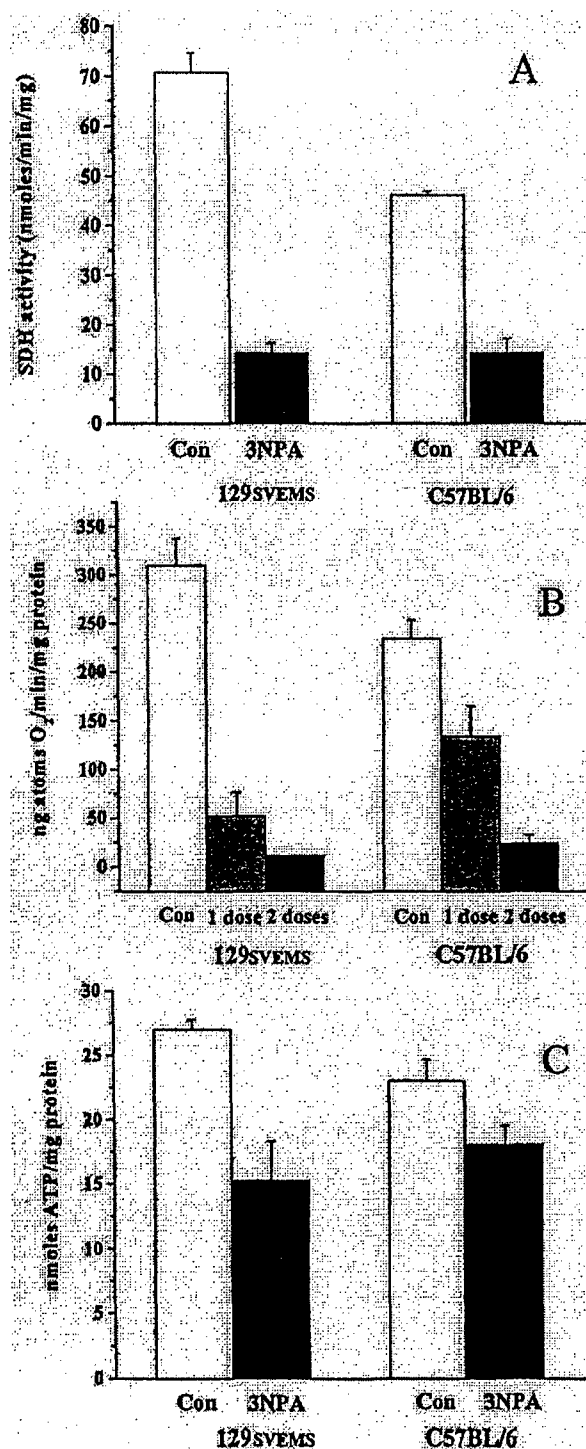


**Figure 5.** 3NPA induces a reduction in heart mitochondrial SDH activity, oxygen consumption, and heart ATP in mice. 129SVEMS and C57BL/6 mice were treated with 3NPA (protocol 1) and heart mitochondria were isolated and analyzed for SDH activity and succinate oxygen consumption rates. 129SVEMS and C57BL/6 mice were treated with 3NPA (protocol 1) and heart ATP was extracted and analyzed by HPLC. **A:** Significant differences were found in SDH activity, control 129SVEMS versus 129SVEMS 3NPA-treated ( $P < 0.001$ ), control C57BL/6 versus C57BL/6 3NPA-treated ( $P < 0.001$ ), control 129SVEMS versus control C57BL/6 ( $P < 0.001$ ). **B:** Significant differences were found in oxygen consumption, control 129SVEMS versus 129SVEMS 3NPA one dose, and two doses ( $P < 0.001$ ), control C57BL/6 versus C57BL/6 3NPA one dose, and two doses ( $P < 0.001$ ). **C:** Significant difference was found in heart ATP, control 129SVEMS versus 129SVEMS 3NPA two doses ( $P < 0.05$ ).

acute 3NPA dose for the mouse is higher than the acute 3NPA dose for the rat (30 mg/kg for two or three injections on consecutive days until neurological signs appear). The mechanisms for the marked differences in species (rat versus mouse) in 3NPA dose exposure required for toxicity are not known. The existence of a 3NPA transporter protein with differential expression between species, between mouse strains and tissues could explain the differences observed in 3NPA toxicokinetics. Additionally, differences in mitochondrial respiration/metabolism and in the requirement for ATP varies between species and possibly between strains, as it does between tissues and this may have an effect on the species differences seen after 3NPA exposure. In terms of potential cardiac toxicity, the heart rate is 600 to 700 beats/minute in the mouse and 300 beats/minute in the rat, thus the mouse may be more susceptible to reductions in cardiac high energy phosphates induced by 3NPA. In humans poisoned by 3NPA, there is a marked interindividual variability in the final neuropathological outcome ranging from diffuse cerebral edema to focal striatal damage.<sup>2,30-33</sup> This marked interindividual variability in humans reflects that seen in other species and is likely related to differences in 3NPA exposure, toxicokinetics, genetic variability, and pre-existing disease.

We found that the mouse strain susceptibility, based on mortality and pathology, is likely driven by 3NPA cardiotoxicity in these four commonly used mouse strains. All mouse strains are sensitive to 3NPA, although the cumulative dose needed to cause cardiac toxicity varies between strains. The ultrastructural changes, including mitochondrial swelling, cellular edema, and myofilament disruption, are more severe in the hearts of the highly sensitive 129SVEMS mice compared to C57BL/6 mice, suggesting the increased cardiac damage may be associated with the increased mortality of this strain. The light microscopic findings of cardiomyocyte cellular swelling, contraction band necrosis, mineralization, and atrial thrombosis are consistent with significant pathological abnormalities seen in other examples of cardiac toxicities.<sup>19,34-41</sup> The cardiac toxin doxorubicin also induces atrial thrombosis in mice.<sup>42</sup> The formation of atrial thrombi in doxorubicin-induced cardiomyopathy is thought to be associated with decreased cardiac contractility, effecting blood flow dynamics and toxic injury to the atrial cardiomyocytes and endothelial surfaces. These mechanisms of injury are likely involved in 3NPA cardiac toxicity.

We found that the mouse strain susceptibility, based on mitochondrial biochemical studies, is likely driven by 3NPA cardiotoxicity when comparing two mouse strains with differential sensitivity. 129SVEMS mice are metabolically more impaired at an earlier time point compared to C57BL/6 mice. The analysis of multiple mitochondrial biochemical endpoints of toxicity at the time point used in the ultrastructural studies revealed significant differences between the strains supporting vulnerability. SDH enzyme activity is significantly reduced in both strains after 3NPA treatment, although 129SVEMS mice have a greater percent reduction compared to controls. Notably, the SDH activity is constitutively higher in this strain that correlates with the higher oxygen consumption rates ob-

served in 129SVEMS mice oxidizing succinate (the substrate for SDH). These data suggest that the 129SVEMS mouse strain may rely more on cardiac SDH activity. 3NPA-treated 129SVEMS mice oxidizing succinate have a significant reduction in oxygen consumption after one dose of 3NPA compared to C57BL/6 mice. In addition, heart ATP levels are significantly reduced in 129SVEMS mice treated with 3NPA compared to controls. These findings correlate well with the 129SVEMS mice strain being more susceptible to 3NPA, although ATP reduction is probably not the only factor involved in this strain's increased sensitivity to 3NPA compared to C57BL/6 mice.

Mitochondrial toxicity is key to 3NPA neurotoxicity<sup>8,43-54</sup> and seems critical in 3NPA cardiac toxicity. 3NPA induces only mitochondrial swelling in some cardiomyocytes. In more severely damaged cells, in addition to mitochondrial swelling, there is also severe disruption in myofilaments. This suggests that 3NPA-induced toxicity in the cardiomyocyte first involves damage to mitochondria, as an early event in toxicity. Further damage to other organelles in this model, may be a sequelae of mitochondrial dysfunction.

There have been no previously published studies evaluating 3NPA *in vivo* cardiac toxicity; yet, 3NPA has been studied in various *in vitro* cardiac systems. 3NPA is a competitive inhibitor of succinoferricyanide oxidoreductase (another name for SDH) activity of Keilin-Hartree mitochondrial particles from rat heart.<sup>55</sup> 3NPA is slowly oxidized by SDH and its oxidation product instantaneously and irreversibly inhibits cardiac SDH.<sup>7,9</sup> Isolated rat atria incubated with 3NPA ( $10^{-4}$  mol/L) in an organ bath for 15 minutes produced bradycardia and significant ATP depletion compared to controls.<sup>56</sup> This finding is consistent with our *in vivo* experiments showing that mice treated with 3NPA have a significant cardiac ATP depletion (129SVEMS mice). Isolated control heart mitochondria exposed to 3NPA  $10^{-2}$  mol/L for a 30-minute incubation produced significant reduction of  $O_2$  consumption in the presence of the substrates malate/glutamate or succinate.<sup>56</sup> This *in vitro* finding also parallels our experiments showing *in vivo* 3NPA treatment reduces oxygen consumption rates in heart mitochondria isolated from treated mice.

Indirect physiological evidence of 3NPA cardiac toxicity has been reported such as models showing bradycardia and a reduction in contractile force in the guinea pig atria,<sup>57</sup> vasodilation in rabbit aortic rings, and hypotension and bradycardia in dogs.<sup>58</sup> Consequently, in light of our more direct evidence of 3NPA inducing cardiac damage, there is substantial evidence that 3NPA cardiac toxicity has the potential to be responsible for cardiac dysfunction and death in animals exposed to this toxin. It is not known if sudden death in mice and rats treated with 3NPA in acute and chronic models (with and without neurological signs) reported by others investigators were because of 3NPA-induced cardiac toxicity<sup>7,11,13,14,51,59,60</sup>. In our protocol, comparable to Gould and Gustine's<sup>7</sup> acute protocol, ultrastructural evidence of cardiac injury is observed at the time point when 129SVEMS mice begin to die acutely, before any significant caudate putamen damage is observed. Caudate putamen infarction never

occurred in our studies (acute and subacute/chronic) in the absence of cardiac toxicity. Any potential relationship between the two lesions needs to be addressed in future studies. The data from our studies show that cardiac toxicity is found in all cases of acute and subacute/chronic 3NPA toxicity in the mouse. The influence of cardiac toxicity (inducing decreased cardiac output) on the development of neurological lesions in the mouse is not known. The incidence of cardiac toxicity in acute and chronic models of 3NPA toxicity in the rat is unknown. Gould and Gustine<sup>7</sup> suggested in the original mouse study, that because 3NPA induced a dramatic decrease in cardiac SDH activity, 3NPA-induced cardiac injury, if severe enough, may decrease cardiac output and cause subsequent caudate putamen ischemic hypoxia-induced striatal damage. Gould and Gustine reported that SDH activity in the mouse heart was reduced to 13% of the controls whereas brain SDH activity was reduced to 20% of the controls. Cardiac pathological lesions were not reported in this study, although it was not clear at what time point heart samples were collected and examined, possibly only after one dose.<sup>7</sup> It should also be noted that the sites of lesions found in the Gould and Gustine<sup>7</sup> 3NPA mouse study, as they point out, are similar to those found as a result of hypoxia.<sup>61</sup> In one of the first studies using 3NPA in rats, Hamilton and Gould<sup>50</sup> observed that the neuronal damage produced by systemic 3NPA histologically resembled that produced either by kainic acid, hypoglycemia, or ischemia. Interestingly, a recent model of global brain ischemia in rats produces cell loss in the striatum that resembles that seen in Huntington's disease.<sup>62</sup>

In general, the striatum is exquisitely sensitive to ischemia and hypoxia.<sup>62-69</sup> The proposed reasons for this increased sensitivity of the striatum to hypoxia and ischemia are: 1) glutamatergic excitotoxicity via NMDA receptor has been attributed to the neuronal cell death and oxidative stress in this area<sup>70,71</sup>; 2) the architecture of the blood supply to the striatum is predominantly end-arterial with few collateral vessels, so this region is susceptible to changes in nutrient perfusion and oxygen delivery<sup>72,73</sup>; 3) the unique connectivity and the level of oxidative metabolism of the striatum<sup>74</sup>; and 4) the striatum is a region in the brain where massive glutamatergic inputs and dopaminergic inputs converge. Dopamine and glutamate are important neurotransmitters in the brain, but when concomitantly over released, each acts as a potent neurotoxin.<sup>75</sup> In fact, the mechanisms attributed to the striatum's generalized vulnerability to ischemia and hypoxia are consistent with those mechanisms found responsible in the pathogenesis of 3NPA striatal neurotoxicity.

Global brain ischemia/hypoxia with striatal damage<sup>76</sup> and increased blood brain barrier permeability<sup>77</sup> can be induced by heart failure. Oxidative stress is a potential outcome of brain hypoperfusion.<sup>78-80</sup> Interestingly, increased protein carbonyls groups indicative of oxidative stress are demonstrated in the cortex and the striatum of 3NPA-treated rats<sup>81</sup> suggesting a more global brain 3NPA effect. Thus, 3NPA intrinsic striatal neurotoxicity needs to be addressed in future studies in the absence of 3NPA cardiac toxicity to rule out the potential influence of cardiac dysfunction and any subsequent possible striatal



hypoperfusion (ischemia/hypoxia) that may occur in the 3NPA neurotoxicity mouse model. It is not known if 3NPA cardiac toxicity-induced deaths observed in mice in a chronic model of 3NPA toxicity developed by Ouay and colleagues,<sup>14</sup> although we observed chronic cardiac injury in mice exposed to 3NPA daily for 21 days.

3NPA may have an intrinsic toxic effect (direct or indirect) on the striatum through its effects on the function of the lateral striatal artery. The potential for a focal disruption of blood flow dynamics involving the lateral striatal artery should be considered. The blood brain barrier of the lateral striatal artery and its tributaries is disrupted in 3NPA toxicity models<sup>44,73</sup> as well as in cardiac arrest/resuscitation models<sup>77</sup> demonstrating the increased sensitivity of this artery to conditions of cardiac dysfunction induced hypoxia/ischemia and 3NPA metabolic inhibition. The mechanisms involved in this blood brain barrier disruption are unknown. Additionally, intermittent cortical vasospasms have been observed after cardiac arrest and global brain ischemia<sup>82,83</sup> and the potential of striatal vasospasms was not evaluated in these studies. 3NPA produces bradycardia and systemic hypotension and vasodilation,<sup>57,84</sup> although regional striatal blood flow dynamics have not been studied. It would be important to evaluate striatal blood flow in 3NPA toxicity, especially in light of cardiac dysfunction, to possibly shed light on the heightened vulnerability of the lateral striatal artery and the striatum.

The finding of strain dependency in 3NPA-induced toxicity is significant because the mouse strains tested in this study are commonly used as background strains for transgenic and knockout mice. For the construction of knockout mice, 129SVEMS mice are most commonly used as the source of the embryonic stem cells. After successful gene targeting, embryonic stem cells are routinely implanted in the blastocysts of C57BL/6 mice.<sup>85</sup> FVB/n mice are also used for the construction of transgenic mice because they have large ova that are easily microinjected with DNA. BALB/c mice are also used as a background strain for nude mice. Differences in the mouse strain genetic background, especially if more than a single parent strain is included, can greatly influence the expression of transgenes and phenotype of knockout mice. Thus, a better understanding of mouse genetics and phenotypes will improve our design and interpretation of studies using genetically engineered mice.

This 3NPA model of cardiac toxicity could be a valuable tool for understanding many issues in cardiac pathophysiology including the mitochondria's role in cardiac cell death (apoptosis and necrosis), oxidative stress, and chemical preconditioning. 3NPA is known for its profound preconditioning effects at low doses (1/25 of the LD-50 dose, ie, gerbils) to protect against subsequent brain ischemia in various rodent models.<sup>86-90</sup> Recently it was found that low doses of 3NPA (1 mg/kg) induces preconditioning and protection in the heart when given before ischemia/reperfusion in rabbits.<sup>91</sup> The stress signals (ie, ATP depletion and reactive oxygen species production) that are induced in 3NPA toxicity may likely be the same signals that induce the preconditioning effect. Thus at high doses, 3NPA is toxic to the brain and heart and at

low doses, 3NPA may be beneficial to the brain and heart. The plant *Astragalus* called "Huang-Qi" in Chinese herbal medicine, known for containing 3NPA, has been used for centuries to precondition the heart. It is not known if the 3NPA in *Astragalus* is inducing this cardiac protective effect.

Remarkably, there are few models of chemical cardiac toxicity. Of those that are well studied, mitochondrial toxicity seems to be of great importance in the heart. Fluoroacetate (1080), a rodenticide and an inhibitor of mitochondrial citric acid cycle enzymes aconitase and SDH, similar to 3NPA, induces damage in the heart and the brain depending on the species studied.<sup>37,92,93</sup> A second cardiac toxin, Doxorubicin (adriamycin) has been shown to redox cycle at complex I producing mitochondrial superoxide, which subsequently damages various complexes of the electron transport chain.<sup>94,95</sup> Thus for its effects on the heart, 3NPA may be another useful compound to study cardiac mitochondrial toxicity and preconditioning.

### Acknowledgments

We thank Brian Schofield of the Johns Hopkins University School of Public Health for his assistance in the preparation of the light microscopy figures, and Frank Barksdale of the Johns Hopkins University School of Medicine for his help with the electron microscopy processing and sectioning.

### References

1. He FZS, Zhang C: Mycotoxin-Induced Encephalopathy and Dystonia in Children. London, Taylor and Francis, 1990
2. Ludolph AC, He F, Spencer PS, Hammerstad J, Sabri M: 3-Nitropropionic acid-exogenous animal neurotoxin and possible human striatal toxin. *Can J Neurol Sci* 1991, 18:492-498
3. Beal MF, Brouillet E, Jenkins BG, Ferrante RJ, Kowall NW, Miller JM, Storey E, Srivastava R, Rosen BR, Hyman BT: Neurochemical and histologic characterization of striatal excitotoxic lesions produced by the mitochondrial toxin 3-nitropropionic acid. *J Neurosci* 1993, 13: 4181-4192
4. Alexi T, Hughes PE, Faull RL, Williams CE: 3-Nitropropionic acid's lethal triplet: cooperative pathways of neurodegeneration. *Neuroreport* 1998, 9:R57-R64
5. Binienda Z, Johnson JR, Tyler-Hashemi AA, Rountree RL, Sapienza PP, Ali SF, Kim CS: Protective effect of L-carnitine in the neurotoxicity induced by the mitochondrial inhibitor 3-nitropropionic acid (3-NPA). *Ann NY Acad Sci* 1999, 890:173-178
6. Borlongan CV, Koutouzis TK, Sanberg PR: 3-Nitropropionic acid animal model and Huntington's disease. *Neurosci Biobehav Rev* 1997, 21:289-293
7. Gould DH, Gustine DL: Basal ganglia degeneration, myelin alterations, and enzyme inhibition induced in mice by the plant toxin 3-nitropropionic acid. *Neuropathol Appl Neurobiol* 1982, 8:377-393
8. Hamilton BF, Gould DH: Nature and distribution of brain lesions in rats intoxicated with 3-nitropropionic acid: a type of hypoxic (energy deficient) brain damage. *Acta Neuropathol* 1987, 72:286-297
9. Coles CJ, Edmondson DE, Singer TP: Inactivation of succinate dehydrogenase by 3-nitropropionate. *J Biol Chem* 1979, 254:5161-5167
10. Alston TA, Mela L, Bright HJ: 3-Nitropropionate, the toxic substance of *Indigofera*, is a suicide inactivator of succinate dehydrogenase. *Proc Natl Acad Sci USA* 1977, 74:3767-3771
11. Alexi T, Hughes PE, Knusel B, Tobin AJ: Metabolic compromise with systemic 3-nitropropionic acid produces striatal apoptosis in

- Sprague-Dawley rats but not in BALB/c ByJ mice. *Exp Neurol* 1998, 153:74-93
12. Bogdanov MB, Ferrante RJ, Kuemmerle S, Klivenyi P, Beal MF: Increased vulnerability to 3-nitropropionic acid in an animal model of Huntington's disease. *J Neurochem* 1998, 71:2642-2644
13. Hickey MA, Morton AJ: Mice transgenic for the Huntington's disease mutation are resistant to chronic 3-nitropropionic acid-induced striatal toxicity. *J Neurochem* 2000, 75:2163-2171
14. Ouary S, Bizat N, Altairac S, Menetrat H, Mitoux V, Conde F, Hant-raye P, Brouillet E: Major strain differences in response to chronic systemic administration of the mitochondrial toxin 3-nitropropionic acid in rats: implications for neuroprotection studies. *Neuroscience* 2000, 97:521-530
15. Schauwecker PE, Steward O: Genetic determinants of susceptibility to excitotoxic cell death: implications for gene targeting approaches. *Proc Natl Acad Sci USA* 1997, 94:4103-4108
16. Sonsalla PK, Heikkila RE: The influence of dose and dosing interval on MPTP-induced dopaminergic neurotoxicity in mice. *Eur J Pharmacol* 1986, 129:339-345
17. Barone FC, Knudsen DJ, Nelson AH, Feuerstein GZ, Willette RN: Mouse strain differences in susceptibility to cerebral ischemia are related to cerebral vascular anatomy. *J Cereb Blood Flow Metab* 1993, 13:683-692
18. Fujii M, Hara H, Meng W, Vonsattel JP, Huang Z, Moskowitz MA: Strain-related differences in susceptibility to transient forebrain ischemia in SV-129 and C57black/6 mice. *Stroke* 1997, 28:1805-1811
19. Herman EH, Zhang J, Chadwick DP, Ferrans VJ: Age dependence of the cardiac lesions induced by minoxidil in the rat. *Toxicology* 1996, 110:71-83
20. Hansford RG, Hogue BA, Mildaziene V: Dependence of H2O2 formation by rat heart mitochondria on substrate availability and donor age. *J Bioenerg Biomembr* 1997, 29:89-95
21. Lowery O, Rosebrough N, Farr A, Randall R: Protein measurement with the folin phenol reagent. *J Biol Chem* 1951, 184:265-275
22. Troughton IA, Kim YL, Jun AS, Wallace DC: Assessment of mitochondrial oxidative phosphorylation in patient muscle biopsies, lymphoblasts, and transmembrane cell lines. *Methods Enzymol* 1996, 264:484-509
23. Harkness JE, Wagner JE: *The Biology and Medicine of Rabbits and Rodents*. Philadelphia, Lea and Febiger, 1995
24. Ally A, Park G: Rapid determination of creatine, phosphocreatine, purine bases and nucleotides (ATP, ADP, AMP, GTP, GDP) in heart biopsies by gradient ion-pair reversed-phase liquid chromatography. *J Chromatogr* 1992, 575:19-27
25. Williams JP, Headrick JP: Differences in nucleotide compartmentation and energy state in isolated and in situ rat heart: assessment by <sup>31</sup>P-NMR spectroscopy. *Biochim Biophys Acta* 1996, 1276:71-79
26. Deschner EE, Hakissian M, Long FC: Genetic factors controlling inheritance of susceptibility to 1,2-dimethylhydrazine. *J Cancer Res Clin Oncol* 1989, 115:335-339
27. Peng YG, Clayton EC, Means LW, Ramsdell JS: Repeated independent exposures to domoic acid do not enhance symptomatic toxicity in outbred or seizure-sensitive inbred mice. *Fundam Appl Toxicol* 1997, 40:63-67
28. Hamre K, Tharp R, Poon K, Xiong X, Smeyne RJ: Differential strain susceptibility following 1-methyl-4-phenyl-1,2,3,6-tetrahydropyridine (MPTP) administration acts in an autosomal dominant fashion: quantitative analysis in seven strains of *Mus musculus*. *Brain Res* 1999, 828:91-103
29. Inoue H, Castagnoli K, Van Der Schyf C, Mabic S, Igarashi K, Castagnoli Jr N: Species-dependent differences in monoamine oxidase A and B-catalyzed oxidation of various C4 substituted 1-methyl-4-phenyl-1,2,3,6-tetrahydropyridine derivatives. *J Pharmacol Exp Ther* 1999, 291:856-864
30. He F, Zhang S, Lui L: Extrapyramidal lesions caused by mildewed sugarcane poisoning (with 3 case reports). *Chin J Med* 1987, 67:395-396
31. He F, Zhang S, Qian F, Zhang C: Delayed dystonia with striatal CT lucencies induced by a mycotoxin (3-nitropropionic acid). *Neurology* 1995, 45:2178-2183
32. Lui X, Luo X, Hu W: Studies on the epidemiology and etiology of moldy sugarcane poisoning in China. *Biomed Environ Sci* 1992, 5:161-177
33. Ming L: Moldy sugarcane poisoning—a case report with a brief review. *Clin Toxicol* 1995, 33:363-367
34. de la Asuncion JG, del Olmo ML, Sastre J, Millan A, Pellin A, Pallardo FV, Vina J: AZT treatment induces molecular and ultrastructural oxidative damage to muscle mitochondria. Prevention by antioxidant vitamins. *J Clin Invest* 1998, 102:4-9
35. Davies KJ, Doroshov JH: Redox cycling of anthracyclines by cardiac mitochondria. I. Anthracycline radical formation by NADH dehydrogenase. *J Biol Chem* 1986, 261:3060-3067
36. Doroshov JH, Davies KJ: Redox cycling of anthracyclines by cardiac mitochondria. II. Formation of superoxide anion, hydrogen peroxide, and hydroxyl radical. *J Biol Chem* 1986, 261:3068-3074
37. Keller DA, Roe DC, Lieder PH: Fluoroacetate-mediated toxicity of fluorinated ethanes. *Fundam Appl Toxicol* 1996, 30:213-219
38. Lewis W, Dalakas MC: Mitochondrial toxicity of antiviral drugs. *Nat Med* 1995, 1:417-422
39. Pai VB, Nahata MC: Cardiotoxicity of chemotherapeutic agents: incidence, treatment and prevention. *Drug Saf* 2000, 22:263-302
40. Tisdale MJ, Brennan RA: Role of fluoroacetate in the toxicity of 2-fluoroethylnitrosoureas. *Biochem Pharmacol* 1985, 34:3323-3327
41. Yuan C, Acosta Jr D: Cocaine-induced mitochondrial dysfunction in primary cultures of rat cardiomyocytes. *Toxicology* 1996, 112:1-10
42. Fujihira S, Yamamoto T, Matsumoto M, Yoshizawa K, Oishi Y, Fujii T, Noguchi H, Mori H: The high incidence of atrial thrombosis in mice given doxorubicin. *Toxicol Pathol* 1993, 21:362-368
43. Schulz JB, Henshaw DR, MacGarvey U, Beal MF: Involvement of oxidative stress in 3-nitropropionic acid neurotoxicity. *Neurochem Int* 1996, 29:167-171
44. Sato S, Gobbel GT, Li Y, Kondo T, Murakami K, Sato M, Hasegawa K, Copin JC, Honkanenmi J, Sharp FR, Chan PH: Blood-brain barrier disruption, HSP70 expression and apoptosis due to 3-nitropropionic acid, a mitochondrial toxin. *Acta Neurochir* 1997, 70(Suppl):S237-S279
45. Matthews RT, Yang L, Jenkins BG, Ferrante RJ, Rosen BR, Kaddurah-Daouk R, Beal MF: Neuroprotective effects of creatine and cyclocreatine in animal models of Huntington's disease. *J Neurosci* 1998, 18:156-163
46. Matthews RT, Yang L, Browne S, Baik M, Beal MF: Coenzyme Q10 administration increases brain mitochondrial concentrations and exerts neuroprotective effects. *Proc Natl Acad Sci USA* 1998, 95:8892-8897
47. Ludolph AC, Seelig M, Ludolph AG, Sabri MI, Spencer PS: ATP deficits and neuronal degeneration induced by 3-nitropropionic acid. *Ann NY Acad Sci* 1992, 648:300-302
48. Klivenyi P, Andreassen OA, Ferrante RJ, Dedeoglu A, Mueller G, Lancelot E, Bogdanov M, Andersen JK, Jiang D, Beal MF: Mice deficient in cellular glutathione peroxidase show increased vulnerability to malonate, 3-nitropropionic acid, and 1-methyl-4-phenyl-1,2,3,6-tetrahydropyridine. *J Neurosci* 2000, 20:1-7
49. Kim GW, Copin JC, Kawase M, Chen SF, Sato S, Gobbel GT, Chan PH: Excitotoxicity is required for induction of oxidative stress and apoptosis in mouse striatum by the mitochondrial toxin, 3-nitropropionic acid. *J Cereb Blood Flow Metab* 2000, 20:119-129
50. Hamilton BF, Gould DH: Correlation of morphologic brain lesions with physiologic alterations and blood-brain barrier impairment in 3-nitropropionic acid toxicity in rats. *Acta Neuropathol* 1987, 74:67-74
51. Gould DH, Wilson MP, Hamar DW: Brain enzyme and clinical alterations induced in rats and mice by nitroaliphatic toxicants. *Toxicol Lett* 1985, 27:83-89
52. Bogdanov MB, Ferrante RJ, Mueller G, Ramos LE, Martinou JC, Beal MF: Oxidative stress is attenuated in mice overexpressing BCL-2. *Neurosci Lett* 1999, 262:33-36
53. Beal MF, Henshaw DR, Jenkins BG, Rosen BR, Schulz JB: Coenzyme Q10 and nicotinamide block striatal lesions produced by the mitochondrial toxin malonate. *Ann Neurol* 1994, 36:882-888
54. Keller JN, Guo Q, Holtsberg FW, Bruce-Keller AJ, Mattson MP: Increased sensitivity to mitochondrial toxin-induced apoptosis in neural cells expressing mutant presenilin-1 is linked to perturbed calcium homeostasis and enhanced oxyradical production. *J Neurosci* 1998, 18:4439-4450
55. Hylin J, Matsumoto H: Inhibition of succinate dehydrogenase by 3-nitropropionate. *Toxicol Appl Pharmacol* 1964, 6:168-171
56. Lopez PS, Castillo CH, Pastelin GH, Hernandez MR, Suarez MJ, Sanchez ML, Escalante BA: Characterization of 3-nitropropionic acid-

- induced bradycardia in isolated atria. *Toxicol Appl Pharmacol* 1998, 148:1-6
57. Castillo C, Reyes G, Rosas-Lezama MA, Valencia I, Hong E: Analysis of the cardiodepressor action of 3-nitropropionic acid. *Proc West Pharmacol Soc* 1994, 37:41-42
58. Hong E, Castillo C, Rivero I, Somanathan R: Vasodilator and antihypertensive actions of 3-nitropropionic acid. *Proc West Pharmacol Soc* 1990, 33:209-211
59. Guyot MC, Hantraye P, Dolan R, Palfi S, Maziere M, Brouillet E: Quantifiable bradykinesia, gait abnormalities and Huntington's disease-like striatal lesions in rats chronically treated with 3-nitropropionic acid. *Neuroscience* 1997, 79:45-56
60. Miller PJ, Zaborsky L: 3-Nitropropionic acid neurotoxicity: visualization by silver staining and implications for use as an animal model of Huntington's disease. *Exp Neurol* 1997, 146:212-229
61. Brierley JB: *Cerebral Hypoxia*. London, Edward Arnold, 1976
62. Meade CA, Figueredo-Cardenas G, Fusco F, Nowak Jr TS, Pulsinelli WA, Reiner A: Transient global ischemia in rats yields striatal projection neuron and interneuron loss resembling that in Huntington's disease. *Exp Neurol* 2000, 166:307-323
63. Burke RE, Karanas AL: Quantitative morphological analysis of striatal cholinergic neurons in perinatal asphyxia. *Ann Neurol* 1990, 27:81-88
64. Burke RE, Kent J, Kenyon N, Karanas A: Unilateral hypoxic-ischemic injury in neonatal rat results in a persistent increase in the density of striatal tyrosine hydroxylase immunoperoxidase staining. *Brain Res Dev Brain Res* 1991, 58:171-179
65. Chesselet MF, Gonzales C, Lin CS, Polsky K, Jin BK: Ischemic damage in the striatum of adult gerbils: relative sparing of somatostatinergic and cholinergic interneurons contrasts with loss of efferent neurons. *Exp Neurol* 1990, 110:209-218
66. Ferriero DM, Arcavi LJ, Sagar SM, McIntosh TK, Simon RP: Selective sparing of NADPH-diaphorase neurons in neonatal hypoxia-ischemia. *Ann Neurol* 1988, 24:670-676
67. Johnston MV, Hudson C: Effects of postnatal hypoxia-ischemia on cholinergic neurons in the developing rat forebrain: choline acetyltransferase immunocytochemistry. *Brain Res* 1987, 431:41-50
68. Mallard EC, Waldevogel HJ, Williams CE, Fauli RL, Gluckman PD: Repeated asphyxia causes loss of striatal projection neurons in the fetal sheep brain. *Neuroscience* 1995, 65:827-836
69. Uemura Y, Kowall NW, Beal MF: Selective sparing of NADPH-diaphorase-somatostatin-neuropeptide Y neurons in ischemic gerbil striatum. *Ann Neurol* 1990, 27:620-625
70. Choi DW: Glutamate neurotoxicity and diseases of the nervous system. *Neuron* 1988, 1:623-634
71. Simpson JR, Isacson O: Mitochondrial impairment reduces the threshold for in vivo NMDA-mediated neuronal death in the striatum. *Exp Neurol* 1993, 121:57-64
72. Hier DB, Davis KR, Richardson Jr EP, Mohr JP: Hypertensive putaminal hemorrhage. *Ann Neurol* 1977, 1:152-159
73. Nishino H, Hida H, Kumazaki M, Shimano Y, Nakajima K, Shimizu H, Ooiwa T, Baba H: The striatum is the most vulnerable region in the brain to mitochondrial energy compromise: a hypothesis to explain its specific vulnerability. *J Neurotrauma* 2000, 17:251-260
74. Portera-Cailliau C, Price DL, Martin LJ: Excitotoxic neuronal death in the immature brain is an apoptosis-necrosis morphological continuum. *J Comp Neurol* 1997, 378:70-87
75. Onley JW: *Neurotoxicity of Excitotoxicity* Amino Acids. New York, Raven Press, 1978
76. Martin LJ, Brambrink AM, Lehmann C, Portera-Cailliau C, Koehler R, Rothstein J, Traystman RJ: Hypoxia-ischemia causes abnormalities in glutamate transporters and death of astroglia and neurons in newborn striatum. *Ann Neurol* 1997, 42:335-348
77. Pluta R, Lossinsky AS, Wisniewski HM, Mossakowski MJ: Early blood-brain barrier changes in the rat following transient complete cerebral ischemia induced by cardiac arrest. *Brain Res* 1994, 633:41-52
78. Karibe H, Chen SF, Zarow GJ, Gafni J, Graham SH, Chan PH, Weinstein PR: Mild intraischemic hypothermia suppresses consumption of endogenous antioxidants after temporary focal ischemia in rats. *Brain Res* 1994, 649:12-18
79. Juurlink BH: Response of glial cells to ischemia: roles of reactive oxygen species and glutathione. *Neurosci Biobehav Rev* 1997, 21:151-166
80. de la Torre J: Cerebral hypoperfusion, capillary degeneration, and development of Alzheimer disease. *Alzheimer Dis Assoc Disord* 2000, 14 (Suppl 1):S72-S81
81. La Fontaine MA, Geddes JW, Banks A, Butterfield DA: 3-nitropropionic acid induced in vivo protein oxidation in striatal and cortical synaptosomes: insights into Huntington's disease. *Brain Res* 2000, 858:356-362
82. Wisniewski HM, Pluta R, Lossinsky AS, Mossakowski MJ: Ultrastructural studies of cerebral vascular spasm after cardiac arrest-related global cerebral ischemia in rats. *Acta Neuropathol* 1995, 90:432-440
83. Arai T, Tsukahara I, Nitta K, Kojo H, Amakawa K: Responsiveness of cerebral vessels to changes of blood pressure and partial pressure of carbon dioxide after a transient period of cardiac arrest in dogs. *Resuscitation* 1985, 12:237-245
84. Castillo C, Valencia I, Reyes G, Hong E: An analysis of the antihypertensive properties of 3-nitropropionic acid, a compound from plants in the genus *Astragalus*. *Arch Inst Cardiol Mex* 1993, 63:11-16
85. Gerlai R: Gene-targeting studies of mammalian behavior: is it the mutation or the background genotype? *Trends Neurosci* 1996, 19:177-181
86. Wiegand F, Liao W, Busch C, Castell S, Knapp F, Lindauer U, Megow D, Meisel A, Redetzky A, Ruscher K, Trendelenburg G, Victorov I, Riepe M, Diener HC, Dirnagl U: Respiratory chain inhibition induces tolerance to focal cerebral ischemia. *J Cereb Blood Flow Metab* 1999, 19:1229-1237
87. Weih M, Bergk A, Isaev NK, Ruscher K, Megow D, Riepe M, Meisel A, Victorov IV, Dirnagl U, Dirnagl U: Induction of ischemic tolerance in rat cortical neurons by 3-nitropropionic acid: chemical preconditioning. *Neurosci Lett* 1999, 272:207-210
88. Sugino T, Nozaki K, Takagi Y, Hashimoto N: 3-Nitropropionic acid induces ischemic tolerance in gerbil hippocampus in vivo. *Neurosci Lett* 1999, 259:9-12
89. Riepe MW, Esclaire F, Kasischke K, Schreiber S, Nakase H, Kempfski O, Ludolph AC, Dirnagl U, Hugon J: Increased hypoxic tolerance by chemical inhibition of oxidative phosphorylation: "chemical preconditioning." *J Cereb Blood Flow Metab* 1997, 17:257-264
90. Riepe MW, Ludolph AC: Chemical preconditioning: a cytoprotective strategy. *Mol Cell Biochem* 1997, 174:249-254
91. Ockali RA, Bhargava P, Kukreja RC: Chemical preconditioning with 3-nitropropionic acid in hearts: role of mitochondrial K(ATP) channel. *Am J Physiol* 2001, 280:H2406-H2411
92. Arellano M, Malet-Martino M, Martino R, Gires P: The anti-cancer drug 5-fluorouracil is metabolized by the isolated perfused rat liver and in rats into highly toxic fluoroacetate. *Br J Cancer* 1998, 77:79-86
93. Jones T, Hunt R: *Veterinary Pathology*, ed 5. Philadelphia, Lea and Febiger, 1983
94. Papadopoulos LC, Theophilidis G, Thomopoulos GN, Tsiftoglou AS: Structural and functional impairment of mitochondria in adriamycin-induced cardiomyopathy in mice: suppression of cytochrome c oxidase II gene expression. *Biochem Pharmacol* 1999, 57:481-489
95. Yen HC, Oberley TD, Galola CG, Szveda LI, St Clair DK: Manganese superoxide dismutase protects mitochondrial complex I against adriamycin-induced cardiomyopathy in transgenic mice. *Arch Biochem Biophys* 1999, 362:59-66

# Mechanisms for neuronal degeneration in amyotrophic lateral sclerosis and in models of motor neuron death (Review)

LEE J. MARTIN<sup>1,2</sup>, ANN C. PRICE<sup>1</sup>, ADEEL KAISER<sup>1</sup>, ARIF Y. SHAIKH<sup>1</sup> and ZHIPING LIU<sup>1</sup>

Departments of <sup>1</sup>Pathology, Division of Neuropathology, and <sup>2</sup>Neuroscience, Johns Hopkins, University School of Medicine, Baltimore, MD, USA

Received October 10, 1999; Accepted November 2, 1999

**Abstract.** Amyotrophic lateral sclerosis (ALS), also referred to as motor neurone disease, is a fatal neurological disease that is characterized clinically by progressive muscle weakness, muscle atrophy, and eventual paralysis. The neuropathology of ALS is primary degeneration of upper (motor cortical) and lower (brainstem and spinal) motor neurons. The amyotrophy refers to the neurogenic atrophy of affected muscle groups, and the lateral sclerosis refers to the hardening of the lateral white matter funiculus in spinal cord (corresponding to degeneration of the corticospinal tract) found at autopsy. Because the mechanisms for the motor neuron degeneration in ALS are not understood, this disease has no precisely known causes and no effective treatments. Very recent studies have identified that the degeneration of motor neurons in ALS is a form of apoptotic cell death that may occur by an abnormal programmed cell death (PCD) mechanism. In order to treat ALS effectively, we need to understand the mechanisms for motor neuron apoptosis more completely. Future studies need to further identify the signals for PCD activation in neurons as they relate to the pathogenesis of ALS and to clarify the molecular pathways leading to motor neuron apoptosis in animal and cell culture model systems. These studies should lead to a better understanding of motor neuron death and to the design of new therapeutic experiments critical for the future treatment of ALS.

## Contents

1. Introduction
2. ALS and mutant SOD1
3. Excitotoxicity and neurodegeneration in ALS
4. ALS and neuronal cell death
5. Apoptosis contributes to the neuronal death in ALS
6. Molecular regulation of apoptosis

7. Autoimmunity and ALS
8. PCD pathways and neuronal apoptosis
9. Oxidative stress induces neuronal apoptosis
10. DNA damage and DNA repair mechanisms in ALS
11. Animal models of neuronal apoptosis in the adult CNS
12. Future hope for the understanding of ALS

## 1. Introduction

ALS is a human disease clinically characterized by progressive weakness, muscle atrophy, and eventual paralysis and death within 3-5 years of clinical onset (1). It is one of the most common neurodegenerative diseases with an adult onset, having an incidence of 1-2 per 100,000 individuals. This disease is neuropathologically characterized by progressive degeneration of upper and lower motor neurons in the brain and spinal cord. The mechanisms leading to degeneration of motor neurons in ALS are not understood. Two major forms of ALS exist: idiopathic (sporadic) and heritable (familial). The vast majority of ALS cases are sporadic with no known genetic component. The familial forms of ALS (FALS) are autosomal dominant and make up about 10-20% of all ALS cases. In a subset of familial ALS cases (about 5-10%), missense mutations have been identified (2) in the gene for superoxide dismutase 1 (SOD1, also known as Cu,Zn SOD).

A variety of hypothesis (Table I) have been proposed for the possible causes of neuronal death in ALS, including SOD1 mutations, abnormal uptake of excitatory amino acids leading to glutamate receptor-mediated excitotoxicity, deficiencies in neurotrophic factors, DNA damage, and autoimmunity. Recently, this laboratory (3) has provided strong evidence that motor neuron degeneration is due to an anomalous activation of programmed cell death (PCD). A better understanding of the pathogenesis of neuronal degeneration in this disease and in animal models that mirror this degeneration of motor neurons found in ALS is critical for the future development of effective therapies for patients with ALS.

## 2. ALS and mutant SOD1

Mutations have been identified in the SOD1 gene in a small subset of individuals with FALS (2,4). Thus, most current ideas

*Correspondence to:* Dr Lee J. Martin, Johns Hopkins University School of Medicine, Department of Pathology, 558 Ross Building, 720 Rutland Avenue, Baltimore, MD 21205-2196, USA

**Key words:** axotomy, DNA damage, excitotoxicity, mitochondria, neuronal apoptosis, oxidative stress, programmed cell death

Table 1. Some leading theories about motor neuron degeneration in ALS.

Mechanism	Comment
SOD1 mutation	Found in a subset of FALS cases. Resulting in a toxic gain-in-function or modified stability of SOD1
Excitotoxicity	Resulting from abnormal glutamate receptor activation and defects in glutamate transport
Neurotrophin withdrawal	Resulting from insufficient muscle cell- or glial cell-derived trophic support or defective neurotrophin receptor signaling
DNA damage/repair defects	Resulting from oxidative stress or inefficient DNA-repair enzyme function. May involve both mitochondrial and nuclear DNA damage
Autoimmunity	Resulting from autoantibodies to motor neuron antigens
Aberrant programmed cell death	May be triggered by all of the above mechanisms

ALS center on the mutant forms of SOD1 found in FALS. Because SOD1 is widely expressed in cells throughout the body, and in CNS tissue the expression is very ubiquitous (5), the basis for the selective vulnerability of motor neurons in the presence of SOD1 mutations is not clear. Initial experiments suggested that mutations in SOD1 lead to motor neuron degeneration by decreasing its enzymatic activity, resulting in toxic effects of superoxide radicals inefficiently scavenged by mutant SOD1 (4). This hypothesis was supported by the finding that down-regulation of SOD1 causes apoptosis in neuronal cell cultures (6) and in slice cultures of spinal cord (7), and by the observation that microinjected normal wild-type SOD1 can delay apoptosis in cultured neurons deprived of trophic factors (8). However, it was observed that FALS-linked mutations in SOD1 do not generally impair enzymatic activity, but instead decrease protein stability (9). More recently, it has been proposed that mutant SOD1 acquires a neurotoxic gain in function. Mutations in SOD1 may convert this enzyme from a protein with antioxidant-antiapoptotic functions to a protein with apoptosis-promoting effects (10). In addition to the dismutation of superoxide, SOD1 also has peroxidase activity, and this peroxidase activity is enhanced in mutant SOD1 compared to normal SOD1 (11). This gain-of-function may lead to enhanced production of hydroxyl, superoxide, and peroxynitrite radicals (11,12). SOD1 catalyzes the nitration of

specific tyrosine residues in protein by peroxynitrite, which may contribute to the damaging gain-of-function resulting from SOD1 mutations (12). Neurofilaments are major structural proteins in motor neurons and, notably, neurofilament L is a target of tyrosine nitration by peroxynitrite (13). Other studies have revealed that  $Zn^{2+}$  affinity of mutant SOD1 is decreased and that neurofilament L binds  $Zn^{2+}$  with sufficient affinity to capture this cofactor from mutant and wild-type SOD1 (14). The loss of  $Zn^{2+}$  from wild-type SOD1 dramatically increases its efficiency for catalyzing peroxynitrite-mediated tyrosine nitration (14). Although neurofilament L is particularly susceptible to peroxynitrite-mediated nitration, tyrosine nitration of this protein is not elevated in spinal cords of sporadic ALS cases compared to controls (15). These altered properties of mutant SOD1 have not yet been causally-linked specifically to motor neuron damage in ALS. However, these observations are relevant to our recent findings that motor neuron degeneration in sporadic ALS and FALS is apoptosis (3) and that induced apoptosis of motor neurons in animal models is associated with peroxynitrite formation and hydroxyl radical damage to DNA (16).

Motor neuron degeneration occurs in mice with forced expression of mutant forms of the gene encoding for SOD1 (17,18). The motor neuron degeneration found in transgenic mice overexpressing the FALS mutant forms of SOD1 (17-19) is different structurally from the degeneration of motor neurons in sporadic and FALS (3). Rather than being a condensational form of death, these mouse motor neurons become swollen and severely vacuolated. Neither morphological nor biochemical evidence for apoptotic death of motor neurons has been shown in any of the SOD1 transgenic mouse models of ALS, and it is still uncertain whether motor neurons in these mouse models die or whether they remain in a severely vacuolated, atrophic state, similar to neurons in some models of axotomy and excitotoxicity (20,21). Although, the survival of FALS mice is prolonged when crossed with mice overexpressing Bcl-2 (22) or a dominant negative inhibitor of caspase-1 (23), the degeneration of motor neurons is not prevented (22), suggesting that neuronal degeneration in FALS mice is not apoptosis controlled by PCD mechanisms. The vacuolar and edematous degeneration of motor neurons in mice overexpressing mutant SOD1 (17-19) more closely resembles excitotoxic neurodegeneration (24,25) or transsynaptic neuronal atrophy (but not death) induced by deafferentation (20,21). It is possible that the prominent neuropathological dissimilarity between motor neuron degeneration in existing transgenic mouse models and in ALS is related to differences in the level of mutant SOD1 expression and the rate of neuronal degeneration. We have found that rate of neuronal injury influences the cell death pathway, with neuronal necrosis evolving acutely and neuronal apoptosis progressing more slowly, despite similar mechanisms such as oxidative stress (26).

### 3. Excitotoxicity and neurodegeneration in ALS

The amino acid glutamate is the major excitatory neurotransmitter in the CNS. Glutamate functions in synaptic neurotransmission by activating glutamate receptors (GluRs). Excessive activation of subtypes of GluRs is excitotoxic to neurons (25-28). GluR-mediated excitotoxicity has been

proposed to explain the patterns of selective neuronal cell death and clinical manifestations of ALS. This hypothesis is based on several different lines of evidence: an exogenous glutamate analogue may be responsible for the damage to upper motor neurons in lathyrism via actions at specific GluR subtypes (29); abnormalities in brain tissue excitatory amino acid metabolism may participate in the pathogenesis of Huntington's disease and olivopontocerebellar atrophy (two slowly progressive, chronic neurodegenerative disorders with selective neuronal vulnerability) (30,31); serum and cerebrospinal fluid concentrations of glutamate have been found to be increased in patients with sporadic ALS in some studies (32-34), although not in other studies (35,36); spinal cord and affected brain regions of patients with ALS have decreased synaptosomal glutamate uptake (37,38); the protein levels of glutamate transporter GLT1 are decreased in vulnerable regions in ALS (39); abnormal RNA processing of GLT1 transcripts may occur in some cases of ALS (40), although other groups have found these 'aberrant' forms of GLT1 transcripts in controls (41,42); and, lastly, the antiglutamate agent riluzole may slow the progression of ALS and improve survival of patients (43).

It still has not been determined satisfactorily if these changes in glutamate levels and glutamate uptake are primary or secondary to the disease process in ALS. For example, defects of glutamate transporter subtypes in ALS (37,38) could reflect a primary loss or inactivation of proteins or secondary effects of neurodegeneration. Neuronal cells have an important modulatory role in astroglial GLT1 expression because neurons liberate soluble factors that signal astroglial expression of GLT1 mRNA and protein (44) and, thus, neuronal loss or synaptic deafferentation may cause a downregulation of GLT1 expression (45,46). Therefore, the argument for glutamate excitotoxicity resulting from GLT1 loss or downregulation as a primary mechanism for neurodegeneration in ALS is, as yet, only speculation, but glutamate toxicity could contribute to the death of motor neurons even if alterations in GluRs or transporters are secondary changes.

The mechanisms through which activation of neuronal GluRs cause cell death involve alterations in cytosolic free  $\text{Ca}^{2+}$  homeostasis and activation of  $\text{Ca}^{2+}$ -sensitive proteases, protein kinases, endonucleases, lipases, and phospholipases (28,47). The acute effects of GluR excitotoxicity have been much better defined than the delayed effects on neurons, whereas the relationships between GluR-mediated excitotoxicity and neuronal death in slow, chronic neurodegeneration are only speculative. The delayed onset of neurodegeneration in patients with ALS could be related synergistically to progressive impairments in mitochondrial oxidative phosphorylation that accompany aging (48), to mutations in SOD1 and ensuing chronic, age-related intracellular damage by reactive free radicals (4), or to cumulative, age-related dysfunctional regulation of glutamate release, transport, and GluR activation (27,28,47,48). This possible synergism between abnormalities is exemplified by a study revealing that SOD1 mutations linked to FALS cause free radical damage to GLT1 and transporter inactivation (49).

However, like the patterns of SOD1 expression in CNS (5), neither differential subunit compositions of ion channel GluRs (AMPA and NMDA receptors) nor differential expressions of glutamate transporters appear to explain sufficiently the

mechanisms that dictate the selective vulnerability of neurons in motor cortex and motor neurons in brainstem and spinal cord in ALS. This conclusion is based on many glutamate receptor/transporter expression and localization studies in animal and human CNS (50-57). The most convincing data indirectly implicating excitotoxicity as having a role in the pathogenesis of ALS is the selective loss of the glutamate transporter GLT1 in vulnerable regions in ALS (38,39). However, loss of synaptosomal glutamate uptake and loss of GLT1 protein also occur in Alzheimer's disease (58,59).

Experimental neuropathological studies have shown the possible consequences of glutamate uptake failure in the regulation of extracellular glutamate and neuronal survival in the CNS. For example, injection of the glutamate transporter inhibitor threo-3-hydroxy-DL-aspartate into rat striatum causes neurodegeneration (60). Mice genetically deficient in GLT1, although they develop normally without motor neuron degeneration, are more susceptible to edema formation than wild-type mice in a model of cold injury to the cerebral cortex (61). Nevertheless, the data in ALS is still indirect evidence for GluR-mediated excitotoxicity, and it is still uncertain whether glutamate transporter changes are related to the consequences of the disease or whether abnormalities in glutamate transporters and potential GluR excitotoxicity contribute mechanistically to the pathogenesis of ALS.

Most patients with ALS are maintained on mechanical ventilation, as a means of relieving symptoms of chronic hypoventilation and prolonging life, but patients die eventually from respiratory insufficiency (62). It has been argued that riluzole improves the survival of ALS patients by acting as a  $\text{Na}^+$  channel blocker and increasing resistance to hypoxia (by reducing energy demand), not by anti-excitotoxic actions (63). Interestingly, there is *in vivo* evidence that GLT1 is preferentially more sensitive to cerebral hypoxia-ischemia than other glutamate transporters in animal models (45,64). It is also important to note that loss of glutamate transporter function and accumulation of extracellular glutamate does not necessarily lead to neurodegeneration (46,65-67). We also found that GluR-mediated excitotoxicity in adult CNS kills neurons by a mechanism that is different structurally from the pattern seen in ALS (3,21,24). Thus, it is possible that changes in astroglial glutamate transporters in individuals with ALS are possibly consequences of neurodegeneration, or, alternatively, these alterations are related to premortem agonal state.

#### 4. ALS and neuronal cell death

Cellular degeneration can result in atrophy or death. Insults to neurons do not necessarily lead to cell death. In the CNS, neurons can survive an insult and exist chronically in an altered, atrophic state (20,21). In ALS, motor neurons die unequivocally and are eliminated (3). The process and molecular causes of motor neuron death in individuals with ALS are not fully understood.

Cell death can occur by different pathways. Depending on the type of cell and on the stimulus, cells die typically in either of two ways, generally described as apoptosis or necrosis (26,68,69). These two forms of cell death are thought to differ fundamentally in structure and mechanisms. Apoptosis is a

structurally organized PCD that is mediated by active, intrinsic mechanisms. However, PCD does not mean that the death is purely genetic and independent of epigenetic or environmental signals. For instance, PCD is often dependent on a variety of trophic factors and cell-cell interactions. In contrast, cellular necrosis is thought to be mechanistically and structurally a more rapid and random degeneration resulting from abrupt pathophysiological perturbations (e.g., osmotic, thermal, toxic, or traumatic) involving energy depletion, disruption of plasma membrane structural and functional integrity, rapid influx of  $\text{Na}^+$ ,  $\text{Ca}^{2+}$  and water, and failure of cell volume homeostasis.

However, within the realm of neuronal cell death structure, 'shades of gray' can be observed (24,26,69,70). Our experiments using an animal model of excitotoxic degeneration of neurons led to the novel concept of an apoptosis-necrosis continuum for neuronal death *in vivo* (24,70). We concluded that excitotoxic death of neurons does not have to be strictly apoptosis or necrosis, according to a traditional binary classification of cell death structure, but it can also occur as intermediate or hybrid forms of cell death with coexisting characteristics that lie along a structural continuum with apoptosis and necrosis at the extremes. Features such as the subtypes of GluR that are activated influence where a dying neuron falls along this continuum. Therefore, excitotoxic neuronal death may not be identical in every neuron, possibly because of the high diversity in the expression, localization, and function of GluR subtypes and second messenger systems in the CNS (50-57). We also discovered that the structure of neuronal death is influenced by CNS maturity, because death of injured adult neurons only rarely occurs with apoptotic structural features that are identical to those seen during naturally occurring PCD in the developing nervous system (26,69). Thus, our concept of the apoptosis-necrosis structural continuum for neuronal cell death may be relevant ultimately for understanding neuronal death in neurodegenerative disorders.

### 5. Apoptosis contributes to the neuronal death in ALS

The ongoing identification of genetic and molecular regulatory mechanisms for PCD (Table II) has fueled the idea that abnormalities in the expression and functioning of cell death proteins may activate anomalous neuronal death in neurodegenerative diseases (26,69,71-73). This possibility is supported by the finding that the genes for neuronal apoptosis inhibitory protein and survival motor neuron are either deleted partially or are mutant in some individuals with spinal muscular atrophy (a pediatric form of motor neuron disease) (72,74). However, it has been uncertain whether the neurodegeneration in ALS is apoptosis and is related causally to abnormalities in the molecular regulation of cell death and whether it is PCD.

We therefore evaluated critically the structure of degenerating motor neurons in postmortem cases of ALS and determined that it is a form of apoptosis (3). Interestingly, the nuclear morphology of degenerating motor neurons in individuals with ALS is not identical to classical neuronal apoptosis found in the developing CNS (26) or to excitotoxicity-induced neuronal apoptosis in the developing brain (26). Therefore, we have concluded that the death of

Table II. Molecular regulation of apoptosis.

Bcl-2 family		Caspase family	IAP family
Antiapoptotic proteins	Proapoptotic proteins		
Bcl-2 <sup>a</sup>	Bax <sup>a</sup>	Apoptosis 'initiators': caspase-2, -8, -9, -10	NAIP
Bcl-x <sub>L</sub> <sup>b</sup>	Bak <sup>a</sup>	Apoptosis 'executioners': caspase-3 <sup>a</sup> , -6, -7	IAP1
Boo	Bcl-x <sub>S</sub> Bad Bid Bik Mtd	Cytokine processors: caspase-1, -4, -5, -11, 12, -14	IAP2 XIAP

<sup>a</sup>Identifies proteins that have been shown to be abnormal in individuals with ALS (3). <sup>b</sup>Identifies proteins that have been shown to be unchanged in ALS (3).

neurons in ALS is a form of apoptosis that may differ slightly from classical apoptosis at the structural level (3). This interpretation is consistent with the concept that neuronal maturity, magnitude of target deprivation, and rate (i.e., progression or timing) of neuronal death may influence the structure of dying cells (26).

We also found that in selectively vulnerable CNS regions in individuals with ALS compared to age-matched controls, the proapoptotic proteins Bax and Bak are elevated in the mitochondrial-enriched membrane compartment but are reduced or unchanged in the cytosol (3). In contrast, the antiapoptotic protein Bcl-2 is decreased in the mitochondrial-enriched membrane compartment of vulnerable regions in ALS but is increased in the cytosol. Coimmunoprecipitation experiments demonstrated that Bax-Bax interactions are greater in the mitochondrial-enriched membrane compartment of ALS motor cortex compared to controls, whereas Bax-Bcl-2 interactions are decreased in the membrane compartment of ALS motor cortex compared to controls. We also found that caspase-3 is activated in ALS. Abnormalities were not found in somatosensory cortex of ALS cases. These measurements were made on discretely microdissected punches throughout the entire lumbar and cervical spinal cord as well as the motor and sensory cortical grey matter mantles. The spinal cord and motor cortical samples were as selective for motor neuron populations as possible without the aid of laser capture microscopy. Thus, we propose that a PCD mechanism, involving cytosol-to-membrane and membrane-to-cytosol redistributions of cell death proteins, participates in the pathogenesis of motor neuron degeneration ALS (3).



## 6. Molecular regulation of apoptosis

Apoptosis is an organized cell death. It is mediated by active, intrinsic PCD mechanisms. Three families of apoptosis-regulating genes have been identified in mammals (75-77). The molecular mechanisms for PCD (Table II) involve the activation of the caspase family of cysteine-containing, aspartate-specific proteases (14 members have been identified to date) and the interactions among cell death proteins in the Bcl-2 family (e.g., Bcl-2, Bcl-x<sub>L</sub>, Bcl-x<sub>S</sub>, Bax, Bak, Bid, and Bad), as well as modulation of cell death by the inhibitor of apoptosis protein (IAP) family.

Caspases exist as constitutively expressed, inactive proenzymes in healthy cells. Caspases are activated through regulated proteolysis (Table II). These proteins function in systematically dismantling and packaging the cell during apoptosis, with 'initiator' caspases activating 'executioner' caspases which subsequently cleave cellular substrates, thereby causing the molecular and structural changes of organized cell death. Active caspases can cleave nuclear proteins [e.g., polyADP-ribose polymerase (PARP), DNA-dependent protein kinases, heteronuclear ribonucleoproteins, or lamins], cytoskeletal proteins (e.g., actin and fodrin), and cytosolic proteins [e.g., other caspases and DNA fragmentation factor 45 (DFF-45)] (75,77). Other caspase family members function in inflammation by processing pro-inflammatory cytokines (Table II). Two different caspase cascades mediate PCD. One pathway is initiated by cytochrome c release from mitochondria, that promotes the activation of caspase-9 through Apaf-1 and then caspase-3 activation (78). Another pathway is initiated by the activation of cell-surface death receptors, including Fas and tumor necrosis factor receptor, leading to caspase-8 activation, that in turn cleaves and activates downstream caspases such as caspase-3, -6, and -7 (79,80).

Another group of apoptosis regulatory genes is the *bcl-2* proto-oncogene family (Table II) (76). Of these genes, *bcl-2*, *bcl-x<sub>L</sub>*, and *boo* are antiapoptotic, whereas *bax*, *bcl-x<sub>S</sub>*, *bad*, *bak*, *bid*, *bik*, and *mtd* are proapoptotic. Membership into the family of Bcl-2-related proteins is defined by homology domains (BH1-BH4), which function in the interactions between members. Bcl-2 family members exist as monomers that form homo- or heterodimers and higher order multimers (76). For example, Bax can form homodimers or heterodimers with either Bcl-2 or Bcl-x<sub>L</sub> (76). When Bax and Bak are present in excess, they can antagonize the antiapoptotic activity of Bcl-2. The formation of Bax homodimers is thought to promote apoptosis, whereas Bax heterodimerization with either Bcl-2 or Bcl-x<sub>L</sub> appears to prevent apoptosis. Thus, the complex, steady-state array of protein-protein interactions among members of the Bcl-2 family functions in dictating whether a cell lives or dies. This complexity is further expanded because some proapoptotic proteins such as Mtd (called matador) can function independently of heterodimerization with survival-promoting Bcl-2 and Bcl-x<sub>L</sub> (81).

Cell death is also regulated by the IAP (inhibitor of apoptosis protein) family (82). This family includes X-chromosome-linked IAP, IAP1, IAP2, and NAIP (neuronal apoptosis inhibitory protein). Survival motor neuron is another apoptosis inhibitory protein. The main identified mechanism by which IAPs suppress apoptosis is by the prevention of

proteolytic processing of specific caspases (83). It appears that procaspase-9 is the major target of IAPs. However, IAPs do not prevent caspase-8-induced proteolytic activation of procaspase-3. IAPs can also block apoptosis by reciprocal interactions with the nuclear transcription factor NFκB (82). NAIP is abnormal in infants and children with spinal muscular atrophy (72-74). It is tempting to speculate about the possibility of IAP inactivation in ALS as a mechanism for motor neuron apoptosis, but this possibility remains to be examined. To date, the deletions in the genes for NAIP and survival motor neuron that have been identified in cases of spinal muscular atrophy have not been found in individuals with ALS (84).

In cell models of apoptosis based on *in vitro* experiments using human cell lines, activation of caspase-3 occurs when caspase-9 proenzyme (also known as Apaf-3) is bound by Apaf-1 in a process initiated by cytochrome c (identified as Apaf-2) and either ATP or dATP (78). Cytosolic ATP or dATP are required cofactors for cytochrome c-induced caspase activation. Apaf-1, a 130 kDa protein, serves as a docking protein for procaspase-9 (Apaf-3) and cytochrome c (78). Apaf-1 becomes activated when ATP is bound and hydrolyzed, with the hydrolysis of ATP and the binding of cytochrome c promoting Apaf-1 oligomerization (85). This oligomeric complex recruits and activates procaspase-9 which disassociates from the complex and becomes available to activate caspase-3. This stage is where IAPs can act to block apoptosis (83). Once activated, caspase-3 cleaves a protein with DNase activity (DFF-45), and this cleavage activates a pathway leading to the internucleosomal fragmentation of genomic DNA (86).

In response to several apoptosis-inducing agents, cytochrome c is released from mitochondria to the cytosol (87,88) through a mechanism that may involve the formation of membrane channels comprised of Bax and mitochondrial permeability transition pores (89). Bcl-2, or the closely related Bcl-x<sub>L</sub>, blocks the release of cytochrome c from mitochondria and thus the activation of caspase-3 (78,90). The blockade of cytochrome c release from mitochondria by Bcl-2 and Bcl-x<sub>L</sub> (90, 91) is possibly due to inhibition of Bax channel-forming activity in the outer mitochondrial membrane (89) or to the regulation of mitochondrial membrane potential and volume homeostasis (91). Bcl-x<sub>L</sub> also has antiapoptotic functions by physically interacting with Apaf-1 and caspase-9 and inhibiting the Apaf-1-mediated maturation of caspase-9 (92). Boo can inhibit Bak- and Bik-induced apoptosis (but not Bax-induced cell death) possibly through heterodimerization and by interactions with Apaf-1 and caspase-9 (93).

Protein phosphorylation can regulate the functions of Bcl-2 family members. Following serine phosphorylation, Bcl-2 loses its antiapoptotic activity, possibly because it cannot maintain its antioxidant function (94). In addition to interacting with homologous proteins, Bcl-2 can associate with non-homologous proteins, including the protein kinase Raf-1 (95). Bcl-2 is thought to target Raf-1 to mitochondrial membranes, allowing this kinase to phosphorylate Bad at serine residues. Phosphorylated Bad translocates to the cytosol and interacts with soluble protein 14-3-3 and, when bound to protein 14-3-3, Bad is unable to interact with Bcl-2 and Bcl-x<sub>L</sub>, thereby promoting survival (96). Non-phosphorylated Bad heterodimerizes with membrane-associated Bcl-2 and Bcl-x<sub>L</sub>, thereby



displacing Bax from Bax-Bcl-2 and Bax-Bcl-x<sub>L</sub> dimers and promoting cell death (97).

Cell death by apoptosis can also be signaled at the cell membrane by surface receptors of the tumor necrosis factor (TNF) receptor family. Fas (CD95/Apo-1) is a member of the TNF receptor family (79). Apoptosis through Fas is independent of new RNA or protein synthesis. The signal for apoptosis is initiated at the cell surface by aggregation of Fas, induced by the binding of the multivalent Fas ligand (FasL), a member of the TNF-cytokine family, expressed on activated T cells and natural killer cells. Clustering of Fas by FasL recruits Fas-associated death domain (FADD), a cytoplasmic adapter molecule that functions in the activation of the caspase 8-Bid pathway, thus forming the 'death-induced signaling complex' (DISC) (80). In this pathway, Bid (a proapoptotic family member that is a substrate for caspase-8) is cleaved in the cytosol, and then truncated Bid translocates to mitochondria, thereby functioning as a transducer of Fas apoptotic signals at the cell plasma membrane to the mitochondria (80). Bid translocation from the cytosol to mitochondrial membranes is associated with a conformational change in Bax (that is prevented by Bcl-2 and Bcl-x<sub>L</sub>) and is accompanied by release of cytochrome c from mitochondria (98). At present it is not clear whether the Fas-caspase-Bid signaling pathway for apoptosis participates in the mechanisms for motor neuron apoptosis in ALS. Our laboratory is actively investigating this possibility.

Apoptosis can also be induced by the oncosuppressor protein p53 (99). This DNA binding protein functions in genome surveillance, DNA repair, and as a transcription factor. p53 commits to death cells that have sustained DNA damage from genotoxic agents and ROS (99). The mechanisms by which p53 induces apoptosis are not fully understood, although it is known that p53 is a direct transcriptional activator of the human *bax* gene (100) and a transcriptional repressor of the *bcl-2* gene (101). This information is important because we have found increased Bax protein levels and decreased Bcl-2 protein in selectively vulnerable CNS regions in ALS (3). Thus, p53 may participate in the mechanisms for motor neuron death in ALS.

## 7. Autoimmunity and ALS

Another theory for the pathogenesis for ALS suggests that degeneration of upper and lower motor neurons is caused by an autoimmune response. Support for this theory is based on studies identifying antibodies to L-type voltage-gated Ca<sup>2+</sup> channels in some patients with sporadic ALS, although the presence of these antibodies is not specific for ALS (102). These Ca<sup>2+</sup> channel antibodies induce Ca<sup>2+</sup>-dependent apoptosis in differentiated motor neurons in culture by a mechanism involving oxidative stress (103). Additional evidence supporting an immune mechanism for neuronal death in ALS is derived from experiments revealing greater numbers of cytotoxic T cells in ALS tissues compared to controls (104). Cytotoxic T cells induce their target cells to undergo PCD by perforin release and granzyme B activation or by Fas signaling (79). It is not yet clear whether Fas signaling contributes to the mechanisms for neuronal apoptosis in ALS. However, caution is warranted in this regard because these data may

signify an immune response in ALS tissues secondary to neurodegeneration, rather than a primary mechanism for motor neuron apoptosis.

Despite data suggesting an immunological contribution to the pathogenesis of ALS, to date, the disease process has not responded to immunosuppressive therapies. However, well recognized immunopathies, such as multiple sclerosis and diabetes, do not respond to known immunosuppression methods. Thus, the possible contributions of immunological abnormalities to the mechanisms for motor neuron death in ALS have yet to be fully explored.

## 8. PCD pathways and neuronal apoptosis

A control of PCD by cell death proteins has been demonstrated in the mammalian nervous system. The numbers of neurons may be increased (presumably resulting from deficient apoptosis) in some CNS regions in transgenic mice that overexpress the *bcl-2* gene (105-107), in mice with *bax* gene ablations (108), and in mice with caspase-3 (109), caspase-9 (110,111), and Apaf-1 (112) gene deletions. Caspase-3, caspase-9, and Apaf-1 deficiencies are embryonic lethal. In contrast, Bcl-2-deficient mice survive and show an interesting progressive degeneration of motor neurons after the PCD period during early postnatal development (113).

Support for the contribution of apoptosis in neurodegeneration is found in axotomy and trophic factor withdrawal experiments. Bcl-2 overexpression ameliorates the motor neuron death in newborn mice induced by facial nerve transection (114), sciatic nerve transection (105), or optic nerve transection (107). Caspases appear to participate in apoptosis of sensory and motor neurons. For example, inhibition of caspase-1 and caspase-2 blocks the apoptosis of dorsal root and sympathetic ganglion neurons when deprived of nerve growth factor (115,116); furthermore, in retina, inhibition of caspase activity protects axotomized ganglion cells from death after optic nerve transection in adult rat (117). Inhibition of caspase-1 also arrests the PCD of motor neurons *in vitro* resulting from trophic factor deprivation and *in vivo* during the period of naturally occurring cell death (118).

## 9. Oxidative stress induces neuronal apoptosis

Oxidative stress is a potent stimulus for apoptosis in a variety of *in vitro* systems, including cultured neurons (119-121). Reactive oxygen species (ROS), such as superoxide anion radical, hydrogen peroxide and hydroxyl radical, can directly damage macromolecules, including DNA, protein, and lipid membranes (122). The balance between endogenous ROS formation and antioxidant defense mechanisms is important for cellular survival. ROS are byproducts of oxidative metabolism. The mitochondrial electron-transfer chain is a primary generator of superoxide and peroxide (123), and damaged mitochondria produce greater amounts of superoxide ion (123). Point mutations in mitochondrial DNA caused by oxidative damage may lead to protein conformational changes and inefficient electron transfer to cytochrome c oxidase (124) and, hence, enhanced superoxide and peroxide formation. These observations are consistent with the idea that mitochondria participate in the effector stages of apoptosis (125)

through changes in apoptotic protein function and cytochrome c release.

## 10. DNA damage and DNA repair mechanisms in ALS

The accumulation of damaged DNA may be a primary abnormality in ALS (126). This damage may be either acquired or inherited. Elevated levels of oxidatively damaged DNA in the form of DNA adducts (e.g., 8-oxodeoxyguanosine) have been found in spinal cord tissue of ALS cases (127). In addition, increased concentrations of hydroxyl radical damaged DNA have been found in the motor cortex of sporadic ALS cases (128). It has been proposed that SOD1 linked FALS mutations cause an altered sensitivity to free radicals; however, lymphoblastoid cells from FALS patients with SOD1 gene mutations do not show impaired abilities to scavenge radiation-induced free radicals and to protect against DNA double-strand breaks (129).

DNA oxidation occurs at a significant rate *in vivo* and is counteracted by specific DNA repair mechanisms (130). Apurinic/apyrimidinic endonuclease (APE) is a critical enzyme in the DNA base-excision repair pathway, which is considered to be the predominant pathway for repair of oxidatively damaged DNA (131). Studies have suggested that DNA repair mechanisms are deficient in individuals with sporadic ALS (132,133), and, interestingly, the possible defects in APE may be cell or tissue type specific (134). Moreover, mutations in APE have been identified in sporadic ALS (135,136), further suggesting a possible role for defective DNA repair in the etiology of ALS.

## 11. Animal models of neuronal apoptosis in the adult CNS

It is important to study neuronal apoptosis in adult animal models because ALS is an adult onset neurodegenerative disease and CNS maturity has major influences on the structure of neuronal death (24,26,69). We found that the degeneration of motor neurons in individuals with ALS (3) has many similarities to the apoptosis of CNS neurons induced by axotomy and target deprivation in adult animals (16,137,138). This induced apoptosis is characterized morphologically by chromatolysis followed by a progressive sequence of neurofilament accumulation, cytoplasmic and nuclear condensation, and cellular shrinkage. Degenerating motor neurons in ALS also undergo chromatolysis and then progressive cytoplasmic and nuclear condensation (3). Affected neurons show cytoskeletal pathology in the form of neurofilament accumulation within the neuronal cell body and axon (139,140). Because motor neuron degeneration in sporadic and FALS is structurally different from the motor neuron degeneration found in transgenic mice overexpressing the FALS mutant forms of SOD1 (3,17-19), animal models for *bona fide* neuronal apoptosis *in vivo* are critical for understanding the neurobiology of disease in ALS.

In two different animal models of axotomy-induced retrograde neuronal apoptosis in the adult CNS, we have found that neuronal death occurs in association with the accumulation of functionally active mitochondria and oxidative stress (16,137, 138). Mitochondrial accumulation within the neuronal cell

body and increased metabolic activity may cause excessive generation of ROS within the vicinity of the neuronal nucleus, depletion of mitochondrial and cytosolic antioxidant mechanisms, and subsequent oxidative damage to DNA (3,138). In both adult CNS models of neuronal apoptosis that are studied in our laboratory, the mitochondria become progressively damaged, as evidenced by the eventual loss of cytochrome c oxidase activity and by the swelling and cristolysis that manifest concurrently with the incipient cytoplasmic compaction of apoptosis, supporting the hypothesis that apoptosis-initiating factor(s) and cytochrome c are sequestered in the mitochondrial intermembrane space (78,90), which upon their release activate a PCD cascade (86-88). The finding that oxidative stress induces neuronal apoptosis *in vitro* (120,121,125) supports our idea that mitochondria may participate in the signaling of injured, chromatolytic motor neurons to enter apoptosis, possibly by releasing cytochrome c from mitochondria (87-88) or by generating excessive ROS and causing DNA damage-induced, p53 activation (99). We now have preliminary data suggesting that this retrograde apoptosis of motor neurons may be dependent on DNA damage-induced p53 activation (Martin LJ, *et al*, Soc Neurosci Abs. 25: 289, 1999). If normal trafficking of mitochondria into axonal and dendritic compartments is not re-established or effectively buffered, a sustained accumulation of active mitochondria in the vicinity of the nucleus may provide a source of DNA damaging ROS as well as Apaf-2. It has been suggested that hydroxyl radical production by microdialysis of hydroxyl radical generators can kill motor neurons in spinal cord (141). However, at present, it is uncertain if mitochondrial-derived ROS can trigger apoptosis of motor neurons *in vivo*.

Induced neuronal apoptosis in the adult CNS is associated with hydroxyl radical damage to DNA (16,138). Among the ROS, hydroxyl radicals are highly reactive and are thought to be genotoxic by interacting with DNA and producing DNA strand breaks and base modifications (122-124). Hydroxyl radicals are products of the transitional metal (e.g., iron)-catalyzed, Haber-Weiss- and Fenton-type reactions that use superoxide and hydrogen peroxide as substrates, respectively (123). Our recent experiments are important because they show the formation of hydroxyl radical-modified DNA during the progression of neuronal apoptosis *in vivo*.

In addition, our experiments indicate that peroxynitrite radicals are formed within motor neurons early after injury at preapoptotic stages of degeneration, based on the transient detection of intense nitrotyrosine immunoreactivity within subsets of ventral root axons and motor neuron cell bodies (16). The appearance of this intense nitrotyrosine immunoreactivity occurs prior to structural evidence for apoptosis in avulsed motor neurons. Nitric oxide synthase is induced in motor neurons after avulsion (142) and in primary cultures of embryonic motor neurons deprived of brain-derived neurotrophic factor (143). In this latter *in vitro* paradigm, motor neurons cultured in the absence of trophic factor exhibit nitrotyrosine immunoreactivity prior to the occurrence of apoptosis (143), similar to our findings *in vivo* (16). Inhibition of nitric oxide synthase reduces motor neuron loss after spinal root avulsion (144). Therefore, the accumulation of active mitochondria within neuronal cell bodies, combined

with nitric oxide induction (142), may lead to peroxynitrite formation and induction of motor neuron apoptosis *in vivo*.

Our observations in models of axotomy-induced neuronal apoptosis in the adult CNS may be important for the understanding of neuronal death in human, adult-onset neurodegenerative diseases such as ALS. Neurodegeneration in ALS has components of axotomy/target deprivation-like retrograde neuronal injury. In addition, evidence for oxidative damage has been found in postmortem brains from individuals with ALS, based on the detection of protein carbonyls, protein nitration, and DNA oxidation (126-128). Important unanswered questions regarding neuronal apoptosis in the adult CNS and in ALS center on the dependence of this process on specific molecules, including p53, Fas, Bax, and caspases. Trophic factor deprivation-induced apoptosis of motor neurons *in vitro* (108,118,143) and *in vivo* (108,118) is caspase- and Bax-dependent, as might be the case for motor neuron apoptosis in ALS (3).

## 12. Future hope for the understanding of ALS

Additional laboratory experiments are necessary to identify possible cellular and molecular causes for motor neuron apoptosis in individuals with ALS by analyzing, in post-mortem CNS tissues, proteins that function in PCD pathways. In parallel, studies need to be conducted to identify the cellular and molecular similarities and differences among motor neuron degeneration in ALS and in animal models in which motor neurons degenerate. For example, mice genetically deficient in Fas/FasL, Bax, and p53, can be used to dissect the contribution of these molecules in controlling apoptosis in motor neurons *in vivo*. Once appropriate animal models for motor neuron apoptosis have been identified and characterized, new drugs or biological agents (caspase inhibitors, antioxidants, immunosuppressants, and neurotrophic factors) can be tested for safety and for their ability to abrogate motor neuron apoptosis. The demonstration that abnormal PCD mechanisms participate in the pathogenesis of motor neuron degeneration in ALS (3), and the clarification of the molecular pathways mediating motor neuron apoptosis, should lead to the identification of alternative treatments or cures for ALS. Our recent experiments with ALS CNS tissues (3) have important therapeutic implications for patients with ALS. Manipulations that cause an elevation and specific activation of Bcl-2 or IAPs and pharmacological treatment with caspase inhibitors may delay the onset or progression of motor neuron apoptosis in patients with ALS. In this regard though, elevations in antiapoptotic proteins may not be meaningful therapeutically unless the subcellular trafficking and targeting (i.e., to mitochondria) of proteins is efficient in motor neurons.

## Acknowledgments

The assistance of Frank Barksdale is appreciated greatly. We thank Drs Carlos Portera-Cailliau, Stephen Ginsberg, Akiko Furuta, Nael Al-Abdulla, Frances Northington, and JoAnne Natale for exciting discussions and experimental contributions in this laboratory. This research was supported by grants from the U.S. Public Health Service (NS34100) and

the U.S. Army Medical Research and Materiel Command (DAMD17-99-1-9553).

## References

- Kuncl RW, Crawford TO, Rothstein JD and Drachman DB: Motor neuron diseases. In: Diseases of the Nervous System. Clinical Neurobiology. Asbury AK, McKhann GM and McDonald WI (eds). WB Saunders, Philadelphia, pp1179-1208, 1992.
- Rosen DR, Siddique T, Patterson D, Figlewicz DA, Sapp P, Hentati A, Donaldson D, Goto J, O'Regan JP, Deng H-X, Rahmani Z, Krizus A, McKenna-Yasek D, Cayabyab A, Gaston AM, Berger R, Tanzi RE, Halperin JJ, Harzfeldt B, van den Bergh R, Hung W-Y, Bird T, Deng G, Mulder DW, Smyth C, Laing NG, Soriano E, Pericak-Vance MA, Haines J, Rouleau GA, Gusella JS, Horvitz HR and Brown RH: Mutations in Cu/Zn superoxide dismutase gene are associated with familial amyotrophic lateral sclerosis. *Nature* 362: 59-62, 1993.
- Martin LJ: Neuronal death in amyotrophic lateral sclerosis is apoptosis: possible contribution of a programmed cell death mechanism. *J Neuropathol Exp Neurol* 58: 459-471, 1999.
- Deng H-X, Hentati A, Tainer JA, Iqbal Z, Cayabyab A, Hung W-Y, Getzoff ED, Hu P, Herzfeldt B, Roos RP, Warner C, Deng G, Soriano E, Smyth C, Parge HE, Ahmed A, Roses AD, Hallewell RA, Pericak-Vance MA and Siddique T: Amyotrophic lateral sclerosis and structural defects in Cu, Zn superoxide dismutase. *Science* 261: 1047-1051, 1993.
- Furuta A, Price DL, Pardo CA, Troncoso JC, Xu Z, Taniguchi N and Martin LJ: Localization of superoxide dismutases in Alzheimer's disease and Down's syndrome neocortex and hippocampus. *Am J Pathol* 146: 357-367, 1995.
- Troy CM and Shelanski ML: Down-regulation of copper/zinc superoxide dismutase causes apoptotic death in PC12 neuronal cells. *Proc Natl Acad Sci USA* 91: 6384-6387, 1994.
- Rothstein JD, Bristol LA, Hosler B, Brown RH and Kuncl RW: Chronic inhibition of superoxide dismutase produces apoptotic death of spinal neurons. *Proc Natl Acad Sci USA* 91: 4155-4159, 1994.
- Greenlund LJS, Deckwerth TL and Johnson EM: Superoxide dismutase delays neuronal apoptosis: a role for reactive oxygen species in programmed neuronal death. *Neuron* 14: 303-315, 1995.
- Borchelt DR, Lee MK, Slunt HS, Guarnieri M, Xu ZS, Wong PC, Brown RH, Price DL, Sisodia SS and Cleveland DW: Superoxide dismutase 1 with mutations linked to familial amyotrophic lateral sclerosis possesses significant activity. *Proc Natl Acad Sci USA* 91: 8292-8296, 1994.
- Rabizadeh S, Butler Gralla E, Borchelt DR, Gwinn R, Valentine JS, Sisodia S, Wong, P, Lee M, Hahn H and Bredesen DE: Mutations associated with amyotrophic lateral sclerosis convert superoxide dismutase from an antiapoptotic gene to a proapoptotic gene: studies in yeast and neural cells. *Proc Natl Acad Sci USA* 92: 3024-3028, 1995.
- Wiedau-Pazos M, Goto JJ, Rabizadeh S, Gralla EB, Roe JA, Lee MK, Valentine JS and Bredesen DE: Altered reactivity of superoxide dismutase in familial amyotrophic lateral sclerosis. *Science* 271: 515-518, 1996.
- Beckman JS, Carson M, Smith CD and Koppenol WH: ALS, SOD and peroxynitrite. *Nature* 364: 584, 1993.
- Crow JP, Ye YZ, Strong M, Kirk M, Barnes S and Beckman JS: Superoxide dismutase catalyzes nitration of tyrosines by peroxynitrite in the rod and head domains of neurofilament-L. *J Neurochem* 69: 1945-1953, 1997.
- Crow JP, Sampson JB, Zhuang Y, Thompson JA and Beckman JS: Decreased zinc affinity of amyotrophic lateral sclerosis-associated superoxide dismutase mutants leads to enhanced catalysis of tyrosine nitration by peroxynitrite. *J Neurochem* 69: 1936-1944, 1997.
- Strong MJ, Sopper MM, Crow, JP, Strong WL and Beckman JS: Nitration of the low molecular weight neurofilament is equivalent in sporadic amyotrophic lateral sclerosis and control cervical spinal cord. *Biochem Biophys Res Commun* 248: 157-164, 1998.
- Martin LJ, Kaiser A and Price AC: Motor neuron degeneration after sciatic nerve avulsion in adult rat evolves with oxidative stress and is apoptosis. *J Neurobiol* 40: 185-201, 1999.
- Gurney ME, Pu H, Chiu AY, Dal Canto MC, Polchow CY, Alexander DD, Caliendo J, Hentati A, Kwon YW, Deng H-X, Chen W, Zhai P, Sufit RL and Siddique T: Motor neuron degeneration in mice that express a human Cu, Zn superoxide dismutase mutation. *Science* 264: 1772-1775, 1994.

18. Wong PC, Pardo CA, Borchelt DR, Lee MK, Copeland NG, Jenkins NA, Sisodia SS, Cleveland DW and Price DL: An adverse property of a familial ALS-linked SOD1 mutation causes motor neuron disease characterized by vacuolar degeneration of mitochondria. *Neuron* 14: 1105-1116, 1995.
19. Dal Canto MC and Gurney ME: Development of central nervous system pathology in a murine transgenic model of human amyotrophic lateral sclerosis. *Am J Pathol* 145: 1271-1280, 1994.
20. Ginsberg SD and Martin LJ: Ultrastructural analysis of the progression of neurodegeneration in the septum following fimbria-fornix transection. *Neuroscience* 86: 1259-1272, 1998.
21. Ginsberg SD, Portera-Cailliau C and Martin LJ: Fimbria-fornix transection and excitotoxicity produce similar neurodegeneration in septum. *Neuroscience* 88: 1059-1071, 1999.
22. Kostic V, Jackson-Lewis V, de Bilbao F, Dubois-Dauphin M and Przedborski S: Bcl-2: prolonging life in a transgenic mouse model of familial amyotrophic lateral sclerosis. *Science* 277: 559-562, 1997.
23. Friedlander RM, Brown RH, Gagliardini V, Wang J and Yuan J: Inhibition of ICE slows ALS in mice. *Nature* 388: 31, 1997.
24. Portera-Cailliau C, Price DL and Martin LJ: Non-NMDA and NMDA receptor-mediated excitotoxic neuronal deaths in adult brain are morphologically distinct: further evidence for an apoptosis-necrosis continuum. *J Comp Neurol* 378: 88-104, 1997.
25. Ikonomidou C, Qin YQ, Labruyere J and Olney JW: Motor neuron degeneration induced by excitotoxin agonists has features in common with those seen in the SOD-1 transgenic mouse model of amyotrophic lateral sclerosis. *J Neuropathol Exp Neurol* 55: 211-224, 1996.
26. Martin LJ, Al-Abdulla NA, Brambrink AM, Kirsch JR, Sieber FE and Portera-Cailliau C: Neurodegeneration in excitotoxicity, global cerebral ischemia, and target deprivation: a perspective on the contributions of apoptosis and necrosis. *Brain Res Bull* 46: 281-309, 1998.
27. Olney JW: Excitatory transmitter neurotoxicity. *Neurobiol Aging* 15: 259-260, 1994.
28. Choi DW: Excitotoxic cell death. *J Neurobiol* 23: 1261-1276, 1992.
29. Chase RA, Pearson S, Nunn PB and Lantos PL: Comparative toxicities of  $\alpha$ - and  $\beta$ -N-oxalyl-L- $\alpha$ , $\beta$ -diaminopropionic acid to rat spinal cord. *Neurosci Lett* 55: 89-94, 1985.
30. Beal MF, Matson WR, Swartz KJ, Gamache PH and Bird ED: Kynurenine pathway measurements in Huntington's disease striatum: evidence for reduced formation of kynurenic acid. *J Neurochem* 55: 1327-1339, 1990.
31. Plaitakis A: Glutamate dysfunction and selective motor neuron degeneration in amyotrophic lateral sclerosis: a hypothesis. *Ann Neurol* 28: 3-8, 1990.
32. Plaitakis A, Constantakakis E and Smith J: The neuroexcitotoxic amino acids glutamate and aspartate are altered in the spinal cord and brain in amyotrophic lateral sclerosis. *Ann Neurol* 24: 446-449, 1988.
33. Rothstein JD, Tsai G, Kuncel RW, Clawson L, Cornblath DR, Drachman DB, Pestronk A, Stauch B and Coyle JT: Abnormal excitatory amino acid metabolism in amyotrophic lateral sclerosis. *Ann Neurol* 28: 18-25, 1990.
34. Rothstein JD, Kuncel RW, Chaudhry V, Clawson L, Cornblath DR, Coyle JT and Drachman DB: Excitatory amino acids in amyotrophic lateral sclerosis: an update. *Ann Neurol* 30: 224-225, 1991.
35. Camu W, Billiard M and Baldy-Moulinier MB: Fasting plasma and CSF amino acid levels in amyotrophic lateral sclerosis: a subtype analysis. *Acta Neurol Scand* 88: 51-55, 1993.
36. Malessa S, Leigh PN, Bertel O, Sluga E and Hornykiewicz O: Amyotrophic lateral sclerosis: glutamate dehydrogenase and transmitter amino acids in the spinal cord. *J Neurol Neurosurg Psychiatry* 54: 984-988, 1991.
37. Rothstein JD, Martin LJ and Kuncel RW: Decreased glutamate transport by the brain and spinal cord in amyotrophic lateral sclerosis. *N Engl J Med* 326: 1464-1468, 1992.
38. Fray AE, Ince PG, Banner SJ, Milton ID, Usher PA, Cookson MR and Shaw PJ: The expression of the glial glutamate transporter protein EAAT2 in motor neuron disease: an immunohistochemical study. *Eur J Neurosci* 10: 2481-2489, 1998.
39. Rothstein JD, van Kammen M, Levey AI, Martin LJ and Kuncel RW: Selective loss of glial glutamate transporter GLT-1 in amyotrophic lateral sclerosis. *Ann Neurol* 38: 73-84, 1995.
40. Lin CL, Bristol LA, Dykes-Hoberg M, Crawford T, Clawson L and Rothstein JD: Aberrant RNA processing in a neurodegenerative disease: the cause for absent EAAT2, a glutamate transporter, in amyotrophic lateral sclerosis. *Neuron* 20: 589-602, 1998.
41. Meyer T, Münch C, Liebau S, Fromm A, Schwalenstöcker B, Völkel H and Ludolph AC: Splicing of the glutamate transporter EAAT2: a candidate gene of amyotrophic lateral sclerosis. *J Neurol Neurosurg Psychiatry* 65: 954, 1998.
42. Nagai M, Abe K, Okamoto K and Itoyama Y: Identification of alternative splicing forms of GLT1 mRNA in the spinal cord of amyotrophic lateral sclerosis. *Neurosci Lett* 244: 165-168, 1998.
43. Bensimon G, Lacomblez L, Meininger V and the ALS/Riluzole Study Group: A controlled trial of Riluzole in amyotrophic lateral sclerosis. *N Engl J Med* 330: 585-591, 1994.
44. Gegelashvili G, Danbolt NC and Schousboe A: Neuronal soluble factors differentially regulate the expression of the GLT1 and GLAST glutamate transporters in cultured astroglia. *J Neurochem* 69: 2612-2615, 1997.
45. Martin LJ, Brambrink AM, Lehmann C, Portera-Cailliau C, Koehler R, Rothstein J and Traystman RJ: Hypoxia-ischemia causes abnormalities in glutamate transporters and death of astroglia and neurons in newborn striatum. *Ann Neurol* 42: 335-348, 1997.
46. Ginsberg SD, Rothstein JD, Price DL and Martin LJ: Fimbria-fornix transections selectively down-regulate subtypes of glutamate transporter and glutamate receptor proteins in septum and hippocampus. *J Neurochem* 67: 1208-1216, 1996.
47. Choi DW: Amyotrophic lateral sclerosis and glutamate: too much of a good thing? *N Engl J Med* 326: 1493-1495, 1992.
48. Beal MF: Does impairment in energy metabolism result in excitotoxic neuronal death in neurodegenerative illness? *Ann Neurol* 31: 119-130, 1992.
49. Trotti D, Rolfs A, Danbolt NC, Brown RH Jr and Hediger MA: SOD1 mutants linked to amyotrophic lateral sclerosis selectively inactivate a glial glutamate transporter. *Nat Neurosci* 2: 427-433, 1999.
50. Blackstone CD, Levey AI, Martin LJ, Price DL and Haganir RL: Immunological detection of glutamate receptor subtypes in human central nervous system. *Ann Neurol* 31: 680-683, 1992.
51. Martin LJ, Blackstone CD, Levey AI, Haganir RL and Price DL: AMPA glutamate receptor subunits are differentially distributed in rat brain. *Neuroscience* 53: 327-358, 1993.
52. Jakowec MW, Fox AJ, Martin LJ and Kalb RG: Quantitative and qualitative changes in AMPA receptor expression during spinal cord development. *Neuroscience* 67: 893-907, 1995.
53. Portera-Cailliau C, Price DL and Martin LJ: N-methyl-D-aspartate receptor proteins NR2A and NR2B are differentially distributed in the developing rat central nervous system as revealed by subunit-specific antibodies. *J Neurochem* 66: 692-700, 1996.
54. Brennan EM, Martin LJ, Johnston MV and Blue ME: The ontogeny of non-NMDA glutamate receptors in rat barrel field cortex. II.  $\alpha$ -AMPA and kainate receptors. *J Comp Neurol* 386: 29-45, 1997.
55. Martin LJ, Furuta A and Blackstone CD: AMPA receptor protein in developing rat brain: GluR1 expression and localization change at regional, cellular, and subcellular levels with maturation. *Neuroscience* 83: 917-928, 1998.
56. Rothstein JD, Martin LJ, Levey AI, Dykes-Hoberg M, Jin L, Wu D, Nash N and Kuncel RW: Localization of neuronal and glial glutamate transporters. *Neuron* 13: 713-725, 1994.
57. Furuta A, Rothstein JD and Martin LJ: Glutamate transporter protein subtypes are expressed differentially during rat CNS development. *J Neurosci* 17: 8363-8375, 1997.
58. Masliah E, Alford M, DeTeresa R, Mallory M and Hansen L: Deficient glutamate transport is associated with neurodegeneration in Alzheimer's disease. *Ann Neurol* 40: 759-766, 1996.
59. Li S, Mallory M, Alford M, Tanaka S and Masliah E: Glutamate transporter alterations in Alzheimer's disease are possibly associated with abnormal APP expression. *J Neuropathol Exp Neurol* 56: 901-911, 1997.
60. McBean GJ and Roberts PJ: Neurotoxicity of L-glutamate and DL-threo-3-hydroxyaspartate in the rat striatum. *J Neurochem* 44: 247-254, 1985.
61. Tanaka K, Watase K, Manabe T, Yamada K, Watanabe M, Takahashi K, Iwama H, Nishikawa T, Ichihara N, Kikuchi T, Okuyama S, Kawashima N, Hori S, Takimoto M and Wada K: Epilepsy and exacerbation of brain injury in mice lacking the glutamate transporter GLT-1. *Science* 276: 1699-1702, 1997.
62. Escarrabill J, Estopa R, Farrero E, Monasterio C and Manresa F: Long-term mechanical ventilation in amyotrophic lateral sclerosis. *Respir Med* 92: 438-441, 1998.

63. Obrenovitch TP: Amyotrophic lateral sclerosis, excitotoxicity and riluzole. *Trends Pharmacol Sci* 19: 9, 1998.
64. Seki Y, Feustel PJ, Keller RW Jr, Tranmer BI and Kimelberg HK: Inhibition of ischemia-induced glutamate release in rat striatum by dihydrokainate and an anion channel blocker. *Stroke* 30: 433-440, 1999.
65. Massieu L, Morales-Villagr n A and Tapia R: Accumulation of extracellular glutamate by inhibition of its uptake is not sufficient for inducing neuronal damage: an *in vivo* microdialysis study. *J Neurochem* 64: 2262-2272, 1995.
66. Levy LM, Lehre KP, Walaas SI, Storm-Mathisen J and Danbolt NC: Down-regulation of glial glutamate transporters after glutamatergic denervation in the rat brain. *Eur J Neurosci* 7: 2036-2041, 1995.
67. Ginsberg SD, Martin LJ and Rothstein JD: Regional deafferentation down-regulates subtypes of glutamate transporter proteins. *J Neurochem* 65: 2800-2803, 1995.
68. Kerr JFR, Wyllie AH and Currie AR: Apoptosis: a basic biological phenomenon with wide-ranging implications in tissue kinetics. *Br J Cancer* 26: 239-257, 1972.
69. Martin LJ, Portera-Cailliau C, Ginsberg SD and Al-Abdulla NA: Animal models and degenerative disorders of the human brain. *Lab Anim* 27: 18-25, 1998.
70. Portera-Cailliau C, Price DL and Martin LJ: Excitotoxic neuronal death in the immature brain is an apoptosis-necrosis morphological continuum. *J Comp Neurol* 378: 70-87, 1997.
71. Bredesen DE: Neural apoptosis. *Ann Neurol* 38: 839-851, 1995.
72. Roy N, Mahadevan MS, McLean M, Shutler G, Yaraghi Z, Farahani R, Baird S, Besner-Johnston A, Lefebvre C, Kang X, Salih M, Aubry H, Tamai K, Guan X, Ioannou P, Crawford TO, de Jong PJ, Surh L, Ikeda J-E, Korneluk RG and MacKenzie A: The gene for neuronal apoptosis inhibitory protein is partially deleted in individuals with spinal muscular atrophy. *Cell* 80: 167-178, 1995.
73. Liston P, Rpy N, Tamai K, Lefebvre C, Baird S, Cherton-Horvat G, Farahani R, McLean M, Ikeda J-E, MacKenzie A and Korneluk RG: Suppression of apoptosis in mammalian cells by NAIP and a related family of IAP genes. *Nature* 379: 349-353, 1996.
74. Lefebvre S, Burglen L, Reboullet S, Clermont O, Burlet P, Viollet L, Benichou B, Cruaud C, Millasseau P, Zeviani M, LePaslier D, Frezal J, Cohen D, Weissenbach J, Munnich A and Melki J: Identification and characterization of a spinal muscular atrophy-determining gene. *Cell* 80: 155-165, 1995.
75. Schwartz LM and Milligan CE: Cold thoughts of death: the role of ICE proteases in neuronal cell death. *Trends Neurosci* 19: 555-562, 1996.
76. Merry DE and Korsmeyer SJ: Bcl-2 gene family in the nervous system. *Annu Rev Neurosci* 20: 245-267, 1997.
77. Wolf BB and Green DR: Suicidal tendencies: apoptotic cell death by caspase family proteinases. *J Biol Chem* 274: 20049-20052, 1999.
78. Li P, Nijhawan D, Budihardjo I, Srinivasula SM, Ahmad M, Alnemri ES and Wang X: Cytochrome c and dATP-dependent formation of Apaf-1/caspase-9 complex initiates an apoptotic protease cascade. *Cell* 91: 479-489, 1997.
79. Cleveland JL and Ihle JN: Contenders in FasL/TNF death signaling. *Cell* 81: 479-482, 1995.
80. Li H, Zhu H, Xu C-J and Yuan J: Cleavage of Bid by caspase 8 mediates the mitochondrial damage in the Fas pathway of apoptosis. *Cell* 94: 491-501, 1998.
81. Inohara N, Ekhterae D, Garcia I, Carria R, Merino J, Merry A, Chen S and N   ez G: Mtd, a novel Bcl-2 family member activates apoptosis in the absence of heterodimerization with Bcl-2 and Bcl-X<sub>L</sub>. *J Biol Chem* 273: 8705-8710, 1998.
82. LaCasse EC, Baird S, Korneluk RG and MacKenzie AE: The inhibitors of apoptosis (IAPs) and their emerging role in cancer. *Oncogene* 17: 3247-3259, 1998.
83. Deveraux QL, Roy N, Stennicke HR, van Arsdalet T, Zhou Q, Srinivasula SM, Alnemri ES, Salvesen GS and Reed JC: IAPs block apoptotic events induced by caspase-8 and cytochrome c by direct inhibition of distinct caspases. *EMBO J* 17: 2215-2223, 1998.
84. Parboosing JS, Meininger V, McKenna-Yasek D, Brown RN Jr and Rouleau GA: Deletions causing spinal muscular atrophy do not predispose to amyotrophic lateral sclerosis. *Arch Neurol* 56: 710-712, 1999.
85. Zou H, Li Y, Liu X and Wang X: An Apaf-1-cytochrome c multimeric complex is a functional apoptosome that activates procaspase-9. *J Biol Chem* 274: 11549-11556, 1999.
86. Liu X, Zou H, Slaughter C and Wang X: DFF, a heterodimeric protein that functions downstream of caspase-3 to trigger DNA fragmentation during apoptosis. *Cell* 89: 175-184, 1997.
87. Kluck RM, Bossy-Wetzel E, Green DR and Newmeyer DD: The release of cytochrome c from mitochondria: a primary site for bcl-2 regulation of apoptosis. *Science* 275: 1132-1136, 1997.
88. Yang J, Liu X, Bhalla K, Kim CN, Ibrado AM, Cai J, Peng T-I, Jones DP and Wang X: Prevention of apoptosis by bcl-2: release of cytochrome c from mitochondria blocked. *Science* 275: 1129-1132, 1997.
89. Antonsson B, Conti F, Ciavatta A, Montessuit S, Lewis S, Martinou I, Bernasconi L, Bernard A, Mermod J-J, Mazzei G, Maundrell K, Gambale F, Sadoul R and Martinou J-C: Inhibition of bax channel-forming activity by bcl-2. *Science* 277: 370-372, 1997.
90. Liu X, Kim CN, Yang J, Jemmerson R and Wang X: Induction of apoptotic program in cell-free extracts: requirement for dATP and cytochrome c. *Cell* 86: 147-157, 1996.
91. Vander Heiden MG, Chandel NS, Williamson EK, Schumacker PT and Thompson CB: Bcl-X<sub>L</sub> regulates the membrane potential and volume homeostasis of mitochondria. *Cell* 91: 627-637, 1997.
92. Hu Y, Benedict MA, Wu D, Inohara N and N   ez G: Bcl-X<sub>L</sub> interacts with Apaf-1 and inhibits Apaf-1-dependent caspase-9 activation. *Proc Natl Acad Sci USA* 95: 4386-4391, 1998.
93. Song Q, Kuang Y, Dixit VM and Vincenz C: Boo, a negative regulator of cell death, interacts with Apaf-1. *EMBO J* 18: 167-178, 1999.
94. Halder S, Jena N and Croce CM: Inactivation of Bcl-2 by phosphorylation. *Proc Natl Acad Sci USA* 92: 4507-4511, 1995.
95. Wang H-G, Rapp UR and Reed JC: Bcl-2 targets the protein kinase raf-1 to mitochondria. *Cell* 87: 629-638, 1996.
96. Zha J, Harada H, Yang E, Jockel J and Korsmeyer SJ: Serine phosphorylation of death agonist Bad in response to survival factor results in binding to 14-3-3 not Bcl-X<sub>L</sub>. *Cell* 87: 619-628, 1996.
97. Yang E, Zha J, Jockel J, Boise LH, Thompson CB and Korsmeyer SJ: Bad, a heterodimeric partner for Bcl-X<sub>L</sub> and Bcl-2, displaces Bax and promotes cell death. *Cell* 80: 285-291, 1995.
98. Desagher S, Osen-Sand A, Nichols A, Eskes R, Montessuit S, Lauper S, Maundrell K, Antonsson B and Martinou J-C: Bid-induced conformational change of bax is responsible for mitochondrial cytochrome c release during apoptosis. *J Cell Biol* 144: 891-901, 1999.
99. Wyllie A: Clues in the p53 murder mystery. *Nature* 398: 237-238, 1997.
100. Miyashita T and Reed JC: Tumor suppressor p53 is a direct transcriptional activator of the human bax gene. *Cell* 80: 293-299, 1995.
101. Miyashita T, Krajewski S, Krajewska M, Wang HG, Lin HK, Liebermann DA, Hoffman B and Reed JC: Tumor suppressor p53 is a regulator of bcl-2 and bax gene expression *in vitro* and *in vivo*. *Oncogene* 9: 1799-1805, 1994.
102. Smith SH, Smith RG, Alexianu MF, Enghardt JI and Stefani E: Autoimmunity as an etiological factor in sporadic amyotrophic lateral sclerosis. In: *Advances in Neurology, Pathogenesis and Therapy of Amyotrophic Lateral Sclerosis*. Serratore GT and Munsat TL (eds). Lippincott-Raven, Philadelphia, pp47-57, 1995.
103. Smith RG, Siklos L, Alexianu ME, Engelhardt JI, Mosier DR, Colom L, Habib MA and Appel SH: Autoimmunity and ALS. *Neurology* 47 (Suppl.): S40-S45, 1996.
104. Kawamata T, Akiyama H, Yamada T and McGeer PL: Immunologic reactions in amyotrophic lateral sclerosis. *Brain and spinal cord. Am J Pathol* 140: 691-707, 1992.
105. Farlie PG, Dringen R, Rees SM, Kannourakis G and Bernard O: Bcl-2 transgene expression can protect neurons against developmental and induced cell death. *Proc Natl Acad Sci USA* 92: 4397-4401, 1995.
106. Martinou J-C, Dubois-Dauphin M, Staple JK, Rodriguez I, Frankowski H, Missotten M, Albertini P, Talbot D, Catsicas S, Pietra C and Huarte J: Overexpression of bcl-2 in transgenic mice protects neurons from naturally occurring cell death and experimental ischemia. *Neuron* 13: 1017-1030, 1994.



107. Bonfanti L, Strettoi E, Chierzi S, Cenni MC, Liu X-H, Martinou J-C, Maffei L and Rabacchi SA: Protection of retinal ganglion cells from natural and axotomy-induced cell death in neonatal transgenic mice overexpressing bcl-2. *J Neurosci* 16: 4186-4194, 1996.
108. Deckwerth TL, Elliott JL, Knudson CM, Johnson EM, Snider WD and Korsmeyer SJ: Bax is required for neuronal death after trophic factor deprivation and during development. *Neuron* 17: 401-411, 1996.
109. Kuida K, Zheng TS, Na S, Kuan C-Y, Yang D, Karasuyama H, Rakic P and Flavell RA: Decreased apoptosis in the brain and premature lethality in CPP32-deficient mice. *Nature* 384: 368-372, 1996.
110. Kuida K, Haydar TF, Kuan C-Y, Gu Y, Taya C, Karasuyama H, Su MS-S, Rakic P and Flavell RA: Reduced apoptosis and cytochrome c-mediated caspase activation in mice lacking caspase-9. *Cell* 94: 325-337, 1998.
111. Hakem R, Hakem A, Duncan GS, Henderson JT, Woo M, Soengas MS, Elia A, de la Pompa JL, Kagi D, Khoo W, Potter J, Yoshida R, Kaufman SA, Lowe SW, Penninger JM and Mak TW: Differential requirement for caspase 9 in apoptotic pathways *in vivo*. *Cell* 94: 339-352, 1998.
112. Yoshio H, Kong Y-Y, Yoshida R, Elia AJ, Hakem A, Hakem R, Penninger JM and Mak TW: Apaf1 is required for mitochondrial pathways of apoptosis and brain development. *Cell* 94: 739-750, 1998.
113. Michaelidis TM, Sendtner M, Cooper JD, Airaksinen MS, Holtmann B, Meyer M and Thoenen H: Inactivation of bcl-2 results in progressive degeneration of motoneurons, sympathetic and sensory neurons during early postnatal development. *Neuron* 17: 75-89, 1996.
114. Dubois-Dauphin M, Frankowski H, Tsujimoto Y, Huarte J and Martinou J-C: Neonatal motoneurons overexpressing the bcl-2 protooncogene in transgenic mice are protected from axotomy-induced cell death. *Proc Natl Acad Sci USA* 91: 3309-3313, 1994.
115. Deshmukh M, Vasilakos J, Deckwerth TL, Lampe PA, Shivers BD and Johnson EM: Genetic and metabolic status of NGF-deprived sympathetic neurons saved by an inhibitor of ICE family proteases. *J Cell Biol* 135: 1341-1354, 1996.
116. Gagliardini V, Fernandez P, Lee RKK, Drexler HCA, Rotello RJ, Fishman MC and Yuan J: Prevention of vertebrate neuronal death by crmA gene. *Science* 263: 826-828, 1994.
117. Kermer P, Klöcker N, Labes M and Bähr M: Inhibition of CPP-32-like proteases rescues axotomized retinal ganglion cells from secondary cell death *in vivo*. *J Neurosci* 18: 4656-4662, 1998.
118. Milligan CE, Prevett D, Yaginuma H, Homma S, Cardwell C, Fritz LC, Tomaselli KJ, Oppenheim RW and Schwartz LM: Peptide inhibitors of the ICE protease family arrest programmed cell death of motoneurons *in vivo* and *in vitro*. *Neuron* 15: 385-393, 1995.
119. Hockenbery DM, Oltvai ZN, Yin X-M, Millman CL and Korsmeyer SJ: Bcl-2 functions in an antioxidant pathway to prevent apoptosis. *Cell* 75: 241-251, 1993.
120. Ratan RR, Murphy TH and Baraban JM: Oxidative stress induces apoptosis in embryonic cortical cultures. *J Neurochem* 62: 376-379, 1994.
121. Bonfoco E, Krainc D, Ankarcrona M, Nicotera P and Lipton SA: Apoptosis and necrosis: two distinct events induced respectively by mild and intense insults with NMDA or nitric oxide/superoxide in cortical cell cultures. *Proc Natl Acad Sci USA* 92: 72162-72166, 1995.
122. Halliwell B and Gutteridge JMC: Oxygen free radicals and iron in relation to biology and medicine: some problems and concepts. *Arch Biochem Biophys* 246: 501-514, 1986.
123. Boveris A and Cadenas E: Cellular sources and steady-state levels of reactive oxygen species. In: *Oxygen, Gene Expression, and Cellular Function*. Biadasz Clerch L and Massaro DJ (eds). Marcel Dekker, New York, pp1-25, 1997.
124. Bandy B and Davison AJ: Mitochondrial mutations may increase oxidative stress: implications for carcinogenesis and aging? *Free Radic Biol Med* 8: 523-539, 1990.
125. Zamzami N, Susin SA, Marchetti P, Hirsch T, Gómez-Monterrey I, Castedo M and Kroemer G: Mitochondrial control of nuclear apoptosis. *J Exp Med* 183: 1533-1544, 1996.
126. Bradley WG and Krasin F: A new hypothesis of the etiology of amyotrophic lateral sclerosis. The DNA hypothesis. *Arch Neurol* 39: 677-680, 1982.
127. Fitzmaurice PS, Shaw IC, Kleiner HE, Miller RT, Monks TJ, Lau SS, Mitchell JD and Lynch PG: Evidence for DNA damage in amyotrophic lateral sclerosis. *Muscle Nerve* 19: 797-798, 1996.
128. Ferrante RJ, Browne SE, Shinobu LA, Bowling AC, Baik MJ, MacGarvey U, Kowall NW, Brown RH Jr and Beal MF: Evidence of increased oxidative damage in both sporadic and familial amyotrophic lateral sclerosis. *J Neurochem* 69: 2064-2074, 1997.
129. Mithal NP, Radunovic A, Figlewicz DA, McMillan TJ and Leigh PN: Cells from individuals with SOD-1 associated familial amyotrophic lateral sclerosis do not have an increased susceptibility to radiation-induced free radical production or DNA damage. *J Neurol Sci* 164: 89-92, 1999.
130. Lindahl T: Instability and decay of the primary structure of DNA. *Nature* 362: 709-715, 1993.
131. Demple B and Harrison L: Repair of oxidative damage to DNA: enzymology and biology. *Annu Rev Biochem* 63: 915-948, 1994.
132. Tandan R, Robison SH, Munzer JS and Bradley WG: Deficient DNA repair in amyotrophic lateral sclerosis cells. *J Neurol Sci* 79: 189-203, 1987.
133. Kisby GE, Milne J and Sweatt C: Evidence of reduced DNA repair in amyotrophic lateral sclerosis brain tissue. *Neuroreport* 8: 1337-1340, 1997.
134. Robison SH, Tandan R and Bradley WG: Repair of N-methylpurines in DNA from lymphocytes of patients with amyotrophic lateral sclerosis. *J Neurol Sci* 115: 201-207, 1993.
135. Olkowski ZL: Mutant AP endonuclease in patients with amyotrophic lateral sclerosis. *Neuroreport* 9: 239-242, 1998.
136. Hayward C, Colville S, Swingle RJ and Brock DJH: Molecular genetic analysis of the APEX nuclease gene in amyotrophic lateral sclerosis. *Neurology* 52: 1899-1901, 1999.
137. Al-Abdulla NA, Portera-Cailliau C and Martin LJ: Occipital cortex ablation in adult rat causes retrograde neuronal death in the lateral geniculate nucleus that resembles apoptosis. *Neuroscience* 86: 191-209, 1998.
138. Al-Abdulla NA and Martin LJ: Apoptosis of retrogradely degenerating neurons occurs in association with the accumulation of perikaryal mitochondria and oxidative damage to the nucleus. *Am J Pathol* 153: 447-456, 1998.
139. Kato T, Hirano A and Kurland LT: Asymmetric involvement of the spinal cord involving both large and small anterior horn cells in a case of familial amyotrophic lateral sclerosis. *Clin Neuropathol* 6: 67-70, 1987.
140. Munoz DG, Greene C, Perl DP and Selkoe DJ: Accumulation of phosphorylated neurofilaments in anterior horn motor neurons of amyotrophic lateral sclerosis. *J Neuropathol Exp Neurol* 47: 9-18, 1988.
141. Liu D, Yang R, Yan X and McAdoo DJ: Hydroxyl radicals generated *in vivo* kill neurons in the rat spinal cord: electrophysiological, histological, and neurochemical results. *J Neurochem* 62: 37-44, 1994.
142. Wu W: Expression of nitric oxide synthase (NOS) in injured CNS neurons as shown by NADPH diaphorase histochemistry. *Exp Neurol* 120: 153-159, 1993.
143. Estévez AG, Spear N, Manuel SM, Radi R, Henderson CE, Barbeito L and Beckman JS: Nitric oxide and superoxide contribute to motor neuron apoptosis induced by trophic factor deprivation. *J Neurosci* 18: 923-931, 1998.
144. Wu W and Li L: Inhibition of nitric oxide synthase reduces motoneuron death due to spinal root avulsion. *Neurosci Lett* 153: 121-124, 1993.

# Delayed Neurodegeneration in Neonatal Rat Thalamus after Hypoxia–Ischemia Is Apoptosis

Frances J. Northington,<sup>1</sup> Donna M. Ferriero,<sup>3</sup> Debra L. Flock,<sup>1</sup> and Lee J. Martin<sup>2</sup>

Eudowood Neonatal Pulmonary Division, Departments of <sup>1</sup>Pediatrics and <sup>2</sup>Pathology, The Johns Hopkins University School of Medicine, Baltimore, Maryland 21287, and <sup>3</sup>Departments of Neurology and Pediatrics, University of California–San Francisco, San Francisco, California 94143

Brain injury in newborns can cause deficits in motor and sensory function. In most models of neonatal brain injury, thalamic damage often occurs. Using the Rice–Vannucci model of neonatal hypoxic–ischemic brain injury, we have shown that neuronal degeneration in somatosensory thalamus is delayed in onset (~24 hr) compared with cortical and striatal injury and exhibits prominent structural features of apoptosis. In the present study, we examined whether cell death in the thalamus has molecular features of apoptosis. Fas death receptor protein expression increased rapidly after neonatal hypoxia–ischemia, in concert with cleavage of procaspase 8 to its active form. Concurrently, the levels of Bax in mitochondrial-enriched cell fractions increase, and cytochrome c accumulates in the solu-

ble fraction. Mitochondria accumulate in a perinuclear distribution by 6 hr after hypoxia–ischemia. Cytochrome oxidase subunit 1 protein levels also increase at 6 hr after hypoxia–ischemia. Increased levels of Fas death receptor, Bax, and cytochrome c, activation of caspase 8, and abnormalities in mitochondria in the thalamus significantly precede the activation of caspase 3 and the appearance of neuronal apoptosis at 24 hr. We conclude that the delayed neurodegeneration in neonatal rat ventral basal thalamus after hypoxic–ischemic injury is apoptosis mediated by death receptor activation.

**Key words:** mitochondria; neonatal brain injury; Bax; Fas death receptor; caspase; cytochrome oxidase

A large amount of investigation has focused on cytokine- and hypoxia–ischemia-mediated injury to the developing cortex and periventricular white matter as the cause of the neurodevelopmental handicaps suffered by infants who have experienced perinatal brain injury. Energy failure, free radical, cytokine, and excitatory amino acid release, and caspase-dependant cell death are known to contribute to injury in the neocortex, striatum, and periventricular white matter (McDonald et al., 1988; Barks and Silverstein, 1992; Hagan et al., 1996; Liu et al., 1996; Martin et al., 1997a, b; Back et al., 1998; Cheng et al., 1998). However, the degeneration of thalamus and other nonforebrain structures after hypoxia–ischemia is studied less frequently. Injury to somatosensory thalamus has been described in human newborns after hypoxia–ischemia (Barkovich, 1995; Roland et al., 1998) and may contribute to sensorimotor deficits in infants with perinatal brain injury and cerebral palsy. Sensorimotor deficits have been detected in neonatal rats subjected to the Rice–Vannucci model (Rice et al., 1981) of hypoxic–ischemic injury (Bona et al., 1997). A few detailed neuropathological studies of animal models have revealed injury to the developing thalamus after neonatal hypoxia–ischemia (Towfighi et al., 1991). In addition, we have demonstrated recently that injury to the thalamus occurs in a delayed manner and exhibits prominent structural features of apoptosis

when compared with the early necrotic cell death seen in the forebrain after hypoxia–ischemia (Northington et al., 2001).

The mechanisms of apoptotic neurodegeneration in the thalamus and other brain regions remote from the forebrain after neonatal hypoxia–ischemia are completely unknown. However, death receptor-activated pathways, altered mitochondrial function, and changes in expression of mitochondrial-related *bcl-2* family proteins are likely important effectors of programmed cell death in the present model of neonatal brain injury (Nelson and Silverstein, 1994; Silverstein, 1998; Felderhoff-Mueser et al., 2000). Fas death receptor protein expression is increased in hippocampus bilaterally during the 24 hr immediately after neonatal hypoxia–ischemia (Felderhoff-Mueser et al., 2000), and administration of cytokine antagonists afford neuroprotection in the present model (Liu et al., 1996). In adult models of apoptosis, mitochondrial accumulation occurs during the critical chromatolytic phase before apoptosis simultaneously with increased expression of the proapoptosis proteins Bax and Bak (Martin, 1999; Martin et al., 1999).

In this study, we investigate whether a cascade of events (including death receptor activation, alteration in the ratio of proapoptosis- and antiapoptosis-regulating proteins in mitochondria, altered mitochondrial activity and location, cytochrome c accumulation, and cleavage of caspases into active subunits) leads to apoptotic neurodegeneration in the thalamus after neonatal hypoxia–ischemia.

## MATERIALS AND METHODS

**Hypoxia–ischemia in 7-d-old rats.** The Rice–Vannucci (Rice et al., 1981) neonatal adaptation of the Levine procedure (Levine, 1960) was used to cause hypoxic–ischemic brain injury in 7-d-old (p7) rats. In brief, rat pups were anesthetized with 2.5% halothane and 15% nitrous oxide in O<sub>2</sub>. The right common carotid artery was permanently ligated (in sham

Received June 27, 2000; revised Dec. 19, 2000; accepted Dec. 21, 2000.

These studies were supported by Johns Hopkins Internal Research Grant funds (F.J.N.), a United Cerebral Palsy Grant (F.J.N.), United States Army Department of Defense Grant DAMD17-99-1-9553, and National Institutes of Health Grants AG 16282 (L.J.M.) and NS 35902 (D.M.F.). We gratefully acknowledge the expert technical assistance of Ann Sheldon, Ann Price, and George Kuck III.

Correspondence should be addressed to Dr. Frances J. Northington, Eudowood Neonatal Pulmonary Division, Department of Pediatrics, CMSC 210, Johns Hopkins Hospital, 600 North Wolfe Street, Baltimore, MD 21287. E-mail: fnorthin@welchlink.welch.jhu.edu.

Copyright © 2001 Society for Neuroscience 0270-6474/01/211931-08\$15.00/0

controls the ligature was passed around the artery and removed). After the wound was sutured, the pups recovered from anesthesia and were returned to the dam. Two hours later, pups were placed in an airtight container in a 37°C water bath through which humidified 8% O<sub>2</sub> and balance nitrogen flowed for 150 min. After hypoxia, pups were returned to the dam until death.

The animals were killed, and the brains were retrieved at 0, 1.5, 3, 6, and 24 hr after the end of hypoxia for histological analysis ( $n = 6$  for each time point) or at 3, 6, and 24 hr after the end of hypoxia for Western blotting. Because of the small size of the immature rat thalamus, three hemithalami per pooled sample were required to generate adequate tissue homogenate for immunoblot analysis. Thus tissue from 12 to 15 animals per time point were used to generate four to five pooled samples at each time point for immunoblotting. The multiple early time points were chosen because our data, as well as that of others, showed a faster progression of injury after hypoxia–ischemia in neonates as compared with adults (Towfighi et al., 1995; Martin et al., 1997a; Northington et al., 2001). Control groups consisted of sham-operated littermates ( $n = 4$ –6 for histological analysis;  $n = 4$  pooled thalami for Western blotting). Because the entire thalamus could be used to create tissue homogenates in sham controls, only eight animals were required to generate adequate tissue samples for immunoblotting. Sham controls were killed on postnatal day 7 to provide age-matched tissue for comparison of expression of apoptosis-related proteins and levels of cytochrome oxidase activity.

All animal studies received previous approval from the Animal Care and Use Committee of Johns Hopkins University School of Medicine and were performed in accordance with the National Institutes of Health *Guide for the Care and Use of Laboratory Animals* (United States Department of Health and Human Services 85-23, 1985).

**Tissue preparation.** Animals were killed with an overdose of pentobarbital (65 mg/kg, i.p.) and exsanguinated with cold 0.1 M PBS, pH 7.4, via intracardiac perfusion. Brains were perfusion fixed with 4% paraformaldehyde in PBS for 30 min at 4 ml/min. The brains were removed, post-fixed in 4% paraformaldehyde overnight, cryoprotected in 30% sucrose, and frozen in isopentane (–30°C). Sixty micrometer coronal sections were cut on a sliding microtome for cresyl violet and immunohistochemical staining.

**Immunoblotting.** Samples of thalamus were rapidly microdissected under a surgical microscope, immediately after death, and frozen on dry ice. Pooled samples (150–200 mg) were homogenized in cold 20 mM Tris-HCl, pH 7.4, containing 10% (w/v) sucrose, 20  $\mu$ g/ml aprotinin (Tray-sol), 20  $\mu$ g/ml leupeptin, 20  $\mu$ g/ml antipain, 20  $\mu$ g/ml pepstatin A, 20  $\mu$ g/ml chymostatin, 0.1 mM phenylmethylsulfonyl fluoride, 10 mM benzamide, 1 mM EDTA, and 5 mM EGTA. Crude homogenates were centrifuged at 1000  $\times$  g for 10 min. The supernatant (S1 fraction) was then centrifuged at 114,000  $\times$  g for 20 min, and the resulting supernatant (S2 soluble fraction) was collected. The pellet (P2, mitochondrial-enriched, membrane fraction) was washed in homogenization buffer (without sucrose) three times by resuspension and centrifugation at 114,000  $\times$  g for 20 min. The P2 fraction was then resuspended fully in homogenization buffer supplemented with 20% (w/v) glycerol. This subcellular fractionation protocol has been verified to be enriched in mitochondria but also contains other organelle constituents (i.e., endoplasmic reticulum and Golgi apparatus) (Martin et al., 2000). Protein concentrations were measured by a Bio-Rad (Hercules, CA) protein assay with bovine serum albumin as a standard.

Samples of membrane or soluble proteins were subjected to SDS-PAGE and electroeluted onto nitrocellulose membranes. The reliability of sample loading and protein transfer was evaluated by staining nitrocellulose membranes with Ponceau S before immunoblotting and by quantification of Coomassie-stained gels and Ponceau-stained blots with OD. Blots were blocked with 2.5% nonfat dry milk with 0.1% Tween 20 in 50 mM Tris-buffered saline, pH 7.4, and incubated overnight at 4°C with antibody. After primary incubation, blots were washed, incubated with peroxidase-conjugated secondary antibodies (0.2  $\mu$ g/ml), and developed with enhanced chemiluminescence. To quantify cell death protein immunoreactivity, films were scanned using Adobe Photoshop, and OD was performed with IP Lab Gel H software. The OD of the corresponding lanes in Coomassie-stained gels or Ponceau-stained blots was used to correct the OD of the cell death protein immunoreactivity for differences in protein loading. Protein levels are thus expressed as relative OD measurements compared with control lanes in the same blot.

**Antibodies.** Anti-Fas death receptor antibody (Santa Cruz Biotechnology, Santa Cruz, CA) is a rabbit polyclonal antibody generated against an epitope mapping to the C terminal of human Fas and is noncross-reactive

with other tumor necrosis factor receptor (TNFR) type-1 receptors. It recognizes a single band at 45 kDa and higher molecular weight bands after SDS-PAGE. Jurkat cells known to express high levels of the Fas death receptor were used as a positive control. Anti-caspase 8 antibody (Santa Cruz Biotechnology) is a rabbit polyclonal antibody raised against a recombinant protein corresponding to amino acids 217–350 of human caspase 8. Anti-Bax (Upstate Biotechnology, Lake Placid, NY) and anti-Bcl-2 antibodies (Santa Cruz Biotechnology) are affinity-purified rabbit polyclonal antibodies generated against a peptide corresponding to amino acids 1–21 of human Bax and a peptide mapping at the N terminal of human Bcl-2, respectively. Anti-Bax antibody recognizes a single 23 kDa band, a faint band at 18.5 kDa representing the cleaved form of Bax, and several less intense high-molecular weight bands in P2 protein fractions. Anti-Bcl-2 antibody recognizes a band at 26 kDa and several less intense high-molecular weight bands in P2 protein fractions. A second rabbit polyclonal anti-Bax antibody (Santa Cruz Biotechnology) generated against a peptide homologous to amino acids 11–30 of human Bax gave results identical to those of the Upstate Biotechnology antibody. Because these proteins were fractionated in denaturing gels, it is unlikely that the high-molecular weight bands represent various Bax and Bcl-2 homodimers and heterodimers. Anti-cytochrome c antibody (Santa Cruz Biotechnology) is a rabbit polyclonal antibody directed against amino acids 1–104 of full-length horse cytochrome c. It recognizes a band at 12–15 kDa. Anti-cytochrome oxidase subunit 1 (anti-COX1) antibody (Molecular Probes, Eugene, OR) is a mouse monoclonal antibody generated against subunit 1 of human cytochrome oxidase. The antibody recognizes only a single band of ~35 kDa in nonboiled P2 protein samples subjected to SDS-PAGE. Anti-caspase 3 antibody (Santa Cruz Biotechnology) is a rabbit polyclonal antibody generated against amino acids 1–277 of full-length human caspase-3, and it recognizes the 32 kDa proenzyme with an intense band of immunoreactivity and the 12, 17, and 20 kDa active fragments with less intense single bands. Cleaved caspase 3 antibody (Cell Signaling Technology, Beverly, MA) is a rabbit polyclonal antibody generated against a synthetic peptide corresponding to residues surrounding the cleavage site of human caspase 3.

**Cytochrome oxidase histochemistry.** To identify the levels of oxidative metabolism and intracellular distribution of oxidatively active mitochondria, we used the cytochrome oxidase histochemical method of Wong-Riley (1979, 1989) as described previously for our laboratory (Martin et al., 1997a). Briefly, brain sections from control and hypoxic–ischemic rat pups were exposed to the assay simultaneously. The enzymatic reaction medium was prepared immediately before each experiment and consisted of 100 mM phosphate buffer, pH 7.4, 0.1% horse heart cytochrome c (Sigma, St. Louis, MO), 117 mM sucrose, and 1.4 mM diaminobenzidine tetrahydrochloride. In this histochemical reaction, *in situ* cytochrome oxidase catalyzes the transfer of electrons (donated by diaminobenzidine) from cytochrome c, provided as substrate, to O<sub>2</sub> to form H<sub>2</sub>O. The donation of electrons from diaminobenzidine is a chromogenic reaction that yields the formation of an insoluble precipitate in the vicinity of cytochrome oxidase activity, thus revealing both the location of the mitochondria and the relative metabolic activity of cytochrome oxidase (Wong-Riley, 1979). Sections were incubated for 2.5 hr at 37°C in a Dubnoff metabolic shaker incubator. After the reaction, sections were rinsed in phosphate buffer, mounted on glass slides, and coverslipped.

**Statistical analysis.** To quantify changes in the expression of Fas death receptor protein, mitochondrial apoptosis-regulating proteins, COX1 protein, and caspase 8 and 3 active fragments, protein expression was corrected for loading differences and then expressed as a percent of control. In some blots, two different controls were used, and the average optical density of the two bands was used for percent control calculations. Mean and SD for protein expression in tissue obtained at similar time points were calculated, and ANOVA was used to compare differences in protein expression over time. *Post hoc* testing for differences in expression at 3, 6, and 24 hr was performed with Fisher's analysis. A *p* value of <0.05 was used to determine significance.

## RESULTS

In the ipsilateral thalamus at 24 hr after neonatal hypoxia–ischemia, many degenerating neurons display light microscopic features of apoptosis (Fig. 1*B*, arrows) (Northington et al., 2001). This contrasts with the normal morphology of thalamic neurons from sham controls (Fig. 1*A*).





**Figure 1.** Thalamic neurons die by apoptosis after neonatal hypoxia-ischemia. *A, B*, Compared with sham controls (*A*), neurons at 24 hr after hypoxia-ischemia (*B*) contain many apoptotic profiles as seen in cresyl violet-stained sections of the ventral basal thalamus (arrows).

### Fas receptor expression is induced in thalamus rapidly after neonatal hypoxia-ischemia

By immunoblotting, Fas death receptor protein expression is increased in the diencephalon after neonatal hypoxia-ischemia (Fig. 2). In membrane protein fractions of newborn rat thalamus, Fas was detected at 45 kDa, corresponding to the known molecular weight of Fas death receptor protein in Jurkat cells. Jurkat cells were chosen as a positive control because they are known to express high levels of Fas death receptor (Felderhoff-Mueser et al., 2000). A comparison of samples from sham-operated controls and p7 rat pups at 3, 6, and 24 hr after hypoxia-ischemia revealed a significant ( $p < 0.05$ ) increase in Fas levels after hypoxia-ischemia (Fig. 2) in the rat thalamus. This increase occurred as early as 3 hr after hypoxia-ischemia. The increase in Fas death receptor was not caused by a generalized increase in similar cytokine receptor expression because expression of the closely related TNF receptor 1 did not change in response to neonatal hypoxia-ischemia (Fig. 2).

### Caspase 8 is cleaved to its active subunits after neonatal hypoxia-ischemia

Procaspase 8 undergoes cleavage and activation in cell culture model systems of apoptosis (Dragovich et al., 1998; Nagata, 1999a,b). Procaspase 8 (54–55 kDa) is cleaved to its 30 and 18 kDa subunits in soluble protein from ipsilateral thalamus after neonatal hypoxia-ischemia (Fig. 3). The levels of procaspase 8 in soluble fractions decrease as the expression of cleaved subunits increases after hypoxia-ischemia (Fig. 3). Jurkat cells, which are

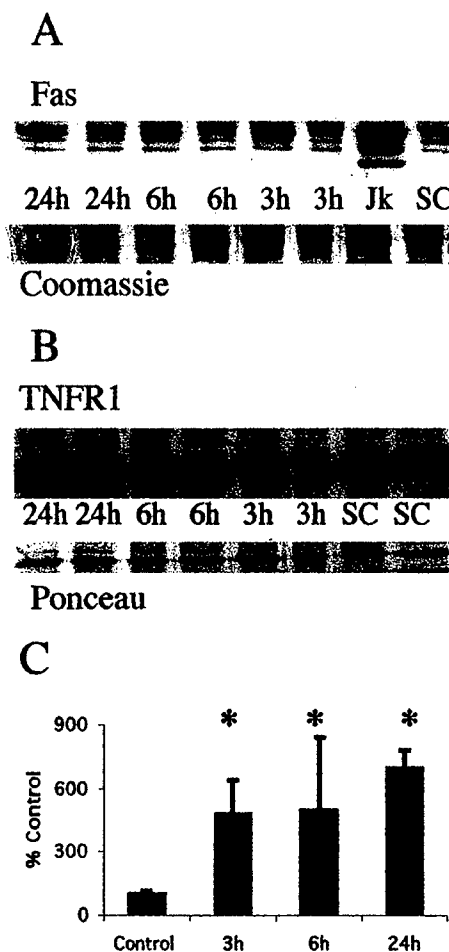


**Figure 2.** Fas death receptor protein levels increase in the thalamus after neonatal hypoxia-ischemia. *A, Top*, Immunoblot showing increased Fas death receptor protein in membrane fractions from thalamic homogenates obtained 3, 6, and 24 hr after neonatal hypoxia-ischemia compared with noninjured control samples. Jurkat cell lysates were used as a positive control, because they express high levels of Fas as detected at 45 kDa. The corresponding 45 kDa band in controls and injured thalamic samples was used for quantification. *Bottom*, The corresponding Coomassie-stained gel. *B, Top*, Immunoblot showing no change in TNFR1 death receptor protein in membrane fractions from thalamic homogenates obtained 3, 6, and 24 hr after neonatal hypoxia-ischemia compared with noninjured control samples. *Bottom*, The corresponding Ponceau-stained blot. For *A* and *B* each lane represents a pooled sample of thalamus from three animals at the indicated time point (i.e., sham control and 3, 6, or 24 hr after hypoxia-ischemia). *C*, Graph representing changes in Fas death receptor protein levels in the thalamus over time after neonatal hypoxia-ischemia. Results are shown as the mean  $\pm$  SD of four to five pooled samples per time point (\* $p < 0.05$  compared with control). *Jk*, Jurkat cell lysates; *SC*, sham control.

highly sensitive to Fas-mediated apoptosis, express both procaspase 8 and the active subunits (Fig. 3).

A potential target of Fas- and caspase 8-mediated apoptosis is the Bcl-2 family protein Bid that has been shown to cause cytochrome c release and subsequent apoptosis (Li et al., 1998). We found no evidence of Bid cleavage in either soluble or mitochondrial-enriched fractions (data not shown).

### Ratio of mitochondrial apoptosis-regulating proteins is altered rapidly after hypoxia-ischemia in the thalamus before the appearance of prominent apoptosis

After neonatal hypoxia-ischemia, levels of the proapoptosis protein Bax rapidly increase in mitochondrial-enriched fractions of

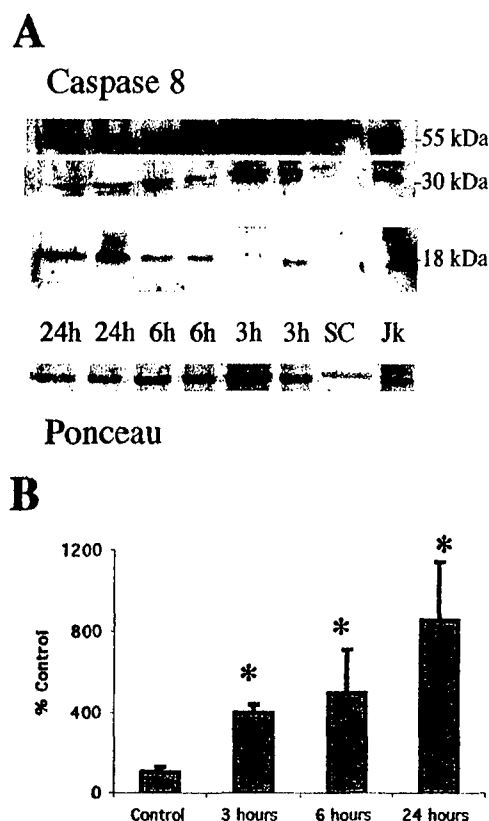


**Figure 3.** Procaspase 8 is cleaved to active fragments in the thalamus after neonatal hypoxia–ischemia. *A*, Immunoblot showing that procaspase 8 (54–55 kDa) levels decrease concurrently with an increase in the levels of the 30 and 18 kDa active fragments of caspase 8 in cytosolic fractions from the thalamus at 3, 6, and 24 hr after neonatal hypoxia–ischemia. There is a progressive increase in expression of the active subunits during the first 24 hr after hypoxia–ischemia compared with controls (SC). Anti-caspase 8 antibody also reacts strongly with a 55, 30, and 18 kDa protein in *Jk* cells consistent with the proenzyme and active fragment forms of caspase 8. *Bottom*, The corresponding Ponceau-stained blot. Each lane represents a pooled sample of thalamus from three animals at the indicated time point (i.e., sham control and 3, 6, or 24 hr after hypoxia–ischemia). *B*, Graph representing changes in abundance of the 18 kDa active subunit of caspase 8 in the thalamus over time after neonatal hypoxia–ischemia. After correcting for protein-loading differences and comparing with control, results are shown as the mean  $\pm$  SD of four to five pooled samples per time point (\* $p$  < 0.05 compared with control).

thalamus (Fig. 4*A*). Additionally, at 24 hr there is faint immunoreactivity of an 18 kDa Bax band (Fig. 4*A*) consistent with a cleaved fragment of Bax reported also to have potent proapoptosis activity (Wood and Newcomb, 2000). This increase in Bax protein, within the mitochondrial fraction, occurs without a concomitant change in the level of the antiapoptosis Bcl-2 protein in the mitochondrial fraction within the same time period (Fig. 4*B*). The increase in expression of Bax and stable expression of Bcl-2 proteins result in a marked shift in protein abundance in favor of proapoptosis Bax (Fig. 4*C*). A significant change in the relative abundance of Bax and Bcl-2 is evident as early as 3 hr after neonatal hypoxia–ischemia.

#### Cytochrome c rapidly accumulates in the soluble fraction of thalamus after neonatal hypoxia–ischemia

Cytochrome c levels increase in the soluble fraction as early as 3 hr after neonatal hypoxia–ischemia (Fig. 5*A*). This increase is coincident with the appearance of cleaved caspase-8 and before the increase in expression of the 12 kDa subunit of caspase 3. The

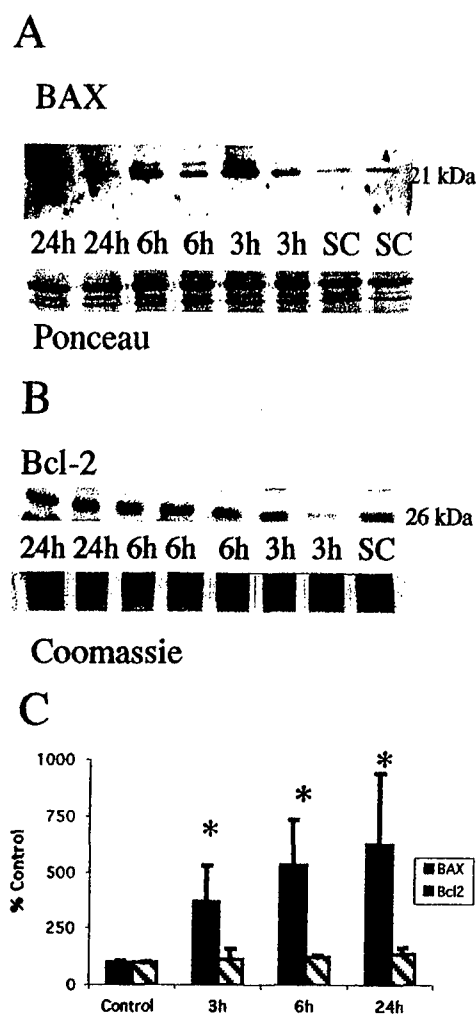


**Figure 4.** Neonatal hypoxia–ischemia causes an elevation in proapoptosis Bax protein levels in the mitochondrial fraction but does not alter levels of antiapoptosis Bcl-2. *A*, *Top*, Immunoblot shows increased Bax protein levels in mitochondrial membrane fractions from the thalamus from homogenates obtained 3, 6, and 24 hr after neonatal hypoxia–ischemia compared with noninjured control samples (SC). Anti-Bax antibody recognizes the expected 21 kDa band corresponding to Bax protein. *Bottom*, The corresponding Ponceau-stained blot is shown. Each lane represents a pooled sample of thalamus from three animals at the indicated time point (i.e., sham control and 3, 6, or 24 hr after hypoxia–ischemia). *B*, In comparison Bcl-2 protein expression is not changed in mitochondrial membrane fractions from thalamus homogenates obtained 3, 6, and 24 hr after neonatal hypoxia–ischemia compared with noninjured control samples (SC). Anti-Bcl-2 antibody recognizes the expected 26 kDa band corresponding to Bcl-2 protein. *Bottom*, The corresponding Coomassie-stained gel is shown. *C*, Graph represents alteration in relative amounts of Bax and Bcl-2 protein in the mitochondrial membrane fraction in the thalamus over time after neonatal hypoxia–ischemia. By 3 hr, there is a significant shift in the Bax/Bcl-2 ratio favoring proapoptosis Bax. After correcting for protein-loading differences and comparing with control, results are shown as the mean  $\pm$  SD of four to five pooled samples per time point (\* $p$  < 0.05 compared with control).

initial increase in the amount of cytochrome c in the soluble fraction at 3 hr is sustained at 6 and 24 hr after neonatal hypoxia–ischemia (Fig. 5*B*).

#### Caspase-3 is cleaved into its active subunits at 24 hr after neonatal hypoxia–ischemia in the thalamus

Caspases 3 and 8 are primary targets of death receptor-mediated apoptosis cascades (Nagata, 1999b; Yamada et al., 1999). When

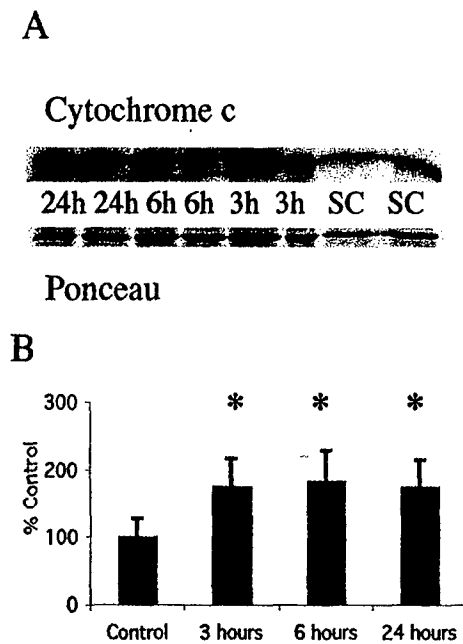


**Figure 5.** Cytochrome c accumulates in the soluble fraction in the thalamus after neonatal hypoxia-ischemia. *A, Top*, Immunoblot showing increased cytochrome c protein in soluble fractions from thalamic homogenates obtained 3, 6, and 24 hr after neonatal hypoxia-ischemia compared with noninjured control samples (SC). *Bottom*, The corresponding Ponceau-stained blot. Each lane represents a pooled sample of thalamus from three animals at the indicated time point (i.e., sham control and 3, 6, or 24 hr after hypoxia-ischemia). *B*, Graph showing the accumulation of cytochrome c in the thalamus over time after neonatal hypoxia-ischemia. After correcting for protein-loading differences and comparing with control, results are shown as the mean  $\pm$  SD of four to five pooled samples per time point (\* $p$  < 0.05 compared with control).

cleaved from its 32 kDa proenzyme form, the active 12, 17, and 20 kDa fragments have a central role in activating DNA fragmentation and other irreversible steps in apoptosis (Du et al., 1997). Caspase 3 is cleaved to its active forms in the thalamus after neonatal hypoxia-ischemia (Fig. 6*A*). Interestingly this activation is found only at 24 hr after hypoxia-ischemia (Fig. 6*B*). This result was confirmed using both the Santa Cruz Biotechnology anti-caspase 3 antibody that recognizes procaspase 3 and the active fragments and an antibody against the 17 kDa cleaved caspase 3 fragment.

#### Mitochondria accumulate at perinuclear locations in thalamic neurons after neonatal hypoxia-ischemia

Using a histochemical detection method for cytochrome oxidase activity to identify mitochondria, we found that neurons in the ventral basal thalamus, after neonatal hypoxia-ischemia, accumulate mitochondria (Fig. 7). These changes occur before the appearance of a significant number of apoptotic profiles at 24 hr (Northington et al., 2001). In normal neurons, cytochrome oxidase activity is evenly distributed throughout the cell soma in ventral basal thalamic neurons (Fig. 7*A*). In contrast, by 3–6 hr after neonatal hypoxia-ischemia, mitochondria within neurons in the ipsilateral ventral basal thalamus exhibit intense cytochrome oxidase activity and form prominent perinuclear aggregates of mitochondria (Fig. 7*B*). These changes are most prominent in neurons in the chromatolytic stage of early neuronal apoptosis (Fig. 7*C*, cytochrome oxidase histochemistry and cresyl violet counterstaining) according to a recently proposed staging scheme for apoptosis of neurons (Al-Abdulla and Martin, 1998; Al-

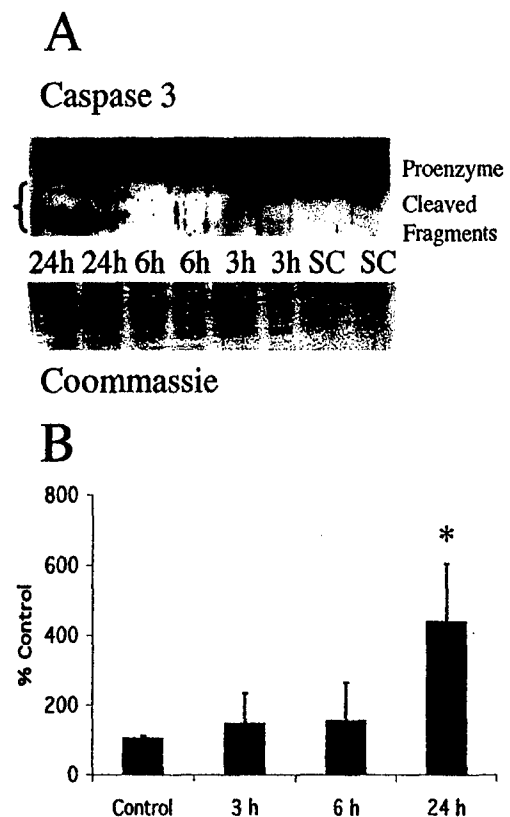


**Figure 6.** Cleavage of procaspase 3 to active fragments occurs at 24 hr after neonatal hypoxia-ischemia. *A, Top*, Immunoblot shows levels of 32 kDa procaspase 3 and its lower molecular weight cleavage products in thalamus cytosolic fractions from homogenates obtained 3, 6, and 24 hr after neonatal hypoxia-ischemia compared with noninjured control samples (SC). *Bottom*, The corresponding Coomassie-stained blot is shown. Each lane represents a pooled sample of thalamus from three animals at the indicated time point (i.e., sham control and 3, 6, or 24 hr after hypoxia-ischemia). *B*, Graph represents change in expression of the 12 kDa cleavage product in the thalamus over time after neonatal hypoxia-ischemia. Not until 24 hr is there a significant increase in the expression of the 12 kDa fragment. After correcting for protein-loading differences and comparing with control, results are shown as the mean  $\pm$  SD of four to five pooled samples per time point (\* $p$  < 0.05 compared with control).

Abdulla et al., 1998; Martin et al., 1999). In these cells, dense cytochrome oxidase-positive aggregates cluster adjacent to peripherally displaced nuclei. By 24 hr, cells in late phases of apoptosis with tightly condensed chromatin aggregates have lost or are losing immunoreactivity for cytochrome oxidase (Fig. 7*D*, cytochrome oxidase histochemistry and cresyl violet counterstaining).

The accumulation of mitochondria in the thalamus after neonatal hypoxia-ischemia was confirmed indirectly by immunoblotting. By immunoblotting, levels of COX1 increased after neonatal hypoxia-ischemia (Fig. 8). Expression of this inner mitochondrial membrane protein increases in the thalamus (Fig. 8*A*). In the thalamus, a significant increase in expression of COX1 is evident at 6 hr after hypoxia-ischemia (Fig. 8*B*) coincident with the peak of cytochrome oxidase activity in neurons in early phases of apoptotic neurodegeneration (Fig. 7*C*).

#### DISCUSSION

We found previously that neuronal degeneration in the neonatal thalamus after hypoxia-ischemia is apoptosis (Northington et al., 2001). In this study, we explored the mechanisms and conclude

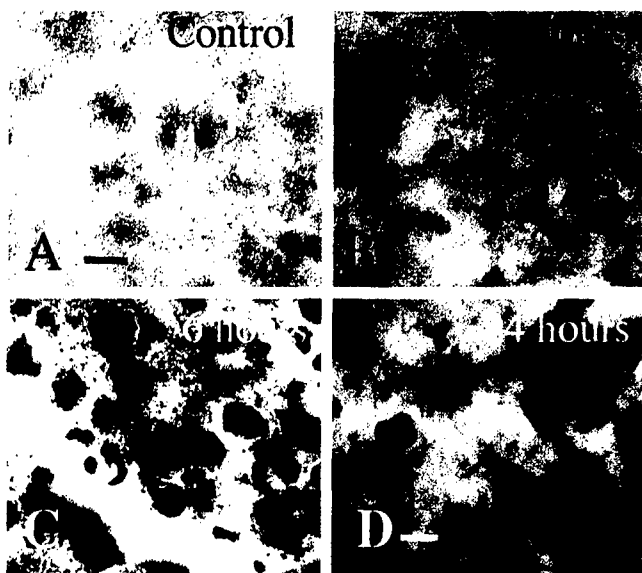


**Figure 7.** Mitochondria accumulate in a perinuclear location in ventral basal thalamic neurons after neonatal hypoxia–ischemia. Histochemistry for cytochrome oxidase activity in the thalamus after neonatal hypoxia–ischemia shows intense cytochrome oxidase activity in mitochondria and alteration in appearance and intracellular location of mitochondria after neonatal hypoxia–ischemia. At 6 hr, mitochondria are densely immunoreactive for cytochrome oxidase, assuming a punctate appearance and clustering near nuclei that are in the chromatolytic phase of apoptosis (*B*, *C*, cytochrome oxidase histochemistry and cytochrome oxidase histochemistry counterstained with cresyl violet, respectively). By 24 hr (*D*), cytochrome oxidase immunoreactivity is dissipating in thalamic neurons undergoing late stages of apoptotic degeneration. Three cells with densely condensed chromatin are shown with variable but decreasing levels of cytochrome oxidase activity. Scale bars: *A*–*C*, 12  $\mu$ m; *D*, 6  $\mu$ m.

that delayed neuronal degeneration in neonatal rat thalamus after hypoxia–ischemia has biochemical and molecular features of apoptosis. The findings that support this conclusion are (1) increased Fas death receptor levels, (2) an alteration in the levels of Bax and Bcl-2 favoring apoptosis-promoting Bax, (3) intracellular redistribution of active mitochondria, (4) accumulation of soluble cytochrome c, and (5) cleavage of caspases 8 and 3 to active forms. This cascade of biochemical and molecular events is consistent with Fas-mediated, mitochondrial-amplified, apoptosis as a major mechanism of delayed neurodegeneration after neonatal hypoxia–ischemia.

Thalamic damage after hypoxia–ischemia in newborns has long been recognized and is particularly important in infants with extrapyramidal cerebral palsy (Malamud, 1950; Volpe, 1995; Roland et al., 1998). Human neuroimaging and neuropathological studies have revealed that the thalamus is among the selectively vulnerable brain regions in the human newborn (Yokochi et al., 1991; Barkovich, 1995; Roland et al., 1998). Despite recognition of injury to the thalamus in children with cerebral palsy, the contribution of delayed injury and injury to nonforebrain regions to the development of cerebral palsy has been less well studied. The ventral basal thalamus contains afferent and efferent connections to the ipsilateral cortex and functions prominently in sensorimotor integration (Erzurumlu and Jhaveri, 1990). Injury to these circuits interrupts cortical sensory function and the integration of sensory information into volitional movement (White, 1989). Damage to motor relay nuclei in the thalamus may lead to movement disorders such as ataxia or dystonia (White, 1989) and when this injury occurs in the immature brain may contribute to

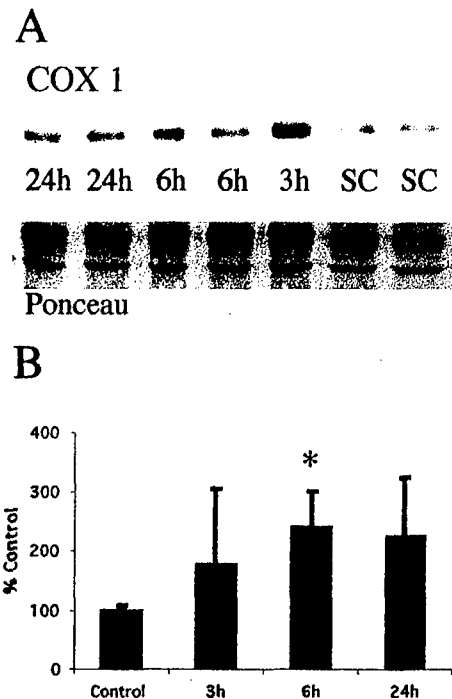


**Figure 8.** COX1 protein increases in thalamic mitochondrial protein fractions coincident with mitochondrial accumulation after neonatal hypoxia–ischemia. *A*, Top, Immunoblot shows an increase in COX1 protein in mitochondria-enriched membrane fractions from the thalamus from homogenates obtained 3, 6, and 24 hr after neonatal hypoxia–ischemia compared with noninjured control samples (*SC*). Bottom, The corresponding Ponceau-stained blot is shown. Each lane represents a pooled sample of thalamus from three animals at the indicated time point (i.e., sham control and 3, 6, or 24 hr after hypoxia–ischemia). *B*, Graph represents changes in COX1 protein levels in the thalamus over time after neonatal hypoxia–ischemia. The maximal increase at 6 hr corresponds nicely with the peak in mitochondrial accumulation seen at 6 hr in Figure 7C. After correcting for protein-loading differences and comparing with control, results are shown as the mean  $\pm$  SD of four to five pooled samples per time point (\* $p < 0.05$  compared with control).

the motor and sensory handicaps suffered by children with cerebral palsy.

In the model of neonatal brain injury used in these studies, the ipsilateral forebrain is the most vulnerable region and clearly represents the ischemic core of the lesion (Rice et al., 1981). However, the thalamus is also damaged in this and most other models of neonatal brain injury (present data) (Myers, 1975; Towfighi et al., 1991, 1995; Martin et al., 1997a; Northington et al., 2001). We postulated that this thalamic injury is apoptosis. We identified increased Fas death receptor protein levels in the ventral basal thalamus after neonatal hypoxia–ischemia. This observation suggests an additional link between cytokine- and hypoxia–ischemia-mediated neonatal brain injury. Previous studies have demonstrated activation of interleukin (IL) (Szafarski et al., 1995) neuroprotection with cytokine antagonists and in the absence of IL-1 $\beta$ -converting enzyme (Liu et al., 1996, 1999). The mechanism of hypoxia–ischemia-induced, cytokine-mediated cell death in the developing brain has not been clearly defined. The present study demonstrates that hypoxia–ischemia induces a cytokine death receptor that functions in apoptosis (Nagata, 1999b). Although we have not shown directly that Fas is induced in thalamic neurons, the rapid induction (by 3 hr) and the sustained elevation over the relevant time preceding thalamic neu-

ronal apoptosis make Fas death receptor induction unlikely to be the result of inflammation.

An elevation in Fas death receptor is a link to multiple pathways of cell death. Fas is a member of the TNFR family. Oligomerization of Fas death receptor and recruitment of FADD/MORT1 and procaspase 8 create the death-inducing signal complex (DISC). DISC is a potent apoptosis stimulus in multiple cell culture models. When procaspase 8 is bound by the DISC, autocleavage to its active fragments occurs. Cleaved caspase 8 then acts directly and indirectly to cleave caspase 3, depending on cell type and injury stimulus (Dragovich et al., 1998; Nagata, 1999a,b). Cleavage of caspase 3 is generally considered one of the irreversible steps immediately responsible for the execution of apoptosis in which the cell develops the morphological features recognizable as late-stage apoptosis (Petit et al., 1996). Our data demonstrate early Fas death receptor elevation and early and progressive cleavage of caspase 8 to its active form, followed by delayed caspase 3 cleavage just at the time of appearance of significant apoptosis in the thalamus after neonatal hypoxia-ischemia. This change is selective for Fas because TNFR1 was not changed. We have not yet shown activation of caspase 8 and caspase 3 specifically in thalamic neurons because of the lack of specific reagents. Fas death receptor protein and downstream caspase 3 cleavage likely bracket an important signaling cascade for apoptotic neurodegeneration in the thalamus.

Direct caspase 8 cleavage of caspase 3 is the original model of Fas-mediated apoptosis signaling (Dragovich et al., 1998); however mitochondrial and mitochondrial apoptosis-regulating proteins of the *bcl-2* family are now known to amplify cell death signals greatly (Susin et al., 1997). Bid, a cytosolic protein with homology to the BH3 domain of the Bcl-2 family, is cleaved in several models of Fas-mediated apoptosis and causes cytochrome c release from the mitochondria (Susin et al., 1997; Nagata, 1999a). We did not find evidence of Bid cleavage in the present model. However, we did find cytochrome c accumulation in the soluble fraction. Most of the *bcl-2* family of proteins that regulate the rate of programmed cell death are normally present within mitochondrial membranes. Several *in vivo* and *in vitro* systems have shown the ratio of the proapoptosis protein Bax and the antiapoptosis proteins Bcl-2 and Bcl-x(l) to be critical in determining cell survival (Krajewski et al., 1995; Vekrellis et al., 1997; Isenmann et al., 1998; Antonawich et al., 1999; Martin, 1999; Shimizu et al., 1999; Almeida et al., 2000).

We find a marked alteration in the balance of proapoptosis and antiapoptosis *bcl-2* proteins in the P2 fraction of thalamus after hypoxia-ischemia. This accumulation of Bax in the mitochondrial-enriched fraction occurs before caspase 3 cleavage and the appearance of large numbers of apoptotic profiles (present data) (Northington et al., 2001). A fourfold increase in the amount of proapoptosis protein Bax in the mitochondrial-enriched fraction was detected by 3 hr after injury, whereas the amount of Bcl-2 in the mitochondria is not changed during the first 24 hr after hypoxia-ischemia. These changes in the relative ratio of Bax to Bcl-2 favors the formation of Bax homodimers, the configuration in which Bax exerts its proapoptosis activity (Gross et al., 1998). Bax normally exists as a cytosolic protein and is translocated to the mitochondria after ligation of Fas receptor. This translocation is inhibited by Bcl-2 (Murphy et al., 2000). The present data suggest active mitochondrial translocation of Bax greatly in excess of the steady-state amount of Bcl-2. This is consistent with a strong death signal and may participate in mitochondrial amplification of Fas-mediated apoptosis. Cleavage of Bax to an 18 kDa

isoform also enhances its cell death potency (Wood and Newcomb, 2000). Although neither antibody used in the present study was designed to detect the 18 kDa isoform, there is weak expression of an 18 kDa Bax band in the diencephalon at 24 hr after neonatal hypoxia-ischemia. The late appearance of this isoform in mitochondrial-enriched fractions is consistent with published reports of calpain-mediated Bax cleavage after translocation of Bax to the mitochondria (Wood and Newcomb, 1999).

Release of cytochrome c and changes in mitochondrial morphology and membrane potential and function precede caspase 3 activation in *in vitro* model systems (Zamzami et al., 1996; Vander Heiden et al., 1997). Cytochrome c has been identified as APAF2, and cytochrome c release is the immediate upstream event preceding caspase 3 cleavage and the execution phase of apoptosis (Susin et al., 1999). Our data show that cytochrome c accumulates in the soluble fraction of thalamus, in concert with caspase 8 cleavage and an altered Bax/Bcl-2 ratio and before the appearance of large amounts of caspase 3 cleavage. In axotomy models of neuronal apoptosis, mitochondrial trafficking is altered with perinuclear accumulation of mitochondria in neurons as they undergo apoptosis (Al-Abdulla and Martin, 1998; Martin et al., 1999), a finding very similar to that of the present study. These previous *in vitro* and *in vivo* observations support our conclusions described here. Within 3–6 hr after neonatal hypoxia-ischemia, neurons in the ventral basal thalamus exhibit marked accumulation of mitochondria (as revealed by intense cytochrome oxidase activity) and simultaneously display altered morphology. The mitochondria assume a prominent punctate appearance and concentrate in a perinuclear location. As thalamic neurons enter late stages of apoptosis, the cytoplasm becomes progressively devoid of COX activity. These data are consistent with immunoblotting for cytochrome oxidase subunit 1 protein, which shows maximal levels at 6 hr after neonatal hypoxia-ischemia in the thalamus. Taken together these data provide evidence of the participation of mitochondria in thalamic neurodegeneration after neonatal hypoxia-ischemia.

In summary, these experiments provide the first evidence of the presence of crucial components of Fas-mediated, mitochondrial-amplified, apoptosis in the thalamus after neonatal brain injury. These findings are important for the further understanding of the mechanisms of neuronal apoptosis in the immature brain. Eventually, these studies may be important for development of appropriately timed and targeted therapies for the protection of the neonatal brain and rescue of neurons after hypoxic-ischemic insults.

## REFERENCES

- Al-Abdulla NA, Martin LJ (1998) Apoptosis of retrogradely degenerating neurons occurs in association with the accumulation of perikaryal mitochondria and oxidative damage to the nucleus. *Am J Pathol* 153:447–456.
- Al-Abdulla NA, Portera-Cailliau C, Martin LJ (1998) Occipital cortex ablation in adult rat causes retrograde neuronal death in the lateral geniculate nucleus that resembles apoptosis. *Neuroscience* 86:191–209.
- Almeida OF, Conde GL, Crochemore C, Demeneix BA, Fischer D, Hassan AH, Meyer M, Holsboer F, Michaelidis TM (2000) Subtle shifts in the ratio between pro- and antiapoptotic molecules after activation of corticosteroid receptors decide neuronal fate. *FASEB J* 14:779–790.
- Antonawich FJ, Federoff HJ, Davis JN (1999) BCL-2 transduction, using a herpes simplex virus amplicon, protects hippocampal neurons from transient global ischemia. *Exp Neurol* 156:130–137.
- Back SA, Li Y, Gan X, Rosenberg PA, Volpe JJ (1998) Maturation-dependent vulnerability of oligodendrocytes to oxidative stress-induced death caused by glutathione depletion. *J Neurosci* 18:6241–6253.
- Barkovich A (1995) Profound asphyxia in the premature infant: image findings. *AJNR Am J Neuroradiol* 95:1837–1846.
- Barks JD, Silverstein FS (1992) Excitatory amino acids contribute to the

- pathogenesis of perinatal hypoxic-ischemic brain injury. *Brain Pathol* 2:235–243.
- Bona E, Johansson BB, Hagberg H (1997) Sensorimotor function and neuropathology five to six weeks after hypoxia-ischemia in seven-day-old rats. *Pediatr Res* 42:678–683.
- Cheng Y, Deshmukh M, D'Costa A, Demaro JA, Gidday JM, Shah A, Sun Y, Jacquin MF, Johnson Jr EM, Holtzman DM (1998) Caspase inhibitor affords neuroprotection with delayed administration in a rat model of neonatal hypoxic-ischemic brain injury. *J Clin Invest* 101:1992–1999.
- Dragovich T, Rudin CM, Thompson CB (1998) Signal transduction pathways that regulate cell survival and cell death. *Oncogene* 17:3207–3213.
- Du Y, Bales KR, Dodel RC, Hamilton-Byrd E, Horn JW, Czilli DL, Simmons LK, Ni B, Paul SM (1997) Activation of a caspase 3-related cysteine protease is required for glutamate-mediated apoptosis of cultured cerebellar granule neurons. *Proc Natl Acad Sci USA* 94:11657–11662.
- Erzurumlu RS, Jhaveri S (1990) Thalamic axons confer a blueprint of the sensory periphery onto the developing rat somatosensory cortex. *Brain Res Dev Brain Res* 56:229–234.
- Felderhoff-Mueser U, Taylor DL, Greenwood K, Kozma M, Stibenz D, Joashi UC, Edwards AD, Mehmet H (2000) Fas/CD95/APO-1 can function as a death receptor for neuronal cells in vitro and in vivo and is upregulated following cerebral hypoxic-ischemic injury to the developing rat brain. *Brain Pathol* 10:17–29.
- Gross A, Jockel J, Wei MC, Korsmeyer SJ (1998) Enforced dimerization of BAX results in its translocation, mitochondrial dysfunction and apoptosis. *EMBO J* 17:3878–3885.
- Hagan P, Barks JD, Yabut M, Davidson BL, Roessler B, Silverstein FS (1996) Adenovirus-mediated over-expression of interleukin-1 receptor antagonist reduces susceptibility to excitotoxic brain injury in perinatal rats. *Neuroscience* 75:1033–1045.
- Iseemann S, Stoll G, Schroeter M, Krajewski S, Reed JC, Bahr M (1998) Differential regulation of Bax, Bcl-2, and Bcl-X proteins in focal cortical ischemia in the rat. *Brain Pathol* 8:49–62, discussion 62–63.
- Krajewski S, Mai JK, Krajewska M, Sikorska M, Mossakowski MJ, Reed JC (1995) Upregulation of bax protein levels in neurons following cerebral ischemia. *J Neurosci* 15:6364–6376.
- Levine S (1960) Anoxic-ischemic encephalopathy in rats. *Am J Pathol* 36:1–17.
- Li H, Zhu H, Xu CJ, Yuan J (1998) Cleavage of BID by caspase 8 mediates the mitochondrial damage in the Fas pathway of apoptosis. *Cell* 94:491–501.
- Liu XH, Eun BL, Silverstein FS, Barks JD (1996) The platelet-activating factor antagonist BN 52021 attenuates hypoxic-ischemic brain injury in the immature rat. *Pediatr Res* 40:797–803.
- Liu XH, Kwon D, Schielke GP, Yang GY, Silverstein FS, Barks JD (1999) Mice deficient in interleukin-1 converting enzyme are resistant to neonatal hypoxic-ischemic brain damage. *J Cereb Blood Flow Metab* 19:1099–1108.
- Malamud N (1950) Status marmoratus: a form of birth injury following either birth injury or inflammation of the central nervous system. *J Pediatr* 37:610.
- Martin LJ (1999) Neuronal death in amyotrophic lateral sclerosis is apoptosis: possible contribution of a programmed cell death mechanism. *J Neuropathol Exp Neurol* 58:459–471.
- Martin LJ, Brambrink AM, Koehler RC, Traystman RJ (1997a) Primary sensory and forebrain motor systems in the newborn brain are preferentially damaged by hypoxia-ischemia. *J Comp Neurol* 377:262–285.
- Martin LJ, Brambrink AM, Lehmann C, Portera-Cailliau C, Koehler RC, Rothstein J, Traystman RJ (1997b) Hypoxia-ischemia causes abnormalities in glutamate transporters and death of astroglia and neurons in newborn striatum. *Ann Neurol* 42:335–348.
- Martin LJ, Kaiser A, Price AC (1999) Motor neuron degeneration after sciatic nerve avulsion in adult rat evolves with oxidative stress and is apoptosis. *J Neurobiol* 40:185–201.
- Martin LJ, Price AC, Kaiser A, Shaikh AY, Liu Z (2000) Mechanisms for neuronal degeneration in amyotrophic lateral sclerosis and in models of motor neuron death (review). *Int J Mol Med* 5:3–13.
- McDonald JW, Silverstein FS, Johnston MV (1988) Neurotoxicity of N-methyl-D-aspartate is markedly enhanced in developing rat central nervous system. *Brain Res* 459:200–203.
- Murphy KM, Streips UN, Lock RB (2000) Bcl-2 inhibits a Fas-induced conformational change in the Bax N-terminus and Bax mitochondrial translocation. *J Biol Chem* 275:17255–17258.
- Myers RE (1975) Four patterns of perinatal brain damage and their conditions of occurrence in primates. *Adv Neurol* 10:223–234.
- Nagata S (1999a) Biddable death. *Nat Cell Biol* 1:E143–E145.
- Nagata S (1999b) Fas ligand-induced apoptosis. *Annu Rev Genet* 33:29–55.
- Nelson C, Silverstein FS (1994) Acute disruption of cytochrome oxidase activity in brain in a perinatal rat stroke model. *Pediatr Res* 36:12–19.
- Northington F, Ferriero D, Graham E, Traystman R, Martin L (2001) Early neurodegeneration after hypoxia-ischemia in neonatal rat is necrosis while delayed neuronal death is apoptosis. *Neurobiol Dis*, in press.
- Petit PX, Susin SA, Zamzami N, Mignotte B, Kroemer G (1996) Mitochondria and programmed cell death: back to the future. *FEBS Lett* 396:7–13.
- Rice JE, Vannucci RC, Brierley JB (1981) The influence of immaturity on hypoxic-ischemic brain damage in the rat. *Ann Neurol* 9:131–141.
- Roland EH, Poskitt K, Rodriguez E, Lupton BA, Hill A (1998) Perinatal hypoxic-ischemic thalamic injury: clinical features and neuroimaging [see comments]. *Ann Neurol* 44:161–166.
- Shimizu S, Narita M, Tsujimoto Y (1999) Bcl-2 family proteins regulate the release of apoptogenic cytochrome c by the mitochondrial channel VDAC [see comments]. *Nature* 399:483–487.
- Silverstein FS (1998) Can inhibition of apoptosis rescue ischemic brain? *J Clin Invest* 101:1809–1810.
- Susin SA, Zamzami N, Castedo M, Daugas E, Wang HG, Geley S, Fassy F, Reed JC, Kroemer G (1997) The central executioner of apoptosis: multiple connections between protease activation and mitochondria in Fas/APO-1/CD95- and ceramide-induced apoptosis. *J Exp Med* 186:25–37.
- Susin SA, Lorenzo HK, Zamzami N, Marzo I, Brenner C, Larochette N, Prevost MC, Alzari PM, Kroemer G (1999) Mitochondrial release of caspase-2 and -9 during the apoptotic process. *J Exp Med* 189:381–394.
- Szafarski J, Burtrum D, Silverstein FS (1995) Cerebral hypoxia-ischemia stimulates cytokine gene expression in perinatal rats. *Stoke* 26:1093–1100.
- Towfighi J, Yager JY, Housman C, Vannucci RC (1991) Neuropathology of remote hypoxic-ischemic damage in the immature rat. *Acta Neuropathol* 81:578–587.
- Towfighi J, Zec N, Yager J, Housman C, Vannucci RC (1995) Temporal evolution of neuropathologic changes in an immature rat model of cerebral hypoxia: a light microscopic study. *Acta Neuropathol* 90:375–386.
- Vander Heiden MG, Chandel NS, Williamson EK, Schumacker PT, Thompson CB (1997) Bcl-xL regulates the membrane potential and volume homeostasis of mitochondria [see comments]. *Cell* 91:627–637.
- Vekrellis K, McCarthy MJ, Watson A, Whitfield J, Rubin LL, Ham J (1997) Bax promotes neuronal cell death and is downregulated during the development of the nervous system. *Development* 124:1239–1249.
- Volpe JJ (1995) *Neurology of the newborn*, pp 314–369. Philadelphia: Saunders.
- White E (1989) *Cortical circuits: synaptic organization of the cerebellar cortex: structure, function, and theory*. Boston: Birkhauser.
- Wong-Riley M (1979) Changes in the visual system of monocularly sutured or enucleated cats demonstrable with cytochrome oxidase histochemistry. *Brain Res* 171:11–28.
- Wong-Riley MT (1989) Cytochrome oxidase: an endogenous metabolic marker for neuronal activity. *Trends Neurosci* 12:94–101.
- Wood D, Newcomb EW (2000) Cleavage of bax enhances its cell death function. *Exp Cell Res* 256:375–382.
- Wood DE, Newcomb EW (1999) Caspase-dependent activation of calpain during drug-induced apoptosis. *J Biol Chem* 274:8309–8315.
- Yamada H, Tada-Oikawa S, Uchida A, Kawanishi S (1999) TRAIL causes cleavage of bid by caspase-8 and loss of mitochondrial membrane potential resulting in apoptosis in BJAB cells. *Biochem Biophys Res Commun* 265:130–133.
- Yokochi K, Aiba K, Kodama M, Fujimoto S (1991) Magnetic resonance imaging in athetotic cerebral palsied children. *Acta Paediatr Scand* 80:818–823.
- Zamzami N, Susin SA, Marchetti P, Hirsch T, Gomez-Monterrey I, Castedo M, Kroemer G (1996) Mitochondrial control of nuclear apoptosis [see comments]. *J Exp Med* 183:1533–1544.

# Early Neurodegeneration after Hypoxia-Ischemia in Neonatal Rat Is Necrosis while Delayed Neuronal Death Is Apoptosis

Frances J. Northington,\* Donna M. Ferriero,<sup>†</sup>  
Ernest M. Graham,<sup>‡</sup> Richard J. Traystman,<sup>§</sup>  
and Lee J. Martin,<sup>¶</sup>

<sup>\*</sup>Departments of Pediatrics Eudowood Neonatal Pulmonary Division, and

<sup>†</sup>Gynecology/Obstetrics, <sup>‡</sup>Anesthesiology/Critical Care Medicine, <sup>§</sup>Neuroscience and

<sup>¶</sup>Pathology, The Johns Hopkins Medical Institutions, Baltimore, Maryland 21287;

<sup>†</sup>Departments of Neurology and Pediatrics, University of California  
at San Francisco, San Francisco, California 94143

Received May 15, 2000; revised November 2, 2000; accepted November 21, 2000; published  
online February 17, 2001

**We used silver staining to demonstrate neuronal cell body, axonal, and terminal degeneration in brains from p7 rat pups recovered for 0, 1.5, 3, 6, 24, 48, 72 h, and 6 days following hypoxia-ischemia. We found that initial injury is evident in ipsilateral forebrain by 3 h following hypoxia-ischemia, while injury in ventral basal thalamus develops at 24 h. A secondary phase of injury occurs at 48 h in ipsilateral cortex, but not until 6 days in basal ganglia. Initial injury in striatum and cortex is necrosis, but in thalamus the neurodegeneration is primarily apoptosis. Degeneration also occurs in bilateral white matter tracts, and in synaptic terminal fields associated with apoptosis in regions remote from the primary injury. These results show that hypoxia-ischemia in the developing brain causes both early and delayed neurodegeneration in specific systems in which the morphology of neuronal death is determined by time, region, and potentially by patterns of neuronal connectivity.** © 2001 Academic Press

## INTRODUCTION

While acute perinatal brain injury does not account for the majority of cerebral palsy (Nelson and Grether, 1999), the neurologic handicaps caused by perinatal anoxia due to asphyxia and lack of cerebral blood flow are severe (Lorenz *et al.*, 1998). The mechanisms for brain injury after hypoxia/ischemia are thought to include energy failure, free radical damage, cytokine and excitotoxicity, and caspase-dependant cell death (Barks and Silverstein, 1992; Cheng *et al.*, 1998; Hagan *et al.*, 1996; Liu *et al.*, 1996; Martin *et al.*, 1997; McDonald *et al.*, 1988). Yet, the mechanisms that underlie the overall distribution and progression of neuronal injury after neonatal hypoxia-ischemia remain unclear. Understanding these mechanisms and a possible role of neuronal connections in the evolution of hypoxic-ischemic injury in the immature brain is neces-

sary to more fully explain the modes of neurodegeneration and the subsequent cognitive, motor, sensory, and attentional disabilities that occur after perinatal brain injury (Lorenz *et al.*, 1998).

Necrosis is a likely cause of acute neuronal cell death in the ipsilateral cortex and basal ganglia after neonatal hypoxic-ischemic injury (Rice *et al.*, 1981; Towfighi *et al.*, 1995), but the structure of cell death in remote regions has not been investigated. Demonstration that caspase inhibitors provide neuroprotection in this model (Cheng *et al.*, 1998), suggests that cell death can occur by both necrosis and apoptosis or by cytokine-mediated inflammatory reactions. Neuronal cell death following trophic factor withdrawal, as occurs after interruption of neuronal connectivity by axotomy and during normal nervous system development, also has characteristics of apoptosis (Eves *et al.*, 1996; Li *et al.*, 1998).



During the perinatal period, neuronal connections are forming between brain regions (Bolz *et al.*, 1990; Shatz, 1996). Developing neurons are highly dependent on trophic support. Interruption of neuronal connectivity and resultant target deprivation causes cell death in the immature brain more rapidly and frequently than in the mature brain (Miller and Kuhn, 1997). Loss of connectivity from deafferentation is also a mechanism of injury in the developing brain (Kotak and Sanes, 1997; Miller and Kuhn, 1997). The potential for neuronal connectivity to dictate the selective distribution of brain injury in the neonate has been suspected (Martin *et al.*, 1997; Oo *et al.*, 1995). However, the role of neuronal connectivity in mediating the timing, pattern, and extent of delayed injury in newborns remains unknown.

Thus, brain damage after hypoxia-ischemia in newborns could result from mechanisms directly related to the hypoxic-ischemic insult per se (e.g., energy failure and acute cell necrosis) and from secondary mechanisms triggered by the resultant early-occurring neurodegeneration. In this study, we tested the hypothesis that the selective vulnerability of different brain regions and the time at which this neurodegeneration emerges segregates as different forms of neuronal cell death, with patterns of distribution that suggest a role for neuronal connectivity in hypoxic-ischemic neurodegeneration in the immature brain.

## METHODS

**Hypoxia-ischemia in p7 rats.** The Rice-Vannucci (Rice *et al.*, 1981) neonatal adaptation of the Levine procedure (Levine, 1960) was used to cause hypoxic ischemic brain injury in 7-day-old (p7) rats. In brief, rat pups were anesthetized with 2.5% halothane, 15% nitrous oxide, in O<sub>2</sub>. The right common carotid artery was permanently ligated (in sham controls the ligature was passed around the artery and removed). After the wound was sutured, the pups recovered from anesthesia and returned to the dam. Two hours later, pups were placed in an air-tight container in a 37°C water bath through which humidified 8% O<sub>2</sub>, balance nitrogen flowed for 150 min. After hypoxia, pups were returned to the dam until sacrifice.

Brains were retrieved at 0, 1.5, 3, 6, 24, 48, 72 h, and 6 days ( $n = 6$  for each time point) following the end of hypoxia. The multiple early time points were chosen because our data, as well as that of others, showed a faster progression of injury after hypoxia-ischemia in neonates as compared to adults (Martin *et al.*, 1997;

Towfighi *et al.*, 1995). These time points would allow detection of small, but possibly important, differences in time of onset of injury within regions undergoing primary acute neurodegeneration. The later time points allow identification of the extent and type of injury in axonal pathways and in remote regions. Control groups consisted of (a) sham-operated littermates, (b) littermates with carotid ligation not exposed to hypoxia, and (c) littermates exposed to hypoxia alone for the same duration as experimental pups. Sham controls were sacrificed on postnatal day 7, 8, 9, 10, and 13 ( $n = 4$  at each age) to control for occurrence of naturally occurring cell death in the developing brain. Hypoxia only controls, sacrificed at 24 and 72 h and 6 days after hypoxia, were used to demonstrate that injury in remote regions is not due to systemic hypoxemia ( $n = 4-6$  at each time point). Ligation-only controls, sacrificed 24 h after surgery, were used to validate our use of the model ( $n = 4$ ).

All animal studies received prior approval from the Animal Care and Use Committee of Johns Hopkins University School of Medicine and were performed in accordance with the NIH "Guide for the Care and Use of Laboratory Animals," U.S. Department of Health and Human Services 85-23, 1985.

**Retrograde tracing.** To reveal the afferent and efferent connections with the ipsilateral cortex, the following procedure was performed. Anesthetized p4 pups ( $n = 6$ ) were secured in a miniature stereotaxic apparatus (Stoelting, Wood Dale, IL), the scalp incised, the skull overlying the parasagittal parietal/occipital cortex removed, and 10 nl of the fluorescent retrograde tracer, Fluorogold (Fluorochrome Inc., Englewood, CO), was injected into the superficial cortex. The scalp was sutured and the pups returned to the dam until p7. To demonstrate the presence of cell death within regions with connections to the ipsilateral cortex, rat pups ( $n = 6$ ) injected with fluorogold on p4 were exposed to hypoxia-ischemia as described above and perfused 48 h after hypoxia for combined fluorogold immunocytochemistry and cresyl violet staining.

**Tissue preparation.** Animals were killed with an overdose of pentobarbital, 65 mg/kg IP, and exsanguinated with cold 0.1 M PBS (pH 7.4) via intracardiac perfusion. Brains were perfusion fixed with 4% paraformaldehyde in PBS for 30 min at 4 ml/min. The brains were removed, postfixed in 4% paraformaldehyde overnight, cryoprotected in 30% sucrose, and frozen in isopentane ( $-30^{\circ}\text{C}$ ). Coronal sections (60  $\mu\text{m}$ ) were cut on a sliding microtome for cresyl violet, immunocytochemistry, and silver staining.

**Immunocytochemistry.** In preparation for detection



of retrograde labeling, sections were washed in 0.05 M TBS (pH = 7.4,  $3 \times 10$  min), endogenous peroxidase activity blocked with cold methanol/ $H_2O_2$ , permeabilized with 0.04% Triton (TX) (30 min), and blocked with 4% normal goat serum (NGS)/0.01% TX (60 min). Tissues were incubated with anti-fluorogold antibody (Chemicon, Temecula, CA) 1:5000 in 2% NGS/0.01% TX overnight at 4°C. Sections were washed (TBS,  $3 \times 10$  min), incubated with GARB (Fab<sub>2</sub>) (ICN-Cappel, West Chester, PA, 1:75, 60 min), washed, and incubated with rabbit peroxidase anti-peroxidase (Sternberger Monoclonals, Baltimore, MD) (1:200, 60 min). Immunoreactivity was detected using diaminobenzidine as the chromagen.

**Apoptotic profiles.** Both silver and cresyl violet staining allowed examination of nuclear morphology in degenerating cells with ready identification of necrotic and apoptotic cells in most cases. Cells meeting the light microscopic morphologic criteria for apoptosis (Martin *et al.*, 1998) were counted in three 400 $\times$  fields within the ventral basal thalamus with the aid of a grid on cresyl violet stained sections. Only cells with a few ( $\leq 3$ ) clearly defined large, regular chromatin clumps were counted as apoptotic. Counts in the three fields were averaged to give a single value for each section. Three sections through the ventral basal thalamus were counted for each animal and averaged for a single value per animal. Potential sampling bias in the counting of apoptotic profiles was minimized by (1) counting apoptotic profiles within a constant reference volume within the ventral basal thalamus and (2) counting cells only once, at the first appearance of the apoptotic nuclei as the tissue was scanned through the Z axis. Split cell counts were minimized because of the thickness of the sections (60  $\mu$ m) and the relative smallness of the apoptotic profiles. Sham control and hypoxia-only controls were counted in identical manner at each of the previously mentioned postnatal ages and posthypoxia time points. Neither sham controls nor hypoxia-only controls showed a change in number of apoptotic profiles over the time courses analyzed, therefore the results for sham and hypoxia-only controls were combined as single values for ease of presentation (Fig. 3A).

**Silver-staining.** Silver staining allows identification of aggregated neurofilament proteins in degenerating neuronal elements within specific neuroanatomical regions. It has been validated and is a highly reproducible technique for identification of neuronal injury (Du *et al.*, 1998). For silver staining, coronal sections were washed repeatedly in PBS for 48 h to remove sucrose. Tissue was reimmersed in 4% paraformaldehyde/0.1

M PBS  $\times$  96 h. FD Neuro Silver kit (FD Neurotechnologies Inc., Baltimore, MD) was used for silver staining. Silver-stained tissue was mounted, coverslipped without dehydration in ETOH, and protected from light.

**Optical densitometry.** Optical densitometry (OD) was used for quantitative analysis of time course of neurodegeneration after hypoxia-ischemia within the cortex, striatum, and thalamus. Previous time courses, in this model have utilized cresyl violet and H&E histochemistry. OD of silver-stained sections allowed the contribution of axonal, terminal, and cell body damage to the overall progression of injury after hypoxia-ischemia to be determined in contrast to the previous methods that primarily evaluated injury to the cell body. Validation of this technique for the purposes of this study is provided in Fig. 3B; see Results.

Silver stained sections from three coronal levels were analyzed. The levels were (1) anterior striatum, (2) midstriatum at the level of the anterior commissure, and (3) the level of hippocampal dentate gyrus, including ventral basal thalamic nuclei. Parasagittal cortex and striatum were analyzed in all three, and two of the three coronal levels, respectively. Within the thalamus, the ventral basal complex including lateral geniculate nucleus, which has major projections to cortex, was analyzed. Time of onset of initial neurodegeneration and additional progression of injury were compared between ipsilateral cortex, striatum, and thalamus.

Sections were digitized using an image analysis system and LA Inquiry Software (Loats Assoc., Westminster, MD). OD measurements were obtained from outlined areas of interest in parasagittal cortex at each of three coronal levels, from striatum in the two anterior-most sections and from the ventral basal thalamus in the most posterior section. The measurements for cortex and striatum were averaged to give one value/region/animal. OD measurements were corrected for background staining by subtracting the OD in a contralateral structure with equal neuronal density but without evidence of injury. This correction for cell density plus the use of an average integrated OD over the entire sample should minimize any contribution of variation in size of area of interest to the results in relation to progression of injury (i.e., edema or atrophy). Based on previous description of the present model (Towfighi *et al.*, 1991) and present data, it was found that cavitory lesions develop in the parasagittal cortex at  $\geq 72$  h, making it impossible to obtain relevant densitometry measurements. Therefore, we

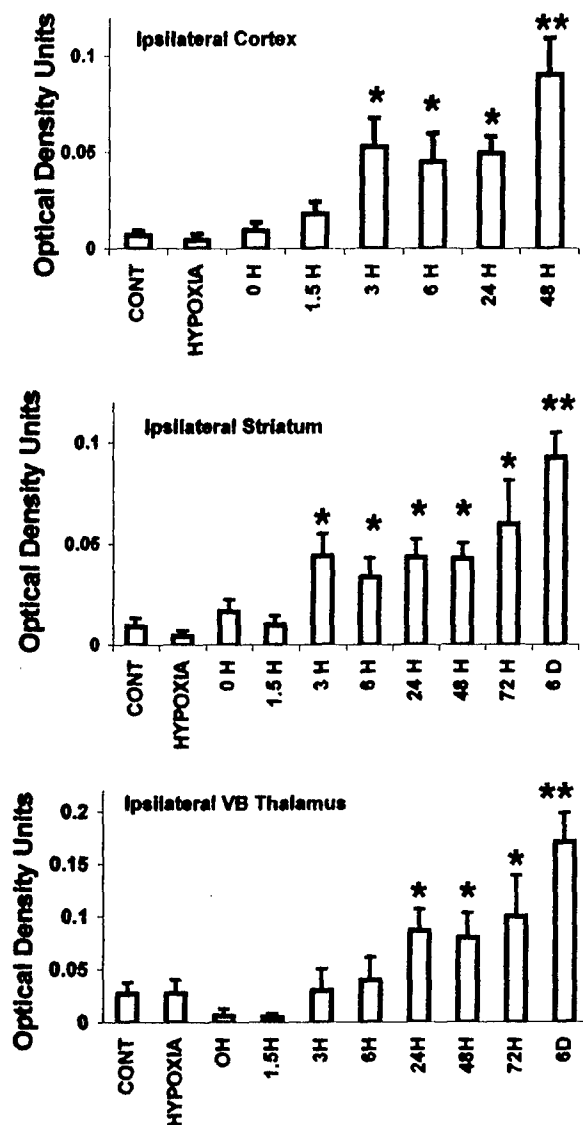


**FIG. 1.** Neonatal hypoxia-ischemia causes neurodegeneration in ipsilateral cortex, striatum, and thalamus, which can be measured densitometrically in silver-stained sections. Optical density measurements from ipsilateral cortex (top panel), ipsilateral striatum (middle panel), and ipsilateral ventral basal thalamus (bottom panel) were obtained from coronal sections of brains perfused at 0, 1.5, 3, 6, 24, 48, 72 h, and 6 days following hypoxia-ischemia and stained with FD Neuro-silver kit. Control groups included animals exposed to no manipulation or to hypoxia-only and survived for 24 h, 72 h, or 6 days. Because animals exposed to hypoxia-only showed no increase in OD at any time point, the results were presented as a single data point. Injury proceeds rapidly in ipsilateral forebrain (cortex and striatum), with an increase in silver deposition detectable by 3 h after hypoxia-ischemia in both regions. Initial evidence for neurodegeneration in thalamus is not found until 24 h after hypoxia-ischemia. Injury continues to progress in all three regions but at significantly different rates. A secondary increase in neurodegeneration is detectable in cortex by 48 h. No further measurements were made in the cortex because by 72 h cystic cavitory lesions were common in the posterior parieto-

made no measurements in the cortical samples after 48 h. The number of animals with cavitory cortical lesions was recorded separately. Age-matched sham and time-matched hypoxia-only controls were analyzed as above, but because of no change in relative optical density with age or at any time following hypoxia-only the results were combined for conciseness of presentation in Fig. 1.

**Electron microscopy.** Sections were processed for electron-microscopy as previously (Al-Abdulla et al., 1998; Portera-Cailliau et al., 1997). Briefly, samples were postfixed (1 h) in 2% osmium tetroxide, dehydrated, and embedded in resin. Plastic-embedded samples were mounted in an Epon block (Electron Microscopy Sciences, Fort Washington, PA) and cut into semithin (1  $\mu$ m) and ultra thin (70 nm) sections for light microscopy and EM, respectively. Semithin sections from ventral basal thalamus were counterstained with toluidine blue and screened by light microscopy to select sections for viewing by EM. Selected ultra-thin sections were stained with uranyl acetate and lead citrate and viewed with a JEOL 100S electron microscope.

**Statistical analysis.** Two-way ANOVA was used to compare OD measurements between control and experimental groups over time and between regions after hypoxia-ischemia. ANOVA was used to compare apoptotic profile counts in the thalamus over time after hypoxia-ischemia. Post hoc testing for individual differences was performed with Fisher's analysis. A  $P$  value  $< 0.05$  was used to determine significance.

## RESULTS

*The onset of damage in the ipsilateral forebrain and thalamus is time-dependent and progressive, and it has an uneven distribution within regions. Forebrain neurodegeneration precedes thalamic neurodegeneration after*

occipital cortex and precluded densitometric analysis. Despite the similarity of time of first appearance of injury in cortex and striatum, secondary injury proceeded much slower in the striatum with a difference not detectable until 6 days after hypoxia-ischemia. A secondary increase in thalamic neurodegeneration also occurs at 6 days following hypoxia-ischemia. In neither forebrain nor thalamus was there a detectable increase in neurodegeneration 24 h after 2.5 h of hypoxic exposure only. The values are mean  $\pm$  standard error of the mean from the regions at matched coronal levels. A single asterisk indicates significant difference ( $P < 0.05$ ) from control and two asterisks indicate significant difference ( $P < 0.05$ ) from first appearance of detectable injury.

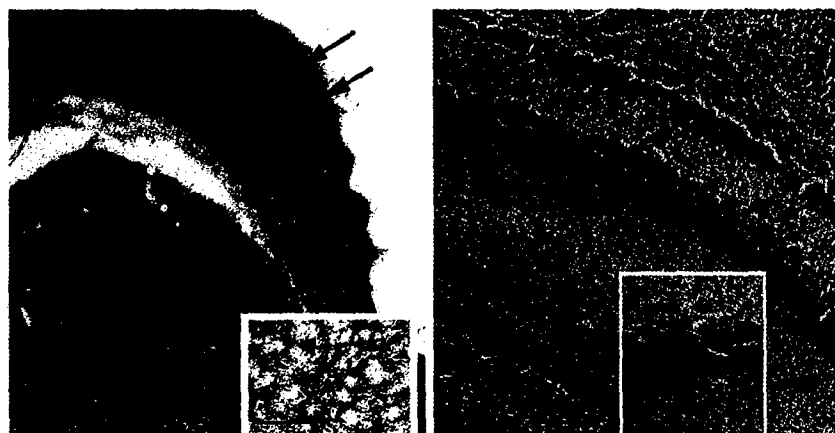


FIG. 2. Forebrain injury after neonatal hypoxia-ischemia is discontinuous with areas of neurodegeneration immediately adjacent to noninjured tissue. (A) Silver-stained coronal section of forebrain shows the previously reported columnar injury in cortex and discrete patches of injury in the adjacent striatum (arrows and arrowheads indicate areas of neurodegeneration). At greater magnification, the close approximation of injured (arrowheads) and noninjured areas of the striatum is apparent (inset). (B) The hippocampus also has a discontinuous distribution of injury after hypoxia-ischemia. Dense silver deposition is seen in the pyramidal cell layer at 24 h (arrows). Scale bar for A, 800  $\mu$ m; A inset, 100  $\mu$ m; B, 200  $\mu$ m; B inset, 40  $\mu$ m.

neonatal hypoxic-ischemic brain injury (Fig. 1). Silver staining can be used as a marker for neurodegeneration. These silver depositions can represent degeneration of neuronal cell bodies and processes (axons, dendrites, and terminals) (Du *et al.*, 1998). In ipsilateral cerebral cortex and striatum silver staining was present by 3 h after hypoxia-ischemia ( $P < 0.05$  vs control) (data are expressed as mean  $\pm$  SEM). Not until 24 h after hypoxia-ischemia did optical density increase in the ventral basal thalamus. Eighty-three percent of rats exhibited cavitory cortical lesions by 72 h after hypoxia-ischemia, therefore no further optical density measurements were obtained after 48 h in the cerebral cortex. Injury progresses in the cortex at 48 h and in the striatum and thalamus at 6 days ( $P < 0.05$  vs OD at time of first appearance of injury), suggesting on-going neurodegeneration after initial injury.

The damage in forebrain is discontinuous (Fig. 2). This pattern cannot be explained by tissue blood flow differences because of the close proximity of viable tissue to injured regions. This is notably evident in the patchy degeneration in both the striatum (Fig. 2A) and hippocampus (Fig. 2B). In Fig. 2 the arrows indicate neurodegeneration in the cortex and hippocampus and arrowheads indicate degeneration in the striatum. Silver deposition within cortical columns within the ipsilateral forebrain is consistent with the columnar injury previously described in this model (Towfighi *et al.*, 1997) and demonstrates that the present techniques

identify the expected areas of injury and allows discrimination of injured from noninjured tissue within regions with a high degree of resolution. The interdigitation of injured and noninjured tissue is evident in both the striatum and hippocampus that is best appreciated at high magnification in the insets (Fig. 2).

The validity of this model and the effect of the chosen duration of hypoxia (2.5 h) to cause a consistent severe injury is demonstrated by the progression of cortical injury to cortical cavitation in 83% of brains obtained  $>48$  h after the end of hypoxia-ischemia and by the relatively small amount of variability in the measures of injury with OD. Additionally, the validity of optical densitometry as a measure of injury was verified with comparison of the initial progression of injury in the thalamus as measured with OD with the appearance of apoptotic profiles within the ventral basal thalamus during the initial 72 h following hypoxia-ischemia (Fig. 3B).

Time of appearance of apoptotic profiles in the thalamus (Fig. 3A) is consistent with the delayed onset of injury in the diencephalon as compared to the forebrain. Utilizing the cresyl violet stained sections to count apoptotic profiles within the thalamus following hypoxia-ischemia, we find that for the first 6 h after hypoxia-ischemia, the numbers of apoptotic profiles are not increased above the baseline number found in age-matched controls or hypoxia-only controls. Apoptosis in hypoxia-only controls did not increase from baseline at 24 and 72 h or 6 days, therefore the data are

presented in a single bar on the graph as discussed in the methods (Fig. 3A). In contrast, from 24 to 72 h after hypoxia-ischemia, a marked increase in number of cells with clearly identifiable apoptotic profiles occurs. By 6 days following the insult, the number of apoptotic profiles is once again at control levels. The initial increase in apoptotic profiles in the thalamus, following hypoxia-ischemia, coincides with the appearance of silver-staining detection of neurodegeneration in the thalamus at 24 h, but lags behind the onset of neurodegeneration in the cortex at 3 h. The presence of increased number of apoptotic profiles in the thalamus continues through progression of injury in the cortex at 48 h.

When the initial progression of injury is graphed utilizing both optical densitometry and appearance of apoptotic profiles (Fig. 3B), the two techniques provide a similar estimation of the rate of progression of injury within the thalamus during the first 72 h after hypoxia-ischemia. A minimal increase in OD and number of apoptotic profiles is seen at 3–6 h followed by a robust increase in both measures of injury during the 24 to 72-h time period. The similarity in pattern of progression of injury as measured by appearance of apoptotic profiles serves to validate our use of OD quantification of silver staining for the purposes of the present study. The validity of the technique is strengthened by the fact that results from the two techniques are quite similar despite measuring different indices of injury (cresyl violet-stained apoptotic profiles-cell soma morphology, silver staining-neurodegeneration of cell soma, processes and nerve terminals).

*In ipsilateral forebrain, neurodegeneration occurring immediately after hypoxia-ischemia is necrosis but delayed neurodegeneration is necrosis and apoptosis.* Analysis of cresyl violet and silver stained sections allows identification of cells demonstrating clear light microscopic morphologic evidence of necrosis or apoptosis. Analysis of the ipsilateral cortex and striatum shows predominant necrosis immediately after hypoxia-ischemia. At 3 h, the major phenotypes of these neurons include irregularly condensed chromatin, argyrophillic cytoplasm, and disintegration of cellular membranes. (Fig. 4A, silver stain-ipsilateral striatum, 3 h after hypoxia-ischemia; Fig. 4B, cresyl violet-ipsilateral cortex, 3 h after hypoxia-ischemia, arrows indicate necrotic neurodegeneration).

In contrast to the early ischemic necrosis seen in ipsilateral cortex and striatum after hypoxia-ischemia, morphology of injury within these regions at later time points is more varied. When examined at the

time of the secondary phase of injury, neurons within upper and lower layers of parasagittal cortex and the striatum exhibit the light microscopic hallmarks of apoptosis and those of a hybrid of apoptosis and necrosis. The latter features have previously been described as part of the cell death continuum in the immature cortex and striatum in response to excitotoxic injury (Portera-Cailliau et al., 1997). Forty-eight h after hypoxia-ischemia, apoptotic and continuum cells are seen in the striatum in contrast to the predominant necrosis seen at 3 h after hypoxia-ischemia. The same is true in the cortex, with many apoptotic and continuum profiles found at delayed time points (Fig. 4C, striatum, 48 h after hypoxia-ischemia, silver stain; Fig. 4D, cortex, 48 h after hypoxia-ischemia-CV, arrows indicate cells with apoptotic and hybrid morphologies).

*Damage occurs in remote locations after hypoxia-ischemia.* Injury occurs in brain regions remote from the areas of acute primary injury. This remote damage occurs in association with damage to interconnected white matter pathways (Fig. 5). Between 24 and 72 h, axonal degeneration and neurodegeneration are identifiable in the mammillary tract and mammillary nucleus, in corpus callosum and contralateral cortex, and in descending corticobulbar tracts and brainstem and cranial nerve nuclei. Axonal degeneration is seen in the contralateral corpus callosum and in the ipsilateral descending corticobulbar tracts (Figs. 5A and 5C) and in their respective target areas, the contralateral cortex (Fig. 5B) and the nucleus of cranial nerve VII (Fig. 5D) (injury indicated by areas of silver deposition, arrows). For comparison, no axonal degeneration is seen in contralateral corpus callosum in controls (Fig. 5a).

*Retrograde transport of fluorogold identifies regions with efferent connections to the ipsilateral cerebral cortex that are at risk for injury after hypoxia/ischemia.* Injury within the lateral geniculate and the ventral basal complex of thalamus occurs in association with columnar cortical injury at 24 h after hypoxia-ischemia (Fig. 6A). Posterior cortical injection of p4 rat pups demonstrates retrograde transport of fluorogold to these same vulnerable areas of ipsilateral thalamus and to contralateral cortex (Figs. 6B and 6E, brown immunoreactivity). Retrograde axonal transport of the fluorogold is confirmed by the presence of abundant immunoreactivity for fluorogold filling the cell body and dendrites of thalamic neurons (Fig. 6C).

Injection of fluorogold prior to hypoxia-ischemia combined with cresyl violet staining of tissue perfused at 48 h after hypoxia/ischemia demonstrates death of neurons with connections to ipsilateral cortex (Fig. 6D,

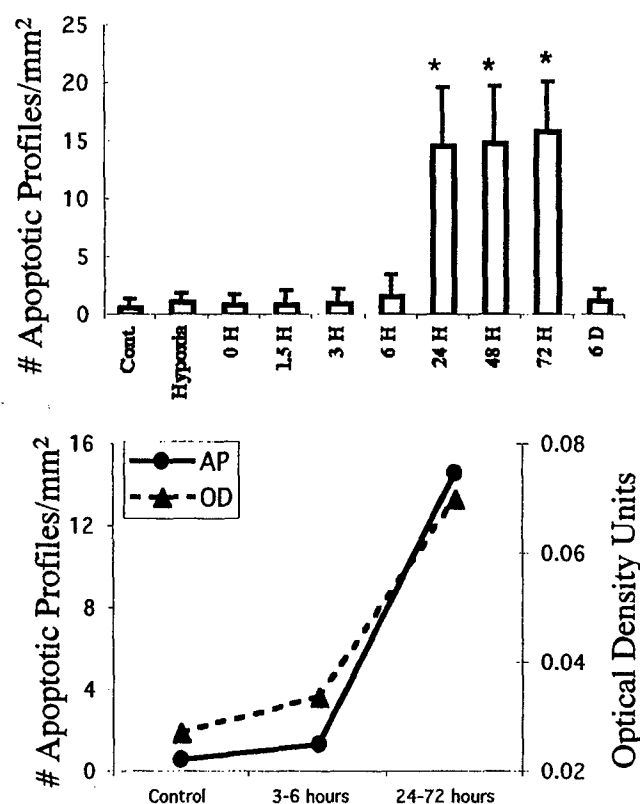


FIG. 3. (A) Appearance of apoptotic profiles in ipsilateral thalamus coincides with initial quantitative evidence of neurodegeneration in thalamus and follows neurodegeneration in ipsilateral forebrain. Not until 24 h after hypoxia-ischemia is there a significant increase in the number of apoptotic profiles in the ipsilateral thalamus. A consistent increase in apoptotic profiles persists at 48 and 72 h. Counts at 0, 1.5, 3, 6 h, and 6 days are not different from those found in age-matched controls and hypoxia-only controls. Hypoxia-only controls were analyzed at 24 h, 72 h, and 6 days. Because there was no increase in number of apoptotic profiles at any of the time points following hypoxia, the data are presented as a single data point for simplicity of presentation. Counts were performed on cresyl violet stained sections of brains at similar coronal levels. The values are mean  $\pm$  standard deviation for each group. A single asterisk indicates significant difference in number of apoptotic profiles from ( $P < 0.05$ ) from control. (B) The appearance of silver staining in the ventral basal thalamus following neonatal hypoxia-ischemia coincides with the appearance of apoptotic profiles in the same region over the first 72 h after injury. These different measures of injury track together, showing a dramatic increase from baseline during the 24 to 72-h period, with the majority of the increase occurring after 6 h. Results at 3 and 6 h and at 24, 48, and 72 h were combined for the purposes of this analysis.

arrows). A cell labeled with flurogold (brown immunoreactivity) and with large chromatin clumps (cresyl violet) can be readily identified, demonstrating directly that cells with cortical connections die with an apoptotic morphology following neonatal hypoxia/ischemia.

*Delayed and remote neurodegeneration in thalamus and brainstem is apoptosis.* In contrast to the initial forebrain injury, initial injury in the thalamus and brainstem is apoptosis beginning 24 h after hypoxia-ischemia (Fig. 4E, silver stain, LGN 24 h after hypoxia-ischemia; Fig. 4F, silver stain, brainstem nuclei, 24 h after hypoxia-ischemia). The light microscopic features displayed by these cells, which are characteristic of apoptosis, including large regular clumps of chromatin, condensation of cytoplasm, and preservation of cytoplasmic membrane. Electron microscopy confirms that thalamic neurons are dying apoptotically at 24 h after hypoxic-ischemia (Fig. 7).

*Remote but interconnected regions also exhibit terminal degeneration at delayed time points.* In addition to apoptotic cell death in regions remote from the ipsilateral forebrain following neonatal hypoxia-ischemia, evidence of terminal degeneration is also found in remote regions at  $\geq 24$  h after the end of hypoxia. Within the respiratory centers of the medulla (Fig. 4G), the ipsilateral globus pallidus (Fig. 4H), and the contralateral cortex (Fig. 4I), primary and pyramidal neurons are found with fine silver deposits covering their surface, indicating degenerating nerve terminals. In some cases, the silver deposits can be seen to decorate the surface of neuronal processes. In the contralateral cortex, cells with an apoptotic morphology are found in the same area as those with terminal degeneration (Fig. 4I).

Control experiments confirm the validity of this model and the lack of contribution of hypoxia alone to remote injury. In age matched control animals (p7, p8, p9, p10, p13), no increase in optical density was found at any age (all control OD data combined, Fig. 1). In control sections, occasional silver-stained cells with apoptotic morphology were found as would be expected because of the previously demonstrated normal period of neuronal cell death that occurs in the first 2 weeks of life in developing rats (Oppenheim, 1991). Neurodegeneration was also not found in animals exposed to hypoxia alone at any of the time points studied (hypoxia-only OD data, Fig. 1; hypoxia-only apoptotic profile counts, Fig. 3). Lack of injury from either hypoxia or ischemia alone is consistent with the original observations made in this model (Rice *et al.*, 1981). Additionally, the lack of injury in hypoxia only controls is evidence that injury found in remote regions following hypoxia-ischemia is not simply the result of systemic hypoxemia. The possibility remains that very delayed neurodegeneration might become ev-

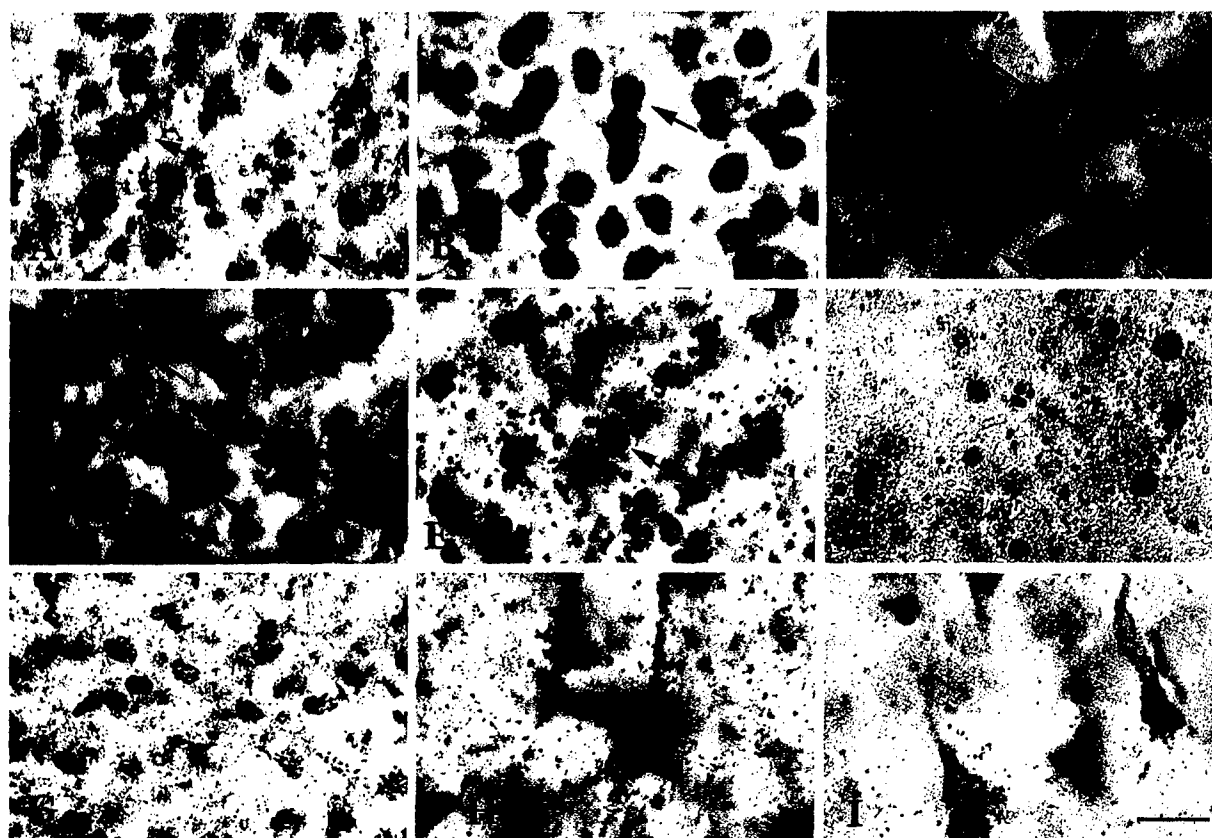


**FIG. 4.** Structure of cell death following neonatal hypoxia-ischemia varies by region and time. Necrosis, apoptosis, and hybrids of apoptosis and necrosis revealing the cell death continuum are seen in both silver and cresyl violet stained sections (A–F). Immediately after hypoxia-ischemia, necrosis is most commonly seen in ipsilateral striatum (A, silver stain) and cortex (B, cresyl violet). These necrotic cells have numerous irregular small chromatin clumps (A, B), a loss of cytoplasmic integrity (A) or swelling of the cytoplasm (B). While necrotic cells can still be found in the forebrain at later time points, cells with fewer, larger, more regular chromatin clumps (C, D) and with pale cytoplasm contained within an apparently intact cellular membrane (D) are found in the hippocampus (C) and cortex (D) at 48 h. Cells of an intermediate morphology with more regularly defined chromatin condensation than that found in necrosis but with smaller and more numerous chromatin aggregates than is typical for apoptosis are also found in the forebrain after 24 h (C, and D, arrows). Ipsilateral thalamus (E) and brainstem (F) exhibit classic apoptosis following neonatal hypoxia-ischemia. Multiple rounded detached cells in both regions have two or three large sharply delineated, uniformly dense, smooth, round chromatin clumps contained within a dense, argyrophillic cytoplasm around which the cytoplasmic membrane is preserved. Cells that have progressed to the final stage of an extruded apoptotic body without apparent cytoplasm are also found. In addition to the neurodegeneration found in forebrain, thalamus and brainstem following hypoxia-ischemia, terminal degeneration is found in regions that receive efferent connections from these injured regions. Respiratory neurons in the medulla (G), neurons in the ipsilateral globus pallidus (H), and layer III pyramidal neurons in the contralateral cortex have multiple tiny silver grains deposited on their surface consistent with silver labeling of degenerating projections to the cell. In contrast to the injured neurons seen in ipsilateral forebrain, thalamus, and brainstem, these neurons have maintained their normal cellular architecture, suggesting that they are intact, not primarily degenerating. For comparison, an apoptotic layer III neuron is seen in (I). While multiple staining techniques allow adequate visualization of nuclear and cytoplasmic structure, silver-staining allows the added ability to visualize degenerating cellular projections. Scale bar, 11  $\mu$ m.

ident in the hypoxia-only animals at a time later than p13.

## DISCUSSION

The most important findings of the present study are that following neonatal hypoxia-ischemia: (1)

brain regional vulnerability is dictated and organized along interconnected neural systems; (2) ipsilateral forebrain injury occurs as two fundamentally different time-dependent patterns: early neuronal necrosis and then delayed apoptotic neuronal death during a secondary injury phase; and (3) delayed cell death can also exist as a hybrid of apoptosis and necrosis. (4) Injury to regions remote from the ipsi-

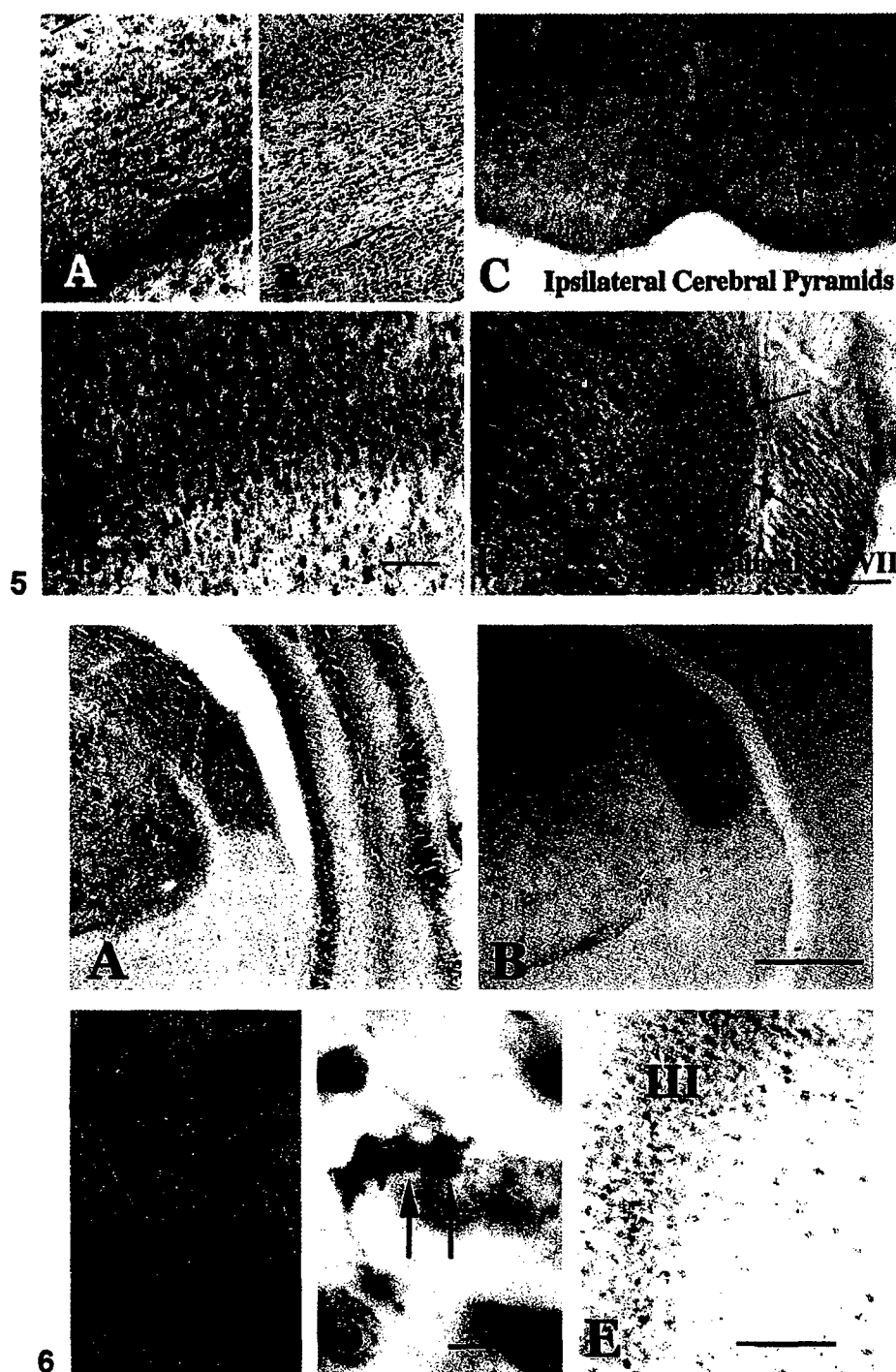


**FIG. 5.** Neurodegeneration occurs in brain regions remote from the primary sites of injury in association with damage to the interconnecting white matter pathways. Axonal degeneration occurs in the contralateral corpus callosum (A) and ipsilateral descending cortico-bulbar tracts (C) along with neurodegeneration in their respective targets, layer III of the contralateral cortex (B), and the nucleus of cranial nerve VII (D). Injury in these target regions is much more focal and circumscribed than that in the primary ipsilateral forebrain. For comparison, no injury is seen in the contralateral corpus callosum of a control (a) or in the contralateral descending cerebral pyramid (C). Scale bar for A, a, and B, 81  $\mu$ m; C and D, 371  $\mu$ m.

**FIG. 6.** Retrograde transport of fluorogold labels two regions that exhibit delayed neurodegeneration following neonatal hypoxia-ischemia. Injection of fluorogold into the ipsilateral posterior parietal-cortex labels ipsilateral posterior and ventral basal thalamus and lateral geniculate nucleus (B) and layer III neurons in the contralateral cortex (E). Neurodegeneration occurs in these regions following hypoxia-ischemia in



lateral forebrain is associated with damage within interconnecting white matter pathways. (5) Cells in remote regions that have connections with ipsilateral cortex and are target deprived, die with a morphology consistent with apoptosis after hypoxia-ischemia.

In the present model of neonatal brain injury, the ipsilateral forebrain clearly represents the ischemic core of the lesion (Nelson and Silverstein, 1994; Rice *et al.*, 1981). Previous neuropathologic studies have demonstrated signs of ischemic necrosis evident as soon as the end of hypoxia within the ipsilateral cortex (Towfighi *et al.*, 1995). Our results are in agreement with this observation and, for the first time, measurements of injury within the ipsilateral forebrain have been made with optical densitometry thereby demonstrating quantifiable injury in both cortex and striatum by 3 h after the end of hypoxia. The simultaneous appearance of injury within ipsilateral cortex and striatum is evidence for the previously described role of hypoxia-ischemia in the initial phase of injury (Towfighi *et al.*, 1991, 1995).

The injury evolves with a different time course in the cortex and striatum, suggesting that different mechanisms control the initial phase of injury versus the subsequent delayed phase of injury in these regions. The coexistence of injured and noninjured tissue within contiguous subregions of striatum and cortex and the different morphology of injury during the initial versus delayed phase (necrosis versus apoptosis) also supports the role for other mechanisms (in addition to acute ischemia) in the overall resultant neuropathology. It is known that within the developing cortex, interconnected neurons provide trophic support for each other (Miller and Kuhn, 1997; Shatz, 1996). It is possible that the rapid necrotic death of an initial population of cortical neurons results in the target deprivation death of connected neurons as is thought to occur in the adult brain (Martin *et al.*, 1998). Our data demonstrating a time-dependent increase in apoptotic cell death in the ipsilateral cortex is consistent with this possibility.

The previously reported effect of delayed administration of pan-caspase inhibitors to provide neuroprotection (Cheng *et al.*, 1998) within a region known to

exhibit early necrotic neurodegeneration (Rice *et al.*, 1981; Towfighi *et al.*, 1995) also suggests alternate mechanism of early vs late injury. Because many members of the caspase family are cytokine processors, caspase inhibition may curtail a more delayed cytokine mediated cell death rather than solely blocking delayed apoptosis (Wolf and Green, 1999). Regardless of the mechanism of caspase neuroprotection, it is obvious that caspase inhibitors have an effect on the neurodegeneration when administered 3 h after hypoxia-ischemia, a time at which early necrosis is well underway in the forebrain (Cheng *et al.*, 1998).

A switch in the mechanism of cell death may also explain the neuropathology found in the ipsilateral striatum. The patchy pattern of cell death may be the result of differential expression patterns of neurotransmitter receptors in the striatal matrix (Martin *et al.*, 1993) or may be the result of heterogeneity of neuronal connectivity (Alloway *et al.*, 1999). The initial columnar neurodegeneration seen in the neocortex (Fig. 2, and (Towfighi *et al.*, 1997)) correlates with areas of incomplete blood supply and patterns of altered NADH metabolism after hypoxia-ischemia in the developing brain (Welsh *et al.*, 1982)). It is known that cortical columns provide afferent striatal input with specific areas of sensory-motor cortex being represented within specific areas of the striatal matrix (Alloway *et al.*, 1999) (Gerfen, 1992). The degeneration of specific cortical columns could lead to degeneration of specific areas within the striatal mosaic during the delayed phase of striatal injury. The more rapid progression of the secondary phase of injury in the cortex than in the striatum supports a temporal framework in which loss of cortical innervation and, thus a deafferentation, could result in striatal neurodegeneration in anatomically discrete regions. Although no quantification of injury within the hippocampus was performed, qualitative analysis reveals timing and structure of injury very similar to that seen in the striatum. Specifically, early evidence of necrosis is abundant, followed by a secondary phase in which cells degenerate with the intermediate "continuum" phenotype (Portera-Cailliau *et al.*, 1997) and with an apoptotic morphology.

---

patterns similar to the pattern of retrograde transport of fluorogold (compare silver-staining of injured ipsilateral thalamus (A) with fluorogold immunoreactivity in thalamus (B) and layer III neurodegeneration in contralateral cortex (Fig. 4B) with fluorogold immunoreactivity in layer III contralateral cortex (E). Retrograde transport of fluorogold occurs specifically to the cell soma and processes (C), none is found in the surrounding neuropil. This specificity of retrograde transport allows identification of neurons with cortical connection to be identified even in late stages of apoptosis (D) when cellular morphology is disturbed. Scale bar A and B, 1 mm; C and D, 11  $\mu$ m; E, 500  $\mu$ m.



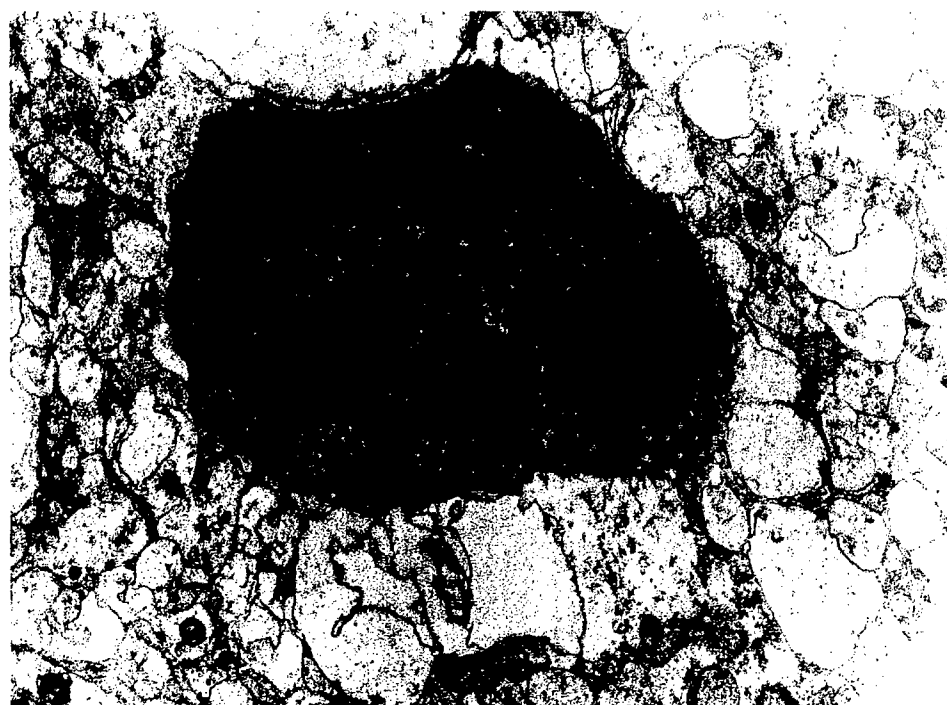


**FIG. 7.** Electron microscopy confirms that the structure of cell death in the ventral basal thalamus at 24 h following hypoxia-ischemia is apoptosis. Degenerating thalamic neurons have several characteristics of apoptosis including (1) an intact but fluted cellular membrane, (2) condensed cytoplasm with intact mitochondria, and (3) highly condensed, large, regularly shaped chromatin clumps.

The possibility that delayed cell death results from secondary mechanisms triggered by the early-occurring neurodegeneration is supported by the present data and previous experiments showing a prominent role for cortical connectivity in neuronal viability in immature thalamus, substantia nigra, and brainstem (Oo *et al.*, 1995; Kolb *et al.*, 1986). Large cortical lesions created in the first week of life result in atrophy of the thalamus and brainstem (Kolb *et al.*, 1986), while even selectively targeted cortical aspiration results in retrograde degeneration within thalamic nuclei (Al-Abdulla *et al.*, 1998). Hypoxia-ischemia results in apoptosis of dopaminergic neurons in the substantia nigra, presumably secondary to loss of trophic support from their striatal inputs (Oo *et al.*, 1995). This is the mechanism that we propose for the remote cell death seen in the present study. Evidence for this mechanism includes: (1) Injury in remote regions always occurs later than primary injury in ipsilateral forebrain. (2) Remote injury is accompanied by injury within interconnecting white matter pathways. (3) Neurons in thalamus that project to ipsilateral forebrain die via apoptosis following hypoxia-ischemia. (4) The structure of the cell death in remote regions was most commonly apoptosis, consistent with target deprivation mediated injury. Apoptosis is present at significant amounts in the

thalamus 21 h following the first increase in injury detectable by OD in the cortex and it continues during the progression of cortical injury to cavitory lesions. (5) In addition to remote cell death, we also find evidence of terminal degeneration on viable principal neurons in remote regions that are known to receive inputs from ipsilateral forebrain (Carpenter, 1983).

Remote neurodegeneration has been reported in the present model and has most often been attributed directly to global ischemic injury (Towfighi *et al.*, 1994, 1991). It is also possible that remote neurodegeneration occurs as the result of seizure activity. However, most evidence suggests that seizures do not exacerbate hypoxic-ischemic brain injury and that seizures may provide neuroprotection if they occur prior to the hypoxic-ischemic insult (Towfighi *et al.*, 1999). Seizure-induced neurodegeneration would not be limited to the ipsilateral forebrain and could occur in the interconnected regions where injury was found in the present study.

If neuronal connectivity does participate in the propagation of neurodegeneration in regions outside of the vascular distribution of the right common carotid, then remote neurodegeneration should only be found in the presence of axonal degeneration in interconnecting white matter pathways between forebrain

and contralateral cortex or brain stem. Because we do not find remote neurodegeneration in the absence of or preceding axonal degeneration, neuronal connectivity-mediated neurodegeneration is possible. Absence of remote injury, in animals exposed to hypoxia only, also supports the hypothesis that neuronal connectivity dictates patterns of degeneration after hypoxia-ischemia. If systemic hypoxemia were the cause of injury to remote regions in the present model, these remote regions should sustain injury when the animals are exposed to hypoxia alone. No evidence has been found of remote neurodegeneration as the result of systemic hypoxemia alone (Towfighi et al., 1994, 1995). The presence of apoptotic neurodegeneration within specific brainstem nuclei also argues for our hypothesis that remote neurodegeneration after hypoxia-ischemia is the result of loss of trophic support from the primarily injured regions.

Neuronal cell death in this model of hypoxia-ischemia occurs as at least three different forms. These different forms of cell death coexist in different regions of brain and sometimes in the same regions. Other studies have revealed the occurrence of necrosis and apoptosis (Rice et al., 1981; Towfighi et al., 1995; Cheng et al., 1998). Support for our conclusion that apoptosis occurs through mechanisms possibly related to connectivity and target deprivation has been found elsewhere (Oo et al., 1995). Our results are entirely consistent with these previous data and they extend our understanding of the neuropathology of neonatal hypoxia-ischemia to include neuroanatomical evidence for necrosis and apoptosis following hypoxia-ischemia and evidence for neurodegeneration within interconnecting axons and terminal projections. This study also shows for the first time that after hypoxia-ischemia, apoptosis and necrosis may coexist within the same cell. This new finding is similar to the observation that a hybrid morphology of cell death, the "continuum" cell, occurs in the forebrain, at delayed time points, in an immature model of glutamate receptor-mediated excitotoxic injury (Portera-Cailliau et al., 1997). The mechanism for the hybrid form of cell death is not yet understood but may relate to relative levels of ATP depletion as has been demonstrated in kidney cell culture *in vitro* (Feldenberg et al., 1999) and the activation of caspase 3 at 6–24 h in the forebrain following neonatal hypoxia-ischemia as shown in the present model (Han et al., 2000).

The methods utilized in the present study to evaluate neurodegeneration differ from the standard use of DNA end-labeling for identification of injury and cell death. We chose not to use TUNEL because it does not differentiate between apoptosis, necrosis, and hybrids of ap-

optosis and necrosis (Martin et al., 1999) and does not provide any information about degeneration of axons or nerve terminals and thus would not provide as much information as would silver staining. We chose to rely on silver staining for quantification of injury because we found it reliable in the prediction of the initial course of thalamic injury when compared with counts of apoptotic profiles. In addition, silver-staining allows identification of degeneration in both cell soma and processes (Du et al., 1998) and intensifies with progression of injury (Fig. 1). Although silver has been reported to label in the absence of cell death (Toth et al., 1998), the transient argyrophilia reported on hippocampal neurons following febrile seizures may represent degenerating nerve terminals which are subsequently eliminated without death of their target neuron. This possibility is supported by our findings of degenerating nerve terminals contacting cells, which appear to be morphologically normal (Figs. 4I and 4J).

In conclusion, this study reveals differences in cell death patterns in ipsilateral forebrain over time following hypoxia-ischemia. Axonal and terminal degeneration occurring along with apoptotic cell death in remote regions after hypoxia-ischemia support the hypothesis that the distribution of neuronal connections dictates the presence of injury, as well as the structure of primary and remote neurodegeneration following neonatal hypoxia-ischemia. These findings have important implications for the development of appropriately timed and targeted therapies for the protection of the neonatal brain and rescue of neurons following hypoxic-ischemic insults.

## ACKNOWLEDGMENTS

The authors gratefully acknowledge the expert technical assistance of Ann Sheldon, Debra Flock, and George Kuck, III. These studies were supported by AG16282 (L.J.M.), US Army Department of Defense DAMD17-99-1-9553 (L.J.M.), and NS 35902 (D.M.F.).

## REFERENCES

- Al-Abdulla, N. A., Portera-Cailliau, C., & Martin, L. J. (1998) Occipital cortex ablation in adult rat causes retrograde neuronal death in the lateral geniculate nucleus that resembles apoptosis. *Neuroscience* 86, 191–209.
- Alloway, K. D., Crist, J., Mutic, J. J., & Roy, S. A. (1999) Corticostriatal projections from rat barrel cortex have an anisotropic organization that correlates with vibrissal whisking behavior [In Process Citation]. *J. Neurosci.* 19, 10908–10922.
- Barks, J. D., & Silverstein, F. S. (1992) Excitatory amino acids contribute to the pathogenesis of perinatal hypoxic-ischemic brain injury. *Brain Pathol.* 2, 235–243.

- Bolz, J., Novak, N., Gotz, M., & Bonhoeffer, T. (1990) Formation of target-specific neuronal projections in organotypic slice cultures from rat visual cortex. *Nature* 346, 359–362.
- Carpenter, M. B., & Sutin, Jerome. (1983) *Human Neuroanatomy* pp. 315–357, 579–611. Williams and Wilkins, Baltimore.
- Cheng, Y., Deshmukh, M., D'Costa, A., Demaro, J. A., Gidday, J. M., Shah, A., Sun, Y., Jacquin, M. F., Johnson Jr, E. M., & Holtzman, D. M. (1998) Caspase inhibitor affords neuroprotection with delayed administration in a rat model of neonatal hypoxic-ischemic brain injury. *J. Clin. Invest.* 101, 1992–1999.
- Du, F., Eid, T., & Schwarcz, R. (1998) Neuronal damage after the injection of aminooxyacetic acid into the rat entorhinal cortex: A silver impregnation study. *Neuroscience* 82, 1165–1178.
- Eves, E. M., Boise, L. H., Thompson, C. B., Wagner, A. J., Hay, N., & Rosner, M. R. (1996) Apoptosis induced by differentiation or serum deprivation in an immortalized central nervous system neuronal cell line. *J. Neurochem.* 67, 1908–1920.
- Feldenberg, L. R., Thevananther, S., del Rio, M., de Leon, M., & Devarajan, P. (1999) Partial ATP depletion induces Fas- and caspase-mediated apoptosis in MDCK cells. *Am. J. Physiol.* 276, F837–F846.
- Gerfen, C. R. (1992) The neostriatal mosaic: Multiple levels of compartmental organization. *Trends Neurosci.* 15, 133–139.
- Hagan, P., Barks, J. D., Yabut, M., Davidson, B. L., Roessler, B., & Silverstein, F. S. (1996) Adenovirus-mediated over-expression of interleukin-1 receptor antagonist reduces susceptibility to excitotoxic brain injury in perinatal rats. *Neuroscience* 75, 1033–1045.
- Han, B. H., D'Costa, A., Back, S. A., Parsadanian, M., Patel, S., Shah, A. R., Gidday, J. M., Srinivasan, A., Deshmukh, M., & Holtzman, D. M. (2000) BDNF blocks caspase-3 activation in neonatal hypoxia-ischemia. *Neurobiol. Dis.* 7, 38–53.
- Kolb, B., Whishaw, I. Q., & van der Kooy, D. (1986) Brain development in the neonatally decorticated rat. *Brain Res.* 397, 315–326.
- Kotak, V. C., & Sanes, D. H. (1997) Deafferentation weakens excitatory synapses in the developing central auditory system. *Eur. J. Neurosci.* 9, 2340–2347.
- Levine, S. (1960) Anoxic-ischemic encephalopathy in rats. *Am. J. Pathol.* 36, 1–17.
- Li, L., Prevette, D., Oppenheim, R. W., & Milligan, C. E. (1998) Involvement of specific caspases in motoneuron cell death *in vivo* and *in vitro* following trophic factor deprivation. *Mol. Cell. Neurosci.* 12, 157–167.
- Liu, X. H., Eun, B. L., Silverstein, F. S., & Barks, J. D. (1996) The platelet-activating factor antagonist BN 52021 attenuates hypoxic-ischemic brain injury in the immature rat. *Pediatr. Res.* 40, 797–803.
- Lorenz, J. M., Wooliever, D. E., Jetton, J. R., & Paneth, N. (1998) A quantitative review of mortality and developmental disability in extremely premature newborns. *Arch. Pediatr. Adolesc. Med.* 152, 425–435.
- Martin, L. J., Al-Abdulla, N. A., Brambrink, A. M., Kirsch, J. R., Sieber, F. E., & Portera-Cailliau, C. (1998) Neurodegeneration in excitotoxicity, global cerebral ischemia, and target deprivation: A perspective on the contributions of apoptosis and necrosis. *Brain Res. Bull.* 46, 281–309.
- Martin, L. J., Blackstone, C. D., Hagan, R. L., & Price, D. L. (1993) The Striatal mosaic in primates: Striosomes and matrix are differentially enriched in ionotropic glutamate receptor subunits. *J. Neurosci.* 13, 782–792.
- Martin, L. J., Brambrink, A. M., Koehler, R. C., & Traystman, R. J. (1997) Primary sensory and forebrain motor systems in the newborn brain are preferentially damaged by hypoxia-ischemia. *J. Comp. Neurol.* 377, 262–285.
- Martin, L. J., Brambrink, A. M., Lehmann, C., Portera-Cailliau, C., Koehler, R. C., Rothstein, J., & Traystman, R. J. (1997) Hypoxia-ischemia causes abnormalities in glutamate transporters and death of astroglia and neurons in newborn striatum. *Ann. Neurol.* 42, 335–348.
- Martin, L. J., Kaiser, A., & Price, A. C. (1999) Motor neuron degeneration after sciatic nerve avulsion in adult rat evolves with oxidative stress and is apoptosis. *J. Neurobiol.* 40, 185–201.
- McDonald, J. W., Silverstein, F. S., & Johnston, M. V. (1988) Neurotoxicity of N-methyl-D-aspartate is markedly enhanced in developing rat central nervous system. *Brain Res.* 459, 200–203.
- Miller, M. W., & Kuhn, P. E. (1997) Neonatal transection of the infraorbital nerve increases the expression of proteins related to neuronal death in the principal sensory nucleus of the trigeminal nerve. *Brain Res.* 769, 233–244.
- Nelson, C., & Silverstein, F. S. (1994) Acute disruption of cytochrome oxidase activity in brain in a perinatal rat stroke model. *Pediatr. Res.* 36, 12–19.
- Nelson, K. B., & Grether, J. K. (1999) Causes of cerebral palsy. *Curr. Opin. Pediatr.* 11, 487–491.
- Oo, T. F., Henschcliff, C., & Burke, R. E. (1995) Apoptosis in substantia nigra following developmental hypoxic-ischemic injury. *Neuroscience* 69, 893–901.
- Oppenheim, R. W. (1991) Cell death during development of the nervous system. *Annu. Rev. Neurosci.* 14, 453–501.
- Portera-Cailliau, C., Price, D. L., & Martin, L. J. (1997) Excitotoxic neuronal death in the immature brain is an apoptosis-necrosis morphological continuum. *J. Comp. Neurol.* 378, 70–87.
- Rice, J. E. d., Vannucci, R. C., & Brierley, J. B. (1981) The influence of immaturity on hypoxic-ischemic brain damage in the rat. *Ann. Neurol.* 9, 131–141.
- Shatz, C. J. (1996) Emergence of order in visual system development. *Proc. Natl. Acad. Sci. USA* 93, 602–608.
- Toth, Z., Yan, X. X., Haftoglou, S., Ribak, C. E., & Baram, T. Z. (1998) Seizure-induced neuronal injury: Vulnerability to febrile seizures in an immature rat model. *J. Neurosci.* 18, 4285–4294.
- Towfighi, J., Housman, C., Mauger, D., & Vannucci, R. C. (1999) Effect of seizures on cerebral hypoxic-ischemic lesions in immature rats. *Brain Res. Dev. Brain Res.* 113, 83–95.
- Towfighi, J., Housman, C., Vannucci, R. C., & Heitjan, D. F. (1994) Effect of unilateral perinatal hypoxic-ischemic brain damage on the gross development of opposite cerebral hemisphere. *Biol. Neonate* 65, 108–118.
- Towfighi, J., Mauger, D., Vannucci, R. C., & Vannucci, S. J. (1997) Influence of age on the cerebral lesions in an immature rat model of cerebral hypoxia-ischemia: A light microscopic study. *Brain Res. Dev. Brain Res.* 100, 149–160.
- Towfighi, J., Yager, J. Y., Housman, C., & Vannucci, R. C. (1991) Neuropathology of remote hypoxic-ischemic damage in the immature rat. *Acta Neuropathol.* 81, 578–587.
- Towfighi, J., Zec, N., Yager, J., Housman, C., & Vannucci, R. C. (1995) Temporal evolution of neuropathologic changes in an immature rat model of cerebral hypoxia: A light microscopic study. *Acta Neuropathol.* 90, 375–386.
- Welsh, F. A., Vannucci, R. C., & Brierley, J. B. (1982) Columnar alterations of NADH fluorescence during hypoxia-ischemia in immature rat brain. *J. Cereb. Blood Flow Metab.* 2, 221–228.
- Wolf, B. B., & Green, D. R. (1999) Suicidal tendencies: Apoptotic cell death by caspase family proteinases. *J. Biol. Chem.* 274, 20049–20052.



## Letter to Neuroscience

### PROJECTION NEURONS AND INTERNEURONS IN THE LATERAL GENICULATE NUCLEUS UNDERGO DISTINCT FORMS OF DEGENERATION RANGING FROM RETROGRADE AND TRANSSYNAPTIC APOPTOSIS TO TRANSIENT ATROPHY AFTER CORTICAL ABLATION IN RAT

N. A. AL-ABDULLA<sup>a,b</sup> and L. J. MARTIN<sup>a,c\*</sup>

<sup>a</sup>Department of Pathology, Division of Neuropathology, Johns Hopkins University School of Medicine, Baltimore, MD 21205-2196, USA

<sup>b</sup>The Wilmer Eye Institute of the Johns Hopkins Hospital, Baltimore, MD 21205-2196, USA

<sup>c</sup>Department of Pathology, Division of Neuroscience, Johns Hopkins University School of Medicine, Baltimore, MD 21205-2196, USA

**Key words:** Alzheimer's disease, amyotrophic lateral sclerosis, axotomy, cell death, DNA damage, traumatic brain injury.

The cytological responses of thalamic interneurons to selective degeneration of thalamocortical projection neurons after cortical damage in the adult brain are poorly understood. We used a unilateral neocortical lesion model (occipital cortex ablation) in the adult rat to test the hypothesis that interneurons and projection neurons in the lateral geniculate nucleus undergo distinct forms of degeneration. *In situ* nuclear DNA fragmentation in neurons in the lateral geniculate occurs maximally at 7 days postlesion. Geniculocortical projection neurons that are identified by the retrograde tracer Fluorogold die primarily with a morphology of endstage apoptosis prominent at 7 days postlesion. In contrast, interneurons, identified by their particular nuclear ultrastructure and by glutamic acid decarboxylase immunoreactivity, undergo an atrophic vacuolar pathology starting early during the period of projection neuron death and peaking after the projection neuron death is complete. This degeneration of interneurons is transient, because these neurons exhibit structural recovery and their numbers are not changed significantly postlesion. A rare subset of interneurons (less than one in 100 interneurons and less than one in 100 apoptotic cells) undergoes

apoptosis concurrently with the projection neurons.

We conclude that different types of neurons within the same thalamic nucleus respond differently to focal cortical target deprivation. Unlike the apoptosis-prone projection neurons, most interneurons undergo transient transsynaptic atrophy and recovery rather than cell death. Nevertheless, a small subset of lateral geniculate interneurons undergoes transsynaptic apoptosis in response to projection neuron apoptosis. The pathological responses of thalamic neurons to cortical trauma vary depending on cell type.

© 2002 IBRO. Published by Elsevier Science Ltd. All rights reserved.

The thalamus is a frequent site of remote neurodegeneration after neocortical damage in humans and animals, occurring after surgical hemidecortication, head trauma, and stroke (Powell, 1952; Adams et al., 2000). Ablation of the visual cortex induces neurodegeneration in thalamus (Lashley, 1941; Barron et al., 1967; Giolli and Guthrie, 1971; Madarász et al., 1983). The geniculocortical projection neurons in the dorsal lateral geniculate nucleus (dLGN) die by a process that resembles apoptosis (Al-Abdulla et al., 1998) which is controlled by *Bax* and *p53* genes (Martin et al., 2001). However, interneurons in the dLGN, which comprise up to 15–25% of the neurons in this region (LeVay and Ferster, 1979; Madarász et al., 1983; Weber and Kalil, 1983) are not usually evaluated after cortical damage. We used a unilateral neocortical lesion model (occipital cortex ablation) to test the hypothesis that interneurons and projection neurons in the LGN undergo distinct forms of degeneration in adult rat. *In situ* nuclear DNA fragmentation in lateral geniculate neurons occurred maxi-

\*Correspondence to: L.J. Martin, Johns Hopkins University School of Medicine, Department of Pathology, 558 Ross Building, 720 Rutland Avenue, Baltimore, MD 21205-2196, USA. Tel.: +1-410-502-5170; fax: +1-410-955-9777.

E-mail address: lmartin@jhmi.edu (L. J. Martin).

**Abbreviations:** CNS, central nervous system; dLGN, dorsal lateral geniculate nucleus; EM, electron microscopy; FG, Fluorogold; GABA,  $\gamma$ -aminobutyric acid; GAD, glutamic acid decarboxylase; LGN, lateral geniculate nucleus; rER, rough endoplasmic reticulum; TUNEL, terminal transferase-mediated deoxyuridine triphosphate nick end labeling.

mally at 7 days postlesion. Geniculocortical projection neurons, identified by the retrograde tracer Fluorogold (FG), were apoptotic by 7 days postlesion. In contrast, interneurons, identified by glutamic acid decarboxylase (GAD) immunoreactivity and nuclear ultrastructure, undergo a transient atrophic vacuolar pathology starting early during the period of projection neuron death and peaking after projection neuron death is complete. Their total numbers did not change significantly postlesion. Therefore, different types of neurons within the same thalamic nucleus respond differently after neocortical damage. The projection neurons are apoptosis-prone, while most interneurons undergo transient transsynaptic atrophy and recovery rather than cell death.

Cell death in the adult rat dLGN was studied using terminal transferase-mediated deoxyuridine triphosphate nick end labeling (TUNEL). TUNEL-positive cells were found within the dLGN ipsilateral to the lesion at 3–30 days postlesion (Figs. 1 and 2A). TUNEL staining of cells in the ipsilateral dLGN was frequent. Many more than a few isolated cells were positive, as shown in panoramic photomicrographs of the ipsilateral dLGN (Fig. 1A), consistent with our earlier studies revealing an ~57% loss of neurons in rat (Al-Abdulla et al., 1998; Martin et al., 2001). These labeled cells were neurons (Figs. 1B and 2A). The TUNEL-positive cells within the ipsilateral dLGN were geniculocortical projection neurons based on the prelabeling with FG (Fig. 2A), confirming earlier observations (Al-Abdulla and Martin, 1998). This labeling was highly specific for the dLGN ipsilateral to the cortical lesion. No labeling was seen in the LGN contralateral to the lesion at any time (Fig. 1C). The number of TUNEL-positive cells changed over time in the ipsilateral dLGN (Fig. 1D). The mean number ( $\pm$  standard deviation) of TUNEL-positive cells per 0.2 mm<sup>2</sup> was  $4.5 \pm 0.7$ ,  $26.0 \pm 4.2$ , and  $2.0 \pm 1.4$  at 3, 7, and 14 days postlesion, respectively. By 30 days postlesion, TUNEL-positive cells were observed infrequently ( $< 1$  darkly stained TUNEL-positive cells/0.2 mm<sup>2</sup>).

We determined if loss of interneurons within the LGN also contributed to the observed cell death. Interneurons in the dLGN were counted to determine if there was a reduction in their number. GAD-positive cells in the dLGN were detected with antibodies (Fig. 2B). Their numbers did not change significantly after occipital cortex lesion. The mean number ( $\pm$  standard deviation) of GAD-positive cells in the dLGN per 0.2 mm<sup>2</sup> was  $20 \pm 4$ ,  $20 \pm 2$ ,  $24 \pm 1$ , and  $20 \pm 2$  at 7, 14, 30 days and 3 months postlesion, respectively (Fig. 3). Thus, loss of GABAergic interneurons did not contribute significantly to the cell death in the dLGN after occipital cortex ablation.

Although the average number of GAD-positive cells did not change significantly in the dLGN after occipital cortex ablation (Fig. 3), interneurons undergo prominent structural abnormalities. This observation was made by light microscopic evaluation of GAD immunostained and Nissl-counterstained sections (Fig. 2C) and by electron microscopy (EM) (Fig. 4). Normal GABAergic interneurons have an ovoid cell body and long slender bifurcating dendrites (Fig. 2B). At 7 days postlesion, GAD-positive cells appeared abnormal, with large den-

dratic and cytoplasmic vacuoles (Fig. 2C). These vacuolated interneurons were found frequently within dLGN areas containing many dying geniculocortical projection neurons. The hydropic atrophy of the majority of interneurons continued through 14 days, and to a lesser

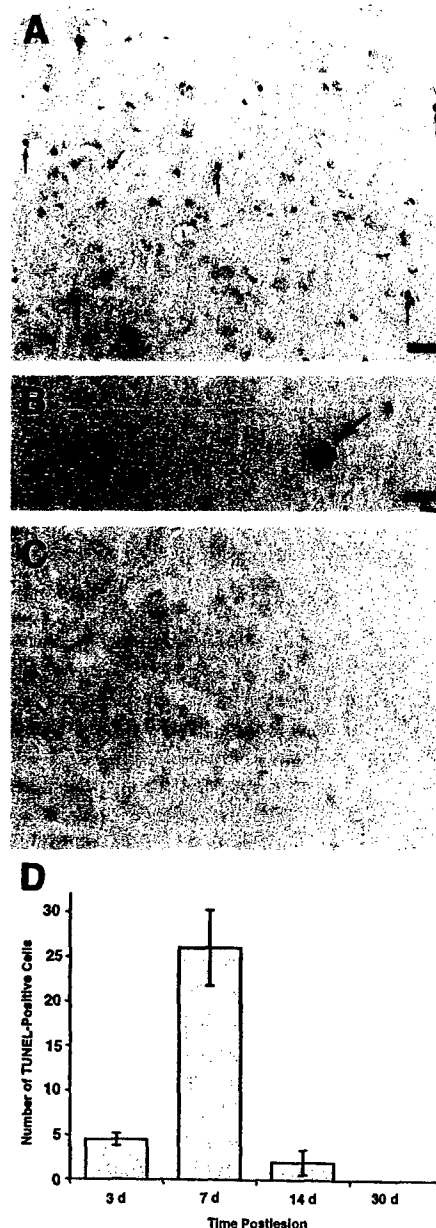


Fig. 1. TUNEL demonstrates that the cell death occurring within the LGN after cortical ablation is copious and is specific for the ipsilateral side. (A) Numerous TUNEL-positive cells (arrows) are present within the ipsilateral LGN at 7 days postlesion (see Fig. 2A for higher magnification photograph illustrating that these TUNEL-positive cells are geniculocortical projection neurons). Scale bar in A (same for C) = 80  $\mu$ m. (B) TUNEL-positive cell (arrow) in the ipsilateral dLGN seen at high magnification. This cell undergoing DNA fragmentation has a large round nucleus typical of a neuron. The DNA is clumped around the margin of the nucleus consistent with apoptosis. Scale bar = 10  $\mu$ m. (C) No TUNEL labeling was seen in the contralateral LGN. (D) Counts of TUNEL-positive cells (mean  $\pm$  S.D.) show that cell death occurs from day 3 to day 30 postlesion, peaking at 7 days postlesion. The value at 30 day is essentially zero. TUNEL-positive cell number at 7 days is significantly different ( $P < 0.05$ ) from other times.

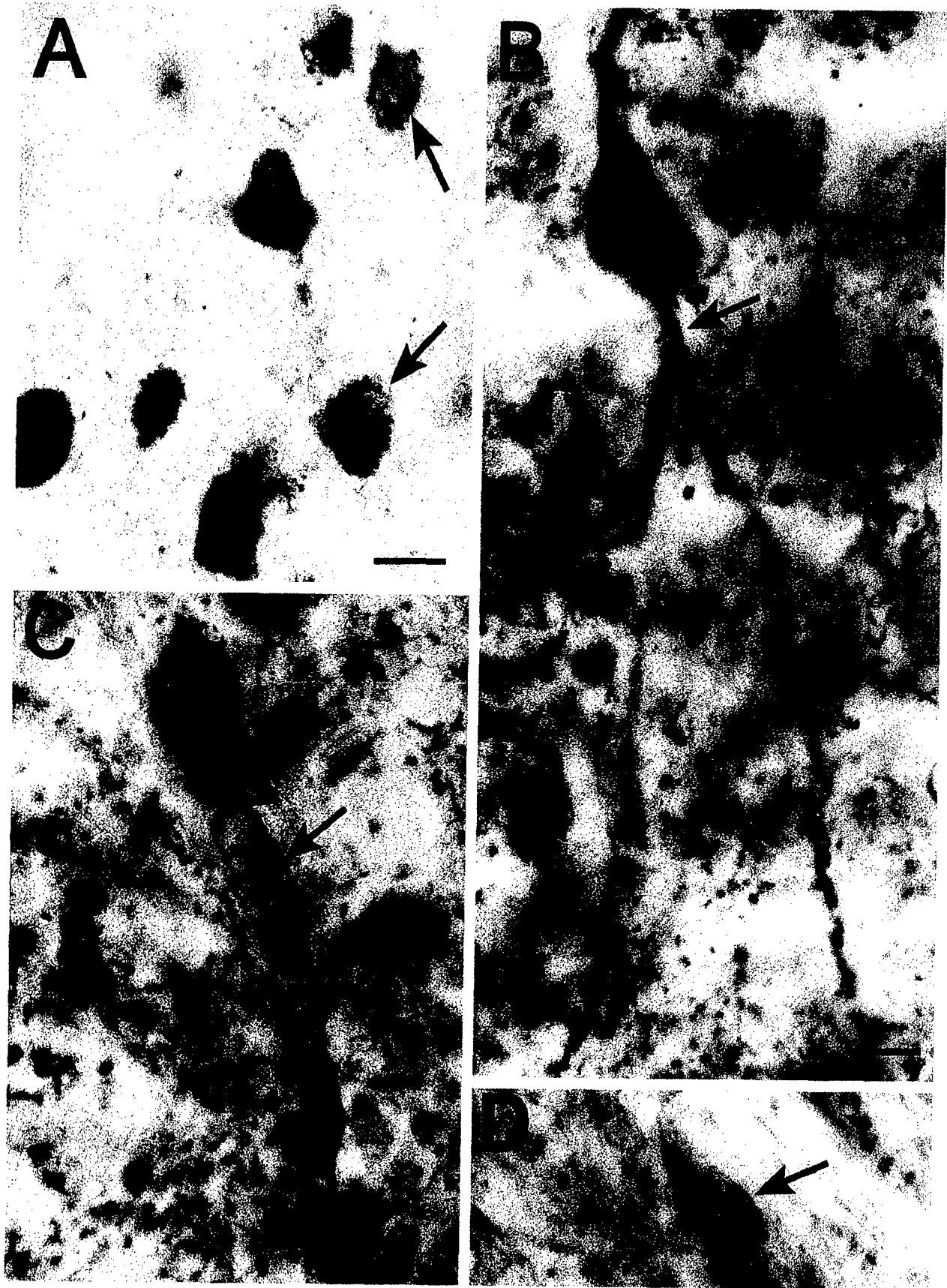


Fig. 2 (Caption overleaf).

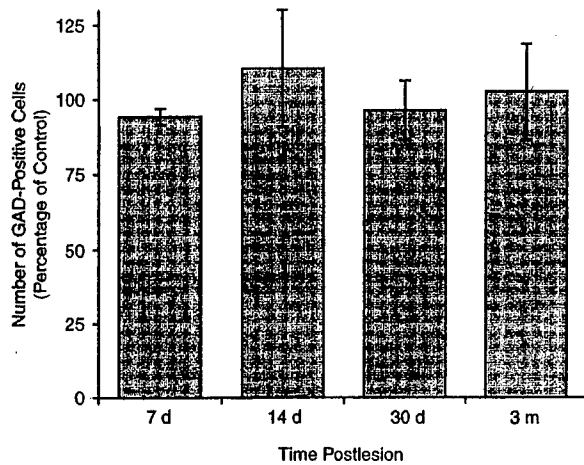


Fig. 3. The number of GAD-positive cells in the dLGN does not change after occipital cortex ablation. Values are reported as mean  $\pm$  S.D. at 7, 14, and 30 days (d) postlesion and 3 months (m) postlesion.

extent at 30 days postlesion (not shown). By 3 months postlesion, interneurons were unremarkable, and interneuron cytopathology was absent (not shown).

Apoptosis of GAD-positive neurons was very infrequent (Fig. 2D), consistent with the failure to detect significant loss of interneurons. These neurons had a condensed cytoplasm and a nucleus with chromatin that was condensed into small round masses (Fig. 2D), characteristic of apoptosis (Martin et al., 1998; Martin et al., 1999; Martin, 2001). Apoptotic interneurons comprised  $<1$  in 100 apoptotic cells and  $<1$  in 100 GAD-positive cells within the ipsilateral dLGN.

EM was used to examine the structure of interneuron pathology for comparison with projection neuron degeneration. Interneurons were identified by a prominent invagination of the nuclear envelope (Fig. 4A, arrow). An indented nuclear envelope is a distinct ultrastructural signature of GAD-positive interneurons (Ohara et al., 1983; Montero and Singer, 1985). It is not known with certainty whether this feature changes in cells responding to an injury. Apoptotic cells had the characteristic dark round chromatin masses (Fig. 4B, asterisk) and condensed cytoplasm. At end-stage apoptosis the cell identity was undecipherable. Thalamic projection neurons and interneurons in the dLGN primarily underwent distinct forms of degeneration after cortical damage. The major form of neurodegeneration was apoptosis, occurring in most projection neurons by 7 days postlesion. A rarefaction pathology, distinct from apoptosis, was a less

frequently occurring form of neurodegeneration (Fig. 4C, D). It occurred in interneurons at 7 and 14 days postlesion. The cytoplasmic pallor appeared to result from dispersion, fragmentation, and apparent loss of the rough endoplasmic reticulum (rER) and Golgi apparatus (Fig. 4C, D). Stacks of rER and Golgi were observed infrequently. Many mitochondria were still present in these pale neurons, but they were dark and condensed (Fig. 4C, D), consistent with a cell responding to injury (Martin et al., 1998). Vacuolar changes were present in the cytoplasm of these interneurons. The nucleus had dispersed chromatin and was weakly contrasted with osmium, resulting in marked nuclear pallor (Fig. 4D). These changes caused the interneurons to appear distinctly lighter than normal neurons. By 30 days postlesion, these degenerative cytoplasmic and nuclear changes were less apparent (vacuoles and mitochondrial condensation dissipated), as these interneurons appeared to recover (Fig. 4H). By 3 months postlesion, interneurons appeared normal, with the rER stacking, mitochondria, Golgi, and nuclear organization appearing unaltered (not shown).

Degeneration of interneurons with an apoptotic morphology was observed infrequently by EM. It could be found only after extensive viewing. When it was found, the structure resembled classic apoptosis similar to LGN projection neuron apoptosis (Al-Abdulla et al., 1998; Martin et al., 1998). In some interneurons at 6 days postlesion, the nucleus contained aggregates of chromatin in nascent compaction (Fig. 4E, F). At early structural stages of apoptosis the nuclear invagination was still present, thus marking these cells as interneurons. By 7 days postlesion, these occasional interneurons had a condensed nucleus with an intact nuclear envelope (Fig. 4G). The nucleus contained multiple dark, moderately dense aggregates of chromatin. Their perikarya were dark and shrunken, consisting of tightly packed organelles within a dark cytoplasmic matrix (Fig. 4G). These structural features of early apoptosis progressed to end-stage apoptosis. At this time apoptotic interneurons and projection neurons were indistinguishable morphologically (Fig. 4B).

Although the occipital cortex ablation model has been employed for over 50 years, this brain injury paradigm can still be used to unravel the mechanisms of neuronal degeneration and recovery within the CNS. This study is novel because it highlights the differential vulnerability of remote thalamic neurons to distant cortical injury. The synchronized apoptosis of projection neurons occurred in

Fig. 2. Geniculocortical projection neurons and GABAergic interneurons degenerate after occipital cortex ablation. (A) Dying cells in the dLGN are geniculocortical projection neurons (arrows). TUNEL-positive cells (brown nuclear labeling) contain the retrograde tracer FG (blue-green cytoplasmic labeling surrounding the nucleus with aggregates of TUNEL staining), indicating that these dying neurons projected to the occipital cortex. Scale bar = 20  $\mu$ m. (B) Normal-appearing GAD-immunopositive interneuron in the dLGN. The cell body is ovoid and the cytoplasm is enriched in GAD immunoreactivity (brown staining). A primary dendrite (arrow) bifurcates into long slender secondary dendrites. Scale bar (same for C and D) = 10  $\mu$ m. (C) A GAD-immunopositive interneuron at 7 days postlesion with large intradendritic vacuoles aligned side-by-side (arrow). The continuity between the vacuolated dendrite and the parent cell body is identified (arrowhead). (D) Apparent apoptosis was observed in very few GAD-immunopositive cells at 7 days postlesion. In immunoperoxidase-labeled sections counterstained with Cresyl Violet, such rare cells (arrow) have a shrunken cell body with residual GAD staining (brown) and a small condensed nucleus, consistent with apoptosis.



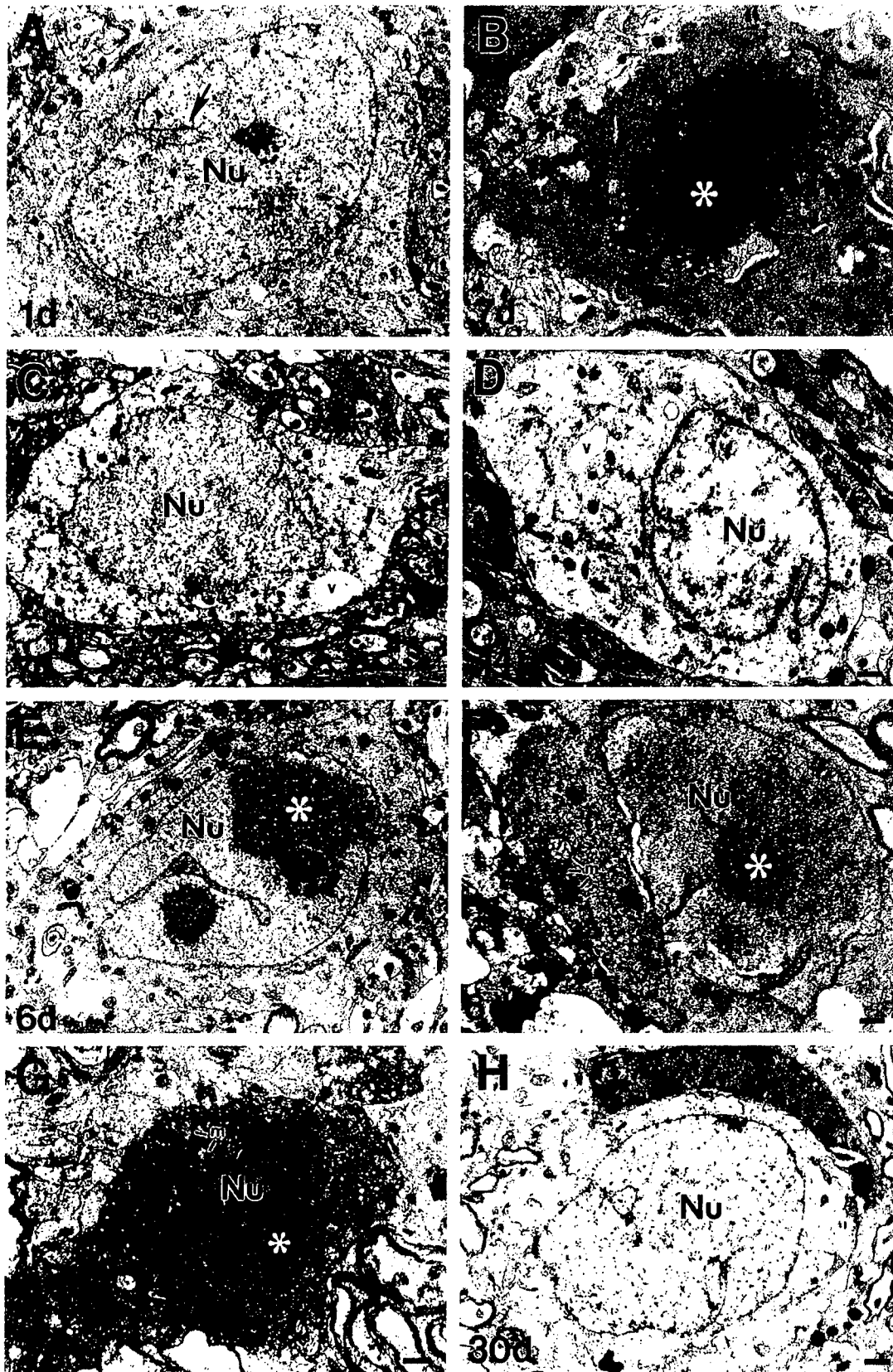


Fig. 4 (Caption overleaf).



association with transient atrophic degeneration and recovery of LGN interneurons. In the presence of widespread apoptosis of geniculocortical projection neurons, the number of GAD-positive cells did not change significantly after occipital cortex ablation; however, EM revealed an interesting pathology in these neurons. This injury in interneurons may be indicative of a transsynaptic retrograde atrophy.

This process of atrophy is similar to that observed in other models of axotomy. After fimbria-fornix transection in rat, neurons in the medial septal nucleus, lateral septal nucleus, and medial mammillary nucleus undergo a sustained vacuolar atrophy (Ginsberg and Martin, 1998; Ginsberg et al., 1999; Ginsberg and Martin, 2002). Unlike the fimbria-fornix model, the interneuronal degeneration in the adult LGN is transient. These abnormalities occur in the apparent absence of nuclear pyknosis and chromatin condensation, in contrast to the apoptotic morphology of projection neurons. Thus, projection neurons and interneurons in the LGN undergo primarily distinct forms of neurodegeneration after occipital cortex lesions. While most geniculocortical projections die by a process that is apoptosis (Martin et al., 2001), most interneurons undergo a hydropic pathology and then recover.

Atrophy of interneurons may be a response to loss of their target neurons, specifically the geniculocortical projection neurons. It is not yet known how many geniculocortical projection neurons are innervated by a single dLGN interneuron and how many relay neurons are required to sustain an interneuron. It is reasonable to suspect that local circuit neurons in the dLGN lose their intrageniculate targets to varying degrees. A transient or sustained decrease in the intrinsic supply of target-derived trophic factors may commit dLGN interneurons to transient degeneration and recovery or to cell death by an apoptotic-like process. Thus, the fate of LGN interneurons may fall along a cell death continuum (Martin et al., 1998; Martin, 2001), depending on the severity of target deprivation and the extent of axonal

collateralization (Fry and Cowan, 1972). Very few dLGN interneurons undergo apoptosis. This death occurs at the end of the wave of geniculocortical projection neuron apoptosis; therefore, this neuronal death of LGN interneurons could be transsynaptic apoptosis. We have described transsynaptic neuronal apoptosis in other models of brain injury (Ginsberg and Martin, 2002).

The mechanisms of interneuron recovery and survival may be related to formation of synaptic interactions with remaining projection neurons or afferents from retinal ganglion cells or corticogeniculate neurons. Interneurons in cerebral cortex respond to apoptosis of their target neurons by up-regulation of the expression of neurotrophin genes (Wang et al., 1998). This transient interneuron degeneration followed by recovery in thalamus may be an important cellular model for isolating *in vivo* mechanisms of neuronal repair and rescue.

## CONCLUSION

This study is novel because it highlights the vulnerability of remote thalamic interneurons to distant cortical injury. The responses of thalamic interneurons to cortical damage are very complex. The process of interneuronal degeneration appears to embrace both transsynaptic neuronal apoptosis as well as transient atrophy with recovery. Although the occipital cortex ablation model has been employed for over fifty years, this brain injury paradigm can still provide extremely useful insights into the mechanisms of neuronal degeneration and recovery within the CNS.

## EXPERIMENTAL PROCEDURES

### Lesion paradigm

An occipital cortex aspiration lesion served as the model for focal neocortical damage and axotomy and target deprivation of LGN projection neurons in adult male Sprague-Dawley rats

Fig. 4. EM demonstrates that neuronal degeneration in the dLGN after occipital cortex ablation can occur as either apoptosis or transient atrophy. These electron micrographs are representative of the different forms of degeneration in the dLGN. (A) Interneurons at 1 day (1d) postlesion have a normal cytoplasm containing organelles, including perinuclear stacking of rER (at lower left of cell), numerous ribosomes, and an open nucleus (Nu) with dispersed chromatin. The nuclear invagination (arrow) flags this neuron as an interneuron in the dLGN. Scale bar = 0.7  $\mu$ m (same for C). (B) Copious end-stage neuronal apoptosis is observed in the dLGN at 7 days (7d) postlesion. Cellular shrinkage and the formation of large chromatin masses (asterisk) characterize this apoptosis. At this stage, the identity of this cell is indeterminate. Scale bar = 0.3  $\mu$ m. (C) At 7 days (7d) postlesion, atrophic changes, occurring in the majority of interneurons, include fragmentation and dispersion of the rER and rarefaction of the cytoplasm. Membrane-bound vacuoles (v) are present. The mitochondria are darker than normal. The nucleus (Nu) appears intact. (D) By 14 days (14d) postlesion, the ultrastructural pathology of injured interneurons is very apparent. Nuclear (Nu) pallor is observed with dispersion and rarefaction of the chromatin, without chromatin compaction. The cytoplasm is pale with some vacuoles (v). Mitochondria are dark but appear intact. Scale bar = 0.8  $\mu$ m (same for E). (E) At 6 days (6d) postlesion, very few interneurons (identified by the conspicuous nuclear invagination) show a darkening of the cytoplasm. Aggregates of chromatin (asterisk) in nascent compaction are observed in the nucleus (Nu) of these rare neurons. (F) Other neurons that could be interneurons based on nuclear invaginations are more advanced (than the neurons shown in E) in their nuclear and cytoplasmic condensation. The nuclear matrix (Nu) is darkening as chromatin aggregates are forming (asterisk). The cytoplasmic matrix becomes darker. Most mitochondria (m) are still intact, although some are degenerating (upper mitochondrion of the three labeled). Scale bar = 0.6  $\mu$ m. (G) At 7 days (7d) postlesion, the apoptosis is structurally advanced. Dense aggregates of chromatin (asterisk) in the nucleus (Nu) have been formed. The cells are shrunken and the cytoplasm is darkly condensed. Most mitochondria (m) are degenerating. Scale bar = 0.5  $\mu$ m. (H) By 30 days (30d) postlesion, interneurons with atrophic cytoplasmic and nuclear changes appear to be recovering based on the cytoplasmic and nuclear (Nu) integrity (compare with neurons shown in A-D). Glial cells (upper cell with dark crescent nucleus) are adjacent to these interneurons. Scale bar = 0.8  $\mu$ m.

(Charles River, Wilmington, MA, USA). The institutional Animal Care and Use Committee approved the animal protocol. This model has been described (Al-Abdulla et al., 1998). The rats were anesthetized with sodium pentobarbital (70 mg/kg, intraperitoneal) and perfused at 1 day, 3, 4, 5, 6, 7, 14, and 30 days and 3 months postlesion ( $n=8$  per time point). To specifically mark geniculocortical projection neurons, the retrograde tract tracer FG (Fluorochrome, Inc., Englewood, CO, USA) was injected into visual cortex as described (Al-Abdulla and Martin, 1998). Three days later the rats ( $n=8$ ) underwent an occipital cortex ablation. FG-injected rats with occipital cortex ablations recovered for 6 days before being perfused. Another set of rats was killed at 1, 3, 5, 6, or 7 days postlesion ( $n=2$  per time point) for EM studies as described (Al-Abdulla et al., 1998; Al-Abdulla and Martin, 1998).

#### Evaluation of neurodegeneration in the dLGN

Brain samples containing the diencephalon were either processed for paraffin histology or were cryopreserved in 30% sucrose in phosphate buffer and frozen in isopentane chilled by dry ice. Roughly half of the brains were processed by one or the other method. Coronal sections (10  $\mu$ m) through the LGN were cut using a rotary microtome from the paraffin-processed brains. These sections were mounted on glass slides coated with Vectabond and were used for identifying DNA fragmentation by TUNEL, a hallmark of cell death (Gavrieli et al., 1992; Martin, 2001), and for dual staining for TUNEL and FG to identify dying corticopetal projection neurons. These methods have been described previously (Martin et al., 1997, 1999; Al-Abdulla et al., 1998; Al-Abdulla and Martin, 1998). DNA fragmentation was visualized with diaminobenzidine (generating an amorphous brown reaction product) and FG was visualized with benzidine dihydrochloride (generating a blue-green crystalline reaction product).

Coronal sections (40  $\mu$ m) through the LGN were cut from the frozen brains using a sliding microtome. These sections were used for immunoperoxidase detection of GAD. GAD is a marker for  $\gamma$ -aminobutyric acid (GABA)-containing interneurons. These sections were processed using a free-floating immu-

noperoxidase method with diaminobenzidine as chromogen. Two different polyclonal antibodies were used (diluted 1:2000). One antibody detects GAD-67 (AB108, Chemicon Inc., Temecula, CA, USA) and the other antibody detects both GAD-65 and GAD-67 (G5163, Sigma, St. Louis, MO, USA).

Stereologic counting of TUNEL-positive cells and GAD-positive neurons was performed using the optical disector methods as previously described (Calhoun et al., 1996; Al-Abdulla et al., 1998; Martin et al., 2001) using a lens with a depth of focus of 1.5  $\mu$ m (Olympus, D Planapo 60). The analysis was done in the ipsilateral dLGN at 7, 14, and 30 days as well as 3 months postlesion ( $n=4$  rats per time group). The contralateral dLGN of the same animal was used as a control. Randomly selected coronal sections through the rostro-caudal axis of the dLGN were used. Systematic random sampling was used to analyze the dLGN. For each adult rat, neuronal profiles were counted at 600 $\times$  magnification. Neuronal counts in the dLGN were used to determine group means and variances and comparisons among groups were performed using a one-way analysis of variance and a Student's *t*-test.

For EM, samples of LGN ipsilateral and contralateral to the cortical lesion were microdissected from each rat, washed in phosphate buffer, placed in 2% osmium tetroxide for 2 h, dehydrated, and embedded in plastic. Semithin sections (1  $\mu$ m) stained with 1% Toluidine Blue were screened for regions of interest, and then thin sections (gold interference color) were cut on an ultramicrotome (Sorvall, Norwalk, CT, USA), contrasted with uranyl acetate and lead citrate, and viewed with a JEOL 100 S electron microscope.

**Acknowledgements**—Supported by grants from the U.S. Public Health Service, National Institutes of Health, National Institute of Neurological Disorders and Stroke (NS34100) and National Institute on Aging (AG16282) and the Department of Defense, U.S. Army Medical Research and Materiel Command (DAMD17-99-1-9553).

#### REFERENCES

- Adams, J.H., Graham, D.I., Jennett, B., 2000. The neuropathology of the vegetative state after an acute brain insult. *Brain* 123, 1327–1338.
- Al-Abdulla, N.A., Martin, L.J., 1998. Apoptosis of retrogradely degenerating neurons occurs in association with the accumulation of perikaryal mitochondria and oxidative damage to the nucleus. *Am. J. Pathol.* 153, 447–456.
- Al-Abdulla, N.A., Portera-Cailliau, C., Martin, L.J., 1998. Occipital cortex ablation in adult rat causes retrograde neuronal death in the lateral geniculate nucleus that resembles apoptosis. *Neuroscience* 86, 191–209.
- Barron, K.D., Doolin, P.F., Oldershaw, J.B., 1967. Ultrastructural observations on retrograde atrophy of lateral geniculate body. I. Neuronal alterations. *J. Neuropathol. Exp. Neurol.* 26, 300–326.
- Calhoun, M.E., Jucker, M., Martin, L.J., Thinakaran, G., Price, D.L., Mouton, P.R., 1996. Comparative evaluation of synaptophysin-based methods for quantification of synapses. *J. Neurocytol.* 25, 821–828.
- Fry, F.J., Cowan, W.M., 1972. A study of retrograde cell degeneration in the lateral mamillary nucleus of the cat, with special reference to the role of axonal branching in the preservation of the cell. *J. Comp. Neurol.* 144, 1–24.
- Gavrieli, Y., Sherman, Y., Ben-Sasson, S.A., 1992. Identification of programmed cell death *in situ* via specific labeling of nuclear DNA fragmentation. *J. Cell Biol.* 119, 493–501.
- Ginsberg, S.D., Martin, L.J., 1998. Ultrastructural analysis of the progression of neurodegeneration in the septum following fimbria-fornix transection. *Neuroscience* 86, 1259–1272.
- Ginsberg, S.D., Portera-Cailliau, C., Martin, L.J., 1999. Fimbria-fornix transection and excitotoxicity produce similar neurodegeneration in the septum. *Neuroscience* 88, 1059–1071.
- Ginsberg, S.D., Martin, L.J., 2002. Axonal transection in adult rat brain induces transsynaptic apoptosis and persistent atrophy of target neurons. *J. Neurotrauma* 19, 99–109.
- Gioli, R.A., Guthrie, M.D., 1971. Organization of subcortical projections of visual areas I and II in the rabbit. An experimental degeneration study. *J. Comp. Neurol.* 142, 351–376.
- Lashley, K.S., 1941. Thalamo-cortical connections of the rat's brain. *J. Comp. Neurol.* 75, 67–121.
- LeVay, S., Ferster, D., 1979. Proportion of interneurons in the cat's lateral geniculate nucleus. *Brain Res.* 164, 304–308.
- Madarász, M., Somogyi, J., Silakov, V.L., Hámori, J., 1983. Residual neurons in the lateral geniculate nucleus of adult cats following chronic disconnection from the cortex. *Exp. Brain Res.* 52, 363–374.
- Martin, L.J., Brambrink, A.M., Lehmann, C., Kocher, R., Rothstein, J., Traystman, R.J., 1997. Hypoxia-ischemia causes abnormalities in glutamate transporters and death of astroglia and neurons in newborn striatum. *Ann. Neurol.* 42, 335–348.
- Martin, L.J., Al-Abdulla, N.A., Brambrink, A.M., Kirsch, J.R., Sieber, F.E., Portera-Cailliau, C., 1998. Neurodegeneration in excitotoxicity, global cerebral ischemia, and target deprivation: a perspective on the contributions of apoptosis and necrosis. *Brain Res. Bull.* 46, 281–309.

- Martin, L.J., Kaiser, A., Price, A.C., 1999. Motor neuron degeneration after sciatic nerve avulsion in adult rat evolves with oxidative stress and is apoptosis. *J. Neurobiol.* 40, 185–201.
- Martin, L.J., Kaiser, A., Yu, J.W., Natale, J.E., Al-Abdulla, N.A., 2001. Injury-induced apoptosis of neurons in adult brain is mediated by p53-dependent and p53-independent pathways and requires bax. *J. Comp. Neurol.* 433, 299–311.
- Martin, L.J., 2001. Neuronal cell death in nervous system development, disease, and injury. *Int. J. Mol. Med.* 7, 455–478.
- Montero, V.M., Singer, W., 1985. Ultrastructural identification of somata and neural processes immunoreactive to antibodies against glutamic acid decarboxylase (GAD) in the dorsal lateral geniculate nucleus of the cat. *Exp. Brain Res.* 59, 151–165.
- Ohara, P.T., Lieberman, A.R., Hunt, S.P., Wu, J.Y., 1983. Neural elements containing glutamic acid decarboxylase (GAD) in the dorsal lateral geniculate nucleus of the rat: immunohistochemical studies by light and electron microscopy. *Neuroscience* 8, 189–211.
- Powell, T.P.S., 1952. Residual neurons in the human thalamus following hemidecortication. *Brain* 75, 571–584.
- Wang, Y., Sheen, V.L., Macklis, J.D., 1998. Cortical interneurons upregulate neurotrophins *in vivo* in response to targeted apoptotic degeneration of neighboring pyramidal neurons. *Exp. Neurol.* 154, 389–402.
- Weber, A.J., Kalil, R.E., 1983. The percentage of interneurons in the dorsal lateral geniculate nucleus of the cat and observations on several variables that affect the sensitivity of horseradish peroxidase as a retrograde marker. *J. Comp. Neurol.* 220, 336–346.

(Accepted 20 March 2002)

Research report

## Altered expression and phosphorylation of *N*-methyl-D-aspartate receptors in piglet striatum after hypoxia–ischemia

Anne-Marie Guerguerian<sup>a</sup>, Ansgar M. Brambrink<sup>a,1</sup>, Richard J. Traystman<sup>a</sup>,  
Richard L. Haganir<sup>b</sup>, Lee J. Martin<sup>b,c,\*</sup>

<sup>a</sup>Department of Anesthesiology and Critical Care Medicine, Johns Hopkins University School of Medicine, Baltimore, MD, USA

<sup>b</sup>Department of Neuroscience, Johns Hopkins University School of Medicine, Baltimore, MD, USA

<sup>c</sup>Department of Pathology, Division of Neuropathology, Johns Hopkins University School of Medicine, Baltimore, MD, USA

Accepted 26 February 2002

### Abstract

The mechanisms for the profound degeneration of striatal neurons after hypoxia–ischemia in newborns are not understood. We hypothesized that this striatal neurodegeneration is related to *N*-methyl-D-aspartate (NMDA) receptor-mediated excitotoxicity. Using a 1-week-old piglet model of hypoxia–ischemia, we evaluated whether the expression and phosphorylation of NMDA receptor subunits in striatum are modified with severity of evolving neuronal injury after hypoxia–ischemia. Protein levels of NR1, phosphorylated NR1<sup>897</sup> serine, NR2A and NR2B in striatum were measured by immunoblotting after piglets underwent hypoxic–asphyxial cardiac arrest, cardiopulmonary resuscitation, and recovery for 3, 6, 12 or 24 h. In membrane fractions isolated from total striatum, mean NR1 and NR2A levels did not change significantly with time after hypoxia–ischemia compared to control; however, the levels of both NR1 and phosphorylated NR1<sup>897</sup> serine correlated with neuronal injury in putamen, with higher levels associated with greater neuronal injury in individual animals. NR2B levels were increased at 24 h after hypoxia–ischemia. Astrocyte expression of NR2B was prominent after hypoxia–ischemia. We conclude that NMDA receptors are changed in striatum after neonatal hypoxia–ischemia and that abnormal NMDA receptor potentiation through increased NR1 phosphorylation may participate in the mechanisms of striatal neuron degeneration after hypoxia–ischemia. © 2002 Elsevier Science B.V. All rights reserved.

**Theme:** Disorders of the nervous system

**Topic:** Ischemia

**Keywords:** Excitotoxicity; Neuronal cell death

### 1. Introduction

Hypoxic–ischemic brain injury in newborns caused by cardiac arrest or perinatal asphyxia leads to clinical neurological disabilities and results in a characteristic

damage of the striatum, with the putamen showing selective vulnerability [10,17]. Because of the extreme difficulty of delineating mechanisms of brain damage in human newborns, animal models must be used. We have developed and characterized a piglet model of hypoxia–ischemia (HI) [4,7,15,18]. This piglet model has a neuropathology comparable to the injury found in human newborns after HI [10]. In this [15,16,18] and other models [5], glutamate receptor mediated excitotoxic cell injury attributable to NMDA receptors is thought to be a main mechanism of neuronal degeneration after HI in newborns.

NMDA receptors, a class of ionotropic glutamate receptors, are composed of three main subunit families:

\*Corresponding author. Johns Hopkins University School of Medicine, Department of Pathology, 558 Ross Building 720 Rutland Avenue, Baltimore, MD, 21205-2196, USA. Tel.: +1-410-502-5170; fax: +1-410-955-9777.

E-mail address: lmartin@jhmi.edu (L.J. Martin).

<sup>1</sup>Current address: Department of Anesthesiology, Johannes Gutenberg-University, Mainz, Germany.

NR1, NR2 (A–D) and NR3A [26]. These receptors are heteromeric protein complexes with individual subunits showing specific pharmacological and electrophysiological properties. Each receptor subunit has characteristic regional and developmental expression profiles in rodents [1,31]. NR1 is the fundamental subunit and is necessary for receptor function. NR2 subunits appear to contribute diversity in NMDA receptor function. NR1 and NR3A have widespread expression throughout the nervous system, whereas NR2A and NR2B are mostly found in the forebrain [24,30]. NR2C is found mainly in the cerebellum and NR2D is essentially complementary to NR2A.

NMDA receptors have been shown to be involved in different models of brain injury such as hypoglycemia-induced neuronal damage [39], carotid ligation ischemia in rodents [35] and hypoxia in piglets [23]. However, neuroprotection experiments using NMDA receptor blockers have generated mixed results in *in vivo* models of brain injury. These divergent results may be related to variations in experimental design, in animal model used and in the specific underlying mechanisms that are involved. For example, MK-801, a noncompetitive NMDA receptor channel blocker, appears to be neuroprotective in adult [6] and neonatal [21,22] rodent models of global ischemia and in adult cat models of focal ischemia [28,29], but MK-801 is not protective in a newborn piglet model of HI [12]. Therefore, despite the widespread literature implicating NMDA receptors in brain injury after HI, more information is needed to delineate the specific mechanisms that define their involvement.

Reliable neuroprotective interventions based on the modulation of NMDA receptor function still need to be carried out in animal models of HI. It remains unclear how NMDA receptors are abnormally activated after an insult such as HI. A demonstration of NMDA receptor activation would provide needed evidence to support a role in HI. Appropriate electrophysiological characterization of NMDA receptor functional activity is extremely difficult in whole animals. However, the phosphorylation state of receptor proteins is known to change as a regulatory mechanism of receptor function [11,36–38]. Notably, phosphorylation plays a role in NR1 activation [9,40]. Protein kinase A (PKA) and protein kinase C (PKC) phosphorylate specific serine residues of the C1 terminal domain of NR1 and can be identified using antibodies specific to each phosphorylated form of NR1 [36]. Therefore in our newborn piglet model of cardiac arrest, we examined the protein levels and phosphorylation status of NMDA receptors after HI. We hypothesized that excitotoxicity mediated by NMDA receptors contributes to the death of neurons in the newborn piglet striatum after HI and that receptor subtype levels and the phosphorylation state of the main receptor, NR1, are modified after HI, with time or severity of neuronal injury. Our experiments show that NR1 phosphorylation is increased with severe neuronal damage.

## 2. Materials and methods

### 2.1. Piglet model of hypoxia–ischemia

The protocol was approved by the Johns Hopkins Medical Institutions Animal Care and Use Committee and has been described and characterized previously [4,16]. One-week-old male or female piglets (~3 kg) were anesthetized with 65 mg/kg intraperitoneal pentobarbital, intubated, and mechanically ventilated. Femoral arterial and venous catheters were placed into the thoracic aorta and inferior vena cava and were tunneled subcutaneously for long-term access; 50 mg/kg cephalothin, *i.v.*, was administered. Oxygenation, ventilation, and acid–base balance were normalized, and animals were maintained normothermic (38.5–39.5 °C). Animals received 10 ml/kg/h of lactated Ringer's solution *i.v.*, with analgesia (10 µg/kg fentanyl *i.v.*) and neuromuscular blockade (0.3 mg/kg pancuronium *i.v.*) as needed. Baseline arterial blood gas, hemoglobin, serum glucose, and pulse and blood pressure were recorded.

Animals were exposed to 30 min of hypoxia by decreasing the fraction of inspired O<sub>2</sub> (FIO<sub>2</sub> 0.1 with an arterial O<sub>2</sub> saturation 30%), then to 5 min of room air ventilation (FIO<sub>2</sub> 0.2 with an arterial O<sub>2</sub> saturation 65%), and to 7 min of airway occlusion (arterial O<sub>2</sub> saturation 5%), resulting in asphyxic cardiac arrest. Ventilation with FIO<sub>2</sub> 1.0, manual chest compressions, 0.1 mg/kg epinephrine, *i.v.* and 1 mequiv./kg sodium bicarbonate *i.v.* were administered for resuscitation until spontaneous circulation returned, usually within 2–3 min. Ventricular fibrillation was treated with 2 J/kg defibrillation, with 1 mg/kg lidocaine *i.v.* if multiple defibrillations were required. Approximately 90% of the piglets were successfully resuscitated. The animals were allowed to awaken and were extubated when able to maintain oxygenation and ventilation, usually within 8 h; they usually drank formula milk within 24 h. Animals were allowed to recover for 3, 6, 12 or 24 h after the return of spontaneous circulation before they were euthanized and brain tissue was harvested.

### 2.2. Brain preparation

Brains were harvested as fresh tissue samples for immunoblotting or were perfusion-fixed for immunocytochemical analysis ( $n=16$  hypoxic–ischemic and  $n=5$  controls). Brain retrieval was done by an investigator blinded to the animal's specific experimental history. For immunoblotting, three to four animals per time point were anesthetized with 65 mg/kg pentobarbital *i.p.* and exsanguinated with cold phosphate-buffered saline (PBS). Brains were removed rapidly and placed on wet ice. The cerebrum was transected midsagittally, and the hemispheres were subdissected to obtain samples from striatum

(putamen, caudate, internal capsule and nucleus accumbens). Samples were frozen quickly in isopentane and stored at  $-70^{\circ}\text{C}$ . From the left hemisphere, a 5-mm thick slab containing striatum was immersion fixed in 5% acrolein, embedded in paraffin, sectioned and stained with hematoxylin and eosin (H&E) for assessment of ischemic neuronal damage (see below).

For immunocytochemical analysis, two to three animals per time point were anesthetized with 65 mg/kg pentobarbital, i.p., exsanguinated with cold PBS, and perfused for 20 min with cold 4% paraformaldehyde–1% glutaraldehyde. The brain was removed, the cerebrum was transected midsagittally, and each hemisphere was cut into 1-cm slabs. The right hemisphere was cryoprotected in 20% glycerol–PBS for 24 h and frozen in isopentane at  $-70^{\circ}\text{C}$ . Serial 40- $\mu\text{m}$  sections through the striatum were cut on a freezing microtome and stored in antifreeze buffer at  $-20^{\circ}\text{C}$ , and subsequently assayed for immunohistochemical staining.

A coronal slab of striatum from the left hemisphere of each animal was paraffin-processed, and 10- $\mu\text{m}$  sections were stained with H&E to quantify ischemic neuronal damage. Neuronal damage was defined as the fraction of neurons with ischemic cytopathology relative to the total number of neurons in microscopic fields in the putamen. Quantification of neuronal damage was done by a blinded investigator unaware of animal recovery time. Neuronal damage was quantified using nonstereological profile counting. In sections that were matched for level, the numbers of neuronal profiles were counted in six nonoverlapping fields of the striatum at  $\times 1000$  [7,16]. In each microscopic field, the fraction of neurons with ischemic cytopathology was determined for each animal. Neurons were distinguished from glial cells by morphology. The criteria for ischemic cytopathology included eosinophilic cytoplasm, cytoplasmic vacuolization and nuclear pyknosis. Six values for each brain were averaged, and this individual number was used to determine the mean value of neuronal damage in the striatum for each animal.

### 2.3. Immunoblotting

Samples (0.4–0.6 g) were homogenized with a Brinkman Polytron homogenizer in cold homogenization buffer (20 mM Tris–HCl, pH 7.4, 10% sucrose, 1 mM EDTA, 5 mM EGTA, 20 U/ml Trayslol, 20  $\mu\text{g}/\text{ml}$  leupeptin, 20  $\mu\text{g}/\text{ml}$  antipain, 20  $\mu\text{g}/\text{ml}$  pepstatin, 20  $\mu\text{g}/\text{ml}$  chymostatin, 0.1 mM phenylmethylsulfonyl fluoride, 10 mM benzamidine) and centrifuged at 1000 g for 10 min at  $4^{\circ}\text{C}$ . The supernatant was collected and centrifuged at 114 000 g for 20 min at  $4^{\circ}\text{C}$ . The second pellet (designated the P2 fraction), the cytoplasmic membrane-enriched fraction, was washed twice with cold sucrose free homogenization buffer and centrifuged at 114 000 g for 20 min at  $4^{\circ}\text{C}$ . The final pellet was suspended in cold homogenization buffer

containing 20% glycerol (rather than sucrose), to a protein concentration of 1–2 mg/ml, as determined by the Bio-Rad protein assay with bovine serum albumin as the standard. Samples were stored at  $-70^{\circ}\text{C}$ .

Aliquots of striatal P2 samples containing 20  $\mu\text{g}$  total protein each were fractionated by sodium dodecyl sulfate–polyacrylamide gel electrophoresis (SDS–PAGE) on 10–12% gels and transferred electrophoretically to nitrocellulose membranes. Each experiment was performed in quadruplicate. To verify uniform protein loading and transfer after SDS–PAGE and electroblotting, gels were stained with Coomassie blue and membranes were stained briefly with Ponceau S. Membranes were washed with 50 mM Tris-buffered saline (TBS) and blocked with blocking buffer (2.5% nonfat milk–0.1% Tween20 in 50 mM TBS). Membranes were incubated for 24 h at  $4^{\circ}\text{C}$  with affinity-purified mouse monoclonal antibody recognizing NR1 protein (Pharmingen) and rabbit affinity-purified polyclonal antibodies recognizing NR2A or NR2B (0.2  $\mu\text{g}/\text{ml}$ ) [31]. To identify possible changes in the phosphorylation status of NR1, we used antiphosphorylated NR1<sup>890</sup>serine and antiphosphorylated NR1<sup>897</sup>serine (0.4  $\mu\text{g}/\text{ml}$ ) rabbit polyclonal affinity-purified antibodies, which recognize NR1 protein phosphorylated at serine residues 890 and 897, respectively [36]. The phosphorylation state specificity of the antibodies in brain extracts was evaluated by transferring proteins to nitrocellulose membranes and treating blots with alkaline phosphatase (80 U/ml, Boehringer Mannheim) which dephosphorylates proteins. Blots with either phosphorylated proteins or dephosphorylated proteins using alkaline phosphatase were then incubated with the phosphorylated state specific antibodies to verify that blots with dephosphorylated proteins had attenuated signals.

The resulting blots were washed and incubated for 1 h at room temperature with either Bio-Rad goat antimouse IgG or antirabbit IgG conjugated to horseradish peroxidase (0.2  $\mu\text{g}/\text{ml}$  in blocking buffer). Blots were washed in blocking buffer and then TBS; immunoreactive proteins were visualized with an Amersham enhanced chemiluminescence detection system, and membranes were exposed to radiographic film.

NR1, phosphorylated NR1, NR2A and NR2B immunoreactivity levels were quantified using Macintosh Adobe PHOTOSHOP and Signal Analytics IP LAB GEL software. Using this digitizing software, protein levels were determined by the average integration of the optical density and the area of immunoreactivity of the band relative to the background density of the radiographic film. Protein levels were expressed as a percentage of control values by comparing the immunodensity of the protein band to the immunodensity of the same band in the control animal lane in the same blot. Moreover, NMDA receptor levels were normalized to relative synaptophysin immunodensity as a quantitative protein loading control. Synaptophysin is a synap-

tic vesicle membrane protein involved in vesicle fusion, levels of which do not change in piglet striatum during the first 24 h after HI [18]. Blots were probed with monoclonal mouse antibody against synaptophysin (Boehringer Mannheim, 0.06 µg/ml in blocking buffer).

#### 2.4. Immunocytochemistry

Free-floating striatal sections were removed from antifreeze buffer, washed in TBS, pretreated with H<sub>2</sub>O<sub>2</sub>–methanol and then sodium borohydride, and blocked in 4% normal goat serum (NGS). Sections were incubated for 48 h at 4 °C with affinity-purified monoclonal antibody against NR1 (10 µg/ml diluted in NGS) and polyclonal rabbit antibody against NR2B (100 µg/ml diluted in NGS). Sections were incubated sequentially with Cappel goat antirabbit IgG F(ab)<sub>2</sub> fragment (10 µg/ml diluted in NGS), and then with affinity-purified monoclonal goat antirabbit antibody conjugated to horseradish peroxidase (Sternberger Monoclonals) at a concentration of 0.2 µg/ml (diluted in NGS). Sites of antibody binding were visualized with H<sub>2</sub>O<sub>2</sub> and diaminobenzidine (DAB). Immunoreactivity of the stained sections was quantified by image analysis using INQUIRY software (Loats, Westminster MD, USA). Under appropriate conditions such as primary and secondary antibody concentrations, concentration of DAB, and time in DAB, this method [2] can detect immunoreactivity which is in the linear range. Each brain section was digitized and then analyzed using the following steps: the putamen and caudate were specifically delineated, excluding the internal capsule, and the optical density of each portion of striatum was quantified relative to the background level of immunoreactivity of the complete section. This allowed for the quantification of the immunoreactivity specifically within different components of the striatum. Immunoreactivity was related to the amount of neurons identified as degenerating in the putamen of each animal.

#### 2.5. Data and statistical analyses

The percent neuronal damage in the putamen at 3, 6, 12 and 24 h after HI, as assessed by H&E staining, was compared to that in controls with the Newman–Keuls test [17]. We compared the immunoreactivity of proteins detected by the antibodies relative to the neuronal damage in putamen for the following reasons. Firstly, up to 24 h after injury, only the putamen shows signs of neuronal damage and the caudate shows no sign of neuronal damage [18]. Secondly, we use the percentage neuronal damage in the putamen as a measure of injury of the striatum. This allows us to classify animals according to their precise damage rather than just by the time after injury.

NMDA receptor protein levels expressed as a percentage of control values, quantified by optical density, were also

compared among groups allowed to recover for 3, 6, 12 or 24 h with the Wilcoxon signed-ranks test (SPSS® version 9.0).

### 3. Results

#### 3.1. Detection of NR1, NR2A and NR2B proteins in piglet striatum

The specificity of the antibody reagents used was characterized in swine tissue because these antibodies were made using rat sequences of NMDA receptors as antigens. We characterized their reactivity with piglet striatal homogenates (Fig. 1). On immunoblots of striatal membrane fractions, a mouse monoclonal antibody against NR1 detected a single band at ~116 kDa, consistent with the size of NR1 in rat CNS [34]. Subunit-specific rabbit polyclonal antibodies against the C-terminus of NR2A and NR2B [31] each detected an immunoreactive band at ~172 kDa, consistent with the size of NR2A and NR2B in rat CNS (Fig. 1). Antibody binding to the NR2A and NR2B receptor proteins on immunoblots of piglet brain homogenates was completely blocked by addition of the homologous C-terminal peptide but not the heterologous peptide (Fig. 1). These results confirmed that each antibody is subunit-specific in the swine brain, recognizing either NR1, NR2A or NR2B. Antibodies for NR1 or NR2B were shown to be sufficiently specific for immunocytochemistry (see full length blots in the upper right corner of Fig. 1).

#### 3.2. Phosphorylated NR1 antibody characterization in piglet brain

We evaluated two antibodies that recognize phosphorylated forms of NR1 as possible reagents to allow us to identify changes in receptor phosphorylation after HI. These antipeptide antibodies were generated from rat sequences for NR1 phosphorylated at <sup>897</sup>serine or <sup>890</sup>serine [36] and respectively identify either PKA-phosphorylated serine residue 897 or PKC-phosphorylated serine residue 890 of the NR1 subunit. Immunoblots of piglet striatal extracts showed that the antibody recognizing the phosphorylated NR1 <sup>897</sup>serine was the most specific and reliable for use in piglet brain homogenates. We exposed protein blots with piglet and rat striatal homogenates to alkaline phosphatase to dephosphorylate the proteins and verify that the antibodies specifically recognized phosphorylated NR1 proteins and not NR1 in its dephosphorylated state. These control dephosphorylation experiments with alkaline phosphatase revealed phosphorylation state related immunodetection of phosphorylated NR1 <sup>897</sup>serine but not <sup>890</sup>serine in piglet homogenates (Fig. 1). In piglet (lanes 1, 3, 5, 7) compared to rodent (lanes 2, 4, 6, 8), the proteins visualized by the antibody recognizing

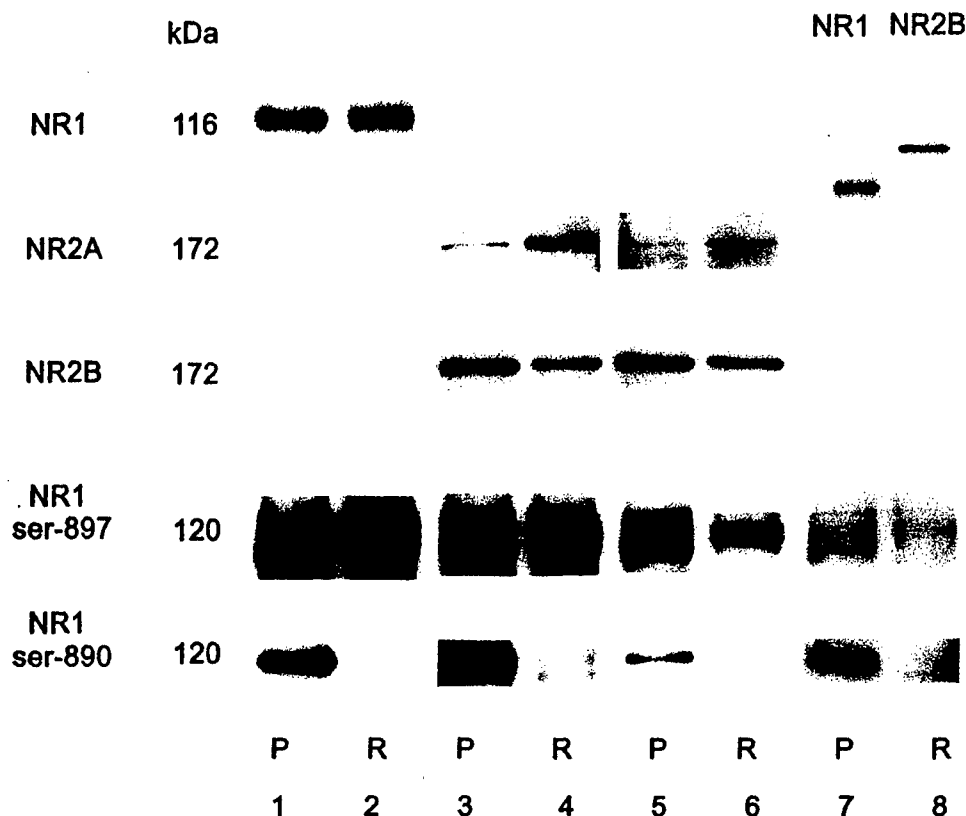


Fig. 1. NR1, NR2A, NR2B, phosphorylated NR1 <sup>897</sup>serine and phosphorylated NR1 <sup>890</sup>serine in piglet and rat forebrain. Reactivity of specific antibodies against NMDA receptors with cytoplasmic membrane-enriched fractions (20 µg protein/lane) of noninjured piglet striatum or rat cerebral cortex after separation by SDS-PAGE is shown. 1st row, specificity of anti-NR1 monoclonal antibody in piglet (P) and rat (R) brain. 2nd and 3rd rows, cell membrane fractions were immunoblotted with NR2A or NR2B affinity-purified antibodies preadsorbed with the homologous peptide (first blot: lanes 1, 2), without any peptide (second blot: lanes 3, 4) or with their heterologous peptide (third blot: lanes 6, 7). 4th and 5th rows, cell membrane fractions from piglet and rat were incubated for 4 h without alkaline phosphatase (lanes 1, 2, 5, 6) to visualize the phosphorylated proteins or with alkaline phosphatase (lanes 3, 4, 7, 8) to dephosphorylate the proteins and verify that the immunoreactivity decreases. Experiments were done at room temperature (lanes 1, 2, 3, 4) and at 37 °C (lanes 5, 6, 7, 8). Membranes were probed with affinity-purified anti-phospho-NR1 <sup>897</sup>serine or anti-phospho-NR1 <sup>890</sup>serine antibodies. In the upper right corner, full-length membranes probed with NR1 or NR2B antibodies are shown to demonstrate the specificity of the antibodies and their suitability for use in immunocytochemistry. Molecular mass markers in kDa are indicated on the left.

phosphorylated <sup>897</sup>serine migrated consistently over a slightly wider range of protein weight.

### 3.3. Expression of NMDA receptor subunits in piglet striatum during early postnatal maturation

Using the characterized antibodies, we examined the expression patterns of NR1, NR2A and NR2B proteins during the early postnatal maturation of the piglet striatum. This experiment was done to identify the presence of NMDA receptors in the striatum in piglets at the ages used to perform the HI experiments. Immunoblots of striatal homogenates obtained on the day of birth and at 1, 2 and 4 weeks of age were probed with subunit-specific antibodies to NMDA receptors (Fig. 2). NR1, NR2A and NR2B are expressed in piglet striatum through 4 weeks of age.

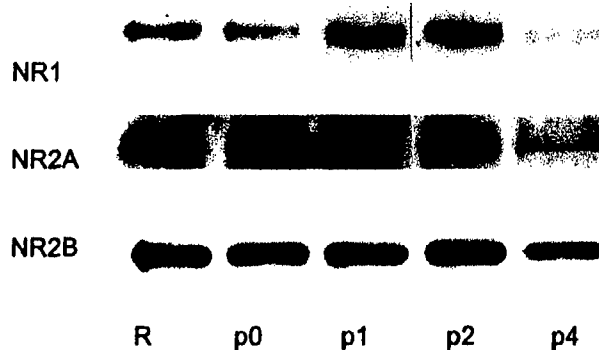


Fig. 2. NR1, NR2A and NR2B in normal (noninjured) piglet striatum at day 0 (p0, day of birth) and at 1–4 weeks (p1–4) of age and in rat (R) forebrain. Cytoplasmic membrane-enriched fractions (20 µg protein/lane) immunoblotted for NR1, NR2A and NR2B show the presence of NR1, NR2A and NR2B.



### 3.4. Neuronal damage in striatum of piglets after HI

Striatal neuronal damage evolves during the first 24 h after HI [18]. Degeneration in this model has been described in detail previously [18]; neuronal damage is characterized as necrosis based on morphology, DNA fragmentation patterns and metabolic deficits. Examples of the characteristic changes seen by H&E staining are shown. The striatum of sham piglets contains many medium-sized (~10–20  $\mu$ m) round neurons with an open nucleus (Fig. 3A). Damaged striatal neurons in piglets after HI have a shrunken pink cell body and a dark condensed nucleus. The amounts of damaged neurons vary in the different piglets with mild to severe injury (Fig. 3B–D).

### 3.5. Expression of NMDA receptors in striatum after HI

The levels of NMDA receptor subunit proteins changed in the striatum of HI piglets. Alterations in NR1 phosphorylation occurred in the striatum after HI. Comparisons

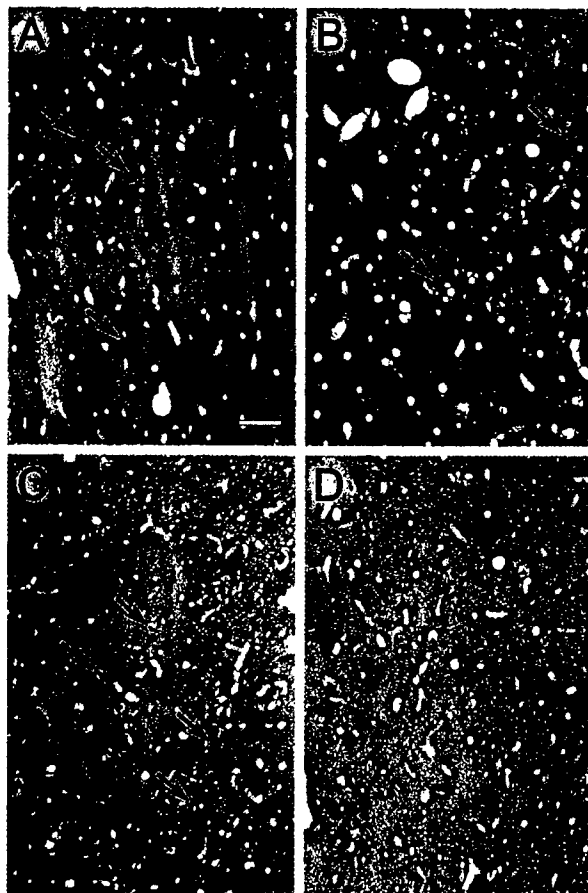


Fig. 3. Striatal neuronal damage. The striatum of piglets was examined by H&E staining. The control striatum (A) has normal appearing neurons (arrows). Representative photomicrographs of HI piglet striatum with neuronal damage (arrows B and C) that is mild (B), moderate (C) and severe (D). Virtually all of the medium-sized neurons in the severe case (D) are damaged. Scale bars in A–D, 200  $\mu$ m.

were made between averages of groups of animals of the same elapsed time after HI as well as among individual animals with known neuropathological outcomes. Some alterations in NMDA receptor levels changed with the progression of neuronal degeneration.

#### 3.5.1. NR1 protein levels

The levels of NR1 in HI piglet striatum were measured by immunoblotting and immunocytochemistry using phosphorylation state independent antibody. On immunoblots of cytoplasmic membrane fractions of total striatum, NR1 levels did not change significantly at 3–24 h recovery after HI compared to controls (Fig. 4). NR1 levels were examined in relation to evolving neuronal cell injury in the putamen. NR1 levels were lower than control at the early stages after HI, when few neurons were damaged, but levels increased as the number of damaged neurons increased (Fig. 4). The highest levels of NR1 protein correlated with the highest number of damaged neurons.

By immunocytochemical staining, NR1 levels were measured in the striatum of control and HI piglets (Fig. 5). Because the anatomical resolution permitted the individual analysis of the different striatal portions, levels of NR1 were measured separately in the putamen and caudate (Fig. 6A). In controls, the putamen and caudate expressed similar amounts of NR1 (Fig. 6A); however, these regions responded differently to HI. NR1 levels in caudate increased transiently at 6 h (Figs. 5B and 6A) and then returned to control levels by 12 h (Figs. 5C and 6A) and remained at control levels at 24 h (Figs. 5D and 6A). In the putamen, NR1 levels were increased at 24 h but not significantly at earlier times (Figs. 5A–D and 6A). This trend followed the counts of damaged neurons in the putamen (Fig. 6B).

Because of an apparent trend between NR1 levels and accumulating neuronal injury and the apparent lack of a simple linear relationship with time after injury, the levels of the phosphorylated form of NR1 subunit were measured by immunoblotting in order to indirectly examine NR1 receptor activation after HI. We analyzed the composite band at 120 kDa as the phosphorylated NR1 receptor. Piglet cytoplasmic membrane fractions of total striatum were probed with antibody recognizing phosphorylated NR1<sup>897</sup> serine (Fig. 7). The number of injured neurons in the putamen correlated with an increase in phosphorylated NR1 levels, suggesting an association between evolving neuronal damage and NR1 activation. The increased phosphorylated NR1 was not associated with the amount of time elapsed after the insult but rather with the specific amount of neuronal damage in the putamen (Fig. 7).

#### 3.5.2. NR2B and NR2A protein levels

To identify whether changes in NMDA receptors are subunit specific, selected NR2 subunits were measured. The levels of NR2 in HI piglet striatum were measured by immunoblotting and immunocytochemistry. On immuno-

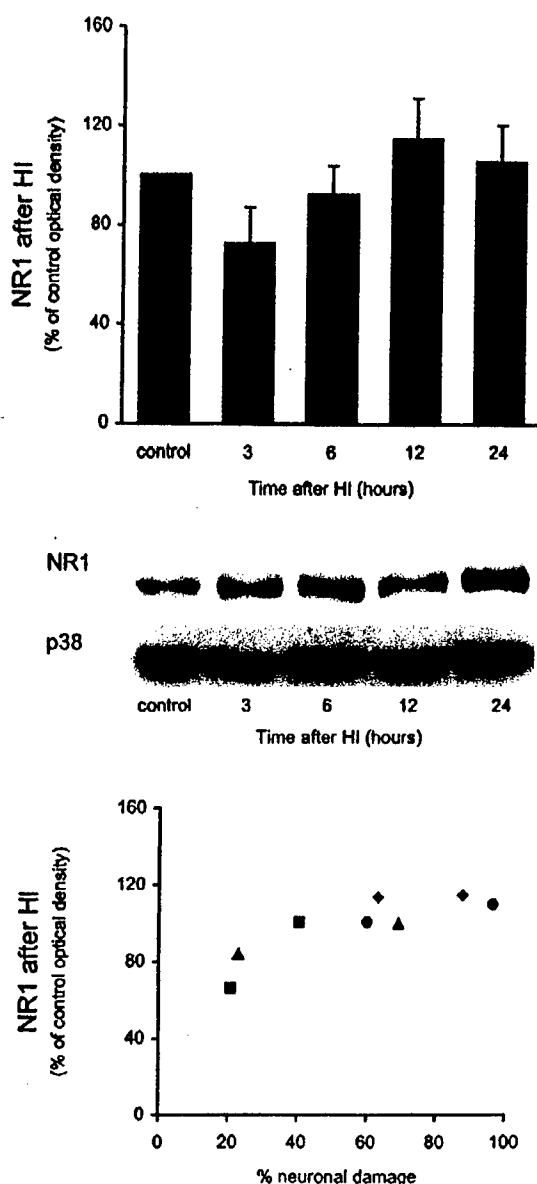


Fig. 4. NR1 immunoreactivity in striatum of control and HI piglets. Cytoplasmic membrane-enriched fractions (20  $\mu$ g protein/lane) of striatum from control and HI piglet brains, collected at 3, 6, 12 or 24 h after HI, were evaluated by Western blot analysis. The histogram shows densitometric quantification of immunoreactive protein levels detected in control and in HI animals in relation to time after injury. A representative blot shows NR1 protein and respective p38 loading control. The dot plot shows the immunoreactivity in cytoplasmic membranes determined by Western blot analysis after HI in relation to percent (%) neuronal damage in the putamen. Percent neuronal damage corresponds to the percentage degenerating neurons in each putamen of these animals analyzed by profile counting (see Methods). Neuronal damage was defined as the fraction of neurons with ischemic cytopathology relative to the total number of neurons in microscopic fields in the putamen. Each animal is plotted according to the time after HI when the sample was harvested (■, 3 h; ▲, 6 h; ♦, 12 h; ●, 24 h). The simple linear regression model obtained with NR1 immunoreactivity (dependent variable) relative percentage neuronal damage is described by the following equation:  $y = 70.3 + 0.49x$ ,  $r^2 = 0.7$ . Immunoreactivity values are expressed as the percent of control optical density  $\pm$  S.E.M.

blots of cytoplasmic membrane fractions of total piglet striatum, NR2B levels did not change appreciably at 3, 6 and 12 h recovery after HI compared to controls (Fig. 8). However, at 24 h after HI, NR2B levels were elevated significantly (29%) above control (Fig. 8). The levels of NR2B were not related to the number of damaged putaminal neurons (Fig. 8). NR2A levels in striatum of HI piglets were not different from control during the 3–24 h evaluation period (Fig. 9).

NR2B immunoreactivity in the putamen and caudate of control and HI piglets was measured by immunocytochemical staining (Fig. 10). The immunocytochemical analysis of NR2B confirmed the immunoblot results. NR2B was increased in the putamen at 24 h after HI (Figs. 10D and 11A). NR2B immunoreactivity in the caudate did not change after HI. No linear relationship was identified using our methods relating the gradual increase in neuronal damage and NR2B immunoreactivity in the putamen (Fig. 11B). NR2B immunoreactivity was prominently elevated in the putamen at a time when the putamen was severely damaged (Fig. 10D and 11A). Because this increase in NR2B did not follow linearly the evolution of neuronal damage (Fig. 11B), we explored its expression in non-neuronal cells. Double-label immunocytochemistry for NR2B and the astroglial protein GFAP showed that astroglia express NR2B in striatum after HI (Fig. 12).

#### 4. Discussion

Our study supports the theory that excitotoxicity mediated by NMDA receptors plays a role in brain damage after HI. In particular, NMDA receptor activation appears to be involved in the death of striatal neurons in the newborn brain after cardiac arrest. Using a piglet model, we found that NMDA receptor subtype expression and phosphorylation are modified after HI according to the severity of the neuronal injury.

NMDA proteins in normal developing piglet striatum were examined by immunoblotting. NR1, NR2A and NR2B are present in piglet striatum up to 4 weeks of age. NMDA receptor protein expression patterns in immature pig striatum are different from those found in rat striatum (using the same NR2A and NR2B antibodies) during postnatal development [31]. In developing rat, NR2A is undetectable until the third and fourth week while NR2B is present at birth and is maintained in adult rodents. These observations emphasize at least two important issues that have bearing on deciphering the roles of NMDA receptors in the developing brain: observations in the developing rat are likely to differ from experiments performed using piglet models, and animals of similar age should be used. This former issue regarding species differences may contribute to the different neuropathological outcomes found in the striatum of rat pups and piglets after HI [16,18,25,27].

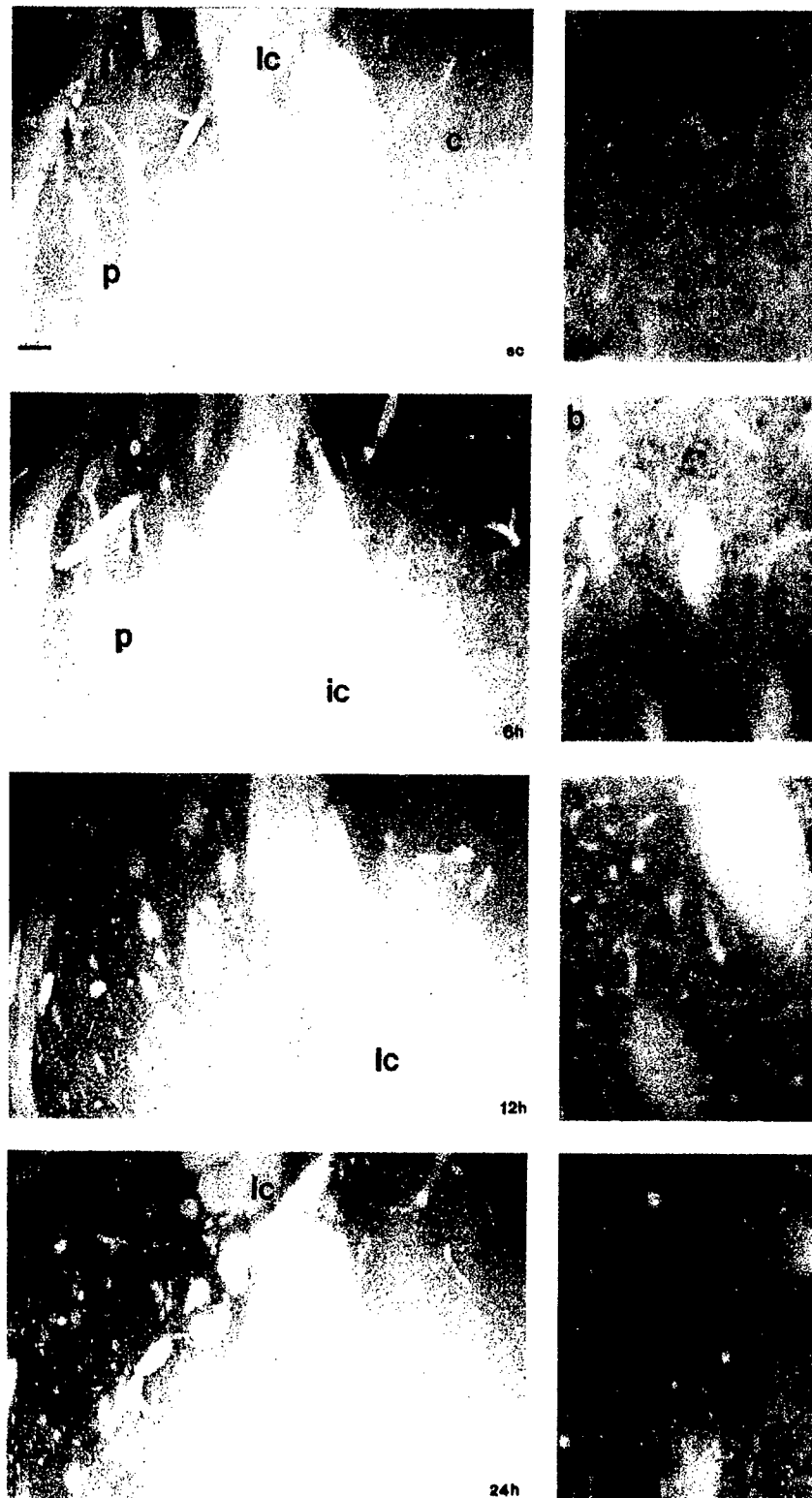


Fig. 5. NR1 immunolocalization in putamen and caudate after HI. Brain sections stained by immunocytochemistry are shown (A–D). NR1 immunoreactivity within the putamen and caudate at low magnification (A–D) and in the putamen at higher magnification (a–d). Scale bars: A–D, 50  $\mu$ m; a–d, 25  $\mu$ m. Brain section from control animal (A, a) shows uniform NR1 labeling. After HI, NR1 labeling decreased slightly in the putamen at 6 h (B, b) and then returned to baseline levels at 12 h (C, c) and 24 h (D, d). NR1 immunoreactivity in the caudate increased slightly at 6 h after HI. Abbreviations: p, putamen; c, caudate; ic, internal capsule.

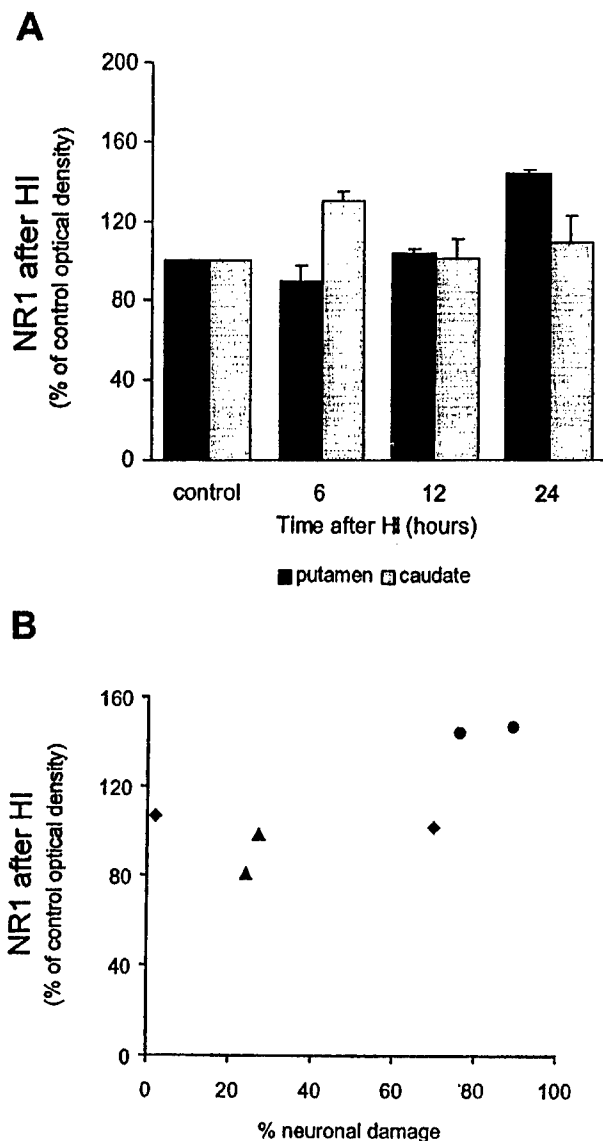


Fig. 6. Quantification of NR1 immunoreactivity in putamen and caudate by immunocytochemistry using densitometry. (A) The histogram shows the optical density of NR1 immunoreactivity (mean  $\pm$  S.E.M.) as a percentage of optical density in control animals. (B) The dot plot shows the relationship of NR1 immunoreactivity relative to the percentage neuronal damage in the putamen after HI. Immunoreactivity was quantified by optical density and stated as percentage of optical density in control animals. The percentage neuronal damage corresponds to the percentage degenerating neurons in the putamen of each piglet plotted individually according to the time after HI when the sample was harvested: (▲, 6 h; ◆, 12 h; ●, 24 h). The single linear regression model with NR1 protein immunoreactivity (dependent variable) relative to the percentage neuronal damage is described by the following equation:  $y = 86.5 + 0.55x$ ,  $r^2 = 0.54$ .

High levels of NMDA receptors which are important for brain development, may predispose the immature brain to NMDA receptor-mediated excitotoxic injury [20]. We hypothesized that the mechanisms for the profound degeneration of striatal neurons after HI may involve NMDA receptor-mediated excitotoxicity [15,18]. Therefore in our

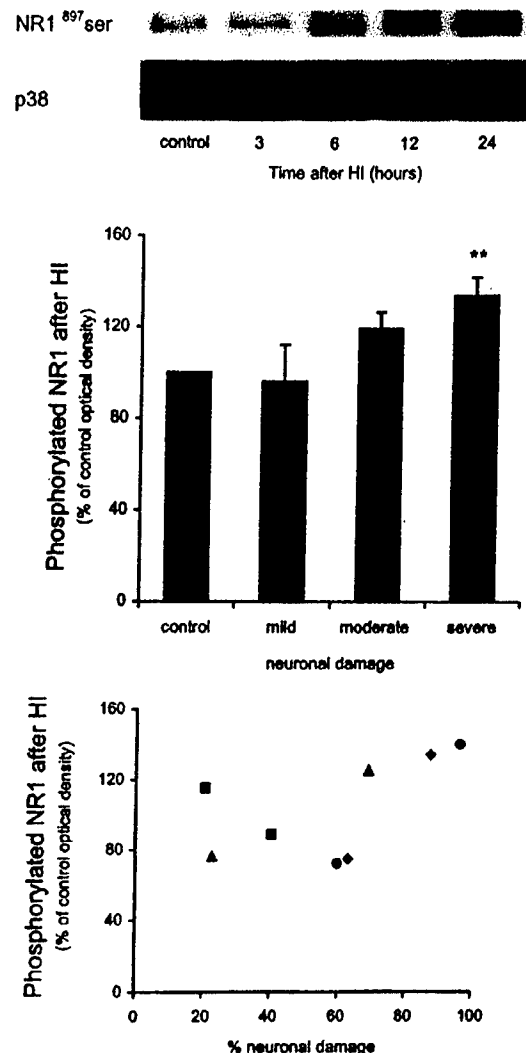


Fig. 7. Phosphorylated NR1<sup>897</sup>serine immunoreactivity in striatum of control and HI piglets. Cytoplasmic membrane-enriched fractions (20  $\mu$ g protein/lane) of striatum from control and HI piglet brains, collected at 3, 6, 12 or 24 h after HI, were evaluated by Western blot analysis. A representative blot shows phosphorylated NR1<sup>897</sup>serine and respective p38 loading control. The dot plot shows the immunoreactivity in cytoplasmic membranes determined by Western blot analysis after HI in relation to percent (%) neuronal damage in the putamen. Percent neuronal damage corresponds to the percentage degenerating neurons in the putamen of each animal that was analyzed by profile counting (see Methods). Neuronal damage was defined as the fraction of neurons with ischemic cytopathology relative to the total number of neurons in microscopic fields in the putamen. Each animal is plotted according to the time after HI when the sample was harvested: (■, 3 h; ▲, 6 h; ◆, 12 h; ●, 24 h). The simple or multiple linear regression models obtained with the phosphorylated NR1<sup>897</sup>serine immunoreactivity (dependent variable) relative percentage neuronal damage are described by the following equations:  $y = 70 + 0.58x$ ,  $r^2 = 0.32$  or  $y = 119.6 + 2.78x + 0.025(100 - x)^2$ . The histogram shows densitometric quantification of the immunoreactive protein levels detected in control and in HI animals in relation to severity of neuronal injury among animals of comparable injury (10–25% neuronal damage=mild injury; 40–65% neuronal damage=moderate injury; 75–100% neuronal damage=severe injury). See Fig. 3 for histopathology. Immunoreactivity values are expressed as the percent of control optical density  $\pm$  S.E.M. The asterisks indicates statistical significance of \*\*,  $P < 0.10$ .

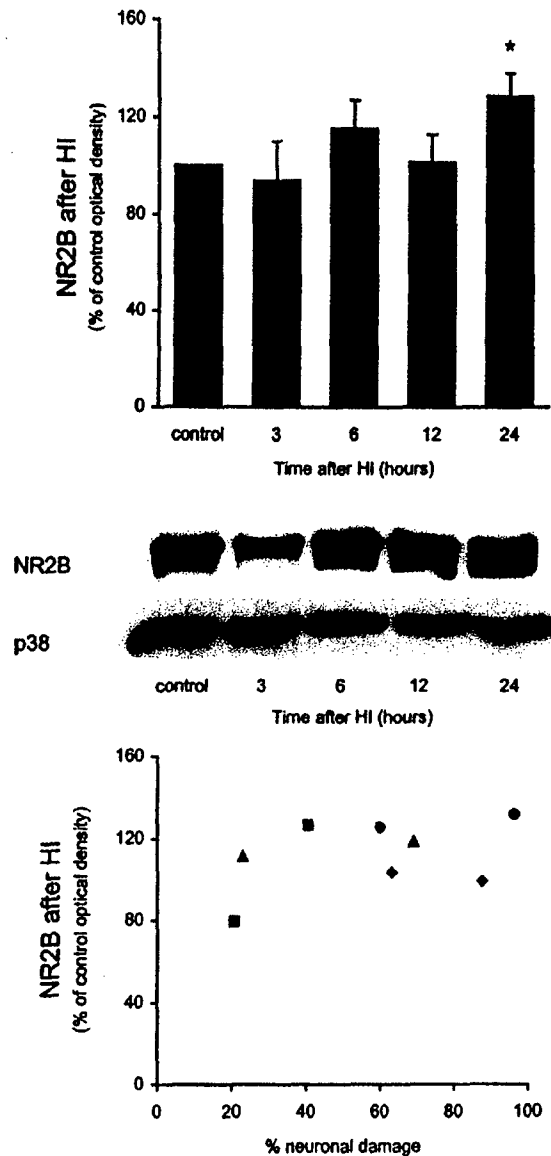


Fig. 8. NR2B immunoreactivity in striatum of control and HI piglets. Cytoplasmic membrane-enriched fractions (20  $\mu$ g protein/lane) of striatum from control and HI piglet brains, collected at 3, 6, 12 or 24 h after HI, were evaluated by Western blot analysis. The histogram shows densitometric quantification of immunoreactive protein levels detected in control and in HI animals in relation to time after injury. A representative blot shows NR2B proteins and respective p38 loading control. The dot plot shows the immunoreactivity in cytoplasmic membranes determined by Western blot analysis after HI in relation to percent (%) neuronal damage in the putamen. Percent neuronal damage corresponds to the percentage degenerating neurons in the putamen for each animal analyzed by profile counting (see Methods). Neuronal damage was defined as the fraction of neurons with ischemic cytopathology relative to the total number of neurons in microscopic fields in the putamen. Each animal is plotted according to the time after HI when the sample was harvested: (■, 3 h; ▲, 6 h; ◆, 12 h; ●, 24 h). The simple regression model obtained with the NR2B protein immunoreactivity (dependent variable) relative percentage neuronal damage is described by the following equation:  $y = 97.7 + 0.25x$ ,  $r^2 = 0.16$ . Immunoreactivity values are expressed as the percent of control optical density  $\pm$  S.E.M. The asterisks indicates statistical significance of \*,  $P < 0.05$ .

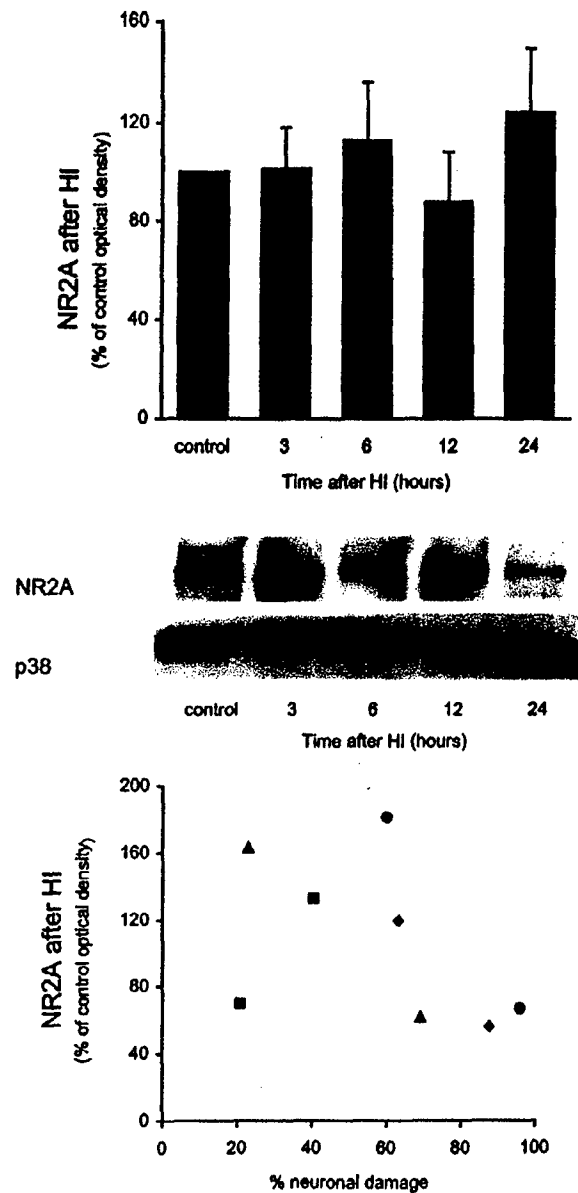


Fig. 9. NR2A immunoreactivity in striatum of control and HI piglets. Cytoplasmic membrane-enriched fractions (20  $\mu$ g protein/lane) of striatum from control and HI piglet brains, collected at 3, 6, 12 or 24 h after HI, were evaluated by Western blot analysis. The histogram shows densitometric quantification of immunoreactive protein levels detected in control and in HI animals, in relation to time after injury. A representative blot shows NR2A proteins and respective p38 loading control. The dot plot shows the immunoreactivity in cytoplasmic membranes determined by Western blot analysis after HI in relation to percent (%) neuronal damage in the putamen. Percent neuronal damage corresponds to the percentage degenerating neurons in the putamen for each animal analyzed by profile counting (see Methods). Neuronal damage was defined as the fraction of neurons with ischemic cytopathology relative to the total number of neurons in microscopic fields in the putamen. Each animal is plotted according to the time after HI when the sample was harvested: (■, 3 h; ▲, 6 h; ◆, 12 h; ●, 24 h). Immunoreactivity values are expressed as the percent of control optical density  $\pm$  S.E.M.

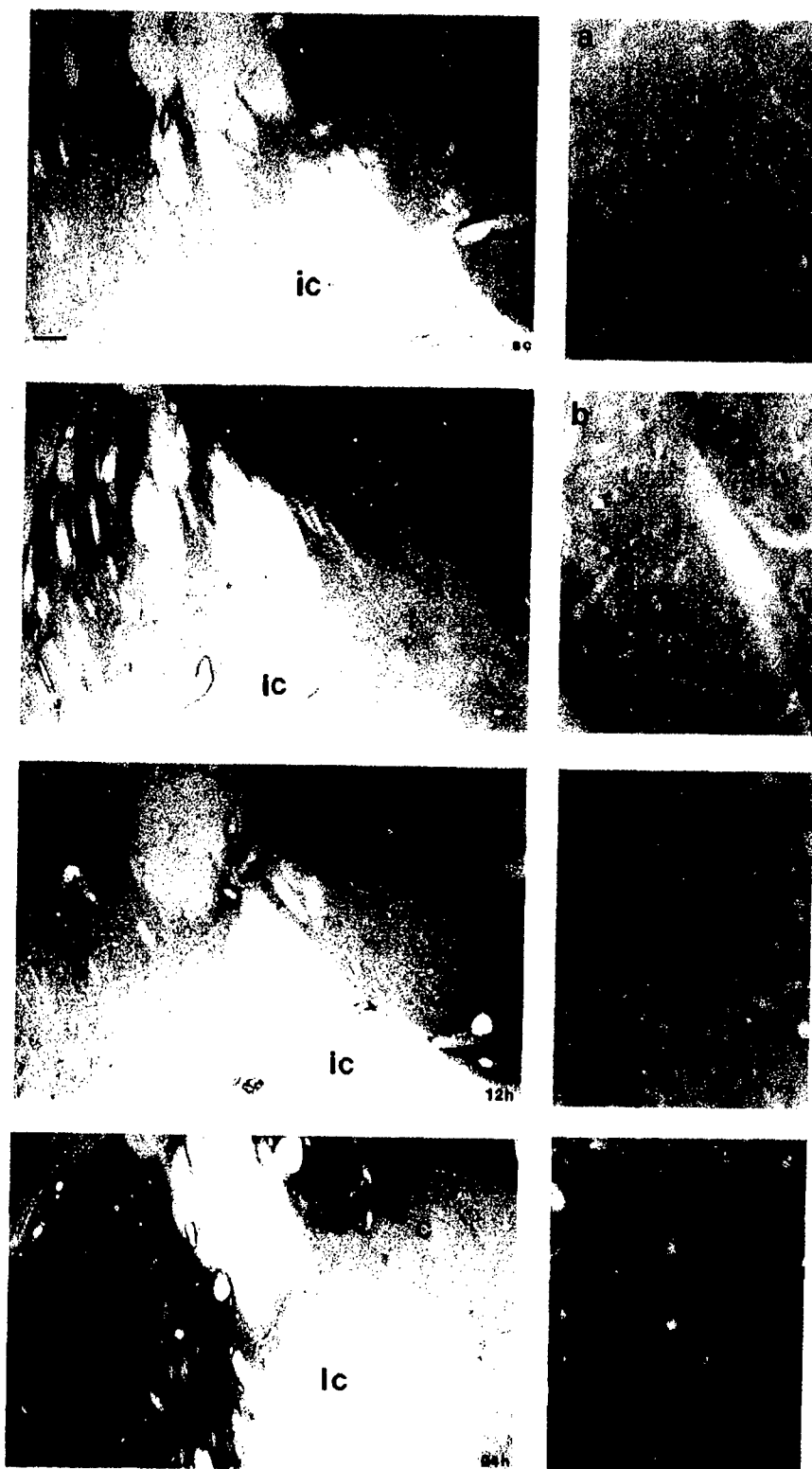


Fig. 10. NR2B immunolocalization in putamen and caudate after HI. Brain sections stained by immunocytochemistry are shown (A–D). NR2B immunoreactivity within the putamen and caudate at low magnification (A–D) and in the putamen at higher magnification (a–d). Scale bars: A–D, 50  $\mu$ m; a–d, 25  $\mu$ m. Brain section of control animal (A, a) shows uniform NR2B labeling. Labeling increased in the putamen at 24 h (D, d) after HI. NR2B immunoreactivity in the caudate was unchanged after HI. Abbreviations: p, putamen; c, caudate; ic, internal capsule. Arrow in (A) identifies an example of a blood vessel. Arrows in (d) identify immunopositive cells.

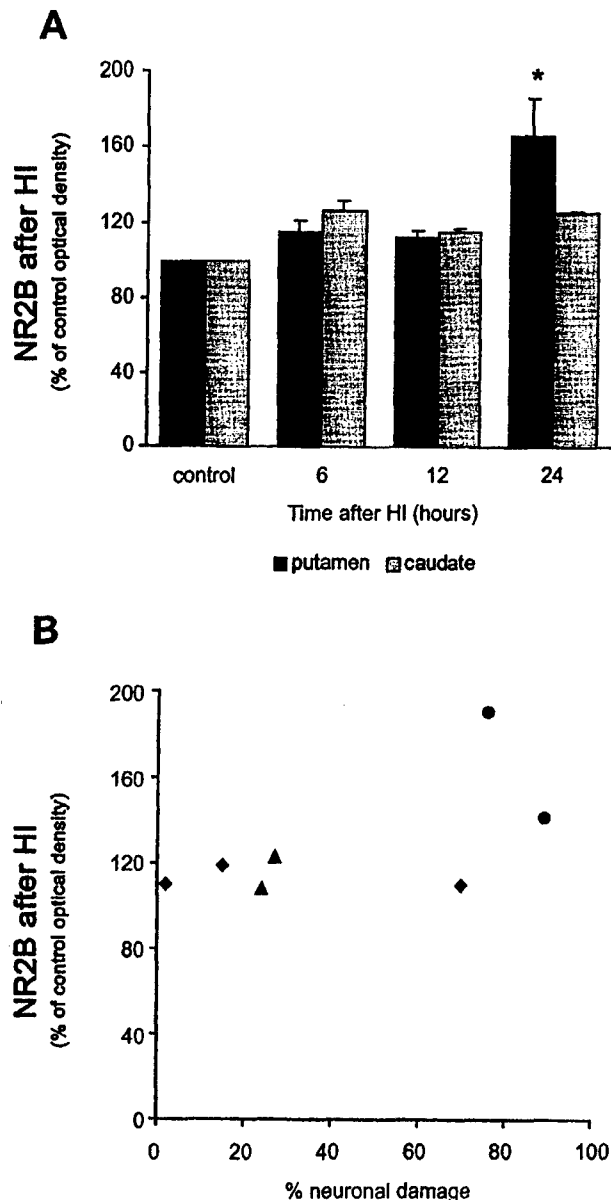


Fig. 11. Quantification of NR2B immunoreactivity in putamen and caudate by immunocytochemistry using densitometry. (A) The histogram shows the optical density of NR2B immunoreactivity (mean  $\pm$  S.E.M.) as a percentage of optical density in control animals. (B) The dot plot shows the relationship of NR2B immunoreactivity relative to the percentage neuronal damage in the putamen after HI. Immunoreactivity was quantified by optical density and stated as percentage of optical density in control animals. The percentage neuronal damage corresponds to the percentage degenerating neurons in the putamen of each piglet plotted individually according to the time after HI when the sample was harvested: ( $\blacktriangle$ , 6 h;  $\blacklozenge$ , 12 h;  $\bullet$ , 24 h). The single linear regression model with NR2B protein immunoreactivity (dependent variable) relative to percentage neuronal damage is described by the following equation:  $y = 106.46 + 0.52x$ ,  $r^2 = 0.40$ . The asterisks indicates statistical significance of \*,  $P < 0.05$ .

newborn piglet model of cardiac arrest, we examined the protein levels and phosphorylation status of NMDA receptors after HI. Our data indicate that NMDA receptor subtypes are changed in relation to the degree of neuronal damage after HI. More specifically, elevated NR1 protein levels in the striatum of HI animals correlated with the severity of neuronal damage, as indicated by the number of actively degenerating neurons identified neuropathologically in brain sections. NR1 levels are lower than baseline when few neurons are damaged, but levels increase when the number of damaged neurons increases. The highest levels of NR1 protein are found with the highest number of neurons showing injury. Because of this apparent trend between NR1 levels and accumulating neuronal injury, the levels of a phosphorylated form of NR1 were measured as a marker of NR1 activation after HI. As neuronal injury emerges, the level of phosphorylated NR1 increases, as detected by an antibody recognizing phosphorylated NR1 at <sup>897</sup>serine. The antibody used allows us to recognize NR1 receptors containing the C1 terminal domain [36]. NR1 splice variants without the C1 cassette would not be recognized. The increased phosphorylated NR1 is not clearly associated with the amount of elapsed time after HI, but rather with the specific amount of neuronal damage in the putamen. These observations are novel and extend the excitotoxicity theory of HI brain damage by showing that the degree of injury is associated with the phosphorylation of NR1 subunit by PKA on serine residue 897 which could further modify selective regional vulnerability to HI. These results suggest that the phosphorylation of NR1 via PKA may be increased with incremental severity of injury and that activation of NMDA receptors may play a role in the excitotoxic death of striatal neurons.

Physiological stimulation of PKA activity shifts the phosphorylation–dephosphorylation equilibrium to the phosphorylation of the NMDA receptor, and PKA antagonizes the effect of calcineurin to decrease channel activity in rat hippocampal neurons [33]. The importance of PKA in increased NMDA receptor activation has been examined in a variety of neuronal models. In primary striatal cultures [13], forskolin, a PKA activator via cAMP stimulation, causes the phosphorylation of NR1 <sup>897</sup>serine in a PKA dependent manner; this forskolin-mediated phosphorylation of the NR1 subunit is blocked by a PKA inhibitor and is not affected by the  $Ca^{2+}$ /calmodulin kinase antagonist. These works, along with others [41], suggest that in neurons subjected to various levels of stimulation the balance of phosphorylation–dephosphorylation may be altered via preferential activation of protein kinases, thereby modulating striatal neuronal signaling. Unfortunately, we were not able to examine PKC phosphorylation of NR1 in these striatal extracts, but we are planning to explore alternative methods to use the specific antibodies to PKC phosphorylated NR1 in striatum of HI piglet.

With regard to striatal neurodegeneration after HI in newborns, it is interesting that in addition to increased

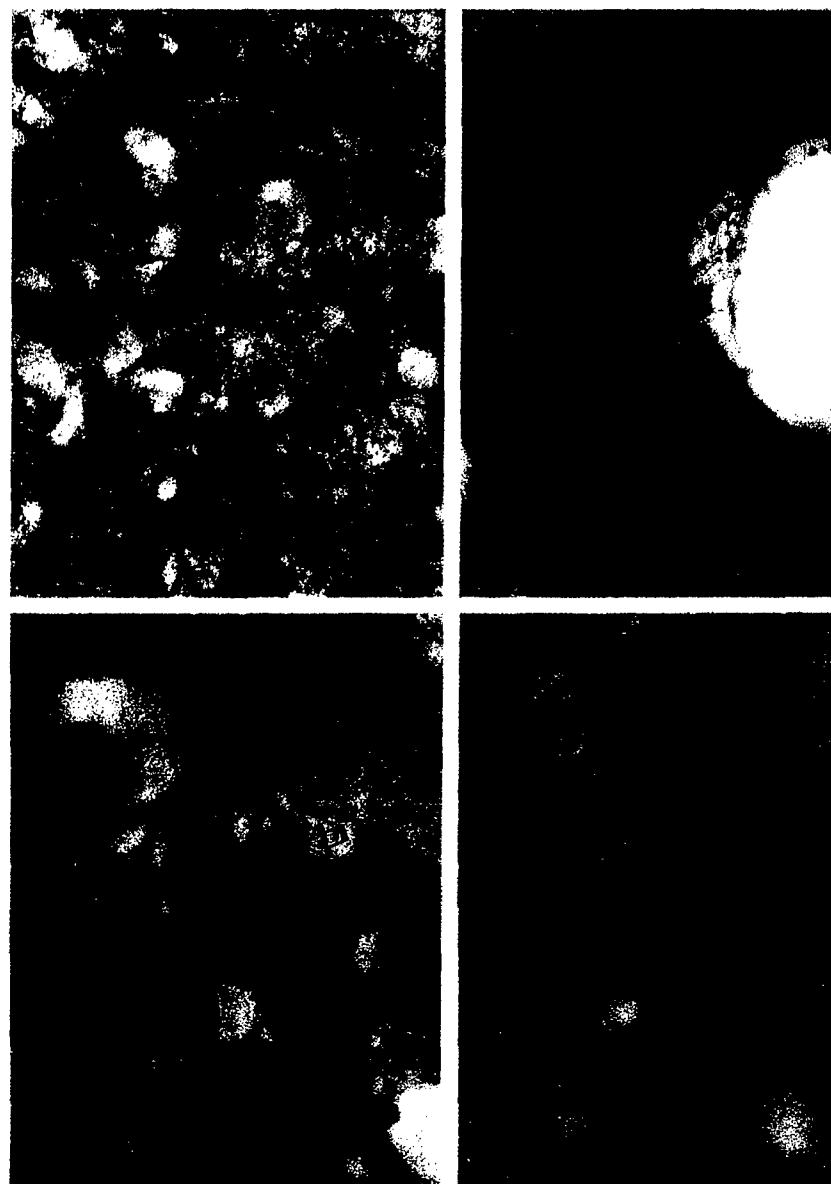


Fig. 12. NR2B is localized in astrocytes in severely damaged putamen after HI. Double-labeling for NR2B (orange/brown staining) and GFAP (dark green stain) immunoreactivities in HI piglet striatum viewed by light microscopy at 50 $\times$  (A) and 400 $\times$  (B–D). GFAP immunoreactivity is found copiously throughout the neuropil. (A and B) Astrocytes express NR2B after HI (solid arrows), some of which are swollen (open arrow). (C) Perivascular astrocytes express NR2B (arrows). (D) Subsets of astrocytes (solid arrow) do not express NR2B.

phosphorylation of NR1, suggesting potentiated or increased receptor activation, we have found evidence for impaired function of striatal Na,K-ATPase early after HI [7]. Furthermore, a downstream consequence of NMDA receptor activation is enhanced NOS activity leading to NO production. In our HI piglet model, we have previously shown evidence for NO toxicity in striatal neurons through the production of peroxynitrite [18]. Moreover, the degree of NMDA receptor activation in striatal neurons after HI may be a driving mechanism for the recently proposed neuronal cell death continuum [14,15,32]. In this continuum excitotoxic and ischemic neuronal death can

emerge as necrosis, apoptosis and hybrids with overlapping apoptotic and necrotic features. The intensity of the activation of NMDA receptors and downstream signaling pathways could influence the mode of cell death after HI, as has been described in *in vitro* models of neurotoxicity [3]. Thus, the developmental expression patterns of NMDA receptors and different activation patterns may have roles in the different contributions of neuronal apoptosis found in models of newborn HI in rodent and swine [19,27].

To identify whether changes in NMDA receptors are subunit specific, selected NR2 subunits were measured. NR2B levels do not change significantly at 3, 6, and 12 h



recovery after HI compared to controls, but NR2B levels are elevated significantly above control at 24 h after HI. The levels of NR2B do not relate to the number of damaged putaminal neurons, but the increase is associated with augmented astroglial expression evolving in parallel with the neuronal damage. Astrocyte expression of NR2B has been described in a rodent model of ischemic brain injury, weeks after the insult [8]. The significance of this finding is still unclear. NR2A levels in striatum of HI piglets are not different from control during the 3–24 h evaluation period.

We conclude that NMDA receptor subunits are changed in the striatum after neonatal HI and we suggest that abnormal NMDA receptor potentiation through increased NR1 phosphorylation participates in the mechanisms of striatal neuron degeneration after HI. Our findings concerning the role of NMDA receptors in ischemic neuronal death add to the existing knowledge on the importance of the NMDA receptor as a major modulator of neuronal injury in HI. Evidence of the activation of NMDA receptors in a relevant *in vivo* model reinforces their participation in the HI pathway to neuronal death. Our data suggest that NR1 phosphorylation increases concurrently with increasing neuronal damage in the striatum of piglets after HI. This is a first step in the functional assessment of these receptors in an *in vivo* model of HI.

We speculate that the severity of the HI insult, and not just time after injury, may be important in the determination of which neuronal death pathway becomes activated or primarily involved in the cell's response to the insult. This concept may be important to consider when investigating novel neuroprotective agents after HI.

## Acknowledgements

The authors are grateful for the outstanding technical support of Ms. Ann Price and Mr. Frank Barksdale and for the editorial support of Dr. Deborah McLellan. This research was supported by grants from the National Institutes of Health, NS34100 (L.J.M.), AG16282 (L.J.M.) and NS20020 (R.J.T.), and from the US Army Medical Research and Materiel Command (DAMD17-99-1-9553, L.J.M.). Anne-Marie Guerguerian is the recipient of a Young Investigator Award from the World Federation of Pediatric Intensive and Critical Care Societies.

## References

- [1] C. Akazawa, R. Shigemoto, Y. Bessho, S. Nakanishi, N. Mizuno, Differential expression of five *N*-methyl-D-aspartate receptor subunit mRNAs in the cerebellum of developing and adult rats, *J. Comp. Neurol.* 347 (1994) 150–160.
- [2] G.P. Ballough, L.J. Martin, F.J. Cann, J.S. Graham, C.D. Smith, C.E. Kling, J.S. Forster, S. Phann, M.G. Filbert, Microtubule-associated protein 2 (MAP-2): a sensitive marker of seizure-related brain damage, *J. Neurosci. Methods* 61 (1995) 23–32.
- [3] E. Bonfoco, D. Krainc, M. Ankarcrona, P. Nicotera, S.A. Lipton, Apoptosis and necrosis: two distinct events induced, respectively, by mild and intense insults with *N*-methyl-D-aspartate or nitric oxide/superoxide in cortical cell cultures, *Proc. Natl. Acad. Sci. USA* 92 (1995) 7162–7166.
- [4] A.M. Brambrink, L.J. Martin, D.F. Hanley, K.J. Becker, R.C. Koehler, R.J. Traystman, Effects of the AMPA receptor antagonist NBQX on outcome of newborn pigs after asphyxial cardiac arrest, *J. Cereb. Blood Flow Metab.* 19 (1999) 927–938.
- [5] L.M. Ford, P.R. Sanberg, A.B. Norman, M.H. Fogelson, MK-801 prevents hippocampal neurodegeneration in neonatal hypoxic-ischemic rats, *Arch. Neurol.* 46 (1989) 1090–1096.
- [6] R. Gill, A.C. Foster, G.N. Woodruff, MK-801 is neuroprotective in gerbils when administered during the postischemic period, *Neuroscience* 25 (1988) 847–855.
- [7] W.C. Golden, A.M. Brambrink, R.J. Traystman, L.J. Martin, Failure to sustain recovery of Na,K-ATPase function is a possible mechanism for striatal neurodegeneration in hypoxic-ischemic newborn piglets, *Brain Res. Mol. Brain Res.* 88 (2001) 94–102.
- [8] M. Gottlieb, C. Matute, Expression of ionotropic glutamate receptor subunits in glial cells of the hippocampal CA1 area following transient forebrain ischemia, *J. Cereb. Blood Flow Metab.* 17 (1997) 290–300.
- [9] C. Hisatsune, H. Umemori, T. Inoue, T. Michikawa, K. Kohda, K. Mikoshiba, T. Yamamoto, Phosphorylation-dependent regulation of *N*-methyl-D-aspartate receptors by calmodulin, *J. Biol. Chem.* 272 (1997) 20805–20810.
- [10] M.V. Johnston, Selective vulnerability in the neonatal brain, *Ann. Neurol.* 44 (1998) 155–156.
- [11] L.F. Lau, R.L. Huganir, Differential tyrosine phosphorylation of *N*-methyl-D-aspartate receptor subunits, *J. Biol. Chem.* 270 (1995) 20036–20041.
- [12] M.H. LeBlanc, V. Vig, B. Smith, C.C. Parker, O.B. Evans, E.E. Smith, MK-801 does not protect against hypoxic-ischemic brain injury in piglets, *Stroke* 22 (1991) 1270–1275.
- [13] J.C. Leveque, W. Macias, A. Rajadhyaksha, R.R. Carlson, A. Barczak, S. Kang, X.M. Li, J.T. Coyle, R.L. Huganir, S. Heckers, C. Konradi, Intracellular modulation of NMDA receptor function by antipsychotic drugs, *J. Neurosci.* 20 (2000) 4011–4020.
- [14] L.J. Martin, Neuronal cell death in nervous system development, disease, and injury, *Int. J. Mol. Med.* 7 (2001) 455–478.
- [15] L.J. Martin, N.A. Al-Abdulla, A.M. Brambrink, J.R. Kirsch, F.E. Sieber, C. Portera-Cailliau, Neurodegeneration in excitotoxicity, global cerebral ischemia, and target deprivation: a perspective on the contributions of apoptosis and necrosis, *Brain Res. Bull.* 46 (1998) 281–309.
- [16] L.J. Martin, A. Brambrink, R.C. Koehler, R.J. Traystman, Primary sensory and forebrain motor systems in the newborn brain are preferentially damaged by hypoxia-ischemia, *J. Comp. Neurol.* 377 (1997) 262–285.
- [17] L.J. Martin, A.M. Brambrink, C. Lehmann, C. Portera-Cailliau, R. Koehler, J. Rothstein, R.J. Traystman, Hypoxia-ischemia causes abnormalities in glutamate transporters and death of astroglia and neurons in newborn striatum, *Ann. Neurol.* 42 (1997) 335–348.
- [18] L.J. Martin, A.M. Brambrink, A.C. Price, A. Kaiser, D.M. Agnew, R.N. Ichord, R.J. Traystman, Neuronal death in newborn striatum after hypoxia-ischemia is necrosis and evolves with oxidative stress, *Neurobiol. Dis.* 7 (2000) 169–191.
- [19] L.J. Martin, F.E. Sieber, R.J. Traystman, Apoptosis and necrosis occur in separate neuronal populations in hippocampus and cerebellum after ischemia and are associated with differential alterations in metabotropic glutamate receptor signaling pathways, *J. Cereb. Blood Flow Metab.* 20 (2000) 153–167.
- [20] J.W. McDonald, M.V. Johnston, Excitatory amino acid neurotoxicity in the developing brain, *NIDA Res. Monogr.* 133 (1993) 185–205.

- [21] J.W. McDonald, F.S. Silverstein, M.V. Johnston, MK-801 protects the neonatal brain from hypoxic–ischemic damage, *Eur. J. Pharmacol.* 140 (1987) 359–361.
- [22] J.W. McDonald, F.S. Silverstein, M.V. Johnston, Neuroprotective effects of MK-801, TCP, PCP and CPP against *N*-methyl-D-aspartate induced neurotoxicity in an in vivo perinatal rat model, *Brain Res.* 490 (1989) 33–40.
- [23] O.P. Mishra, M. Delivoria-Papadopoulos, Cellular mechanisms of hypoxic injury in the developing brain, *Brain Res. Bull.* 48 (1999) 233–238.
- [24] E. Morikawa, H. Mori, Y. Kiyama, M. Mishina, T. Asano, T. Kirino, Attenuation of focal ischemic brain injury in mice deficient in the epsilon1 (NR2A) subunit of NMDA receptor, *J. Neurosci.* 18 (1998) 9727–9732.
- [25] W. Nakajima, A. Ishida, M.S. Lange, K.L. Gabrielson, M.A. Wilson, L.J. Martin, M.E. Blue, M.V. Johnston, Apoptosis has a prolonged role in the neurodegeneration after hypoxic ischemia in the newborn rat, *J. Neurosci.* 20 (2000) 7994–8004.
- [26] S. Nakanishi, Molecular diversity of glutamate receptors and implications for brain function, *Science* 258 (1992) 597–603.
- [27] F.J. Northington, D.M. Ferriero, E.M. Graham, R.J. Traystman, L.J. Martin, Early neurodegeneration after hypoxia–ischemia in neonatal rat is necrosis while delayed neuronal death is apoptosis, *Neurobiol. Dis.* 8 (2001) 207–219.
- [28] C.K. Park, D.G. Nehls, D.I. Graham, G.M. Teasdale, J. McCulloch, Focal cerebral ischaemia in the cat: treatment with the glutamate antagonist MK-801 after induction of ischaemia, *J. Cereb. Blood Flow Metab.* 8 (1988) 757–762.
- [29] C.K. Park, D.G. Nehls, D.I. Graham, G.M. Teasdale, J. McCulloch, The glutamate antagonist MK-801 reduces focal ischemic brain damage in the rat, *Ann. Neurol.* 24 (1988) 543–551.
- [30] R.S. Petralia, Y.X. Wang, R.J. Wenthold, The NMDA receptor subunits NR2A and NR2B show histological and ultrastructural localization patterns similar to those of NR1, *J. Neurosci.* 14 (1994) 6102–6120.
- [31] C. Portera-Cailliau, D.L. Price, L.J. Martin, *N*-Methyl-D-aspartate receptor proteins NR2A and NR2B are differentially distributed in the developing rat central nervous system as revealed by subunit-specific antibodies, *J. Neurochem.* 66 (1996) 692–700.
- [32] C. Portera-Cailliau, D.L. Price, L.J. Martin, Excitotoxic neuronal death in the immature brain is an apoptosis–necrosis morphological continuum, *J. Comp. Neurol.* 378 (1997) 70–87.
- [33] I.M. Raman, G. Tong, C.E. Jahr,  $\beta$ -Adrenergic regulation of synaptic NMDA receptors by cAMP-dependent protein kinase, *Neuron* 16 (1996) 415–421.
- [34] S.J. Siegel, N. Brose, W.G. Janssen, G.P. Gasic, R. Jahn, S.F. Heinemann, J.H. Morrison, Regional, cellular, and ultrastructural distribution of *N*-methyl-D-aspartate receptor subunit 1 in monkey hippocampus, *Proc. Natl. Acad. Sci. USA* 91 (1994) 564–568.
- [35] R.P. Simon, J.H. Swan, T. Griffiths, B.S. Meldrum, Blockade of *N*-methyl-D-aspartate receptors may protect against ischemic damage in the brain, *Science* 226 (1984) 850–852.
- [36] W.G. Tingley, M.D. Ehlers, K. Kameyama, C. Doherty, J.B. Ptak, C.T. Riley, R.L. Huganir, Characterization of protein kinase A and protein kinase C phosphorylation of the *N*-methyl-D-aspartate receptor NR1 subunit using phosphorylation site-specific antibodies, *J. Biol. Chem.* 272 (1997) 5157–5166.
- [37] W.G. Tingley, K.W. Roche, A.K. Thompson, R.L. Huganir, Regulation of NMDA receptor phosphorylation by alternative splicing of the C-terminal domain, *Nature* 364 (1993) 70–73.
- [38] Y.T. Wang, M.W. Salter, Regulation of NMDA receptors by tyrosine kinases and phosphatases, *Nature* 369 (1994) 233–235.
- [39] T. Wieloch, Hypoglycemia-induced neuronal damage prevented by an *N*-methyl-D-aspartate antagonist, *Science* 230 (1985) 681–683.
- [40] S. Zhang, M.D. Ehlers, J.P. Bernhardt, C.T. Su, R.L. Huganir, Calmodulin mediates calcium-dependent inactivation of *N*-methyl-D-aspartate receptors, *Neuron* 21 (1998) 443–453.
- [41] X. Zou, Q. Lin, W.D. Willis, Enhanced phosphorylation of NMDA receptor 1 subunits in spinal cord dorsal horn and spinothalamic tract neurons after intradermal injection of capsaicin in rats, *J. Neurosci.* 20 (2000) 6989–6997.

# Neurodegeneration in the Thalamus following Neonatal Hypoxia-Ischemia Is Programmed Cell Death

Frances J. Northington<sup>a</sup> Donna M. Ferriero<sup>d</sup> Lee J. Martin<sup>b,c</sup>

Eudowood Neonatal Pulmonary Division, Departments of <sup>a</sup>Pediatrics, <sup>b</sup>Pathology and <sup>c</sup>Neuroscience, Johns Hopkins University School of Medicine, Baltimore, Md., and <sup>d</sup>Departments of Neurology and Pediatrics, University of California, San Francisco, Calif., USA

## Key Words

Apoptosis · Bax · Caspase · Cytochrome C oxidase · Fas death receptor · Mitochondria

## Abstract

We studied neuronal cell body, axonal, and terminal degeneration in brains from 7-day-old rat pups recovered for 0, 1.5, 3, 6, 24, 48, 72 h, and 6 days following hypoxia-ischemia and identified proteins involved in the delayed neurodegeneration in the thalamus. We found that injury is biphasic with initial necrosis in the ipsilateral forebrain by 3 h following hypoxia-ischemia, in contrast to more delayed and apoptotic-like injury in the ventral-basal thalamus, brainstem, and other remote non-forebrain regions. Prior to the appearance of large numbers of apoptotic profiles in the ventral-basal thalamus, expression of Fas death receptor protein, activated forms of caspase 8 and caspase 3, and pro-apoptotic Bcl-2 proteins are increased. This manuscript combines our data on hypoxic-ischemic injury in the developing brain and presents evidence for at least two forms of neurodegeneration, namely, acute necrosis in the forebrain and delayed neurodegeneration in the thalamus, which is death-receptor-mediated programmed cell death.

Copyright © 2001 S. Karger AG, Basel

## Introduction

It is now understood that acute perinatal brain injury is a relatively rare cause of cerebral palsy [1], however, the neurologic handicaps caused by perinatal anoxia due to asphyxia and lack of cerebral blood flow are severe and lifelong [2]. Mechanisms for hypoxic-ischemic brain injury include energy failure, free radical damage, cytokine and excitotoxicity and caspase-mediated cell death [3–9]. These mechanisms have been primarily investigated in the rapidly and severely injured forebrain regions. Degeneration of neurons in regions other than the forebrain (i.e. diencephalon) after hypoxia-ischemia is studied much less frequently in newborn asphyxia models. The somatosensory thalamus is injured in human newborns after hypoxia-ischemia [10, 11], and this damage may contribute to sensory-motor deficits common in infants with neonatal brain injury and cerebral palsy. Neuropathologic studies of animal models have revealed injury to the developing diencephalon, substantia nigra and brainstem following hypoxia-ischemia in neonatal rats [12–15] and piglets [16, 17]. However, the timing, structure and mechanisms responsible for neurodegeneration in non-forebrain regions after neonatal hypoxia-ischemia have only recently begun to be understood [14, 15, 18].

## KARGER

Fax +41 61 306 12 34  
E-Mail [karger@karger.ch](mailto:karger@karger.ch)  
[www.karger.com](http://www.karger.com)

© 2001 S. Karger AG, Basel

Accessible online at:  
[www.karger.com/journals/dne](http://www.karger.com/journals/dne)

Frances J. Northington, MD  
Eudowood Neonatal Pulmonary Division  
Department of Pediatrics, CMSC 210, Johns Hopkins Hospital, 600 N. Wolfe Street  
Baltimore, MD 21287 (USA)  
Tel. +1 410 955 5259, Fax +1 410 955 0298, E-Mail [fnorthin@jhmi.edu](mailto:fnorthin@jhmi.edu)

We report here our combined recent findings [15, 18] that support the hypothesis that remote neurodegeneration segregates from initial forebrain injury as different forms of neuronal cell death, with patterns of distribution that suggest a role for neuronal connectivity in hypoxic-ischemic neurodegeneration in the immature brain and involve activation of proteins known to participate in programmed cell death.

## Methods

The Rice-Vannucci [19] neonatal adaptation of the Levine procedure [20] was used to cause hypoxic-ischemic brain injury in 7-day-old (p7) rats. The animals were killed with an overdose of pentobarbital 0, 1.5, 3, 6, 24, 48 and 72 h and 6 days following the end of hypoxia. All animal studies received prior approval from the Animal Care and Use Committee of the Johns Hopkins University School of Medicine and were performed in accordance with the NIH Guide for the Care and Use of Laboratory Animals, US Department of Health and Human Services 85-23, 1985. The brains were retrieved for histological and histochemical analysis, and for immunoblotting. A minimum of 6 animals/time point were used for immunohistochemical analysis, and a minimum of 4 pooled samples ( $n = 8$  animals)/time point were used for immunoblotting experiments.

Silver staining [21] (FD Neuro Silver Kit; FD Neurotechnologies, Baltimore, Md., USA) and cresyl violet staining were used for the identification of injured brain regions in histological preparations. Sections were digitized using an image analysis system and LA Inquiry Software (Loats, Westminster, Md., USA). Optical density (OD) measurements were obtained from outlined areas of interest in the parasagittal cortex at each of three coronal levels and from the ventral-basal thalamus in the most posterior section. The measurements for the cortex were averaged to give one value/region/animal. OD measurements were corrected for background staining by subtracting the OD in a contralateral structure with equal neuronal density but without evidence of injury.

Electron microscopy was used to confirm the apoptotic morphology [17, 22]. Retrograde labeling with fluorogold was used to identify thalamic neurons with cortical connections. The cytochrome oxidase histochemical method of Wong-Riley [23, 24] was used to identify levels of oxidative metabolism and intracellular distribution of oxidatively active mitochondria in thalamic neurons following hypoxia-ischemia.

Immunoblotting [25] was used to identify changes in the expression of proteins involved in programmed cell death. 150–200 mg pooled thalamic samples ( $n = 2$ /pooled sample) were homogenized in cold 20 mM Tris HCl (pH 7.4) containing (10% w/v) sucrose, and a cocktail of protease inhibitors including 20  $\mu$ M/ml aprotinin (Trasyol), 20  $\mu$ M/ml leupeptin, 20  $\mu$ M/ml antipain, 20  $\mu$ M/ml pepstatin A, 20  $\mu$ M/ml chymostatin, 0.1 mM phenylmethylsulfonyl fluoride, 10 mM benzamide, 1 mM EDTA, and 5 mM EGTA. Homogenates were centrifuged at 1,000 g for 20 min, and the resulting supernatant (S2 soluble protein fraction) collected. The pellet (P2 mitochondrial-enriched, membrane fraction) was washed in homogenization buffer (without sucrose) 3 times by resuspension and centrifugation at 114,000 g for 20 min and then resuspended fully in homogenization buffer supplemented with 20% (w/v) glycerol. This subcellular frac-

tionation protocol has been verified to be enriched in mitochondria, but also contains other organelle constituents (i.e. endoplasmic reticulum and Golgi apparatus) [26]. Protein concentrations were measured by a Bio-Rad protein assay with bovine serum albumin as a standard.

Samples of membrane or soluble proteins were subjected to SDS-PAGE and electroblotted onto nitrocellulose membranes. After primary incubation, blots were washed, incubated with peroxidase-conjugated secondary antibodies (0.2  $\mu$ g/ml) and developed with enhanced chemiluminescence. To quantify cell death protein immunoreactivity, films were scanned using Adobe Photoshop and OD performed with IP Lab Gel H software. The OD of the corresponding lanes in Coomassie-stained gels or Ponceau-stained blots was used to correct the OD of the cell death protein immunoreactivity for differences in protein loading. Protein levels are thus expressed as relative OD measurements compared to control lanes in the same blot.

Antibodies used to determine the involvement of death receptors, mitochondrial-apoptosis-related proteins and caspase cleavage in thalamic neurodegeneration following neonatal hypoxia-ischemia included: anti-Fas death receptor antibody, anti-caspase 8 antibody, anti-Bcl 2 antibody (Santa Cruz Biotechnology, Santa Cruz, Calif., USA), anti-Bax (Upstate Biotechnology, Lake Placid, N.Y., USA) and cleaved caspase 3 antibody (Cell Signaling Technology, Beverly, Mass., USA) Jurkat cells known to express high levels of the Fas death receptor protein, and other constituents of programmed cell death cascades were used as a positive control.

**Retrograde Tracing.** As described previously, 10 nl of the fluorescent retrograde tracer, Fluorogold (Fluorochrome, Englewood, Colo., USA), were injected into the superficial parietal, occipital cortex. The scalp was sutured and the pups returned to the dam until p7. To demonstrate the presence of cell death within regions with connections to the ipsilateral cortex, rat pups ( $n = 6$ ) injected with fluorogold on p4 were exposed to hypoxia-ischemia as described above and perfused 48 h after hypoxia for combined fluorogold immunocytochemistry (anti-fluorogold antibody; Chemicon, Temecula, Calif., USA) and cresyl violet staining.

## Results and Discussion

*Regional Differences in Timing and Structure of Neurodegeneration following Neonatal Hypoxia-Ischemia.* As reported by others [27] necrotic neurons are found within the ipsilateral cortex immediately following neonatal hypoxia-ischemia (fig. 1C). Using silver staining, neurodegeneration is evident within 3 h in the cortex following hypoxia-ischemia (fig. 1A). This early and rapid neurodegeneration in the forebrain contrasts with the ipsilateral thalamus where neurodegeneration is evident at 24 h following neonatal hypoxia-ischemia, a time at which many thalamic neurons show the light-microscopic features of apoptosis (fig. 1D). Densitometric analyses of the progression of injury as measured by increased silver deposition are shown in figure 1A, B and most prominent structures of cell death are shown in figure 1C, D.

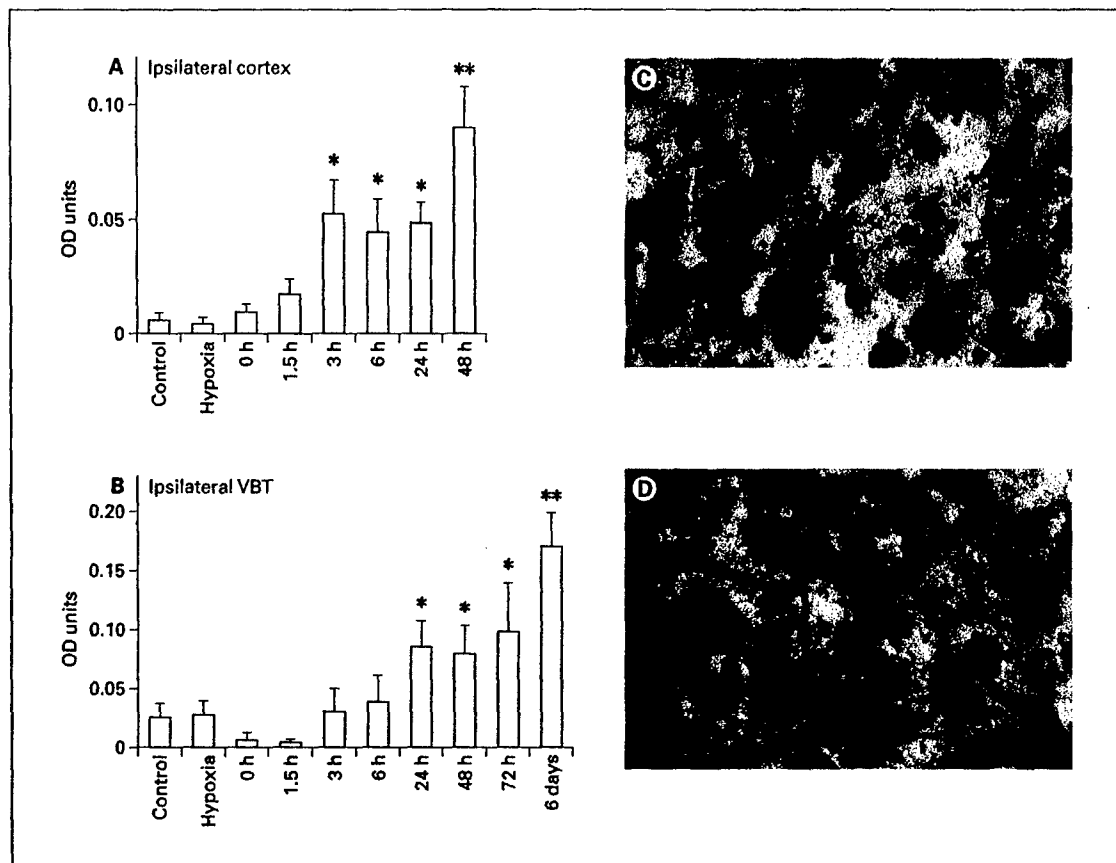


**Fig. 1.** Onset and structure of neurodegeneration following neonatal hypoxia-ischemia differ in the cortex and ventral-basal thalamus (VBT). Increased silver deposition on injured neuronal elements as measured by an increased OD is evident in the cortex by 3 h after hypoxia-ischemia (**A**) but not until 24 h in the ipsilateral ventral basal thalamus (**B**). A further increase in the amount of injury also occurs more rapidly in the cortex, at 48 h, compared to the thalamus, 6 days. Densitometric analysis of silver deposition in injured structures is presented (**A**, **B**). Photomicrographs demonstrating the primary structure of cell death in the region, at the time of first detection of increased silver deposition (**C**, ipsilateral cortex, necrosis at 3 h, **D** ipsilateral VBT, apoptosis 24 h following neonatal hypoxia-ischemia). For densitometric analysis, \*  $p \leq 0.05$  vs. control (= non-ligated, non-hypoxic littermates). Hypoxia = Non-ligated, hypoxia-exposed littermates,  $n = 6$  at each time point.

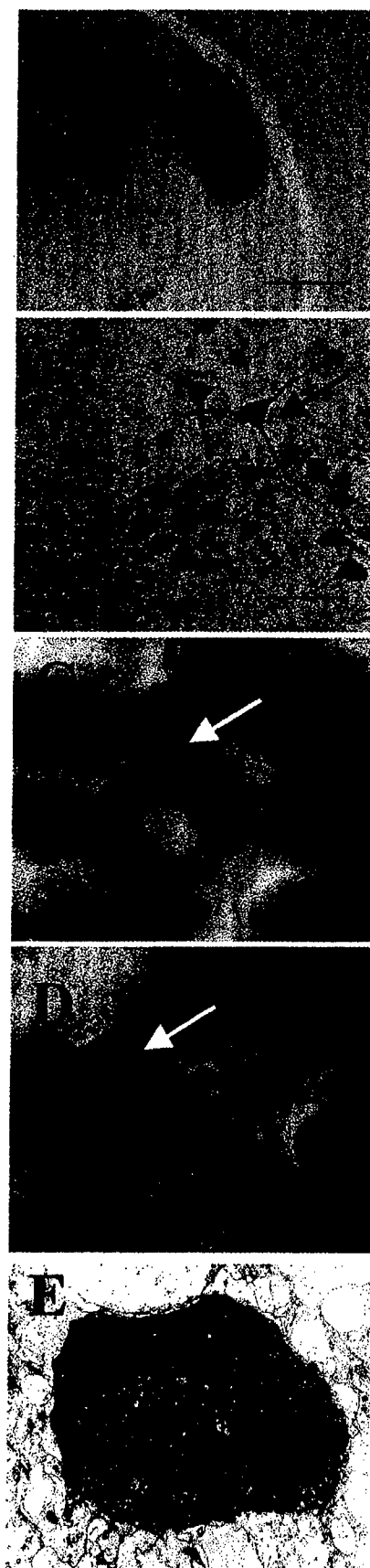
*Dying Thalamic Neurons Have Cortical Connections.* Using retrograde labeling, it can be demonstrated that many neurons in the lateral geniculate nucleus and the ventral tier of thalamic nuclei have cortical connections (fig. 2A, B; fluorogold immunohistochemistry in thalamic neurons following cortical injection of retrograde tracer). Following neonatal hypoxia-ischemia, many thalamic neurons with cortical connections die apoptotically (fig. 2C, neurons double labeled with brown immunoreactivity for fluorogold and cresyl-violet-stained condensed chromatin clumps which are characteristic of late-stage apoptosis).

*From Early Chromatolytic to Late Stages of Apoptosis, Thalamic Neurons Have Increased Cytochrome Oxidase Activity.* Stages of apoptotic neurodegeneration were classified as our laboratory has done previously. In the pre-apoptotic chromatolytic phase, neuronal soma and dendrites shrink. Rounded neurons with scalloped membranes and a loss of Nissl substance are in the early stages of apoptosis, while at end-stage apoptosis, the cell consists of two or three closely apposed, small, round nuclear fragments surrounded by a thin rim of cytoplasm [28]. Chromatolytic and apoptotic thalamic neurons also have increased cytochrome oxidase activity 6–24 h following hypoxia-ischemia (fig. 2D, double labeling with brown

immunoreactivity for cytochrome oxidase activity in cresyl-violet-stained thalamic neurons with distinct large chromatin clumps). Electron microscopy confirms that the thalamic neurons found to have light-microscopic features of apoptosis also have an ultrastructure consistent with apoptosis 24 h following neonatal hypoxia-ischemia (fig. 2E).

*Multiple Biochemical Markers of Apoptosis Are Expressed in the Thalamus in the First 24 h following Neonatal Hypoxia-Ischemia.* As we have reported [18], by 3 h following hypoxia-ischemia, increased expression of Fas death receptor protein occurs in the membrane fractions of ipsilateral thalamus by SDS-PAGE (fig. 3A). This increase coincides with caspase 8 cleavage to its active fragments (fig. 3C, expression of 18-kD active fragment of caspase 8). There is a concomitant decrease in the amount of pro-caspase 8 (54–55 kD) in the soluble protein fraction during the first 24 h following neonatal hypoxia-ischemia (not shown). There is also a progressive increase in the level of pro-apoptosis BAX in the mitochondria-enriched membrane fraction from 3 to 24 h following injury (fig. 3B, solid bars), while the levels of the anti-apoptosis Bcl<sub>2</sub> (fig. 3B, open bars) did not change. Thus, there is a large increase in the relative abundance of BAX, greatly favoring apoptosis [29]. By 24 h, this cascade of pro-apoptotic biochemical events also includes cleavage of caspase 3 to its active forms (fig. 3D). A pan caspase 3 antibody recognizing the pro-enzyme and its active forms and an antibody specific for the 17-kD cleaved fragment of caspase 3 gave identical results.

**Fig. 2.** Thalamic neurons, which die following neonatal hypoxia-ischemia, have cortical connections and also have transiently increased cytochrome oxidase activity. Cortical injection of fluorogold results in retrograde transport to the thalamus (**A**, brown immunoreactivity for retrogradely transported fluorogold in lateral geniculate and nuclei, LGN, and ventral-basal thalamus, VBT). Cortical injection specifically labels thalamic neurons, filling the cell bodies and processes with fluorogold (brown immunoreactivity, **B**). When animals are exposed to hypoxia-ischemia after injection of retrograde tracer, apoptotic thalamic neurons containing fluorogold are seen (**C**, brown immunoreactivity for fluorogold present in thalamic neurons with condensed chromatin labeled with cresyl violet). 6–24 h after neonatal hypoxia-ischemia, thalamic neurons in the mid to late stages of apoptosis have increased cytochrome oxidase activity, which then dissipates at the latest stages of apoptosis (**D**, brown immunoreactivity for cytochrome oxidase activity in neurons with large rounded cresyl-violet-stained chromatin clumps). When examined by electron microscopy, dying thalamic neurons have the ultrastructural features of apoptosis (**E**).



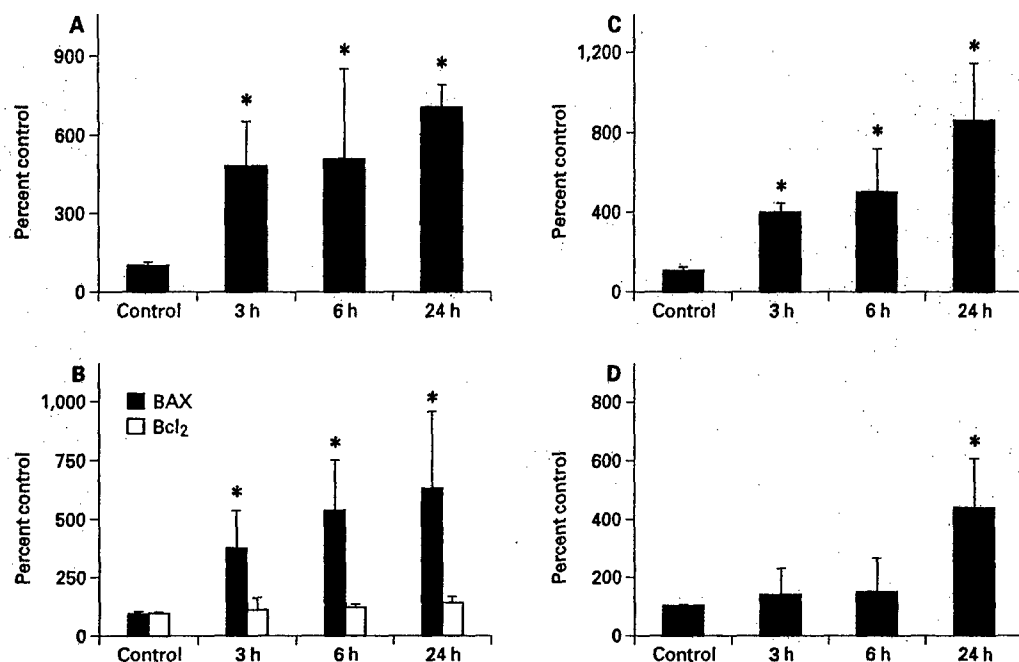


**Fig. 3.** Pro-apoptosis Fas death receptor protein, activated caspases and BAX are expressed in thalamus following neonatal hypoxia-ischemia. By 3 h after hypoxia-ischemia there is an increased expression of Fas death receptor protein (**A**) and a simultaneous increase in the expression of the 18-kD activated form of caspase 8 (**C**) in the membrane and soluble protein fractions from the ipsilateral thalamus. The ratio of pro- and anti-apoptosis *Bcl<sub>2</sub>* family proteins is altered, favoring the expression of pro-apoptosis BAX (**B**). These events significantly precede increased expression of the activated form caspase 3, 24 h following neonatal hypoxia-ischemia (**D**). Results are expressed as percent of control, compared with ANOVA, \*  $p \leq 0.05$  vs. simultaneously run control tissues; 6 samples of ipsilateral thalamic tissue were examined with each antibody, at each time point.

These data extend previous observations of neurodegeneration following neonatal hypoxia-ischemia by (1) using silver staining to quantify the difference in the time of onset and progression injury in cortex versus thalamus [15], (2) demonstrating significant differences in structure of neurodegeneration in cortex versus thalamus [15], and (3) showing that expression of key apoptosis-regulating proteins is increased, consistent with delayed programmed cell death in the thalamus [18]. Because thalamic neurons, which have cortical connections, die via apoptosis following hypoxia-ischemia, retrograde neurodegeneration following cortical damage may contribute to the delayed injury seen in the thalamus. Additionally, the transient phase of increased cytochrome oxidase activity in concert with the pro-apoptosis alteration of mitochondrial-apoptosis-regulating proteins further suggest an important role for mitochondria in delayed thalamic neu-

rodegeneration [18]. These data have implications for the development of targeted therapies designed to rescue specific neuronal populations following neonatal hypoxia-ischemia.

### Acknowledgments

The authors gratefully acknowledge the expert technical assistance of Debra Flock, Ann Price, Frank Barksdale and George Kuck, III. This work was supported by United Cerebral Palsy (F.J.N.), R03HD 39672 (F.J.N.), US army Department of Defense DAMD 17-99-1-9553 and NIH AG61282 (L.J.M.) and NS 35902 (D.M.F.).

## References

- Nelson KB, Grether JK: Causes of cerebral palsy. *Curr Opin Pediatr* 1999;11:487-491.
- Lorenz JM, Wooliever DE, Jetton JR, Paneth N: A quantitative review of mortality and developmental disability in extremely premature newborns. *Arch Pediatr Adolesc Med* 1998;152:425-435.
- Barks JD, Silverstein FS: Excitatory amino acids contribute to the pathogenesis of perinatal hypoxic-ischemic brain injury. *Brain Pathol* 1992;2:235-243.
- Cheng Y, Deshmukh M, D'Costa A, Demaro JA, Gidday JM, Shah A, Sun Y, Jacquin MF, Johnson EM Jr, Holtzman DM: Caspase inhibitor affords neuroprotection with delayed administration in a rat model of neonatal hypoxic-ischemic brain injury. *J Clin Invest* 1998;101:1992-1999.
- Hagan P, Barks JD, Yabut M, Davidson BL, Roessler B, Silverstein FS: Adenovirus-mediated over-expression of interleukin-1 receptor antagonist reduces susceptibility to excitotoxic brain injury in perinatal rats. *Neuroscience* 1996;75:1033-1045.
- Liu XH, Eun BL, Silverstein FS, Barks JD: The platelet-activating factor antagonist BN 52021 attenuates hypoxic-ischemic brain injury in the immature rat. *Pediatr Res* 1996;40:797-803.
- Martin LJ, Brambrink AM, Lehmann C, Portera-Cailliau C, Koehler RC, Rothstein J, Traystman RJ: Hypoxia-ischemia causes abnormalities in glutamate transporters and death of astroglia and neurons in newborn striatum. *Ann Neurol* 1997;42:335-348.
- McDonald JW, Silverstein FS, Johnson MV: Neurotoxicity of N-methyl-D-aspartate is markedly enhanced in developing rat central nervous system. *Brain Res* 1988;459:200-203.
- Ishida A, Ishiwa S, Trescher WH, Nakajima W, Lange MS, Blue ME, Johnston MV: Delayed increase in neuronal nitric oxide synthase immunoreactivity in thalamus and other brain regions after hypoxic-ischemic injury in neonatal rats. *Exp Neurol* 2001;168:323-333.
- Barkovich A: Profound asphyxia in the premature infant: Image findings. *AJNR Am J Neuroradiol* 1995;95:1837-1846.
- Roland EH, Poskitt K, Rodriguez E, Lupton BA, Hill A: Perinatal hypoxic-ischemic thalamic injury: Clinical features and neuroimaging (see comments). *Ann Neurol* 1998;44:161-166.
- Oo TF, Henchcliffe C, Burke RE: Apoptosis in substantia nigra following developmental hypoxic-ischemic injury. *Neuroscience* 1995;69:893-901.
- Towfighi J, Yager JY, Housman C, Vannucci RC: Neuropathology of remote hypoxic-ischemic damage in the immature rat. *Acta Neuropathol* 1991;81:578-587.
- Nakajima W, Ishida A, Lange MS, Gabrielson KL, Wilson MA, Martin LJ, Blue ME, Johnston MV: Apoptosis has a prolonged role in the neurodegeneration after hypoxic ischemia in the newborn rat. *J Neurosci* 2000;20:7994-8004.
- Northington FJ, Ferriero DM, Graham EM, Traystman RJ, Martin LJ: Early neurodegeneration after hypoxia-ischemia in neonatal rat is necrosis while delayed neuronal death is apoptosis. *Neurobiol Dis* 2001;8:207-219.
- Martin LJ, Brambrink AM, Koehler RC, Traystman RJ: Primary sensory and forebrain motor systems in the newborn brain are preferentially damaged by hypoxia-ischemia. *J Comp Neurol* 1997;377:262-285.
- Martin LJ, Al-Abdulla NA, Brambrink AM, Kirsch JR, Sieber FE, Portera-Cailliau C: Neurodegeneration in excitotoxicity, global cerebral ischemia, and target deprivation: A perspective on the contributions of apoptosis and necrosis. *Brain Res Bull* 1998;46:281-309.
- Northington FJ, Ferriero DM, Flock DL, Martin LJ: Delayed neurodegeneration in neonatal rat thalamus after hypoxia-ischemia is apoptosis. *J Neurosci* 2001;21:1931-1938.
- Rice JE, Vannucci RC, Brierley JB: The influence of immaturity on hypoxic-ischemic brain damage in the rat. *Ann Neurol* 1981;9:131-141.
- Levine S: Anoxic-ischemic encephalopathy in rats. *Am J Pathol* 1960;36:1-17.
- Du F, Eid T, Schwarcz R: Neuronal damage after the injection of aminooxyacetic acid into the rat entorhinal cortex: A silver impregnation study. *Neuroscience* 1998;82:1165-1178.
- Portera-Cailliau C, Price DL, Martin LJ: Excitotoxic neuronal death in the immature brain is an apoptosis-necrosis morphological continuum. *J Comp Neurol* 1997;378:70-87.
- Wong-Riley M: Changes in the visual system of monocularly sutured or enucleated cats demonstrable with cytochrome oxidase histochemistry. *Brain Res* 1979;171:11-28.
- Wong-Riley MT: Cytochrome oxidase: An endogenous metabolic marker for neuronal activity. *Trends Neurosci* 1989;12:94-101.
- Martin LJ: Neuronal death in amyotrophic lateral sclerosis is apoptosis: Possible contribution of a programmed cell death mechanism. *J Neuropathol Exp Neurol* 1999;58:459-471.
- Martin LJ, Price AC, Kaiser A, Shaikh AY, Liu Z: Mechanisms for neuronal degeneration in amyotrophic lateral sclerosis and in models of motor neuron death (review). *Int J Mol Med* 2000;5:3-13.
- Towfighi J, Zec N, Yager J, Housman C, Vannucci RC: Temporal evolution of neuropathologic changes in an immature rat model of cerebral hypoxia: A light microscopic study. *Acta Neuropathol* 1995;90:375-386.
- Martin LJ, Kaiser A, Price AC: Motor neuron degeneration after sciatic nerve avulsion in adult rat evolves with oxidative stress and is apoptosis. *J Neurobiol* 1999;40:185-201.
- Gross A, Jockel J, Wei MC, Korsmeyer SJ: Enforced dimerization of BAX results in its translocation, mitochondrial dysfunction and apoptosis. *Embo J* 1998;17:3878-3885.



## Research report

## Failure to sustain recovery of Na,K-ATPase function is a possible mechanism for striatal neurodegeneration in hypoxic–ischemic newborn piglets

W. Christopher Golden<sup>a</sup>, Ansgar M. Brambrink<sup>b,1</sup>, Richard J. Traystman<sup>b</sup>, Lee J. Martin<sup>c,d,\*</sup><sup>a</sup>*Department of Pediatrics, Eudowood Neonatal Pulmonary Division, Johns Hopkins University School of Medicine, Baltimore, MD 21205, USA*<sup>b</sup>*Department of Anesthesiology and Critical Care Medicine, Johns Hopkins University School of Medicine, Baltimore, MD 21205, USA*<sup>c</sup>*Department of Pathology, Division of Neuropathology, Johns Hopkins University School of Medicine, 558 Ross Building, 720 Rutland Avenue, Baltimore, MD 21205, USA*<sup>d</sup>*Department of Neuroscience, Johns Hopkins University School of Medicine, Baltimore, MD 21205, USA*

Accepted 9 January 2001

### Abstract

Hypoxia–ischemia (HI) in the newborn can lead to a variety of sensorimotor abnormalities, including movement and posture disorders. Striatal neurons undergo necrosis after HI in piglets, but mechanisms for this neuronal death are not understood. We tested the hypothesis that Na,K-ATPase is defective in striatum early after HI. Piglets (1 week old) were subjected to 30 min hypoxia (arterial oxygen saturation 30%) and then 7 min of airway occlusion (oxygen saturation 5%), producing asphyxic cardiac arrest. Animals were resuscitated and recovered for 3, 6, 12, and 24 h, respectively. Neuronal necrosis in the striatum is progressive [14]. Na,K-ATPase activity (percent of control) was 60, 98, 51, and 54% at 3, 6, 12, and 24 h after HI, respectively. Intrastratial differences in enzyme activity were detected histochemically, with the putamen showing greater loss of Na,K-ATPase activity than caudate after 12 h recovery. Immunoblotting showed that the levels of the  $\alpha_3$  isoform (localized exclusively to neurons) were 85, 115, 101, and 79% of sham control at 3, 6, 12, and 24 h, respectively. Levels of  $\beta_1$ , the predominant  $\beta$  isoform, were similar to  $\alpha_3$ , while levels of the  $\alpha_1$  subunit, the catalytic isoform found in neurons and glia, were 182, 179, 226, and 153% at the same recovery times. We conclude that early inactivation of Na,K-ATPase function participates in the pathogenesis of striatal neuron necrosis, but that loss of enzyme function early after HI is not caused by depletion of composite  $\alpha/\beta$  subunits. © 2001 Elsevier Science B.V. All rights reserved.

**Theme:** Disorders of the nervous system**Topic:** Ischemia**Keywords:** Cerebral palsy; Excitotoxicity; Nitric oxide; Neuronal cell death; Oxidative stress; Peroxynitrite

### 1. Introduction

Perinatal hypoxic–ischemic encephalopathy (HIE) contributes significantly to mortality in the newborn period and to the development of long-term neurological handicaps in children. Systemic asphyxia resulting from a disruption in placental gas exchange occurs perinatally in two to four per 1000 full-term infants [29]. Approximately

15–20% of infants who develop HIE subsequently die during the newborn period, with up to 25% of survivors exhibiting permanent neurological disabilities (such as cerebral palsy) [28].

Using an animal model of neonatal HIE, we have discovered that primary sensory and forebrain motor structures that regulate posture and movement are preferentially damaged [13]. However, the selective vulnerability of these cortical and subcortical sensorimotor structures does not reflect the involvement of a particular vascular distribution. Instead, these regions exhibit higher basal levels of oxidative metabolism (identified by high concentrations of cytochrome oxidase and sodium–potassium ATPase (Na,K-ATPase)) and have particular con-

\*Corresponding author. Tel.: +1-410-502-5170; fax: +1-410-955-9777.

E-mail address: lmartin@jhmi.edu (L.J. Martin).

<sup>1</sup>Present address: Department of Anesthesiology, Johannes Gutenberg-University, Mainz, Germany.

nections with other brain regions [12,13]. These findings suggest that intrinsic metabolic status and connectivity contribute to brain regional vulnerability after hypoxia–ischemia (HI) in newborns.

Cerebral HI in the newborn has profound molecular consequences, including glutamate receptor-mediated abnormalities in intracellular ion and water flux and the generation of reactive oxygen species (ROS) [22,28]. However, the exact molecular mechanisms resulting in neuronal death remain unclear. ROS are generated from many sources, including impaired function of cytochrome oxidase in the initial stages of HIE, as well as through prostaglandin synthesis and xanthine oxidase activity during the reperfusion of ischemic regions [28]. ROS cause protein damage through direct modification, decreasing molecular stability and facilitating intracellular proteolysis [4]. Cerebral antioxidant levels are lower in neonates relative to adults [18,25], thus the newborn brain may be more vulnerable to ROS. Unmitigated oxidative stress can possibly damage cellular enzymes responsible for homeostasis, leading to the neurodegeneration seen in HIE.

Na,K-ATPase is a ubiquitous cell membrane enzyme responsible for establishment of ion gradients necessary for cell function, including maintenance of the resting membrane potential of neurons. The enzyme contains two major subunits: a larger  $\alpha$  protein responsible for the majority of the catalytic activity, and a smaller, glycosylated  $\beta$  protein required for maturation of the enzyme and transport to the cell surface [10]. Multiple  $\alpha$  and  $\beta$  isoforms have been identified in mammalian brain [16,20], likely reflecting both the heterogeneity of cell subtypes and the possible need for variability in enzyme expression based on tissue-specific requirements [10].

Previous experiments have shown that Na,K-ATPase activity is diminished in cortical synaptosomes isolated from animals exposed acutely to hypoxia in a non-survival model [21]. At present, however, little is known regarding the role of the ATPase-driven Na/K ion pump in the evolution of selective neuronal death after HI in newborns. The striatum, a brain region which functions in the planning and initiation of coordinated movements through integration of neocortical and thalamic signals, demonstrates both Na,K-ATPase activity and particular vulnerability to degeneration after HIE [11–14]. In this study, we tested the hypothesis that abnormalities in Na,K-ATPase activity and protein subunit isoform levels occur in newborn piglet striatum during the first 24 h after HI.

## 2. Materials and methods

### 2.1. Animal model of newborn hypoxia–ischemia

All animal protocols were approved by the Animal Use and Care Committee of the Johns Hopkins University

School of Medicine. One-week-old piglets (~2.5 kg) were anesthetized with sodium pentobarbital (65 mg/kg intraperitoneally, i.p.). These animals were subsequently intubated and mechanically ventilated to maintain normal oxygenation and ventilation. Under sterile conditions, femoral incisions were made, and catheters were advanced to the level of the thoracic aorta and the vena cava. The piglets received intravenous cephalothin for antibiotic coverage, fentanyl (10  $\mu$ g/kg intravenous) for anesthesia, and pancuronium bromide (0.3 mg/kg i.v.) to produce muscle paralysis. Maintenance i.v. fluids consisting of lactated Ringer's solution (10 cc/kg per h) were also administered. The animals were placed on a warming blanket, keeping rectal temperatures normothermic (38.5–39.5°C) for the piglets. Baseline measurements of arterial blood gases, hemoglobin concentration, oxygen content, glucose, blood pressure, heart rate, and temperature were recorded.

One set of piglets ( $n=5$ ) not subjected to hypoxic–ischemic injury served as surgical sham controls. The others ( $n=5$  per time point at 3, 6, 12, and 24 h recovery post insult) were exposed to 30 min of hypoxia (arterial  $O_2$  saturation 30%), 5 min of room air saturation ( $O_2$  saturation 65%) followed by 7 min of airway occlusion ( $O_2$  saturation 5%) resulting in cardiac arrest. At this point, ventilation was initiated with 100% oxygen, and epinephrine was injected as a bolus (0.1 mg/kg i.v.), followed by continuous infusion (40  $\mu$ g/kg per min). Sternal chest compressions were performed manually at a rate of 100/min. Upon recovery of spontaneous circulation, sternal chest compressions were terminated, and when arterial pressure exceeded 60 mmHg, the epinephrine infusion was discontinued. To maintain arterial pH at 7.4 after resuscitation, sodium bicarbonate (1 mEq/kg) was infused. Fentanyl was infused (5  $\mu$ g/kg per h) for 4 h. The animals were allowed to awaken (generally between 6 and 8 h) and subsequently weaned from ventilatory support. Animals usually drank water between 12 and 24 h and drank formula milk afterwards (if allowed to survive to that point).

### 2.2. Piglet brain preparation

The brains were prepared as described [14] and used for determination of Na,K-ATPase biochemical activity, Na,K-ATPase subunit protein levels, and in situ Na,K-ATPase histochemistry. For the enzyme activity and immunoblot analyses, sham control ( $n=2$ ) and HI piglets ( $n=2$  at 3, 6, 12, and 24 h) were anesthetized with sodium pentobarbital and then perfused briefly with cold phosphate-buffered saline. The brain was rapidly removed and subdissected, and the striatum (caudate, putamen, internal capsule, and nucleus accumbens) was transferred to cold homogenization buffer containing 20 mM Tris–HCl (pH 7.4) with 10% (w/v) sucrose, 1 mM EDTA, 5 mM EGTA, and a cocktail of protease inhibitors (20 U/ml Trasylol, 20

$\mu\text{g/ml}$  leupeptin, 20  $\mu\text{g/ml}$  antipain, 20  $\text{mg/ml}$  chymostatin, 0.1  $\text{mM}$  phenylmethylsulfonyl fluoride, 10  $\text{mM}$  benzamidine). The tissue was then homogenized and centrifuged at  $1000\times g$  for 10 min at  $4^\circ\text{C}$ . The nuclear-enriched pellet (P1) was frozen, and the supernatant (S1 fraction) then was centrifuged for 20 min at  $114\,000\times g$  at  $4^\circ\text{C}$ . The resulting membrane-enriched fraction (P2 fraction) was then washed with sucrose-free homogenization buffer twice by resuspension, with subsequent centrifugation at  $114\,000g$ . The final pellet was resuspended in homogenization buffer containing 20% (w/v) glycerol instead of sucrose to a protein concentration of 1.5–3  $\text{mg/ml}$ . Protein concentrations were then determined by Bio-Rad assay (with bovine serum albumin as the standard).

To generate brain sections for enzyme histochemistry, sham controls ( $n=3$ ) and HI piglets at 6, 12, or 24 h ( $n=3$  per time point) were perfused intra-aortically with cold 4% paraformaldehyde and 1% glutaraldehyde as described [14]. Sufficient numbers of brains at a 3-h time point were not available for analysis using enzyme histochemistry. After fixation, the brains were dissected midsagittally, and the striata from each animal were sliced coronally throughout the forebrain. From the left striatum of each animal, neurodegeneration was quantified using hematoxylin and eosin (H&E) staining and *in situ* DNA fragmentation [14]. These animals were also analyzed using electron microscopy [14]. The right striatum of each animal was cryoprotected in phosphate-buffered 20% glycerol for 24 h, frozen in isopentane, and stored at  $-80^\circ\text{C}$ . These samples were cut serially at 40  $\mu\text{m}$  on a sliding microtome and subsequently assayed for histochemical activity.

### 2.3. Na,K-ATPase biochemical assay

We measured using the method of Mishra and Delivoria-Papadopoulos [17] the biochemical activity of Na,K-ATPase in the striatum of control and HI piglets. Cell membrane-enriched homogenate (50  $\mu\text{g}$  of protein) from each animal was reacted in 1 ml of buffer containing 50  $\text{mM}$  Tris-HCl (pH 7.4), 100  $\text{mM}$  NaCl, 20  $\text{mM}$  KCl, 3  $\text{mM}$   $\text{MgCl}_2$ , and 0.2  $\text{mM}$  EGTA. The reaction was carried out in the presence and absence of 1.0  $\text{mM}$  ouabain. KCl was not added to the reaction samples containing ouabain. The reaction was carried out in the presence of 3  $\text{mM}$  ATP for 5 min at  $37^\circ\text{C}$ . The enzymatic hydrolysis was terminated by ice cold 12.5% trichloroacetic acid, and the samples were centrifuged at 15 000 rpm for 10 min. Enzymatic activity was measured as a function of liberated inorganic phosphate ( $\text{P}_i$ ) by the colorimetric reaction described by Taussky and Shorr [27]. For each ouabain-containing and ouabain-free sample for each animal, a separate reaction tube containing the reaction mixture and ATP without homogenate was assayed to account for spontaneous ATP hydrolysis. Samples from all animals were done in triplicate.

### 2.4. Na,K-ATPase histochemistry

To identify levels of regional Na,K-ATPase activity within the striatum, we used a histochemical method for the detection of ouabain-sensitive ATPase by a reaction involving the ATP analog *p*-nitrophenyl phosphate in the presence of lead acetate [5]. Brain sections containing mid-caudate and putamen from control and HI piglets were washed in 100  $\text{mM}$  Tris, 100  $\text{mM}$  sucrose and subsequently incubated in a solution of 25% DMSO, 200  $\text{mM}$  levamisole, 1  $\text{mM}$  potassium citrate, 2  $\text{mM}$  glycine, 100  $\text{mM}$  lead acetate, and 10  $\text{mM}$  *p*-nitrophenyl phosphate for 1 h at  $37^\circ\text{C}$  in a Dubnoff metabolic incubator shaker. After the reaction, the sections were rinsed in Tris-sucrose thrice for 10 min, followed by incubation in 1% ammonium sulfate. The sections were then rinsed in deionized water, mounted on glass slides, and coverslipped. The detection of this enzymatic reaction product is completely abolished by ouabain [12].

Densitometric quantification of Na,K-ATPase activity in brain sections was accomplished using an image analysis system as described [13]. The reacted slides were placed on a light box, and video images of sections (matched for striatal level) were captured on a Dage 68 video camera. Digitized images were then displayed in gray scale, and an average of sample density at each time point post injury was determined.

### 2.5. Western blot analysis

To measure Na,K-ATPase subunit levels in striatum of control and HI piglets, samples of striatal homogenates (5 or 20  $\mu\text{g}$ ) were fractionated by sodium dodecyl sulfate-polyacrylamide gel electrophoresis (SDS-PAGE). The proteins were then transferred by electroelution to nitrocellulose overnight at  $4^\circ\text{C}$  or for 3 h at room temperature. Confirmation of uniform transfer was accomplished by Ponceau S. The blots were washed with 0.05 M Tris-buffered saline (TBS, pH 7.3–7.4) and then blocked with 0.05 M TBS, 2.5% non-fat milk, 0.1% Tween-20 for 2 h. They were incubated subsequently overnight at  $4^\circ\text{C}$  with either a polyclonal antibody (dilution 1: 20 000) made against rabbit kidney Na,K-ATPase (Research Diagnostics, Flanders, NJ), a monoclonal antibody (0.1  $\mu\text{g/ml}$  IgG) against the Na,K-ATPase  $\alpha_3$  subunit (Affinity Bioreagents, Golden, CO), or a monoclonal antibody (0.084  $\mu\text{g/ml}$  IgG) against the  $\beta_1$  subunit of the enzyme (Upstate Biotechnology, Lake Placid, NY). All antibodies were diluted in Tris-milk-Tween solution. After incubation, the blots were washed in blocking solution and subsequently incubated with goat anti-mouse or goat anti-rabbit horseradish peroxidase-conjugated IgG (BioRad) for 1 h. The blots were washed again, and the immunoreactive proteins were visualized with a chemiluminescent detection system (Pierce Chemical, Rockford, IL, or Amersham Pharmacia Biotech, Piscataway, NJ) and subsequent exposure to

radiographic film. Synaptophysin (for the rabbit polyclonal antibody to Na,K-ATPase and  $\alpha_3$  monoclonal blots) or SNAP-25 (for the  $\beta_1$  antibody blots) were used as quantitative loading controls for each sample; levels of these proteins are not changed before 24 h recovery [11,13]. An optical density standard curve using increasing concentrations of striatal protein was generated for both the  $\alpha_3$  and  $\beta_1$  subunits. Protein levels were quantified by densitometry (using the Macintosh AdobePhotoshop and IP Lab Gel programs) and expressed as a percentage of loading control by comparing the optical density of the scanned isoform band to the synaptophysin (or SNAP-25) band of the same lane and blot.

### 2.6. Statistical analysis

Statistical analysis of differences in biochemical and histochemical activity as well as isoform subunit levels was accomplished using a two-tailed Student's *t*-test (two-tailed). Statistical significance was defined as  $P \leq 0.05$ .

## 3. Results

### 3.1. Striatal Na,K-ATPase is transiently inactivated, reestablishes normal activity, and then activity is lost after HI

Striatal neuron death is rapid, progressive necrosis during the first 24 h after HI [14]. This degeneration has been detailed previously [14]. This neuronal death is characterized as necrosis based on morphology, DNA fragmentation patterns and metabolic deficits [14]. At 3, 6, 12, and 244 h after recovery of spontaneous circulation 16, 31, 47, and 79% of neurons are damaged, respectively, as shown by H&E staining [14]. Ultrastructurally, neuronal death appears to be initiated by ~3 h post insult with cytoplasmic vacuolization and cellular edema [14]. At 6 h, the onset of significant neurodegeneration occurs, with fusiform changes in the cellular shape, continued vacuolization, fragmentation of the rough endoplasmic reticulum, and condensation of the mitochondria. Between 12 and 24 h, the injured cell disintegrates, with cytoplasmic dissolution, chromatin clumping, and ultimate karyolysis.

To identify the possible early mechanisms of striatal neuron death after HI, we measured Na,K-ATPase activity in synaptosomal membrane fractions in control and HI piglets (Fig. 1). Control piglet striatum has enzyme activity of 29.12  $\mu\text{mol P}_i/\text{mg protein per h}$ . At 3 h after HI, Na,K-ATPase activity is decreased significantly ( $P < 0.05$ ) to 62% of control. At 6 h after HI, striatal Na,K-ATPase activity is 98% of control. During the remainder of the early recovery time course, striatal Na,K-ATPase activity is reduced significantly ( $P < 0.05$ ) to ~50–55% of control enzyme activity.

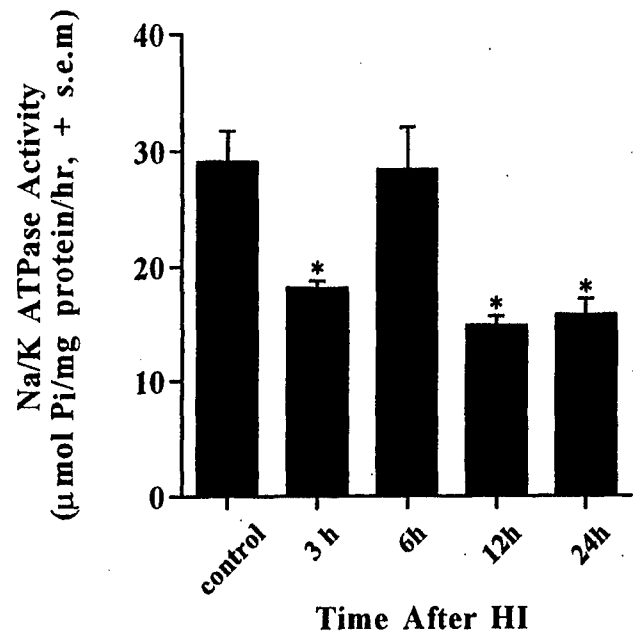


Fig. 1. Na/K-ATPase activity in striatal membrane fractions from 1-week-old piglets exposed to HI. Each bar represents mean ATPase activity (plus standard error of the mean) as measured by net inorganic phosphate ( $\text{P}_i$ ) production, excluding effects of Mg-ATPase and spontaneous ATP hydrolysis ( $n=2$  animals per time point). Controls are sham piglets not exposed to HI. An asterisk (\*) represents a statistically significant ( $P \leq 0.05$ ) difference between enzyme activity of HI piglets compared to control piglets. Na/K-ATPase undergoes early inactivation, a short period of recovery, and then sustained loss of function dysfunction after HI.

### 3.2. Na,K-ATPase activity in putamen is more vulnerable than in caudate to HI

The neuropathology after HI is different in distinct components of the striatum [13]. The putamen in newborn piglets is extremely vulnerability to HI [13]. We evaluated changes in membrane-associated ATPase activity in specific regions of the striatum by measuring histochemical activity of the enzyme in brain slices containing the striatum (Fig. 2). This activity represents the mean optical density from mid-striatum after reaction with the ATP analog *p*-nitrophenyl phosphate in situ. Membrane activity in the caudate nucleus was 83% of control at 6 h after HI, with recovery to normal or above normal values at 12 and 24 h. These changes were not significant. The putamen showed a similar loss and then recovery of ATPase activity (69 and 98% of control at 6 and 12 h, respectively), but then activity declined to 67% of control at 24 h after HI. The decrease in ATPase histochemical activity in the putamen at 24 h was nearly significant in comparison to control activity in that region ( $P=0.09$ ).

### 3.3. Na,K-ATPase subunit levels do not decrease in striatum during 24 h recovery after HI

To evaluate whether decreased Na,K-ATPase activity

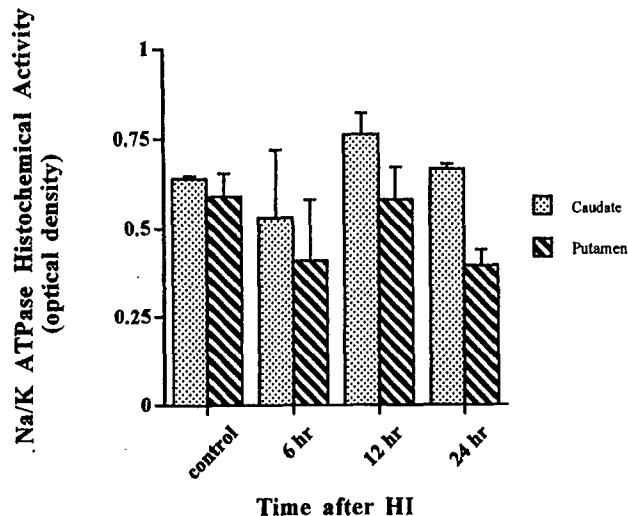


Fig. 2. In situ ouabain-sensitive ATPase activity in mid-striatal coronal sections of 1-week-old piglets after HI. Images of each section were analyzed digitally to determine optical density (plus standard error of the mean) as a representation of enzyme activity in caudate (dotted bars) and putamen (striped bars). Time represents h after HI ( $n=2-3$  piglets per time point). Controls are sham piglets not exposed to HI. The data demonstrate a differential loss of Na,K-ATPase activity within the putamen at 24 h recovery, corresponding to the preferential necrosis in the putamen observed neuropathologically [13,14].

during recovery from HI coincides with the loss of Na/K ATPase subunits, we measured the levels of a ubiquitous  $\alpha$  isoform ( $\alpha_1$ ) and the neuron specific  $\alpha$  and  $\beta$  subunits. Standard curves for  $\alpha_3$  and  $\beta_1$  were generated to demonstrate that our assay conditions were appropriate (Fig. 3A), by measuring the level of immunoreactivity for these isoforms as a function of increasing striatal protein concentration. The  $\alpha_3$  subunit was identified on Western blots as a single band corresponding to a 110-kDa protein, while the  $\beta_1$  subunit migrated as a broad 50–60-kDa band (corresponding to the glycosylated form of the protein). The immunoblot assay saturates for  $\alpha_3$  (Fig. 3a, left) and  $\beta_1$  (Fig. 3a, right) isoforms as protein concentration approaches 20  $\mu$ g.

To determine whether changes in protein levels occur in response to HI, striatal homogenates from both control and HI piglets were measured in the same blots. With 5  $\mu$ g of protein, the striatal levels of both  $\alpha_3$  and  $\beta_1$  (Fig. 3b, two lowest blot sets) at each time point after HI are similar

qualitatively, as are the levels of immunoreactivity for synaptophysin and SNAP-25 across time. When represented as a ratio of Na,K-ATPase subunit to loading control (Fig. 4, left), the immunoreactivity of each isoform at each time point after HI is similar ( $P \geq 0.32$  for both subunits in HI-exposed animals versus sham controls). These results were reproduced using 20  $\mu$ g protein (Fig. 3b, blot sets 2 and 3; Fig. 4, right, dotted and striped bars), with no statistical difference between control and HI piglets ( $P \geq 0.24$  for both subunits). The level of  $\alpha_1$  isoform in HI piglet striatum was similar to control at all recovery times, except at 3 h (Fig. 3b, upper blot set; Fig. 4, right, solid bars), at which time a significant increase ( $P=0.02$ ) was detected. The  $\alpha_1$  results were most reliably quantitated using the higher protein concentration because of the lower abundance of this isoform in striatum. These data demonstrate that the loss of Na,K-ATPase subunits does not account for the decrease in ATPase activity during recovery from HI.

#### 4. Discussion

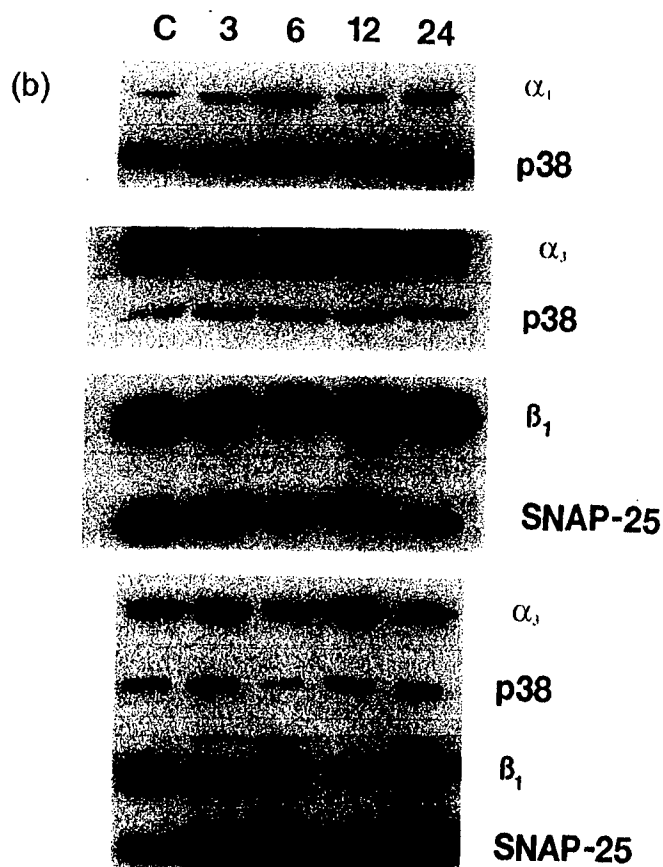
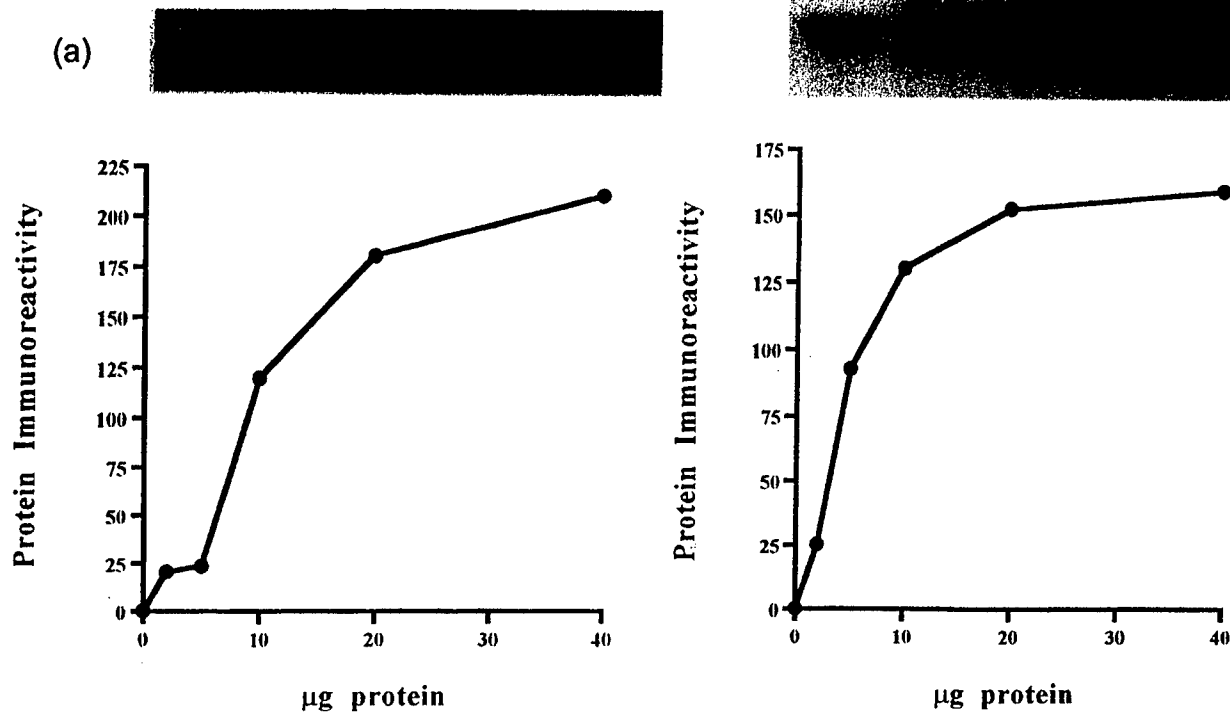
Perinatal HI initiates cellular and molecular perturbations in neurons that eventually cause neuronal death, gliosis, and atrophy, particularly in striatum [11–14]. We study biochemical and molecular defects in the striatum after HI, because the degeneration of this brain region is likely to be important for the long-term abnormalities in posture and movement and sensorimotor deficits that result from perinatal HI. Here, we focused on Na,K-ATPase because this enzyme may be a key molecular target in the pathobiology of HIE. This enzyme establishes cell membrane electrochemical gradients for  $\text{Na}^+$  and  $\text{K}^+$ . This gradient is crucial for maintaining membrane potential and function of neurons. Excessive influx of  $\text{Na}^+$  into neurons initiated by glutamate release and glutamate receptor activation during and after HI, coupled with failed membrane ion pumps, result in an accumulation of intracellular  $\text{Na}^+$ , cellular edema [2], and possible striatal neuron necrosis [11,14].

We have identified a loss of Na,K-ATPase activity in striatum at 3 h after HI. This defect coincides with the onset of cellular edema seen by electron microscopy in our piglet model of HIE [14]. The loss of ATPase activity at

Fig. 3. Na,K-ATPase subunit isoform immunoreactivity. (A) Western blot analysis of increasing concentrations of membrane protein from newborn piglet striatum was used to determine the optimal assay conditions for detection of ATPase subunit isoforms using chemiluminescence. Lanes were loaded with 2, 5, 10, 20, and 40  $\mu$ g protein, subjected to SDS-PAGE, transferred to nitrocellulose, and blotted with antibodies to the  $\alpha_3$  (left) and  $\beta_1$  (right) isoforms. The standard curves and protein blots (inserts) demonstrate a steep increase in protein immunoreactivity between 5 and 20  $\mu$ g. (B) ATPase subunit immunoreactivity of striatal membrane fractions. Samples were subjected to SDS-polyacrylamide gel electrophoresis, electrophoretically transferred to nitrocellulose membranes, and probed with either a rabbit polyclonal antibody against the  $\alpha_1$  subunit or a mouse monoclonal antibody against the  $\alpha_3$  or  $\beta_1$  subunit. Membranes were then incubated in a horseradish peroxidase-conjugated secondary antibody, with visualization of protein bands accomplished by chemiluminescence and autoradiography. Each blot was probed for the respective subunit as well as a known invariant synaptosomal protein (synaptophysin [p38] for the  $\alpha$  subunits, SNAP-25 for the  $\beta$  subunit); the subsequent images were analyzed digitally to determine optical density. The first three sets of blots represent immunoreactivity quantitated using 20  $\mu$ g protein per lane; the last two sets reflect quantitation using 5- $\mu$ g samples in each lane.

this time of recovery occurs prior to appreciable ischemic neurodegeneration; thus, we interpret this abnormality as a mechanism, rather than a consequence, of neuronal death. Additionally, our *in vitro* assay indicates that this loss of

activity is not related to the known decrease in high-energy phosphate levels (ATP substrate) that occurs during HI. The near complete recovery of activity at 6 h suggests that a reversible modification of the enzyme (e.g., perhaps



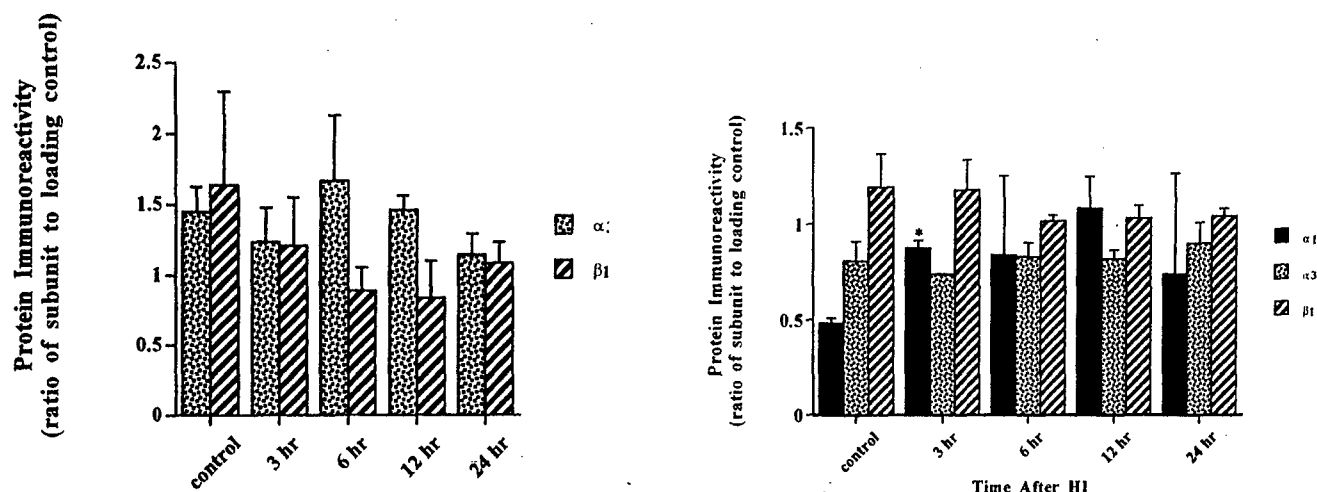


Fig. 4. Na/K-ATPase subunit immunoreactivity in 5- $\mu$ g (left) and 20- $\mu$ g (right) aliquots of striatal membrane fractions from 1-week-old piglets exposed to HI. Samples ( $n=2$ ) from HI and control (unexposed) animals were subjected to Western blot analysis. Protein levels of the  $\alpha_3$  (dotted bars),  $\beta_1$  (striped bars) and  $\alpha_1$  isoforms (solid bars) were represented as the ratio of the mean optical density of the subunit to control (plus standard error of the mean). For each subunit, three to five blots were used to measure immunoreactivity. An asterisk (\*) represents a statistically significant ( $P \leq 0.05$ ) increase in isoform level in the HI-exposed animals relative to control. No significant changes occurred with  $\alpha_3$  and  $\beta_1$ , while  $\alpha_1$  immunoreactivity in HI piglets shows a significant increase relative to control at 3 h recovery.

phosphorylation or nitration) is at least partially responsible for the early loss of function seen at 3 h. At 12 and 24 h, striatal Na,K-ATPase activity was again decreased, coinciding with the destruction of striatal neurons [14]. We have found that cytochrome oxidase (COX), a key mitochondrial enzyme that is also enriched in striatum, undergoes a similar biphasic pattern of activity after HI [14]. Therefore, we conclude that some, yet to be identified, critical pathological events, possibly oxidative stress mediated by NMDA receptor activation, are initiated in the striatum by 3 h after HI. The elucidation of these early pathological processes will be critical for the future identification of neuroprotection strategies that may be beneficial for newborns that have experienced HI episodes.

We evaluated Na,K-ATPase activity using two different methods. We used a biochemical assay on striatal homogenates and an in situ assay on brain sections. The different techniques have advantages and disadvantages. The biochemical method is a more direct and sensitive assay for Na,K-ATPase compared to the histochemical method, but the latter assay offers spatial and regional localization of activity. For example, the biochemical assay detects total ouabain-sensitive Na,K-ATPase activity in tissue extracts, whereas the histochemical assay reflects only membrane-associated Na,K-ATPase activity. However, the histochemical assay can yield information on a subregional level (e.g., putamen versus caudate), while, as used here, the biochemical assay measures Na,K-ATPase in striatal membrane fractions that include putamen and caudate nucleus. Some discrepancy in the results on Na,K-ATPase activity after HI was found with the two different assays. Biochemically, total ouabain-sensitive Na,K-ATPase activity is decreased at 3 h, returns to control level at 6 h, and then

decreases again at 12 and 24 h. Histochemically, membrane-associated Na,K-ATPase in putamen is lower than control (although not significantly reduced) at 6 h, recovers to control levels at 12 h, and then again is lower than control at 24 h. By histochemical assay, Na,K-ATPase activity in the caudate is relatively invariant compared to putamen. Although putamen and caudate have near normal levels of activity at 12 h, the putamen does not sustain this activity. The explanation for the discrepant findings with the different assays is not completely clear. It is possible that these assays detect Na,K-ATPase in different cellular constituents. For example, the biochemical assay has a greater synaptosomal neuronal component compared to the histochemical assay, with the latter assay perhaps reflecting more glial Na,K-ATPase. In any event, the important message with the histochemical assay is that Na,K-ATPase in the putamen has a greater vulnerability than Na,K-ATPase in the caudate nucleus and that the putamen fails to sustain the recovery of Na,K-ATPase function after HI.

Na,K-ATPase is a ubiquitous enzyme with in the CNS. All three  $\alpha$  isoenzymes ( $\alpha_1$ ,  $\alpha_2$ , and  $\alpha_3$ ) are expressed throughout the CNS [26]. Both  $\beta$  isoforms ( $\beta_1$  and  $\beta_2$ ) are also found within nervous tissue, with  $\beta_2$  expression occurring selectively in cerebellum, pineal gland, and in photoreceptors [20,26]. At present, information on Na,K-ATPase subunit isoform localization and function in striatum is limited to biochemical studies characterizing three enzyme forms with 'very high', 'high', and 'low' affinities for ouabain [19]. Therefore, we used multiple antibodies to detect subunit levels in the newborn piglet. We identified high expression levels of the  $\alpha_3$  and  $\beta_1$  isoforms in swine striatum.

We examined whether Na,K-ATPase subunit proteins

are reduced after HI to account for the loss of Na,K-ATPase function. Western blot analysis, however, revealed little or no change in  $\alpha_3$  or  $\beta_1$  immunoreactivity. An increase in  $\alpha_1$  subunit levels was found. Previous studies of focal cerebral ischemia in mouse [8] have also demonstrated loss of Na,K-ATPase activity without changes in subunit isoform expression. These data suggest that modifications of Na,K-ATPase subunits or perturbations in subunit interactions cause the inactivation of Na,K-ATPase function early after HI.

Excitotoxic excitatory amino acids (i.e., glutamate) have been implicated as a major contributor to the pathogenesis of HIE [1,15]. One pathway for excitotoxicity is the generation of ROS. This phenomenon has been demonstrated in cultured neurons after activation of the NMDA receptor [22]. One particular signal transduction pathway activated by NMDA receptors is nitric oxide (NO) generation [2]. Na,K-ATPase activity can be inhibited by NO-producing compounds [23], and modified by mechanisms involving superoxide dismutase (via tyrosine residues) in the presence of the NO derivative peroxynitrite [6]. The possible links between NMDA receptor activation and the generation of NO, superoxide, and peroxynitrite need to be explored in greater detail in this clinically relevant animal model of newborn HIE.

Previous experiments from our laboratory using this piglet model have revealed depletion of glutathione stores at 3 h recovery after HI and peroxynitrite-mediated oxidative damage to intracellular proteins (tubulin and Golgi apparatus associated protein) [14]. Given this evidence for oxidative stress, it is plausible that HI-induced ROS modify mature, membrane-associated Na,K-ATPase or nascent enzyme heterodimers during processing through the Golgi apparatus. Transport of the complete enzyme from the endoplasmic reticulum to the plasma membrane requires at least 40–60 min [3], coinciding with the onset of decreased Na,K-ATPase activity seen in striatum at 3 h after HI. Recovery of enzyme function at 6 h may be related to reversal of protein modification, recovery of mitochondrial function (decreasing the ROS production), or rapid turnover of the defective membrane Na,K-ATPase. As disruption of the nucleus, cytoskeletal structure, and organelles progresses between 6 and 24 h [14], production of cellular enzymes ceases, resulting in the sustained decrease in Na,K-ATPase function seen over the remainder of the time course.

We have strong evidence that in newborn piglets, striatal neurons sustain profound peroxynitrite-mediated damage [14]. Several domains in both Na,K-ATPase subunits may serve as targets for peroxynitrite modification. In rat brain, three tyrosine substitutions in the  $\alpha_3$  isoform occur relative to  $\alpha_1$  [24]. The  $\beta$  subunit, known more for its role in trafficking, facilitates cation occlusion through a specific interaction with a region of the carboxy terminus of the  $\alpha$  subunit [3]. The interactive region of the rat  $\beta$  subunit contains tyrosine residues; thus, peroxynitrite attack on this

region would result in failed heterodimer interaction and enzymatic activity. Lipid peroxidation in conjunction with loss of Na,K-ATPase activity after HI also has been described [7,21]; thus, damage to membrane phospholipids may potentiate defects in subunit interactions and failure of enzyme function.

An alternative explanation for the diminished enzyme activity involves the balance of catalytic subunit expression. Despite elevated in  $\alpha_1$  levels in striatum after HI, a concomitant rise in biochemical activity was not found over time. The presence of multiple isoforms of Na,K-ATPase has been postulated as a mechanism whereby tissues can regulate enzyme activity [10]. Jewell and Lingrel have further hypothesized that the  $\alpha_3$  isoform, which has a lower affinity for  $\text{Na}^+$  than the  $\alpha_1$  or  $\alpha_2$  isoform, is recruited by neurons during period of higher  $\text{Na}^+$  influx, such as repetitive action potentials [9]. Since excess glutamate potentiates both the production of ROS and an increased influx of  $\text{Na}^+$ , oxidative stress resulting from excitotoxicity and subsequent damage to the  $\alpha_3$  isoform would decrease the total ATPase activity. The absence of a contribution from  $\alpha_3$  isoform would alter the normal stoichiometry of the catalytic subunits, thus explaining the failure of enzyme function despite the increase in  $\alpha_1$  subunit levels seen in our study. With diminished cortical Na,K-ATPase activity after HI, loss of a ouabain inhibitory site has been demonstrated, theoretically occurring secondary to modification of a 'high affinity' ( $\alpha_2$  or  $\alpha_3$ ) isoform [8].

In summary, we have identified that Na,K-ATPase function is inactivated early after HI in a subcortical brain region that sustains preferential damage. This alteration in enzyme function appears to be mediated by factors other than the levels of its composite subunits. Further investigations are necessary to determine the molecular modifications occurring in the specific  $\alpha$  and  $\beta$  isoforms and the relationships between different  $\alpha/\beta$  heterodimers and total Na,K-ATPase activity. These experiments may prove valuable in designing therapies to target brain regions vulnerable to neonatal asphyxia, which would significantly reduce the incidence of HIE and its long-term sequelae.

## Acknowledgements

The authors are grateful for the technical support of Ms. Ann Price and Mr. Frank Barksdale. This work was supported by grants from the National Institutes of Health, NS34100 (L.J.M.), AG16282 (L.J.M.) and NS20020 (R.J.T.), and from the US Army Medical Research and Materiel Command (DAMD17-99-1-9553, L.J.M.). Dr. Golden is the recipient of a Bauernschmidt Fellowship from the Eudowood Board, Johns Hopkins Hospital.



## References

- [1] D.W. Choi, Calcium-mediated neurotoxicity: relationship to specific channel types and role in ischemic damage, *Trends Neurosci.* 11 (1988) 465–469.
- [2] D.W. Choi, Excitotoxic cell death, *J. Neurobiol.* 9 (1992) 1261–1276.
- [3] D.C. Chow, J.G. Forte, Functional significance of the  $\beta$ -subunit for heterodimeric P-type ATPases, *J. Exp. Biol.* 198 (1995) 1–17.
- [4] K.J.A. Davies, Protein damage and degradation by oxygen radicals: general aspects, *J. Biol. Chem.* 262 (1987) 9895–9901.
- [5] K. Inomata, H. Mayanara, K. Fujimoto, K. Ogawa, Ultrastructural localization of ouabain-sensitive potassium-dependent *p*-nitrophenylphosphatase ( $\text{Na}^+$ - $\text{K}^+$ -ATPase) activity in the central nervous system of the rat, *Acta Histochem. Cytochem.* 16 (1983) 277–284.
- [6] H. Ischiropoulos, L. Zhu, J. Chen, M. Tsai, J.C. Martin, C.D. Smith, J.S. Beckman, Peroxynitrite-mediated tyrosine nitration catalyzed by superoxide dismutase, *Arch. Biochem. Biophys.* 298 (1992) 431–437.
- [7] I. Jamme, E. Petit, D. Divoux, A. Gerbi, J.M. Maixent, A. Nouvelot, Modulation of mouse cerebral  $\text{Na}^+$ ,  $\text{K}^+$  ATPase activity by oxygen free radicals, *Neuroreport* 7 (1995) 333–337.
- [8] I. Jamme, O. Barbery, P. Trouve, D. Charlemange, J.M. Maixent, E.T. Mackenzie, L. Pellerin, A. Nouvelot, Focal cerebral ischemia induces a decrease in activity and a shift in ouabain affinity of  $\text{Na}^+$ ,  $\text{K}^+$  ATPase isoforms without modifications in mRNA and protein expression, *Brain Res.* 819 (1999) 132–142.
- [9] E.A. Jewell, J.B. Lingrel, Comparison of substrate dependence properties of rat  $\text{Na}$ ,  $\text{K}$ -ATPase  $\alpha 1$ ,  $\alpha 2$ , and  $\alpha 3$  isoforms expressed in HeLa cells, *J. Biol. Chem.* 266 (1991) 16925–16930.
- [10] J.B. Lingrel,  $\text{Na}$ ,  $\text{K}$ -ATPase: isoform structure, function, and expression, *J. Bioenerg. Biomembr.* 24 (1992) 263–270.
- [11] L.J. Martin, A.M. Brambrink, C. Lehmann, C. Portera-Cailliau, R. Koehler, J. Rothstein, R.J. Traystman, Hypoxia-ischemia causes abnormalities in glutamate transporters and death of astroglia and neurons in newborn striatum, *Ann. Neurol.* 42 (1997) 335–348.
- [12] L.J. Martin, A. Brambrink, R.C. Koehler, R.J. Traystman, Neonatal asphyxial brain injury is neural system preferential and targets sensory-motor networks, in: D.K. Stevenson, P. Sunshine (Eds.), *Fetal and Neonatal Brain Injury: Mechanisms, Management, and the Risks of Practice*, Oxford University Press, New York, 1997, pp. 374–399.
- [13] L.J. Martin, A. Brambrink, R.C. Koehler, R.J. Traystman, Primary sensory and forebrain motor systems in the newborn brain are preferentially damaged by hypoxia-ischemia, *J. Comp. Neurol.* 377 (1997) 262–285.
- [14] L.J. Martin, A.M. Brambrink, A.C. Price, A. Kaiser, D.M. Agnew, R.N. Ichord, R.J. Traystman, Neuronal death in newborn striatum after hypoxia-ischemia is necrosis and evolves with oxidative stress, *Neurobiol. Dis.* 7 (2000) 169–191.
- [15] G.J. McBean, P.J. Roberts, Chronic infusion of L-glutamate causes neurotoxicity in rat striatum, *Brain Res.* 290 (1984) 372–375.
- [16] K.M. Mc Grail, J.M. Phillips, K.J. Sweadner, Immunofluorescent localization of three  $\text{Na}$ ,  $\text{K}$ -ATPase isoenzymes in the rat central nervous system: both neurons and glia can express more than one  $\text{Na}$ ,  $\text{K}$ -ATPase, *J. Neurosci.* 11 (1991) 381–391.
- [17] O.P. Mishra, M. Delivoria-Papadopoulos,  $\text{Na}^+$ ,  $\text{K}^+$  ATPase in developing fetal guinea pig brain and the effect of maternal hypoxia, *Neurochem. Res.* 13 (1988) 765–770.
- [18] A. Nishida, Y. Misaki, H. Kuruta, Developmental expression of copper, zinc-superoxide dismutase in human brain by chemiluminescence, *Brain Dev.* 16 (1994) 40–44.
- [19] S. Peckovic, N. Nedeljkovic, G. Nikezic, A. Horvat, M. Stojiljkovic, L. Rakic, J.M. Martinovic, Biochemical characterization of the hippocampal and striatal  $\text{Na}$ ,  $\text{K}$ -ATPase reveals striking differences in kinetic properties, *Gen. Physiol. Biophys.* 16 (1997) 227–240.
- [20] L. Peng, P. Martin-Vasallo, K.J. Sweadner, Isoforms of  $\text{Na}$ ,  $\text{K}$ -ATPase  $\alpha$  and  $\beta$  subunits in the rat cerebellum and in granule cell cultures, *J. Neurosci.* 17 (1997) 3488–3502.
- [21] B. Razdan, P.J. Marro, O. Tammela, R. Goel, O.M. Mishra, M. Delivoria-Papadopoulos, Selective sensitivity of synaptosomal membrane function to cerebral cortical hypoxia in newborn piglets, *Brain Res.* 600 (1993) 308–314.
- [22] I.J. Reynolds, T.G. Hastings, Glutamate induces the production of reactive oxygen species in cultured forebrain neurons following NMDA receptor activation, *J. Neurosci.* 15 (1995) 3318–3327.
- [23] T. Sato, Y. Kamata, M. Irifune, T. Nishikawa, Inhibitory effect of several nitric oxide-generating compounds on purified  $\text{Na}^+$ ,  $\text{K}^+$ -ATPase activity from porcine cerebral cortex, *J. Neurochem.* 68 (1997) 1312–1318.
- [24] G.E. Shull, J. Greeb, J.B. Lingrel, Molecular cloning of three distinct forms of the  $\text{Na}^+$ ,  $\text{K}^+$ -ATPase  $\alpha$ -subunit from rat brain, *Biochemistry* 25 (1986) 8125–8132.
- [25] C.V. Smith, T.N. Hansen, N.E. Martin, H.W. McMicken, S.J. Elliot, Oxidant stress responses in premature infants during exposure to hyperoxia, *Pediatr. Res.* 34 (1993) 360–364.
- [26] K.J. Sweadner, Overview: subunit diversity in the  $\text{Na}$ ,  $\text{K}$ -ATPase, in: *The Sodium Pump: Structure, Mechanism, and Regulation*, Vol. 46, Rockefeller University Press, New York, 1991, pp. 63–76.
- [27] H.H. Taussky, E. Shorr, A microcolorimetric method for the determination of inorganic phosphorus, *J. Biol. Chem.* 202 (1953) 675–685.
- [28] R.C. Vannucci, Hypoxia-ischemia: clinical effects, in: A.A. Fanaroff, R.J. Martin (Eds.), *Neonatal-Perinatal Medicine: Diseases of the Fetus and Infant*, Mosby-Year Book, St. Louis, MO, 1997, pp. 877–891.
- [29] R.C. Vannucci, J.M. Perlman, Interventions for perinatal hypoxic-ischemic encephalopathy, *Pediatrics* 100 (1997) 1004–1014.

## Apoptosis and Necrosis Occur in Separate Neuronal Populations in Hippocampus and Cerebellum After Ischemia and Are Associated With Differential Alterations in Metabotropic Glutamate Receptor Signaling Pathways

\*†Lee J. Martin, ‡Frederick E. Sieber, and ‡Richard J. Traystman

Departments of \*Pathology (Division of Neuropathology), †Neuroscience, and ‡Anesthesiology/Critical Care Medicine, Johns Hopkins University School of Medicine, Baltimore, Maryland, U.S.A.

**Summary:** It was evaluated whether postischemic neurodegeneration is apoptosis and occurs with alterations in phosphoinositide-linked metabotropic glutamate receptors (mGluRs) and their associated signaling pathways. A dog model of transient global incomplete cerebral ischemia was used. The CA1 pyramidal cells and cerebellar Purkinje cells underwent progressive delayed degeneration. By *in situ* end-labeling of DNA, death of CA1 and Purkinje cells was greater at 7 days than 1 day after ischemia, whereas death of granule neurons in dentate gyrus and cerebellar cortex was greater at 1 than at 7 days. Ultrastructurally, degenerating CA1 pyramidal neurons and cerebellar Purkinje cells were necrotic; in contrast, degenerating granule neurons were apoptotic. In agarose gels of regional DNA extracts, random DNA fragmentation coexisted with internucleosomal fragmentation. By immunoblotting of regional homogenates, mGluR1 $\alpha$ , mGluR5, phospholipase C $\beta$  (PLC $\beta$ ),

and G $\alpha_{q/11}$  protein levels in hippocampus at 1 and 7 days after ischemia were similar to control levels, but in cerebellar cortex, mGluR1 $\alpha$  and mGluR5 were decreased but PLC $\beta$  was increased. By immunocytochemistry, mGluR and PLC $\beta$  immunoreactivity dissipated in CA1 and cerebellar Purkinje cell/molecular layers, whereas immunoreactivities for these proteins were enhanced in granule neurons. It was concluded that neuronal death after global ischemia exists as two distinct, temporally overlapping forms in hippocampus and cerebellum: necrosis of pyramidal neurons and Purkinje cells and apoptosis of granule neurons. Neuronal necrosis is associated with a loss of phosphoinositide-linked mGluR transduction proteins, whereas neuronal apoptosis occurs with increased mGluR signaling. **Key Words:** Bax—Excitotoxicity—Glutamate receptors—Granule neuron—Phospholipase C—Programmed cell death.

The mechanisms for delayed neuronal death (DND) after global cerebral ischemia in the adult CNS are not understood. Structurally and mechanistically, cellular degeneration resulting from hypoxia-ischemia has been thought to be a form of necrosis (Laiho and Trump, 1975; Wyllie et al., 1980; Kerr and Harmon, 1991; Deshpande et al., 1992); but recently postischemic DND has been considered to be a form of apoptosis mediated by programmed cell death (PCD) mechanisms (Héron et al., 1993; MacManus et al., 1995; Nitatori et al., 1995; Krajewski et al., 1995). However, the idea that selectively vulnerable neurons undergo apoptosis after ischemia is very controversial (Deshpande et al., 1992; Martin et al., 1998; Ishimaru et al., 1999), although ischemic DND might be more easily classified according to the concept of the apoptosis-necrosis continuum (MacManus et al., 1995; Portera-Cailliau et al., 1997a,b). The accurate identification of the contributions of apoptosis and necrosis to neuronal death in the adult central nervous system after ischemia has very important therapeutic relevance.

Neuronal cell death after ischemia involves perturbations in intracellular Ca<sup>2+</sup> homeostasis and impairments in protein synthesis, possibly resulting from excitotoxic activation of neuronal glutamate receptors (GluRs)

Received March 17, 1999; final revision received July 13, 1999; accepted July 13, 1999.

Supported by grants from the U.S. Public Health Service (NS 34100 and NS 20020), the U.S. Army Medical Research and Materiel Command (DAMD17-99-9553), and the American Heart Association, Maryland affiliate (grant-in-aid MDSG5597).

Address correspondence and reprint requests to Dr. Lee J. Martin, Division of Neuropathology, Department of Pathology, Johns Hopkins University School of Medicine, 720 Rutland Ave., 558 Ross Research Bldg., Baltimore, MD 21205-2196, U.S.A.

**Abbreviations used:** DND, delayed neuronal death; GluR, glutamate receptor; mGluR, metabotropic glutamate receptor; NMDA, *N*-methyl-D-aspartate; PCD, programmed cell death; PLC, phospholipase C; TUNEL, terminal transferase-mediated biotin-dUTP nick end-labeling.

(Diemer et al., 1993). The GluRs that modulate intracellular  $\text{Ca}^{2+}$  levels within neurons are the ion channel receptors [*N*-methyl-*D*-aspartate (NMDA) and  $\alpha$ -amino-3-hydroxy-5-methyl-4-isoxazole propionate receptors] and the G protein-coupled, phosphoinositide-linked metabotropic GluRs (mGluRs) (Nakanishi, 1992). Within the central nervous system, excitotoxic activation of GluRs delineates an apoptosis–necrosis continuum for neuronal death in which the structure of neuronal degeneration is influenced by the subtype of GluR that is activated (Portera-Cailliau et al., 1997a,b). A possible role for excessive activation of GluRs in the mechanisms for postischemic DND is supported by studies showing that blockade of  $\alpha$ -amino-3-hydroxy-5-methyl-4-isoxazole propionate receptors is neuroprotective after forebrain ischemia in adult rodents (Sheardown et al., 1990), that abnormalities in phosphoinositide signaling pathways occur in hippocampus after ischemia (Kirino et al., 1992), and that mGluR antagonists are neuroprotective in *in vitro* hippocampal slice models of hypoxia–hypoglycemia (Opitz et al., 1995) and *in vivo* models of excitotoxicity and transient global ischemia (Bruno et al., 1999).

Some forms of PCD are  $\text{Ca}^{2+}$  dependent (Sen, 1992), and activation of mGluRs and heterotrimeric GTP-binding proteins (G proteins) can regulate neuronal apoptosis *in vitro* (Copani et al., 1995; Yan et al., 1995). Therefore, we evaluated whether ischemic DND is apoptosis structurally and whether DND is possibly associated mechanistically with abnormalities in phosphoinositide-linked mGluRs and their downstream intracellular signal transduction proteins, including the functionally coupled G proteins and phospholipase C (PLC). Thus, the goal of this study was to provide insight into the possible contribution of apoptosis to neurodegeneration after ischemia and the possible molecular mechanisms for this DND.

## METHODS

### Model of ischemia

A model of temporary global incomplete cerebral ischemia in dogs was used (Sieber et al., 1995). All animal procedures were conducted in accordance with the *NIH Guide for the Care and Use of Laboratory Animals*, and protocols were approved by the institutional animal care and use committee. Under sterile conditions, anesthetized (1 to 2% inspired halothane), mechanically ventilated, normothermic (epidural temperature at 37 to 38°C), adult beagles ( $n = 20$ ) were subjected to transient incomplete global cerebral ischemia by intraventricular infusion of prewarmed sterile artificial cerebrospinal fluid into the lateral ventricle, producing an intracranial pressure of 10 mm Hg below mean arterial blood pressure (Sieber et al., 1995). The intracranial pressure was maintained, keeping cerebral perfusion pressure constant at 10 mm Hg for 20 minutes. To start reperfusion, the cerebrospinal fluid pressure reservoir was disconnected, and intracranial pressure was allowed to normalize. Six dogs were used as nonischemic sham controls.

### Neuropathology, TUNEL, and electron microscopy

To evaluate neuropathology, sham control dogs ( $n = 3$ ) and ischemic dogs surviving for 1 day ( $n = 5$ ) or 7 days ( $n = 9$ ) were anesthetized with pentobarbital, vasodilated with sodium nitrite, anticoagulated with heparin, and perfused intraaortically with phosphate-buffered saline followed by a mixture of 4% paraformaldehyde and 0.5% glutaraldehyde. The brains were divided midsagittally, and each hemisphere was cut into 1-cm-thick coronal slabs. In this model of ischemia, neuronal damage is similar bilaterally (Sieber et al., 1995). From the left hemisphere, samples of midhippocampus (containing the septal and temporal hippocampus) and cerebellum (at the level of the vermis) were used for paraffin histology. For quantification of postischemic neurodegeneration in hippocampus and cerebellar cortex (Fig. 1), sections (10  $\mu\text{m}$  thick) were stained with hematoxylin and eosin or the terminal transferase-mediated biotin-dUTP nick end-labeling (TUNEL) method for *in situ* detection of nuclear DNA fragmentation as described (Portera-Cailliau et al., 1997a,b; Martin et al., 1997a; Al-Abdulla et al., 1998). The TUNEL method was used to identify dying cells after ischemia, although this technique is not specific for apoptosis (Martin et al., 1998).

Profile counting was used to estimate ischemic neuronal damage in hematoxylin and eosin-stained sections in the stratum pyramidale of CA1 (in six microscopic fields at 600 $\times$ ; see Fig. 1A) and in the Purkinje cell layer of the anterior vermis of cerebellar cortex (in four microscopic fields at 400 $\times$ ; see Fig. 1B). Because Purkinje cells are arranged in only a single layer (Fig. 1B), the cerebellar sections were counted at a lower magnification so that a greater number of Purkinje cell could be analyzed per microscopic field. The percentage of neurons with ischemic cytopathology was determined using as criteria microvacuolar change within the soma, peripheralization of Nissl substance, nuclear pyknosis, perinuclear eosinophilia, or perikaryal shrinkage with cytoplasmic eosinophilia (Sieber et al., 1995; Martin et al., 1997a,b, 1998). The percentage neuronal damage was estimated by identifying the fraction of neurons with ischemic cytopathology relative to the total number of neurons in microscopic fields of the CA1 and cerebellar cortex. The percentage neuronal damage in each region was averaged for each animal, and a group mean was calculated. The number of neurons per square millimeter was calculated for each region in control and ischemic dogs, and the percentage of remaining neurons following ischemia was calculated. Neuropathology scores between groups and regions at each time point were analyzed using the Mann–Whitney test.

In TUNEL preparations counterstained with cresyl violet, the densities of cells showing DNA fragmentation were determined by counting TUNEL-positive nuclei in six microscopic fields at 1,000 $\times$  in the stratum pyramidale of CA1 and CA2–superior CA3, the granule cell layer of the dentate gyrus, and the Purkinje cell and granule cell layers of cerebellar cortex (Fig. 1). The TUNEL sections were counted at 1,000 $\times$  so that TUNEL-positive nuclei could be easily identified and the type of cell could be recognized. The number of TUNEL-positive cells per square millimeter in each region was averaged for each animal, and a group mean was calculated. The TUNEL scores between groups and regions at each time point were analyzed using the Mann–Whitney test.

To determine whether DND has the structure of apoptosis, necrosis, or a hybrid form of degeneration, samples (3 mm<sup>3</sup>) of hippocampus and cerebellar cortex from the left hemisphere were osmicated immediately, embedded in plastic, and evaluated by electron microscopy. Ischemic DND was evaluated using ultrastructural criteria described previously in models of

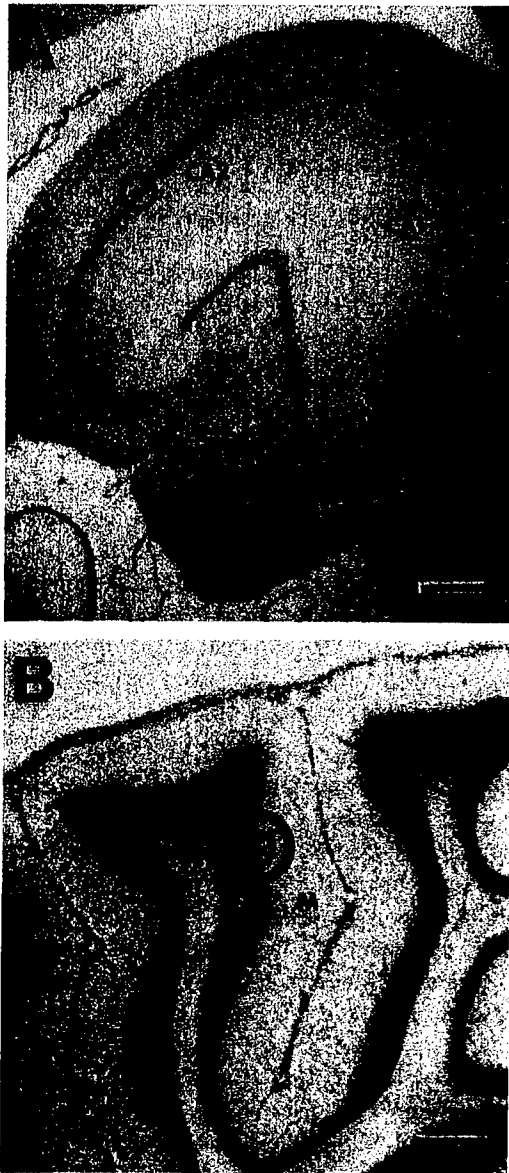


**FIG. 1.** Locations in hippocampus (A) and cerebellar cortex (B) where cell counts were made in hematoxylin and eosin and terminal transferase-mediated biotin-dUTP nick end-labeling (TUNEL) sections. CA1–CA4, Ammon's horn subfields 1 to 4; DG, dentate gyrus; m, molecular layer; p, Purkinje cell layer; g, granule cell layer. Bars = 12 mm. Circles with three different diameters are shown. The smallest circle (shown in A and B) corresponds to the 1,000 $\times$  microscopic fields in which the counts of TUNEL-positive cells were made in CA1, CA2 and CA3, and dentate gyrus of hippocampus and in the granule cell and Purkinje cells layers of cerebellar cortex. This magnification was used to best identify TUNEL labeling in the nucleus. The intermediate circle (shown in A), corresponding to the 600 $\times$  magnification fields, was used to determine in larger sample sizes the neuronal density and percentage neuronal damage in CA1. The largest circle (shown in B), corresponding to the 400 $\times$  magnification fields, was used to determine the neuronal density and percentage neuronal damage in the Purkinje cell layer. For this purpose, a larger microscopic field (i.e., lower magnification) was used so that a greater number of Purkinje cells per field could be analyzed.

unequivocal neuronal apoptosis (Portera-Cailliau et al., 1997a,b; Al-Abdulla et al., 1998; Martin et al., 1998, 1999).

#### DNA isolation and agarose gel electrophoresis

Because the TUNEL method identifies DNA fragmentation independent of mechanisms (Portera-Cailliau et al., 1997b; Martin et al., 1998), we evaluated regional neuropathology based on DNA fragmentation patterns in agarose gels. Genomic DNA was isolated from samples of hippocampus (septal and temporal) and cerebellar cortex from control dogs ( $n = 2$ ) and dogs at 1 day ( $n = 2$ ) and 7 days ( $n = 2$ ) after ischemia. Two additional animals were killed at 6 hours after ischemia. Tissue samples were homogenized in DNA extraction buffer containing 10 mmol/L Tris (pH 7.4), 10 mmol/L NaCl, 25 mmol/L ethylenediaminetetraacetate, 1% sodium dodecyl sulfate, and 1 mg/ml proteinase K and incubated in the same buffer overnight at 37°C. DNA was extracted with an equal volume of salt-saturated phenol/chloroform/isoamyl alcohol (10:10:1), and the recovered aqueous phase was extracted with diethyl ether. The DNA was precipitated with ethanol (2.5 volumes). The DNA pellet was dissolved in 0.1 $\times$  saline–sodium citrate and incubated (37°C) with DNase-free RNase A (0.1 mg/mL) for 1 hour and then overnight (37°C) with 0.1 mg/mL proteinase K. DNA was reextracted, precipitated, and dissolved in Tris/ethylenediaminetetraacetate buffer. The DNA samples ( $\sim 1.0$   $\mu$ g) were 3' end-labeled with digoxigenin-11-dideoxy-uridine-5'-triphosphate using terminal transferase (Boehringer-Mannheim, Indianapolis, IN, U.S.A.), precipitated, resuspended in Tris/ethylenediaminetetraacetate buffer, fractionated by agarose gel (1.2%) electrophoresis, and transferred to nylon membrane followed by ultraviolet cross-linking. Membranes were incubated in 2% nucleic acid blocking reagent (Boehringer-Mannheim) and then in blocking reagent containing 75 mU/mL antidigoxigenin Fab fragments conjugated to alkaline phosphatase (Boehringer-Mannheim). After washing, membranes were reacted with chemiluminescent substrate for alkaline phosphatase detection reagent (Boehringer-Mannheim) and exposed to Kodak X-OMAT film to visualize DNA.

#### Immunoblotting

To evaluate possible mechanisms for DND, we studied by immunoblotting the expression of the proapoptotic protein Bax as well as mGluRs and their related intracellular signaling proteins. We focused on mGluR1 and mGluR5 because these receptors are G protein-coupled receptors that operate through heterotrimeric GTP-binding proteins and PLC activation, which regulates intracellular  $\text{Ca}^{2+}$  by phosphoinositide hydrolysis (Tanabe et al., 1992; Pin and Duvoisin, 1995). Activation of phosphoinositide-linked mGluRs initiates a cascade of events including the activation of PLC $\beta$  by  $G_q$  proteins, generation of inositol triphosphate and diacylglycerol, and subsequent mobilization of  $\text{Ca}^{2+}$  from nonmitochondrial intracellular stores (Pin and Duvoisin, 1995). Control dogs ( $n = 3$ ) and ischemic dogs at 1 day ( $n = 2$ ) and 7 days ( $n = 2$ ) of recovery were anesthetized with pentobarbital, ventilated, and exsanguinated by intraaortic perfusion of ice-cold phosphate-buffered saline. The brains were quickly removed from the skull and placed on ice, and the hippocampus (septal) and anterior lobule of the cerebellum were isolated and frozen in isopentane. The samples were homogenized and subjected to differential centrifugation (Portera-Cailliau et al., 1996), and subcellular fractions were assayed for protein concentration using a Bio-Rad (Hercules, CA, U.S.A.) detection method. For immunoblotting, mitochondria-enriched membrane fractions or synaptic plasma membrane fractions (10, 12, or 15  $\mu$ g of protein) were subjected to sodium dodecyl sulfate polyacrylamide gel electro-

phoresis (8, 10, or 15% gels) and transferred to nitrocellulose membrane by electroblotting (Martin et al., 1992, 1997a). Samples of control and ischemic dogs were always run in the same gel. To ensure that equivalent amounts of protein were loaded in each lane and that transfer was comparable, membranes were stained with Ponceau S before immunoblotting. Blots were then blocked with 2.5% nonfat dry milk with 0.1% Tween 20 in 50 mmol/L Tris-buffered saline (pH 7.4) and incubated overnight at 4°C with antibodies to mGluR1 $\alpha$ , mGluR5, PLC $\beta_1$ , or G $\alpha_{q/11}$ . Affinity-purified rabbit polyclonal antibodies to the C-terminal domains of mGluR1 $\alpha$  and mGluR5 were used at a concentration of 0.5  $\mu$ g IgG/mL (Martin et al., 1992; Blue et al., 1997). Affinity-purified antipeptide rabbit polyclonal antibodies to PLC $\beta_1$  and G $\alpha_{q/11}$  were obtained from commercial sources (Santa Cruz Biotechnology, Santa Cruz, CA, U.S.A.) and were used at concentrations of 33 or 20 ng IgG/mL, respectively. In the same samples, the levels of proapoptotic protein Bax were measured, using commercial antibodies (Santa Cruz Biotechnology) at 150 ng IgG/mL, to evaluate whether changes in mGluR signaling proteins are associated with alterations in cell death protein levels. After the primary antibody incubation, membranes were washed and incubated with peroxidase-conjugated secondary goat anti-rabbit IgG (0.2  $\mu$ g/mL) for 1 hour and developed with enhanced chemiluminescence (Amersham, Piscataway, NJ, U.S.A.). All blots were then reprobated with synaptophysin antibody (Boehringer-Mannheim) for a quantitative loading control.

Western blots were quantified densitometrically to evaluate brain regional changes in the levels of these proteins in post-ischemic animals relative to controls. Films were scanned using a Macintosh Adobe Photoshop program and an Agfa Arcus Plus scanner (Ridgefield Park, NJ, U.S.A.). Densitometric analysis was performed using Signal Analytics IP Lab Gel software (Scanalytics, Fairfax, VA, U.S.A.). Protein levels were expressed as relative optical density measurements, determined by comparing the density and area of the immunoreactive band in each lane scanned with control lanes in the same blot. The relative values for each animal were replicated in at least four immunoblotting experiments. Bax protein levels and signal transduction protein levels were expressed as percentages of control values. Mean percentages were compared among the recovery groups by a Wilcoxon signed rank test with the significance level set at  $P < 0.05$ .

### Immunocytochemistry

From perfusion-fixed dogs (same as those used for hematoxylin and eosin staining and TUNEL), the right hemisphere was cut into 1-cm-thick coronal slabs, cryoprotected in 20% phosphate-buffered glycerol, and frozen in isopentane. Forebrain and cerebellar samples were cut at 40  $\mu$ m on a sliding microtome, and sections were placed in antifreeze buffer for storage ( $-20^\circ\text{C}$ ) until immunocytochemical processing. A peroxidase antiperoxidase method (Martin et al., 1992; Fotuhi et

al., 1993) was used to detect mGluR1 $\alpha$ , mGluR5, and PLC $\beta_1$  immunoreactivities in hippocampus and cerebellar cortex of sham and ischemic dogs. The polyclonal antibodies to Bax were not used for immunocytochemical experiments because they recognize several proteins in addition to the proteins at 21 and 23 kDa. Affinity-purified goat anti-rabbit IgG F(ab) $_2$  fragments (Cappel, West Chester, PA, U.S.A.) were used as secondary antibodies. Immunoreactivity was visualized with diaminobenzidine as chromogen. At least four sections from each brain region from each dog in each experimental group were processed concurrently using the same batches of reagents to obviate tissue section variability in antigen localization. Immunocytochemical negative controls included omission of primary antibodies and competition of antibodies with synthetic peptides corresponding to the antigenic C-terminal domains of mGluR1 $\alpha$ , mGluR5, and PLC $\beta_1$ .

## RESULTS

Twenty dogs were subjected to 20 minutes of global incomplete cerebral ischemia. All dogs had similar severities of ischemia and were similar to those described previously (Sieber et al., 1995). Epidural temperature during ischemia was maintained at normothermic values. No ischemic dogs were eliminated from the study, and all dogs recovered for the designated survival time after ischemia.

### CA1 pyramidal neuron and Purkinje cell degeneration overlaps with granule neuron death after global ischemia

The neuronal damage after transient global incomplete ischemia was progressive, as evidenced by the delayed reduction in neuronal density and the greater amount of ischemic cytopathology in neurons at 7 than at 1 day after ischemia (Table 1). At 1 day after ischemia, CA1 pyramidal neuron and cerebellar Purkinje cell densities were not significantly different from control values (Table 1). At 7 days after ischemia, 43% of CA1 pyramidal cells remained, while Purkinje cell densities were 78% of control (Table 1). The percentage of CA1 pyramidal neurons with ischemic cytopathology increased from 13% at 1 day of recovery to 52% at 7 days of recovery (Table 1). In cerebellum, the percentage of Purkinje cells with cytopathology was 24% at 1 day and 69% at 7 days after ischemia (Table 1). In hematoxylin and eosin sections of control animals, background neuronal injury (possibly due to the anesthesia, perfusion-

TABLE 1. Neuropathology in dog hippocampus and cerebellum after global incomplete ischemia

	CA1 neurons			Cerebellar Purkinje cells		
	Control	1 Day	7 Day	Control	1 Day	7 Day
% Neurons remaining	100 $\pm$ 2	97 $\pm$ 10	43 $\pm$ 10†	100 $\pm$ 8	82 $\pm$ 16	78 $\pm$ 16
% Neurons damaged	2 $\pm$ 1	13 $\pm$ 10*	52 $\pm$ 10†	3 $\pm$ 2	24 $\pm$ 11*	69 $\pm$ 6†

Values are mean  $\pm$  SD. The percent neurons remaining is percent of baseline control. The percent neurons damaged is the percent of remaining neurons with ischemic cytopathology.

\* Significantly different from control ( $P < 0.05$ ).

† Significantly different from control and 1 day ( $P < 0.05$ , Mann-Whitney test).

fixation, brain compression during removal from the skull, or histological processing) was  $\leq 3\%$  in CA1 and cerebellum (Table 1).

Neurons in hippocampus and cerebellar cortex were undergoing nuclear DNA fragmentation at 1 and 7 days after ischemia, as determined by TUNEL (Figs. 2 and 3). In hippocampus, subsets of neurons in the pyramidal cell layer of CA1 and CA2–superior CA3 (CA3a) were TUNEL-positive as well as subsets of granule neurons in the hippocampal dentate gyrus. In CA1, the number of TUNEL-positive cells/mm<sup>2</sup> was significantly greater ( $P < 0.05$ ) at 7 than at 1 day, whereas more dentate gyrus granule neurons were TUNEL-positive at 1 than at 7 days (Fig. 3). In cerebellar cortex, the number of TUNEL-positive Purkinje cells at 7 days after ischemia was approximately twofold higher than at 1 day, whereas TUNEL-positive cells in the granule cell layer were nearly twofold higher at 1 than at 7 days (Fig. 3).

In pyramidal neurons of hippocampus and in Purkinje cells, the TUNEL-positive nuclei usually had reaction product that was random in distribution, with irregularly shaped aggregates, or had uniform and nonaggregated labeling, unlike the organized spherical clumping or crescentic capping of chromatin that was found in granule neurons (Figs. 2A and 5F–5H) and is characteristic of neuronal apoptosis (Portera-Cailliau et al., 1997a,b; Al-Abdulla et al., 1998; Martin et al., 1999).

In agarose gels, random (smearing) and internucleo-

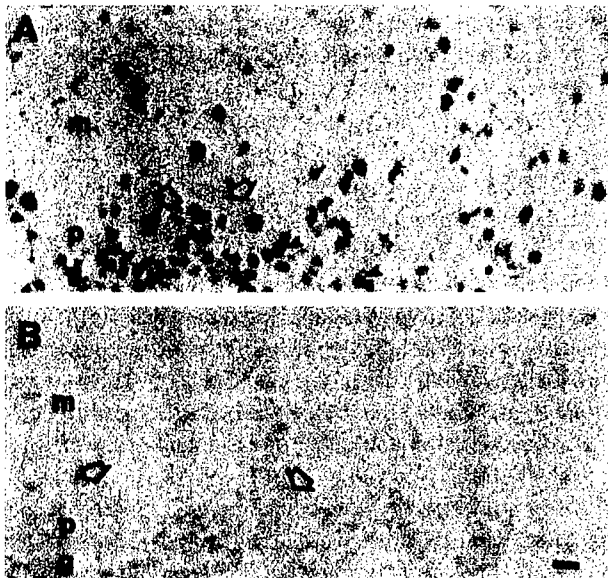


**FIG. 2.** Nuclear DNA fragmentation in dog cerebellar cortex after global incomplete ischemia. m, molecular layer; p, Purkinje cell layer; g, granule cell layer. (A): At 7 days after ischemia, terminal transferase-mediated biotin-dUTP nick end-labeling (TUNEL)-positive cells are detected in the three layers of cerebellar cortex. Purkinje cells (arrows) and a subset of granule neurons (arrowheads) are TUNEL-positive. (B): Granule neurons and Purkinje cells (arrows) are not TUNEL-positive in sham control dog cerebellum. Bar = 14  $\mu$ m.

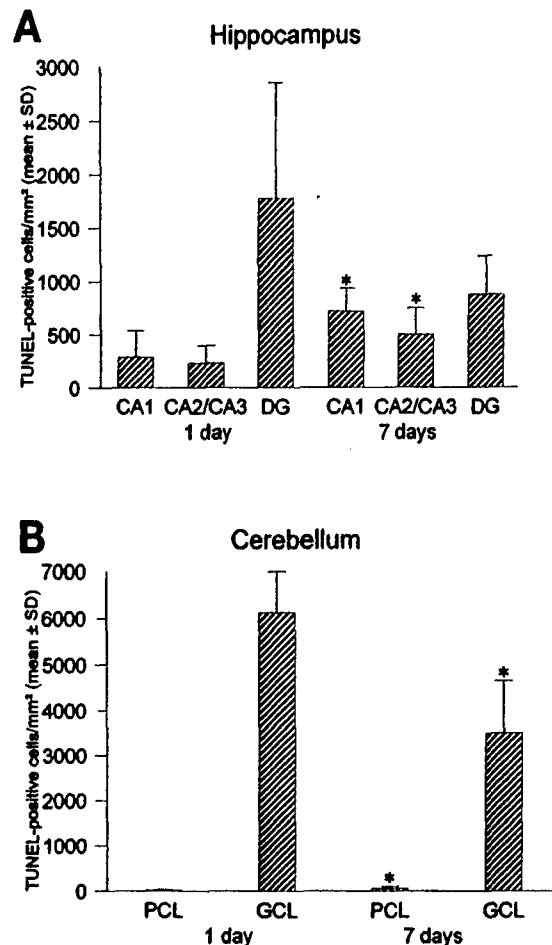


**FIG. 3.** Quantification of terminal transferase-mediated nick end-labeling (TUNEL)-positive cells in hippocampus (A) and cerebellum (B) at 1 and 7 days after ischemia. Cresyl violet-counterstained TUNEL preparations were used to count TUNEL-positive cells in CA1, CA2–superior CA3 (CA3a), and dentate gyrus (DG) granule neuron layer of hippocampus and in the Purkinje cell layer (PCL) and granule cell layer (GCL) of cerebellar cortex. Values are means  $\pm$  SD. Asterisks indicate that the values at 7 days were significantly different ( $P < 0.05$ , Mann–Whitney test) from corresponding values at 1 day.

somal fragmentation of DNA was detected in genomic DNA extracts of dog hippocampus and cerebellar cortex after ischemia (Fig. 4, lanes 2 and 4). These different patterns of DNA degradation coexisted, most prominently at 7 days after ischemia. The internucleosomal fragmentation was similar to the pattern detected during developmental PCD of neurons (Fig. 4, lane 1). No DNA fragmentation was detected in control dog hippocampus and cerebellar cortex (Fig. 4, lanes 3 and 5), and no fragmentation of DNA was observed at 6 hours after ischemia (data not shown).

#### CA1 pyramidal neuron and Purkinje cell death is necrosis, but granule neuron death is apoptosis after ischemia

With use of criteria for neuronal apoptosis established in previous experiments (Portera-Cailliau et al., 1997a,b;

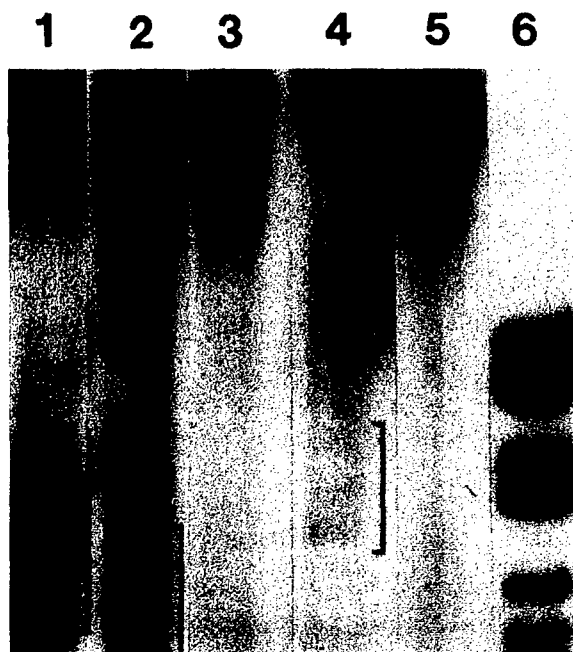


**FIG. 4.** Analysis of DNA fragmentation patterns in dog hippocampus and cerebellar cortex by agarose gel electrophoresis. Genomic DNA was isolated and fractionated from ischemic dog hippocampus (lane 2) and cerebellar cortex (lane 4) at 7 days of recovery and from control dog hippocampus (lane 3) and cerebellar cortex (lane 5). Programmed cell death in developing rat retina at postnatal day 19 served as a positive control for internucleosomal fragmentation of DNA (lane 1). Brackets delineate internucleosomal fragments (lanes 1, 2, and 4). Smearing of DNA is also seen in ischemic dog hippocampus and cerebellar cortex (lanes 2 and 4). Base pair molecular mass markers (lane 6) are (top to bottom): 2,176, 1,766, 1,230, 1,033, 653, 517, and 453.

Al-Abdulla et al., 1998; Martin et al., 1998, 1999), the degeneration of CA1 pyramidal neurons and Purkinje cells after ischemia was not apoptosis (Fig. 5). The degeneration of these neurons was consistent with necrosis (Figs. 5A–5C). Whereas nuclear pyknosis and chromatin condensation into irregular clumps were observed in these dying neurons, this pattern was very dissimilar to that found in unequivocal neuronal apoptosis (Portera-Cailliau et al., 1997a,b; Al-Abdulla et al., 1998; Martin et al., 1998, 1999). These ultrastructural observations are consistent with the hematoxylin and eosin staining and TUNEL patterns found in CA1 pyramidal neurons and cerebellar Purkinje cells, indicating a nonapoptotic structure, as shown previously (Martin et al., 1997a, 1998). In contrast, granule neuron degeneration in the dentate gyrus and cerebellar cortex was apoptosis (Fig. 5D–H). For example, early structural changes were chromatin margination and crescentic capping of chromatin at the nuclear envelope and dispersion of many ribosomes within the cytoplasm (Fig. 5F and G). These changes occurred in the presence of maintained mitochondrial morphology (Fig. 5G). Later in the progression of apoptosis, granule neurons underwent condensation of chro-

matin into large, round clumps and convolution of the nuclear envelope and then budding (Fig. 5H).

To further evaluate the presence or absence of indicators for neuronal apoptosis after cerebral ischemia, immunoblotting was used to evaluate the levels of Bax protein expression in hippocampus and cerebellum. A representative immunoblot of Bax expression in control and ischemic dogs is shown in Fig. 6. Bax levels at 1 and 7 days after ischemia did not differ significantly from control levels in homogenates of dorsal hippocampus, as quantified by comparing the density and area of the immunoreactive band in each lane of ischemic dog homogenate scanned with values of control dog lanes in the same blot. Bax protein levels (in relative optical density units, means  $\pm$  SD) in hippocampus were  $32.4 \pm 6.2$  (control),  $27.9 \pm 8.0$  (1 day after ischemia), and  $32.1 \pm 10.5$  (7 days after ischemia). In contrast, Bax protein expression was significantly ( $P < 0.05$ ) increased to  $128 \pm 5\%$  of control cerebellum values at 7 days after ischemia but not at 1 day after ischemia.

#### Alterations in metabotropic glutamate receptor signaling pathways occur in hippocampus and cerebellum after ischemia

In homogenates of whole septal hippocampal formation, mGluR1 $\alpha$  protein levels (detected as an immunoreactive band at 142 kDa) were unchanged, with values 108 and 114% of control at 1 and 7 days after ischemia, respectively (Table 2; Fig. 7); similarly, mGluR5 protein levels (detected as an immunoreactive band at 148 kDa) were unchanged, with values 105 and 112% of control at 1 and 7 days of recovery, respectively (Table 2; Fig. 7). The PLC $\beta_1$  and G $\alpha_{q11}$  protein levels in hippocampus were also not changed significantly after ischemia. At 1 and 7 days after ischemia, PLC $\beta_1$  protein values (detected as an immunoreactive 80-kDa band) were 95 and 122% of controls, respectively, and G $\alpha_{q11}$  protein values (detected as an immunoreactive 45-kDa band) were 98 and 81% of control values at 1 and 7 days after ischemia, respectively (Table 2; Fig. 7). The maintenance of mGluR1 $\alpha$ , mGluR5, PLC $\beta_1$ , and G $\alpha_{q11}$  protein levels, notably at 7 days after ischemia, occurred despite neuronal degeneration and death in the dorsal hippocampus (Table 1; Figs. 2 and 3).

In homogenates of cerebellar cortex, mGluR1 $\alpha$  and mGluR5 protein levels were significantly reduced after ischemia. mGluR1 $\alpha$  levels were 75 and 68% of controls at 1 and 7 days after ischemia, respectively (Table 2; Fig. 8), whereas mGluR5 was reduced to 22% of control at 1 day and then returned to 55% of control levels by 7 days (Table 2; Fig. 8). In contrast, PLC $\beta_1$  levels in cerebellar cortex were increased significantly to 173 and 213% of control at 1 and 7 days after ischemia, respectively, whereas G $\alpha_{q11}$  was reduced to 80% of control at 1 day



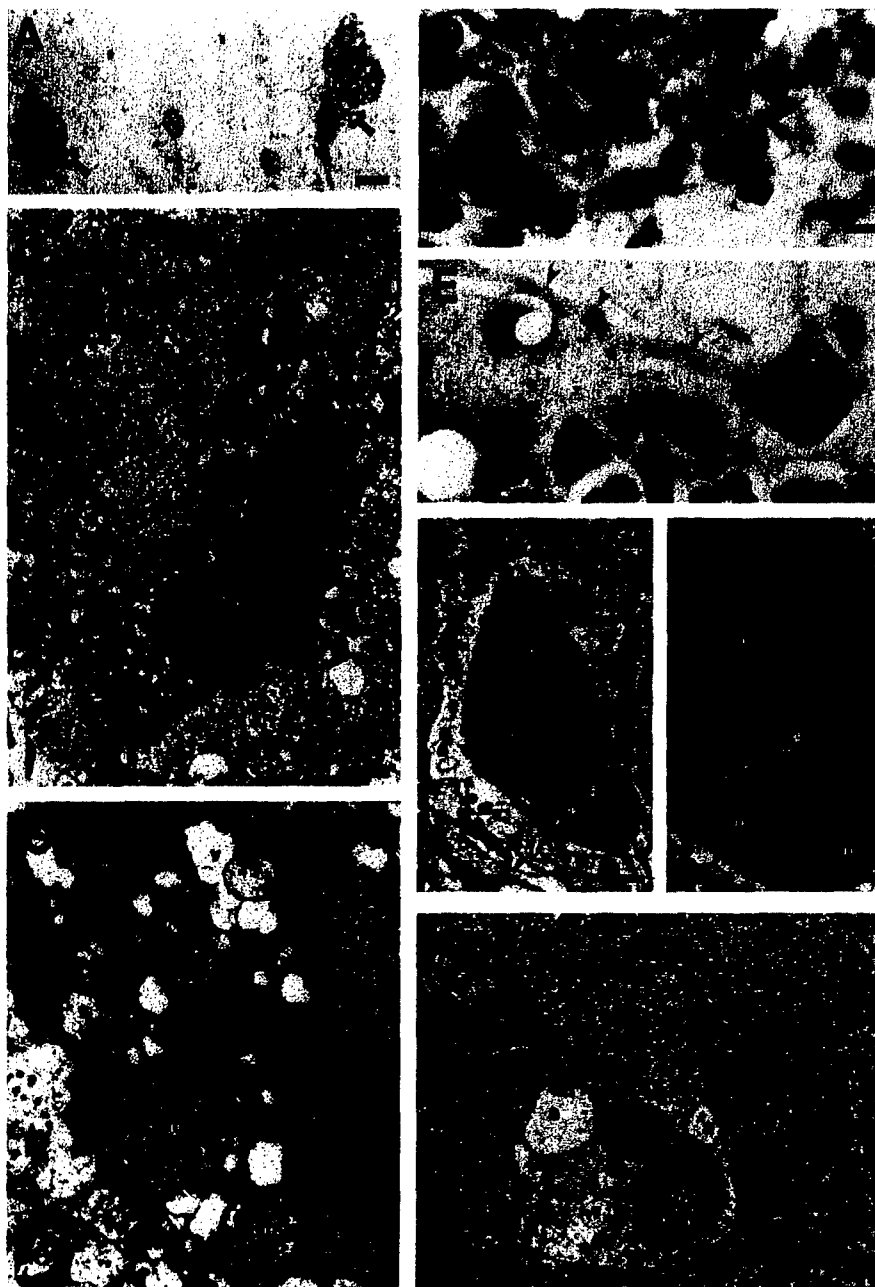


**FIG. 5.** Necrosis and apoptosis occur in distinct populations of neurons after ischemia. **(A)** Plastic section (1  $\mu\text{m}$  thick) shows degenerating CA1 pyramidal neurons (arrows). The nucleus (arrowheads) in these neurons is dark and pyknotic, and the cytoplasm contains many small, clear vacuoles (corresponding to degenerating mitochondria and fragmented Golgi; see B) and dark granules (corresponding to lysosomes). These changes are consistent with cellular necrosis (Kerr et al., 1991; Wyllie et al., 1980; Portera-Cailliau et al., 1997b; Martin et al., 1998). Bar = 8  $\mu\text{m}$ . **(B and C)** By electron microscopy, degeneration of CA1 neurons is morphologically necrotic. The cytoplasm of this representative neuron contains many swollen, degenerating mitochondria (m) and vacuoles (v). The pyknotic nucleus (Nu) contains many dispersed and irregularly shaped aggregates of chromatin throughout the nucleus (asterisks). Area in brackets is shown in C at higher magnification. Bars = 1.0  $\mu\text{m}$  (B) and 0.2  $\mu\text{m}$  (C). **(D)** Granule neuron degeneration in the hippocampal dentate gyrus after ischemia is apoptotic. Apoptotic granule neurons (arrows) are shrunken, and the nucleus displays chromatin clumping into dark, round aggregates. This neurodegeneration (arrows) occurs as isolated cells in a field of normal granule neurons. Bar = 5  $\mu\text{m}$ . **(E)** Granule neuron degeneration in cerebellar cortex at 7 days after ischemia is also apoptotic. An isolated apoptotic cerebellar granule neuron (arrow) is shrunken, and the nucleus contains dark, round clumps of chromatin. Above this neuron is an injured Purkinje cell (P) showing ischemic degeneration of its dendrite (arrowheads). Bar = 6  $\mu\text{m}$ . **(F)** The ultrastructure of granule neuron degeneration is consistent with apoptosis. At early morphologic stages of apoptosis, the cytoplasm and the nucleus (Nu) become dark and condensed, but the overall ultrastructural integrity of the neuron is not disrupted, in contrast to necrosis (cf. B and C). Apoptotic neurons are isolated from the surrounding neuropil by astrocytic processes (a). The chromatin aggregates (asterisks) as round clumps or crescents often at the periphery of the nucleus. Area in brackets is shown at higher magnification in G. Bar = 0.6  $\mu\text{m}$ . **(G)** At higher magnification, the condensed chromatin (asterisk) within the nucleus (Nu) abuts the nuclear envelope (in contrast to the random aggregation of chromatin throughout the nucleus in necrosis; see B and C). Cisterns form in some areas at the cytoplasmic surface of the nuclear envelope (arrowheads). The mitochondria (m) remain intact (unlike the swelling and dissolution of the mitochondria in necrosis; see B and C) and are embedded in a cytoplasmic matrix that appears striated due to the organization of the cytoskeleton. These changes are typical of apoptosis in neurons (Portera-Cailliau et al., 1997a; Al-Abdulla et al., 1998; Martin et al., 1998). Bar = 0.3  $\mu\text{m}$ . **(H)** At end-stage apoptosis, the nucleus (Nu) of granule neurons shows advanced chromatin condensation into round and crescentic aggregates (asterisks), some of which are extruded from the nucleus as the nuclear envelope ruptures (arrowheads). The residual cytoplasm, containing cytoskeletal and membranous debris and only few vacuoles (v), becomes infiltrated or enveloped by astrocytic processes (a). Nearby granule neurons (g) appear normal. Bar = 1.2  $\mu\text{m}$ .



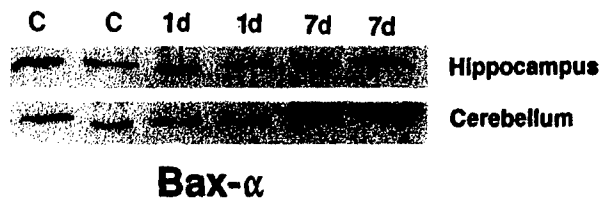


**FIG. 6.** Immunoblot analysis of Bax expression in mitochondria-enriched subcellular fractions of hippocampus (15  $\mu$ g of protein/lane) and cerebellar cortex (12  $\mu$ g of protein/lane) from sham control (c) and ischemic dogs at 1 day (1 d) and 7 days (7 d) of recovery. In hippocampus, Bax levels are unchanged at 1 and 7 days after ischemia. In cerebellar cortex, Bax levels are increased at 7 days after ischemia.

and then returned to control levels by 7 days (Table 2; Fig. 8).

The maintenance of some protein levels in regional homogenates, despite neuronal degeneration, suggested the possibility that changes occur in the cellular localization of mGluR1 $\alpha$ , mGluR5, and PLC $\beta_1$  after ischemia. We used immunocytochemistry to determine the localization of mGluR1 $\alpha$ , mGluR5, and PLC $\beta_1$  in hippocampus and cerebellum. In control dog hippocampus, mGluR1 $\alpha$  is localized primarily within the stratum oriens of CA1 and in the dentate gyrus hilus, with only faint immunolabeling of granule cells (Fig. 9A). This pattern of mGluR1 $\alpha$  localization in dog hippocampus is similar to the pattern shown in rat brain (Martin et al., 1992). In ischemic dogs, granule cell immunolabeling is augmented compared with controls (Fig. 9B), whereas the intensity of mGluR1 $\alpha$  immunoreactivity in the neuropil of CA1 is diminished. In control dogs, mGluR5 is highly enriched in CA1 pyramidal cell bodies and in the neuropil of stratum oriens and stratum radiatum (corresponding to the dendritic fields of CA1 pyramidal neurons), whereas dentate gyrus granule neurons are less intensely immunoreactive than CA1. After ischemia, mGluR5 immunoreactivity in the CA1 pyramidal cell body and dendritic layers is reduced as compared with controls, but the dentate gyrus molecular layer, subiculum, and parahippocampal gyrus are more intensely im-

## Hippocampus

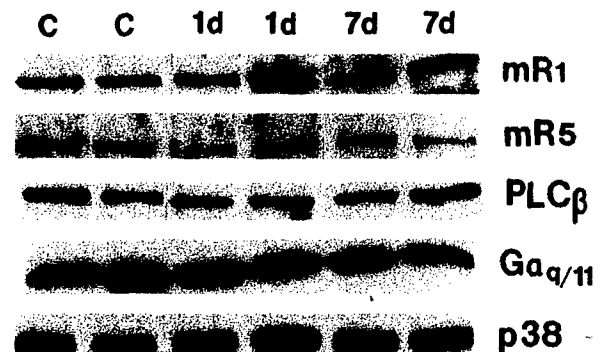


**FIG. 7.** Immunoblot analysis of metabotropic glutamate receptor (mGluR) 1 $\alpha$  (mR1), mGluR5 (mR5), phospholipase C $\beta$  (PLC $\beta$ ), and G $\alpha_{q/11}$  proteins in synaptic membrane fractions (10  $\mu$ g of protein/lane) of hippocampus from sham control (c) and ischemic dogs at 1 day (1 d) and 7 days (7 d) of recovery. Blots were probed for synaptophysin (p38) as a loading control.

munoreactive compared with control (data not shown). In normal hippocampus, PLC $\beta_1$  is highly enriched in cell bodies and proximal dendrites of pyramidal neurons and in the neuropil of CA1 (Fig. 9C) and is localized less intensely in the granule cells of the dentate gyrus (Fig. 9E). After ischemia, PLC $\beta_1$  immunoreactivity is lost in the pyramidal cell body and dendritic (radiatum) layers of CA1 (Fig. 9D); in contrast, PLC $\beta_1$  immunoreactivity is increased in the granule cell and molecular layers of the dentate gyrus (Fig. 9F) and in other locations corresponding to the distribution of the perforant path (not shown), suggesting an augmented presynaptic localization of PLC $\beta_1$  after ischemia.

In control dog cerebellar cortex, mGluR1 $\alpha$  is enriched in the neuropil of the molecular layer and in Purkinje cell bodies, but in the granule cell layer, occasional Golgi type II cells are immunopositive and granule cells are only weakly immunoreactive for mGluR1 $\alpha$  (Fig. 9G). This pattern of mGluR1 $\alpha$  localization in dog cerebellum

**TABLE 2.** Quantitative immunoblot analysis of phosphoinositide-linked mGluR signal transduction proteins after global incomplete ischemia

	Hippocampus			Cerebellar cortex		
	Control	1 Day	7 Days	Control	1 Day	7 Days
mGluR1 $\alpha$	164.4 $\pm$ 10.8	177.5 $\pm$ 0.4 (108%)	187.1 $\pm$ 5.3 (114%)	38.7 $\pm$ 11.6	29.2 $\pm$ 4.0* (75%)	26.1 $\pm$ 4.4* (68%)
mGluR5	148.6 $\pm$ 6.6	156.3 $\pm$ 10.0 (105%)	166.0 $\pm$ 16.9 (112%)	60.3 $\pm$ 21.2	13.3 $\pm$ 8.5* (22%)	32.9 $\pm$ 11.3* (55%)
PLC $\beta$	78.4 $\pm$ 16.5	74.2 $\pm$ 8.2 (95%)	95.9 $\pm$ 26.0 (122%)	44.3 $\pm$ 5.0	76.9 $\pm$ 6.8* (173%)	94.3 $\pm$ 3.8* (213%)
G $\alpha_{q/11}$	123.8 $\pm$ 20.4	121.4 $\pm$ 1.0 (98%)	99.9 $\pm$ 7.5 (81%)	110.3 $\pm$ 0.3	87.7 $\pm$ 12.6* (80%)	104.5 $\pm$ 21.9 (95%)

Values are mean  $\pm$  SD of the relative optical density measurements of the immunoreactive bands at the appropriate molecular mass. Numbers in parentheses are percent of control value.

\* Indicates significantly different from control ( $P < 0.05$ , Wilcoxon signed rank test).

## Cerebellum

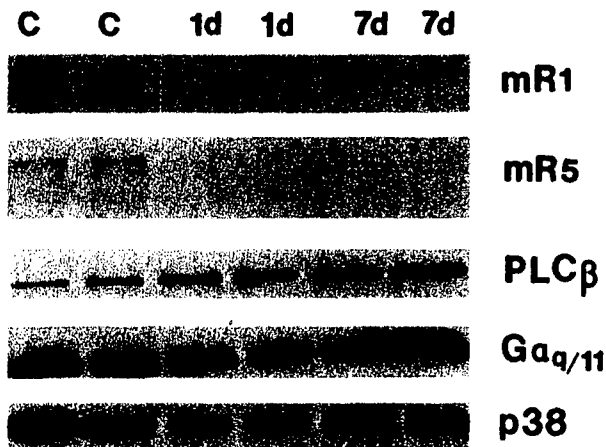
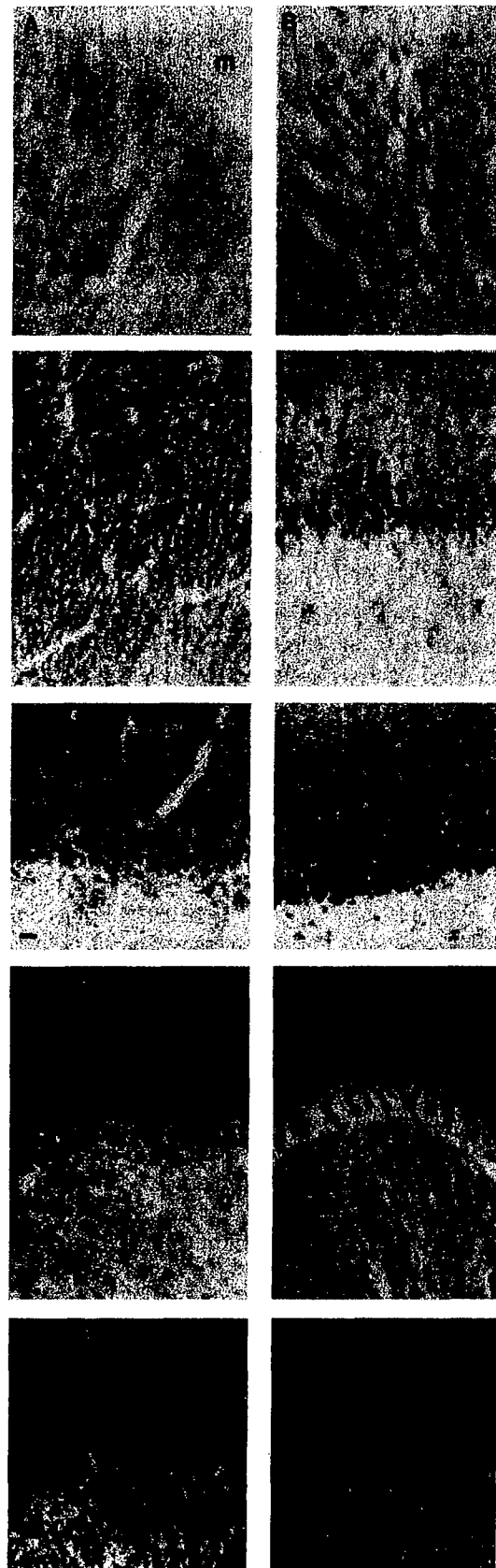


**FIG. 8.** Immunoblot analysis of metabotropic glutamate receptor (mGluR) 1 $\alpha$  (mR1), mGluR5 (mR5), phospholipase C $\beta$  (PLC $\beta$ ), and G $\alpha_{q/11}$  proteins in synaptic membrane fractions (10  $\mu$ g of protein/lane) of cerebellar cortex from sham control (c) and ischemic dogs at 1 day (1 d) and 7 days (7 d) of recovery. Blots were probed for synaptophysin (p38) as a loading control.

is similar to the pattern shown in rat brain (Martin et al., 1992). After ischemia, mGluR1 $\alpha$  immunoreactivity is reduced in the neuropil of the molecular layer but is increased in the granule cell layer (Fig. 9H). Like mGluR1 $\alpha$ , mGluR5 staining in the cerebellum was less intense in the molecular layer after ischemia compared with control (data not shown). The PLC $\beta_1$  level in control cerebellum is highly enriched in Purkinje cell bodies and dendrites extending throughout the molecular layer, which also contains diffuse neuropil immunoreactivity,

**FIG. 9.** Alterations occur in the regional and cellular localization of metabotropic glutamate receptor (mGluR) 1 $\alpha$  and phospholipase C $\beta$  (PLC $\beta$ ) in hippocampus and cerebellar cortex at 7 days after global ischemia in dog. Photomicrographs on the left (A, C, E, G, and I) are from control dogs, and photomicrographs on the right (B, D, F, H, and J) are from ischemic dogs. The varying shades of darkness in these black-and-white photomicrographs reflect the intensity of immunoreactivity. In hippocampal dentate gyrus after ischemia (B), granule cells (arrowheads) show increased mGluR1 $\alpha$  immunoreactivity as compared with normal dogs (A). m, molecular layer; g, granule cell layer. Bar (A) = 7  $\mu$ m. In CA1 after ischemia (D), PLC $\beta$  immunoreactivity is reduced in the pyramidal cell body layer (p) and in the apical dendritic layer (stratum radiatum; r) as compared with controls (C). Bar (C) = 33  $\mu$ m. In hippocampal dentate gyrus after ischemia (F), granule cells in the granule cell layer (g) and the neuropil of the molecular layer (m) have increased PLC $\beta$  immunoreactivity as compared with nonischemic dogs (E). Bar (E) = 16  $\mu$ m. In the cerebellar cortex of posts ischemic dogs (H) compared with control dogs (G), mGluR1 $\alpha$  immunoreactivity is diminished in the molecular layer (m), corresponding to a reduction in immunoreactive dendrites of Purkinje cells. In contrast, mGluR1 $\alpha$  immunoreactivity in granule cells (g) is markedly increased after ischemia. Bar (G) = 18  $\mu$ m. In the cerebellar cortex of posts ischemic dogs (J), immunoreactivity for PLC $\beta$  is enhanced in both the molecular layer (m) and the granule cell layer (g) as compared with nonischemic dogs (I). Bar (I) = 18  $\mu$ m.



and the granule cell layer is not uniformly immunoreactive (Fig. 9I). After ischemia, PLC $\beta_1$  immunoreactivity is increased in the neuropil of the molecular layer and in granule cells, whereas Purkinje cell labeling for PLC $\beta_1$  is prominently decreased (Fig. 9J).

## DISCUSSION

These experiments demonstrate that global ischemia results in two temporally overlapping, but distinct, forms of neuronal cell degeneration: necrosis of selectively vulnerable neurons (CA1 pyramidal neurons and cerebellar Purkinje cells) and apoptosis of granule neurons in dentate gyrus and cerebellum. Neuronal cell death in these regions is accompanied by differential changes in phosphoinositide-linked mGluR transduction mechanisms. Necrosis of CA1 neurons and Purkinje cells occurs in association with a loss of PLC-coupled mGluR signaling proteins, whereas apoptosis of granule neurons occurs in association with increases in proteins involved in PLC-coupled mGluR signaling.

### Ischemic delayed degeneration of selectively vulnerable neurons is necrosis

The CA1 neurons undergo selective DND after ischemia in rodents (Ito et al., 1975; Kirino, 1982) and in dogs (Sato et al., 1990). The DND of cerebellar Purkinje cells is not studied commonly in rodent forebrain models of ischemia, but our study in dogs provided a novel opportunity to compare similarities among neuronal degeneration in hippocampus and cerebellum after ischemia. Our results show that ischemic delayed degeneration of CA1 pyramidal neurons and cerebellar Purkinje cells is similar structurally. The same conclusion has been made using a model of global complete ischemia in cats (Martin et al., 1998). Furthermore, our data demonstrate that the DND of selectively vulnerable neurons following global ischemia is cellular necrosis rather than apoptosis or a hybrid of apoptosis and necrosis. This degeneration of CA1 pyramidal neurons and Purkinje cells after ischemia is very distinct from neuronal apoptosis (Portera-Cailliau et al., 1997a; Al-Abdulla et al., 1998; Martin et al., 1998, 1999); it is also distinct from non-NMDA GluR-mediated excitotoxic neuronal apoptosis (Portera-Cailliau et al., 1997b; Martin et al., 1998), but it is very similar to NMDA receptor-mediated excitotoxic neuronal necrosis (Portera-Cailliau et al., 1997b; Martin et al., 1998; Ginsberg et al., 1999). Both the nucleus and the cytoplasm undergo ultrastructural perturbations consistent with cellular necrosis, with the main features being irregular clumping of chromatin, swelling and degeneration of organelles, extensive cytoplasmic vacuolation, destruction of plasma membrane integrity, and eventual dissolution of the cell. Moreover, dying CA1 neurons do not bud to form discrete, round nuclear fragments, as in apoptosis (cf. Fig. 4C and H) (Wyllie et al., 1980; Kerr

and Harmon, 1991; Martin et al., 1998). The nuclear pyknosis with condensation of chromatin into many small, irregularly shaped clumps in ischemic neurons contrasts with the formation of few, uniformly dense, and regularly shaped chromatin aggregates that occurs in neuronal apoptosis (Portera-Cailliau et al., 1997a; Al-Abdulla et al., 1998; Martin et al., 1998, 1999).

The cell plasma membrane and cytoplasmic organelles are damaged in necrotic neurons after ischemia. The immunocytochemically identified loss of mGluR-PLC signaling proteins in hippocampal pyramidal neurons in CA1 and Purkinje cells (as well as the loss of immunolabeling in their dendritic fields) is consistent with plasma membrane damage. The mitochondria swell and the inner mitochondrial membrane undergoes cristaeolysis. These mitochondrial abnormalities have been demonstrated in cellular necrosis (Laiho et al., 1971; Laiho and Trump, 1975) and can be produced when plasma membrane function and ATP synthesis are impaired (Laiho and Trump, 1975). Our observations are also consistent with previous findings showing that organelles that function in protein synthesis and posttranslational modification become structurally abnormal early in the course of ischemic neurodegeneration and are persistently abnormal during the process of neurodegeneration (Kirino et al., 1984; Martin et al., 1998). These structural changes are consistent with the finding that total protein synthesis is severely reduced by 6 hours after transient global forebrain ischemia and is reduced persistently in CA1 neurons, with the vast majority of pyramidal neurons never regaining their normal biosynthetic activity (Thilmann et al., 1986; Araki et al., 1990; Johansen and Diemer, 1990; Furuta et al., 1993). Cytoskeletal disintegration also occurs early after ischemia, particularly in dendrites, before the degeneration of neuronal cell bodies (Kitagawa et al., 1989; Yamamoto et al., 1990). This rapid disassembly and proteolysis of the cytoskeleton after ischemia (Kitagawa et al., 1989) contrast with the organized structure of the cytoskeleton and the cytoskeletal accumulation in neurons undergoing apoptosis (see Fig. 4G) (Al-Abdulla et al., 1998; Martin et al., 1998, 1999).

Nevertheless, previous studies have suggested that DND in hippocampus is apoptosis. The first observation suggesting this possibility was the finding that systemic treatment with protein synthesis inhibitors protected against CA1 neuron loss after global ischemia (Goto et al., 1990; Shigeno et al., 1990), although the hypothermic effects of protein synthesis inhibitors were not considered. However, other experiments have shown that protein and RNA synthesis inhibitors do not ameliorate postischemic DND in CA1 and that this neurodegeneration is not PCD (Deshpande et al., 1992). More recent studies have focused on DNA fragmentation. By *in situ* DNA end-labeling methods, many studies

have shown that selectively vulnerable populations of neurons undergo nuclear DNA fragmentation after global cerebral ischemia in the adult brain (Héron et al., 1993; MacManus et al., 1995; Nitatori et al., 1995). However, *in situ* end-labeling methods for DNA fail to discriminate among apoptotic and necrotic cell deaths (Grasl-Kraupp et al., 1995; Portera-Cailliau et al., 1997b; Martin et al., 1998) and can also detect DNA fragments during DNA synthesis (Lockshin and Zakeri, 1994); thus, these results *per se* cannot be interpreted as solely apoptosis. DNA integrity after global ischemia in adult brain has also been studied by gel electrophoresis. In DNA extracts of adult rat or gerbil brain, internucleosomal fragmentation has been found after transient global forebrain ischemia and has been interpreted as apoptosis occurring by PCD mechanisms (Okamoto et al., 1993; Héron et al., 1993; MacManus et al., 1995; Nitatori et al., 1995; Bhat et al., 1996). However, it is also uncertain whether internucleosomal DNA fragmentation is specific for apoptosis, because it occurs in ischemic liver necrosis (Fukuda et al., 1993), in NMDA receptor-mediated excitotoxic neuronal necrosis in adult brain (Portera-Cailliau et al., 1997b) and in culture (Gwag et al., 1997; Sohn et al., 1998), and in cells undergoing necrosis induced by calcium ionophores and heat shock (Collins et al., 1992). The analysis of DNA fragmentation patterns (and protein levels) in brain extracts is further confounded by tissue homogenization of heterogeneous cell systems, which precludes the evaluation of cell death on a cell-by-cell basis. Nonneuronal cells (e.g., astrocytes, oligodendrocytes, inflammatory cells, and vascular cells) also die following central nervous system injury, including ischemia-reperfusion and axotomy-target deprivation, and some of these nonneuronal cells die apoptotically (Martin et al., 1997a, 1998; Al-Abdulla et al., 1998). The interpretation of DNA fragmentation data is limited by the specificity and the caveats of the assay system, and, as concluded in previous studies (Kerr and Harmon, 1991; Collins et al., 1992; Portera-Cailliau et al., 1997b; Martin et al., 1998), cell structure is still the best indicator for classifying cell death *in vivo*. In our experiments, we found coexisting random and internucleosomal DNA fragmentation, and we attribute these different patterns to necrosis of pyramidal neurons and Purkinje cells and apoptosis of granule neurons within these regions. Our electron microscopic data support this conclusion.

This and previous ultrastructural studies illustrate that ischemic neurodegeneration in selectively vulnerable regions is not apoptosis (Kirino, 1982; Kirino and Sano, 1984; Kirino et al., 1984; Deshpande et al., 1992; Martin et al., 1998). These studies demonstrate that ischemic neurodegeneration has the typical features of cellular necrosis, consistent with the acute parenchymal cell death found in other organs after ischemia (Wyllie et al., 1980).

Yet, other studies with electron microscopic data have asserted that DND of CA1 pyramidal neurons after ischemia is apoptosis (Nitatori et al., 1995), although unambiguous ultrastructural evidence of apoptosis in these neurons in the adult brain has not been demonstrated. This discrepancy regarding whether DND fits the pattern of apoptosis is likely to be due to differences in criteria for identifying neuronal apoptosis and to the detail of the electron microscopic analysis. Alternatively, DND after ischemia may fall along a structural and mechanistic apoptosis-necrosis continuum (MacManus et al., 1995; Portera-Cailliau et al., 1997a,b; Martin et al., 1998). For example, GluR-mediated excitotoxic death of neurons occurs along an apoptosis-necrosis continuum, and the structure of excitotoxic neuronal degeneration is influenced by the subtype of GluR that is activated (Portera-Cailliau et al., 1997a,b). In the adult rat brain, the degeneration of neurons caused by NMDA receptor activation is structurally necrotic; however, the neuronal death produced by non-NMDA GluR activation is distinct from that caused by NMDA receptor stimulation. This non-NMDA receptor-mediated neuronal death in adult brain has some cytoplasmic and nuclear features reminiscent of neuronal apoptosis (Portera-Cailliau et al., 1997b). Thus, like non-NMDA GluR-mediated excitotoxicity, DND after ischemia could be a hybrid of apoptosis and necrosis, with the death of these neurons not strictly apoptosis or necrosis, according to a traditional binary classification of cell death, but occurring as intermediate or hybrid forms with coexisting characteristics that lie along a structural continuum with apoptosis and necrosis at the extremes. Because this continuum is influenced by the subtype of glutamate receptor that is activated, DND after ischemia may not be identical in every neuron, possibly because of the high diversity in the expression, localization, and function of GluR subtypes or the diversity in second messenger systems in the central nervous system. Surprisingly, however, we did not find ultrastructural evidence that ischemic DND resembles non-NMDA GluR-mediated excitotoxic neuronal death, but rather it is structurally very similar to NMDA receptor-mediated excitotoxic necrosis (Portera-Cailliau et al., 1997a,b; Martin et al., 1998).

#### **Granule neurons undergo apoptosis after ischemia**

The degeneration of granule neurons in dentate gyrus and cerebellum after global ischemia sharply contrasts with the degeneration of CA1 neurons and Purkinje cells. Granule neuron death after ischemia closely resembles apoptosis. Thus, granule neurons provide an internal standard for classic apoptosis with which CA1 pyramidal neuron and cerebellar Purkinje cell degeneration after ischemia can be compared to demonstrate that the death of these latter neurons is not apoptosis. As with apoptosis in nonneuronal tissues (Kerr and Harmon, 1991), in de-

veloping brain during naturally occurring PCD of neurons (Portera-Cailliau et al., 1997a), and in some neuronal groups after axotomy–target deprivation (Al-Abdulla et al., 1998; Martin et al., 1999), apoptosis of granule neurons was characterized morphologically by nuclear and cytoplasmic condensation. The most prominent alterations were condensation of chromatin into few, large, round clumps or crescentic caps, aggregation and lamination of the cytoskeleton, and cellular shrinkage. Membranous organelles, including mitochondria, remained intact until the late stages of apoptosis. Neurodegeneration after global ischemia involves entire neural systems, and neuronal connectivity as well as metabolic factors possibly dictate the pattern of selective vulnerability (Martin et al., 1997b). Granule neuron death may be a direct consequence of the ischemia, or it may be secondary to necrotic degeneration of hippocampal pyramidal neurons and cerebellar Purkinje cells and thus is a form of target deprivation-induced apoptosis (Martin et al., 1998, 1999; Al-Abdulla et al., 1998), because the targets of dentate granule neurons include hippocampal pyramidal neurons and the targets of cerebellar granule neurons are Purkinje cells. This possibility is supported by *in vitro* studies showing that, in response to serum deprivation, cerebellar granule neurons undergo transcription-dependent apoptosis (D'Mello et al., 1993; Watson et al., 1998) by activation of a pathway involving c-Jun phosphorylation (Watson et al., 1998). Similar mechanisms seem to be operative in a related *in vitro* paradigm (i.e., low potassium) of cerebellar granule neuron apoptosis (D'Mello et al., 1993; Watson et al., 1998), and, interestingly, activation of phosphoinositide-linked mGluRs blocks this neuronal apoptosis (Copani et al., 1995). Thus, augmented mGluR expression in cerebellar and hippocampal granule neurons after cerebral ischemia may signify a physiological attempt at neuroprotection rather than an event mediating the apoptosis.

#### Contribution of programmed cell death mechanisms in ischemic neurodegeneration

Gene products that regulate PCD of mammalian cells have been studied after ischemia. Bax mRNA is increased in both vulnerable and less vulnerable regions after ischemia (Chen et al., 1996). Changes in mRNA after cerebral ischemia are difficult to interpret in light of damage to organelles that function in protein synthesis and posttranslational processing, thereby potentially rendering the translation and formation of mature products inefficient. By immunoblotting, Bax protein in hippocampus is increased transiently at 6 hours after ischemia but then returns to control levels (Krajewski et al., 1995). We found no changes in Bax protein levels in hippocampus at 1 and 7 days after ischemia, but we observed an increase in Bax in cerebellum at 7 days after ischemia. A possible explanation for a lack of detection of changes in

Bax protein levels in hippocampus by immunoblotting is that apoptotic death of dentate gyrus granule neurons is less frequent than granule neuron death in cerebellum (see Fig. 3). Also, granule neurons compose a greater population of cells in cerebellum than in hippocampus (West et al., 1991; Korbo et al., 1993). However, a sustained postischemic increase in Bax protein levels has been shown in hippocampus but not cerebellum (Chen et al., 1996), although the contributions of different cells to this observation have not been identified. Important in this regard is the finding that mRNA and protein levels for the proapoptotic cysteine protease ICE interleukin-1 converting enzyme (caspase-1) are increased in hippocampus after global ischemia in gerbils, but this change is associated with inflammatory cells rather than selectively vulnerable CA1 pyramidal neurons (Bhat et al., 1996). In addition, after global ischemia in rat, caspase-3 mRNA levels are progressively elevated in CA1 at 24 to 72 hours, although most of the neurons are already lost by 72 hours, whereas caspase-3 mRNA is transiently elevated in dentate gyrus granule cells at 8 hours after ischemia (Chen et al., 1998). This latter pattern would be more consistent with a role for caspase-3 in the granule neuron apoptosis that we have identified. On the other hand, Bcl-2 overexpression in transgenic mice reduces hippocampal pyramidal neuron degeneration after global ischemia (Kitagawa et al., 1998), although this effect of Bcl-2 cannot yet be specifically ascribed to antiapoptotic activity, because this protein has additional functions in injured neurons (Chen et al., 1997). It is still uncertain, however, whether the absence of a classic apoptotic structure in selectively vulnerable neurons after ischemia is sufficient evidence to exclude the possibility that PCD may be operative, because all forms of PCD may not occur via apoptosis (Schwartz et al., 1993).

#### Metabotropic glutamate receptor signaling pathways after ischemia

The distinct forms of degeneration in different populations of hippocampal and cerebellar neurons after ischemia were accompanied by differential changes in proteins involved in phosphoinositide-coupled mGluR signal transduction. These changes were more easily identified by immunocytochemistry rather than by immunoblotting (except for PLC $\beta$  in cerebellum), perhaps because of overlapping and differential contributions of distinct populations of neurons that are not divisible in gel analyses of regional homogenates. Necrosis of CA1 neurons and Purkinje cell is associated with a loss of mGluRs and PLC $\beta$ . In contrast, apoptosis in granule cell populations in hippocampus and cerebellum is paralleled by increased expression of these proteins. Our results are consistent with the reported loss of mGluR1 and mGluR5 mRNA in CA1 after global ischemia (Iversen et al., 1994). This observation is not surprising when con-

sidering the postsynaptic, somatodendritic localization of these proteins (Martin et al., 1992; Blue et al., 1997) and the rapid damage to dendritic membranes and the cytoskeletal proteolysis that occur in these neurons after ischemia (Kitagawa et al., 1989; Yamamoto et al., 1990). These abnormalities further support our conclusion that hippocampal pyramidal neurons and Purkinje cells undergo necrosis after ischemia. In contrast, in granule neurons of dentate gyrus and cerebellum, immunoreactivity for mGluRs and PLC $\beta$  is enhanced. This finding is consistent with the concept that apoptosis results from the *de novo* expression or activation of a PCD program (Sen, 1992), but it is not clear whether changes in PLC-coupled mGluRs participate directly in the mechanisms for apoptosis in these neurons or whether these changes reflect the activation of compensatory survival signaling pathways (Copani et al., 1995).

The possible roles for PLC-coupled mGluRs in the mechanisms for necrotic degeneration of selectively vulnerable neurons after ischemia are uncertain. Activation of mGluRs is necessary for Purkinje cell survival *in vitro* (Mount et al., 1993) and protects neurons from oxidative stress (Sagara and Schubert, 1998). Thus, a loss of somatodendritic phosphoinositide-linked mGluRs in Purkinje cells and CA1 neurons may have a role in the necrosis of these neurons after ischemia. Alternatively, this loss is possibly a consequence of necrotic degeneration of these neurons. It is possible that augmented activity of PLC-coupled mGluR signal transduction proteins does not participate in the primary mechanisms for DND of CA1 pyramidal neurons and cerebellar Purkinje cells after ischemia. This conclusion is supported by the finding that neither pharmacological blockade of mGluRs nor ablation of the mGluR1 gene reduces ischemic and excitotoxic brain injury *in vivo* (Ferraguti et al., 1997). However, other observations suggest that endogenous activation of mGluR1 contributes to ischemic and excitotoxic neuronal degeneration (Bruno et al., 1999). Additional work is necessary to precisely identify the role of mGluR signaling in neurodegeneration after ischemia.

**Acknowledgments:** The authors thank Ann Price and Dawn Spicer as well as the technical staff of the Department of Pathology electron microscope core facility (Marilyn Miller, Barbara Plantholt, and Gerald Horne) for their assistance.


## REFERENCES

- Al-Abdulla NA, Portera-Cailliau C, Martin LJ (1998) Occipital cortex ablation in adult rat causes retrograde neuronal death in the lateral geniculate nucleus that resembles apoptosis. *Neuroscience* 86:191–209
- Araki T, Kato H, Inoue T, Kogure K (1990) Regional impairment of protein synthesis following brief cerebral ischemia in the gerbil. *Acta Neuropathol* 79:501–505
- Bhat RV, DiRocco R, Marcy VR, Flood DG, Zhu Y, Dobrzanski P, Siman R, Scott R, Contreras PC, Miller M (1996) Increased expression of IL-1 $\beta$  converting enzyme in hippocampus after ischemia: selective localization in microglia. *J Neurosci* 16:4146–4154
- Blue ME, Martin LJ, Brennan EM, Johnston MV (1997) Ontogeny of non-NMDA glutamate receptors in rat barrel field cortex: I. Metabotropic receptors. *J Comp Neurol* 386:16–28
- Bruno V, Battaglia G, Kingston A, O'Neill MJ, Catania MV, Di Grezia R, Nicoletti F (1999) Neuroprotective activity of the potent and selective mGluR1a metabotropic glutamate receptor antagonist, (+)-2-methyl-4-carboxyphenylglycine (LY367385): comparison with LY357366, a broader spectrum antagonist with equal affinity for mGluR1a and mGluR5 receptors. *Neuropharmacology* 38:199–207
- Chen DF, Schneider GE, Martinou J-C, Toneyawa S (1997) Bcl-2 promotes regeneration of severed axons in mammalian CNS. *Nature* 385:434–439
- Chen J, Zhu RL, Nakayama M, Kawaguchi K, Jin K, Stetler RA, Simon RP, Graham SH (1996) Expression of the apoptosis-effector gene, *bax*, is up-regulated in vulnerable hippocampal CA1 neurons following global ischemia. *J Neurochem* 67:64–71
- Chen J, Nagayama T, Jin K, Stetler RA, Zhu RL, Graham SH, Simon RP (1998) Induction of caspase-3-like protease may mediate delayed neuronal death in the hippocampus after transient cerebral ischemia. *J Neurosci* 18:4914–4928
- Collins RJ, Harmon BV, Gobé VC, Kerr JFR (1992) Internucleosomal DNA cleavage should not be the sole criterion for identifying apoptosis. *Int J Radiat Biol* 61:451–453
- Copani A, Bruno VMG, Barresi V, Battaglia G, Condorelli DF, Nicoletti F (1995) Activation of metabotropic glutamate receptors prevents neuronal apoptosis in culture. *J Neurochem* 64:101–108
- Deshpande J, Bergstedt K, Linden T, Kalimo H, Wieloch T (1992) Ultrastructural changes in the hippocampal CA1 region following transient cerebral ischemia: evidence against programmed cell death. *Exp Brain Res* 88:91–105
- Diemer NH, Valente E, Bruhn T, Berg M, Jürgensen MB, Johansen FF (1993) Glutamate receptor transmission and ischemic nerve cell damage: evidence for involvement of excitotoxic mechanisms. *Prog Brain Res* 96:105–123
- D'Mello SR, Galli C, Ciotti T, Calissano P (1993) Induction of apoptosis in cerebellar granule neurons by low potassium: inhibition of death by insulin-like growth factor I and cAMP. *Proc Natl Acad Sci USA* 90:10989–10993
- Ferraguti F, Pietra C, Valerio E, Corti C, Chiamulera C, Conquet F (1997) Evidence against a permissive role of the metabotropic glutamate receptor 1 in acute excitotoxicity. *Neuroscience* 79:1–5
- Fotuhi M, Dawson TM, Sharp AH, Martin LJ, Graybiel AM, Snyder SH (1993) Phosphoinositide second messenger system is enriched in striosomes: immunohistochemical demonstration of inositol 1,4,5-trisphosphate receptors and phospholipase C  $\beta$  and  $\gamma$  in primate basal ganglia. *J Neurosci* 13:3300–3308
- Fukuda K, Kojima M, Chiu J-F (1993) Demonstration of extensive chromatin cleavage in transplanted Morris hepatoma 7777 tissue: apoptosis or necrosis? *Am J Pathol* 142:935–946
- Furuta S, Ohta S, Hatakeyama T, Nakamura K, Sakaki S (1993) Recovery of protein synthesis in tolerance-induced hippocampal CA1 neurons after transient forebrain ischemia. *Acta Neuropathol* 86:329–336
- Ginsberg SD, Portera-Cailliau C, Martin LJ (1999) Fimbria-fornix transection and excitotoxicity produce similar neurodegeneration in the septum. *Neuroscience* 88:1059–1071
- Goto K, Ishige A, Sekiguchi K, Iizuka S, Sugimoto A, Yuzurihara M, Aburada M, Hosoya E, Kogure K (1990) Effects of cycloheximide on delayed neuronal death in rat hippocampus. *Brain Res* 534:299–302
- Grasl-Kraupp B, Ruttkay-Nedecky B, Koudelka H, Bukowska K, Bursch W, Schulte-Hermann R (1995) *In situ* detection of fragmented DNA (TUNEL assay) fails to discriminate among apoptosis, necrosis, and autolytic cell death: a cautionary note. *FASEB J* 21:1465–1468
- Gwag BJ, Koh JY, DeMaro JA, Ying HS, Jacquin M, Choi DW (1997)

- Slowly triggered excitotoxicity occurs by necrosis in cortical cultures. *Neuroscience* 77:393-401
- Héron A, Pollard H, Dessi F, Moreau J, Lasbennes F, Ben-Ari Y, Charriaut-Marlangue C (1993) Regional variability in DNA fragmentation after global ischemia evidenced by combined histological and gel electrophoresis observations in the rat brain. *J Neurochem* 61:1973-1976
- Ishimaru MJ, Ikonomidou C, Tenkova TI, Der TC, Dikranian K, Sesma MA, Olney JW (1999) Distinguishing excitotoxic from apoptotic neurodegeneration in the developing rat brain. *J Comp Neurol* 408:461-476
- Ito U, Spatz M, Walker JT, Klatzo I (1975) Experimental cerebral ischemia in Mongolian gerbils. I. Light microscopic observations. *Acta Neuropathol* 32:209-223
- Iversen L, Mulvihill E, Haldeman B, Diemer NH, Kaiser F, Sheardown M, Kristensen P (1994) Changes in metabotropic glutamate receptor mRNA levels following global ischemia: increase of a putative presynaptic subtype (mGluR4) in highly vulnerable rat brain areas. *J Neurochem* 63:625-633
- Johansen FF, Diemer NH (1990) Temporal profile of interneuron and pyramidal cell protein synthesis in rat hippocampus following cerebral ischemia. *Acta Neuropathol* 81:14-19
- Kerr JFR, Harmon BV (1991) Definition and incidence of apoptosis: an historical perspective. In: *Apoptosis: the molecular basis of cell death* (Tomei LD, Cope FO, eds), Cold Spring Harbor: Cold Spring Harbor Laboratory Press, pp 5-29
- Kirino T (1982) Delayed neuronal death in the gerbil hippocampus following ischemia. *Brain Res* 239:57-69
- Kirino T, Sano K (1984) Fine structural nature of delayed neuronal death following ischemia in the gerbil hippocampus. *Acta Neuropathol* 62:209-218
- Kirino T, Tamura A, Sano K (1984) Delayed neuronal death in rat hippocampus following transient forebrain ischemia. *Acta Neuropathol* 64:139-147
- Kirino T, Robinson HPC, Miwa A, Tamura A, Kawai N (1992) Disturbance of membrane function preceding ischemic delayed neuronal death in the gerbil hippocampus. *J Cereb Blood Flow Metab* 12:408-417
- Kitagawa K, Matsumoto M, Niinobe M, Mikoshiba K, Hata R, Ueda H, Handa N, Fukunaga R, Isaka Y, Kimura K, Kamada T (1989) Microtubule-associated protein 2 as a sensitive marker for cerebral ischemic damage. Immunohistochemical investigation of dendritic damage. *Neuroscience* 31:401-411
- Kitagawa K, Matsumoto M, Tsujimoto Y, Ohtsuki T, Kuwabara K, Matsushita K, Yang G, Tanabe H, Martinou J-C, Hori M, Yanagihara T (1998) Amelioration of hippocampal neuronal damage after global ischemia by neuronal overexpression of Bcl-2 in transgenic mice. *Stroke* 29:2616-2621
- Korbo L, Andersen BB, Ladefoged O, Miller A (1993) Total number of various cell types in rat cerebellar cortex estimated using an unbiased stereological method. *Brain Res* 609:262-268
- Krajewski S, Mai JK, Krajewska M, Sikorska M, Mossakowski MJ, Reed JC (1995) Upregulation of bax protein levels in neurons following cerebral ischemia. *J Neurosci* 15:6364-6376
- Laiho KU, Trump BJ (1975) Studies on the pathogenesis of cell injury. Effects of inhibitors of metabolism and membrane function on the mitochondria of Ehrlich ascites tumor cells. *Lab Invest* 32:163-182
- Laiho KU, Shelburne JD, Trump BJ (1971) Observations on cell volume, ultrastructure, mitochondrial conformation and vital-dye uptake in Ehrlich ascites tumor cells. *Am J Pathol* 65:203-230
- Lockshin RA, Zakeri A (1994) Programmed cell death: early changes in metamorphosing cells. *Biochem Cell Biol* 72:589-596
- MacManus JP, Hill IE, Preston E, Rasquinha I, Walker T, Buchan AM (1995) Differences in DNA fragmentation following transient cerebral ischemia or decapitation ischemia in rats. *J Cereb Blood Flow Metab* 15:728-737
- Martin LJ, Blackstone CD, Hagan RL, Price DL (1992) Cellular localization of a metabotropic glutamate receptor in rat brain. *Neuron* 9:259-270
- Martin LJ, Brambrink AM, Lehmann C, Portera-Cailliau C, Koehler R, Rothstein J, Traystman RJ (1997a) Hypoxia-ischemia causes abnormalities in glutamate transporters and death of astroglia and neurons in newborn striatum. *Ann Neurol* 42:335-348
- Martin LJ, Brambrink A, Koehler RC, Traystman RJ (1997b) Primary sensory and forebrain motor systems in the newborn brain are preferentially damaged by hypoxia-ischemia. *J Comp Neurol* 377:262-285
- Martin LJ, Al-Abdulla NA, Brambrink AM, Kirsch JR, Sieber FE, Portera-Cailliau C (1998) Neurodegeneration in excitotoxicity, global cerebral ischemia, and target deprivation: a perspective on the contributions of apoptosis and necrosis. *Brain Res Bull* 46:281-309
- Martin LJ, Kaiser A, Price AC (1999) Motor neuron degeneration after sciatic nerve avulsion in adult rat evolves with oxidative stress and is apoptosis. *J Neurobiol* 40:185-201
- Mount HTJ, Dreyfus CF, Black IB (1993) Purkinje cell survival is differentially regulated by metabotropic and ionotropic excitatory amino acid receptors. *J Neurosci* 13:3173-3179
- Nakanishi S (1992) Molecular diversity of glutamate receptors and implications for brain function. *Science* 258:597-603
- Nitatori T, Sato N, Waguri S, Karasawa Y, Araki H, Shibani K, Kominami E, Uchiyama Y (1995) Delayed neuronal death in the CA1 pyramidal cell layer of the gerbil hippocampus following transient ischemia is apoptosis. *J Neurosci* 15:1001-1011
- Okamoto M, Matsumoto M, Ohtsuki T, Taguchi A, Mikoshiba K, Yanagihara T, Kamada T (1993) Internucleosomal DNA cleavage involved in ischemia-induced neuronal death. *Biochem Biophys Res Commun* 196:1356-1362
- Opitz T, Richter P, Carter AJ, Kozikowski AP, Shiozaki H, Reymann KG (1995) Metabotropic glutamate receptor subtypes differentially influence neuronal recovery from in vitro hypoxia/hypoglycemia in rat hippocampal slices. *Neuroscience* 68:989-1001
- Pin J-P, Duvoisin R (1995) The metabotropic glutamate receptors: structure and functions. *Neuropharmacology* 34:1-26
- Portera-Cailliau C, Price DL, Martin LJ (1996) N-Methyl-D-aspartate receptor proteins NR2A and NR2B are differentially distributed in the developing rat central nervous system as revealed by subunit-specific antibodies. *J Neurochem* 66:692-700
- Portera-Cailliau C, Price DL, Martin LJ (1997a) Excitotoxic neuronal death in the immature brain is an apoptosis-necrosis morphological continuum. *J Comp Neurol* 378:70-87
- Portera-Cailliau C, Price DL, Martin LJ (1997b) Non-NMDA and NMDA receptor-mediated excitotoxic neuronal deaths in adult brain are morphologically distinct: further evidence for an apoptosis-necrosis continuum. *J Comp Neurol* 378:88-104
- Sagara Y, Schubert D (1998) The activation of metabotropic glutamate receptors protects nerve cells from oxidative stress. *J Neurosci* 18:6662-6671
- Sato M, Hashimoto H, Kosaka F (1990) Histological changes of neuronal damage in vegetative dogs induced by 18 minutes of complete global brain ischemia: two-phase damage of Purkinje cells and hippocampal CA1 pyramidal cells. *Acta Neuropathol* 80:527-534
- Schwartz LM, Smith SW, Jones MEE, Osborne BA (1993) Do all programmed cell deaths occur via apoptosis? *Proc Natl Acad Sci USA* 90:980-984
- Sen S (1992) Programmed cell death: concept, mechanism and control. *Biol Rev* 67:287-319
- Sheardown MJ, Nielsen EØ, Hansen AJ, Jacobsen P, Honoré T (1990) 2,3-Dihydroxy-6-nitro-7-sulfamoyl-benzo(F)quinoxaline: a neuroprotectant for cerebral ischemia. *Science* 247:571-574
- Shigeno T, Yamasaki Y, Kato G, Kusaka K, Mima T, Takakura K, Graham DI, Furukawa S (1990) Reduction of delayed neuronal death by inhibition of protein synthesis. *Neurosci Lett* 120:117-119
- Sieber FE, Palmon SC, Traystman RJ, Martin LJ (1995) Global incomplete cerebral ischemia produces predominantly cortical neuronal injury. *Stroke* 26:2091-2096
- Sohn S, Kim EY, Gwag BJ (1998) Glutamate neurotoxicity in mouse cortical neurons: atypical necrosis with DNA ladders and chromatin condensation. *Neurosci Lett* 240:147-150
- Tanabe Y, Masu M, Ishii T, Shigemoto R, Nakanishi S (1992) A family of metabotropic glutamate receptors. *Neuron* 8:169-179
- Thilmann R, Xie Y, Kleihues P, Kiessling M (1986) Persistent inhibi-

- tion of protein synthesis precedes delayed neuronal death in post-ischemic gerbil hippocampus. *Acta Neuropathol* 71:88-93
- Tominaga T, Kure S, Narisawa K, Yoshimoto T (1993) Endonuclease activation following focal ischemic injury in the rat brain. *Brain Res* 608:21-26
- Watson A, Eilers A, Lallemand D, Kyriakis J, Rubin LL, Ham J (1998) Phosphorylation of c-jun is necessary for apoptosis induced by survival signal withdrawal in cerebellar granule neurons. *J Neurosci* 18:751-762
- West MJ, Slomianka L, Gundersen HJG (1991) Unbiased stereological estimation of the total number of neurons in the subdivisions of the rat hippocampus using the optical fractionator. *Anat Rec* 231:482-497
- Wyllie AH, Kerr JFR, Currie AR (1980) Cell death: the significance of apoptosis. *Int Rev Cytol* 68:251-306
- Yamamoto K, Hayakawa T, Mogami H, Akai F, Yanagihara T (1990) Ultrastructural investigation of the CA1 region of the hippocampus after transient cerebral ischemia in gerbils. *Acta Neuropathol* 80:487-492
- Yan G-M, Lin S-Z, Irwin RP, Paul SM (1995) Activation of G proteins bidirectionally affects apoptosis of cultured cerebellar granule neurons. *J Neurochem* 65:2425-2431





# Peptides, Hormones, and the Brain and Spinal Cord

LEE J. MARTIN

*Johns Hopkins University School of Medicine*

- 
- I. Introduction
  - II. Brain Peptides Occur as Many Different Kinds with Many Different Functions
  - III. Neuroactive Brain Peptides Are Made from Protein Precursors That Undergo Proteolytic Processing
  - IV. Brain Peptides and Hormones Act at Cell Membrane Receptors
  - V. Brain Peptides Provide a Biochemical Fingerprint for Many Brain Regions and Reveal New Features about the Parcelling of the Brain
  - VI. Abnormalities in Brain Peptides Occur in Behavioral, Psychiatric, and Neurodegenerative Disorders of Humans
  - VII. Brain Peptides Modulate Neuronal Degeneration and Regeneration in Experimental Models
  - VIII. The Future of CNS Peptide Research Has Great Promise

## GLOSSARY

**astrocyte** A class of nonneuronal glial cell in the central nervous system that has long, radial processes that ensheath neurons and synaptic complexes, regulate the extracellular chemical and ionic environment, and secrete brain peptides, growth factors, cytokines, and chemokines.

**central nervous system** The brain and spinal cord.

**chemokine** A chemoattractant small peptide or protein cytokine.

**cytokine** Extracellular signaling peptide or protein that acts as a local mediator in cell-cell communication.

**glial cell** Nonneuronal cell in the nervous system (e.g., astrocyte, oligodendrocyte, microglial cell, and Schwann cell).

**growth factor** An extracellular peptide or protein that functions as a cell survival factor that can maintain cell survival or stimulate a cell to grow or proliferate.

**hormone** A chemical produced by a cell to regulate the functioning of another cell.

**microglia** the resident small phagocytic cells of the central nervous system that are related to the mononuclear phagocyte lineage and function as immune accessory cells that secrete cytokines and chemokines.

**neuromodulator** A chemical signal that modulates the response of a neuron to a neurotransmitter.

**neuropeptide** Peptide secreted by neurons or nonneuronal cells as either a synaptic or nonsynaptic cell-cell signaling molecule.

**neurotransmitter** Signaling molecule secreted by the presynaptic terminal of a neuron at chemical synapses to relay a signal to a postsynaptic neuron.

**oligodendrocyte** Glial cells that provide myelin sheaths for axons within the CNS and secrete peptide growth factors.

**programmed cell death** A form of cell death that is mediated by the activation of intrinsic mechanisms.

**Schwann cell** Glial cells that provide myelin sheaths for axons within the peripheral nervous system and that secrete peptide growth factors.

**tyrosine kinase** Enzyme that transfers the terminal phosphate of ATP to a specific tyrosine residue in a target protein.

**Brain peptides are amino-acid-comprised molecules that are synthesized and released by neuronal and nonneuronal cells that function as intercellular signaling molecules, serving as neurotransmitters, neuromodulators, neurohormones, cytokines, chemokines, or growth factors.**

## I. INTRODUCTION

The field of brain peptide research has been revolutionary in neuroscience. Many fundamentally new concepts about brain organization and function, as well as abnormal function and disease, have been revealed by studying brain peptides. Through brain peptides, new interactions have been disclosed between the nervous system and endocrine system, the nervous system and gastrointestinal system, and the nervous system and immune system. New principles about cell-cell signaling and intracellular signal transduction pathways have come to light from studies of brain peptides and related molecules. These studies are particularly important because a variety of these naturally occurring chemicals have been implicated in modulating basic nervous system functions such as sensibility, emotions, and behavior, and they most likely participate in the pathobiology of neurologic and psychiatric diseases in humans. The accumulating information on brain peptides may have ramifications as far-reaching as the further understanding of the pathophysiology of Alzheimer's disease, amyotrophic lateral sclerosis, multiple sclerosis, stroke, acquired immune deficiency syndrome (AIDS), obesity, anorexia, sleeping disorders, and brain-spinal cord trauma.

At the same time, however, advances in the field of brain peptides tend to cloud the conventional classification of intercellular signaling molecules within the body. For example, the tachykinins are a family of peptides including substance P and neurokinins that are present widely throughout the body, including the brain and spinal cord. These peptides have several clearly identified functions outside the central nervous system (CNS) and within the CNS, participating in cardiovascular function and inflammation. In the spinal cord, tachykinins function in the synaptic transmission of nociceptive (pain) information and, thus, are important neurotransmitters. Yet tachykinins (as well as several other well-known brain peptides) also function in neuromodulation, participating in the regulation of neuronal excitability by modulating glutamatergic excitatory synaptic transmission via glutamate receptors, and they also function in neuronal survival akin to neurotrophic factors. Another example that emphasizes the breakdown of the walls of conventional classification of brain peptides is illustrated by the functions of vasoactive intestinal peptide. An early identified function of vasoactive intestinal peptide was the regulation of blood flow in the autonomic nervous system and CNS. Now, it has been shown that vasoactive intestinal

peptide has diverse neurotransmitter, neuromodulator, cytokine, and neurotrophic factor actions that regulate neuronal survival and growth as well as glial activation and release of glial-cell-derived soluble factors. Work has revealed exciting new evidence that vasoactive intestinal peptide can prevent neuronal death induced by the AIDS virus envelope protein gp120, and another more recently identified vasoactive intestinal peptide family member (i.e., pituitary adenylate cyclase activating polypeptide) can block apoptosis of cultured granule neurons and necrosis of hippocampal pyramidal neurons after cerebral ischemia. These few examples highlight the fact that the highly diverse actions of brain peptides can make it difficult to discretely classify these naturally occurring brain chemicals. Furthermore, these examples emphasize their pathophysiological and potential therapeutic importance in disorders of the human CNS.

The discovery of each brain peptide involves its isolation, chemical characterization, anatomical localization, gene cloning, receptor identification and cloning, and functional assessment at the micro (electrophysiological and intracellular signaling) and macro-levels (behavior). Substance P was the first neuroactive peptide found in nervous tissue. Originally, there was considerable debate about the suitability of referring to brain peptides as neurotransmitters. Many of these peptides had been identified previously as peripheral tissue hormones with physiological actions at target organs outside the brain. Cholecystokinin, somatostatin, and insulin-like growth factors are only a few examples in this regard (Table I).

The possibility that small peptides acted as neurotransmitters was a new concept in the early emerging field of neuroscience (Fig. 1). Generally, four criteria should be fulfilled for a chemical to be considered a neurotransmitter: (1) a neurotransmitter is synthesized in neurons (Fig. 2); (2) a neurotransmitter is present in the presynaptic terminal and is released after depolarization in quantities sufficient to effect a response postsynaptically (Fig. 1); (3) exogenous application of a candidate neurotransmitter at physiological concentrations mimics the actions of endogenously released chemical; and (4) the action of the candidate neurotransmitter at the synapse is terminated by a specific mechanism. Many different types of brain peptides (old and recently identified) have now been shown to be neurotransmitters (Table I).

More than one neurotransmitter may coexist in neurons. Neuroactive peptides and small-molecule

**Table I**  
Classical Neuroactive Peptides<sup>a</sup>

Peptide	Size <sup>b</sup>	Family	Major functions
Vasopressin	9	Neurohypophyseal hormone	Renal H <sub>2</sub> O resorption, vasoconstriction
Oxytocin	9	Neurohypophyseal hormone	Uterine contraction, milk ejection, natriuretic effects
Gonadotropin-releasing hormone	10	Hypothalamic peptide	Stimulates secretion of FSH and LH
Thyrotrophin-releasing hormone	3	Hypothalamic peptide	Stimulates TSH secretion
Corticotropin-releasing hormone	41	Hypothalamic peptide	Stimulates ACTH secretion
$\beta$ -Endorphin	30	Endogenous opioid	Analgesia, stress response, inhibition of dopamine release
Dynorphin	17	Endogenous opioid	Analgesia, inhibition of dopamine release
Enkephalin	5	Endogenous opioid	Analgesia, primary afferent modulation
Cholecystokinin	8	Gastrointestinal peptide gastrin	Inhibition of feeding
Neuropeptide Y	36	Gastrointestinal peptide	Feeding behavior, modulation of neuronal excitability
Neurotensin	13	Gastrointestinal peptide	Modulation of dopaminergic neurons
Somatostatin	14	Gastrointestinal-hypothalamic peptide	Inhibits growth hormone release, inhibits synaptic transmission, neurotrophin
Substance P	11	Gastrointestinal-tachykinin peptide	Pain transmission, neurotrophin
Vasoactive intestinal peptide	28	Gastrointestinal-secretin peptide	Cerebral blood flow regulation
Insulin-like growth factor	67-70	Insulin	Neuronal survival

<sup>a</sup>Represents only a selection of the more than 50 classical neuroactive peptides that have been identified.

<sup>b</sup>Number of amino acid residues.

neurotransmitters are often found within the same neuron (Fig. 1). This observation was iconoclastic because, until this discovery, it was believed that each neuron used only one neurotransmitter. Now it is known that, at synapses, peptides are stored in dense-core vesicles that contain ATP. These dense-core vesicles (called dense-core because they appear to have a dark core when viewed in the electron microscope) are usually much less numerous than small, clear synaptic vesicles that contain neurotransmitters such as acetylcholine, GABA, and glutamate (Fig. 1). Peptide-containing dense-core vesicles are large (100–150 nm) compared to small, clear synaptic vesicles (40–60 nm). Dense-core vesicles are released at higher frequencies of stimulation of the axon and are not released solely at the presynaptic active zone like small-molecule neurotransmitters, because they do not require the presynaptic membrane specialization for their exocytotic release. The inactivation of the neuroactive peptide at the synapse occurs extracellularly and is slower than the inactivation of the small-molecular-weight neurotransmitter; thus, peptides act over a longer period of time than classical neurotransmitters.

## II. BRAIN PEPTIDES OCCUR AS MANY DIFFERENT KINDS WITH MANY DIFFERENT FUNCTIONS

The diversity of brain peptides is extensive (Tables I–IV). These peptides can be grouped into families. One way to classify neuroactive peptides is based on structural similarities, notably, commonalities in amino acid sequences (i.e., primary structure). Similarities in the physiological responses (i.e., biological activities) that are evoked by different brain peptides are another way to group these chemical messengers, although each brain peptide can have multiple physiological actions. More recently, similarities in the nucleotide base sequences in the genes that encode precursors of neuroactive peptides are used to identify membership in peptide families.

### A. Classical and More Recently Discovered Neuropeptides

The classical brain peptides can be grouped into broad families such as the hypothalamic-releasing hormones,

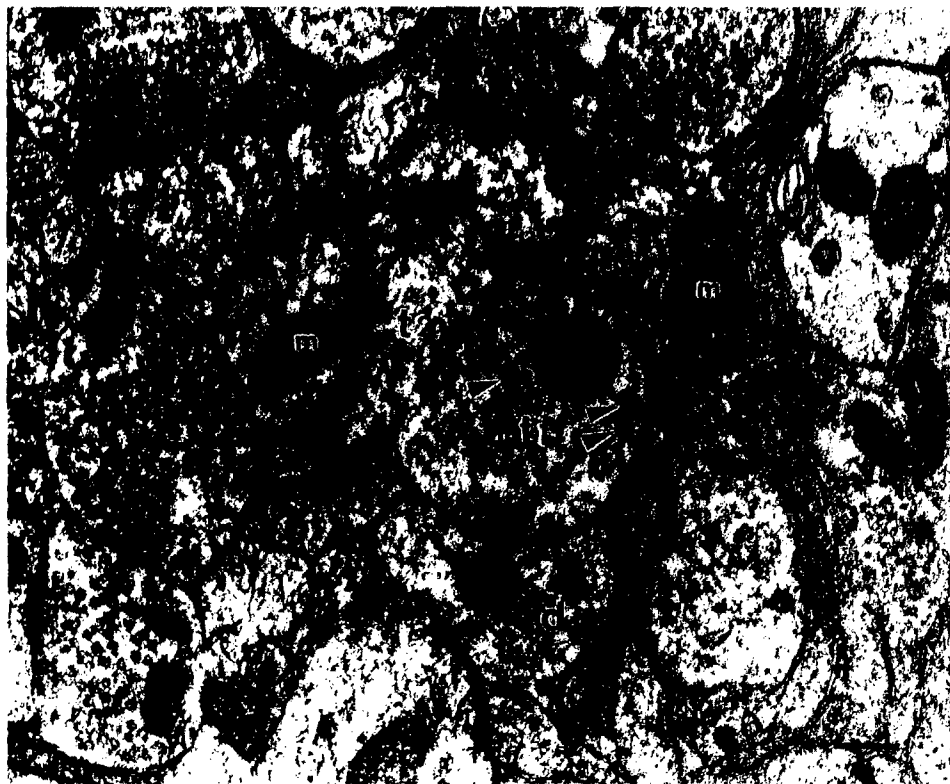


**Figure 1** Synaptic structure as revealed by electron microscopic examination of rhesus monkey cerebral cortex. Nerve terminals (t1 and t2) contain numerous small, clear, round synaptic vesicles (t2, small, black arrowheads) but only a few dense-core synaptic vesicles that can contain neuropeptides (t1, black-on-white arrowheads). Mitochondria (m) are present in nerve terminals for the energy-dependent release of synaptic vesicles. Nerve terminals form synaptic contacts with dendrites (d). The active zone of the synapse (t1 and t2, open arrow) is the site of synaptic vesicle exocytosis. Scale bar = 0.4  $\mu$ m.

the neurohypophyseal hormones, the pituitary peptides, the gastrointestinal peptides, the opioids, and the tachykinins (Table I). The classical brain peptides are located differentially throughout the CNS (Fig. 3). For example, forebrain structures (cerebral cortex, striatum, and amygdala) tend to have greater diversity in neuropeptides than hindbrain structures (cerebellum and spinal cord). Remarkably, regions that have the same embryonic derivation within the diencephalon (thalamus versus hypothalamus) can have vastly different neuropeptide profiles (Fig. 3).

Major advances have been made in understanding brain peptide regulation of feeding and body weight. In the 1950s a recessive obesity mutation was identified that results in profound obesity and adult-onset (type II) diabetes. It was thus postulated that an obese gene product may be a component in a signaling pathway regulating body fat deposition. Mice with mutations in the obese gene are obese and diabetic and are found to have reduced activity, metabolism, and body temperature. It was discovered that leptin, a 16-kDa secreted

protein hormone, is the product of the obese gene and is believed to be synthesized only in adipose tissue. Leptin is an integral component in a homeostatic loop that regulates body weight. Leptin acts to control food intake and energy expenditure by both classical and newly discovered neuropeptides in the hypothalamus. One classical neuropeptide that functions in weight control is neuropeptide Y (Table I).

The brain neuropeptides that function in this loop are the orexins (or hypocretins because they are hypothalamic neuropeptides similar to the gut hormone secretin). Orexin-A and orexin-B are peptides of 33 and 28 amino acid residues, respectively, that are derived from the proteolytic processing of a single prepro-orexin precursor protein. These peptides are produced exclusively by a specific group of neurons in the lateral hypothalamus (Fig. 3) called the perifornical nucleus. These orexin-utilizing neurons have widespread projections to the olfactory bulb, cerebral cortex, thalamus, hypothalamus, and brain stem. These brain peptides are endogenous ligands for two

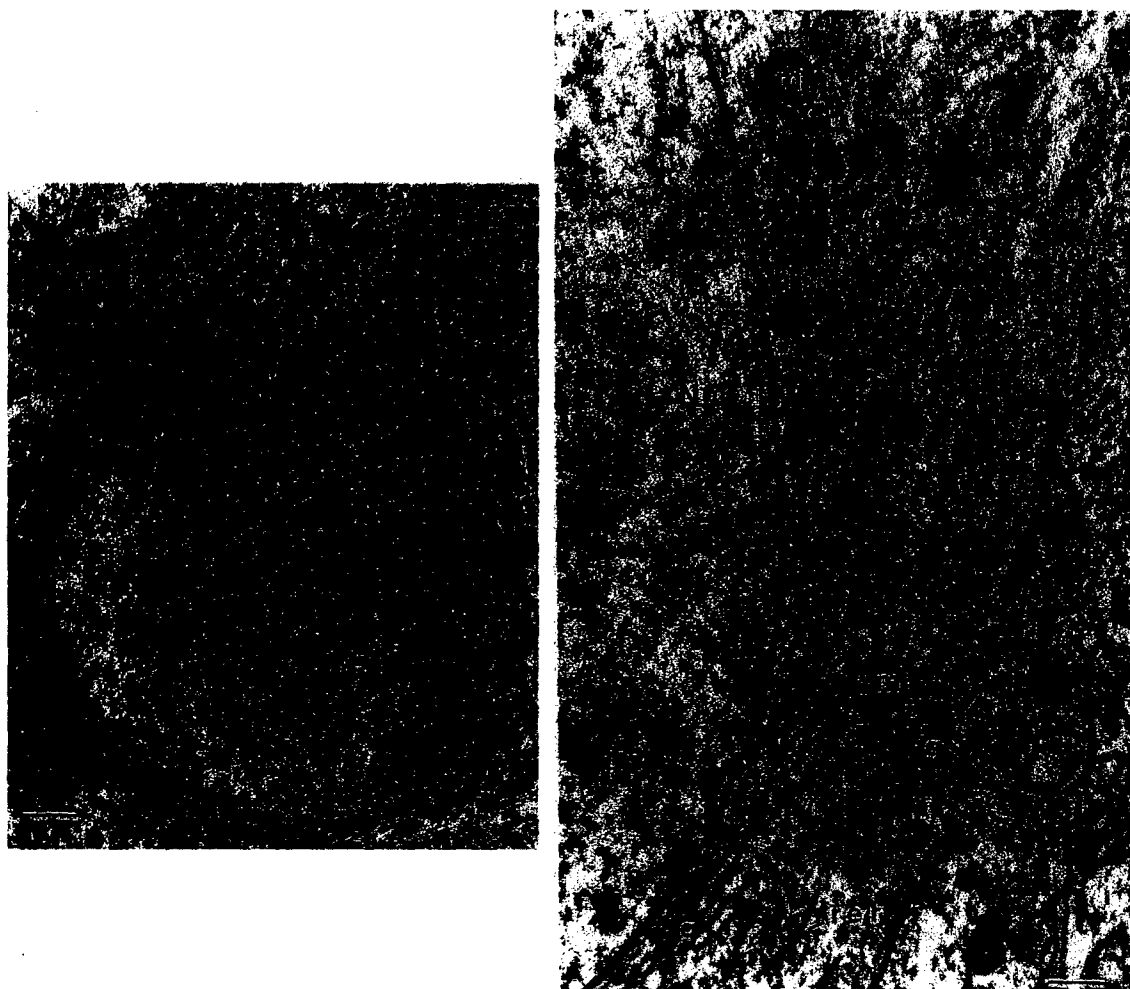


**Figure 2** Electron microscopic identification of subcellular organelles in neurons of piglet striatum. Low-magnification view (left panel) of a primary neuron found in the striatum. At higher magnification (right panel), these neurons have abundant polyribosomes distributed throughout the cytoplasmic matrix (small granules), arrays of rough endoplasmic reticulum (rer), stacks of Golgi complex (g) with budding secretory vesicles (black-on-white arrowhead), and mitochondria (m). The nucleus (Nu) has a predominantly pale matrix and is surrounded by a continuous, bilaminar nuclear membrane that contains nuclear pores (arrows). Scale bars = 0.85  $\mu$ m (left panel) and 0.25  $\mu$ m (right panel).

G-protein-coupled receptors found in the brain that function at synapses to increase the presynaptic release of GABA and glutamate.

In addition to these peptides functioning in energy homeostasis, it has been discovered that the orexin neuropeptide-receptor system functions in sleep regulation. Two animal models dramatically highlight this point. Mice deficient in the orexin gene display abnormal sleep-wakeful states, and autosomal recessive mutations of the hypocretin (orexin) receptor-2 gene cause a sleep disorder in Doberman Pinschers. Both of these abnormalities are believed to cause sleep disorders similar to narcolepsy in humans. Support for

this conclusion is derived from studies showing that orexin is undetectable in many people with narcolepsy.

## B. Growth Factors

A growth factor is a secreted peptide or protein that functions as a cell survival factor and can stimulate cell growth, differentiation, or proliferation (Table II). In the nervous system, growth factors are called neurotrophins. They can act locally as autocrine or paracrine regulators of cell function. The first neurotrophin to be isolated, chemically characterized, and physiologically

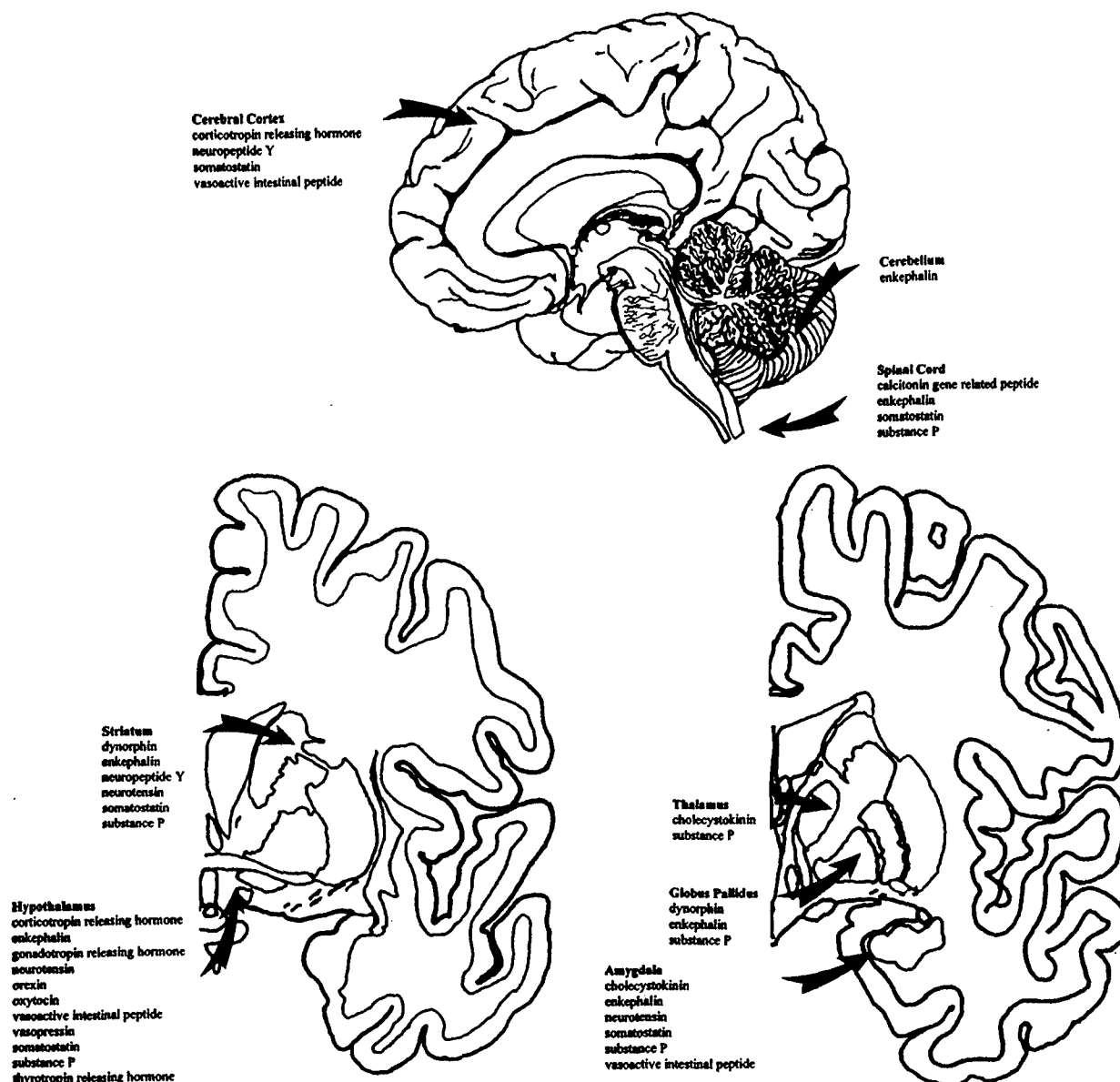


**Figure 3** General locations of some classical neuropeptides in the human CNS. The top image is a view of the brain and upper spinal cord from a midsagittal perspective, and the two lower panels are transverse views through the forebrain and anterior or mid-diencephalon. Some of the major neuropeptides found in these regions are indicated.

evaluated was nerve growth factor. Neurotrophins act as target- or afferent-derived growth factors for specific populations of neurons and can have survival-promoting effects on immature and adult neurons. In general, the effects of neurotrophins are mediated by binding to a specific high-affinity tyrosine kinase receptor on the presynaptic terminal (Fig. 1), followed by internalization and then retrograde transport of the neurotrophin-receptor complex to the neuronal cell

body (Fig. 2), where it can regulate neuronal differentiation and survival according to the traditional neurotrophin concept. Some neurotrophins (e.g., brain-derived neurotrophic factor) regulate the expression of neuropeptides (e.g., somatostatin and neuropeptide Y) in neurons. More recent discoveries, however, have now altered this concept. Neurotrophins can be transported away from the neuronal cell body down the axon, stored in nerve terminals, and then released

**Table II**  
Survival Peptides and Growth Factors for Neurons

Growth factor	Cellular sources	Responsive cell populations
Nerve growth factor (NGF)	Schwann cells, neurons in hippocampus, neocortex, olfactory bulb	Neurons in peripheral ganglia, basal forebrain magnocellular complex (BFMC), striatum
Ciliary neurotrophic factor (CNTF)	Schwann cells, astroglia	Peripheral ganglion neurons, motor neurons, hippocampal neurons, astroglia, oligodendroglia
Brain-derived neurotrophic factor (BDNF)	Neurons in neocortex, hippocampus, BFMC, striatum, hypothalamus, cerebellum	Neurons in peripheral ganglia, retina, BFMC, substantia nigra, cerebellum
Neurotrophin-3 (NT-3)	Neurons in hippocampus, cerebellum	Neurons in peripheral and enteric ganglia, hippocampus, cerebellum, motor neurons
Neurotrophin-4/5 (NT-4/5)	Neurons in neocortex, hippocampus, BFMC	Peripheral ganglion neurons, BFMC, motor neurons
Glial-cell-derived neurotrophic factor (GDNF)	Neurons in neocortex, hippocampus, striatum, peripheral ganglia, motor neurons, chromaffin cells, muscle	Peripheral ganglion neurons, motor neurons, substantia nigra neurons, cerebellar neurons
Insulin-like growth factor (IGF)	Schwann cells, muscle	Motor neurons, astroglia, oligodendroglia
Leukemia inhibitory factor (LIF)	Astroglia, microglia, Schwann cells	Peripheral ganglion neurons, spinal motor neurons, astroglia, oligodendroglia, microglia
Fibroblast growth factor (FGF)	Peripheral ganglion neurons, motor neurons, muscle	Peripheral ganglion neurons, motor neurons

presynaptically, thus functioning as afferent-derived (instead of target-derived) growth factors or neurotransmitters.

areas, whereas other cytokines (e.g., interleukin-1 $\alpha$ , interleukin-1 $\beta$ , and tumor necrosis factor- $\alpha$ ) are produced predominantly by activated microglia.

### C. Cytokines

Cytokines are a highly diverse group of extracellular signaling molecules that act as local mediators in cell-cell communication (Table III). These molecules are peptide hormones that regulate a wide variety of inflammatory and immune processes. Furthermore, they can function by modulating cellular responses to growth factors by either potentiating or antagonizing signals. Their activity is mediated by binding to specific, high-affinity cell surface receptors on target cells. The production of cytokines is triggered by an activation event, broadly including brain injury or infection. In the nervous system, cytokines are produced by glial cells (astrocytes, microglia, oligodendrocytes, and Schwann cells), and their cellular targets can be other glial cells and neurons. They can initiate, propagate, and suppress inflammatory and immune responses. Some cytokines that are synthesized by astrocytes (e.g., interleukin-1, interleukin-6, and granulocyte macrophage colony stimulating factor) participate in the recruitment of microglia into damaged

### D. Chemokines

Chemokines are small peptides or proteins that are members of a superfamily of inducible, secreted, proinflammatory cytokines that function as cellular chemoattractant signals (Table IV). These highly diverse inflammatory molecules are classified, according to the topology of cysteine residues, into four groups: C, C-C, C-X-C, and C-X<sub>3</sub>-C. The C subfamily lacks the first and third cysteine residues of the conserved motif, whereas the C-C subfamily members have the first two cysteines adjacent. In the C-X-C group, the first two of four cysteine residues are separated by a single amino acid, and in the C-X<sub>3</sub>-C group the first two cysteines are separated by three amino acid residues. By activating G-protein-coupled membrane receptors on their target cells, chemokines can signal cells to migrate to or remain at the site of chemokine production. An important example for chemokine activity is the governing of inflammatory cell accumulation during immune-mediated demyelination of axons.

**Table III**  
Cytokines<sup>a</sup>

Cytokine	Cellular sources	Functions
Tumor necrosis factor $\alpha$ (TNF- $\alpha$ )	Astroglia, microglia	Inflammation, cell death through necrosis or apoptosis
Fas ligand (FasL)	T-cells	Promote apoptosis
Interleukins	Astroglia, microglia, endothelial cells	Promote or suppress inflammation, modulate chemokine production, molecule specific (at least 15 interleukins have been identified)
Interferon- $\gamma$	T-cells	Antiviral activity, antiproliferation, immunomodulation, microglial activation
Transforming growth factor $\beta$ (TGF- $\beta$ )	Neurons, astroglia, microglia, Schwann cells	Regulate extracellular matrix and proliferation of astroglia and Schwann cells, suppress inflammation, modulate chemokine production
Leukemia inhibitory factor (LIF)	Astroglia, microglia, Schwann cells	Promote neuronal repair

<sup>a</sup>Represents a tabulation of only selected cytokines found in brain.

### III. NEUROACTIVE BRAIN PEPTIDES ARE MADE FROM PROTEIN PRECURSORS THAT UNDERGO PROTEOLYTIC PROCESSING

Neuroactive peptide hormones are generated from precursor proteins. Several different neuroactive peptides are usually encoded by a single continuous mRNA that is translated into a large, inactive protein precursor. Prior to translation, these mRNA transcripts can undergo alternative RNA splicing within the nucleus to generate different mature mRNAs that encode protein precursors with different amino acid sequences. These secretory proteins are formed in the cell bodies of neurons and nonneuronal cells on polyribosomes attached to the cytosolic surface of

the endoplasmic reticulum (Fig. 2). Neuroactive peptides or their precursors, like other secretory proteins, are processed in the endoplasmic reticulum and then shuttled to the Golgi apparatus for further processing (Fig. 2). The processing of larger precursor proteins occurs through specific, regulated proteolytic cleavage by serine proteases, thiol endopeptidases, amino peptidases, and carboxypeptidases. These cleavages are thought to begin in the *trans*-Golgi network, and they continue in the secretory vesicles. Proteins destined for secretory dense-core vesicles (Fig. 1) are packaged into appropriate vesicles in the Golgi apparatus by a sorting signal mechanism involving the selective aggregation of secretory proteins. The peptide-containing secretory vesicles leave the

**Table IV**  
Chemokines in the Brain<sup>a</sup>

Chemokine	Cellular expression	Functions
Macrophage inflammatory protein-1 (MIP1)	T-cells, monocytes, macrophages, platelets, astroglia, microglia	Attraction of T-cells, monocytes, basophils, eosinophils, natural killer cells
Monocyte chemoattractant protein-1 (MCP1)	Monocytes, macrophages, endothelial cells, astroglia	Attraction and activation of monocytes, lymphocytes, basophils
Interferon inducible protein-10 (IP10)	Astroglia	Attraction of T-cells
RANTES <sup>b</sup>	Astroglia, microglia, Schwann cells, endothelial cells	Monocyte chemoattraction, neuronal migration
Fractalkine	T-cells, endothelial cells, neurons, microglia	Suppression of inflammation and microglial activation

<sup>a</sup>Only selected cytokines are shown.

<sup>b</sup>RANTES: regulated upon activation, normal T-cell expressed and secreted.



*trans*-Golgi apparatus by a process involving clathrin-coated budding (Fig. 2). After the immature secretory vesicles bud from the Golgi apparatus, their contents undergo rapid and extreme condensation resulting from acidification of the vesicle lumen by the activity of a vesicle membrane ATP-driven  $H^+$  pump. In neurons, the mature vesicles are then moved to the presynaptic terminal (Fig. 1) by fast axonal transport. This traveling along the axon occurs by kinesin motor proteins attached to the surface of the secretory vesicle that propel them along microtubules. The release of the peptide-containing vesicle at the axon terminal occurs by exocytosis in response to a depolarization-induced local increase in intracellular  $Ca^{2+}$ .

#### IV. BRAIN PEPTIDES AND HORMONES ACT AT CELL MEMBRANE RECEPTORS

The signal transduction mechanisms through which most neuroactive brain peptides operate involve G-protein-linked receptors or enzyme-linked receptors. Most classical neuroactive peptides (Table I, e.g., substance P-neurokinins, somatostatin, neurotensin, opioid pentapeptides, vasopressin, and angiotensin) and some cytokine peptides (interleukin-8) are ligands for G-protein-linked receptors. These receptors activate a chain of events that alters the concentration of one or more small, intracellular, second messenger signaling molecules that, in turn, amplify the signal and pass it on by altering the functioning of specific proteins. Two of the most widely used second messengers for classical neuroactive peptides are  $Ca^{2+}$  and cyclic adenosine monophosphate (AMP). The effects of somatostatin, vasopressin, and adrenocorticotrophic hormone are mediated by cyclic AMP.

In contrast, enzyme-linked receptors function directly as enzymes or as receptor-associated enzymes when activated. Neuropeptides, growth factors, cytokines, and chemokines can operate through one of five known classes of enzyme-linked receptors, including the following: (1) receptor guanylyl cyclases that catalyze the production of cyclic guanosine monophosphate (GMP) in the cytosol; (2) receptor tyrosine kinases that phosphorylate specific tyrosine residues on a small set of signaling proteins; (3) tyrosine-kinase-associated receptors that interact with proteins that have tyrosine kinase activity; (4) receptor tyrosine phosphatases that remove phosphate groups (dephosphorylate) from tyrosine residues of signaling proteins; and (5) receptor serine-threonine kinases that phosphorylate serine or threonine residues in specific proteins.

#### V. BRAIN PEPTIDES PROVIDE A BIOCHEMICAL FINGERPRINT FOR MANY BRAIN REGIONS AND REVEAL NEW FEATURES ABOUT THE PARCELING OF THE BRAIN

Very important and novel information about the nervous system has been obtained by charting the location of brain peptides (Figs. 4–7). Generally, these data are gleaned immunocytochemically by using highly specific antibodies that recognize unique amino acid sequences in brain peptides and proteins. Such experiments can provide critical information on the brain regions that contain peptides–proteins and their detailed cellular and subcellular localizations in experimental animal and post mortem human brain and spinal cord tissues. Over the past two decades, exciting results on brain peptides have been obtained that feature how the brains of humans and animals are organized, how they function, and how they are changed in abnormal conditions. Many prominent examples can be provided about how the charting of brain peptides reveals novel information on brain organization and the abnormalities in brain peptides that occur in experimental animals with profound neurobehavioral disorders. Two forebrain regions, the amygdala–bed nucleus complex and the striatum, provide informative examples.

##### A. The Amygdala–Bed Nucleus of the Stria Terminalis (BST) Complex

By studying the chemical neuroanatomy of the basal forebrain of humans and monkeys, it was discovered that the bed nucleus of the stria terminalis (BST) and the amygdala form a large, multidivisional complex (Figs. 4 and 5). This complex has been also called the extended amygdala by other investigators. The BST is continuous with the central and medial divisions of the amygdala through the ventral forebrain substantia innominata, and it intermingles with the nucleus basalis of Meynert of the basal forebrain magnocellular complex. The amygdala–BST continuum is a hotbed of neuropeptides, including somatostatin, enkephalins, substance P, neurotensin, cholecystikinin, vasoactive intestinal peptide, and galanin (Figs. 4 and 5). Specific chemically delineated zones and cellular compartments contain these brain peptides. The locations of these brain peptides reveal that the amygdala–BST complex is a very prominent and discretely compartmental structure in the basal

forebrain of humans and monkeys (Figs. 4 and 5). On the basis of neuropeptide distribution and cytology, this complex can be divided into at least 10 subdivisions. Furthermore, both subtle and dramatic differences in brain peptides are found in the amygdala–BST complex in different species, with humans having unique patterns that differ from those of animals.

Prominent gender differences (sexual dimorphisms) occur in the BST of humans and experimental animals. In humans, some divisions of BST are ~2.5 larger in the male brain than in the female brain. Major differences in the neuropeptide composition of the BST occur as well. These differences are thought to be caused by gonadal steroid hormones and also by glial-cell-derived peptide growth factors and cytokines such

as transforming growth factor- $\beta$ . Neurons of the BST and centromedial amygdala are among the chief testosterone- and estradiol-concentrating cells in animal brains. The sexual differentiation of the human brain takes place much later than originally believed, suggesting that, in addition to genetic factors, environmental and psychosocial factors may have ample opportunity to exert a profound influence on the sexual differentiation of the brain. This information is important because it could have implications for the determination of sexual orientation, and the BST is known to participate in sexually dimorphic functions, including aggressive behavior, sexual behavior, and feeding behavior. Furthermore, a relatively well-identified role of the amygdala–BST complex is the mediation of stress, fear, and anxiety responses, which

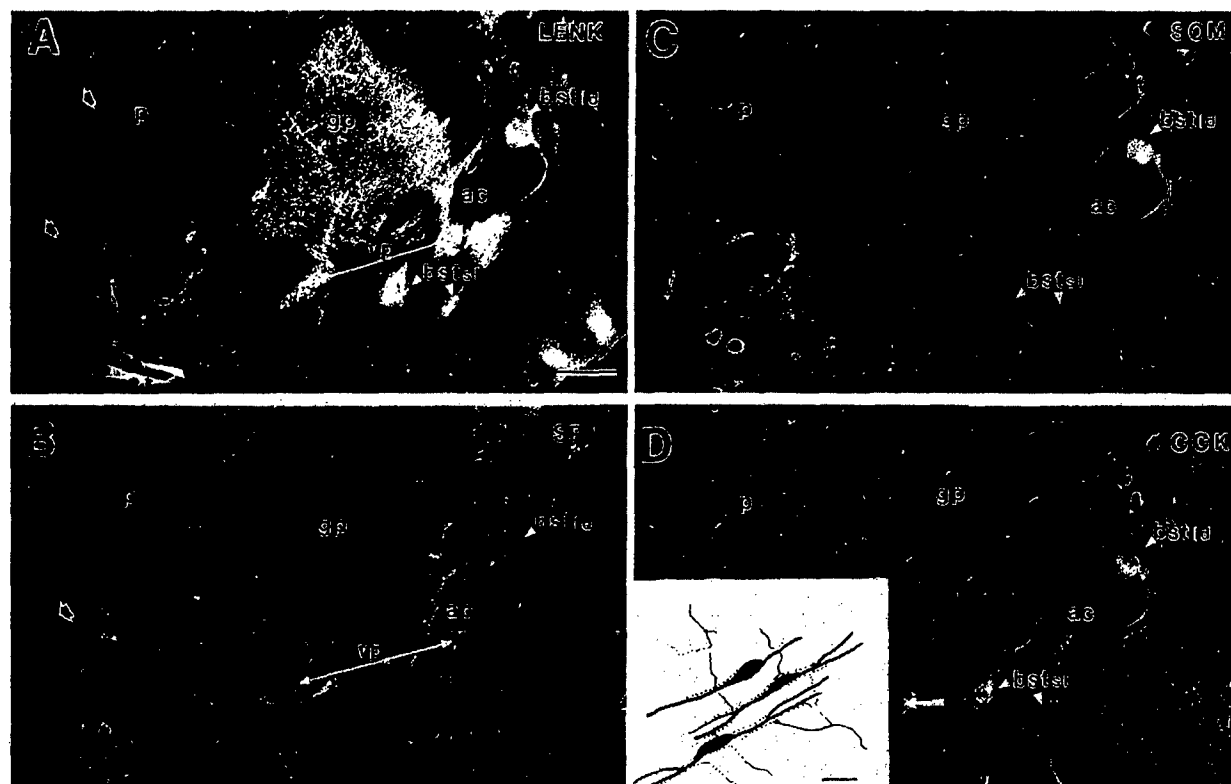


**Figure 4** Neuropeptides delineate the compartments within in the basal forebrain and basal ganglia of humans. Antibodies were used to identify leucine-enkephalin (LENK, A), substance P (SP, B), somatostatin (SOM, C), and cholecystikinin (CCK, D) in postmortem human brain sections. Abbreviations: ac, anterior commissure; bstld, bed nucleus of the stria terminalis, lateral dorsal division; bstsl, bed nucleus of the stria terminalis, subnucleus division; gp, globus pallidus; p, putamen; vp, ventral pallidum. White areas represent neuropeptide immunoreactivity. The globus pallidus, its ventral extension (the ventral pallidum), and the bed nucleus are enriched in enkephalin. The striatal mosaic in the putamen (A, white, open, arrowheads) can be identified by enkephalin. The bed nucleus and its subnucleus extension are clearly divisible from the globus pallidus and the ventral pallidum by the presents of somatostatin and cholecystikinin. Somatostatin and cholecystikinin specifically mark the subnucleus division of the BST, so that it can be distinguished from the ventral pallidum. The inset (D) shows the typical distributions of LENK, SOM, and CCK in the BST subnucleus. These neuropeptides are highly concentrated in many nerve terminals (small dots) that innervate neuronal cell bodies and dendrites that form the cellular columns that bridge the BST and amygdala in the human basal forebrain. Scale bars = 2.5 mm (A, same for B–D) and 40  $\mu$ m (inset).

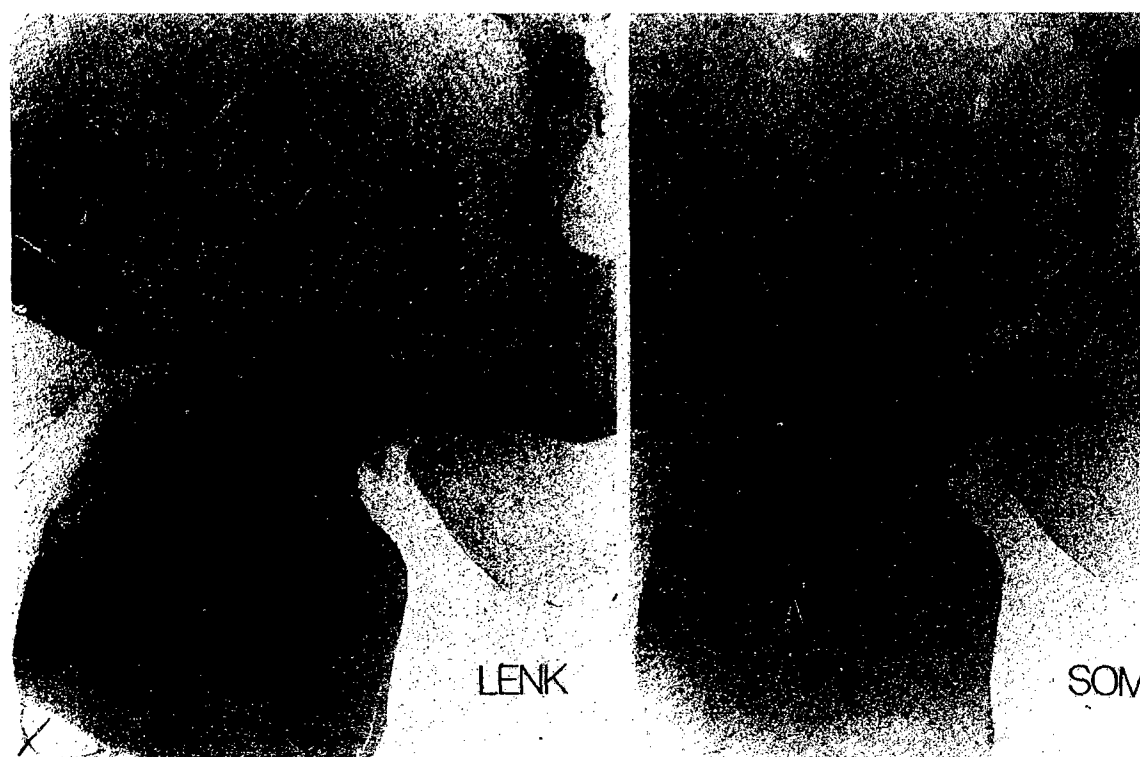


**Figure 5** Neuropeptides delineate the amygdala-bed nucleus complex within in the basal forebrain of nonhuman primates. Antibodies were used to identify leucine-enkephalin (LENK, left panel) and somatostatin (SOM, right panel) in brain sections of rhesus monkeys. Abbreviations: A, amygdala; A-Bst, amygdala-bed nucleus continuum; Bst, bed nucleus of the stria terminalis; GP, globus pallidus; H, hypothalamus; P, putamen. Black areas represent neuropeptide immunoreactivity. The amygdala-bed nucleus continuum and the globus pallidus are both enriched in enkephalin. The amygdala-bed nucleus complex is specifically identified by the high concentration of somatostatin. Scale bar = 1.3 mm.

are likely to be regulated by brain peptides such as corticotrophin-releasing hormone.

### B. The Striatal Mosaic

The basal ganglia are subcortical brain regions that function in sensory-motor integration, planning and initiation of somatic movements, cognition, and some types of social-emotional and species-typical behaviors. The striatum (caudate nucleus, putamen, and nucleus accumbens), globus pallidus (external and internal divisions and ventral pallidum), substantia nigra (pars compacta and reticulata), and subthalamic nucleus are the major components of the basal ganglia (Figs. 6 and 7). The striatum is divisible into at least two primary compartments designated as striosomes (patches) and matrix (Figs. 6 and 7). This forebrain region, thus, is like a jigsaw puzzle because it has different pieces that fit together, comprising a structure called the striatal mosaic. Neurons within striosomes

and matrix differ with respect to their time of embryogenesis, connections with other brain regions, and expression of brain peptides. Striosomes are much more enriched in substance P and enkephalins than the striatal matrix, whereas the matrix is more enriched in somatostatin and neuropeptide Y than the striosomes. These general neuropeptide patterns change when comparing the dorsal striatum (caudate and putamen) with the ventral striatum (nucleus accumbens) (Figs. 6 and 7).

An important relationship exists between the regulation of gene expression for brain peptides within neurons of the striatal mosaic and the expression of excitatory glutamate receptors. Inputs into the striatum participate in the steady-state regulation of peptide expression in medium-spiny, striatal neurons, which are the principal neurons of the striatum. For example, ablation of corticostriatal projections reduces preprotachykinin and preproenkephalin mRNA in neurons of rodent striatum. Synaptic activity and membrane depolarization regulate neural gene

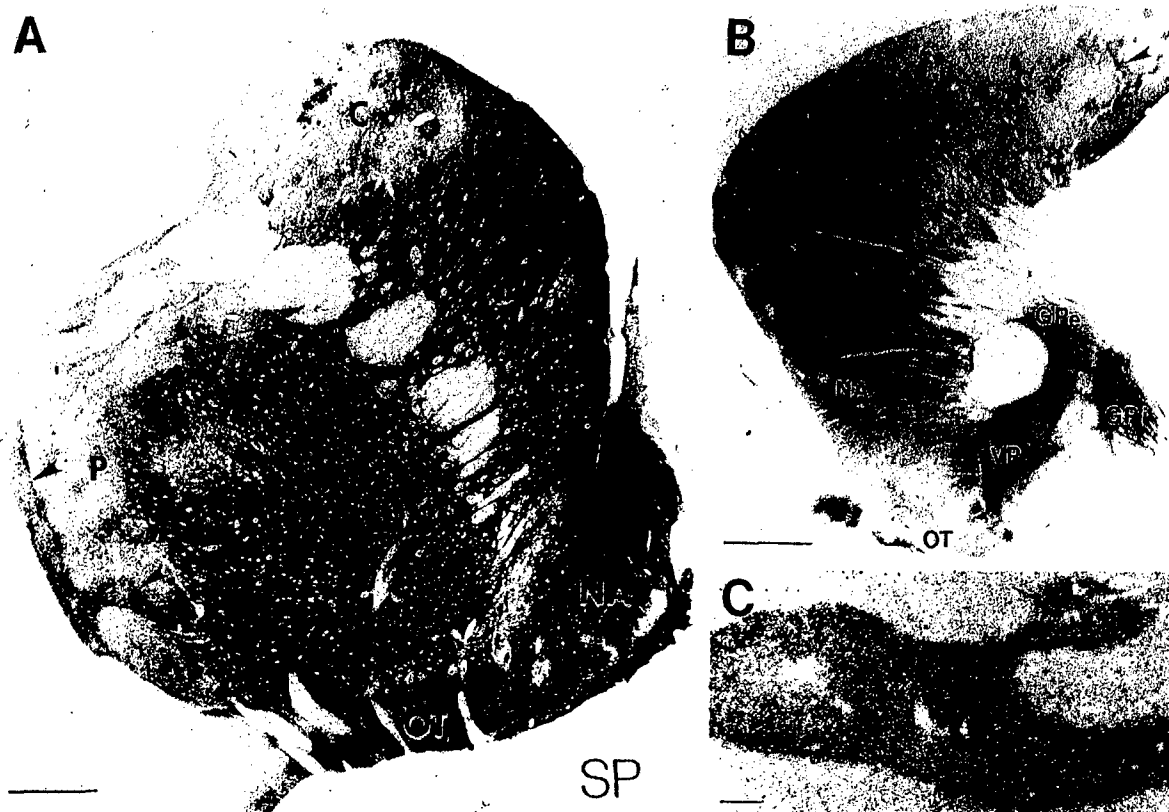


**Figure 6** The localization of substance P reveals that the striatum is a mosaic and extends to the ventral surface of the brain. Antibodies were used to identify substance P in brain sections of rhesus monkeys. Shown are photographs of striatum in the transverse (A) and parasagittal (B) planes and a higher magnification view of a striosome (C). Abbreviations: C, caudate nucleus; GPe, globus pallidus external part; GPi, globus pallidus internal part; NA, nucleus accumbens; OT, olfactory tubercle; VP, ventral pallidum. Black-gray areas represent neuropeptide immunoreactivity. These photographs illustrate the discrete topography and heterogeneity of the striosome (A and B, black arrowheads) and matrix compartments throughout the dorsal striatum (caudate nucleus and putamen) and the ventral striatum (nucleus accumbens and olfactory tubercle). The chemical organization of striosomes is different in the dorsal striatum from the ventral striatum. In the caudate and putamen, striosomes are enriched in substance P or they have a ring (dark) and hollow (pale) pattern compared to the surrounding matrix. The more uniform striosomes contain numerous neurons with substance P (C, small black arrowheads) that are embedded in a dense plexus of nerve terminals containing substance P. In the nucleus accumbens, striosomes are poor in substance P compared to the surrounding matrix (B). Scale bars = 1.7 mm (A), 2.2 mm (B) and 130  $\mu$ m (C).

expression, possibly through a  $\text{Ca}^{2+}$ -dependent mechanism that may involve calmodulin. Striatal neurons are enriched in calmodulin. Thus, excitatory glutamatergic neurotransmission may directly regulate, in an activity-dependent manner, neuropeptide expression within subsets of striatal neurons. Support for this idea is derived from our studies showing that glutamate receptors are expressed by substance P- and enkephalin-containing neurons within striosomes. This enrichment of glutamate receptors at postsynaptic sites within striosomes of the dorsal striatum may reflect a more dominant glutamatergic regulatory control of neuropeptide expression within striosomal neurons than within matrix neurons. An informative example in this regard is provided by striatal dopamine

receptors. Dopamine receptors regulate the relative levels of expression of opiate and tachykinin peptides in subsets of striatal neurons through cyclic AMP, protein kinase A, and cyclic AMP response-element-binding protein. Several genes for striatal neuropeptides contain cyclic AMP response elements, including dynorphin, enkephalin, and somatostatin. Although the activation of different molecular subtypes of glutamate receptors may engage signal transduction pathways for neuropeptide gene expression in striatal neurons, the intracellular signaling pathways have not been identified completely.

For many years, the neuropeptide organization of the forebrain in normal monkeys and humans has been studied, thereby laying a foundation for concepts

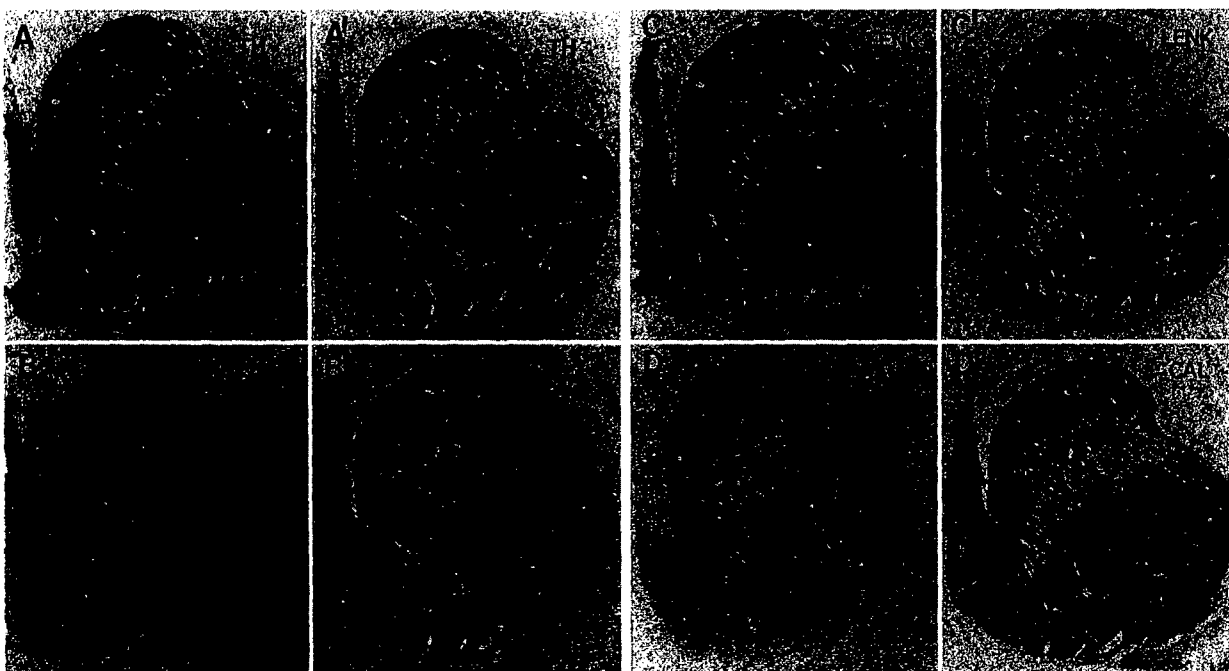


**Figure 7** The primate striatum undergoes prominent remodeling of its chemical structure after birth. Antibodies were used to identify tyrosine hydroxylase (TH, a marker of dopamine innervation of the striatum), substance P (SP), leucine-enkephalin (LENK), and the calcium-binding protein calbindin (CAL, a striatal matrix marker) in brain sections of rhesus monkeys. The left image of each pair (A–D) shows the relative amounts and distributions of these striatal peptides–proteins in a monkey 4 months of age. The right images (A'–D') show the same chemicals in the striatum of an adult monkey. In each pair, the caudate nucleus is on the left and the putamen is on the right. (A, A') The dopaminergic innervation of the striatum is not fully established at 4 months of age, nor is the adultlike striosome–matrix organization. In the infant, the striosomes are slightly more enriched in dopaminergic innervation than the surrounding matrix. The reverse pattern is present in adults. (B, B') The substance P pattern at 4 months is immature compared to the adult, but the differences appear to be of degree (intensity) and not in basic pattern (like TH). The caudate nucleus in the infant and adult has numerous striosomes enriched in substance P; however, striosomes in the infant putamen are less developed than the striosomes in the adult putamen. Furthermore, the matrix in the infant caudate and putamen is deficient in substance P compared to adult. Furthermore, the ventral striatum (the nucleus accumbens and olfactory tubercle) has not yet attained adultlike levels of substance P. (C, C') The distribution and relative amount of enkephalin in the infant striatum are very different from those found in adults. In the 4-month-old monkey, the caudate nucleus has striosomes that are poor in enkephalin and a matrix that is enriched in enkephalin. The reverse pattern is present in the caudate nucleus in adults. (D, D') The distributions of calbindin in the infant striatum and adult striatum also differ. At both ages the striosomes have less calbindin relative to the matrix; however, in the infant, the striosomes are essentially devoid of calbindin compared to those in the adult, and the infant striosomes are much larger. In the infant putamen (lateral region), the level of calbindin is deficient compared to that in the adult.

about areas of the brain that could be selectively vulnerable to environmental conditions and experiences in early life. We have put forth a hypothesis that neuropeptide transmitter systems in the striatum of infant rhesus monkeys undergo prolonged postnatal maturation, which may render this brain region highly vulnerable to environmental and experiential influences. So far, our studies of developing rhesus monkeys have revealed that peptide neurotransmitters undergo remarkable remodeling during the first year of postnatal life (Fig. 7). Many brain peptides in the striatal mosaic are present in early stages of life, but they need time to develop their proper distributions, amounts, and roles (Fig. 7).

It was hypothesized that an insufficient social environment for infant monkeys might interfere with the development of neurotransmitters in the basal ganglia, because animals raised under such conditions have abnormal movements and social behaviors. The brains of two groups of monkeys with different environmental rearing conditions have been studied: one group of monkeys that experienced social deprivation when they were infants and had many abnormal behaviors, and another group of monkeys that was raised in a highly social environment and behaved like normal monkeys.

It was discovered that the development of the structural organization of peptide neurotransmitter

systems of the basal ganglia is highly vulnerable to early postnatal experience. The normal compartmental arrangements of brain peptides of the major output striatal neurons and the localization of neuropeptides within synaptic targets of the striatum (globus pallidus and substantia nigra) are altered selectively in adult rhesus monkeys that experienced severe sensory-social deprivation during the first year of infancy (Fig. 8). Immature rhesus monkeys that have insufficient infant-mother and infant-peer interactions during early development manifest psychosocial abnormalities and motor impairments, including withdrawal and fearfulness, lack of play, apathy, learning deficits, stereotypic movements, and self-injurious behavior. Furthermore, as adults, these monkeys do not show appropriate parental behavior and are indifferent and abusive to their offspring. Certain brain areas are more vulnerable to the effects of social deprivation than other brain regions. Surprisingly, the neuropeptides in the amygdala-BST complex (Fig. 5) did not appear vulnerable, but the same neuropeptides were profoundly vulnerable in the striatal mosaic (Fig. 8). Because monkeys that experienced social-sensory deprivation have neurochemical alterations in their basal ganglia, and because the behavioral dysfunction induced by social-sensory deprivation of infant primates persists into adulthood and suggests functional abnormalities of the basal ganglia, it has been suggested that the normal postnatal development of peptide neurotransmitter systems in the basal ganglia, particularly the neostriatum, is partly dictated by the environment and experience.

These results were very novel and interesting because they showed, for the first time in a well-controlled experiment, that social deprivation can produce changes in brain chemistry in selectively vulnerable regions in animals that have brains very similar in many respects to the human brain. These changes may underlie the abnormal social, repetitive, and self-harmful behaviors of these monkeys, and they may be related to similar abnormal behaviors of children with developmental problems. Certain peptide neurotransmitters in the striatal mosaic and other basal ganglia areas of monkeys raised with insufficient social contacts do not develop and mature like they do in socially raised monkeys. Some of these altered neurotransmitters have important functions in signaling aversive messages. These findings are important because these animals, as well as children with some developmental disorders, can harm themselves. These experiments are also exciting because similar numbers of neurons are present in both groups of monkeys (i.e.,

they do not degenerate or die), although some neurons are unable to make the appropriate neurotransmitter. Lithium can increase the expression of enkephalin and substance P in neurons of the striatum of rats. Because the neurons appear to be still alive in these monkeys, they could be stimulated by drugs so that they can make their normal neurotransmitter, thereby possibly modifying the abnormal behaviors of these monkeys.

This seminal study by Martin and colleagues explored important relationships between the early experience of infants, the postnatal maturation of the brain, and the susceptibility of some neurotransmitters in certain brain areas to environmental factors. There are growing concerns about the long-term effects of parental-peer neglect or abuse and exposure to drugs or environmental toxins in early childhood on the development of brain structure and function. As a result of this study, it is now known that the basal ganglia is very vulnerable in infants. The implications may be profound. For example, environmental factors (social-sensory deprivation of varying severity) can interfere with the normal postnatal progression of brain peptides and other neurotransmitters in the maturing basal ganglia. However, the specific events producing these changes are not clear, and considerably more work is needed on how external or environmental experiences can turn on and off vulnerable genes in immature neurons of the brain. The normal maturational events that occur with neuropeptides in the basal ganglia of primates during postnatal development must be understood more completely before this theory of experience-dependent neurodevelopment of the basal ganglia can be clarified and before the possible cellular and molecular mechanisms responsible for the mutability of basal ganglia organization by early postnatal experience can be understood.

Several disorders that affect young people are characterized by abnormal conduct such as repetitive or stereotyped movements, poor skills in communication, self-preoccupation or withdrawal from family and society, and self-inflicted harm. Children with mental retardation and autism, Rett syndrome, and Lesch-Nyhan syndrome show some or all of these abnormal behaviors. In the United States, it was estimated that 160,000 young individuals with developmental disabilities exhibited harmful behaviors involving aggression toward themselves, other people, and property. The self-harmful behaviors of people with these disorders are primary reasons for institutionalization, failure in school environments,

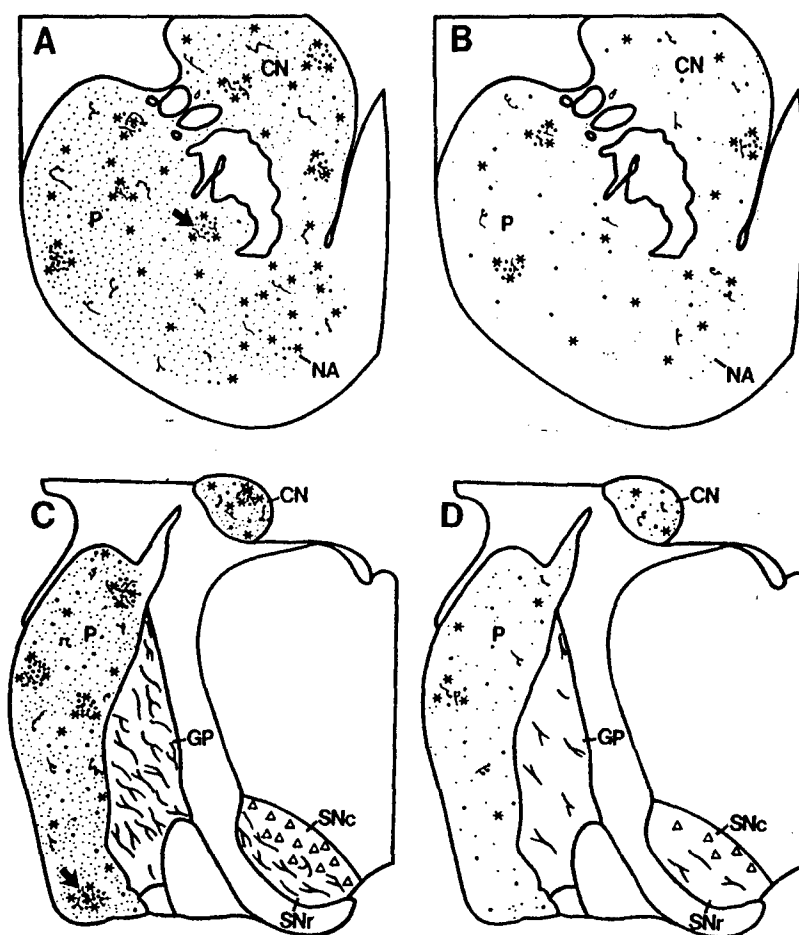


**Figure 8** The chemical composition and structural organization of the primate basal ganglia are highly vulnerable to early postnatal experiences and environmental conditions. This diagram depicts some of the organizational features of the primate basal ganglia in monkeys raised in a socially healthy environment and their changes in monkeys raised in an inappropriate social environment. Abbreviations: CN, caudate nucleus; GP, globus pallidus; P, putamen; SNc, substantia nigra compact part; SNr, substantia nigra reticular part. In normal rhesus monkeys (A and C), substance-P-containing neurons (asterisks), processes (short, beaded lines), and axonal terminals (solid circles) are concentrated in some foci forming discrete patches (striosomes, black arrow) in the caudate and putamen. Striosomes are also enriched in enkephalin. The neuronal elements that comprise striosomes are found in lower amounts and diffuse throughout the surrounding matrix (the compartment that makes up the majority of the striatum). The nucleus accumbens has a matrix very enriched in substance P and enkephalin. The striatum receives an extensive synaptic terminal innervation (fine, small dots) from dopamine-utilizing neurons in the substantia nigra compact part (triangles). The neurons in the striatum that contain substance P and enkephalin innervate the globus pallidus and substantia nigra reticular part (smooth, branching lines). In monkeys that were raised in a socially inadequate environment (B and D), this organization of the basal ganglia is abnormal. These monkeys have fewer striosomes, they have less substance P and enkephalin in the matrix, and the dopamine innervation from the substantia nigra is deficient in the striatum. Also, striatal target regions (e.g., the globus pallidus and substantia nigra reticular part) are deficient in substance P and enkephalin due to the loss of innervation from substance-P- and enkephalin-expressing striatal neurons. The ability of neurons in the substantia nigra to make dopamine is impaired, although the neurons remain. [Reproduced with permission from *J. Neurosci.* 11(11), 3344–3358, 1991, copyright the Society for Neuroscience].

and improper adjustment in communities. In some communities, 6–21 individuals out of 100 people have behavioral and emotional disorders, with a tendency for higher numbers in groups subject to social deprivation. The causes of these behavioral problems are unknown, although animal model experiments suggest a likely connection with brain peptides.

## VI. ABNORMALITIES IN BRAIN PEPTIDES OCCUR IN BEHAVIORAL, PSYCHIATRIC, AND NEURODEGENERATIVE DISORDERS OF HUMANS

The participation of brain peptide neurotransmitters, cytokines, and growth factors in many forms of

behavioral and neurological disorders is now very evident (Tables V and VI). The most widely studied disorders in which brain peptides have been implicated are schizophrenia, mood disorders, Huntington's disease, Alzheimer's disease, and multiple sclerosis.

In schizophrenia, cholecystokinin neuronal systems seem to be the most vulnerable by some reports and are prominently depleted in the temporal cortex and hippocampus. Somatostatin, vasoactive intestinal peptide, substance P, neurotensin, and thyrotropin-releasing hormone have been reported to be abnormal in cerebral cortex, amygdala, and basal ganglia. Some of these findings have not been replicated. It is also very possible that ongoing drug treatment of patients diagnosed with schizophrenia will confound observations on brain peptide levels.

In depression, the hypothalamic-pituitary-adrenal axis and the hypothalamic-pituitary-thyroid axis have been examined thoroughly. It is believed that corticotropin-releasing hormone and thyrotropin-releasing hormone are hypersecreted in individuals with major depression. Furthermore, prodynorphin mRNA expression is elevated in the striosomal compartment of the striatal mosaic in individuals that commit suicide. Thus, dysfunction of the endogenous opioid dynorphin system might contribute to depression and the risk of suicide.

In neurodegenerative diseases, the major brain areas affected by the disease process tend to exhibit changes in neuropeptide systems. In Huntington's disease, substance-P- and enkephalin-containing neurons are lost in the striatum. Neurons in neocortex that contain neuropeptides are depleted in Alzheimer's disease,

**Table V**  
**Behavioral, Psychiatric, and Neurological Disorders Involving Brain Peptides**

Abnormality	Possible brain peptides involved
Stress-anxiety	Corticotropin-releasing hormone
Obesity	Neuropeptide Y
Anorexia-cachexia	Orexins, tumor necrosis factor- $\alpha$ , interleukins, leukemia inhibitory factor, ciliary neurotrophic factor
Sleep disorders	Orexins
Epilepsy	Substance P, somatostatin, galanin, neuropeptide Y
Migraine headache	Calcitonin gene-related peptide
Schizophrenia	Cholecystokinin
Mood disorders	Corticotropin-releasing hormone, thyrotropin-releasing hormone, dynorphin

**Table VI**  
**Neurodegenerative Disorders Involving Brain Peptides**

Disorder	Brain peptide groups involved
AIDS dementia	Classical neuropeptides, cytokines, chemokines
Alzheimer's disease	Classical neuropeptides, growth factors, cytokines, chemokines
Amyotrophic lateral sclerosis	Growth factors, cytokines
Cerebral ischemia (cardiac arrest and stroke)	Growth factors, cytokines
CNS trauma	Growth factors, cytokines, chemokines
Multiple sclerosis	Cytokines, chemokines
Parkinson's disease	Growth factors

with somatostatin and corticotropin-releasing hormone showing high vulnerability. In neurodegenerative diseases of the human CNS that have prominent inflammatory components, such as multiple sclerosis, Alzheimer's disease, and AIDS, the proinflammatory cytokine tumor necrosis factor- $\alpha$  is up-regulated. Thus, brain and spinal cord inflammation and autoimmune reactions participate in the nervous system degeneration in these diseases. This idea is greatly emphasized by the finding that nonsteroidal anti-inflammatory drugs (such as aspirin, ibuprofen, and indomethacin) strongly protect against Alzheimer's disease.

The observation that anti-inflammatory drugs are helpful in Alzheimer's disease could be related to the discovery that astroglia and microglia are primary generators of amyloid deposits in the aging brain. Amyloid (A $\beta$ ) is a protein fragment fibril made up of a 4-kDa peptide consisting of 40–42 amino acid residues that is derived proteolytically from the amyloid precursor protein. A $\beta$  is a major component of senile plaques, which are brain lesions that occur in individuals with Alzheimer's disease, Down's syndrome, and, less frequently, people aging normally. In addition to A $\beta$ , these lesions have a complex composition, consisting of dystrophic neurites (damaged and swollen dendrites or axon terminals) and activated astrocytes and microglia. Our studies of aging monkeys revealed that senile plaques are dynamic brain lesions that evolve from early synaptic defects within the neuropil to mature plaques and extracellular deposits of A $\beta$ . The staging of these lesions is thought to be the degeneration of neuritic structures, followed by the attraction of reactive glia, and the subsequent deposition of extracellular A $\beta$  derived from microglia or



astrocytes. These experiments demonstrated that structural and biochemical perturbations within neuronal and nonneuronal cells occur before the deposition of extracellular A $\beta$  fibrils. Furthermore, our results suggest that focal abnormalities in synaptic contacts within the neuropil (synaptic disjunction) may initiate a complex series of inflammatory events resulting in the formation of diffuse senile plaques and deposits of A $\beta$ . In response to synaptic disjunction in the aged brain, astroglia and microglia produce A $\beta$ . This event may be signaled by cytokines.

## VII. BRAIN PEPTIDES MODULATE NEURONAL DEGENERATION AND REGENERATION IN EXPERIMENTAL MODELS

Classical neuropeptides as well as brain peptide growth factors and cytokines play important roles in neuronal degeneration and brain repair. It is now very evident that numerous small, diffusible peptide-protein factors modulate the growth, differentiation, survival, proliferation, and migration of neurons and/or glial cells. In the developing nervous system, neuronal death occurs normally and is thought to be necessary for regulating the size of neuronal groups in relation to target size and synaptic inputs. This developmental neuronal death is thought to be partially controlled by growth factors, including the conventional neurotrophic factors (Table II), as well as by some of the classical neuropeptides (Table I, e.g., somatostatin and vasoactive intestinal peptide). After brain and spinal cord injury, many cellular and molecular responses occur simultaneously or in phases, some of which are degenerative and others regenerative events. The vague concept for the release of tissue-soluble factors that may play a role in the degeneration, regeneration, and survival of nerve cells was introduced in the early 1900s by Santiago Ramón y Cajal. Subsequently, Levi-Montalcini, Hamburger, Prestige, and others established this concept. Many of the current ideas about the critical dependence of neurons on survival molecules or trophic factors (Table II) have been developed from experiments of cultured neurons and injured motor neurons *in vivo*.

### A. Cell Culture Models

When neurons are removed from the developing nervous system, they require survival factors to grow

in a dish. Some of these neuronal survival factors are neuroactive peptides and proteins (Tables I and II). Immature sympathetic ganglion neurons, cerebellar granule neurons, and cortical and hippocampal neurons are used commonly for culture experiments. The classical example for this concept is the survival of sympathetic ganglion neurons being dependent on serum factors such as nerve growth factor. When these cells are deprived of serum or nerve growth factor, they undergo apoptosis by a programmed cell death (PCD) mechanism that is dependent on specific cell death molecules. Bax and caspase-3 are critical for neuronal death by apoptosis, involving Bax translocation to mitochondria and mitochondrial release of cytochrome *c* to participate in the activation of caspase-3, which subsequently activates proteins including DNA fragmentation factor-45 that cleave genomic DNA. Nerve growth factor also controls sympathetic neuron survival by Ras suppression of a p53-mediated cell death pathway. Serum or potassium deprivation of cerebellar granule neurons and cortical neurons also results in apoptosis. Roles for neuropeptides in neuronal survival pathways have come to light. Apoptosis of granule neurons *in vitro* can be delayed by angiotensins II and IV, and angiotensinogen knockout mice have fewer granule neurons in the cerebellum and hippocampus than wildtype-mice, suggesting that the renin-angiotensin system has a role in neuronal survival by preventing apoptosis during the period of developmental cell death. In addition, pituitary adenylate cyclase activating polypeptide can block apoptosis of sympathetic ganglion and granule neurons by activation of the extracellular signal-regulated (ERK) type of MAP kinase via a cyclic-AMP-dependent pathway and proteasome-mediated degradation of caspase-3.

### B. Animal Models

In animal models of spinal cord and nerve injury, brain peptide hormones, growth factors, and cytokines can be studied for their roles in degeneration and for their applicability for therapeutics. The extent of neuronal death or of regeneration and survival after spinal cord injury is influenced by the age of the animal at the time of injury and the location of axonal trauma in relation to motor neurons. Motor neurons with axonal damage in the immature CNS die rapidly. In contrast, in some settings, axotomized motor neurons in the adult CNS are more likely to persist in some altered form. This observation

could have major importance with regard to the recovery of neurological function in infants, children, and adults.

Cytokines (Table III) have stimulated much excitement in the pathobiology of spinal cord and peripheral nerve injury. A cytokine called leukemia inhibitory factor might be important for the successful regeneration of injured sensory and motor axons in immature and adult animals by altering neuronal gene expression. Other molecules that may be relevant to neuronal degeneration and regeneration after spinal cord and peripheral nerve injury are inflammatory factors. Tissue inflammation is believed to be a critical component of the degenerative process after nervous system injury. Following CNS damage, a variety of changes occur, including the extravasation of serum proteins through the compromised blood-brain barrier, activation of neuroglial cells, and rapid synthesis and liberation of proinflammatory cytokines. A major proinflammatory cytokine in the CNS is tumor necrosis factor- $\alpha$ , which promotes inflammation and cell death through its p55 receptor. Tumor necrosis factor- $\alpha$  also promotes cell death by inhibiting receptor signals initiated by key survival peptides such as insulin-like growth factor. Thus, brain peptide cytokines can interact antagonistically or synergistically with brain peptide growth factors. Interestingly, the remarkable anti-inflammatory and antipyretic actions of  $\alpha$ -melanocyte-stimulating hormone occur by inhibition of glial-derived tumor necrosis factor- $\alpha$ . Other cytokines function as potent anti-inflammatory factors. Interleukin-10 reduces the production of tumor necrosis factor- $\alpha$  by astroglia. Interleukin-10 reduces inflammation and improves functional outcome in humans and in animal models of spinal cord injury. In contrast, interleukin-3 appears to cause spinal cord damage. Overexpression of interleukin-3 in mice leads to motor neuron degeneration and progressive muscular atrophy, suggesting that an autoimmune reaction may participate in the degenerative process in humans with amyotrophic lateral sclerosis.

### VIII. THE FUTURE OF CNS PEPTIDE RESEARCH HAS GREAT PROMISE

The use of animal models will be necessary to advance our understanding of brain peptide function and their roles in nervous system development, maturation, degeneration, and repair. An interesting feature of the different classical neuropeptide systems is that many of

these brain peptides undergo prominent changes during development (Fig. 7). However, it is not yet clear whether these changes direct maturational events involved in the pattern formation of brain structure or whether changes in the expression are consequences of brain maturation. For example, brain peptides and hormones may be critical for pattern formation during development of the cerebral cortex and striatum, and abnormalities may cause neurodevelopmental defects. With regard to CNS degeneration, paradigms should include animal models of brain and spinal cord injury and aging. Animal models of CNS degeneration are crucial for improving our understanding of the mechanisms and stages of degenerative and repair processes. These models can provide an *in vivo* system to identify how neurons and neuroglia change in paradigms that mirror certain neuropathological and clinical features of neurological conditions that occur in humans (Table VI). With animal models, the process of nervous system degeneration and repair can be studied directly at the structural and molecular levels, the roles for brain peptides and hormones can be identified, and the model subsequently can be used to test new therapies to prevent the neuropathology and improve neurologic recovery in a biologically relevant system. In addition, the application of molecular genetics and transgenic mouse technology will be essential. The development of transgenic mouse systems for peptide growth factors and cytokines should be expanded.

Pharmaceutical drug development centering around neuroactive brain peptides holds immense promise for the future treatment of a wide range of neurobehavioral, neurological, and neurodegenerative disorders (Tables V and VI). For example, the design of drugs that mimic the actions of satiety neuropeptides could be useful for weight management in obesity or blocking the functions of brain satiety peptides for the treatment of anorexia or cachexia in chronically or terminally ill patients. The neuropeptides that function in sleep-wakefulness could be targets for sleep disorders. The anti-inflammatory actions of certain cytokines and the blockade of proinflammatory cytokines could be exploited for the treatment of Alzheimer's disease, multiple sclerosis, head and spinal cord injury, and cerebral ischemia after stroke and cardiac arrest. Furthermore, the well-known neuronal survival actions of neurotrophins should continue to be targets for drug discovery as well as the neuronal survival effects of classical and more recently identified brain peptides. The application of research on survival peptides has enormous potential for the treatment of

Alzheimer's disease, Parkinson's disease, amyotrophic lateral sclerosis, and cerebral ischemia, and CNS trauma (Table VI).

The current inability to effectively and rationally help people with nervous system abnormalities is in large part due to the lack of understanding of how neurons communicate with other neurons and how neurons communicate with neuroglia or other non-neuronal cells. It is very likely that future discoveries in brain peptides and hormones will add to the formulation of new therapies for humans with neurobehavioral disorders and neurodegenerative conditions.

### See Also the Following Articles

ASTROCYTES • CHEMICAL NEUROANATOMY • CIRCADIAN RHYTHMS • ENDORPHINS AND THEIR RECEPTORS • GLIAL CELL TYPES • HOMEOSTATIC MECHANISMS • NEUROPEPTIDES AND ISLET FUNCTION • NEUROTRANSMITTERS • PSYCHONEUROENDOCRINOLOGY • SEXUAL DIFFERENTIATION, HORMONES AND • STRESS: HORMONAL AND NEURAL ASPECTS

### Acknowledgments

Dr. Martin is supported by grants from the U.S. Public Health Service, National Institutes of Health (NS34100 and AG16282), and the U.S. Army Medical Research and Material Command (DAMD17-99-1-9553). The photographic assistance of Frank

Barksdale is appreciated greatly. This article is dedicated to the tireless efforts of my wife Laura.

### Suggested Reading

- Heimer, L., de Olmos, J., Alheid, G. F., and Záborszky, L. (1991). "Perestroika" in the basal forebrain: Opening the border between neurology and psychiatry. *Prog. Brain Res.* **87**, 109-165.
- Hökfelt, T. (1991). Neuropeptides in perspective: The last ten-years. *Neuron* **7**, 867-879.
- Martin, L. J., Spicer, D. M., Lewis, M. H., Gluck, J. P., and Cork, L. C. (1991). Social deprivation of infant rhesus monkeys alters the chemoarchitecture of the brain: I. Subcortical regions. *J. Neurosci.* **11**, 3344-3358.
- Martin, L. J., Powers, R. E., Dellovade, T. L., and Price, D. L. (1991). The bed nucleus-amygdala continuum in human and monkey. *J. Comp. Neurol.* **309**, 445-485.
- Martin, L. J., Hadfield, M. G., Dellovade, T. L., and Price, D. L. (1991). The striatal mosaic in primates: Patterns of neuropeptide immunoreactivity differentiate the ventral striatum from the dorsal striatum. *Neuroscience* **43**, 397-417.
- Martin, L. J., Pardo, C. A., Cork, L. C., and Price, D. L. (1994). Synaptic pathology and glial responses to neuronal injury precede the formation of senile plaques and amyloid deposits in the aging cerebral cortex. *Am. J. Pathol.* **145**, 1358-1381.
- Martin, L. J., Portera-Cailliau, C., Ginsberg, S. D., and Al-Abdulla, N. A. (1998). Animal models and degenerative disorders of the human brain. *Lab Animal* **27**, 18-25.
- Martin, L. J., Price, A. C., Kaiser, A., Shaikh, A. F., and Liu, Z. (2000). Mechanisms for neuronal degeneration in amyotrophic lateral sclerosis and in models of motor neuron death. *Int. J. Mol. Med.* **5**, 3-13.
- McGeer, E. G., and McGeer, P. L. (1998). Inflammation in the brain in Alzheimer's disease: Implications for therapy. *NeuroScience News* **1**, 29-35.



# Neurodegenerative Disorders

LEE J. MARTIN

*Johns Hopkins University School of Medicine*

- 
- I. Introduction
  - II. Alzheimer's Disease Is a Progressive Neurodegenerative Disease of Elderly Individuals That Causes Synapse Defects and Dementia
  - III. ALS Is a Disease of Motor Neurons
  - IV. Neurodegenerative Diseases of the Basal Ganglia Cause Movement Disorders
  - V. Neuronal Death Occurs in Different Forms
  - VI. Programmed Cell Death Occurs Normally during Nervous System Development
  - VII. Glutamate Receptor Excitotoxicity Kills Neurons
  - VIII. Neuronal Degeneration Can Occur as an Apoptosis–Necrosis Continuum
  - IX. Apoptosis May Have Important Contributions to Neurodegenerative Disorders in Humans
  - X. Animal Models of Neurodegeneration Are Necessary to Understand How Neurons Die
  - XI. The Future Is Promising for Understanding the Causes of Neurodegenerative Disorders in Humans and Identifying Treatments

## GLOSSARY

**antioxidant** An enzyme or chemical that inactivates reactive oxygen species.

**apoptosis** A form of programmed cell death that has a characteristic structural appearance and occurs through the activation of intrinsic cell death pathways.

**apoptosis–necrosis continuum** The concept that neuronal cell death can occur as typical apoptosis, typical necrosis, or as intermediates or hybrids of cell death with varying, overlapping contributions of apoptosis and necrosis.

**astroglia** Glial cells in the central nervous system that have long radial processes that ensheath neurons and synaptic complexes.

Astroglia regulate the extracellular chemical and ionic environment and secrete peptides, growth factors, cytokines, and chemokines.

**axotomy** Experimental injury to the neuronal axon (or bundles of axons) by transection, avulsion, or trauma.

**central nervous system** The brain and spinal cord.

**death protein** A protein that regulates programmed cell death.

**excitotoxicity** A neurotoxic process that is mediated by excessive activation of excitatory glutamate receptors.

**experimental neuropathology** The study of neurodegeneration in animal or cell culture model systems.

**glial cell** Nonneuronal cell in the nervous system (e.g., astrocyte, oligodendrocyte, microglial cell, Schwann cell).

**glutamate receptor** A family of cell membrane proteins located on neurons and glia that bind glutamate or related chemicals, causing depolarization by ionic conductance or activation of enzymes resulting in the production or release of intracellular second messengers.

**microglia** The resident small phagocytic cells of the brain and spinal cord that are related to the mononuclear phagocyte lineage and function as immune accessory cells that secrete cytokines and chemokines.

**mutation** Change in the DNA nucleotide sequence of a gene.

**necrosis** A form of cell death that has a characteristic structural appearance and occurs through the failure of homeostatic mechanisms (e.g., energy production, cell volume).

**neurotransmitter** Signaling molecule secreted by the presynaptic terminal of a neuron at chemical synapses to relay a signal to a postsynaptic neuron (e.g., glutamate).

**NMDA receptor** A type of ion channel glutamate receptor that controls neuronal excitation and is very important for synaptic plasticity. It regulates intracellular  $\text{Ca}^{2+}$ . Overactivation of NMDA receptors causes excitotoxic neuronal death.

**oligodendroglia** Glial cells that provide myelin sheaths for axons within the CNS and secrete peptide growth factors.

**programmed cell death** A form of cell death that is brought about by intrinsic cellular pathways involving specific death proteins.

**reactive oxygen species** An oxygen molecule containing an odd number of electrons rendering it chemically reactive due to an open bond (e.g., superoxide, hydroxyl radical, nitric oxide).

**stem cell** Relatively undifferentiated cell that can divide into daughter cells that can undergo terminal differentiation into particular cell types (e.g., neurons).

**target deprivation** The removal or ablation of a brain region or peripheral tissue that is the site with which a group of neurons connects.

**Neurodegeneration is the pathology of neurons instigated by an acute insult or a chronic perturbation in cell function.** The process of neurodegeneration can be rapid or it can be slow and progressive, and it can result in neuronal loss and neuronal dysfunction with neurological consequences. Acute neurodegeneration is caused by cerebral ischemia (stroke and cardiac arrest), toxins, and trauma. Chronic neurodegeneration is caused by diseases such as Alzheimer's disease, amyotrophic lateral sclerosis, Huntington's disease, and Parkinson's disease. In different neurological disorders, different groups of neurons are selectively vulnerable to the molecular pathology of the degenerative process. The basis for this selective vulnerability may be intrinsic to the different groups of neurons. Models of experimental neuropathology are essential for discovering the mechanisms for selective neuronal vulnerability to injury and neurodegenerative disease.

## I. INTRODUCTION

A variety of neurodegenerative disorders affect the brain or spinal cord of humans (Tables I–III). The degeneration of nervous tissue can result from acute injury and from chronic disease. Acute neuropathology in adults, children, and infants can arise from head or spinal cord trauma, infection, toxicity, liver failure, and cerebral ischemia resulting from stroke, cardiac arrest, or asphyxiation. Chronic, progressive neuropathology occurs in adult disorders such as Alzheimer's disease, amyotrophic lateral sclerosis (Lou Gehrig's disease), Huntington's disease, multiple sclerosis, and Parkinson's disease and in infants and children with spinal muscular atrophy. These disease processes involve the degeneration of neurons and glial cells. Different populations of neurons in different nervous system regions have differential susceptibilities to disease and injury (Table I). This differential susceptibility of groups of neurons provides the basis for the yet to be understood concept of selective

vulnerability (Table I). The underlying mechanisms for selective vulnerability are possibly related to specific properties of neurons, including size, axonal length, connections, metabolism, and gene mutations. This neuronal degeneration causes tragic neurological and behavioral disabilities ranging from memory loss to paralysis. For example, neuronal degeneration is responsible for the memory disturbances that occur in individuals with Alzheimer's disease (AD) and in people that have experienced cardiac arrest, asphyxiation, or strokes. Nerve cell loss is also responsible for the profound abnormalities in movement that occur in individuals with amyotrophic lateral sclerosis (ALS), Parkinson's disease, or Huntington's disease and in children with cerebral palsy or spinal muscular atrophy.

The impact of neurodegenerative disorders on our society is revealed by epidemiological studies. AD affects approximately 4 million adults (most are > 65 years of age) and is the 4th-leading cause of death in the United States. AD accounts for > 100,000 deaths annually. ALS affects approximately 30,000 Americans (4–6 people in 100,000), whereas Huntington's disease annually affects 4–7 people per 100,000. Estimates of the incidence of Parkinson's disease vary depending on the populations of individuals studied, with the annual incidence ranging from 7 to 19 affected people per 100,000. More than 100,000 Americans under the age of 18 years have some degree of neurological disability attributable to cerebral palsy.

**Table I**  
Selective Vulnerability of the Human Central Nervous System in Neurodegenerative Conditions

Neurodegenerative disorder	Vulnerable neurons–brain regions
Alzheimer's disease	Neocortex, hippocampus, amygdala, basal forebrain cholinergic neurons, brain stem monoaminergic neurons
Amyotrophic lateral sclerosis	Lower motor neurons (spinal cord and brain stem) and upper motor neurons (motor cortex)
Cerebral ischemia (cardiac arrest and stroke)	Neocortex, hippocampus, striatum, cerebellum
Huntington's disease	Striatum
Multiple sclerosis	White matter
Parkinson's disease	Substantia nigra
Spinal muscular atrophy	Lower motor neurons (spinal cord and brain stem)

No drugs are available yet that can prevent the degeneration of neurons in the brain and spinal cord in people with these neurodegenerative disorders (Table I).

## II. ALZHEIMER'S DISEASE IS A PROGRESSIVE NEURODEGENERATIVE DISEASE OF ELDERLY INDIVIDUALS THAT CAUSES SYNAPSE DEFECTS AND DEMENTIA

Alzheimer's disease is the most common cause of dementia occurring in middle and late life. About 70% of all cases of dementia are due to AD. It affects 7–10% of individuals >65 years of age and up to 40% of people >80 years of age. The prevalence of AD is increasing proportionally to increased life expectancy. AD thus will continue to be a major health concern because estimates predict that ~25% of the population will be >65 years of age in the year 2050. AD now affects >4 million people in the United States. Most cases of AD have unknown etiology and are called sporadic; however, some cases of AD, particularly those with early onset, are familial and are inherited as an autosomal dominant disorder linked to mutations in the gene that encodes amyloid precursor protein or in the genes that encode for presenilin proteins (Table II). For late-onset sporadic cases, a variety of risk factors have been identified in addition to age. The apolipoprotein E (apoE) allele is a susceptibility locus with the apoE4 type showing dose-dependent contributions. Cardiovascular disease and head trauma are additional risk factors for AD.

The mechanisms that cause the profound brain atrophy (Fig. 1), neuronal degeneration and progressive impairments in memory and intellect that occur with AD are not understood. Atrophy of the cerebral cortex (i.e., loss of cerebral cortex volume) correlates strongly with cognitive decline. Normal cognition and memory, as well as neuronal survival, depend on synapses (Fig. 2A). Regulated release of neurotransmitter-containing vesicles is necessary for normal synaptic function. Some proteins that control synaptic operation are abnormal in AD (Fig. 2B). These proteins function in the presynaptic terminal by controlling the regulated exocytosis of neurotransmitter packets. Particular proteins are reduced in the hippocampus of individuals with AD who have moderate to severe abnormalities in memory (Figs. 2 and 3). Another important discovery is that the synaptic proteins that control neurotransmitter vesicle translocation and priming at the release site of the presynaptic nerve terminal are more vulnerable than proteins involved in vesicle exocytosis at the cell membrane. It appears that these proteins begin to be lost in individuals in the early stages of AD who do not yet have detectable cognitive impairments, but as the synaptic defects progressively become more severe, individuals manifest more severe memory impairment. Abnormalities in the presynaptic proteins that regulate neurotransmitter release may be an early pathological process in the development of AD (Fig. 2).

A variety of brain lesions occur in people with AD. The major lesions are called neurofibrillary tangles and senile plaques (Fig. 4). These brain lesions are formed abundantly in individuals with AD and patients with Down's syndrome and less frequently in people aging

**Table II**  
Gene Mutations Associated with Some Neurodegenerative Diseases

Neurodegenerative disease	Gene mutation-deletion	Prevalence
Familial amyotrophic lateral sclerosis <sup>a</sup>	Copper-zinc superoxide dismutase	10% of all FALS cases
Familial Alzheimer's disease <sup>b</sup>	Amyloid precursor protein	<10% of all familial AD cases
Familial Alzheimer's disease	Presenilin-1	<10% of all familial AD cases
Familial Alzheimer's disease	Presenilin-2	<10% of all familial AD cases
Huntington's disease	Huntingtin	100% of cases
Parkinson's disease	$\alpha$ -Synuclein	Very rare
Spinal muscular atrophy	Survival motor neuron, neuronal apoptosis inhibitory protein	Majority of cases

<sup>a</sup>ALS occurs as a familial or sporadic disease. Approximately 5–10% of all ALS cases are familial. The majority of cases are sporadic, with no yet identified mutations.

<sup>b</sup>AD occurs as a familial or sporadic disease. Approximately 10% of all AD cases are familial. The majority of AD cases are sporadic.



**Figure 1** Severe atrophy of the brain occurs in Alzheimer's disease. (A) Midsagittal view of the brain from an 86-year-old normal, individual. The cerebral cortex is normal, with broad gyri and narrow sulci. Scale bar = 23 mm (same for B). (B) Midsagittal view of the brain from an 85-year-old individual with Alzheimer's disease. The cerebral cortex is atrophic, as indicated by widening of the sulci and narrowing of the gyri (white arrowheads).

normally. Pyramidal neurons in the neocortex and hippocampus (Fig. 4A, Table I) are highly vulnerable to the formation of neurofibrillary tangles. Neurofibrillary tangles are abnormal bundles of protein filaments that occur within neurons (Fig. 4B). These tangled masses consist of paired helical filaments containing  $\tau$  protein (Fig. 4C). Senile plaques are formed throughout the brain parenchyma, and in AD they occur in large numbers (Fig. 4D). The composition of senile plaques is very complex (Figs. 4D and 5), consisting of dystrophic neurites

(damaged and swollen dendrites or axon terminals), activated astrocytes and microglia, and extracellular deposits of insoluble amyloid. Amyloid occurs as fibrils composed of a small peptide ( $A\beta$ ) consisting of 40–42 amino acid residues. This abnormal protein fragment is derived proteolytically from the amyloid precursor protein (APP), a cell surface protein. APP may participate directly in the pathogenesis of AD because mutations have been identified in the APP gene that are linked to early-onset AD in some families (Table II).

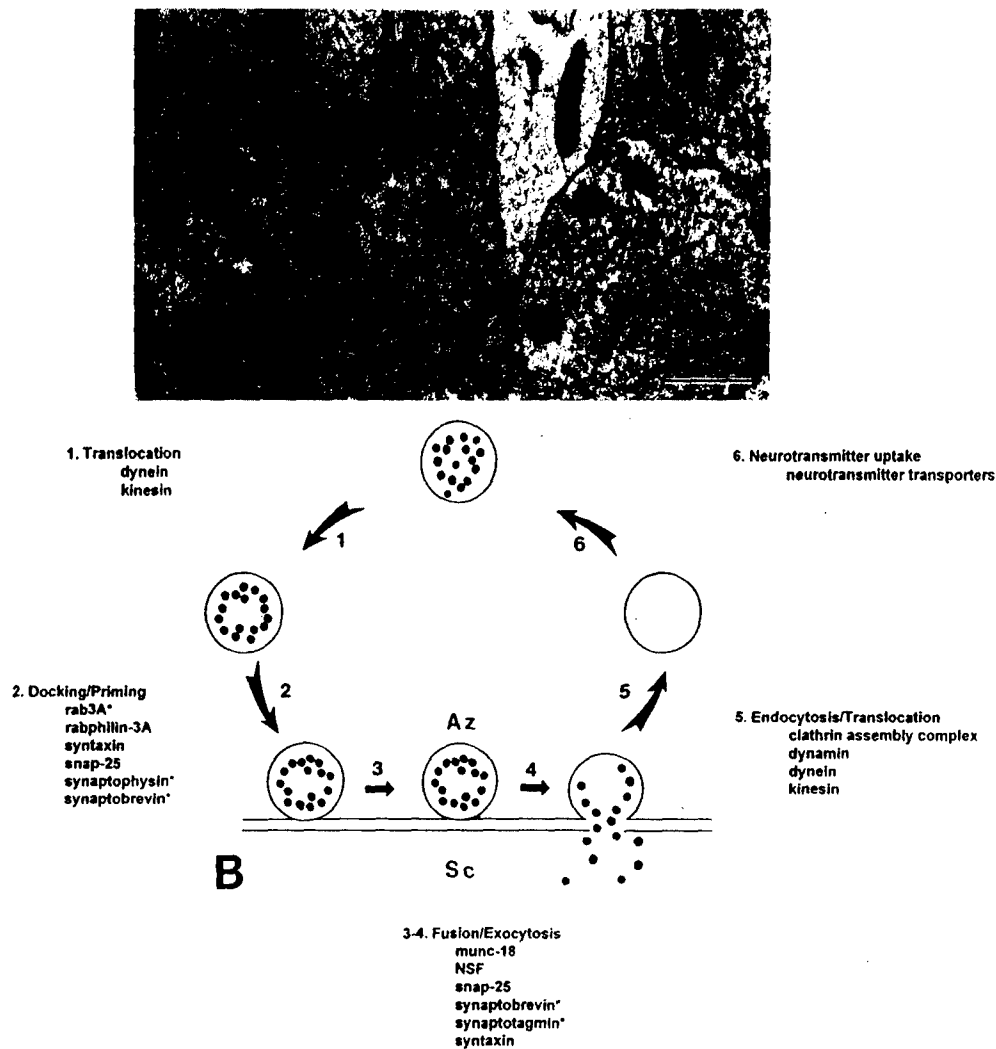


**Figure 2** The synaptic vesicle cycle may be abnormal in Alzheimer's disease. (A) Electron micrographs of synapses in the cerebral cortex of a rhesus monkey. Axon terminals (T), containing many small clear synaptic vesicles (arrowheads), from synapses (open arrow) with postsynaptic structures. Synaptic vesicles cluster at the active zone of the presynaptic membrane. The narrow space between the presynaptic and postsynaptic components is the synaptic cleft. Scale bar = 1.0  $\mu$ m. (B) Diagram of the synaptic vesicle cycle. This cycle functions in the regulated release of neurotransmitter-containing vesicles (filled circles) from the presynaptic terminal. Abbreviations: Az, synaptic active zone; Sc, synaptic cleft. The synaptic vesicle cycle can be divided into six major components, as indicated. Some of the specific proteins that function at each phase of the cycle are indicated. Some of these proteins (indicated by the asterisk) appear to be selectively vulnerable in individuals with Alzheimer's disease.

The functions of APP are still not well-defined, although it appears that APP functions at synapses. APP is an abundant and ubiquitous protein within CNS and other tissues. APP has structural features similar to some cell surface receptors and may be a G-protein-coupled receptor. Secreted and nonsecreted forms of APP exist, with different APP derivatives having neurotrophic or neurotoxic actions. APP is incorporated into the extracellular matrix and, thus, may have roles in cell-cell and cell-substrate adhesion. Furthermore, APP may function in the regulation of neurite outgrowth, perhaps by modulating the effects

of neurotrophins and cytokines in the responses of neurons and glia to brain injury.

In cell culture, APP normally undergoes constitutive proteolytic cleavage by an  $\alpha$ -secretase. This enzyme cleaves APP within the A $\beta$  region at or near the plasma membrane, thereby generating secreted forms of APP and precluding the formation of full-length A $\beta$  peptide fragments. APP is also metabolized by an endosomal-lysosomal pathway that, unlike the  $\alpha$ -secretase pathway, yields amyloidogenic fragments of A $\beta$  that are deposited in senile plaques (Fig. 4D). A $\beta$  can be formed normally *in vivo* and *in vitro*, and studies of



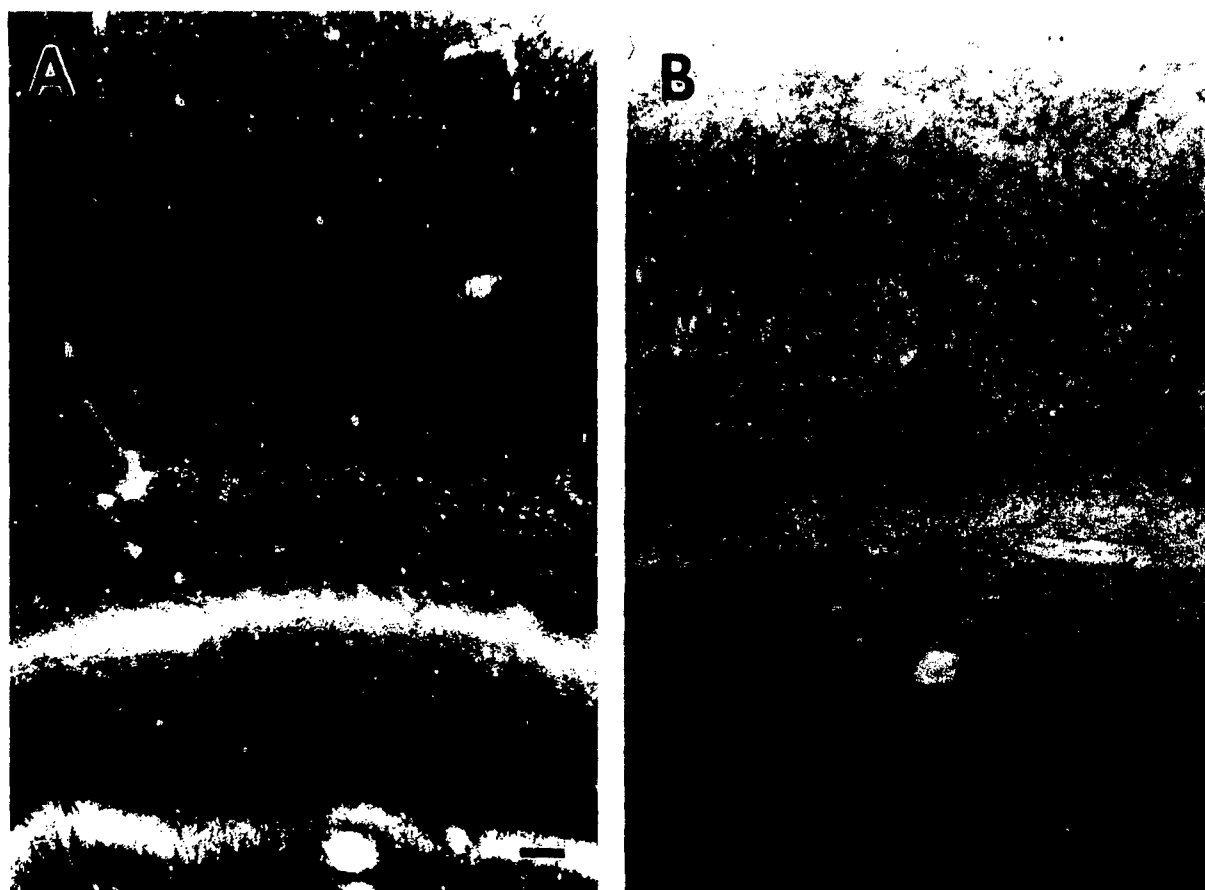


**Figure 3** Synapses in the hippocampus of individuals with Alzheimer's disease are abnormal. (A) The hippocampus of normal, aged control humans has very high levels of synapses, as revealed by the synaptic vesicle protein synaptophysin (the intensity of the black staining reflects the amount of synaptophysin immunoreactivity). Scale bar = 42  $\mu$ m (same for B). (B) The hippocampus of an individual with Alzheimer's disease shows a marked depletion of synaptophysin immunoreactivity (as reflected by the less intense black staining).

cultured human cells and aged non-human primates show that it is generated intracellularly.

Although  $A\beta$  has been shown to be neurotoxic in cell culture, a causal role for  $A\beta$  in neuronal degeneration within the brain remains speculative. A  $\beta$ -secretase cleaves APP at the N-terminus of  $A\beta$ , and a  $\gamma$ -secretase cleaves APP at the C-terminus of  $A\beta$ , causing the formation of  $A\beta$  that is either 40 or 42 amino acids long. This pathway for APP metabolism is found within the endoplasmic reticulum and Golgi apparatus of neurons. Mutant presenilins (Table II) promote  $A\beta_{42}$  generation. Presenilins, which are present at relatively low levels in the brain, localize to the endoplasmic reticulum and Golgi apparatus. Mutant presenilin is processed differently from normal presenilin, and fragments that are normally subject to endoproteolytic cleavage tend to accumulate. Thus, metabolism of APP through the  $\beta$ - and  $\gamma$ -secretase pathways may be promoted by *presenilin-1* and

*presenilin-2* gene mutations linked to early-onset familial AD (Table II).

We and others have shown that APP is present in essentially all neurons and in some astroglia, microglia, and vascular endothelial cells. The most prominent neuronal localization of APP is within cell bodies and dendrites and is particularly enriched postsynaptically at some synapses. The expression of APP in nonneuronal cells in the brain is low in comparison to the dominant expression of APP within neurons and their processes. It appears that astroglia and microglia constitutively express APP at low levels in the resting state. However, the relative enrichment of APP within these neuroglial cells changes in response to brain injury and synaptic abnormalities. This idea is supported by our finding that APP is expressed prominently by activated astroglia and microglia within senile plaques of aged nonhuman primates and by other reports showing that APP is localized to

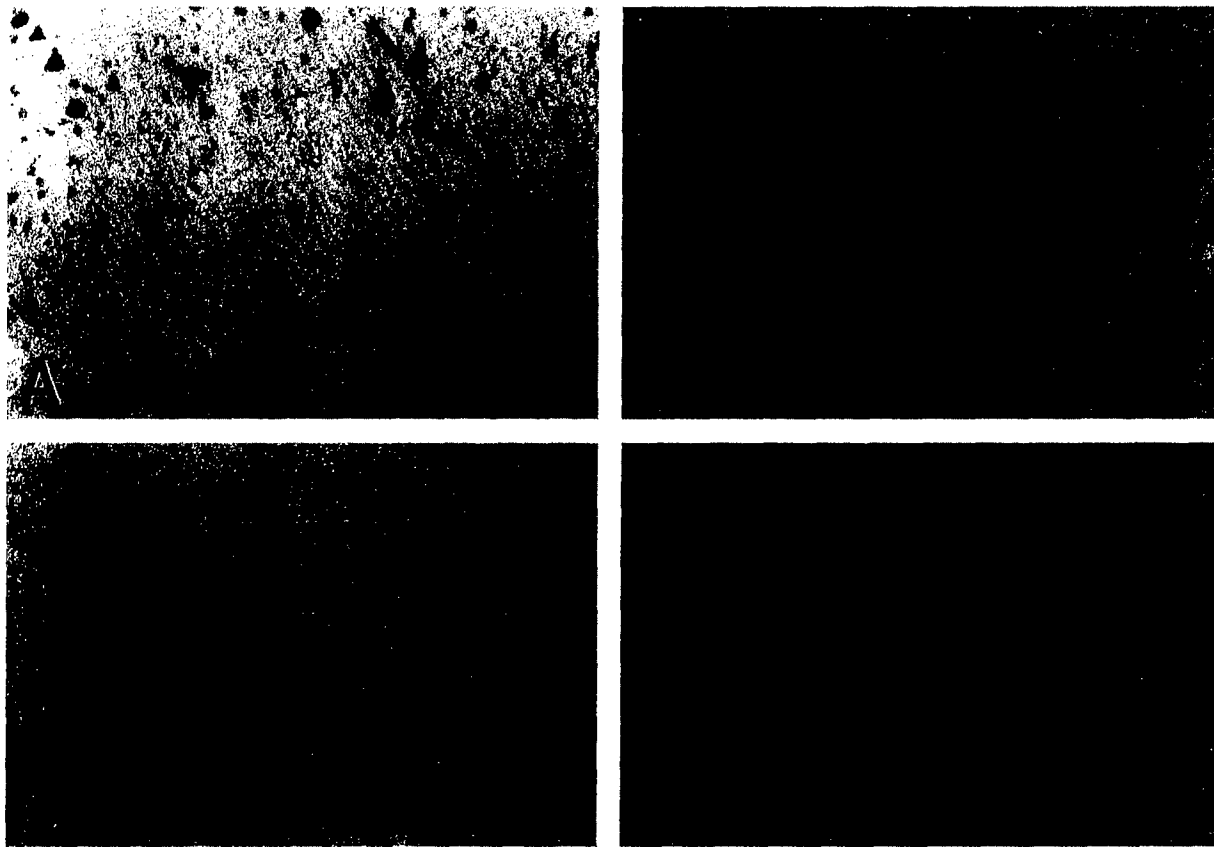


**Figure 4** Neurofibrillary tangles and amyloid deposits are brain lesions that are formed in patients with Alzheimer's disease. (A) Pyramidal neurons in the neocortex (arrows) are vulnerable in individuals with Alzheimer's disease. Scale bar = 50  $\mu$ m. (B) Neurofibrillary tangles, which are abnormal intracellular aggregates of protein (arrows), are formed in pyramidal neurons in patients with Alzheimer's disease. Scale bar = 50  $\mu$ m. (C) Neurofibrillary tangles are composed of  $\tau$  proteins (arrows). Scale bar = 100  $\mu$ m. (D) Individuals with Alzheimer's disease form numerous abnormal extracellular deposits of  $A\beta$  amyloid protein in the brain (arrows). Scale bar = 200  $\mu$ m.

astrocytes in senile plaques in cases of AD. Other studies have shown that some forms of APP are expressed in reactive astrocytes in the early stages of brain damage. Because levels of APP in some neurons and nonneuronal cells are increased by the cytokine interleukin-1, it is likely that the expression of APP is inducible in glia when these cells are activated in response to neuronal injury.

Several theories for the formation of senile plaques and  $A\beta$  deposits have been presented. The genesis of senile plaques may begin with the abnormal processing of APP via  $\beta$ -secretase and the formation of extracellular  $A\beta$  before the degeneration of cellular elements within these brain lesions. Alternatively,  $A\beta$  may be derived from degenerating axonal nerve terminals or dendrites containing APP that evolve into neurite-rich foci that form  $A\beta$  at the cell plasma membrane by aberrant processing of APP within neurons. In addition, invading reactive microglia and

astroglia as well as capillaries may actively produce  $A\beta$  from APP.

We have found that senile plaques are dynamic brain lesions that evolve from early defects in synapses within the neuropil to mature plaques and extracellular deposits of  $A\beta$  (Figs. 4D and 5). The staging of these lesions is thought to be the degeneration of neuritic structures, followed by the attraction of reactive glia and the subsequent deposition of extracellular  $A\beta$  derived from microglia or astrocytes. Studies demonstrate that structural and biochemical perturbations within neuronal and non-neuronal cells, importantly glia, occur before the deposition of extracellular  $A\beta$  fibrils. Furthermore, these results suggest that focal abnormalities in synaptic contacts within the neuropil (synaptic disjunction) may instigate this complex series of events resulting in the formation of diffuse senile plaques and deposits of  $A\beta$  (Figs. 4D and 5). In



**Figure 5** Electron microscopy reveals the complexity of the senile plaques that are formed in the cerebral cortex. Extracellular amyloid (A) is surrounded by numerous dystrophic, swollen neurites (dn), which are filled with abnormal membranous organelles. Microglia (m) infiltrate into the plaques. A nearby neuron (N) appears structurally normal. Scale bar = 4  $\mu$ m.

response to synaptic disjunction in the aged brain, astroglia and microglia produce  $A\beta$ . The molecular pathology we and others have identified at the synaptic level in humans with AD (Figs. 2 and 3)

may be related to senile plaque lesions and  $A\beta$  deposits (Figs. 4D and 5). Defects in the synaptic vesicle cycle (Fig. 2) and synaptic disjunction in the neuropil may lead to abnormal APP processing

within neuroglia and could be early events in the formation of senile plaques and A $\beta$  lesions.

### III. ALS IS A DISEASE OF MOTOR NEURONS

ALS is a fatal neurological disease that causes a movement disorder (Table III) characterized by progressive muscle weakness, muscle atrophy, and eventual paralysis. Individuals affected with ALS die within 3–5 years of clinical onset. This disease is neuropathologically characterized by progressive degeneration of the upper and lower motor neurons in the brain and spinal cord (Table I, Fig. 6). The neuropathology of ALS is primary degeneration of the upper (motor cortical) and lower (brain stem and spinal) motor neurons. The amyotrophy refers to the neurogenic atrophy of affected muscle groups, and the lateral sclerosis refers to the hardening of the lateral white matter funiculus in the spinal cord (corresponding to degeneration of the corticospinal tract) found at autopsy. Because the mechanisms for the motor neuron degeneration in ALS are not understood, this disease has no precisely known causes and no effective treatments. Two major forms of ALS exist: idiopathic (sporadic) and heritable (familial). The vast majority of ALS cases are sporadic with no known genetic component. The familial forms of ALS (FALS) are autosomal dominant and make up about 10–20% of all ALS cases. In a subset of familial ALS cases (about 5–10%), missense mutations have been identified in the gene for superoxide dismutase 1 (SOD1), also called copper–zinc superoxide dismutase (Table II).

A variety of theories have been proposed for the possible causes of neurodegeneration in ALS (Table VI). A major center of attention is the mutant forms of SOD1 found in FALS. Because SOD1 is widely expressed in cells throughout the body and in CNS tissue the expression is very ubiquitous, the basis for the selective vulnerability of motor neurons in the presence of SOD1 mutations is still not clear. Initial experiments hinted that mutations in SOD1 could lead to motor neuron degeneration by decreasing enzy-

matic activity, resulting in neurotoxicity of reactive oxygen species, notably superoxide radicals that are inefficiently scavenged by mutant SOD1. However, it was found that FALS-linked mutations in SOD1 generally do not impair enzymatic activity but instead decrease protein stability. It was then proposed that mutant SOD1 acquires a neurotoxic gain in function. Mutations in SOD1 may convert this enzyme from a protein with antioxidant–antiapoptotic functions to a protein with apoptosis-promoting effects. In addition to the dismutation of superoxide, SOD1 also has peroxidase activity, and this peroxidase activity is enhanced in mutant SOD1 compared to normal SOD1. This gain of function could lead to the enhanced production of reactive oxygen species that could damage motor neurons. In mice with forced expression of mutant forms of the gene encoding for SOD1, motor neuron degeneration does occur. Unfortunately, however, this degeneration in transgenic mice overexpressing mutant forms of SOD1 is neuropathologically different from the degeneration of motor neurons in people with sporadic and familial ALS.

Studies have identified that the degeneration of motor neurons in ALS is a form of apoptotic cell death that appears to occur by a programmed cell death (PCD) mechanism (Fig. 7). PCD is a type of cell death that is triggered by intrinsic cellular pathways involving specific death proteins. This PCD of motor neurons in ALS could be due to a gain in function of the tumor suppressor protein p53. p53 is a DNA-binding phosphoprotein that functions in genome surveillance, DNA repair, and gene transcription. p53 commits to death cells that have sustained DNA damage from genotoxic agents and reactive oxygen species. DNA lesions have been found in individuals with ALS possibly because of free radical damage and defective DNA repair. Thus, p53 may participate in the mechanisms for motor neuron death in ALS in response to DNA damage. The gene expression of some cell death proteins is promoted by p53. For example, the levels of a protein called Bax (see Table IV) are regulated by p53. Bax is critical for neuronal

**Table III**  
Classification of Some Movement Disorders in Humans

Motor neuron diseases	Akinetic disorders	Hyperkinetic disorders	Ataxic disorders
Amyotrophic lateral sclerosis	Parkinson's disease	Huntington's disease	Spinocerebellar degeneration
Spinal muscular atrophy	Progressive supranuclear palsy	Dystonia	Ataxia–telangiectasia

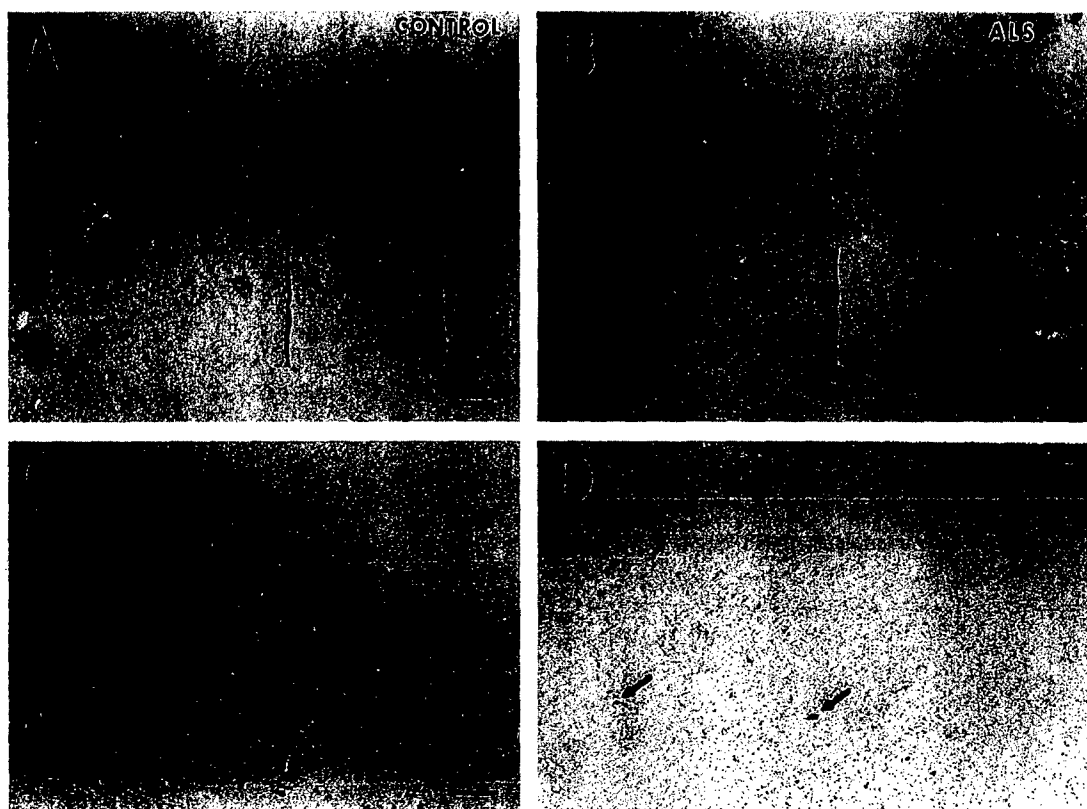


**Figure 6** Motor neurons degenerate in patients with ALS. (A) In normal control individuals, the anterior horn of the spinal cord (brackets) is populated with many neurons (black dots within brackets). Scale bar = 0.7 mm (same for B). (B) In ALS, the anterior horn is depleted of neurons (brackets). (C) The anterior horn of the spinal cord in normal subjects is populated with large, multipolar motor neurons (arrows). Scale bar = 200  $\mu$ m (same for D). (D) In ALS, the anterior horn contains many shrunken neurons (arrows) instead of large multipolar cells.

apoptosis. In ALS, we have found that p53 levels are elevated and that this p53 has competent DNA binding activity; moreover, Bax levels are elevated in individuals with ALS. This information is novel and is conceptually very important for further understanding

the pathobiology of motor neuron death in ALS. It suggests that critical molecular mechanisms for regulating human cancer are overactive in vulnerable CNS regions in a human-age-related neurodegenerative disease. This theory may advance the

**Table IV**  
Leading Theories on the Possible Causes of Motor Neuron Degeneration in ALS

Mechanism	Comment
SOD1 mutation	Found in some FALS cases. Resulting in a toxic gain in function or modified stability of SOD1.
Excitotoxicity	Resulting from abnormal glutamate receptor activation and defects in glutamate transport.
Neurotrophin withdrawal	Resulting from insufficient muscle cell- or glial-cell-derived trophic support or defective neurotrophin receptor signaling.
DNA damage-repair defects	Resulting from oxidative stress or inefficient DNA repair enzyme function. May involve both mitochondrial and nuclear DNA damage.
Autoimmunity	Resulting from autoantibodies to motor neuron antigens.
Aberrantly occurring programmed cell death	May be triggered by all of the precedings mechanisms.

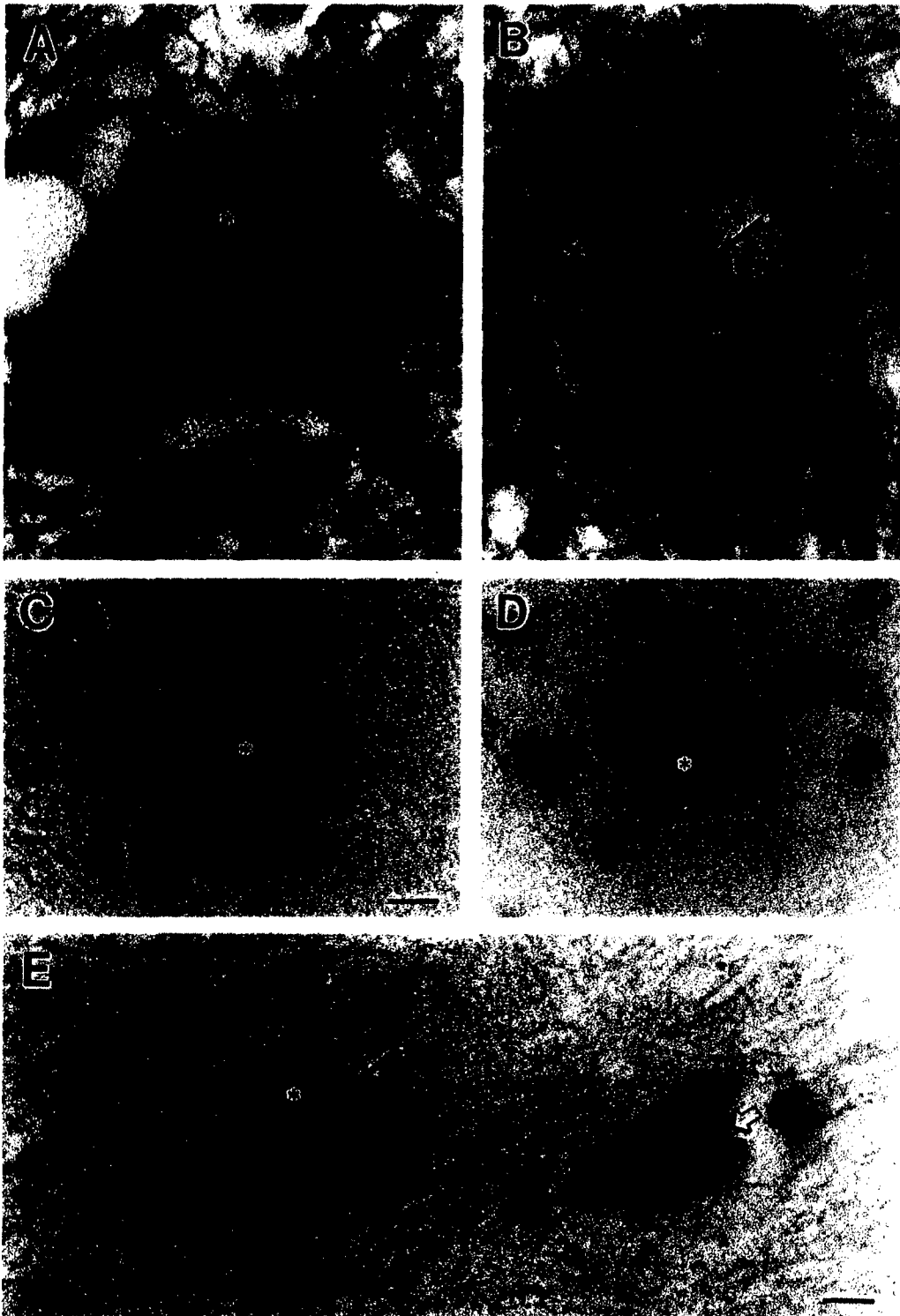


**Figure 7** Motor neuron degeneration in ALS is a form of apoptosis that may be mediated by a p53-dependent mechanism. (A) Normal appearing spinal motor neuron with a large, multipolar cell body and a large nucleus (asterisk) containing a reticular network of chromatin and a large nucleolus. Scale bar = 7  $\mu$ m (same for B). (B) Near end stage apoptotic motor neuron in ALS (arrow). The cell has shrunk to about 10% of normal size and has become highly condensed. (C and D) Nuclear DNA fragmentation (asterisk) occurs in motor neurons in patients with ALS as the nucleus condenses (asterisks) and the cell shrinks. Scale bar = 7  $\mu$ m. (E) In individuals with ALS, p53 accumulates in the nuclei (asterisk) of motor neurons (arrow). The nearby neuron (open arrow) has an unlabeled nucleus for comparison. Scale bar = 10  $\mu$ m. (See color insert in Volume 1).

understanding of motor neuron degeneration in ALS and perhaps other age-related neurodegenerative disorders in which chronic and progressive DNA damage may occur.

#### IV. NEURODEGENERATIVE DISEASES OF THE BASAL GANGLIA CAUSE MOVEMENT DISORDERS

The basal ganglia are subcortical brain structures that function in sensory-motor integration and in the planning and initiation of skeletal muscle movements. The striatum (caudate nucleus and putamen), globus pallidus (external and internal divisions), substantia nigra (pars compacta and reticulata), and subthalamic nucleus are the major components of the basal ganglia (Fig. 8). The basal ganglia do not control movement through direct connections with lower motor neurons, but rather the functions of the basal ganglia are

executed by the frontal cortex through corticobulbar and corticospinal projections to brain stem and spinal motor neurons, respectively. The operation of the basal ganglia involves forebrain-diencephalon-mid-brain circuitry loops. The different circuits within the basal ganglia utilize different neurotransmitters (Table V). The primary input to the basal ganglia originates from the neocortex and is directed to the striatum (Fig. 8). This corticostriatal projection uses the excitatory neurotransmitter glutamate. The primary output center of the basal ganglia is the globus pallidus, which conveys signals back to the neocortex through the thalamus (Fig. 8). The pallidothalamic projection is inhibitory; in contrast, the thalamocortical projection is excitatory (Table V). Thus, the globus pallidus functions to inhibit the excitatory thalamic drive of neocortex. Somatic movements occur when thalamic neurons are released from tonic inhibition. This release occurs when corticostriatal projections excite striatal neurons that can phasically inhibit the neurons in the

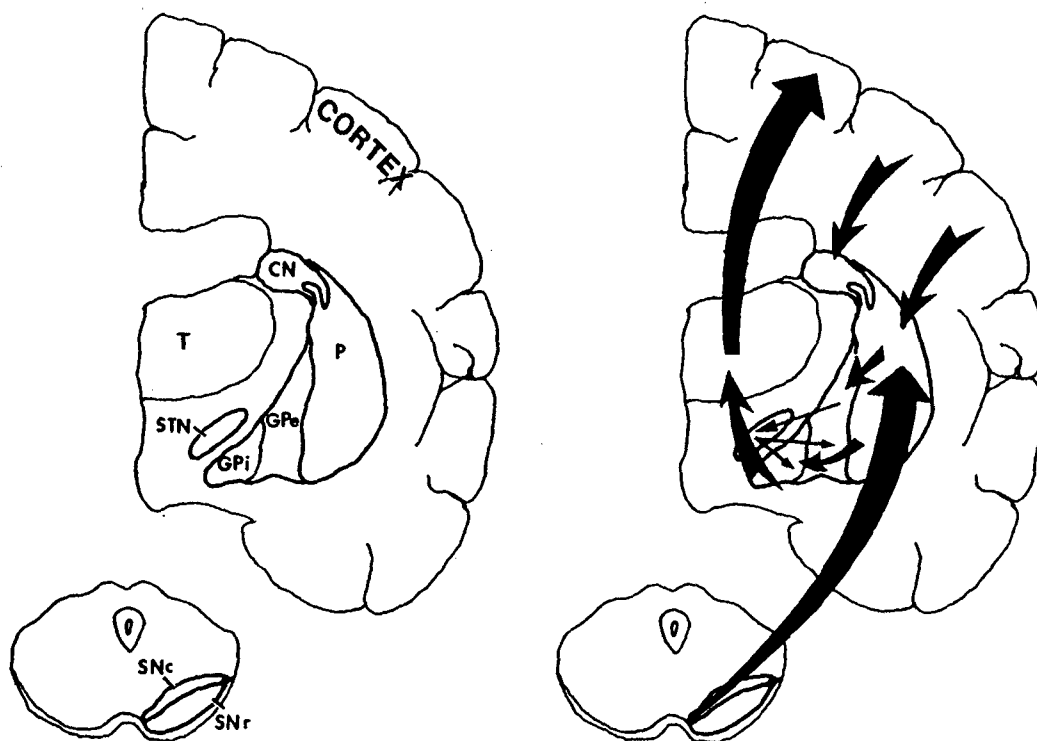


**Figure 8** Basal ganglia circuits control movements. The basal ganglia comprise (left panel) the caudate nucleus (CN), putamen (P), globus pallidus external (GPe) and internal (GPi) divisions, the subthalamic nucleus (STN), and the substantia nigra compacta (SNc) and reticular (SNr) divisions. The cerebral cortex and thalamus (T), although not part of the basal ganglia, participate in the connectivity loops (right panel). See Table V for connections. The major excitatory input to the striatum (the caudate nucleus and putamen) is from the cerebral cortex (right panel). The striatum in turn projects to the globus pallidus and the substantia nigra reticular division. Striatal activity is modulated by extensive dopaminergic input from the substantia nigra compacta. The major output of the basal ganglia is directed toward the thalamus, originating from GPi and SNr (not shown). The thalamic projection to the cerebral cortex (premotor and supplementary motor areas) drives the activity of the motor cortex, which executes somatic movements.

**Table V**  
**Primary Connections of the Basal Ganglia and Their Major Neurotransmitters<sup>a</sup>**

Projection	Neurotransmitter
Neocortex to striatum (corticostriatal)	glutamate
Striatum to globus pallidus (striatopallidal)	GABA <sup>b</sup> -neuropeptides <sup>c</sup>
Globus pallidus externa to subthalamic nucleus (pallidosubthalamic)	GABA
Subthalamic nucleus to globus pallidus externa-interna (subthalamopallidal)	Glutamate
Subthalamic nucleus to substantia nigra reticulata (subthalamonigral)	Glutamate
Substantia nigra compacta to striatum (nigrostriatal)	Dopamine
Substantia nigra reticulata to thalamus (nigrothalamic)	GABA
Globus pallidus interna to thalamus (pallidothalamic)	GABA

<sup>a</sup>See Fig. 8 for illustration of connections.

<sup>b</sup> $\gamma$ -Aminobutyric acid.

<sup>c</sup>Principal striatal neurons coexpress a variety of neuropeptide transmitters, including enkephalins, tachykinins, and dynorphin (see the article on Neuropeptides and Hormones in the Brain and Spinal Cord).

globus pallidus that inhibit thalamic neurons. The resulting activation of thalamocortical projections excites the premotor and supplementary motor areas of frontal neocortex that activate the motor cortex, thereby facilitating movement.

There are two major circuits within the basal ganglia, designated as the direct and the indirect pathways. These two pathways counterbalance each another. The direct pathway is the striatal projection to the globus pallidus (internal segment) and the substantia nigra reticulata, which in turn project to the thalamus (Fig. 8). Activation of the direct pathway results in the activation of thalamocortical projections and the facilitation of movement. The substantia nigra dopaminergic neurons activate striatal neurons of the direct pathway, thus functioning to facilitate movement. The indirect pathway, in contrast, involves a loop with the subthalamic nucleus (Fig. 8), which changes the physiological outcome in the thalamus. In the indirect pathway, the striatum inhibits the globus pallidus (external segment), which functions to inhibit the subthalamic nucleus. The subthalamic nucleus projects back to the globus pallidus (both segments) and to the substantia nigra reticulata to activate these regions; the internal segment of the globus pallidus and

the substantia nigra reticulata then inhibit the thalamus. Thus, activation of the indirect pathway decreases movement. The substantia nigra dopaminergic neurons inhibit striatal neurons of the indirect direct pathway, thus opposing the activation of the indirect pathway and functioning to facilitate movement.

Diseases of the basal ganglia can cause involuntary movements, lack of movement, or slowness of movement (Table III). In Parkinson's disease, degeneration of the dopaminergic neurons in the substantia nigra results in the loss of dopamine in the striatum. Parkinson's disease causes involuntary movements (tremors), lack of movement (akinesia), and slowness of movement (bradykinesia). Some of the neurological features of Parkinson's disease are thought to arise from the loss of dopamine inhibition of striatal neurons in the indirect pathway (Fig. 8), resulting in increased inhibition of the globus pallidus external segment and greater excitatory drive of the subthalamic nucleus on the globus pallidus interna and substantia nigra reticulata. Moreover, the loss of dopamine results in decreased activity of striatal neurons in the direct pathway, leading to increased pallidothalamic inhibition. In Huntington's disease, degeneration of subsets of the principal neurons in the striatum may lead to decreased activity of the globus pallidus internal segment via the indirect pathway (Fig. 8). This failure to suppress thalamocortical activity is thought to cause slow writhing movements of the extremities (athetosis) and abrupt movements of the limbs and facial muscles (chorea).

## V. NEURONAL DEATH OCCURS IN DIFFERENT FORMS

Neurons can die in different ways (Fig. 9). The death of cells has been classified generally as two distinct types: apoptosis and necrosis. These two forms of cellular degeneration are classified differently because they are believed to differ structurally and biochemically. Apoptosis is generally regarded as physiological cell death and is considered to be an organized PCD that is mediated by active, intrinsic mechanisms through which certain molecular pathways are activated to initiate apoptosis (Table VI). In contrast, necrosis is cell death resulting from a failure to sustain homeostasis due to extrinsic insults to the cell (e.g., osmotic, thermal, toxic, traumatic). The process of cellular necrosis involves damage to the structural and functional integrity of the cell plasma membrane, a rapid influx of ions and H<sub>2</sub>O, and, subsequently, dissolution



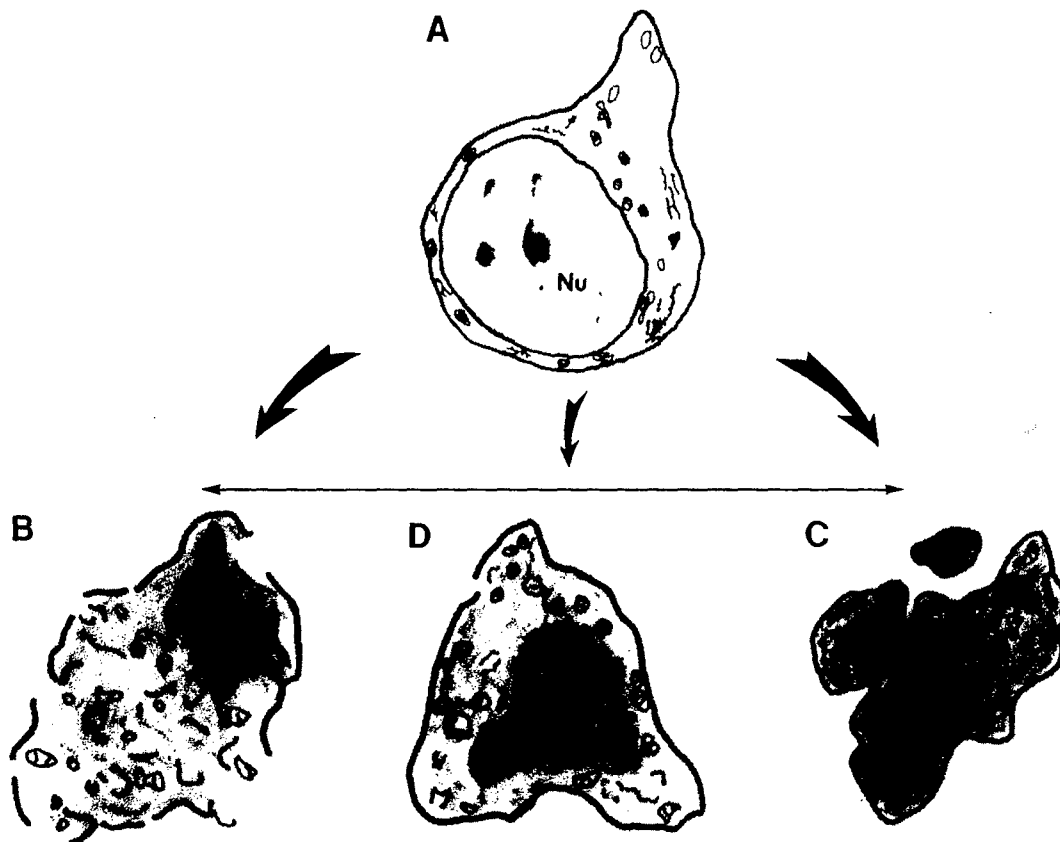


**Figure 9** Neuronal cell death occurs as an apoptosis–necrosis continuum. According to the traditional binary scheme for cell death, a neuron (A) can die by either necrosis (B) or apoptosis (C). These forms of cell death were thought to be structurally distinct (representative images of cells are shown) and mutually exclusive. With cellular necrosis (B), which occurs as groups of cells, massive damage to organelles and the plasma membrane occurs with the release of cellular constituents. The nucleus (Nu) undergoes fragmentation, with the condensation of nuclear material being irregular and distinct from that occurring in apoptosis. In necrotic neurons the nucleolus can remain intact. In contrast, apoptosis (C) is an organized form of cell death that occurs generally as isolated cells within groups of cells. The nucleus containing the DNA is packaged into uniformly condensed masses (shown by the round or elliptical black structures), and the surrounding cytoplasm becomes shrunken and condensed (shown by the gray) with the organelles generally preserved until end stage apoptosis. Small fragments of cell cytoplasm surrounding packaged chromatin bud from the dying cell and are engulfed by glial cells. The concept of the apoptosis–necrosis continuum is based on the observation that neurons can die with a structure that is a hybrid of apoptosis and necrosis (D). The nuclear (Nu) and cytoplasmic changes are intermediate between those occurring in apoptosis and necrosis. The packaging of the chromatin occurs as large irregular masses in the nucleus. In the cytoplasm, some mitochondria remain intact whereas others are swollen.

of the cell. Thus, cellular necrosis is induced not by an intrinsic program within the cell *per se* (as in PCD) but by abrupt or slow homeostatic perturbations and departures from physiological conditions. It has been realized that an abnormal activation of PCD in brain and spinal cord neurons may also play a role in the disease process in humans with neurodegenerative disorders; therefore, deciphering of the contributions of the different types of cell death in degenerative diseases of the human CNS could help to develop treatments for these diseases. These treatments could possibly be drugs that inhibit the actions of key enzymes, ion channels in cell membranes, or numerous

other proteins, as well as drugs (e.g., antioxidants) that block or inactivate the production of toxic chemicals (e.g., free oxygen radicals) that are generated during the process of neuronal death.

## VI. PROGRAMMED CELL DEATH OCCURS NORMALLY DURING NERVOUS SYSTEM DEVELOPMENT

Naturally occurring apoptotic degeneration of neurons occurs normally in the developing nervous system (Fig. 10). Animals are born with excess numbers of

Table VI  
Molecular Regulation of Programmed Cell Death

Bcl-2 family		Caspase family	IAP family	Tumor suppressor family
Antiapoptotic proteins	Proapoptotic proteins			
Bcl-2 <sup>a</sup>	Bax <sup>a</sup>	Apoptosis "initiators:" caspase-2, -8, -9, -10	NAIP	p53 <sup>a</sup>
Bcl-x <sub>L</sub> <sup>b</sup>	Bak <sup>a</sup>	Apoptosis "executioners:" caspase-3 <sup>a</sup> , -6, -7	IAP1	p63
Boo	Bcl-x <sub>S</sub>	Cytokine processors: caspase-1, -4, -5, -11, -12, -14	IAP2	p73
	Bad			
	Bid		XIAP	
	Bik			

<sup>a</sup>Proteins that have been shown to be abnormal in individuals with ALS.

<sup>b</sup>Proteins that have been shown to be unchanged in ALS.

neurons. The elimination of these supernumerary neurons in the developing nervous system occurs by normal programmed neurodegeneration at specific times. This normal neurodegeneration is thought to be important for matching the size of neuronal groups to the size of their targets (other groups of neurons to which they are connected by axons and nerve terminal synapses) as well as to their own synaptic inputs from other regions. This developmental neuronal death (particularly of spinal and sympathetic ganglion neurons and motor neurons) is thought to be partially controlled by the supply of sustaining neurotrophic factors that are synthesized by the target axon-associated glial cells or by the input regions. Thus, an insufficient supply of neurotrophic molecules triggers an apoptotic process within interconnected groups of neurons by PCD.

Apoptosis is regulated by specific molecules within cells (Table VI). Several genes that regulate apoptosis were originally identified in a nematode worm. Homologous genes have been identified in mammalian cells. The molecular mechanisms for apoptosis involve the participation of at least three groups of proteins that are made from three different gene families. One set of proteins is the caspase family of cysteine-containing, aspartate-specific proteases (14 members have been identified to date). A second group includes the death-promoting and death-suppressing proteins in the *Bcl-2* family (e.g., *Bcl-2*, *Bcl-x<sub>L</sub>*, *Bax*, *Bak*, *Bad*, *Boo*). A third group of proteins is designated as the inhibitor of apoptosis protein (IAP) family.

Caspases exist as dormant proenzymes in healthy cells and are activated through regulated proteolysis. These proteins function in the execution phase of apoptosis with "initiator" caspases activating "effec-

tor" caspases, which subsequently cleave a variety of proteins, thereby causing the molecular and structural changes of apoptosis. Once activated, caspases act on nuclear proteins, cytoskeletal proteins, or cytosolic proteins. Two different caspase cascades mediate PCD. One pathway involves the regulated release of cytochrome c from mitochondria that promotes the activation of caspase-9 through Apaf-1 and then caspase-3 activation. Another pathway is initiated by the activation of cell-surface death receptors, including Fas and tumor necrosis factor receptor, leading to caspase-8 activation, which in turn cleaves and activates downstream caspases such as caspase-3, -6, and -7.

Apoptosis regulation by the *bcl-2* protooncogene family is a very complex and exciting process (Table VI). Of these genes, *bcl-2* and *bcl-x<sub>L</sub>* are antiapoptotic (death-suppressing), whereas *bax*, *bcl-x<sub>S</sub>*, *bad*, *bak*, and *bik* are proapoptotic (death-promoting). Membership into the family of Bcl-2-related proteins is defined by homology domains within their amino acid sequences. These domains function in the interactions (i.e., binding) between members. Bcl-2 family members exist as monomers (single proteins) that form homodimers (two of the same proteins bound together), heterodimers (two different proteins bound together), and higher order multimers (more than two interacting proteins). For example, Bax forms homodimers or forms heterodimers with either Bcl-2 or Bcl-x<sub>L</sub>. When Bax is present in excess, it antagonizes the antiapoptotic activity of Bcl-2. The formation of Bax homodimers promotes apoptosis, whereas Bax heterodimerization with either Bcl-2 or Bcl-x<sub>L</sub> blocks apoptosis. Thus, the complex steady-state array of protein-protein interactions among members of the

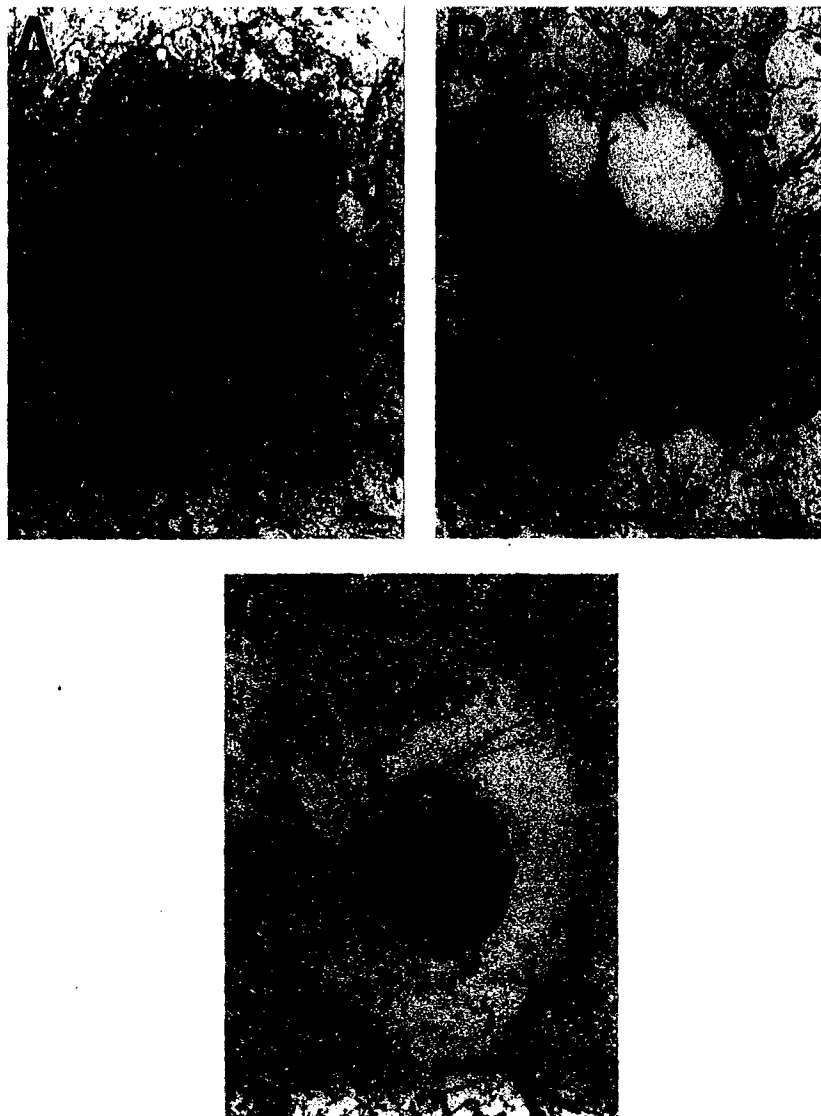


**Figure 10** Neurodegeneration in the form of apoptosis is important for the normal development of the nervous system. By electron microscopy this naturally occurring programmed cell death has very characteristic features. (A) In the developing rat striatum, degenerating neurons in the early stages of apoptosis are characterized by chromatin condensation into crescentic caps (arrowhead) abutting the nuclear envelope and into round aggregates (asterisk). The surrounding cytoplasm condenses (as indicated by the uniformly dark staining), although most of the mitochondria remain intact. Scale bar = 2.5  $\mu$ m. (B) As apoptosis progresses, major changes occur in the nucleus and cytoplasm. The chromatin packaging into dense round clumps (asterisk) becomes more advanced, and the integrity of the nuclear envelope is lost. The cytoplasm becomes more condensed and the mitochondria become damaged. Astrocytic processes (a) begin to surround the degenerating cell. Scale bar = 3.0  $\mu$ m. (C) At end stage apoptosis, fragments of cells consist of round packages of chromatin (asterisk) surrounded by condensed cytoplasm. These apoptotic fragments are engulfed by astrocytic processes (a). Scale bar = 4.0  $\mu$ m.

Bcl-2 family functions in dictating whether a cell lives or dies by apoptosis.

Cell death is also regulated by the IAP (inhibitor of apoptosis protein) family (Table VI). This family includes X-chromosome-linked IAP, IAP1, IAP2, and NAIP (neuronal apoptosis inhibitory protein). Survival motor neuron is another apoptosis inhibitory

protein. The primary mechanism identified by which IAPs suppress apoptosis is the prevention of proteolytic processing of specific caspases. It appears that procaspase-9 is the major target of IAPs. However, IAPs do not prevent caspase-8-induced proteolytic activation of procaspase-3. IAPs can also block apoptosis by reciprocal interactions with the nuclear

transcription factor NF $\kappa$ B. NAIP is abnormal in infants and children with spinal muscular atrophy (Table II).

The regulation of PCD in the mammalian nervous system by caspases and *bcl-2* family members has been substantiated by using transgenic mouse technology and neuronal culture systems. In mice, deficiencies in the genes for caspase-3 and caspase-9 result in perinatal death and cerebral malformations, possibly caused by reduced PCD during brain development. Inhibition of caspase-1 and caspase-2 blocks the apoptosis of cultured dorsal root and sympathetic ganglion neurons when deprived of the neurotrophin nerve growth factor; furthermore, inhibition of caspase-1 arrests the PCD of motor neurons in cell culture resulting from neurotrophic factor deprivation and in the nervous system during the period of naturally occurring cell death. Mice that overexpress the *bcl-2* gene or have the *bax* gene eliminated fail to exhibit normal PCD of neurons in some nervous system regions, whereas *bcl-2*-deficient mice show progressive neurodegeneration after the period of PCD.

## VII. GLUTAMATE RECEPTOR EXCITOTOXICITY KILLS NEURONS

Neurons communicate by neurotransmission at synapses (Fig. 2A). In the CNS, the amino acid glutamate is the major excitatory neurotransmitter that is packaged into small clear synaptic vesicles (Fig. 2A). Glutamate is released from nerve terminals into the synaptic cleft by regulated exocytosis of synaptic

vesicles (Fig. 2B). Concentrations of glutamate at the synaptic cleft have been estimated to be approximately 1 mM, whereas the concentration of interstitial glutamate is about 1  $\mu$ M. Glutamate can bind and activate several types of glutamate receptors (GluRs) on neurons (Table VII). These GluRs are classified broadly as either ion channel or metabotropic G-protein-coupled receptors. These classes of GluRs have distinct molecular compositions and distinct signal transduction mechanisms.

The ion channel GluRs are the *N*-methyl-D-aspartate (NMDA) receptors and the non-NMDA receptors. The non-NMDA GluRs are further divided into the  $\alpha$ -amino-3-hydroxy-5-methyl-4-isoxazole propionate (AMPA) and kainate (KA) receptors (Table VII). The ion channel GluRs all form monovalent cation (Na<sup>+</sup>, K<sup>+</sup>) conducting channels, but they have differences in their permeabilities to divalent cations (Ca<sup>2+</sup>). The activation of ion channel GluRs directly changes the conductance of specific ions through the receptor-ion channel complex, thereby inducing membrane depolarization. Fast, short-lived (1–10 msec) excitatory postsynaptic currents in most neurons in the CNS are mediated by these receptors. These receptors are oligomers, most likely pentameric heterooligomers, of homologous subunits encoded by distinct genes. The NMDA receptor subunits are NR1, NR2A–NR2D, and NR3, the AMPA receptor subunits are GluR1–GluR4 (or GluRA–GluRD), and the kainate receptor subunits are GluR5–GluR7 and KA1–KA2.

The metabotropic GluRs (mGluRs) are G-protein-coupled receptors that are single proteins encoded by

Table VII  
Molecular Classification of Glutamate Receptors

Ion channel (ionotropic) receptors			G protein-coupled (metabotropic) receptors		
NMDA	Non-NMDA		Group I	Group II	Group III
	AMPA	Kainate			
Receptor subunits					
NR1	GluR1	GluR5	mGluR1	mGluR2	mGluR4
NR2A	GluR2	GluR6	mGluR5	mGluR3	mGluR6
NR2B	GluR3	GluR7			mGluR7
NR2C	GluR4	KA1			mGluR8
NR2D		KA2			
NR3					

single genes. The mGluRs do not form ion channels but are instead linked to signal transduction molecules within the plasma membrane. mGluRs have slower electrophysiological characteristics (latencies >100 msec) than ion channel GluRs. Group I mGluRs (mGluR1 and mGluR5) operate through activation of phospholipase C (PLC) by  $G_q$  proteins, phosphoinositide hydrolysis and generation of inositol 1,4,5-triphosphate and diacylglycerol, and subsequent mobilization of  $Ca^{2+}$  from nonmitochondrial intracellular stores. Group II mGluRs (mGluR2 and 3) and group III mGluRs (mGluR4 and 6–8) function by  $G_i$ - or  $G_o$ -protein-mediated inhibition of adenylyl cyclase and modulation of ion channel activity.

Although glutamate and GluR activation are critical for normal nervous system function, glutamate is toxic to neurons at abnormally high concentrations if the GluRs on neurons are excessively activated. This process is called excitotoxicity. The excessive stimulation of GluRs by glutamate or chemical analogs of glutamate produces abnormalities in intracellular ions, pH, protein phosphorylation, energy levels, and reactive oxygen species. Acute excitotoxicity causes degeneration in neuronal cultures of animal brain and spinal cord and after intracerebral delivery of GluR activators into the CNS of experimental animals. In addition, excitotoxicity participates in the mechanisms for neuronal degeneration in animal models of cerebral ischemia, as well as brain and spinal cord trauma, and in the neurotoxicity in humans resulting from consumption of mussels contaminated with the KA receptor activator domoic acid. Excitotoxicity is also suspected as a culprit in the nerve cell loss associated with AD, ALS, Huntington's disease, and Parkinson's disease.

The precise mechanisms for GluR-mediated excitotoxic degeneration of neurons are not understood. Both neuronal culture and animal model data are discordant with regard to whether excitotoxic neuronal death is apoptosis or necrosis. Activation of neuronal GluRs kills neurons by pathways that may involve alterations in cytosolic free  $Ca^{2+}$  homeostasis and activation of  $Ca^{2+}$ -sensitive proteases, protein kinases, endonucleases, lipases, and phospholipases. Excitotoxicity results in an activation of endonucleases (DNA-cleaving enzymes) and internucleosomal digestion of genomic DNA into 180–200 base pair fragments 12–48 hr after intracerebral injections of excitotoxins in rats. Internucleosomal fragmentation of DNA also occurs in cultures of cortical neurons, although others have not found internucleosomal DNA fragmentation in cell culture.

The structural changes that occur in neurons in the adult rat brain after an excitotoxic insult include swelling and vacuolation of the cell body and dendrites, fragmentation of the nucleus into irregular clumps of chromatin, and damage to membranous organelles including the Golgi apparatus, endoplasmic reticulum, and mitochondria. This damage is thought to be typical of cellular necrosis (Fig. 9). However, in the immature brain, excitotoxicity can cause neuronal death very similar to apoptosis.

## VIII. NEURONAL DEGENERATION CAN OCCUR AS AN APOPTOSIS-NECROSIS CONTINUUM

We have developed the concept that neuronal degeneration is influenced by brain maturity and GluR subtype. We tested the hypothesis that GluR-mediated excitotoxicity in the brain induces neuronal death with characteristics that vary depending on the maturity of the brain at the time of the insult and the GluR subtype that is activated. In the newborn rat brain, excitotoxic activation of NMDA and non-NMDA GluRs (Table VII) causes neuronal death with phenotypes ranging from apoptosis to necrosis (Fig. 9). Three structurally different forms of dying neurons were identified initially: a classic apoptotic form, a vacuolated form, and a classic necrotic form. When the progression of excitotoxin-induced neuronal death in the newborn brain was evaluated, it was found that the vacuolated form is a precursor stage of apoptosis, which has many similarities to the PCD that occurs naturally in the developing brain. Thus, some neurons die as a hybrid of apoptosis and necrosis. In contrast, when the adult rat brain is exposed to excitotoxins, the degeneration of neurons caused by NMDA receptor activation is morphologically necrotic; however, the neuronal death produced by non-NMDA receptor activation (Table VII) is distinct from that caused by NMDA receptor stimulation. Non-NMDA receptor-mediated neuronal death in the adult brain has some cytoplasmic and nuclear features reminiscent of neuronal apoptosis in the excitotoxically injured newborn brain, although non-NMDA receptor excitotoxic neurodegeneration in the adult brain and naturally occurring apoptosis in the developing brain are very different structurally. Surprisingly, both NMDA and non-NMDA receptor-mediated excitotoxic neurodegeneration occur in the presence of apoptotic-like internucleosomal DNA fragmentation.

Our experiments using this animal model of excitotoxic degeneration of neurons led to the novel concept of an apoptosis–necrosis continuum for neuronal death in the CNS. We concluded that the excitotoxic death of neurons does not have to be strictly apoptotic or necrotic, according to a traditional binary classification of cell death (Fig. 9), but it can also occur as intermediate or hybrid forms of cell death with coexisting characteristics that lie along a structural continuum with apoptosis and necrosis at the extremes. This continuum is influenced by the subtype of GluR that is activated (Table VII); hence, excitotoxic neuronal death may not be identical in every neuron, possibly because of the high diversity in the expression, localization, and function of GluR subtypes and second messenger systems in the CNS. We also concluded that the structure of neuronal death is influenced by CNS maturity, because excitotoxic degeneration of adult neurons does not occur with apoptotic structural features that closely resemble those seen during naturally occurring cell death in the developing nervous system.

This new concept may be important for understanding how neuronal degeneration occurs in neurological disorders that affect the human brain and spinal cord (Table I) and, thus, may be important for future studies aimed at the prevention of neuronal loss in human neurodegenerative diseases. The clarification of the relationships between mechanisms of neuronal death (active or passive) and the resulting structure of dying neurons in human neurodegenerative disease is important, particularly when addressing hypotheses as to whether PCD and apoptosis are equivalent and whether apoptosis and necrosis are mutually exclusive forms of neuronal cell death. Furthermore, if brain maturity dictates how neurons die, then, in humans, neuronal degeneration in adults may be fundamentally different from neuronal degeneration in newborns or children. For example, mature neurons appear to be less capable than immature neurons of displaying an apoptotic structure after an excitotoxic insult. An injury that produces a hybrid of apoptosis and necrosis in the adult CNS is more likely to elicit primarily apoptosis in the immature CNS. We speculate that PCD mechanisms may be activated more readily after an injury to the immature brain than to the mature brain, because immature neurons are closer than mature neurons to the period of naturally occurring developmental PCD.

## IX. APOPTOSIS MAY HAVE IMPORTANT CONTRIBUTIONS TO NEURODEGENERATIVE DISORDERS IN HUMANS

It has been discovered that the degeneration of neurons in ALS is a form of apoptosis (Fig. 7). Vulnerable brain and spinal cord regions in ALS (Table I) have abnormalities in the balance of Bcl-2, Bax, and Bak proteins and abnormalities in their interactions (Table IV). However, the initial molecular pathology and upstream signals for motor neurons to engage PCD mechanisms are not known, although we suspect DNA damage. Furthermore, it is still unknown whether the neuronal degeneration in other age-related neurological disorders such as AD, Parkinson's disease, and Huntington's disease is related causally to an abnormal activation of PCD pathways in selectively vulnerable neurons.

Much uncertainty also centers around the possible role of apoptosis in the nerve cell degeneration resulting from cerebral ischemia caused by heart failure, asphyxiation, and stroke. Historically, cellular degeneration resulting from these abnormalities has been considered a form of cellular necrosis, but it has been suggested that postischemic neurodegeneration is apoptosis possibly mediated by a PCD mechanism. However, the contribution of apoptosis to the selective degeneration of neurons after ischemia is not yet resolved.

## X. ANIMAL MODELS OF NEURODEGENERATION ARE NECESSARY TO UNDERSTAND HOW NEURONS DIE

Animal models of neuronal degeneration are crucial for improving our understanding of the mechanisms and progressive stages of neuronal death. These models provide an experimental system to identify how nerve cells die in paradigms that mirror certain neuropathological and clinical features of a neurological disorder that occurs in humans (Tables I and VIII). With animal models, the process of nerve cell death can be studied at the structural, biochemical, and molecular levels, and then subsequently the model can be used to test new therapies to prevent the degeneration of neurons in a biologically relevant system.

### A. Neuronal Degeneration in Models of Axotomy and Target Deprivation

Animal models of axotomy (axon cutting or transection) and target deprivation (target removal) provide

insight into the mechanisms of progressive neuronal degeneration and are relevant to acute and slow, chronic degenerative disorders that affect the human brain or spinal cord (Table VIII). The progression of axotomy–target deprivation-induced neuronal degeneration and the likelihood of subsequent neuronal death or survival are influenced by several variables, including whether the cell body of an axotomized neuron resides within the peripheral nervous system (PNS) or CNS, the age of the animal at the time of injury, the location of axonal trauma in relation to the cell body, and the animal species. In the immature brain and spinal cord, axotomized neurons often die rapidly. Axotomy-induced degeneration of motor neurons in the immature CNS appears to be apoptosis on the basis of structural evidence in mouse and chick and the finding that overexpression of the *bcl-2* gene reduces motor neuron death in newborn mice in response to facial nerve transection or sciatic nerve transection. In contrast, in the adult nervous system, axotomized neurons can recover or persist in some altered form or they can undergo apoptosis. The outcome depends upon the type of model. Thus, in general, neuronal apoptosis is induced more easily by axotomy in the immature or newborn CNS than in the mature or adult CNS. Differences in the fate of target-deprived neurons in the developing and adult CNS may be related to the extent of target deprivation and collateral connections of deprived neurons with other brain regions and related to the differential ability to activate a PCD pathway.

Interruption of specific axonal pathways by transection in rodents and nonhuman primates can be used as

a model for some forms of neuronal degeneration and behavioral deficits found in humans with certain neurological disorders (Table VIII). The hippocampal formation and septum form a neural system in the brain that functions in learning and memory. This system is vulnerable in AD (Table I). These brain regions are interconnected by an axon pathway called the fimbria–fornix. Transection of the fimbria–fornix is a model of target deprivation–axotomy that results in degeneration of neurons in the basal forebrain cholinergic complex and partial removal of glutamate-utilizing synaptic inputs (deafferentation) to neurons in the lateral septal nucleus. By using this model in rats, we have shown that these neurons that are deprived of their target or of inputs undergo chronic atrophy rather than death. They shrink but survive in a sickly state. Thus, long-term damage occurs within the cell bodies and dendrites (the major synapse-receiving areas) of these neurons, including the formation of vacuolar pathology, but they do not die. This is encouraging because, if the process is reversible, therapeutic interventions could restore these neurons to a normal healthy condition.

This neuronal injury within the septal complex of rat brain after fimbria–fornix transection has some pathological similarities to neuronal damage caused by excitotoxic GluR activation (Table VII), suggesting a mechanistic overlap. This idea has been confirmed by experiments showing that a drug that blocks NMDA receptors reduces the neuronal damage in the septum after fimbria–fornix transection. This work shows that, following interruption of the fimbria–fornix, the neuronal damage that occurs within the septum is

**Table VIII**  
Human Neurodegenerative Disorders and Animal Models

Neurological condition	Age of onset	Major vulnerable CNS regions	Animal model
Alzheimer's disease	Adult (mid to late life)	Neocortex, hippocampus, amygdala, basal forebrain	Axotomy/target deprivation, excitotoxicity, aging nonhuman primates, transgenic mice
Amyotrophic lateral sclerosis	Adult (midlife)	Motor neurons in spinal cord and brain stem, motor cortex	Axotomy–target deprivation, excitotoxicity, transgenic mice
Parkinson's disease	Adult (midlife)	Substantia nigra dopaminergic neurons	Target deprivation, excitotoxicity, MPTP poisoning, transgenic mice
Huntington's disease	Adult (midlife)	Striatum (caudate nucleus)	Excitotoxicity, metabolic toxins, transgenic mice
Spinal muscular atrophy	Infancy–childhood	Motor neurons in spinal cord and brain stem	Axotomy–target deprivation, transgenic mice
Cerebral ischemia	Any age	Cerebral cortex, striatum, cerebellum, thalamus	Global cerebral ischemia, focal cerebral ischemia (stroke), excitotoxicity, axotomy–target deprivation
CNS trauma	Any age	Cerebral cortex, striatum, cerebellum, thalamus, spinal cord	Contusion–compression injury, excitotoxicity, axotomy–target deprivation

partly caused by a sublethal excitotoxic process involving NMDA receptors. Although GluR activation has been implicated in a variety of neurodegenerative processes within the CNS, these experiments have identified important links between degenerative processes in neurons caused by axon transection, target deprivation, and deafferentation (removal of inputs) and those caused by excitotoxic mechanisms that may be relevant to the neurodegeneration in AD.

It was discovered that the neuronal degeneration in ALS has structural features of apoptosis and molecular characteristics of PCD. Because ALS is an adult-onset neurodegenerative disease, and because of the newly developed concept of the apoptosis-necrosis continuum, it is necessary to study the mechanisms of neuronal apoptosis in the CNS of adult animals. Therefore, models of *bona fide* neuronal apoptosis in the adult brain and spinal cord have been developed. In one model, the neocortex is damaged by unilaterally ablating the visual cortex in the rat. This model axotomizes and deprives thalamic relay neurons in the dorsal lateral geniculate nucleus of their neocortical target. In another model, the sciatic nerve is removed by avulsion. This model axotomizes and deprives motor neurons in the lumbar spinal cord of vital muscle- and Schwann-cell-derived survival factors.

By using these models of retrograde neuronal degeneration, it has been discovered that neuronal apoptosis occurs in association with the accumulation of functionally active mitochondria and oxidative (free radical) damage to the DNA in the cell nucleus. An important new theory of neuronal degeneration has been developed on the basis of these animal models of definitive neuronal apoptosis. Mitochondrial accumulation within the neuronal cell body and increased cytochrome c oxidase activity may result in overwhelming generation of reactive oxygen species within the vicinity of the neuronal nucleus, depletion of mitochondrial and cytosolic antioxidant mechanisms, subsequent oxidative damage to proteins and nucleic acids, and failure of DNA repair mechanisms. The mitochondria become progressively damaged, as evidenced by their swelling and lysis of the inner membrane that manifest concurrently with incipient condensation of the neuronal cytoplasm, supporting the hypothesis that apoptosis-initiating factors are sequestered within the mitochondrial intermembrane space, which upon their release activate an apoptotic cell death cascade. Damage to DNA then activates a p53-dependent form of PCD in injured neurons. At present, it is still not known whether this process truly mimics the condition in humans with a

neurodegenerative disease, but this idea is being actively studied.

The process of axotomy-induced neuronal apoptosis is associated with hydroxyl radical damage to DNA. Hydroxyl radicals are products of the transition metal (e.g., iron) catalyzed, Haber-Weiss- and Fenton-type reactions that use superoxide and hydrogen peroxide as substrates, respectively. Among the reactive oxygen species, hydroxyl radicals are highly reactive and are thought to be genotoxic by interacting with DNA and producing DNA strand breaks and base modifications. Our experiments are very important because they show, for the first time, the formation of hydroxyl-radical-modified DNA during the progression of neuronal apoptosis in animal models that are relevant to both AD and ALS.

## B. Neuronal Degeneration in Models of Cerebral Ischemia

An interruption in the normal supply of oxygen to the brain resulting from abnormal blood flow or low amounts of oxygen in the blood causes cerebral hypoxia-ischemia. If the entire brain is affected, as in heart failure or asphyxiation, the abnormality is called global cerebral hypoxia-ischemia. If only specific regions are affected as in stroke, the perturbation is called focal cerebral ischemia. The mechanisms by which cerebral ischemia produces irreversible neuronal death are still not fully understood. Interestingly, only certain regions of the brain are selectively damaged by global cerebral hypoxia-ischemia (Table I).

We have studied neuronal degeneration by using models of global ischemia in experimental animals. The degeneration of pyramidal neurons in the neocortex and hippocampus, Purkinje cells in the cerebellum, and medium spiny neurons in the striatum after global ischemia (Table I) pathologically is a form of cellular necrosis rather than apoptosis. We have observed patterns of DNA fragmentation, with a progression that is very consistent with acute damage by reactive oxygen species and subsequent neuronal necrosis. The degeneration of selectively vulnerable neurons after ischemia (Table I) evolves in association with damage to organelles that function in protein synthesis, posttranslational modification, and secretion. Disaggregation of polyribosomes and fragmentation or vesiculation of the endoplasmic reticulum and Golgi apparatus are prominent examples of this subcellular pathology that would likely alter protein



synthesis-processing capabilities. This degeneration of neurons after ischemia is structurally similar in the different brain regions, regardless of the severity of the ischemia and whether the degeneration occurs acutely ( $\leq 24$  hr) or is delayed (3–7 days). Thus, the acute and delayed neuronal deaths after cerebral ischemia are structurally, and perhaps mechanistically, identical. In several models of global cerebral ischemia, neuronal degeneration in selectively vulnerable regions is indistinguishable structurally from the neuronal death caused by excitotoxicity, and, specifically, it closely resembles the neuronal necrosis caused by NMDA GluR activation in the adult brain.

In the same animal models, apoptotic cell death occurs in some neuronal groups that are not typically regarded as selectively vulnerable to ischemia. For example, subsets of granule cells in the hippocampal dentate gyrus and cerebellar cortex and subsets of neurons in the thalamus undergo apoptosis. In addition, prominent apoptotic death of white matter oligodendrocytes can occur. It has been theorized that apoptosis in these groups of cells after global ischemia is a form of PCD caused by target deprivation and axonal degeneration in response to necrotic degeneration of selectively vulnerable populations of neurons (Table I). Thus, necrosis and apoptosis, occurring as secondary degeneration in remote or distant brain areas resulting from target deprivation, both contribute to the neurodegeneration after cerebral ischemia.

Interestingly, cell death in the different settings of naturally occurring and pathological neuronal degeneration may be mechanistically distinct, or some of the underlying mechanisms in these different settings of neuronal degeneration may be shared to varying degrees, but they differ in the rate at which the primary mechanisms of injury occur (e.g., how fast an oxidative stress occurs). For example, oxidative stress and free radical damage in neuronal death caused by target deprivation-axotomy evolve slowly, and the corresponding neuronal death is apoptosis; in contrast, if oxidative stress evolves rapidly, as in the death of striatal neurons after ischemia, then the neuronal death is necrosis.

An important, unresolved question regarding the pathobiology of neuronal degeneration is whether the absence of the classic apoptotic structure in vulnerable populations of neurons is sufficient evidence to exclude the possibility that PCD participates in the pathogenesis of neuronal degeneration. All forms of PCD may not occur via apoptosis. For example, the death of T cells during negative selection in mouse thymus and the death of intersegmental muscles during metamorpho-

sis in the moth *Manduca sexta* both occur by PCD; however, these cell populations die with distinct structural and biochemical features. Thus, some cells can die by a PCD mechanism that is not associated with the structure of classic apoptosis. Clearly, much more work using animal and cell models is needed to answer this complex question as it may relate to neuronal degeneration in disorders of the human brain and spinal cord.

## XI. THE FUTURE IS PROMISING FOR UNDERSTANDING THE CAUSES OF NEURODEGENERATIVE DISORDERS IN HUMANS AND IDENTIFYING TREATMENTS

Unfortunately, no effective treatments are available to prevent or cure any of these neurological disorders that affect humans. Molecular genetics studies are likely to identify additional gene mutations or deletions that are associated with progressive neurodegenerative disorders (Table II). Animal models of experimental neuropathology will remain critical for studying how nerve cells die in the brain and spinal cord. Neurons within the CNS can be damaged by neurotoxin exposure, by cutting nerves and white matter pathways, by reducing blood flow to the brain producing oxygen deprivation, by forcing brain cells to express mutant genes, and by deleting genes. These animal models of neuronal degeneration are relevant to several neurological disorders that affect humans, including Alzheimer's disease, ALS, and cerebral ischemia (Table VIII). A better understanding of the pathogenesis of neuronal degeneration in human diseases and in animal models that mirror this degeneration is critical for the future development of effective therapies for patients with Alzheimer's disease, ALS, and other conditions. A more complete understanding of the characteristics and mechanisms of neuronal death within the CNS, provided by animal models of injury and transgenic gene expression-deletion, is important for the subsequent development of effective pharmacological and biological treatments to prevent or limit neurodegeneration in human neuropathological conditions.

It is still generally believed that, once neurons die in the mature CNS of mammals, these neurons cannot be replaced by nearby neurons (unlike the liver for example) because the remaining neurons are postmitotic (i.e., after neurons have achieved their mature

state, they cannot enter back into the cell cycle and undergo cell division). However, nervous tissue grafting or stem cell implantation as a means for neuronal replacement is an experimental approach that offers some hope, though much work needs to be done to evaluate the feasibility and efficacy of this approach. Importantly, it remains to be shown whether the immature or adult CNS provides a permissive environment for the appropriate integration of exogenous or grafted cells into a functional neural system.

### See Also the Following Articles

ALZHEIMER'S DISEASE, NEUROPSYCHOLOGY OF •  
BASAL GANGLIA • GLIAL CELL TYPES • MOTOR  
CONTROL • MOTOR NEURON DISEASE • MOTOR SKILL •  
MULTIPLE SCLEROSIS • NEURAL TRANSPLANTATION •  
NEURON • NEUROTRANSMITTERS • PARKINSON'S  
DISEASE • STROKE

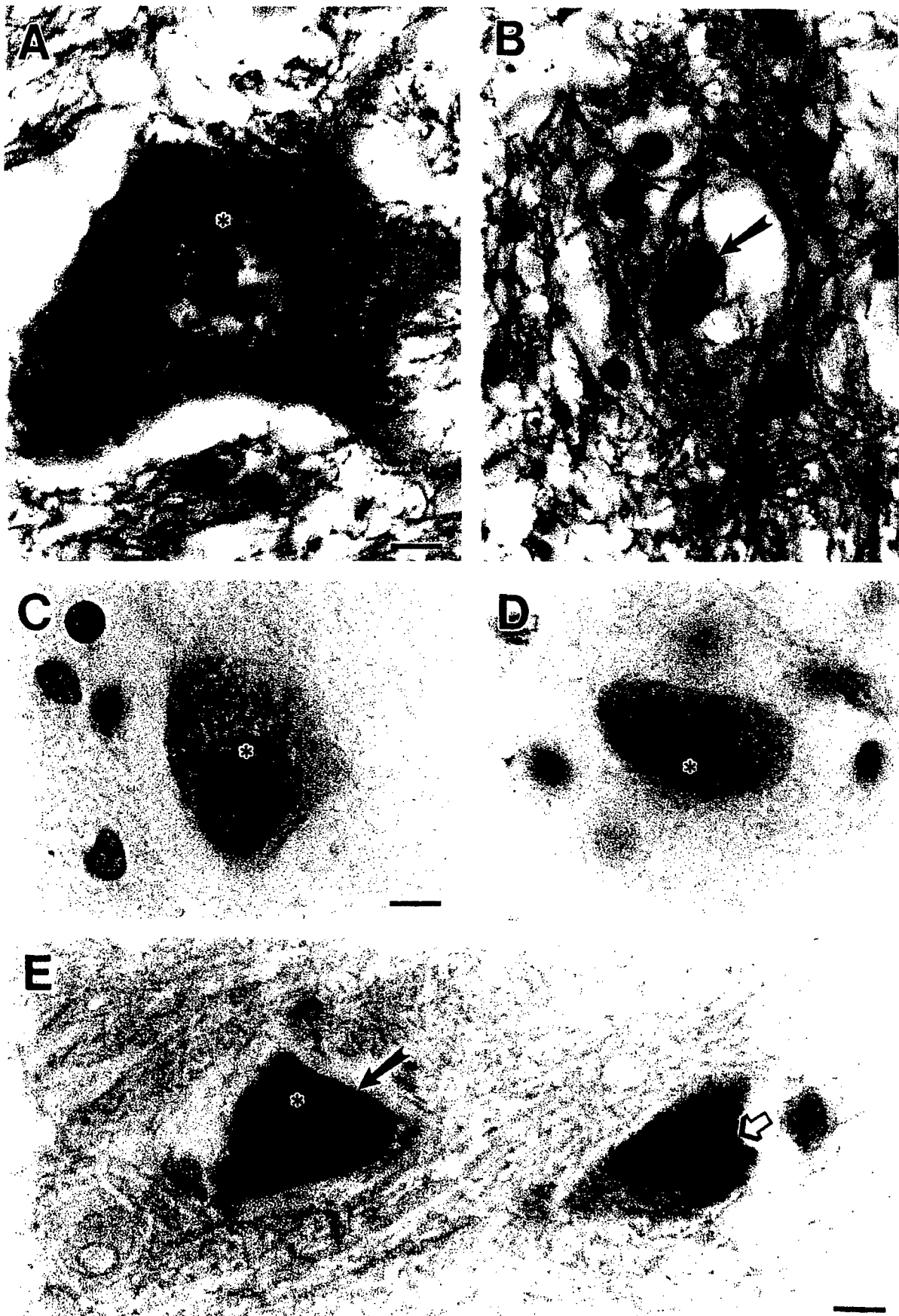
### Acknowledgments

Dr. Martin is supported by grants from the U.S. Public Health Service, National Institutes of Health, National Institute of Neurological Disorders and Stroke (NS 34100), National Institute on Aging (AG16282), and the U.S. Army Medical Research and Material Command (DAMD17-99-1-9553). The author is grateful for the expert assistance of Ann Price, Frank Barksdale, and Adeel Kaiser, and he thanks Drs. Carlos Portera-Cailliau, Stephen Ginsberg, Chun-I Sze, Akiko Furuta, Nael Al-Abdulla, Frances Northington, JoAnne Natale, and Ansgar Brambrink for their contributions to his laboratory. This chapter is dedicated to my wonderful twin daughters, Gabrielle and Isabella.

### Suggested Reading

Martin, L. J., Pardo, C. A., Cork, L. C., and Price, D. L. (1994). Synaptic pathology and glial responses to neuronal injury precede the formation of senile plaques and amyloid deposits in the aging cerebral cortex. *Am. J. Pathol.* **145**, 1358–1381.

- Martin, L. J., Brambrink, A. M., Lehmann, C., Portera-Cailliau, C., Koehler, R., Rothstein, J., and Traystman, R. J. (1997). Hypoxia-ischemia causes abnormalities in glutamate transporters and death of astroglia and neurons in newborn striatum. *Ann. Neurol.* **42**, 335–348.
- Martin, L. J., Al-Abdulla, N. A., Brambrink, A. M., Kirsch, J. R., Sieber, F. E., and Portera-Cailliau, C. (1998a). Neurodegeneration in excitotoxicity, global cerebral ischemia, and target deprivation: A perspective on the contributions of apoptosis and necrosis. *Brain Res. Bull.* **46**, 281–309.
- Martin, L. J., Portera-Cailliau, C., Ginsberg, S. D., and Al-Abdulla, N. A. (1998b). Animal models and degenerative disorders of the human brain. *Lab Animal* **27**, 18–25.
- Martin, L. J. (1999). Neuronal death in amyotrophic lateral sclerosis is apoptosis: Possible contribution of a programmed cell death mechanism. *J. Neuropathol. Exp. Neurol.* **58**, 459–471.
- Martin, L. J., Price, A. C., Kaiser, A., Shaikh, A. Y., and Liu, Z. (2000a). Mechanisms for neuronal degeneration in amyotrophic lateral sclerosis and in models of motor neuron death. *Int. J. Mol. Med.* **5**, 3–13.
- Martin, L. J., Sieber, F. E., and Traystman, R. J. (2000b). Apoptosis and necrosis occur in separate neuronal populations in hippocampus and cerebellum after ischemia and are associated with alterations in metabotropic glutamate receptor signaling pathways. *J. Cereb. Blood Flow Metab.* **20**, 153–167.
- Martin, L. J., Brambrink, A. M., Price, A. C., Kaiser, A., Agnew, D. M., Ichord, R. N., and Traystman, R. J. (2000c). Neuronal death in newborn striatum after hypoxia-ischemia is necrosis and evolves with oxidative stress. *Neurobiol. Disease* **7**, 169–191.
- Mouton, P. R., Martin, L. J., Calhoun, M. E., Dal Forno, G., and Price, D. L. (1998). Cognitive decline strongly correlates with cortical atrophy in Alzheimer's disease. *Neurobiol. Aging* **19**, 371–377.
- Portera-Cailliau, C., Price, D. L., and Martin, L. J. (1997). Excitotoxic neuronal death in the immature brain is an apoptosis-necrosis morphological continuum. *J. Comp. Neurol.* **378**, 70–87.
- Sze, C.-I., Troncoso, J. C., Kawas, C., Mouton, P., Price, D. L., and Martin, L. J. (1997). Loss of the presynaptic vesicle protein synaptophysin in hippocampus correlates with cognitive decline in Alzheimer's disease. *J. Neuropathol. Exp. Neurol.* **56**, 933–994.
- Sze, C.-I., Bi, H., Kleinschmidt-DeMasters, B. K., Filley, C. M., and Martin, L. J. (2000). Selective regional loss of exocytotic presynaptic vesicle proteins in Alzheimer's disease brains. *J. Neurol. Sci.* **175**, 81–90.



Motor neuron degeneration in ALS (amyotrophic lateral sclerosis) is a form of apoptosis that may be mediated by a p53-dependent mechanism triggered by DNA damage. See article *NEURODEGENERATIVE DISORDERS*.

## Synaptic and Neuroglial Pathobiology in Acute and Chronic Neurological Disorders

---

Lee J. Martin

### 1. INTRODUCTION

Pathology at the molecular and cellular level is the fundamental basis of disorders that effect the brain or spinal cord of humans. A pathophysiological event can target specific molecules and groups of cells, causing neuronal dysfunction and degeneration and resulting in acute and chronic neurological and behavioral disabilities ranging from memory loss to paralysis. For example, Alzheimer's disease (AD) is associated with loss of forebrain neurons and the formation of brain lesions consisting of abnormal deposits of glial- or -neuronal generated amyloid  $\beta$  protein, possibly in response to gene mutations, synaptic perturbations, oxidative stress, or neuronal cytoskeletal defects (1-5). The degeneration of motor neurons in amyotrophic lateral sclerosis (ALS) is associated with impairments in glutamate reuptake by astroglia (6,7), gene mutations in superoxide dismutase-1 (8), and abnormal apoptosis of motor neurons that appears to be mediated by programmed cell death mechanisms (9,10). The nerve cell damage in adults and children that have experienced cardiac arrest, asphyxiation, strokes, and head or spinal cord trauma may be caused by failure of astroglial glutamate transport, excessive stimulation of glutamate receptors, abnormal activation or impaired function of intracellular signaling pathways, toxic generation of free oxygen radicals, and structural damage to target molecules within selectively vulnerable populations of neurons (11). Epidemiological studies reveal the impact that neurodegenerative disorders have on our society. For example, AD affects ~4 million adults (most are >65-yr-of-age) and is the fourth-leading cause of death in the United States, accounting for >100,000 deaths annually (12). ALS affects approx 30,000 Americans (4-6 people in 100,000) (13). Stroke is the third leading cause of death in industrialized populations and is a major cause of long term neurological disability (14).

No cures or therapies (e.g., synthetic drugs or biological factors) are available yet that can prevent the degeneration of neurons in the human brain and spinal cord and that can improve the quality of life for individuals with these neurological disorders. The current inability to effectively and rationally manage and treat individuals with these nervous system abnormalities is due to insufficient information on how neurons and glia become dysfunctional or degenerate and the synaptic and molecular mecha-

nisms for this pathobiology. This chapter will focus on synaptic and neuroglial perturbations in two broad settings of neurodegeneration: Acute neuronal cell death after cerebral ischemia and chronic, progressive neuronal degeneration that occurs in age-related disorders of the nervous system, such as AD and ALS. Treatments for these disorders will be forthcoming eventually through a more complete understanding of the normal cellular and molecular organization of the nervous system and of cellular and molecular neuropathology.

## 2. ORGANIZATION OF THE CENTRAL SYNAPSE

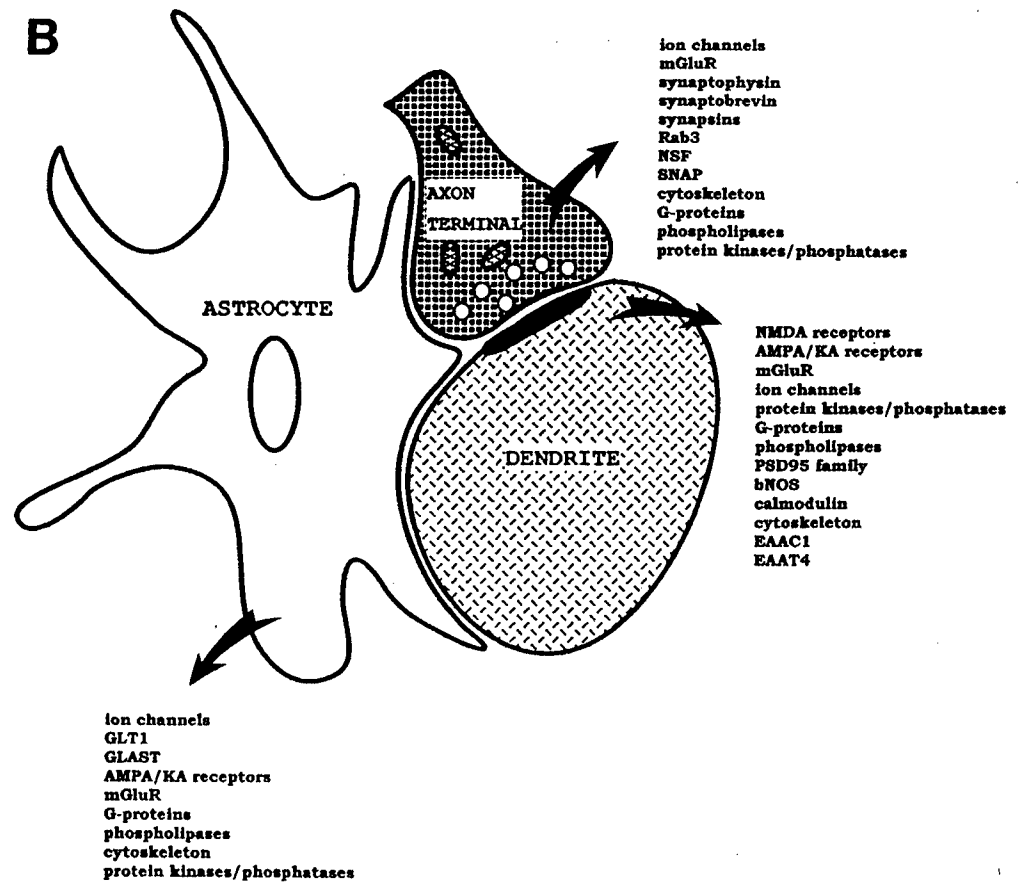
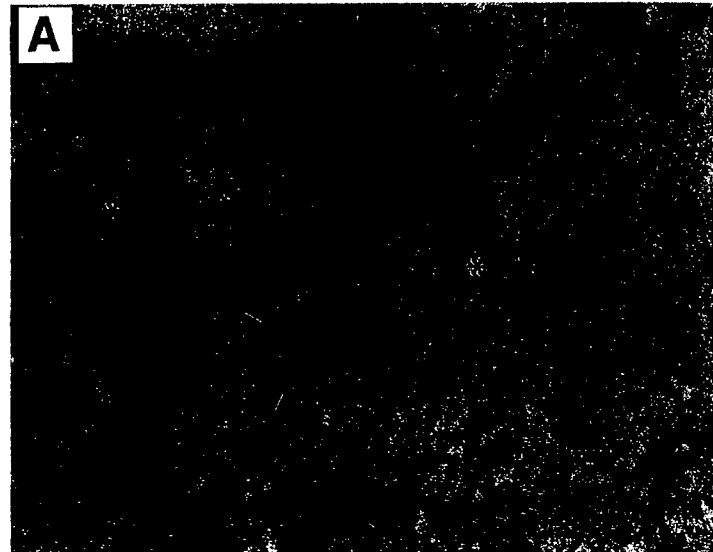
### 2.1. Structural and Molecular Design of the Synapse

Synapses are the principal units of intercellular communication in neural circuits. The structural organization of a central nervous system (CNS) synapse consists of a presynaptic component (the axon terminal), a synaptic cleft (~20–40 nm in width), a postsynaptic component (a neuronal cell body or process), and an astroglial sheath (Fig. 1). Each of these components has its own elaborate structural organization and molecular specifications. The presynaptic and postsynaptic membranes have thickenings on their cytoplasmic surfaces (Fig. 1), and these specialized membranes together with the synaptic cleft form the synaptic junction. These membrane specializations are the presynaptic grid or active zone and the postsynaptic density.

The presynaptic nerve terminal (Fig. 1A), containing several hundred neurotransmitter vesicles, is the principal site of regulated release of excitatory or inhibitory neurotransmitters. A complex ensemble of proteins (Fig. 1B) within the presynaptic nerve terminal functions in exocytosis of neurotransmitter-containing vesicles (15). Synaptic vesicles dock at the active zone. Specific proteins function in neurotransmitter vesicle docking, priming, fusion, and exocytosis and endocytosis. This process is called the synaptic vesicle cycle (15).

Dendrites receive the vast majority of excitatory synapses in the mammalian CNS (Figs. 1 and 2). Like the presynaptic terminal, the postsynaptic element contains an equally staggering array of proteins that function in inter- and intracellular signaling. These proteins are neurotransmitter receptors (ionotropic and metabotropic receptors), ion channels ( $\text{Ca}^{2+}$ ,  $\text{Na}^+$ ,  $\text{K}^+$ , and  $\text{Cl}^-$  channels), and other signal transduction molecules, including protein kinases, protein phosphatases, heterotrimeric GTP-binding proteins (G-proteins), phospholipases, nitric oxide synthase (NOS), calmodulin, and cytoskeletal proteins (Fig. 1B). At the postsynaptic site, the postsynaptic density is an

**Fig. 1. (Right)** Organization of a central nervous system synapse (A) Electron micrograph illustrating the synaptic complex. Two presynaptic axon terminals (t), containing numerous neurotransmitter vesicles (arrows) which are ~50 nm in diameter, form synaptic junctions with dendrites (d). The dark thickening at the dendritic side of the junction is the postsynaptic density. The synaptic cleft of one junction is identified (arrowheads). Astroglial processes (asterisks) ensheath the synaptic complex. (B) Simplified synaptic organization in forebrain as represented by an presynaptic axon terminal (with synaptic vesicles and mitochondria) forming an asymmetrical synapse with a dendrite (seen in cross sectional profile). An astrocyte partially envelops the synapse. Each component of the central synapse has a complex ensemble of proteins integral to their function. Although the lists are incomplete, some important proteins are identified.



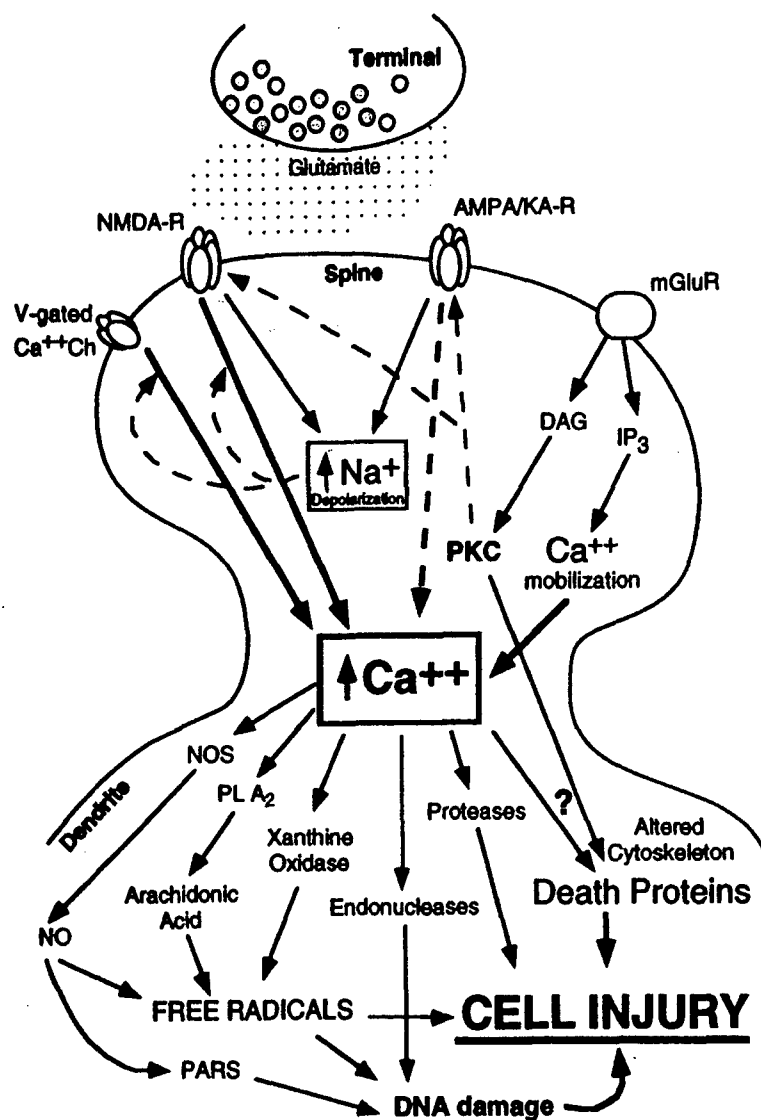


**Fig. 2.** Summary diagram of synaptic mechanisms related to excitotoxic neuronal degeneration. The diagram summarizes the prominent postsynaptic intracellular pathways that lead to neuronal injury and death resulting from excitotoxic activation of GluR. Abbreviations: AMPA/KA-R,  $\alpha$ -amino-3-hydroxy-5-methyl-4-isoxazole propionate and kainate receptors; DAG, diacylglycerol;  $IP_3$ , inositol trisphosphate; mGluR, metabotropic glutamate receptor; NMDA-R, *N*-methyl-*D*-aspartate receptor; NO, nitric oxide, NOS, NO synthase, PARS, poly (ADP-ribose) synthetase also known as PARP, poly(ADP-ribose) polymerase; PKC protein kinase C;  $PLA_2$ , phospholipase  $A_2$ ; V-gated  $Ca^{++}$  ch, voltage-gated  $Ca^{2+}$  channel.

electron-dense meshwork of fine filaments that underlies the plasma membrane and is thought to anchor and cluster neurotransmitter receptors (16–18).

Astroglia have a critical role in synaptic function and neuronal survival. Astroglia are the most numerous cellular element of the mammalian CNS. They outnumber

neurons by ten to one and comprise up to 50% of the total tissue volume in some brain regions, with the volume of the astroglial compartment increasing with phylogenetic development (19,20). Astroglial processes ensheath the cell bodies and processes of neurons, envelop synapses (Fig. 1), invest the nodes of Ranvier of myelinated axons, and form glial limiting membranes over the meninges and parenchymal vasculature. The known functions of astrocytes are numerous, including regulation of synaptic neurotransmission, extracellular pH, ion concentration and osmolarity, production and secretion of extracellular matrix proteins, neurotrophic factors and cytokines, detoxification of toxic metabolites (e.g., ammonia, glutamate, and free radicals), and immune/inflammatory response mechanisms (19,20). Astrocytes express functional ligand-gated and metabotropic receptors to neurotransmitters, including glutamate receptors, and they express voltage-gated and other ion channels, including  $\text{Ca}^{2+}$ ,  $\text{Na}^+$ ,  $\text{K}^+$ , and  $\text{Cl}^-$  channels. Astroglia also possess uptake systems for neurotransmitters for terminating synaptic neurotransmission. Astrocytes respond to a wide variety of potentially injurious stimuli in an effort to restore normal physiological set points. Perturbations in astroglial functions may participate directly in the pathobiology of neuronal degeneration in disease. Important topics that will be discussed in this chapter are astroglial uptake of glutamate and production of amyloid  $\beta$  protein.

## 2.2. Glutamate Receptor Subtypes

The amino acid glutamate is the major excitatory neurotransmitter in the CNS (21,22). In normal circumstances, glutamatergic synaptic transmission occurs by regulated release of glutamate from presynaptic axon terminals (Figs. 1 and 2). Concentrations of neurotransmitter glutamate at the synaptic cleft have been estimated to be ~1 mM, whereas the concentration of interstitial glutamate is ~1  $\mu\text{M}$  (23). At synapses, glutamate binds and activates several molecular subtypes of glutamate receptors (GluRs) located on the plasma membranes of neurons and some glial cells (24). These receptors are categorized as members of one of two families, the ionotropic receptors and metabotropic receptors, which differ structurally (distinct molecular compositions) and functionally (distinct signal transduction mechanisms) (24,25).

Ionotropic GluRs form monovalent cation ( $\text{Na}^+$ ,  $\text{K}^+$ )-conducting channels, but the different subtypes have differences in their permeabilities to divalent cations ( $\text{Ca}^{2+}$ ) (24,25). The activation of ionotropic GluRs directly changes conductance of specific ions through the receptor-ion channel complex, thereby inducing membrane depolarization. The ionotropic GluRs are the *N*-methyl-*D*-aspartate (NMDA) receptors and the non-NMDA receptors ( $\alpha$ -amino-3-hydroxy-5-methyl-4-isoxazole propionate [AMPA] and kainate receptors). These receptors are oligomers, most likely pentameric heterooligomers, of homologous subunits encoded by distinct genes. The NMDA receptor subunits are NR1 and NR2A-NR2D, the AMPA receptor subunits are GluR1-GluR4 (or GluRA-GluRD), and the kainate receptor subunits are GluR5-GluR7 and KA1-2 (24,25). Variants of AMPA receptor subunits (designated as "flip" and "flop") are generated by alternate splicing of GluR1-GluR4 mRNA (26). These two versions of subunits are different minimally in a 38-amino acid transmembrane sequence, but the "flip" variant shows less desensitization and larger currents (26). Additional diversity in GluR function is generated by RNA editing (25). GluR2 is a



negative regulator of  $\text{Ca}^{2+}$  permeability through non-NMDA receptors (i.e., its presence in the pentameric receptor assembly blocks  $\text{Ca}^{2+}$  flux) (25,27–29). The molecular mechanism for the  $\text{Ca}^{2+}$  impermeability of GluR2 is RNA editing. The genomic sequence of GluR2 differs from the cDNA in the coding sequence between transmembrane domains 1 and 2, and this editing of mRNA transcripts results in an arginine instead of a glutamine, thereby changing the channel properties (27–29).

In most neurons in the CNS, activation of glutamate-gated ion channels produces fast, short-lived, excitatory postsynaptic currents with latency periods ranging from 1–10 msec; excitatory postsynaptic currents of non-NMDA receptors have greater amplitudes and shorter durations than NMDA receptors. AMPA and kainate receptor channels are voltage-independent, whereas the NMDA receptor is voltage-dependent because of a  $\text{Mg}^{2+}$  block at resting membrane potentials (24,25). Because the non-NMDA receptor channels are permeable to monovalent cations,  $\text{Na}^+$  enters the cell following its electrochemical gradient, thereby depolarizing the postsynaptic plasma membrane and activating voltage-sensitive ion channels, including NMDA receptors,  $\text{Ca}^{2+}$  channels, and  $\text{Na}^+$  channels (Fig. 2).

Other GluRs do not form ion channels but are instead linked to signal transduction molecules within the plasma membrane. These metabotropic GluRs (mGluRs) are G protein-coupled receptors that are single proteins encoded by single genes (30,31). mGluRs have slower electrophysiological characteristics (latencies >100 msec) than ion channel GluRs. Group I mGluRs (mGluR1 and mGluR5) operate through activation of phospholipase C (PLC) by  $G_q$  proteins, phosphoinositide hydrolysis and generation of inositol-1,4,5 triphosphate and diacylglycerol, and subsequent mobilization of  $\text{Ca}^{2+}$  from nonmitochondrial intracellular stores (31). Group II mGluRs (mGluR 2 and 3) and Group III mGluRs (mGluR 4 and 6–8) function by  $G_i$  or  $G_o$  protein-mediated inhibition of adenylyl cyclase and modulation of ion channel activity (30,31).

### 2.3. Glutamate Transporter Subtypes

Excitatory synaptic transmission is largely terminated by high-affinity,  $\text{Na}^+$ -dependent transport of glutamate into cells (neurons and astroglia), thereby preventing extracellular concentrations of synaptic glutamate from reaching neurotoxic levels (Fig. 1B). Five distinct high affinity,  $\text{Na}^+$ -dependent glutamate transporters have been cloned from animal and human tissue (GLAST, GLT1, EAAC1, EAAT4, and EAAT5), and these proteins differ in structure, pharmacological properties, and tissue distribution (32–34). Under physiological conditions in normal adult CNS, immunohistochemical studies have shown that GLAST and GLT1 are expressed primarily in astrocytes, whereas EAAC1 is widely distributed in neurons (35–38). EAAT4 is expressed mainly in cerebellar Purkinje cells (37,39), and EAAT5 is primarily a retinal glutamate transporter (34). Thus, the dominant astroglial and neuronal glutamate transporters in cerebellum are GLAST and EAAT4, respectively, whereas GLT1 and EAAC1 are the primary astroglial and neuronal glutamate transporters, respectively, in forebrain, brainstem, and spinal cord.

The different molecular subtypes of glutamate transporters have very distinct, but coordinated, regional patterns of expression during CNS development. The cell-type specificity in the expression of distinct glutamate transporter subtypes is generally similar in the developing and adult CNS. However, one major exception to this conclu-

sion is that GLT1 is also expressed transiently in a variety of neurons in the developing CNS (37,38,40).

#### **2.4. Synaptic Pathobiology: GluR-Mediated Excitotoxicity and Glutamate Toxicity**

Abnormalities in synaptic function (Fig. 2) can kill neurons in animal models and in humans. Although glutamate and GluR activation are critical for normal brain function, glutamate is toxic to neurons at abnormally high concentrations (41,42). When GluRs are activated excessively, a process called excitotoxicity ensues (41,42). Acute excitotoxicity causes degeneration in cultures of neurons from animal brain and spinal cord and after in vivo delivery of GluR agonists into the CNS of experimental animals (42–45). In addition, excitotoxicity participates in the mechanisms for neuronal degeneration in animal models of cerebral ischemia and traumatic brain injury (11,42,43) and in the neurotoxicity of humans resulting from ingestion of mussels contaminated with the GluR agonist domoic acid (46). In humans, GluR-mediated excitotoxic mechanisms have also been suspected to be responsible for epilepsy, for the neuronal death in the brain resulting from cardiac arrest and stroke, and for neuronal degeneration occurring in individuals with AD, ALS, Huntington's disease, and Parkinson's disease (11,14,42,43,47).

The excessive interaction of glutamate or chemical analogs of glutamate with subtypes of GluRs produces abnormalities in intracellular ionic concentrations, pH, protein phosphorylation, molecular stability, and energy metabolism (42,43). Excitotoxically challenged cells (Fig. 2) undergo rapid osmotic perturbations and swell, reflecting the influx of  $\text{Na}^+$ ,  $\text{Cl}^-$ , and  $\text{H}_2\text{O}$  (43). An increase in cytosolic free  $\text{Ca}^{2+}$ , resulting from activation of  $\text{Ca}^{2+}$ -permeable AMPA receptors and voltage-sensitive ion channels including NMDA receptors and  $\text{Ca}^{2+}$  channels, causes increased enzymatic activity of  $\text{Ca}^{2+}$ -sensitive proteases, protein kinases, and phosphatases, endonucleases, and phospholipases (Fig. 2). Through the activation of proteins with DNase activity, excitotoxicity results in internucleosomal DNA fragmentation in cultures of cortical neurons (48,49) and cerebellar granule cells (50,51), although others have not found internucleosomal DNA fragmentation in cerebellar granule cell cultures (52). In vivo, internucleosomal and random fragmentation of genomic DNA occur 12–48 h after intracerebral injections of excitotoxins (44,45,53,54), and this pattern can persist to 5 d postlesion (54). The activation of other  $\text{Ca}^{2+}$ -dependent enzyme systems, such as phospholipase  $\text{A}_2$ , cyclo-oxygenase, and xanthine oxidase, can generate highly toxic reactive oxygen species (ROS) (55,56). Another pathway for the production of ROS, namely nitric oxide (NO), is activation of  $\text{Ca}^{2+}$ /calmodulin-dependent NOS (57).

Oxidative stress is a potent stimulus for neuronal death in cultured neurons (58,59). ROS (e.g., superoxide anion radical, hydrogen peroxide, hydroxyl radical, NO, and peroxynitrite) can cause direct oxidative damage to macromolecules, including DNA, protein, and lipid membranes (55–57). The balance between the formation of endogenous free radicals and antioxidant defense mechanisms is important for cellular survival. ROS are also products of oxidative metabolism. The mitochondrial electron-transfer chain is a primary generator of superoxide and peroxide, and damaged mitochondria are believed to produce greater amounts of superoxide ion (60). Damage to mitochondrial DNA caused by ROS may lead to protein conformational

changes usually associated with an inefficient electron transfer to cytochrome c oxidase (61) and, hence, enhanced superoxide and peroxide formation. Other critical molecular targets for oxidative damage include glutamate transporters (62),  $\text{Na}^+/\text{K}^+$  ATPase (63), glucose transporters (64), cytoskeletal proteins (65,66), and superoxide dismutase-1 (67). ROS can also mediate trophic factor deprivation-induced apoptosis of sympathetic neurons in vitro (68), and we have implicated ROS in target deprivation-induced apoptosis of brain and spinal cord neurons in vivo (69,70). Because neuronal survival depends on trophic factors (71,72), some of which are glial-derived, abnormalities in neurotrophic support may result in apoptotic death of neurons by inducing a PCD mechanism involving the generation of ROS (68–70).

Another mechanism through which glutamate can cause death of neuronal cells is oxidative glutamate toxicity. In this process, glutamate alters cellular metabolism by interacting with the cystine-glutamate antiporter, resulting in depletion of intracellular cystine/cysteine and reduced levels of the cysteine-containing tripeptide glutathione (73). Oxidative stress results from depletion of intracellular pools of the antioxidant glutathione (73). Activation of phosphoinositide-linked mGluRs generates a cellular response that protects against oxidative glutamate toxicity; in contrast, group I mGluR antagonists potentiate glutamate toxicity (74).

### 3. NEUROGLIAL AND SYNAPTIC MECHANISMS FOR NEURONAL DEGENERATION AFTER CEREBRAL ISCHEMIA

#### 3.1. Abnormalities in Glutamate Transport and Astroglia Occur after Global Cerebral Ischemia

Numerous overlapping mechanisms for neuronal injury are likely to be operative in ischemic brain damage. Here, the focus will be on impaired glutamate transport, excitotoxicity, and the associated perturbations in intracellular signal transduction. In models of transient global cerebral ischemia, extracellular glutamate levels are increased transiently (75–78), possibly resulting in excitotoxic activation of neuronal GluR (79). Abnormally high concentrations of extracellular glutamate may be the result of vesicular exocytosis of glutamate (80), reversed glutamate transporter function (81), defective uptake of glutamate (82–84), or astrocyte swelling (85). Of these possible mechanisms, impaired glutamate transporter function has received considerable attention.

Impaired glutamate transport is thought to cause neurodegeneration. For example, intrastriatal delivery of the glutamate transport inhibitor DL-threo-3-hydroxyaspartate causes neuronal degeneration in rat (86). Lethal spontaneous seizures and increased susceptibility to acute cortical injury occur in some mice deficient in GLT1 (87), and GLAST gene-ablation exacerbates retinal damage after ischemia in mice (88). However, we have shown that transient reductions in glutamate transporter function and astroglial glutamate transporter (GLAST and GLT1) protein expression can occur in the absence of neuronal degeneration in models of axotomy and deafferentation (89,90).

Alterations occur in glutamate transporters after cerebral ischemia. In adult rat,  $D$ - $[^3\text{H}]$ aspartate binding sites are increased in hippocampus within 5 min after forebrain ischemia (91), but the levels of GLT1 mRNA and protein are reduced in hippocampus at 3–6 h postischemia (92). In rat pups (7-d-of-age), high-affinity glutamate transport is

transiently reduced in striatum during hypoxia-ischemia and after one hour of recovery (82). In hypoxic-ischemic piglets (1-wk-old), high-affinity glutamate transport in striatal synaptosomes is defective functionally by 6 to 12 h recovery (84), and GLT1 and EAAC1 protein levels are reduced in striatum at 24 h recovery and thereafter (83). In contrast, GLAST protein expression is maintained in striatum after hypoxic-ischemic injury (84). Therefore, the evolution of neuronal degeneration in some brain regions after hypoxia-ischemia is paralleled by sustained abnormalities in glutamate transport during the first 24 h of recovery. These defects in glutamate transporters are molecular subtype specific (83,84).

A functional defect in glutamate uptake could be mediated by inactivation of glutamate transporters. For example, covalent modification of glutamate transporters by glycosylation influences their function. *N*-linked glycosylation of EAAC1 (93), but not *N*-glycosylation of GLAST (94), appears to be required for transporter activity. We have shown that the Golgi apparatus within striatal neurons undergoes fragmentation and vesiculation by 3–6 h after hypoxia-ischemia. Furthermore, during this time course, tubulin undergoes extensive oxidative damage (i.e., protein nitration) through a NO-associated toxic pathway. Therefore, posttranslational processing as well as targeting and transport of proteins may be abnormal early after hypoxia-ischemia (11,95).

Covalent modification of glutamate transporters by phosphorylation has subtype-specific modulatory effects on activity. Protein kinase C (PKC) activation results in direct phosphorylation of GLAST and inhibits GLAST function (96); in contrast, phosphorylation of GLT1 by PKC stimulates GLT1 function (97). We have found increases in PKC activity as well as increases in membrane protein phosphorylation at serine sites in vulnerable brain regions at 24 h after global ischemia (98). Thus, phosphorylation of astroglial GLAST, but not GLT1, by PKC may be a mechanism for reduced glutamate uptake in vulnerable brain regions after hypoxia-ischemia (84).

Another possibility is that glutamate transporter function may be impaired by direct structural damage to the proteins. In cell culture systems, oxygen radicals decrease high-affinity glutamate transport (99). Peroxynitrite (formed by the combination of superoxide and NO) is a potent inhibitor of GLAST, GLT1, and EAAC1 function (62,100). We have found evidence for peroxynitrite-mediated oxidative damage to membrane proteins within the piglet striatum early (3 to 6 h) after hypoxia-ischemia (95). Some of these proteins have not yet been identified. It is interesting that the molecular mass of some of these proteins is in the range of glutamate transporters (i.e., ~65–73 kDa). These abnormalities in protein nitration and in the expression or function of glutamate transporters may participate in striatal neurotoxicity after hypoxia-ischemia.

Abnormal control of extracellular glutamate concentrations by astroglia could be an early mechanism for neuronal degeneration after ischemia. In our piglet model of hypoxia-ischemia, striatal astrocytes are damaged early, as evidenced by their swelling, fragmentation, and death as well as by the loss of GLT1 protein at 24 h recovery (83). Astroglia in culture survive exposures to excitotoxins at concentrations sufficient to kill most neurons, suggesting that astrocytes are more resistant than neurons to excitotoxicity; however, overactivation of AMPA receptors is lethal to astrocytes, when receptor desensitization is blocked (101). In addition, astrocytes *in vivo* are damaged by acidosis (102), and prolonged, severe acidosis is lethal to astrocytes *in vitro* (103).

Astroglial swelling occurs within minutes of hypoxia-ischemia, suggesting that initial astrocytic abnormalities may contribute to the evolution of neuronal damage (104). In piglets, principal striatal neurons and astrocytes have a similar time course of injury and death at one to two days following hypoxia-ischemia (83,84,95). Cell culture studies show that neurons in an astrocyte-poor environment are more vulnerable to excitotoxicity than neurons cultured with astrocytes (105) and that uptake of glutamate by astrocytes improves neuronal survival in an excitotoxic environment (106). The finding that astroglial and neuronal injury occur concurrently within brain further strengthens the concept that abnormalities in astroglia could participate in the evolution of neuronal degeneration after hypoxia-ischemia (83,104). Astroglial damage and defective glutamate transport would favor excitotoxic neuronal cell death after hypoxia-ischemia, and oxidative damage to astroglial proteins could be a potential molecular mechanism for this defect (83,84,95).

### ***3.2. Glutamate Receptor-Mediated Excitotoxicity as a Mechanism for Neuronal Cell Death After Cerebral Ischemia***

Neuronal cell death after ischemia involves perturbations in intracellular  $\text{Ca}^{2+}$  homeostasis and impairments in protein synthesis. The GluRs that modulate intracellular  $\text{Ca}^{2+}$  levels within neurons are the ion channel receptors (NMDA and AMPA) and the group I mGluRs (24–31). In models of transient global cerebral ischemia a possible role for excessive activation of GluRs in the mechanisms for delayed neuronal death is supported by studies showing that blockade of AMPA receptors is neuroprotective following forebrain ischemia in adult rodents (107) and that abnormalities in phosphoinositide signaling pathways occur in hippocampus after ischemia (108). In models of focal ischemia (stroke), antisense oligodeoxynucleotide knockdown of NR1 production (109), targeted disruption of the NR2A gene (110), and selective pharmacological antagonism of NR2B (111) attenuate forebrain damage, thus a decrease in the number of functional NMDA receptors appears to mediate this neuroprotection.

We have demonstrated that excitotoxic activation of GluRs causes an apoptosis-necrosis continuum for cell death in which the structure of neuronal degeneration is influenced by the subtype of GluR that is activated and the age (maturity) of the CNS at the time of the insult (44,45). In the developing rat CNS, excitotoxic activation of NMDA and non-NMDA GluRs causes neuronal death with phenotypes ranging from apoptosis to necrosis. Excitotoxic neuronal death occurs as three structurally different forms: Classic apoptosis, classic necrosis, and a hybrid of apoptosis and necrosis (11,44,15,47). In contrast, in the adult rat CNS, the degeneration of neurons caused by NMDA receptor activation is necrosis morphologically; however, the neuronal death produced by non-NMDA receptor activation appears to be a structural hybrid of apoptosis and necrosis and is distinct from the death caused by NMDA receptor stimulation.

Interestingly, neuronal death after cerebral ischemia may not follow the apoptosis-necrosis continuum for excitotoxic neuronal death. We have shown with three different animal models of transient global ischemia that neuronal cell death within selectively vulnerable brain regions (e.g., CA1 pyramidal neurons, cerebellar Purkinje cells, and striatal neurons) is identical structurally to excitotoxic neuronal cell necrosis mediated by NMDA receptor activation, and, in the vulnerable neuronal populations, classic apoptosis and hybrids of apoptosis-necrosis rarely occur (11,47,112). However, in sev-

eral different paradigms of global ischemia, we and others have been unable to rescue these neurons from degeneration using noncompetitive antagonists to NMDA receptors (113,114) or competitive antagonists to NMDA receptors (115,116), AMPA receptors (117–119), and group I mGluRs (120). Some of our data even suggest that antagonists to NMDA receptors (116), AMPA receptors (118,119) and mGluRs (120) worsen neurologic outcome after ischemia. Yet, other studies have shown that AMPA receptor antagonism is neuroprotective in adult rodent models of global ischemia (107,114). The lack of neuroprotection and the deleterious effects of GluR antagonists in *in vivo* animal models are difficult to interpret and may be related to several variables associated with experimental design, including the dosage, solubility, delivery, administration route, and systemic pharmacokinetics of the drug. Although GluR-mediated excitotoxicity and glutamate toxicity continue to be potential mechanisms for neurodegeneration after hypoxia-ischemia, the pathobiology of this neuronal cell death remains poorly understood. The future clarification of the structural and molecular mechanisms of neuronal death after ischemia and the neuroglial participation in these mechanisms will lead to a rational and effective design of experiments for the protection of neurons and glia.

### 3.3. Possible Roles for Protein Kinases in Neurodegeneration After Ischemia

Protein kinases function in cell growth and differentiation, and, in nervous tissue, additional functions are regulation of neurotransmitter receptors and ion channels as well as modulation of neuronal excitability, neurotransmitter release, and synaptic plasticity (Fig. 2; for review *see* refs. 121,122). Protein kinase activation may thus play a role in GluR-mediated excitotoxic neuronal death (123,124) and in neuronal degeneration after ischemia (98,122,125). GluR stimulation causes increased intracellular  $\text{Ca}^{2+}$  and activation of  $\text{Ca}^{2+}$ /calmodulin protein kinase II (CaM kinase II) and causes increased activity of phospholipase  $\text{A}_2$  and PLC (Fig. 2), leading to the accumulation of diacylglycerol and activation of PKC (24,31,43). Mild ischemia induces a persistent translocation of CaM kinase II from the cytosol to synaptic plasma membranes (126,127). We have identified a sustained increase in PKC activity, an isoform-specific translocation to the plasma membrane, as well as increased protein phosphorylation at serine residues in plasma membranes of selectively vulnerable brain regions after ischemia (98). Astroglia may contribute to some of these changes (98). Other studies have suggested that protein kinases that are membrane-translocated after ischemia function improperly (126,128). However, changes in brain protein kinase activity may depend on the severity of ischemia and energy failure (98).

Several studies have shown that phosphorylation of AMPA, kainate, and NMDA receptors by CAM kinase II, PKC, or cAMP-dependent protein kinase A causes positive modulation of receptor function by potentiating activation (129–134). This enhancement of receptor function is transient because of the activity of postsynaptic protein phosphatases (134). In contrast, PKC-mediated phosphorylation of PLC-coupled mGluRs causes desensitization to glutamate (135,136). The integrative actions of different molecular subtypes of GluRs are also being revealed. Activation of PLC-coupled mGluRs increases NMDA receptor function through PKC activation (137,138). PKC potentiates NMDA receptor function by increasing the probability of channel openings and by reducing the voltage-dependent  $\text{Mg}^{2+}$  block (139).

The possible relevance of these observations to neuronal and astroglial degeneration after ischemia is provocative but still only speculative. We have found increases in PLC and PKC after ischemia (98,140), and other groups have found abnormalities in phosphoinositide signaling pathways after ischemia (108). Electrophysiological studies of neuronal activity in vulnerable regions after transient ischemia are discrepant. By extracellular recording in vivo, studies have shown that spontaneous firing rate in CA1 is increased (141), whereas other studies show that spontaneous firing rate and evoked responses are suppressed (142,143). By intracellular recording, CA1 neuronal activities and evoked synaptic potentials are suppressed after in vitro hypoxia-ischemia (144); similarly, in spiny striatal neurons in vivo, spontaneous activities and evoked postsynaptic potentials are suppressed and excitability is decreased after transient ischemia (145). However, whole-cell recordings reveal that CA1 pyramidal neurons have abnormal excitatory postsynaptic currents produced by activation of non-NMDA receptors that mediate  $\text{Ca}^{2+}$  influx (146). It is still uncertain whether changes in protein kinases after ischemia mediate these functional abnormalities and contribute directly to the mechanisms of neuronal death or whether they reflect secondary degenerative or regenerative processes in injured or surviving neurons and/or changes due to activation of glial cells. Based on the knowledge that protein kinases modulate GluR receptor and glutamate transporter function, ion channel function,  $\text{Na}^+/\text{K}^+$  ATPase activity, and neurotransmitter release (to name only a few critical functions for protein kinases), much more work is needed to identify the possible contributions of protein kinases to the mechanisms for neuronal degeneration after ischemia (Fig. 2).

#### ***3.4. Participation of NO-Mediated Mechanisms in the Pathobiology of Neurodegeneration After Ischemia***

NO is a short-lived, membrane-permeant ROS that functions in synaptic neurotransmission, synaptic plasticity, cell-mediated immune response, and cerebrovascular regulation (57,147,148). NO is generated by the catalytic activity of NOS, of which three molecular isoforms exist. Brain or neuronal NOS (NOS1) is constitutively expressed in subsets of neurons, inducible NOS (NOS2) is an inflammatory/glial cell isoform, and endothelial NOS (NOS3) is constitutively expressed in vascular endothelial cells (57,148–150). Neuronal NOS activity is regulated by intracellular  $\text{Ca}^{2+}$  (149). NMDA receptor activation results in NOS activation (Fig. 2; 151), and mGluR activation enhances NO production, possibly involving a  $\text{Ca}^{2+}$ -induced  $\text{Ca}^{2+}$  release amplification of mGluR-associated intracellular signals (152). NO has presynaptic actions as well by stimulation of synaptic vesicle exocytosis in a process involving cGMP (153). NO functions by forming covalent linkages and redox interactions with intracellular proteins (154). Excessive generation of NO is thought to be toxic to cells in vivo and may be an important mediator of neuronal degeneration resulting from cerebral ischemia (57,155–157), CNS inflammation (158), and axotomy/target deprivation (70). A predominant mechanism by which NO toxicity occurs is by the diffusion-limited reaction of NO with superoxide to generate peroxynitrite anion, which is a strong and relatively long-lived oxidant that directly damages the structure of a variety of proteins (57). Peroxynitrite decomposes to form secondary oxidants, including the particularly toxic hydroxyl radical (57), which we have shown to damage neuronal DNA and RNA after cerebral ischemia (95,159) and axonal injury (69,70).

In studies of cerebral ischemia, the results supporting a role for neurotoxic actions of NO *in vivo* are discrepant. In settings of focal ischemia, mice deficient in neuronal NOS (155) or inducible NOS (156) have slightly smaller infarct volumes than controls, and pharmacological inhibition of NOS has been shown to decrease brain damage volume in some studies (160) but not in other experiments (161,162). In settings of global ischemia, mice with targeted disruption of the neuronal NOS gene have less CA1 damage than wild-type mice (163). However, in rat and gerbil, pharmacological inhibition of NOS is not protective (162,164). We have been unable to show that an inhibitor of NOS results in neuroprotection in hippocampus and cerebellum after global ischemia (165). However, we have found that peroxynitrite-mediated damage to striatal membrane proteins occurs strongly by 6 h after hypoxic-asphyxic cardiac arrest (95,159). In addition, we discovered that the critical cytoskeletal protein tubulin is a target of peroxynitrite (159). It is therefore possible that the participation of NO-mediated toxicity is different in acute vs delayed neuronal degeneration after cerebral ischemia, and, thus, onset and severity of oxidative stress may influence rate of neuronal death on a regional basis, because striatal damage evolves faster than CA1 neuron and Purkinje cell damage (11).

#### 4. SYNAPTIC PATHOBIOLOGY IN PROGRESSIVE, AGE-RELATED NEURODEGENERATIVE DISEASES

##### 4.1. *Synaptic Dysfunction in AD*

AD is the most common type of dementia occurring in middle and late life (166), and it affects 7–10% of individuals >65 years of age and possibly 40% of people >80 years of age (12,167). The prevalence of AD is increasing proportionally to increased life expectancy (estimates predict that ~25% of the population will be >65 years of age in the year 2050). AD now affects >4 million people in the United States (168). Although most cases of AD have unknown etiologies and are called sporadic, some cases of AD, particularly those with early onset, are familial and are inherited as autosomal dominant disorders linked to mutations in the gene that encodes amyloid precursor protein (169–171) or genes that encode for proteins called presenilins (172,173). For late onset sporadic cases, a variety of risk factors have been identified in addition to age. The apolipoprotein E (apoE) allele is a susceptibility locus with the apoE4 type showing dose-dependent contributions (174). Cardiovascular disease and head trauma are additional risk factors for AD (166).

The mechanisms that cause the profound neuronal degeneration and the progressive impairments in memory and intellect that occur with sporadic and familial AD are not understood. Neuronal survival and normal memory and cognition depend on synaptic function. Regulated exocytosis of neurotransmitter-containing vesicles (Fig. 1A) is obligate for normal synaptic function (15). Synaptophysin (p38), an integral membrane glycoprotein of small synaptic vesicles in the presynaptic terminal (15), is one protein of many that functions in regulated exocytosis (Fig. 1B). We have found that synaptophysin is reduced in the hippocampus of individuals with AD who have moderate to severe deficits in memory (5). This finding is not surprising in light of the vulnerability of the hippocampus in advanced AD (1,3,4,166). A more exciting finding is the loss of synaptic marker in individuals with early AD (or possible AD)



who had no detectable cognitive impairment (5). The severity of this abnormality in synaptophysin in hippocampus correlates strongly with the severity of memory impairment in individuals with AD. Defects in other presynaptic components for regulated exocytosis of neurotransmitters (Fig. 1B) may also occur in the hippocampus of individuals with early AD. We also have interesting new data suggesting that synaptobrevin, synaptotagmin, syntaxin, and Rab3a are abnormal in the hippocampus of AD, but synapsin I, SNAP25, and SV2 levels are normal (175). Thus, presynaptic vesicles appear to be more vulnerable in AD than the presynaptic membrane that contains the active zone where vesicle docking occurs. In addition, we have discovered in individuals with AD selective abnormalities in the levels of the NR2B subunit of the NMDA receptor in the hippocampus as well as abnormalities in NMDA receptor phosphorylation (176). These synaptic molecule defects in subjects with early AD may foreshadow the clinical appearance of memory/cognitive impairment. Ultimately, structural loss of the entire synaptic complex could contribute to the atrophy of the cerebral cortex (i.e., cortical volume loss) which correlates strongly with cognitive decline (177).

#### ***4.2. Cellular Dynamics of Senile Plaque Formation and Amyloid Deposition within the Brain During Aging***

Senile plaques (SP) are brain lesions that occur in individuals with AD, patients with Down's syndrome (DS), and, less frequently, in people aging normally (1,4,178,179, *see ref. 2* for additional references). These lesions have a complex composition, consisting of dystrophic neurites (damaged and swollen dendrites or axon terminals), activated astrocytes and microglia, and extracellular deposits of insoluble amyloid fibrils (179, *see ref. 2* for additional references). These fibrils are composed of a 4-kDa peptide (A $\beta$ ) (180–182) consisting of 40–42 amino acid residues (183). This protein fragment is derived proteolytically from the amyloid precursor protein (APP), a cell surface protein with a large N-terminal extracellular domain that contains 22 residues of A $\beta$ , a hydrophobic membrane-spanning region including the transmembrane portion of the A $\beta$  region, and a short C-terminal cytoplasmic segment (184–186). The APP gene is located on human chromosome 21 (187–189), and mRNA gene products are spliced alternatively to generate ~5 different forms of APP transcripts and protein isoforms (184,189). A role for APP in the pathogenesis of AD is supported further by the identification of mutations in the APP gene linked to early-onset AD in some families (169–171).

The functions of APP are still not well defined, although it appears that APP functions at synapses (2,190). APP is an abundant and ubiquitous protein within CNS and other tissues. However, mice deficient in APP show no major neurological or neuropathological abnormalities (191), possibly due to homologous proteins. APP has structural features similar to some cell surface receptors (184) and may be a G protein-coupled receptor (192). Secreted and nonsecreted forms of APP exist (193,194), with different APP derivatives showing neurotrophic or neurotoxic actions. APP is incorporated into the extracellular matrix (195) and, thus, may have roles in cell-cell and cell-substrate adhesion (193,196–199). Furthermore, APP may function in the regulation of neurite outgrowth (200–201), perhaps by mediating the effects of nerve growth factor (202) and in neuronal and glial responses to brain injury (203–205).

In cell culture, APP normally undergoes constitutive proteolytic cleavage (186,190,193) by an  $\alpha$ -secretase, an enzyme that cleaves APP within the A $\beta$  region at or near the plasma membrane (206–208), thereby generating secreted forms of APP and precluding the formation of full-length A $\beta$  peptide fragments (206,208). APP is also metabolized by an endosomal-lysosomal pathway that, unlike the  $\alpha$ -secretase pathway, yields amyloidogenic fragments of A $\beta$  (209,210). A $\beta$  can be formed normally in vivo and in vitro (211,212), and studies of cultured human cells show that it is generated intracellularly (213,214). Although A $\beta$  has been shown to be neurotoxic in cell culture, a causal role for A $\beta$  in neuronal degeneration in vivo remains speculative. A  $\beta$ -secretase cleaves APP at the N-terminus of A $\beta$ , and a  $\gamma$ -secretase cleaves APP at the C-terminus of A $\beta$ , causing the formation of A $\beta$  that is either 40 amino acids or 42 amino acids long (215). This pathway for APP metabolism is found within the endoplasmic reticulum and Golgi apparatus of neurons (216,217). Interestingly, presenilins, which are present at relatively low levels in brain (218), localize to the endoplasmic reticulum and Golgi apparatus (219), and mutant presenilins promote A $\beta$ 42 generation (220). Mutant presenilin is processed differently than normal presenilin, and fragments that are normally subject to endoproteolytic cleavage tend to accumulate (221). Thus, metabolism of APP through the  $\beta$ - and  $\gamma$ -secretase pathways may be promoted by presenilin-1 and presenilin-2 gene mutations linked to early onset familial AD.

We and others have shown that APP is expressed by neurons and by subsets of astroglia, microglia, and vascular endothelial cells (2,196,222–224). The most prominent neuronal localization of APP is within cell bodies and dendrites and is particularly enriched postsynaptically at subsets of synapses (2,205). The expression of APP in nonneuronal cells in brain is low in comparison to the dominant expression of APP within neurons and their processes. It appears that astroglia and microglia constitutively express APP at low levels in the resting state (2,222). However, an important finding is that the relative enrichment of APP within these neuroglial cells changes in response to brain injury and synaptic abnormalities (2,204). This idea is supported by our finding that APP is expressed prominently by activated astroglia and microglia within SP of aged nonhuman primates (2,224) and by other reports (225) showing that APP is localized to astrocytes in SP in cases of AD. Other studies have shown that APP isoforms containing the Kunitz protease inhibitor domain are expressed in reactive astrocytes in early stages of brain damage (204). Because levels of APP in some neurons and nonneuronal cells are increased by the cytokine interleukin-1 (226), it is likely that the expression of APP is inducible in glia when these cells are activated in response to neuronal injury.

Several hypotheses for A $\beta$  deposition and SP formation have been presented. The genesis of SP may begin with the formation of extracellular A $\beta$  before the degeneration of cellular elements within these lesions (227,228). Alternatively, A $\beta$  may be derived from degenerating axonal nerve terminals or dendrites containing APP that evolve into neurite-rich foci that form A $\beta$  at the cell plasma membrane by aberrant processing of APP within neurons (181,223,229). In addition, invading reactive microglia (2,179,230,231) and astroglia (2) as well as capillaries (232) may actively produce A $\beta$  from APP. In one scheme for SP formation, A $\beta$  (in a nonfibrillar form and then a fibrillar form) is deposited before neuronal neuritic damage occurs, and thus is a cause of neuronal degeneration (233,234). We have not identified extracellular A $\beta$  (even as

sparse, scattered bundles of fibrils) before the appearance of synaptic abnormalities and dendritic/axonal neurites (2,224). We believe that astroglia and microglia are primary generators of A $\beta$  deposits in the aging brain (2,224). In early diffuse plaques, we have identified A $\beta$ -containing transformed astrocytes and microglia after neuritic defects have appeared. Our experiments with aging nonhuman primates are concordant with studies of SP in the cerebral cortex from cases of AD (179,230).

These studies reveal that SP are dynamic brain lesions that evolve from early synaptic defects within the neuropil to mature plaques and extracellular deposits of A $\beta$ . The staging of these lesions is thought to be the degeneration of neuritic structures, followed by the attraction of reactive glia, and the subsequent deposition of extracellular A $\beta$  derived from microglia (2,179,230) or astrocytes (2). Our studies demonstrate that structural and biochemical perturbations within neuronal and nonneuronal cells occur before the deposition of extracellular A $\beta$  fibrils (2,224). Furthermore, our results suggest that focal abnormalities in synaptic contacts within the neuropil (synaptic disjunction) may initiate this complex series of events resulting in the formation of diffuse SP and deposits of A $\beta$ . In response to synaptic disjunction in the aged brain, astroglia and microglia produce A $\beta$  (2). The molecular pathology that we and others have identified at the synaptic level in humans with AD (5,175,176,235) may be related to SP lesions and A $\beta$  deposits. For example, we found a strong inverse correlation between synaptophysin loss and the density of neuritic and diffuse plaques in hippocampus. It is not surprising to find an inverse correlation between SP density and synaptophysin immunoreactivity, because synaptic disjunction in the neuropil and abnormal APP processing within neuroglia may be early events in the formation of SP (2,224).

#### 4.3. Oxidative Stress in the AD Brain

Neurons have a particularly high risk for structural damage caused by ROS, because of high rates of oxygen consumption and high contents of polyunsaturated fatty acids that are susceptible to lipid peroxidation; therefore, a free radical hypothesis has been suggested as a mechanism for compromised CNS functioning with aging (3,11,47,66). Some experimental evidence is available to support this argument. For example, superoxide dismutase-1 (SOD1) activity is elevated in fibroblasts from individuals with familial AD (236), and the SOD1 gene is located on human chromosome 21 (237), which individuals with DS possess an extra copy, and a gene dosage effect on lipid peroxidation has been observed in brain tissue of patients with DS (238). ROS have been implicated in the induction of neuronal death by apoptosis in DS (239) and in *in vitro* (58,59) and *in vivo* models (11,69,70). Mitochondria may participate in the effector stage of apoptosis by directly providing a rich source of ROS or by changes in mitochondrial membrane cell death proteins that prevent apoptosis by an antioxidant mechanism, or that suppress apoptosis by blocking release of cytochrome c (a required molecule for apoptosis in cell culture systems) or by regulating membrane potential and volume homeostasis of mitochondria (for references see 10,11,69,71).

Cellular oxidative stress and antioxidant enzyme regulation are relevant to age-related neurodegenerative disorders because abnormalities in antioxidant enzyme systems (e.g., superoxide dismutase) and oxidative injury may provide mechanisms for neuronal degeneration. Cytosolic copper/zinc-superoxide dismutase (SOD1) and mitochondrial manganese-superoxide dismutase (SOD2) are localized predominantly to

neocortical and hippocampal pyramidal neurons, but are scarcely seen in glial cells in normal human brain (3). In AD and DS, the cellular expressions of these two forms of SOD are very different from normal individuals (3). SOD1 is highly enriched in pyramidal neurons undergoing degeneration, whereas SOD2 is more enriched in reactive astrocytes than in neurons. In SP, astrocytes highly enriched in SOD2 surround SOD1-enriched neurites. Some pyramidal neurons coexpress SOD and the cytoskeletal protein tau, and some SOD1-enriched structures in SP are tau-positive (3). Microglia infrequently show expression of high levels of superoxide dismutase. These findings in AD and DS support a role for oxidative stress in neuronal degeneration and SP formation. The differential localizations of SOD1 and SOD2 in sites of degeneration in diseased brain suggest that the responses of cells to oxidative stress is antioxidant enzyme-specific and cell type-specific and that these two forms of superoxide dismutase may have different functions in brain antioxidant mechanisms in response to injury.

A glial expression of SOD has been reported in AD brain (240). Our studies have shown that SOD protein is rarely seen in glial cells in control brain (3). However, in AD and DS brain, SOD2 is induced strongly in reactive astrocytes in cerebral cortex and white matter. This change in the astroglial expression of SOD2 in the brains of AD and DS cases is a major difference between control and diseased tissue, and is possibly due to metabolic activation of reactive astrocytes, because SOD2 is localized within the mitochondrial matrix (241). SOD1-expressing astrocytes are also seen, but this expression is weaker than that of SOD2. Because SOD2 mRNA is induced by tumor necrosis factor- $\alpha$  and interleukin-1, SOD2 is thought to have a cytoprotective function against various microglia/macrophage-derived inflammatory mediators (242,243) that may participate in the pathogenesis of AD and DS (244). Our findings that SOD2 may be downregulated in pyramidal neurons and upregulated in reactive astrocytes in AD and DS brain (3) may relate to the selective cytotoxicity of microglia-derived cytokines (e.g., tumor necrosis factor- $\alpha$  and interleukin-1) (245). Activated microglia secrete superoxide radicals (246), and stimulated neutrophils disrupt SOD structure in cell culture (247), but reactive microglia-macrophage cells that are widely distributed in AD and DS cases, show scarce evidence for expression of SOD (3). Thus, modulation of glial expression of SOD appears to be relatively selective for astrocytes, because in AD and DS, astroglia show the greatest increase in SOD2 expression.

#### 4.4. Synaptic and Astroglial Pathobiology in ALS

ALS is a disease that causes progressive weakness, muscle atrophy, and eventual paralysis. Death occurs within 3 to 5 years of onset and is characterized neuropathologically by progressive degeneration of upper and lower motor neurons in the brain and spinal cord (13,248). The mechanisms leading to the selective degeneration of motor neurons in ALS are not known. Some forms of ALS are inherited (8,9). Mutant forms of SOD1 have been identified in a small subset (10–20%) of individuals with familial ALS which occurs in 5–10% of all patients with ALS (8,9). Forced expression of mutant forms of the gene encoding SOD1 results in degeneration of motor neurons in mice (249,250). A toxic gain in function of mutant SOD1 might initiate this neurodegeneration (249,251). In cultured cells, expression of mutant SOD1 can induce abnormalities in the production of ROS and neuronal apoptosis (251,252). Oxidative stress

resulting from downregulation of normal SOD1 can also cause apoptosis in cell culture (253). Other possible causes for neuronal death in ALS are neurofilament abnormalities (254–256), defective uptake of glutamate by astroglia (6,7) leading to GluR-mediated excitotoxic neuronal death, or deficiencies in neurotrophic factors (257).

We have found (10) that the degeneration of motor neurons in sporadic and familial ALS is different structurally from the motor neuron degeneration found in transgenic mice overexpressing the familial ALS mutant forms of SOD1 (249,250) and in transgenic mice overexpressing normal and mutant neurofilament proteins (254–256). SOD1 and neurofilament transgenic mouse models of ALS have not revealed structural or biochemical changes for apoptotic death of motor neurons similar to those we have discovered in humans with ALS (10). In fact, it is still uncertain whether motor neurons in these mouse models die or whether they remain in a severely atrophic state. The survival of mice with familial ALS mutations is prolonged when crossed with mice overexpressing Bcl-2 (258) or a dominant negative inhibitor of caspase-1 (259), although the degeneration of motor neurons is not prevented (258), suggesting that neuronal degeneration in these mice is not apoptosis controlled by programmed cell death mechanisms. The prominent vacuolar and edematous degeneration of motor neurons in mice overexpressing mutant SOD1 (249,250) or neurofilament protein (254–257) more closely resembles excitotoxic neurodegeneration (45) or transsynaptic neuronal atrophy (but not death) in response to deafferentation (260).

We and others have proposed that excitotoxicity may explain the selective neuronal cell death in ALS (6,7,11,42,47). This hypothesis was formulated based on background information showing that abnormal activation of GluR can kill neurons (41–43) and that exogenous glutamate analogs may be responsible for the damage to upper motor neurons in lathyrism via actions at specific GluRs (42,261). Subsequently, studies revealed that serum and cerebrospinal fluid concentrations of glutamate are increased in some patients with sporadic ALS (262,263), but this change was not found in other studies (264,265). In more recent studies, it has been shown that spinal cord and affected brain regions of patients with sporadic ALS have reduced high-affinity glutamate uptake (6) and a selective reduction in GLT1 (7). It has also been reported that aberrant splicing of astroglial GLT1 mRNA is ALS-specific and is the cause for reduced expression of GLT1 protein and even possibly the cause of motor neuron degeneration (266). However, defective astroglial glutamate uptake and loss of GLT1 occur also in brain regions selectively vulnerable in AD (267), in brain regions vulnerable to hypoxia-ischemia (83,84), and even in brain regions that do not develop neuronal degeneration after axotomy and deafferentation in experimental animals (89,90). In addition, splicing of GLT1 mRNA transcripts is highly variable in human CNS tissue, and variant transcripts considered to be “aberrant” are found in normal individuals and in other species (268–270). Furthermore, the degeneration of motor neurons in individuals with ALS is structurally very different from excitotoxic neuronal degeneration in the adult CNS (10). Thus, it is unlikely that the abnormalities in astroglial GLT1 and GluR-mediated excitotoxicity are the specific causes for motor neuron degeneration in ALS.

Over the years it has become increasingly clear that selective neuronal vulnerability in ALS is not simply related to excitotoxic processes. Neither differential subunit compositions of ion channel GluRs (AMPA and NMDA receptors) nor differential expres-

sions of glutamate transporters appear to explain sufficiently the mechanisms that dictate the selective vulnerability of neurons in motor cortex and motor neurons in brainstem and spinal cord in ALS. This conclusion is based partly on glutamate receptor/transporter expression and cellular localization studies in animal and human CNS performed by us (35,37,38,40,271,273) and by others (36,274,275). The foundation for the excitotoxicity theory in the pathogenesis of ALS is built on experiments showing a selective loss of the astroglial glutamate transporter GLT1 in vulnerable regions in ALS (7). Nevertheless, this observation is still indirect evidence for GluR-mediated excitotoxicity, and the explanations for this abnormality and the disease specificity for motor neurons are controversial. It is also still uncertain whether this abnormality is related to the causes or the consequences of the disease. Most patients with ALS are maintained on mechanical ventilation, as a means of relieving symptoms of chronic hypoventilation and for prolonging life (276), but patients with ALS die eventually from respiratory insufficiency (10,276). In fact, it has been argued that riluzole, a drug that may improve the survival of ALS patients, acts as a Na<sup>+</sup> channel blocker and increases resistance to hypoxia (by reducing energy demand), not by anti-excitotoxic actions (277). In support of this recent interpretation (277), we have observed in a physiologically well-characterized animal model of cerebral hypoxia-asphyxia that regionally selective abnormalities occur in astroglial GLT1 expression (83,84). Moreover, our new data reveal that non-NMDA and NMDA GluR toxicity in adult CNS neurons is structurally different from the pattern seen in ALS (10,11,45). Thus, it is possible that changes in astroglial glutamate transporters in individuals with ALS are consequences of neurodegeneration, or, alternatively, these changes are related to premortem agonal state.

We have found recently in adult animal models of peripheral nerve avulsion that motor neuron degeneration is induced by oxidative stress and is apoptosis (70). We have also found that motor neuron death in ALS is apoptosis that may be mediated by programmed cell death mechanisms (9,10,282). The neuronal degeneration in ALS closely resembles neuronal apoptosis induced by target deprivation in the mature CNS (10,11,69,70) and could be related to the deficiency in neurotrophic factors that is found in individuals with ALS (257). Some of these neurotrophic factors are produced by neuroglia. Trophic factor deprivation-induced motor neuron apoptosis in cell culture and in developing animals (278–280) is caspase-, Bax-, and p53-dependent, as might be the case for motor neuron apoptosis in ALS (10,281,282). Our model of motor neuron apoptosis in the spinal cord will be useful for identifying the synaptic and molecular pathobiology of neuronal apoptosis in the adult CNS and thereby will provide insight into the mechanisms, including the roles for neuroglial-derived trophic factors, for the neuronal degeneration in ALS (281,282).

## ACKNOWLEDGMENTS

This research was supported by grants from the U.S. Public Health Service (NS 34100, and A61682) and the U.S. Army Medical Research and Materiel Command (DAMD17-99-1-9553). The author thanks Ann Price and Adeel Kaiser for technical assistance and Drs. Carlos Portera-Cailliau, Stephen Ginsberg, Nael Al-Abdulla, Chun-I Sze, Akiko Furuta, Frances Northington, JoAnne Natale, Ansgar Brambrink, Frederick Sieber, Jeffrey Kirsch, and Stephen Hays for their contributions in his laboratory.

## REFERENCES

1. Price, D.L., Martin, L.J., Clatterbuck, R.E., et al. (1992) Neuronal degeneration in human diseases and animal models. *J. Neurobiol.* **23**, 1277-1294.
2. Martin, L.J., Pardo, C.A., Cork, L.C., and Price, D.L. (1994) Synaptic pathology and glial responses to neuronal injury precede the formation of senile plaques and amyloid deposits in the aging cerebral cortex. *Am. J. Pathol.* **145**, 1358-1381.
3. Furuta, A., Price, D.L., Pardo, C.A., et al. (1995) Localization of superoxide dismutases in Alzheimer's disease and Down's syndrome neocortex and hippocampus. *Am. J. Pathol.* **146**, 357-367.
4. Terry, R.D. (1996) The pathogenesis of Alzheimer disease: an alternative to the amyloid hypothesis. *J. Neuropathol. Exp. Neurol.* **55**, 1023-125.
5. Sze, C.-I., Troncoso, J.C., Kawas, C., Mouton, P., Price, D.L., and Martin, L.J. (1997) Loss of the presynaptic vesicle protein synaptophysin in hippocampus correlates with cognitive decline in Alzheimer's disease. *J. Neuropathol. Exp. Neurol.* **56**, 933-994.
6. Rothstein, J.D., Martin, L.J., and Kuncel, R.W. (1992) Decreased glutamate transport by the brain and spinal cord in amyotrophic lateral sclerosis. *N. Engl. J. Med.* **326**, 1464-1468.
7. Rothstein, J.D., Van Kammen, M., Levey, A.I., Martin, L.J., and Kuncel, R.W. (1995) Selective loss of glial glutamate transporter GLT-1 in amyotrophic lateral sclerosis. *Ann. Neurol.* **38**, 73-84.
8. Rosen, D.R., Siddique, T., Patterson, D., et al. (1993) Mutations in Cu/Zn superoxide dismutase gene are associated with familial amyotrophic lateral sclerosis. *Nature* **362**, 59-62.
9. Martin, L.J. (2000) p53 is abnormally elevated and active in the CNS of patients with amyotrophic lateral sclerosis. *Neurobiol. Disease* **7**, 613-622.
10. Martin, L.J. (1999) Neuronal death in amyotrophic lateral sclerosis is apoptosis: possible contribution of a programmed cell death mechanism. *J. Neuropathol. Exp. Neurol.* **58**, 459-471.
11. Martin, L.J., Al-Abdulla, N.A., Brambrink, A.M., Kirsch, J.R., Sieber, F.E., and Portera-Cailliau, C. (1998) Neurodegeneration in excitotoxicity, global cerebral ischemia, and target deprivation: a perspective on the contributions of apoptosis and necrosis. *Brain Res. Bull.* **46**, 281-309.
12. Evans, D.A., Funkenstein, H.H., Albert, M.S. et al. (1989) Prevalence of Alzheimer's disease in a community population of older persons. Higher than previously reported. *JAMA* **262**, 2551-2556.
13. Williams, D.B. and Windebank, A.J. (1993) Motor neuron disease, in *Peripheral Neuropathy* (Dyck, P.J., Thomas, P.K., Griffin, J.W., Low, P.A., and Poduslo, J.F. eds.), Saunders, Philadelphia, pp. 1028-1050.
14. Kalimo, H., Kaste, M., and Haltia, M. (1997) Vascular diseases, in *Greenfields Neuropathology*, (Graham, D.I. and Lantos P.L., eds.), Arnold, London, pp. 315-396.
15. Sudhof, T.C. (1995) The synaptic vesicle cycle: a cascade of protein-protein interactions. *Nature* **375**, 645-653.
16. Kim, E., Naisbitt, S., Hsueh Y.-P., et al. (1997) GKAP, a novel synaptic protein that interacts with the guanylate kinase-like domain of the PSD95/SAP90 family of channel clustering molecules. *J. Cell Biol.* **136**, 669-678.
17. Ehlers, M.D., Fung, E.T., O'Brien, R.J., and Huganir, R.L. (1998) Splice variant-specific interaction of the NMDA receptor subunit NR1 with neuronal intermediate filaments. *J. Neurosci.* **18**, 720-730.
18. Wechsler, A. and Teichberg V.I. (1998) Brain spectrin binding to the NMDA receptor is regulated by phosphorylation, calcium and calmodulin. *EMBO J.* **17**, 3931-3939.
19. Montgomery, D.L. (1994) Astrocytes: form, functions, and roles in disease. *Vet. Pathol.* **31**, 145-167.

20. Norenberg, M.D. (1994) Astrocyte responses to CNS injury. *J. Neuropathol. Exp. Neurol.* **53**, 213–220.
21. Curtis, D.R., Phillis, J.W., and Watkins, J.C. (1959) Chemical excitation of spinal neurons. *Nature* **183**, 611–612.
22. Watkins, J.C. and Evans, R.H. (1981) Excitatory amino acid transmitters. *Ann. Rev. Pharmacol. Toxicol.* **21**, 165–204.
23. Clements, J.D., Lester, R.A.J., Tong, G., Jahr, C.E., and Westbrook, G.L. (1992) The time course of glutamate in the synaptic cleft. *Science* **258**, 1498–1501.
24. Nakanishi, S. (1992) Molecular diversity of glutamate receptors and implications for brain function. *Science* **258**, 597–603.
25. Seeburg, P.H. (1993) The molecular biology of mammalian glutamate receptor channels. *TINS* **16**, 359–365.
26. Sommer, B., Keinänen, K., Verdoorn, T.A., et al. (1990) Flip and flop: a cell-specific functional switch in glutamate-operated channels of the CNS. *Science* **249**, 1580–1585.
27. Hollman, M., Hartley, M. and Heinemann, S. (1991)  $\text{Ca}^{2+}$  permeability of KA-AMPA-gated glutamate receptor channels depends on subunit composition. *Science* **252**, 851–853.
28. Sommer, B., Köhler, M., Sprengel, R., and Seeburg, P.H. (1991) RNA editing in brain controls a determinant of ion flow in glutamate-gated channels. *Cell* **67**, 11–19.
29. Burnashev, N., Monyer, H., Seeburg, P.H., and Sakmann, B. (1992) Divalent ion permeability of AMPA receptor channels is dominated by the edited form of a single subunit. *Neuron* **8**, 189–198.
30. Tanabe, Y., Masu, M., Ishii, T., Shigemoto, R., and Nakanishi, S. (1992) A family of metabotropic glutamate receptors. *Neuron* **8**, 169–179.
31. Pin, J.-P., and Duvoisin, R. (1995) The metabotropic glutamate receptors: structure and functions. *Neuropharmacol.* **34**, 1–26.
32. Kanai, Y., Smith, C.P. and Hediger, M.A. (1993) A new family of neurotransmitter transporters: the high-affinity glutamate transporters. *FASEB J.* **7**, 1450–1459.
33. Danbolt, N.C. (1994) The high affinity uptake system for excitatory amino acids in the brain. *Prog. Neurobiol.* **44**, 377–396.
34. Arriza, J.L., Eliasof, S., Kavanaugh, M.P., and Amara, S.P. (1997) Excitatory amino acid transporter 5, a retinal glutamate transporter coupled to a chloride conductance. *Proc. Natl. Acad. Sci. USA* **94**, 4155–4160.
35. Rothstein, J.D., Martin, L., Levey, A.I., et al. (1994) Localization of neuronal and glial glutamate transporters. *Neuron* **13**, 713–725.
36. Chaudhry, F.A., Lehre, K.P., van Lookeren Campagne, M., Ottersen, O.P., Danbolt, N.C., and Storm-Mathisen, J. (1995) Glutamate transporters in glial plasma membranes: highly differentiated localizations revealed by quantitative ultrastructural immunocytochemistry. *Neuron* **15**, 711–720.
37. Furuta, A., Rothstein, J.D., and Martin, L.J. (1997) Glutamate transporter protein subtypes are expressed differentially during rat CNS development. *J. Neurosci.* **17**, 8363–8375.
38. Northington, F.J., Traystman, R.J., Koehler, R.C., Rothstein, J.R., and Martin, L.J. (1998) Regional and cellular expression of glial (GLT1) and neuronal EAAC1 glutamate transporter proteins in ovine fetal brain. *Neuroscience* **85**, 1183–1194.
39. Furuta, A., Martin, L.J., C.-L. G., Lin, Dykes-Hoberg, M., and Rothstein, J.D. (1997) Cellular and synaptic localization of the neuronal glutamate transporters, excitatory amino acid transporters 3 and 4. *Neuroscience* **81**, 1031–1042.
40. Northington, F.J., Traystman, R.J., Koehler, R.C., and Martin, L.J. (1999) GLT1, glial glutamate transporter, is transiently expressed in neurons and develops astrocyte specificity only after midgestation in the ovine fetal brain. *J. Neurobiol.* **39**, 515–526.



41. Lucas, D.R. and Newhouse, J.P. (1957) The toxic effect of sodium *L*-glutamate on the inner layers of the retina. *AMA Arch. Ophthalmol.* **58**, 193–201.
42. Olney, J.W. (1994) Excitatory transmitter neurotoxicity. *Neurobiol. Aging* **15**, 259–260.
43. Choi, D.W. (1992) Excitotoxic cell death. *J. Neurobiol.* **23**, 1261–1276.
44. Portera-Cailliau, C., Price, D.L., and Martin, L.J. (1997) Excitotoxic neuronal death in the immature brain is an apoptosis-necrosis morphological continuum. *J. Comp. Neurol.* **378**, 70–87.
45. Portera-Cailliau, C., Price, D.L., and Martin, L.J. (1997) Non-NMDA and NMDA receptor-mediated excitotoxic neuronal deaths in adult brain are morphologically distinct: further evidence for an apoptosis-necrosis continuum. *J. Comp. Neurol.* **378**, 88–104.
46. Stewart, G.R., Zorumski, C.F., Price, M.T., and Olney, J.W. (1990) Domoic acid: a dementia-inducing excitotoxic food poison with kainic acid receptor specificity. *Exp. Neurol.* **110**, 127–138.
47. Martin, L.J., Portera-Cailliau, C., Ginsberg, S.D., and Al-Abdulla, N.A. (1998) Animal models and degenerative disorders of the human brain. *Lab Animal* **27**, 18–25.
48. Gwag, B.J., Koh, J.Y., DeMaro, J.A., Ying, H.S., Jacquin, M., and Choi, D.W. (1997) Slowly triggered excitotoxicity occurs by necrosis in cortical cultures. *Neuroscience* **77**, 393–401.
49. Kure, S., Tominaga, T., Yoshimoto, T., Tada, K., and Narisawa, K. (1991) Glutamate triggers internucleosomal DNA cleavage in neuronal cells. *Biochem. Biophys. Res. Commun.* **179**, 39–45.
50. Ankarcrona, M., Dypbukt, J.M., Bonfoco, E., et al. (1995) Glutamate-induced neuronal death: a succession of necrosis or apoptosis depending on mitochondrial function. *Neuron* **15**, 961–973.
51. Simonian, N.A., Getz, R.L., Leveque, J.C., Konradi, C., and Coyle, J.T. (1996) Kainate induces apoptosis in neurons. *Neuroscience* **74**, 675–683.
52. Dessi, F., Charriaut-Marlangue, C., Khrestchatsky, M., and Ben-Ari, Y. (1993) Glutamate-induced neuronal death is not a programmed cell death in cerebellar culture. *J. Neurochem.* **60**, 1953–1955.
53. Ferrer, I., Martin, F., Serrano, T., et al. (1995) Both apoptosis and necrosis occur following intrastriatal administration of excitotoxins. *Acta Neuropathol.* **90**, 504–510.
54. van Lookeren Campagne, M., Lucassen, P.J., Vermeulen, J.P., and Balázs, R. (1995) NMDA and kainate induced internucleosomal DNA cleavage associated with both apoptotic and necrotic cell death in the neonatal rat brain. *Eur. J. Neurosci.* **7**, 1627–1640.
55. Halliwell, B. and Gutteridge, J.M.C. (1986) Oxygen free radicals and iron in relation to biology and medicine: some problems and concepts. *Arch. Biochem. Biophys.* **246**, 501–514.
56. McCord, J.M. (1985) Oxygen-derived free radicals in postischemic tissue injury. *N. Engl. J. Med.* **312**, 159–163.
57. Beckman, J.S., Chen, J., Ischiropoulos, H., and Conger, K.A. (1992) Inhibition of nitric oxide synthesis and cerebral neuroprotection, in *Pharmacology of Cerebral Ischemia* (Kriegstein, J. and Oberpichler-Schwenk, H., eds.), Wissenschaftliche Verlagsgesellschaft, Stuttgart, pp. 383–394.
58. Ratan, R.R., Murphy, T.H., and Baraban, J.M. (1994) Macromolecular synthesis inhibitors prevent oxidative stress-induced apoptosis in embryonic cortical neurons by shunting cysteine from protein synthesis to glutathione. *J. Neurosci.* **14**, 4385–4392.
59. Bonfoco, E., Krainc, D., Ankarcrona, M., Nicotera, P., and Lipton, S.A. (1995) Apoptosis and necrosis: two distinct events induced respectively by mild and intense insults with NMDA or nitric oxide/superoxide in cortical cell cultures. *Proc. Natl. Acad. Sci. USA* **92**, 72162–72166.
60. Boveris, A. and Cadenas, E. (1997) Cellular sources and steady-state levels of reactive oxygen species, in *Oxygen, Gene Expression, and Cellular Function* (Biadasz Clerch, L. and Massaro, D.J., eds.), Marcel Dekker, New York, pp. 1–25.

61. Bandy, B. and Davison, A.J. (1990) Mitochondrial mutations may increase oxidative stress: implications for carcinogenesis and aging? *Free Rad. Biol. Med.* **8**, 523–539.
62. Trotti, D., Danbolt, N.C., and Volterra, A. (1998) Glutamate transporters are oxidant-vulnerable: a molecular link between oxidative and excitotoxic neurodegeneration. *TIPS* **19**, 328–334.
63. Sato, T., Kamata, Y., Irifune, M., and Nishikawa, T. (1997) Inhibitory effects of several nitric oxide-generating compounds on purified Na<sup>+</sup>, K<sup>+</sup>-ATPase activity from porcine cerebral cortex. *J. Neurochem.* **68**, 1312–1318.
64. Mark, R.J., Pang, Z., Geddes, J.W., Uchida, K., and Mattson, M.P. (1997) Amyloid  $\beta$ -peptide impairs glucose transport in hippocampal and cortical neurons: involvement of membrane lipid peroxidation. *J. Neurosci.* **17**, 1046–1054.
65. Mirabelli, F., Salis, A., Perotti, M., Taddei, F., Bellomo, G., and Orrenius, S. (1998) Alterations of surface morphology caused by the metabolism of menadione in mammalian cells are associated with the oxidation of critical sulfhydryl groups in cytoskeletal proteins. *Biochem. Pharmacol.* **37**, 3423–3427.
66. Troncoso, J.C., Costello, A.C., Kim, J.H., and Johnson, G.V.W. (1995) Metal-catalyzed oxidation of bovine neurofilaments in vitro. *Free Rad. Biol. Med.* **18**, 891–899.
67. Salo, D.C., Pacifici, R.E., Lin, S.W., Giulivi, C., and Davies, K.J.A. (1990) Superoxide dismutase undergoes proteolysis and fragmentation following oxidative modification and inactivation. *J. Biol. Chem.* **265**, 11919–11927.
68. Greenlund, L.J.S., Deckwerth, T.L., and Johnson, E.M. (1995) Superoxide dismutase delays neuronal apoptosis: a role for reactive oxygen species in programmed neuronal death. *Neuron* **14**, 303–315.
69. Al-Abdulla, N.A. and Martin, L.J. (1998) Apoptosis of retrogradely degenerating neurons occurs in association with the accumulation of perikaryal mitochondria and oxidative damage to the nucleus. *Am. J. Pathol.* **153**, 447–456.
70. Martin, L.J., Kaiser, A., and Price, A.C. (1999) Motor neuron degeneration after sciatic nerve avulsion in adult rat evolves with oxidative stress and is apoptosis. *J. Neurobiol.* **40**, 185–201.
71. Hamburger, V. (1975) Cell death in the development of the lateral motor column of the chick embryo. *J. Comp. Neurol.* **160**, 535–546.
72. Yan, Q., Elliot, J.L., Matheson C, et al. (1993) Influences of neurotrophins on mammalian motoneurons in vivo. *J. Neurobiol.* **24**, 1555–1577.
73. Murphy, T.H., Miyamoto, M., Sastre, A., Schnaar, R.L., and Coyle, J.T. (1989) Glutamate toxicity in a neuronal cell line involves inhibition of cystine transport leading to oxidative stress. *Neuron* **2**, 1547–1558.
74. Sagara, Y. and Schubert, D. (1998) The activation of metabotropic glutamate receptors protects nerve cells from oxidative stress. *J. Neurosci.* **18**, 6662–6671.
75. Benveniste, H., Drejer, J., Schousboe, A., and Diemer, N.H. (1984) Elevation of the extracellular concentrations of glutamate and aspartate in rat hippocampus during transient cerebral ischemia monitored by intracerebral microdialysis. *J. Neurochem.* **43**, 1369–1374.
76. Drejer, J., Benveniste, H., Diemer, N.H., and Schousboe, A. (1985) Cellular origin of ischemia-induced glutamate release from brain tissue in vivo and in vitro. *J. Neurochem.* **45**, 145–151.
77. Globus, M.Y.-T., Busto, R., Dietrich, W.D., Martinez, E., Valdes, I., and Ginsberg, M.D. (1988) Intra-ischemic extracellular release of dopamine and glutamate is associated with striatal vulnerability to ischemia. *Neurosci. Lett.* **91**, 36–40.
78. Mitani, A., Andou, Y., and Kataoka, K. (1992) Selective vulnerability of hippocampal CA1 neurons cannot be explained in terms of an increase in glutamate concentration during ischemia in the gerbil: brain microdialysis study. *Neuroscience* **48**, 307–313.
79. Diemer, N.H., Valente, E., Bruhn, T., Berg, M., Jørgensen, M.B., and Johansen, F.F. (1993) Glutamate receptor transmission and ischemic nerve cell damage: evidence for involvement of excitotoxic mechanisms. *Prog. Brain Res.* **96**, 105–123.

80. Rothman, S.M. (1984) Synaptic release of excitatory amino acid neurotransmitter mediates anoxic neuronal death. *J. Neurosci.* **4**, 1884–1891.
81. Szatkowski, M. and Attwell, D. (1994) Triggering and execution of neuronal death in brain ischaemia: two phases of glutamate release by different mechanisms. *TINS* **17**, 359–365.
82. Silverstein, F.S., Buchanan, K., and Johnston, M.V. (1986) Perinatal hypoxia-ischemia disrupts striatal high-affinity <sup>3</sup>H-glutamate uptake into synaptosomes. *J. Neurochem.* **47**, 1614–1619.
83. Martin, L.J., Brambrink, A.M., Lehmann, C., Portera-Cailliau, C., Koehler, R., Rothstein, J., and Traystman, R.J. (1997) Hypoxia-ischemia causes abnormalities in glutamate transporters and death of astroglia and neurons in newborn striatum. *Ann. Neurol.* **42**, 335–348.
84. Martin, L.J. (2001) Mechanisms of brain damage in animal models of hypoxia-ischemia in newborns. In: *Fetal and neonatal brain injury: Mechanisms, management, and the risks of practice* (Stevenson, D.K. and Sunshine, P., eds.), 2nd edition. Oxford University Press, *in press*.
85. Kimelberg, H.K., Goderie, S.K., Higman, S., Pang, S., and Waniewski, R.A. (1990) Swelling-induced release of glutamate, aspartate, and taurine from astrocyte cultures. *J. Neurosci.* **10**, 1583–1591.
86. McBean, G.J. and Roberts, P.J. (1985) Neurotoxicity of L-glutamate and DL-threo-3-hydroxy-aspartate in the rat striatum. *J. Neurochem.* **44**, 247–254.
87. Tanaka, K., Watase, K., Manabe, T., et al. (1997) Epilepsy and exacerbation of brain injury in mice lacking the glutamate transporter GLT-1. *Science* **276**, 1699–1702.
88. Harada, T., Harada, C., Watanabe, M., et al. (1998) Functions of the two glutamate transporters GLAST and GLT-1 in the retina. *Proc. Natl. Acad. Sci. U.S.A.* **95**, 4663–4666.
89. Ginsberg, S.D., Martin, L.J., and Rothstein, J.D. (1995) Regional deafferentation down-regulates subtypes of glutamate transporter proteins. *J. Neurochem.* **65**, 2800–2803.
90. Ginsberg, S.D., Rothstein, J.D., Price, D.L., and Martin, L.J. (1996) Fimbria-fornix transections selectively down-regulate subtypes of glutamate transporter and glutamate receptor proteins in septum and hippocampus. *J. Neurochem.* **67**, 1208–1216.
91. Anderson, K.J., Nellgård, B., and Wieloch, T. (1993) Ischemia-induced upregulation of excitatory amino acid transport sites. *Brain Res.* **662**, 93–98.
92. Torp, R., Lekieffre, D., Levy, L.M., et al. (1995) Reduced postischemic expression of a glial glutamate transporter, GLT1, in the rat hippocampus. *Exp. Brain Res.* **103**, 51–58.
93. Ferrer-Martinez, A., Felipe, A., Nicholson, B., Casado, J., Pastor-Anglada, M., and McGivan, J. (1995) Induction of the high-affinity Na<sup>+</sup>-dependent glutamate transport system XAG by hypertonic stress in the renal epithelial cell line NBL-1. *Biochem. J.* **310**, 689–692.
94. Conradt, M., Storck, T., and Stoffel, W. (1995) Localization of N-glycosylation sites and functional role of the carbohydrate units of GLAST-1, a cloned rat brain L-glutamate/L-aspartate transporter. *Eur. J. Biochem.* **229**, 682–687.
95. Martin, L.J., Brambrink, A.M., Price A.C., et al. (2000) Neuronal death in newborn striatum after hypoxia-ischemia is necrosis and evolves with oxidative stress. *Neurobiol. Disease* **7**, 169–191.
96. Conradt, M. and Stoffel, W. (1997) Inhibition of the high-affinity brain glutamate transporter GLAST-1 via direct phosphorylation. *J. Neurochem.* **68**, 1244–1251.
97. Casado, M., Bendahan, A., Zafra, F., et al. (1993) Phosphorylation and modulation of brain glutamate transporters by protein kinase C. *J. Biol. Chem.* **268**, 27313–27317.
98. Sieber, F.E., Traystman, R.J., Brown, P.R., and Martin, L.J. (1998) Protein kinase C expression and activity after global incomplete cerebral ischemia in dogs. *Stroke* **29**, 1445–1453.
99. Volterra, A., Trotti, D., Tromba, C., Floridi, S., and Racagni, G. (1994) Glutamate uptake inhibition by oxygen free radicals in rat cortical astrocytes. *J. Neurosci.* **14**, 2924–2932.
100. Trotti, D., Rossi, D., Gjesdal, O., et al. (1996) Peroxynitrite inhibits glutamate transporter subtypes. *J. Biol. Chem.* **271**, 5976–5979.

101. David, J.C., Yamada, K.A., Bagwe, M.R., and Goldberg, M.P. (1996) AMPA receptor activation is rapidly toxic to cortical astrocytes when desensitization is blocked. *J. Neurosci.* **16**, 200–209.
102. Kalimo, H., Rehnström, S., Soderfeldt, B., Olsson, Y., and Siesjö, B.K. (1981) Brain lactic acidosis and ischemic cell damage: 2. Histopathology. *J. Cereb. Blood Flow Metabol.* **1**, 313–327.
103. Norenberg, M.D., Mozes, L.W., Gregorios, J.B., and Norenberg, L.B. (1987) Effects of lactic acid on astrocytes in primary culture. *J. Neuropathol. Exp. Neurol.* **46**, 154–166.
104. Brown, A.W. and Brierley, J.B. (1973) The earliest alterations in rat neurones and astrocytes after anoxia-ischaemia. *Acta Neuropathol.* **23**, 9–22.
105. Rosenberg, P.A., Amin, S., and Leitner, M. (1992) Glutamate uptake disguises neurotoxic potency of glutamate agonists in cerebral cortex in dissociated cell culture. *J. Neurosci.* **12**, 56–61.
106. Sugiyama, K., Brunori, A., and Mayer, M.L. (1989) Glial uptake of excitatory amino acids influences neuronal survival in cultures of mouse hippocampus. *Neuroscience* **32**, 779–791.
107. Sheardown, M.J., Nielsen, E.Ø., Hansen, A.J., Jacobsen, P., and Honoré, T. (1990) 2,3-Dihydroxy-6-nitro-7-sulfamoyl-benzo(F)quinoxaline: a neuroprotectant for cerebral ischemia. *Science* **247**, 571–574.
108. Kirino, T., Robinson, H.P.C., Miwa, A., Tamura, A., and Kawai, N. (1992) Disturbance of membrane function preceding ischemic delayed neuronal death in the gerbil hippocampus. *J. Cereb. Blood Flow Metabol.* **12**, 408–417.
109. Wahlestedt, C., Golanov, E., Yamamoto, S., et al. (1993) Antisense oligodeoxynucleotides to NMDA-R1 receptor channel protect cortical neurons from excitotoxicity and reduce focal ischaemic infarctions. *Nature* **363**, 260–263.
110. Morikawa, E., Mori, H., Kiyama, Y., Mishina, M., Asano, T., and Kirino, T. (1998) Attenuation of focal ischemic brain injury in mice deficient in the  $\epsilon 1$  (NR2A) subunit of NMDA receptor. *J. Neurosci.* **18**, 9727–9732.
111. Di, X., Bullock, R., Watson, J., et al. (1997) Effect of CP101,606, a novel NR2B subunit antagonist of the *N*-methyl-*D*-aspartate receptor, on the volume of ischemic brain damage and cytotoxic brain edema after middle cerebral artery occlusion in the feline brain. *Stroke* **28**, 2244–2251.
112. Martin, L.J., Sieber, F.E., and Traystman, R.J. (2000) Apoptosis and necrosis occur in separate neuronal populations in hippocampus and cerebellum after ischemia and are associated with alterations in metabotropic glutamate receptor signaling pathways. *J. Cereb. Blood Flow Metab.* **20**, 153–167.
113. Buchan, A. and Pulsinelli, W.A. (1990) Hypothermia but not the *N*-methyl-*D*-aspartate antagonist, MK-801, attenuates neuronal damage in gerbils subjected to transient global ischemia. *J. Neurosci.* **10**, 311–316.
114. Sheardown, M.J., Suzdak, P.D., and Nordholm, L. (1993) AMPA, but not NMDA, receptor antagonism is neuroprotective in gerbil global ischaemia, even when delayed 24 h. *Eur. J. Pharmacol.* **236**, 347–353.
115. LeBlanc, M.H., Vig, V., Smith, B., Parker, C.C., Evans, O.B., and Smith, E.E. (1991) MK-801 does not protect against hypoxic-ischemic brain injury in piglets. *Stroke* **22**, 1270–1275.
116. Helfaer, M.A., Ichord, R.N., Martin, L.J., Hurn, P.D., Castro, A., and Traystman, R.J. (1998) Treatment with the competitive NMDA receptor antagonist GPI 3000 does not improve outcome after cardiac arrest in dog. *Stroke* **29**, 824–829.
117. LeBlanc, M.H., Li, X.Q., Huang, M., Patel, D.M., and Smith, E.E. (1995) AMPA antagonist LY293558 does not affect the severity of hypoxic-ischemic injury in newborn pigs. *Stroke* **26**, 1908–1915.
118. Martin, L.J., Brambrink, A., Koehler, R.C., and Traystman, R.J. (1997) Neonatal asphyxial brain injury is neural system preferential and targets sensory-motor networks, in *Fetal and Neonatal*

*Brain Injury: Mechanisms, Management, and the Risks of Practice* (Stevenson, D.K. and Sunshine, P. eds.), Oxford University Press, pp 374-399.

119. Brambrink, A.M., Martin, L.J., Hanley, D.F., Becker, K.J., Koehler, R.C., and Traystman, R.J. (1999) Effects of the AMPA receptor antagonist NBQX on outcome of newborn pigs after asphyxic cardiac arrest. *J. Cereb. Blood Flow Metab.* **19**, 927-938.
120. Sieber, F.E., Brown, P.R., Ichord, R.N., Traystman, R.J., and Martin, L.J. (1998) Antagonists to metabotropic glutamate receptors worsen neurologic outcome following global ischemia. *Soc. Neurosci.* **24**, 897.
121. Kaczmarek, L.K. (1987) The role of protein kinase C in the regulation of ion channels and neurotransmitter release. *TINS* **10**, 30-34.
122. Saitoh, T., Masliah, E., Jin, L.-W., Cole, G.M., Wieloch, T., and Shapiro, I.P. (1991) Protein kinases and phosphorylation in neurologic disorders and cell death. *Lab. Invest.* **64**, 596-616.
123. Candeo, P., Favaron, M., Lengyel, I., Manev, R.M., Rimland, J.M., and Manev, H. (1992) Pathological phosphorylation causes neuronal death: effect of okadaic acid in primary culture of cerebellar granule cells. *J. Neurochem.* **59**, 1558-1561.
124. Hajimohammadreza, I., Probert, A.W., Coughenour, L.L., et al. (1995) A specific inhibitor of calcium/calmodulin-dependent protein kinase-II provides neuroprotection against NMDA- and hypoxia/hypoglycemia-induced cell death. *J. Neurosci.* **15**, 4093-4101.
125. Hara, H., Onodera, H., Yoshidomi, M., Matsuda, Y., and Kogure, K. (1990) Staurosporine, a novel protein kinase C inhibitor, prevents postischemic neuronal damage in the gerbil and rat. *J. Cereb. Blood Flow Metab.* **10**, 646-653.
126. Hu, B.-R. and Wieloch, T. (1995) Persistent translocation of  $\text{Ca}^{2+}$ /calmodulin-dependent protein kinase II to synaptic junctions in the vulnerable hippocampal CA1 region following transient ischemia. *J. Neurochem.* **64**, 277-284.
127. Hu, B.-R., Kamme, F., and Wieloch, T. (1995) Alterations of  $\text{Ca}^{2+}$ /calmodulin-dependent protein kinase II and its messenger RNA in the rat hippocampus following normo- and hypothermic ischemia. *Neuroscience* **68**, 1003-1016.
128. Wieloch, T., Cardell, M., Bingren, H., Zivin, J., and Saitoh, T. (1991) Changes in the activity of protein kinase C and the differential subcellular redistribution of its isozymes in the rat striatum during and following transient forebrain ischemia. *J. Neurochem.* **56**, 1227-1235.
129. Wang, L.-Y., Taverna, F.A., Huang, X.-P., MacDonald, J.F., and Hampson, D.R. (1993) Phosphorylation and modulation of a kainate receptor (GluR6) by cAMP-dependent protein kinase. *Science* **259**, 1173-1175.
130. Raymond, L.A., Blackstone, C.D., and Haganir, R.L. (1993) Phosphorylation and modulation of recombinant GluR6 glutamate receptors by cAMP-dependent protein kinase. *Nature* **361**, 637-641.
131. Tingley, W.G., Roche, K.W., Thompson, A.K., and Haganir, R.L. (1993) Regulation of NMDA receptor phosphorylation by alternative splicing of the C-terminal domain. *Nature* **364**, 70-73.
132. Blackstone, C., Murphy, T.H., Moss, S.J., Baraban, J.M., and Haganir, R.L. (1994) Cyclic AMP and synaptic activity-dependent phosphorylation of AMPA-preferring glutamate receptors. *J. Neurosci.* **14**, 7585-7593.
133. Tan, S.-E., Wenthold, R.J., and Soderling, T.R. (1994) Phosphorylation of AMPA-type glutamate receptors by calcium/calmodulin-dependent protein kinase II and protein kinase C in cultured hippocampal neurons. *J. Neurosci.* **14**, 1123-1129.
134. Wyllie, D.J.A. and Nicoll, R.A. (1994) A role for protein kinases and phosphatases in the  $\text{Ca}^{2+}$ -induced enhancement of hippocampal AMPA receptor-mediated synaptic responses. *Neuron* **13**, 635-643.
135. Desai, M.A., Burnett, J.P., Mayne, N.G., and Schoepp, D.D. (1996) Pharmacological characterization of desensitization in a human mGluR1  $\alpha$ -expressing non-neuronal cell line co-transfected with a glutamate transporter. *Br. J. Pharmacol.* **118**, 1558-1564.

136. Gereau, R.W., IV and Heinemann, S.F. (1998) Role of protein kinase C phosphorylation in rapid desensitization of a metabotropic glutamate receptor 5. *Neuron* **20**, 143–151.
137. Kelso, S.R., Nelson, T.E., and Leonard, J.P. (1992) Protein kinase C-mediated enhancement of NMDA currents by metabotropic glutamate receptors in *Xenopus oocytes*. *J. Physiol.* **449**, 705–718.
138. Aniksztejn, L., Otani, S., Ben-Ari, Y. (1992) Quisqualate metabotropic receptors modulate NMDA currents and facilitate induction of long-term potentiation through protein kinase C. *Eur. J. Neurosci.* **4**, 500–505.
139. Chen, L., and Huang, L.-Y. M. (1992) Protein kinase C reduces  $Mg^{2+}$  block of NMDA-receptor channels as a mechanism of modulation. *Nature* **356**, 521–523.
140. Sieber, F.E., Traystman, R.J., and Martin, L.J. (1997) Delayed neuronal death following global incomplete ischemia in dogs is accompanied by changes in phospholipase C protein expression. *J. Cereb. Blood Flow Metab.* **17**, 527–533.
141. Chang, H.S., Sasaki, T., and Kassel, N.F. (1989) Hippocampal unit activity after transient ischemia in rats. *Stroke* **20**, 1951–1958.
142. Omon, H., Mitani, A., Andou, Y., Arai, T., and Kataoka, K. (1991) Delayed neuronal death is induced without postischemia hyperexcitability: continuous multiple-unit recording from ischemic CA1 neurons. *J. Cereb. Blood Flow Metab.* **11**, 819–823.
143. Mitani, A., Imon, H., Iga, K., Kubo, H., and Kataoka, K. (1990) Gerbil hippocampal extracellular glutamate and neuronal activity after transient ischemia. *Brain Res. Bull.* **25**, 319–324.
144. Urban, L., Neill, K.H., Crain, B.J., Nadler, J.V., and Somjen, G.G. (1989) Postischemic synaptic physiology in area CA1 of the gerbil hippocampus studied *in vitro*. *J. Neurosci.* **9**, 3966–3975.
145. Xu, Z.C. (1995) Neurophysiological changes of spiny neurons in rat neostriatum after transient forebrain ischemia: an *in vivo* intracellular recording and staining study. *Neuroscience* **67**, 823–836.
146. Tsubokawa, H., Ogura, K., Masuzawa, T., and Kawai, N. (1994)  $Ca^{2+}$ -dependent non-NMDA receptor-mediated synaptic currents in ischemic CA1 hippocampal neurons. *J. Neurophysiol.* **71**, 1190–1196.
147. Schmidt, H.H.H.W. and Walter, U. (1994) NO at work. *Cell* **78**, 919–925.
148. Vincent, S.R. (1994) Nitric oxide: a radical neurotransmitter in the central nervous system. *Prog. Neurobiol.* **42**, 129–160.
149. Bredt, D.S., and Snyder, S.H. (1992) Nitric oxide, a novel neuronal messenger. *Neuron* **8**, 3–11.
150. Northington, F.J., Koehler, R.C., Traystman, R.J., and Martin, L.J. (1996) Nitric oxide synthase 1 and nitric oxide synthase 3 protein expression is regionally and temporally regulated in fetal brain. *Dev. Brain Res.* **95**, 1–14.
151. Garthwaite, J., Garthwaite, G., Palmer, R.M.J., and Moncada, S. (1989) NMDA receptor activation induces nitric oxide synthesis from arginine in rat brain slices. *Eur. J. Pharmacol.* **172**, 413–416.
152. Bhardwaj, A., Northington, F.J., Martin, L.J., Hanley, D.F., Traystman, R.J., and Koehler, R.C. (1997) Characterization of metabotropic glutamate receptor mediated nitric oxide production *in vivo*. *J. Cereb. Blood Flow Metab.* **17**, 153–160.
153. Meffert, M.K., Calakos, N.C., Scheller, R.H., and Schulman, H. (1996) Nitric oxide modulates synaptic vesicle docking/fusion reactions. *Neuron* **16**, 1229–1236.
154. Stamler, J.S. (1994) Redox signaling: nitrosylation and related target interactions of nitric oxide. *Cell* **78**, 931–936.
155. Huang, A., Huang, P.L., Panahian, N., Dalkara, T., Fishman, M.C., and Moskowitz, M.A. (1994) Effects of cerebral ischemic in mice deficient in neuronal nitric oxide synthase. *Science* **265**, 1883–1885.
156. Iadecola, C., Zhang, F., Casey, R., Nagayama, M., and Ross, M.E. (1997) Delayed reduction of ischemic brain injury and neurological deficits in mice lacking the inducible nitric oxide synthase gene. *J. Neurosci.* **17**, 9157–9164.

158. Hooper, D.C., Bagasra, O., Marini, J.C., et al. (1997) Prevention of experimental allergic encephalomyelitis by targeting nitric oxide and peroxynitrite: implications for the treatment of multiple sclerosis. *Proc. Natl. Acad. Sci. USA* **94**, 2528–2533.
159. Martin, L.J. (2001) The apoptosis-necrosis continuum in CNS development, injury, and diseases: contributions and mechanisms. In: *Neuroprotection* (Lo, E. and Marwah, J., eds.) Prominent Press, in press.
160. Yoshida, T., Limmroth, V., Irkura, K., and Moskowitz, M.A. (1994) The NOS inhibitor, 7-nitroindazole, decreases focal infarct volume but not the response to topical acetylcholine in pial vessels. *J. Cereb. Blood Flow Metab.* **14**, 924–929.
161. Kuluz, J.W., Prado, R.J., Dietrich, W.D., Schleien, C.L., and Watson, B.D. (1993) The effect of nitric oxide synthase inhibition on infarct volume after reversible focal cerebral ischemia in conscious rats. *Stroke* **24**, 2023–2029.
162. Buchan, A.M., Gertler, S.Z., Huang, Z.-G., Li, H., Chaundy, K.E., and Xue, D. (1994) Failure to prevent selective CA1 neuronal death and reduce cortical infarction following cerebral ischemia with inhibition of nitric oxide synthase. *Neuroscience* **61**, 1–11.
163. Panahian, N., Yoshida, T., Huang, P.L., et al. (1996) Attenuated hippocampal damage after global cerebral ischemia in mice mutant in neuronal nitric oxide synthase. *Neuroscience* **72**, 343–354.
164. Sancesario, G., Iannone, M., Morello, M., Nisticò, G., and Bernardi, G. (1994) Nitric oxide inhibition aggravates ischemic damage of hippocampal but not of NADPH neurons in gerbils. *Stroke* **25**, 436–444.
165. Kirsch, J.R., Bhardwaj, A., Martin, L.J., Hanley, D.F., and Traystman, R.J. (1997) Neither L-arginine nor L-NAME affect neurological outcome after global ischemia in cats. *Stroke* **28**, 2259–2264.
166. Katzman, R. (1993) Education and the prevalence of dementia and Alzheimer's disease. *Neurology* **43**, 13–20.
167. McKhann, G., Drachman, D., Folstein, M., Katzman, R., Price, D., and Stadlan, E.M. (1984) Clinical diagnosis of Alzheimer's disease: report of the NINCDS-ADRDA work group under the auspices of the Department of Health and Human Services task force on Alzheimer's disease. *Neurology* **34**, 939–944.
168. Olshansky, S.J., Carnes, B.A., and Cassel, C.K. (1993) The aging of the human species. *Sci. Am.* **268**, 46–52.
169. Chartier-Harlin, M.-C., Crawford, F., Houlden, H., et al. (1991) Early-onset Alzheimer's disease caused by mutations at codon 717 of the  $\beta$ -amyloid precursor protein gene. *Nature* **353**, 844–846.
170. Goate, A., Chartier-Harlin, M.-C., Mullan, M., et al. (1991) Segregation of a missense mutation in the amyloid precursor protein gene with familial Alzheimer's disease. *Nature* **349**, 704–706.
171. Naruse, S., Igarashi, S., Kobayashi, H., et al. (1991) Mis-sense mutation Val->Ile in exon 17 of amyloid precursor protein gene in Japanese familial Alzheimer's disease. *Lancet* **337**, 978–979.
172. Campion, D., Flaman, J.M., Brice, A., et al. (1995) Mutations of the presenilin 1 gene in families with early-onset Alzheimer's disease. *Hum. Mol. Genet.* **4**, 2373–2377.
173. Sherrington, R., Rogaev, E.I., Liang, Y., et al. (1995) Cloning of a gene bearing missense mutations in early-onset familial Alzheimer's disease. *Nature* **375**, 754–760.
174. Roses, A.D. (1996) Apolipoprotein E alleles as risk factors in Alzheimer's disease. *Annu. Rev. Med.* **47**, 387–400.
175. Sze, C.-I., Bi, H., Kleinschmidt-DeMasters, B.K., Filley, C.M., and Martin, L.J. (2000) Selective regional loss of exocytotic presynaptic vesicle proteins in Alzheimer's disease. *J. Neurol. Sci.* **175**, 81–90.

176. Sze, C.-I., Bi, H., Filley, C.M., Kleinschmidt-DeMasters, B.K., and Martin, L.J. (2001) *N*-Methyl-*D*-aspartate receptor subunits and their phosphorylation status are altered selectively in Alzheimer's disease brain. *J. Neurol. Sci.* **182**, 151–159.
177. Mouton, P.R., Martin, L.J., Calhoun, M.E., Dal Forno, G., and Price, D.L. (1998) Cognitive decline strongly correlates with cortical atrophy in Alzheimer's disease. *Neurobiol. Aging* **19**, 371–377.
178. Alzheimer, A. (1907) Über eine eigenartige Erkrankung der Hirnrinde *Allg. Z. Psychiatrie Psychiatrisch-Gerichtlich Med.* **64**, 146–148.
179. Wisniewski, H.M. and Terry, R.D. (1973) Reexamination of the pathogenesis of the senile plaque, in *Progress in Neuropathology* (Zimmerman, H.M., ed.), Grune & Stratton, New York, pp. 1–26.
180. Allsop, D., Landon, M., and Kidd, M. (1983) The isolation and amino acid composition of senile plaque core protein. *Brain Res.* **259**, 348–352.
181. Masters, C.L., Simms, G., Weinman, N.A., Multhaup, G., McDonald, B.L., and Beyreuther, K. (1985) Amyloid plaque core protein in Alzheimer disease and Down syndrome. *Proc. Natl. Acad. Sci. USA* **82**, 4245–4249.
182. Wong, C.W., Quaranta, V., and Glenner, G.G. (1985) Neuritic plaques and cerebrovascular amyloid in Alzheimer disease are antigenically related. *Proc. Natl. Acad. Sci. USA* **82**, 8729–8732.
183. Müller-Hill, B. and Beyreuther, K. (1989) Molecular biology of Alzheimer's disease. *Annu. Rev. Biochem.* **58**, 287–307.
184. Kang, J., Lemaire, H.-G., Unterbeck, A., et al. (1987) The precursor of Alzheimer's disease amyloid A4 protein resembles a cell-surface receptor. *Nature* **325**, 733–736.
185. Dyrks, T., Weidemann, A., Multhaup, G., et al. (1988) Identification, transmembrane orientation and biogenesis of the amyloid A4 precursor of Alzheimer's disease. *EMBO J.* **7**, 949–957.
186. Weidemann, A., König, G., Bunke, D., et al. (1989) Identification, biogenesis, and localization of precursors of Alzheimer's disease A4 amyloid protein *Cell* **57**, 115–126.
187. Goldgaber, D., Lerman, M.I., McBride, O.W., Saffiotti, U., and Gajdusek, D.C. (1987) Characterization and chromosomal localization of a cDNA encoding brain amyloid of Alzheimer's disease. *Science* **235**, 877–880.
188. Tanzi, R.E., Gusella, J.F., Watkins, P.C., et al. (1987) Amyloid  $\beta$  protein gene: cDNA, mRNA distribution, and genetic linkage near the Alzheimer locus. *Science* **235**, 880–884.
189. Kitaguchi, N., Takahashi, Y., Tokushima, Y., Shiojiri, S., and Ito, H. (1998) Novel precursor of Alzheimer's disease amyloid protein shows protease inhibitory activity. *Nature* **331**, 530–532.
190. Schubert, W., Prior, R., Weidemann, A., et al. (1991) Localization of Alzheimer  $\beta$ A4 amyloid precursor protein at central and peripheral synaptic sites. *Brain Res.* **563**, 184–194.
191. Zheng, H., Jiang, M.-H., Trumbauer, M.E., et al. (1995)  $\beta$ -amyloid precursor protein-deficient mice show reactive gliosis and decreased locomotor activity. *Cell* **81**, 525–531.
192. Nishimoto, I., Okamoto, T., Matsuura, Y., et al. (1993) Alzheimer amyloid protein precursor complexes with brain GTP-binding protein  $G_O$ . *Nature* **362**, 75–79.
193. Schubert, D., Jin, L.-W., Saitoh, T., and Cole, G. (1989) The regulation of amyloid  $\beta$  protein precursor secretion and its modulatory role in cell adhesion. *Neuron* **3**, 689–694.
194. Kametani, F., Haga, S., Tanaka, K., and Ishii, T. (1990) Amyloid  $\beta$ -protein precursor (APP) of cultured cells: secretory and non-secretory forms of APP *J. Neurol. Sci.* **97**, 43–52.
195. Klier, F.G., Cole, G., Stalleup, W., and Schubert, D. (1990) Amyloid  $\beta$ -protein precursor is associated with extracellular matrix. *Brain Res.* **515**, 336–342.
196. Shivers, B.D., Hilbich, C., Multhaup, G., Salbaum, M., Beyreuther, K., and Seeburg, P.H. (1988) Alzheimer's disease amyloidogenic glycoprotein: expression pattern in rat brain suggests a role in cell contact. *EMBO J.* **7**, 1365–1370.



197. Octave, J.-N., de Sauvage, F., and Maloteaux, J.-M. (1989) Modification of neuronal cell adhesion affects the genetic expression of the A4 amyloid peptide precursor. *Brain Res.* **486**, 369–371.
198. Breen, K.C., Bruce, M., and Anderton, B.H. (1991) Beta amyloid precursor protein mediates neuronal cell-cell and cell-surface adhesion. *J. Neurosci. Res.* **28**, 90–100.
199. Chen, M. and Yankner, B.A. (1991) An antibody to  $\beta$  amyloid and the amyloid precursor protein inhibits cell-substratum adhesion in many mammalian cell types. *Neurosci. Lett.* **125**, 223–226.
200. Saitoh, T., Sundsmo, M., Roch, J.-M., et al. (1989) Secreted form of amyloid  $\beta$  protein precursor is involved in the growth regulation of fibroblasts. *Cell* **58**, 615–622.
201. Masliah, E., Mallory, M., Ge, N., and Saitoh, T. (1992) Amyloid precursor protein is localized in growing neurites of neonatal rat brain. *Brain Res.* **593**, 323–328.
202. Milward, E.A., Papadopoulos, R., Fuller, S.J., et al. (1992) The amyloid protein precursor of Alzheimer's disease is a mediator of the effects of nerve growth factor on neurite outgrowth. *Neuron* **9**, 129–137.
203. Siman, R., Card, J.P., Nelson, R.B., and Davis, L.G. (1989) Expression of  $\beta$ -amyloid precursor protein in reactive astrocytes following neuronal damage. *Neuron* **3**, 275–285.
204. Kawarabayashi, T., Shoji, M., Harigaya, Y., Yamaguchi, H., and Hirai, S. (1991) Expression of APP in the early stage of brain damage. *Brain Res.* **563**, 334–338.
205. Shigematsu, K., McGeer, P.L., and McGeer, E.G. (1992) Localization of amyloid precursor protein in selective postsynaptic densities of rat cortical neurons. *Brain Res.* **593**, 353–357.
206. Esch, F.S., Keim, P.S., Beattie, E.C., et al. (1990) Cleavage of amyloid  $\beta$  peptide during constitutive processing of its precursor. *Science* **248**, 1122–1124.
207. Wang, R., Meschia, J.F., Cotter, R.J., and Sisodia, S.S. (1991) Secretion of the  $\beta$ /A4 amyloid precursor protein. Identification of a cleavage site in cultured mammalian cells. *J. Biol. Chem.* **266**, 16960–16964.
208. S.S. Sisodia (1992)  $\beta$ -amyloid precursor protein cleavage by a membrane-bound protease. *Proc. Natl. Acad. Sci. USA* **89**, 6075–6079.
209. Cole, G.M., Huynh, T.V., and Saitoh, T. (1989) Evidence for lysosomal processing of amyloid  $\beta$ -protein precursor in cultured cells. *Neurochem. Res.* **14**, 933–939.
210. Golde, T.E., Estus, S., Younkin, L.H., Selkoe, D.J., and Younkin, S.G. (1992) Processing of the amyloid protein precursor to potentially amyloidogenic derivatives. *Science* **255**, 728–730.
211. Haass, C., Schlossmacher, M.G., Hung, A.Y., et al. (1992) Amyloid  $\beta$ -peptide is produced by cultured cells during normal metabolism. *Nature* **359**, 322–325.
212. Shoji, M., Golde, T.E., Ghiso, J., et al. (1992) Production of the Alzheimer amyloid  $\beta$  protein by normal proteolytic processing. *Science* **258**, 126–129.
213. Knauer, M.F., Soreghan, B., Burdick, D., Kosmoski, J., and Glabe, C.G. (1992) Intracellular accumulation and resistance to degradation of the Alzheimer amyloid A4/ $\beta$  protein. *Proc. Natl. Acad. Sci. USA* **89**, 7437–7441.
214. Turner, R.S., Suzuki, N., Chyung, A.S.C., Younkin, S.G., and Lee, V.M.-Y. (1996) Amyloids  $\beta$ 40 and  $\beta$ 42 are generated intracellularly in cultured human neurons and their secretion increases with maturation. *J. Biol. Chem.* **271**, 8966–8970.
215. Seubert, P., Oltersdorf, T., Lee, M.G., et al. (1993) Secretion of  $\beta$ -amyloid precursor protein cleaved at the amino terminus of the  $\beta$ -amyloid peptide. *Nature* **361**, 260–263.
216. Yang, Y., Turner, R.S., and Gaut, J.R. (1998) The chaperone BiP/GRP78 binds to amyloid precursor protein and decreases A $\beta$ 40 and A $\beta$ 42 secretion. *J. Biol. Chem.* **273**, 25552–25555.
217. Doan, A., Thinakaran, G., Borchelt, D.R., et al. (1996) Protein topology of presenilin 1. *Neuron* **17**, 1023–1030.
218. Lee, M.K., Slunt, H.H., Martin, L.J., et al. (1996) Expression of presenilin 1 and 2 (PS1 and PS2) in human and murine tissues. *J. Neurosci.* **16**, 7513–7525.

219. Thinakaran, G., Borchelt, D.R., Lee, M.K., et al. (1996) Endoproteolysis of presenilin 1 and accumulation of processed derivatives in vivo. *Neuron* **17**, 181–190.
220. Borchelt, D.R., Thinakaran, G., Eckman, C.B., et al. (1996) Familial Alzheimer's disease-linked presenilin 1 variants elevate A $\beta$ 1-42/1-40 ratio in vitro and in vivo. *Neuron* **17**, 1005–1013.
221. Lee, M.K., Borchelt, D.R., Kim, G., et al. (1997) Hyperaccumulation of FAD-linked Presenilin 1 variants in vivo. *Nature Med.* **3**, 756–760.
222. Card, J.P., Meade, R.P. and Davis, L.G. (1998) Immunocytochemical localization of the precursor protein for  $\beta$ -amyloid in the rat central nervous system. *Neuron* **1**, 835–846.
223. Martin, L.J., Sisodia, S.S., Koo, E.H., et al. (1991) Amyloid precursor protein in aged nonhuman primates. *Proc. Natl. Acad. Sci. USA* **88**, 1461–1465.
224. Martin, L.J. (1993) Cellular dynamics of senile plaque formation and amyloid deposition in cerebral cortex: an ultrastructural study of aged nonhuman primates. *Neurobiol. Aging* **14**, 681–683.
225. Yamaguchi, H., Yamazaki, T., Ishiguro, K., Shoji, M., Nakazato, Y., and Hirai, S. (1992) Ultrastructural localization of Alzheimer amyloid $\beta$ /A4 protein precursor in the cytoplasm of neurons and senile plaque-associated astrocytes. *Acta Neuropathol.* **85**, 15–22.
226. Goldgaber, D., Harris, H.W., Hla, T., et al. (1988) Interleukin 1 regulates synthesis of amyloid-protein precursor mRNA in human endothelial cells. *Proc. Natl. Acad. Sci. USA* **86**, 7606–7610.
227. Allsop, D., Haga, S.-I., Haga, C., Ikeda, S.-I., Mann, D.M.A., and Ishii, T. (1989) Early senile plaques in Down's syndrome brains show a close relationship with cell bodies of neurons. *Neuropathol. Appl. Neurobiol.* **15**, 531–542.
228. Yamaguchi, H., Nakazato, Y., Hirai, S., Shoji, M., and Harigaya, Y. (1989) Electron micrograph of diffuse plaques. Initial stage of senile plaque formation in the Alzheimer brain. *Am. J. Pathol.* **135**, 593–597.
229. Probst, A., Langui, D., Ipsen, S., Robakis, N., and Ulrich, J. (1991) Deposition of  $\beta$ /A4 protein along neuronal plasma membranes in diffuse senile plaques. *Acta Neuropathol.* **83**, 21–29.
230. Wisniewski, H.M., Wegiel, J., Wang, K.C., Kujawa, M., and Lach, B. (1989) Ultrastructural studies of the cells forming amyloid fibers in classical plaques. *Can. J. Neurol. Sci.* **16**, 535–542.
231. Frackowiak, J., Wisniewski, H.M., Wegiel, J., Merz, G.S., Iqbal, K., and Wang, K.C. (1992) Ultrastructure of the microglia that phagocytose amyloid and the microglia that produce  $\beta$ -amyloid fibrils. *Acta Neuropathol.* **84**, 225–233.
232. Miyakawa, T., Shimoji, A., Kuramoto, R., and Higuchi, Y. (1982) The relationship between senile plaques and cerebral blood vessels in Alzheimer's disease and senile dementia. Morphological mechanism of senile plaque production. *Virchows Arch. (Cell Pathol.)* **40**, 121–129.
233. Yamaguchi, H., Nakazato, Y., Hirai, S., and Shoji, M. (1990) Immunoelectron microscopic localization of amyloid  $\beta$  protein in the diffuse plaques of Alzheimer-type dementia. *Brain Res.* **508**, 320–324.
234. Yamaguchi, H., Nakazato, Y., Shoji, M., Takatama, M., and Hirai, S. (1991) Ultrastructure of diffuse plaques in senile dementia of the Alzheimer type: comparison with primitive plaques. *Acta Neuropathol.* **82**, 13–20.
235. Troncoso, J.C., Martin, L.J., Dal Forno, G., and Kawas, C.H. (1996) Neuropathology in controls and demented subjects from the Baltimore Longitudinal Study of Aging. *Neurobiol. Aging* **17**, 365–371.
236. Zemlan, F.P., Thienhaus, O.J., and Bosmann, H.B. (1989) Superoxide dismutase activity in Alzheimer's disease: possible mechanism for paired helical filament formation. *Brain Res.* **476**, 160–162.
237. Tan, Y.H., Tischfield, J., and Ruddle, F.H. (1973) The linkage of genes for the human interferon induced antiviral protein and indophenol oxidase-B traits to chromosome G-21. *J. Exp. Med.* **137**, 317–330.

238. Brooksbank, B.W.L. and Balazs, R. (1984) Superoxide dismutase, glutathione peroxidase and lipoperoxidation in Down's syndrome fetal brain. *Dev. Brain Res.* **16**, 37-44.
239. Busciglio, J. and Yankner, B.A. (1995) Apoptosis and increased generation of reactive oxygen species in Down's syndrome neurons in vitro. *Nature* **378**, 776-779.
240. Pappolla, M.A., Omar, R.A., Kim, K.S., and Robakis, N.K. (1992) Immunohistochemical evidence of antioxidant stress in Alzheimer's disease. *Am. J. Pathol.* **140**, 621-628.
241. Weisiger, R.A. and Fridovich, I. (1973) Superoxide dismutase, organelle specificity. *J. Biol. Chem.* **248**, 3582-3592.
242. Wong, G.H.W. and Goeddel, D.V. (1988) Induction of manganous superoxide dismutase by tumor necrosis factor: possible protective mechanism. *Science* **242**, 941-944.
243. Masuda, A., Longo, D.L., Kobayashi, Y., Appella, E., Oppenheim, J.J., and Matsushima, K. (1988) Induction of mitochondrial manganese superoxide dismutase by interleukin 1. *FASEB J.* **2**, 3087-3090.
244. McGeer, E.D. and McGeer, P.L. (1998) Inflammation in the brain in Alzheimer's disease: implications for therapy. *NeuroScience News* **1**, 29-35.
245. Sawada, M., Kondo, N., Suzumura, A., and Marunouchi, T. (1989) Production of tumor necrosis factor- $\alpha$  by microglia and astrocytes in culture. *Brain Res.* **491**, 394-397.
246. Colton, C.A. and Gilbert, D.L. (1987) Production of superoxide anions by a CNS macrophage, the microglia. *FEBS Lett.* **223**, 284-288.
247. Sharonov, B.P. and Churilova, I.V. (1992) Inactivation and oxidative modification of Cu,Zn superoxide dismutase by stimulated neutrophils: the appearance of new catalytically active structures. *Biochem. Biophys. Res. Commun.* **189**, 1129-1135.
248. Kuncel, R.W., Crawford, T.O., Rothstein, J.D., and Drachman, D.B. (1992) Motor neuron diseases, in *Diseases of the Nervous System. Clinical Neurobiology* (Asbury, A.K., McKhann, G.M., and McDonald, W.I., eds.), WB Saunders, Philadelphia, pp. 1179-1208.
249. Gurney, M.E., Pu, H., Chiu, A.Y., et al. (1994) Motor neuron degeneration in mice that express a human Cu,Zn superoxide dismutase mutation. *Science* **264**, 1772-1775.
250. Wong, P.C., Pardo, C.A., Borchelt, D.R., et al. (1995) An adverse property of a familial ALS-linked SOD1 mutation causes motor neuron disease characterized by vacuolar degeneration of mitochondria. *Neuron* **14**, 1105-1116.
251. Rabizadeh, S., Butler Gralla, E., Borchelt, D.R., et al. (1995) Mutations associated with amyotrophic lateral sclerosis convert superoxide dismutase from an antiapoptotic gene to a proapoptotic gene: studies in yeast and neural cells. *Proc. Natl. Acad. Sci. USA* **92**, 3024-3028.
252. Ghadge, G.D., Lee, J.P., Bindokas, V.P., et al. (1997) Mutant superoxide dismutase-1-linked familial amyotrophic lateral sclerosis: molecular mechanisms of neuronal death and protection. *J. Neurosci.* **17**, 8756-8766.
253. Troy, C.M. and Shelanski, M.L. (1994) Down-regulation of copper/zinc superoxide dismutase causes apoptotic death in PC12 neuronal cells. *Proc. Natl. Acad. Sci. USA* **91**, 6384-6387.
254. Xu, Z., Cork, L.C., Griffin, J.W., and Cleveland, D.W. (1993) Increased expression of neurofilament subunit NF-L produces morphological alterations that resemble the pathology of human motor neuron disease. *Cell* **73**, 23-33.
255. Côté, F., Collard, J.-F., and Julien, J.-P. (1993) Progressive neuronopathy in transgenic mice expressing the human neurofilament heavy gene: a mouse model of amyotrophic lateral sclerosis. *Cell* **73**, 35-46.
256. Lee, M.K., Marszalek, J.R., and Cleveland, D.W. (1994) A mutant neurofilament subunit causes massive, selective motor neuron death: implications for the pathogenesis of human motor neuron disease. *Neuron* **13**, 975-988.
257. Anand, P., Parrett, A., Martin, J., et al. (1995) Regional changes of ciliary neurotrophic factor and nerve growth factor levels in post mortem spinal cord and cerebral cortex from patients with motor disease. *Nature Med.* **1**, 168-172.

258. Kostic, V., Jackson-Lewis, V., de Bilbao, F., Dubois-Dauphin, M., and Przedborski, S. (1997) Bcl-2: prolonging life in a transgenic mouse model of familial amyotrophic lateral sclerosis. *Science* **277**, 559–562.
259. Friedlander, R.M., Brown, R.H., Gagliardini, V., Wang, J., and Juan, J. (1997) Inhibition of ICE slows ALS in mice. *Nature* **388**, 31.
260. Ginsberg, S.D., Portera-Cailliau, C., and Martin, L.J. (1999) Fimbria-fornix transection and excitotoxicity produce similar neurodegeneration in the septum. *Neuroscience* **88**, 1059–1071.
261. Chase, R.A., Pearson, S., Nunn, P.B., and Lantos, P.L. (1985) Comparative toxicities of  $\alpha$ - and  $\beta$ -N-oxalyl-L- $\alpha,\beta$ -diaminopropionic acids to rat spinal cord. *Neurosci. Lett.* **55**, 89–94.
262. Plaitakis, A. (1990) Glutamate dysfunction and selective motor neuron degeneration in amyotrophic lateral sclerosis: a hypothesis. *Ann. Neurol.* **28**, 3–8.
263. Rothstein, J.D., Tsai, G., Kuncl, R.W., et al. (1990) Abnormal excitatory amino acid metabolism in amyotrophic lateral sclerosis. *Ann. Neurol.* **28**, 18–25.
264. Camu, W., Billiard, M., and Baldy-Moulinier, M. (1993) Fasting plasma and CSF amino acid levels in amyotrophic lateral sclerosis: a subtype analysis. *Acta Neurol. Scand.* **88**, 51–55.
265. Perry, T.L., Krieger, C., Hansen, S., and Eisen, A. (1990) Amyotrophic lateral sclerosis: amino acid levels in plasma and cerebrospinal fluid. *Ann. Neurol.* **28**, 12–17.
266. Lin, C.-L., Bristol, L.A., Jin, L., et al. (1998) Aberrant RNA processing in neurodegenerative disease: the cause for absent EAAT2, a glutamate transporter, in amyotrophic lateral sclerosis. *Neuron* **20**, 589–602.
267. Shi, L., Mallory, M., Alford, M., Tanaka, S., and Masliah, E. (1997) Glutamate transporter alterations in Alzheimer's disease are possibly associated with abnormal APP expression. *J. Neuropathol. Exp. Neurol.* **56**, 901–911.
268. Nagai, M., Abe, K., Okamoto, K., and Itoyama, Y. (1998) Identification of alternative splicing forms of GLT-1 mRNA in the spinal cord of amyotrophic lateral sclerosis patients. *Neurosci. Lett.* **244**, 165–168.
269. Meyer, T., Münch, C., Knappenberger, B., Liebau, S., Völkel, H., and Ludolph, A.C. (1998) Alternative splicing of the glutamate transporter EAAT2. *Neurosci. Lett.* **241**, 68–70.
270. Meyer, T., Münch, C., Liebau, S., et al. (1998) Splicing of the glutamate transporter EAAT2: a candidate gene of amyotrophic lateral sclerosis. *J. Neurol. Neurosurg. Psychiatry* **65**, 920.
271. Blackstone, C.D., Levey, A.I., Martin, L.J., Price, D.L., and Haganir, R.L. (1992) Immunological detection of glutamate receptor subtypes in human central nervous system. *Ann. Neurol.* **31**, 680–683.
272. Martin, L.J., Blackstone, C.D., Levey, A.I., Haganir, R.L., and Price, D.L. (1993) AMPA glutamate receptor subunits are differentially distributed in rat brain. *Neuroscience* **53**, 327–358.
273. Portera-Cailliau, C., Price, D.L., and Martin, L.J. (1996) *N*-methyl-D-aspartate receptor proteins NR2A and NR2B are differentially distributed in the developing rat central nervous system as revealed by subunit-specific antibodies. *J. Neurochem.* **66**, 692–700.
274. Williams, T.L., Ince, P.G., Oakley, A.E., and Shaw, P.J. (1996) An immunocytochemical study of the distribution of AMPA selective glutamate receptor subunits in the normal human motor system. *Neuroscience* **74**, 185–198.
275. Petralia, R.S., Wang, Y.-X., and Wenthold, R.J. (1994) The NMDA receptor subunits NR2A and NR2B show histological and ultrastructural localization patterns similar to those of NR1. *J. Neurosci.* **14**, 6102–6120.
276. Escarrabill, J., Estopa, R., Farrero, E., Monasterio, C., and Manresa, F. (1998) Long-term mechanical ventilation in amyotrophic lateral sclerosis. *Respir. Med.* **92**, 438–441.
277. Obrenovitch, T.P. (1998) Amyotrophic lateral sclerosis, excitotoxicity and riluzole. *TIPS* **19**, 9.
278. Milligan, C.E., Prevette, D., Yaginuma, H., et al. (1995) Peptide inhibitors of the ICE protease family arrest programmed cell death of motoneurons in vivo and in vitro. *Neuron* **15**, 385–393.